Emanuel Tschopp

MSc in Paleontology

Evolution of Diplodocid Sauropod Dinosaurs with Emphasis on Specimens from Howe Ranch, Wyoming (USA)

Dissertação para obtenção do Grau de Doutor em Geologia, especialidade de Paleontologia

Orientador: Prof. Octávio Mateus, CICEGe-FCT, Universidade Nova de Lisboa

Júri:

Presidente:	Prof. Doutora Maria Paula Pires dos Santos Diogo
Arguentes:	Prof. Doutor Paul Upchurch
	Prof. Doutor Louis Jacobs
Vogais:	Prof. Doutor Rogério Rocha
	Prof. Doutor João Pais
	Doutor Fidel Torcida Fernández-Baldor
	Prof. Doutor Octávio Mateus

FACULDADE DE CIÊNCIAS E TECNOLOGIA
UNIVERSIDADE NOVA DE LISBOA

Outubro 2013

LOMBADA

Evolution of Diplodocid Sauropod Dinosaurs

Emanuel Tschopp

2013

Emanuel Tschopp

MSc in Paleontology

Evolution of Diplodocid Sauropod Dinosaurs with Emphasis on Specimens from Howe Ranch, Wyoming (USA)

Dissertação para obtenção do Grau de Doutor em Geologia, especialidade de Paleontologia

Orientador: Prof. Octávio Mateus, CICEGe-FCT, Universidade Nova de Lisboa

Júri:

Presidente:	Prof. Doutora Maria Paula Pires dos Santos Diogo
Arguentes:	Prof. Doutor Paul Upchurch
	Prof. Doutor Louis Jacobs
Vogais:	Prof. Doutor Rogério Rocha
	Prof. Doutor João Pais
	Doutor Fidel Torcida Fernández-Baldor
	Prof. Doutor Octávio Mateus

FACULDADE DE CIÊNCIAS E TECNOLOGIA
UNIVERSIDADE NOVA DE LISBOA

Outubro 2013

dedicata a te

per la tua pazienza infinita
per il tuo sostegno e supporto straordinario

per il tuo amore

grazie

Acknowledgment

A Ph.D. thesis cannot be undertaken without a supervisor, so my first, big "thank you" goes to Octávio Mateus, who was a thoughtful and understanding mentor. He found the perfect equilibrium between tight guidance and leaving room for my own decisions, and thereby easily managed to keep my interest in science very strong.

Further thanks go to the remaining members of the doctoral committee, which are Martin Sander (Bonn, Germany), João Pais, Rogerio Rocha (both CICEGe), and Louis Jacobs (Dallas, USA). They were there when I needed further advice or help with administrative things.

Besides them, most importantly, I want to thank Köbi Siber (or Kirby for the English speaking readers), and anybody else from the Sauriermuseum Aathal (Switzerland), not only for the possibility to study material under their care during my Ph.D. thesis, but especially for their continuing support and inspiration during my entire (yet still short) scientific career. I obtained my first preparation skills in the museum, the first professional paleontological excavation I took part was at the Howe Ranch, I held my first scientific presentation at the Stegosaur Symposium in Aathal in 2009, and my first scientific paper was a result from the studies done for the symposium in material from the Sauriermuseum. I was allowed to photograph, laser scan, drill, CT scan, take samples for SEM, and museum staff was always available for help. Through the museum, and especially thanks to Köbi, I got to know many important paleontologists on my way, among which was also my present supervisor Octávio Mateus. Finally, the Sauriermuseum also provided financial support for some of my studies, or for travels to field work or conferences, which I greatly acknowledge.

From the Sauriermuseum staff I want to thank in particular, and specifically for the work done for my Ph.D. thesis: Esther Premru for the outstanding work during the preparation of the bones and the drawing of the quarry map of the holotype specimen of *Kaatedocus siberi* SMA 0004, Ben Pabst for the stunning reconstruction of its skull, and Martin Kistler and Ben Pabst for the help with the dismantling of SMA 0004 for the structured light scanning. Martin Kistler and his team also helped a lot with opening boxes for the study of SMA 0011. Preparation of that specimen was led by Yoli Siber, together with Maya Siber, Esther Wolfensberger, and myself back in 2001 and 2002. Specimen SMA 0087 is being prepared by Christina Egli and Yoli Siber, quarry maps of both SMA 0011 and 0087 were drawn by Esther Premru.

I furthermore want to thank the staff of the Museu da Lourinhã for their companionship, and the technical support during my stay in Lourinhã. Particular thanks go to the entire Mateus family for hospitality, and to João Russo and Simão Mateus for their help with the thesis formatting and printing.

I highly appreciated the work with my co-authors and collaborators for some of the papers published during the time of my Ph.D.: Gordon Dzemski (Flensburg, Germany) introduced me to 3D scanning and reproduction, which lead to two articles (Tschopp and Dzemski, 2012; Tschopp et al., 2013). João Russo (CICEGe) contributed the part on deforming a Dodo cervical vertebra to the retrodeformation paper, which is part of the present thesis (Tschopp et al., 2013). Inspiring artistic collaborations were made with Davide Bonadonna (Milan, Italy), Andrea Pirondini (Bologna, Italy), and Simão Mateus (ML). Bonadonna provided the highly accurate skull life reconstruction of *Kaatedocus siberi* for the description (Tschopp and Mateus, 2012b: fig. 12), and with an extended version of this life reconstruction, arranged as a poster by Pirondini, he won the 2013 Lanzendorf PaleoArt Award of the Society of Vertebrate Paleontology in the category Scientific Illustration. A second piece with *Kaatedocus siberi* in his environment at the Howe Quarry locality was used as background for the new permanent exhibit around the holotype specimen at SMA, and was awarded the 2013 Lanzendorf PaleoArt Award of SVP in the category 2D Illustration. Simão Mateus created the beautiful reconstruction of the skull of *Galeamopus shellensis*.

I am very grateful for all the help provided for the publications during my Ph.D., and the comments and corrections for the yet unpublished thesis chapters. Louis Jacobs, Mike Polcyn, and Ricardo Araújo (South. Methodist Univ., Dallas, Texas, USA) provided access to high end 3D software and computers at the Visualization Lab of the Huffington Department of Earth Sciences, and made helpful comments on a first draft of the manuscript of the retrodeformation paper. Andreas Christian and Jan-Thomas Möller (Univ. of Flensburg, Germany), helped with the dismantling and scanning of SMA 0004. I am indebted to David Allan (DNSM) and Leon Claessens (Holy Cross, Worcester, USA) for providing the 3D model of the Dodo cervical. David Wiley (Univ. of California) was providing references and further information concerning the retrodeformation tools. Comments on an early version of the description of *Kaatedocus* by Phil Mannion (Imperial Coll., London), John Whitlock (Mt. Aloysius Coll., Cresson) and Paul Upchurch (Univ. Coll. London) improved the quality of the final paper considerably. João Marinheiro (CICEGe) and Matthias Meier (Wetzikon, Switzerland) assisted with photography and taking measurements during the description of *Kaatedocus*. Laura Redish was of great help concerning the Crow/Absaroka language and the naming of *Kaatedocus*. I greatly acknowledge the fruitful discussions with Matthew Vickaryous (Univ. of Guelph, Canada) on interclavicular development, and with

Regina Fechner (Univ. Bochum, Germany) on sauropodomorph gastralia and sternal ribs, and for her comments on a first draft of the clavicles manuscript. Ricardo Araújo and Jasmina Hugi (Winterthur, Switzerland) were of great help with finding literature on the embryological development of the various chest bones in reptiles, birds and mammals. Emanuele Minari (Turin, Italy) translated the description of the clavicle of *Datousaurus* in Dong and Tang (1984). Octávio Mateus, Christophe Hendrickx (CICEGe), Steve Brusatte (Univ. of Edinbourgh), Jay Nair (Univ. of Queensland), and Mike Taylor (Univ. of Bristol) reviewed an earlier version of portions of the dissertation. Ioannis Michelis shared information concerning *Barosaurus* and the Howe Quarry material. Remo Forster (Zürich, Switzerland) helped with some figures of the specimen SMA 0087. Lara Couldwell (ML), Holly Barden (Univ. of Manchester), Steve Brusatte, Jay Nair, and Mike Taylor provided corrections for the English. I also want to thank the editorial staffs of the Journal of Paleontological Techniques, the Journal of Systematic Palaeontology, the Journal of Anatomy, and Palaeontologia Electronica for their help, as well as four anonymous reviewers for thoughtful and detailed reviews of the published papers.

A specimen-based phylogenetic analysis as performed herein is highly dependent on personal observations of the specimens included. Although it was not possible to see all of them, many collection visits were possible thanks to the help and hospitality from the following people: Kate Wellspring (AC), Carl Mehling, Mark Norell, and Alana Gishlick (AMNH), Ted Daeschler and Ned Gilmore (ANS), Amy Henrici, Matthew Lamanna, and Dan Pickering (CM), Rafael Royo-Torres and Edoardo Espilez (CPT), Daniela Schwarz-Wings (MB.R.), Virginia Tidwell and Logan Ivy (DMNS), David Temple (HMNS), Margarita Belinchón (MCNV), Paul Barrett and Sandra Chapman (NHMUK), Matt Carrano and Mike Brett-Surman (USNM), Ralf Kosma, Achim Ritter, and Ulrich Joger (SNHM), Bill Wahl and Malcolm Bedell (WDC), and Dan Brinkman and Marilyn Fox (YPM). Several people shared numerous pictures of specimens I was not able to see myself: Christophe Hendrickx, Carl Mehling, Dave Lovelace (Univ. of Wisconsin), Henry Galiano (Dinosauria International), Heiner Mallison (MB.R.), José Carballido (MPEF), Jean Le Loeuff (Esperaza, France), Jay Nair, John Whitlock, Kelli Trujillo (Univ. of Wyoming), Mattia Baiano (Inst. Cat. Pal, Barcelona), Mike Brett-Surman, Matt Wedel (West. Univ. of Health Sciences, Pomona), Nils Knötschke (Dinopark Münchehagen), Octávio Mateus, Phil Mannion, Pong Suteethorn (Univ. of Mahasarakham, Thailand), Regina Fechner, Ralf Kosma, Takehito Ikejiri (Univ. of Alabama), Virginia Tidwell, William Gearty (YPM), and William Simpson (FMNH).

I thank the Willy Hennig Society for making the phylogeny software TNT freely accessible, and Andrea Cau (Museo Geologico "Cappellini", Bologna), Jay Nair, and especially José Carballido for invaluable help with phylogenetic techniques.

This study would not have been possible without the financial support throughout my Ph.D. through the doctoral fellowship from the Fundação para a Ciência e a Tecnologia of the Ministério de Educação e Ciência, Portugal (SFRH / BD / 66209 / 2009), under which I also received additional travel subsidies for my stay at South. Methodist Univ. Many thanks go to the Jurassic Foundation for the funding of a project of 3D digitalization and the study of serial variation in sauropod cervical and caudal vertebrae. Travel subsidies were kindly provided by the following institutions: European Science Foundation (a short visit grant for a histology course at Univ. of Bonn, Germany), Jackson School of Geosciences (for the attendance and poster presentation at the SVP conference in Pittsburgh, 2010), Synthesys (DE-TAF-1150; for a collection visit at Museum für Naturkunde, Berlin), Fundação Lusoamericana (for a talk at the Romer Prize Session at the SVP conference in Los Angeles, 2013), and the Sauriermuseum Aathal and Siber & Siber (for the participation at excavations in Wyoming, 2010, and the attendance at the SVP conference in Los Angeles, 2013).

Last but not least, thousand thanks to all my friends and family. Your moral support gave me the strength to go on this journey (or these many journeys), which sometimes seemed never-ending.

Resumo

Os Diplodocidae estão entre os dinossauros saurópodes mais conhecidos. Várias espécies foram descritas no final do século XIX ou início de XX. Desde então, numerosos espécimes outros foram recuperados nos EUA, Tanzânia, Portugal, bem como, possivelmente de Espanha, Inglaterra e Ásia. Até à data, o clado inclui 12 a 15 espécies diferentes, algumas delas com estatuto taxonómico questionável como, por exemplo, '*Diplodocus*' *hayi* ou *Dyslocosaurus polyonychius*. No entanto, as relações intragenéricas de géneros multi-específicos e icónicos como *Apatosaurus* e *Diplodocus* ainda são pouco conhecidos. A maneira de resolver este desafio é uma análise filogenética baseada em espécimes, o que foi feito para *Apatosaurus*, mas aqui é realizada pela primeira vez para todo o clado Diplodocidae.

Novo material de diferentes localidades e níveis estratigráficos (em Howe Ranch, Shell, Wyoming, EUA) aumenta o conhecimento sobre a evolução dos Diplodocidae. Três novos espécimes são aqui descritos, aumentando consideravelmente o nosso conhecimento da anatomia do grupo. Os novos espécimes (SMA 0004, SMA 0011 e SMA 0087) representam duas, possivelmente três novas espécies de diplodocídeos, e compreendem material ósseo de todas as partes do esqueleto, incluindo dois crânios quase completos, bem como membros anteriores e posteriores bastante completos, o que é geralmente raro em diplodocídeos. Desta forma, os espécimes permitem um aumento consideravel da sobreposição anatómica entre holótipos que amiúde são incompletos, o que permite obter resultados significativos nesta análise filogenética com base em espécimes. Além disso, são identificados os ossos clavícula e interclavícula, sendo este último aqui reportado pela primeira vez em dinossauros. A sua presença parece restrita aos primeiros saurópodes, Flagellicaudata e Macronaria basais, e pode por isso ser um caso de retenção de plesiomorfia, com a perda destes ossos como sinapomorfia dos Titanosauriformes e possivelmente Rebbachisauridae.

Os novos espécimes permitem testar anteriores hipóteses filogenéticas dos diplodocídeos. Com esse objectivo, todos os espécimes-tipo previamente propostos como diplodocídeos foram incluído no estudo, assim como outros espécimes relativamente completos de forma a aumentar a sobreposição anatómica entre eles. Espécimes ulteriormente sugeridos como saurópodes não-diplodocídeos, foram incluídos como grupos externos. A análise filogenética resultante inclui, assim, 76 unidades taxonómicas operacionais, 45 das quais pertencem a Diplodocidae. Cada espécime foi codificado para 477 caracteres morfológicos, o que representa uma das mais extensas análises filogenéticas de dinossauros saurópodes. O cladograma resultante recupera o arranjo clássico das relações filogenéticas dos diplodocídeos.

Foi realisada uma abordagem numérica para reduzir a subjetividade na decisão de separação específica ou genérica, para as espécies que historicamente têm sido incluídas em géneros conhecidos, como *Apatosaurus* ou *Diplodocus*, tendo algumas resultado serem genericamente diferente. Desse modo, o famoso género *Brontosaurus* é ressuscitado, e as evidências sugerem, ainda que também *Elosaurus parvus* (anteriormente designados *Apatosaurus*) ou *'Diplodocus' hayi* representam géneros únicos. O estudo aumenta o conhecimento sobre a variação individual, e ajuda a decidir como classificar géneros multi-específicos. Este tipo de análise filogenética baseada em espécimes provou ser uma ferramenta valiosa para validar espécies históricas em saurópodes, e na paleontologia como um todo.

Palavras-chave: Dinossauros saurópodes, Diplodocidae, filogenia baseada em espécimes, Formação Morrison, Howe Quarry, *Kaatedocus*, espécie, taxonomia.

Abstract

Diplodocidae are among the best known sauropod dinosaurs. Several species were described in the late 1800s or early 1900s. Since then, numerous additional specimens were recovered in the USA, Tanzania, Portugal, as well as possibly Spain, England, and Asia. To date, the clade includes about 12 to 15 different species, some of them with questionable taxonomic status (e.g. '*Diplodocus*' *hayi* or *Dyslocosaurus polyonychius*). However, intrageneric relationships of the multi-species, iconic genera *Apatosaurus* and *Diplodocus* are still poorly known. The way to resolve this issue is a specimen-based phylogenetic analysis, which was done for *Apatosaurus*, but is here performed for the first time for the entire clade of Diplodocidae.

New material from different localities and stratigraphic levels on the Howe Ranch (Shell, Wyoming, USA) sheds additional light on the evolution of Diplodocidae. Three new specimens are described herein, considerably increasing our knowledge of the anatomy of the group. The new specimens (SMA 0004, SMA 0011, and SMA 0087) represent two, to possibly three new diplodocid species. They preserve material from all parts of the skeleton, including two nearly complete skulls, as well as fairly complete manus and pedes, material which is generally rare in diplodocids. Thereby, they considerably increase anatomical overlap between the sometimes fragmentary holotype specimens of the earlier described diplodocid species, allowing for significant results in a specimen-based phylogenetic analysis. Furthermore, clavicles and interclavicles are identified, the latter for the first time in dinosaurs. Their presence seems restricted to early sauropods, flagellicaudatans, and early Macronaria, and might thus be a retained plesiomorphy, with the loss of these bones being synapomorphic for Titanosauriformes and possibly Rebbachisauridae.

The new material allows to test previous hypotheses of diplodocid phylogeny. In order to do so, any type specimen previously proposed to belong to Diplodocidae was included in the study, as are relatively complete referred specimens, in order to increase the degree of overlapping material. For specimens subsequently suggested to be non-diplodocid sauropods, their hypothesized sister taxa were included as outgroups. The current phylogenetic analysis thus includes 76 operational taxonomic units, 45 of which belong to Diplodocidae. The specimens were scored for 477 morphological characters, representing one of the most extensive phylogenetic analyses done within sauropod dinosaurs.

The resulting cladogram recovers the classical arrangement of diplodocid relationships. Basing on a newly developed numerical approach to reduce subjectivity in the decision of specific or generic separation, species that have historically been included into well-known genera like *Apatosaurus* or *Diplodocus*, were detected to be actually generically different. Thereby, the famous genus *Brontosaurus* is resuscitated, and evidence further suggests that also *Elosaurus parvus* (previously referred to *Apatosaurus*) or '*Diplodocus*' *hayi* represent unique genera. The study increases our knowledge about individual variation, and helps to decide how to score multi-species genera. Such a specimen-based phylogenetic analysis thus proves a valuable tool to validate historic species in sauropods, and in paleontology as a whole.

Keywords: Sauropod dinosaurs, Diplodocidae, specimen-based phylogeny, Morrison Formation, Howe Quarry, *Kaatedocus*, species, taxonomy.

Chapters

Figures

(d) SMA L 22-3; (e) SMA L 27-7. Scale bar = 10 cm. Gray areas in (a) indicate broken surfaces. Note the bifurcate end on top and the spatulate end at the bottom.

Figure 4.4: Photographs of morphotype A element AMNH 30900. Scale bar = 10 cm.

Figure 4.5: Photographs of morphotype A element SMA I 24-4. Scale bar = 10 cm.

Figure 4.6: Photographs of morphotype A element SMA M 25-3. Scale bar = 10 cm.

Figure 4.7: Photographs of morphotype A element SMA L 22-3. Scale bar = 10 cm.

Figure 4.8: Photographs of morphotype A element SMA L 27-7. Scale bar = 10 cm.

Figure 4.9: Drawings of the pair of morphotype B elements SMA K 24-3 (outer bone) and SMA K 24-6 (inner bone) in internal (a) and external (b) view. Short leg of L-shaped bones shown in perpendicular view below. Note the considerable bend of this portion in respect to the main axis of the bone. Scale bar = 10 cm.

Figure 4.10: Photographs of the morphotype B element SMA K 24-6. Scale bar = 5 cm.

Figure 4.11: Photographs of the morphotype B element SMA K 24-3. Scale bar = 10 cm.

Figure 4.12: Drawings of the pair of morphotype B elements AMNH 30789 in internal (a) and external (b) view. Scale bar = 10 cm.

Figure 4.13: Photographs of the left morphotype B element AMNH 30789. Scale bar = 10 cm.

Figure 4.14: Photographs of the right morphotype B element AMNH 30789. Scale bar = 10 cm.

Figure 4.15: Morphotype B elements of the diplodocid DQ-SB, articulated with the acromia (arrowheads) of the scapulae, as they were found. Co, coracoid; MB, morphotype B element; Sc, scapula. Picture courtesy of H. Galiano.

Figure 4.16: Coracoid with taphonomically attached morphotype B element (MB) of the non-somphospondylian macronarian SMA 0009 in posteroventral (a) and lateral (b) view. Coracoid made semitransparent in order to visualize better the morphotype B element. Arrows indicate brightly colored matrix present between the MB and the coracoid. CF, coracoid foramen; GL, glenoid surface. Scale bar = 2 cm.

Figure 4.17: Drawings of morphotype C elements SMA H 20-7 (a) and L 21-5 (b). Both elements are incomplete, fracture surface at the top is indicated by the gray area. Scale bar = 10 cm.

Figure 4.18: Photographs of the morphotype C element SMA H 20-7. Scale bar = 10 cm.

Figure 4.19: Photographs of the morphotype C element SMA L 21-5. Scale bar = 10 cm.

Figure 4.20: Drawings of morphotype D elements SMA D 28-5 (a), M 21-2 (b) and M 21-8 (c). The bottom end of M 21-8 is broken. Scale bar = 10 cm.

Figure 4.21: Photographs of the morphotype D element SMA D 28-5. Scale bar = 10 cm.

Figure 4.22: Photographs of the morphotype D element SMA M 21-2. Scale bar = 10 cm.

Figure 4.23: Photographs of the morphotype D element SMA M 21-8. Scale bar = 10 cm.

Figure 4.24: Proposed articulation between two morphotype D elements (left, SMA D 28-5; right, SMA D 28-14) in three views (internal/dorsal view in the center, gray lines indicate the same morphological landmarks on the respective elements). Note the similarity to the central portion of the fused morphotype D element (Fig. 4.23). Scale bar = 5 cm.

Figure 4.25: Drawings of morphotype E elements SMA H 21-3 (a), N 22-12 (b) and M 21-15 (c). Note the irregular shapes that do not allow an assignation to any other morphotype. Dotted lines in (a) indicate direction of the broken hook-like projection. Scale bar = 10 cm.

Figure 4.26: Photographs of morphotype E element SMA M 21-15. Scale bar = 10 cm.

Figure 4.27: Photographs of morphotype E element SMA N 22-12. Scale bar = 10 cm.

Figure 4.28: Reconstruction of the pectoral girdle and the chest region of an indeterminate diplodocid sauropod, based on the finds reported. Light gray elements represent pectoral girdle elements not discussed in the paper, dark gray elements mark the bones identified as chest bone morphotypes in this paper. Anterior (a) and ventral (b) view. Abbreviations: aDR, anterior dorsal ribs; Cl, clavicle (morphotype B); Co, coracoid; DR, dorsal rib; Ga, gastralia (morphotype D); In, interclavicle (morphotype A); pDR, posterior dorsal ribs; Sc, scapula; SP,

sternal plates; SR, sternal ribs (morphotypes C and E); VC, vertebral column. Modified from Schwarz et al. (2007a; a) and Filla and Redman (1994; b).

Figure 4.29: Evolution of the furcula, comparison between the two hypotheses. Note the gap within Dinosauriformes in the furcula-interclavicle hypothesis. Line drawings scaled to same size. Eaton and Stewart (1960: *Hesperoherpeton*); Chatterjee (1978: *Parasuchus*); Klima (1987: *Ornithorhynchus*); Rieppel (1992: *Lacerta*); Steyer et al. (2000: *Aphanerama*); Benton and Walker (2002: *Erpetosuchus*); Martz (2002: *Typothorax*); Vickaryous and Hall (2006: *Dimetrodon*; 2010: *Alligator*, *Basilicus*, *Gallus*, *Leptoceratops*); Remes (2008: *Euparkeria*); Dilkes and Sues (2009: *Doswellia*).

Figure 5.1: Quarry map of SMA 0011, indicating the single bones found. Note the separation of the cervical series and the skull from the dorsal column and the appendicular skeleton. Color code: skull (orange), CV (red), DV (violet), DR and SR (yellow), PcG (light green), PvG (dark green), Fl (light blue), Hl (dark blue). Abb.: Bc, braincase; co, coracoid; CR, cervical rib; CV, cervical vertebra; DR, dorsal ribs; DV, dorsal vertebra; fe, femur; fi, fibula; Fl, forelimb; h, humerus; Hl, hindlimb; il, ilium; is, ischium; Ma, manus; PcG, pectoral girdle; Pe, pes; pu, pubis; PvG, pelvic girdle; r, radius; sc, scapula; SR, sternal ribs; SV, sacral vertebrae; tb, tibia; u, ulna. Map drawn by Esther Premru.

Figure 5.2: Quarry map of SMA 0087, without bones of other specimens found close-by. Abb.: DR, dorsal ribs; DV, dorsal vertebra; fe, femur; fi, fibula; il, ilium; is, ischium; Pe, pes; pu, pubis; SR, sternal ribs; SV, sacral vertebrae; tb, tibia. Map drawn by Esther Premru.

Figure 5.3: Skull bones of SMA 0011 before mounting. Black elements were lacking and reconstructed for the mounted skull. Abb.: an, angular; aof, antorbital fenestra; at, atlas; Bc, braincase; d, dentary; f, frontal; j, jugal; la, lacrimal; m, maxilla; na, nasal; pf, prefrontal; pm, premaxilla; pra, proatlas; q, quadrate; qj, quadratojugal; sa, surangular; T, teeth. Scale bar = 10 cm. Photo by Urs Möckli.

Figure 5.4: Skull of SMA 0011 as usually figured in anterodorsal (top), posterodorsal (left), right lateral (bottom center), and rostral views (right). Dark elements were lacking and reconstructed for the mounted skull. Abb.: an, angular; aof, antorbital fenestra; bo, basioccipital; bpr, basipterygoid process; d, dentary; ex, exoccipital; f, frontal; j, jugal; ltf, laterotemporal fenestra; m, maxilla; n, external nares; na, nasal; o, orbit; os, orbitosphenoid; p, parietal; paof, preantorbital fossa; pf, prefrontal; pm, premaxilla; po, postorbital; popr, paroccipital process; pro, prootic; q, quadrate; qj, quadratojugal; sa, surangular; so, supraoccipital; sq, squamosal; stf, supratemporal fenestra. Scale bar = 10 cm.

Figure 5.5: Skull of SMA 0011 in supposed habitual pose in dorsal (top), anterior (left), left lateral (bottom center), and posterior views (right). Dark elements were lacking and reconstructed for the mounted skull. Abb.: an, angular; aof, antorbital fenestra; bo, basioccipital; bpr, basipterygoid process; bt, basal tubera; cpr, crista prootica; d, dentary; ex, exoccipital; f, frontal; fm, foramen magnum; j, jugal; ltf, laterotemporal fenestra; m, maxilla; n, external nares; na, nasal; o, orbit; os, orbitosphenoid; p, parietal; pf, prefrontal; pm, premaxilla; po, postorbital; popr, paroccipital process; pro, prootic; ptf, posttemporal fenestra; q, quadrate; qj, quadratojugal; sa, surangular; so, supraoccipital; sq, squamosal; stf, supratemporal fenestra. Scale bar = 10 cm.

Figure 5.6: Skull reconstruction of *Galeamopus shellensis* in dorsal and lateral view, created by Simao Mateus (ML), and based on SMA 0011. Lacking bones were reconstructed after *Diplodocus* (Whitlock, 2011b).

Figure 5.7: Maxillary canal in the skull of SMA 0011 (arrow in the inlet) in right lateral view. The canal is herein interpreted as an autapomorphy of *Galeamopus shellensis*. Abb.: aof, antorbital fenestra; j, jugal; m, maxilla; paof, preantorbital fossa. Scale bar in skull overview = 10 cm.

Figure 5.8: Unusual development of sagittal nuchal crest in the skull of SMA 0011 (arrow in the inlet) in posterodorsal view. The complex structure indicates that there might have been an additional element lacking, but no such bone has yet been described in any sauropod skull. Abb.: f, frontal; p, parietal; so, supraoccipital. Scale bar in skull overview = 10 cm.

Figure 5.9: Right pterygoid of SMA 0011 in lateral (A) and medial (B) views. The element is only partly prepared, the lighter color is matrix adhered to the darker bone. Abb.: ar, anterior ramus; er, ectopterygoid ramus; qr, quadrate ramus. Scale bar = 5 cm.

Figure 5.10: Right hyoid of SMA 0011 in medial (A) and lateral (B) views. Abb.: ar, anterior ramus; sqr, squamosal ramus. Scale bar = 10 cm.

Figure 5.11: Right ?prearticular of SMA 0011 in lingual view. Note the shallow longitudinal canal (arrows). Scale bar = 5 cm.

Figure 5.12: Teeth of SMA 0011. They were found disarticulated from the skull. Abb.: tc, tooth crown; tr, tooth root. Scale bar = 2 cm.

Figure 5.13: Right proatlas of SMA 0011 in lateral (A) and medial (B) views. Note the elongate and narrow distal tip. Scale bar = 2 cm.

Figure 5.14: Atlas and axis of SMA 0011. A shows the two elements in an articulated state, B show the neurapophyses in lateral (B1) and medial (B2) views. Abb.: acdl, anterior centrodiapophyseal lamina; at, atlas; avl, anteroventral lip; ax, axis; axr, axial rib; cpol, centropostzygapophyseal lamina; di, diapophysis; dip, distal process; epi, epipophyses; lsp, lateral spur; mp, medial process; ncs, neurocentral synostosis; pl, pleurocoel; podl, postzygodiapophyseal lamina; poz, postzygapophysis; prdl, prezygodiapophyseal lamina; prsl, prespinal lamina; spol, spinopostzygapophyseal lamina; vk, ventral keel. Scale bars = 10 cm.

Figure 5.15: Cervical vertebrae 3 to 6 of SMA 0011 in right lateral view. Abb.: acdl, anterior centrodiapophyseal lamina; apf, anterior pneumatic fossa; cpol, centropostzygapophyseal lamina; cprl, centroprezygapophyseal lamina; di, diapophysis; dsf, dorsal spinal fossa; epi, epipophysis; naf, neural arch foramen; ncs, neurocentral synostosis; pap, parapophysis; pcdl, posterior centrodiapophyseal lamina; pl, pleurocoel; podl, postzygodiapophyseal lamina; poz, postzygapophysis; ppf, posterior pneumatic fossa; prdl, prezygodiapophyseal lamina; pre, pre-epipophysis; prsl, prespinal lamina; prz, prezygapophysis; pvf, posteroventral flange; pvfo, posteroventral fossa; spol, spinopostzygapophyseal lamina; sprl, spinoprezygapophyseal lamina; vk, ventral keel; vsf, ventral spinal fossa. Scale bar = 10 cm.

Figure 5.16: Cervical vertebrae 8 and 9 of SMA 0011 in right lateral view. Note the open neurocentral synchondrosis. Abb.: acdl, anterior centrodiapophyseal lamina; al, accessory lamina; apf, anterior pneumatic fossa; asl, accessory spinal lamina; bns, bifid neural spine; cpol, centropostzygapophyseal lamina; cprl, centroprezygapophyseal lamina; di, diapophysis; epi, epipophysis; naf, neural arch foramen; ncs, neurocentral synchondrosis; pap, parapophysis; pcdl, posterior centrodiapophyseal lamina; podl, postzygodiapophyseal lamina; poz, postzygapophysis; ppf, posterior pneumatic fossa; prdl, prezygodiapophyseal lamina; pre, pre-epipophysis; prz, prezygapophysis; pvf, posteroventral flange; pvfo, posteroventral fossa; spol, spinopostzygapophyseal lamina; sprl, spinoprezygapophyseal lamina; vsf, ventral spinal fossa. Scale bar = 10 cm.

Figure 5.17: Cervical vertebrae 11 and 12 of SMA 0011 in right lateral view. Abb.: al, accessory lamina; apf, anterior pneumatic fossa; asl, accessory spinal lamina; bns, bifid neural spine; cpol, centropostzygapophyseal lamina; cprl, centroprezygapophyseal lamina; di, diapophysis; mt, median tubercle; naf, neural arch foramen; pap, parapophysis; pcdl, posterior centrodiapophyseal lamina; podl, postzygodiapophyseal lamina; poz, postzygapophysis; ppf, posterior pneumatic fossa; prdl, prezygodiapophyseal lamina; pre, pre-epipophysis; prz, prezygapophysis; pvf, posteroventral flange; pvfo, posteroventral fossa; spol, spinopostzygapophyseal lamina; sprl, spinoprezygapophyseal lamina. Scale bar = 10 cm.

Figure 5.18: Cervical vertebra 15 of SMA 0011 in right lateral view. Articulated DV 1 shaded. Abb.: acdl, anterior centrodiapophyseal lamina; al, accessory lamina; cpol, centropostzygapophyseal lamina; cprl, centroprezygapophyseal lamina; di, diapophysis; ncs, neurocentral synostosis; pap, parapophysis; pcdl, posterior centrodiapophyseal lamina; pl, pleurocoel; podl, postzygodiapophyseal lamina; poz, postzygapophysis; prdl, prezygodiapophyseal lamina; prz, prezygapophysis; pvf, posteroventral flange; spol, spinopostzygapophyseal lamina; sprl, spinoprezygapophyseal lamina. Scale bar = 10 cm.

Figure 5.19: Neurocentral synostosis in CV 5 of SMA 0011. Detail of the vertebra in right lateral view. Note the higher degree of fusion in the posterior portion compared to the anterior part (arrows). Abb.: apf, anterior pneumatic fossa; cpol, centropostzygapophyseal lamina; di, diapophysis; pcdl, posterior centrodiapophyseal lamina; podl, postzygodiapophyseal lamina; poz, postzygapophysis; ppf, posterior pneumatic fossa; pvfo, posteroventral fossa.

Figure 5.20: Neural arch foramina in CV 9 of SMA 0011, in posterodorsal view. The foramina are highlighted with the semi-transparent overlay. Abb.: bns, bifid neural spine; epi, epipophysis; mt, median tubercle; naf, neural arch foramen; pap, parapophysis; poz, postzygapophysis; ppf, posterior pneumatic fossa; prdl, prezygodiapophyseal lamina; prz, prezygapophysis; pvfo, posteroventral fossa; spol, spinopostzygapophyseal lamina; sprl, spinoprezygapophyseal lamina. Scale bar = 10 cm.

Figure 5.21: Dorsal vertebra 1 of SMA 0011 in right lateral view. Articulated CV 15 and DV 2 shaded. Abb.: acdl, anterior centrodiapophyseal lamina; al, accessory lamina; cpol, centropostzygapophyseal lamina; cprl, centroprezygapophyseal lamina; pap, parapophysis; pcdl, posterior centrodiapophyseal lamina; pl, pleurocoel; podl, postzygodiapophyseal lamina; poz, postzygapophysis; prdl, prezygodiapophyseal lamina; prz,

prezygapophysis; pvf, posteroventral flange; spol, spinopostzygapophyseal lamina; sprl, spinoprezygapophyseal lamina. Scale bar = 10 cm.

Figure 5.22: Dorsal vertebra 2 of SMA 0011 in right lateral view. Articulated DV 1 and DV 3 shaded. The right metapophysis is lacking, only the medial face of the left one is visible. Note the broken diapophysis that reveals the inner structure. Abb.: cpol, centropostzygapophyseal lamina; cprl, centroprezygapophyseal lamina; di, diapophysis; pap, parapophysis; pl, pleurocoel; poz, postzygapophysis; prdl, prezygodiapophyseal lamina; prz, prezygapophysis; spol, spinopostzygapophyseal lamina; sprl, spinoprezygapophyseal lamina. Scale bar = 10 cm.

Figure 5.23: Dorsal vertebra 3 of SMA 0011 in right lateral view. Articulated DV 2 and partial DV 4 shaded. The right metapophysis is lacking, only the medial face of the left one is visible. The broken right prezygapophysis is present on top of the broken diapophysis. Abb.: DV, dorsal vertebra; ncs, neurocentral suture; pap, parapophysis; pl, pleurocoel; prz, prezygapophysis; spol, spinopostzygapophyseal lamina; sprl, spinoprezygapophyseal lamina; vk, ventral keel. Scale bar = 10 cm.

Figure 5.24: Dorsal vertebral centrum 4 of SMA 0011 in anterior (A), dorsal (B), and left lateral (C) views. The element is still partly preserved within matrix. Abb.: nc, neural canal; ncs, neurocentral synostosis; pl, pleurocoel. Scale bar = 10 cm.

Figure 5.25: Dorsal vertebra 5 of SMA 0011 in posterolateral (A) and right lateral view (B). The element lacks the right half of the neural spine, and is partly mounted in matrix. Grey lines indicate the probable extensions of the right half. Note that the tip of the left diapophysis is reconstructed. Abb.: di, diapophysis; nc, neural canal; pap, parapophysis; pl, pleurocoel; poz, postzygapophysis; prz, prezygapophysis; spdl, spinodiapophyseal lamina; spol, spinopostzygapophyseal lamina; sprl, spinoprezygapophyseal lamina. Scale bar = 10 cm.

Figure 5.26: Dorsal vertebrae 6 to 10 of SMA 0011 in right lateral (A), posterolateral (B), and anterolateral view (C). The elements are partly preserved in matrix. Note the open neurocentral synchondrosis in DV 7 to DV 10. Abb.: cpol, centropostzygapophyseal lamina; DV, dorsal vertebra; lspol, lateral spinopostzygapophyseal lamina; pap, parapophysis; pcdl, posterior centrodiapophyseal lamina; pcpl, posterior centroparapophyseal lamina; pl, pleurocoel; podl, postzygodiapophyseal lamina; posl, postspinal lamina; poz, postzygapophysis; prdl, prezygodiapophyseal lamina; prpl, prezygoparapophyseal lamina; prsl, prespinal lamina; spdl, spinodiapophyseal lamina; sprl, spinoprezygapophyseal lamina. Scale bar in A = 10 cm, DV 6 in A and C, and DV 10 in A and B are scaled to the same vertebral height.

Figure 5.27: Scapula and coracoid of SMA 0011 in right lateral view. Lacking parts indicated with dashed lines. Abb.: acr, acromion ridge; CF, coracoid foramen; co, coracoid; GL, glenoid; sc, scapula. Scale bar = 20 cm.

Figure 5.28: Forelimb of SMA 0011 in anterior view: A) humerus, B) antebrachium and manus (as mounted within matrix). Note that the carpal was probably mounted upside down. Abb.: c, carpal; dpc, deltopectoral crest; hh, humeral head; lr, lateral ridge; mc, metacarpal; mr, medial ridge; phm, manual phalanx; r, radius; rt, tubercle for articulation with radius; u, ulna; ut, tubercle for articulation with ulna. Scale bar (valid for both A and B) = 20 cm.

Figure 5.29: Left manual phalanx I-1 of SMA 0011 in posterior view. Note the distinct posteroventral lip and posterolateral crest. Abb.: lco, lateral condyle; mco, medial condyle; plc, posterolateral crest; pvl, posteroventral lip. Scale bar = 2 cm.

Figure 5.30: Possible preservation of keratinous sheet on left manual ungual I-2 of SMA 0011 (medial view). Note the different surface texture at the tip (arrow), compared to more posterior portions. Abb.: dg, distal groove; pas, proximal articular surface. Scale bar = 5 cm.

Figure 5.31: Right pubis (A) and left ischium (B) of SMA 0011 in medial view. The distal end of the ischium is reconstructed. Abb.: ac, acetabular surface; amb, ambiens process; ip, iliac peduncle; isa, ischial articular surface; of, obturator foramen; pua, pubic articulation. Scale bar = 20 cm.

Figure 5.32: Left hindlimb of SMA 0011: A) femur in posterior view; B) tibia and fibula in anterior view, as mounted. The lacking greater trochanter of the femur is indicated by the dashed line. Abb.: cc, cnemial crest; ec, epicondyle; fh, femoral head; fi, fibula; fic, fibular condyle; icg, intercondylar groove; tb, tibia; tic, tibial condyle. Scale bar = 20 cm.

Figure 5.33: Left astragalus of SMA 0011 in anterior (A) and lateral (B) view. Due to the mounted state, a portion of the tibia, obscuring a posterodorsal part of the astragalus is masked as semitransparent. Abb.: asp, ascending process; dro, distal roller; fif, fibular facet; tb, tibia; tif, tibial facet. Scale bar = 5 cm.

Figure 5.34: Left metatarsals of SMA 0011 in anterior/dorsal view: A) mt I, B) mt II, C) mt III, D) mt IV, E) mt

V. Elements partially overlapping the other bones are marked by a black line. Abb.: dlr, dorsolateral ridge; icg, intercondylar groove; mts, metatarsal; nf, nutrient foramen; plp, posterolateral process. Scale bar = 10 cm.

Figure 5.35: Left pedal phalanges of SMA 0011 in dorsal view, as mounted. Php IV-1 could actually also be php III-2 or php V-1 (see text). Abb.: php, pedal phalanx; ung, ungual. Scale bar = 10 cm.

Figure 5.36: Dorsal centrum 6 of SMA 0087 in left, posterior, right, anterior (top left to right), and ventral view (bottom). Abb.: cpol, centropostzygapophyseal lamina; cprl, centroprezygapophzseal lamina; nc, neural canal; pl, pleurocoel. Scale bar = 10 cm.

Figure 5.37: Dorsal neural spine 6 of SMA 0087 in left, right, and ventral (bottom) view. Note the anterior and dorsal spurs on the diapophysis. Abb.: cpol, centropostzygapophyseal lamina; das, diapophysis anterior spur; dds, diapophysis dorsal spur; di, diapophysis; hya, hypantrum; hys, hyposphene; lspol, lateral spol; mspol, medial spol; pap, parapophysis; pcdl, posterior centrodiapophyseal lamina; pcpl, posterior centroparapophyseal lamina; podl, postzygodiapophyseal lamina; posl, postspinal lamina; poz, postzygapophysis; prdl, prezygodiapophyseal lamina; prpl, prezygoparapophyseal lamina; prsl, prespinal lamina; prz, prezygapophysis; spdl, spinodiapophyseal lamina; spol, spinopostzygapophyseal lamina; sprl, spinoprezygapophyseal lamina. Scale bar = 10 cm.

Figure 5.38: Caudal vertebra 5 of SMA 0087 in anterior, left lateral, and posterior view (from left to right). Note the foramen that pierces the ventral surface, and the dorsally expanded transverse processes. Abb.: chf, chevron facet; nf, nutrient foramen; posl, postspinal lamina; poz, postzygapophysis; prsl, prespinal lamina; prz, prezygapophysis; spol, spinopostzygapophyseal lamina; sprl, spinoprezygapophyseal lamina; tp, transverse process. Scale bar = 10 cm.

Figure 5.39: Caudal vertebra 7 of SMA 0087 in posterior, right lateral, and anterior view (left to right). Abb.: cpol, centropostzygapophyseal lamina; cprl, centroprezygapophyseal lamina; posl, postspinal lamina; poz, postzygapophysis; prsl, prespinal lamina; prz, prezygapophysis; spol, spinopostzygapophyseal lamina; sprl, spinoprezygapophyseal lamina; tp, transverse process. Scale bar = 10 cm.

Figure 5.40: Caudal vertebra 16 of SMA 0087 in dorsal (top), posterior (left) and right lateral view (bottom right). Note the presence of two weak longitudinal ridges on the centrum. Abb.: chf, chevron facets; lr, lateral ridge; prsl, prespinal lamina; prz, prezygapophysis; poz, postzygapophysis; sprl, spinoprezygapophyseal lamina; vlr, ventrolateral ridge. Scale bar = 10 cm.

Figure 5.41: Anterior chevron of SMA 0087 in anterior, right lateral, and posterior view (left to right). This chevron was found between Cd 2 and 3. Note the bridged over haemal canal. Abb.: hc, haemal canal. Scale bar = 10 cm.

Figure 5.42: Mid-chevron of SMA 0087 in anterior, left lateral, posterior, right lateral (top, left to right), and ventral view (bottom). This chevron was recovered associated with Cd 16 to 18. Note the ventral slit visible in ventral view. Abb.: ap, anterior process; hc, haemal canal; pp, posterior process. Scale bar = 10 cm.

Figure 5.43: Sternal rib of SMA 0087. Corresponds to Morphotype C of Tschopp and Mateus (2013). Scale bar = 10 cm.

Figure 5.44: Sternal or gastral rib of SMA 0087. Corresponds to morphotype C of Tschopp and Mateus (2013). Note the longitudinal sulcus (arrow), which might indicate a gastral instead of a sternal origin. Scale bar = 10 cm.

Figure 5.45: Right astragalus of SMA 0087 in dorsal (top), posterior (center left), ventral (bottom), and anterior view (center right). Abb.: af, astragalar foramen; asp, ascending process; dro, distal roller; fif, fibular facet; tif, tibial facet. Scale bar = 10 cm.

Figure 5.46: Right metatarsal I of SMA 0087 in proximal (top), dorsal, medial, plantar, lateral (center left to right), and distal view (bottom). Abb.: dlr, dorsolateral ridge; nf, nutrient foramen; plp, posterolateral process. Scale bar = 10 cm.

Figure 5.47: Right metatarsal II of SMA 0087 in proximal (top), dorsal, medial, plantar, lateral (center left to right), and distal view (bottom). Abb.: dlr, dorsolateral ridge; plp, posterolateral process. Scale bar = 10 cm.

Figure 5.48: Right metatarsal V of SMA 0087 in proximal (top), dorsal, medial, plantar, lateral (center left to right), and distal view (bottom). Scale bar = 10 cm.

Figure 5.49: Right pedal phalanx I-1 of SMA 0087 in proximal (top), dorsal, medial, plantar, lateral (center left to right), and distal view (bottom). Abb.: pvl, posteroventral lip. Scale bar = 5 cm.

Figure 5.50: Right pedal phalanx II-1 of SMA 0087 in proximal (top), dorsal, medial, plantar, lateral (center left to right), and distal view (bottom). Abb.: nf, nutrient foramen. Scale bar = 5 cm.

Figure 5.51: Right pedal phalanx II-2 of SMA 0087 in proximal (top), dorsal, medial, plantar, lateral (center left to right), and distal view (bottom). Scale bar = 5 cm.

Figure 5.52: Right pedal ungual I-2 of SMA 0087 in dorsal (top), medial, lateral (center left, right), and plantar view (bottom). Abb.: ps, proximal spur; Scale bar = 10 cm.

Figure 5.53: Right pedal ungual II-3 of SMA 0087 in dorsal (top), medial, lateral (center left, right), and plantar view (bottom). Scale bar = 10 cm.

Figure 6.1: Skulls of *Mamenchisaurus youngi* (A; modified from Ouyang and Ye, 2002), *Camarasaurus* sp. USNM 13786 (B; photo from O. Mateus), *Giraffatitan brancai* (C; modified from Janensch, 1935), *Diplodocus* sp. CM 11161 (D), and *Galeamopus shellensis* SMA 0011 (E) in lateral view, illustrating the states of the characters 1, 5, 13, 14, 15, 19, 20, 21, 37, 38, 39, 45, 46, 55, 113. Not to scale.

Figure 6.2: Anterior portions of premaxillae of *Camarasaurus* (A; modified from Madsen et al., 1995) and *Galeamopus shellensis* SMA 0011 (B) in anterodorsal view, illustrating the states of characters 2 and 3. Not to scale.

Figure 6.3: Skulls (A, C-E) or maxilla (B) of *Camarasaurus* sp. SMA 0002 (A; photo by O. Mateus), *Dicraeosaurus hansemanni* MB.R.2336 (B), *Kaatedocus siberi* SMA 0004 (C), *Galeamopus shellensis* SMA 0011 (D; photo by O. Mateus), and *Diplodocus* sp. CM 11161 (E) in anterolateral view, illustrating the states of the characters 6, 9, 10, 11, 12, 16, 17, 48. Not to scale.

Figure 6.4: Premaxillae of *Suuwassea emilieae* ANS 21122 (A), *Dicraeosaurus hansemanni* MB.R.2337 (B), and *Diplodocus* sp. USNM 2673 (C, left element reversed) in lateral view, illustrating the states of character 7. Not to scale.

Figure 6.5: Skulls of *Camarasaurus* (A; modified from Wilson and Sereno, 1998), *Limaysaurus tessonei* MUCPv-205 (B; photo by J. Whitlock), *Dicraeosaurus hansemanni* MB.R.2379 (C), *Kaatedocus siberi* SMA 0004 (D) and *Diplodocus* sp. CM 11161 (E) in dorsal view, illustrating the states of the characters 8, 26, 29, 30, 34, 35, 36, 66. Not to scale.

Figure 6.6: Skull roof of *Diplodocus* sp. CM 11161 (A; based on Wilson and Sereno, 1998) and *Limaysaurus tessonei* MUCPv-205 (B; based on Calvo and Salgado, 1995) in dorsal view. Note the anteromedial hook in the prefrontal of CM 11161 (A; C23-1), and the differently shaped frontal-nasal suture (straight to anteriorly bowed in A, C28-0; bowed posteriorly in B, C28-1). Abb.: f, frontal; na, nasal; pf, prefrontal. Scaled to the same skull roof length.

Figure 6.7: Left (F, H-K) and right (A-E, G) diplodocoid frontals in dorsal view, anterior to the front. The upper row shows elements with an anteriorly restricted posterior process of the prefrontal (C23-0), the lower row have elongated posterior processes (C23-1). Additional states are illustrated from the characters 24, 31, 33. Frontals figured in strict perpendicular view, and scaled to the same anteroposterior length.

Figure 6.8: Left jugal of *Diplodocus* USNM 2672 in lateral view, illustrating the large contribution of the jugal to the antorbital fenestra (C40-1), the narrow and elongate posteroventral process (C42-1), the dorsal process of the jugal (C43-0), and the anterior spur (C44-1). Abb.: aof, antorbital fenestra; j, jugal; la, lacrimal; ltf, laterotemporal fenestra; m, maxilla; o, orbit; po, postorbital; qj, quadratojugal.

Figure 6.9: Skulls of *Shunosaurus lii* ZG 65430 (A; modified from Chatterjee and Zheng, 2002) and *Diplodocus* sp. CM 11161 (B) in ventral view. Note the anteriorly displaced position of the ectopterygoid ramus of the pterygoid, and the ectopterygoid itself, in *Diplodocus* (B; C41-1 and C102-1), as well as the vomer that articulates with the premaxilla in *Shunosaurus* (A; C103-0), but with the maxilla in *Diplodocus* (B; C103-1). Abb.: aof, antorbital fenestra; bo, basioccipital; bpr, basipterygoid process; bt, basal tuber; ep, ectopterygoid; er, ectopterygoid ramus; j, jugal; m, maxilla; pa, palate; pm, premaxilla; popr, paroccipital process; pt, pterygoid; qj, quadratojugal; v, vomer. Pictures scaled to the same skull length.

Figure 6.10: Quadrate articular surface shapes of *Camarasaurus* sp. SMA 0002 (left, quadrangular, C49-0), *Suuwassea emilieae* ANS 21122 (center, roughly triangular, C49-1), and *Nigersaurus taqueti* GAD512-7 (right, crescent-shaped, C49-2). Figures of *Suuwassea* and *Nigersaurus* traced from Harris (2006a) and Sereno et al. (2007), respectively.

Figure 6.11: Quadrates of *Camarasaurus* sp. SMA 0002 (A) and Diplodocidae indet. SMA D27-7 (B) in

posterior view, illustrating the transverse ridge (B, inlet; C50-1), and the deep (A; C51-0) versus shallow (B; C51-1) quadrate fossa. Not to scale.

Figure 6.12: Quadrates of *Camarasaurus* sp. SMA 0002 (A) and Diplodocidae indet. SMA D27-7 (B) in medial view, illustrating the second medial fossa (B; C52-1), the shape of the dorsal margin (C53, concave versus convex), and the stocky versus slender posterior ramus (C54). Scaled to the same height.

Figure 6.13: Squamosal and adjacent bones in *Mamenchisaurus youngi* (A; traced from Ouyang and Ye, 2002), *Camarasaurus lentus* CM 11338 (B; traced from Madsen et al., 1995), *Amargasaurus cazaui* MACN-N15 (C; traced from Salgado an Bonaparte, 1991), and Diplodocinae indet. CM 3452 (D; traced from a 3D model from L. Witmer), in right (A, C) and left (B, D) lateral view; illustrating the states of the characters 56, 57, and 58. Abb.: po, postorbital; q, quadrate; qj, quadratojugal; sq, squamosal. Not to scale.

Figure 6.14: Sauropod skulls of *Spinophorosaurus nigerensis* GCP-CV-4229 (A; traced from Knoll et al. 2012); *Suuwassea emilieae* ANS 21122 (B; traced from Harris, 2006a); *Limaysaurus tessonei* MUCPv-205 (C; after Calvo and Salgado, 1995); *Kaatedocus siberi* SMA 0004 (D); *Apatosaurus louisae* CM 11162, (E, reversed); *Diplodocus* sp. CM 11161 (F) in posterior view. Note the participation (C; C59-0) or exclusion (D; C59-1) of the parietal to the posttemporal fenestra; the straight (A; C62-0) or convex (D; C62-1) dorsal edge of the posterolateral process of the parietal; the outwards curve of the distal end of the posterolateral process of the parietal (B; C64-1); the distally expanded (C; C68-0) or straight paroccipital processes (F; C68-1); the dorsally vaulted supraoccipital (E; C73-0); and the narrow contribution of the basioccipital to the dorsal surface of the condyle (B; C78-1). Skulls scaled to the same occipital condyle width.

Figure 6.15: Transverse ridge of the parietal (arrow, C65-1) of *Kaatedocus siberi* SMA 0004 in posterolateral view. Abb.: anp, antotic process; bo, basioccipital; f, frontal; p, parietal; ppfo, postparietal foramen; po, postorbital; popr, paroccipital process; pra, proatlas; snc, sagittal nuchal crest; so, supraoccipital; stf, supratemporal fenestra.

Figure 6.16: Oblique ridge on paroccipital process (arrow, C67-1) of *Kaatedocus siberi* SMA 0004 in posterior view. Abb.: CV, cervical vertebrae; f, frontal; p, parietal; ppfo, postparietal foramen; po, postorbital; popr; paroccipital process; pra, proatlas; ptf, post-temporal fenestra; q, quadrate; qj, quadratojugal; so, supraoccipital; sq, squamosal; stf, supratemporal fenestra.

Figure 6.17: Braincase of *Suuwassea emilieae* ANS 21122 (A) and *Tornieria africana* MB.R.2386 (B) in right (A) and left (B) lateral view, illustrating the curved lateral end of the paroccipital process (A; C68-1), and the short (A; C79-0) and elongate basioccipital (B; C79-1). Abb.: anp, antotic process; bo, basioccipital; bpr, basipterygoid process; bt, basal tuber; cpr, crista prootica; f, frontal; os, orbitosphenoid; p, parietal; popr, paroccipital process. Scale bar = 5 cm.

Figure 6.18: Braincase of *Diplodocus* sp. CM 11161 (A) and *Tornieria africana* MB.R.2386 (B) in dorsal view. Note the concave anterior margin of the supraoccipital in *Diplodocus* (A; C72-0), in contrast to the convex edge of *Tornieria* (B; C72-1). The left frontal of MB.R.2386 is lacking. Abb.: f, frontal; na, nasal; os, orbitosphenoid; p, parietal; pf, prefrontal; po, postorbital; popr, paroccipital process; so, supraoccipital; sq, squamosal; stf, supratemporal fenestra. Not to scale.

Figure 6.19: Skulls of *Diplodocus* sp. CM 11161 (A) and *Dicraeosaurus hansemanni* MB.R.2379 (B) in posterior view, illustrating the development of the sagittal nuchal crest (C74), and the supraoccipital foramina (C75). Abb.: bo, basioccipital; ex, exoccipital; fm, foramen magnum; p, parietal; po, postorbital; popr, paroccipital process; ptf, post-temporal fenestra; so, supraoccipital; sq, squamosal. Skulls scaled to the same skull width.

Figure 6.20: Basal tubera and basisphenoid of *Dicraeosaurus hansemanni* MB.R.2379 in posteroventral (A), left lateral (B), and anterodorsal view (C). Note the lateral expansion of the anteroventral end of the crista prootica (C76-1), the narrowly diverging, and elongate basipterygoid processes (C92-2 and C94-2, respectively), the deep slot-like cavity separating the bases of the processes (A, arrowhead; C95-1), and the groove on the dorsal surface of the parasphenoid rostrum (C; C99-1). Abb.: bt, basal tuber; bpr, basipterygoid process; cpr, crista prootica; psr, parasphenoid rostrum. Scale bar = 5 cm.

Figure 6.21: Braincase of *Camarasaurus* sp. UUVP 4286 (A; modified from Madsen et al., 1995) and *Tornieria africana* MB.R.2386 (B) in a view perpendicular to the dorsal surface of the occipital condyle, illustrating the distinctly offset articular surface (arrow in A; C77-0), in contrast to the derived condition of diplodocoids (B; C77-1). Abb.: ex, exoccipital; f, frontal; fm, foramen magnum; oc, occipital condyle; os, orbitosphenoid; p, parietal; pf, prefrontal; popr, paroccipital process. Skulls scaled to same breadth of occipital condyle.

Figure 6.22: Braincase of *Losillasaurus giganteus* MCNV Lo-26 in posterolateral (A) and posterior (B) view. Note the lateral basioccipital depression between the foramen magnum and the basal tubera (A; C80-1); the laterally curving distal ends of the basipterygoid processes (B; C97-1), as well as their distinct transverse expansion (B; 98-1). Abb.: bo, basioccipital; bpr, basipterygoid process; bt, basal tuber; ex, exoccipital; fm, foramen magnum; popr, paroccipital process; psr, parasphenoid rostrum; so, supraoccipital. Scale bar = 10 cm.

Figure 6.23: Hypothetical diplodocid basioccipital-basisphenoid complex in posteroventral view, showing the locations of pits sometimes present in diplodocid specimens: between occipital condyle and basal tubera (C81-1), in the notch between basal tubera (C90-1), and on the basisphenoid, between the bases of the basipterygoid processes (termed 'basipterygoid recess' by Wilson, 2002; C91-1). Abb.: bo, basioccipital; bpr, basipterygoid process; bs, basisphenoid; bt, basal tuber; cpr, crista prootica; ex, exoccipital; popr, paroccipital process.

Figure 6.24: Basal tubera of *Camarasaurus grandis* YPM 1905 (A; modified from Madsen et al., 1995), *Suuwassea emilieae* ANS 21122 (B), and *Kaatedocus siberi* SMA 0004 (C; photo by J. Marinheiro) in posterior view. Note the globose (B; C82-0) compared to the box-like shape (C; C82-1) of the tubera, the transverse ridge on their posterior face (C; C86-1), and the ventrolateral (A; C89-0) in contrast to ventral orientation (C; C89-1). Abb.: bo, basioccipital; bpr, basipterygoid process; bs, basisphenoid; bt, basal tuber; ex, exoccipital; fm, foramen magnum; oc, occipital condyle; popr, paroccipital process. Pictures scaled to same distance between dorsal face of occipital condyle and basal tubera.

Figure 6.25: Skulls of *Nigersaurus taqueti* (A; modified from Schmitt, 2012) and *Diplodocus* sp. USNM 2673 (B) in occipital view. Note the reduced basal tubera in *Nigersaurus* (A; C84-1), and the convex (A; C 85-0), or concave (B; C85-2) posterior face of the tubera. Abb.: bpr, basipterygoid process; bt, basal tuber; cpr, crista prootica; fm, foramen magnum; oc, occipital condyle; popr, paroccipital process; so, supraoccipital. Skulls scaled to same occipital condyle height.

Figure 6.26: Basioccipital-basispenoid complex of *Apatosaurus louisae* CM 11162 (A), *Kaatedocus siberi* SMA 0004 (B; traced from a photo by J. Marinheiro), and *Diplodocus* sp. CM 11161 (C) in posteroventral view. Note the differing orientations of the longest axes of the basal tubera (B; C87-0; in contrast to C; C87-1), as well as the concave (A; C88-1) versus the straight to slightly convex anterior edge of the tubera (B; C88-0). Abb.: bo, basioccipital; bpr, basipterygoid process; bs, basisphenoid; bt, basal tuber; ex, exoccipital. Drawings not to scale.

Figure 6.27: Basisphenoid of *Kaatedocus siberi* SMA 0004 (A; traced from a photo by J. Marinheiro), and *Diplodocus* sp. CM 11161 (B) in posteroventral view. Note the parallel proximal portion of the basipterygoid processes and the accompanying outwards curve in *Kaatedocus* (A; C96-1), in contrast to the straight processes of CM 11161 (B; C96-0). Abb.: bo, basioccipital; bpr, basipterygoid process; bs, basisphenoid; bt, basal tuber. Scaled to the same process length.

Figure 6.28: Braincases of *Suuwassea emilieae* ANS 21122 (A), and *Tornieria africana* MB.R.2386 (B; traced from Janensch, 1935) in anterior view. Note the unpaired optic foramen of *Suuwassea* (A; C100-1), in contrast to the paired foramen in *Tornieria* (B; C100-0). Abb.: anp, antotic process; bs, basisphenoid; can, crista antotica; cpr, crista prootica; ls, laterosphenoid; olf, olfactory foramen; opf, optic foramen; os, orbitosphenoid; popr, paroccipital process; pro, prootic. Scaled to the same width of the orbitosphenoids.

Figure 6.29: Left pterygoid of *Camarasaurus lentus* DNM 28 in medial view. Note the presence of a hook-like process at the articulation surface for the basipterygoid process (C101-1). Diplodocidae, on the other hand, only have shallow articular facets without hooks. Abb.: ap, anterior process; bph, basipterygoid hook; er, ectopterygoid ramus; qr, quadrate ramus. Picture traced from Madsen et al. (1995). Scale bar = 10 cm.

Figure 6.30: Left dentary of *Camarasaurus lentus* DNM 28 (A; traced from Madsen et al., 1995), *Dicraeosaurus hansemanni* MB.R.2372 (B; traced from Janensch, 1935), and *Nigersaurus taqueti* MNN GAD512-10 (C; traced from Sereno et al., 2007) in lingual view. Note the chin-like ventral process in *Dicraeosaurus* (B; C104-1), the different shapes of the symphysis (C105-1 to 3), and the high elevation of the coronoid eminence in *Camarasaurus* (A; C108-0). Abb.: an, angular; d, dentary; sa, surangular; sym, symphysis; t, tooth. Scaled to the same anteromedial height of the dentary.

Figure 6.31: Left dentary of *Dicraeosaurus hansemanni* MB.R.2372 (A), and *Nigersaurus taqueti* MNN GAD512-10 (B; traced from Sereno et al., 2007) in dorsal view. Note the labial tubercle in *Dicraeosaurus* (A; C106-1), the dentigerous portion that expands laterally in *Nigersaurus* (B; C107-1), and the anterolaterally displaced tooth row, compared to the usual curvature in both taxa (C112-1). Abb.: sym, symphysis; t, tooth. Scaled to the same anteroposterior length.

Figure 6.32: Left lower jaw of *Camarasaurus lentus* CM 11338 (A; modified from Madsen et al., 1995),

Nigersaurus taqueti MNN GAD-512 (B; traced from Sereno et al., 2007), and SMA 0011 (C; traced from a photo by O. Mateus) in lateral view. Note the surangular foramen in A and B (C109-1), the external mandibular fenestra in *Nigersaurus* (B; C110-0), the strongly overlapping teeth of *Camarasaurus* (A; C120-0) in contrast to the more widely spaced teeth of diplodocids (C; C120-1), and the anterior inclination of the the diplodocid teeth in respect to the jaw axis (C; C122-1). Abb.: an, angular; d, dentary; emf, external mandibular fenestra; sa, surangular; saf, surangular foramen; t, tooth. Scaled to the same mandibular length.

Figure 6.33: Tooth of *Omeisaurus tianfuensis* T5705 (A; traced from He et al., 1998), *Camarasaurus* sp. SMA 0002 (B; traced from a photo by O. Mateus), and Diplodocinae indet. CM 3452 (C) in lingual view. Note the V-shaped wear facets in *Camarasaurus* (B; C117-0), in contrast to the single, planar facet in diplodocids (C; C117-1), the longitudinal grooves in *Omeisaurus* and *Camarasaurus* (A, B; C123-1), and the marginal tooth denticles in *Omeisaurus* (A; C125-0). Abb.: ato, anterior tooth; dt, denticles; pto, posterior tooth; tc, tooth crown; tr, tooth root; wf, wear facet. Teeth scaled to the same crown length.

Figure 6.34: Tooth of *Nigersaurus* in labial (A) and lingual (B) view, showing the paired, planar wear facets typical for Rebbachisauridae (C117-1; C118-0). Abb.: wf, wear facet. Figure traced from Whitlock (2011b).

Figure 6.35: Tooth cross-section of *Camarasaurus* sp. AMNH 5764 (A), and *Demandasaurus darwini* MDS-RVII,438 (B; traced from Torcida Fernández-Baldor et al., 2011). Note the D-shaped crown of *Camarasaurus* (A; C121-0) in contrast with the rounded cross-section of diplodocoids (B; C121-0), and the asymmetric disposition of the enamel typical for rebbachisaurids (B; C124-1). The camarasaur tooth has the same specimen number as *Amphicoelias altus* holotype, but not the same individual (see text). Abb.: de, dentin; en, enamel. Scaled to the same mesiodistal width.

Figure 6.36: Posterior cervical vertebra (CV ?12) of SMA 0011 in right lateral view, showing the pleurocoel typical for advanced eusauropods (C129-1), but highly subdivided (C171-2), the elongate posteroventral fossa present in diplodocines (C131-1), the anteriorly restricted pcdl (C135-0), in contrast to the more posteriorly reaching pcdl of *Apatosaurus*, the dorsally excavated parapophysis (C173-0), the large foramen connecting the pocdf and the spof (C191-1), and the accessory laminae connecting the podl and the sprl (C197-1), and the pcdl and the podl (C199-1). Abb.: apf, anterior pneumatic fossa; di, diapophysis; pap, parapophysis; pcdl, posterior centrodiapophyseal lamina; pocdf, postzygapophyseal centrodiapophyseal fossa; podl, postzygodiapophyseal lamina; poz, postzygapophysis; prdl, prezygodiapophyseal lamina; pre, pre-epipophysis; prz, prezygapophysis; pvf, posteroventral flange; sdf, spinodiapophyseal fossa; spof, spinopostzygapophyseal fossa; spol, spinopostzygapophyseal lamina; sprl, spinoprezygapophyseal lamina; tpol, interpostzygapophyseal lamina.

Figure 6.37: Mid- to posterior cervical vertebrae cross-section of *Supersaurus vivianae* WDC DMJ-021 (A; modified from Lovelace et al., 2007), and *Brachiosaurus* sp. BYU 12866 (B; modified from Wedel, 2009). Sections at base of diapophysis. Note the different internal pneumatic structure, with few but large cavities in *Supersaurus* (A; C128-1), in contrast to the many irregularly small fossa typical for titanosauriforms (B; C128-2). The differences shown here in cervical vertebrae apply as well for dorsal vertebrae (C228). Pictures scaled to the same centrum height. Abbreviations see page XXXII.

Figure 6.38: Mid- to posterior cervical vertebrae of *Dicraeosaurus hansemanni* MB.R.4886 (A; photo by J. Harris), *Kaatedocus siberi* SMA 0004 (B), and *Barosaurus lentus* YPM 429 (C) in ventral view (anterior to the top). Note the different developments of the ventral keels (prominent in *Dicraeosaurus*, A, C132-0; shallow, single in *Kaatedocus*, B, C132-1 and 175-0; double in *Barosaurus*, C, C175-1), the ventral sulcus typical for diplodocines (B, C; C133-1), the pneumatic foramina accompanying the ventral keel in *Dicraeosaurus* (A; C176-1), the posteroventral flanges (C179-1), and the numerous accessory laminae subdividing the prezygapophyseal centrodiapophyseal fossa in *Barosaurus* (C; C184-2). Vertebrae scaled to same centrum length. Abbreviations see page XXXII.

Figure 6.39: Mid- to posterior cervical vertebrae of *Apatosaurus ajax* YPM 1860 (A; traced from a photo by M. Taylor), and *Kaatedocus siberi* SMA 0004 (B; CV 13, traced from Tschopp and Mateus, in press) in dorsal view (anterior to the top). Note the triangular posterior projection on the diapophysis in *Kaatedocus* (B; C134-1), the transversely compressed (B; C142-0) in contrast to rounded (A; C142-1) neural spine summits, the transverse sulcus accompanying the prezygapophyseal facet posteriorly in *Kaatedocus* (B; C195-1), the anterior bulge of the sprl, just below the spine summit, characterizing most diplodocines (B; C196-1), and the median tubercle visible in *Apatosaurus* (A; C210-1). Abb.: bns, bifid neural spine; CR, cervical rib; di, diapophysis; epi, epipophysis; pcdl, posterior centrodiapophyseal lamina; podl, postzygodiapophyseal lamina; prdl, prezygodiapophyseal lamina; prz, prezygapophysis; spol, spinopostzygapophyseal lamina; sprl, spinoprezygapophyseal lamina; tpol, interpostzygapophyseal lamina; tprl, interprezygapophyseal lamina. Vertebrae scaled to same total length.

Figure 6.40: Cervical vertebra 11 of *Apatosaurus louisae* CM 3018 (A; modified from Gilmore, 1936) and *Diplodocus carnegii* (B; modified from Hatcher, 1901) in left (A) and right (B) lateral view. Note the posteriorly extending posterior centrodiapophyseal lamina in *Apatosaurus* (A; C135-1), the anteriorly restricted pneumatic foramen typical for most apatosaurs (A; C172-1), the pre-epipophysis (A; C181-1), the subdivided prezygapophyseal centrodiapophyseal fossa, characterizing *A. louisae* (A; C184-1), the posteriorly expanded interpostzygapophyseal lamina of *Diplodocus* (B; C190-1), the posteriorly restricted prezygapophysis of *A. louisae* (A; C194-1), compared to the state in *Diplodocus*, where it reaches the anterior edge of the condyle (B; C194-0), the vertical accessory spinal lamina marking *Diplodocus* (B; C203-1), the different positions of the cervical ribs (ventrally projecting, A, C216-1; or level with centrum, B, C216-0), and the absence (A; C219-1) or presence (B; C219-0) of the anterior process of the cervical rib. Vertebrae scaled to same posterior cotyle height. Abbreviations see page XXXII.

Figure 6.41: Cervical vertebra 6 of *Australodocus bohetii* MB.R.2455 (A) and SMA 0011 (B) in left (A) and right (B) lateral view. Note the short second pcdl in *Australodocus* (A; C136-1), the foramen piercing the podl (A; C137-1), the projection formed by the epipophysis (B; C138-1), the low (A; C164-0), and high (B; C164-1) neural spines, and the cervical rib, which is slightly longer than the centrum in SMA 0011 (B; C215-1). Abb.: acdl, anterior centrodiapophyseal lamina; apf, anterior pneumatic fossa; cpol, centropostzygapophyseal lamina; cprl, centroprezygapophyseal lamina; CR, cervical rib; naf, neural arch foramen; pcdl, posterior centrodiapophyseal lamina; podl, postzygodiapophyseal lamina; poz, postzygapophysis; ppf, posterior pneumatic fossa; prz, prezygapophysis; spol, spinopostzygapophyseal lamina; sprl, spinoprezygapophyseal lamina; tpol, interpostzygapophyseal lamina. Vertebrae scaled to the same centrum length.

Figure 6.42: Mid- to posterior cervical vertebrae of *Barosaurus lentus* YPM 429 (A) and *Diplodocus carnegii* CM 84 (B) in left posterolateral (A) and left dorsolateral view (B). Note the differently pneumatized epipophyses (C139-1), the transversely compressed epipophysis (B; C202-1), and the horizontal ridge below the neural spine summit in *Diplodocus* (B; C205-1). The cervical vertebra of *B. lentus* is partly covered by matrix and plaster. Abb.: apf, anterior pneumatic fossa; CR, cervical rib; pap, parapophysis; pcdl, posterior centrodiapophyseal lamina; ppf, posterior pneumatic fossa; prdl, prezygodiapophyseal lamina; prz, prezygapophysis; pvf, posteroventral flange; pvfo, posteroventral fossa; spol, spinopostzygapophyseal lamina; sprl, spinoprezygapophyseal lamina. Vertebrae scaled to the same posterior cotyle height.

Figure 6.43: Cervical vertebra 5 of *Suuwassea emilieae* ANS 21122 (A) and *Kaatedocus siberi* SMA 0004 (B; modified from Tschopp and Mateus, in press) in anterior view. Note the transversely widening (A; C141-1) instead of straight (B; C141-0) neural spine, and the presence of a prespinal lamina in *Kaatedocus* (B; C161-1). The neural spine of *Suuwassea* (A) is not bifurcated, but broken (as indicated by the dashed line). Abb.: cprl, centroprezygapophyseal lamina; pap, parapophysis; poz, postzygapophysis; prdl, prezygodiapophyseal lamina; prz, prezygapophysis; sprl, spinoprezygapophyseal lamina. Vertebrae scaled to the same anterior condyle length.

Figure 6.44: Proatlas of ?*Kaatedocus* SMA P29-1 (A) and SMA 0011 (B) in medial view, illustrating the broad (A; C143-0) and narrow distal tips (B; C143-1). Abb.: pas, proximal articular surface. Scaled to the same articular surface height.

Figure 6.45: Atlas of *Camarasaurus* sp. UUVP 10070 (A; modified from Madsen et al., 1995), and *Galeamopus shellensis* AMNH 969 (B) in posterior (left) and right lateral view (right, A shows left side reversed). Note the distinct anteroventral lip characterizing diplodocids (B; C144-1), and the foramen between the posterior ventrolateral processes in AMNH 969 (B; C144-1). Abb.: ncs, neurocentral synchondrosis; pvlp, posterior ventrolateral process. Scaled to the same centrum height.

Figure 6.46: Neurapophyses of *Apatosaurus louisae* CM 3018 (A; modified from Gilmore, 1936), *Kaatedocus siberi* SMA 0004 (B; traced from 3D model provided by G. Dzemski), and SMA 0011 (C) in lateral (A; left side reversed), and dorsolateral view (B, C). Note the weak (B; C146-0) in contrast to well-developed medial process (C; C146-1), the subtriangular lateral spur in SMA 0011 (C; C147-1), the different shapes of the distal process (tapering, B, C148-0; wide, C, C148-1), and the foramen characterizing *A. louisae* (A; C149-1). Abb.: dip, distal process; ncs, neurocentral synchondrosis. Scaled to the same anteroposterior length.

Figure 6.47: Axis of *Diplodocus carnegii* CM 84 in posterolateral view, illustrating the pneumatic slot-like fossa posterior to the parapophysis (C150-1), and the presence of a postspinal lamina (C152-1). Abb.: at, atlas; CV 3, cervical vertebra 3; pap, parapophysis; pl, pleurocoel; poz, postzygapophysis; prdl, prezygodiapophyseal lamina; prsl, prespinal lamina; spol, spinopostzygapophyseal lamina.

Figure 6.48: Axis of *Galeamopus shellensis* AMNH 969 in dorsal (top), right lateral (bottom left), and anterior (bottom right) view, illustrating the anteriorly expanded prespinal lamina (C151-1), and the anteriorly restricted

neural spine summit (C153-2). Abb.: di, diapophysis; epi, epipophysis; pap, parapophysis; pcdl, posterior centrodiapophyseal lamina; pl, pleurocoel; poz, postzygapophysis; prsl, prespinal lamina; prz, prezygapophysis. Scale bar = 10 cm.

Figure 6.49: Cervical vertebra 4 of *Dicraeosaurus hansemanni* MB.R.4886 (A) and SMA 0011 (B) in right lateral view. Note the differently inclined posterior border of the anterior condyle (A, C156-0; B, C156-1), the subdivision of the pleurocoel in SMA 0011 (B; C157-1), which is absent in anterior cervical vertebrae of *Dicraeosaurus* (A; C157-0), the anterior pneumatic fossa that extends onto the parapophysis (B; C158-0), the presence of a prespinal lamina in SMA 0011 (B; C161-1), and the posteriorly projecting spur on the dorsal edge of the posterior process of the cervical rib of *Dicraeosaurus* (A; C217-1). Abb.: acdl, anterior centrodiapophyseal lamina; apf, anterior pneumatic fossa; cprl, centroprezygapophyseal lamina; CR 3, cervical rib 3; CV 3, cervical vertebra 3; epi, epipophysis; naf, neural arch foramen; pl, pleurocoel; podl, postzygodiapophyseal lamina; poz, postzygapophysis; ppf, posterior pneumatic fossa; prdl, prezygodiapophyseal lamina; prz, prezygapophysis; spol, spinopostzygapophyseal lamina; sprl, spinoprezygapophyseal lamina. Vertebrae scaled to the same cotyle height.

Figure 6.50: Cervical vertebra 6 of *Dicraeosaurus hansemanni* MB.R.4886 (A) and SMA 0011 (B) in right lateral view. Note the large, rounded pneumatic foramen marking the anterior end of the posterior pneumatic fossa in SMA 0011 (B; C162-1), the elongate foramen in the neural spine (B; C165-1), the right (A; C170-1), or acute angles (B; C170-0) between the spinopostzygapophyseal and the postzygodiapophyseal laminae, and the vertical (A; C218-0) or posteriorly inclined tuberculum (B; C218-1). Abb.: acdl, anterior centrodiapophyseal lamina; apf, anterior pneumatic fossa; cprl, centroprezygapophyseal lamina; CR, cervical rib; CV 5, cervical vertebra 5; pap, parapophysis; pl, pleurocoel; poz, postzygapophysis; ppf, posterior pneumatic fossa; prz, prezygapophysis; pvf, posteroventral flanges; sprl, spinoprezygapophyseal lamina. Scaled to the same cotyle height.

Figure 6.51: Mid-cervical vertebrae of *Kaatedocus siberi* SMA 0004 (A; CV 10, modified from Tschopp and Mateus, in press) and *Diplodocus carnegii* CM 84 (B; CV 8) in right lateral (A) and left laterodorsal view (B). Note the reduced spinoprezygapophyseal lamina (B; C163-1), the pre-epipophysis (C181-1), which is anteriorly expanded in *K. siberi* (A; C167-1), the distinct fossa posterolaterally to the prezygapophysis (A; C183-1), which is absent in CM 84 (B; C183-0), and the short cervical ribs (B; 214-1). Abb.: apf, anterior pneumatic fossa; cprl, centroprezygapophyseal lamina; CR, cervical rib; CV 7, cervical vertebra 7; podl, postzygodiapophyseal lamina; poz, postzygapophysis; ppf, posterior pneumatic fossa; prz, prezygapophysis; pvf, posteroventral flanges; spol, spinopostzygapophyseal lamina; sprl, spinoprezygapophyseal lamina. Not to scale.

Figure 6.52: Cervical vertebra 8 of *Dicraeosaurus hansemanni* MB.R.4886 (A) and *Kaatedocus siberi* SMA 0004 (B) in right lateral view. Note the different inclinations of the neural spine (C169), and the small tuberosity marking the anterodorsal corner of the centrum in *Kaatedocus* (B; C178-1). Abb.: cpol, centropostzygapophyseal lamina; CV 7, cervical vertebra 7; epi, epipophysis; mt, median tubercle; podl, postzygodiapophyseal lamina; poz, postzygapophysis; pre, pre-epipophysis; prz, prezygapophysis; pvf, posteroventral flanges; spol, spinopostzygapophyseal lamina; sprl, spinoprezygapophyseal lamina. Scaled to the same cotyle height.

Figure 6.53: Cervical vertebra 14 of *Dinheirosaurus lourinhanensis* ML 414 in lateroventral view, illustrating the particular ventral morphology with posteriorly located paired pneumatic foramina (C176-1), lateral grooves posterior to the parapophyses (C177-1), a posteriorly restricted ventral keel (C193-1), and the elongated lateral spinal cavity (C204-1). Abb.: acdl, anterior centrodiapophyseal lamina; CR, cervical rib; pap, parapophysis; poz, postzygapophysis; prz, prezygapophysis; pvf, posteroventral flanges; pvfo, posteroventral fossa.

Figure 6.54: Cervical vertebra 11 of *Jobaria tiguidensis* MNN TIG (A; traced from photo by J. Carballido), *Camarasaurus supremus* AMNH 5671 (B; based on Osborn and Mook, 1921), and *Diplodocus carnegii* CM 84 (C; based on Hatcher, 1901) in anterior view. Note the straight (A; C180-0), in contrast to convex prezygapophyseal facet (C; C180-1), and the different morphologies of the centroprezygapophyseal lamina (single, A, C185-0; divided, and connecting to tprl, B, C185-1; divided with both branches connecting to prezygapophysis, C, C185-2). Abb.: di, diapophysis; nc, neural canal; pap, parapophysis; podl, postzygodiapophyseal lamina; poz, postzygapophysis; prdl, prezygodiapophyseal lamina; prz, prezygapophysis; spol, spinopostzygapophyseal lamina; sprl, spinoprezygapophyseal lamina. Scaled to the same condyle height.

Figure 6.55: Cervical vertebra 12 of *Kaatedocus siberi* SMA 0004 in lateral anterodorsal view. Note the laterally tilted anterior portion of the sprl (C182-1), the lateral fossa marking the anterior end of the spinodiapophyseal fossa (C183-1), and the transverse sulcus accompanying the prezygapophyseal facet posteriorly (C195-1). Abb.: cpol, centropostzygapophyseal lamina; CR, cervical rib; epi, epipophysis; poz, postzygapophysis; prdl, prezygodiapophyseal lamina; pre, pre-epipophysis; prz, prezygapophysis; spol, spinopostzygapophyseal lamina;

sprl, spinoprezygapophyseal lamina. 3D digital model provided by G. Dzemski.

Figure 6.56: Cervical vertebra 12 of *Apatosaurus louisae* CM 3018 (A; based on Gilmore, 1936), and *Kaatedocus siberi* SMA 0004 (B; based on Tschopp and Mateus, in press) in posterior view. Note the separated (A; C186-1) or connected pcdl and podl (B; C186-0), the divided (A; C189-1) or single cpol (B; C189-0), the accessory lamina in the postzygapophyseal centrodiapophyseal fossa (B; C198-1), and the tpol that connects directly (B; C201-0) or indirectly with the neural canal roof (A; C201-1). Abb.: CR, cervical rib; pcdl; posterior centrodiapophyseal lamina; podl, postzygodiapophyseal lamina; poz, postzygapophysis; prdl, prezygodiapophyseal lamina; spol, spinopostzygapophyseal lamina; tpol, interpostzygapophyseal lamina. Scaled to the same posterior cotyle height.

Figure 6.57: Posterior cervical vertebra of *Barosaurus lentus* YPM 429 in right lateral view, illustrating the short horizontal accessory lamina within the spinodiapophyseal fossa (C187-1), the anteriorly bifurcated posterior centrodiapophyseal lamina (C188-1), and the anteriorly restricted postzygapophyses (C200-1). Abb.: cpol, centropostzygapophyseal lamina; pap, parapophysis; podl, postzygodiapophyseal lamina; prdl, prezygodiapophyseal lamina; prz, prezygapophysis; pvf, posteroventral flanges; spol, spinopostzygapophyseal lamina; sprl, spinoprezygapophyseal lamina. Scale bar = 10 cm.

Figure 6.58: Posterior cervical vertebrae of *Kaatedocus siberi* SMA 0004 (A), and *Barosaurus lentus* YPM 429 (B) in dorsal view. Note the dorsoventral ridge on the medial side of the metapophysis (A; C206-1) and the anterior projection lateral to the prezygapophyseal facet (B; C213-1). Abb.: di, diapophysis; epi, epipophysis; podl, postzygodiapophyseal lamina; prdl, prezygodiapophyseal lamina; prz, prezygapophysis; spol, spinopostzygapophyseal lamina; sprl, spinoprezygapophyseal lamina. Scaled to the same total length.

Figure 6.59: Dorsal vertebra 1 of *Apatosaurus louisae* CM 3018 (A; modified from Gilmore, 1936), and *Diplodocus carnegii* CM 84 (B; modified from Hatcher, 1901) in left and right lateral view, respectively. Note the roughened prdl (B; C208-1), and the different location of the pleurocoels (C240). Abb.: cpol, centropostzygapophyseal lamina; di, diapophysis; pap, parapophysis; pcdl; posterior centrodiapophyseal lamina; pl, pleurocoel; poz, postzygapophysis; spol, spinopostzygapophyseal lamina. Scaled to same posterior cotyle height.

Figure 6.60: Anterior dorsal vertebrae of *Suuwassea emilieae* ANS 21122 (A), *Apatosaurus* sp. UW 15556 (B; modified from Gilmore, 1936), and *Apatosaurus ajax* YPM 1860 (C) in anterior view. Note the prespinal lamina (A and C; C209-1), the diverging (B; C211-0) or parallel neural spines (A; C211-1), the wide (C; C212-0) or narrow (A; C212-1) distance between the spine tops, and the ridge on the medial side of the neural spine (C; C245-1). Abb.: di, diapophysis; nc, neural canal; pap, parapophysis; pcdl; posterior centrodiapophyseal lamina; prdl, prezygodiapophyseal lamina; prpl, prezygoparapophyseal lamina; prz, prezygapophysis; sprl, spinoprezygapophyseal lamina; tprl, interprezygapophyseal lamina. Scaled to same anterior condyle height.

Figure 6.61: Posterior cervical ribs of *Apatosaurus* sp. UW 15556 (A; after Gilmore, 1936) and *A. louisae* CM 3018 (B; after Gilmore, 1936) in right lateral view (B inverted). Note the short, reduced anterior projection (A; C220-1), the pointed anterior process (A; C221-1), the ventrolateral process (B; C222-1), and the downwards curving posterior process (A; C223-1). Abb.: cap, capitulum; tub, tuberculum. Scaled to same length.

Figure 6.62: Dorsal vertebra 3 of *Shunosaurus lii* T5401 (A; modified from Zhang, 1988), and *Apatosaurus* sp. UW 15556 (B; modified from Gilmore, 1936) in left (A) and right (B) lateral view. Note the slightly concave lateral surface of the centrum in *Shunosaurus* (A; C227-0), in contrast to the well-defined pneumatopore in *Apatosaurus* (B; C227-1), and the different locations of the parapophyses (C246). Abb.: cpol, centropostzygapophyseal lamina; di, diapophysis; pcdl, posterior centrodiapophyseal lamina; poz, postzygapophysis. Scaled to the same total vertebral height.

Figure 6.63: Posterior dorsal vertebrae of *Haplocanthosaurus priscus* CM 572 (A; modified from Hatcher, 1903), *Demandasaurus darwini* MDS-RVII 798 (B; modified from Torcida Fernández-Baldor et al., 2011), and *Apatosaurus louisae* CM 3018 (C; modified from Gilmore, 1936) in posterior view. Note the paired pneumatic foramen dorsolateral to the neural canal in *Demandasaurus* (B; C229-1), the different orientations of the diapophyses in *Haplocanthosaurus* (A; C230-1) and *Apatosaurus* (C; C230-0), the single lamina that supports the hyposphene from below (C; C238-0), the dorsal spur on the tip of the transverse process (A; C264-1), the small triangular lateral projections at the spine top (A; C267-1), or their absence (C; C267-0), the rhomboid (C; C276-0) in contrast to laminar (B; C276-1) hyposphene, and the ventrally forked spol (B; C277-1). Abb.: cpol, centropostzygapophyseal lamina; nc, neural canal; pap, parapophysis; posl, postspinal lamina; poz, postzygapophysis; spdl, spinodiapophyseal lamina; spol, spinopostzygapophyseal lamina. Scaled to same posterior centrum height.

Figure 6.64: Dorsal vertebra 8 of *Camarasaurus supremus* AMNH 5760 (A; traced from Osborn and Mook, 1921) and *Apatosaurus louisae* CM 3018 (B; traced from Gilmore, 1936) in anterior view. Note the separated (A; C231-0) or dorsally united spinoprezygapophyseal laminae (B; C231-1), the fossa between them (B; C233-0), and the triangular processes of the neural spine, that project further than the zygapophyses (A; C267-2). Abb.: acpl, anterior centroparapophyseal lamina; cprl, centroprezygapophyseal lamina; nc, neural canal; pap, parapophysis; prsl, prespinal lamina; prz, prezygapophysis; spdl, spinodiapophyseal lamina; tp, transverse process. Scaled to same anterior condyle height.

Figure 6.65: Dorsal neural arches of *Diplodocus carnegii* CM 84 (A; traced from Hatcher, 1901) and *Nopcsaspondylus alarconensis* holotype specimen (B; traced from Nopcsa, 1902) in anterior view. Note the festooned spdl typical for rebbachisaurids (B; C232-1), in contrast to the plesiomorphic state (A; C232-0), and the notched (A; C281-1), or straight to convex spine summits (B; C281-0). Abb.: cprl, centroprezygapophyseal lamina; prdl, prezygodiapophyseal lamina; prsl, prespinal lamina; tp, transverse process. Not to scale.

Figure 6.66: Posterior dorsal vertebrae of *Losillasaurus giganteus* MCNV Lo-11 (A), and *Apatosaurus louisae* CM 3018 (B; modified from Gilmore, 1936) in posterior view. Note the concave dorsal end of the posl (A; C234-1), the horizontal (A; C275-0), instead of angled (B; C275-1) postzygapophyseal facets, and the medial spinopostzygapophyseal lamina (B; C278-1). Abb.: cprl, centroprezygapophyseal lamina; hys, hyposphene; lspol, lateral spinopostzygapophyseal lamina; posl, postspinal lamina; poz, postzygapophysis; spdl, spinodiapophyseal lamina. Scaled to same posterior cotyle height.

Figure 6.67: Dorsal vertebra 4 of *Dinheirosaurus lourinhanensis* ML 414 in ventral view, illustrating the ventral keel (C242-1) in anterior dorsal vertebrae. Abb.: DV, dorsal vertebra; pcdl, posterior centrodiapophyseal lamina; pl, pleurocoel; podl, postzygodiapophyseal lamina; tp, transverse process.

Figure 6.68: Dorsal vertebra 1 of *Apatosaurus louisae* CM 3018 (A) and *A.* sp. UW 15556 (B; both traced from Gilmore, 1936) in posterior view. Note the different positions of the transverse processes (high, A, C243-0; low, B, C243-1), and the varying width of the base of the bifurcated spines (wide, A, C244-0; narrow, B, C244-1). Abb.: di, diapophysis; pcdl, posterior centrodiapophyseal lamina; podl, postzygodiapophyseal lamina; poz, postzygapophysis; prz, prezygapophysis. Scaled to same posterior cotyle height.

Figure 6.69: Mid-dorsal vertebrae of *Dinheirosaurus lourinhanensis* ML 414 (A; traced from photo by O. Mateus) and *Galeamopus shellensis* SMA 0011 (B) in lateral view. Note the pleurocoels that are entirely situated on the centrum (A; C247-0), or invade the neural arch (B; C247-1), the accessory spinal lamina connecting to the junction of spol and spdl (A; C251-1), the vertical lamina subdividing the pleurocoel (A; C253-1), the anteriorly displaced parapophysis (A; C256-1) in contrast to its usual position above the anterior edge (B; C256-0), and the horizontal accessory lamina connecting the hyposphene with the pcdl (A; C260-1). Abb.: cpol, centropostzygapophyseal lamina; pcdl, posterior centrodiapophyseal lamina; pcpl, posterior centroparapophyseal lamina; podl, postzygodiapophyseal lamina; spol, spinopostzygapophyseal lamina. Scaled to same vertebral height.

Figure 6.70: Posterior dorsal vertebrae of *Apatosaurus louisae* CM 3018 (A; traced from Gilmore, 1936) and *Supersaurus vivianae* BYU 9044 (B; traced from Jensen, 1985) in left (A) and right (B) lateral view. Note the prpl (A; C255-1), the anteriorly displaced parapophysis (B; C256-1), the acpl (A; C257-1), the pcpl (B; C258-1), the lateral branch of the cpol (B; C261-1), the pronounced opisthocoely (B; C270-2), and the anteriorly inclined base of the neural spine (A; C280-1). Abb.: cpol, centropostzygapophyseal lamina; hys, hyposphene; pl, pleurocoel; posl, postspinal lamina; poz, postzygapophysis; spdl, spinodiapophyseal lamina. Scaled to same posterior cotyle height.

Figure 6.71: Posterior dorsal vertebrae of *Giraffatitan brancai* MB.R.3822 (A), *Apatosaurus louisae* CM 3018 (B; traced from Gilmore, 1936), and *Diplodocus carnegii* CM 84 (C; traced from Hatcher, 1901) in right lateral view. Note the double pcpl (C; C258-2), the accessory lamina in the parapophyseal centrodiapophyseal fossa (C; C259-1), the accessory lamina connecting the hyposphene with the pcdl (C; C260-1), the infradiapophyseal pneumatic foramen (A; C262-1), the dorsally tapering neural spine (A; C265-1), the different shapes of the pleurocoels (C271), and the ventrally open parapophyseal, centrodiapophyseal fossa (B; C273-0). Abb.: cprl, centroprezygapophyseal lamina; lspol, lateral spinopostzygapophyseal lamina; posl, postspinal lamina; poz, postzygapophysis; prsl, prespinal lamina; prz, prezygapophysis; spdl, spinodiapophyseal lamina; tp, transverse process. Scaled to same total height.

Figure 6.72: Posterior dorsal vertebra of *Elosaurus parvus* CM 566 in lateral anterodorsal view. Note the greatly reduced spinoprezygapophyseal lamina, which does not reach the prezygapophysis (C274-0). Only the base of the neural arch is preserved (see Peterson and Gilmore, 1902). Abb.: lspol, lateral spinopostzygapophyseal

lamina; podl, postzygodiapophyseal lamina; posl, postspinal lamina; poz, postzygapophysis; prdl, prezygodiapophyseal lamina.

Figure 6.73: Dorsal rib heads of *Suuwassea emilieae* ANS 21122 (A; modified from Harris, 2006b), *Apatosaurus louisae* CM 3018 (B; modified from Gilmore, 1936) and *Barosaurus* sp. AMNH 6341 (C, fragment) in anterior (A, B) and posterior (C) view. Note the transverse ridge (C; C283-1), the pneumatic foramen (B; C284-1), and two of three different orientations of the tuberculum in respect to the rib shaft (C285). Grey lines in C indicate the continuation of the rib if complete. Abb.: cap, capitulum; tub, tuberculum. Not to scale.

Figure 6.74: Sacrum of *Brontosaurus amplus* YPM 1981 in ventral view (modified from Ostrom and McIntosh 1966), illustrating the oblique ridge on sacral rib III (C288-1). Abb.: DV, dorsal vertebra; SV, sacral vertebra, sy, sacricostal yoke. Scale bar = 20 cm.

Figure 6.75: Sacra of *Apatosaurus* sp. UW 15556 (A; modified from Hatcher, 1903) and *Diplodocus* sp. AMNH 223 (B; modified from Osborn, 1899) in left lateral view. Note the flat (A; C289-0) instead of ornamented sacral neural spine top (B; C289-1), the spdl that extends ventrally to the diapophysis (A; C290-1), and the parallel (A; C291-0) in contrast to converging neural spines (B; C291-1). Abb.: DR, dorsal rib; il, ilium; SV, sacral vertebra. Scaled to the same height.

Figure 6.76: Anterior caudal vertebra of *Diplodocus carnegii* CM 94 in left lateral view, illustrating various characters typical for the genus: a depression between the lateral spinal lamina and the postspinal lamina (C292-1), the large pleurocoel (C297-1), an additional pneumatic foramen posterodorsally in the caudal centrum (C298-1), the accessory lamina between pre- and postzygapophysis (C301-1), a dorsally widened lateral spinal lamina (C303-1), a pre-epipophysis (C311-1), the double anterior centrodiapophyseal lamina (C314-1), the distinct spinoprezygapophyseal lamina that extends onto the lateral surface of the spine (C318-1) and contacts the spinopostzygapophyseal lamina (C319-1), the presence of a prespinal lamina (C320-1) with a thickened anterior rim (C321-1), and the presence of a postspinal lamina (C323-1). Scale bar = 10 cm.

Figure 6.77: Anterior caudal vertebrae of *Demandasaurus darwini* MDS-RVII,610 (A; traced from Torica Fernandéz-Baldor et al., 2011), *Brontosaurus excelsus* YPM 1980 (B; traced from Ostrom and McIntosh, 1966), and *Diplodocus carnegii* CM 84 (C; traced from Hatcher, 1901) in anterior view. Note the lateral triangular processes (B; C293-1), the mostly rectangular outline of the spine (B; C294-0), the wing-like transverse processes (A; C299-1), the convex prezygapophyses (B; C310-1), the laterally (C; C312-0) or dorsally directed ventral surface of the transverse process (A; C312-1), the notched neural spine top (C; C326-1), the gradual (C; C328-0) or abrupt distal expansion of the spine (B; C328-1), and the foramen piercing the transverse process (B; C350-0). Abb.: prsl, prespinal lamina; prz, prezygapophysis; sprl, spinoprezygapophyseal lamina; tp, transverse process. Scaled to same total height.

Figure 6.78: Anterior caudal vertebrae of *Apatosaurus ajax* YPM 1860 (A) and *Diplodocus* sp. DMNS 462 (B) in ventral view. Note the ventral keel (A; C296-1), the ventral foramen (B; C305-1) within the ventral longitudinal hollow (B; C330-1), and the anteroposteriorly expanded distal end of the transverse process (A; C316-1). Abb.: ns, neural spine. Scaled to same centrum length.

Figure 6.79: Anterior caudal vertebrae of *Dicraeosaurus hansemanni* MB.R.3774 (A), *Apatosaurus* sp. NHMUK R.3211 (B), and *Barosaurus lentus* YPM 429 (C) in left lateral view. Note the reduced (B; C307-0) or large pneumatopores (C; C307-1), the distinct posterior centrodiapophyseal and postzygodiapophyseal laminae (C; C315-1), and the postspinal lamina that projects dorsally (A; C324-1). Abb.: prz, prezygapophysis; sprl, spinoprezygapophyseal lamina; tp, transverse process. Scaled to same posterior centrum height.

Figure 6.80: Anterior caudal vertebra of *Dicraeosaurus hansemanni* MB.R.3774 in posterior view, illustrating the hyposphenal ridge (C325-0). Abb.: cpol, centropostzygapophyseal lamina; posl, postspinal lamina; poz, postzygapophysis; tp, transverse process. Scale bar = 10 cm.

Figure 6.81: Mid-caudal vertebra of SMA 0087 (A) and *Diplodocus* sp. AMNH 223 (B) in right (A) and left (B) lateral view. Note the ventrolateral (A; C329-1) and lateral ridges (A; C333-1), the flat ventral border of the centrum (B; 335-1), the anteriorly shifted neural arch (B; C337-1), the differing inclinations of the neural spine (C340), which overhang the postzygapophyses (A; C343-0), or not (B; C343-1). Abb.: ns, neural spine; prz, prezygapophysis. Scaled to the same anterior articular surface height.

Figure 6.82: Mid-caudal vertebrae of *Losillasaurus giganteus* MCNV Lo-32 (A), *Isisaurus colberti* ISIR335/42 (B; traced from Jain and Bandyopadhyay, 1997), *Diplodocus* sp. AMNH 655 (C), and *Barosaurus lentus* AMNH 6341 (D) in anterior view, illustrating the four states of character 334 (A, circular; B, quadrangular; C, trapezoidal; D, flat ventral margin with rounded lateral edges). Abb.: nc, neural canal; ns, neural spine; prz,

prezygapophysis. Scaled to same anterior surface height.

Figure 6.83: Mid-caudal vertebra of *Diplodocus longus* YPM 1920 in dorsal view, illustrating the transverse ridge connecting the prezygapophyses posteriorly (C338-1). Abb.: poz, postzygapophysis; prz, prezygapophysis; sprl, spinoprezygapophyseal lamina. Scale bar = 5 cm.

Figure 6.84: Mid-caudal vertebrae of *Cetiosauriscus stewarti* NHMUK R.3078 (A; traced from Woodward, 1905) and *Supersaurus vivianae* WDC DMJ-021 (B; traced from a photo by D. Lovelace) in left lateral view, illustrating the anterodorsal projection on the spine top (B; C341-1), and the posteriorly elongated neural spine (A; C344-0). Abb.: lr, lateral ridge; poz, postzygapophysis; prz, prezygapophysis. Scaled to same total vertebral height.

Figure 6.85: Anterior chevron of *Apatosaurus ajax* YPM 1860 in anterior, right lateral, and posterior view (left to right). Note the crus bridging the haemal canal dorsally (broken here; C352-0), the anterior, longitudinal median ridge (C354-1), and the step-like posterior expansion of the distal blade (C355-1). Abb.: db, distal blade; hc, haemal canal. Scale bar = 10 cm.

Figure 6.86: Mid-chevron of *Diplodocus* sp. AMNH 223 in dorsal, left lateral, and ventral view (top-bottom). Note the anterior and posterior projections (C353-1), the rugose horizontal ridge (C356-1), and the medial fossa (C357-1). Abb.: pas, proximal articular surface. Scale bar = 5 cm.

Figure 6.87: Scapula outlines of *Haplocanthosaurus priscus* CM 879 (A), *Limaysaurus tessonei* MUCPv-205 (B), *Apatosaurus louisae* CM 3018 (C; all traced from Mannion, 2009), and *Diplodocus* sp. AMNH 223 (D; traced from Osborn, 1899). Note the concave dorsal border of the acromion process (B; C363-1), the acromion process that reaches almost half the scapular length (D; C364-1), the different shapes of the acromial edge (straight, C, C367-0; with rounded expansion distally, A, C367-1; raquet-shaped, B, C367-2), the ventrally curving ventral margin (A; C368-1), and the subtriangular process (D; C370-1). Abb.: acm, acromion; ca, coracoid articulation; db, distal blade. Scaled to same scapular length.

Figure 6.88: Right scapulae of *Elosaurus parvus* CM 566 (A) and *Brontosaurus excelsus* YPM 1980 (B) in lateral view. Note the excavated area between the acromial edge and the distal blade (A; C365-0) and the flat muscle scar at the base of the distal blade (B; C369-1). Abb.: acr, acromial ridge; db, distal blade. Scaled to same length.

Figure 6.89: Left coracoids of *Amphicoelias altus* AMNH 5764? (A) and *Apatosaurus ajax* YPM 1860 (B; traced from Bakker, 1998) in anterolateral view. Note the rounded (A; C372-0) instead of rectangular shape (B; C372-1), and the deep (A; C373-1) in contrast to shallow infraglenoid groove (B; C373-0). Abb.: CF, coracoid foramen. Scaled to the same height.

Figure 6.90: Right (A, B) and left (C) sternal plates of *Giraffatitan brancai* MB.R.2181 (A; modified from Janensch, 1961), *Brontosaurus amplus* YPM 1981 (B), and *Tornieria africana* MB.R.2726 (C) in ventral view. Note the different shapes (oval, B, C374-0; triangular, C, C374-1; crescentic, A, C374-2), the longitudinal ridge (A; C375-1), the anterior dorsoventral thickening (C; C376-1), and the straight posterior border (C; C377-1). Scaled to same length.

Figure 6.91: Humeri of *Turiasaurus riodevensis* CPT 1195-1210 (A; traced from Royo-Torres et al., 2006) and *Suuwassea emilieae* ANS 21122 (B; traced from Harris, 2007) in anterior view. Note the pronounced proximolateral corner (B; C383-1), the symmetrical proximal transverse expansion (B; C384-1), the unexpanded (A; C385-1) or expanded lateral edges (B; C385-0), and the tubercle marking the center of the proximal concavity (B; C386-1). Abb.: dpc, deltopectoral crest. Scaled to same length.

Figure 6.92: Distal half of radius of *Dyslocosaurus polyonychius* AC 663 illustrating the very weak ridges for the articulation with the ulna (C392-0). Scale bar = 10 cm.

Figure 6.93: Carpal elements of SMA 0011 (A) and *Apatosaurus* sp. UW 15556 (B; traced from Bonnan, 2003) in anterior view, illustrating the two different shapes described in C396: 0) block-like (A), and 1) disc-like (B). Scaled to the same transverse width.

Figure 6.94: Articulated metacarpals III-V of *Apatosaurus louisae* CM 3018 in proximal view (traced from Gilmore, 1936), showing the greatly enlarged mc V, in comparison to mc III and IV (C403-1).

Figure 6.95: Manual phalanx phm I-1 of *Apatosaurus* sp. NSMT-PV 20375 in medial view (traced from Upchurch et al., 2004b), showing the proximoventral lip-like projection (C404-1).

Figure 6.96: Right (A) and left (B) ilium of *Brachiosaurus altithorax* FMNH P25107 (A; modified from Riggs,

1904) and *Diplodocus* sp. DMNS 1494 (B) in lateral view. Note the pointed (B; C406-0) or semicircular preacetabular process (A; C406-1), the straight (A; C409-0) or strongly convex dorsal edge (B; C409-1), the location of the highest point (anterior to pubic peduncle, A, C410-1; posterior to pubis peduncle, B, C410-1), the triangular fossa on the pubic peduncle base (B; C412-1), and the tubercle in the postacetabular region (A; C413-1). Abb.: prap, preacetabular process; pup, pubic peduncle. Scaled to same height.

Figure 6.97: Left (A, C) and right (B, reversed) pubis of *Camarasaurus supremus* AMNH 5761 (A; modified from Osborn and Mook, 1921), *Dicraeosaurus hansemanni* MB.R.4886 (B; modified from Janensch, 1961), and *Brontosaurus excelsus* YPM 1980 (C; modified from Ostrom and McIntosh, 1966) in lateral view. Note the different sizes of the ambiens process (C414, arrowheads: absent, A; hook-like, B; incipient, C). Abb.: ac, acetabular surface; ip, iliac peduncle; isa, ischial articular surface; of, obturator foramen. Scaled to same length.

Figure 6.98: Left ischium of *Haplocanthosaurus priscus* CM 572 (A; modified from Hatcher, 1903), *Demandasaurus darwini* MPS-RVII,18 (B; modified from Pereda Suberbiola et al., 2003), and *Brontosaurus excelsus* YPM 1980 (C; modified from Ostrom and McIntosh, 1966) in lateral (left) and distal (right) view. Note the flat (C; C418-0) in contrast to strongly concave acetabular margin (B; C418-1), the constricted neck of the iliac tubercle (B; C419-1), the elongate muscle scar on the proximal shaft (A; C421-1), the lateral fossa at the base of the blade (C; C422-1), the blade-like (B; C423-0) or medially expanded distal ends (C; C423-1), which form a more or less straight line (B; C424-1) or a V (C; C424-0), and can be straight (A; C426-0) or expanded dorsoventrally as well as transversely (C; C425-1). The light gray line in B indicates the distal view of the right ischium. Scaled to same length.

Figure 6.99: Right femur of *Giraffatitan brancai* MB.R. St291 (A), *Dicraeosaurus hansemanni* MB.R.4886 (B; both modified from Janensch, 1961), and *Tornieria africana* SMNS 12140 (C; modified from Fraas, 1908) in anterior view. Note the lateral bulge (A; C428-1), the medial deflection of the femoral head (A; C429-1), the different positions of the highest point of the femoral head (C431), the stepped ventral margin of the head (B; C432-1), the nutrient foramen (B; C434-1), the fourth trochanter, which is visible in anterior view (A; C436-0), and the anteriorly extended distal articular surface of the condyle (C; C439-1). Scaled to same length.

Figure 6.100: Tibia of *Omeisaurus tianfuensis* T5701 (A; traced from He et al., 1988), *Dyslocosaurus polyonychius* AC 663 (B), and *Apatosaurus louisae* CM 3018 (C; traced from Gilmore, 1936) in proximal view. Note the different outlines (anteroposteriorly compressed, A, C441-1; subtriangular, B, C442-1; subrectangular, C, C442-0), and the projection posterior to the cnemial crest (B; C446-0). Abb.: cc, cnemial crest. Scaled to same anteroposterior length.

Figure 6.101: Distal end of tibia of *Dyslocosaurus polyonychius* AC 663 in medial view, illustrating the transverse ridge on the anteromedial surface, close to the distal end (C443-1). Scale bar = 10 cm.

Figure 6.102: Tibia of *Zapalasaurus* sp. MOZ-Pv 1244 (A; traced from Salgado et al., 2012) and *Tornieria africana* MB.R.2572 (B; traced from Remes, 2006) in anterolateral view, illustrating the different shapes of the cnemial crest (widely rounded, A, C444-0; triangular, B, C444-1). Scaled to same length.

Figure 6.103: Proximal end of the tibia of *Suuwassea emilieae* ANS 21122 in posterolateral view, showing the distinct fibular trochanter on the posterior surface of the cnemial crest (C445-1). Scale bar = 10 cm.

Figure 6.104: Astragalus of SMA 0087 (A) and *Dyslocosaurus polyonychius* AC 663 (B) in dorsal (top) and posterior (bottom) view. Note the triangular shape in both views (B; C449-1, C450-1), the ascending process that reaches the posterior border (A; C453-1), the anterior border of the fibular facet, which is visible in posterior view (B; C454-1), the presence (B; C455-0) or absence (A; 455-1) of a sheet underlying the fibula, and the blunt (A; C456-0) in contrast to elongate medial end (B; C456-1). Scaled to the same proximodistal height.

Figure 6.105: Metatarsal I of *Cetiosauriscus stewarti* NHMUK R3078 in dorsal/anterior view. Note the foramina (C459-1), the angled proximal (C460-0) and distal articular surfaces (C462-0), and the distinct posterolateral process on the distal articular surface (C464-1). Scale bar = 5 cm.

Figure 6.106: Right (A) and left (B) metatarsal II of SMA 0087 (A) and *Dyslocosaurus polyonychius* AC 663 in dorsal/anterior view. Note the dorsolateral rugosity (C465-1) with its different developments (reduced, laterally, A, C468-0; prominent, reaching center or shaft, B, C468-1), or the posterolateral process (absent, A, C469-0; present, B, C469-1). Scaled to same proximodistal length.

Figure 6.107: Right (A) and left (B) metatarsal II of *Suuwassea emilieae* ANS 21122 (A) and *Dyslocosaurus polyonychius* AC 663 (B) in proximal view, illustrating the concave (A) and straight (B) lateral margins (arrows; C467). Scaled to the same dorsoventral height.

Tables

Table 6.60: Pedal phalanges, ratios.

Table 6.61: Clades recovered, support values, and differences.

Supplementary material

S2.1: Video renderings of the original, deformed, and the retrodeformed 3D models of CV 14 from *Kaatedocus siberi* SMA 0004 in right lateral view. The sequence runs from the original, deformed model, to the SAM-16, MM-16, and back to the original.

S2.2: Video renderings of the original, deformed, and the retrodeformed 3D models of CV 14 from *Kaatedocus siberi* SMA 0004 in dorsal view. The sequence runs from the original, deformed model, to the SAM-16, MM-16, and back to the original.

S2.3: Video renderings of the original, deformed, and the retrodeformed 3D models of CV 14 from *Kaatedocus siberi* SMA 0004 in posterior view. The sequence runs from the original, deformed model, to the SAM-16, MM-16, and back to the original.

S3.1: Phylogenetic matrix of diplodocid sauropod dinosaurs, based on Whitlock (2011a), with *Kaatedocus siberi* added. This is a preliminary version of the specimen-based phylogenetic analysis presented later in this thesis.

S6.1: Specimen-based phylogenetic matrix, mesquite file.

Abbreviations

Institutional:

AC, Beneski Museum of Natural History, Amherst College, Amherst, Massachusetts, USA; **AMNH**, American Museum of Natural History, New York City, New York, USA; **ANS**, Academy of Natural Sciences, Philadelphia, Pennsylvania, USA; **AODF**, Australian Age of Dinosaurs Fossil; **BYU**, Brigham Young University, Museum of Paleontology, Provo, Utah, USA; **CEU**, College of Eastern Utah, Prehistoric Museum, Price, Utah, USA; **CM**, Carnegie Museum of Natural History, Pittsburgh, Pennsylvania, USA; **CMC**, Cincinnati Museum Center, Cincinnati, Ohio, USA; **CMNH**, Cleveland Museum of Natural History, Cleveland, Ohio, USA; **CPT**, Conjunto Paleontológico de Teruel, Dinópolis, Teruel, Spain; **DGO**, Museo de Geologia de la Universidad de Oviedo, Oviedo, Spain; **DMNS**, Denver Museum of Nature and Science, Denver, Colorado, USA; **DNM**, Dinosaur National Monument, Jensen, Utah, USA; **DNSM**, Durban Natural Science Museum, South Africa; **DQ**, Dana Quarry, Dinosauria International Inc., Tensleep, Wyoming, USA; **FMNH**, Field Museum of Natural History, Chicago, Illinois, USA; **GMNH**, Gunma Museum of Natural History, Gunma, Japan; **GPIT**, Institut für Geowissenschaften, Eberhard-Karls-Universität Tübingen, Tübingen, Germany; **HMNS**, Houston Museum of Nature and Science, Houston, TX, USA; **IPGAN**, Institute of Paleobiology, Georgian Academy of Sciences, Tbilisi, Georgia; **IVPP**, Institute of Vertebrate Paleontology and Paleoanthropology, Chinese Academy of Sciences, Beijing, China; **KUVP**, Kansas University Natural History Museum, Lawrence, Kansas, USA; **LACM**, Natural History Museum, Los Angeles County, Los Angeles, California, USA; **MB.R.**, Museum für Naturkunde, Berlin, Germany; **MCNV**, Museo de Ciencias Naturales, Valencia, Spain; **MIGM**, Museu Geológico do Instituto Geológico e Mineiro de Portugal, Lisboa, Portugal; **ML**, Museu da Lourinhã, Lourinhã, Portugal; **MOR**, Museum of the Rockies, Bozeman, Montana, USA; **MWC**, Museum of Western Colorado, Grand Junction, Colorado, USA; **NHM**, Natural History Museum, London, United Kingdom; **NMMNH**, New Mexico Museum of Natural History and Science, Albuquerque, New Mexico, USA; **NSMT**, National Museum if Nature and Science, Tokyo, Japan; **OMNH**, Sam Noble Oklahoma Museum of Natural History, Norman, Oklahoma, USA; **PMU**, Evolutionsmuseet Paleontologi, University of Uppsala, Uppsala, Sweden; **ROM**, Royal Ontario Museum, Toronto, Canada; **SDSM**, South Dakota School of Mines and Technology, Rapid City, South Dakota, USA; **SMA**, Sauriermuseum Aathal, Aathal, Switzerland; **SNHM**, Staatliches Naturhistorisches Museum, Braunschweig, Germany; **Tate**, Tate Geological Museum, Casper College, Casper, Wyoming, USA; **UCL**, University College, London, UK; **UCM**, University of Colorado Museum of Natural History, Boulder, Colorado, USA; **UMNH**, Utah Museum of Natural History, Salt Lake City, Utah, USA; **USNM**, United States National Museum, Smithsonian Institution, Washington DC, USA; **UUVP**, University of Utah, Salt Lake City, Utah, USA; **UW**, University of Wyoming Geological Museum, Laramie, Wyoming, USA; **WDC**, Wyoming Dinosaur Center, Thermopolis, Wyoming, USA; **YPM**, Yale Peabody Museum, New Haven, Connecticut, USA.

Anatomical:

a, articular; **aal**, acetabular articulation surface length; **ac**, acetabular surface; **aCd,** anterior caudal vertebrae; **acdl**, anterior centrodiapophyseal lamina; **acf**, anterior condyle fossa; **acl**, acromion length; **acm**, acromion; **acr**, acromial ridge; **aCV**, anterior cervical vertebrae; **adt**, anterodorsal tuberosity; **aDV,** anterior dorsal vertebrae; **af**, astragalus foramen; **al**, accessory lamina; **amb**, ambiens process; **amc**, amphicoelous; **amCd**, anterior-most caudal vertebrae; **amp**, amphiplatyan; **an**, angular; **anp**, antotic process; **aof**, antorbital fenestra; **ap**, anterior process; **apd**, anteroposterior depth; **apf**, anterior pneumatic fossa; **apl**, anterior process length; **ar**, anterior ramus; **asl**, accessory spinal lamina; **asp**, ascending process; **at**, atlas; **ato**, anterior tooth; **avl**, anteroventral lip; **ax**, axis; **axr**, axial rib; **Bc,** braincase; **bic**, biconvex; **bns**, bifid neural spine; **bo**, basioccipital; **bph**, basipterygoid hook; **bpr**, basipterygoid process; **bs**, basisphenoid; **bt**, basal tuber; **c**, carpal; **ca**, coracoid articulation; **can**, crista antotica; **cap**, capitulum; **cc**, cnemial crest; **cdf**, centrodiapophyseal fossa; **CF**, coracoid foramen; **Ch**, chevrons; **chf**, chevron facet; **co**, coracoid; **cpr**, crista prootica; **cprf**, centroprezygapophyseal fossa; **cprl**, centroprezygapophyseal lamina; **CR**, cervical ribs; **CV**, cervical vertebra; **d**, dentary; **dapd**, distal anteroposterior depth; **das**, anterior spur on diapophysis; **db**, distal blade; **dCd**, distal caudal vertebrae; **dds**, dorsal spur on diapophysis; **de**, dentin; **dg**, distal groove; **di**, diapophysis; **dip**, distal process; **dlr**, dorsolateral ridge; **dp**, diapophysis posterior process; **dpc**, deltopectoral crest; **dpcl**, length deltopectoral crest; **DR**, dorsal ribs; **dro**, distal roller; **dsf**, dorsal spinal fossa; **dt**, denticles; **DV**, dorsal vertebra; **dw**, distal width; **ec**, epicondyle; **EFS**, external fundamental system; **emf,** external mandibular fenestra; **en**, enamel; **ep**, ectopterygoid; **epi**, epipophysis; **er**, ectopterygoid ramus; **ex**, exoccipital; **f**, frontal; **fe**, femur; **fh**, femoral head; **fi**, fibula; **fic**, fibular condyle; **fif**, fibular facet; **Fl**, forelimb; **fm**, foramen magnum; **FS**, facial skull; **ft**, fourth trochanter; **GL**, glenoid; **h**, humerus; **hc**, haemal canal; **hh**, humeral head; **Hl**, hindlimb; **hya**, hypantrum; **hys**, hyposphene; **icg**, intercondylar groove; **il**, ilium; **int sprl**, interrupted spinoprezygapophyseal lamina; **ip**, iliac peduncle; **is**, ischium; **isa**, ischial articular surface; **isal**, ischial articular surface length; **j**, jugal; **la**, lacrimal; **lco**, lateral condyle; **LJ**, lower jaw; **lpl**, lateral process length; **lprzc**, lateral prezygapophyseal cavity; **lr**, lateral ridge; **ls**, laterosphenoid; **lsc**, lateral spine cavity; **lsp**, lateral spur; **lspol**, lateral spinopostzygapophyseal lamina; **ltf**, laterotemporal fenestra; **m**, maxilla; **Ma**, manus; **MB**, morphotype B element; **mc**, metacarpal; **mCd**, mid-caudal vertebrae; **mco**, medial condyle; **mCV**, mid-cervical vertebrae; **mDV**, mid-dorsal vertebrae; **mp**, medial process; **mr**, medial ridge; **mspol**, medial spinopostzygapophyseal lamina; **msw**, midshaft width; **mt**, median tubercle; **mts**, metatarsal; **n**, external nares; **na**, nasal; **naf**, neural arch foramen; **nc**, neural canal; **ncs**, neurocentral synchondrosis; **nf**, nutrient foramen; **ns**, neural spine; **o**, orbit; **of**, obturator foramen; **olf**, olfactory foramen; **opc**, opisthocoelous; **opf**, optic foramen; **os**, orbitosphenoid; **p**, parietal; **pa**, palate; **pabh**, preacetabular blade height; **pap**, parapophysis; **papd**, proximal anteroposterior depth; **paof**, preantorbital fossa; **par bns**, parallel bifurcated neural spine; **pas**, proximal articular surface; **pCd**, posterior caudal vertebrae; **pcdl**, posterior centrodiapophyseal lamina; **PcG**, pectoral girdle; **pcpl**, posterior centroparapophyseal lamina; **pCV**, posterior cervical vertebrae; **pdd**, proximodistal depth; **pDV**, posterior dorsal vertebrae; **Pe**, Pes; **pf**, prefrontal; **phm**, manual phalanx; **php**, pedal phalanx; **pl**, pleurocoel; **plc**, posterolateral crest; **plp**, posterolateral process; **pm**, premaxilla; **pnf**, pneumatic foramina; **po**, postorbital; **podl**, postzygodiapophyseal lamina; **popr**, paroccipital process; **posl**, postspinal lamina; **poz**, postzygapophysis; **pp**, posterior process; **ppapd**, pubic peduncle anteroposterior depth; **ppf**, posterior pneumatic fossa; **ppfo**, postparietal foramen; **pph**, pneumatopore height; **ppl**, pneumatopore length; **ppw**, pubic peduncle transverse width; **pra**, proatlas; **prap**, preacetabular process; **prapl**, preacetabular process length; **prc**, procoelous; **prcdf**, prezygapophyseal centrodiapophyseal fossa; **prdl**, prezygodiapophyseal lamina; **pre**, pre-epipophysis; **pro**, prootic; **prpl**, prezygoparapophyseal lamina; **prsl**, prespinal lamina; **prz**, prezygapophysis; **ps**, proximal spur; **psr**, parasphenoid rostrum; **ptc**, platycoelous; **ptf**, posttemporal fenestra; **pto**, posterior tooth; **ptr**, vertical distance from proximal articular surface to trochanter; **pts**, prezygapophysis transverse sulcus; **pu**, pubis; **pua**, pubic articular surface; **pual**, pubic articular surface length; **pup**, pubic peduncle; **pupl**, pubic peduncle length; **pvf**, posteroventral flanges; **pvfo**, posteroventral fossa; **PvG**, pelvic girdle; **pvl**, posteroventral lip; **pvlp**, posterior ventrolateral process; **pw**, proximal width; **q**, quadrate; **qj**, quadratojugal; **qr**, quadrate ramus; **r**, radius; **rt**, tubercle for articulation with radius; **sa**, surangular; **saf**, surangular foramen; **sc**, scapula; **sdf**, spinodiapophyseal fossa; **sh**, shaft height; **snc**, sagittal nuchal crest; **so**, supraoccipital; **spof**, spinopostzygapophyseal fossa; **spol**, spinopostzygapophyseal lamina; **sprl**, spinoprezygapophyseal lamina; **sprl ab**, spinoprezygapophyseal lamina anterior bulge; **sq**, squamosal; **sqr**, squamosal ramus; **SR**, sternal ribs; **stf**, supratemporal fenestra; **SV**, sacral vertebrae; **sw**, shaft width; **sym**, symphysis; **T**, teeth; **tb**, tibia; **tc**, tooth crown; **tic**, tibial condyle; **tif**, tibial facet; **tp**, transverse process; **tpol**, interpostzygapophyseal lamina; **tprl**, interprezygapophyseal lamina; **tr**, tooth root; **tub**, tuberculum; **u**, ulna; **ung**, ungual; **ut**, tubercle for articulation with ulna; **vk**, ventral keel; **vlh**, ventral longitudinal hollow; **vlr**, ventrolateral ridge; **vmc**, ventral median constriction; **vsf**, ventral spinal fossa; **wf**, wear facet.

Other:

EI, elongation index; **HOS**, histological ontogenetic stage; **HQ**, Howe Quarry; **HScQ**, Howe-Scott Quarry; **HStQ**, Howe-Stephens Quarry; **mdA**, more derived Apatosaurines; **mdD**, more derived Diplodocoidea; **mdE**, more derived Eusauropoda; **MM**, Motani Method; **OTU**, operational taxonomic unit; **RI**, robustness index; **SAM**, Single Axis Method; **SI**, slenderness index; **SHQ**, Spring Hill Quarry.

Introduction

Overview of diplodocid sauropods

The sauropod dinosaur clade Diplodocidae includes some of the most iconic sauropods. With their greatly elongated necks and tails, diplodocids constitute the typical image of sauropod dinosaurs. The clade is historically important, having provided the first published reconstruction of an entire sauropod skeleton ('*Brontosaurus*' *excelsus*; Marsh, 1883), the first complete sauropod skull to be described (*Diplodocus*; Marsh, 1884), and the first mounted sauropod specimen (*Apatosaurus* AMNH 460; Matthew, 1905). Diplodocids range from relatively small to gigantic sauropod species (*Kaatedocus siberi* Tschopp and Mateus, 2012b, to *Supersaurus vivianae* Jensen, 1985, respectively), and include the well-known genera *Apatosaurus* Marsh, 1877a, *Diplodocus* Marsh, 1878, and *Barosaurus* Marsh, 1890. Their possible first occurrence dates to the Middle Jurassic of England (*Cetiosauriscus stewarti* Charig, 1980; but see Heathcote and Upchurch, 2003, or Rauhut et al., 2005, for a differential identification of *Cetiosauriscus*). Diplodocidae reaches a peak in diversity in the Late Jurassic, with finds from North America, Tanzania, Zimbabwe, Portugal, Spain, as well as possibly England, Georgia, and China (Upchurch and Mannion, 2009; Mannion et al., 2012). To date, no convincing evidence exists for their presence in the Cretaceous (Whitlock et al., 2011), but their probable extinction at the Jurassic-Cretaceous boundary still remains a mystery (Taylor et al., 2011).

In recent phylogenetic trees, Diplodocidae consistently forms the sister group to the possibly exclusively Gondwanan clade Dicraeosauridae, with which they form Flagellicaudata, which in turn is included, together with the Rebbachisauridae, in Diplodocoidea (e.g. Upchurch, 1998; Wilson, 2002, 2005; Harris and Dodson, 2004; Upchurch et al., 2004a; Rauhut et al., 2005; Harris, 2006c; Sereno et al., 2007; Whitlock, 2011a; Carballido et al., 2012b; Mannion et al., 2012; Tschopp and Mateus, 2012b). The taxonomy of the clade was historically somewhat confused, with "Diplodocidae" being used in the same way as Diplodocoidea today (see e.g. McIntosh, 1990a, b). In the following, I use the taxonomy and definitions as clarified by Taylor and Naish (2005).

Whereas the vast majority of diplodocid species were described in the late 1800s and early 1900s, additional taxa still continue to be discovered (see Tab. 1.1). The high rate of early descriptions, particularly during the so-called bone wars in the late 1800s, resulted also in a high amount of species that are now considered invalid, questionable, or synonymous (Taylor, 2010). Species recognition is furthermore hampered by the fact that many of the holotype specimens are incomplete and fragmentary (e.g. *Diplodocus longus* YPM 1920), or appear to include bones of more than one individual (e.g. *Apatosaurus ajax* YPM 1860). Due to the absence of field notes or quarry maps in many of these cases, it remains difficult or even impossible to confidently assign the individual bones to particular animals. Given that the majority of the sites in the Upper Jurassic Morrison Formation, which yielded about three quarters of the reported diplodocid genera, are multi-taxon assemblages, it is possible that some of these holotype specimens include material from different species. This renders meaningful diagnoses for the species and thus the identification of new material highly difficult. However, the detailed studies of original material and their corresponding field notes by McIntosh and Berman (1975), Berman and McIntosh (1978), McIntosh (1981, 1990a, 1995, 2005), and McIntosh and Carpenter (1998), provided a wealth of important information concerning the composition of diplodocid holotype specimens and species recognition. Nonetheless, only one study that tested the validity of single species by means of phylogenetic methods has been published to date, focusing on the genus *Apatosaurus* only (Upchurch et al., 2004b). By using individual specimens as operational taxonomic units (OTUs), Upchurch et al. (2004b) succeeded in obtaining a significant result, which generally supported the traditional view of *Apatosaurus* intrarelationships.

The specimen-based phylogenetic analysis is herein extended to the entire clade of Diplodocidae, and combined with the most recent analyses of diplodocoid interrelationships (Whitlock, 2011a; Mannion et al., 2012; Tschopp and Mateus, 2012b). It includes all holotype specimens of every single putative diplodocid species ever described (see Tab. 1.2). The phylogenetic analysis is furthermore expanded by adding reasonably complete and articulated referred specimens from various sites in the Morrison Formation (e.g. *Diplodocus* sp. AMNH 223, Osborn, 1899; or

Barosaurus sp. AMNH 6341, McIntosh, 2005). Among the additional OTUs are also four specimens from the Howe Ranch in the vicinity of Shell (Bighorn Basin, Wyoming), three of which are herein reported or described for the first time.

Table 1.1: Species historically described as belonging to Diplodocidae

Species	Most recent taxonomic opinion	Reference	Occurrence	Comments
Dystrophaeus viaemalae Cope, 1877b	Sauropoda incertae sedis	Upchurch et al., 2004a	USA	genotype of *Dystrophaeus*
Amphicoelias altus Cope, 1877a	Diplodocoidea incertae sedis	Tschopp and Mateus, in press	USA	genotype of *Amphicoelias*
Amphicoelias latus Cope, 1877a	synonym of *Camarasaurus supremus*	Osborn and Mook, 1921	USA	
Apatosaurus ajax Marsh, 1877a	Apatosaurinae	Upchurch et al., 2004b	USA	genotype of *Apatosaurus*
Apatosaurus grandis Marsh, 1877a	Misassigned, => *Camarasaurus grandis*	Marsh, 1878; Upchurch et al., 2004b	USA	
Amphicoelias fragillimus Cope, 1878	synonym of *A. altus*	Osborn and Mook, 1921	USA	
Atlantosaurus immanis Marsh, 1878	synonym of *A. ajax*	McIntosh, 1995; Upchurch et al., 2004b	USA	
Diplodocus longus Marsh, 1878	Diplodocinae	McIntosh and Carpenter, 1998	USA	genotype of *Diplodocus*
Brontosaurus excelsus Marsh, 1879	*Brontosaurus* = *Apatosaurus*; species referred to *Apatosaurus* (*A. excelsus*)	Riggs, 1903; Upchurch et al., 2004b	USA	genotype of *Brontosaurus*
Apatosaurus laticollis Marsh, 1879	synonym of *A. ajax*	McIntosh and Berman, 1975; Upchurch et al., 2004b	USA	
Brontosaurus amplus Marsh, 1881	synonym of *A. excelsus*	McIntosh and Berman, 1975; Upchurch et al., 2004b	USA	
Diplodocus lacustris Marsh, 1884	nomen dubium	McIntosh, 1990a	USA	originally described as *Stegosaurus armatus* teeth (Marsh, 1877b; McIntosh, 1990a)
Barosaurus lentus Marsh, 1890	Diplodocinae	Tschopp and Mateus, in press	USA	genotype of *Barosaurus*
Barosaurus affinis Marsh, 1899	synonym of *B. lentus*	McIntosh, 1990a	USA	
Diplodocus carnegii Hatcher, 1901	unambiguous differential diagnosis from *D. longus* not yet demonstrated	Gilmore, 1932; McIntosh, 1990a	USA	sometimes called *D. carnegiei* (e. g. Janensch, 1961)
Elosaurus parvus Peterson and Gilmore, 1902	*Elosaurus* = *Apatosaurus;* => *A. parvus*	Upchurch et al., 2004b	USA	genotype of *Elosaurus*
Gigantosaurus africanus Fraas, 1908	*Gigantosaurus* preoccupied, => *Tornieria africana*; included into *Barosaurus* (*Barosaurus africanus*); generic distinction proved valid, => *Tornieria africana*	Sternfeld, 1911; Janensch, 1922; Remes, 2006	Tanzania	genotype of *Tornieria*
Apatosaurus louisae Holland, 1915a	Apatosaurinae	Upchurch et al., 2004b	USA	
Apatosaurus minimus Mook, 1917	misassigned, Macronaria incertae sedis	McIntosh, 1990a; Mannion et al., 2012	USA	
Diplodocus hayi Holland, 1924	possibly new genus	Holland, 1924; McIntosh, 1990a	USA	
Apatosaurus alenquerensis Lapparent and Zbyzsewski, 1957	Misassigned, => *Camarasaurus alenquerensis*; later new genus erected: *Lourinhasaurus alenquerensis* (Macronaria)	McIntosh, 1990b; Dantas et al., 1998; Mocho et al., 2013	Portugal	genotype of *Lourinhasaurus*
Barosaurus gracilis Russell et al., 1980	nomen nudum	Remes, 2006	Tanzania	initially described as *B. africanus* var. *gracilis* (Janensch, 1961)
Cetiosauriscus stewarti Charig, 1980	Non-neosauropod Eusauropoda; originally described as *Cetiosaurus leedsi*	Rauhut et al., 2005	United Kingdom	genotype of *Cetiosauriscus*
Supersaurus vivianae Jensen, 1985	Diplodocidae	Tschopp and Mateus, in press	USA	genotype of *Supersaurus*
Dystylosaurus edwini Jensen, 1985	synonym of *S. vivianae*	Curtice and Stadtman, 2001	USA	genotype of *Dystylosaurus*
Seismosaurus halli Gillette, 1991	*Seismosaurus* = *Diplodocus*, possibly *D. longus*, or *D. hallorum*	Lucas et al., 2006; Lovelace et al., 2007	USA	genotype of *Seismosaurus*; should be called *S. hallorum* (Gillette, 1994, after a personal comment of G. Olshevsky)
Dyslocosaurus polyonychius McIntosh et al., 1992	Diplodocoidea incertae sedis	Upchurch et al., 2004a	USA	genotype of *Dyslocosaurus*
Apatosaurus yahnahpin Filla and Redman, 1994	new genus: *Eobrontosaurus* (Diplodocidae)	Bakker, 1998	USA	genotype of *Eobrontosaurus*
Dinheirosaurus lourinhanensis Bonaparte and Mateus, 1999	Diplodocidae	Tschopp and Mateus, in press	Portugal	genotype of *Dinheirosaurus*
Losillasaurus giganteus Casanovas et al., 2001	Turiasauria, sister taxon to *Turiasaurus*	Royo-Torres and Upchurch, 2012	Spain	genotype of *Losillasaurus*
Suuwassea emilieae Harris and Dodson, 2004	Dicraeosauridae	Tschopp and Mateus, in press	USA	genotype of *Suuwassea*
Australodocus bohetii Remes, 2007	Titanosauria incertae sedis	Mannion et al., in press	Tanzania	genotype of *Australodocus*
Kaatedocus siberi Tschopp and Mateus, 2012b	Diplodocinae	Tschopp and Mateus, in press	USA	genotype of *Kaatedocus*

Howe Ranch: a rediscovered diplodocid Eldorado

The Howe Ranch sites have produced a high number of partially to almost completely articulated dinosaur skeletons, sometimes even with soft tissue preservation (see Brinkmann and Siber, 1992; Ayer, 2000; Schwarz et al., 2007c; Tschopp, 2008; Siber and Möckli, 2009; Christiansen and Tschopp, 2010; Tschopp and Mateus, 2012b). Three sites proved particularly productive: the Howe Quarry, the Howe-Stephens Quarry, and the Howe-Scott Quarry (Fig. 1.1). The Howe Quarry was first worked by Barnum Brown for the American Museum of Natural History (New York, USA) in 1934, and was later relocated and completely excavated by a team from the Sauriermuseum Aathal (Switzerland), led by Hans-Jakob 'Kirby' Siber (Brown, 1935; Ayer, 2000; Michelis, 2004; Tschopp and Mateus, 2012b). The other two sites, as well as several smaller, less productive spots at various stratigraphy levels within the Morrison Formation, have since been discovered nearby and excavated by the SMA (Ayer, 2000; Siber and Möckli, 2009; Christiansen and Tschopp, 2010; Fig. 1.2). All three major sites yielded well-preserved and at least partially articulated diplodocid specimens, both apatosaurine and diplodocine, of varying ontogenetic stages (Fig. 1.3; Tab. 1.3). Only one of these specimens has yet been formally described (even including the AMNH material from 1934), and is part of this doctoral thesis (Tschopp and Mateus, 2012b).

Table 1.2: Type material of diplodocid species, ordered according to year of description

Species	Holotype	Holotype material	Comments holotype	Other type material
Dystrophaeus viaemalae Cope, 1877b	USNM 2364	frag. DV, scapula, ulna, radius, metacarpals		
Amphicoelias altus Cope, 1877a	AMNH 5764	Tooth?, 2 DV, L scapulacoracoid?, ulna?, pubis?, femur		
Amphicoelias latus Cope, 1877a	AMNH 5765	4 Cd (two missing), femur		
Apatosaurus ajax Marsh, 1877a	YPM 1860	Bc?, frontals?, quadrates, CV 12-14, DV 1-4, 6-10, SV 1-5, 18 Cd, CR, DR, 6 Ch, scapulae, R coracoid, R ulna, ilia, L pubis, R ischium, frag. L femur, L tibia, L fibula	braincase might be from another quarry (Lakes Quarry 1)	
Apatosaurus grandis Marsh, 1877a	YPM 1901	Bc, DV, DR, partial sacrum, Cd 1-27, scapulae, humerus, radius, ulna, femora, tibia, fibula, manus (one carpal, mc III)		YPM 1905 (paratype)
Amphicoelias fragillimus Cope, 1878	AMNH 5777	dorsal neural arch	lost, not included into phylogenetic analysis	
Atlantosaurus immanis Marsh, 1878	YPM 1840	frag. anterior CV, CV 9, 10, 13, 15; D 1, 3, 5-10; S 1; several Cd, DR, 3 Ch, coracoids, pubes, ischia, L femur, R tibia, L fibula, pedal phalanx		
Diplodocus longus Marsh, 1878	YPM 1920	mCd, Ch		
Brontosaurus excelsus Marsh, 1879	YPM 1980	CV 5 to Cd 19, DR, sternal ribs, Ch, scapulae, coracoids, sternal plates, humeri, R radius, frag. L ilium, ischia, pubes, femora, tibiae, fibulae, astragali		
Apatosaurus laticollis Marsh, 1879	YPM 1861	part. mid- or posterior CV		
Brontosaurus amplus Marsh, 1881	YPM 1981	8 DV, SV 1-5, 12 aCd, DR, Ch, frag. R scapula, L coracoid, sternal plate, L humerus, L mc II, L ilium, frag. R ilium, L pubis, L ischium, L femur, L tibia, L fibula, L astragalus		
Diplodocus lacustris Marsh, 1884	YPM 1922	teeth		
Barosaurus lentus Marsh, 1890	YPM 429	CV 13-16, DV1, 4, 5, 7-9, Cd 2, 6-13, 15-17, 19, 20, 23, 25, 28, 32, and some dCd; Ch, DR, sternal L, part scapula, sacrum, part ilium, part pubis R, part ischium L, femur, tibia, part fibula L		
Barosaurus affinis Marsh, 1899	YPM 419	Mt I and V		
Diplodocus carnegii Hatcher, 1901	CM 84	CV 2-15, DV 1-10, SV 1-5, Cd 1-12, 18 DR, L scapula, L coracoid, R Ilium & frag of L, pubes, ischia, R femur, sternal plates, interclavicle		CM 94 (cotype)
Elosaurus parvus Peterson and Gilmore, 1902	CM 566	mCV, pDV, 2 SV, R scapula, humeri, R ulna, frag. ilium, frag. pubis, R femur, L fibula	young juvenile	
Gigantosaurus africanus Fraas, 1908	SMNS 12141a, 12145a, 12143, 12140, 12142	centrum of Cd 2, frag. DR, R ischium, R femur, R fibula	individual also contains R astragalus (SMNS 12145c); L scapula (MB.R.2728); R humerus (MB.R.2672); R ilium (MB.R.2713)	
Apatosaurus louisae Holland, 1915a	CM 3018	CV 1-15, DV 1-10, SV 1-5, Cd 1-64, 18 DR, Ch 1-3, scapulae, coracoids, humeri, L radius, ulna & manus, ilia, pubes, ischia, R femur, tibia & fibula, L pes	might include the skull CM 11162	
Apatosaurus minimus Mook, 1917	AMNH 675	SV, ilia, L pubis, L ischium		
Diplodocus hayi Holland, 1924	HMNS 175	part. skull, 10 CV, 5 DV, SV, 33 Cd, scapulae, coracoids, sternal plates, interclavicle, humeri, radii, L ulna & Mc, ilia, pubes, ischia, frag. R femur, L tibia, L fibula, R pes	previously CM 662, interclavicle and some other single bones still housed at CM	
Apatosaurus alenquerensis Lapparent and Zbyzsewski, 1957	no holotype assigned			MIGM 4956-7, 4970, 4975, 4979-80, 4983-4 and 5780-1 (lectotype)
Barosaurus gracilis Russell et al., 1980	no type		initially used to distinguish two morphotypes of *'B.' africanus* (Janensch, 1961)	
Cetiosauriscus stewarti Charig, 1980	NHMUK R.3078	frag. DV and SV, aCd to mCd, Ch, L scapulacoracoid, L humerus, L ulna, L ilium, L femur, L tibia, L fibula, L astragalus, L pes		
Supersaurus vivianae Jensen, 1985	BYU 12962	R scapulacoracoid		
Dystylosaurus edwini Jensen, 1985	BYU 4503	aDV	old specimen number: BYU 5750	
Seismosaurus halli Gillette, 1991	NMMNH 3690	8 DV, SV, Cd 1-8, 12-16, 20-27, DR, 5 Ch, ilia, ischia, pubis, 230 gastroliths		
Dyslocosaurus polyonychius McIntosh et al., 1992	AC 663	part. ?L ulna and radius, part. L femur, part. L tibia, part. R tibia, L astragalus, L Mt I-III, part. mt IV, L phalanges I-1, III-1, IV-1, unguals of I, II, III (proximal half), IV, possible ungual V	not sure if same individual, or even same locality	
Apatosaurus yahnahpin Filla and Redman, 1994	Tate-001	3 CV, 7 DV, DR, sternal ribs, L & part. R scapulacoracoid, sternal plates, L humerus, L ulna, L radius, L manus, pubis, L tibia, L fibula, R astragalus, R pes		
Dinheirosaurus lourinhanensis Bonaparte and Mateus, 1999	ML 414	2 pCV, DV 2-10, Cd centrum, ribs		
Losillasaurus giganteus Casanovas et al., 2001	MCNV Lo-5	aCd	individual also contains CV, DV, mCd and pCd, sternal plate, humerus, radius, ulna, ischium	MCNV Lo.10 and Lo-23 (paratypes)
Suuwassea emilieae Harris and Dodson, 2004	ANS 21122	frag. skull, CV 1-3, 5-7, pCV; DV 1-3; aCd, mCd, and pCd, DR, Ch, R scapula, R coracoid, R sternal plate, interclavicle, R humerus, L femur, L tibia, L fibula, L calcaneum, L pes		
Australodocus bohetii Remes, 2007	MB.R.2455	mCV		MB.R.2454 (paratype)
Kaatedocus siberi Tschopp and Mateus, 2012b	SMA 0004	part. skull, proatlas, CV 1, 3-14		

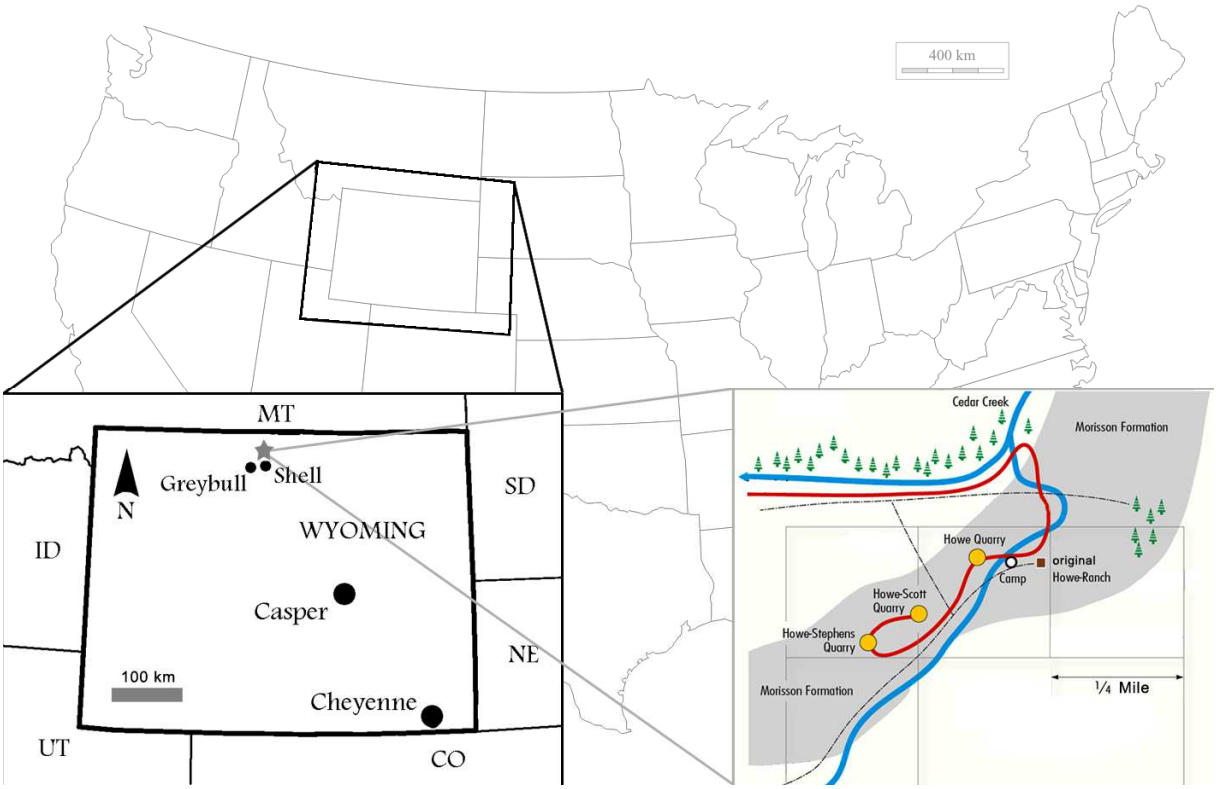

Figure 1.1: Locality of the Howe Ranch in the vicinity of Shell, Wyoming (lower left, star), with a detailed map of the three most important sites on the Ranch (lower right). Left inlet modified from Christiansen and Tschopp, 2010, right inlet courtesy of the Sauriermuseum Aathal.

Due to the good preservation of the SMA material, the addition of these specimens to a specimen-based phylogenetic analysis as attempted herein is of great importance. By doing so, the anatomical overlap among different OTUs is greatly increased – a very welcome fact, when many of the holotypes are fragmentary and only include few bones, as is the case in Diplodocidae. In particular two specimens with articulated and almost complete skulls (SMA 0004 and 0011) yield important new data. Although the clade Diplodocidae has produced the most skulls within sauropods (Whitlock et al., 2010), only two diplodocine (CM 3452, HMNS 175) and three apatosaurine specimens (CM 3018/11162, CMC 7180, YPM 1860) with possibly articulated skull material were reported to date (Holland, 1906, 1924; McIntosh and Berman, 1975; Berman and McIntosh, 1978; Barrett et al., 2011). Other than CM 11162, which is probably the skull of CM 3018 (Berman and McIntosh, 1978), none of them has yet been described in detail. This renders the identification of disarticulated skull material extremely difficult, and impedes specimen-based phylogenetic analyses. The new specimens described herein thus finally allow detailed reassessments of fragmentary material, including type skeletons and disarticulated skulls.

Structure of the thesis

The thesis itself includes both published papers written during the time of my Ph.D. and original contributions. Citations to the published papers are given below the title of the corresponding chapter. The main sections of the thesis are the introduction, a short methods part on retrodeformation as a test to evaluate numerical characters, the descriptions of the new specimens from the Howe Ranch, and finally, the specimen-based phylogenetic analysis, with its taxonomic implications and updated diagnoses for the species and genera of Diplodocidae.

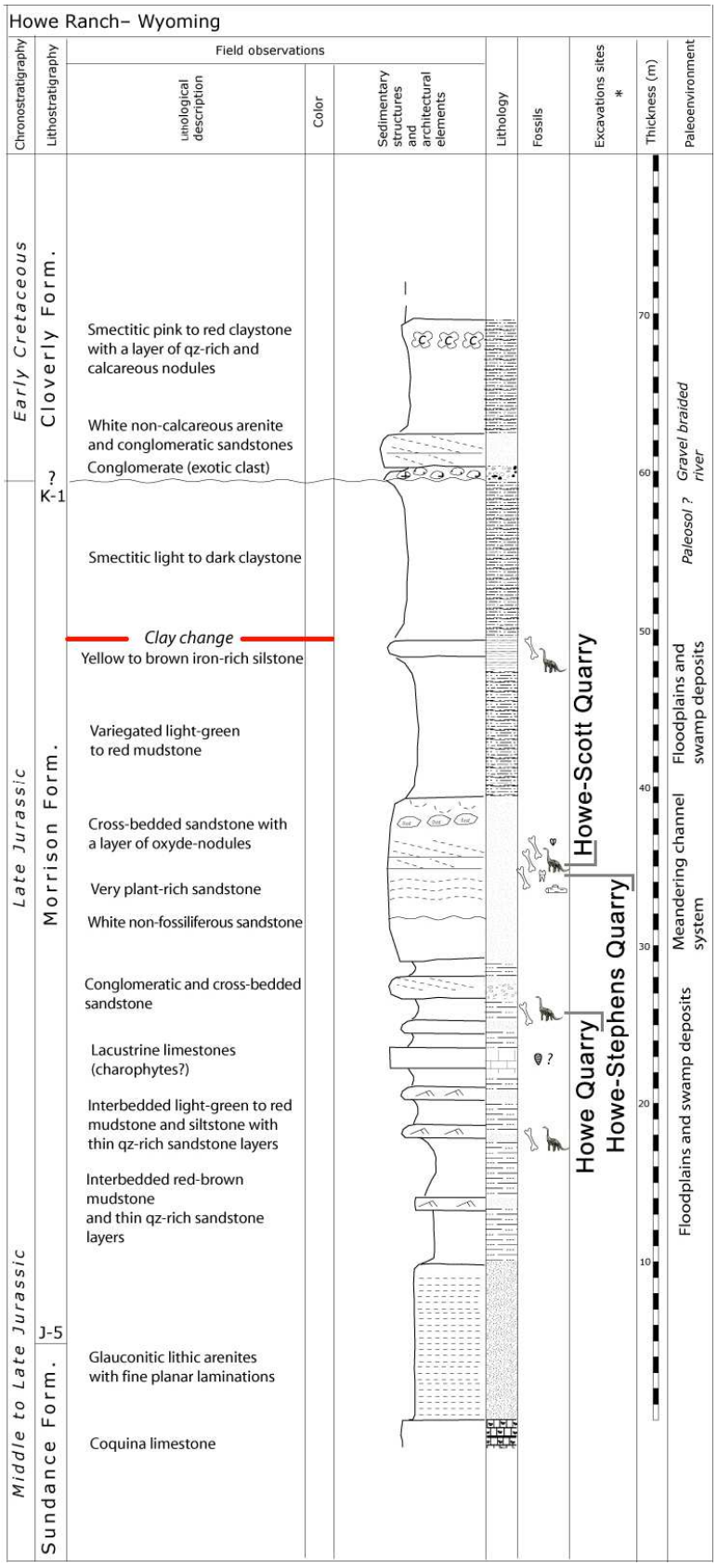

Figure 1.2: Stratigraphic log of the Howe Ranch sites showing the levels of the three most important quarries. The red line marks the clay change which has been proposed as marker bed to correlate sites across the Morrison Formation. Copyright by Jacques Ayer.

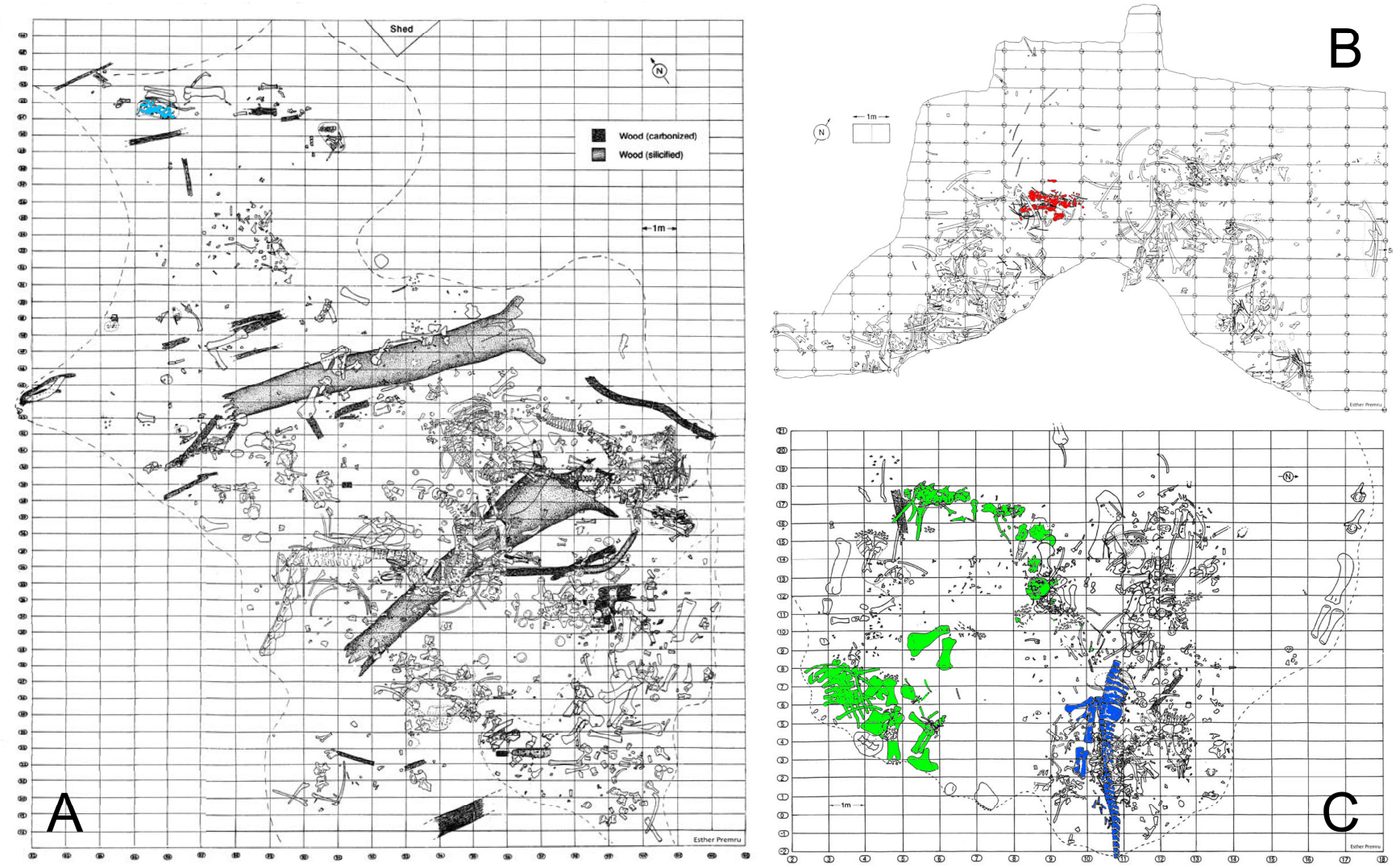

Figure 1.3: Quarry maps of the Howe-Stephens Quarry (a), Howe Quarry (b), and the Howe-Scott Quarry (c), highlighting the specimens included in the phylogenetic analysis (A, light blue: SMA 0009; B, red: SMA 0004; C, green: SMA 0011; C, dark blue: SMA 0087). Quarry maps drawn by Esther Premru, copyright by Sauriermuseum Aathal.

Table 1.3: Diplodocid specimens at SMA from the Howe Ranch sites.

Apatosaurinae					
Specimen number	Bones preserved	Articulation	Ontogenetic age	Site	References
SMA 0014	Hindleg including pes	partly articulated	adult	HScQ	
SMA 0084	Hindleg			HScQ	
SMA 0086	Hindleg		subadult	HStQ	
SMA 0087*	Pelvis, hindleg, tail	perfectly articulated	adult, HOS 10-11	HScQ	Klein and Sander, 2008

Diplodocinae					
Specimen number	Bones preserved	Articulation	Ontogenetic age	Site	References
SMA 0003	composite skeleton	partly articulated		HQ	Klein and Sander, 2008; Hohn-Schulte, 2010; Carballido et al., 2012a
SMA 0004*	cervical series including skull	articulated	subadult	HQ	Ayer, 2000; Klein et al., 2012; Tschopp and Dzemski, 2012; Tschopp et al., 2013; Tschopp and Mateus, in press
SMA 0007	partial postcranial skeleton	partly articulated	adult	HStQ	Klein and Sander, 2008
SMA 0008	partial postcranial skeleton	partly articulated		SHQ	Klein and Sander, 2008
SMA 0011*	Skeleton lacking the tail	partly articulated	subadult, HOS 8	HScQ	Klein and Sander, 2008
SMA 0013	partial postcranial skeleton	partly articulated		HStQ	Sander and Tückmantel, 2003; Klein and Sander, 2008
SMA 0083	partial postcranial skeleton	scattered		HStQ	

Diplodocidae?					
Specimen number	Bones preserved	Articulation	Ontogenetic age	Site	References
SMA 0009*	nearly complete postcranial skeleton	articulated	early juvenile, HOS 4	HStQ	Schwarz et al., 2007c; Klein and Sander, 2008; Galiano and Albersdörfer, 2010; Carballido et al., 2012a; Mannion et al., 2012; Woodruff and Fowler, 2012

Asterisks mark specimens included in the phylogenetic analysis. Abb.: HOS, histological ontogenetic stage; HQ, Howe Quarry; HScQ, Howe-Scott Quarry; HStQ, Howe-Stephens Quarry; SHQ, Spring Hill Quarry.

Retrodeformation as a test for the validity of phylogenetic characters: an example from diplodocid sauropod vertebrae

published in Palaeontologia Electronica:

Tschopp, E., J. Russo, and G. Dzemski. 2013. Retrodeformation as a test for the validity of phylogenetic characters: an example from diplodocid sauropod vertebrae. Palaeontologia Electronica, 16 (1, 2T): 1-23. palaeo-electronica.org/content/2013/352-retrodeformation-and-phylogeny

Abstract

Tectonic strain is ubiquitous in rock formations, leading to deformations, faults and cracks at small as well as large scales. Fossils embedded in these strata will passively participate in these deformations, and are thus rarely been found undistorted. This affects ratios used in phylogenetic analyses. As a case study, diplodocid (Dinosauria: Sauropoda) cervical vertebrae were subjected to two different methods of retrodeformation, and the same methods were tested with a manually deformed digital model of a Dodo (*Raphus cucullatus* Linnaeus, 1758) cervical vertebra. The results indicate that shape changes considerably in all dimensions. The tests showed that generally, retrodeformation restored symmetry, but increased deformation induced by compression. By comparing the trends obtained by the *Raphus cucullatus* analysis with the results from the diplodocid vertebrae, phylogenetic characters that are more prone to various types of deformations were identified. Phylogenetic analyses without these questionable characters generally yielded better resolution, shorter most parsimonious trees, and higher supporting values. Ratios used for character definitions, as well as other character information possibly affected by deformation, have therefore to be applied very carefully, and highly susceptible ratios should be avoided a priori. As shown in this study, retrodeformation can work as a tool to identify such ratios and characters, but has to be simultaneously tested with similar bones from extant taxa.

Introduction

During the process of preservation, biological hard tissue usually undergo a certain amount of taphonomic deformation, which can induce a loss of biologically important information (Hughes and Jell, 1992; Dunlavey et al., 2004; Angielczyk and Sheets, 2007; Boyd and Motani, 2008; Arbour and Currie, 2012). Quantifying the amount of distortion is crucial for studies of taxonomy, ontogeny, or biomechanics of these organisms, and numerous studies proposed different methods of how to achieve that aim (e.g., Sdzuy, 1966; Williams, 1990; Cooper, 1990; Hughes and Jell, 1992; Rushton and Smith, 1993; Motani, 1997; Ponce de León and Zollikofer, 1999; Zollikofer and Ponce de León, 2005; Srivastava and Shah, 2006; Ogihara et al., 2006; Angielczyk and Sheets, 2007; Gunz et al., 2009; Kazhdan et al., 2009; Arbour and Currie, 2012; Molnar et al., 2012). The various approaches were categorized under the term retrodeformation by Williams (1990), implying that they deform the fossil another time, but in the reverse direction, ideally recovering the original undeformed shape (Ponce de León and Zollikofer, 1999). Most of these techniques focused on the reconstruction of the original shape of two-dimensional images of rather simply shaped invertebrates (e.g., Cooper, 1990; Rushton and Smith, 1993), or on the calculation of strains in the matrix preserving the fossils (e.g., Sdzuy, 1966; Srivastava and Shah, 2006). In certain cases, retrodeformation methods resulted in considerable systematic changes, enabling the researchers to unite various taxa that were previously distinguished based on distorted length ratios (Hughes and Jell, 1992; Motani, 1997). In more complexly shaped, three-dimensionally preserved fossils, the probability that different parts are deformed in non-uniform ways is higher. Furthermore, since tectonic events rarely deform rocks in a homogeneous way, fossils with high relief or varying mechanical properties from the matrix are particularly susceptible to plastic as well as brittle deformation (Hughes and Jell, 1992; Boyd and Motani, 2008). Whereas the former changes the shape of the fossil without breaking it, the latter fractures the object and displaces the parts relative to each other (Zollikofer and Ponce de León, 2005; Boyd and Motani, 2008; Arbour and Currie, 2012). Some of the increasing number of attempts to reconstruct the original shape of three-

dimensional fossils were made with plesiosaur cervical vertebrae (Motani et al., 2005), a skull of a snake (Polcyn et al., 2005), a vertebra of an early tetrapod (Molnar et al., 2012), and most importantly, primate skulls (e.g., Ponce de León and Zollikofer, 1999; Zollikofer and Ponce de León, 2005; Zollikofer et al., 2005, 2009; Ogihara et al., 2006; Gunz et al., 2009). Recently, retrodeformation was also shown to be useful to detect areas with high probabilities of being deformed, thereby allowing to validate taxonomic affinities (Arbour and Currie, 2012).

Sauropod, and particularly diplodocid cervical vertebrae exhibit extremely complex structures with numerous laminae and cavities (Wilson, 1999). Vertebral morphology thus contributes a large part of phylogenetic analyses of sauropods (e.g., Wilson, 2002; Upchurch et al., 2004b). However, since such complex structures are more susceptible to deformation, information obtained from distorted elements has to be interpreted with special care. In the present case study, 3D models of the holotype neck of the diplodocid sauropod *Kaatedocus siberi* Tschopp and Mateus, 2012b were subjected to two different retrodeformation tools provided within the geometric morphometrics software Landmark™ (Motani et al., 2005; Wiley et al., 2005: www.idav.ucdavis.edu/research/EvoMorph). These tools address plastic deformation based on bilaterally symmetric points on the surface of the element, in order to reconstruct its initial shape. In order to evaluate the results, the same methods were applied to a digitally deformed 3D model of a cervical vertebra of *Raphus cucullatus* (Aves, Columbiformes). This allowed to identify phylogenetic characters that are based on ratios highly susceptible to deformation processes.

Material & Methods

This case study is based on the articulated neck of the holotype of *Kaatedocus siberi* (SMA 0004; Tschopp and Mateus, 2012b) found at Howe Quarry close to Shell in north-central Wyoming. The site lies in the Upper Jurassic Morrison Formation, and the vertebrae were subject to both plastic and brittle deformation (Fig. 2.1). The specimen was scanned in 3D using a structured light scanner (Tschopp and Dzemski, 2012). The obtained digital models were imported into Landmark™ (Motani et al., 2005; Wiley et al., 2005), a program facilitating the placing of landmarks on three-dimensional surfaces for geometric morphometric analyses, as well as providing tools for retrodeformation of distorted specimens. The retrodeformation tools offer two methods called Single Axis (SAM) and Motani Method (MM), and are both based on bilateral symmetry. The SAM assumes that the object under study was compressed during fossilization, and that this compression took place in a single axis (for detailed mathematical backgrounds see Kazhdan et al., 2009), a hypothesis which has also been used by Zollikofer and Ponce de León (2005). Since no additional information is given or referred to concerning the MM (only an abstract mentioning it: Motani et al., 2005), interested readers are further referred herein to an earlier publication on retrodeformation of 2D photographs of distorted fossils by Motani (1997), which is mainly based on two assumptions: homogenous/linear deformation within the study area, and that the undeformed shape of vertebral centra is cylindrical (Motani, 1997; Motani et al., 2005).

In order to apply these methods, 16 bilaterally symmetric landmark pairs were chosen on the vertebrae (Fig. 2.2). Retrodeformed models were produced using SAM and MM for the cervical vertebrae 3 to 14, and will herein be called SAM-16, or MM-16 models respectively. In order to further analyze the methods behind the tools, obtained retrodeformed models of CV 12 were subjected to a second iteration with the respective method (hereinafter called 2xSAM or 2xMM), and restored models of CV 12 were produced using different numbers of defining landmarks (four and nine pairs; herein called SAM-4 and MM-4, or SAM-9 and MM-9, respectively).

Comparisons were conducted using 2D imaging software: pictures of corresponding views of original and retrodeformed models were stacked and certain landmarks as well as the outline traced in order to visualize induced shape changes (Figs 2.3, 2.4). The retrodeformed models of CV 14 were also imported into LightWave 3D™ (NewTek). Videos of CV 14 in right lateral, dorsal, and posterior view were rendered by changing transparency between the original and the retrodeformed models, to highlight occurred shape changes (Supplementary material S2.1-2.3).

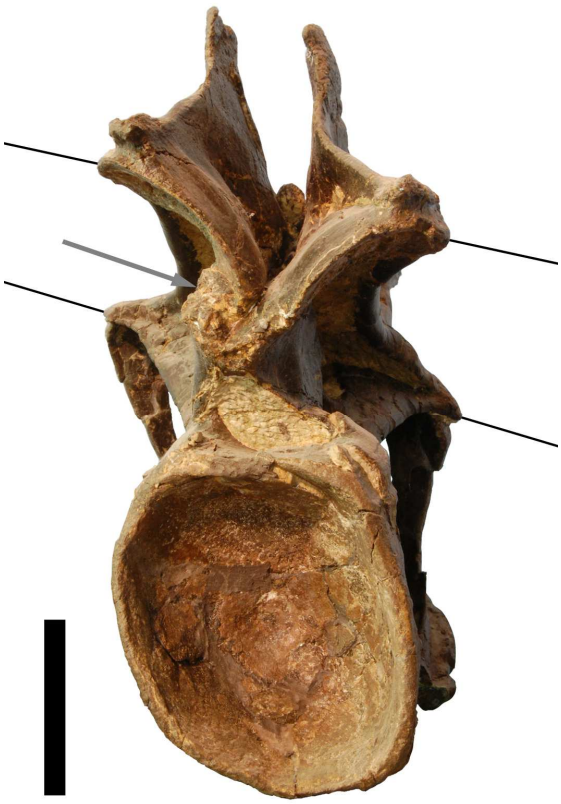

Figure 2.1: Posterior view of CV 12 of *Kaatedocus siberi* SMA 0004, showing brittle (arrow) and plastic deformation (lines; indicate the originally horizontal plane of postzygapophyses (above) and transverse processes (below)). Scale bar equals 5 cm.

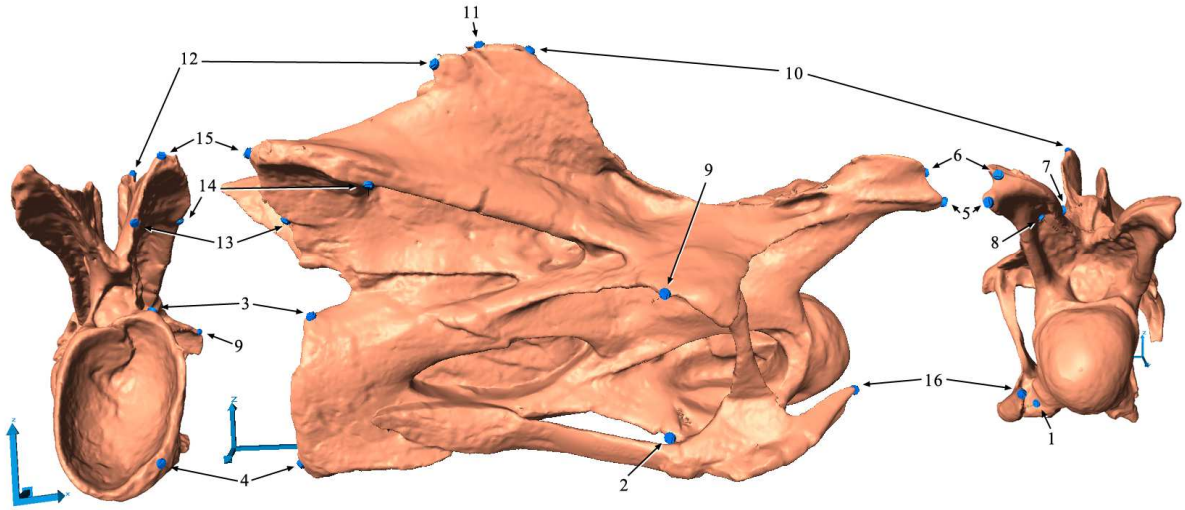

Figure 2.2: Landmarks used for the retrodeformation methods, shown in CV 10 of *Kaatedocus siberi* SMA 0004 in posterior, right lateral, and anterior view (from left to right). Only landmarks on right side are shown. The landmarks on the centrum are: 1) anteromedial corners of the parapophyses; 2) posterior ends of the parapophyses; 3) dorsolateral corner of the border of the cotyle, where the centropostzygapophyseal laminae converge with the centrum; 4) ventrolateral corner of the cotyle, where the posterolateral flanges of the ventral surface of the centrum merge with the border of the cotyle. The landmarks on the neural arch are: 5) anterior ends of prezygodiapophyseal laminae; 6) anterior-most points of prezygapophyses; 7) medial-most point of prezygapophyses; 8) medial sides of insertion of centroprezygapophyseal laminae into prezygapophyses; 9) posterolateral-most points of transverse processes; 10) anterior-most points of the neural spine summit; 11) small protrusions at the center of the neural spine summit; 12) posterior-most point of the neural spine summit; 13) posteromedial corners of postzygapophyses; 14) anterolateral corners of postzygapophyses; 15) posterior ends of spinopostzygapophyseal laminae. The landmark on the cervical rib is its anterior-most tip (16).

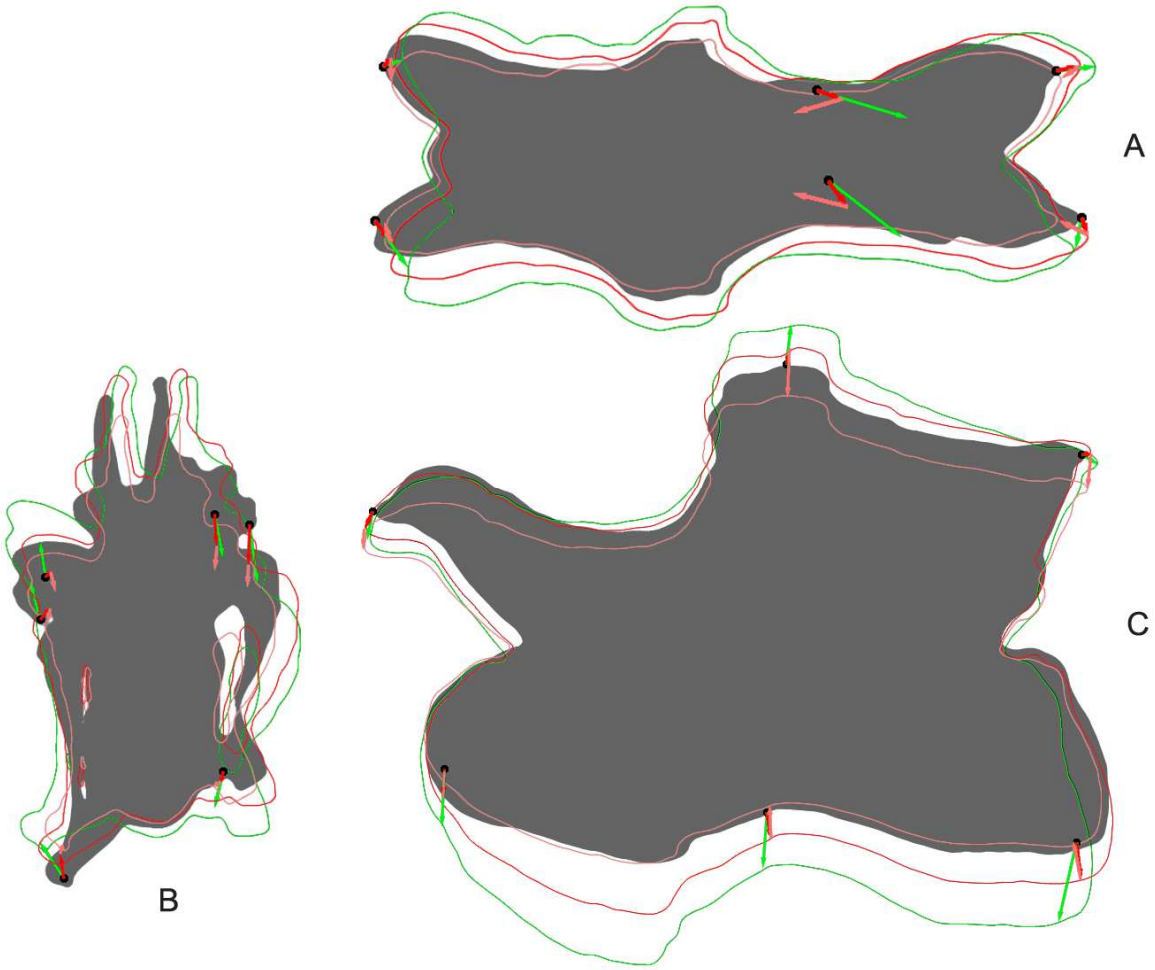

Figure 2.3: Shape changes after two retrodeformation steps in CV 12 of *Kaatedocus siberi* SMA 0004 in dorsal (A), anterior (B), and left lateral (C) view. The full shape marks the original deformed model, the outlines show the shape of the retrodeformed models (green: SAM, dark and light red: MM, two steps).

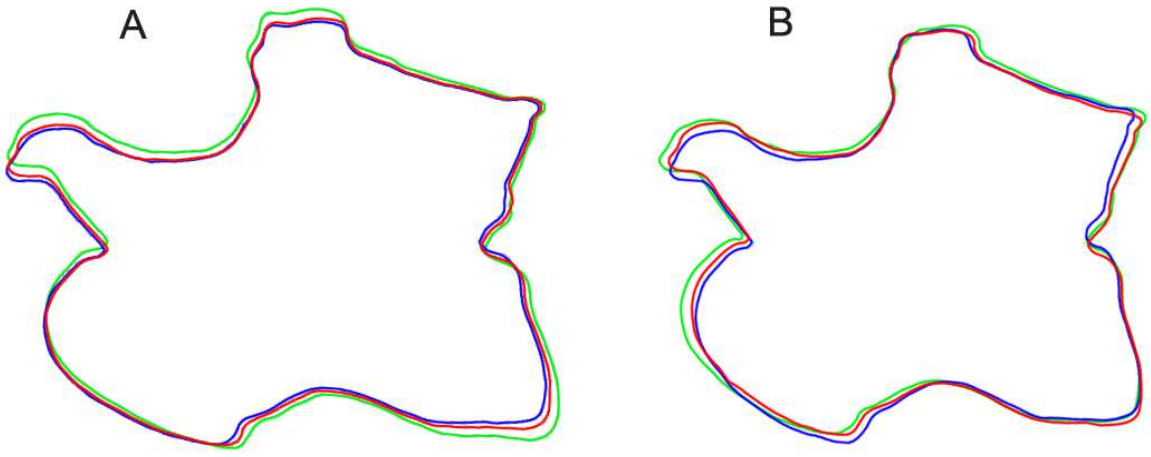

Figure 2.4: Outlines of different retrodeformed models of CV 12 of *Kaatedocus siberi* SMA 0004 obtained by using 4 (green), 9 (blue), or 16 (red) landmarks to define the midsagittal plane. A: results of the MM, B: results of the SAM.

In order to evaluate the applied retrodeformation tools, the same methods as above described were used on a manually deformed 3D model of a cervical vertebra of a Dodo (*Raphus cucullatus* Linnaeus, 1758; DNSM Ornithology 2366). The original model was generously provided by Aves 3D (www.aves3D.org) and the DNSM. In order to deform the model, two modifying tools in LightWave Modeler® were used, based on the deformation of the vertebrae of SMA 0004. Three different deformed models of the *Raphus cucullatus* vertebra were produced by applying shear, compression, as well as shear and compression combined (already implemented tools in the LightWave Modeler, compression can be introduced by using the stretch tool). For the combination of both, shearing was applied before compression. The amount of deformation was chosen trying to mimic the deformed diplodocid vertebrae.

Five ratios used to define numerical characters describing cervical vertebra shape in three different phylogenetic analyses (Upchurch et al., 2004b; Harris, 2006c; Whitlock, 2011a) were tested for their susceptibility to changes during taphonomic deformation and automated retrodeformation. The ratios of the original model of *Raphus cucullatus* were compared to the respective ratios obtained from both the deformed and retrodeformed models, in order to identify questionable characters. The trends recovered in the *Raphus cucullatus* test were compared to the trends seen in the diplodocid analysis, resulting in the identification of possibly inverted shape changes relative to the true, but in this case unknown, original form. Two characters were identified as questionable (H112, and H114, which is basically the same as W90; Tabs 2.1, 2.2). For both datasets (Harris, 2006c; Whitlock, 2011a), two phylogenetic analyses were performed with and without the questionable characters, using WinClada (version 1.00.08; www.cladistics.com), and the results, as well as the tree length, bootstrap values, consistency index, and retention index of the recovered strict consensus trees were compared (Tab. 2.3).

Table 2.1: Numerical characters used in phylogenetic analyzes, with the corresponding ratios of the original vertebrae of the *Kaatedocus siberi* SMA

Character	Borders as set in character	Vertebra	Original	Retrodeformed		Comparison with trends		Comments
				MM	SAM	MM	SAM	
H112	1,25	CV 3	1,29	1,59	1,38	=		SMA 0004 ambiguous, retrodeformation enhances ambiguity, but is questioned by Dodo analysis
		CV 4	1,08	1,16	1,05	=	≠	
		CV 5	1,10	1,04	0,95	≠		
H114 (=W90)	4 in Harris (2006c), Whitlock (2011a) leaves gap: 2.5-3, or 4+ as plesio- or apomorphic states, respectively	CV 6	4,13	3,38	3,20	=		Original ambiguous, retrodeformation shifts mid-cervicals into plesiomorphic state of H114, W90 only applicable with SAM models and original of CV 6, but SAM appears to give false trends according to Dodo analysis
		CV 7	3,66	3,81	2,81	≠	=	
		CV 8	3,31	3,02	2,68	=		
		CV 9	3,51	3,70	2,83	≠	=	
		CV 10	3,00	3,66	2,90	≠	=	
H115	1	CV 6	1,38	1,42	1,35	=	=	Retrodeformation generally strengthens assignment of SMA 0004 to apomorphic state, although this seems to be the wrong trend, according to Dodo analysis. However, deformation would have to be very strong for SMA 0004 to fall within plesiomorphic state
		CV 7	1,29	1,45	1,50	=	≠	
		CV 8	1,23	1,34	1,28	=	≠	
		CV 9	1,38	1,41	1,45	=	≠	
		CV 10	1,32	1,44	1,18	=	=	
H118 (=W87)	no explicit border in Harris (2006c), but described to be around 1; Whitlock (2011a) restricts character to anterior cervicals, but leaves gap: <1, or 1.5 as plesio-, or apomorphic states, respectively	CV 3	0,68	0,60	0,71	≠	=	Retrodeformation ambiguous in its trends in anterior and mid-cervicals, but shifts ratios of posterior cervicals towards upper end of plesiomorphic state of H118. However, this appears to be the wrong trend, according to the Dodo analysis. SMA 0004 can thus be safely scored as plesiomorphic
		CV 4	0,72	0,69	0,69	≠		
		CV 5	0,61	0,55	0,58	≠		
		CV 6	0,55	0,55	0,52	≠		
		CV 7	0,60	0,48	0,59	≠		
		CV 8	0,61	0,66	0,67	=		
		CV 9	0,67	0,59	0,66	≠		
		CV 10	0,60	0,52	0,55	≠		
		CV 11	0,67	0,73	0,78	=		
		CV 12	0,80	0,86	0,89	=		
		CV 13	0,84	0,89	0,96	=		
		CV 14	0,94	0,97	1,00	=		
U1	1,5	CV 3	0,48	0,61	0,62	≠		No changes, weak trend to wider vertebrae through retrodeformation (especially when applying the SAM), which appears to be right according the the Dodo analysis
		CV 4	0,62	0,61	0,66	=	≠	
		CV 5	0,65	0,70	0,69	≠		
		CV 6	0,64	0,78	0,70	≠		
		CV 7	0,61	0,61	0,62	≠		
		CV 8	0,76	0,75	0,82	=	≠	
		CV 9	0,68	0,71	0,75	≠		
		CV 10	0,69	0,74	0,83	≠		
		CV 11	0,62	0,62	0,69	≠		
		CV 12	0,62	0,70	0,71	≠		
		CV 13	0,73	0,77	0,79	≠		
		CV 14	0,74	0,68	0,70	=		

Trends recovered by retrodeformation are compared to the *Raphus cucullatus* test, green indicates probable real trends for SMA 0004. Abb.: H112, character 112 of Harris (2006c); U1, character 1 of Upchurch et al. (2004b); W87, character 87 of Whitlock (2011a).

Table 2.2: Numerical characters used in phylogenetic analyses, with the corresponding ratios of the original vertebra of *Raphus cucullatus*, the deformed models, the MM models, and the SAM models.

Character	Character definitions	Undeformed original	Deformed models		RD models		Difference from undeformed original (in percent)			Comments on character	RD trends		Comments on retrodeformation
					MM	SAM	deformed	MM	SAM		MM	SAM	
H112	Height/width posterior articular surface	0,61	C	**1,27**	1,30	1,28	210,20%	215,09%	211,25%	highly susceptible, should be deleted	↙↙	↙	increases transverse compression even more, both MM and SAM indicate trend if shear only
			S	0,84	0,75	**0,69**	139,25%	124,65%	114,11%		↗	↗↗	
			CS	**1,16**	1,18	1,18	190,85%	194,52%	195,19%		↙	↙	
H114 (=W90)	Centrum length/height of posterior articular surface	2,00	C	1,45	**1,63**	1,45	72,32%	81,25%	72,73%	susceptible, use with care	↗↗		bad performance if shear involved, MM indicates trend if compression only
			S	**2,09**	2,33	2,38	104,65%	116,67%	119,23%		↙	↙↙	
			CS	**1,44**	1,23	1,20	72,00%	61,32%	59,80%		↙	↙↙	
H115	Height neural arch/height of posterior articular surface	1,33	C	**1,36**	1,18	1,29	102,48%	88,91%	97,38%	relatively constant, can be used	↙↙	↙	generally wrong, inverted trends, but on a low error level
			S	**1,33**	1,31	1,34	100,00%	98,65%	101,25%		↙↙	↙	
			CS	1,42	1,43	**1,40**	107,35%	108,18%	105,90%		↙	↗↗	
H118 (=W87)	Total height/centrum length	1,47	C	1,76	**1,47**	1,75	119,57%	100,18%	119,06%	highly susceptible if CS, should be deleted in this case (or scored ?)	↗↗	↗	bad performance if shear involved, MM indicates trend if compression only
			S	**1,28**	1,16	1,23	86,93%	79,13%	83,40%		↙↙	↙	
			CS	**2,05**	2,22	2,37	139,52%	151,18%	160,92%		↙	↙↙	
U1	Total width/total height	1,31	C	0,87	**0,94**	0,91	66,17%	71,50%	68,96%	susceptible, use with care	↗↗	↗	bad performance if shear involved, MM indicates trend if compression only
			S	**1,38**	1,49	1,57	104,97%	113,84%	119,73%		↙	↙↙	
			CS	**0,97**	0,92	0,89	73,67%	69,89%	68,14%		↙	↙↙	

The closest fit with the original vertebra is marked with bold numbers. Differences between the deformed/retrodeformed models and the original are given in percent, with high deviations (>50%) marked in red, and low differences (<5%) in green. The similarity of the retrodeformed models with the original vertebra is given compared with the deviance of the deformed model (arrows pointing upwards indicate a closer fit between retrodeformed models and original vertebra, arrows pointing down show that the retrodeformation increased deformation even more; two arrows show higher (green) or lower (red) accuracy of the respective retrodeformation method compared with the other one). Abb.: H112, character 112 of Harris (2006c); RD, retrodeformation; U1, character 1 of Upchurch et al. (2004b); W87, character 87 of Whitlock (2011a).

Table 2.3: Support values of the performed phylogenetic analyses with and without the questionable characters (H112, H114 for Harris, 2006c; W90 for Whitlock, 2011a).

Phylogenetic analysis		Tree length	Number of MPTs	Consistency index	Retention index
Harris (2006c)	with	965	50	44	62
	without	899	6	47	66
Whitlock (2011a)	with	354	1	70	83
	without	350	1	71	83

Abb.: MPT, most parsimonious tree.

Results

Retrodeformation. Retrodeformed models obtained by application of the SAM are much more bilaterally symmetrical than both the original fossil and the MM-16 models. Landmarks are brought to almost the same horizontal and vertical level after applying SAM-16, whereas MM-16 usually yielded intermediate results between the original bones and the SAM-16 models (Figs 2.5-2.9). SAM-16 reconstructions are generally shorter, broader transversely, and at least as high as the original version. The direction of the induced shape changes (more gracile vs. more robust) by the MM appears to be more variable (Tab. 2.1): MM-16 of CV 10, for example, produced a more slender reconstruction compared to the original element (Fig. 2.5). Condyle and cotyle outlines get more rounded with both methods (Figs 2.5-2.9).

Whereas a second iteration of SAM did not affect the results, shape changes considerably between MM-16 and 2xMM models. With 2xMM, symmetry was slightly more restored, although still not to the degree as in the SAM-16 models. Unexpectedly, in the case of CV 12, where the first step yielded a more robust model, the 2xMM model inverted this trend, producing a reconstruction even more slender than the original fossil (Fig. 2.3).

Using different numbers of defining landmarks showed very few differences between the obtained models when applying the SAM. On the other hand, MM-9 and MM-16 models are much more similar to each other than to the MM-4 models. They are shorter and more slender than MM-4 models, which are relatively robust with a pronounced posteroventral corner of the vertebral centrum, and an elevated neural spine summit (Fig. 2.4).

The retrodeformed models of *Raphus cucullatus* generally compared very badly with the original bone. Whereas overall symmetry was restored to a large degree during the retrodeformation process, the same cannot be said for the proportions (Figs 2.10-2.12; Tab. 2.2). The only retrodeformed model that matched the original state more than the respective deformed model, was MM-16 applied to the transversely compressed vertebra – mainly due to the disproportionately elongated posteroventral edge of the centrum (Tab. 2.2). Both methods thus appear very weak in coping with shear, which is the most evident deformation present in *Kaatedocus* SMA 0004.

Analyzing the implied shape changes, it becomes evident that the more dimensions are involved in measuring the dimensions, the more these ratios are prone to deformation (Tab. 2.2). Height of the neural arch to height of the posterior articular surface of the centrum (character H115), for example, can be measured on one single line, and the majority of the changes introduced by deformation and retrodeformation are below five percent. On the other hand, height to width of the posterior articular surface (character H112), has to be measured in a plane, and shape changes considerably.

Comparing the recovered trends from the *Raphus cucullatus* test with the trends obtained by retrodeforming the *Kaatedocus* vertebrae, reveals that they are inverted in many cases (Tab. 2.1). As the deformation introduced to the *Raphus cucullatus* model was chosen to mimic taphonomic distortion of the SMA 0004 elements, a comparison of the recovered trends allows validation of the retrodeformation of the diplodocid vertebrae. Given this, it appears that depending on the ratios, both SAM-16 and MM-16 can recover real trends, but the true dimensions still remain impossible to determine. Based on these comparisons, the following characters were identified as questionable: H112, because of a very high susceptibility to deformation, and ambiguity in the trends of retrodeformation; and H114 (or W90), due to relatively bad results in the test, and false trends and/or intermediate, inapplicable ratios of the retrodeformed models of SMA 0004 (Tabs 2.1, 2.2).

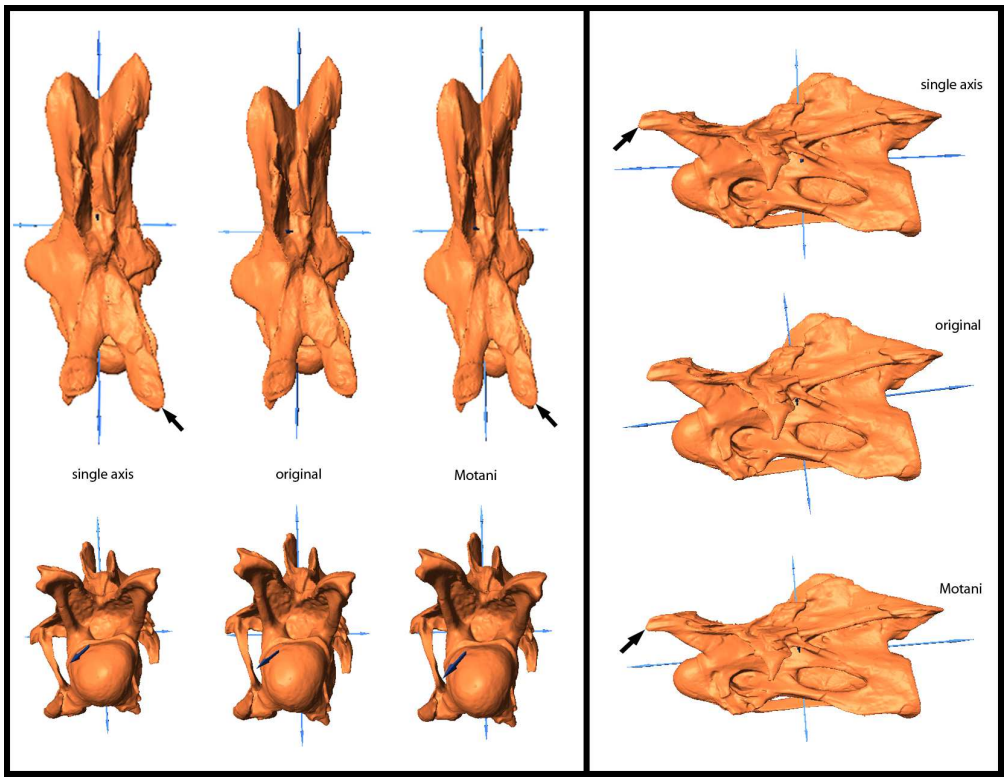

Figure 2.5: Original and retrodeformed models of CV 10 of *Kaatedocus siberi* SMA 0004 in dorsal (top left), anterior (bottom left), and lateral view (right). Note the elongation of the prezygapophysis in the retrodeformed models (arrow) and the slenderness of the model produced by the MM. Vertebrae not to scale

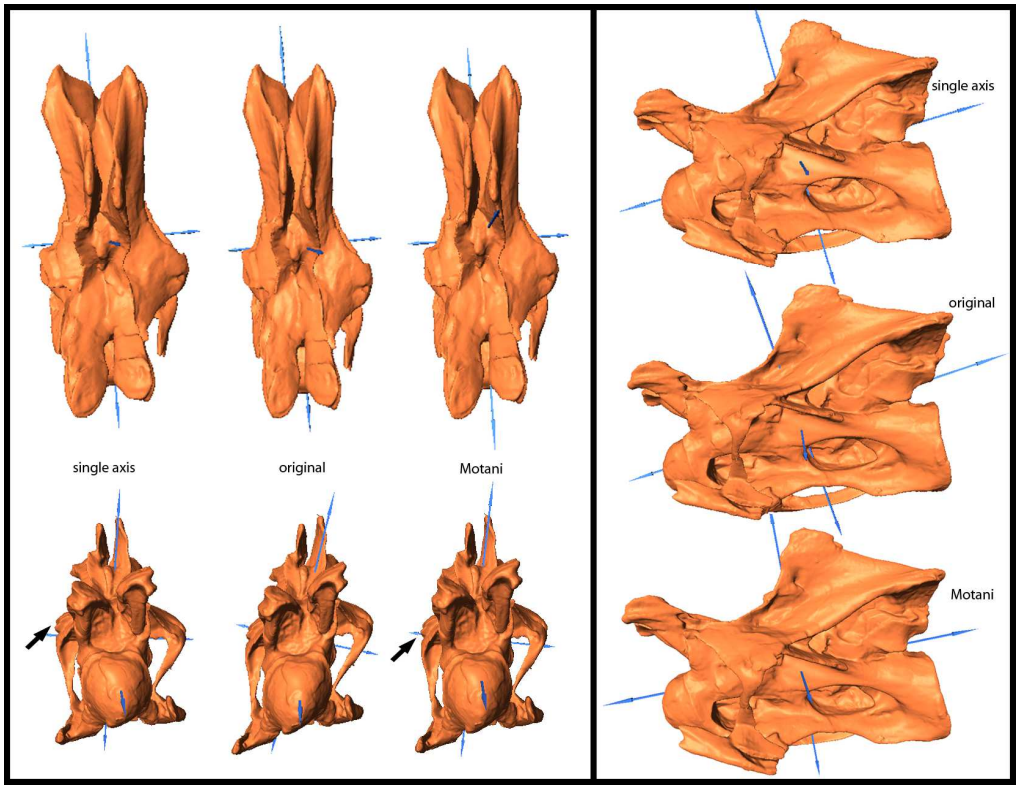

Figure 2.6: Original and retrodeformed models of CV 11 of *Kaatedocus siberi* SMA 0004 in dorsal (top left), anterior (bottom left), and lateral view (right). Note the leveling of the transverse processes in the retrodeformed models (arrows). Vertebrae not to scale.

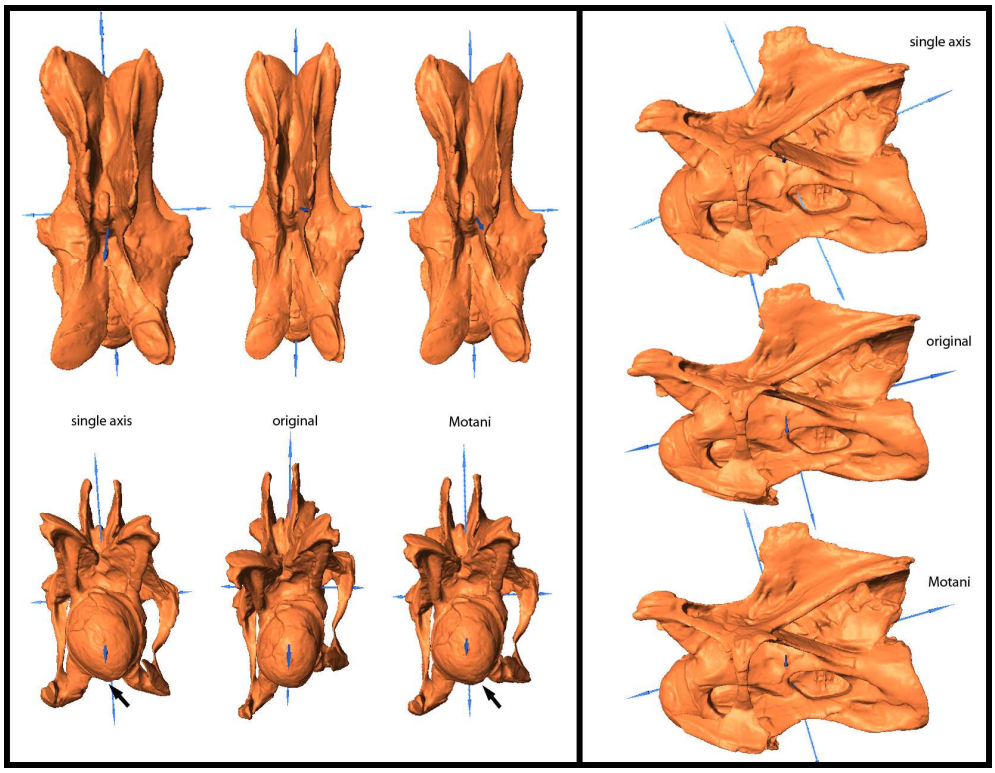

Figure 2.7: Original and retrodeformed models of CV 12 of *Kaatedocus siberi* SMA 0004 in dorsal (top left), anterior (bottom left), and lateral view (right). Note the more rounded condyles (arrows) and the pronounced robustness of the model produced by the SAM. Vertebrae not to scale.

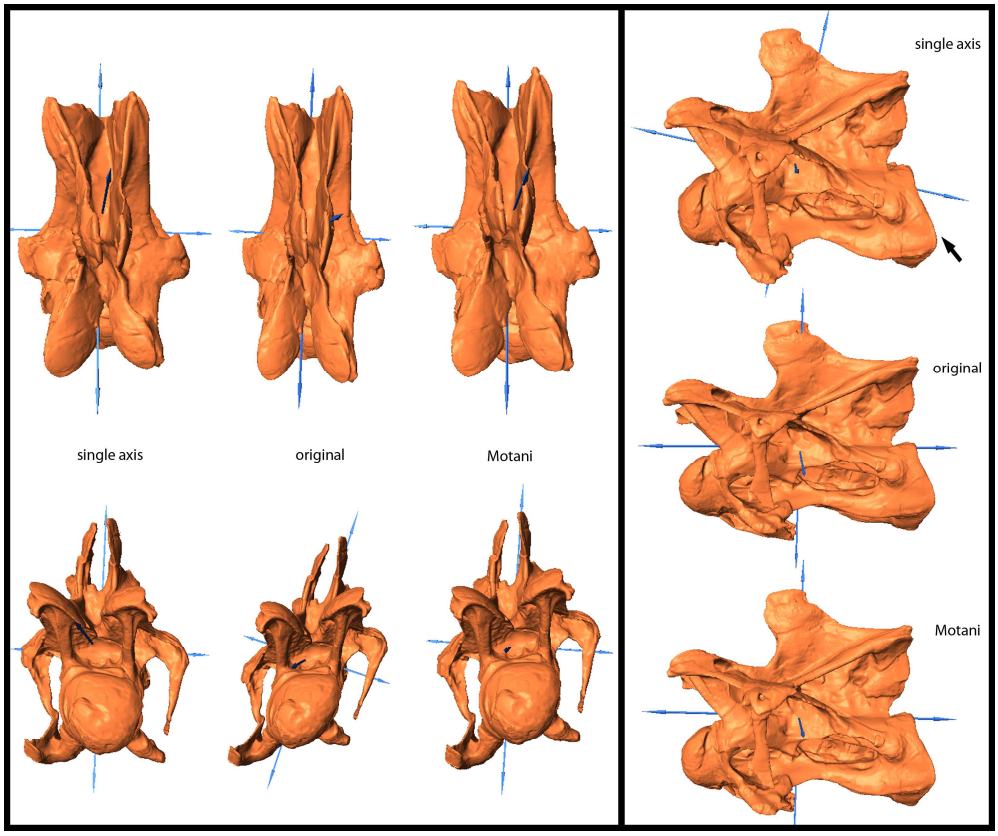

Figure 2.8: Original and retrodeformed models of CV 13 of *Kaatedocus siberi* SMA 0004 in dorsal (top left), anterior (bottom left), and lateral view (right). Note the more pronounced posteroventral corner in the SAM (arrow). Vertebrae not to scale.

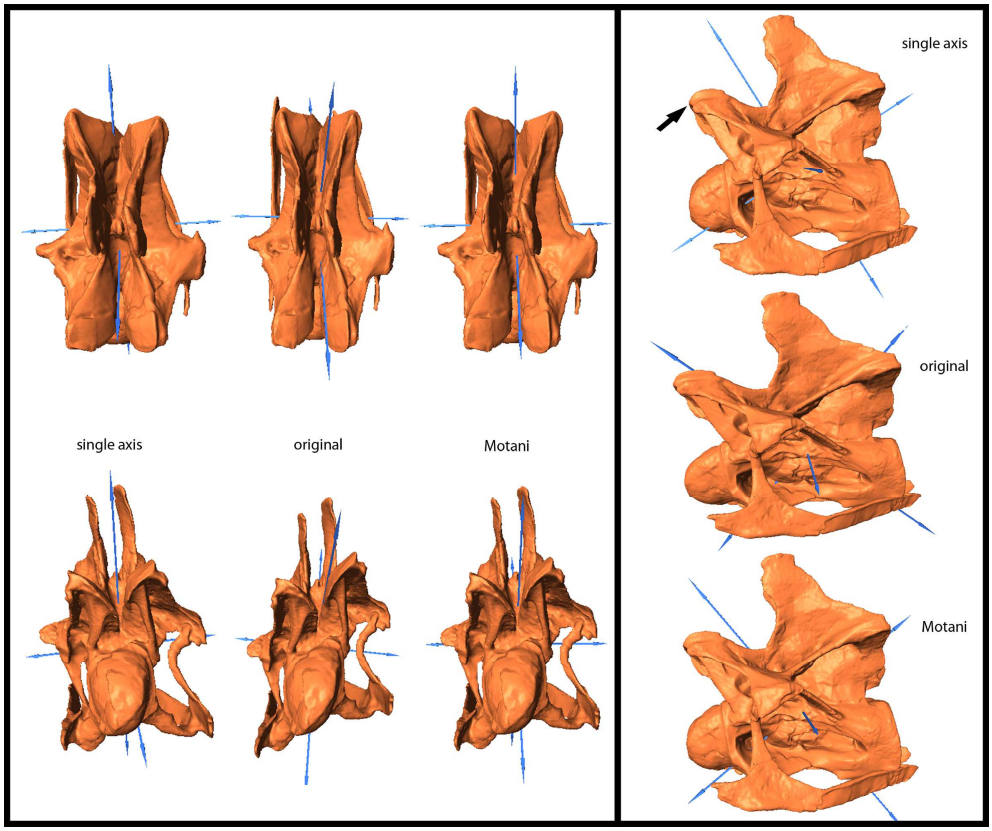

Figure 2.9: Original and retrodeformed models of CV 14 of *Kaatedocus siberi* SMA 0004 in dorsal (top left), anterior (bottom left), and lateral view (right). Note the retraction of the prezygapophyses in the retrodeformed models (arrows) and the robustness of the model produced by the SAM. Vertebrae not to scale.

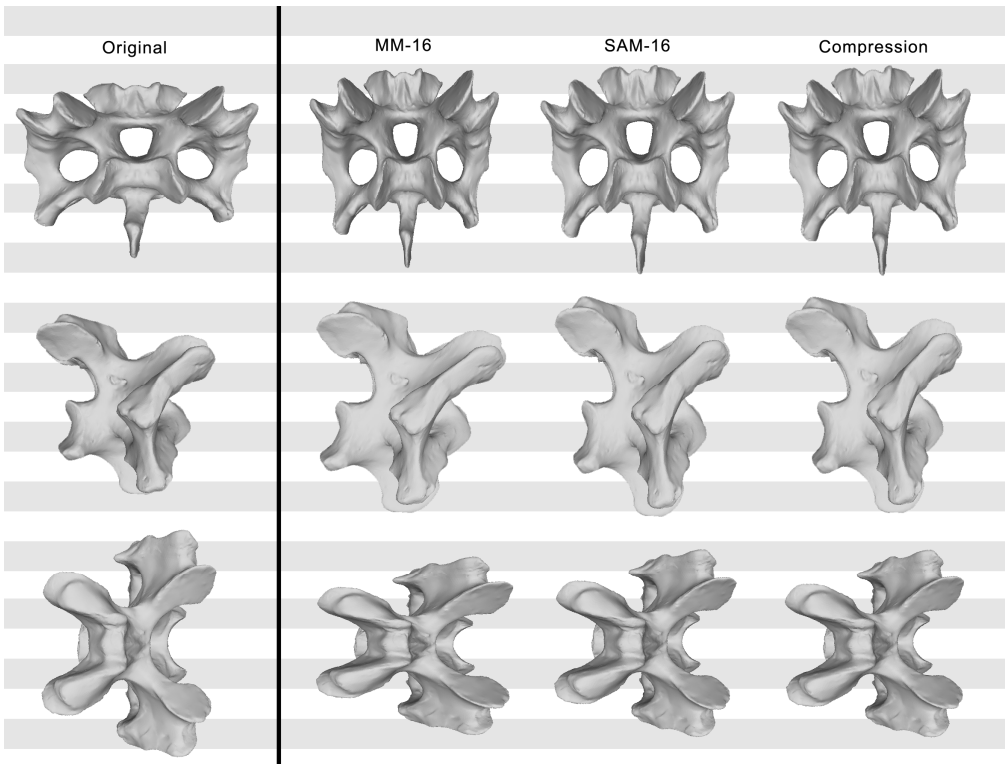

Figure 2.10: Original, deformed (using compression), and retrodeformed models of a cervical vertebra of *Raphus cucullatus* (DNSM Ornithology 2366) in anterior (top), right lateral (center), and dorsal (bottom) view. Note the transversely more compressed retrodeformed models compared to the deformed model.

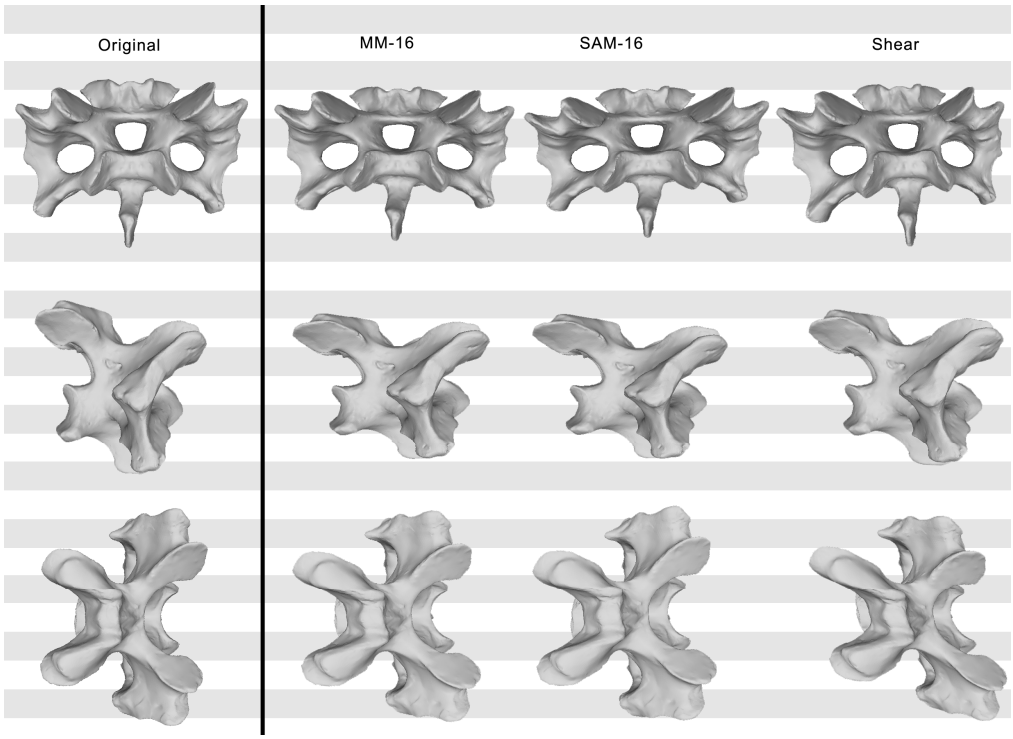

Figure 2.11: Original, deformed (using shear), and retrodeformed models of a cervical vertebra of *Raphus cucullatus* (DNSM Ornithology 2366) in anterior (top), right lateral (center), and dorsal (bottom) view. Note the dorsoventrally more compressed retrodeformed models compared to the deformed model.

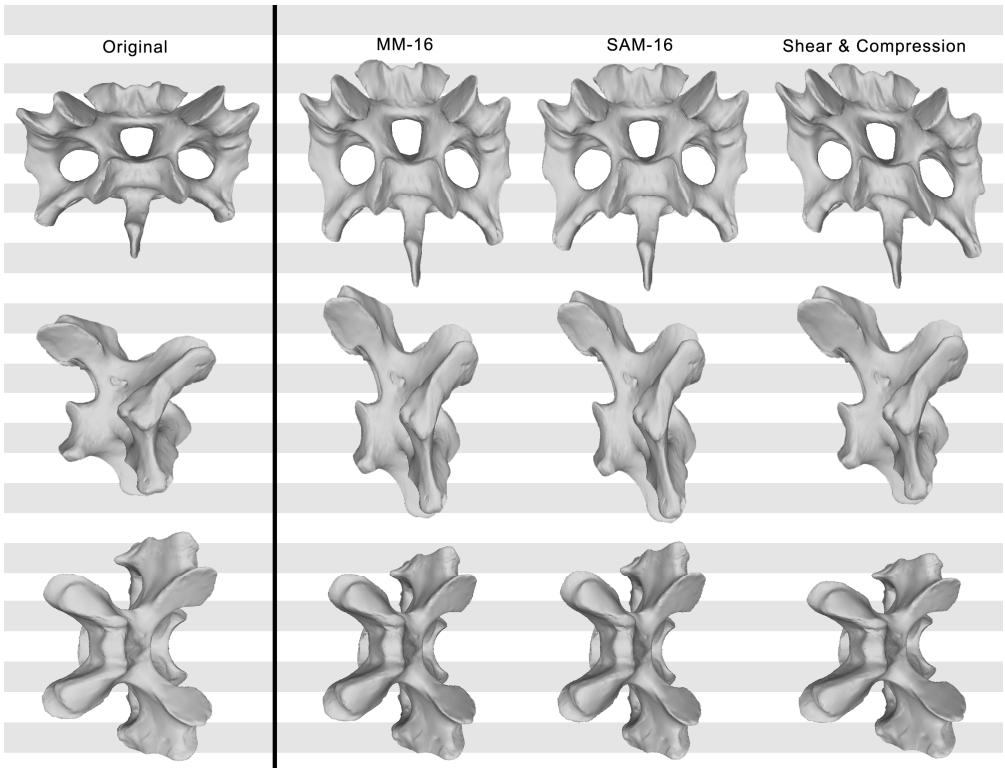

Figure 2.12: Original, deformed (compression and shear combined), and retrodeformed models of a cervical vertebra of *Raphus cucullatus* (DNSM Ornithology 2366) in anterior (top), right lateral (center), and dorsal (bottom) view. Note the dorsoventrally higher, and anteroposteriorly shorter retrodeformed models compared to the deformed model.

Phylogeny. Phylogenetic analyses usually contain a mix of qualitative and quantitative characters. As retrodeformation and thus deformation sometimes considerably change dimensions, especially scores for numerical characters can be affected. The two analyses performed with each the Harris (2006c) and the Whitlock (2011a) matrices, in- and excluding the questionable characters, yielded slightly varying tree topologies (Figs 2.13, 2.14). Using Harris (2006c) without the questionable characters, resolution of the tree increases, tree length of the strict consensus tree decreases considerably, and consistency and retention indexes are slightly higher. Bootstrap values are higher for high-level taxa like Neosauropoda, Titanosauriformes, and Diplodocoidea, whereas lower level taxa have lower support when excluding the questionable characters (Fig. 2.13, Tab. 2.3). Performing the analysis of Whitlock (2011a), the differences are smaller, but the same trends are observable: a shorter tree, higher consistency index (Tab. 2.3), as well as generally higher bootstrap values for high-level taxa (in this case: *Jobaria* + Neosauropoda, Flagellicaudata, Dicraeosauridae, and Diplodocidae; Fig. 2.14). The diplodocine intrarelationships are different in the two analyses based on Whitlock (2011a), but bootstrap values are less than 50% in both recovered trees, indicating that more thorough taxonomic research is needed within this clade.

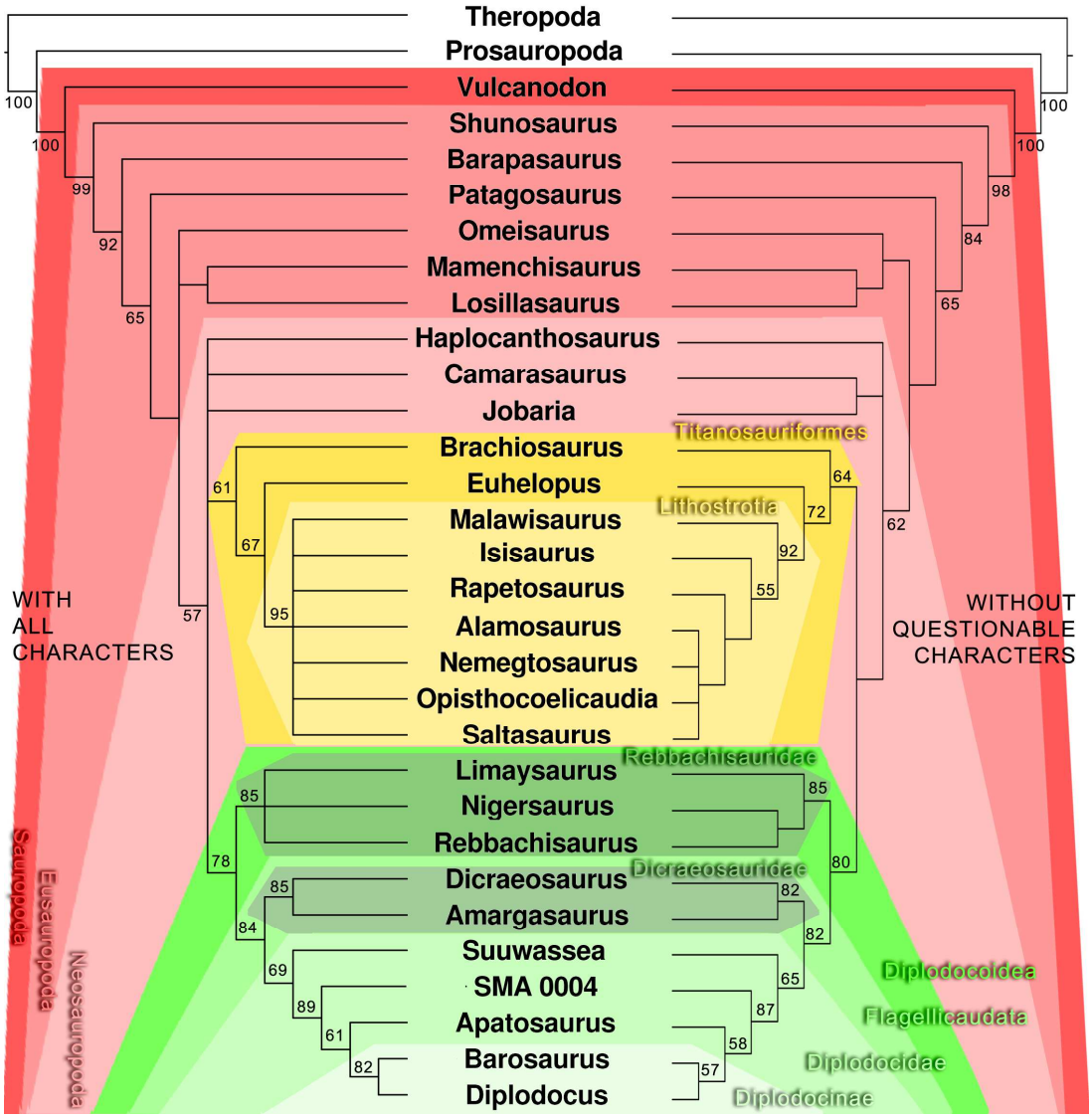

Figure 2.13: Phylogenetic trees (based on Harris, 2006c) recovered with (left) and without (right) the questionable characters (H112 and H114). Bootstrap values indicated if > 50. Note the better resolved tree without the questionable characters. Bootstrap values in the right tree are higher for high-level, but lower for low-level taxa.

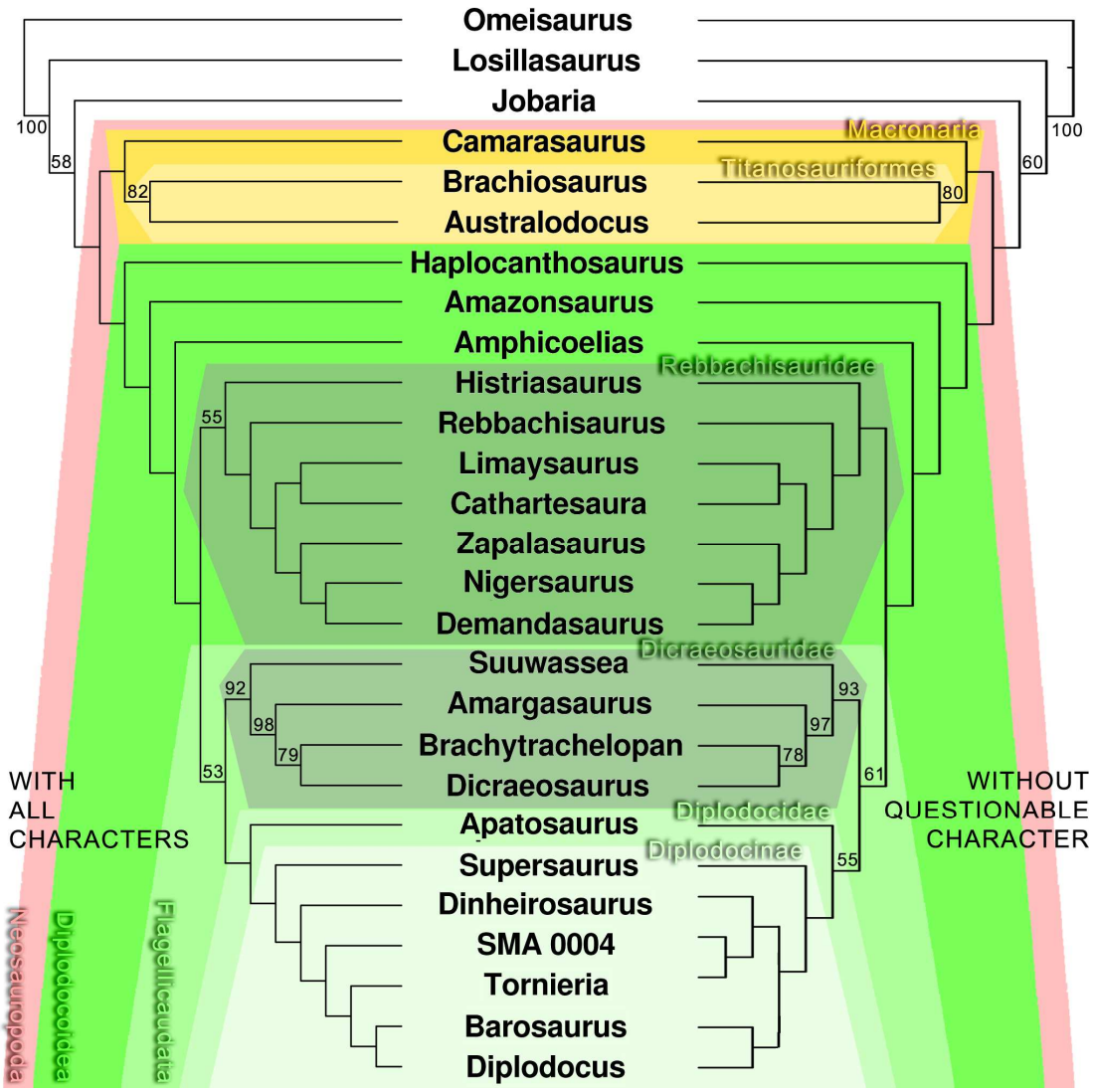

Figure 2.14: Phylogenetic trees (based on Whitlock, 2011a) recovered with (left) and without (right) the questionable character (W90). Bootstrap values indicated if > 50. Note the differences in diplodocine intrarelationships. Bootstrap values in the right tree are higher for high-level, but lower for low-level taxa.

Discussion

Retrodeformation. One of the basic problems of the reconstruction of deformed fossils is the fact that the original undeformed shape of the elements is unknown. Therefore, any retrodeformation technique has to rely on certain assumptions. The vast majority of these methods (including SAM and MM) assume that the objects under study are bilaterally symmetrical. Problematic issues concerning retrodeformation thus include asymmetrical elements or symmetrical deformation like compression. Partly due to this, automated retrodeformation sometimes even yields models that are less similar to the original shape than the deformed elements, as shown by Angielczyk and Sheets (2007) and the *Raphus cucullatus* test in this study.

The methods employed here require at least four pairs of bilaterally symmetric landmarks for the calculation of the midsagittal plane. However, the calculated plane, on which the retrodeformation is based, often does not pass through landmarks like the median tuberosity in the middle of the bifurcate neural spines (Fig. 2.15). The number of constraining points in the methods included into Landmark™, and thereby also the quality of the retrodeformation process, could be considerably augmented by including single landmarks on the sagittal plane, as implemented in the method of Ogihara et al. (2006).

Our results obtained by defining a varying number of landmark pairs do not confirm that the

more landmarks you define to constrain the plane of symmetry, the more accurate the outcome (Motani et al., 2005; Ogihara et al., 2006; Gunz et al., 2009). In fact, where differences are visible (using MM), models obtained by MM-9 and MM-16 are more slender, and tightly reproduce the false trends recovered by the *Raphus cucullatus* test. The method in itself thus appears to be more thorough and consistent when using more landmark pairs, but one has to pay attention to not take this as indication for higher accuracy of the retrodeformation. The fact that a second application of the MM to an already retrodeformed object often changes its shape in almost opposing directions sheds additional doubts on the validity of the MM. In order to verify this accuracy, a test of the method has to be performed with manually deformed, morphologically similar elements, mimicking as closely as possible the taphonomy of the study objects.

Unexpectedly, the trends recovered by the diplodocid case study, and the *Raphus cucullatus* test are often opposite to each other (Tabs 2.1, 2.2). This is surprising, especially since bird vertebrae are the most similar in morphology you can get to sauropod vertebrae within extant animals, and also because digital deformation of the *Raphus cucullatus* vertebra was designed to mimic as closely as possible the taphonomic processes that affected SMA 0004. Two possible explanations are imaginable: first, it is conceivable that different algorithms in automated retrodeformation tools yield differing, but still bilaterally symmetrical models. However, applying the methods with the same default settings to all elements under study, it would be odd if they would produce opposite trends. Second, it could be that the varying trends are due to the additional brittle deformation in SMA 0004, which was not attempted to reproduce in the manually deformed *Raphus cucullatus* vertebra. In order to cope with brittle deformation, previous researchers disassembled and retrodeformed single parts independently, before applying automated retrodeformation tools to the reassembled object. To our knowledge, this was only done with hominoid skulls (e.g., Zollikofer et al., 1998, 2005; Ponce de León and Zollikofer, 1999; Ogihara et al., 2006; Gunz et al., 2009), which are often the only elements recovered from the entire skeleton. Whereas such complex and time-consuming reconstructions are justifiable in such cases, they are hardly appropriate for large numbers of elements as the 15 cervical vertebrae in diplodocid sauropod necks as considered here. However, since methodological errors can most probably be excluded as reasons for the differing trends, retrodeformation can be used to test the validity of length ratios, and thus the usefulness of morphological characters used in phylogenetic analyses.

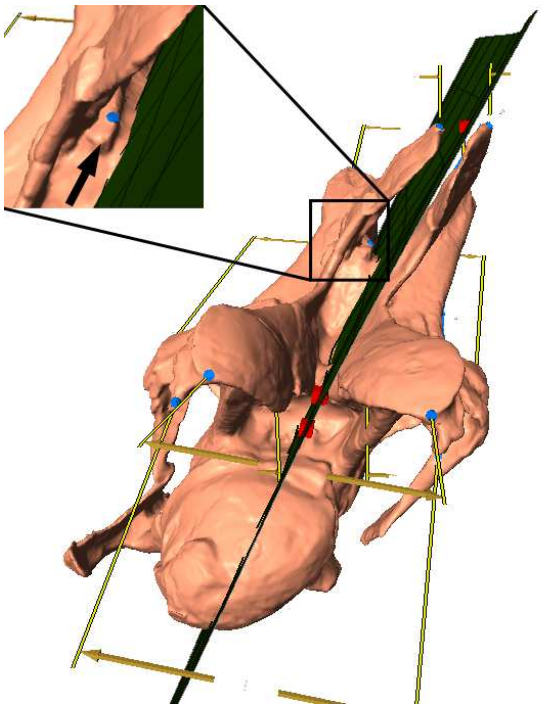

Figure 2.15: Calculated midsagittal plane on original model of CV 13 of *Kaatedocus siberi* SMA 0004 in oblique anterodorsal view. The used symmetrical pairs of landmarks are indicated in yellow and blue, the midsagittal plane in green. Note the medial tuberosity (arrow in close-up), which is supposed to lie on the midsagittal plane, but the methods used herein do not allow to include single points.

Phylogeny. The increased resolution and support values of the recovered phylogenetic trees, when excluding the questionable characters, imply that deformation negatively affects the accuracy of phylogenetic analyses. However, the fact that bootstrap values for lower-level taxa appear to decrease considerably in some cases (e.g., Diplodocinae, Figs 2.13, 2.14), indicates that these questionable characters might still be phylogenetically informative at lower taxonomical levels. The question then rises if it would not be possible to circumvent the exclusion of these characters. One possibility would be to apply the same methods as proposed here, including the *Raphus cucullatus* test, for all the taxa included in the phylogenetic analysis. By doing so, deformation of the vertebrae could be assessed taxon by taxon. To date, however, only very few sauropod bones are available as 3D models. Therefore, taxa for which no retrodeformation data is available would have to be scored as unknown for this character. In some cases this might result in characters scored for only one or two taxa, such that no additional phylogenetic value would be generated. Nonetheless, this will be a promising approach for the future. In the case of character H114 (or W90), a different approach was chosen by Tschopp and Mateus (2012b). H114 describes the elongation of the vertebral centra. Their definitions of the states vary in the two analyses: Harris (2006c) defines the states as "<4.0 (0); ≥ 4.0 (1)", and Whitlock (2011a) as "2.5–3 (0); 4 + (1)". In the case of SMA 0004, both of these definitions appear to be problematic, because both the original elements as well as the MM-16 models fall between the borders as set by Whitlock (2011a) to distinguish diplodocine taxa from e.g., *Apatosaurus*. Since the *Raphus cucullatus* test indicates that MM-16 produced a reasonable model in this case (Tab. 2.1), the intermediate state of SMA 0004 between the short cervical vertebrae of *Apatosaurus* and the very elongated ones of the more derived diplodocines *Diplodocus*, *Barosaurus*, or *Tornieria*, appears taxonomically significant. Thus, if one would use Harris' (2006c) definition, this intermediate state, would not be resolved. Tschopp and Mateus (2012b) therefore added an intermediate state to Whitlock's (2011a) definition: ≤3 (0); 3.1-3.9 (1); ≥4 (2). This shows that retrodeformation – if tested simultaneously with extant material – can serve as a tool to validate phylogenetic characters, and modify them accordingly.

Conclusions

Although many different approaches were made to reconstruct deformed fossils automatically, many of them only consider two dimensions. When applying retrodeformation to 3D objects, it gets obvious that shape can change considerably in all dimensions, affecting also ratios used for phylogenetic characters. Testing the used retrodeformation methods with manually deformed, morphologically similar elements, allows validation of trends recovered for the fossils under study, and helps to identify phylogenetic characters that are highly susceptible to deformation. In this case study, deletion of such questionable characters lead to better resolved trees with generally higher support values, which confirms the usefulness of retrodeformation as tool for testing the validity of phylogenetic characters.

The skull and neck of a new flagellicaudatan sauropod from the Morrison Formation and its implication for the evolution and ontogeny of diplodocid dinosaurs

published in the Journal of Systematic Palaeontology:
Tschopp, E., and O. Mateus. 2012b. The skull and neck of a new flagellicaudatan sauropod from the Morrison Formation and its implication for the evolution and ontogeny of diplodocid dinosaurs. Journal of Systematic Palaeontology 1–36.

Abstract

A new taxon of diplodocid sauropod, *Kaatedocus siberi* gen. et sp. nov., is recognized based on well-preserved cervical vertebrae and skull from the Morrison Formation (Kimmeridgian, Late Jurassic) of northern Wyoming, USA. A phylogenetic analysis places it inside Diplodocinae (Sauropoda: Flagellicaudata: Diplodocidae), as a sister taxon to a clade uniting *Tornieria africana* and the classical diplodocines *Barosaurus lentus* and *Diplodocus*. The taxon is diagnosed by a unique combination of plesiomorphic and derived traits, as well as the following unambiguous autapomorphies within Diplodocidae: frontals separated anteriorly by a U-shaped notch; squamosals restricted to the post-orbital region; presence of a postparietal foramen; a narrow, sharp and distinct sagittal nuchal crest; the paired basal tuber with a straight anterior edge in ventral view; anterior end of the prezygapophyses of mid- and posterior cervical vertebrae is often an anterior extension of the pre-epipophysis, which projects considerably anterior to the articular facet; anterodorsal corner of the lateral side of the posterior cervical vertebrae marked by a rugose tuberosity; posterior margin of the prezygapophyseal articular facet of posterior cervical vertebrae bordered posteriorly by conspicuous transverse sulcus; posterior cervical neural spines parallel to converging. The inclusion of *K. siberi* and several newly described characters into a previously published phylogenetic analysis recovers the new taxon as basal diplodocine, which concurs well with the low stratigraphical position of the holotype specimen. *Dinheirosaurus* and *Supersaurus* now represent the sister clade to *Apatosaurus* and Diplodocinae and therefore the most basal diplodocid genera. The geographical location in the less known northern parts of the Morrison Fm., where *K. siberi* was found, corroborates previous hypotheses on faunal provinces within the formation. The probable subadult ontogenetic stage of the holotype specimen allows analysis of ontogenetic changes and their influence on diplodocid phylogeny.

Introduction

Diplodocids were most abundant and diverse during the Late Jurassic. Many specimens have been found in the USA, Portugal, Tanzania and possibly Asia (McIntosh, 1990b; Upchurch et al., 2004a; Upchurch and Mannion, 2009; Whitlock, 2011a; Mannion et al., 2012). The taxa of Late Jurassic Diplodocidae usually considered valid are: *Apatosaurus ajax* Marsh, 1877a (type species), *A. excelsus* (Marsh, 1879), *A. louisae* Holland, 1915, *A. parvus* Peterson and Gilmore, 1902), *Barosaurus lentus* Marsh, 1890, *Dinheirosaurus lourinhanensis* Bonaparte and Mateus, 1999, *Diplodocus longus* Marsh, 1878 (type species), *Diplodocus carnegii* Hatcher, 1901, *Diplodocus hayi* Holland, 1924, *Diplodocus hallorum* (Gillette, 1991), *Supersaurus vivianae* Jensen, 1985, *Tornieria africana* (Fraas, 1908), and probably *Dyslocosaurus polyonychius* McIntosh et al., 1992 (McIntosh, 1990b; Upchurch et al., 2004a, 2004b; Lucas et al., 2006). Most of these come from the Morrison Formation of southern Wyoming, Colorado or Utah, and only few skeletons are known from other parts of the world, even from northern Wyoming or Montana. The American Museum of Natural History, New York (AMNH) conducted one of their most productive field seasons in the Morrison Formation in north central Wyoming (Brown, 1935). According to Brown (1935), more than 3000 bones of primarily diplodocids were recovered from the Howe Quarry near Shell, Wyoming, but none of the specimens have since been properly described, and many of them were lost subsequently during a fire at the AMNH (Michelis, 2004). The site was later abandoned and only reopened in 1990 by a team of the Sauriermuseum Aathal, Switzerland (Ayer, 2000; Christiansen and Tschopp, 2010). Among the several dozens of bones excavated in 1990 and 1991 was a well-preserved and partly articulated neck and

associated skull bones including both braincase and rostral elements (Fig. 3.1; Ayer, 2000; Michelis, 2004). As the specimen (SMA 0004, nick-named 'HQ 2') is relatively small, it was usually considered to be a juvenile *Diplodocus* (Ayer, 2000), or *Barosaurus* (Michelis, 2004). The present, detailed study of the morphology of SMA 0004 revealed that it can be clearly distinguished from both of these classical Late Jurassic diplodocines. The new taxon thereby increases both the taxonomic and morphological diversity in the Morrison Formation.

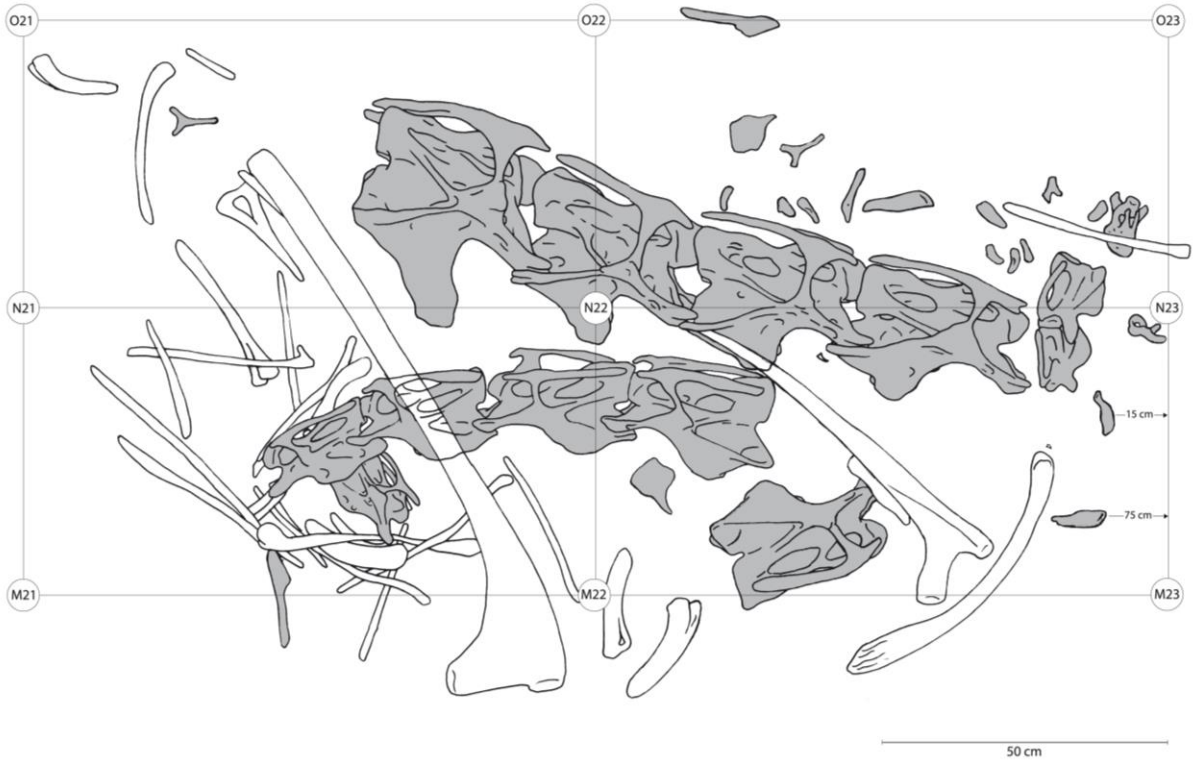

Figure 3.1: Quarry map of the holotype of *Kaatedocus siberi*, SMA 0004. Gray elements represent cervical vertebrae and disarticulated skull elements. Two of the latter were found 15 and 75 cm to the right of this grid (see arrows on the lower right side). SMA 0004 was associated with dorsal ribs, an interclavicle, sternal ribs and chevrons of maybe another individual. Drawing by Esther Premru. Scale bar = 50 cm.

Geological Setting

The geological members of the Morrison Formation, as identified further south, are difficult to recognize in northern Wyoming. The only layer that has been used for stratigraphical correlation between the Howe Quarry and the various quarries in southern Wyoming, Colorado, Utah, South Dakota, Oklahoma and New Mexico is a clay change that was interpreted to divide the Morrison Formation into lower and upper parts (Turner and Peterson, 1999; but see Trujillo, 2006 for critiques). Such a clay change is present approximately 20 m above the Howe Quarry (Fig. 3.2). If Turner and Peterson (1999) prove to be right in interpreting this geological marker as useful for long distance correlation of the sites in the Morrison Formation, the Howe Quarry would be among the stratigraphically oldest fossil sites of the entire Morrison Formation (Turner and Peterson, 1999; J. Ayer pers. comm. 2005). However, several authors propose a higher stratigraphical position for the Howe Quarry (Dodson et al., 1980; Swierc and Johnson, 1996; Wilborn, 2008). Swierc and Johnson (1996) dated the Howe Quarry as being 145.7 Ma, but this date groups all of the sites on the Howe Ranch together and does not take into account that the different quarries are situated at varying stratigraphical levels (see Fig.1.2). Kvale et al. (2001) interpreted a second site approximately 10 m higher in stratigraphy (Howe-Stephens Quarry, see Schwarz et al., 2007c; Christiansen and Tschopp, 2010) as being of 147 Ma in age. This implies a latest Kimmeridgian to earliest Tithonian age for the Howe Quarry. Due to the fact that SMA 0004 is the first specimen of the Howe Quarry to be properly described and identified, previous synopses of the faunal assemblage of the site have to be regarded as provisional. An updated list of reported dinosaurs includes the sauropods *Camarasaurus*, *Apatosaurus*,

Kaatedocus and possibly *Diplodocus* and *Barosaurus* (if they do not prove to be *Kaatedocus* as well), the theropods *Allosaurus* and a smaller taxon (represented by footprints and shed teeth), and the ornithopod *Camptosaurus* (Brown, 1935; Foster, 1998; Michelis, 2004). Non-dinosaurian remains include carbonized wood fragments and a dental plate of the dipnoid fish *Ceratodus robustus* (Foster, 1998; Michelis, 2004).

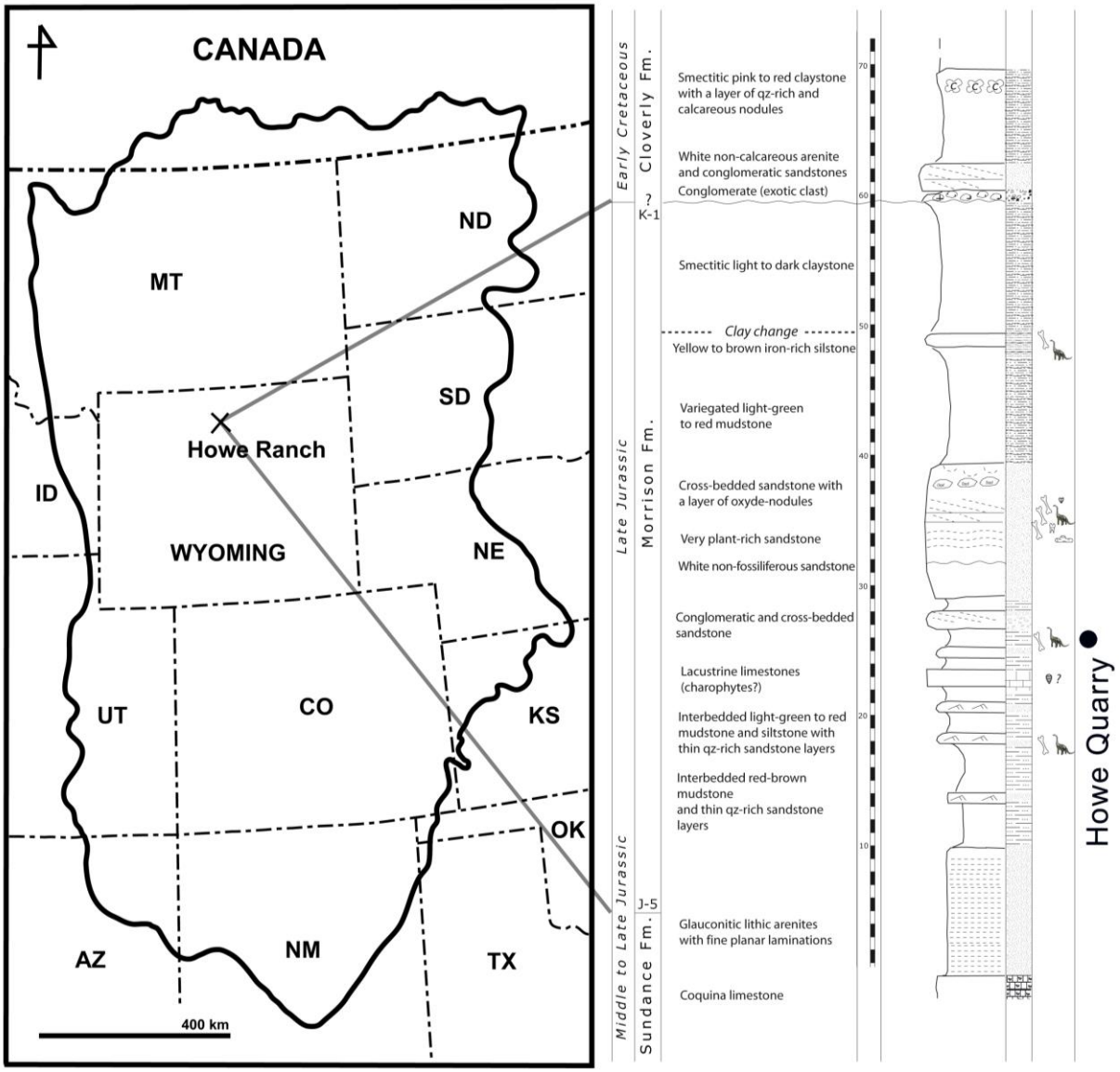

Figure 3.2: Geographical and geological setting of the Howe Quarry within the Upper Jurassic Morrison Formation. The Howe Quarry is located in North Central Wyoming, and stratigraphically well below the clay change. Modified from Schwarz *et al.* (2007c).

Systematic paleontology

Dinosauria Owen, 1842
Sauropoda Marsh, 1878
Eusauropoda Upchurch, 1995
Neosauropoda Bonaparte, 1986
Diplodocoidea Marsh, 1884 (see Upchurch, 1995)
Flagellicaudata Harris and Dodson, 2004
Diplodocidae Marsh, 1884
Kaatedocus gen. nov.
Type species. *Kaatedocus siberi* sp. nov.

Diagnosis. See diagnosis for type and only species below.

Kaatedocus siberi gen. et sp. nov.
(Figs 3.3-3.23)

Diagnosis. Diplodocid sauropod with the following features not found in other sauropods: U-shaped notch separating the frontals anteriorly (Fig. 3.5); a rugose tuberosity that marks the anterodorsal corner of the lateral surface of the posterior cervical vertebrae (Fig. 3.19); posterior margin of the prezygapophyseal articular facet of posterior cervical vertebrae bordered posteriorly by a conspicuous transverse sulcus, separating the facet from the prezygapophyseal process (Fig. 3.19).

The following features are unique to *Kaatedocus* among Flagellicaudata or more inclusive clades: squamosals are restricted to the post-orbital region (unique for Diplodocoidea; Fig. 3.3); a straight anterior margin of the paired basal tuber in ventral view; anterior end of the prezygapophyses in mid- and posterior cervical vertebrae is formed by an accessory ventral process of the pre-epipophysis, that projects considerably anterior to the prezygapophyseal articular facet (Fig. 3.13).

The following features are unique to *Kaatedocus* among Diplodocidae: postparietal foramen present (Fig. 3.6); narrow, sharp and distinct sagittal nuchal crest on the supraoccipital (Figs 3.5, 3.6); and the narrowly diverging to subparallel posterior cervical neural spines (Fig. 3.19).

Furthermore, the new taxon can be distinguished from adult *Apatosaurus* and *Diplodocus* by its closed or very reduced preantorbital fenestra (Fig. 3.4); the dorsal portion of lateral edge of the lacrimal that bears a dorsoventrally short laterally projecting spur (Fig. 3.6); the relatively rounded snout (Fig. 3.5); a second small fossa in the quadrate, medially at the base of the pterygoid ramus; and the ratio of length/maximum basal diameter of the basipterygoid processes being less than four. In contrast to *Apatosaurus*, *Kaatedocus* exhibits spinoprezygapophyseal laminae that are reduced to a ridge, or totally interrupted at the base of the prezygapophysis of anterior and mid-cervical vertebrae (Figs 3.9, 3.13). *Kaatedocus* is different from *Diplodocus* due to the presence of at least 12 maxillary and dentary teeth that are not restricted to the anterior-most part of the jaw (Fig. 3.3). It can be distinguished from *Diplodocus*, *Tornieria* and *Barosaurus* due to its relatively short mid-cervical centra (Elongation Index (EI) = centrum length/height of posterior cotyle < 4).

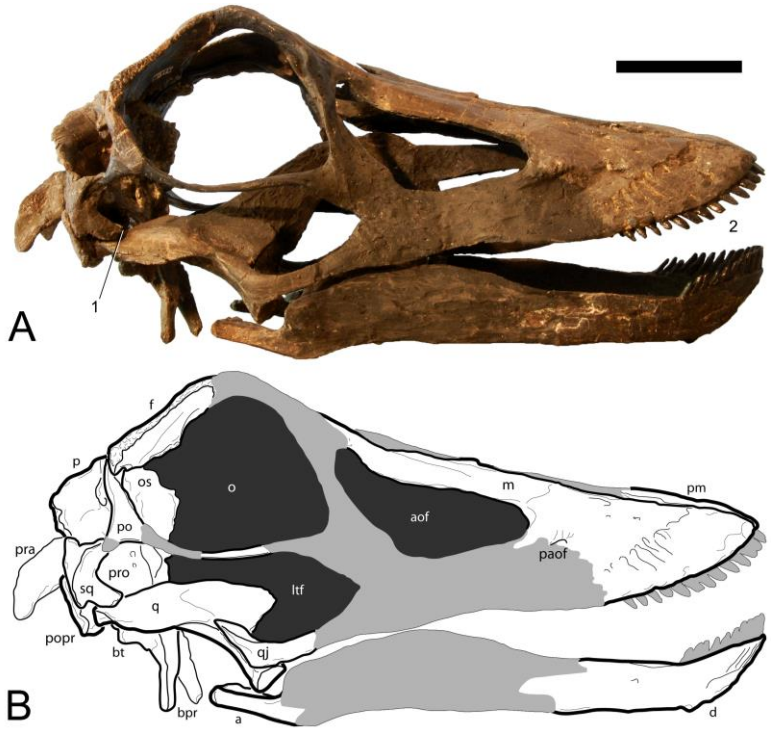

Figure 3.3: A, Photograph and B, drawing of the reconstructed skull of the holotype of *Kaatedocus siberi* (SMA 0004) in right lateral view. Light gray areas in B are reconstructed parts. The right surangular is mistakenly mounted as left angular. Notes corresponding to diagnostic features: (1) anteriorly restricted squamosal; (2) high tooth count, teeth not restricted to anterior-most jaw. Scale bar = 5 cm.

Etymology. 'Kaate' means in the Crow (Absaroka) language, one of the Native American tribes of northern Wyoming. 'Docus' is an allusion to *Diplodocus* and the Greek dokos/*δοκος* 'beam'. '*Siberi*' is after Hans-Jakob 'Kirby' Siber, b. 1942, doctor honoris causa of the University of Zurich, Switzerland. Siber is the founder and director of the Sauriermuseum Aathal, Switzerland, and organized and funded the excavation, preparation and curation of the holotype specimen of *Kaatedocus siberi*.

Holotype. SMA 0004: partial skull (right premaxilla, both maxillae, left lacrimal, both frontals, both postorbitals, both quadratojugals, both quadrates, both squamosals, both parietals, complete braincase, both dentaries, right surangular, both articulars (Figs 3.3-3.6), and cervical series from proatlas to cervical vertebra 14 (Figs 3.7-3.23).

The only elements that were not found articulated are one proatlantal element and the axis. They were included in the mount as they fit in size and morphology. The assignment of the axis to the holotype is provisional pending the discovery of a second specimen including this element. However, as no character in the phylogenetic analysis used herein describes axial morphology, the attribution of these elements to the holotype does not affect the phylogenetic position of *Kaatedocus siberi*.

Locality and horizon. SMA 0004 was recovered from the Howe Quarry in the vicinity of Shell, Bighorn County, north-central Wyoming, USA (44◦ 40 2.95 N/107◦ 49 8.12 W). The site is interpreted to be of Late Kimmeridgian or Early Tithonian age, in the upper part of the lower Morrison Formation (Fig. 3.2; Schwarz et al., 2007c; J. Ayer pers. comm. 2005).

Ontogeny. The ontogenetic stage of SMA 0004 is ambiguous as the specimen exhibits an intermediate morphology with osteological features that have been interpreted historically as indicators of either juvenile or adult ontogenetic stages.

Compared to other diplodocids, a young age is implied by the small size (combined skull and neck length approximately 3.8 m, estimated body length 14 m, based on intermediate cervical vertebrae elongation between *Apatosaurus* and *Diplodocus*) and the relatively large orbit. With a total length of 30 cm, the skull is slightly larger than the juvenile *Diplodocus* CM 11255, and reaches approximately 58% of the length of the adult *Diplodocus* skull CM 11161 (Holland, 1906; Whitlock et al., 2010). In addition, the incomplete fusion of the parietals, the rounded muzzle (in contrast to the squared snout of adult *Diplodocus* and *Apatosaurus*), the restriction of the bifurcation of cervical neural spines to mid- and posterior cervical vertebrae, and relatively shorter cervical centra have recently been interpreted to be typical for a juvenile ontogenetic stage (Wedel et al., 2000; Whitlock et al., 2010; Woodruff and Fowler, 2012). On the other hand, the complete co-ossification in all cervical vertebrae, and the presence of rugose tubercles, or roughened areas on laminae edges on both cranial and cervical elements indicate a higher ontogenetic age (Varricchio, 1997; Ikejiri et al., 2005; Schwarz et al., 2007c).

Taking all of the above mentioned features into account, the juvenile traits are generally seen as well on adult specimens of other taxa (like the more rounded snout of dicraeosaurids, or the less developed bifurcation of the cervical vertebrae in *Barosaurus*; Janensch, 1935; McIntosh, 2005), whereas the indicators for a subadult stage of SMA 0004 (in particular the advanced co-ossification and the conspicuous rugosities on both skull bones and vertebrae) are not reported from any specimens of young age, to our knowledge. In fact, adult alligators (Ikejiri, 2012), and a juvenile *Allosaurus* (Birkemeier, 2011) have recently been reported to possess open neurocentral synchondroses in cervical vertebrae, but fused centra and neural spines in caudal and/or dorsal elements. This indicates that neurocentral closure proceeds from the back to the front, with the cervical vertebrae being the last to co-ossify (Birkemeier, 2011; Ikejiri, 2012). On the other hand, the subadult flagellicaudatan *Suuwassea emilieae* ANS 21122 was reported to have fused cervical arches, but unfused mid-caudal vertebrae, which might contradict the developmental model supported by the above-mentioned taxa (Harris, 2006a). However, based on the available material, we still interpret SMA 0004 as a subadult specimen that retained a small body size. This is in agreement with the ontogenetic stages as described for *Camarasaurus* in Ikejiri et al. (2005). According to these authors, neurocentral closure in cervical vertebrae, as well as the subdivision of cervical pleurocoels, happens in subadult to adult stages.

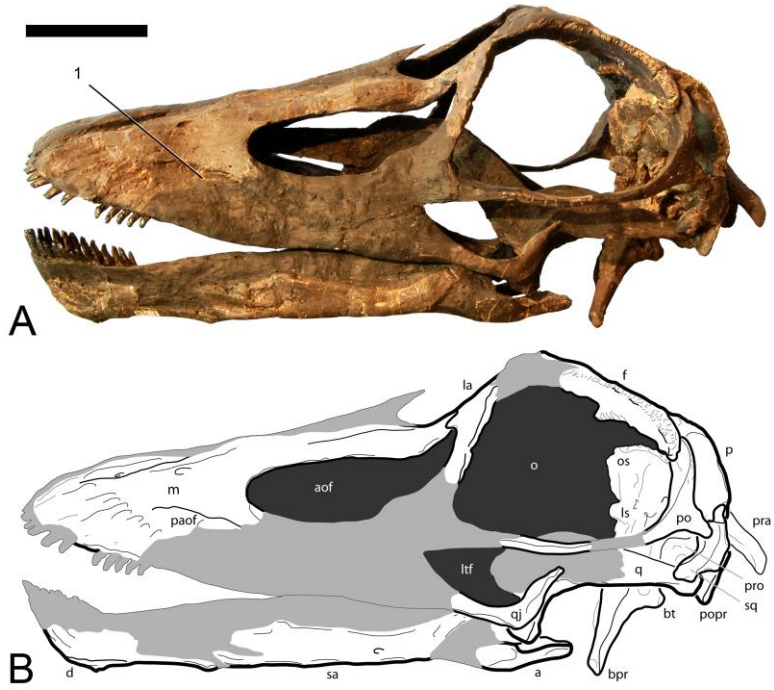

Figure 3.4: A, Photograph and B, drawing of the reconstructed skull of the holotype of *Kaatedocus siberi* (SMA 0004) in left lateral view. Light gray areas in B are reconstructed parts. The right surangular is mistakenly mounted as left angular. Note corresponding to diagnostic features: (1) closed or reduced preantorbital foramen. Scale bar = 5 cm.

Figure 3.5: A, Photograph and B, drawing of the reconstructed skull of the holotype of *Kaatedocus siberi* (SMA 0004) in dorsal view. Light gray areas in B are reconstructed parts. Notes corresponding to diagnostic features: (1) U-shaped frontal notch; (2) rounded snout; (3) narrow, distinct sagittal nuchal crest. Scale bar = 5 cm.

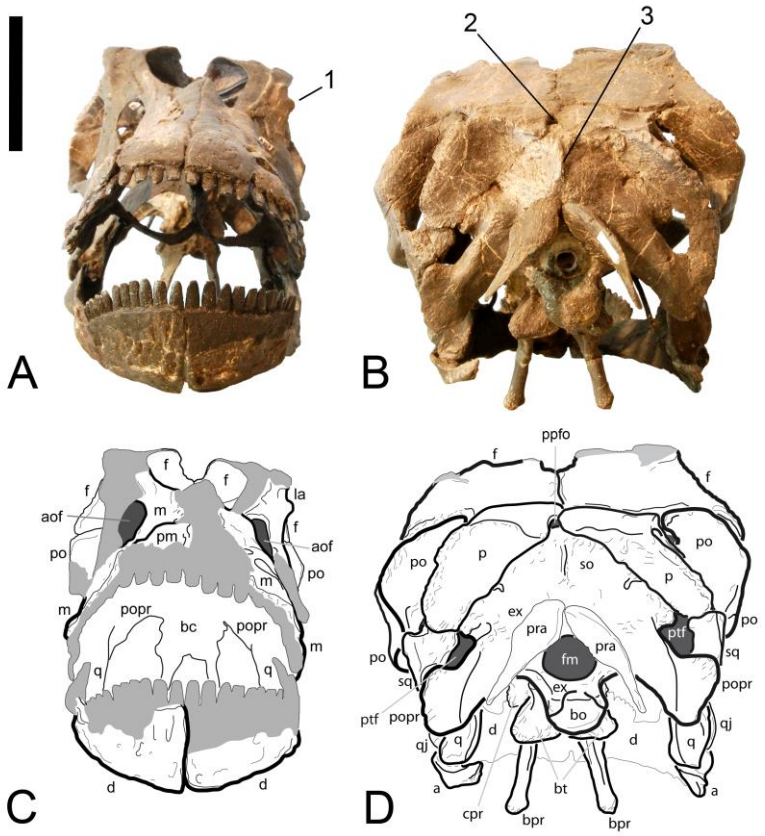

Figure 3.6: A, B, Photographs and C, D, drawings of the reconstructed skull of the holotype of *Kaatedocus siberi* (SMA 0004) in anteroventral (A, C), and posterodorsal (B, D) views. Light gray areas in C and D are reconstructed parts. Notes corresponding to diagnostic features: (1) lateral lacrimal spur; (2) postparietal foramen; (3) narrow, distinct sagittal nuchal crest. Scale bar = 5 cm.

Description

Terminology follows the standard nomenclature generally used (anterior and posterior instead of cranial and caudal). For the names of the vertebral lamina and fossae, we follow Wilson (1999) and Wilson et al. (2011), respectively, with two exceptions: instead of intrapre- and intrapost-zygapophyseal lamina we use the terms interpre- and interpostzygapophyseal lamina, as the prefix inter- describes better the arrangement between the two zygapophyses. To keep confusion to a minimum we keep the abbreviations proposed by Wilson (1999): tprl (interprezygapophyseal lamina) and tpol (interpostzygapophyseal lamina).

Skull

The general shape of the skull is highly similar to *Diplodocus* or *Apatosaurus*, elongated and having retracted external nares. Some obvious differences compared to adult skulls (e.g. AMNH 969, CM 11161, 11162, USNM 2672, 2673) include the larger orbit and the teeth that reach further backwards, although these are still restricted to the anterior-most part of the skull (Figs 3.3, 3.4).

Premaxilla. The right premaxilla preserves the anterior portion, and lacks the anterior-most dorsal border and the teeth. The main body is simple, without a sinuous curve forming a muzzle. It is broadest anteriorly, and its straight lateral and medial edges slightly converge posteriorly, including a very acute angle of approximately 10◦. The dorsal surface does not bear any anteroventrally extending grooves as are present in *Dicraeosaurus hansemanni* MB.R.2337. Four alveoli are visible, oriented such that the teeth would be procumbent. There is no indication of an anterior dorsoventral expansion as in *Diplodocus* USNM 2673 or *Dicraeosaurus hansemanni* MB.R.2337.

Maxilla. Both maxillae lack their posteroventral ramus and teeth. From the main body, the lamina-like dorsal ramus projects posteriorly and tapers until it meets the lacrimal. Its ventral edge is convex, resulting in a concave dorsal border of the antorbital fenestra as in most diplodocid skulls (e.g. CM

3452, 11161, 11162, 11255; USNM 2672). Slightly lateral to the border with the premaxilla, both the subnarial and the anterior maxillary foramen are well visible and closely spaced. A third, small foramen is situated just lateroventrally of the subnarial foramen. The preantorbital fossa is a longitudinal depression marked by an acute step bordering it dorsally. Such a development has been considered autapomorphic for *Diplodocus* (Mannion et al., 2012), but there it roofs a relatively large preantorbital fenestra (e.g. CM 3452, 11161, 11255; Berman and McIntosh, 1978; Whitlock et al., 2010; pers. obs. 2011), which is not present in SMA 0004. It does not open into a fenestra as in *Diplodocus* (e.g. CM 3452, 11161, 11255; Berman and McIntosh, 1978). In this respect, *Kaatedocus siberi* is very similar to *Dicraeosaurus* (MB.R.2336; pers. obs. 2011), where a very reduced foramen-like opening is present in the posterior-most extension of a dorsally well-defined fossa. The posterior-most portion is not preserved in SMA 0004 and could also exhibit such a small opening. The rostral portion of the main body of the maxilla shows the wavy surface typical for the part containing the replacement teeth. At least 12 alveoli can be counted in the right element.

Quadratojugal. Only the posterior halves of both quadratojugals have been preserved. They are L-shaped bones that cover the quadrate laterally with the shorter dorsal ramus, and would extend anteriorly to meet the jugal and the maxilla if completely preserved. The two arms of the L are transversely compressed and form an angle of approximately 110◦. The dorsal ramus projects dorsoposteriorly, as in *Diplodocus* or *Apatosaurus*, and curves slightly more backwards in its upper half. From there, it tapers to an acute tip, which does not extend far posteriorly, and thus remains well separated from the anteroventral projection of the squamosal – a typical feature in diplodocids, which is also present in *Suuwassea* (ANS 21122, pers. obs. 2011; contrary to the interpretation of Harris, 2006c). The preserved portion of the anterior ramus is dorsoventrally shortest close to where it grades into the dorsal process, and expands slightly towards the anterior end.

Lacrimal. The left lacrimal preserves the dorsal part that articulates with the maxilla anteriorly, the nasal medially, and the prefrontal posteriorly. The anterior edge of the lacrimal is straight until it reaches the posterodorsal-most end of the antorbital fenestra. The posterior border becomes thicker towards the upper end, where it develops a concavity that holds the lacrimal foramen. Lateral to this foramen, the lacrimal develops a blunt bony spur projecting laterally, a feature that is only seen in the juvenile diplodocid skulls CM 3452 and 11255, but not in adults (CM 11161, 11162; Berman and McIntosh, 1978; pers. obs. 2011).

Frontal. Both frontals are completely preserved. Anteroposterior length is about equal to maximum transverse width. The dorsal surface is flat and relatively smooth. The anterior and posterior margins are straight and subparallel at their medial portions. The lateral-most quarter of the anterior edge is marked by a distinct, acute V-shaped invagination that would receive the posterior process of the prefrontal, which does not extend far posteriorly as in *Diplodocus*, but remains well distant from the parietal. The posterior edge of the frontal also curves inward, but to a lesser degree than the anterior one. This indentation is gently rounded and forms the articulation facet for the dorsomedial process of the postorbital. The medial edges are straight along their posterior half and form an approximate right angle with the frontal–parietal suture. Anteriorly, they curve laterally, such that between the frontals a U-shaped notch develops. The edge is extremely thin, and neither exhibits any indication of fracturing nor is it undulose as sutures often are. Thus, the notch either enclosed a posterior process of the nasals, having a straight suture, or remained open as a posterior extension of the external nares, so that the nasals did not contact each other medially. The only sauropod with a similar development is *Spinophorosaurus nigerensis*, which has a narrow, V-shaped notch between the frontals (Knoll et al., 2012). The wider, U-shaped notch of *Kaatedocus siberi* can thus be considered an unambiguous autapomorphy. The straight lateral margins contribute to a major part of the dorsal edge of the orbit, and exhibit a similar rugosity as is typical for bone sutures, present in most diplodocoid skulls (e.g. AMNH 969, 7530, CM 3452, MB.R.2386, 2387, pers. obs. 2011). This indicates the existence of a cartilaginous palpebral element (homologue to the ossified palpebral bones in ornithischian dinosaurs; see Maidment and Porro, 2010). In ventral view it becomes clear that the frontal supports the end of the posterior process of the prefrontal from below. From there, a conspicuous, sharp ridge passes the ventral surface obliquely until it reaches the anterior end of the articulation surface for the anterodorsal part of the braincase, which is highly rugose and stands almost perpendicularly to this ridge.

Postorbital. Both postorbitals preserve their dorsomedial process and parts of the anterior process that forms the ventral border of the orbit. It covers the frontal posteriorly, and overlies the anterodorsal-most corner of the squamosal laterally. The left element also shows the posterior process. The dorsomedial process is relatively high dorsoventrally and compressed anteroposteriorly. It extends medially to reach the frontal–parietal suture, thereby excluding the frontal from the margin of the supratemporal fenestra. It is dorsoventrally convex posteriorly and concave anteriorly. The anterior process is a dorsoventrally compressed, subtle structure that extends nearly straight and subparallel to the dorsal margin of the orbit up to the point where it would reach the jugal, which is not preserved in SMA 0004. Posteriorly, the postorbital anterior process curves gently upwards, and expands slightly transversely. The posterior ramus is very short and acute. It projects almost straight posteriorly in dorsal view, and curves to a small degree ventrally in lateral aspect.

Parietal. Both parietals are complete and not fused. They contact the frontals anteriorly, the supraoccipital and exoccipital medioventrally, and the postorbitals and squamosals laterally. The parietals are dorsally flat bones on the posterior skull roof with a short anterolateral and a longer posterolateral process, which together enclose a major portion of the supratemporal fenestra. The frontal–parietal suture is more or less straight, and partly obscured due to the restoration and mounting of the skull, but appears to have been open in lifetime (B. Pabst, pers. comm., 2011). There is no trace visible of a pineal foramen, which would be situated where the paired frontals and parietals meet. A postparietal foramen can be observed posteriorly between the parietals and the supraoccipital, similar to the condition in *Dicraeosaurus*, *Amargasaurus* and *Suuwassea* (Janensch, 1935; Salgado and Bonaparte, 1991; Harris, 2006c; Whitlock, 2011a). The medial borders of the parietals bend slightly laterally in their posterior half, somewhat anterior to where they meet the supraoccipital, which they overlap to a small degree. The posterior border of the dorsal portion of the parietals is transversely concave in dorsal view. From there, the posterolateral process extends in a right angle ventrally, and laterally, following the oblique dorsolateral edge of the supraoccipital, and forming the posterior margin of the supratemporal fenestra. The posterior aspect of this process has a subequal or greater surface area than the flat dorsal portion. It is anteroposteriorly compressed, dorsomedially–ventrolaterally convex, and dorsolaterally–ventromedially concave. The dorsal edge extends straight dorsomedially–ventrolaterally, such that the supratemporal fenestra faces somewhat posteriorly as well, unlike the condition in *Diplodocus* CM 3452, but similar to *Apatosaurus* CM 11162 (Berman and McIntosh, 1978). The ventrolateral end of the posterolateral process is rounded and overlaps the squamosal laterally. The anterior surface gently curves into the anteroposteriorly concave medial side of the parietal, which is well separated by a distinct ridge from the dorsal flat area of the same bone. In its anterior part, it bears the short anterolateral process, which projects ventrolaterally forming the anterior edge of the supratemporal fenestra, together with the postorbital.

Squamosal. The squamosals are complete except for their dorsal-most part, which is not preserved on either side. It connects with the postorbital anterodorsally, with the quadrate anteroventrally, with the parietal dorsomedially, and with the paroccipital process posteroventrally. Dorsally, the squamosal forms the posterolateral corner of the supratemporal fenestra, ventromedially the dorsolateral edge of the posttemporal fenestra, and anteriorly the posterior-most corner of the infratemporal fenestra. It is a strongly transversely curved bone, with its convex side facing outwards, forming part of the posterolateral edge of the skull. In lateral view, the anterodorsal process of the squamosal bears a dorsoventral concavity for the reception of the postorbital. The ventral process tapers to a blunt tip that points slightly anteriorly as well, but does not exceed the posterior border of the orbit as in other diplodocoids (e.g. Berman and McIntosh, 1978; Salgado and Bonaparte, 1991). Both its anterior and posterior borders are straight, before they curve frontwards and backwards, respectively. In the posterior margin this happens slightly earlier, and the posterior process is thus dorsoventrally longer than the anterior ramus. The squamosal therefore bears a short posteroventral process but does not form such a distinct ‘prong’ as present in *Amargasaurus* (Salgado and Bonaparte, 1991; Whitlock, 2011a). In posterior view, the squamosals are dorsoventrally convex, with the dorsomedial process projecting medially to meet the parietal.

Quadrate. Both quadrates lack their anterodorsal portions of the wing-like anterodorsal ramus, but are otherwise complete. They are triradiate bones forming the jaw articulation with the articular ventrally, contacting the pterygoids anteromedially, and the squamosal posteriorly. The articular facet for the

mandibular joint is subtriangular, lacking a medial process as the one seen in some rebbachisaurids (Whitlock, 2011a; Mannion et al., 2012). It is located at the ventral end of the relatively stout ventral ramus, which is oriented at an angle of about 90◦ to the skull roof. The anteroventral projection of the quadrate shaft is covered laterally almost completely by the dorsal ramus of the quadratojugal, and exhibits a shallow concavity on its posterior side. This concavity extends onto the ventral side of the posterior process, forming a shallow quadrate fossa as in other diplodocids (Wilson, 2002; Upchurch et al., 2004a). Posteriorly, the ramus tapers both in dorsoventral and in mediolateral directions. It curves slightly medially as well, so that the whole lateral side of the quadrate becomes antero-posteriorly slightly convex. The wing-like pterygoid flange is a very thin lamina originating at the lateral edge of the posterior ramus. Medially it borders another shallow fossa that lies on the quadrate shaft and becomes deeper anteriorly. Such a cavity has not been described in any diplodocid sauropod, and personal observations showed it to be absent in most diplodocid skulls (e.g. AMNH 969; CM 11161, 11162, 11255; USNM 2672, 2673). However, the possible *Diplodocus* skull CM 3452, as well as the quadrates assigned to the holotype of *Apatosaurus ajax* YPM 1860, show similar features.

Braincase and occiput

Supraoccipital and exoccipital-opisthotic complex. The supraoccipital is complete and well fused to the exoccipital-opisthotic complex, so that sutures are difficult to observe. The whole fused element is subtriangular, contacting the parietals anterolaterally, bordering the posttemporal fenestrae with the dorsolateral margin of the paroccipital processes, and contributing to the upper portion of the occipital condyle ventrally. It roofs the braincase posteriorly, encloses the foramen magnum, and bears two oblique, ellipsoid facets right dorsolaterally of the foramen magnum for the articulation with the wing-like proatlas. Together, these facets form an inverted V-shape and reproduce more or less the angle included by the paroccipital processes. Dorsal to these proatlantal facets, the supraoccipital bears a narrow sagittal nuchal crest, very similar to the state in *Suuwassea emilieae* ANS 21122 (Harris, 2006c). This ridge extends dorsally to the dorsomedial, rounded corner of the supraoccipital, which also borders the postparietal foramen posteriorly. From here, the oblique dorsolateral borders extend ventrolaterally, bearing a short posttemporal process at their outer ends that meets the squamosal, and thereby excludes the parietal from the anterior margin of the posttemporal fenestra. Close to the dorsolateral border, at about midlength, there is a foramen like the one interpreted as an external occipital foramen in the *Apatosaurus* BYU 17096 (Balanoff et al., 2010). Another small foramen is situated between the latter and the proatlas facets, near the base of the paroccipital process.

The paroccipital processes are anteroposteriorly flat structures that project ventrolaterally, and slightly posteriorly to meet the squamosal and the quadrate. Their dorsal and ventral margins are subparallel in posterior view, and also parallel to a line projecting in continuation from the dorsolateral edges of the supraoccipital. The ventrolateral ends of the processes are expanded both dorsally and ventrally. The dorsal expansion is more abrupt and distinct than the ventral one, so that the paroccipital process, together with the posttemporal process of the supraoccipital–exoccipital–opisthotic complex encloses the ellipsoid posttemporal fenestra on three sides. The posterior side of the paroccipital process is dorsolaterally–ventromedially convex, and bears a ridge that originates at the dorsolateral corner of its base, and extends almost vertically to where the slight ventral extension of the outer end begins. This ridge is weakly rugose and might thus represent some muscle insertion. In ventral view, the edge of the paroccipital process expands anteroposteriorly and develops distinct ridges to enclose a fossa, which contains at least two deep foramina (probably for cranial nerves IX–XI; Janensch, 1935; Upchurch et al., 2004a). The anterior-most crest extends onto the neighboring bones of the braincase to form the crista prootica.

Basioccipital and basisphenoid. The basioccipital forms the main body of the occipital condyle. The sutures with the exoccipital are unclear but appear to extend obliquely, so that the exoccipital contributes to only the laterodorsal-most corners of the occiput, as is the case in all known sauropods (Wilson and Sereno, 1998; Upchurch et al., 2004a). The entire condyle has a straight dorsal margin, so that the outline becomes semicircular. Towards the foramen magnum, the neck of the occipital condyle develops a very slight midline concavity that leads into the endocranium. Two foramina are placed lateroventrally on the base of the neck of the occipital condyle, where also the paroccipital processes originate. These foramina are usually interpreted as the openings for cranial nerve XII (Janensch, 1935; Upchurch et al., 2004a; Harris, 2006c). The ventral face of the occipital neck curves gradually to

form a deep and narrow U-shaped concavity between the basal tubera and the occipital condyle, when seen in lateral view. Towards the paired basal tubera, the basisphenoid expands laterally so that the paired tubera equal about twice the width of the occipital condyle, which is considerably more than in any other diplodocid and might thus represent an additional autapomorphy of *Kaatedocus siberi* (see Mannion, 2011: tab. 1). From their ventrolateral corners, the basipterygoid processes extend anteroventrally for a short distance before curving outwards (forming an acute angle of about 26◦) and finally exceed the width of the basal tubera. The tubera are only slightly distinct in ventral view, but appear as posteriorly projecting rugose knobs in lateral aspect. They are parallel to each other in ventral view, and separated by a narrow notch. Unlike in *Apatosaurus* YPM 1860, *Diplodocus hayi* HMNS 175 (= CM 662) and the flagellicaudatan braincase MB.R.2387, no foramen is present in this notch (Holland, 1906; Remes, 2009; pers. obs. 2011).

The bases of the slender basipterygoid processes are subtriangular and about a third to half of the width of their corresponding tuber. The processes become subcircular more distally, but maintain more or less the same width until they expand to a small degree transversely at their distal end. Although the mounted skull gives the impression that they would project directly ventrally, the disarticulated braincase and frontals clearly show that they actually were at an angle of about 45◦ to the skull roof. The basipterygoid processes are united at their bases by a thin bony sheet, originating at their ventral edges and extending anteroventrally to the point where the processes curve outwards. In anterodorsal view, this bony sheet bears the ventral-most point of the parasphenoid rostrum, which is broken off. From there, a thin but distinct ridge extends posterodorsally, until it reaches a small midline foramen around midlength of the entire braincase, posterior to the larger opening for the optic nerve. This ridge borders two large oval symmetrical fossae extending from the base of the basipterygoid processes to a point slightly anteroventral to the small foramen mentioned above. The fossae probably include the foramen for cranial nerve VI. They are symmetrical, and laterally bordered by the crista prootica that connects posterodorsally to the anterior side of the paroccipital processes.

Orbitosphenoid. The orbitosphenoids are paired bones that floor the braincase anteriorly and connect it with the frontals dorsally. The oblique posterolateral edges of the orbitosphenoids contact the laterosphenoids, but no clear suture is visible. In ventral view, the two orbitosphenoids form a transversely convex trapezoid structure with subparallel anterodorsal and posteroventral margins. The longer anterodorsal edge attaches to the frontals laterally and forms the ventral margin of the opening for cranial nerve I medially. At its midlength, a deep narrow notch is well marked, separating the two elements. The notch almost reaches the foramina for the cranial nerve II, which are medially conjoined and form a single opening, unlike *Apatosaurus* BYU 17096 (Balanoff et al., 2010) but similar to *Suuwassea* ANS 21122 (Harris, 2006c); pers. obs. 2011).

Laterosphenoid. The laterosphenoids floor the braincase lateroventrally, being capped by the frontals and parietals dorsally, and contacting the orbitosphenoid and prootic anteromedially and posteromedially, respectively. At the posterior-most corner of the barely recognizable suture with the orbitosphenoid, slightly dorsally to posterodorsally of the foramen for the cranial nerve II, a smaller, ellipsoid fossa appears to bear two foramina for the cranial nerve III and IV. These foramen are usually thought to mark the suture between orbitosphenoid and laterosphenoid (Upchurch et al., 2004a), but are located more anteriorly in, for example, *Suuwassea emilieae* ANS 21122 (Harris, 2006c). The lateral edge of the laterosphenoid bears a conspicuous lateroventrally projecting process that tapers towards its end, and that in vivo would probably have contacted the medial end of the ventral margin of the postorbital dorsomedial process. This process marks the origin of the crista antotica, which then extends ventrally along the lateral side of the braincase to merge with the crista prootica. The crista antotica thereby separates the more posteriorly situated foramen for cranial nerve V from the two anteroventrally placed foramina for cranial nerves III and IV.

Prootic. The two prootics floor the braincase lateroventrally and do not show any midline contact. They meet the basisphenoid ventrally, the laterosphenoid anteriorly, and at least the exoccipital–opisthotic complex dorsally, and are separated by the midline ridge originating at the parasphenoid rostrum, and the adjacent fossae for cranial nerve VI. Its sutures are difficult to observe, the only hints to them are the various foramina that have previously been interpreted to pierce the prootic at the base of the paroccipital process, towards the ventral midline of the braincase and anterodorsally (see above and Upchurch et al., 2004a; Carabajal et al., 2008). The prootic bears a major part of the crista prootica

that originates at the base of the paroccipital processes and from there passes laterally on the prootic in the direction of the basal tubera, bordering the trigeminal foramen posterodorsally on its way. Further ventrally, it merges with the crista antotica and develops a thin bony shelf lateral to the basal tubera, distinct, but without a conspicuous lateral process as present in *Dicraeosaurus* (Janensch, 1935; Upchurch et al., 2004a) or *Amargasaurus* (Salgado and Bonaparte, 1991; Upchurch et al., 2004a).

Mandible

Dentary. Both dentaries are only partially preserved, the right element lacking a median portion of the tooth-bearing dorsal edge, and the posterior-most part. The left element only preserves the anteroventral portions. The bones are labiolingually compressed, and slightly thicker dorsally than ventrally, where they taper to a sharp edge. In ventral view the dentaries gently curve medially at their anterior ends, similar to the juvenile *Diplodocus* CM 11255 (Whitlock et al., 2010), but in contrast to the squared shape of the lower jaw of *Diplodocus* CM 11161 (McIntosh and Berman, 1975; Whitlock, 2011a). In lateral view, the ventral margins of the dentaries develop a weak posteroventrally projecting process close to the symphysis, so that the entire border is slightly concave anteroposteriorly. This process does not form such a sharp 'chin' as described in *Diplodocus* or *Dicraeosaurus* (Janensch, 1935; Upchurch, 1998; Whitlock, 2011a), but is still distinctive. The symphysis itself has a sub-rectangular outline, and is oriented obliquely in a way that its dorsal end projects further anteriorly than the ventral 'chin'. It marks also the highest part of the dentaries, which become gradually constricted dorsoventrally up to the posterior-most alveolus. Although in both elements the total number of alveoli is not preserved, the position of the posterior-most alveolus in the right jaw and the accompanying grooves on the ventral portion indicate that 12 or 13 dentary teeth were present. They do not reach as far back as the maxillary teeth, so that a crown-to-crown occlusion does not appear to have occurred. Posteriorly, there is no indication of a prominent coronoid eminence, as is the case within all Diplodocoidea (Upchurch et al., 2004a). However, due to its incomplete preservation, an abrupt dorsal expansion for a shallow eminence similar to the one present in *Diplodocus* CM 11161 (McIntosh and Berman, 1975) cannot be excluded.

Surangular. The probable right surangular is mistakenly mounted as a left angular. It is anteroposteriorly straight and contributes the posterior part of the dorsal edge of the lower jaw. This dorsal margin is mostly straight in lateral view, only at its posterior-most fifth of the entire length it first curves weakly laterally, before it turns to project ventrally and slightly medially, to cover the outer surface of the articular, and to initiate the medial bowing of the retroarticular process of the jaw. The ventral border is highly concave, with the most constricted part close to the point where the opposing edge bows ventrally. Slightly anterior to this point, there is a well-developed foramen at the anterodorsal end of a short oblique groove. Not far anterior to this foramen, accompanied by the dorsoventral expansion of the anterior portion of the surangular, a shallow dorsoventral concavity develops, which extends up to the anterior-most visible part.

Articular. Both articulars of SMA 0004 are preserved. They bear the articulation surface for the joint with the quadrate, and bow medially in respect to the long axis of one ramus of the lower jaw. The articular facet lies slightly below the level of the tooth row in lateral view. In addition to the concave facet for the articulation with the quadrate, also the medial and lateral sides bear shallow dorsoventral concavities. The lateral side is less high in this respect than the medial one, but reaches further posteriorly in lateral aspect, which is mostly due to the medial bowing of the posterior end of the bone. The posterior end has a subtriangular cross section, with a very narrow ventral surface and the two slightly inclined lateral and medial sides. This inclination gives room for the further needed mediolateral expansion towards its anterior end, where the articular facet is situated.

Cervical series

Proatlas. SMA 0004 only preserves the left proatlas, but the mount at SMA includes a right element of a pair of proatlases (Figs 3.3-3.6) found approximately 7 m east of where the holotype of *Kaatedocus siberi* was found. The left element lacks its distal tip but is otherwise complete. To our knowledge, this is the first reported proatlas of any diplodocid sauropod. The proatlas consists of two symmetrical, wing-like bones with a relatively broad base and bluntly pointed, backwards, outwards and downwards pointing distal ends. The proatlas attaches to the exoccipital-opisthotic complex, just

above the foramen magnum. The general shape of the proatlas in SMA 0004 is very similar to proatlases of *Dicraeosaurus*, *Giraffatitan* and *Camarasaurus* (Janensch, 1929, 1950; Madsen et al., 1995). The base of the proatlantal elements is broader mediodorsally than lateroventrally, so that its cross section is ovoid. Whereas the outer surface remains shallowly convex, the inner side flattens after approximately one third of its entire length and even becomes slightly concave towards its distal end, where it caps the anterior-most part of the atlantal neural arch. In dorsal view, the entire bone is curved with its anterior and posterior edges being concave and convex, respectively.

Atlas–axis complex. The atlas–axis complex is complete, except for the ribs (Figs 3.7, 3.8). The general morphology is similar to that of *Apatosaurus louisae* CM 3018 and *Suuwassea emilieae* ANS 21122 (Gilmore, 1936; Harris, 2006a). The atlas anterior articulation tapers anteroventrally, forming the acute ventral 'lip' typical for flagellicaudatans (Fig. 3.7B; Whitlock, 2011a; Mannion et al., 2012). In ventral view, the parapophyses project ventroposteriorly. Dorsal to this, small and shallow pneumatopores occupy the posterior half of the centrum. The centrum is fused to the atlantal neurapophysis. These have a wing-like shape, with a long posterior and a very short anterior projection. The neurapophyses do not meet at the midline.

The axial centrum is long (more than three times its dorsoventral height), with a long, undivided pleurocoel occupying most of the lateral aspect. In ventral view, the centrum is hourglass-shaped and flat. The anterior expansion is confluent with the parapophysis, whereas the posterior expansion has two small longitudinal ridges, which on more posterior vertebrae form the posteroventral flanges. The anterior condyle of the centrum has a midline dorsal projection that articulates with the atlas. The neural arch pedicels are short anteroposteriorly, occupying only half of the dorsal side of the centrum. This is in contrast to other diplodocids, such as *Apatosaurus louisae* CM 3018 or *Diplodocus carnegii* CM 84, where they cover almost the entire centrum (Hatcher, 1901; Gilmore, 1936). The posterodorsal and anterodorsal sections of the axial centrum of SMA 0004 are therefore free and not attached to the pedicels, unlike most diplodocids.

The axial neural arch is tall (more than 2.5 times the height of the centrum). The neural spine summit has a paired projection giving a bifid aspect. Anteriorly, there is a midline prespinal lamina that is straight in lateral view. The neural spine is inclined posterodorsally at an angle of 45◦. Posteroventrally, the spinopostzygapophyseal laminae enclose a deep spof. Small epipophyses and pre-epipophyses are present. The diapophyses are mound-like posterolateral projections situated at the base of the neural arch and in the middle of the vertebra in lateral view.

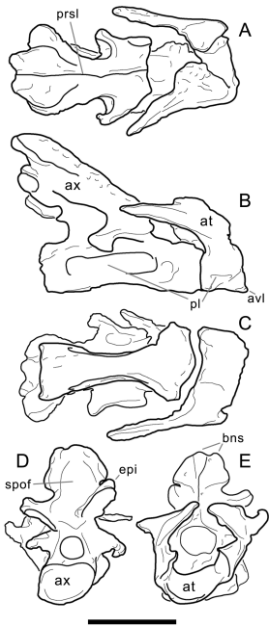

Figure 3.7: Drawings of the atlas–axis complex of the holotype of *Kaatedocus siberi* (SMA 0004; assignment of axis uncertain, see text) in A, dorsal, B, right lateral, C, ventral, D, posterior, and E, anterior views. Scale bar = 4 cm.

Figure 3.8: Photographs of the atlas-axis complex of the holotype of *Kaatedocus siberi* (SMA 0004; assignment of axis uncertain, see text) in posterior (left), dorsal (top), right lateral (center), ventral (bottom), and anterior (right) views. Scale bar = 4 cm.

Anterior cervical vertebrae (CV 3-5). The anterior cervical vertebrae are complete and only slightly deformed (Fig. 3.9; Tab. 3.1). The cervical ribs are fused to the vertebrae, only marked by a rugose and slightly expanded area. The neurocentral synostosis is closed and not discernible. The vertebrae are longer than high, with the cervical ribs not projecting far beneath the ventral-most point of the centrum. The opisthocoelous centra have EI values between 3.1 and 3.6 (Tab. 3.2). The posterior extremities are higher than wide, and broader dorsally than ventrally, forming a subtrapezoidal outline. Whereas the hemispherical anterior condyle is continuous with the centrum in CV 3 (Fig. 3.10), it is separated from the rest of the centrum by a shallow ridge in CV 4 and 5 (Figs 3.11, 3.12). Its surface is slightly more irregular compared to the other portions. The condyle of CV 5 shows two distinct invaginations dorsomedially (Fig. 3.9, B5). As there is no other element that bears such a structure on its condyle, a taphonomic cause is probable, although the more dorsally located indentation lies more or less on the midline and resembles a foramen. However, a connection with the internal structures cannot be identified with certainty.

The lateral sides of the centra of CV 3 to 5 are straight dorsally but have a somewhat sinuous outline ventrally. The ventral edge extends ventrally from the anterior condyle backwards to where the parapophysis is situated. At the posterior end of the parapophysis, it becomes strongly concave, with the most constricted point slightly anterior to the centrum midlength. The posterior portion is again expanded ventrally but curves back dorsally to a very small degree just before reaching the postero-ventral corner. The median constriction is more pronounced the more posterior the element is in the cervical column. The lateral surfaces of the centra bear a large pleurocoel, which is undivided in CV 3 and 4 but separated into two by a median ridge in CV 5. The pleurocoels are bordered medially by a

very thin wall and occupy almost the entire length of the vertebral centra. Whereas the anterior border of the coels in CV 3 and 4 is clearly defined, the posterior end is created by the gradual curvature of the cotyle. Following the overall aspect of the lateral surface of the centra, the pleurocoels expand dorsoventrally posteriorly. In CV 5, an oblique, shallow ridge divides the pleurocoel into a shorter anterior and a longer posterior pneumatic fossa (Fig. 3.9, B2). The anterior depression has a very distinct and continuously rounded anterior edge. Its posterior end is more pointed due to the antero-dorsally–posteroventrally extending ridge that divides the pleurocoel. This ridge reaches the ventral margin of the centrum at its most dorsoventrally constricted point and is more or less continuous with the posterior part of this concave portion of the ventral edge. The posterior pneumatic fossa of CV 5 has thus a subtriangular outline, with its hypotenuse being formed by the separating ridge and the ventral margin of the lateral surface. The horizontal dorsal margin is more distinct than the ventral margin.

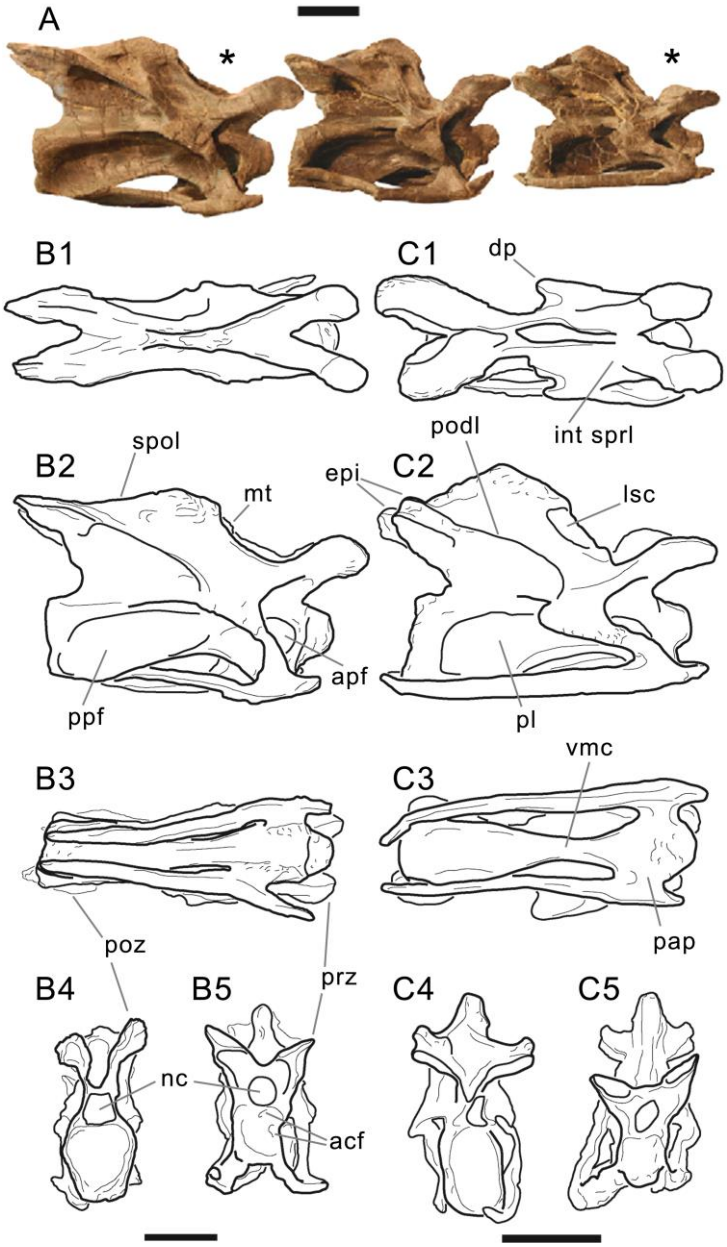

Figure 3.9: A, Photograph and B, C, drawings of the anterior cervical vertebrae of the holotype of *Kaatedocus siberi* (SMA 0004). Photographs in lateral view and to scale, elements shown in the drawings are indicated by an asterisk. Drawings of CV 5 (B), and CV 3 (C) in dorsal (1), lateral (2), ventral (3), posterior (4) and anterior (5) views; scaled to the same centrum length, in order to highlight changes of proportions. Scale bars = 4 cm.

Table 3.1: Measurements of CV 3-14 of the holotype of *Kaatedocus siberi* (SMA 0004).

	measurements (mm)															
element	gl	gh	cl	cmw	wd	wpr	wpo	ppl	pph	wct	hct	wcd	hcd	hns	cl wo cd
CV 3	134	89	113	8	43	49	44	90	18	28	36	19	23	48	110
CV 4	151	92	131	11	57	43	51	103	20	36	39	20	27	59	118
CV 5	206	97	165	14	63	58	51	129	27	42	46	29	35	59	135
CV 6	227	108	194	14	69	49	64	134	22	49	47	37	38	65	184
CV 7	268	134	227	17	82	71	62	151	25	40	62	48	43	80	203
CV 8	297	138	245	23	105	77	79	161	39	49	74	49	49	91	213,5
CV 9	309	161	270	39	109	80	82	168	28	40	77	50	54	106	231
CV 10	338	183	273	40	126	94	92	176	30	60	91	62	63	120	241
CV 11	324	202	298	50	125	74	92	172	37	78	100	68	84	124	253
CV 12	327	221	314	60	138	108	108	169	35	85	102	71	95	147	264
CV 13	309	250	322	67	182	116	98	182	28	84	125	76	102	172	269
CV 14	302	273	312	68	203	113	112	155	28	84	118	70	110	182	244
	ratios														
	wd/gh	wd/gl	gh/cl	cl/wct	hct/wct	cl wo cd/hct	cl/hct	hns/hct	ppl/cl	gl/cl	hns/gl	wd/wct	hns/wd	hns/gh	gh/gl
CV 3	0,48	0,32	0,79	4,04	1,29	3,06	3,14	1,33	0,80	1,19	0,36	1,54	1,12	0,54	0,66
CV 4	0,62	0,38	0,70	3,64	1,08	3,03	3,36	1,51	0,79	1,15	0,39	1,58	1,04	0,64	0,61
CV 5	0,65	0,31	0,59	3,93	1,10	2,93	3,59	1,28	0,78	1,25	0,29	1,50	0,94	0,61	0,47
CV 6	0,64	0,30	0,56	3,96	0,96	3,91	4,13	1,38	0,69	1,17	0,29	1,41	0,94	0,60	0,48
CV 7	0,61	0,31	0,59	5,68	1,55	3,27	3,66	1,29	0,67	1,18	0,30	2,05	0,98	0,60	0,50
CV 8	0,76	0,35	0,56	5,00	1,51	2,89	3,31	1,23	0,66	1,21	0,31	2,14	0,87	0,66	0,46
CV 9	0,68	0,35	0,60	6,75	1,93	3,00	3,51	1,38	0,62	1,14	0,34	2,73	0,97	0,66	0,52
CV 10	0,69	0,37	0,67	4,55	1,52	2,65	3,00	1,32	0,64	1,24	0,36	2,10	0,95	0,66	0,54
CV 11	0,62	0,39	0,68	3,82	1,28	2,53	2,98	1,24	0,58	1,09	0,38	1,60	0,99	0,61	0,62
CV 12	0,62	0,42	0,70	3,69	1,20	2,59	3,08	1,44	0,54	1,04	0,45	1,62	1,07	0,67	0,68
CV 13	0,73	0,59	0,78	3,83	1,49	2,15	2,58	1,38	0,57	0,96	0,56	2,17	0,95	0,69	0,81
CV 14	0,74	0,67	0,88	3,71	1,40	2,07	2,64	1,54	0,50	0,97	0,60	2,42	0,90	0,67	0,90

Abb: cl, centrum length; cl wo cd, centrum length without condyle; cmw, centrum minimum width; gh, greatest height; gl, greatest length; hcd, height anterior condyle; hct, height posterior cotyle; hns, height neural spine; pph, pneumatopore height; ppl, pneumatopore length; wcd, width anterior condyle; wct, width posterior cotyle; wd, width across diapophyses; wpo, width across postzygapophyses; wpr, width across prezygapophyses

Table 3.2: Elongation indices of the CV of the holotype of *Kaatedocus*				
		EI	mean EI	
Anterior	CV 3	3,14	3,36	
	CV 4	3,36		
	CV 5	3,59		
Middle	CV 6	4,13	3,52	
	CV 7	3,66		
	CV 8	3,31		
	CV 9	3,51		
	CV 10	3		
Posterior	CV 11	2,98	2,88	
	CV 12	3,08		
	CV 13	2,58		
	CV 14	2,64		

Figure 3.10: Photographs of CV 3 of the holotype of *Kaatedocus siberi* (SMA 0004) in posterior (left), dorsal (top), right lateral (center), ventral (bottom), and anterior (right) views. Scale bar = 4 cm.

Figure 3.11: Photographs of CV 4 of the holotype of *Kaatedocus siberi* (SMA 0004) in posterior (left), dorsal (top), right lateral (center), ventral (bottom), and anterior (right) views. Scale bar = 4 cm.

Figure 3.12: Photographs of CV 5 of the holotype of *Kaatedocus siberi* (SMA 0004) in posterior (left), dorsal (top), right lateral (center), ventral (bottom), and anterior (right) views. Scale bar = 4 cm.

The ventral side of the centra of CV 3 to 5 is marked by a strong constriction slightly anterior to midlength and posterior to the parapophyses, so that the centrum has an irregular hourglass-shaped outline in ventral aspect, which is most pronounced in CV 4. Whereas the parapophyses are attached to the anterior condyle in CV 3, they become detached in the subsequent vertebrae. In all three elements, the parapophyses project ventrolaterally and are longer than wide. Together with the posterior end of the condyle they enclose a shallow subtriangular concavity. The dorsal surfaces of the parapophyses of CV 5 are concave, forming an extension of the pneumatic fossa. An indistinct ridge separates the fossa into two smaller depressions. The transverse constriction of the ventral sides occupies mainly the anterior second fourth of the surface, and is flat to slightly convex in CV 3 and 4, but concave in CV 5. Posterior to the constriction, the lateral edges develop ventrally to lateroventrally projecting, thin flanges that border a second, larger cavity. These flanges become oriented subparallel in the last fourth of the ventral surface, and gradually disappear shortly before they reach the posterior edge of the centrum. In posterior view, they almost reach the ventral level of the cervical rib shafts.

The neural arches of CV 3 to 5 exceed both the length and the height of the centra by two to four centimeters. The spine summit is elevated above the postzygapophyses in CV 3 and 4, but is at about the same height in CV 5. It is slightly anteriorly inclined in CV 4 and 5. With the exception of CV 3, where the prezygapophyses mark the widest point of the vertebra, all cervical vertebrae are widest across their diapophyses. The outline of the prezygapophyseal facets is highly variable, being subrectangular in CV 3 (with the longer diameter extending anteroposteriorly), subtriangular in CV 4 (with the anterior end pointed and the posterior edge straight), and rather rounded in CV 5. The facets are well separated from the prezygapophyseal process in CV 3 but less so in the subsequent elements. As in all diplodocines that preserve cervical vertebrae, the prezygapophyseal facet surfaces are somewhat convex both anteroposteriorly and transversely (e.g. Hatcher, 1901; McIntosh, 2005). In anterior view they face inwards and upwards, at an angle of about 45◦ to the horizontal. The prezygapophyses are supported by a stout single centroprezygapophyseal lamina extending anteriorly as well as dorsally and laterally until it curves to project almost straight anteriorly. The cprl unites with the anterior end of the prdl ventral to the posterior-most point of the articular facet in CV 3. This cannot be observed in CV 4 and 5, because the prdl disappears towards its anterior end. The course of the prdl cannot be followed further than to a point lateroventral to the posterior-most extension of the articular facets. The tprl develops approximately at midlength of and ventral to the articular facets, and extends backwards to the base of the process where the two portions of the right and the left side unite in a very acute angle. Together with the cprl and the neural canal roof, the tprl forms two small centroprezygapophyseal fossae (cprf).

The sprl originates on the posterolateral corner of the prezygapophyseal facet but disappears shortly posteriorly. Its course is difficult to follow in CV 3 and 4. In CV 3 a median, slightly bifid crest originates posterior to where the right and left parts of the tprl unite. It is posteriorly inclined at about 50◦ to the base of the neural canal. At midlength, the bifurcation becomes suddenly somewhat deeper and the inclination of the sprl decreases to approximately 40◦ while proceeding to the spine summit. In CV 4 a trifid median crest develops behind the union of the tprl. It is slightly inclined posteriorly in its ventral portion, which is longer than the corresponding structure of CV 3. The median ridge on the trifid crest disappears dorsally, where the lateral edges become suddenly more developed, and even project anteriorly to a small degree, before they extend straight posterodorsally to reach the spine summit. The sprl of CV 5 are the easiest to observe. At the base of the spine, they turn to proceed dorsally at an angle of 25–30◦ towards the spine summit. Shortly before the sprl meet at the dorsal-most point of the neural spine, a median bony structure appears and projects somewhat anteriorly (Fig. 3.9, B2). From this point the sprl bend and proceed straight dorsally before turning backwards to reach the uppermost point of the vertebra. In all three anterior cervical vertebrae the two sprl meet the spol at the spine summit where they are interconnected such that the spine cannot be interpreted as being entirely bifid. This contrasts with the state in *Diplodocus* and dicraeosaurids where the bifurcation of the cervical vertebrae also affects the anterior-most elements (e.g. Hatcher, 1901; Janensch, 1929).

The spine summit is transversely compressed and forms a blunt apex in lateral view. It is located posterior to the posterior-most point of the diapophysis. The lateral side of the neural spine bears a distinct, dorsoventrally elongated fossa posteriorly adjacent to the sprl. Additional, shallower cavities are present in CV 4 and 5, ventral and posterior to the distinct fossa, respectively. The diapophysis is situated on the anterior second quarter of the vertebral centrum. It is defined by the prdl anteriorly, the

podl posterodorsally, the nearly horizontal pcdl posteriorly, and a very short acdl anteroventrally. The pcdl is relatively short compared to its length in more posterior elements and disappears considerably anterior to the posterior-most extension of the pleurocoels. In lateral view the diapophysis of CV 3 describes a strong backwards curve due to a rounded posterior projection and the strongly anteroventrally protruding articular end. Whereas the latter remains similar in the following vertebrae, the posterior edge of the diapophyses of CV 4 and 5 bear subsequently less-developed posterior projections. The podl of CV 3 to 5 is gently curved. It originates at an acute angle with the diapophysis (approximately 55◦ to the horizontal), and becomes almost horizontal at the postzygapophyses.

The postzygapophyses are inclined posteriorly and bear large and suboval facets, with their longest diameter oriented anteroposteriorly. The facets face downwards and somewhat outwards and backwards. They are concave mediolaterally, and extend anteriorly to a point almost straight above the posterior-most point of the pedicels of the neural arch. In posterior view, the tpol continues the curvature of the facets until the two sides unite, where they meet the roof of the neural canal. Dorsally, the postzygapophyseal facets are capped by very distinct epipophyses that overhang the facets both laterally and posteriorly. Their lateral margins are confluent with the podl. Whereas the posterior edge of the epipophysis is rounded in CV 3, it becomes more and more pointed in the subsequent elements. Such a strong development of the epipophyses is rarely seen in other diplodocids. Although epipophyses are present in most taxa, they usually do not form a pointed posterior end that overhangs the articular facet (e.g. AMNH 6341; CM 84, 94, 11984; DNMS 492, 1494; Hatcher, 1901; McIntosh, 2005; pers. obs. 2011). In CV 5 the spol and the podl unite at the very acute posterior end of the epipophysis. The spol extends straight and includes an acute angle of approximately 40◦ with the podl in lateral view in CV 3. In the more posterior elements this angle decreases to about 35◦ in CV 4 and 30◦ in CV 5.

Mid-cervical vertebrae (CV 6-10). Some of the mid-cervical vertebrae show minor compression, caused by shearing (CV 7, 8) or weak crushing (CV 10), but are completely preserved. They are well fused with the neural arches and the cervical ribs (Fig. 3.13). The vertebrae are longer than high, and higher than wide (Tab. 3.1). The opisthocoelous centra are axially long and somewhat higher than wide at their posterior end. With a mean EI of 3.5, the mid-cervical vertebrae constitute the most elongated centra of the series, which lies between the values reported for *Apatosaurus* or *Diplodocus* and *Barosaurus* (McIntosh, 1990b, 2005; Wedel et al., 2000). CV 6 is the most elongated element of the cervical column (Tab. 3.2).

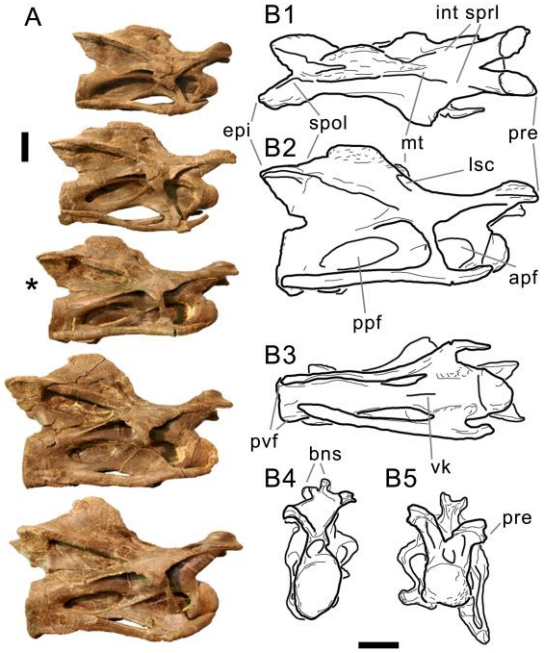

Figure 3.13: A, Photograph and B, drawings of the mid-cervical vertebrae of the holotype of *Kaatedocus siberi* (SMA 0004). Photograph in lateral view and to scale, CV 8 shown in the drawings is indicated by an asterisk. Drawings of CV 8 (B) in dorsal (1), lateral (2), ventral (3), posterior (4) and anterior (5) views. Scale bars = 4 cm.

In CV 7 to 10, the well-developed, hemispherical anterior condyle is separated from the rest of the centrum by a weak but easily discernible ridge extending anterodorsally–posteroventrally (CV 7 to 9), or subvertically (CV 10) on its lateral sides, and straight transversely dorsally and ventrally. Whereas in CV 6 to 9 the outline of the condyle is subcircular in anterior view, in CV 10 it is broader dorsally than ventrally. The surface of the articular ball and around its posterior ridge is irregular. The subdivision of the pleurocoel becomes subsequently more distinct from anterior to posterior, with even a weak subdivision of the anterior coel in CV 10. Here, faint ridges are located at about mid-height both anteriorly and posteriorly. Between the two pleurocoels, a relatively wide bony shelf develops in CV 8 (Fig. 3.13, B2) and more posterior elements, bearing an oblique, anteriorly inclined ridge extending from the posterodorsal corner of the anterior pneumatic fossa downwards and backwards, before it diminishes in about the middle of the bony shelf. The anterior pneumatic fossa of CV 8 to 10 shows a very gradual transition onto the bony shelf between the two depressions. Whereas in all mid-cervical vertebrae the pneumatic fossae are completely separated ventrally, a combined dorsal margin can still be seen in CV 6 and 7 (Figs 3.14, 3.15). The posterior fossa becomes more restricted posteriorly in more posterior elements, so that both the anterior and posterior portion together occupy less and less of the entire centrum length. The shape of their outlines remains practically the same in all mid-cervical vertebrae: the anterior coel is subcircular and relatively short, whereas the posterior coel is more lens-shaped with pointed ends anterodorsally and posteroventrally. In CV 8 the upper edge of the posterior pleurocoel is more curved than the lower margin (Fig. 3.13, B2).

In ventral view the vertebral centrum is broadest anteriorly where the parapophyses are situated. The transverse constriction of the mid-cervical centra migrates more posteriorly than the more anterior elements, so that it now marks the middle third. Whereas in CV 6 this portion is slightly transversely convex, it is flat to shallowly concave in more posterior vertebrae. The depression between the parapophyses is interrupted medially by a shallow ridge. This is only visible between the posterior end of the parapophyses and the narrowest point of the centrum but becomes more pronounced in the more posterior elements of the cervical series. The parapophyses point lateroventrally and are longer than wide. They are located beneath the anterior pneumatic fossa in lateral view, which extends slightly onto the dorsal surface of the parapophyses. At the base of the parapophysis a shallow ridge divides this extended coel into a dorsal portion (lying on the centrum) and a ventral part lying on the parapophysis.

Figure 3.14: Photographs of CV 6 of the holotype of *Kaatedocus siberi* (SMA 0004) in posterior (left), dorsal (top), right lateral (center), ventral (bottom), and anterior (right) views. Scale bar = 4 cm.

Figure 3.15: Photographs of CV 7 of the holotype of *Kaatedocus siberi* (SMA 0004) in posterior (left), dorsal (top), right lateral (center), ventral (bottom), and anterior (right) views. Scale bar = 4 cm.

The neural arch of CV 6 to 8 is dorsoventrally shorter relative to centrum length compared to the anterior cervical vertebrae and the more posterior elements. In all mid-cervical vertebrae it exceeds the centrum in length anteriorly but only very little posteriorly. The prezygapophyses project anteriorly, dorsally, and slightly laterally, beyond the anterior condyle. The articular facets are anteroposteriorly elongated and well offset from the rest of the prezygapophysis. The facets are transversely as well as anteroposteriorly convex and are supported ventrally by the cprl. Like the anterior cervical vertebrae the prezygapophyses of CV 6 are laterally flat and smooth. On the other hand, CV 7 to 10 exhibit an initially shallow, but in more posterior elements pronounced horizontal ridge that extends ventral and parallel to the articular facet, connecting the sprl with the prdl (Figs 3.15-3.18). Together they form a distinct anteriorly projecting spur that extends considerably beyond the anterior edge of the prezygapophyseal articular facet. A similar ridge and spur is also present in the holotype of *Australodocus bohetii* (MB.R.2455; Remes, 2007; pers. obs. 2011) and appears homologous to the pre-epipophysis described in *Euhelopus* and other titanosauriforms (Wilson and Upchurch, 2009; Whitlock, 2011c). Whereas the ridge is also present in a number of diplodocids (e.g. *Apatosaurus* sp. AMNH 550; *Diplodocus carnegii* CM 84; *Barosaurus* sp. CM 11984; pers. obs. 2011), it does not project beyond the anterior margin of the facets in these taxa. The spur can thus be considered a local autapomorphy of *Kaatedocus siberi*.

Posteroventral to the pre-epipophyseal ridge in CV 9 and 10 a distinct cavity marks the anterior-most extension of the sdf, which is relatively shallow. The cavity is bordered dorsally by the posterior-most extension of the pre-epipophysis and by the here laterally inclined anterior-most portion of the sprl. In CV 10 a second, indistinct crest is present subparallel to and between the facet and the pre-epipophysis. The anterior spur in CV 7 to 10 is ventrally confluent with the cprl as well, which borders the deep cprf. The tprl of all mid-cervical vertebrae form a V-shape in dorsal view, and meet the roof of the neural canal at their posterior-most extension.

The sprl becomes reduced to a shallow ridge towards the base of the prezygapophysis, before it curves dorsally again (Fig. 3.13, B1). Anteriorly, it connects to the posterolateral corner of the articular facet, as in the anterior cervical vertebrae. The curvature of the sprl in lateral view becomes more pronounced in the more posterior elements. The sudden posterior bend that marks the sprl of the previous cervical vertebrae also occurs in CV 6 and 7 but even closer to the level of the neural spine top, so that

the lamina extends almost horizontally towards the dorsal-most point of the spine. In CV 8 and 9 this last portion of the sprl is oriented straight horizontally, and thus forms the spine summit, whereas in CV 10 the sprl develops another backwards bend anteroventral to the summit. The lateral cavity of CV 6 and 7 is situated more dorsally than in the anterior cervical vertebrae but remains restricted to the lower half of the sdf in CV 8 to 10. It is much more distinct than in *Diplodocus carnegii* CM 84, and more ventrally located compared to *Barosaurus* sp. CM 11984 (Hatcher, 1901; McIntosh, 2005; pers. obs. 2011). Anterior and medial to the sprl, the median ridge is more developed than in any previous element, and bears a distinct anterior projection in CV 6 and 7. The ridge connects posteriorly with the now anteroposteriorly elongated area, where both sprl and spol unite to create a single neural spine summit. In CV 8 to 10, the anterior projection becomes lost, and the sprl and spol begin to develop dorsal projections that exceed the median ridge laterally, so that CV 8 and more posterior elements are the first to exhibit more and more bifurcated neural spines. This con-figuration shows that the median ridge probably represents the true neural spine, and is equivalent to the structure termed by Schwarz et al. (2007b) the median tuberosity, a flagellicaudatan synapomorphy (Whitlock, 2011a; Mannion et al., 2012). As with the lateral cavity within the sdf, the median tuberosity becomes reduced again in CV 8 to 10, and both structures remain restricted to about the same height.

The mid-cervical spine summit is rugose laterally and posteriorly offset from the rest of the spol. In anterior view, the transversely narrow metapophyses are subparallel to slightly laterally inclined. In dorsal view, the metapophyses of CV 8 to 10 have a very transversely compressed but subtriangular cross section, with a flat outer surface and an angled medial side. From this medial-most point a step-like structure extends anteroventrally and connects the top with the posterior corner of the true neural spine. The summit sits above the central third of the centrum length in CV 6 and 7, above the posterior second fifth in CV 8 and 9, and slightly more anteriorly in CV 10.

Figure 3.16: Photographs of CV 8 of the holotype of *Kaatedocus siberi* (SMA 0004) in posterior (left), dorsal (top), right lateral (center), ventral (bottom), and anterior (right) views. Scale bar = 4 cm.

Figure 3.17: Photographs of CV 9 of the holotype of *Kaatedocus siberi* (SMA 0004) in posterior (left), dorsal (top), right lateral (center), ventral (bottom), and anterior (right) views. Scale bar = 4 cm.

Figure 3.18: Photographs of CV 10 of the holotype of *Kaatedocus siberi* (SMA 0004) in posterior (left), dorsal (top), right lateral (center), ventral (bottom), and anterior (right) views. Scale bar = 4 cm.

The diapophysis overlaps the anterior second quarter of the centrum. It is formed by the prdl anteriorly, the podl posterodorsally, the pcdl posteriorly, and a short acdl anteroventrally. The podl is anteroposteriorly concave in dorsal view. In lateral aspect, it is gently curved in CV 6 and 7 but straight in CV 8 to 10. The angle that the podl forms with the base of the neural canal decreases from approximately 25◦ in CV 6 to 20◦ in CV 7 to 9 and finally to about 18◦ in CV 10. In the latter the podl is supported by a small accessory lamina immediately after it originates on the base of the diapophysis. This accessory lamina is well visible in posterolateral view, and its free edge faces posteriorly. The acdl separates the well-developed prcdf and the cdf. It extends upwards and backwards in its anterior portion, but curves to become almost vertical below the diapophysis. With the exception of CV 9 and the right side of CV 8, the posterior edge of the mid-cervical diapophyses develops a very short posterior projection similar to but much less pronounced than in CV 3 and 4. The articulation with the tuberculum in the mid-cervical vertebrae is weakly posterodorsally inclined.

The postzygapophyses are transversely deeply concave in posterior view. Whereas the postzygapophyses of CV 6 have rounded posterior edges in dorsal view, they are more pointed in CV 7 to 10. The articular facets are subtriangular, and wider than long. Their anterior edges mark the posterior extent of the postzygapophyseal centrodiapophyseal fossa. The tpol unite medially straight above the posterior edge of the centrum, and not slightly inset as in the previous vertebrae. In lateral aspect the neural arch thus describes a regular U-shape in its posteroventral corner, before it bends dorsally to follow the posterior margin of the postzygapophyseal articular facets. The epipophyses are less developed than in the anterior cervical vertebrae, but still overhang the articular facets both laterally and posteriorly. As in the anterior cervical vertebrae, both spol and podl insert in the epipophysis. The spol is straight in CV 6 and 10, but slightly convex in CV 7 to 9 (most so in the left spol of CV 7, where it forms a step-like configuration).

Posterior cervical vertebrae (CV 11-14). The posterior cervical vertebrae (Fig. 3.19) are complete and well preserved, although the bone surface is mildly crushed and slightly deformed in most elements. The vertebrae and cervical ribs are well-fused and the transition is rugose but not well marked by a line. The vertebrae as a whole are longer than high, and higher than wide, exhibiting increasing ratios towards a more posterior position in the cervical column (Tab. 3.1). The centra are strongly opisthocoelous and slightly higher than wide in posterior view. The EI of the posterior cervical vertebrae is approximately 3 in CV 11 and 12, decreasing to 2.6 in CV 13 and 14 (Tab. 3.2). The anterior condyle is very pronounced, hemispherical, and bordered by a ridge that is slightly anteriorly inclined (in CV 11 to 13) to almost vertical (in CV 14; Fig. 3.19, B2), and conspicuous in lateral and dorsal views but absent ventrally. The bone surface of the articular condyle is more rugose than the centrum.

Laterally, the centra of the posterior cervical vertebrae bear progressively more complex arrangements of laminae, ridges and depressions. In CV 11 two large pneumatic fossae form the main structure (Figs 3.19, C2; 3.20), together occupying about 60% of the lateral side. The anterior pneumatic fossa possesses two interior laminae that extend horizontally, the dorsal lamina being longer and more prominent. The anterodorsal rim of the pneumatic fossa is deep and well defined. The posteroventral part becomes shallower and grades into the ventrolateral wall of the centrum and the parapophysis. The upper part of the pneumatic fossa is axially longer than the ventral part and is pointed posteriorly. The posterior pneumatic fossa is approximately 1.5 times longer than the anterior, and has a lens-like shape. The posterior and anterior ends form an acute angle and the entire pneumatic fossa is deep and well invaginated. The two pneumatic fossae are separated by a 3 cm wide longitudinal shelf that progresses diagonally in an anterodorsal–posteroventral direction and is reinforced by a ridge.

The anterior pneumatic fossa of CV 12 (Fig. 3.21) is highly similar to its corresponding structure in CV 11. It has tall margins anteriorly and dorsally, but grades onto a bony shelf posteroventrally. It is extended ventrally to also occupy the dorsal surface of the parapophysis, and subdivided into three areas by two unequally developed horizontal ridges. The posterior pneumatic fossa of CV 12, on the other hand, is different from the previous one. Two depressions are well separated from each other, but still united dorsally, where an anteroposteriorly long margin extends from the anterodorsal-most point of the posterior pneumatic fossa backwards and slightly downwards until it disappears at about mid-height on the centrum, below the posterior-most point of the pedicels. The anterior half of this crest roofs a very distinct, subtriangular (on the right side) to rhomboidal (on

the left) depression. This depression is situated almost entirely beneath the pcdl, and bordered anteroventrally by the oblique bony shelf that also in the previous cervical vertebrae divides the anterior from the posterior coel. Ventrally, a broad ridge separates the larger anterodorsal subdivision of the posterior pneumatic fossa from a small oval depression posteroventral to it.

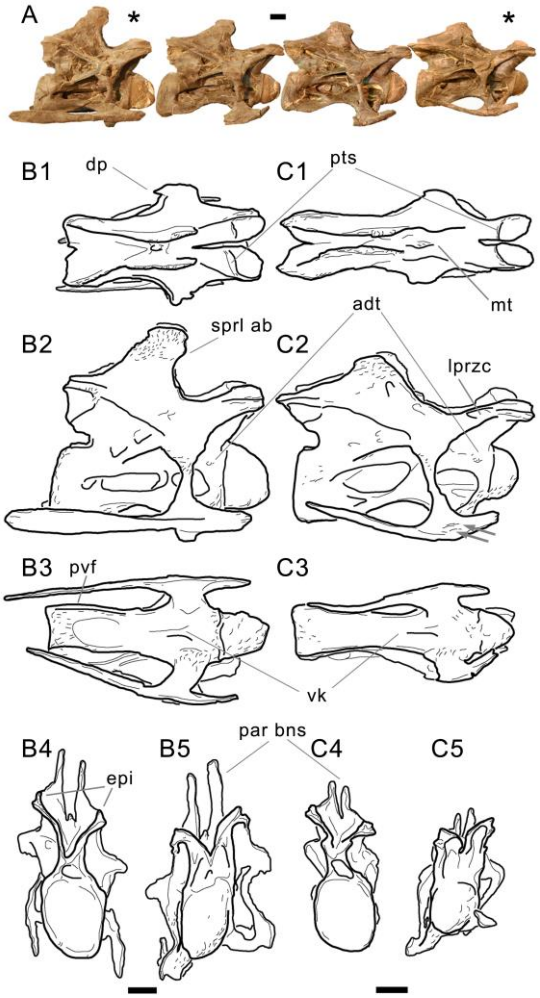

Figure 3.19: A, Photographs and B, C, drawings of the posterior CV of the holotype of *Kaatedocus siberi* (SMA 0004). Photographs in lateral view and to scale, elements shown in the drawings indicated by an asterisk. Drawings of CV 14 (B), and CV 11 (C) in dorsal (1), lateral (2), ventral (3), posterior (4) and anterior (5) views; scaled to the same centrum length, in order to highlight changes of proportions. Arrows in C2 mark possible bite marks. Scale bars = 4 cm.

The lateral surfaces of CV 13 are marked by two deep pneumatic fossae anteriorly and posteriorly, which are subdivisions of more extended depressions that include smaller cavities as well (Fig. 3.22). The general arrangement of these divided coels resembles the state in CV 12, except that the two most dorsal fossae are the most distinct and more anteroposteriorly elongated than in the previous element. Contrary to the state in CV 12, the more posterior of the two coels in CV 13 extends backwards beyond the posterior-most point of the pcdl. The small fossa that was clearly visible posteroventral to the subtriangular larger part of the posterior pneumatic fossa of CV 12 is reduced to a shallow concavity, of which the margins are unclear in CV 13. The portion of the centrum length that is occupied by the entire pleurocoelous structure decreases more or less continuously within the cervical column from 80% in CV 3 to 57% in CV 13.

In CV 14, two deeply invaginated pneumatic fossae represent the most distinct structures of the lateral surface (Figs 3.19, B2; 3.23). They are located anteriorly and posteriorly at the same level around mid-height on the centrum. Whereas both pneumatic fossae are of approximately the same dorsoventral height, the anterior coel is shorter anteroposteriorly by a third relative to the posterior

one. It is of rhomboidal shape and subdivided into smaller cavities by three ridges: an oblique, anteriorly inclined crest that separates the posterodorsal corner; a horizontal ridge that extends from the posteroventral end of the previous ridge anteriorly; and a shallow ridge originating at the same point but proceeding anteroventrally. As in the preceding vertebrae with subdivided pleurocoels, the two major pneumatic fossae of CV 14 are separated from each other by a ventrally oriented bony shelf. The latter bears a crest that originates at the posterodorsal corner of the anterior pneumatic fossa, and then proceeds ventrally before curving backwards to reach the posteroventral corner of the bony shelf. Here the ridge unites with the ventral edge of the posterior pneumatic fossa, which is antero-posteriorly elongated and slightly taller at the front than at the back. The dorsal edge of the posterior pneumatic fossa is straight and develops an almost horizontal bony strut at about midlength, which then proceeds anteriorly. Posteriorly, the dorsal rim exceeds the main coel to border a smaller depression behind the posterior pneumatic fossa, as in CV 12 and 13. This smaller cavity is sub-triangular in CV 14, with an acute posterior end, and an almost vertical anterior rim that separates it from the main posterior pneumatic fossa. In the middle of the latter coel, a narrow horizontal crest is visible that does not connect to other morphological landmarks. It might thus also represent taphonomic deformation as the median wall separating the pleurocoels of the two sides at the centrum midline is extremely thin.

In all posterior cervical vertebrae, a rugose tuberosity is situated at the anterodorsal corner of the lateral side of the centrum (Fig. 3.19, B2 and C2). This tuberosity would be in line with a straight, imaginary extension of the anterior portion of the acdl. In CV 12 and 13 a weak striation connects these two structures. The only taxon that shows a similar feature is the probable dicraeosaurid *Suuwassea emilieae* (ANS 21122, pers. obs. 2011), but only in mid-cervical vertebrae (posterior cervical vertebrae are unknown in this taxon; Harris, 2006a). The anterodorsal tuberosity can thus be considered at least a local autapomorphy (within Diplodocidae) of *Kaatedocus siberi*.

Figure 3.20: Photographs of CV 11 of the holotype of *Kaatedocus siberi* (SMA 0004) in posterior (left), dorsal (top), right lateral (center), ventral (bottom), and anterior (right) views. Scale bar = 4 cm.

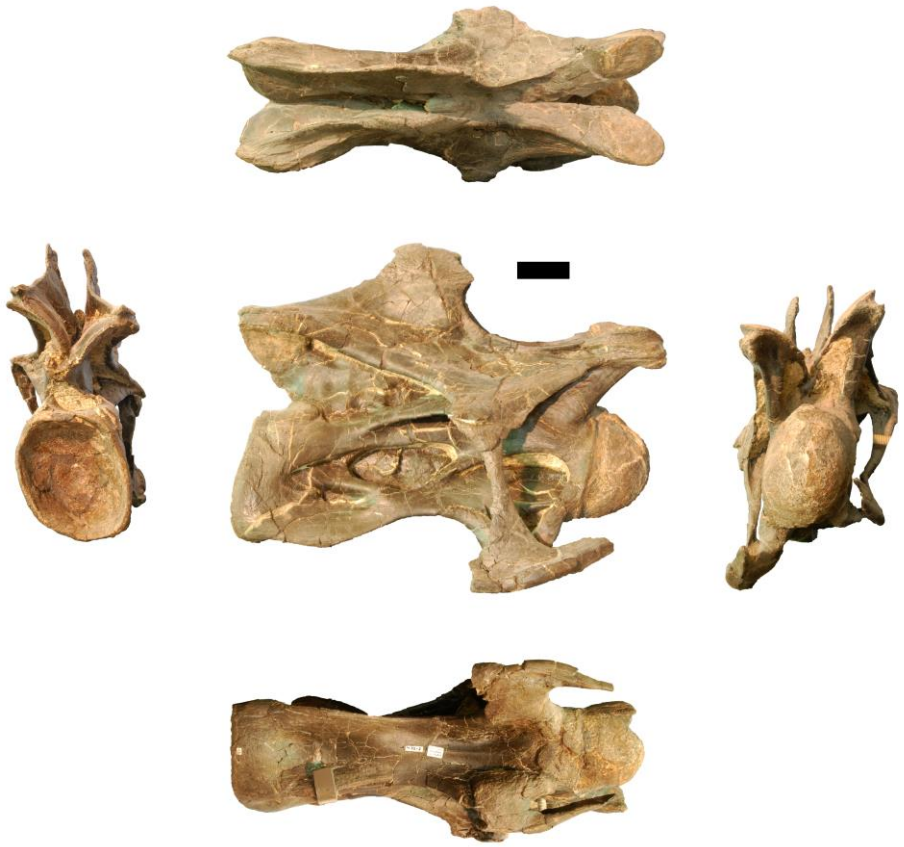

Figure 3.21: Photographs of CV 12 of the holotype of *Kaatedocus siberi* (SMA 0004) in posterior (left), dorsal (top), right lateral (center), ventral (bottom), and anterior (right) views. Scale bar = 4 cm.

Figure 3.22: Photographs of CV 13 of the holotype of *Kaatedocus siberi* (SMA 0004) in posterior (left), dorsal (top), right lateral (center), ventral (bottom), and anterior (right) views. Scale bar = 4 cm.

Figure 3.23: Photographs of CV 14 of the holotype of *Kaatedocus siberi* (SMA 0004) in posterior (left), dorsal (top), right lateral (center), ventral (bottom), and anterior (right) views. Scale bar = 4 cm.

In ventral view the centrum of the posterior cervical vertebrae of SMA 0004 is hourglass-shaped with a medium transverse constriction, which becomes less pronounced in more posterior elements. The surface is marked by two deep concavities, an anterior one bordered by the condyle and the two parapophyses, and a posterior one enclosed by the cotyle and two posteroventral flanges. The anterior concavity is subdivided by a midline ridge, which is located in the second quarter of the centrum length, and disappears at or somewhat anteriorly to the most constricted portion of the ventral surface. It is more distinct in more posterior vertebrae. The pair of flanges projects ventrally from each lateral side of the posteroventral corner of the centrum, but does not extend to the ventral-most rim of the cotyle. The flanges seem to clasp the distal end of the cervical ribs in some elements, but to what degree this is caused by taphonomic deformation is difficult to discern. If this represents the actual morphology it would probably be another autapomorphy of the new taxon. The parapophyses are at least twice as long as they are dorsoventrally high. They are positioned below the anterior pneumatic fossa in the first half of the centrum, and project to a small degree ventrolaterally.

The neural arch undergoes considerable changes throughout the posterior cervical vertebral series. It becomes both anteroposteriorly shortened, as well as dorsally elongated, and wider across the diapophyses towards more posterior positions. Whereas in CV 11 and 12 the neural arch still slightly surpasses the anterior or posterior rims of the centrum, CV 13 and 14 have subequally long arches and centra. The neural arch height/greatest length ratio remains around 30–40% in CV 3 to 11, but increases to 45% in CV 12, 56% in CV 13, and 60% in the last preserved vertebra. A similar increase can be observed in the width across diapophyses/greatest length ratio: this steadily rises from 30% in CV 6 to 39% in CV 11 and 42% in CV 12, after which it rises significantly to 59% in CV 13 and 67% in CV 14. In lateral view, also the orientation of the bifurcated neural spine changes within the

posterior cervical vertebrae. In CV 11 (as also in the mid-cervical elements), the anterior corner of the spine summit marks the posterior-most extension of the sprl (Fig. 3.19, C2). In CV 12, the summit is located more anteriorly, arriving vertically above the posterior-most point of the now considerably curved sprl. This trend continues in CV 13 and 14, where the spine tops become even anteriorly inclined.

The prezygapophyseal facets are oblong to subtriangular, straight laterally and tapering somewhat posteromedially. They face dorsomedially and are slightly convex transversely. In anterior view the facets thus form a V. The distance between the two prezygapophyses is shorter than the width of a single zygapophysis, but this might be due to transverse taphonomic compression. The posterior rim of the articular facet is well marked and bordered by a ridge followed by a transverse sulcus. To our knowledge such a sulcus is not present in any other diplodocid species, nor has it been reported from other sauropod taxa. It can thus be considered a true autapomorphy of *Kaatedocus siberi*. On the lateral aspect of the prezygapophyses of the CV 11 and 12 of SMA 0004, a second, parallel ridge – dorsal to the pre-epipophysis – progresses horizontally and subparallel to the articular facets. This second ridge is less conspicuous than the pre-epipophysis. The upper ridge is confluent with the sprl posteriorly. As in CV 10, the sdf in CV 11 to 13 forms a deep cavity posteroventrally to the pre-epipophysis and the second ridge. The pre-epipophysis extends slightly anterior to the prezygapophysis and forms the anterior-most point of CV 11 to 13. It gets slightly reduced in CV 14. Its anterior end unites with the prdl in CV 11 and 12, but remains independent in CV 13 and 14. Ventrally, the prezygapophysis is supported by strong cprl that remain undivided in CV 11, but show shallow centroprezygapophyseal lamina fossae in CV 12 to 14. The relative strengths of the medial and lateral branches of the cprl change from one vertebra to the other. In all three elements, the right cprl is more divided than the left, forming a left–right asymmetry. In CV 12 both branches are subequally developed, CV 13 has a stronger medial, and CV 14 a slightly better built lateral portion. The division of the cprl was considered synapomorphic for Diplodocidae (Wilson, 2002; Remes, 2007; Sereno et al., 2007; Whitlock, 2011a). Medially, the prezygapophyses are united by a thin tprl.

Whereas the sprl is interrupted at the base of the prezygapophysis in CV 11, it can be followed without problems throughout its entire length in the more posterior elements. The sprl gets progressively more curved from CV 11 to 14, and almost describes a U-shape in last two preserved elements. At its dorsal end, just below the neural spine summit, the sprl develops a rounded (CV 13 and 14) to rather pointed (CV 11 and 12) anterior bulge, similar to the state in *Diplodocus carnegii* CM 84 and *Barosaurus lentus* YPM 429 (Hatcher, 1901; pers. obs. 2011). This anterior bulge can thus be considered a diplodocine synapomorphy.

Between the two metapophyses of the divided posterior neural spine of SMA 0004 the true neural spine is atrophied into a median tubercle. Each one of the metapophysis summits is much longer than broad. In lateral view, the summit is topped by a horizontal table. The metapophyses are laminar, and very compressed transversely. Whereas the lateral surface of the posterior neural spines does not bear such distinct, dorsoventrally long cavities as in the mid-cervical vertebrae, CV 11 still exhibits a small anterior indentation, dorsal to the uppermost extension of the median tubercle (Fig. 3.19, C2). This depression is somewhat set back from the sprl and thus is probably not homologous to the elongated fossa on the posteroventral to the sprl of the previous elements. More anteriorly, where the homologous structure would be expected, there is a much less defined and more rounded depression in CV 11, which can also be observed in the more posterior elements. The distal end of the metapophyses is laterally marked by a rugose surface that extends ventrally to a height just below the anterior bulge of the sprl. On their medial side the metapophyses of all posterior cervical vertebrae bear a ridge formed by a step like structure that extends to meet the median tubercle. While the spine summit migrates anteriorly, the median tubercle remains located above the middle of the centrum in lateral view. The ridge on the medial surface of the metapophyses therefore changes its orientation within the series. In CV 11 and more anterior elements, it extends anteroventrally to meet the posterior extension of the median tubercle. In CV 12, it is oriented vertically, and in CV 13 and 14, it is anteriorly inclined and connects to the anterior end of the median tubercle.

The diapophysis of the posterior cervical vertebrae is situated in the second quarter of the vertebra, above the posterior portion of the anterior pneumatic fossa. It is axially long but not very projected transversely and bends ventrally towards its lateral end, forming a gentle curve. The articular end projects slightly anteroventrally in CV 11 and 12, and vertically in CV 13 and 14. The diapophysis

unites four laminae: the prdl anterodorsally, the podl posterodorsally, the acdl anteroventrally, and the pcdl posteroventrally. Whereas the pcdl as well as the prdl are oriented relatively straight horizontally in CV 11 to 13, CV 14 has considerably elevated diapophyses and prezygapophyses. Both the prdl and pcdl are thus distinctly anteriorly inclined. In CV 13 and 14, the prdl borders a deep prcdf together with the cprl medially and the acdl posteriorly. The prcdf is further marked by one (CV 13) or two (CV 14) distinct depressions on its medial wall. In all posterior cervical vertebrae, the acdl originates on the centrum and proceeds subparallel with the podl until it reaches the center of the ventral surface of the diapophysis. There it bends to extend vertically outwards onto the diapophysis–tuberculum complex, so that the dorsal portion of the latter has a subtriangular cross section. No posterior projection is present in CV 11 and 12, and only a short but pointed spur or a slight rugosity are visible in the left diapophysis of CV 14 and the right of CV 13, respectively. The pcdl and the podl of CV 11 have a small vertical lamina that unites them, with the free edge facing posteriorly. This accessory lamina thus subdivides the pocdf into two smaller cavities. The more posterior elements do not show this feature, but exhibit short ridges originating around midlength on the dorsal face of the pcdl and extending vertically before disappearing on the lateral wall of the neural canal. The cdf of CV 11 to 14 is deeply invaginated, and marked by a progressively more distinct, small cavity at its dorsomedial acute corner.

The postzygapophyses form a V in posterior view and are strongly concave transversely. Dorsally to the postzygapophyses the epipophysis is confluent with the spol, as well as with a horizontal ridge connecting to the podl that is subparallel to the postzygapophyseal facet. The epipophysis forms a pointed posterior projection overhanging the zygapophysis in CV 11 to 13, but not in CV 14. The articular facets are distinct from the postzygapophyseal process dorsally, but grade into the tpol ventrally. The latter connects the two postzygapophyses ventrally above the midline of the neural canal, but projects posteriorly and terminates above the posterior edge of the centrum. It forms a U-shaped notch in lateral view, with the rounded portion facing anteriorly, and the two parallel sides being represented by the horizontal dorsal centrum and the posteriorly projecting tpol. The course of the spol is bipartite in CV 11 and 12, being straight along most of its extent in both lateral and dorsal view, until it curves dorsally (in lateral view) to support the horizontal table of the neural spine summit. In CV 13 and 14, the spol extends anteriorly in a very acute angle to the podl, to a position above the posterior-most extension of the pcdl, at about half of its length. There it curves more dorsally and becomes somewhat convex. Below the summit table, it bends straight dorsally as in CV 11 and 12.

Cervical ribs

The ribs are well fused to the vertebra, which renders the distinction between the tuberculum and diapophysis difficult. The cervical ribs are usually shorter than the centrum length. However, in CV 3, 12 and 14, they protrude slightly beyond the posterior centrum wall (Figs 3.9, C2, C3; 3.19, B2, B3). Due to the dorsoventrally higher posterior than anterior end of the vertebral centrum, the ribs – although protruding somewhat ventrally at the parapophyses – do not increase the maximum height of the vertebrae to a significant degree. However, overhanging cervical ribs are absent in other diplodocid taxa apart from *Dinheirosaurus*. The latter and *Kaatedocus siberi* can thus be considered plesiomorphic for this trait. Whereas in the anterior cervical ribs the tuberculum is inclined distinctly posteriorly to meet the diapophysis, in mid-cervical and posterior cervical ribs the inclination decreases and CV 13 and 14 have an almost vertical diapophysis–tuberculum complex. The proximal end of the tuberculum is slightly subtriangular in cross section initially but becomes transversely flattened ventrally. The tuberculum is at least three times longer than the capitulum, which is axially long, dorsoventrally short and moderately projected medially. All cervical ribs have a pronounced anterior projection that represents from about one-fifth of the length of the rib in CV 3, 7 and 11, to approximately one-third in CV 5 and 8. The rib shaft is often somewhat deformed but appears to be slightly bowed, with the anterior and posterior extremes curving dorsally and often ending above the ventral-most point of the posteroventral flanges of the centrum. In anterior to mid-cervical ribs the shaft is slender and subcircular to subtriangular in cross section with the longer side facing medially, and the shorter sides laterodorsally and ventrolaterally. Posterior elements are more robust and mediolaterally flattened. The depth of the shaft is constant in lateral view, so its dorsal and ventral rims are subparallel until they taper at their ends. The only exceptions are CV 8 to 10 where the cervical

ribs show a distinct dorsoventral expansion shortly after midlength, before they taper towards their posterior extreme. A few cervical ribs show special morphologies that do not appear on other elements: cervical rib 4 exhibits a distinct bend and slightly rugose area that probably represents reactive bone growth after a fracture of the cervical rib shaft (Fig. 3.11). Furthermore, the lateral side of cervical rib 11 exhibits two slot-like depressions on the right ventrally to the tuberculum (Fig. 3.19, C2, arrows). These might represent bite marks, which would be the only ones in the specimen.

Phylogenetic analysis

The phylogenetic analysis is based on Whitlock (2011a; modified by Mannion et al., 2012),with the addition of some characters from Upchurch et al. (2004b), Harris (2006b), Lovelace et al. (2007), Whitlock and Harris (2010), Whitlock (2011a) and 23 newly defined characters based on the description of SMA 0004 (see Supplementary Material). Previously performed preliminary analyses using unchanged existing matrices (Upchurch et al., 2004b; Harris, 2006b; Whitlock, 2011a) recovered SMA 0004 consistently inside Diplodocinae (Tschopp et al., 2013). Therefore, several changes concerning terminal taxa were introduced. The incomplete basal diplodocoid *Haplocanthosaurus* and all rebbachisaurids except for *Limaysaurus* were omitted as their positions in the past have been controversial (Wilson, 2002; Upchurch et al., 2004a) or poorly resolved (Mannion et al., 2012). The relatively complete *Nigersaurus* and *Brachytrachelopan* were deleted from the matrix because they represent very specialized forms within Rebbachisauridae and Dicraeosauridae, respectively, and therefore bear little additional information on diplodocid ingroup relationships. Furthermore, outgroup taxa with respect to Diplodocoidea were reduced to the very well-known basal macronarian *Camarasaurus* and the non-neosauropod eusauropod *Omeisaurus.* Within Diplodocidae, the multi-species genera *Apatosaurus* and *Diplodocus* are considered monophyletic, which was supported for *Apatosaurus* in the specimen-based phylogenetic analysis of Upchurch et al. (2004b). Additional coding for modified and new characters of *Apatosaurus* was based on *A. louisae*, as this species is the most complete and best reported in the genus. In contrast, *Diplodocus* is still pending a detailed review of its species-level taxonomy. As this would exceed the scope of the current study, we have adopted the coding of the original studies for the unmodified characters, but concentrate on *D. carnegii* in the coding for the modified and new characters. The final analysis thus includes 14 taxa and 234 characters. The sources for the modified scoring in original characters as well as the coding in the modified and new characters are given in table 3.3.

Two different analyses were conducted using the heuristic search in WinClada 1.00.08 with 50 replicates. In the first, all multi-state characters were treated as unordered, whereas in the second run, nine of the total 22 multi-state characters were ordered, seven based on the fact that they describe either continuous ratios or vertebral counts. The remaining two ordered characters are 34 and 97. The former describes the laterally projecting spur, which is most probably an extension of the dorso-ventrally elongated lateral ridge (character state 1) present in, for example, *Diplodocus*. Character 97 describes the bifurcation of the cervical vertebrae, which starts in anterior elements in *Diplodocus* but more posteriorly in SMA 0004 and other taxa. The bifurcation is considered to happen continuously from the back to the front (Woodruff and Fowler, 2012) during ontogeny. Basing on Haeckel's rule that phylogeny recapitulates ontogeny, the development of this bifurcation in adult specimens should replay this continuous change, and an ordering of this character therefore appears reasonable.

Both analyses produced the same result (Fig. 3.24). *Kaatedocus siberi* is therefore recovered within Diplodocinae, as sister group to a polytomy including *Tornieria africana* + *Barosaurus lentus* + *Diplodocus*. The recovered Nelsen consensus tree (based on six equally parsimonious trees retained in the original analysis) has a length of 388 steps, a consistency index of 64%, and a retention index of 57%.

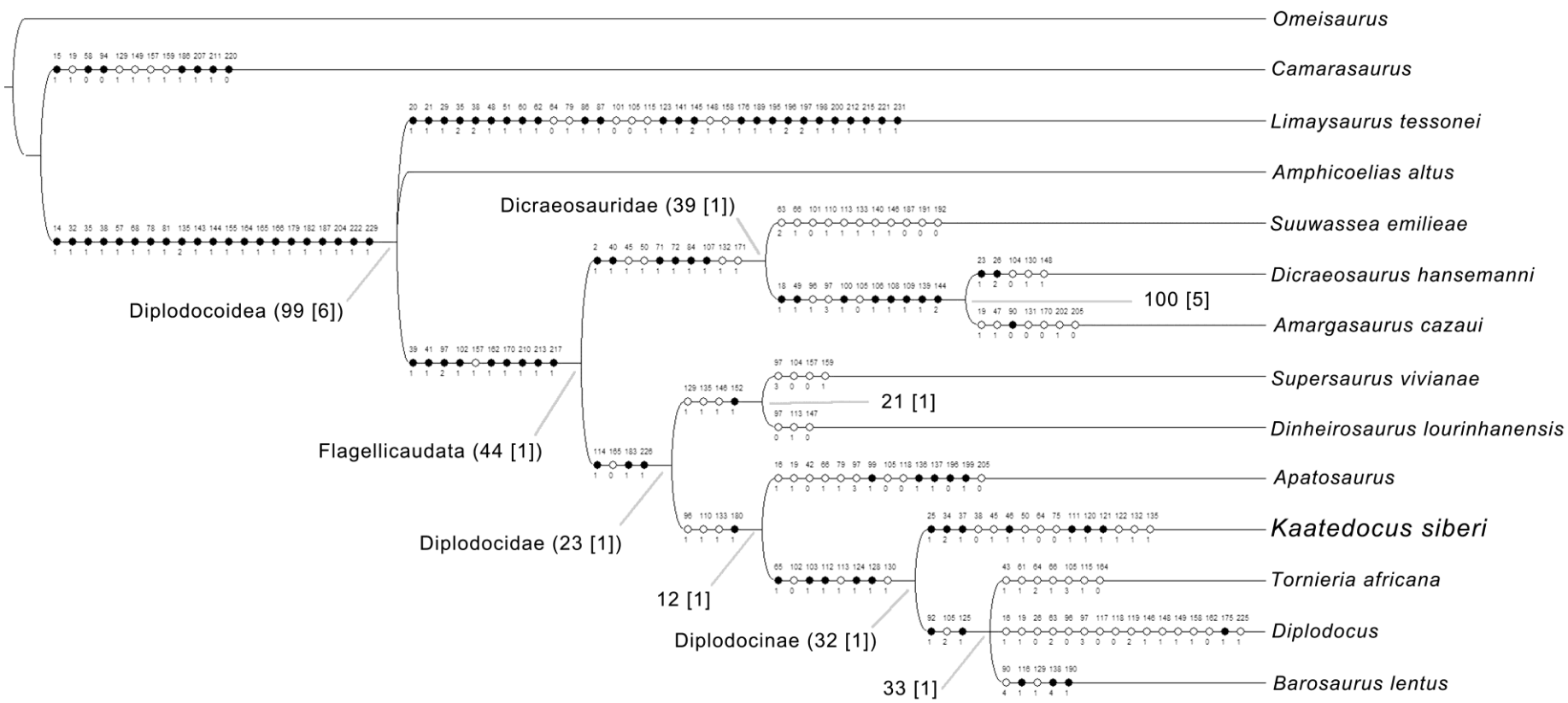

Figure 3.24: Nelsen Consensus tree obtained from a heuristic search in WinClada (six most parsimonious trees; tree length = 388; CI = 64%; RI = 57%). Dots indicate ambiguous (white) and unambiguous (black) synapomorphies, and autapomorphies of the respective clade. The corresponding character number and scoring is indicated above and below the dots, respectively. Main clades are indicated by their name, and bootstrap as well as Bremer Support values are given for each node (Bremer Support in square brackets). *Kaatedocus siberi* is resolved as Diplodocinae more basal than *Tornieria africana*, *Barosaurus lentus* and *Diplodocus*.

Comparison with other diplodocids

The Morrison Formation has produced the most diverse diplodocid fauna worldwide, including at least 12 taxa currently considered valid (see above). The vast majority of described taxa of this clade come from this Upper Jurassic formation, with only a few exceptions from Europe and Africa. The abundance of diplodocids and their diversity was recognized in the early years of palaeontology (Marsh, 1877a, 1878, 1890; Osborn, 1899; Hatcher, 1901; Holland, 1915; Gilmore, 1932, 1936), and new diplodocid or closely related taxa are still being recovered (Jensen, 1985; McIntosh et al., 1992; Filla and Redman, 1994; Harris and Dodson, 2004).

Although several diplodocid species have been reported previously, specimen SMA 0004 can be undoubtedly distinguished from all of these (Fig. 3.24). The present phylogenetic analysis recovers 15 autapomorphies in SMA 0004, seven of them unambiguous (but see detailed discussion below). It can be confidently identified as diplodocid, due to the hooked posterior process of the prefrontal, the absence of a contact between the squamosal and the quadratojugal, the 14–15 cervical vertebrae, and the divided cprl in mid- and posterior cervical vertebrae (Upchurch, 1995, 1998; Wilson, 2002; Harris, 2006b; Whitlock, 2011a; Mannion et al., 2012). It is easily distinguishable from *Apatosaurus* by its more slender cervical vertebra, and cervical ribs that do not project far ventrally (Gilmore, 1936; Upchurch et al., 2004b). An attribution of SMA 0004 to *Supersaurus* can be excluded due to its small size and the much less elongated mid-cervical centra (see Lovelace et al., 2007). *Dinheirosaurus* differs from *Kaatedocus siberi* as it appears to have unbifurcated neural spines, as well as a groove posterior to the parapophyses, marking the ventrolateral edges of the posterior cervical centra (Mannion et al., 2012) – both local autapomorphies of *Dinheirosaurus* within Diplodocidae. *K. siberi* differs from the more derived *Barosaurus*, *Tornieria* and *Diplodocus* in the absence of a small, anteroposteriorly elongate fossa posteroventral and separate from the main pleurocoel, relatively short mid-cervical vertebrae, and the lack of a vertical accessory lamina posterior to the sprl of posterior cervical vertebrae (unknown in *Tornieria*).

As some of the distinguishing features have previously been interpreted as ontogenetic, a more detailed comparison is appropriate between SMA 0004 and more derived diplodocine species (including *Tornieria africana*, *Diplodocus longus*, *D. carnegii*, *D. hayi* and *Barosaurus lentus*). Whereas *T. africana* was found in Tanzania (Fraas, 1908; Sternfeld, 1911; Remes, 2006), all species of *Diplodocus* as well as *B. lentus* are only known from the Morrison Formation (Marsh, 1878, 1890; Hatcher, 1901; Holland, 1924). The two latter genera were reported from the Howe Quarry by Brown (1935) but this identification was not accompanied or followed by a thorough scientific analysis and description. Two well-preserved necks from the AMNH 1934 excavation at Howe Quarry are tentatively identified as *Barosaurus* (AMNH 7530 and 7535; Michelis, 2004). Both are of approximately the same size as SMA 0004, show disarticulated skull material, but have never been described in detail (Brown, 1935; Michelis, 2004). Other diplodocine specimens comparable in size to SMA 0004 are very rare. The only other well-described specimen is a juvenile *Diplodocus* skull (CM 11255; Whitlock et al., 2010).

Comparison of *Kaatedocus siberi* with *Barosaurus lentus* and *Tornieria africana* is hampered due to little overlap in the incomplete reported specimens, which is probably also the reason for the relatively low bootstrap values in the recovered phylogenetic tree (see Fig. 3.24). Both of these taxa show very elongated cervical vertebrae (McIntosh, 2005; Remes, 2006). Wedel et al. (2000) reported an increase of the EI in *Apatosaurus* of 35–60%, comparing very young individuals to adults. SMA 0004 has an elongation index about 82% of that of *Diplodocus carnegii* CM 84, and 66% of *B. lentus* AMNH 6341 (Hatcher, 1901; Wedel et al., 2000; McIntosh, 2005). The increase during ontogeny would thus be 22% to reach the ratio in *Diplodocus*, or 52% for *Barosaurus*. As a very young age for SMA 0004 can be excluded due to the complete neurocentral fusion, the ratio has to be lower than that spanning practically the entire ontogeny in *Apatosaurus* (Wedel et al., 2000). An allometric growth strong enough to reach the elongation of *Barosaurus* or *Tornieria* thus appears improbable. Furthermore, the braincase identified as *T. africana* (MB.R.2386; Remes, 2006) can be distinguished from SMA 0004 by the curved instead of straight dorsal edge of the posterolateral process of the parietal, the narrow width of the basal tubera and their U-shaped anterior border, as well as the presence of a foramen in the notch separating them (Janensch, 1935; Remes, 2006). Besides having a much more elongated centrum, the only preserved cervical vertebra of *T. africana* (MB.R.3816; Remes, 2006) does not show a ventral ridge (Remes, 2006). Of the possible additional *Tornieria*

specimens, a dentary (MB.R.2347) is less squared than that of *Diplodocus* CM 11161 but also less rounded than that of SMA 0004. However, assignment of MB.R.2347 to *T. africana* is uncertain (Remes, 2009), and therefore this difference remains doubtful. Besides the cervical vertebral elongation and the snout shape, none of the aforementioned characters have previously been interpreted as being affected by ontogenetic changes in sauropods. These characters are thus considered sufficiently distinct and independent from ontogeny that a generic separation from *T. africana* is reasonable for *K. siberi*.

A separation of *Kaatedocus siberi* from *Barosaurus lentus* is equally well supported. Apart from the improbable enormous allometric growth necessary for the cervical vertebrae of SMA 0004 to reach the elongation index of *B. lentus* (McIntosh, 2005), three more morphological characters can be put forward to distinguish these two taxa (plus the unambiguous autapomorphies of *K. siberi*). *B. lentus* YPM 429 exhibits a bifurcate anterior end of the pcdl, and postzygapophyses that terminate anterior to the posterior margin of the posterior cervical centra (Lull, 1919; pers. obs. 2011). Furthermore, the ventral keels in the cervical vertebrae of the *B. lentus* holotype YPM 429 show a quite different morphology from the single anterior ridge in SMA0004: in YPM 429 two crests extend obliquely from between the parapophyses posterolaterally to unite with the posteroventral flanges (Lull, 1919; pers. obs. 2011). Adding the recovered autapomorphies of *K. siberi*, a generic distinction from *Barosaurus* can be justified.

Diplodocus is the most abundant diplodocine sauropod in the Morrison Formation. The initial provisional identification of SMA 0004 as *Diplodocus* by Ayer (2000) shows that a separation from this taxon is the most difficult. *Diplodocus* is the only diplodocine for which a juvenile skull has been reported (CM 11255), and this specimen superficially looks much like SMA 0004 (Whitlock et al., 2010). Differences between CM 11255 and *Diplodocus* skulls of older individuals (CM 3452 and 11161) include a rounder snout shape, maxillary teeth that reach further posteriorly, and a relatively larger orbit (Whitlock et al., 2010). These are traits that also distinguish *Kaatedocus siberi* from *Diplodocus*. More detailed comparisons of SMA 0004 with the subadult and juvenile *Diplodocus* skulls CM 3452 and 11255 show that some of the recovered autapomorphies of *K. siberi* are actually shared with the latter specimens, and might therefore be ontogenetic. These include the lateral spur on the lacrimal, the ridge on the paroccipital processes, and the straight orientation of the anterior edge of the basal tubera, traits present in both CM 3452 and 11255 but absent in adult *Diplodocus* skulls (AMNH 969; CM 11161; USNM 2672, 2673; pers. obs. 2011). Furthermore, the shallow fossa medial to the pterygoid ramus of the quadrate is also observable in CM 3452, but neither in CM 11255 nor in the above mentioned adult specimens (pers. obs. 2011). Other more widespread features shared with the juvenile and absent in the adult stages are the prefrontal that does not reach far posteriorly, and relatively more elongate frontals in CM 3452 and SMA 0004 (both unknown in CM 11255). The shallow groove that accommodates both the subnarial and the anterior maxillary foramen in CM 3452, 11161, as well as USNM 2672, is lacking in CM 11255 and SMA 0004 (Whitlock et al., 2010; pers. obs. 2011). The basipterygoid processes of SMA 0004 resemble more their corresponding structures in CM 11255, than in CM 3452 and 11161. In the latter, subadult to adult specimens, the processes are straight along their entire extent, and without a curved shelf that connects the base of the processes. In SMA 0004 and CM 11255, such a shelf is present, and throughout its extent, it keeps the processes subparallel in ventral view, before they curve laterally.

Other osteological features in SMA 0004 more closely resemble adult *Diplodocus* skulls than CM 11255. The squamosal of CM 11255 was shown to have an elongated anterior process that almost contacts the quadratojugal, whereas in adult skulls (and also in SMA 0004) these two bones are well separated (Whitlock et al., 2010; CM 11161; USNM 2672, 2673, pers. obs. 2011). Furthermore, the dorsal margin of the quadrate is concave in lateral view in CM 11255 but fairly straight in adult *Diplodocus* and *Kaatedocus siberi* (Whitlock et al., 2010; CM 11161; USNM 2672; pers. obs. 2011). The foramen present on the surangular in SMA 0004 appears to be lacking in CM 11255 (Whitlock et al., 2010), which indicates that in *Diplodocus* this foramen only develops during ontogeny.

Despite these similarities, several features present in SMA 0004 but absent in any *Diplodocus* skull indicate that the specimen described here is distinct from *Diplodocus.* The location of the frontal–parietal suture is more similar to its position in MB.R.2386 than in the *Diplodocus* skulls CM 11161 and 11255. Whereas in the *Diplodocus* skulls the suture is quite anteriorly placed with respect to the supratemporal fenestra, in both SMA 0004 and MB.R.2386 it is situated more posteriorly, around

the center of the opening in dorsal view (Remes, 2006; Whitlock et al., 2010; pers. obs. 2011). The basal tubera are closer to the occipital condyle in SMA 0004, resembling more the state in *Suuwassea emilieae* ANS 21122 than in *Diplodocus* skulls CM 11161 and 11255 (Harris, 2006c; Whitlock et al., 2010; pers. obs. 2011). There is no indication of a basipterygoid recess posterior to the basal tubera, a trait previously used to distinguish *Apatosaurus* from *Diplodocus* where such a recess is present (Wilson, 2002; Whitlock et al., 2010). Additionally, SMA 0004 has a closed preantorbital fossa, similar to the state in *Dicraeosaurus hansemanni* MB.R.2336. As both *Apatosaurus* (CM 11162) and *Diplodocus* (including the juvenile CM 11255) show a distinct, open, oval preantorbital fenestra (Berman and McIntosh, 1978; Whitlock et al., 2010), the retention of the plesiomorphic state in SMA 0004 can be considered taxonomically important. Furthermore, the tooth count in both the maxillae and the dentaries of SMA 0004 is higher than usual for *Diplodocus* (12–13 versus 9–11; Holland, 1924; Barrett and Upchurch, 1994; Calvo, 1994; Whitlock et al., 2010; CM 11161, 11255, pers. obs. 2011), and appears equal to *Apatosaurus* CM 11162 (Berman and McIntosh, 1978; Calvo, 1994; pers. obs. 2011). Although a reduction in the number of teeth during ontogeny was proposed for *Camarasaurus* (McIntosh et al., 1996), the fact that CM 11255 shows the average number of teeth known in adult *Diplodocus* skulls indicates that the higher number in SMA 0004 most probably represents taxonomic diversity.

Possible diplodocid species from North America that were not included in this analysis are *Eobrontosaurus yahnahpin*, *Dystrophaeus viaemalae* and *Dyslocosaurus polyonychius*. However, *E. yahnahpin* has previously been interpreted as being a camarasaurid (Upchurch et al., 2004a), and thus most probably cannot be considered a diplodocine. Moreover, a distinction is easily made using the elongated neural spines in the anterior cervical vertebrae and the widely transversely projecting parapophyses (Filla and Redman, 1994; P. Mannion, pers. comm. 2011). Comparisons with the other two taxa are impossible as they are very fragmentary and do not show any overlap (Cope, 1877b; McIntosh et al., 1992). Nonetheless, both remains are of larger animals than SMA 0004, and the difference appears too much to be explained by individual or sexual variation, even considering that SMA 0004 might still have been in the growth phase.

Autapomorphies of *Kaatedocus siberi*

The recovered autapomorphies of *Kaatedocus siberi* are discussed in detail below. As the discussion will show, some of these features are actually shared with farther related taxa that were not included into the present phylogenetic analysis, or with single specimens of included genera. They were therefore excluded or defined as local autapomorphies in the diagnosis of *K. siberi* (see above).

The U-shaped notch anteriorly between the frontals is recovered as an unambiguous autapomorphy. Diplodocid skulls usually have frontals that contact each other and fuse along their entire medial edge so that their anterior borders form a single straight line that connects to the nasals (Berman and McIntosh, 1978; Wilson and Sereno, 1998; Whitlock et al., 2010). In SMA 0004 the medial margin of the frontals curve laterally in their anterior half. A similar morphology can be seen in the partial skull of *Spinophorosaurus nigerensis* (Knoll et al., 2012) and the holotype specimen of *Diplodocus hayi* HMNS 175, but in these specimens it is V- and W shaped, respectively, and not U-shaped as in *Kaatedocus siberi*. *D. hayi* has previously been doubted to be congeneric with *Diplodocus* (Foster, 1998). The difference in the frontals indicates that this hypothesis might prove to be correct, and its similarity to SMA 0004 could imply that HMNS 175 should group with *Kaatedocus siberi*. On the other hand, several differences in the rest of the skull (e.g. orientation of the basipterygoid processes) and also the cervical vertebrae (e.g. dorsally expanded bifid neural spines already in anterior cervical vertebrae) preclude an assignment of SMA 0004 to *D. hayi* (Holland, 1906, 1924; HMNS 175, pers. obs. 2010). The only partially conjoined frontals in SMA 0004 could also be interpreted as not entirely fused, and indicate an early juvenile age for the animal. However, embryonic skulls of the basal sauropodomorph *Massospondylus* show tightly appressed right and left frontals along their entire medial edge (Reisz et al., 2005), and the subadult skull of the titanosauriform *Bonitasaura salgadoi* has a frontal with an entirely straight medial margin (Gallina and Apesteguía, 2011). This indicates that the outwards curve in the frontal of SMA 0004 is not an ontogenetic feature but is instead taxonomically significant and an unambiguous autapomorphy of *K. siberi*.

The laterally projecting spur is another unambiguous autapomorphy as recovered from the phylogenetic analysis. However, as stated above, the juvenile and subadult *Diplodocus* skulls CM 11255 and 3452 also show this feature, and therefore the influence of ontogeny cannot be ruled out, even though bony spurs and an increased development of ridges and crests are usually interpreted to be typical of older individuals (Varricchio, 1997). Given that lacrimals are unknown in *Suuwassea*, *Supersaurus*, *Dinheirosaurus*, *Tornieria* and *Barosaurus*, a decision on the taxonomic importance of this morphological feature remains difficult. Furthermore, a similar spur is present in the camarasaurid SMA 0002 and some specimens mentioned in Madsen et al. (1995) as '*Camarasaurus*-like'. An interpretation of this lacrimal spur as locally autapomorphic within Diplodocoidea might thus be possible but must await further finds of definitively adult specimens of *K. siberi*, or juvenile skulls of more diplodocid taxa.

A third recovered unambiguous autapomorphy of *Kaatedocus siberi* is the small fossa present medially to the sheetlike pterygoid ramus of the quadrate. However, this character is also present in the subadult skull CM 3452. Its absence in both juvenile and adult *Diplodocus* specimens (CM 11161, 11255; USNM 2672, 2673; pers. obs. 2011) might imply that this feature is only developed in subadult specimens. A similar development can also be seen in the large quadrates belonging to the holotype of *Apatosaurus ajax* (YPM 1860), which also appears to be a juvenile to subadult specimen (McIntosh, 1990b). The development of such a medial quadrate cavity in subadult stages might thus be a synapomorphy of the entire Diplodocidae, and its interpretation as an autapomorphy of *Kaatedocus siberi* cannot be entertained with certainty at present.

The short anterior process of the squamosal appears as a local autapomorphy within Diplodocoidea. This process exceeds the posterior border of the orbit considerably in all known diplodocoid skulls, and even extends beyond the anterior orbital edge in the rebbachisaurs *Limaysaurus tessonei* and *Nigersaurus taqueti* (Calvo and Salgado, 1995; Sereno et al., 2007). The retention of a short anterior process therefore appears to be a real local autapomorphy of *Kaatedocus siberi*.

The presence of a postparietal foramen is an ambiguous autapomorphy shared with *Dicraeosaurus*, *Amargasaurus* and *Suuwassea* in the present data matrix. It has thus been traditionally interpreted as a synapomorphy of Dicraeosauridae (Salgado and Bonaparte, 1991; Remes, 2009; Whitlock, 2011a). Upchurch et al. (2004a) also reported a postparietal foramen in *Tornieria* but of the braincases found at Tendaguru, Tanzania, only MB.R.2387 shows such a foramen (Janensch, 1935; Remes, 2009; pers. obs. 2011). MB.R.2387 has subsequently been identified as Flagellicaudata indet. as it could not be confidently referred to *Tornieria* based on the situation of the quarry, and because it shows a mix of dicraeosaurid and diplodocid characters (Remes, 2009). The morphology of the foramen in SMA 0004 strongly resembles its corresponding structure in MB.R.2387, where it is considerably smaller than in *Suuwassea* and *Dicraeosaurus*. The presence of this foramen in SMA 0004 might also be due to incomplete fusion of the parietals in this specimen and thus be ontogenetic. However, the small *Diplodocus* skull CM 11255 does not show such a foramen, which is yet another characteristic that helps distinguish these two taxa. Awaiting a definitive taxonomic assignment of MB.R.2387, and finds of skulls of *Supersaurus*, *Dinheirosaurus* and *Barosaurus*, the postparietal foramen in *K. siberi* is provisionally regarded as a local autapomorphy within Diplodocidae.

The distinct oblique posterior ridges on the paroccipital processes of SMA0004 are another recovered unambiguous autapomorphy, which is actually shared with the juvenile *Diplodocus* specimens (see above). A detailed analysis of the development and distribution of this character among juvenile to subadult individuals of different species has thus to be postponed until more material is found and described.

As with the postparietal foramen, the narrow and distinct sagittal nuchal crest is also a shared feature of *Kaatedocus siberi* and Dicraeosauridae (Salgado and Bonaparte, 1991; Harris, 2006c; Whitlock, 2011a; Mannion et al., 2012). Furthermore, the indeterminate flagellicaudatan MB.R.2388 also exhibits a similar shape of the nuchal crest (Remes, 2009). The state of this character is unknown in *Supersaurus*, *Dinheirosaurus* and *Barosaurus* as their skeletons are only known from postcranial material. The occurrence of such a distinct nuchal crest in SMA 0004 is the first reported for any diplodocid. The low and broad nuchal crest of *Apatosaurus* and diplodocines more derived than *K. siberi* indicates that either the acquisition of this feature, or its loss, happened twice independently within Flagellicaudata. Interestingly, in contrast to the adult *Diplodocus* skull CM 11161, the juvenile *Diplodocus* CM 11255 does show a more developed sagittal nuchal crest (Whitlock et al., 2010). This

implies that the high nuchal crest can also be an ontogenetic character that decreased in size during growth. This would mean that the well-developed crest in SMA 0004 could still become somewhat weaker and broader during ontogeny, and thus approach the state in *Tornieria africana* or *Diplodocus*. However, the development of the crest in CM 11255 does not equal its counterpart in SMA 0004, and such a pronounced change from a subadult to the adult stage seems improbable. Moreover, the opposite development has been shown to happen in *Massospondylus* and *Psittacosaurus* (Gow, 1990; Varricchio, 1997), and the closely related dicraeosaurids also show a well-developed crest in adult individuals. Therefore, even though it seems to be an ontogenetic feature in *Diplodocus* this might be different in *K. siberi*, of which the derived state can be considered locally autapomorphic within Diplodocidae.

The straight anterior edge of the basal tuber is shared with *Limaysaurus tessonei* in the present analysis. However, it is equally expressed in both juvenile and subadult *Diplodocus* (CM 11255, 3452, pers. obs. 2011), as well as *Nigersaurus taqueti* (Sereno et al., 2007). It might thus be that juveniles and subadult *Diplodocus* retain the plesiomorphic trait present in the more basal rebbachisaurs. The decision on how the appearance of this character in *Kaatedocus siberi* should be treated (ontogenetic character or retained plesiomorphy) should await future finds of adult *Kaatedocus* or juvenile basal diplodocid specimens.

The more rounded snout shape, with a premaxilla–maxilla index (PMI; see Whitlock, 2011b for a detailed explanation) of less than 70% is shared with the juvenile specimen CM 11255 and CMC VP 8300 (Whitlock et al., 2010). With a PMI of 68%, *Kaatedocus siberi* is slightly beneath the border set by Whitlock (2011a) to define the plesiomorphic state. Based on the reconstructions of Whitlock (2011b), the PMI in SMA 0004 is very close to that of *Tornieria* (71%; Whitlock, 2011b), which falls in the gap of the borders set for this character, but would rather group with the plesiomorphic taxa. *Suuwassea* is considered to have a slightly higher index of 74% by the same author, and is thus closer to the apomorphic state. These ratios are not included in this analysis as the reconstructions in Whitlock (2011b) are based on incomplete material. Nonetheless, they describe a general trend towards gradually more squared snouts during the evolution of Diplodocoidea, becoming extreme in *Nigersaurus*, *Apatosaurus* and *Diplodocus* (Whitlock, 2011b). The retention of the plesiomorphic state in *K. siberi* and probably *Tornieria* therefore appears to be the exception to this rule, but the rounded snout in the juvenile *Diplodocus* skulls CM 11255 and CMC VP 8300 indicates that this might also be an ontogenetic feature (Whitlock et al., 2010). CM 11255 has a PMI of only 56%, which is even lower than in *Camarasaurus* or *Brachiosaurus* (Whitlock et al., 2010; Whitlock, 2011b). Even though this might be partly due to transverse compression of the skull, it implies that juvenile *Diplodocus* develop the typical squared snout only during ontogeny. However, as *Tornieria* appears to show a similar value, a coding of *K. siberi* as plesiomorphic in this character can be justified, and can be regarded as local autapomorphy of *K. siberi*, and perhaps *Tornieria* too.

The anteriorly projecting pre-epipophysis that forms the anterior-most point of the entire mid-cervical vertebrae is another unambiguous autapomorphy in the phylogenetic analysis. Its distribution is unknown in *Supersaurus*, *Dinheirosaurus* and *Tornieria*, but the preserved vertebrae in the first two of these taxa indicate that such a spur was probably not present. This feature was described as autapomorphic within Diplodocidae in *Australodocus*, where it is very pronounced (Remes, 2007). It is also present in *Haplocanthosaurus* (Hatcher, 1903). As *Australodocus* is currently considered a titanosauriform, the spur is herein interpreted to be a local autapomorphy of *K. siberi* within the clade uniting all diplodocoids more derived than *Haplocanthosaurus*. An alternative interpretation of this spur as a juvenile character is improbable as such traits usually develop late in ontogeny (Varricchio, 1997).

The small, rugose tuberosity placed anterodorsally to the anterior pneumatic fossa on the lateral surfaces of the posterior cervical vertebrae represents another unambiguous autapomorphy of *Kaatedocus siberi*. Comparisons with various diplodocid specimens (e.g. *Apatosaurus* CM 3018; *Diplodocus* CM 84, DMNS 492, 1494, HMNS 175; *Barosaurus* AMNH 6341, YPM 429) indicate that this feature is unique in *K. siberi*. The only taxon with a similar trait is the basal dicraeosaurid *Suuwassea*, where the mid-cervical vertebrae bear a tubercle in the same position (ANS 21122, pers. obs. 2011). The fragmentary posterior cervical centra of ANS 21122 do not preserve this region in enough detail to discern their state. Therefore, an interpretation of this feature as local autapomorphy of *K. siberi* within Diplodocidae is relatively well supported, only lacking information about its

distribution in *Supersaurus*, *Dinheirosaurus* and *Tornieria*. *Dinheirosaurus* ML 414 shows a fractured surface in this region, and the only preserved cervical vertebra of *Tornieria africana* is badly crushed, so the presence or absence of this tubercle cannot be determined in these taxa.

The sulcus posterior to the prezygapophyseal facets of the posterior cervical vertebrae is considered an additional unambiguous autapomorphy in the present analysis. Personal observations showed this trait to be absent in *Suuwassea*, *Apatosaurus*, *Diplodocus* and *Barosaurus* (AMNH 550; ANS 21122; CM 84, 94, 3018; YPM 429, 1860). In the holotype material of *Dinheirosaurus lourinhanensis* (ML 414) the prezygapophysis is partly covered by matrix and somewhat distorted but such a sulcus does not appear to be present. Furthermore, the detailed description of the cervical vertebrae of *Dicraeosaurus* (Janensch, 1929) does not mention any similar structure in these taxa. In *Nigersaurus*, as a representative of a more distantly related diplodocoid, the distinct articular facets of the prezygapophysis are well offset from the prezygapophyseal process, but no transverse sulcus is present (Sereno et al., 2007). Neither the presence nor the absence of such sulci has previously been considered valuable for characterizing either adults or juveniles. This autapomorphy of *Kaatedocus siberi* can thus be assumed to unambiguous.

The posteriorly facing accessory lamina between the pcdl and the podl is shared between *Kaatedocus siberi* and *Dinheirosaurus*. However, such a lamina is also present in the *Apatosaurus* specimens UW 15556, YPM 1840, 1860 and 1861 (Gilmore, 1936; Wedel and Sanders, 2002; pers. obs. 2011). This character is thus not considered an autapomorphy of *K. siberi*.

The narrowly diverging neural spines of SMA 0004 resemble more closely the state in dicraeosaurids than in diplodocids. The possibility cannot be excluded that this character was affected and exaggerated by taphonomy; therefore, a question mark has to be placed over its designation as a local autapomorphy within Diplodocidae. However, as the diapophysis of CV 14 in particular does not seem to be highly deformed, a narrower angle between the metapophyses can still be assumed. On the other hand, the supposed *Barosaurus* sp. CM 11984 also exhibits less widely diverging neural spines compared to other diplodocids. A decision on the validity of this autapomorphy is thus not possible yet.

The cervical ribs that in some vertebrae exceed the posterior end of the centra are another ambiguous autapomorphy of *Kaatedocus siberi*. The only other diplodocoids with the same trait are *Supersaurus* and *Dinheirosaurus*, which are recovered as a sister group to Diplodocidae in the present phylogenetic analysis (contrary to previous analyses, see below). Elongated cervical ribs were also reported in *Eobrontosaurus yahnahpin* (Bakker, 1998), the taxonomic affinity of which has yet to be resolved. At present, this feature thus represents a local autapomorphy within Diplodocidae.

To summarize, *Kaatedocus siberi* can be confidently identified by three general unambiguous autapomorphies: (1) the U-shaped notch between the frontals; (2) the lateral rugose tubercle on anterodorsal corner of posterior cervical centra; and (3) the sulcus bordering the prezygapophyseal facets posteriorly in posterior cervical vertebrae. Furthermore, the diagnosis is strengthened with local autapomorphies or retained plesiomorphies (see above).

Phylogenetic implications

In the majority of the phylogenetic analyses on Sauropoda, the clade Diplodocidae was well resolved and easily distinguishable from other clades. This was mainly due to the inclusion of a limited number of diplodocid taxa, using only the best-known genera *Apatosaurus*, *Diplodocus* and *Barosaurus* (Upchurch, 1995, 1998; Wilson and Sereno, 1998; Wilson, 2002, 2005; Upchurch et al., 2004a). Recent studies have looked in detail at the intrarelationships of this group, including more incomplete taxa, even single specimens such as *Supersaurus*, '*Seismosaurus*' (Lovelace et al., 2007), and different apatosaur species (Upchurch et al., 2004b). Only two detailed phylogenetic analyses have included a larger set of ingroup taxa, representing the most inclusive diplodocid phylogenies published to date (Whitlock, 2011a; Mannion et al., 2012). Although Whitlock (2011a) helped in resolving uncertainties within the more basal diplodocoid clade Rebbachisauridae, Diplodocidae was not fully resolved, with *Dinheirosaurus*, *Tornieria* and a clade comprising the classical diplodocines *Diplodocus* and *Barosaurus* forming a trichotomy. Mannion et al. (2012), based on Whitlock's (2011a) matrix, redescribed *Dinheirosaurus* in detail and were therefore able to update and correct some character states used in the earlier study. *Dinheirosaurus* was recovered as a sister taxon to *Supersaurus*, and together they form the most basal subclade within Diplodocinae, followed by *Tornieria* and

(*Diplodocus* + *Barosaurus*). The addition of *Kaatedocus* and several new characters to the matrix corroborates this result in parts (Fig. 3.24): in the Nelsen consensus tree, the clade comprising *Dinheirosaurus* and *Supersaurus* is recovered more basal than *Apatosaurus* – and would therefore form the basal-most clade within Diplodocidae (following the recommended definition by Taylor and Naish, 2005). This corroborates the assumption of Mannion et al. (2012) that the assignment of *Dinheirosaurus* to Diplodocinae has still to be considered uncertain, as this taxon shares a number of traits with more basal diplodocoids. However, the low bootstrap values imply that more detailed studies are still needed in order to resolve diplodocid phylogeny in a convincing way. The fact that *Kaatedocus* exhibits features previously identified as dicraeosaurid synapomorphies indicates that some of them were actually already present in basal flagellicaudatans and subsequently lost in diplodocids other than *Kaatedocus*.

The basal position of *Kaatedocus siberi* in the diplodocid clade is consistent with the low stratigraphical position (Fig. 3.2), considered older than most sauropod occurrences in the Morrison Formation. *K. siberi* thus makes a nice example of Cope's Rule as well, as a small sized, more basal taxon, compared with the large, advanced diplodocines *Barosaurus* and *Diplodocus*. However, as already mentioned, the stratigraphy of the northern exposures of the Morrison Formation is ambiguous, and long distance correlation with the better known southern sites is difficult (Turner and Peterson, 1999; Trujillo, 2006). As the few reported specimens from northern Wyoming or Montana comprise previously unknown or rare species (Wilson and Smith, 1996; Harris, 2006b), long distance correlation by proposed faunal zones (see Foster, 1998; Turner and Peterson, 1999) appears difficult as well. The recent descriptions of new taxa from these areas (e.g. Harris and Dodson, 2004; this study) therefore highlights the importance of a more detailed exploration and analysis of the northern Morrison Formation, both for a better understanding of diplodocid phylogeny and stratigraphical correlation of the various fossil sites and faunal changes within the formation.

Skull reconstruction

Some of the skull elements bear features that are reported for the first time in diplodocid sauropods. The majority of these characters would have been hidden in vivo, like the posterior expansion of the nasal opening, the anteriorly restricted squamosal, and the morphology of the braincase and the quadrate. However, the lacrimal spur and the rugose lateral surface of the frontal, which indicates the presence of a palpebral element, are traits that affected the outward aspect of the living *Kaatedocus*. Fig. 3.25 shows a skull reconstruction, undertaken in cooperation with the Italian artist Davide Bonadonna, showing these features.

Conclusions

Kaatedocus siberi is a new diplodocid sauropod from the little-known northern exposures of the Upper Jurassic Morrison Formation of Wyoming, USA. It was found at the historic Howe Quarry, relatively low in the stratigraphy, and therefore fills both a spatial as well as temporal gap from which only few sauropod specimens have been reported. *K. siberi* represents a basal diplodocine, and forms the sister taxon to a clade including *Tornieria africana*, *Barosaurus lentus* and the multi-species genus *Diplodocus*. With its smaller size compared to the more derived taxa, it is an example of Cope's Rule, which predicts a body size increase during evolution. The holotype comprises a disarticulated but nearly complete skull and an associated cervical vertebral column (including the first record of a proatlas in diplodocid dinosaurs), and is interpreted as a subadult individual. Newly identified, possibly ontogenetic features include a shallow excavation on the quadrate shaft, medial to the pterygoid ramus, oblique ridges on the external side of the paroccipital processes, and a straight anterior margin of the basal tubera in ventral view. *K. siberi* furthermore shares characters that were previously interpreted as dicraeosaurid synapomorphies. The presence of a postparietal foramen, as well as the narrow but distinct sagittal nuchal crest, therefore probably represents the plesiomorphic state in Flagellicaudata. An updated phylogenetic analysis recovers the clade uniting *Supersaurus* and *Dinheirosaurus* as the most basal Diplodocidae.

The highly rugose lateral margins of the frontal are considered equivalent to the attachment sites of palpebral bones on frontals in ornithischian dinosaurs. This is the first such interpretation for sauropod dinosaurs, and a skull reconstruction of *Kaatedocus siberi* was therefore attempted, which shows a palpebral element covering the eye anterodorsally. SMA 0004 is the only specimen from the

historic Howe Quarry to be completely described and properly identified to date. The fact that it represents a new diplodocid taxon highlights the importance of this site, but further studies are needed to understand better the implications for diplodocid phylogeny as well as faunal changes in the Morrison Formation through space and time.

Figure 3.25: Life reconstruction of the skull of *Kaatedocus siberi*. Note the lateral spur on the lacrimal and the palpebral element covering the orbit. Illustration by Davide Bonadonna (Milan).

Addendum – unpublished

The prefrontal of *Kaatedocus*

Among additional skull elements recovered from the Howe Quarry was a partial right prefrontal and articulated dorsal end of the lacrimal (SMA field number N 22). These elements were associated with the holotype skull of *Kaatedocus siberi* (SMA 0004), where this portion of the skull is unknown and reconstructed in the mount. As they fit in size, the prefrontal and dorsal end of the lacrimal are herein referred to the holotype.

The prefrontal is lacking its posterior process, which would articulate with the frontal. Anteriorly, the prefrontal caps the dorsal end of the lacrimal dorsomedially. In a complete skull, the prefrontal would articulate furthermore with the nasal anteromedially. The prefrontal is a relatively slender, anteroposteriorly curved bone, with a pointed posterior, and a transversely wider anterior end. It increases in dorsoventral thickness from posterior to anterior. The anterior end bears a deep fossa for the reception of the lacrimal, which is dorsally and medially capped by two subtriangular sheets of bone projecting anteriorly. The distinct ventral edge of the medial sheet also forms the ventral margin of the lateral surface, which is facing lateroventrally. Thus, the cross-section of the bone is sub-triangular anteriorly. The lateral surface is slightly concave anteroposteriorly. Its dorsal edge is acute, and forms the anterodorsal corner of the orbital margin, which is short compared to the contribution of the frontal. The medial face bears an elongate and shallow, lens-shaped fossa just ventral to the dorsal edge, approximately at midlength. The fossa is anteriorly bordered by a weak medially projecting tubercle.

The prefrontal of *Kaatedocus siberi* can be distinguished from other diplodocid prefrontals in that its medial edge does not curve considerably medially at its anterior end, and in its slenderness. *Diplodocus* or *Apatosaurus* have transversely wider main bodies, and a more distinct hook-like shape of their posterior process (Holland 1906, 1924; Berman and McIntosh, 1978; Whitlock, 2011b).

Clavicles, interclavicles, gastralia, and sternal ribs in sauropod dinosaurs: new reports from Diplodocidae and their morphological, functional and evolutionary implications

published in the Journal of Anatomy:
Tschopp, E., and O. Mateus. 2013. Clavicles, interclavicles, gastralia, and sternal ribs in sauropod dinosaurs: new reports from Diplodocidae and their morphological, functional and evolutionary implications. Journal of Anatomy 222:321-340.

Abstract

Ossified gastralia, clavicles, and sternal ribs are known in a variety of reptilians, including dinosaurs. In sauropods, however, the identity of these bones is controversial. The peculiar shapes of these bones complicate their identification, which led to various differing interpretations in the past. Here we describe different elements from the chest region of diplodocids, found near Shell, Wyoming, USA. Five morphotypes are easily distinguishable: (A) elongated, relatively stout, curved elements with a spatulate and a bifurcate end resemble much the previously reported sauropod clavicles, but might actually represent interclavicles; (B) short, L-shaped elements, mostly preserved as a symmetrical pair, probably are the real clavicles, as indicated by new findings from diplodocids; (C) slender, rod-like bones with rugose ends are highly similar to elements identified as sauropod sternal ribs; (D) curved bones with wide, probably medial ends constitute the fourth morphotype, herein interpreted as gastralia; and (E) irregularly shaped elements, often with extended rugosities, are included into the fifth morphotype, tentatively identified as sternal ribs and/or intercostal elements. To our knowledge, the bones previously interpreted as sauropod clavicles were always found as single bones, which sheds doubt on the validity of their identification. Various lines of evidence presented herein suggest they might actually be interclavicles – which are single elements. This would be the first definitive evidence of interclavicles in dinosauromorphs. Previously supposed interclavicles in the early sauropodomorph *Massospondylus* or the theropods *Oviraptor* and *Velociraptor* were later reinterpreted as clavicles or furculae. Independent from their identification, the existence of the reported bones has both phylogenetic and functional significance. Their presence in non-neosauropod Eusauropoda and Flagellicaudata and probable absence in rebbachisaurs and Titanosauriformes shows a clear character polarity. This implicates that the ossification of these bones can be considered plesiomorphic for Sauropoda. The proposed presence of interclavicles in sauropods may give further support to a recent study, which finds a homology of the avian furcula with the interclavicle to be equally parsimonious to the traditional theory that furcula were formed by the fusion of the clavicles. Functional implications are the stabilizing of the chest region, which coincides with the development of elongated cervical and caudal vertebral columns or the use of the tail as defensive weapon. The loss of ossified chest bones coincides with more widely spaced limbs, and the evolution of a wide-gauge locomotor style.

Introduction

The plesiomorphic composition of the chest region in early reptiles includes various elements of the pectoral girdle (scapula, suprascapula, pro- and metacoracoids, cleithrum, clavicle, and the interclavicle), the sternal apparatus (sternal plates and ribs) and other chest bones (gastralia; Romer, 1956; Vickaryous and Hall, 2006; see Tab. 4.1 for a summary of pectoral and sternal elements in Reptilia). The term chest bones is here informally used to include gastralia, sternal plates, and ribs, clavicles, and interclavicles based on the topographic position, and independent from their embryological or evolutionary origin.

Table 4.1: Bones present in the chest regions of tetrapods.

	Embryological origin	Phylogenetic bracket	Bone connection	Previously identified in Sauropoda	General shape and distinction	Paired/single. Number
Clavicles	Dermal bone	Basal Sauropodomorpha: present Birds/Theropoda: fused to form furcula (?) Crocodylia: absent Basal Archosauria: present	Dorsal to coracoids (covering it sometimes), between cleithrum, scapula, and interclavicle in basal reptiles	Yes	Curved element	Paired, can fuse into one (furcula, questioned herein). One pair present
Interclavicles	Dermal bone	Basal Sauropodomorpha: ? Birds/Theropoda: = furcula? Crocodylia: present Basal Archosauria: present	Between the clavicles. Connects to the coracoid and/or sternal plates posteriorly	No	Variable. Diamond shaped in early tetrapods, rod-like with or without transverse processes in crocodylians and lacertilians	Single (very rarely paired). Only one present
Sternal Ribs	Endochondral	Basal Sauropodomorpha: absent? Birds/Theropoda: present Crocodylia: present Basal Archosauria: present	Connects the sternal plates with the dorsal ribs or intercostal elements	Yes	Irregularly shaped, often rugose	Paired. Maximum one per dorsal rib, often less
Intercostal elements	Endochondral	Basal Sauropodomorpha: absent Birds/Theropoda: absent Crocodylia: present: Basal Archosauria: present	Connects sternal ribs with dorsal ribs	No	Irregularly shaped, often rugose	Paired. Maximum one per dorsal rib, often less
Gastralium	Dermal bone	Basal Sauropodomorphs: present Birds/Theropoda: present Crocodylia: present Basal Archosauria: present	Articulate among themselves and through cartilage to dorsal ribs, as well as maybe the sternal apparatus	Yes	Slender, slightly curved bones. Medial elements with expanded medial end for articulation with corresponding gastralia. Anteriormost sometimes fused	Four elements per row (2 lateral, 2 medial). Up to 21 rows in large theropods
Cleithrum	Dermal bone	Basal Sauropodomorphs: absent Birds/Theropoda: absent Crocodylia: absent Basal Archosauria: absent	Capping scapulacoracoid, attaches to clavicles	No	Spoon-shaped	Paired. Only one pair present
Sternal plates	Endochondral	Basal Sauropodomorphs: present Birds/Theropoda: present Crocodylia: present Basal Archosauria: present	Articulate among themselves, sternal ribs attached to them, sometimes touching the interclavicle anteriorly	Yes	Shield-like: flat oval or reniform	Paired or single. One single or two mirrored elements
Scapulacoracoid	Endochondral	Basal Sauropodomorphs: present Birds/Theropoda: present Crocodylia: present Basal Archosauria: present	Dorsal and external to sternal apparatus, connected medially by cleithrum, clavicles, and interclavicle	Yes	Large, flat, subcircular acromion with a elongate, more narrow posterodorsal projection	Paired. One pair present

In Diapsida, the cleithrum was lost, and pro- and metacoracoids fused to form a single element (Vickaryous and Hall, 2006; Remes, 2008). The interclavicle is generally interpreted to have been lost in Dinosauriformes (Nesbitt, 2011). A supposed absence of clavicles was often used as synapomorphy of Dinosauria or even more inclusive clades, and as reason against the ancestry of this clade to birds (see Sereno, 1991; Novas, 1996; Yates and Vasconcelos, 2005). However, numerous reports of clavicles in various dinosaur clades imply that these elements are plesiomorphically present, and that it is mostly due to diagenetic or taphonomic reasons that they are not recovered (Yates and Vasconcelos, 2005; Remes, 2008). On the other hand, a recent study on the embryology of the avian furcula and the crocodilian interclavicle revealed that an interpretation of the furcula as derived interclavicle would be equally parsimonious as the traditional hypothesis, where the furcula represents the medially fused clavicles (Vickaryous and Hall, 2010). The suggestion of Vickaryous and Hall (2010) that all previously reported dinosaurian clavicles might actually be interclavicles would bring back the earlier stated hypothesis that the absence of clavicles would be synapomorphic for Dinosauriformes, paralleled by extant crocodilians. However, the evidence remains ambiguous, and especially Sauropodomorpha appear to have both ossified clavicles and interclavicles (Huene, 1926; Yates and Vasconcelos, 2005; this study).

In the Sauropodomorpha, pectoral girdles usually only preserve the scapula and the coracoid, which in sauropods generally fuse during ontogeny (Ikejiri et al., 2005; Schwarz et al., 2007a, c; Remes, 2008). Putative clavicles are predicted to connect the scapulae dorsal to the coracoids but, until recently, no articulated pair has been reported in sauropods (Remes, 2008; but see Galiano and Albersdörfer, 2010 for an articulated specimen). Unpaired rod-like structures interpreted as clavicles were found in a variety of sauropod taxa, sometimes associated with the pectoral girdle (Hatcher, 1901, 1903; Dong and Tang, 1984; He et al., 1988; Zhang, 1988; Sereno et al., 1999; Harris, 2007; Remes et al., 2009). However, most of these identifications rely solely on the similarity to previously reported 'clavicles' – which themselves are not beyond doubt.

The sauropod scapulacoracoid articulates posteroventrally with the sternal plates, which are connected with the dorsal ribs through usually cartilaginous sternal ribs (Schwarz et al., 2007a; Remes, 2008; Hohn-Schulte, 2010). As they remain mostly cartilaginous, sternal ribs are very rarely preserved in the fossil record. The only reports are from the *Apatosaurus excelsus* holotype YPM 1980 (Marsh, 1896), a set of ribs associated with the holotype of *A. louisae* (Holland, 1915a), a sternal rib fused to a sternal plate in a probable early macronarian (Tschopp and Mateus, 2012a), and maybe from the holotype of *Eobrontosaurus yahnahpin* (Filla and Redman, 1994; Claessens, 2004). Filla and Redman (1994) initially interpreted these structures to be gastralia, based on superficial similarity to gastralia in theropods, non-sauropod sauropodomorphs, and other archosaurs like crocodilians or sphenodonts. Gastralia were also reported from *Gongxianosaurus shibeiensis* and *Jobaria tiguidensis* (He et al., 1998; Sereno et al., 1999), but Claessens (2004) and Fechner (pers. comm., 2011), based on a detailed comparison with theropod and non-sauropod sauropodomorph gastralia, recently questioned this identification, and suggested them to be ossified sternal ribs instead. In short, the evolutionary and developmental origin of these elements is hotly debated, and the sauropod chest bones other than the scapulacoracoid remain poorly understood.

Herein we describe five morphotypes of bones from the chest region, and state their most probable identifications. This classification helps identifying disarticulated elements. It yields important new information on the proper reconstruction of the sauropod pectoral girdle.

Locality

The new material described herein comes exclusively from the Howe Quarry in the Bighorn Basin of Wyoming, USA (Fig. 4.1). Two periods of extensive excavation were conducted at this site. In 1934 Barnum Brown collected 3000–4000 bones at the Howe Quarry for the American Museum of Natural History, NY, USA (AMNH; Brown, 1935; Michelis, 2004). In 1990 Hans-Jakob Siber reopened the site with a team from the Sauriermuseum Aathal, Switzerland (SMA) and excavated another 700–800 elements (Ayer, 2000; Michelis, 2004; Tschopp and Mateus, 2012b). Only one of the specimens found during these two periods has since been described in detail, and was identified as subadult specimen of a new diplodocine species (Tschopp and Mateus, 2012b). Brown (1935) tentatively identified the majority as Diplodocinae, except for some elements belonging to *Apatosaurus* or *Camarasaurus* (see

also Michelis, 2004; Tschopp and Mateus, 2012b).

Both the AMNH and the SMA expeditions yielded various sets of bones resembling the gastralia or sternal ribs described from *Eobrontosaurus yahnahpin* (Filla and Redman, 1994; Fig. 4.2). Furthermore, five single elements like the bones previously identified as sauropod clavicles, as well as two pairs of L-shaped, symmetrical elements were recovered, the identity of which is discussed below (Tab. 4.2). Although such an accumulation of chest bones is unusual, none of these bones from the Howe Quarry has been reported to date. Given the predominance of Diplodocidae in the Howe Quarry, and the close association of some of the clusters of gastralia/sternal ribs and the clavicles to diplodocid cervical vertebrae, an attribution of these elements to this group can be considered highly probable.

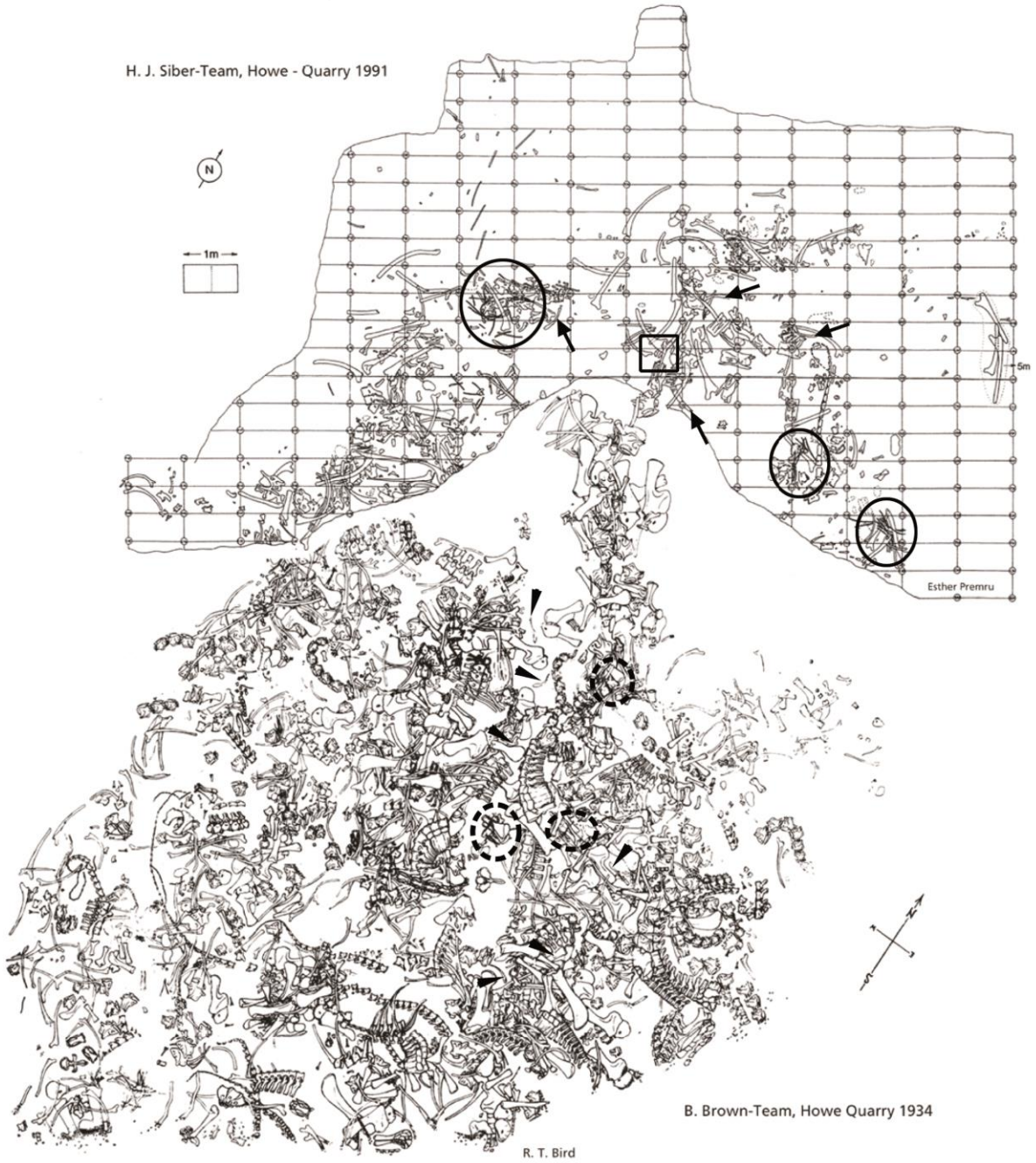

Figure 4.1: Compiled quarry map of the two excavation periods at the Howe Quarry (AMNH map below; SMA map above). Arrows indicate supposed clavicles at SMA, arrowheads possible locations of the supposed clavicle at AMNH. Circles indicate gastral or sternal baskets (full circles: SMA; dashed circles: AMNH), rectangle marks the SMA pair of symmetrical bones. AMNH map modified from Bird (1985); SMA map drawn by Esther Premru.

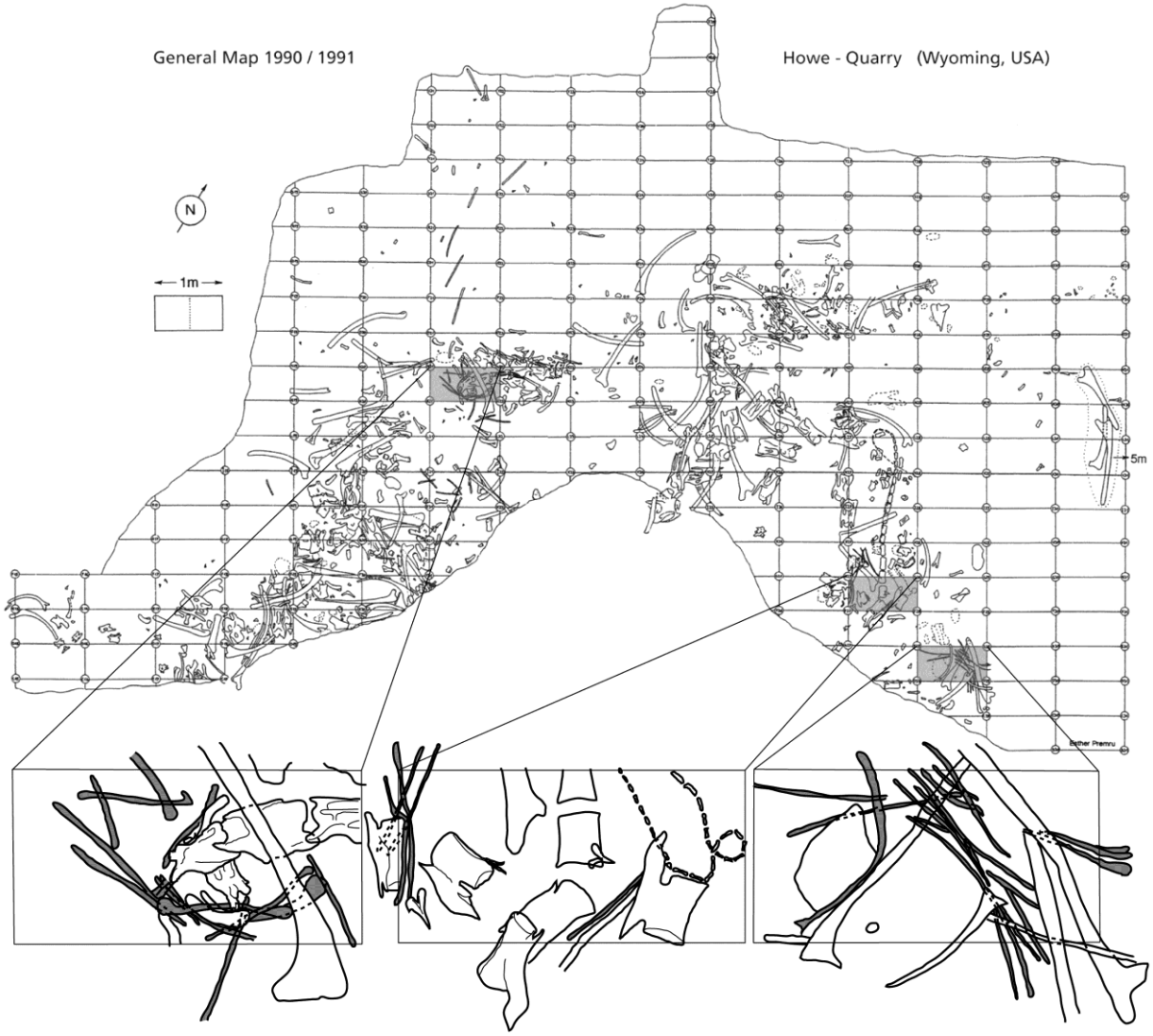

Figure 4.2: Detail of the 1991 quarry map, with sections producing associated morphotype C–E elements enlarged (from left to right: clusters M 21, F 27 and D 28). The morphotype C–E elements are highlighted in gray in the enlarged sections.

Description and discussion

Morphotype A
Previous identification: clavicles, sternal ribs, os penis (baculum; Figs 4.3-4.8; Tab. 4.3)
Our interpretation: interclavicles.

General morphology. Morphotype A elements are relatively stout, elongated bones. They are usually bowed, and exhibit a spatulate and a bifurcate end. Assuming that the concave side follows the curvature of the body, this side can be regarded as internal. The spatulate end bears more or less linear, rugose striations for muscle or ligament attachment. The shafts are suboval in cross-section at mid-length, and achieve their greatest breadth at two-thirds to three quarters of their total length, toward the spatulate end. The notch in the bifurcated end is usually only visible in internal or external view.

Morphotype A elements show some superficial similarities to dorsal ribs. They can be distinguished from ribs by the presence of the spatulate and bifid ends, the more circular cross-section at midlength, and the striated rugosities present on the spatulate end.

Table 4.2: New and already reported chest bones of sauropods, ordered by morphotype and first mention. Reported chest bones of unknown morphotype are listed in the end.

	Specimen Number	Taxonomy	References	first identified as	Comments
	CM 84	*Diplodocus carnegii*	Hatcher, 1901, 1903; Nopsca, 1905; Holland, 1906; McIntosh, 1981	clavicle	
	HMNS 175 (= CM 662)	'*Diplodocus*' *hayi*	Hatcher, 1903; Nopsca, 1905; Holland, 1906	clavicle	stored at CM
	?	*Mamenchisaurus sp.*	Dong et al., 1983	clavicle	
	?	*Omeisaurus junghsiensis*	Dong et al., 1983	clavicle	three elements mentioned
	IVPP V7262	*Datousaurus bashanensis*	Dong and Tang, 1984	clavicle	
	IVPP V7263	*Datousaurus bashanensis*	Dong and Tang, 1984	clavicle	
	T5704	*Omeisaurus tianfuensis*	He et al., 1988	clavicle	
	T5401	*Shunosaurus lii*	Zhang, 1988	clavicle	
	ANS 21122	*Suuwassea emilieae*	Harris, 2007	clavicle	
	NMB-1698-R	*Spinophorosaurus nigerensis*	Remes et al., 2009	clavicle	
	AMNH 30900	?diplodocid	Tschopp and Mateus, 2013	interclavicle	
	SMA I 24-4	?diplodocid	Tschopp and Mateus, 2013	interclavicle	
	SMA L 22-3	?diplodocid	Tschopp and Mateus, 2013	interclavicle	
	SMA L 27-7	?diplodocid	Tschopp and Mateus, 2013	interclavicle	
	SMA M 25-3	?diplodocid	Tschopp and Mateus, 2013	interclavicle	
Morphotype A	?	Titanosauria indet.	K. Voegele, pers. comm., 2012	interclavicle	patagonian titanosaur
	SMA Arapo	Diplodocinae indet.	new	interclavicle	found together with morphotype B elements
	WDC		R. Wilhite, pers. comm., 2012	interclavicle	4 elements
	SMA 0009	Non-somphospondylian macronarian	Schwarz et al. 2007c, Tschopp and Mateus, 2013	possible furcula	pair recovered
	GCP-CV 4229	*Spinophorosaurus nigerensis*	Remes et al., 2009	tail spikes	two elements, possibly not symmetrical
	DQ-SB	Diplodocidae indet.	Galiano and Albersdörfer, 2010	clavicle	pair recovered
	DQ-TY	Diplodocidae indet.	Galiano and Albersdörfer, 2010	clavicle	
	SMA K 24-3 and 6	?diplodocid	Tschopp and Mateus, 2013	clavicle	pair recovered
	AMNH 30789	?diplodocid	Tschopp and Mateus, 2013	clavicle	pair recovered
Morphotype B	KUVP 129716	*Camarasaurus* sp.	A. Maltese, pers. comm., 2012 in Tschopp and Mateus, 2013	clavicle	pair recovered
	ANS 21122	*Suuwassea emilieae*	D. Lovelace, pers. comm., 2013	clavicle	possible pair recovered
	SMA Arapo	Diplodocinae indet.	new	clavicle	pair recovered
	AMNH 5760/5761	*Camarasaurus supremus*	Osborn and Mook, 1921	sternal/ventral rib	single element
	Tate 001	*Eobrontosaurus yahnahpin*	Filla and Redman, 1994	gastralia	almost complete set including morphotype E as well
	GMNH 101	*Camarasaurus grandis*	McIntosh et al., 1996a	gastralia	
	AMNH 30901	?diplodocid	Tschopp and Mateus, 2013	?sternal rib	fragmentary
	SMA ?	?diplodocid	Tschopp and Mateus, 2013	?sternal rib	various unnumbered elements
	SMA C 17-5	?diplodocid	Tschopp and Mateus, 2013	?sternal rib	
	SMA D 28-6 to 11	?diplodocid	Tschopp and Mateus, 2013	?sternal rib	part of D 28-cluster
	SMA D 28-18 to 19	?diplodocid	Tschopp and Mateus, 2013	?sternal rib	part of D 28-cluster
	SMA E 19-9	?diplodocid	Tschopp and Mateus, 2013	?sternal rib	
	SMA E 21-2 to 3	?diplodocid	Tschopp and Mateus, 2013	?sternal rib	
Morphotype C	SMA F 19-10	?diplodocid	Tschopp and Mateus, 2013	?sternal rib	

Table 4.2: continued.

	SMA F 19-21	?diplodocid	Tschopp and Mateus, 2013	?sternal rib	
	SMA F 20-9	?diplodocid	Tschopp and Mateus, 2013	?sternal rib	
	SMA F 27-16 to 17	?diplodocid	Tschopp and Mateus, 2013	?sternal rib	part of F 27-cluster
	SMA F 27-33 to 35	?diplodocid	Tschopp and Mateus, 2013	?sternal rib	part of F 27-cluster
	SMA G 21-2	?diplodocid	Tschopp and Mateus, 2013	?sternal rib	
	SMA G 27-3 to 4	?diplodocid	Tschopp and Mateus, 2013	?sternal rib	probably part of F 27-cluster
	SMA G 27-22 to 23	?diplodocid	Tschopp and Mateus, 2013	?sternal rib	probably part of F 27-cluster
	SMA H 20-7	?diplodocid	Tschopp and Mateus, 2013	?sternal rib	
	SMA H 21-2	?diplodocid	Tschopp and Mateus, 2013	?sternal rib	
	SMA H 21-5	?diplodocid	Tschopp and Mateus, 2013	?sternal rib	bears a foramen
	SMA H 21-9 to 10	?diplodocid	Tschopp and Mateus, 2013	?sternal rib	
	SMA H 21-12	?diplodocid	Tschopp and Mateus, 2013	?sternal rib	
	SMA L 21-3 to 5	?diplodocid	Tschopp and Mateus, 2013	?sternal rib	probably part of M 21-cluster
	SMA M 21-4	?diplodocid	Tschopp and Mateus, 2013	?sternal rib	part of M 21-cluster
	SMA M 21-6 to 7	?diplodocid	Tschopp and Mateus, 2013	?sternal rib	part of M 21-cluster
	SMA M 21-11	?diplodocid	Tschopp and Mateus, 2013	?sternal rib	part of M 21-cluster
	SMA M 21-13	?diplodocid	Tschopp and Mateus, 2013	?sternal rib	part of M 21-cluster
	SMA N 22-2	?diplodocid	Tschopp and Mateus, 2013	?sternal rib	probably part of M 21-cluster
	SMA P 19-1	?diplodocid	Tschopp and Mateus, 2013	?sternal rib	
	SMA P 21-1	?diplodocid	Tschopp and Mateus, 2013	?sternal rib	
	SMA S 22-3	?diplodocid	Tschopp and Mateus, 2013	?sternal rib	
	SMA V 21-1	?diplodocid	Tschopp and Mateus, 2013	?sternal rib	
	YPM 1901	*Camarasaurus grandis*	M. Fox, pers. comm., 2012	?sternal rib	
	WDC FS-42		R. Wilhite, pers. comm., 2012	?sternal rib	
	SMA Arapo	Diplodocinae indet.	new	?sternal rib	several elements
	SMA 0087	Apatosaurinae indet.	new	?sternal rib	several elements
Morphotype D	SMA D 28-5	?diplodocid	Tschopp and Mateus, 2013	gastralia	part of D 28-cluster
	SMA D 28-14 to 15	?diplodocid	Tschopp and Mateus, 2013	gastralia	part of D 28-cluster
	SMA F 19-11 to 12	?diplodocid	Tschopp and Mateus, 2013	gastralia	
	SMA G 21-3	?diplodocid	Tschopp and Mateus, 2013	gastralia	
	SMA M 21-2	?diplodocid	Tschopp and Mateus, 2013	gastralia	part of M 21-cluster
	SMA M 21-8	?diplodocid	Tschopp and Mateus, 2013	gastralia	part of M 21-cluster, fused element
	SMA M 21-16	?diplodocid	Tschopp and Mateus, 2013	gastralia	part of M 21-cluster, fused element
	SMA N 21-3	?diplodocid	Tschopp and Mateus, 2013	gastralia	probably part of M 21-cluster
	SMA Arapo	Diplodocinae indet.	new	gastralia	Several fused and single elements, fused sometimes with central slit
Morphotype E	YPM 1980	*Apatosaurus excelsus*	Marsh, 1883, 1896	sternal ribs	several elements
	Tate 001	*Eobrontosaurus yahnahpin*	Filla and Redman, 1994	gastralia	almost complete set including morphotype C as well
	SMA H 21-1	?diplodocid	Tschopp and Mateus, 2013	sternal rib	associated with SMA H 21-3 and morphotype C elements
	SMA H 21-3	?diplodocid	Tschopp and Mateus, 2013	sternal rib	associated with SMA H 21-1 and morphotype C elements
	SMA M 21-15	?diplodocid	Tschopp and Mateus, 2013	sternal rib	part of M 21-cluster
	SMA N 22-12	?diplodocid	Tschopp and Mateus, 2013	sternal rib	probably part of M 21-cluster

Table 4.2: continued

unknown	?CM 3018	*?Apatosaurus louisae*	Holland, 1915a	sternal ribs	several elements, not described/figured
	?	*Gongxianosaurus shibeiensis*	He et al., 1998	gastralia	several elements, not described, inadequately figured
	?	*Jobaria tiguidensis*	Sereno et al., 1999	clavicle	not described, inadequately figured
	?	*Jobaria tiguidensis*	Sereno et al., 1999	gastralia	several elements, not described/figured
	DNM ?	*?Camarasaurus*	Claessens, 2004	sternal ribs	several elements in the wall, not described/figured, possibly the same as the ones mentioned by Holland 1915a?
	DNM 3755	?	Michelis, 2004	gastralia	preserved in the wall, possibly the same as mentioned by Claessens 2004
	AODF 603	*Diamantinasaurus matildae*	Hocknull et al., 2009	gastralia	fragmentary, not described/figured
	DQ-TY	Diplodocidae indet.	Galiano and Albersdörfer, 2010	sternal ribs	several elements, not described/figured
	DQ-SB	Diplodocidae indet.	Galiano and Albersdörfer, 2010	gastralia or sternal ribs	several elements, not described/figured
	DQ-EN	Diplodocidae indet.	Galiano and Albersdörfer, 2010	sternal ribs	several elements, not described/figured
	DMNS 59329	*Diplodocus carnegii*	Tschopp and Mateus, 2013	clavicle	not described/figured; probably morphotype A

Howe Quarry material. Five elements were located in the collections of the AMNH and the SMA (AMNH 30900; SMA field numbers I 24-4, L 22-3, L 27-7 and M 25-3; Figs 4.3-4.8). Whereas the provenance and association of the AMNH element within the Howe Quarry is unclear, the SMA specimens were found close to dorsal ribs and an associated but disarticulated series of diplodocid cervical vertebrae (I 24-4); neck and skull remains of a new diplodocine sauropod (Tschopp and Mateus, 2012b), and a gastral/sternal rib cage (L 22-3); anterior cervical vertebrae, a dorsal rib, some skull remains and a metatarsal (L 27-7); and dorsal ribs, posterior diplodocid cervical vertebrae and an articulated series of mid-caudal vertebrae (M 25-3). All these elements were found as single elements, which is consistent with the earlier findings of similar finds in other sauropod taxa.

Previous reports. Several bones belonging to morphotype A have been reported in the literature, and were usually identified as sauropod clavicles (Tab. 4.2). The species preserving morphotype A elements are the non-neosauropod Eusauropoda *Shunosaurus lii*, *Spinophorosaurus nigerensis*, *Omeisaurus junghsiensis*, *O. tianfuensis*, *Mamenchisaurus* sp. and *Datousaurus bashanensis*, as well as the Flagellicaudata *Diplodocus carnegii*, *D. hayi* and *Suuwassea emilieae* (Hatcher, 1901, 1903; Dong et al., 1983; Dong and Tang, 1984; He et al., 1988; Zhang, 1988; Harris, 2007; Remes et al., 2009). In none of these taxa, morphotype A elements were recovered in pairs, even though some of the specimens were reasonably complete and articulated.

Variation in morphology. Two different orientations of the spatulate end can be observed in the five elements from the Howe Quarry, as well as in previously reported bones belonging to morphotype A: perpendicular to the curvature of the bone, so that its thin edges face internally and externally (e.g. SMA L 22-3; Figs 4.3d, 4.7), or turned 90° (e.g. SMA I 24-4; Figs 4.3b, 4.5). The spatulate end can bear a deep slot-like concavity on its internal side (e.g. in SMA M 25-3 and L 22-3; Figs 4.3c, d, 4.6, 4.7), giving the impression of a deeply bifurcated end on this side as well, in internal view. In other elements, the internal side of the spatulate end bears shallow (*Diplodocus hayi* HMNS 175 or *Spinophorosaurus nigerensis* NMB-1698-R) to distinct ridges (*Suuwassea emilieae* ANS 21122) with varying lengths (Hatcher, 1903; Harris, 2007; Remes et al., 2009). Differences in curvature (see the straight element SMA I 24-4 or the outwards curve in SMA L 27-7; Figs 4.3b, e, 4.5, 4.8) are most probably of taphonomic origin.

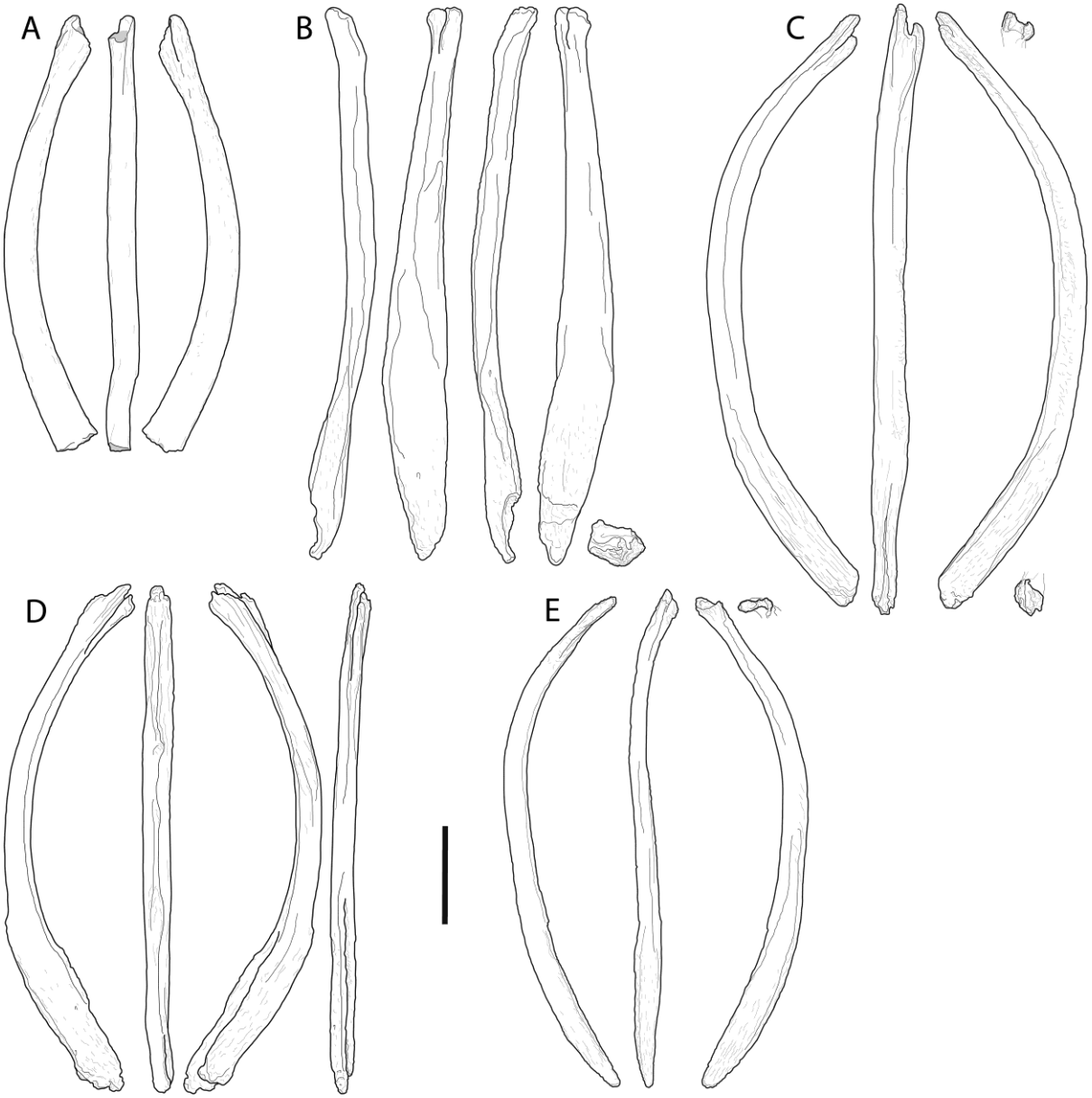

Figure 4.3: Drawings of morphotype A elements, to scale. (a) AMNH 30900; (b) SMA I 24-4; (c) SMA M 25-3; (d) SMA L 22-3; (e) SMA L 27-7. Scale bar = 10 cm. Gray areas in (a) indicate broken surfaces. Note the bifurcate end on top and the spatulate end at the bottom.

Identification. The first reported element of morphotype A was found associated with the scapula-coracoid of *Diplodocus carnegii* CM 84 and was tentatively identified as clavicle (Hatcher, 1901). Although this interpretation has never been definitely confirmed, it has become generally accepted, and subsequent finds of similar bones continued to be identified as clavicles (Hatcher, 1903; Dong et al., 1983; Dong and Tang, 1984; He et al., 1988; Zhang, 1988; Harris, 2007; Remes et al., 2009). The suggestions of Nopcsa (1905) or Holland (1906) that morphotype A elements represent the os penis or sternal ribs, respectively, are improbable given the absence of bacula in extant reptiles, and because they are relatively much more massive compared with articulated sternal ribs of pterosaurs or crocodilians (Claessens et al., 2009; *Crocodylus niloticus*, NHM, unregistered display specimen, ET, pers. obs.).

The five elements recovered as single bones in the Howe Quarry, as well as the corresponding elements of *Diplodocus carnegii* (CM 84), *D. hayi* (HMNS 175), *Spinophorosaurus nigerensis* (NMB-1698-R) and *Suuwassea emilieae* (ANS 21122), are slightly asymmetrical (see also Hatcher, 1901, 1903; Holland, 1906), but have a longitudinal midline extending through the bifid end and dividing the expanded spatulate end in two halves. These bones could therefore also represent elements of the chest

region that lie on the body midline, and their continuous findings as single elements might have been no coincidence. The two areas abutting to the right and left of the ridges subdividing the spatulate end in the elements of *Suuwassea* and *Spinophorosaurus* resemble articulation surfaces, implying that the morphotype A elements covered two symmetrical elements externally, and medially. The absence of such a ridge in the other taxa might be of taxonomic significance.

Figure 4.4: Photographs of morphotype A element AMNH 30900. Scale bar = 10 cm.

Figure 4.5: Photographs of morphotype A element SMA I 24-4. Scale bar = 10 cm.

Figure 4.6: Photographs of morphotype A element SMA M 25-3. Scale bar = 10 cm.

Figure 4.7: Photographs of morphotype A element SMA L 22-3. Scale bar = 10 cm.

Figure 4.8: Photographs of morphotype A element SMA L 27-7. Scale bar = 10 cm.

The only median pectoral element in the non-avian shoulder girdle is the interclavicle. As the morphotype A elements, also *Alligator* interclavicles have slightly asymmetrical outlines (Vickaryous and Hall, 2010; R. Wilhite, pers. comm. 2012). Whereas early tetrapods had diamond-shaped interclavicles (Steyer et al., 2000), crocodylomorphs and some lepidosaurs developed rod-like shapes without lateral processes (Vickaryous and Hall, 2010), similar to the elements described herein. Following this interpretation, the bifurcated end probably represents the reduced lateral processes, and the spatulate end would articulate with either the coracoids or the sternal plates – covering them externally and anteromedially.

A bone found in the pectoral girdle of the early sauropodomorph *Massospondylus carinatus* shows a similar spatulate expansion on one end, and in fact has first been interpreted as interclavicle (Cooper, 1981). Sereno (1991) and Yates and Vasconcelos (2005) subsequently reinterpreted this element as a clavicle, based on its similarity to paired, articulated clavicles in both *Plateosaurus* and other specimens of *Massospondylus*. The articulated specimens connect to the acromion process of the scapulae, which is typical for clavicles, but almost never the case in interclavicles (Tab. 4.1; Romer, 1956). The only reported exception is the interclavicle in some monotreme mammals, where the transverse processes reach the acromion (Klima, 1973). The articulation of these elements with the acromia of the scapulae in both *Massospondylus* (Yates and Vasconcelos, 2005) and *Plateosaurus* (B. Pabst, pers. comm., 2011; ET, pers. obs.) thus make an interpretation as clavicles more probable. However, given that sauropods appear to have both clavicles and interclavicles, Cooper's (1981) interpretation of the single *Massospondylus* 'interclavicle' might have to be reconsidered.

An alternative hypothesis would be that morphotype A represents a neomorphic element, independently developed in Sauropoda. This would be the case if interclavicles would really have gotten lost in Dinosauriformes. However, given the incompleteness of the finds of early dinosauriforms and dinosaurs, it cannot be ruled out that the absence of an ossified interclavicle is due to taphonomy. Therefore, and since the presence of an interclavicle is plesiomorphic for tetrapods, an interpretation of the sauropod morphotype A elements as interclavicle seems more appropriate.

Morphotype B

Not previously recognized (Figs 4.9-4.14).

Our interpretation: clavicles.

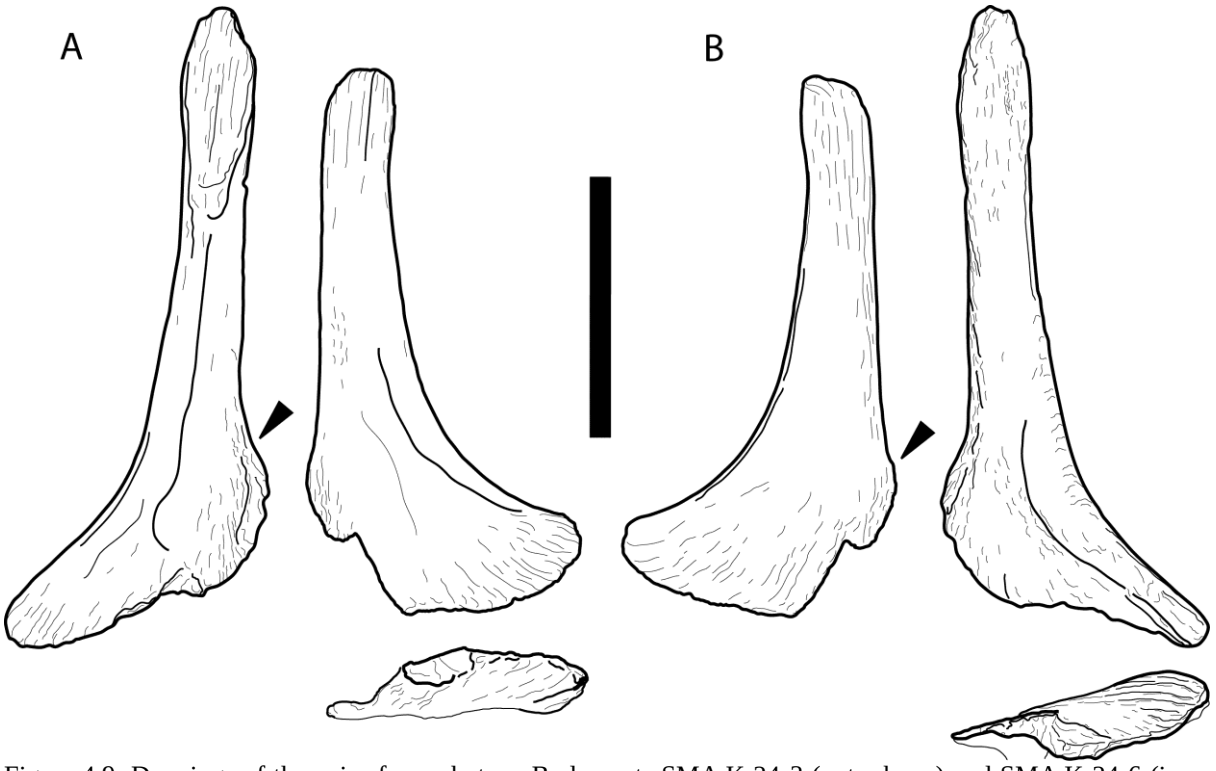

Figure 4.9: Drawings of the pair of morphotype B elements SMA K 24-3 (outer bone) and SMA K 24-6 (inner bone) in internal (a) and external (b) view. Short leg of L-shaped bones shown in perpendicular view below. Note the considerable bend of this portion in respect to the main axis of the bone. Scale bar = 10 cm.

Figure 4.10: Photographs of the morphotype B element SMA K 24-6. Scale bar = 5 cm.

General morphology. Morphotype B elements are L-shaped, and of similar thickness as morphotype A, but shorter. They are concave on one side, and convex on the opposite surface, and are usually found in pairs. Morphotype B elements have a D- to crescentic-shaped cross-section at midlength. The convex side is hereinafter interpreted as external, the flat to slightly concave surface as internal. Towards the end of the longer leg of the L, a striated rugosity develops on both sides, and the bone expands slightly. This end is broken pre-burial in one of the SMA elements (K 24-6; Figs 4.9, 4.10), and postmortem in both AMNH elements, so that they appear shorter and stouter (Fig. 4.12). The shorter leg of the L is expanded 'backwards' as well, especially so in the SMA specimen, forming a somewhat heel-like, rounded flange (Figs 4.9, 4.12). Towards the tip of the short leg, the bone curves externally. This portion shows a similar but stronger striated rugosity as in the longer leg of the L.

Morphotype B elements have a peculiar morphology. The most similar bones are the anterior- or posterior-most dorsal ribs, but neither capitulum nor tuberculum are present on the morphotype B. Furthermore, the striations marking soft tissue attachment do not occur on dorsal ribs.

Howe Quarry material. Two pairs of morphotype B elements were found at this site. The first specimen was found in 1934 by the AMNH (AMNH 30789), the other pair was recovered in the SMA excavation and bear the field numbers SMA K 24-3 and K 24-6. Whereas it is clear that the two bones of AMNH 30789 were found together (this collection number was given to all bones in a plaster jacket bearing the field number 151), their placement within the Howe Quarry is impossible to locate to date.

AMNH 30789 also includes chevrons and pedal material. The SMA specimens were found closely together, below several dorsal ribs, and between posterior cervical and anterior dorsal diplodocid vertebrae.

Figure 4.11: Photographs of the morphotype B element SMA K 24-3. Scale bar = 10 cm.

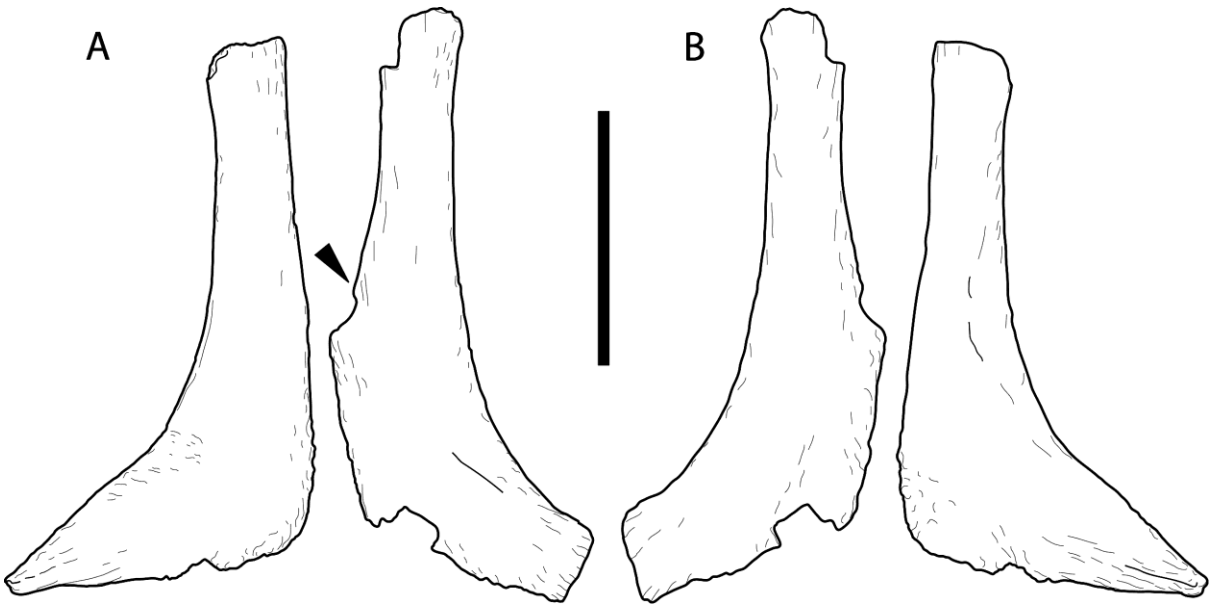

Figure 4.12: Drawings of the pair of morphotype B elements AMNH 30789 in internal (a) and external (b) view. Scale bar = 10 cm.

Figure 4.13: Photographs of the left morphotype B element AMNH 30789. Scale bar = 10 cm.

Figure 4.14: Photographs of the right morphotype B element AMNH 30789. Scale bar = 10 cm.

Previous reports. Not much is known about the occurrence of morphotype B elements in sauropods. The only formal reports of similar elements concerns an element recovered with an early juvenile sauropod (Schwarz et al., 2007c), as well as two bones belonging to the holotype of *Spinophorosaurus nigerensis* (Remes et al., 2009). Due to superficial affinities to elements in *Shunosaurus lii*, Remes et al. (2009) tentatively identified the *Spinophorosaurus* elements as tail spikes. Recently, Galiano and Albersdörfer (2010) informally reported three elements (one pair and a single bone) found associated with indeterminate diplodocid sauropods.

Variation in morphology. One of the AMNH elements develops a conspicuous ridge towards the tip of the short leg of the L. In its counterpart, this end is broken off. Contrary to the state in the AMNH elements, the same end is transversely expanded in the single morphotype B bone reported by Galiano and Albersdörfer (2010; H. Galiano, pers. comm. 2011).

The SMA specimens bear a thickened portion resembling an articulation facet at about midlength of the shorter leg of the L (Figs 4.9-4.11). As the AMNH elements show broken edges in this region, this facet might also constitute to the general morphology (Figs 4.12-4.14).

Identification. The three morphotype B elements recently reported by Galiano and Albersdörfer (2010) include a set of paired bones articulated between the acromia of the scapulae of a diplodocid specimen (DQ-SB; Fig. 4.15), where clavicles are supposed to attach (Romer, 1956; Vickaryous and Hall, 2006). Similarly, detailed examination of the juvenile sauropod SMA 0009 revealed that a second, L-shaped element is actually present attached to the dorsal corner of the right coracoid (Fig. 4.16). Schwarz et al. (2007c), in their initial description of SMA 0009, described this bone as 'dorsally pointing tip' of the coracoid, but a thin layer of matrix between the elements indicates that they are taphonomically pressed onto each other. A third pair of morphotype B elements, articulated between the scapulae, appears to be present in a *Camarasaurus* (KUVP 129716, Bader et al., 2009; A. Maltese, pers. comm., 2012).

The topology and paired appearance of these morphotype B elements strongly suggests that they fit an identification as clavicles better than morphotype A. Such an interpretation would also match previous findings of similarly shaped clavicles in ceratopsian dinosaurs (Chinnery and Weishampel, 1998: fig. 6; Vickaryous and Hall, 2010: fig. 5). On the other hand, paired finds of non-sauropod sauropodomorph clavicles appear to be more straight (Huene, 1926; Yates and Vasconcelos, 2005; Martínez, 2009; B. Pabst, pers. comm., 2011), but without the bifurcated end – resembling the elements recovered from *Jobaria tiguidensis* (Sereno et al., 1999: fig. 3e). However, other than the report of the presence of this bone in *J. tiguidensis*, no other information about which bones it was associated with, and no detailed description has been provided to date.

Another explanation would be that morphotype B comprises sternal ribs. However, a taphonomical shifting of sternal ribs into a position equal to the clavicular articulation typical for tetrapods (as is the case in the specimen DQ-SB) is highly improbable. Therefore, an interpretation of morphotype B elements as the true sauropod clavicles is the most convincing. This interpretation challenges Hatcher's (1901, 1903) identification of the morphotype A bones. As the gross morphology of the shoulder girdle remains similar in the majority of Sauropoda, a high diversity in the shape of clavicles seems improbable. Therefore, an interpretation of the morphotype A elements as interclavicles is supported as well by the presence of morphotype B bones as the true clavicles.

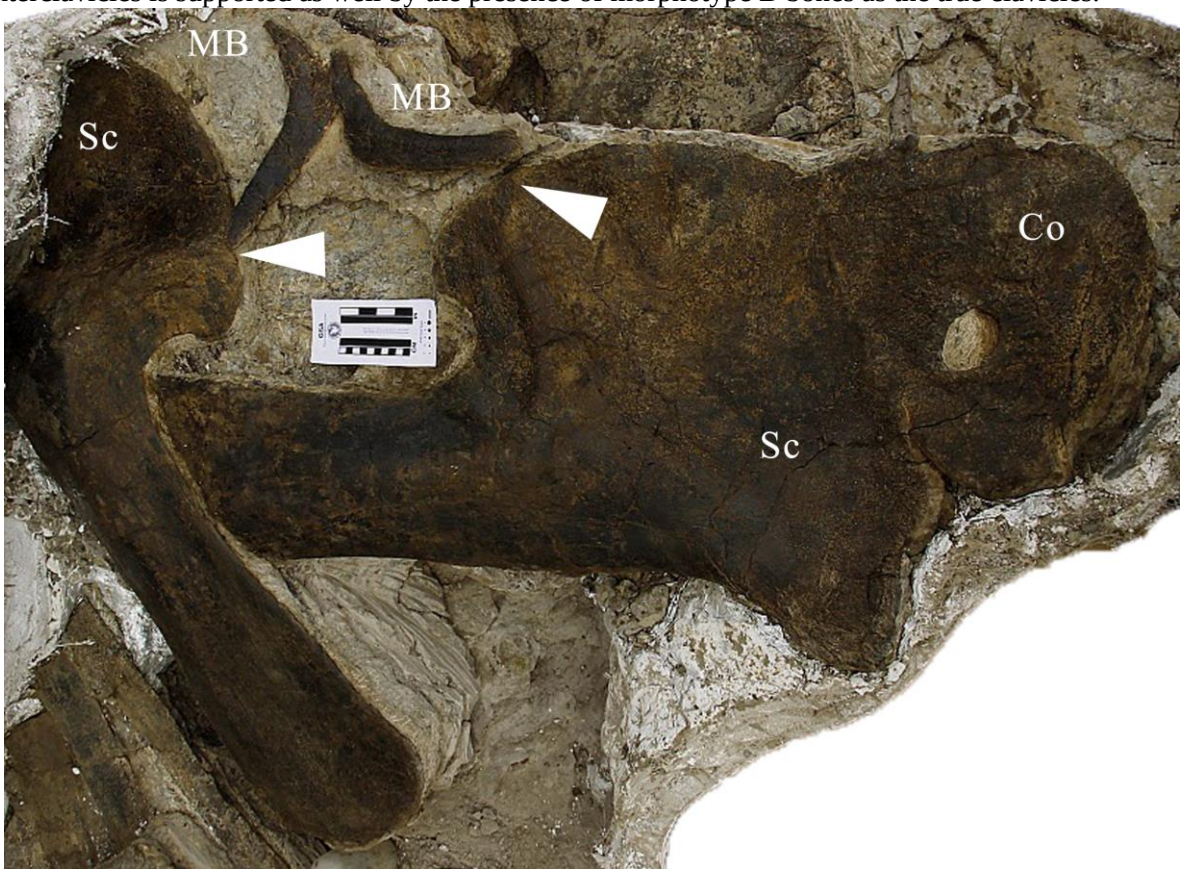

Figure 4.15: Morphotype B elements of the diplodocid DQ-SB, articulated with the acromia (arrowheads) of the scapulae, as they were found. Co, coracoid; MB, morphotype B element; Sc, scapula. Picture courtesy of H. Galiano.

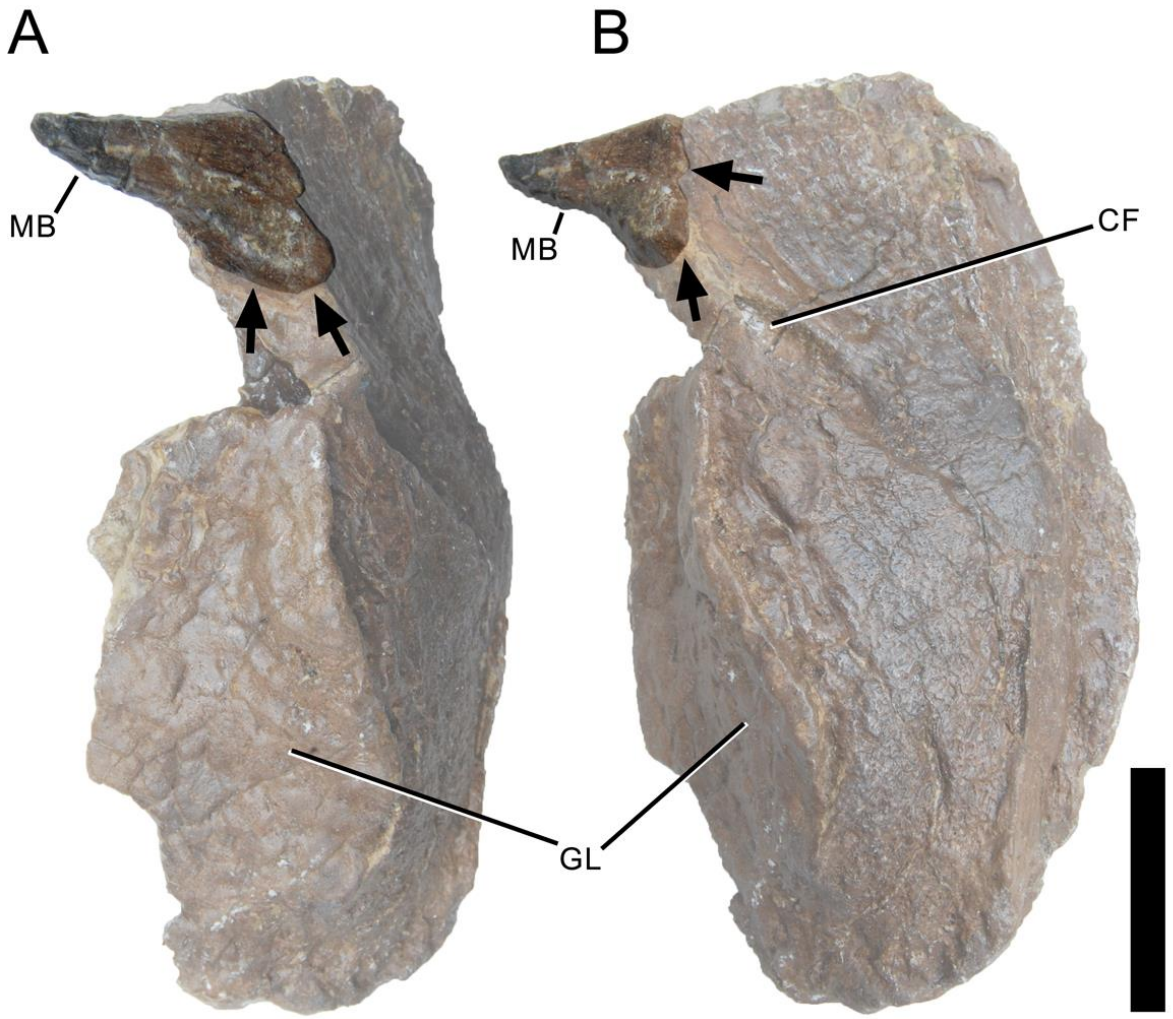

Figure 4.16: Coracoid with taphonomically attached morphotype B element (MB) of the non-somphospondylian macronarian SMA 0009 in posteroventral (a) and lateral (b) view. Coracoid made semitransparent in order to visualize better the morphotype B element. Arrows indicate brightly colored matrix present between the MB and the coracoid. CF, coracoid foramen; GL, glenoid surface. Scale bar = 2 cm.

Morphotype C
Previous identification: gastralia, ventral ribs, sternal ribs (Figs 4.17-4.19).
Our identification: sternal ribs.

General morphology. Morphotype C elements are elongated, rod-like bones with a suboval cross-section. The smooth shafts are generally slightly curved, in some elements (e.g. SMA D 28-6, D 28-7) in two directions forming a weak S-shape. Both ends are rugose and irregular. One end is flattened and often shows differing degrees of rugosity on the two sides of the flattened portion.

The most similar bones to morphotype C elements would be cervical ribs or ossified tendons. However, cervical ribs are usually concave dorsally. Ossified tendons are often attached to other bones, or do not exhibit expanded ends, but if only a portion of the shaft of a morphotype C element is found, distinguishing between the two might be difficult.

Howe Quarry material. In the Howe Quarry sample, three clusters of gastralia/sternal ribs were found by the SMA (around field area D 28, F 27 and M 21; Fig. 4.2). All three clusters contain about 15 single elements. Within these clusters, morphotype C elements constitute the majority of the recovered bones. They (as well as elements belonging to morphotypes D and E) were always found in association with dorsal ribs. In the field area F 27, also two distal tail segments of different sizes as well as single posterior cervical vertebrae were recovered in the vicinity of the gastral/sternal rib cage.

The M 21 cluster was associated with the skull and neck of a diplodocine sauropod, as well as single (probably diplodocid) anterior chevrons. Additional morphotype C elements come from various areas within the Howe Quarry, and were found more scattered.

Previous reports. Such elements were usually described as sternal or gastral ribs, and are often associated with bones of morphotypes D and E. Taxa reported to preserve morphotype C elements include the non-neosauropod eusauropod *Jobaria tiguidensis*, the diplodocids *Apatosaurus louisae*, *Eobrontosaurus yahnahpin*, as well as the macronarian *Camarasaurus supremus* and *Diamantinasaurus matildae* (Holland, 1915a; Osborn and Mook, 1921; Filla and Redman, 1994; Sereno et al., 1999; Hocknull et al., 2009).

Variation in morphology. Instead of being slightly curved, some morphotype C elements remain straight during their entire length. Toward the non-flattened ends, some of the elements remain straight, whereas others show a distinct bend.

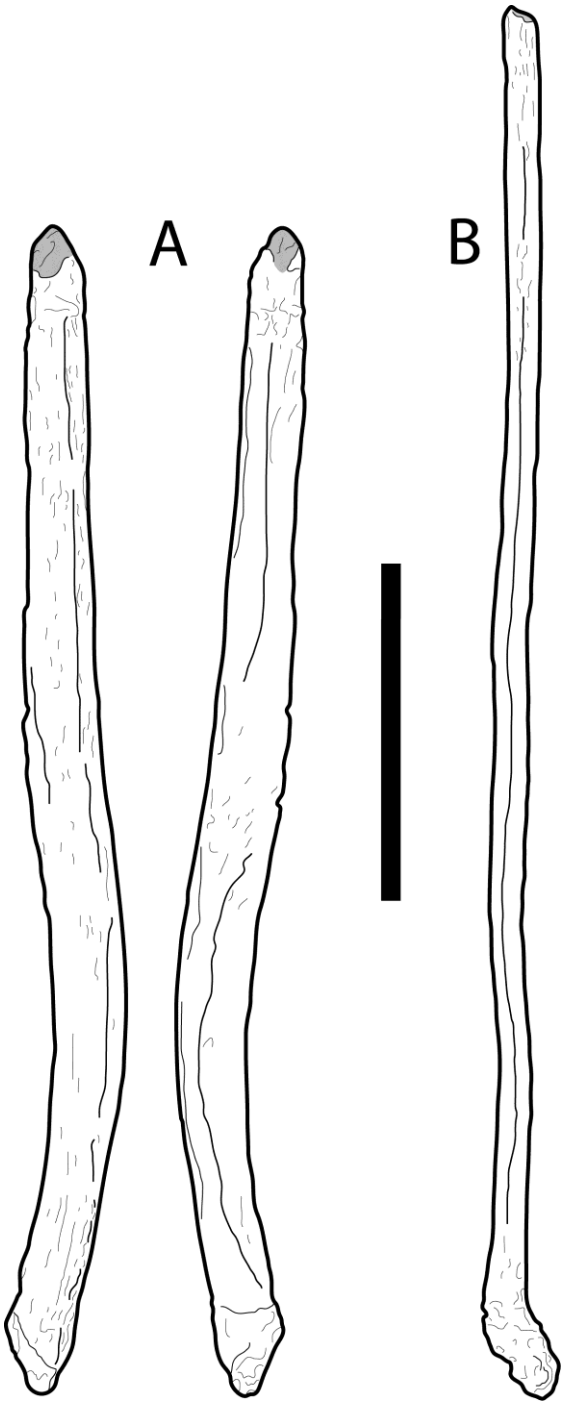

Figure 4.17: Drawings of morphotype C elements SMA H 20-7 (a) and L 21-5 (b). Both elements are incomplete, fracture surface at the top is indicated by the gray area. Scale bar = 10 cm.

Figure 4.18: Photographs of the morphotype C element SMA H 20-7. Scale bar = 10 cm.

Figure 4.19: Photographs of the morphotype C element SMA L 21-5. Scale bar = 10 cm.

Identification. Probable sauropod gastralia and/or sternal ribs have been reported more often than clavicles, and in a wider range of taxa (Tab. 4.2). As mentioned above, their interpretation as gastralia has been challenged by Claessens (2004), pointing out their anatomical differences compared with non-sauropod sauropodomorph or theropod gastralia. Claessens (2004) proposes that Marsh (1896) was right in identifying such elements as sternal ribs.

Sternal ribs are of endochondral origin, and present in both extant birds and crocodilians, but remain often cartilaginous (Claessens, 2004; Claessens et al., 2009; R. Fechner, pers. comm., 2011). They connect the distal tips of the anterior dorsal ribs with the sternum, either directly as in birds, or articulating with the dorsal ribs through generally cartilaginous intercostal elements (Claessens et al., 2009; R. Fechner, pers. comm., 2011; pers. obs.). Within dinosaurs, only very few reports of sternal ribs exist besides the ones from Marsh (1883, 1896): they are described in hypsilophodont Ornithischia (e.g. Parks, 1926; Galton and Jensen, 1973; Weishampel and Heinrich, 1992), and Theropoda (e.g. Clark et al., 1999; Ruben et al., 2003).

Gastralia are dermal bones embedded in the abdominal musculature, and are usually thought to support the breathing apparatus and/or protect the belly (Claessens, 2004; Claessens et al., 2009). As sternal ribs, also gastralia are present in both birds and crocodilians (Claessens, 2004). Unambiguous evidence for gastralia in dinosaurs appears to exist only in Theropoda and early Sauropodomorpha ('prosauropods'; Claessens, 2004; R. Fechner, pers. comm., 2011). None of the bones of morphotype C exhibit the typical longitudinal articulation facets that occur between the medial and lateral elements of theropod or early sauropodomorph gastralia (Claessens, 2004). On the other hand, for a birdlike sternal rib configuration, 15 elements are too many: in birds, distally expanded dorsal ribs usually connect to sternal segments through cartilage (Parks, 1926; Clark et al., 1999; Schwarz et al., 2007a), and straight or converging distal rib ends mark free ribs. Fully articulated ribcages of *Apatosaurus* and *Diplodocus* show transversely expanded ends only in the first five to seven dorsal ribs (Gilmore, 1936; Schwarz et al., 2007a) – which would allow a maximum number of 14 sternal ribs. However, the about 15 elements recovered per cluster include at least three morphotype D elements. Given that the latter most probably are not sternal ribs (see below), the maximum number of sternal ribs per individual would not be exceeded. An identification of morphotype C elements as sternal ribs is thus the most convincing.

Morphotype D
Not previously recognized (Figs 4.20-4.23).
Our identification: gastralia.

General morphology. Morphotype D elements are more irregularly formed than morphotype C, shorter and thicker. They are curved bones with both ends expanded and rugose. The expansions are not equal on the two extremities, one of them being wider than the other. The wider end is flattened, very irregularly expanded, and with strong rugosities. On one side, this end is slightly convex, indicating that this side was not articulating with any other element. These bones all show some curvature at the opposite end, resulting in an outward pointing extremity.

Morphotype D elements can be very similar to bones belonging to morphotype C, and thus also to ossified tendons and cervical ribs. The wide, probably medial (see below) extremity is the best characteristic to define morphotype D. It is more irregular, wider and resembles more bony overgrowth than what is usually present in morphotype C.

Howe Quarry material. Morphotype D elements are less frequently found. However, all three gastral/sternal rib clusters in the SMA collection contain morphotype D elements. Two bones of the cluster D 28 are symmetrical, and can be nicely articulated at their wider ends (D 28-5 and 14; Fig. 4.24).

Previous reports. To our knowledge, elements of this morphotype are described for the first time in this paper. It is possible, however, that previously mentioned sets of 'gastralia' or 'sternal ribs' include morphotype D elements, but that these were not recognized as such and not figured (see Tab. 4.2).

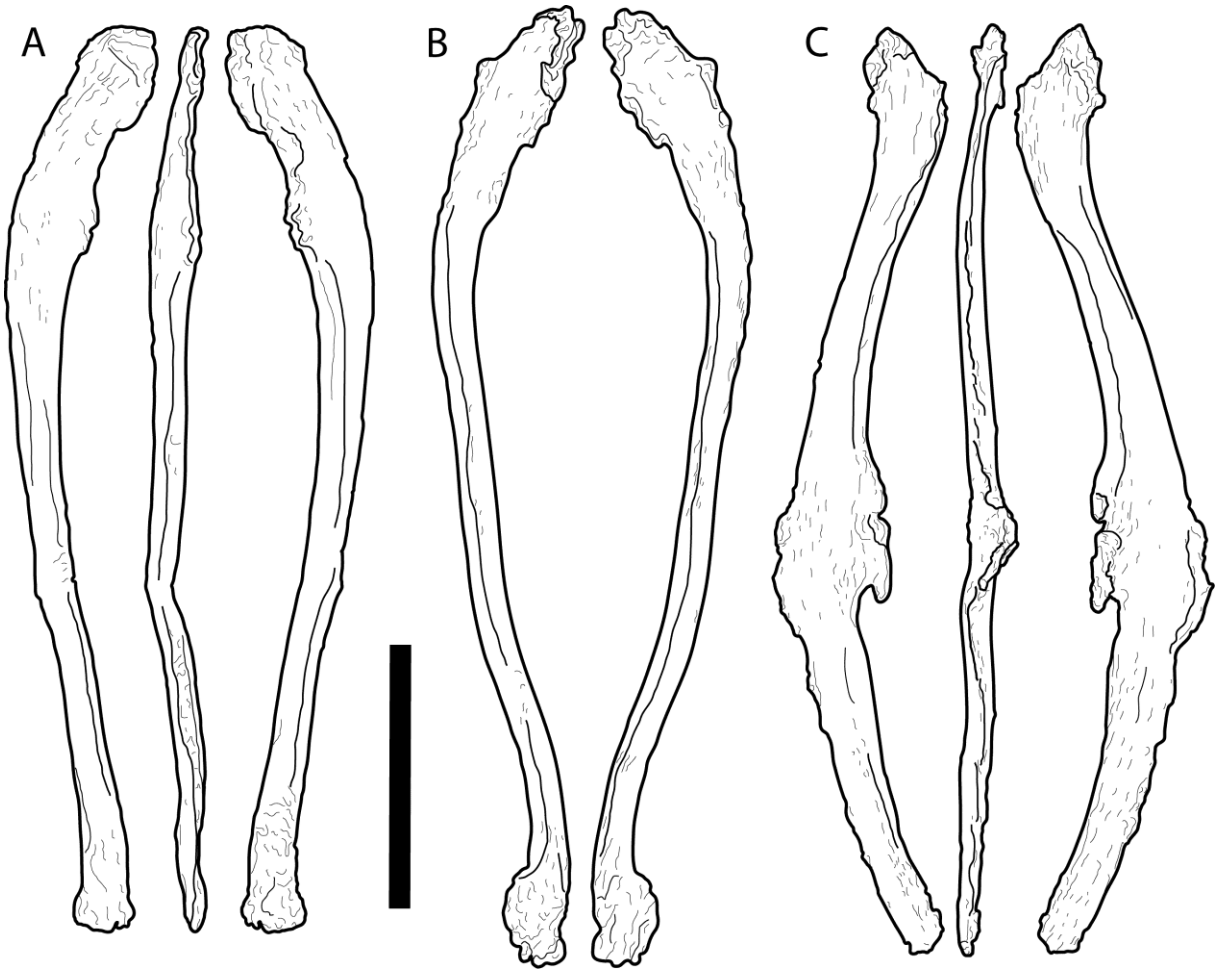

Figure 4.20: Drawings of morphotype D elements SMA D 28-5 (a), M 21-2 (b) and M 21-8 (c). The bottom end of M 21-8 is broken. Scale bar = 10 cm.

Variation in morphology. Certain elements in the M 21-basket (e.g. SMA M 21-8; Figs 4.20c, 4.23) appear to be fused symmetric elements. They reproduce the slight upward curvature of two articulated opposing elements similar to the pair SMA D 28-5 and 14, and exhibit an outgrowth in the middle of the bone, which would come to lie on the body midline. This outgrowth resembles somewhat pathological bony overgrowth but also the shape of two unfused anterior or posterior gastralia with their enlarged medial ends. Towards the extremities the curvature of the bone becomes inverted in a way that the expanded ends are pointing somewhat downwards again (or probably straightly outwards when articulated). This results in a slightly sinuous curve, similar to tyrannosaur furculae described by Makovicky and Currie (1998).

Identification. Although associated with the probable sternal ribs belonging to morphotype C, bones like SMA M 21-8 (Figs 4.20c, 4.23), which seem to be composed of two fused elements like D 28-5 or M 21-2 (Figs 4.20a, 4.21, or 4.20b, 4.22 respectively), have no equivalent in previously described sternal ribs known to us. Sternal ribs sometimes connect to other, more anteriorly placed elements, instead of articulating directly with the sternal plates (Galton and Jensen, 1973; Clark et al., 1999; Claessens et al., 2009), but no specimen has been reported to date exhibiting fused left and right ribs.

Manual manipulation of the two corresponding elements SMA D 28-5 and 14 shows that the expanded ends would articulate relatively nicely in a way similar to the midline joint of two gastralia in non-sauropod sauropodomorphs and theropods (Fig. 4.24). Median gastralia of the anterior-most row were previously shown to fuse in certain cases, thereby forming irregularly shaped and asymmetric sutures (e.g. Makovicky and Currie, 1998; Claessens, 2004). Such a development resembles much the herein described fused elements. Morphotype D is thus most convincingly interpreted as the anterior-most gastralia, close to the sternal apparatus.

Figure 4.21: Photographs of the morphotype D element SMA D 28-5. Scale bar = 10 cm.

Figure 4.22: Photographs of the morphotype D element SMA M 21-2. Scale bar = 10 cm.

Figure 4.23: Photographs of the morphotype D element SMA M 21-8. Scale bar = 10 cm.

Figure 4.24: Proposed articulation between two morphotype D elements (left, SMA D 28-5; right, SMA D 28-14) in three views (internal/dorsal view in the center, gray lines indicate the same morphological landmarks on the respective elements). Note the similarity to the central portion of the fused morphotype D element (Fig. 4.23). Scale bar = 5 cm.

Morphotype E
Previous identification: gastralia, sternal ribs (Figs 4.25-4.27).
Our identification: sternal ribs and/or intercostal elements.

General morphology. Bones belonging to morphotype E have irregular shapes that cannot be included in any of the above defined morphotypes. Peculiar morphologies include projections (e.g. SMA H 21-1; Fig. 4.25a), irregular expansions (SMA N 22-12; Figs 4.25b, 4.27), and bifurcated ends (SMA M 21-15; Figs 4.25c, 4.26). Due to their particular shapes, morphotype E elements do not resemble any other bone in the sauropod skeleton.

Howe Quarry material. Few of these elements were recovered at the Howe Quarry, always in association with bones of the morphotypes C and D. SMA H 21-1 and 3 form a symmetrical pair.

Previous reports. Similar elements include bones of *Apatosaurus excelsus*, identified as sternal ribs by Marsh (1883, 1896), and some of the elements of the gastral basket of *Eobrontosaurus yahnahpin* described by Filla and Redman (1994).

Variation in morphology. SMA H 21-1 and H 21-3 develop a projection approximately at one-third to two-fifths of their entire length, which appears to proceed at an acute angle to the longer portion of the bone (Fig. 4.25a). How long this projection is remains unclear, as their ends are broken in both elements. M 21-15 is a rather thick bone of medium length, compared with the usual gastralia/sternal ribs. Both ends are flattened, one of them is markedly and slightly asymmetrically bifurcated (Figs 4.25c, 4.26). On the edge running from the longer portion of the bifurcation, somewhat inwards, a tubercle can be seen with fractured bone surface so that the original expansion of this feature cannot

be determined. The opposing end is irregular as well, exhibiting a very shallow notch. N 22-12 is a short and very thin bone, with one end greatly expanded in two dimensions, forming a spatulate shape with irregular margins, and a weak, radiating striation extending from the center of the bone towards the outer margins on both sides (Figs 4.25b, 4.27). At the base of this expansion, both sides are marked by well visible foramina, which lie on the same level in regard to the long axis of the bone, and only very slightly displaced perpendicular to the long axis. Towards the other end, at about two-thirds of the entire length, there is a rugose tubercle. Further towards this end, the bone curves and becomes more rugose again.

Identification. Considering a crocodilian arrangement, morphotype E elements (like the particularly shaped SMA N 22-12, and maybe also the short elements described by Filla and Redman (1994: fig. 11h,i,q,r) might represent intercostal elements. Furthermore, the two SMA elements with the projection (H 21-1 and H 21-3), as well as the very irregularly shaped bone figured by Marsh (1896: figs 12, 13) resemble somewhat the posterior sternal ribs in the pterosaur *Rhamphorhynchus* (Claessens et al., 2009: fig. 2d). The projections as well as the bifurcations might have articulated with more anterior sternal ribs.

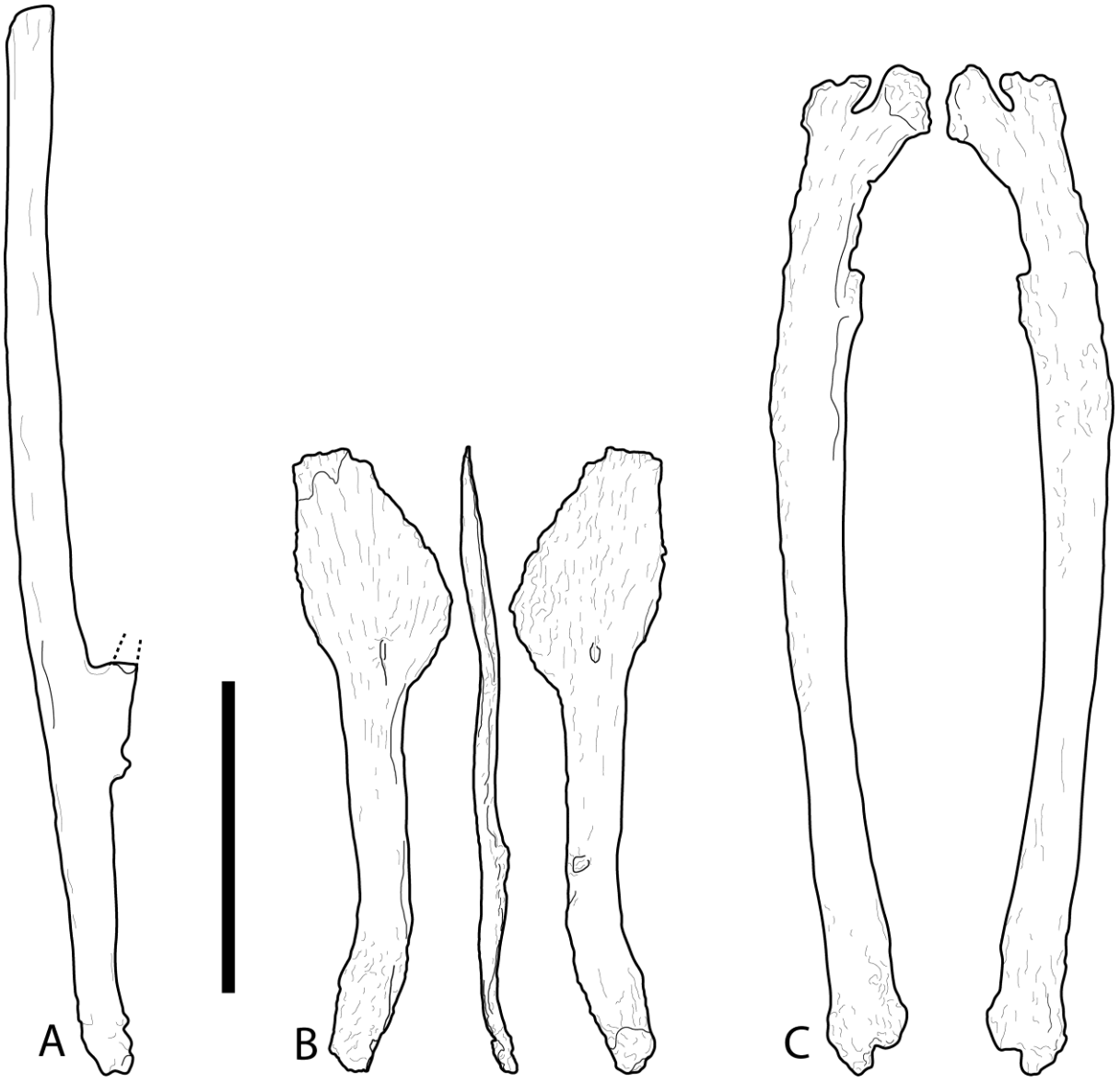

Figure 4.25: Drawings of morphotype E elements SMA H 21-3 (a), N 22-12 (b) and M 21-15 (c). Note the irregular shapes that do not allow an assignation to any other morphotype. Dotted lines in (a) indicate direction of the broken hook-like projection. Scale bar = 10 cm.

As gastral and sternal ribs have differing developmental origins (Tab. 4.1), a histological analysis might yield more definitive results concerning the identity of morphotypes C–E, but should include elements of all of them. However, histological sections of dermal and endochondral bones are difficult to distinguish in a fully ossified state (T. Scheyer, pers. comm., 2009). Such a study has thus to await further analyses and comparisons of known gastralia and sternal ribs in extant animals, and lies outside the scope of this paper.

Figure 4.26: Photographs of morphotype E element SMA M 21-15. Scale bar = 10 cm.

Figure 4.27: Photographs of morphotype E element SMA N 22-12. Scale bar = 10 cm.

Morphological implications

The rarity of finds of ossified chest elements other than the scapulacoracoid or the sternal plates render proper identifications difficult, especially due to the fact that they are often recovered disarticulated from the corresponding pectoral girdle. This might imply that the soft tissue connection between them and the pectoral girdle or the sternal apparatus was not very strong during lifetime – and as a consequence, chest bones were possibly easily disarticulated if not lost entirely before burial. When pre-served and found, the indistinct shape and consequential difficulties identifying these elements make them more likely to not be reported or not even collected, increasing such a taphonomic bias even more. Nonetheless, the herein reported bones indicate that additional elements like the clavicles, inter-clavicle, sternal ribs, gastralia, and possibly intercostal elements do ossify in some sauropod taxa. However, it must be noted that no articulated sauropod specimen has yet been reported preserving both morphotype A (interclavicles) and B elements (clavicles; but see addendum). The finds, where clavicles were found articulated (DQ-SB, KUVP 129716) or associated (SMA 0009) with the scapulacoracoids, do not appear to preserve an interclavicle. In the Howe Quarry sample described herein, all the elements were found disarticulated in a bonebed. Nonetheless, the tight association with diplodocid material suggests that if not from the same individuals, they were at least from the same taxon. A novel reconstruction of the diplodocid pectoral girdle and sternal apparatus, taking these interpretations into account, is shown in Fig. 4.28.

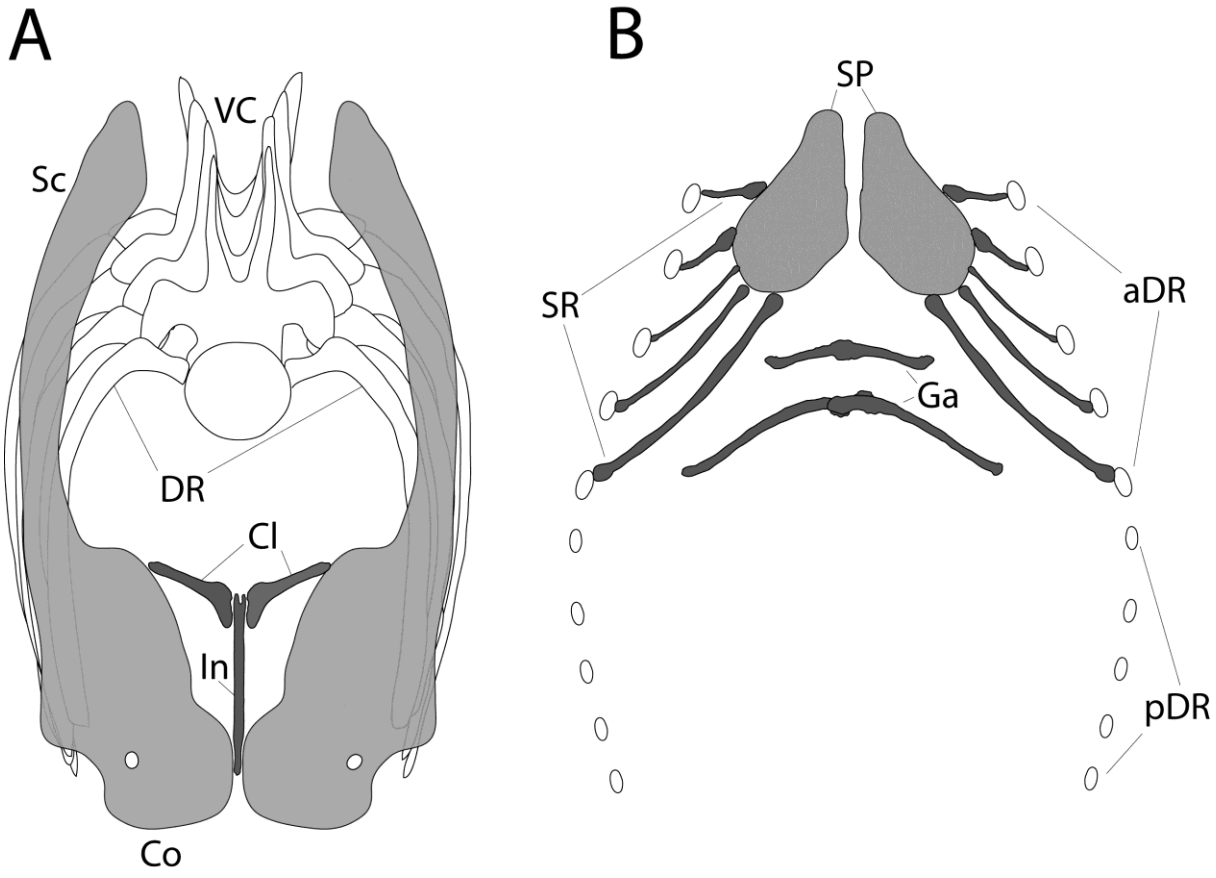

Figure 4.28: Reconstruction of the pectoral girdle and the chest region of an indeterminate diplodocid sauropod, based on the finds reported. Light gray elements represent pectoral girdle elements not discussed in the paper, dark gray elements mark the bones identified as chest bone morphotypes in this paper. Anterior (a) and ventral (b) view. Abbreviations: aDR, anterior dorsal ribs; Cl, clavicle (morphotype B); Co, coracoid; DR, dorsal rib; Ga, gastralia (morphotype D); In, interclavicle (morphotype A); pDR, posterior dorsal ribs; Sc, scapula; SP, sternal plates; SR, sternal ribs (morphotypes C and E); VC, vertebral column. Modified from Schwarz et al. (2007a; a) and Filla and Redman (1994; b).

The only species from which both types of bones are reported is *Spinophorosaurus nigerensis*, but they are from two different individuals (Remes et al., 2009). The somewhat L-shaped elements of the holotype of *Spinophorosaurus nigerensis* appear to be of considerably different sizes, which was one of the reasons leading to their identification as tail spikes (Remes et al., 2009; R. Kosma and A. Ritter, pers. comm., 2011). However, the *Spinophorosaurus* elements resemble much more the L-shaped bones found at the Howe Quarry than the supposed *Shunosaurus* tail spikes (Zhang, 1988). They do not bear the typical osteoderm surface rugosity as seen in thyreophorans and sauropods, neither shows the specimen any club-like distal extension as present in *Shunosaurus*. Compared with the Howe Quarry material, the base of the *Spinophorosaurus* elements (which would correspond to the shorter leg of the L) is slightly broader, and the two legs curve gently into each other, giving the entire bone a rather triangular outline. Also, the obviously broken edges of the preserved elements shed some doubt on them being of considerably different size as described by Remes et al. (2009). Given that these elements were found below the scapula (Remes et al., 2009), an interpretation as clavicles seems possible for the *Spinophorosaurus* elements, and the original material should be reassessed under the light of the new findings.

Functional implications

An ossification of such a variety of chest elements creates anchor attachments for musculature and stabilizes the entire pectoral girdle, the sternal apparatus and in case of ossified gastralia also the rest of the trunk. A substitution of soft tissues (probably cartilage or ligaments in the case of the sauropod pectoral apparatus) by bone helps to cope with higher loads (Romer, 1956; Haines, 1969). The sauropod taxa exhibiting ossification of the various chest elements show some correlation with taxa usually interpreted to use their tail as laterally swinging defensive weapon, indicated by the presence of tail clubs (*Shunosaurus, Omeisaurus, Mamenchisaurus*; Zhang, 1988; Dong et al., 1989; Xing et al., 2009), possible tail spikes (*Shunosaurus, Spinophorosaurus*; Zhang, 1988; Remes et al., 2009; but see above) or whip-lash tails (*Suuwassea, Diplodocus*; Hatcher, 1901; Harris, 2006b). Lateral movements of the tail might request a firm trunk in order to not disequilibrate the entire animal. Since the pelvic girdle – in contrast to the shoulder girdle – is co-ossified with the vertebral column, reinforcements would be particularly essential in the pectoral girdle. Furthermore, a posteriorly located center of mass, as present especially in diplodocids, appears to induce important lateral stresses to the pectoral girdle during locomotion (Sander et al., 2011).

The loss of ossified chest elements coincides with the evolution of the particular wide-gauge locomotor style of titanosauriform sauropods (Wilson and Carrano, 1999; Carrano, 2005). The question remains, if the loss of ossified chest bones allowed the wider spacing of the legs, or if the latter enhanced stability enough to render the ossification useless. The presence of clavicles and/or interclavicles in *Datousaurus*, *Jobaria*, and *Camarasaurus* might just represent an example of retained plesiomorphies without strong functional significance.

Phylogenetic implications

The proposed presence of ossified elements in the chest region of some sauropods has also phylogenetic implications – even in case some of the above-stated interpretations would remain controversial. Although a taphonomic bias leading to the absence of chest bones in titanosauriforms and rebbachisaurs cannot be excluded to date, their distinctly taxonomically restricted appearance appears striking. As an ossification of additional chest elements in diplodocids and early eusauropods does also make sense in a functional point of view (see above), their presence is herein interpreted as plesiomorphic for Sauropoda, whereas the loss of ossified clavicles, interclavicles, sternal and/or gastral ribs might result a synapomorphy for Titanosauriformes, and maybe Rebbachisauridae as well. The single findings of sternal ribs in the lithostrotian *Diamantinasaurus* (Hocknull et al., 2009) remain doubtful, or might represent exceptions to the rule.

The presence of interclavicles in dinosaurs is herein stated for the first time with direct morphological evidence. The other reported possible dinosaurian interclavicles were reinterpreted as clavicles or furculae, and thus their identification remains ambiguous (Cooper, 1981; Yates and Vasconcelos, 2005). This supports Vickaryous and Hall (2010) statement that the theropod and avian

furcula could also be homologous to the interclavicle instead of representing the fused clavicles, as generally proposed (Yates and Vasconcelos, 2005; Nesbitt et al., 2009). The evolutionary gap between non-dinosauriform interclavicles and theropod furculae, for which we did not have conclusive data before, is shortened by the presence of interclavicles in sauropods. If the interclavicle-furcula homology would get confirmed by future studies, theropods would have reduced the stem-like central body of the interclavicle as seen in sauropods to the hypocleidium, and the transverse processes would have been enlarged, and would have substituted the clavicles, which would have gotten lost early in theropod evolution. However, because both clavicles and interclavicles are present in sauropods, conclusions have to await finds of articulated specimens of early dinosaurs, or dinosauriforms, which might shed more light on the evolution of the theropod pectoral girdle. The strongest evidence against the furcula-interclavicle homology are the topology of the furcula (it articulates with the acromion as clavicles do; see Nesbitt et al., 2009), and the pairs of bones found in *Massospondylus* and early theropods, which articulate with the scapular acromion laterally, and among themselves medially (Yates and Vasconcelos, 2005; Nesbitt et al., 2009). Since in articulation, they resemble much the theropod furcula, and Nesbitt et al. (2009) interpreted them as an intermediate evolutionary state between unfused clavicles and the furcula. The competing hypotheses are summarized in Fig. 4.29.

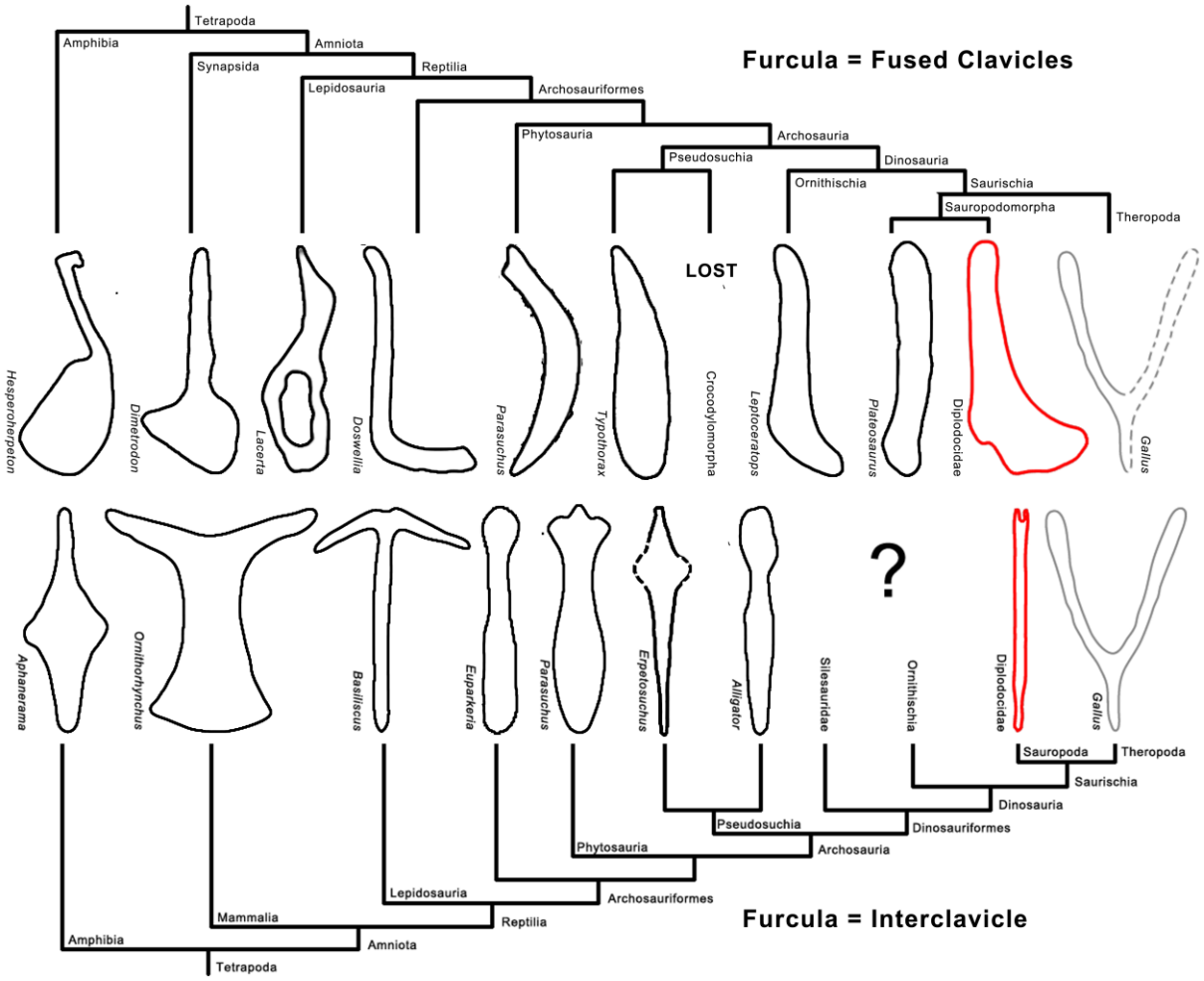

Figure 4.29: Evolution of the furcula, comparison between the two hypotheses. Note the gap within Dinosauriformes in the furcula-interclavicle hypothesis. Line drawings scaled to same size. Eaton and Stewart (1960: *Hesperoherpeton*); Chatterjee (1978: *Parasuchus*); Klima (1987: *Ornithorhynchus*); Rieppel (1992: *Lacerta*); Steyer et al. (2000: *Aphanerama*); Benton and Walker (2002: *Erpetosuchus*); Martz (2002: *Typothorax*); Vickaryous and Hall (2006: *Dimetrodon*; 2010: *Alligator*, *Basilicus*, *Gallus*, *Leptoceratops*); Remes (2008: *Euparkeria*); Dilkes and Sues (2009: *Doswellia*).

Conclusions

Several elements recovered at the Howe Quarry (Bighorn County, Wyoming, USA) resemble bones previously identified as sauropod clavicles, as well as gastralia and/or sternal ribs. The finding of pairs of symmetric bones associated with pectoral girdle elements sheds new light on these old interpretations. In fact, detailed investigations lead to the conclusion that the bones previously supposed to represent clavicles, most probably are interclavicles, with the symmetrical, L-shaped pairs being the true claviculae. This supports the result of developmental studies of Vickaryous and Hall (2010), which questions the loss of the interclavicle in Dinosauria – and proposes a homology between the avian furcula and the reptilian interclavicle. This would change the usual interpretation that the furcula represents the fused clavicles.

A review of the occurrence of such bones within Sauropoda implies that the tendency to ossify interclavicles, clavicles, and sternal and/or gastral ribs has a distinct taxonomic distribution, with non-neosauropod Eusauropoda and Flagellicaudata representing the plesiomorphic state, and Titanosauriformes as well as possibly Rebbachisauridae exhibiting the derived condition. Functional implications of retaining the ossified chest bones include the stabilization of the trunk in order to have a firm base for lateral movements of elongated necks and tails. On the other hand, the loss of these osseous elements could have allowed the evolution of the wide-gauge locomotion in Macronaria.

Addendum – unpublished

Two specimens are now known to show one morphotype A and a set of two morphotype B elements from the same individual: a diplodocid skeleton from Dana Quarry (SMA Arapo, pers. obs., 2013), and *Suuwassea emilieae* ANS 21122 (D. Lovelace, pers. comm., 2013). Furthermore, also a titanosaur skeleton was informally reported to possibly preserve an interclavicle (K. Voegele, pers. comm., 2012; see the updated table 4.2). The presence of one morphotype A element and two morphotype B elements in SMA Arapo, and ANS 21122 further corroborates the hypothesis that the morphotype A bones are interclavicles. In SMA Arapo, they were found during preparation, below anterior dorsal vertebrae, close to the right scapula (R. Lillich, pers. comm., 2013). The exact location and association of the probable *Suuwassea* clavicles is not known to date.

If the identification of an interclavicle in a titanosaur is confirmed, the proposed correlation of the loss of clavicles and interclavicles and the evolution of the wide-gauge locomotion mode typical for titanosauriform sauropods would become much weaker. Taphonomic reasons for the lack of such elements in titanosauriforms known to date might then be more probable than real absence.

Two new specimens of diplodocid sauropods from the northern exposures of the Morrison Formation (Upper Jurassic; Wyoming, USA)

Locality

The two new specimens described in the following (SMA 0011, SMA 0087) were found at the Howe-Scott quarry, one of three major sites on the Howe Ranch, north of Shell, Wyoming. The Howe-Scott quarry is located between the better known Howe Quarry (Brown, 1935; Ayer, 2000; Michelis, 2004; Tschopp and Mateus, 2012b) and the Howe-Stephens quarry (Ayer, 2000; Schwarz et al., 2007c; Christiansen and Tschopp, 2010; Fig. 1.1). The site was found in 1995 by a team from the Saurier-museum Aathal, Switzerland, and excavated in three periods (1995, 2000, 2002-2003). Stratigraphically, it lies just slightly above the Howe-Stephens quarry, 30 meters above the J-5, and 30 meters below the K-1 unconformities, which define the lower and upper limits of the Morrison Formation, respectively (Michelis, 2004; J. Ayer, pers. comm. 2007; Fig. 1.2). In addition to SMA 0011 and 0087, four fragmentary diplodocid specimens (mostly appendicular material), a possible brachiosaur hindlimb, two partly-to-almost complete *Hesperosaurus* (Ornithischia, Stegosauria), some *Othnielosaurus* bones (Ornithischia, Neornithischia), numerous shed theropod teeth, carbonized wood, and various freshwater shells were recovered at the Howe-Scott quarry (Michelis, 2004; H.-J. Siber, pers. comm., 2003; pers. obs., 2003). However, none of these specimens has yet been formerly described or identified.

Material

SMA 0011

The specimen SMA 0011 consists of an almost complete, disarticulated skull, eleven cervical vertebrae (probably CV 1-6, 8, 9, 11, 12, and 15, see below), the complete dorsal column, including several dorsal and sternal ribs, a partial sacrum, the right scapula and coracoid, both humeri, the left ulna, radius and manus, the right ilium and pubis, a left ischium, femur, tibia, fibula and nearly complete pes. The specimen was found in two parts: 1) skull and vertebral column from the atlas to DV 3, and 2) dorsal vertebrae 4 to 10, sacrum, and appendicular elements (Fig. 5.1). It is interpreted to belong to a single individual due to matching size, no overlap of elements, and an extremely similar pattern of neurocentral closure in cervical and dorsal vertebrae (see below). The specimen SMA 0011 was excavated in 1995 and 2000.

SMA 0087

The specimen SMA 0087 consists of an articulated series of 35 dorsal, sacral, and caudal vertebrae. In addition, some dorsal and sternal ribs, several chevrons, the right ilium and pubis, both ischia, and a completely articulated right hindlimb and associated pes were recovered (Fig. 5.2). The specimen was overlying an articulated stegosaur specimen (SMA 0092). The material is partly prepared to date. Dorsal vertebrae 5 to 8, portions of the sacral neural arches, anterior to middle caudal vertebrae, as well as the femur, lower hindlimb and pes are accessible and described herein. The skeleton was found in 2002, and completely excavated in 2003. It was found lying below SMA 0011, in a layer about one meter deeper.

Systematic Paleontology

Dinosauria Owen, 1842
Sauropoda Marsh, 1878
Eusauropoda Upchurch, 1995
Neosauropoda Bonaparte, 1986
Diplodocoidea Marsh, 1884 (see Upchurch, 1995)
Flagellicaudata Harris and Dodson, 2004
Diplodocidae Marsh, 1884

Diplodocinae Marsh, 1884
Galeamopus gen. nov.
Type species. *Galeamopus hayi* (Holland, 1924)

Diagnosis. *Galeamopus* is diagnosed by the following autapomorphies: portion of the parietal contributing to the skull roof is practically inexistent (unique among Flagellicaudata), a foramen in the notch that separates the two basal tubera (unique among Diplodocinae), well-developed anteromedial processes on the atlantal neurapophyses, which are distinct from the posterior wing (unique among Diplodocoidea), the posterior wing of atlantal neurapophyses remains of subequal width along most of its length (unambiguous), and the axial prespinal lamina develops a transversely expanded, knob-like tuberosity at its anterior end (unambiguous).

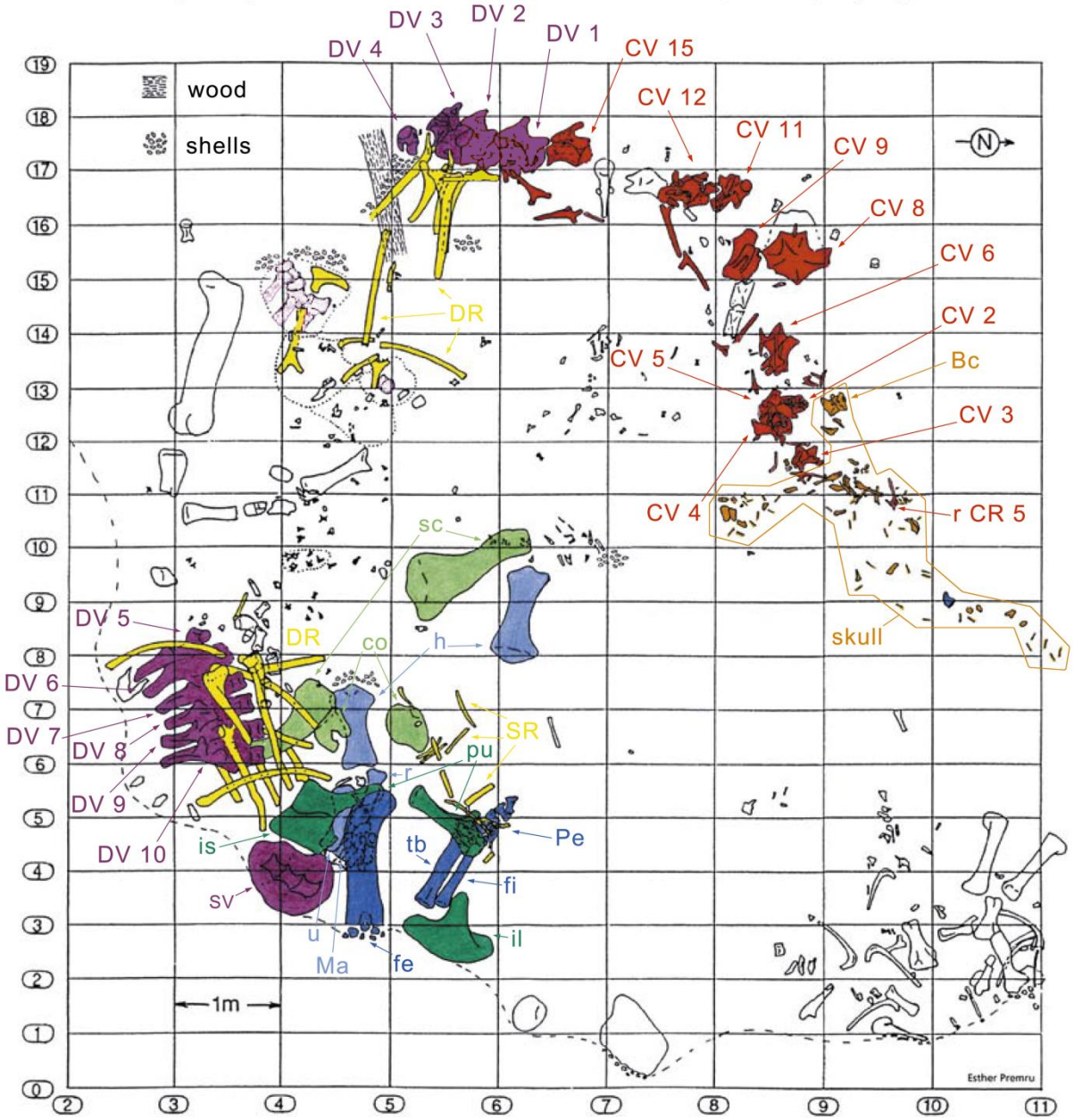

Figure 5.1: Quarry map of SMA 0011, indicating the single bones found. Note the separation of the cervical series and the skull from the dorsal column and the appendicular skeleton. Color code: skull (orange), CV (red), DV (violet), DR and SR (yellow), PcG (light green), PvG (dark green), Fl (light blue), Hl (dark blue). Abb.: Bc, braincase; co, coracoid; CR, cervical rib; CV, cervical vertebra; DR, dorsal ribs; DV, dorsal vertebra; fe, femur; fi, fibula; Fl, forelimb; h, humerus; Hl, hindlimb; il, ilium; is, ischium; Ma, manus; PcG, pectoral girdle; Pe, pes; pu, pubis; PvG, pelvic girdle; r, radius; sc, scapula; SR, sternal ribs; SV, sacral vertebrae; tb, tibia; u, ulna. Map drawn by Esther Premru.

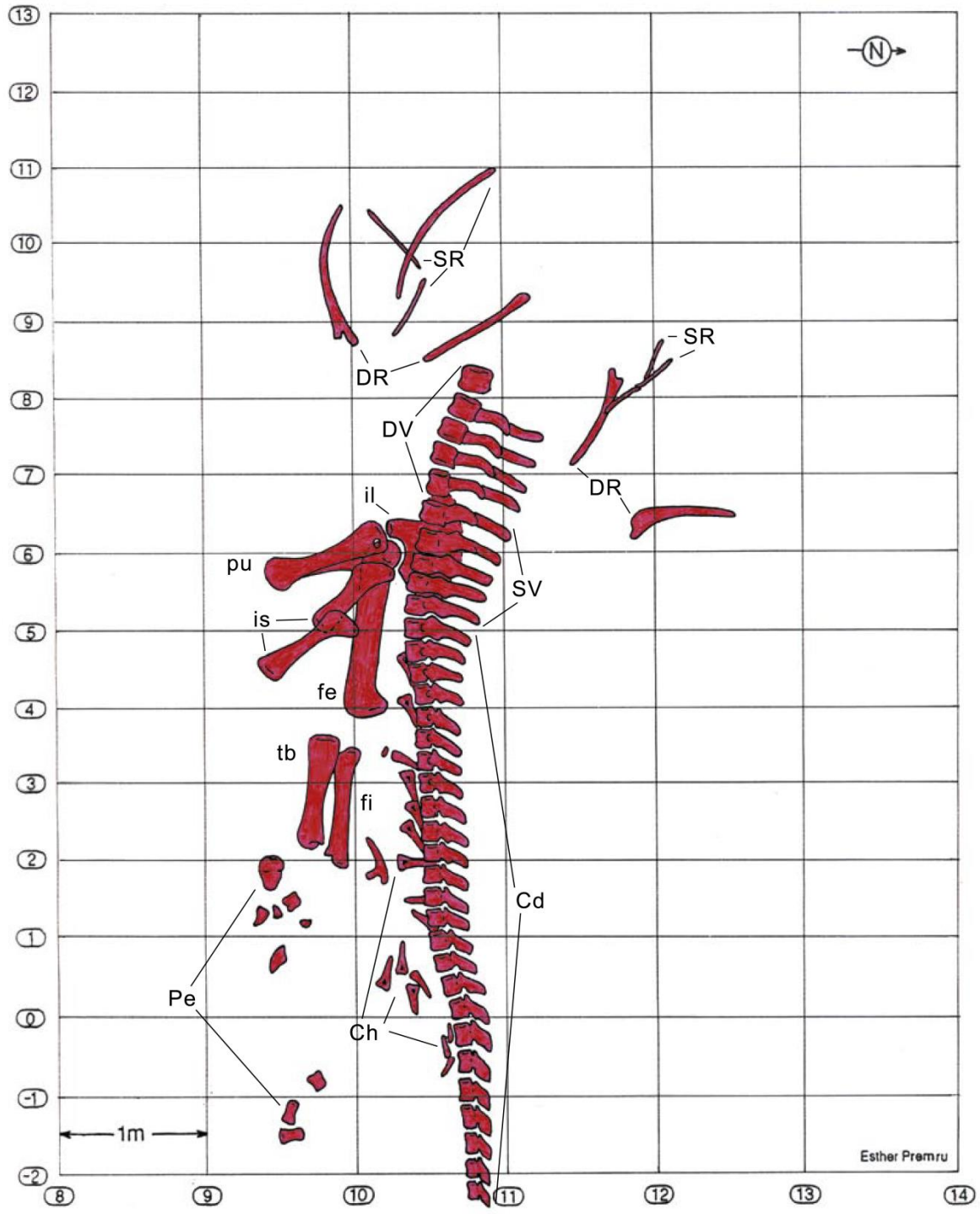

Figure 5.2: Quarry map of SMA 0087, without bones of other specimens found close-by. Abb.: DR, dorsal ribs; DV, dorsal vertebra; fe, femur; fi, fibula; il, ilium; is, ischium; Pe, pes; pu, pubis; SR, sternal ribs; SV, sacral vertebrae; tb, tibia. Map drawn by Esther Premru.

Etymology. 'Galeam' means helmet, and 'opus' need, necessity in Latin, remembering and honoring the two 'Williams' intimately connected with the genoholotype specimen HMNS 175: William H. Utterback and William J. Holland. The English name 'William' derives from the German name 'Wilhelm', meaning "want helmet, protection". Utterback found HMNS 175 in 1902 and Holland described its braincase in 1906, and named the holotype species *G. hayi* as *Diplodocus hayi* in 1924 – although already stating that the morphological differences between *G. hayi* and *Diplodocus* might prove to allow the erection of a new genus in future. *Galeamopus* is also an allusion to the fact that the fragile braincase is the only described part of the holotype skeleton to date. Last but not least, the referred specimen SMA 0011 was informally called "Max", after the kid's story 'Max and Moritz' from the German writer Wilhelm Busch.

Galeamopus shellensis sp. nov.
Figs 5.3-5.35

Diagnosis. *Galeamopus shellensis* can be diagnosed by the following autapomorphies: horizontal canal connecting the preantorbital and the antorbital fenestra laterally on the maxilla (unambiguous), mid- and posterior cervical vertebrae with a large foramen connecting the postzygapophyseal centrodiapo-physeal fossa and the spinopostzygapophyseal fossa (unambiguous), a robust humerus (unique within Diplodocinae), absence of a shallow, but distinct rugose tubercle at the center of the concave proximal portion of the anterior surface of the humerus (unique within Diplodocinae), and the maximum diameter of the proximal end of the radius divided by its greatest length equals 0.3 or greater (unique within Diplodocinae).

Holotype. SMA 0011: partial skull, 11 cervical vertebrae, 10 dorsal vertebrae, partial sacrum, dorsal and sternal ribs, the right scapula and coracoid, both humeri, the left ulna, radius, and manus, the right ilium and pubis, the left ischium, the left femur, tibia, fibula, and pes.

Etymology. The species name 'shellensis' derives from Shell, the small town in Big Horn County, Wyoming, that lies closest to the Howe Ranch sites. People from Shell always supported the team from the Sauriermuseum Aathal both with manpower as well as morally.

Referred specimen. AMNH 969, a nearly complete skull (see next chapter).

Locality and horizon. *Galeamopus shellensis* is known from two quarries in the Upper Jurassic Morrison Formation of Wyoming: the Howe-Scott Quarry (SMA 0011) on the western slopes of the Bighorn mountains and the Bone Cabin Quarry in Albany County (AMNH 969). Both sites were previously interpreted to lie relatively low stratigraphically in the Morrison Formation (Turner and Peterson, 1999; Schwarz et al., 2007c). However, correlation of excavation sites in northern Wyoming, Montana, and South Dakota with quarries from more southern exposures remains difficult, and further studies are needed to confirm their respective stratigraphic positions (Turner and Peterson, 1999; Trujillo, 2006). Nonetheless, the fact that both quarries produced the same species implies that they are from similar stratigraphic levels.

Description of SMA 0011

Skull (Figs 5.3-5.12; Tab. 5.1)
The skull of *Galeamopus shellensis* SMA 0011 has a typically diplodocid shape. It is elongate, with the external nares retracted and dorsally facing, and slender, peg-like teeth (Figs 5.3-5.5). Given the completeness of the skull, a reconstruction was created in cooperation with the Portuguese illustrator Simão Mateus (ML; Fig. 5.6). When comparing with recent reconstructions of the skull of *Diplodocus* (Wilson and Sereno, 1998; Whitlock, 2011b), it can be seen that *Galeamopus* has a more triangular skull outline in lateral view, and more sinuous ventral maxillary edges in dorsal view (Fig. 5.6).

Premaxilla. The premaxillae are completely preserved. They are anteroposteriorly long and transversely narrow elements that contact each other medially and the maxillae laterally. The posterior end of the premaxillae delimits the nasal opening anteriorly. In dorsal view, the elements are narrow in their central part and widen anteriorly and posteriorly. The anterior edge is straight to slightly convex, whereas the posterior margin is deeply concave, such that the two premaxillae together form a

triangular process that enters the nasal opening. The medial margin is straight, and the lateral one concave due to the central narrowing of the element. Some nutrient foramina are present on the anterior-most portion of the dorsal surface, as is a groove originating at the premaxillary-maxillary contact, and extending obliquely anteromedially. The groove is faint and relatively short, not reaching either the anterior or the medial margin. Such a groove was usually interpreted as typical for dicraeosaurids (Remes, 2009; Whitlock, 2011a), but is also present in other diplodocids (pers. obs. 2011). However, a fading out is uncommon in dicraeosaurids, where the groove is distinct (Janensch, 1935; Remes, 2009). Ventrally, the anterior portion of the premaxillae thickens slightly dorsoventrally in order to bear the replacement teeth, but not to the extent seen in USNM 2673 (ET, pers. obs., 2011). Five teeth are mounted, but only four alveoli are present in the left element, whereas the right premaxilla appears to show five. The alveoli of the articulated premaxillae do not contact each other medially, such that there would be space for two more teeth in between, or a gap. At the border with the maxilla, where the premaxilla narrows from the broader anterior part to the narrow central part, the two bones form an elongated fossa which bears the subnarial and the anterior maxillary foramen. Both foramina lie on the medial edge of the maxilla, very close together.

Figure 5.3: Skull bones of SMA 0011 before mounting. Black elements were lacking and reconstructed for the mounted skull. Abb.: an, angular; aof, antorbital fenestra; at, atlas; Bc, braincase; d, dentary; f, frontal; j, jugal; la, lacrimal; m, maxilla; na, nasal; pf, prefrontal; pm, premaxilla; pra, proatlas; q, quadrate; qj, quadratojugal; sa, surangular; T, teeth. Scale bar = 10 cm. Photo by Urs Möckli.

Maxilla. Only the right maxilla is preserved, and complete. The broad anterior portion bears a posterior process, which contacts the jugal and quadratojugal, and a posterodorsal process, which contacts the lacrimal, nasal and possibly the prefrontal. The maxilla forms the dorsal, anterior, and anteroventral margins of the antorbital fenestra, and completely encloses the preantorbital fossa and fenestra. Unlike *Kaatedocus* and *Dicraeosaurus*, the preantorbital fossa is pierced by a large fenestra, and dorsally capped by a distinct ridge similar to *Diplodocus*, but unlike *Apatosaurus*. This distinct dorsal edge was previously thought to represent an autapomorphy of *Diplodocus*, but was shown to be present in other taxa as well (Tschopp and Mateus, 2012b). The preantorbital fenestra does not fill the entire preantorbital fossa: the anterior-most area remains closed by a thin bony wall. The fossa is anterodorsally accompanied by a short, narrow groove more or less following the curvature of the anterior end of the dorsal rim of the fossa. The posterior end of the fossa is interconnected with the central portion of the antorbital fenestra by a distinct groove that extends posterodorsally to the dorsal corner of the posterior process, which is regarded as an autapomorphy herein (Fig. 5.7). Remaining parts of the dorsal surface of the maxilla do not bear other distinctive morphological features, with the exception of the anterior-most portion, where a few nutrient foramina can be seen, similar to those present on the premaxilla.

Prefrontal. Both prefrontals are present and complete. They contact the frontals posteriorly, the nasals medially, the lacrimal laterally, and the maxilla anterolaterally. The prefrontals are short, anteroposteriorly convex elements. Their lateral margin is straight, the medial one with an anterior and a posterior concavity for the attachment of the nasal and the frontal, respectively. A sharply pointed, medially projecting process separates the two concavities. The posterior edge is anterolaterally-posteromedially oriented, forming a hook-like posteromedial process as is typical for Diplodocidae (Wilson, 2002; Whitlock, 2011a). The process almost reaches the frontal midlength, as is the case in the putative *Diplodocus* skulls CM 3452 and 11161 (ET, pers. obs. 2011). Anteriorly, the prefrontal tapers to a narrow tip, which is slightly dorsoventrally expanded. The left element bears a small nutrient foramen on the dorsal surface of the anterior part. The ventromedial edge is very distinct.

Frontal. Both frontals are completely preserved. They contact the prefrontal anterolaterally, the nasal anteromedially, the other frontal medially, the parietal posteromedially, and the postorbital posterolaterally. Ventrally, the frontal makes contact with the braincase, articulating with the orbitosphenoid. The frontals have a smooth dorsal surface, which is slightly convex posterolaterally-anteromedially. Their medial border is generally straight, but curves laterally at its posterior and anterior ends. Both a pineal fenestra (as in dicraeosaurids; width 14mm) and an anterior notch are thus present (as in *Kaatedocus*; length 18mm). The anterior notch is rather V-shaped than U-shaped as in *Kaatedocus*, and wider than in *Spinophorosaurus* (Knoll et al., 2012; Tschopp and Mateus, 2012b). The anterior margin of the frontal is strongly convex in order to accommodate the posterior, hook-like process of the prefrontal anterolaterally. From the posterior-most point of the posterior process of the prefrontal, the frontal has a straight edge extending obliquely anterolaterally, before it reaches the lateral edge, with which it includes a very acute angle. The lateral border is distinctly concave in dorsal view, smooth in its anterior part, but becoming highly rugose posteriorly, close to where it articulates with the postorbital. Posteriorly, the lateral and posterior edges form an acute angle. The lateral portion of the posterior margin is slightly displaced anteriorly, compared to the medial portion, resulting in a somewhat sinuous posterior edge. Ventrally, the frontals are marked by a distinct ridge, extending obliquely from the anterolateral corner, below the posterior process of the prefrontal, to an elevated, broad area for the attachment of the braincase.

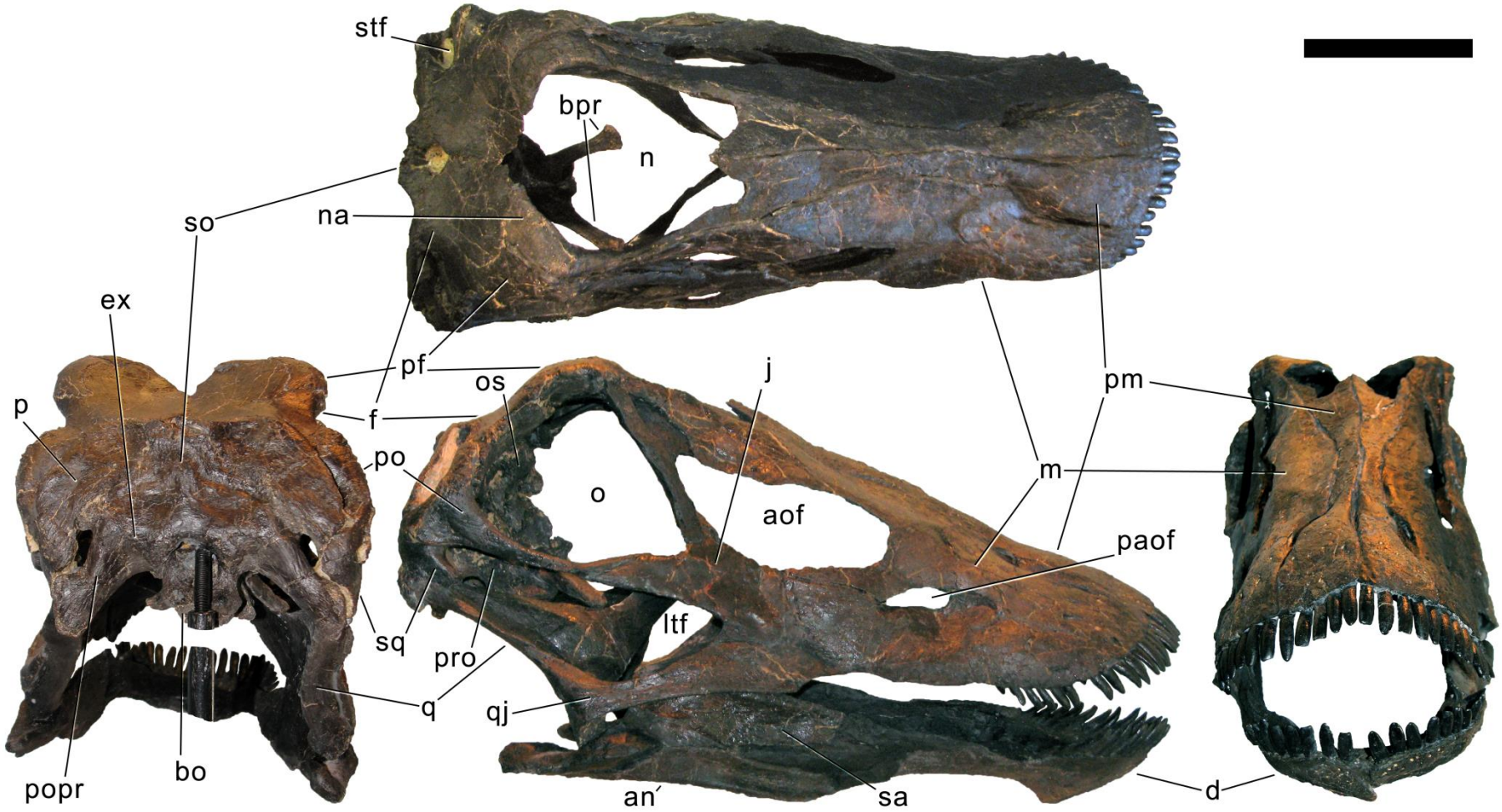

Figure 5.4: Skull of SMA 0011 as usually figured in anterodorsal (top), posterodorsal (left), right lateral (bottom center), and rostral views (right). Dark elements were lacking and reconstructed for the mounted skull. Abb.: an, angular; aof, antorbital fenestra; bo, basioccipital; bpr, basipterygoid process; d, dentary; ex, exoccipital; f, frontal; j, jugal; ltf, laterotemporal fenestra; m, maxilla; n, external nares; na, nasal; o, orbit; os, orbitosphenoid; p, parietal; paof, preantorbital fossa; pf, prefrontal; pm, premaxilla; po, postorbital; popr, paroccipital process; pro, prootic; q, quadrate; qj, quadratojugal; sa, surangular; so, supraoccipital; sq, squamosal; stf, supratemporal fenestra. Scale bar = 10 cm.

Postorbital. Both elements are complete. The postorbital is a triradiate bone with an anterior process articulating with the jugal, a posterior process overlapping the squamosal laterally, and a dorsomedial process covering the frontal posteriorly and connecting to the anterolateral process of the parietal posteromedially, thereby excluding the frontal from the margin of the supratemporal fenestra. Anteromedially, the dorsomedial process abuts the antotic process of the braincase. The anterior process has a subtriangular cross section, long dorsally and ventrally, with a narrow lateral and an even thinner medial margin. The anterior process is dorsally slightly concave. Towards anterior, it tapers to a point. The posterior process is short and triangular. At its base, one (on the right postorbital) or two (on the left element) nutrient foramina can be seen. The process is compressed transversely. The dorsomedial process is dorsoventrally concave anteriorly and convex posteriorly. It is relatively high dorsoventrally, but narrow anteroposteriorly. It is anteroposteriorly broader laterally than medially. The anterior face of the dorsomedial process is marked by a horizontal ridge at its base. The ridge supports the posterior edge of the frontal.

Jugal. Both jugals are preserved and complete. The jugal is a flat, relatively large bone with a posterior process contacting the postorbital, and a dorsal process articulating with the lacrimal. The main portion connects to the quadratojugal ventrally and the maxilla anteriorly. The jugal forms the anteroventral rim of the orbit, the posteroventral border of the antorbital fenestra, as well as the anterodorsal edge of the laterotemporal fenestra. The bases of the dorsal and posterior processes are relatively broad, before they taper dorsally and posteriorly, respectively. The anterior edge of the jugal is slightly concave, as is the anteroventral margin. Therefore, these two edges include an acute angle.

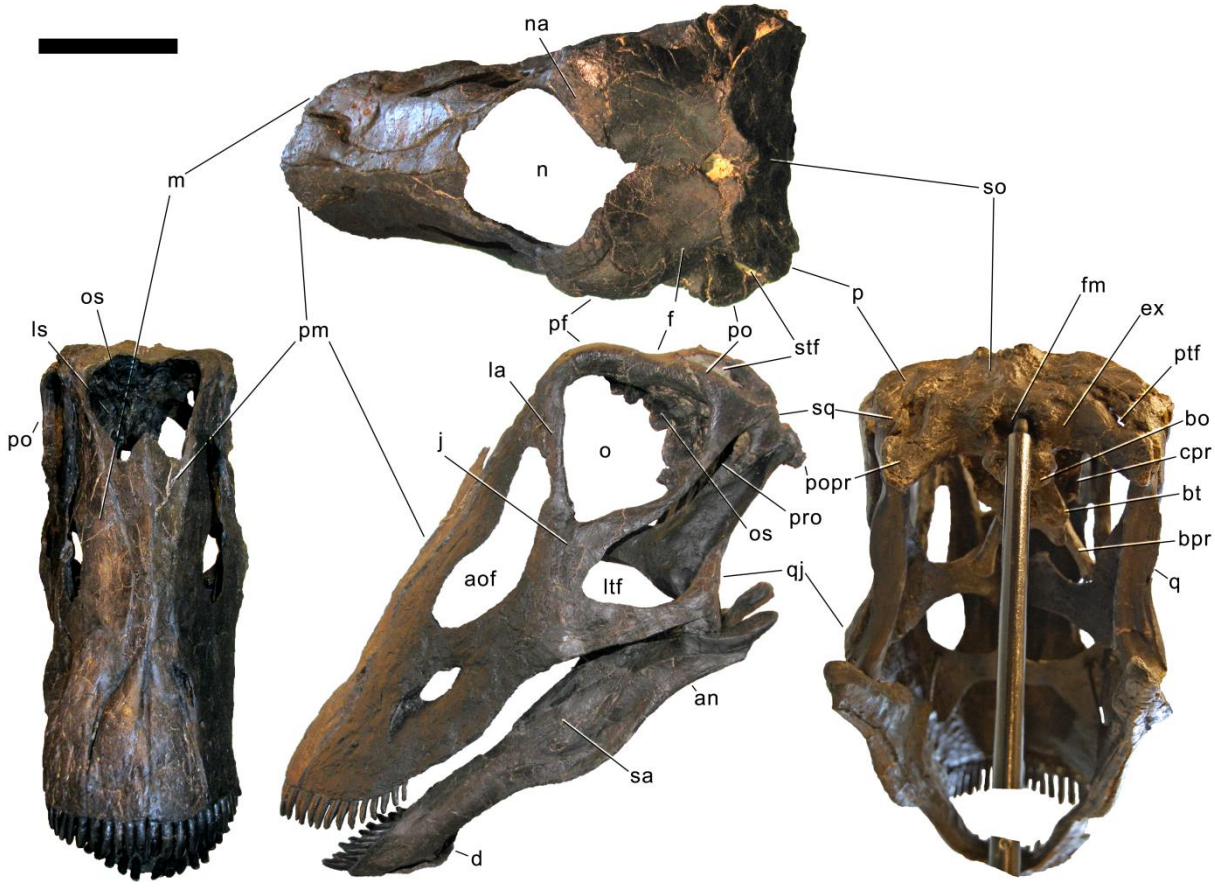

Figure 5.5: Skull of SMA 0011 in supposed habitual pose in dorsal (top), anterior (left), left lateral (bottom center), and posterior views (right). Dark elements were lacking and reconstructed for the mounted skull. Abb.: an, angular; aof, antorbital fenestra; bo, basioccipital; bpr, basipterygoid process; bt, basal tubera; cpr, crista prootica; d, dentary; ex, exoccipital; f, frontal; fm, foramen magnum; j, jugal; ltf, laterotemporal fenestra; m, maxilla; n, external nares; na, nasal; o, orbit; os, orbitosphenoid; p, parietal; pf, prefrontal; pm, premaxilla; po, postorbital; popr, paroccipital process; pro, prootic; ptf, posttemporal fenestra; q, quadrate; qj, quadratojugal; sa, surangular; so, supraoccipital; sq, squamosal; stf, supratemporal fenestra. Scale bar = 10 cm.

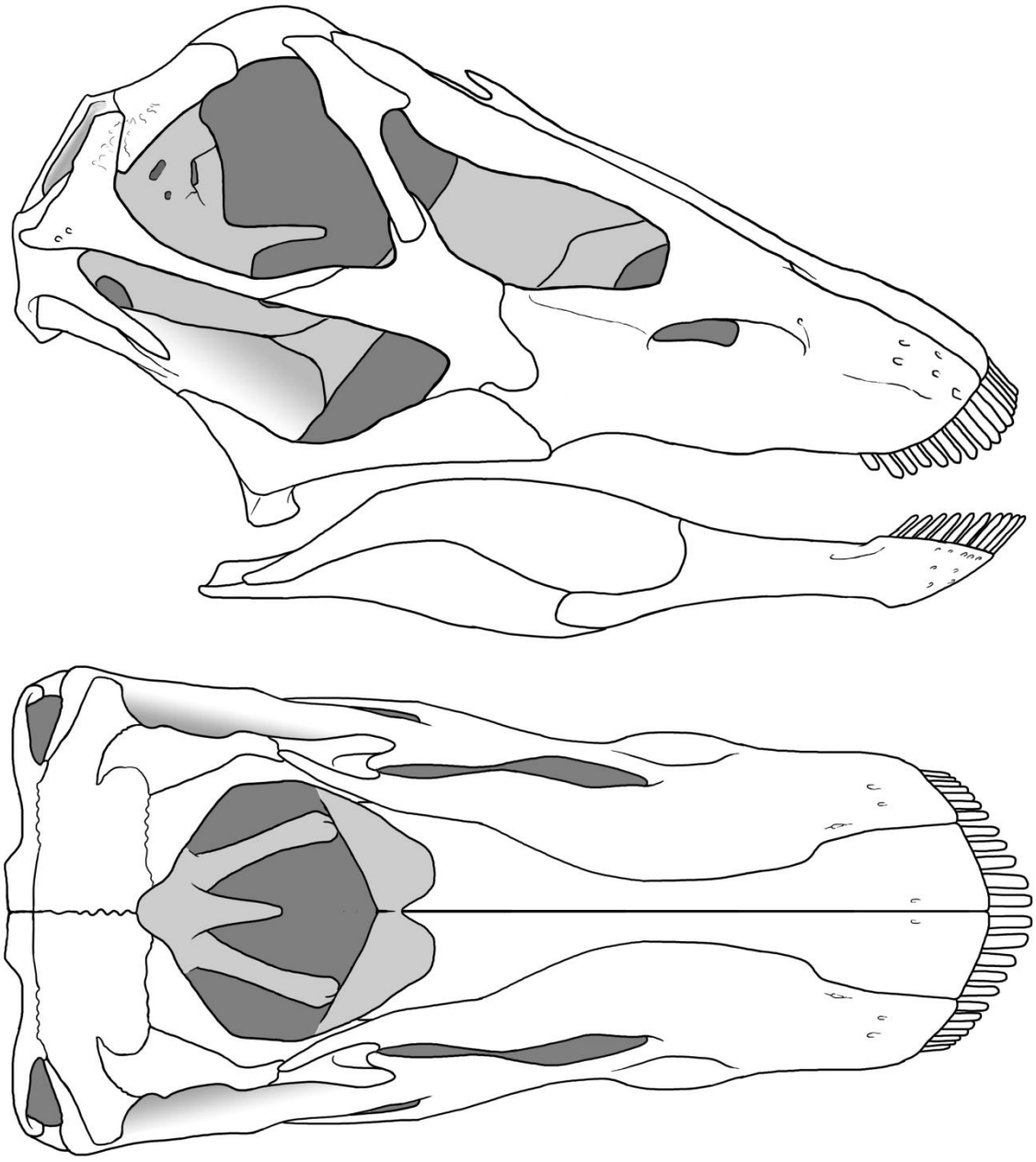

Figure 5.6: Skull reconstruction of *Galeamopus shellensis* in dorsal and lateral view, created by Simao Mateus (ML), and based on SMA 0011. Lacking bones were reconstructed after *Diplodocus* (Whitlock, 2011b).

Quadratojugal. The quadratojugals are both complete. They are transversely thin bones with a posterior dorsal process overlying the quadrate laterally, and a long anterior ramus contacting the jugal dorsally and the maxilla anteriorly. The quadratojugals form the anteroventral margins of the laterotemporal fenestra, and the ventral border of the skull. The anterior ramus of the quadratojugal is narrow at its base but extends dorsoventrally towards its anterior end. The ventral edge is almost straight; it is thus the concave dorsal margin of the anterior ramus that accounts mostly for this dorsoventral expansion. The shape of the anterior margin is not discernible in the mounted skull. The dorsal process is less than half the length of the anterior process. It is inclined posterodorsally, as in all diplodocids (Upchurch, 1998; Wilson, 2002; Whitlock, 2011a). It is anteroposteriorly convex externally, relatively broad at its base, and tapers to a point dorsally, reaching about midlength of the quadrate shaft.

Lacrimal. Only the dorsal half of the left lacrimal is present. It is a narrow element expanding towards its dorsal end, where it contacts the posterodorsal process of the maxilla anteriorly, the prefrontal dorsally, and possibly the nasal medially. Ventrally, the lacrimal would contact the jugal, if preserved. The lacrimal is the element separating the orbit from the antorbital fenestra. It is anteroposteriorly narrow in its ventral half, with a triangular cross section, being flat externally but bearing a distinct dorsoventral ridge internally. The anterior edge develops a short, but dorsoventrally high, anterior process at its dorsal end. The posterior margin is generally straight, with only a weak bulge on its dorsal portion. The dorsal-most end curves backwards, below the prefrontal. The internal ridge becomes slightly higher dorsally, posteriorly enclosing the lacrimal foramen, which is small and shallow in SMA 0011.

Quadrate. Only the right quadrate is preserved, but it is complete. It has a complex anatomy, with a quadrate shaft articulating with the squamosal and the paroccipital process posterodorsally and posteroventrally, respectively; a pterygoid flange interconnecting the outer skull with the pterygoid medially; and a ventral ramus being overlapped by the quadratojugal externally and bearing the articulating surface with the lower jaw ventrally. The quadrate shaft is elongate posteriorly, and has concave dorsal and lateroventral surfaces. The lateral edge is a thin crest, where it is not capped by the squamosal or the quadratojugal. The posterior surface of the quadrate shaft and the ventral ramus is shallowly concave, forming the quadrate fossa. The pterygoid flange originates on the medial half of the quadrate shaft. It is very thin mediolaterally, but anteroposteriorly long, and curves medially at its dorsal tip. The dorsal edge of the flange is straight and more or less horizontally oriented. The medial side of the pterygoid flange is concave, but does not form such a distinct fossa like that which is present autapomorphically in *Kaatedocus* (Tschopp and Mateus, 2012b). The ventral ramus is subtriangular in cross-section, with concave anterior and posterolateral surfaces. It has a thinner lateral than medial margin. The articular surface is subtriangular, with a concave anterior border, and a pointed posterior corner. The entire ventral ramus of the quadrate of SMA 0011 is posterodorsally inclined, as in all diplodocids (Upchurch, 1998; Wilson, 2002; Whitlock, 2011a).

Figure 5.7: Maxillary canal in the skull of SMA 0011 (arrow in the inlet) in right lateral view. The canal is herein interpreted as an autapomorphy of *Galeamopus shellensis*. Abb.: aof, antorbital fenestra; j, jugal; m, maxilla; paof, preantorbital fossa. Scale bar in skull overview = 10 cm.

Squamosal. Both squamosals are preserved, but lack a part of their anterior process (the right one more so than the left). The squamosals form the posteroventral corner of the skull. They have a complicated morphology, having to accommodate a variety of elements from the braincase and outer skull. The anterior process overlies the posterior end of the quadrate. Dorsally, the squamosal is laterally covered by the posterior process of the postorbital, and forms the external margin of the supratemporal fenestra. Posteriorly it touches the paroccipital processes, and dorsoposteriorly the posterolateral process of the parietal. The squamosal is strongly curved posterolaterally. The anterior process appears to be the longest of all squamosal processes, even though it is not preserved in its entire length. The ventral edge of the squamosal develops a short ventral projection at its posterior end, similar to, but much less distinct than the ventral prong as present in advanced dicraeosaurids (Salgado and Calvo, 1992; Whitlock, 2011a). A concave area appears to be present on the laterodorsal surface, in order to accommodate the posterior process of the postorbital. Other morphological features are difficult to observe in the articulated and reconstructed skull of SMA 0011.

Parietal. Both parietals are complete but slightly distorted. They are tightly sutured with the frontals anteriorly, and develop a short anterolateral process to contact the dorsomedial process of the postorbital, with which they form the anterior margin of the supratemporal fenestra. The posterior face of the parietal contacts the exoccipital and the supraoccipital medioventrally. The posterolateral process of the parietal forms the posterior margin of the supratemporal fenestra and reaches the squamosal laterally. The dorsal portion of the parietal in SMA 0011 is very narrow. The two elements do not touch each other medially, but this appears to be due to postmortem breakage of the extremely thin bone behind the parietal fenestra, which the parietals form together with the frontals. The dorsal portion is flat, and not well separated from the posterior surface by a ridge like that present in *Kaatedocus*. It widens anteroposteriorly at its lateral end, where it develops a short anterolateral and a long and dorsoventrally deep posteroventral process. The parietal thus contributes most to the margin of the supratemporal fenestra. The posterior surface has an oblique ventromedial border, which has a very sinuous suture together with the supraoccipital. The dorsal margin of the posterolateral process is straight as well, and does not cover the anterior border of the supratemporal fenestra in posterior view. Their ventral edges are excluded from the posttemporal fenestra by the squamosal and a laterally projecting spur of the exoccipital.

Supraoccipital. The supraoccipital is complete, and fused with the parietals, and the exoccipital-opisthotic complex. It is a somewhat hexagonal bone, that contacts the parietals dorsolaterally, the exoccipital-opisthotic complex ventrolaterally, and borders the foramen magnum ventrally. The supraoccipital is fused with the exoccipital-opisthotic, and the suture is barely visible. The dorsolateral edges of the supraoccipital are slightly concave. The ventrolateral edges are only laterally indicated. More medially, the suture is not traceable up to the foramen magnum, but probably extended below the two distinct tubercles located dorsolaterally to the foramen magnum. These tubercles served for the attachment of the proatlases. The tubercles are ellipsoid, and oriented with their long axes extending dorsomedially-ventrolaterally. The elevation is much more distinct ventrally than dorsally. The dorsal portion of the supraoccipital bears a complex arrangement of ridges and concavities, as if it would lack an additional element topping this structure. No distinct sagittal ridge is present, but if an element is lacking, it could be this element that forms the crest (Fig. 5.8). However, it has never been reported that the sagittal nuchal crest derives from an additional skull element. This would thus be highly unusual and possibly autapomorphic. The supraoccipital is widest slightly more ventrally than dorsally. No distinct foramina are present close to the border with the parietal, unlike in *Kaatedocus* (Tschopp and Mateus, 2012b). The dorsolateral edges of the supraoccipital are straight, not concave as in *Apatosaurus* CM 11162, or MB.R.2388, where it forms a distinct dorsal elevation (Berman and McIntosh, 1978; Remes, 2009).

Exoccipital-opisthotic complex. This outer portion of the braincase is completely preserved. No sutures can be seen between the exoccipital and the opisthotic. They bear two elongate paroccipital processes that extend lateroventrally to articulate with the squamosal and the posterior end of the quadrate. Ventrally, the exoccipital-opisthotic borders almost the entire the foramen magnum except for a small dorsal contribution of the supraoccipital. The exoccipital contributes the dorsolateral corners to the occipital condyle. As in *Suuwassea* and *Diplodocus* CM 11161, the exoccipital almost excludes the basioccipital from the participation in the dorsal surface of the occipital condyle (Harris,

2006a). The paroccipital processes have slightly convex external surfaces, but do not bear a ridge as in *Kaatedocus* (Tschopp and Mateus, 2012b). The ventral edge is straight, only the dorsal corner of the distal end is expanded dorsally, resulting in a distinctly concave dorsal edge. The lateral margin of the paroccipital process is subtriangular, with a longer, vertically oriented dorsal portion, and a shorter, laterally inclined ventral part. In lateral view, it is straight, unlike the curved ends of *Suuwassea* (Harris, 2006a; ANS 21122, pers. obs., 2011).

Figure 5.8: Unusual development of sagittal nuchal crest in the skull of SMA 0011 (arrow in the inlet) in posterodorsal view. The complex structure indicates that there might have been an additional element lacking, but no such bone has yet been described in any sauropod skull. Abb.: f, frontal; p, parietal; so, supraoccipital. Scale bar in skull overview = 10 cm.

Basioccipital and basisphenoid. The basioccipital forms the main portion of the occipital condyle. It is relatively short and connects the articular surface of the occipital condyle with the basal tubera, which are of about the same width. The articular surface is offset from the condylar neck. Narrow ridges connect the central part of the condylar neck with the posteromedial corner of the basal tubera, and the lateral face with the posterolateral corner. The posterior surface of the basal tubera is therefore concave, as are the lateral surfaces of the basioccipital. The basal tubera are box-like, and separated by a distinct, but relatively narrow, notch. The ventral edges of the tubera form a relatively straight line in posterior view, whereas the anterior edges are angled in a wide V-shaped manner in ventral view. Anteriorly, the basipterygoid processes attach to the tubera. In the reconstructed skull, they are mounted slightly dorsal to their actual location, above the anteroventral end of the crista prootica. When articulated properly, they would be elongate (5.3 times longer than wide) and straight, and would also include a narrower angle than as mounted. This is important as shorter and more widely diverging basipterygoid processes are typical for *Apatosaurus*, whereas narrower angles are present in *Diplodocus* (Berman and McIntosh, 1978). The processes are not as well connected at their base as is the case in *Kaatedocus* (Tschopp and Mateus, 2012b). The distal ends of the basipterygoid processes are expanded.

Orbitosphenoid. The orbitosphenoids delimit the endocranial cavity anteriorly, and attach to the frontals and parietals dorsally, themselves medially, and the laterosphenoids lateroventrally. Each orbitosphenoid is relatively wide dorsally and develops an anteroventral process, which is expanded at its end and separates the two openings for cranial nerves II medially (the optic foramen) and III laterally (the trigeminal foramen; Janensch, 1935; Harris, 2006a; Balanoff et al., 2010). Other than in *Suuwassea* (Harris, 2006a), the optic foramen is bridged over by bone medially. Anterodorsally, the two orbitosphenoids form the olfactory fenestra together with the frontals (Janensch, 1935; Balanoff et al., 2010), and posterolaterally, at the junction with the laterosphenoid, the foramen for cranial nerve IV (the trochlear foramen; Balanoff et al., 2010) defines the outline of the orbitosphenoid.

Laterosphenoid. The laterosphenoid mainly consists of a crest that develops the antotic process posterodorsally and extends anteroventrally to join the crista prootica. It connects to the parietal posteriorly, the orbitosphenoid anterodorsally, and the prootic posteroventrally. As the orbitosphenoid, also the laterosphenoid outline is defined by various openings: the cranial nerves III and IV anterodorsally at the junction with the orbitosphenoid, the facial foramen posterodorsally (cranial nerve V; Balanoff et al., 2010), as well as the oculomotor foramen and the abducens foramen anteroventrally (Balanoff et al., 2010).

Prootic. The prootic lies between the laterosphenoid anterodorsally, the parietal and paroccipital processes posterodorsally, and the basisphenoid anteroventrally. It bears the well-developed crista prootica, which extends relatively far laterally, but is very thin dorsoventrally. It does not end in an additional transverse expansion anteriorly, as is typical for dicraeosaurids (Janensch, 1935). Posteriorly, the crista prootica extends to the base of the paroccipital processes, where it separates foramina IX to XI from XII (Janensch, 1935; Harris, 2006a).

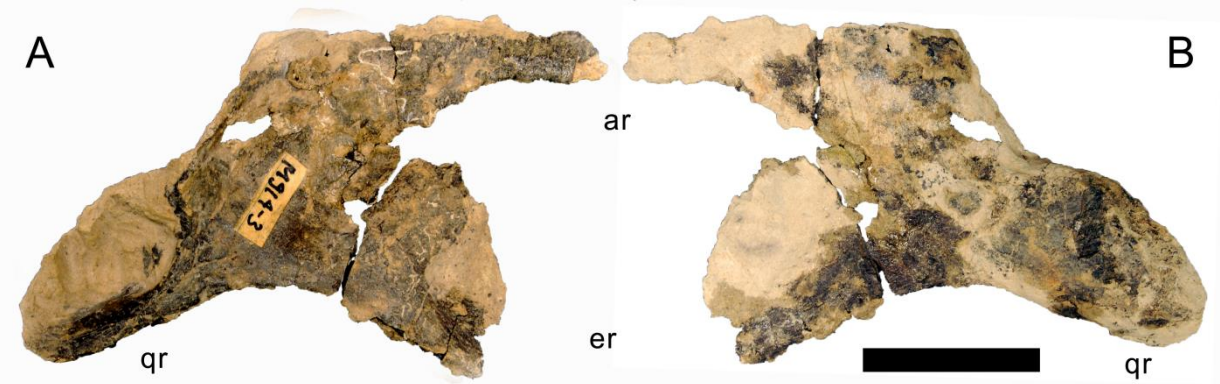

Figure 5.9: Right pterygoid of SMA 0011 in lateral (A) and medial (B) views. The element is only partly prepared, the lighter color is matrix adhered to the darker bone. Abb.: ar, anterior ramus; er, ectopterygoid ramus; qr, quadrate ramus. Scale bar = 5 cm.

Pterygoid. The left pterygoid is preserved, but is only partly prepared (Fig. 5.9). The pterygoid connects the quadrate posterolaterally with the basipterygoid processes posteromedially, the ectopterygoid and palatine anterolaterally, and the vomer anteromedially. The two elements would join along the midline of the skull. The pterygoid of SMA 0011 resembles this bone in CM 3452 in its dorsoventrally deeper shape than in *Camarasaurus* and *Giraffatitan* (McIntosh and Berman, 1975). It bears a shallow articulation facet for the basipterygoid processes, without a hook-like process as present in dicraeosaurids and *Camarasaurus* (Wilson, 2002; Whitlock, 2011a).

Hyoid. Only the right hyoid is preserved, but appears to be almost complete (Fig. 5.10). It is a narrow bone, with a distinct upward curve at midlength. The anterior ramus becomes transversely flattened towards its anterior end, which bears a shallow longitudinal groove on the medial side. The hyoid slightly widens dorsoventrally where it curves upwards and towards the squamosal, as was shown in *Tapuiasaurus* (Zaher et al., 2011). The posterodorsal end is rounded and offset from the shaft by a distinct rim.

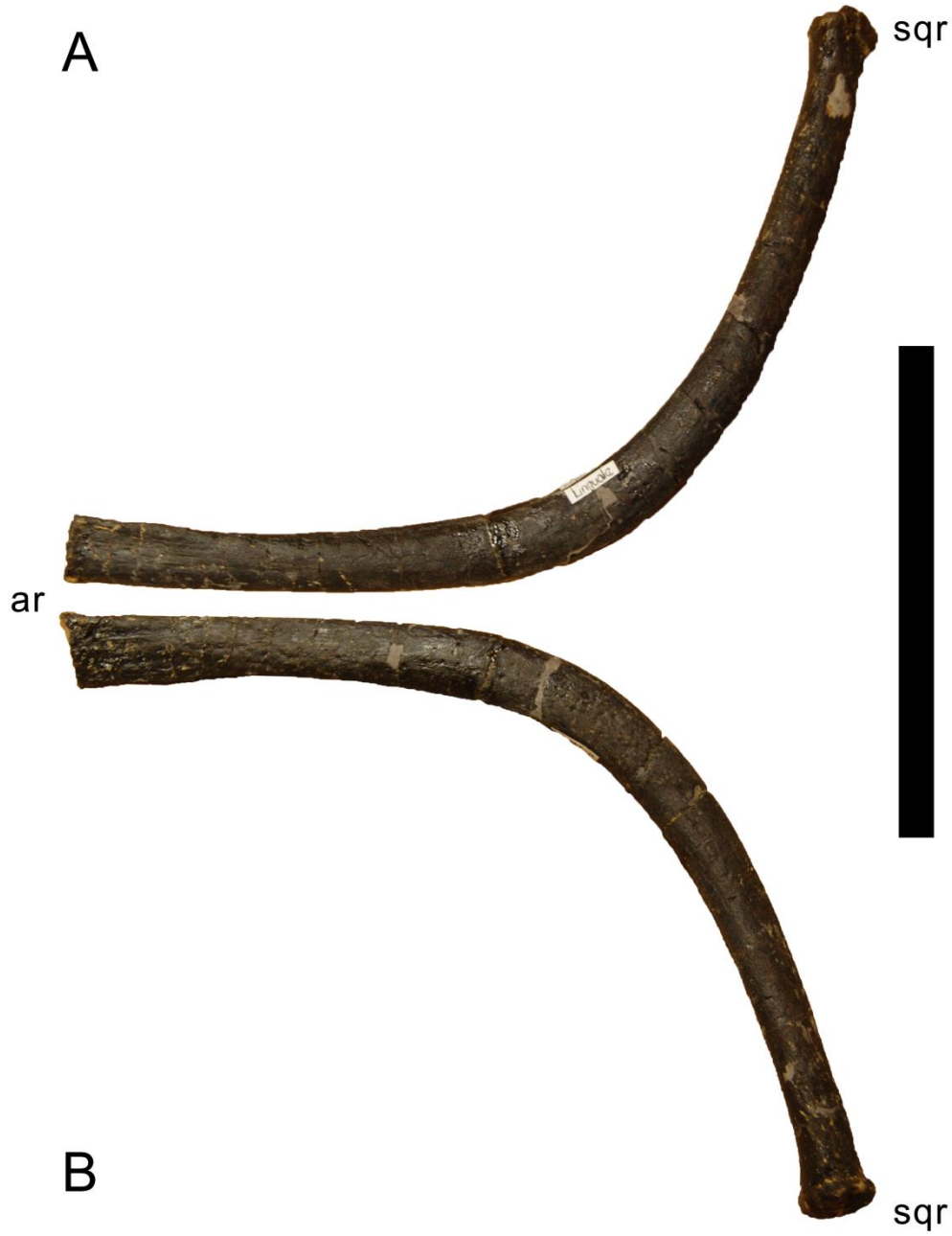

Figure 5.10: Right hyoid of SMA 0011 in medial (A) and lateral (B) views. Abb.: ar, anterior ramus; sqr, squamosal ramus. Scale bar = 10 cm.

Mandible

Dentary. Both dentaries are preserved. The dentary is the anterior-most bone of the lower jaw and the only one bearing teeth. Posteriorly, it is followed by the surangular dorsally and the angular ventrally. Internally, it is overlain by the splenial ventrally. The dentary is a thin bone with a dorsoventrally high dentigerous portion, developing the typical 'chin' of flagellicaudatans (Upchurch, 1998; Whitlock, 2011a). Posterior to the tooth bearing portion, the dentary tapers dorsoventrally, the right one much more so than the left. The symphysis is oblong and strongly anteriorly inclined.

Surangular. Both surangulars are present. This bone is very flat transversely, curves ventrally at its posterior end and bears a foramen at its highest point, which is also the highest point of the entire lower jaw. The jaw thus does not develop a coronoid eminence.

Angular. Both angulars are preserved but incomplete anteriorly. They are concave externally, due to the laterally curving ventral edge. They taper relatively continuously anteriorly, but abruptly at their posterior ends, where they expand transversely in order to accommodate the articular, which is not preserved.

?Prearticular. Both prearticulars appear to be present, but are partly hidden in the mount or only partially prepared (Fig. 5.11). They are very thin, elongate bones that taper posteriorly. A very shallow groove marks the probable lingual surface, extending anteroposteriorly, following the somewhat sinuous curve of the dorsal edge of the bone. In its anterior half, the bone becomes slightly thicker and curves outwards.

Figure 5.11: Right ?prearticular of SMA 0011 in lingual view. Note the shallow longitudinal canal (arrows). Scale bar = 5 cm.

Teeth. The teeth have the typical diplodocoid, peg-like shape (Fig. 5.12). They are slightly wrinkled but do not have denticles. Worn teeth usually have one single wear facet at a low angle to the long axis of the tooth, but some teeth also show two facets that are conjoined medially. In these teeth, the lingual facet is more steeply inclined than the labial one. The crown tips are slightly wider than deep, which is especially well visible in replacement and/or unworn teeth, which have a very weakly spatulate uppermost crown. The enamel is distributed evenly on all sides, and no grooves mark the lingual face. In the jaws, the teeth are inclined anteriorly compared to the long axis of the jaw, and set side-by-side without overlapping each other. There are at least 11, possibly 12, dentary teeth.

Cervical vertebrae (Figs 5.13-5.20; Tab. 5.2)

Proatlas. The right proatlas is preserved and complete (Fig. 5.13). It is strongly curved and tapers distally. The proximal articular surface is ovoid, with the largest width located in the dorsal half. The medial surface is concave, the lateral one convex. The proatlas of SMA 0011 is different from the element in *Kaatedocus* due to its much narrower distal tip.

Atlas. The atlantal centrum is not fused to the neurapophyses (Fig. 5.14). It has a well-developed anteroventral process as is typical for diplodocids, but convergently present in various other sauropods (Mannion, 2011; Whitlock, 2011a). A large foramen lies between the posterior knobs of the intercentrum. The lateral surface of the centrum is concave and bears a foramen as well. The neurapophyses have a relatively wide base, and turn upwards and backwards to articulate with the prezygapophyses of the axis. A wide medial process develops anteriorly, as in AMNH 969 (Holland, 1906). This process serves for articulation with the proatlas, and is much better developed than in *Kaatedocus* or *Diplodocus carnegii* CM 84 (Hatcher, 1901; Tschopp and Mateus, 2012b). A small but distinct subtriangular process is present on the opposite side of the medial process, projecting laterally.

Axis. The axis of SMA 0011 (Fig. 5.14A) has a closed but still slightly visible neurocentral synostosis, and separate cervical ribs. The centrum is opisthocoelous. The pleurocoel extends over almost the entire centrum, with short horizontal ridges at its anterior and posterior end. No vertical subdivision of the pleurocoel is present. Anteriorly, the pleurocoel extends onto the parapophysis. The ventral surface of the centrum bears a distinct longitudinal keel in its posterior portion. The parapophysis is rounded, and faces anterolaterally and slightly ventrally. The neural arch is high and slightly posteriorly inclined. The prezygapophyses are not preserved. The only well-defined lamina is the podl. The prsl is slightly expanded transversely at its anterior end, similar to, but not as distinct as in AMNH 969 (pers. obs. 2011). The diapophysis projects somewhat posteriorly, but does not have a distinct posterior process. In lateral view, the anterior edge of the neural spine is slightly concave at the bottom, and straight in the upper part. The spine top is rugose, slightly expanded transversely, and entirely restricted anterior to the postzygapophyseal facets. This anterior restriction is unusual for sauropods, but present in *Diplodocus carnegii* CM 84 (Hatcher, 1901), and could thus represent a diplodocine synapomorphy. Other than in CM 84, however, the neural spine summit of SMA 0011 develops a posterior projection, similar to *Giraffatitan* (Janensch, 1950). The spol is strongly concave, becoming vertical on the upper part. Small epipophyses are present laterally above the postzygapophyses, which do not project backwards. A large rugose area is present on the lateral side of spine, slightly above mid-height. It is of subtriangular shape, broader towards the spol, and with a pointed, elongate tip towards the center of the sdf. This rugosity could be homologous to the distal lateral expansion in the axis of *Suuwassea* or *Camarasaurus* (Madsen et al., 1995; Harris, 2006b), just that the neural spine top is much more elevated in SMA 0011. Such a rugosity appears to be absent in the element of *Diplodocus carnegii* (Hatcher, 1901). The postzygapophyses of the axis of SMA 0011 slightly overhang the centrum posteriorly, and bear subtriangular facets with a straight border anteriorly.

Postaxial cervical vertebrae. Eleven cervical vertebrae are present. They were found in four blocks, with CV 1-6 constituting the first one (Figs 5.14, 5.15), CV 8 and 9 the second (Fig. 5.16), CV 11 and 12 the third set (Fig. 5.17), and CV 15 (Fig. 5.18) was recovered articulated with the first three dorsal vertebrae. The interpretation of the gaps is mainly based on the position of the bones in the quarry, and on the fact that diplodocid cervical series are interpreted to comprise 15 vertebrae (Hatcher, 1901; Gilmore, 1936; Upchurch, 1998; Wilson, 2002; Whitlock, 2011a). However, since only two nearly complete, and largely articulated diplodocid necks have been reported to date (*Diplodocus carnegii* CM 84, lacking the atlas, Hatcher, 1901); *Apatosaurus louisae* CM 3018, Gilmore, 1936), this count may also have been different in diplodocid genera other than *Apatosaurus* or *Diplodocus*. A more detailed study of the morphological changes within the cervical column will be needed to show if the present assignment is correct, but is out of the scope of this description. For a phylogenetic assessment of the specimen, it is sufficient to order the single vertebrae in anterior, mid-, and posterior cervical vertebrae, which is perfectly possible in the present case.

The cervical centra are all opisthocoelous and relatively elongate. As is typical for nearly all sauropods, the most elongated elements are the mid-cervical vertebrae. All cervical centra have well-developed pleurocoels extending over the entire length of the centrum, and also invading the dorsal surfaces of the parapophyses. The internal structure of the pleurocoel varies along the column: the anterior and posterior horizontal ridges described in the axis disappear by CV 4, and a vertical subdivision in anterior and posterior pneumatic fossae becomes visible in CV 3, and is pronounced from CV 5 backwards. The subdividing ridge is oriented anterodorsally-posteroventrally, as in *Kaatedocus* (Tschopp and Mateus, 2012b). The posterior pneumatic fossae of CV 5 and 6 bear a large, slightly ellipsoid foramen at its anterior end, and becomes pointed posteriorly, due to the development of a shallow posteroventral fossa, which is synapomorphic for diplodocines more derived than *Kaatedocus*, according to Tschopp and Mateus (2012b). From CV 6 backwards, the anterior pneumatic fossa becomes subdivided by a horizontal ridge at about mid-height. The ventral portion of the anterior fossa becomes vertically divided in CV 11. The latter is also the first element in the series to show a separation of the posterior-most portion of the posterior pneumatic fossa. In addition, CV 12 also has a horizontally subdivided posteroventral fossa. In CV 15, the pleurocoel becomes less ramified again.

Figure 5.12: Teeth of SMA 0011. They were found disarticulated from the skull. Abb.: tc, tooth crown; tr, tooth root. Scale bar = 2 cm.

Figure 5.13: Right proatlas of SMA 0011 in lateral (A) and medial (B) views. Note the elongate and narrow distal tip. Scale bar = 2 cm.

Table 5.1: Skull measurements SMA 0011 (in mm, asterisks indicates estimated dimensions)

Element		apL	Lap	Lv	Ltb	Ll-oc	Lpp	min apW	max apW	aW	minW	maxW	pW	dW	Wn	minH	maxH	Hap	dH	Hvr	Hdlp	Hdmp	L aop	L cpr	pp-fp	comments
Premaxilla	R	325								47	13		46													
	L	320								47	12		45													
Maxilla	R	354		225	120		246										210									Lpp: distance posterior process to anterior margin; Lv: measured along curvature; maxH: distance posteroventral corner to posterodorsal corner
Preantorbital fossa	R	73																								
Preantorbital fenestra	R	45																								
Prefrontal	R	63				53						37													37	
	L	67				43						34													37	
Frontal	R	73				41					69	90														
	L	74				44					68	84														
Postorbital	R	139								20		41					63	10				36				Hap: measured at lateral edge
	L	116								24		42					68	11				36				Hap: measured at lateral edge
Jugal	R	121					58										81									Lpp: measured from anteriormost point of orbit to posteriormost extension of jugal
	L	133					68										93									Lpp: measured from anteriormost point of orbit to posteriormost extension of jugal
Quadratojugal	R	182	154														59									maxH: length dorsal process
	L	149	106														51									maxH: length dorsal process
Lacrimal	L	62						12			13	15					10*	56								apL measured at dorsal end
Quadrate	R	148																		29						apL: distance from posterior-most point of shaft to anterior-most point of ventral ramus
Squamosal	R	>40										23					63									anterior process incomplete
	L	>59										22					60									anterior process incomplete
Parietal	R						69	3	19												39					Hdlp: measured at base of process; Lpp: measure along dorsal edge of posterolateral process; min & max apW measured dorsally
	L						62	6	15												41					Hdlp: measured at base of process; Lpp: measure along dorsal edge of posterolateral process; min & max apW measured dorsally
Supraoccipital	-													28			59									maxH: distance foramen magnum-parietal suture
Exoccipital-opisthotic complex	-											150														maxW: measured across paroccipital processes
Paroccipital process	R															23			inc							
	L															23			34							
Occipital condyle	-	29									39	42														minW: measured at neck
Foramen magnum	-											27					17									
Posttemporal fenestra	R											23														
	L											24														
Basioccipital	-										30															
Basal tubera	-											42			8											maxW: paired tubera
Basipterygoid process	R	64								16	11	17														aW: measured at distal tip; maxW: measured at base, dorsoventrally
	L	def								19	10	16														aW: measured at distal tip; maxW: measured at base, dorsoventrally
Orbitosphenoid	R												36													pW: measure posterodorsally
	L												38													pW: measure posterodorsally
Laterosphenoid	R																						30			
Prootic	R																							42		
	L																							42		
Dentary	R															22	62									maxH: at symphysis
	L															37	67									maxH: at symphysis
Surangular	R															44										
	L															41										
Angular	R	180																								
	L	170																								

Abb: apL, anteroposterior length; apL paofe, anteroposterior length preantorbital fenestra; apL paofo, anteroposterior length preantorbital fossa; aW, anterior width; def, deformed; dH, distal dorsoventral height; dW, dorsal width; Hap, dorsoventral height anterior process; Hdlp, dorsoventral height dorsolateral process; Hdmp, dorsoventral height dorsomedial process; Hvr, dorsoventral length ventral ramus; inc, incomplete; L aop, length antotic process; L cpr, length crista prootica; Lap, length anterior process; Ll-oc, lateral length contributing to orbit; Lpp, length posterior process; Ltb, length tooth-bearing portion; Lv, length ventral edge; max apW, maximum anteroposterior width; maxH, maximum dorsoventral height; maxW, maximum transverse width; min apW, minimum anteroposterior width; minH, minimum dorsoventral height; minW, minimum transverse width; pp-fp, distance posterior process to frontoparietal suture; pW, posterior width; Wn, width notch.

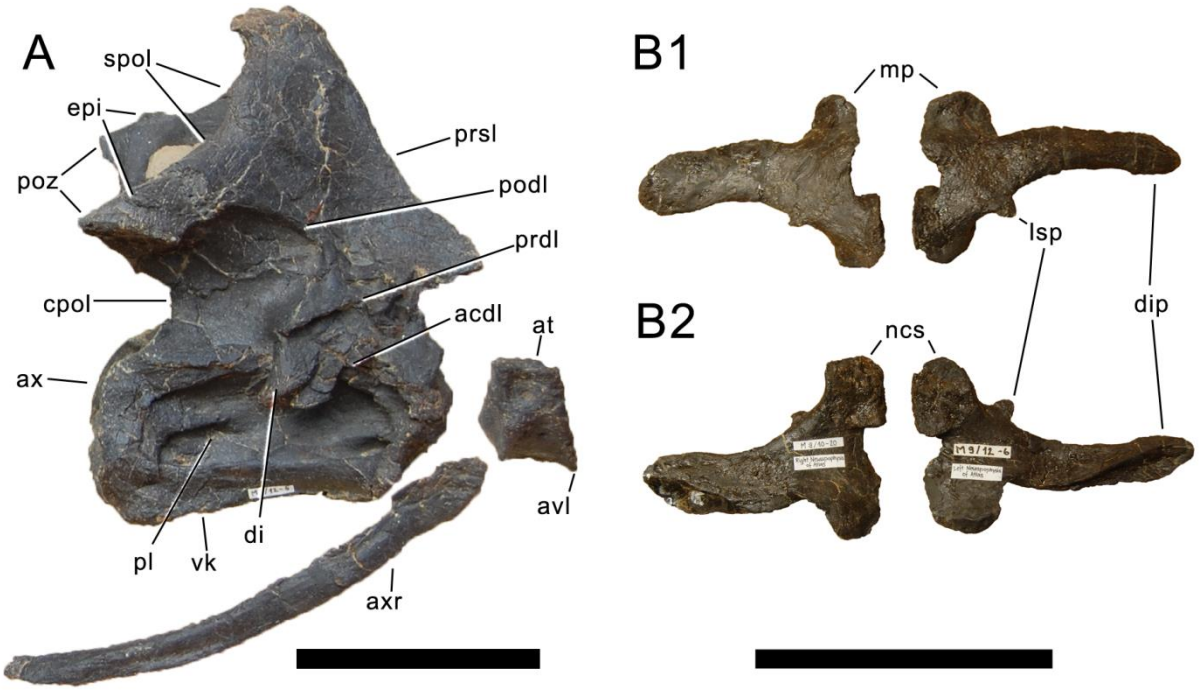

Figure 5.14: Atlas and axis of SMA 0011. A shows the two elements in an articulated state, B show the neurapophyses in lateral (B1) and medial (B2) views. Abb.: acdl, anterior centrodiapophyseal lamina; at, atlas; avl, anteroventral lip; ax, axis; axr, axial rib; cpol, centropostzygapophyseal lamina; di, diapophysis; dip, distal process; epi, epipophyses; lsp, lateral spur; mp, medial process; ncs, neurocentral synostosis; pl, pleurocoel; podl, postzygodiapophyseal lamina; poz, postzygapophysis; prdl, prezygodiapophyseal lamina; prsl, prespinal lamina; spol, spinopostzygapophyseal lamina; vk, ventral keel. Scale bars = 10 cm.

In CV 15, the anterior condyle is damaged, so that it reveals the internal structure. The condyle is composed of large internal cavities, surrounded by 2-4 mm thick, relatively dense bony struts. The arrangement appears symmetric, with a subtriangular cavity dorsomedially, and two subcircular cavities following both medially and laterally.

The parapophyses become slightly anteroposteriorly elongate in CV 3 and 4. They project ventrolaterally in all elements, and are interconnected with the anterior condyle through a transversely wide, somewhat rugose area. The fossa on its dorsal surface is subdivided by a short, oblique ridge from CV 6 backwards. In CV 11 and 12, the parapophysis is subtriangular, being long antero-posteriorly, and wider posteriorly than anteriorly.

The ventral surface is hourglass-shaped and relatively narrow in anterior and mid-cervical vertebrae, but becomes relatively wide posteriorly. In anterior cervical vertebrae, it bears a distinct longitudinal keel on its anterior half, with well visible pneumatic foramina lateral to it in CV3, but less so in more posterior elements. In CV 3, a shallow ventral ridge is also present on the posterior end, but already in CV 4 this ridge cannot be seen anymore. The ventral surfaces of CV 5 and more posterior vertebrae are concave without any traces of ridges or pneumatic foramina. Posteriorly, they are bordered by distinct posteroventral flanges, which is a synapomorphy of Diplodocinae, according to Tschopp and Mateus (2012b). These flanges become rugose ventrally in CV 15.

None of the centra are fused with the corresponding cervical ribs. The neurocentral synostosis is closed but visible in the anterior and posterior cervical vertebrae, whereas in posterior mid-cervical vertebrae it is completely open. Where it is closed, the zigzagging neurocentral synostosis is better visible anteriorly than posteriorly (Fig. 5.19). In the most anterior and posterior elements, the synostosis becomes extremely faint to completely obliterated posteriorly. It lies on top of the centrum, such that the entire pedicels of the neural arches are detached in the unfused elements. The synostosis line is highest in the anterior half and descends anteriorly and posteriorly.

The neural arch is high in anterior cervical vertebrae, but becomes lower posteriorly. In all elements, it appears very fragile and slender, with very thin but distinct lamination. In posterior cervical vertebrae, the neural arch is somewhat displaced anteriorly, reaching close to the anterior condyle, but being well distant from the posterior edge of the centrum. The displacement reaches its maximum in CV 15.

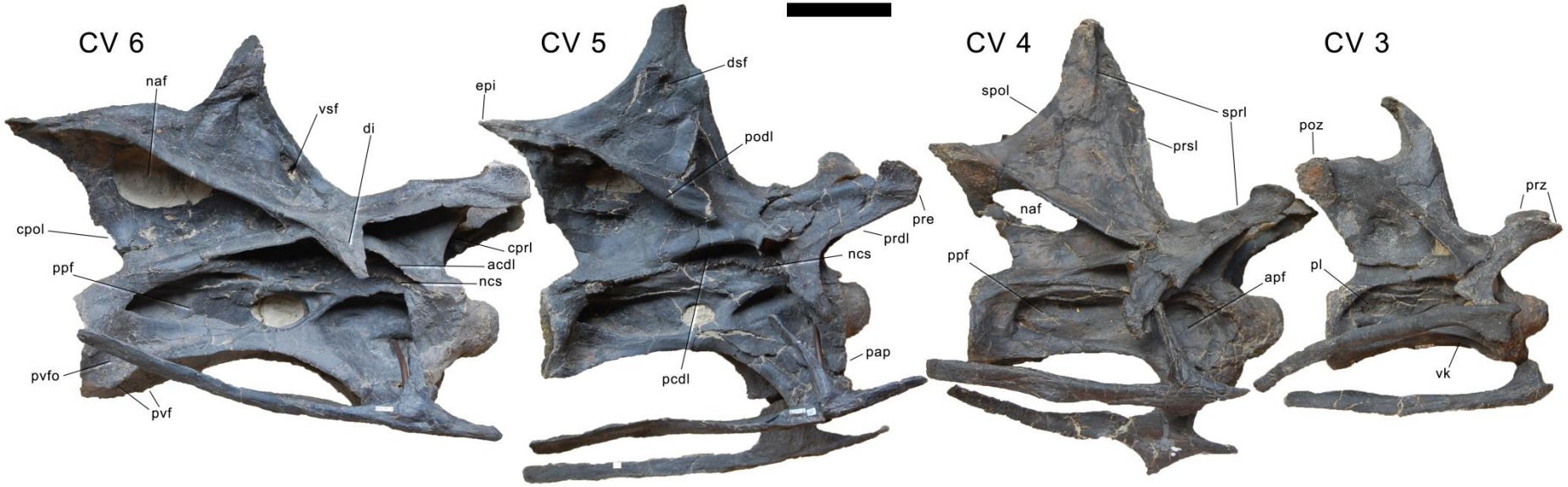

Figure 5.15: Cervical vertebrae 3 to 6 of SMA 0011 in right lateral view. Abb.: acdl, anterior centrodiapophyseal lamina; apf, anterior pneumatic fossa; cpol, centropostzygapophyseal lamina; cprl, centroprezygapophyseal lamina; di, diapophysis; dsf, dorsal spinal fossa; epi, epipophysis; naf, neural arch foramen; ncs, neurocentral synostosis; pap, parapophysis; pcdl, posterior centrodiapophyseal lamina; pl, pleurocoel; podl, postzygodiapophyseal lamina; poz, postzygapophysis; ppf, posterior pneumatic fossa; prdl, prezygodiapophyseal lamina; pre, pre-epipophysis; prsl, prespinal lamina; prz, prezygapophysis; pvf, posteroventral flange; pvfo, posteroventral fossa; spol, spinopostzygapophyseal lamina; sprl, spinoprezygapophyseal lamina; vk, ventral keel; vsf, ventral spinal fossa. Scale bar = 10 cm.

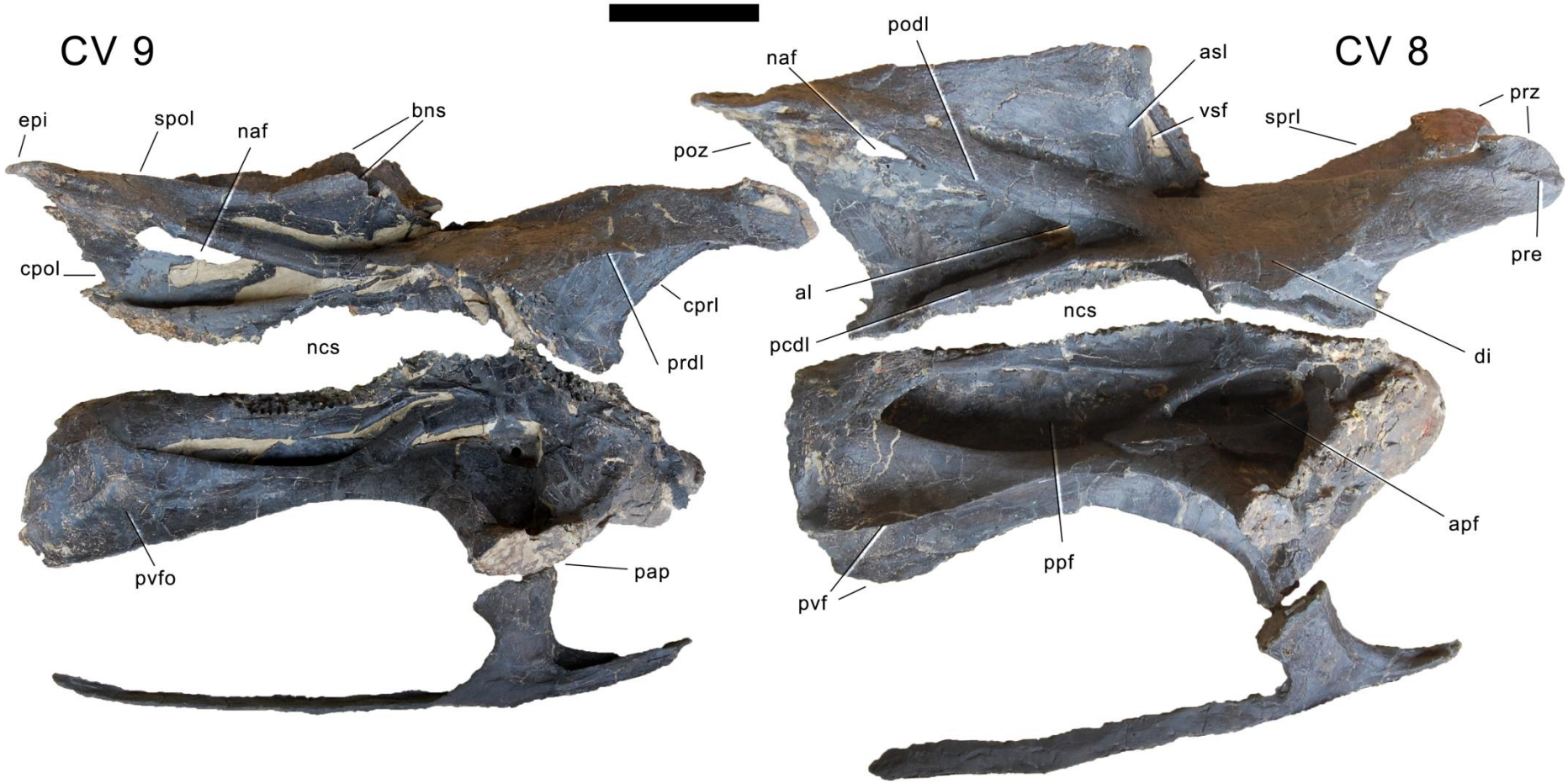

Figure 5.16: Cervical vertebrae 8 and 9 of SMA 0011 in right lateral view. Note the open neurocentral synchondrosis. Abb.: acdl, anterior centrodiapophyseal lamina; al, accessory lamina; apf, anterior pneumatic fossa; asl, accessory spinal lamina; bns, bifid neural spine; cpol, centropostzygapophyseal lamina; cprl, centroprezygapophyseal lamina; di, diapophysis; epi, epipophysis; naf, neural arch foramen; ncs, neurocentral synchondrosis; pap, parapophysis; pcdl, posterior centrodiapophyseal lamina; podl, postzygodiapophyseal lamina; poz, postzygapophysis; ppf, posterior pneumatic fossa; prdl, prezygodiapophyseal lamina; pre, pre-epipophysis; prz, prezygapophysis; pvf, posteroventral flange; pvfo, posteroventral fossa; spol, spinopostzygapophyseal lamina; sprl, spinoprezygapophyseal lamina; vsf, ventral spinal fossa. Scale bar = 10 cm.

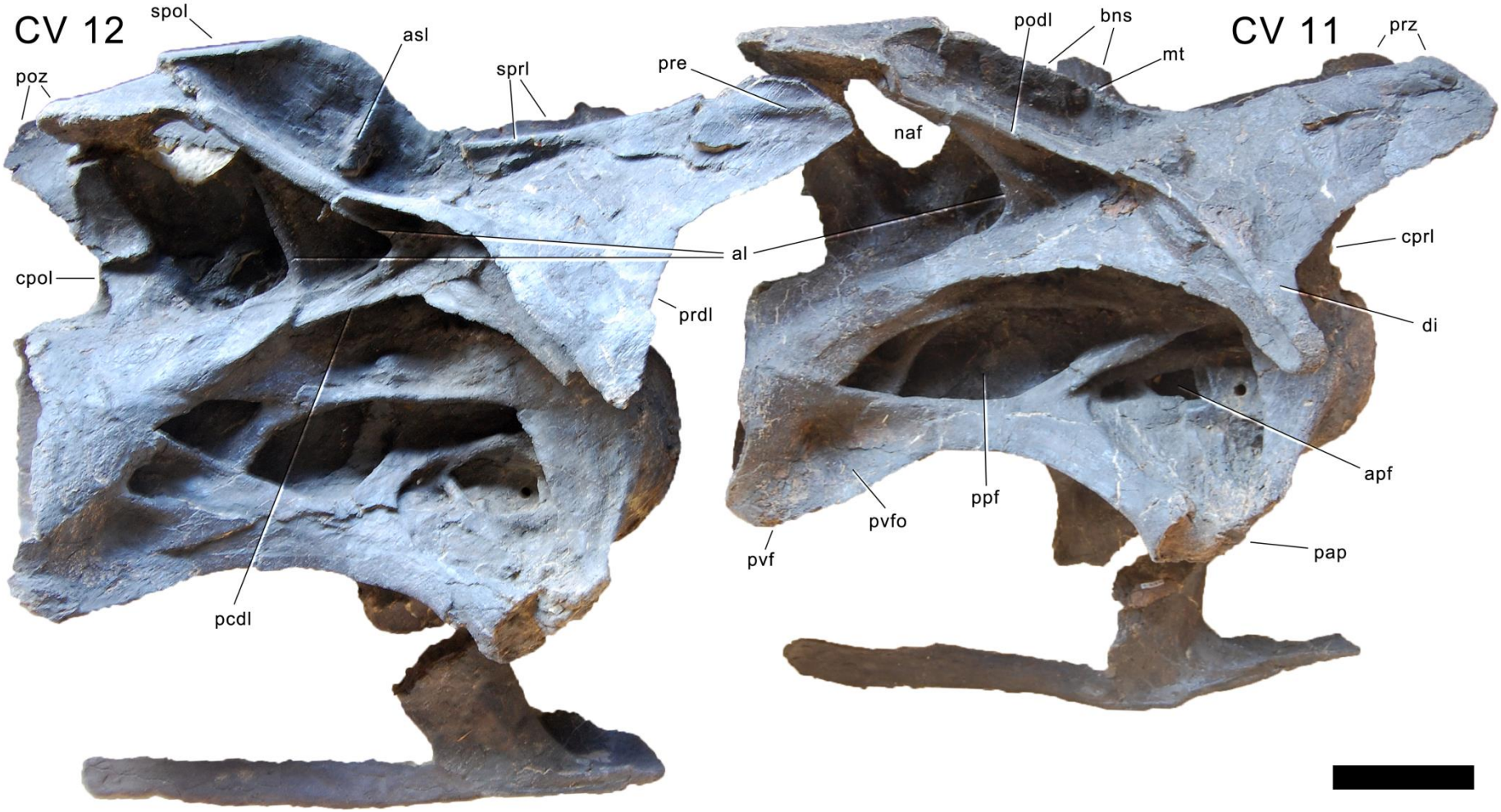

Figure 5.17: Cervical vertebrae 11 and 12 of SMA 0011 in right lateral view. Abb.: al, accessory lamina; apf, anterior pneumatic fossa; asl, accessory spinal lamina; bns, bifid neural spine; cpol, centropostzygapophyseal lamina; cprl, centroprezygapophyseal lamina; di, diapophysis; mt, median tubercle; naf, neural arch foramen; pap, parapophysis; pcdl, posterior centrodiapophyseal lamina; podl, postzygodiapophyseal lamina; poz, postzygapophysis; ppf, posterior pneumatic fossa; prdl, prezygodiapophyseal lamina; pre, pre-epipophysis; prz, prezygapophysis; pvf, posteroventral flange; pvfo, posteroventral fossa; spol, spinopostzygapophyseal lamina; sprl, spinoprezygapophyseal lamina. Scale bar = 10 cm.

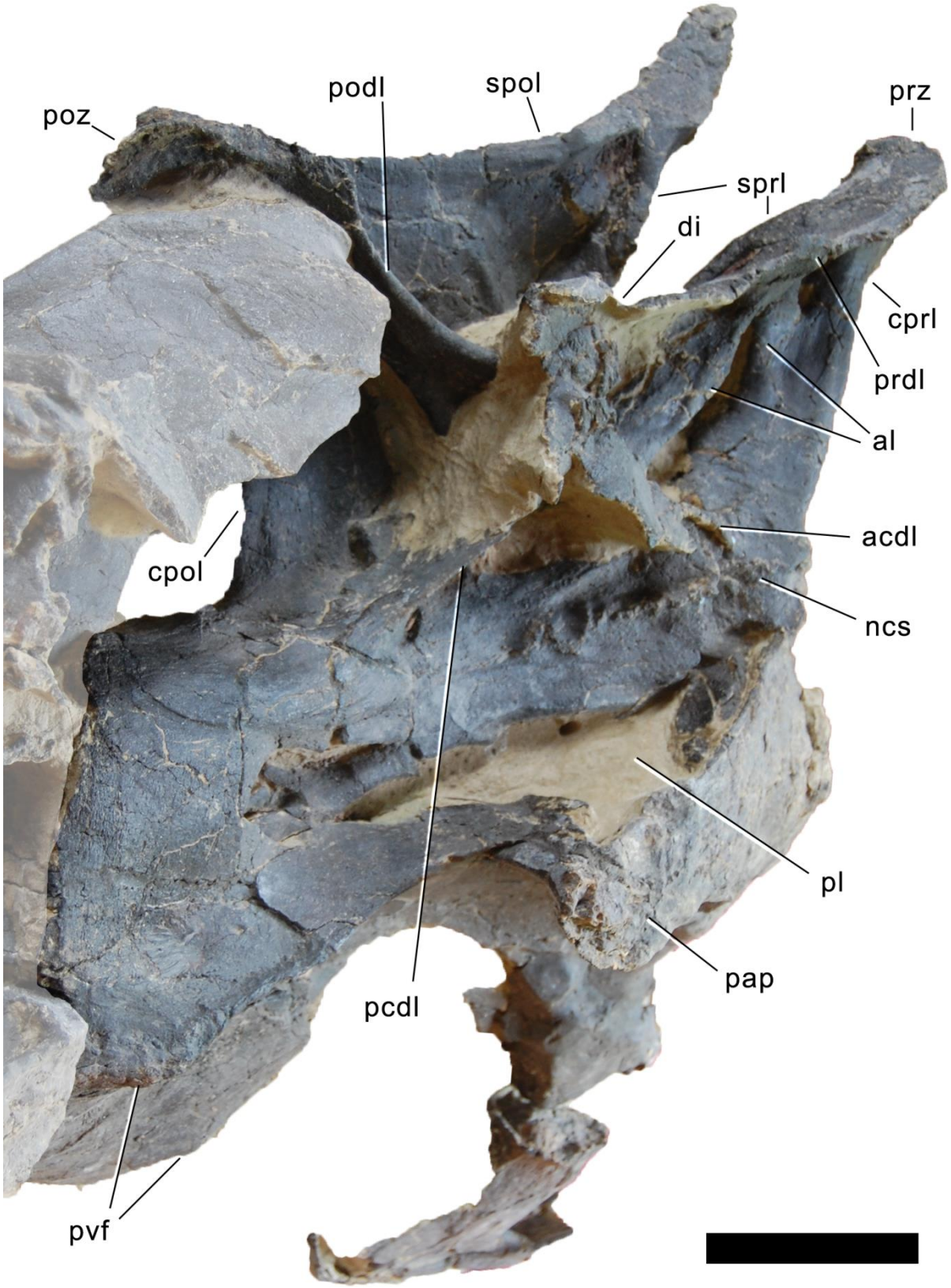

Figure 5.18: Cervical vertebra 15 of SMA 0011 in right lateral view. Articulated DV 1 shaded. Abb.: acdl, anterior centrodiapophyseal lamina; al, accessory lamina; cpol, centropostzygapophyseal lamina; cprl, centroprezygapophyseal lamina; di, diapophysis; ncs, neurocentral synostosis; pap, parapophysis; pcdl, posterior centrodiapophyseal lamina; pl, pleurocoel; podl, postzygodiapophyseal lamina; poz, postzygapophysis; prdl, prezygodiapophyseal lamina; prz, prezygapophysis; pvf, posteroventral flange; spol, spinopostzygapophyseal lamina; sprl, spinoprezygapophyseal lamina. Scale bar = 10 cm.

The prezygapophyses project anteriorly and slightly dorsally in most elements. Close to the cervico-dorsal transition, they become more elevated. They bear suboval facets in CV 3, with the long axis extending anteroposteriorly. From CV 4 onwards, the facets become subtriangular, with the tip located medially. The facets are convex as in all diplodocines (McIntosh, 1990b; Wilson, 2002; Whitlock, 2011a). Only in CV 5 are they concave, but this appears to be due to taphonomic distortion. In CV 8 and 9, the articular facets are elevated on pedestals, but no transverse sulcus is present posteriorly, unlike in *Kaatedocus* (Tschopp and Mateus, 2012b). The prezygapophyses cap the prcdf dorsally, which in CV 5 and 6 is subdivided by a vertical accessory lamina connecting acdl and prdl right at the diapophysis. Anteriorly, the prezygapophyses are ventrally supported by the cprl, which is single in anterior cervical vertebrae. From CV 8 backwards, the cprl is divided, with one distinct and few short, weak accessory lamina in the prcdf. The accessory laminae subdividing the prcdf become stronger in more posterior elements. Weak pre-epipophyses mark the lateral surface anteriorly in CV 4 and more posterior elements. Only in CV 10 do they extend anterior to the prezygapophyseal facet. This is in contrast to *Kaatedocus*, where the majority of mid- and posterior cervical vertebrae bear anteriorly projecting pre-epipophyses (Tschopp and Mateus, 2012b). Posteriorly on the prezygapophyseal process, the anterior portion of the sdf develops a deep, but not well defined fossa in CV 3.

The sprl is distinct on the prezygapophyseal process, disappears around midlength of the dorsal portion, and becomes visible again on the spine top in anterior cervical vertebrae. In mid-cervical vertebrae, the sprl is weak to almost absent on the prezygapophyseal process, as is typical for Diplodocinae (Tschopp and Mateus, 2012b). In posterior cervical vertebrae, the sprl is again better developed. Due to a backwards curve of the spine top in anterior cervical vertebrae, the sprl has a somewhat sinuous appearance in lateral view in these elements. Below the backwards curve, the sprl extends almost vertically in CV 3 to 5, but becomes posteriorly inclined in more posterior vertebrae. A prsl is present at the base of neural arch in unbifurcated spines, which reach back to CV 8, as in *Barosaurus* (McIntosh, 2005).

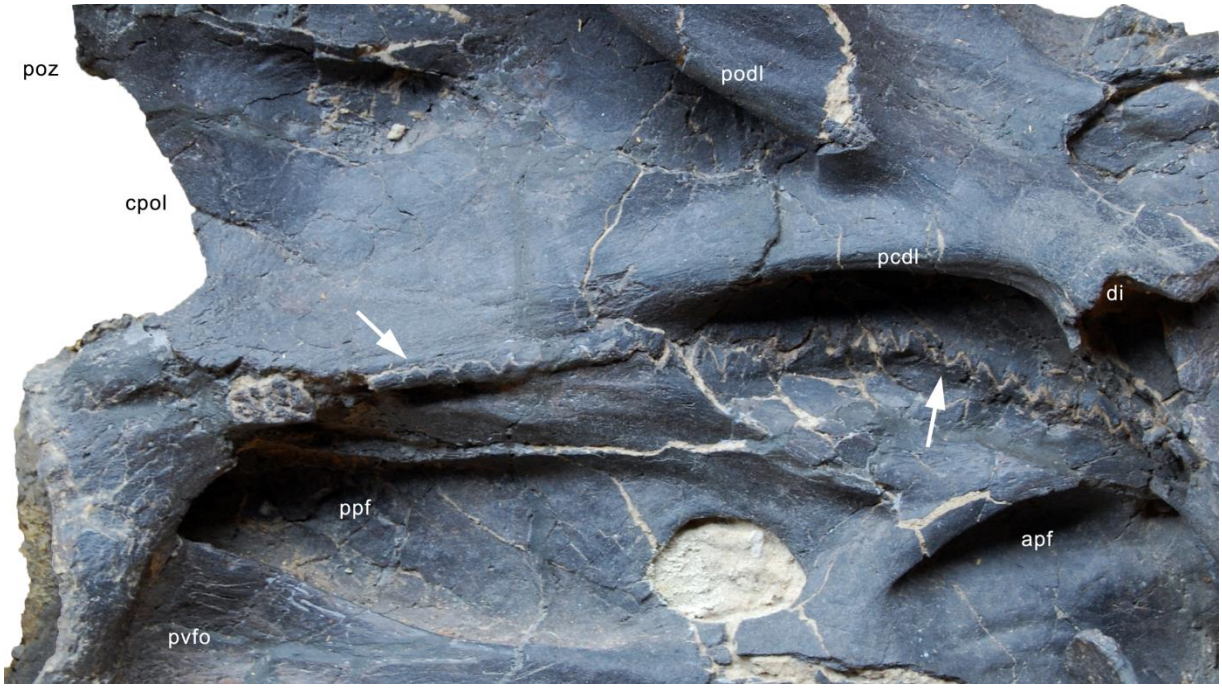

Figure 5.19: Neurocentral synostosis in CV 5 of SMA 0011. Detail of the vertebra in right lateral view. Note the higher degree of fusion in the posterior portion compared to the anterior part (arrows). Abb.: apf, anterior pneumatic fossa; cpol, centropostzygapophyseal lamina; di, diapophysis; pcdl, posterior centrodiapophyseal lamina; podl, postzygodiapophyseal lamina; poz, postzygapophysis; ppf, posterior pneumatic fossa; pvfo, posteroventral fossa.

The diapophysis is entirely located in the anterior half of the vertebra. It is supported by distinct acdl, prdl, podl, and pcdl. The acdl and prdl are separated along their entire length, a feature typical for *Apatosaurus*, and usually absent in diplodocines. The pcdl is almost horizontal, and the podl steeply inclined in CV 3, but in CV 4 and more posterior elements, they approach each other, forming a more acute angle anteriorly. In anterior elements, the podl and pcdl unite before curving laterally, but more posteriorly they remain separate as the acdl and prdl, and the pocdf is therefore extended onto posterior surface of diapophysis. They do not form such distinct posterior processes such as those present in *Kaatedocus* (Tschopp and Mateus, 2012b). The pcdl bifurcates anteriorly in the mid-cervical vertebrae, whereas in more posterior elements two parallel pcdl are present. This sheds new light on serial variation of these characters, as they are used to distinguish different species in some cases (e.g. *Apatosaurus parvus* or *Australodocus bohetii*; Upchurch et al., 2004b; Remes, 2007). However, since in the majority of cases (*Apatosaurus parvus* UW 15556, or *Barosaurus lentus* AMNH 6341 and YPM 429; Gilmore, 1936; Upchurch et al., 2004b; pers. obs., 2011) only one of these states is present, they are still considered as taxonomically informative. The cdf lies directly ventral to the diapophyseal process. In CV 15 of SMA 0011, a short but stout accessory lamina is present in the posterior portion of the fossa. In mid- and posterior vertebrae of SMA 0011, an accessory lamina is present between the pcdl and podl, facing posteriorly. In CV 12, there is even a second vertical accessory lamina subdividing the pocdf. Dorsomedial to the accessory lamina, the pocdf is pierced by a large foramen, such that the pocdf is interconnected with the spof. A similar state appears to be present in the anterior cervical vertebrae of *Dicraeosaurus* MB.R. 4886 (pers. obs., 2011), a partial mid-cervical vertebra of *Suuwassea* ANS 21122 (Harris, 2006b: fig. 8B), and *Eobrontosaurus* Tate-001 (P. Mannion, pers. comm., 2011) but in these taxa, the borders of the opening seem to be broken (pers. obs.). Fossae at the same location are present in many taxa, including *Diplodocus* or *Supersaurus* (Hatcher, 1901; D. Lovelace, pers. comm., 2012), but none of them opens up into a large foramen as in SMA 0011 (Fig. 5.20).

The sdf is of generally simple morphology. In CV 5 and 6, a shallow but dorsally well offset fossa is located close to the spine summit. In CV 6 and 8, the sdf bears a distinct, dorsoventrally elongate fossa posterolateral to the sprl, at about mid-height of the metapophysis. From CV 8 backwards, a vertical accessory lamina follows the sprl posteriorly, as in *Diplodocus carnegii* CM 84 (Hatcher, 1901). No subfossae are present in the sdf of posterior cervical vertebrae, but in CV 15, the sdf becomes clearly delimited dorsally, just below the anteroposterior narrowing of spine top.

The neural spine undergoes distinct changes in development and orientation from anterior to posterior. In anterior cervical vertebrae, it is vertical, and dorsoventrally elongate, reaching well above the postzygapophyses. The axis, as well as CV 3 and 4 have a distinctly posteriorly turning spine summit, as can also be seen in the corresponding elements of *Eobrontosaurus* (P. Mannion, pers. comm., 2011). There is an abrupt change in height from CV 5 to 6, resulting in a smaller total height of CV 6 compared to CV 5. Such a development has only been described in *Dicraeosaurus* (Janensch, 1929a), but neural spines are often incomplete, where anterior cervical vertebrae have been found (e.g. *Diplodocus carnegii* CM 84, *Apatosaurus louisae* CM 3018; Hatcher, 1901; Gilmore, 1936), which makes a thorough assessment of this character difficult. However, SMA 0011 is clearly different from the state in *Kaatedocus siberi* SMA 0004, as well as the indeterminate diplodocines AMNH 7530, 7535, and CM 3452, where the anterior cervical neural spines are low, and total vertebral height continuously increases throughout the vertebral column (Tschopp and Mateus, 2012b; pers. obs., 2011). From CV 6 backwards, the cervical neural spines of SMA 0011 decrease in relative length, compared to pedicel height, but remain vertical. Towards the cervico-dorsal transition, neural spine height increases again, such that CV 15 has a highly elevated spine summit. In this vertebra, the spine summit is also strongly anteriorly inclined. The distal-most part of the neural spine of CV 15 is anteroposteriorly short but elongated dorsoventrally. Bifurcation of the spine is present, but only from CV 9 backwards, as is the case in *Barosaurus* AMNH 6341 (McIntosh, 2005). Unbifurcated neural spines slightly expand transversely towards their distal end, similar to the state in *Suuwassea emilieae* (Harris, 2006b). Posteriorly, the spol are thin but project far posterodorsally, and connect to each other across the spine summit. Therefore, they enclose a distinct and deep spof. Elements with bifid neural spines have a median tubercle. The lateral surface of the neural spine summits becomes rugose in posterior vertebrae.

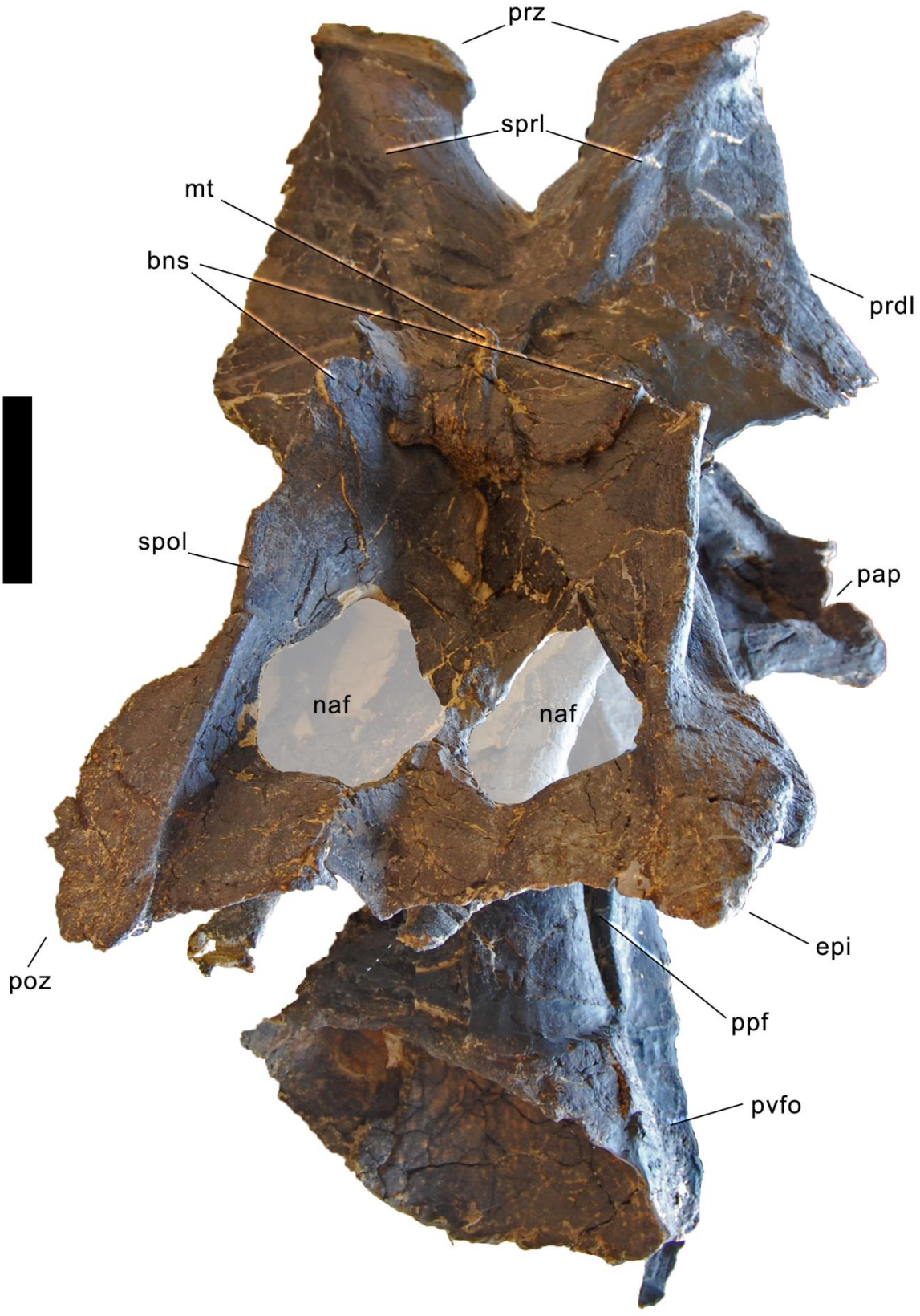

Figure 5.20: Neural arch foramina in CV 9 of SMA 0011, in posterodorsal view. The foramina are highlighted with the semi-transparent overlay. Abb.: bns, bifid neural spine; epi, epipophysis; mt, median tubercle; naf, neural arch foramen; pap, parapophysis; poz, postzygapophysis; ppf, posterior pneumatic fossa; prdl, prezygodiapophyseal lamina; prz, prezygapophysis; pvfo, posteroventral fossa; spol, spinopostzygapophyseal lamina; sprl, spinoprezygapophyseal lamina. Scale bar = 10 cm.

Table 5.2: Measurements of cervical vertebrae of SMA 0011.

CV	gl	gh	cl	cmw	wpr	wpo	ppl	pph	wct	hct	wcd	hcd	hns	cl wo cd	hna
Atlas			25							15		28		25	
Axis	146	204	129				86	29	29 (def)	54 (def)		44	133	115	45
CV 3	240	251	195	32	83		140	42	45	71		55	178	170	115
CV 4	330	330	264				170	35	54	71	38	56	255	228	116
CV 5	409	400	320	33	def		241	45	63	85		64	256	286	150
CV 6	465	325	388	42	127		258	52	97	89	52	65	200	348	138
CV 8	476	300	410	55	185		260	50		103	86	63	150	340	30
CV 9	497	inc	430	72	240	235	258	25 (comp)	150 (def)	90 (comp)	105 (def)	53 (comp)	inc	380	80 (comp)
CV 11	450	327	400	79	175		259	61	153	140		113	inc	363	188
CV 12	500 (est)	380 (est)	379		190 (def)	190 (est)	225	57	160	160		150 (def)	195	354	170
CV 15	415	380	400	116			230	34		185	180	165	240	370	208

Abb: cl, centrum length; cl wo cd, centrum length without condyle; cmw, centrum minimum width; comp, compressed; def, deformed; est, estimated; gh, greatest height; gl, greatest length; hcd, height anterior condyle; hct, height posterior cotyle; hna, height neural arch (below poz); hns, height neural spine; pph, pneumatopore height; ppl, pneumatopore length; wcd, width anterior condyle; wct, width posterior cotyle; wpo, width across postzygapophyses; wpr, width across prezygapophyses

Following the changing orientation and elevation of the spine, the spol also has a quite variable morphology from anterior to posterior cervical vertebrae: it is strongly concave in CV 3, and less so in CV 4, due to the more expressed backwards leaning of the spine top in CV 3. The spol is gently curved in CV 5, but forms a 90° angle in CV 6. Due to the low spine top, the spol is almost horizontal in CV 8 to 12. In CV 15, it becomes concave again, but remains almost horizontal posteriorly, where it unites with the epipophysis. The latter is well developed in all cervical vertebrae, often overhanging the postzygapophyses. It constitutes the posterior end of the spol, and is often pointed. The postzygapophyseal facets are suboval to subcircular in the anterior cervical vertebrae, but become subtriangular more posteriorly, with the tip pointing medially. They are concave and thus face both downwards and outwards. They are ventrally supported by a vertical, single cpol.

Dorsal vertebrae (Figs 5.21-5.26; Tab. 5.3)

Dorsal vertebrae 1 and 2. The first two dorsal vertebrae are still embedded in matrix, and only the right sides are prepared (Figs 5.21, 5.22). The diapophysis is not preserved in either vertebra, and DV 2 also lacks the right metapophysis and postzygapophysis. The anterodorsal part of the right lateral surface of the centrum of DV 2 is reconstructed, including the neurocentral synostosis.

The dorsal vertebrae 1 and 2 more closely resemble the cervical vertebrae than more posterior elements of the dorsal sequence. Compared to the last cervical vertebra, DV 1 and 2 have a considerably deeper diapophysis, and less distinct epipophyses. Their centra are opisthocoelous, and have an intermediate elongation compared to the last cervical and DV 3. The lateral surface is marked by elongate pleurocoels that occupy the central and anterior portion of the centrum. In DV 2, the pleurocoel is more restricted towards the anterior than in DV 1, being almost entirely situated above the parapophysis. The parapophysis lies anteroventral to the pleurocoels, which extend onto its dorsal face. Posteroventral flanges are present, but become less distinct in DV 2. The ventral surface is concave and broad, with a shallow longitudinal ridge located anteriorly.

The neural arch height is more or less equal to centrum length, not counting the condyle. As in anterior and posterior cervical vertebrae, the neurocentral synostosis is closed, but still visible in its anterior half. The neural spine is divided. The prezygapophysis is broad, and projects slightly anterior to the condyle in both vertebrae, although it is more vertically oriented in DV 2. A weak pre-epipophysis is present, but does not extend beyond the prezygapophyseal facet. The sprl is strongly concave, due to the strong anterior inclination of the spine top. The prdl does not contact the acdl directly, but they are interconnected by a vertical lamina below the diapophysis. The latter is thus slightly elevated above the centrum, and dorsoventrally high. The broken diapophysis of DV 2 reveals large open spaces that are surrounded by narrow laminae of relatively dense bone tissue. Both the acdl and the pcdl are only slightly inclined. The pocdf is subdivided by a strong, laterally facing, almost vertical accessory lamina, forming a posteroventral branch of the podl. This differs from the posterior cervical vertebrae, where the accessory lamina in the pocdf faces posteriorly. Unlike the mid- and posterior cervical vertebrae, DV 1 and 2 do not have any fenestra connecting the pocdf with the spof. The spine summit is anteroposteriorly narrow, and inclined anteriorly, but the inclination decreases in DV 2 and more posterior elements. The lateral surface of the spine is marked by the sdf, which is well delimited dorsally, similar to the state in CV 15. From the top of the sdf, the spine of DV 1 and 2 forms a narrow anterodorsal projection. The medial surface of the spine (visible in DV 2) is slightly convex and smooth, unlike the subtriangular shape present in most *Apatosaurus* (e.g. NSMT-PV 20375; Upchurch et al., 2004b).

Dorsal vertebrae 3 and 4. Both elements are broken and deformed such that it is difficult to understand their morphology in detail (Figs 5.23, 5.24). Dorsal vertebra 3 lacks the right diapophysis and neural spine, such that the internal surface of the left spine is visible in the mount. The dorsal portion of the centrum and ventral half of the neural arch are crushed, and various pieces of each became intermingled. Dorsal vertebra 4 preserves a very deformed centrum, mounted in anteroventral view, which is not fused with the neural arch. A part of the neural arch is preserved intermingled with the fractured pieces of DV 3.

The dorsal vertebrae from DV 3 towards the sacrum are considerably shorter than DV 1 and 2, but remain of about the same length (not considering the condyle). DV 3 has a strongly opisthocoelous centrum, but DV 4 is only slightly opisthocoelous. A distinct pleurocoel is present on the anterodorsal corner of the lateral side, but it is shorter than in DV 1 or 2. The position of the parapophysis is

difficult to see, but appears to be still on the centrum, above the pleurocoel in DV 3, whereas the centrum of DV 4 does not show any traces of a parapophysis. The ventral side of DV 3 is well delimited by posterior ridges between the lateral and ventral surfaces. A broad, but relatively distinct midline ridge marks the anterior half of the ventral side of the centrum of DV 3. The articulation surface of the centrum of DV 4 for the neurocentral synchondrosis is broad and curved. The neural canal is narrowest at midlength of the centrum.

The neural arch of DV 3 is higher, but more anteroposteriorly compressed, than in DV 2. The prezygapophysis is relatively short. The sprl is oriented almost vertically, and no strong anterior inclination of the neural spine is present anymore. The medial side of the neural spine of DV 3 is gently convex, and slightly wider anteroposteriorly than in DV 2. Postzygapophyses are not preserved.

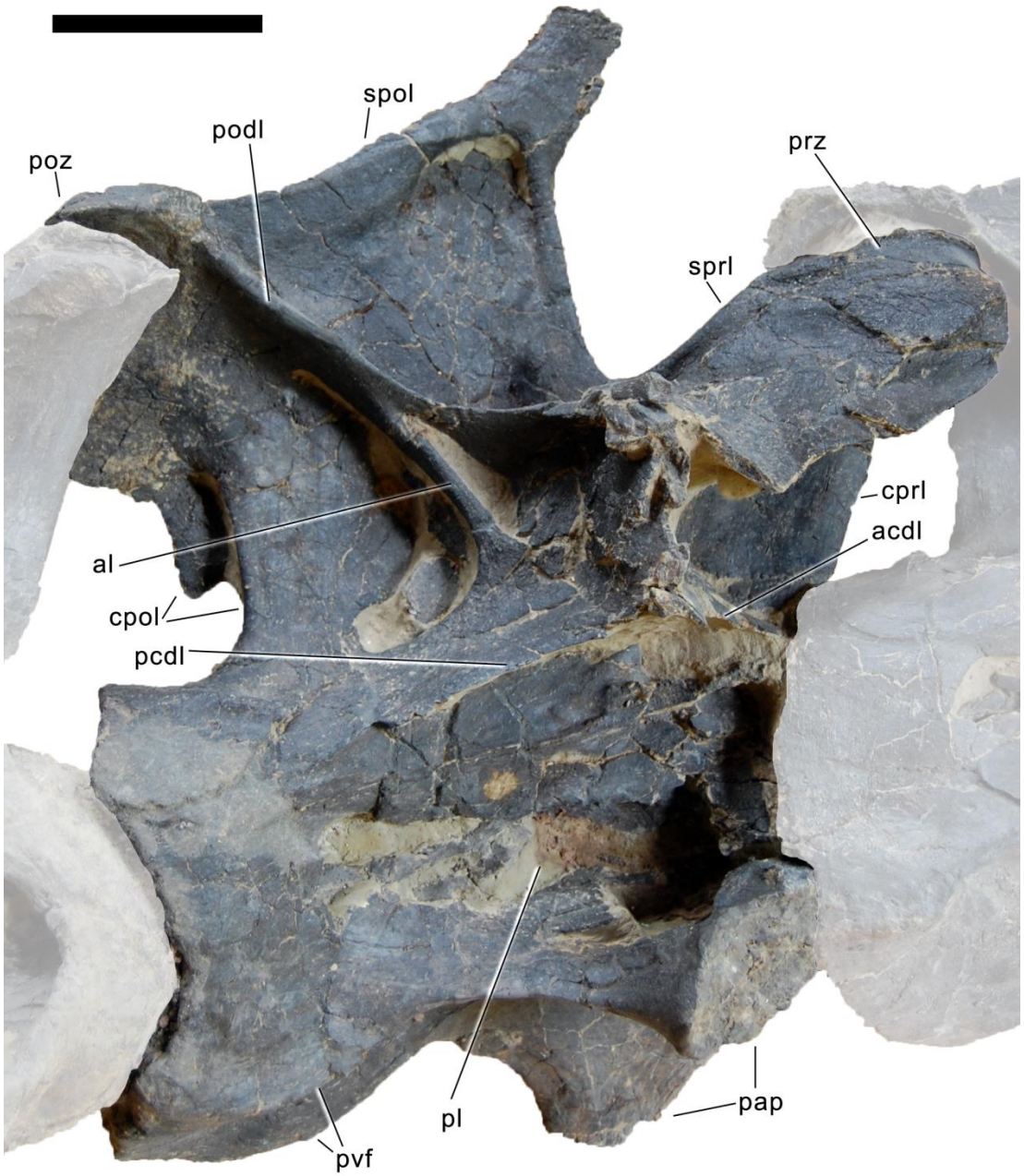

Figure 5.21: Dorsal vertebra 1 of SMA 0011 in right lateral view. Articulated CV 15 and DV 2 shaded. Abb.: acdl, anterior centrodiapophyseal lamina; al, accessory lamina; cpol, centropostzygapophyseal lamina; cprl, centroprezygapophyseal lamina; pap, parapophysis; pcdl, posterior centrodiapophyseal lamina; pl, pleurocoel; podl, postzygodiapophyseal lamina; poz, postzygapophysis; prdl, prezygodiapophyseal lamina; prz, prezygapophysis; pvf, posteroventral flange; spol, spinopostzygapophyseal lamina; sprl, spinoprezygapophyseal lamina. Scale bar = 10 cm.

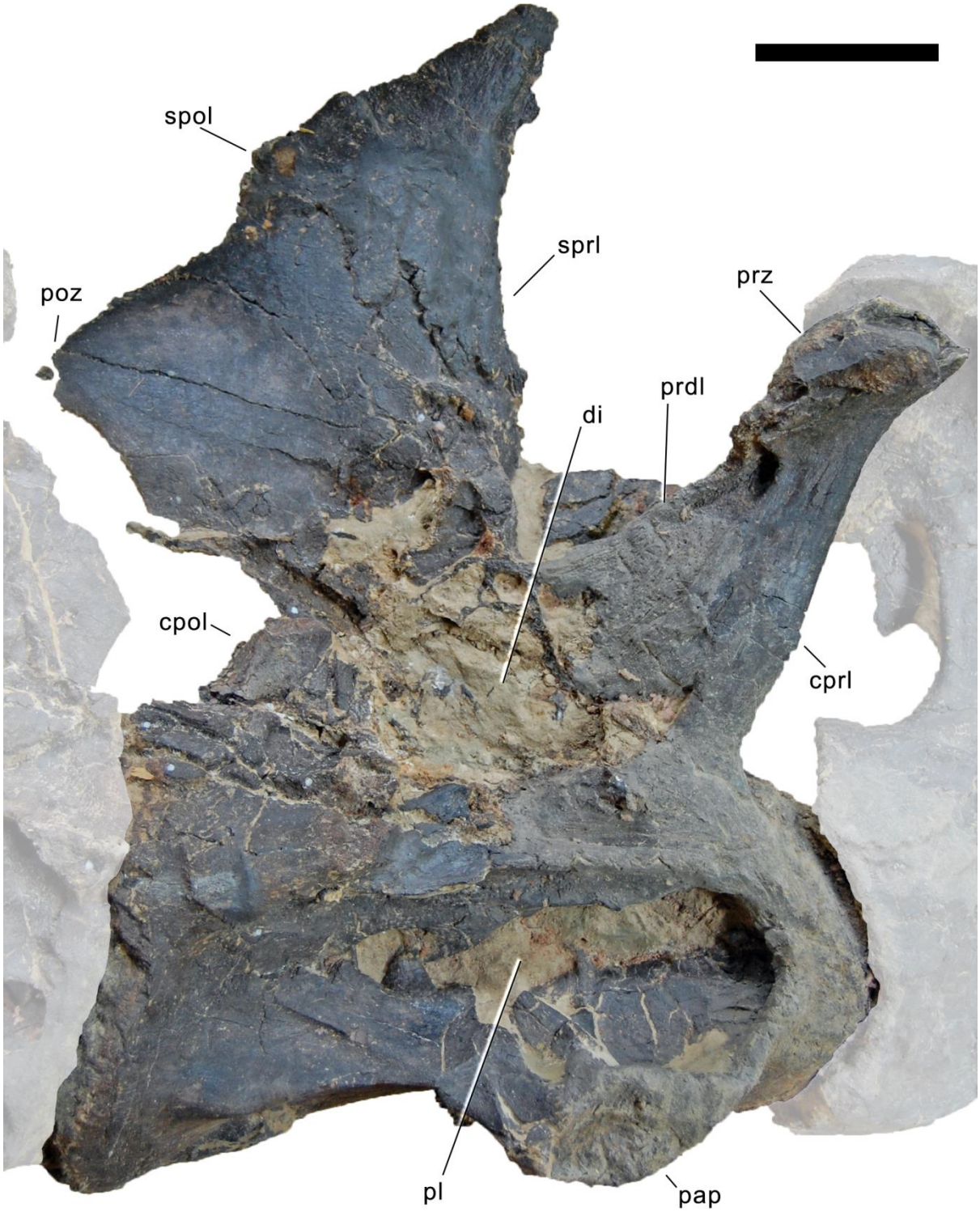

Figure 5.22: Dorsal vertebra 2 of SMA 0011 in right lateral view. Articulated DV 1 and DV 3 shaded. The right metapophysis is lacking, only the medial face of the left one is visible. Note the broken diapophysis that reveals the inner structure. Abb.: cpol, centropostzygapophyseal lamina; cprl, centroprezygapophyseal lamina; di, diapophysis; pap, parapophysis; pl, pleurocoel; poz, postzygapophysis; prdl, prezygodiapophyseal lamina; prz, prezygapophysis; spol, spinopostzygapophyseal lamina; sprl, spinoprezygapophyseal lamina. Scale bar = 10 cm.

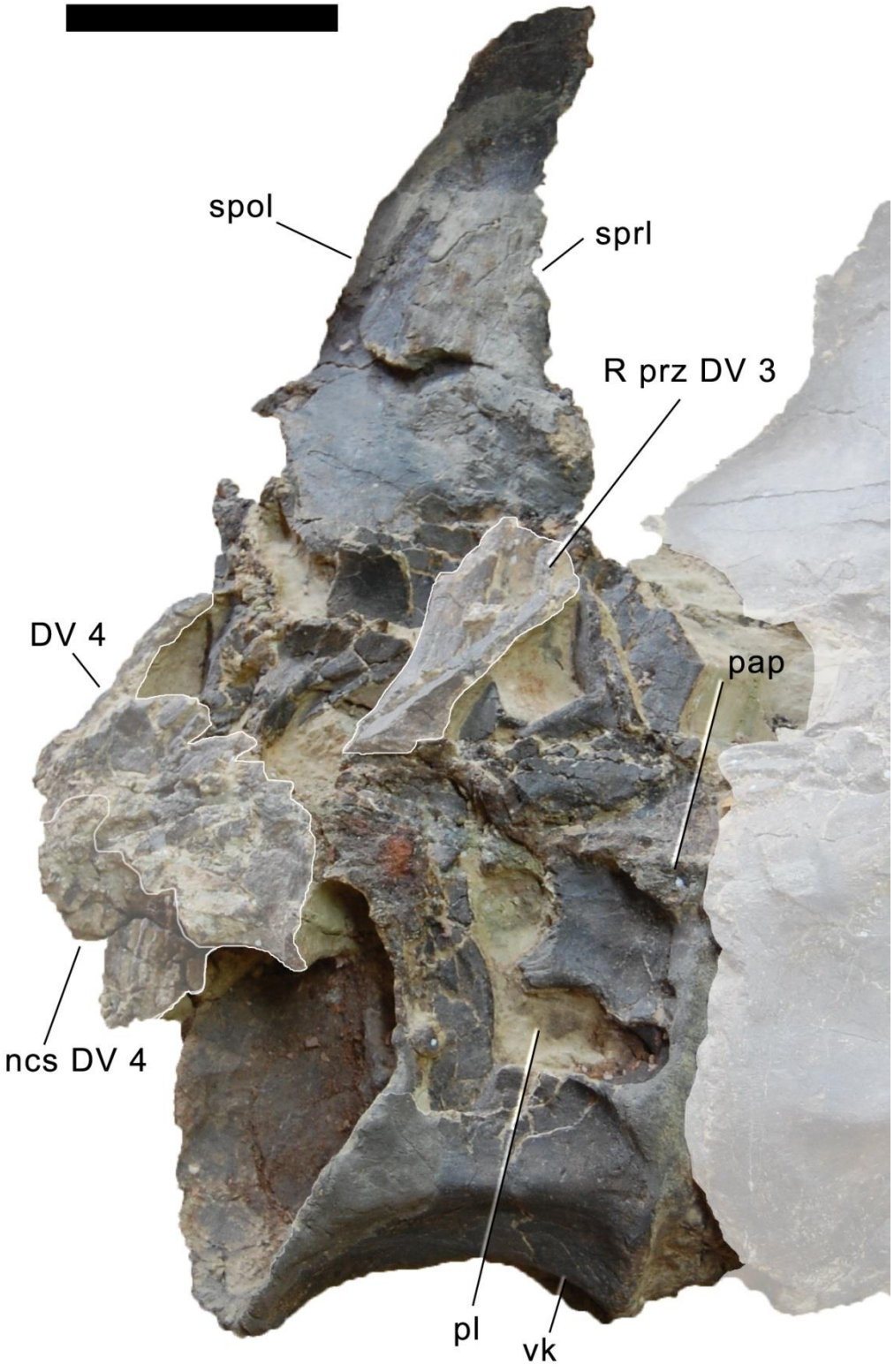

Figure 5.23: Dorsal vertebra 3 of SMA 0011 in right lateral view. Articulated DV 2 and partial DV 4 shaded. The right metapophysis is lacking, only the medial face of the left one is visible. The broken right prezygapophysis is present on top of the broken diapophysis. Abb.: DV, dorsal vertebra; ncs, neurocentral synchondrosis; pap, parapophysis; pl, pleurocoel; prz, prezygapophysis; spol, spinopostzygapophyseal lamina; sprl, spinoprezygapophyseal lamina; vk, ventral keel. Scale bar = 10 cm.

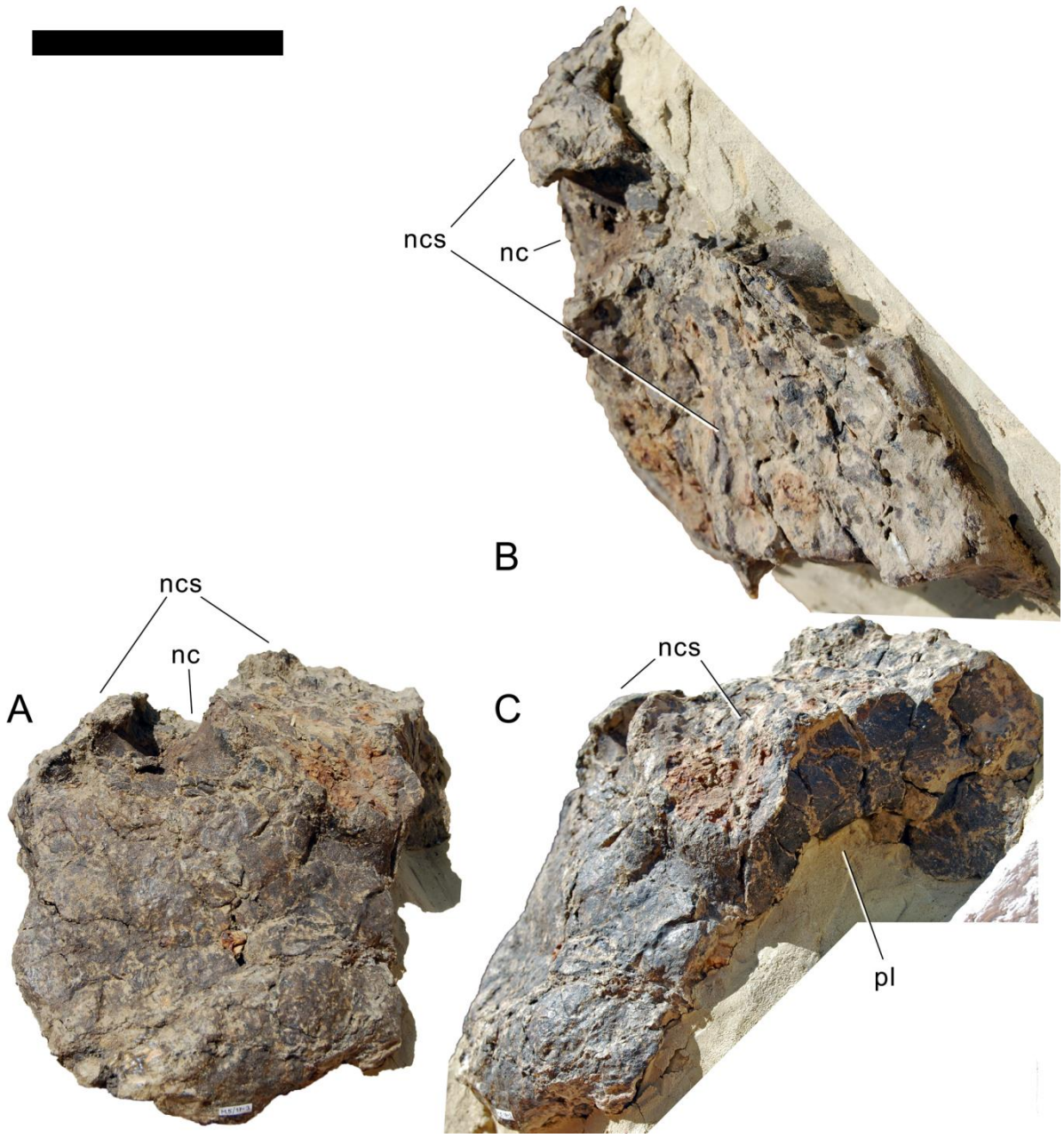

Figure 5.24: Dorsal vertebral centrum 4 of SMA 0011 in anterior (A), dorsal (B), and left lateral (C) views. The element is still partly preserved within matrix. Abb.: nc, neural canal; ncs, neurocentral synchondrosis; pl, pleurocoel. Scale bar = 10 cm.

Mid- to posterior dorsal vertebrae (DV 5 to 10). Dorsal vertebra 5 is lacking its right neural arch, diapophysis, and spine, as well as the distal tip of the left diapophysis (Fig. 5.25). Dorsal vertebra 6 lacks the anterior part of the centrum, the right diapophysis, parapophysis, and prezygapophysis, and the spine top. In dorsal vertebra 7, the right diapophysis, parapophysis, and the spine top are missing. Dorsal vertebrae 8 and 9 lack the right diapophysis and parapophysis. The last dorsal vertebra lacks the neural spine process, whereas the arch below the postzygapophysis, the diapophysis, and the prezygapophyses are preserved (Fig. 5.26).

The mid- and posterior dorsal centra are short, and generally amphiplatyan to amphicoelous. Only DV 5 shows a weak anterior condyle. The pleurocoel is largest in DV 6 to 8, occupies the dorsal half of the centrum, and extends slightly onto the pedicels, but below the neurocentral synchondrosis. The ventral surface is convex, and not well separated from the lateral side. The centrum is slightly shorter ventrally than at mid-height. In DV 6 and 7, a zigzagged line marks the neurocentral synostosis

at the dorsal edge of the centrum. Dorsal vertebrae 8 to 10 have unfused neurocentral synchondroses. The neural arch is high, with highly elevated postzygapophyses, resulting in longer pedicels than neural spines in at least DV 5 to 8. Pre- and postzygapophyses are on more or less a horizontal line. The pedicels below do not show a strong lamination, but the acpl, pcdl, and cpol can be well distinguished. Dorsal vertebrae 6 to 9 furthermore show a weakly developed pcpl. An accessory lamina can be found in DV 7, connecting the pcdl with the podl, and in DV 8 between the prpl and the prdl. The presence and development of the hyposphene-hypantrum articulation cannot be distinguished due to the articulated state of the vertebrae. The parapophysis lies at mid-height on the pedicels in DV 6, at two thirds in DV 7 and at three fourths in DV 8. More posteriorly, the parapophysis seems to have been attached to the prezygapophysis. The spine is relatively low in DV 5 to 8, and only in DV 9 and probably 10 does it exceed the pedicel height. The spines are situated above the posterior-most portion of the centrum, and are vertically oriented. This differs from the strongly anteriorly inclined posterior dorsal neural spines of *Diplodocus* (Hatcher, 1901; Gilmore, 1932). The sprl is vertical in DV 6, strongly dorsoventrally convex in DV 7 and 8, and slightly convex in DV 9. The spdl is short and only expressed at its ventral end. Dorsally it merges with the spol, which extends onto the lateral surface of the spine. The posl, or possibly medial spol, is straight and vertical. Due to the preservation and mounting, it cannot be distinguished at this point how far back the bifurcation proceeds. The last definitively bifid neural spines are present in DV 5.

Table 5.3: Measurements of dorsal vertebrae of SMA 0011.

Dorsals	gl	gh	cl	cmw	ppl	pph	wct	hct	wcd	hcd	hns	cl wo cd	hna
DV 1	450	475		95	185	57		195			325	310	222
DV 2		485	355	108	185	40		190		160	365	305	170 (est)
DV 3		630			65		120	220 (est)		200	458 (def)	140	250 (est)
DV 4					53 (def)				185 (def)	180 (def)			
DV 5		730	157		50	83	160 (def)	195				150 (est)	
DV 6		800			106	150		210			545 (est)	160	330
DV 7		810			110	160		225			605 (est)	170	345
DV 8		900			138	148		225			665	163	330
DV 9		900			112	130		212			665	160	290
DV 10					140	130		216				175	260 (est)

Abb: cl, centrum length; cl wo cd, centrum length without condyle; cmw, centrum minimum width; comp, compressed; def, deformed; est, estimated; gh, greatest height; gl, greatest length; hcd, height anterior condyle; hct, height posterior cotyle; hna, height neural arch (below poz); hns, height neural spine; pph, pneumatopore height; ppl, pneumatopore length; wcd, width anterior condyle; wct, width posterior cotyle.

Ribs

Cervical ribs. The cervical ribs are thin, fragile elements. The axial cervical rib has almost no tuberculum, and is thus a straight, elongate, and transversely compressed sheet of bone (Fig. 5.14). Anterior to mid-cervical ribs are longer than their corresponding centrum, but they only overlap a small portion of the following vertebra (Figs 5.14, 5.15). The anterior process is distinct, but very short in CR 3, and pointed in anterior and mid-cervical ribs. It becomes very broad and rounded anteriorly in posterior cervical ribs, with a central longitudinal lamina connecting to the capitulum. The tuberculum is posteriorly inclined in anterior cervical ribs, and subtriangular in cross-section at midlength. The rib itself is concave internally, with a lamina connecting the tuberculum with the capitulum internally, producing two separate fossae anteriorly and posteriorly. Cervical rib 6 bears a pneumatic foramen internally on the capitulum.

Dorsal ribs. Several ribs have been recovered associated with the dorsal series, but the correct position of the single elements cannot be confidently determined at this point. There is some information from the quarry maps that the rib associated with DV 1 (as interpreted herein) looks much like a cervical rib. It is short, with a straight shaft, and has the typical anterior process of cervical ribs. However, the rib is detached from the centrum, as in all presacral vertebrae of SMA 0011. Also, if the vertebra herein described as DV 1 would actually be the last cervical vertebra, the second dorsal vertebra would be considerably shorter than the first. Such an early length decrease in the dorsal column would be unusual, and different from *Diplodocus* or *Barosaurus*, where this happens between DV 2 and 3 (CM 84, or AMNH 6341; Hatcher, 1901; McIntosh, 2005). The cervical-like rib shape of

DR 1 is thus interpreted to be due to cervicalization, which appears to be an important evolutionary trend within diplodocids (McIntosh, 2005).

More posterior ribs are transversely compressed to slightly subtriangular at midshaft. Some of the elements have anteroposteriorly expanded distal ends (probably the anterior ribs, see Schwarz et al., 2007a), whereas others taper to a point. The capitulum is generally elongate, and the tuberculum low, but distinct. Between them, a relatively thin sheet of bone forms a triangular bony plate, which in at least some of the elements bears a ridge, as present in *Barosaurus* AMNH 6341, but absent in apatosaurs like *A. excelsus* YPM 1980 (pers. obs., 2011).

Sternal ribs. Several morphotype C elements (sensu Tschopp and Mateus, 2013) were recovered associated with SMA 0011, but remain unprepared. They are elongate, narrow bones. No additional information can be gleaned to date that would help to confirm or discard the interpretation of Claessens (2004) and Tschopp and Mateus (2013) that these elements are sternal ribs.

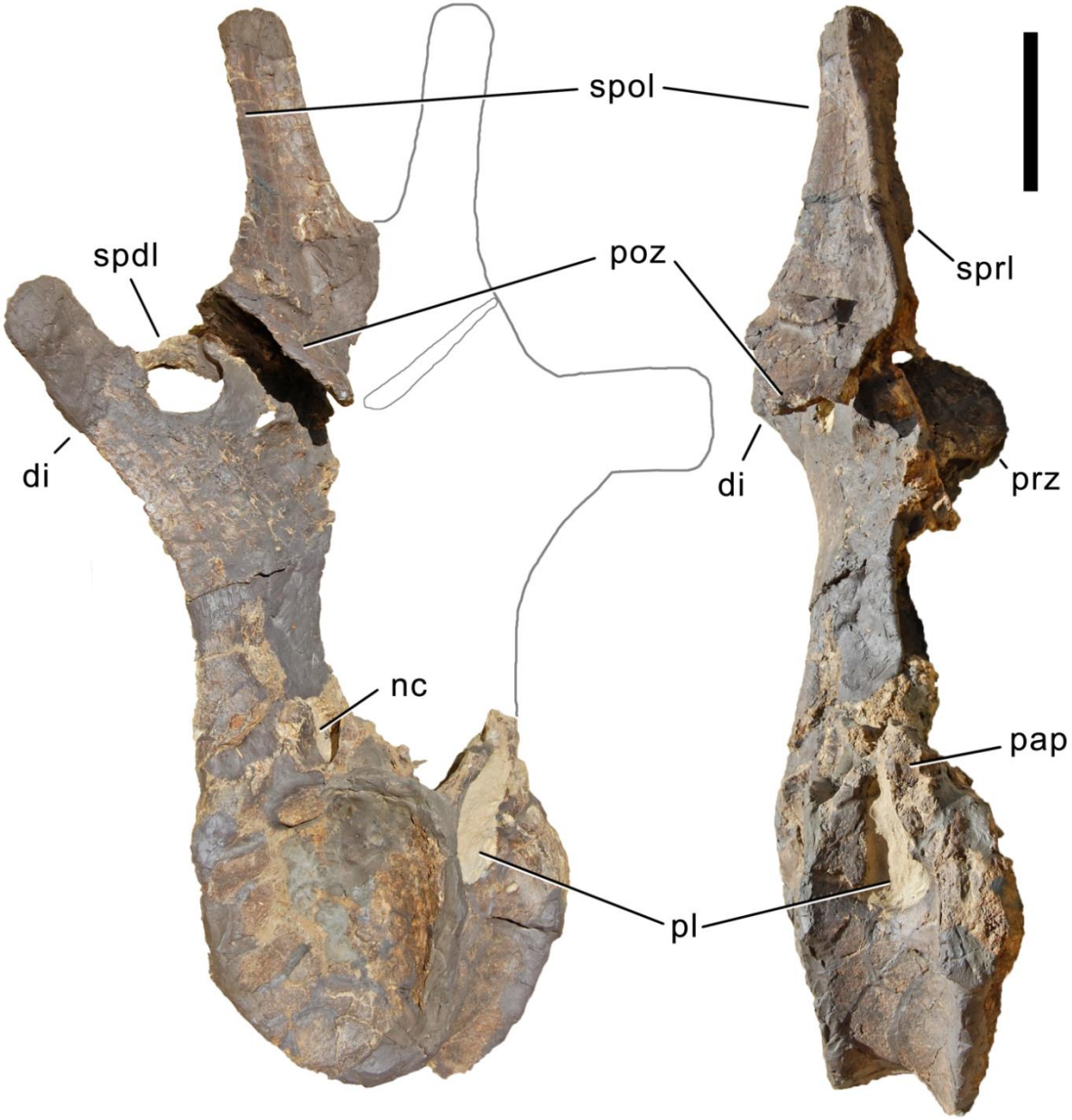

Figure 5.25: Dorsal vertebra 5 of SMA 0011 in posterolateral (A) and right lateral view (B). The element lacks the right half of the neural spine, and is partly mounted in matrix. Grey lines indicate the probable extensions of the right half. Note that the tip of the left diapophysis is reconstructed. Abb.: di, diapophysis; nc, neural canal; pap, parapophysis; pl, pleurocoel; poz, postzygapophysis; prz, prezygapophysis; spdl, spinodiapophyseal lamina; spol, spinopostzygapophyseal lamina; sprl, spinoprezygapophyseal lamina. Scale bar = 10 cm.

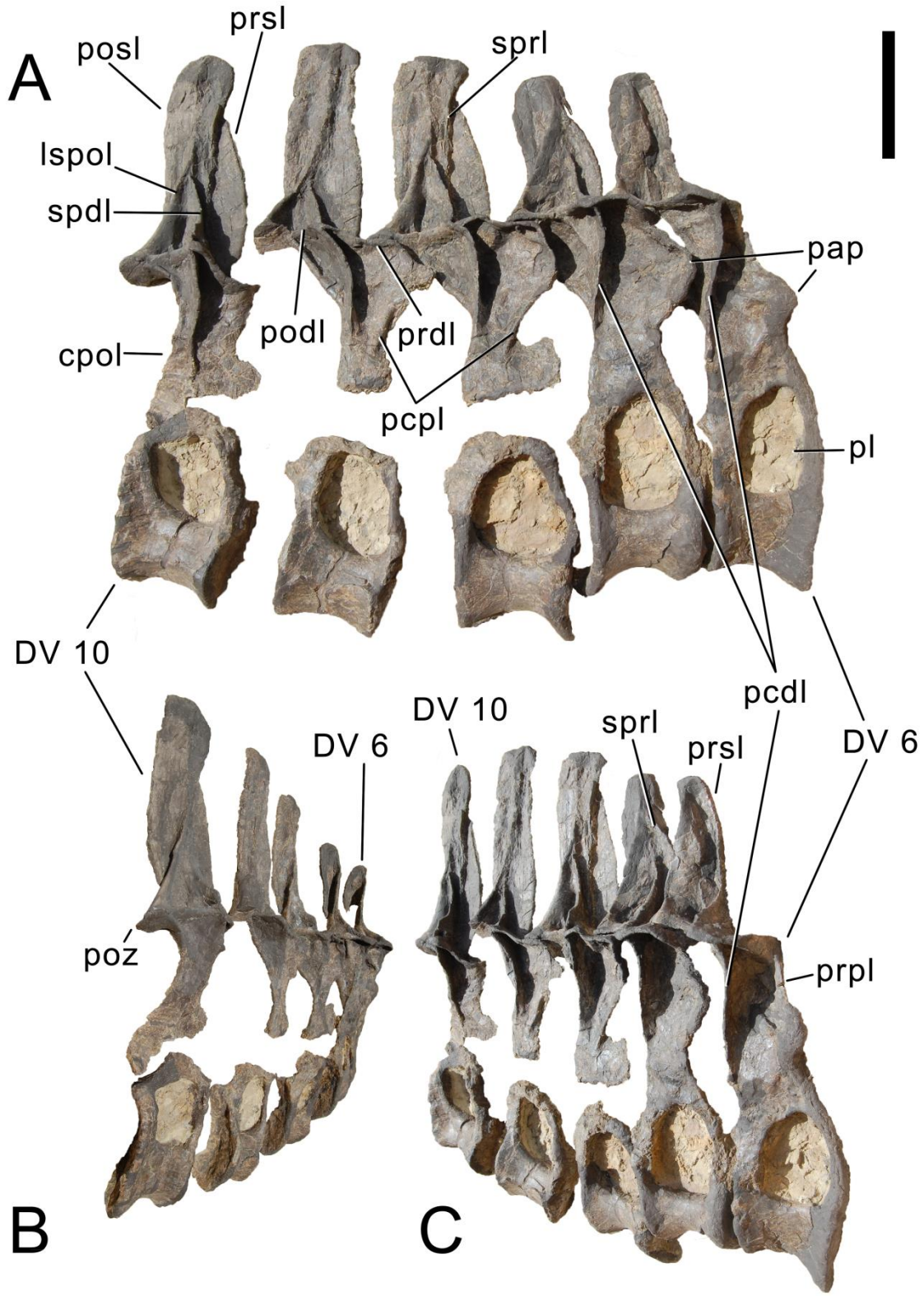

Figure 5.26: Dorsal vertebrae 6 to 10 of SMA 0011 in right lateral (A), posterolateral (B), and anterolateral view (C). The elements are partly preserved in matrix. Note the open neurocentral synchondrosis in DV 7 to DV 10. Abb.: cpol, centropostzygapophyseal lamina; DV, dorsal vertebra; lspol, lateral spinopostzygapophyseal lamina; pap, parapophysis; pcdl, posterior centrodiapophyseal lamina; pcpl, posterior centroparapophyseal lamina; pl, pleurocoel; podl, postzygodiapophyseal lamina; posl, postspinal lamina; poz, postzygapophysis; prdl, prezygodiapophyseal lamina; prpl, prezygoparapophyseal lamina; prsl, prespinal lamina; spdl, spinodiapophyseal lamina; sprl, spinoprezygapophyseal lamina. Scale bar in A = 10 cm, DV 6 in A and C, and DV 10 in A and B are scaled to the same vertebral height.

Forelimb (Figs 5.27-5.30; Tab. 5.4)

Scapula R, external view. The right scapula lacks the dorsal part of the acromion and of the distal end of the blade (Fig. 5.27). The acromion and the blade form an acute angle, but the acromial ridge is only very slightly developed. The area anterior to the acromial ridge is concave. The posteroventral edge is mostly straight, and does not bear a triangular process as present in some *Camarasaurus* specimens, or *Dystrophaeus* (Osborn and Mook, 1921; McIntosh, 1997). The distal end of the blade is slightly curving ventrally as in *Apatosaurus excelsus* YPM 1980 (Upchurch et al., 2004b). The anterodorsal, or acromial edge of the scapula is much more concave, due to the stronger extensions of both the dorsal portion of the acromion, as well as the indicated widening of the distal shaft, which starts more anteriorly in this edge than on the posteroventral one. No oval rugose tubercle is present on the base of the shaft as in *Apatosaurus excelsus* YPM 1980 (Upchurch et al., 2004b; pers. obs., 2011).

Coracoid R, external view. The coracoid is somewhat tear-drop shaped (Fig. 5.27), with a concave anterodorsal edge, and a strongly, continuously convex, narrow dorsal margin, unlike the squared coracoids of apatosaurs (Riggs, 1903; Bakker, 1998). The coracoid foramen is completely enclosed, but the coracoid is not fused with the scapula. The bone is gently convex dorsoventrally. It curves slightly medially at its anterior margin. No distinct notch is present anterior to the glenoid surface. The glenoid is strongly transversely expanded at its center, and tapers dorsally and ventrally. The glenoid surface and the articulation surface with the scapula enclose an angle of about 155°.

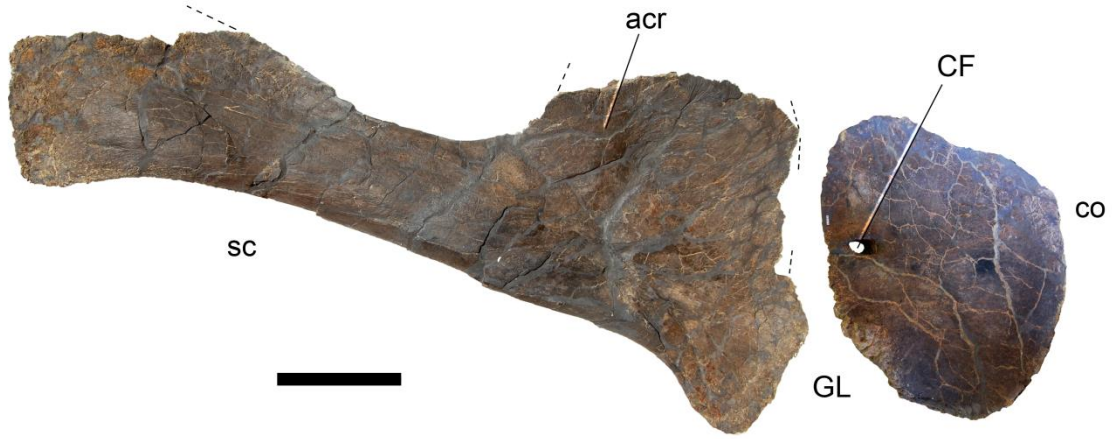

Figure 5.27: Scapula and coracoid of SMA 0011 in right lateral view. Lacking parts indicated with dashed lines. Abb.: acr, acromion ridge; CF, coracoid foramen; co, coracoid; GL, glenoid; sc, scapula. Scale bar = 20 cm.

Humerus R, anterior view. The right humerus is complete but slightly compressed anteroposteriorly (Fig. 5.28A). It is widely expanded at its proximal end, both laterally and medially. The distal end is expanded as well, but less so. The proximal portion is concave transversely, and does not bear a central rugose tubercle as present in *Apatosaurus* AMNH 6114 (pers. obs., 2011). The deltopectoral crest does not extend to midshaft. Its distal end is distinct and follows the lateral margin. It is not transversely expanded as typical for titanosaurids (Wilson, 2002; Curry Rogers, 2005). The crest is concave laterally, but this depression is exaggerated taphonomically. Two ridges mark the distal end anteriorly, indicating the extension of the medial and lateral condyles. The ridges are relatively well visible and extend proximally. The medial condyle is much more prominent than lateral one.

Ulna L, anterior view. The ulna lacks the proximal-most portion of the anterior arm of the condylar processes. The bone is strongly transversely compressed in its proximal half (Fig. 5.28B). It is generally slender, with a triradiate proximal end. The anterior arm is considerably longer than the lateral one, even though this is enhanced due to compression. The ulna has relatively strongly concave anterolateral and posterolateral surfaces. The lateral arm is somewhat wider than the anterior one. The distal part of the anteromedial surface bears two strong and elevated, longitudinal ridges. They proceed both distally and proximally, but narrower and with a smooth surface. Proximally, the more lateral of the two ridges extends above midlength. Distally, the more medial ridge is more pronounced, reaching the distal articular surface. The distal end is expanded medially and somewhat transversely. The articular surface is subtriangular in outline.

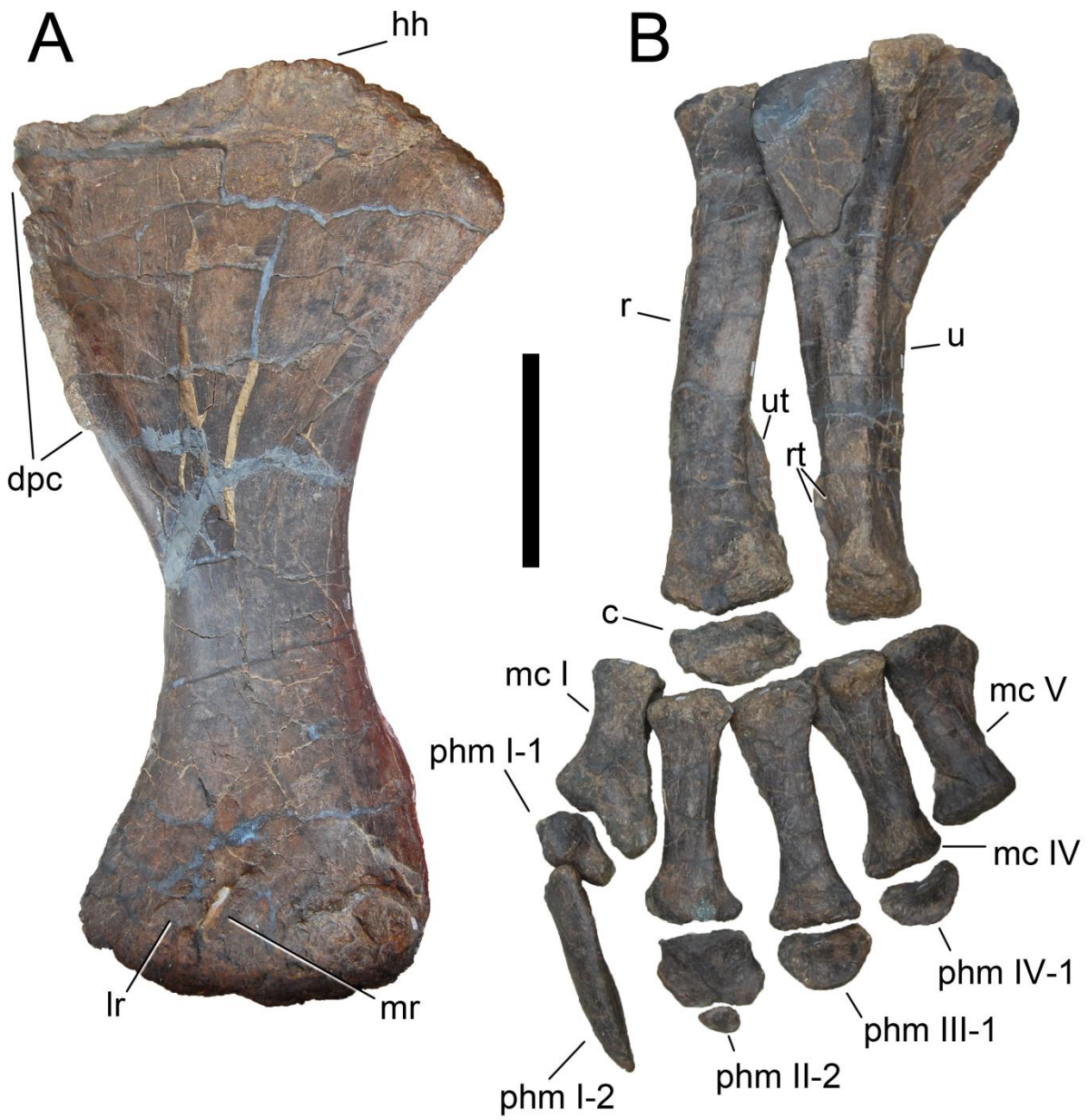

Figure 5.28: Forelimb of SMA 0011 in anterior view: A) humerus, B) antebrachium and manus (as mounted within matrix). Note that the carpal was probably mounted upside down. Abb.: c, carpal; dpc, deltopectoral crest; hh, humeral head; lr, lateral ridge; mc, metacarpal; mr, medial ridge; phm, manual phalanx; r, radius; rt, tubercle for articulation with radius; u, ulna; ut, tubercle for articulation with ulna. Scale bar (valid for both A and B) = 20 cm.

Radius L, anterior view. The radius is complete, but its proximal end is compressed (Fig. 5.28B). It has thus a narrow, ellipsoid outline, but would probably be subcircular if undeformed. The shaft appears subrectangular in cross-section. As in the ulna, also the distal end of the radius is slightly expanded. The posterolateral surface bears at least one longitudinal ridge on its distal portion for the articulation with the ulna (more is obscured due to the mounting in matrix).

Carpal L. The carpal is a block-like element (Fig. 5.28B). Only one has been found in the otherwise articulated manus. The entire bone is relatively rugose and articulates with the radius. Comparison with the carpal elements found in other diplodocids (Hatcher, 1902; Gilmore, 1936; Bedell and Trexler, 2005) would suggest that it has been mounted upside down, although it was mounted as found, according to the quarry maps. If the mount is correct, it has a flat proximal, and an irregular, but transversely convex distal surface, contrary to the case in other diplodocids (Hatcher, 1902; Gilmore, 1936; Bedell and Trexler, 2005). It is anteroposteriorly wider at its medial end than laterally. There are

no distinct articulation surfaces for the metacarpals as seen in *Camarasaurus* (Tschopp, 2008). The carpal of SMA 0011 is longer proximodistally than the element known from *Apatosaurus* CM 3018 or UW 15556 (Hatcher, 1902; Gilmore, 1936). The anterior surface is concave transversely. Other than in *Apatosaurus*, where the carpal articulated with both the ulna and the radius, and caps the median three metacarpals proximally (Hatcher, 1902; Gilmore, 1936), the carpal of SMA 0011 appears to overlie metacarpals I, II, and possibly III. This is the same arrangement as found in the articulated manus of WDC-FS001A (Bedell and Trexler, 2005).

Metacarpals L, anterior view. All metacarpals are complete and articulated (Fig. 5.28B). They are relatively elongate bones, but less than in *Camarasaurus* (Tschopp, 2008). Metacarpal III is the longest, followed by mc II, IV, I, and V (Tab. 5.4). Metacarpal I and II have subrectangular proximal articulation surfaces, mc III and IV triangular ones. Metacarpal I is relatively stout, with distinct anterior, lateral and medial surfaces. The lateral condyle is much longer proximodistally than the medial one. This results in a strongly inclined distal surface, such that the phalanges project posteromedially in the articulated manus. Metacarpal II has very distinct, straight anteromedial and anterolateral edges. The proximal and distal ends are slightly expanded in all directions. The distal surface slightly curves into the anterior surface. Its lateral and medial condyles are only visible in distal and posterior view. The proximal portions of both the medial and lateral surfaces are concave, laterally more than medially. Metacarpal III has a very distinct posterior corner of the proximal surface, probably connecting to a median ridge on the posterior surface, as is typical for Sauropoda (Upchurch et al., 2004a). Whereas no distinct transition from the anterior onto the medial surface occurs on mc III, the lateral face is clearly separated. The proximally and distal articular surfaces are slightly twisted. The distal surface is ellipsoid, and does not extend considerably onto the anterior face. Metacarpal IV has a triangular proximal articulation surface, with a concave medial edge. As in mc III the shaft of mc IV is twisted, and a distinction of the anterior face is not possible. The distal articular surface is subtriangular as well, with the apex anteriorly, and inclined medial and lateral edges. Two condyles are visible posteriorly. The apex of the distal articular surface curves onto the anterior face. Metacarpal V is short and widely expanded transversely at its proximal end. The distal end is lacking, but the preserved parts indicate that it is transversely expanded. This expansion occurs perpendicular to the proximal one.

Manual non-ungual phalanges L, anterior view. The manual non-ungual phalanges are relatively short and stocky (Fig. 5.28B). They are wider than long, as is typical for the eusauropod manus (Bonnan, 2003). The manual phalanx I-1 is mounted in posterior view. The proximal surface is concave anteroposteriorly. The phalanx I-1 has a concave posterior surface, with a proximally projecting ventral lip. Its medial surface is shorter than the lateral one, enhancing the outwards twist of the ungual phalanx even more. Well-developed medial and lateral condyles are present distally. The lateral extension of the posterolateral edge forms a thin, short crest (Fig. 5.29). Nothing similar is present in the manus of *Camarasaurus* (Osborn, 1904; Tschopp, 2008), but too few articulated proximal manual phalanges are known in diplodocids in order to decide if this might be autapomorphic in SMA 0011 or is instead more widespread within the clade. A phalanx figured by Jensen (1985: fig. 1E) appears to show a similar development of the posterolateral edge, but has not been identified below Sauropod indet. (Jensen, 1985). The manual phalanx II-1 has a concave proximal surface, which is probably ovoid in outline (only the dorsal portion can be seen as it is currently mounted). It is only minimally wider than the shaft. The medial surface is broader, but shorter than the lateral one. The anterior surface is convex transversely. The distal articular surface is expanded transversely, and the well-developed condyles extend onto the lateral surfaces. The manual phalanx II-2 is a vestigial, suboval bony nubbin. A distinct ridge separates the proximal and distal surfaces. The manual phalanges III-1 and IV-1 are very similar, with III-1 being slightly larger. They have concave proximal articular surfaces, transversely more so than anteroposteriorly. The surfaces are suboval in outline, and their anterior margins are pronounced medially. The anterior surfaces are concave proximodistally, but slightly convex transversely. The distal surfaces are without condyles. They have a continuous, rounded surface, which curves proximally at its medial and lateral end, almost reaching the proximal articular surface. The medial and lateral surfaces are thus practically nonexistent. The lack of medial and lateral condyles implies that there were no vestigial terminal phalanges in these digits, unlike in *Camarasaurus* (Tschopp, 2008). The unusual shape of phm III-1

and IV-1 (as mounted) resembles phm V-1 in *Camarasaurus* SMA 0002 (Tschopp, 2008). Given that no additional phalanx was found to mount with digit V, the elements mounted on the third and fourth digit might actually represent phm IV-1 and V-1. Both of these bones were not found articulated with their corresponding metacarpals, which makes a definitive assignment difficult. However, given that the manus would otherwise be complete, the mount is herein interpreted to be right, and no, or only a vestigial phalanx would have been present in digit V. Comparing with the manus of *Camarasaurus* SMA 0002, this would indicate that the peculiar shape without distal condyles of phm III-1, and IV-1 of SMA 0011, or phm V-1 of SMA 0002 represent an intermediate stadium of phalangeal reduction, between the usual phalangeal shape and the nubbin-like vestigial elements found with digits two of both SMA 0011 and SMA 0002 (Tschopp, 2008).

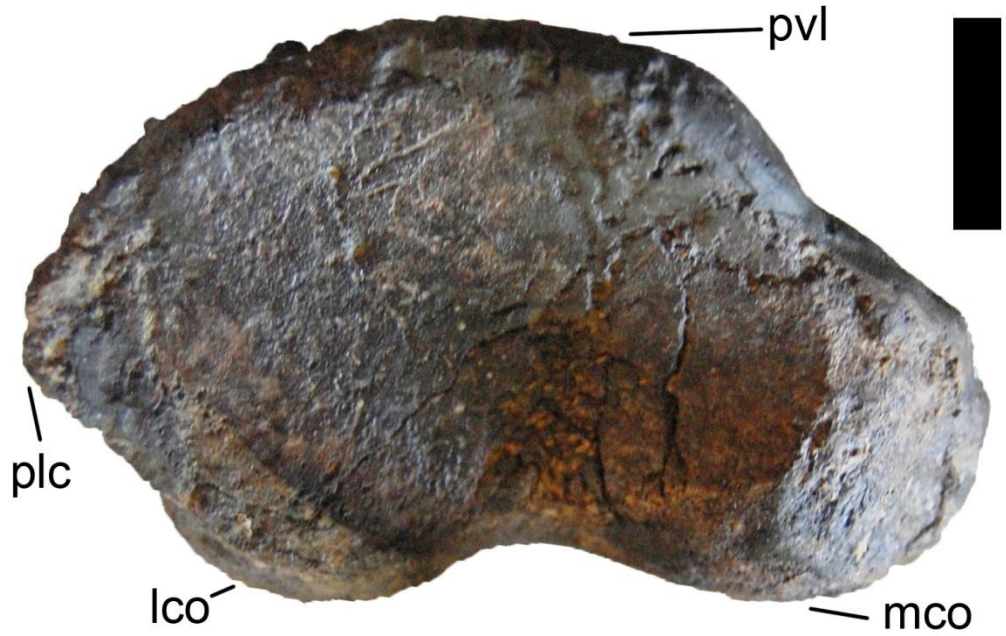

Figure 5.29: Left manual phalanx I-1 of SMA 0011 in posterior view. Note the distinct posteroventral lip and posterolateral crest. Abb.: lco, lateral condyle; mco, medial condyle; plc, posterolateral crest; pvl, posteroventral lip. Scale bar = 2 cm.

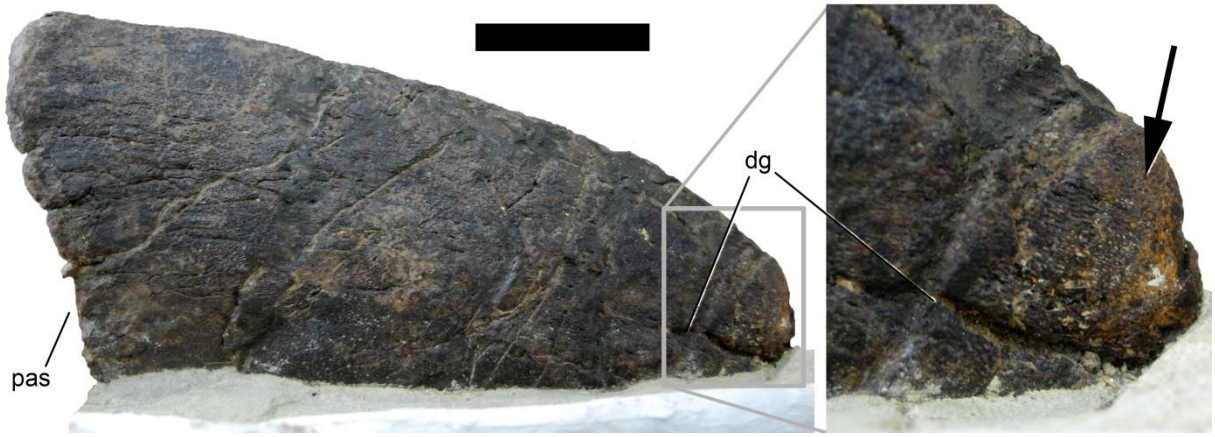

Figure 5.30: Possible preservation of keratinous sheet on left manual ungual I-2 of SMA 0011 (medial view). Note the different surface texture at the tip (arrow), compared to more posterior portions. Abb.: dg, distal groove; pas, proximal articular surface. Scale bar = 5 cm.

Manual ungual L, anterior view. One ungual is present, and situated on the first digit (Fig. 5.28B). It is a long, high, and transversely compressed element. The proximal surface is tear-drop shaped, with a laterally curving anterior tip, and a widened posterior portion, where the articular surface lies. Anterior to the articular surface, the proximal surface projects somewhat proximally, and is rugose. This rugosity extends as a short ridge posteriorly, into the articular surface. The medial surface is convex anteroposteriorly. A short groove marks the distal-most portion, which is slightly elevated (about 1 mm) above the more proximal portion of the claw, and shows a different surface texture (Fig. 5.30). The latter might represent fossilized remnants of the keratinous sheet covering the claw. The lateral surface is almost plane, with a long, proximodistally extending, straight groove covering the distal half of the surface.

Table 5.4: Forelimb measurements of SMA 0011, in mm.

	gl	acl	min sw	max sw	min apd	pw	dw	dpcl	apl	lpl	max pdd	papd	dapd	Comments
Scapula	1375	620 (inc)	178	240 (inc)										
Humerus	870		174		70 (est)	474	309	310						
Radius	601		82			165	137							
Ulna	603						94		280 (def)	170 (def)				
Carpal				131							62			
Mc I	186		54	108		70	108					60 (est)		
Mc II	218		54	104		99	101					60 (est)	54	
Mc III	230		41	86		80	86					70 (est)	40	
Mc IV	208		33	85		68	85					95 (def)		
Mc V	180		40	113		113								
phm I-1	53			89		86	75							
phm II-1	78		91	111		93	111							
phm III-1	51		93	95		93								
phm IV-1	35		78	80		78								
phm V-1 manual ungual	202/220			43		43								gl measured straight/ along curvature
phm II-2	17			40		40								

Abb.: acl, acromion length; apd, anteroposterior depth; apl; anterior process length; dapd; distal anteroposterior depth; dpcl, length deltopectoral crest; dw, distal transverse width; gl, greatest length; lpl, lateral process length; papd, proximal anteroposterior depth; pdd, proximodistal depth; pw, proximal transverse width; sw, shaft width.

Hindlimb (Figs 5.31-5.35; Tab. 5.5)

Ilium R, external view. The ilium lacks a large part of its posterior upper portion. The preacetabular process has a very pointed apex, which is pointing anterolaterally. The anterior portion is strongly concave, with the ventral margin facing laterally. The ventral preacetabular border and the pubic process form an angle of 90°, which is uncommon in *Diplodocus*, but present in the holotype of '*Diplodocus*' *hayi* (Hatcher, 1901; HMNS 175, pers. obs., 2010). A triangular depression is located laterally at the base of the pubic process, with horizontal and medio- and lateroventrally inclined sides. This is similar to the putative diplodocid ilium from Spain (CPT-1074; Royo-Torres and Cobos, 2004; pers. obs., 2012). The pubic peduncle is distinctly concave transversely at its posterior end, but breaks indicate that the concavity is exaggerated and that the transverse width of the pubic peduncle would be slightly larger. The ischial tubercle is facing slightly laterally. The acetabular margin is thinnest just posterior to the pubic peduncle, and extends transversely both posteriorly and anteroventrally, reaching the articulation surfaces of the ischium and pubis.

Pubis R, internal view. The right pubis is almost complete. Its anterodorsal corner is slightly eroded, and the middle portion of the ischial articulation is missing. The entire bone is relatively slender (Fig. 5.31A). The pubic foramen is closed, and located in the proximal third of the ischial articulation. Even though eroded, the anterodorsal corner does not seem to bear a very pronounced ambiens process, as seen in *Diplodocus* or *Supersaurus* (Hatcher, 1901; Lovelace et al., 2007). This corner is laterally expanded, and from here, the pubis slightly tapers along the acetabular surface. The medial surface of the proximal half of the bone is proximodistally concave, and transversely slightly convex. The latter convexity becomes more pronounced towards midlength, where the ventral margin curves back from the expanded ischial articulation to the narrow midshaft. The dorsal edge of the pubis is gently concave. Its anterior end is expanded both transversely and anteroposteriorly. The narrowest portion of the shaft lies at about two thirds of the entire length of the pubis.

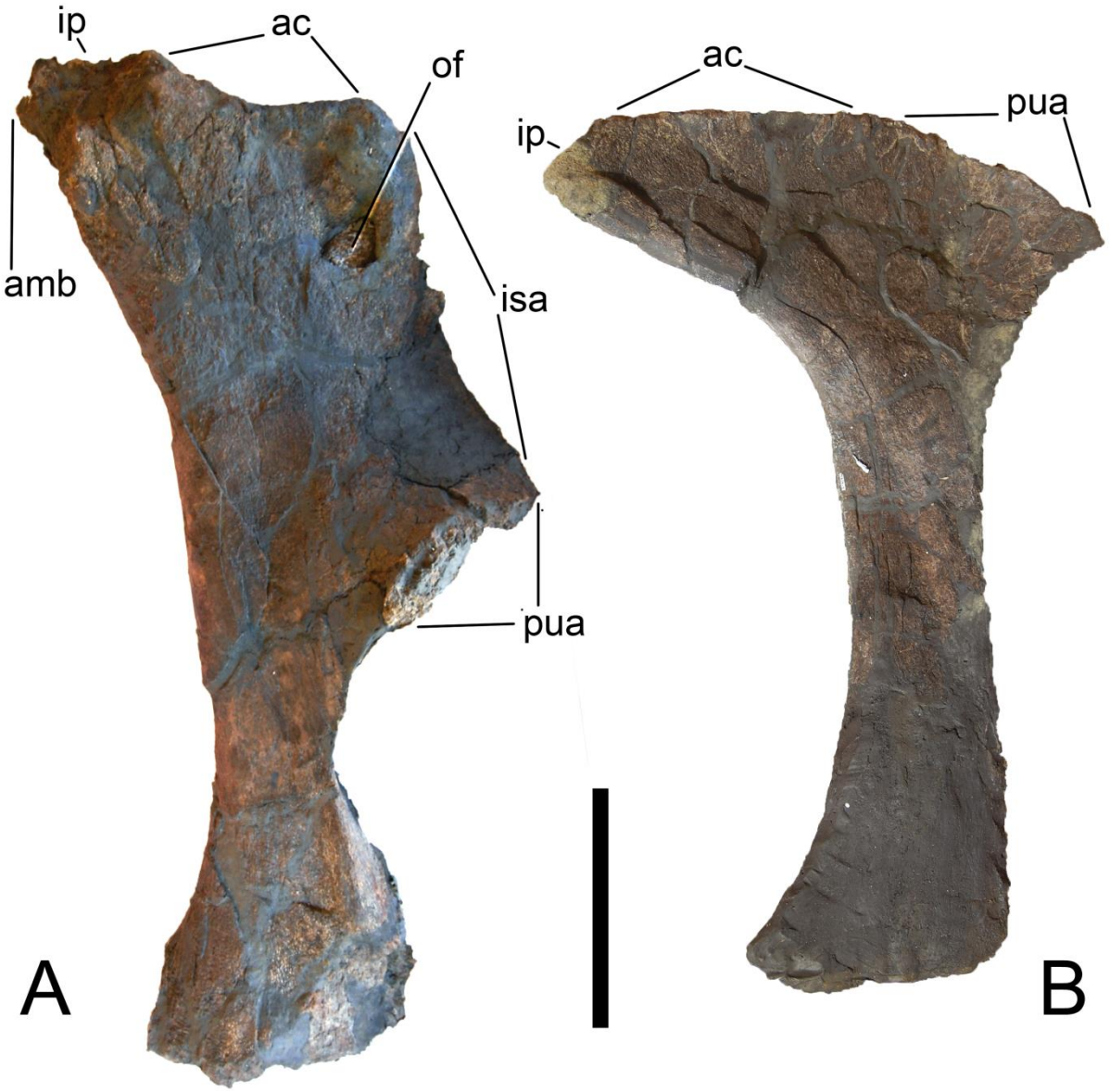

Figure 5.31: Right pubis (A) and left ischium (B) of SMA 0011 in medial view. The distal end of the ischium is reconstructed. Abb.: ac, acetabular surface; amb, ambiens process; ip, iliac peduncle; isa, ischial articular surface; of, obturator foramen; pua, pubic articulation. Scale bar = 20 cm.

Ischium L, internal view. The ischium lacks the posterior half of the shaft (Fig. 5.31B). Its proximal portion is wide and concave. The acetabular surface is inclined, such that the medial border forms a thin crest. This crest is relatively straight in medial view, but concave and curved in proximal view. Unlike the state in rebbachisaurids, the acetabular surface does not expand towards the articulation surfaces for the ilium and the pubis (Calvo and Salgado, 1995; Whitlock, 2011a). The iliac process has thus no distinct neck, and is relatively narrow. The pubic articulation is much longer, and straight in medial view. It curves slightly medially towards its ventral end. The shaft is weakly convex at its base, separating the concave acetabular portion from the again shallowly concave posterior shaft. The dorsal and ventral margins are parallel, only the posterior-most preserved portion of the dorsal edge indicates a slight dorsal expansion towards the end, as is typical for diplodocids (McIntosh, 1990a, b; Upchurch, 1998; Wilson, 2002). No distinct ridges or scars can be seen on the internal surface. Oblique, minuscule elongated cavities indicate the presence of a now eroded shallow ridge extending from about midlength of the ventral edge of the shaft proximodorsally onto the convex base of the shaft and ending on the dorsal margin where it curves into the acetabular portion.

Femur L, posterior view. The greater trochanter and the intercondylar groove are missing in the femur of SMA 0011 (Fig. 5.32A). The medial edge is gently curved below the femoral head, not as distinct as in *Dyslocosaurus* (McIntosh et al., 1992). The head is not well separated from the shaft ventrally. The fourth trochanter terminates slightly above midlength. It is entirely located on the posterior surface of the shaft, but close to the medial border proximally. The distal end of the fourth trochanter curves distinctly laterally. The distal condyles of the femur project far posteriorly. The lateral condyle bears an epicondyle. Both condyles expand slightly outwards, and the medial one projects further distally than the lateral one. In posterior view, the two condyles are slightly inclined medially.

Tibia L, anterior view. The tibia is complete (Fig. 5.32B). It is slightly expanded at both ends. A small convexity marks the distal end of the medial edge, similar, but broader and less distinct than in *Dyslocosaurus* (AC 663, pers. obs., 2011). The cnemial crest is somewhat displaced distally, and distally thicker than proximally. The proximal end appears longer transversely than anteroposteriorly, but not the entire surface is visible. This also precludes the assessment of the outline of the proximal articular surface, which is subrectangular in apatosaurines, whereas it is subtriangular in diplodocines (Lovelace et al., 2007), and would thus yield further information on the correct taxonomic assignment of SMA 0011.

Fibula L, anterior view. The fibula is a slender bone, with a strongly expanded proximal end, and less so distally (Fig. 5.32B). The proximal end is transversely compressed. The attachment site for the iliofibularis muscle is situated slightly above midheight, as in *Diplodocus* (Whitlock, 2011a).

Astragalus L, anterior view. The astragalus is wedge-shaped in both anterior and proximal views (Fig. 5.33). The anteromedial corner is reduced. Proximally, the astragalus is marked by a high ridge connecting to the ascending process, which extends backwards to the posterior end. The high, broad ridge separates the two fossae for the articulation with the tibia medially and the fibula laterally. The tibial fossa is larger, and subdivided by a more shallow, anteroposteriorly oriented ridge in a medial and a lateral portion. The fibular fossa is relatively uniform, with the anterior edge more developed than the posterior one. It is thus visible in posterior view, a diplodocoid synapomorphy, convergently acquired by *Jobaria* (Whitlock, 2011a).

Metatarsals L, anterior view. All left metatarsals were recovered complete (Fig. 5.34). The metatarsals III and IV are the longest, mt I and II the stoutest elements (Tab. 5.5). Metatarsal I is very stocky, and has a D-shaped proximal surface. The anterior surface is considerably shorter medially than laterally, resulting in angled proximal and distal surfaces, compared to the long axis of the shaft. The anterior surface bears few nutrient foramina, as is the case in *Cetiosauriscus* and *Suuwassea*, but not in *Camarasaurus* (Harris, 2007; Tschopp, 2008; NHMUK R3078, pers. obs., 2011). Distally, the lateral condyle projects much further than the medial, and develops a distinct posterolateral process, as typical for diplodocids (McIntosh, 1990a, b). The medial surface is slightly convex, the lateral one concave for the reception of mt II. The distal articular surface bears a distinct intercondylar groove visible in anterior view. Metatarsal II has a more squared proximal surface, and also the anterior surface is less trapezoidal than in mt I. However, the proximal and distal articular surfaces are still angled to the long-axis of the shaft. As mt I, also mt II has a strong posterolateral process. The distal portion of the anterolateral edge bears a distinct rugosity, which does not extend onto the anterior surface as in *Dyslocosaurus* AC 663 or *Cetiosauriscus* NHMUK R3078 (McIntosh et al., 1992; pers. obs., 2011). Metatarsal II of SMA 0011 has a very distinct anteromedial edge, but a less developed anterolateral one. No intercondylar groove can be seen between the distal condyles in anterior view. Metatarsal III is elongate, with a narrow shaft and greatly expanded proximal and distal ends. The proximal and distal articular surfaces stand perpendicular to the shaft axis. The proximal articular surface is subrectangular to subtriangular, with the posterior margin being shorter than the anterior one. It is relatively flat, and does not show distally curving edges as in mt I and II. A weak, narrow rugosity marks the distal end of the anterolateral edge. Metatarsal IV is similarly elongate as mt III, but the proximal expansion reaches further down the shaft. The proximal end seems slightly twisted in respect to the long axis. It is subtriangular in outline, with a concave posterior margin, resembling the shape of mt IV of the camarasaur SMA 0002, but with a less well-developed concavity (Tschopp, 2008). The surface is flat, as in mt III. The shaft is smooth, without any distinct rugosities. The distal

end does only have incipient condyles, which are hardly recognizable in both anterior and distal views. The metatarsal V has the typical paddle-shaped outline known from almost all sauropods (Bonnan, 2005). The proximal articulation surface is subtriangular, with the apex anteriorly. From there, a ridge extends distally, separating the proximal portion of the anterior surface from the medial one. The ridge disappears in the distal half. The shaft is smooth unlike in mt V of the camarasaur SMA 0002 (Tschopp, 2008). The distal surface is a single, convex facet.

Figure 5.32: Left hindlimb of SMA 0011: A) femur in posterior view; B) tibia and fibula in anterior view, as mounted. The lacking greater trochanter of the femur is indicated by the dashed line. Abb.: cc, cnemial crest; ec, epicondyle; fh, femoral head; fi, fibula; fic, fibular condyle; icg, intercondylar groove; tb, tibia; tic, tibial condyle. Scale bar = 20 cm.

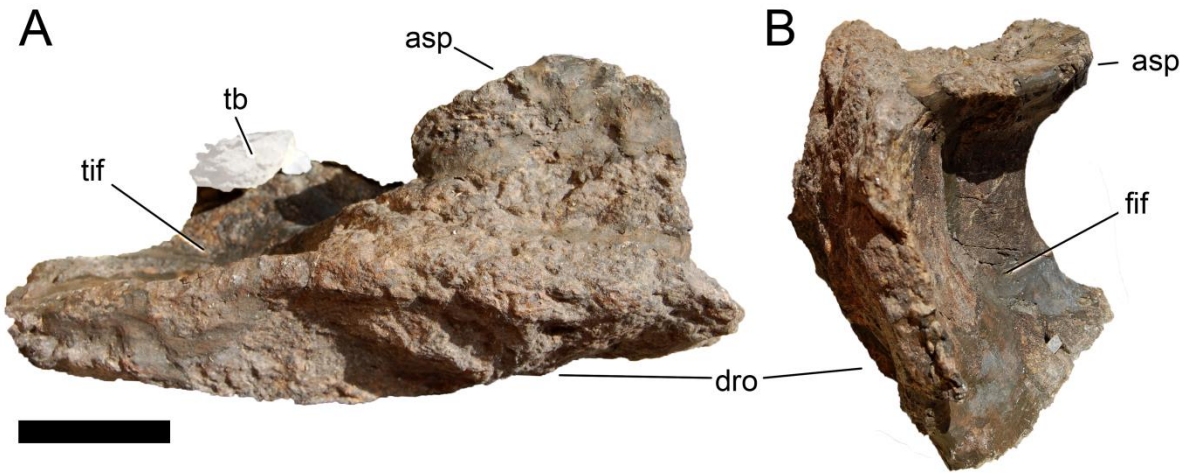

Figure 5.33: Left astragalus of SMA 0011 in anterior (A) and lateral (B) view. Due to the mounted state, a portion of the tibia, obscuring a posterodorsal part of the astragalus is masked as semitransparent. Abb.: asp, ascending process; dro, distal roller; fif, fibular facet; tb, tibia; tif, tibial facet. Scale bar = 5 cm.

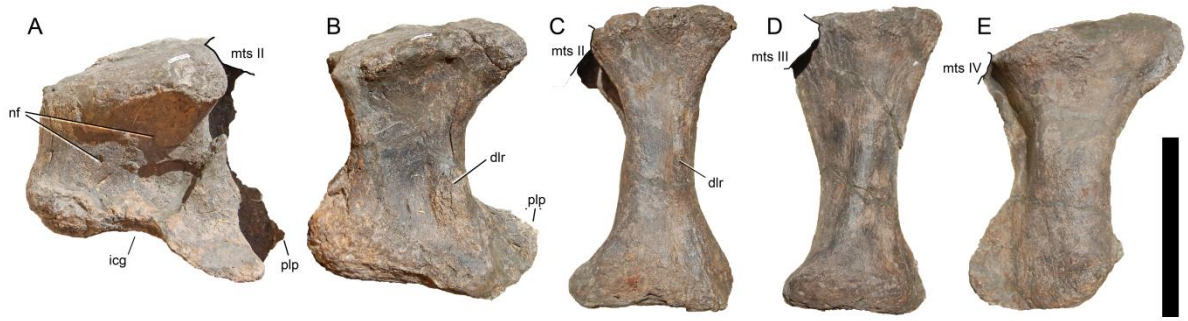

Figure 5.34: Left metatarsals of SMA 0011 in anterior/dorsal view: A) mt I, B) mt II, C) mt III, D) mt IV, E) mt V. Elements partially overlapping the other bones are marked by a black line. Abb.: dlr, dorsolateral ridge; icg, intercondylar groove; mts, metatarsal; nf, nutrient foramen; plp, posterolateral process. Scale bar = 10 cm.

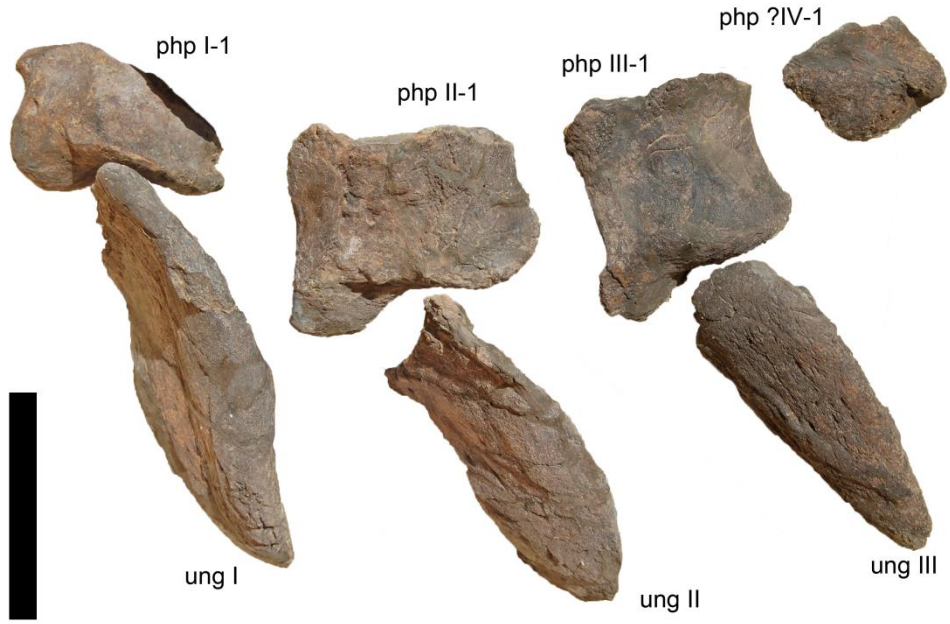

Figure 5.35: Left pedal phalanges of SMA 0011 in dorsal view, as mounted. Php IV-1 could actually also be php III-2 or php V-1 (see text). Abb.: php, pedal phalanx; ung, ungual. Scale bar = 10 cm.

Table 5.5: Hindlimb measurements of SMA 0011, in mm.

	gl	pupl	ppapd	ppw	prapl	min sw	max sw	isal	pual	pw	dw	aal	ptr	papd	dapd	pdd	apd	Comments
Ilium	885	340	105	120 (est)	335													prapl measured ventrally
Pubis	835					129		320										
Ischium									244	482		197						
Femur	1370					206				435	344		657					ptr: measured to distal end 4th trochanter
Tibia	845					133				255	238							
Fibula	850					85							350	218	145			ptr: measured to center of iliofibular trochanter
Astragalus							250									100	105	sw corresponds to maximum transverse width
mt I L	119					80				96	124						110 (est)	
mt II L	145					55				105	115						94	
mt III L	158					40				80	90						68	
mt IV L	162					40					79							
mt V L	148					44												
php I-1 L	69					73				91	74							
php II-1 L	87					84				87	98							
Php III-1 L	88					69				76	80							
php IV-1 L	36																	
pedal ungual I	190/210																130	gl measured straight proximodistally/oblique from proximal-most to distal-most point
pedal ungual II	157/173																	gl measured straight proximodistally/oblique from proximal-most to distal-most point
pedal ungual III	144/150																	gl measured straight proximodistally/oblique from proximal-most to distal-most point

Abb.: aal, acetabular articulation surface length; apd, anteroposterior depth; dapd, distal anteroposterior surface length; dw, distal transverse width; est, estimated; gl, greatest length; isal, ischial articular surface length; papd, proximal anteroposterior depth; pdd, proximodistal depth; ppapd, pubic peduncle anteroposterior depth; ppw, pubic peduncle transverse width; prapl, preacetabular process length; ptr, vertical distance from proximal articular surface to trochanter; pual, pubic articular surface length; pupl, pubic peduncle length; pw, proximal transverse width; sw, shaft width.

Pedal non-ungual phalanges L, anterior view. The left pes of SMA 0011 preserves four proximal non-ungual phalanges (Fig. 5.35). They are relatively short bones with a flat proximal articular surface, and subsequently less well-developed distal condyles, from php I-1 to php IV-1. The pedal phalanx I-1 is slightly wedge-shaped, with a considerably shorter lateral than medial surface. Therefore, the distal condyles face laterodistally, resulting in the typical lateral deflection of the pedal unguals in eusauropods (Bonnan, 2005). The anterior surface is transversely narrower than the posterior surface. Due to the semi-emerged mounting method, which covers the posterior half of the phalanx, the angle between the posterior and the proximal surface cannot be determined. Pedal phalanges II-1 and III-1 are similar in general shape. The former is slightly broader than php III-1, which has subequal widths and lengths (Tab. 5.5). The medial condyle of both phalanges is transversely compressed, but projects further distally than the lateral one. The phalanx mounted as php IV-1 has a similar outline as php II-1, but is about half its size. The surfaces are relatively undefined, and distal condyles are barely distinguishable. This implies that if a second phalanx was present in the same digit, it was most probably vestigial. The indistinct shape of this element suggests that it might actually also represent php III-2 or php V-1. In *Apatosaurus* and *Camarasaurus*, php IV-1 has a distinct shape in being the only element with a longer lateral than medial surface (Gilmore, 1936; Tschopp, 2008). It usually also shows distinct medial and lateral condyles, at least in distal view (Hatcher, 1901; Gilmore, 1936; Janensch, 1961; Bonnan, 2005; Tschopp, 2008), unlike the element mounted as php IV-1 in the pes of SMA 0011.

Pedal unguals L, anterior view. Three unguals are present in the left pes of SMA 0011 (Fig. 5.35). As mounted, this amounts to a pedal phalangeal formula of 2-2-2-1-0. This, however, is most probably underestimated, as comparisons with other diplodocid feet, and the questionable assignment of php IV-1 imply (Hatcher, 1901; Gilmore, 1936; Janensch, 1961; Bonnan, 2005). The pedal unguals are sickle-shaped, and decreasing in length from the first to the third. They are strongly transversely compressed, but this is possibly slightly exaggerated due to taphonomy. The anterior edge is strongly curved and narrow. The medial surfaces are convex, the lateral sides concavoconvex anteroposteriorly. The pedal unguals are wider transversely in their plantar half, especially at the proximal end, where the wider area bears the proximal articular surface. The ungual III is the most stout element, as the proximal width remains more or less the same from ungual I to III, whereas the length decreases.

Ontogeny

The specimen SMA 0011 shows a variety of features that were previously reported to indicate a juvenile age of the animal. Cranial ontogeny in diplodocids was extensively discussed by Whitlock et al. (2010), who proposed the following juvenile features in *Diplodocus*: a relatively rounded snout, with tooth rows that reach further back, and a large orbit. Whereas the latter is typical for most amniotes (Varricchio, 1997; Whitlock et al., 2010), the first two characteristics also occur in adults of

more basal diplodocines, showing that at least in *Diplodocus*, ontogeny is recapitulating phylogeny (Tschopp and Mateus, 2012b). The skull of SMA 0011 has an orbit of about the same relative size as CM 11161, and thus relatively smaller than the juvenile CM 11255 (Whitlock et al., 2010). However, the snout is more rounded, reaching only 72% in the PMI, compared to more than 80% in CM 11161 (Whitlock, 2011b). Taken together, this indicates a more basal phylogenetic position of SMA 0011 compared to *Diplodocus* CM 11161. One feature in the skull of SMA 0011 deserves special notion: the canal connecting the preantorbital fossa with the antorbital fenestra. This canal could indicate that the posterior and dorsal processes of the maxilla start growing out of the main body of the maxilla independently, and that only later in ontogeny, they fuse posteriorly.

Osteological characteristic of young age in the postcranial skeleton of SMA 0011 include unfused vertebral centra and neural arches, unfused cervical ribs, the ilium, which is detached from the sacrum, and separate scapula and coracoids (Gilmore, 1925; Janensch, 1961; McIntosh, 1990b; Wedel and Taylor, 2013). Other characteristics often proposed to be an indicator for a young age, but absent in SMA 0011, are the open coracoid and pubic foramina, or relatively smooth articular surfaces of the long bones (Hatcher, 1903; McIntosh, 1990b; Bonnan, 2003; Schwarz et al., 2007c). Furthermore, the lacking fusion of sacral vertebrae was shown to reflect ontogeny (Riggs, 1903; Mook, 1917; Wedel and Taylor, 2013), and the sternal plates are thought to adopt their definitive shape in adult animals only (Wilhite, 2003, 2005), but neither the sacrum nor any sternal plate are preserved in SMA 0011. Carpenter and McIntosh (1994) also proposed that the longitudinal ridges on the distal shafts of radius and ulna develop during ontogeny, but this could also be a taxonomically valid character, given that *Dyslocosaurus* or *Diplodocus* appear to have them much less developed than *Apatosaurus* (pers. obs., 2011). Wilson (1999), Bonnan (2007), Schwarz et al. (2007c), and Carballido and Sander (2013) showed that vertebral lamination and pneumaticity increases during ontogeny, but only the smallest neosauropod specimens show largely reduced pleurocoels and laminae (equivalent to the MOS 1; Schwarz et al., 2007c; Carballido and Sander, 2013; CM 566, SMA 0009, pers. obs., 2011). Wedel et al. (2000) reported an increase in cervical centra elongation of 35-65% in *Apatosaurus*. However, their calculation was based on juvenile vertebrae from Oklahoma, identified as *Apatosaurus* by Carpenter and McIntosh (1994), but some of them might actually belong to *Camarasaurus* (Upchurch et al., 2004b). Increase in centrum elongation was also shown to happen during ontogeny of *Europasaurus* (Carballido and Sander, 2013). Recently, it has furthermore been suggested that the bifurcation of the neural spine is ontogenetically controlled (Woodruff and Fowler, 2012).

Given the presence of both open neurocentral synchondroses as well as closed synostoses in some cervical and dorsal vertebrae of SMA 0011, the present specimen qualifies for MOS 3 and 4 of (Carballido and Sander, 2013), which in *Europasaurus* already show all phylogenetically significant characters of the species (Carballido and Sander, 2013). The same was hypothesized for *Suuwassea emilieae* ANS 21122 (Hedrick et al., 2012) and *Bonitasaura salgadoi* (Gallina, 2011, 2012) and is thus here regarded to be valid as well for SMA 0011. Contrary to Woodruff and Fowler (2012), the immature state of some vertebrae of SMA 0011 does thus not appear to be correlated with the posterior onset of neural bifurcation, which is herein regarded as phylogenetically significant. Furthermore, Woodruff and Fowler (2012) based their assessment on material that has not yet been identified to genus or species level, and given that this feature changes among different genera (McIntosh, 2005), their results remain doubtful.

Histology. The histology of the scapula, humerus and femur of SMA 0011 has been studied by Klein and Sander (2008). This allows for an accurate comparison of morphological and histological ontogenetic markers. Both the humerus as well as the femur of SMA 0011 were classified within HOS stage 9, whereas the scapula showed a varying degree of remodeling from medial to lateral (Klein and Sander, 2008). This is the same age as suggested for *Suuwassea* (Hedrick et al., 2012) and *Bonitasaura* (Gallina, 2012), and is probably the stage, where sexual maturity is reached (Klein and Sander, 2008), although the timing of sexual maturity is still a matter of debate (Hedrick et al., 2012).

Timing of neurocentral closure. The pattern of neurocentral closure is variable among archosaurs (Brochu, 1996; Irmis, 2007; Birkemeier, 2011; Ikejiri, 2012). Even within Sauropoda, varying patterns have been reported (Harris, 2006b; Irmis, 2007; Gallina, 2011; Carballido and Sander, 2013). The incomplete nature and rare finds of immature specimens result in additional difficulties, and only very little information is available from articulated or associated vertebral columns (Gilmore, 1925; Harris,

2006b; Schwarz et al., 2007c; Gallina, 2011; Carballido et al., 2012a). The current specimen is thus of special importance for the study of neurocentral closure in sauropods.

SMA 0011 has closed, but visible neurocentral synostoses in anterior and posterior cervical vertebrae, and in anterior and mid-dorsal vertebrae. Mid-cervical, one mid-dorsal, and all posterior dorsal vertebrae of SMA 0011 have open neurocentral synchondroses. No cervical rib is fused to its corresponding centrum. Given that long bone histology revealed that SMA 0011 already reached sexual maturity (Klein and Sander, 2008), it seems that open synchondroses still occurred in sexually mature sauropods. In *Suuwassea*, the same is the case for caudal vertebrae, but all preserved presacral vertebrae are fused (Harris, 2006b). However, only fragmentary mid- and posterior cervical, and no mid- and posterior dorsal vertebrae are preserved in ANS 21122, which are the only elements still showing unfused centra and neural arches in SMA 0011. As ANS 21122, also SMA 0011 has unfused cervical ribs, a separate scapula and coracoid, but a closed coracoid foramen and relatively rugose articular surfaces of the longbones (Harris, 2006b, 2007; Hedrick et al., 2012). The two specimens therefore seem to be of about the same individual age. The titanosaur *Bonitasaura* MPCA-460 appears to show a slightly different pattern of neurocentral closure, with a completely fused axis, but open anterior cervical and dorsal vertebrae, and closed posterior elements (Gallina, 2011). However, also MPCA-460 was shown to fit into HOS 9 (Gallina, 2012). These three specimens therefore indicate that neurocentral closure was delayed and only completed after sexual maturity in sauropods. They also show that the pattern of closure is not as simple as previously thought: based on comparisons with crocodiles, and on partial finds of specimens with open synchondroses and closed neurocentral synostoses, a posterior-to-anterior sequence was postulated (Brochu, 1996; Irmis, 2007; Birkemeier, 2011; Ikejiri, 2012; Tschopp and Mateus, 2012b). However, SMA 0011 shows that - at least in diplodocids - in both the cervical and the dorsal column, the middle elements fuse last, and that within one single vertebra, the fusion starts posteriorly and progresses anteriorly (Fig. 5.19). Adding the information from *Suuwassea* ANS 21122, anterior cervical vertebrae appear to fuse first (also in SMA 0011, these are the ones where the synchondroses are the least visible), followed by anterior dorsal and posterior cervical vertebrae, posterior dorsal vertebrae, whereas mid-cervical, mid-dorsal, and anterior to mid-caudal vertebrae fuse last. This varies from *Bonitasaura*, where a posterior-to-anterior pattern was proposed both within the postaxial cervical and in the dorsal columns (Gallina, 2011). A general posterior-to-anterior fusion pattern also appears to be present in at least one *Camarasaurus* (Trujillo et al., 2011), and the small juvenile, probably basal titanosauriform SMA 0009, which already have closed, but still visible synchondroses in anterior caudal vertebrae (Schwarz et al., 2007c; Carballido et al., 2012a). Different fusion patterns might thus prove to be a taxonomically valid character, with Macronaria showing a faster neurocentral closure than Diplodocoidea, and following a more strict posterior-to-anterior pattern, at least in the single vertebral regions. However, too few specimens are known to date, where neurocentral closure can be directly compared with histology, in order to evaluate this character statistically. Nonetheless, these finds have further implications for the individual age of the holotype specimen of *Kaatedocus siberi*, SMA 0004 (see above). The latter does not show any traces of neurocentral synostoses in any cervical vertebra, and also has completely fused cervical ribs (Tschopp and Mateus, 2012b). Being a diplodocine, this implies that Tschopp and Mateus (2012b) were right in identifying SMA 0004 as at least subadult specimen, which retained a relatively small size. Moreover, as (Carballido and Sander, 2013) showed for *Europasaurus*, sauropod vertebrae already show the majority of the phylogenetically informative characters of their respective species before the completion of the neurocentral closure.

Systematic Paleontology

Apatosaurinae Huene, 1927
Incertae sedis.

Description of SMA 0087

Axial skeleton (Figs 5.36-5.44)

Dorsal vertebrae (Tab. 5.6). The dorsal vertebrae of SMA 0087 have relatively short centra with highly elevated neural arches. Their centra are amphicoelous, and have flat to slightly convex ventral

surfaces (Fig. 5.36). Deep pleurocoels extend onto the neural arch. Unlike in *Supersaurus*, *Dinheirosaurus*, and certain *Apatosaurus* specimens (Mannion et al., 2012; pers. obs., 2011), no vertical lamina separates the pleurocoel internally. The neural arch appears extremely fragile (Fig. 5.37), but has probably been altered diagenetically, indicated by the presence of numerous, small and rounded pits. Therefore, also many of the laminae originally present are now difficult to identify. However, the centrum is connected with the transverse process through the cprl anteriorly, the oblique pcpl, the pcdl, and the cpol, which does not unite with its counterpart below the hyposphene. The transverse process is horizontal and formed by the prdl and the podl. It forms a largely dorsoventrally widened lateral end, with two spurs projecting dorsally and anteriorly. They might have been the origin of the prdl anteriorly and the spdl dorsally, given the fact that many of the laminae appear dissolved or eaten away by necrophagous organisms. However, the laminae would then have to be very extended towards the transverse process, and would significantly reach above the level of the zygapophyses. To my knowledge, the only similar morphology is shown in an apatosaur dorsal vertebra from Oklahoma (OMNH 1670; Stovall, 1938), and to a lesser degree in UW 15556 (Gilmore, 1936). It is unknown in any other diplodocid, where dorsal transverse processes are preserved (Osborn, 1899; Hatcher, 1901; Riggs, 1903; Gilmore, 1936; Ostrom and McIntosh, 1966; Jensen, 1985; Upchurch et al., 2004b). The neural spine is flattened transversely, but would have been of at least equal width and length at its distal end when preserved entirely. The bifurcation passes from distinct to nonexistent in what are most probably dorsal vertebrae 5 and 6, based on the usual count of 10 vertebrae in diplodocids. This is typical for apatosaurines, and distinct from diplodocines like *Barosaurus* or *Diplodocus* (Hatcher, 1901; Gilmore, 1936; McIntosh, 2005). The prsl is distinct and rugose, and widens distally. The sprl unite with the prsl at about midlength of the spinal process. At the same height, the spdl meets the spol, from where a single lamina continues dorsally and forms a triangular, laterally projecting process connected with the spine top by a dorsally widening, rugose sheet of bone. A medial spol is only present in DV 6 on the left side. The lateral spol are undivided ventrally. Pre- and postzygapophyses are oriented obliquely and are relatively straight, unlike the curved and laterally horizontal facets of diplodocines. The hyposphene-hypantrum articulation is present and a well-defined rhomboid structure.

Figure 5.36: Dorsal centrum 6 of SMA 0087 in left, posterior, right, anterior (top left to right), and ventral view (bottom). Abb.: cpol, centropostzygapophyseal lamina; cprl, centroprezygapophzseal lamina; nc, neural canal; pl, pleurocoel. Scale bar = 10 cm.

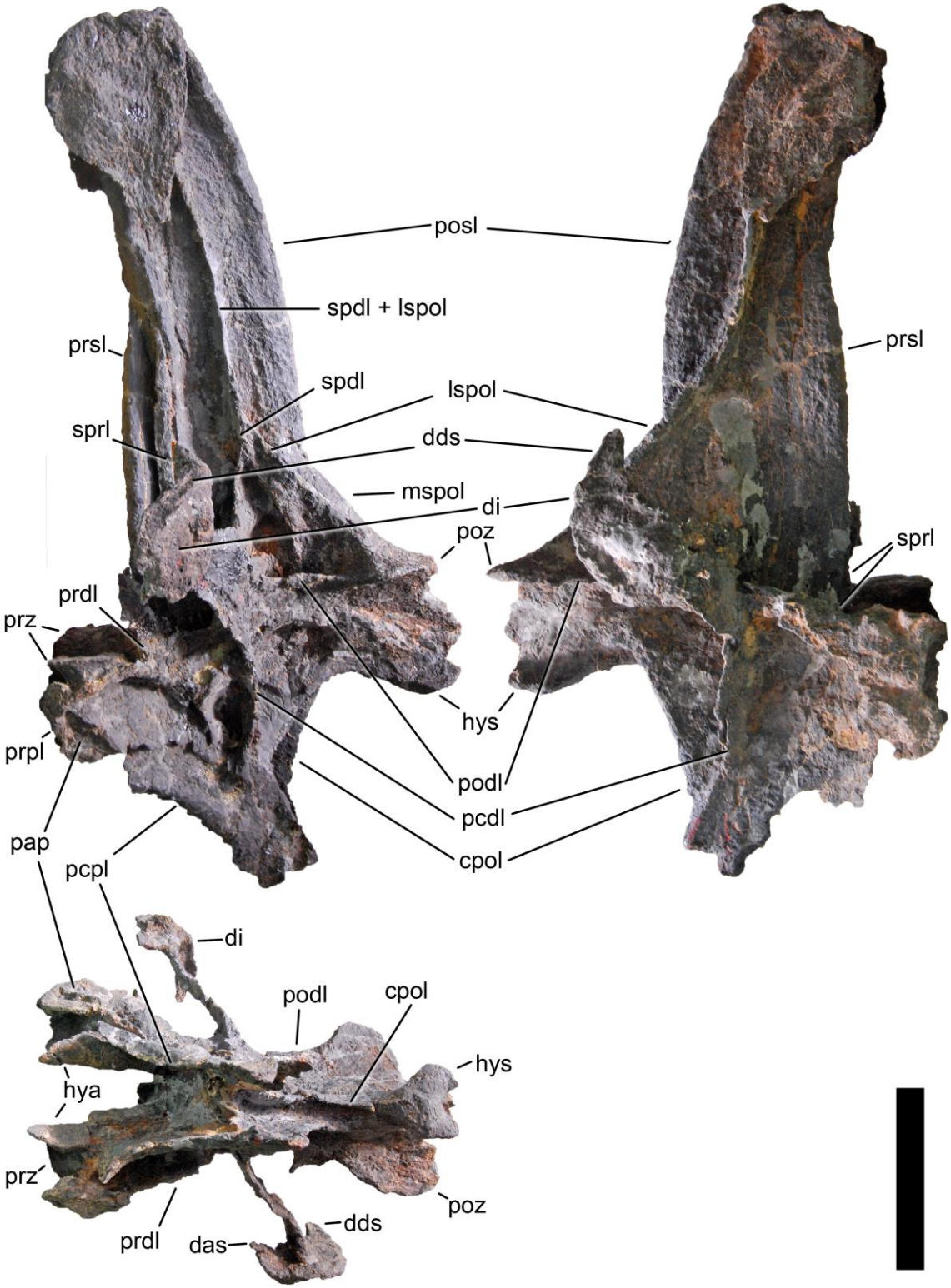

Figure 5.37: Dorsal neural spine 6 of SMA 0087 in left, right, and ventral (bottom) view. Note the anterior and dorsal spurs on the diapophysis. Abb.: cpol, centropostzygapophyseal lamina; das, diapophysis anterior spur; dds, diapophysis dorsal spur; di, diapophysis; hya, hypantrum; hys, hyposphene; lspol, lateral spol; mspol, medial spol; pap, parapophysis; pcdl, posterior centrodiapophyseal lamina; pcpl, posterior centroparapophyseal lamina; podl, postzygodiapophyseal lamina; posl, postspinal lamina; poz, postzygapophysis; prdl, prezygodiapophyseal lamina; prpl, prezygoparapophyseal lamina; prsl, prespinal lamina; prz, prezygapophysis; spdl, spinodiapophyseal lamina; spol, spinopostzygapophyseal lamina; sprl, spinoprezygapophyseal lamina. Scale bar = 10 cm.

Table 5.6: Measurements of dorsal vertebrae of SMA 0087, in mm.

	gh	cl	wd	wpr	wpo	ppl	pph	hct	wct	wcd	hcd	hns	hna	wns	lns
DV 5	665	155	240 (def)	100	120	102	95	160 (def)	122	88 (def)	158	525	225	72	74
DV 6	735	150	290 (def)	125	130	105	98	150 (def)	136		154			74	71
DV 7	760	150		125	105	110	102	165	150		155	590	235	59	73
DV 8	795	135	220 (est)		145	92	98	165	155		160	620	250	51	78
DV 9	770	140									158			51	95
DV 10	740														

Abb: cl, centrum length; def, deformed; gh, greatest height; hcd, height anterior condyle; hct, height posterior cotyle; hna, height neural arch (below poz); hns, height neural spine; lns, anteroposterior length neural spine (at summit); pph, pneumatopore height; ppl, pneumatopore length; wcd, width anterior condyle; wct, width posterior cotyle; wd, width across diapophyses; wns, width neural spine (at summit); wpo, width across postzygapophyses; wpr, width across prezygapophyses.

Dorsal ribs. The dorsal ribs are only partly prepared. They are slender and their heads flat, without the conspicuous ridges as present in diplodocines (AMNH 223, 6341, pers. obs., 2011). No indication of pneumatization is visible.

Sacral vertebrae. Not much has been prepared yet from the sacral vertebrae. A single, broken sacral rib has a highly rugose lateral end, where the ilium would attach. A wide, dorsoventral groove at its medial end indicates that the fusion between the rib and the centrum was incomplete. No ridge is present on its ventral surface. Three fused neural spines do not converge distally and form a relatively flattened sheet of bone only marked by the vertical and narrow spdl, which slightly expands distally.

Caudal vertebrae (Tab. 5.7). Anterior caudal vertebrae (herein defined as the elements with transverse processes) are procoelous/distoplatyan, becoming amphicoelous distally (Figs 5.38, 5.39). The centra are higher than wide, and without large pleurocoels, but various foramina that pierce the lateral surfaces. The ventral surface is convex and shows irregularly placed foramina, but no distinct ridges as in *Tornieria, Barosaurus* or *Diplodocus* (Remes, 2006; YPM 429, CM 94, pers. obs.). The transverse processes are wing-like in the six anterior-most vertebrae (Fig. 5.38). In more distal anterior caudal vertebrae, the transverse processes are anteroposteriorly expanded at their lateral ends, and entirely situated on the centrum. No foramina are present that pierce the wing-like anterior-most transverse process as in *Apatosaurus excelsus* YPM 1980 (Upchurch et al., 2004b). Only the prdl and the acdl are moderately well-developed in anterior-most vertebrae, but become reduced as soon as the wing-like processes disappear. The pedicels of the neural arch are low and above the middle of the centrum. The zygapophyses face inwards (prezygapophysis) or outwards (postzygapophysis), and are dorsoventrally high. Towards posterior, they decrease in height. In Cd 12, and more posteriorly, the zygapophyseal facets become tilted to face dorsomedially and ventrolaterally. Distinct sprl that extend onto the lateral side of the spine are present up to Cd 12 (which is also the second last to show a reduced, bump-like transverse process). The prespinal lamina is rugose and distinct and projects dorsally until there is no transverse process anymore at all. The spol is distinct and contacts the sprl in Cds 1-13. All anterior caudal vertebrae have distinct and rugose posl, which project dorsally. Together with the prsl, this creates a anteroposteriorly concave spine summit.

Mid-caudal vertebrae have higher than wide centra with two weak longitudinal ridges on their lateral faces (Fig. 5.40). The first element to show these ridges is also the first in the series without transverse processes. The centra are slightly amphicoelous, with rounded articulation facets. They are about 1.5 times as long as high. The ventral surface is narrow, and bears a shallow concavity resembling the diplodocine ventral hollow but much less deep and much narrower. They are similarly developed as in *Supersaurus vivianae* WDC DMJ-021 (Lovelace et al., 2007; D. Lovelace, pers. comm.). The chevron facets are well developed posteriorly, but almost nonexistent anteriorly. No caudal ribs are present anymore. The neural arch is situated above the midlength of the centrum, whereas the pedicels are slightly shifted anteriorly. The prezygapophyses are narrow, anteriorly projecting spurs. They do not project anterior to the centrum, and are not interconnected posteriorly as in *Diplodocus longus* YPM 1920 (pers. obs., 2011). The neural spine is relatively wide antero-posteriorly, and overhangs the postzygapophyses considerably. It is posteriorly inclined and has distinct anterior, dorsal and posterior edges in more anterior regions of the tail, whereas more posterior

elements have anterior and dorsal edges that continuously curve into each other. The postzygapophyses extend posteriorly to the vertebral centrum, and form two distinct, concave, ventrally facing facets for the articulation with the prezygapophyses of the following vertebra. More posteriorly, they become less distinct, but still overhang the centrum posteriorly.

Chevrons. Anterior chevrons are connected proximally to completely surround the haemal canal (Fig. 5.41). They curve slightly posteriorly at their distal ends. The anterior edge is very narrow and does not show the widened area with the median ridge as present in some diplodocines (e.g. *Diplodocus* AMNH 223, pers. obs., 2011). Middle chevrons have anterior and posterior processes as typical for Flagellicaudata (Fig. 5.42). They have no internal concavity as present in AMNH 223. The posterior chevrons have a slit-like opening ventrally between the right and left branches, which are fused anteriorly and posteriorly. In one case, only the anterior processes are fused and the slit is open posteriorly.

Sternal ribs (Tab. 5.8). Several elongate but narrow elements with slightly expanded ends can be identified as morphotype C bones of Tschopp and Mateus (2013; Figs 5.43, 5.44). Following their interpretation, they probably represent sternal ribs. However, they are much larger than the elements described therein. Also, the fact that no anterior dorsal vertebrae and ribs are present in the specimen sheds some doubt on this identification, and until no clearly articulated specimen is found, an interpretation as gastralia cannot be ruled out completely. One of the two elements bears a longitudinal groove, similar to the grooves serving as articulation surfaces between medial and lateral gastralia in non-sauropod sauropodomorphs and theropods (Claessens, 2004; Fig. 5.44). However, given that such a groove is absent in the other element figured, it could also be a bite mark.

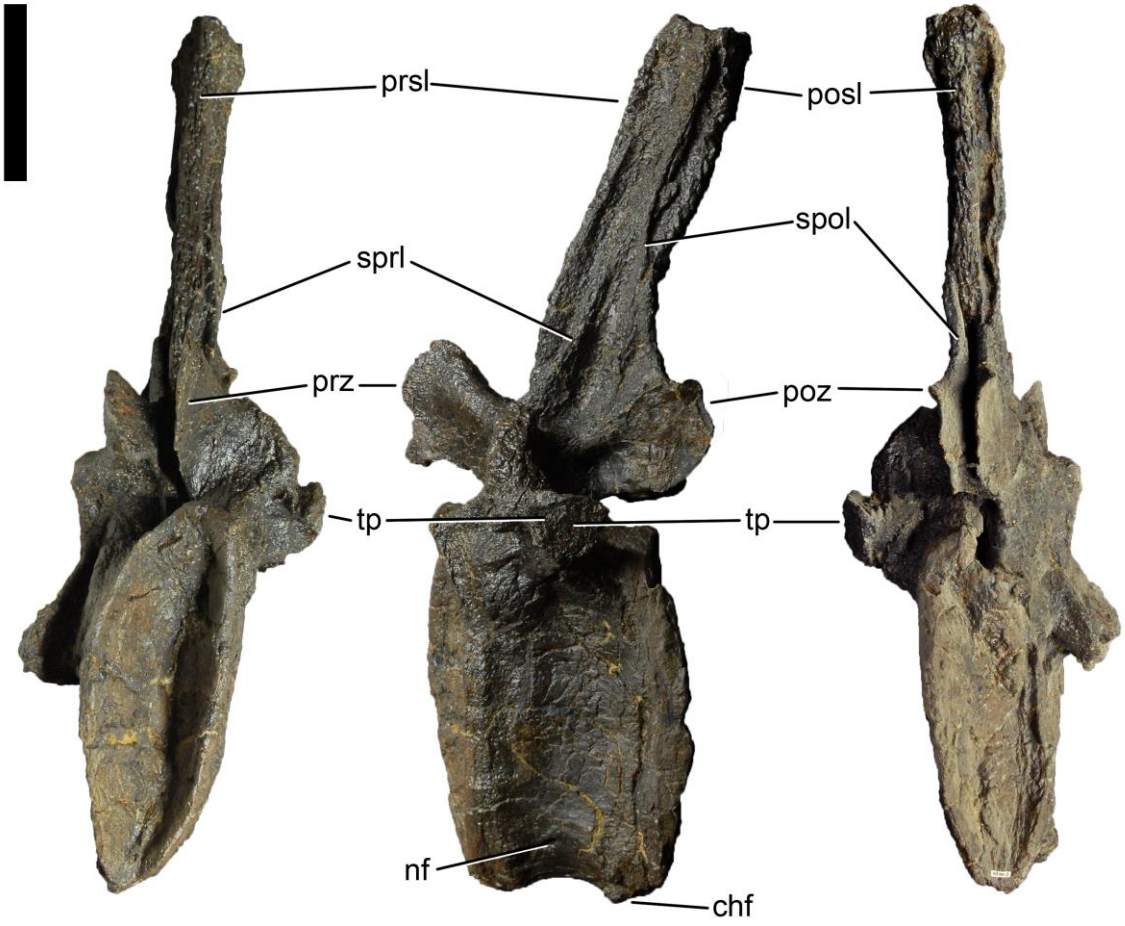

Figure 5.38: Caudal vertebra 5 of SMA 0087 in anterior, left lateral, and posterior view (from left to right). Note the foramen that pierces the ventral surface, and the dorsally expanded transverse processes. Abb.: chf, chevron facet; nf, nutrient foramen; posl, postspinal lamina; poz, postzygapophysis; prsl, prespinal lamina; prz, prezygapophysis; spol, spinopostzygapophyseal lamina; sprl, spinoprezygapophyseal lamina; tp, transverse process. Scale bar = 10 cm.

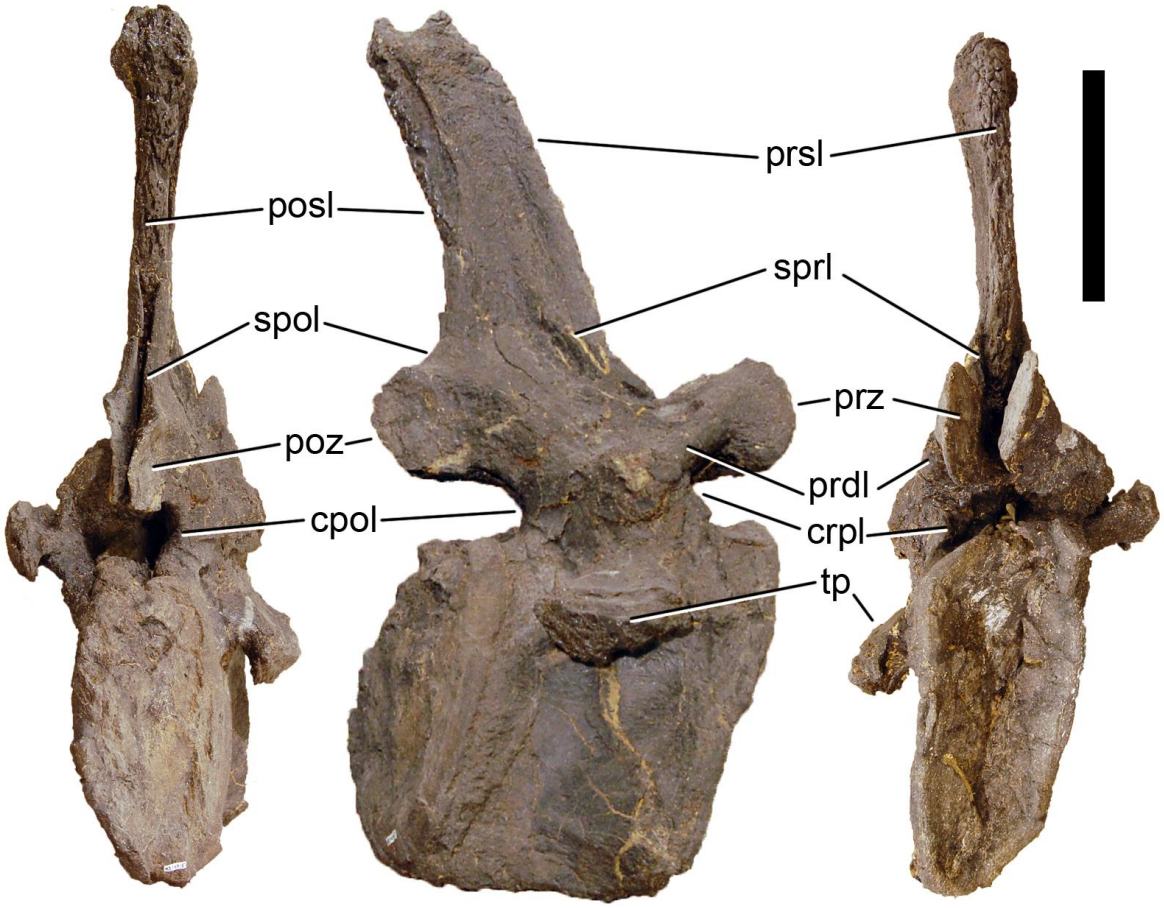

Figure 5.39: Caudal vertebra 7 of SMA 0087 in posterior, right lateral, and anterior view (left to right). Abb.: cpol, centropostzygapophyseal lamina; cprl, centroprezygapophyseal lamina; posl, postspinal lamina; poz, postzygapophysis; prsl, prespinal lamina; prz, prezygapophysis; spol, spinopostzygapophyseal lamina; sprl, spinoprezygapophyseal lamina; tp, transverse process. Scale bar = 10 cm.

Table 5.7: Measurements of caudal vertebrae of SMA 0087, in mm.

	gl	cl	gh	wcd	hcd	wct	hct	wd	max wns	min wns	lns	comments
Cd 2		131		130*	211	141	225					transversely compressed, spine missing
Cd 3	195	140	606	151	215	140	225	220*	38	24	68	transversely compressed
Cd 4	214	134	558	132	233	102	220	190*	47	33	85	transversely compressed
Cd 5	198	124	512	100	213	95	189	185*	46	24	64	transversely compressed
Cd 6	187	136	470	94	198	82	174	163	43	25	65	transversely compressed
Cd 7	195	138	428	85	185	70	164	180	40	20	58	transversely compressed
Cd 8	185	140	399	98	177	88	148	188	37	21	65	transversely compressed
Cd 9	183	140	378	95	162	79	150	171	34	17	54	transversely compressed
Cd 10	177	139	368	96	154	83	149	150	39	18	55	transversely compressed
Cd 11	181	134	367	98	148	85	144		32	16	55	transversely compressed
Cd 12	210	134	341	88	148	80	154		23	13	62	transversely compressed
Cd 13	236	142	335	64	150	83	152		20	10	60	transversely compressed
Cd 14	218	148	308	67	157	80	149					transversely compressed
Cd 15	233	138	291	83	130	84	129					transversely compressed
Cd 16	243	142	269	84	120	82	123					transversely compressed
Cd 17		143		80	119	79	117					

Abb: cl, centrum length; gh, greatest height; hcd, height anterior condyle; hct, height posterior cotyle; lns, anteroposterior length neural spine (at summit); wcd, width anterior condyle; wct, width posterior cotyle; wd, width across diapophyses; wns, width neural spine.

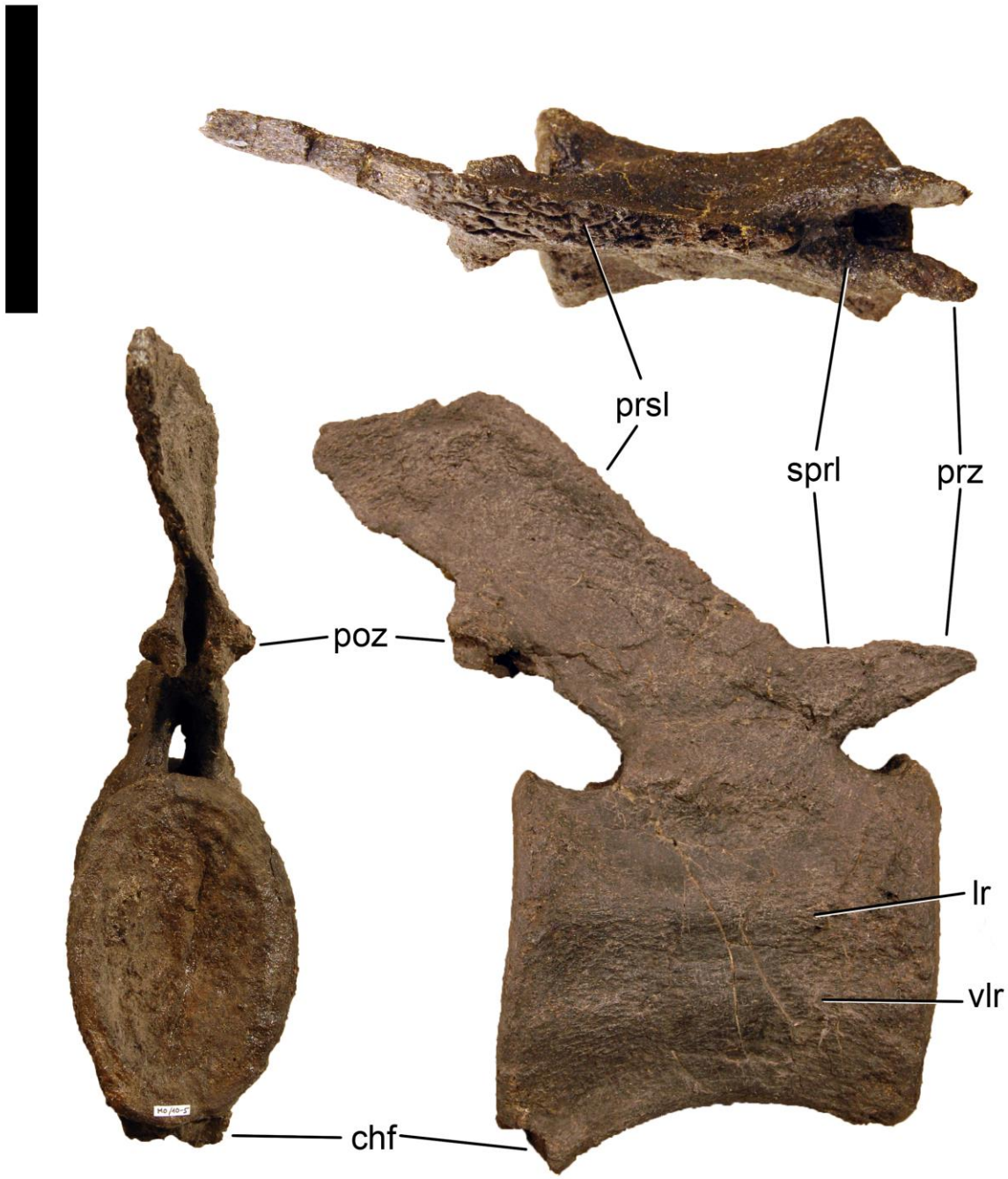

Figure 5.40: Caudal vertebra 16 of SMA 0087 in dorsal (top), posterior (left) and right lateral view (bottom right). Note the presence of two weak longitudinal ridges on the centrum. Abb.: chf, chevron facets; lr, lateral ridge; prsl, prespinal lamina; prz, prezygapophysis; poz, postzygapophysis; sprl, spinoprezygapophyseal lamina; vlr, ventrolateral ridge. Scale bar = 10 cm.

Table 5.8: Measurements of sternal ribs of SMA 0087, in mm.

Field number	gl	min sh	msw	Comments
SMA M5/9-1	592	19	14	gl measured across curvature
SMA M3/9-5	623	16	16	gl measured across curvature

Abb.: gl, greatest length; msw, midshaft width; sh, shaft height.

Figure 5.41: Anterior chevron of SMA 0087 in anterior, right lateral, and posterior view (left to right). This chevron was found between Cd 2 and 3. Note the bridged over haemal canal. Abb.: hc, haemal canal. Scale bar = 10 cm.

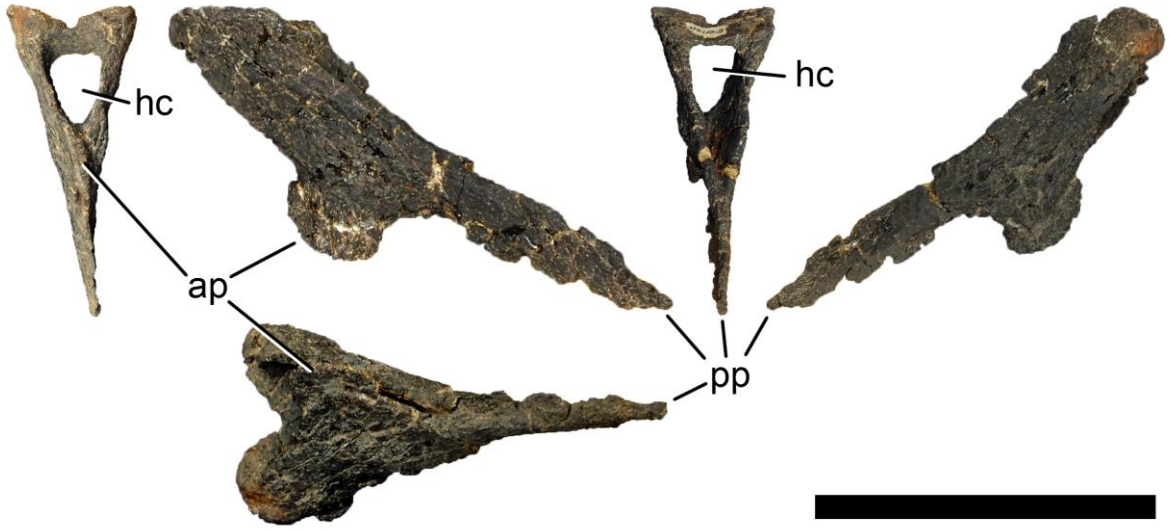

Figure 5.42: Mid-chevron of SMA 0087 in anterior, left lateral, posterior, right lateral (top, left to right), and ventral view (bottom). This chevron was recovered associated with Cd 16 to 18. Note the ventral slit visible in ventral view. Abb.: ap, anterior process; hc, haemal canal; pp, posterior process. Scale bar = 10 cm.

Figure 5.43: Sternal rib of SMA 0087. Corresponds to Morphotype C of Tschopp and Mateus (2013). Scale bar = 10 cm.

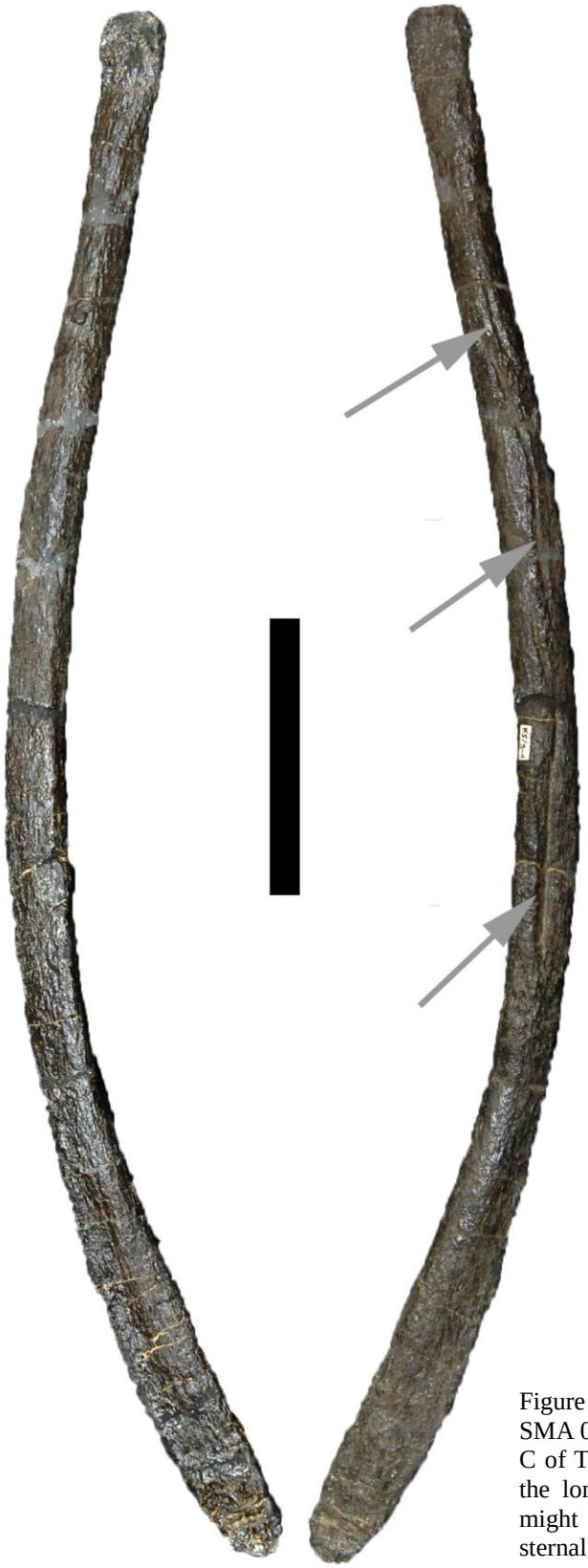

Figure 5.44: Sternal or gastral rib of SMA 0087. Corresponds to morphotype C of Tschopp and Mateus (2013). Note the longitudinal sulcus (arrow), which might indicate a gastral instead of a sternal origin. Scale bar = 10 cm.

Appendicular skeleton (Tab. 5.9)

Ischium. The ischium shows the typical distal expansion and V-shaped orientation of Diplodocidae (Gilmore, 1936; McIntosh, 1990b). More details cannot be seen at the current state of preparation.

Femur. The femur is severely crushed transversely. It has a distinct and well-offset head, forming a step ventrally. The fourth trochanter is almost entirely located on the proximal half of the shaft and curves laterally towards the center at its distal end. It is reduced and not visible in anterior view. The distal condyles are rounded posteriorly, but restricted to the distal surface anteriorly. A deep intercondylar groove separates the two condyles posteriorly.

Tibia. The tibia is only prepared in anterior view. It is diagenetically flattened anteroposteriorly, and thus has a wide proximal end. The cnemial crest projects laterally, and extends straight outwards from the proximal articular surface. It is gently rounded, but not to the degree as in the rebbachisaur *Zapalasaurus* (Salgado et al., 2012). The shaft is narrowest in its distal half and expands again distally. In anterior view, the distal articular surface is angled in comparison with the longitudinal axis, with the medial condyle projecting farther distally.

Fibula. As the tibia, the fibula is only prepared anteriorly. It is flat and expanded proximally. At about midlength, a trochanter is present on the anterolateral edge. This trochanter is usually interpreted to mark the attachment site of the M. iliofibularis. The distal end is expanded in all directions, unlike the proximal one. It is thus of about equal width and depth.

Astragalus. The astragalus tapers medially in both anterior and dorsal view (Fig. 5.45). It is mostly rugose, with only the ascending process being smooth. The ascending process extends to the posterior surface, and a large foramen marks the tibial facet close to the process. The medial end is blunt, as is typical for *Apatosaurus* (Gilmore, 1936; Remes, 2006).

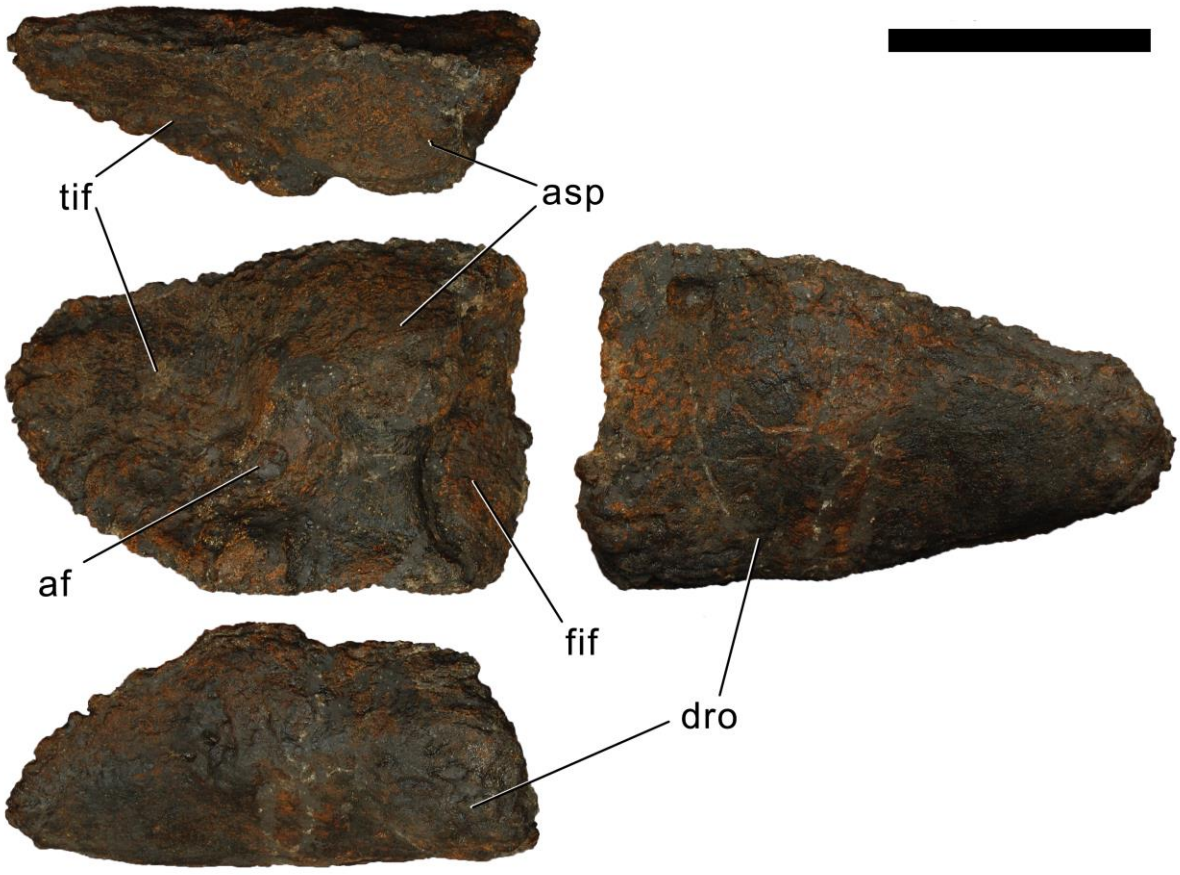

Figure 5.45: Right astragalus of SMA 0087 in dorsal (top), posterior (center left), ventral (bottom), and anterior view (center right). Abb.: af, astragalar foramen; asp, ascending process; dro, distal roller; fif, fibular facet; tif, tibial facet. Scale bar = 10 cm.

Metatarsals. Metatarsals I, II, and V are prepared. The metatarsal I is very broad and stout, with angled proximal and distal articulation surfaces (Fig. 5.46). Dorsally, it bears a few irregularly placed foramina, and the lateral distal condyle develops the pointed distolateral process typical for Flagellicaudata (McIntosh, 1990b; McIntosh et al., 1992). The proximal articular surface is D-shaped, with a slightly concave lateral margin, for the attachment of mt II. Metatarsal II is stout as well, but considerably less so than mt I (Fig. 5.47). It is longer and slightly narrower. It has a trapezoid proximal surface, and the dorsal side is marked by a short and relatively weak lateral rugosity toward its distal end. The distal condyles are distinct but do not develop a laterodistal condyle as is usually the case in diplodocids (Nair and Salisbury, 2012). Metatarsal V has the paddle-shape typical for eusauropods, with the widely enlarged proximal surface (Fig. 5.48). The latter is triangular in proximal view, flat posteriorly, and with a distinct ridge on the dorsal surface, which reaches onto the shaft. The distal surface is only slightly expanded, and no distinct condyles are present.

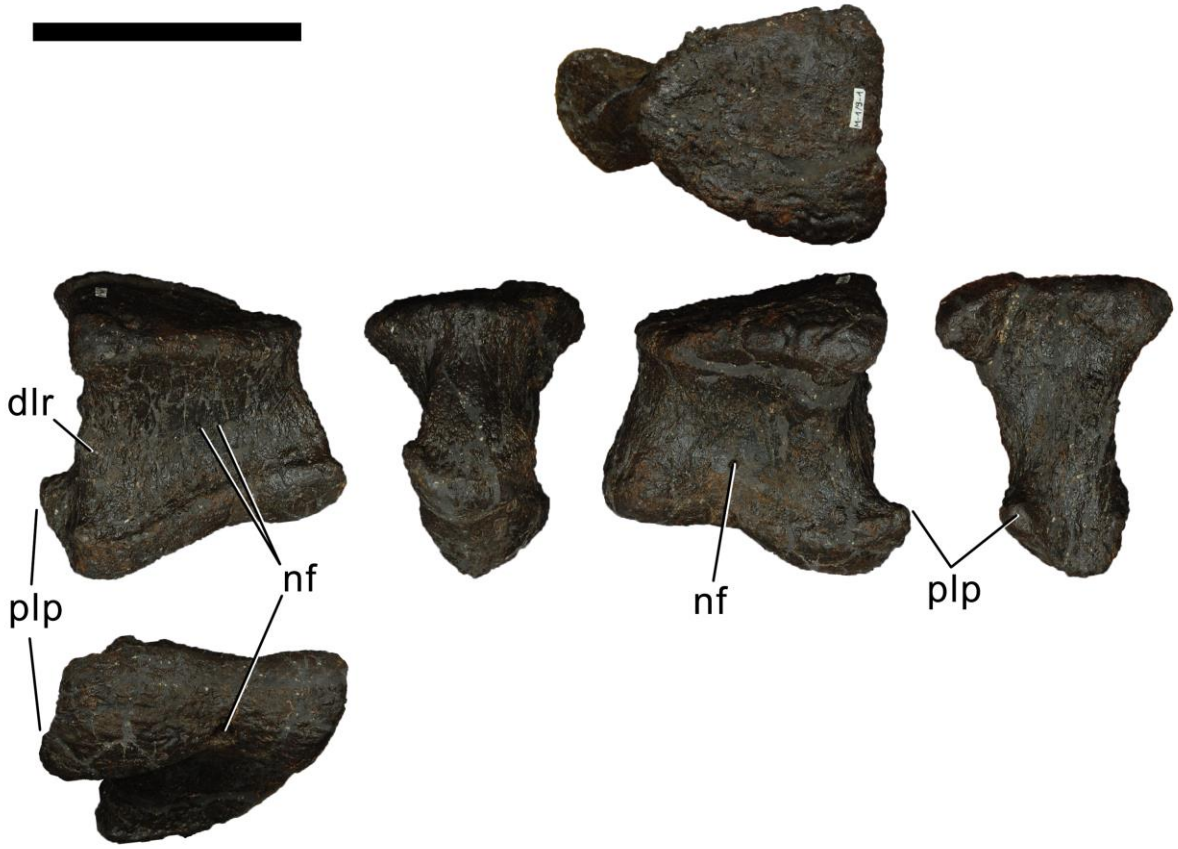

Figure 5.46: Right metatarsal I of SMA 0087 in proximal (top), dorsal, medial, plantar, lateral (center left to right), and distal view (bottom). Abb.: dlr, dorsolateral ridge; nf, nutrient foramen; plp, posterolateral process. Scale bar = 10 cm.

Pedal phalanges. The pedal phalanx I-1 is narrow dorsally and somewhat wider plantarly (Fig. 5.49). The proximal surface is concave, with the posterior edge projecting further proximally than the anterior one. The dorsal surface is marked by two longitudinal ridges that demarcate the lateral edges. Two distal condyles are well-distinguishable, and in an angle to each other. Pedal phalanx II-1 is wider than long, and anteroposteriorly compressed (Fig. 5.50). It is flat to slightly concave proximally. The medial surface is distinct, whereas the lateral one curves gradually into the dorsal face. This leads to two distal condyles that are oriented in an angle to each other, with the medial one almost vertical and the lateral one medially inclined. The distal articular surface is therefore wider posteriorly than anteriorly. The pedal phalanx II-2 is very short proximodistally, especially so at its lateral side, such that the proximal and distal ends almost contact each other (Fig. 5.51). The proximal surface is convex transversely, and concave anteroposteriorly. The distal surface bears two condyles.

Figure 5.47: Right metatarsal II of SMA 0087 in proximal (top), dorsal, medial, plantar, lateral (center left to right), and distal view (bottom). Abb.: dlr, dorsolateral ridge; plp, posterolateral process. Scale bar = 10 cm.

Figure 5.48: Right metatarsal V of SMA 0087 in proximal (top), dorsal, medial, plantar, lateral (center left to right), and distal view (bottom). Scale bar = 10 cm.

Figure 5.49: Right pedal phalanx I-1 of SMA 0087 in proximal (top), dorsal, medial, plantar, lateral (center left to right), and distal view (bottom). Abb.: pvl, posteroventral lip. Scale bar = 5 cm.

Figure 5.50: Right pedal phalanx II-1 of SMA 0087 in proximal (top), dorsal, medial, plantar, lateral (center left to right), and distal view (bottom). Abb.: nf, nutrient foramen. Scale bar = 5 cm.

Figure 5.51: Right pedal phalanx II-2 of SMA 0087 in proximal (top), dorsal, medial, plantar, lateral (center left to right), and distal view (bottom). Scale bar = 5 cm.

Figure 5.52: Right pedal ungual I-2 of SMA 0087 in dorsal (top), medial, lateral (center left, right), and plantar view (bottom). Abb.: ps, proximal spur; Scale bar = 10 cm.

Pedal unguals. Two pedal unguals are prepared. Based on their size, they are herein interpreted as the first and the second (Figs 5.52, 5.53). They are flattened transversely, and appear diagenetically compressed dorsoventrally. Dorsal to the proximal articular surface, which occupies the lower about two thirds of the entire proximal surface, there is a relatively distinct proximal extension, somewhat similar to the possible ossified tendon insertion in the right, third ungual of the *Camarasaurus* SMA 0002 (Tschopp, 2008). The entire proximal face is tilted laterally, such that the unguals are directed laterally in the living animal. No canal is present on the medial side of the claw, but laterally, there is a distinct canal following the curvature of the dorsal edge (better visible on ungual II).

Figure 5.53: Right pedal ungual II-3 of SMA 0087 in dorsal (top), medial, lateral (center left, right), and plantar view (bottom). Scale bar = 10 cm.

Table 5.9: Measurements of appendicular elements of SMA 0087, in mm. Asterices indicate estimated measurements.

	gl	ptr	max w	apd	pdd	pw	min sw	dw	papd	min adp	dadp	comments
Femur, R	1210*	560										highly transversely compressed
Tibia R	756					250	128	215				
Fibula R	790						78	125				
Astragalus R			205	105	64							
Metatarsal I R	119					95	86	111	90	42	53	
Metatarsal II R	152					87	56	80	103	56	70	
Metatarsal V R	164					129	54	70	49	34		
Php I-1 R	74					68	52	52	60	52	49	
Php II-1 R	72					73	69	85	48	30	39	
Php II-2 R	30					58	43	47	52	51	51	
Ungual pI R	192					45	10	10	81*			
Ungual pII R	147					27	9	9	81			

Abb.: apd, anteroposterior depth; dapd, distal anteroposterior surface length; dw, distal transverse width; gl, greatest length; max w, maximum transverse width; papd, proximal anteroposterior depth; pdd, proximodistal depth; ptr, vertical distance from proximal articular surface to trochanter; pw, proximal transverse width; sw, shaft width.

Ontogeny

A core sample was taken from the femur of SMA 0087. The histology shows little remodeling, but an EFS, which is initiating to form (Klein and Sander, 2008). The occurrence of an EFS, even in its initial stages, shows that the animal was adult (Klein and Sander, 2008). SMA 0087 was thus included in HOS 12 (Klein and Sander, 2008; Stein and Prondvai, 2013). However, as identification of an EFS in its initial form is difficult, the true HOS of SMA 0087 might also be slightly lower (N. Klein, pers. comm., 2013). Still, an adult age can be inferred with relatively high confidence, based on its histology.

Dorsal vertebrae are fused, without any visible suture, corresponding to MOS 4 of Carballido and Sander (2013). MOS 4 is the only mature ontogenetic stadium known in dorsal vertebrae (Carballido and Sander, 2013). However, the sacrum is not fused to the ilium, and also sacral rib fusion to the centra does not appear to be complete.

A Specimen-Based Phylogenetic Analysis of Diplodocidae (Dinosauria, Sauropoda)

Methods

The phylogenetic analysis is based on Whitlock (2011a), with changes introduced by Mannion et al. (2012) and Tschopp and Mateus (2012b), and combined with the specimen-based analysis of *Apatosaurus* by Upchurch et al. (2004b). The taxon list was extended in order to include all holotypes of putative diplodocid taxa, as well as reasonably complete specimens previously assigned to any diplodocid taxon (Tab. 1.1). The OTU slots for the diplodocid genera and species used in the previously published analyses were substituted by single specimens. Based on earlier publications or personal observations of the specimens, 243 characters were added to the version published in Tschopp and Mateus (2012b). Changes and character deletions proposed by Tschopp et al. (2013) were applied. Operational taxonomic units were scored based on personal observations where possible, on published descriptions where existing, or on photos from fellow researchers (Tab. 6.1).

Phylogenetic analysis

The phylogenetic analysis was performed with the software TNT (Goloboff et al., 2008), using the New Technology Search tool and enabling all options (Sect. Search, Ratchet, Drift, and Tree Fusing). Of the 53 multi-state characters, 23 were treated as ordered (explained in the character descriptions below). The consensus tree was stabilized five times with factor 75.

Main analyses. Several preliminary analyses were run in order to test previous hypotheses that unified several specimens into one individual (see below). By doing so, the data set was reduced from 81 operational taxonomic units to 76, which decreased the percentage of highly incomplete taxa and increased taxon overlap, which would otherwise have been very low (Tab. 6.2). The final reduced data set was again analyzed with the above stated settings. Additionally, in order to find all possible shortest trees, the TNT script ‘bbreak’ was used with tree bisection and reconnection (command: bbreak=tbr safe). A reduced consensus tree was produced by using the heuristic method (Trees > Comparison > Agreement subtrees). Specimens not represented in the reduced consensus were added one by one to check their possible phylogenetic positions. Subsequently, pruned trees were generated (Trees > Comparison > Pruned Trees), with the parameters different from the default set as follows: up to 4 taxa, list as text. Since the three taxon combinations proposed by the 'pruned tree analysis' include only six specimens in total, a strict consensus tree was generated excluding all of these six OTUs a posteriori.

Given the low consistency index (CI) and thus high number of homoplasies in the dataset, an additional analysis with the same settings, but under implied weighting was conducted. Implied weighting calculates and adapts the weight of the characters during the analysis, based on the consistency index of the single characters (Goloboff, 1993). As characters with a high number of homoplasies in a specimen-based analysis are possibly coding for individual variation, and thus not phylogenetically significant, downweighting of these characters would be expected to yield more accurate results. Furthermore, as ontogenetic changes generally occur in a similar way in closely related taxa, and given that the dataset includes several juvenile to subadult specimens (YPM 1901, SMA 0009, CM 566, and possibly ANS 21122, SMA 0004, CM 3452, SMA 0011, AMNH 7530, AMNH 7535, SMA O25-8, SMA D16-3), characters describing them are probably more homoplastic than others and thus downweighted as well.

Support values. For both analyses, symmetric resampling was preferred over bootstrapping or jackknifing for quantifying node support (Analyze > Resample; using the default settings). Symmetric resampling is not affected by differential weighting of the characters, and thus a more meaningful value for the analysis with implied weights (Goloboff et al., 2003). For better comparison between the trees of the two methods, the same method was used for both analyses.

Table 6.1: Taxa and specimens included as OTUs in the phylogenetic analysis, with sources used for their coding.

OTU	Personal observations	Additional references	Additional pictures
Shunosaurus lii		Zhang, 1988; McIntosh, 1990a; Zheng, 1996; Chatterjee and Zheng, 2002; Rauhut et al., 2005; Carballido et al. 2012b; Mannion et al. 2012	
Spinophorosaurus nigerensis	NMB-1698-R; NMB-1699-R	Remes et al., 2009; Knoll et al., 2012	O. Mateus, 2011
Omeisaurus		He et al., 1988; McIntosh, 1990a; Rauhut et al., 2005; Remes et al., 2009; Whitlock, 2011a; Carballido et al., 2012b; Mannion et al., 2012	
Mamenchisaurus		Young, 1958; McIntosh, 1990a; Russell and Zheng, 1993; Ouyang and Ye, 2002; Rauhut et al., 2005; Remes et al., 2009; Carballido et al., 2012b	
Jobaria tiguidensis	NMB-1695-R	Sereno et al., 1999; Rauhut et al., 2005; Remes et al., 2009; Whitlock, 2011a; Carballido et al., 2012b; Mannion et al., 2012; Wilson, 2012	NMB-1695-R, O. Mateus, 2011; MNN TIG, J. Carballido, 2013
Turiasaurus riodevensis	CPT-1195 to 1261	Royo-Torres et al., 2006; Carballido et al., 2012b; Royo-Torres and Upchurch, 2012	
Losillasaurus giganteus type	MCNV Lo-1 to 26	Casanovas et al., 2001; Harris, 2006c; Remes et al., 2009; Carballido et al., 2012b	
Cetiosauriscus stewarti , NHMUK R3078	yes	Woodward, 1905; Charig, 1980; Mannion et al., 2012; Nair and Salisbury, 2012	
Dystrophaeus viaemalae , USNM 2364	yes	Cope, 1877a; Huene, 1904; McIntosh, 1997	
Camarasaurus	SMA 0002	Osborn and Mook, 1921; Madsen et al., 1995; McIntosh et al., 1996a, b; Wilson and Sereno, 1998; Bonnan, 2001; Ikejiri, 2004; Whitlock, 2011a; Carballido et al., 2012b; Mannion et al., 2012	CM 11338, A. Henrici, 2008; WDC A & B, T. Ikejiri, 2008; USNM 13768, O. Mateus, 2011
Amphicoelias latus AMNH 5765	limited	Cope, 1877b; Osborn and Mook, 1921	
Apatosaurus grandis YPM 1901		Marsh 1877a, 1878; Ostrom and McIntosh, 1966; Madsen et al., 1995; Bonnan, 2001	M. Fox, 2012
Lourinhasaurus alenquerensis lectotype	MIGM 4956-7, 4970, 4975, 4979-80, 4983-84, 5780-81		O. Mateus, 2011
Giraffatitan brancai	MB.R.2180-81, 2635, 2713, 2727, 3689, 3736, 3822, 3824	Janensch 1929b, 1935, 1950, 1961; McIntosh, 1990a; Wilson and Sereno, 1998; Bonnan, 2003; Taylor, 2009; Carballido et al., 2012b; D'Emic, 2012	
Brachiosaurus sp. SMA 0009	yes	Schwarz et al., 2007c; Carballido et al., 2012a; Tschopp and Mateus, 2013	
Brachiosaurus altithorax		Riggs, 1904; Carpenter and Tidwell, 1998; Bonnan and Wedel, 2004; Taylor, 2009; Carballido et al., 2012b; D'Emic, 2012	D. Lovelace, 2013
Australodocus bohetii type	MB.R.2454 & 2455	Remes, 2007; Whitlock, 2011a, b; Mannion et al., 2012, 2013	
Ligabuesaurus leanzai		Bonaparte et al., 2006; Carballido et al., 2012b; D'Emic, 2012	
Isisaurus colberti		Jain and Bandyopadhyay, 1997; Carballido et al., 2012b; D'Emic, 2012	
Haplocanthosaurus priscus		Hatcher, 1903; McIntosh, 1990a; Upchurch, 1995; Gallina and Apesteguía, 2005; Whitlock, 2011a; Carballido et al., 2012b; Mannion et al., 2012	
Limaysaurus tessonei		Calvo and Salgado, 1995; Whitlock, 2011a; Carballido et al., 2012b; Mannion et al., 2012	MUCPv-205, O. Mateus, 2011; J. Whitlock, 2012
Cathartesaura anaerobica		Gallina and Apesteguía, 2005; Whitlock, 2011a; Carballido et al., 2012b; Mannion et al., 2012	
Zapalasaurus bonapartei		Salgado et al., 2006, 2012; Whitlock, 2011a; Carballido et al., 2012b; Mannion et al., 2012	
Nigersaurus taqueti		Sereno et al., 1999, 2007; Rauhut et al., 2005; Sereno and Wilson, 2005; Wilson et al., 2011; Whitlock, 2011a; Carballido et al., 2012b; Mannion et al., 2012	
Demandasaurus darwini		Pereda Suberbiola et al., 2003; Torcida Fernandez-Baldor et al., 2011; Whitlock, 2011a; Carballido et al., 2012b; Mannion et al., 2012	
Amphicoelias altus AMNH 5764	yes	Cope, 1877b; Osborn and Mook, 1921; Rauhut et al., 2005; Whitlock, 2011a; Mannion et al., 2012	O. Mateus, 2011
Amphicoelias altus AMNH 5764 ext	yes	Cope, 1877b; Osborn and Mook, 1921; Rauhut et al., 2005; Whitlock, 2011a; Mannion et al., 2012	O. Mateus, 2011
Dicraeosaurus hansemanni	MB.R.2336-37, 2372, 2379, 3739, 3774, 4886	Janensch, 1929a, b, 1935, 1961; McIntosh, 1990a; Gallina and Apesteguía, 2005; Rauhut et al., 2005; Schwarz-Wings, 2009; Whitlock, 2011a; Carballido et al., 2012b; Mannion et al., 2012	J. Harris, 2013
Brachytrachelopan mesai		Rauhut et al., 2005; Whitlock, 2011a; Carballido et al., 2012b; Mannion et al., 2012	J. Carballido, 2013
Amargasaurus cazaui		Salgado and Bonaparte, 1991; Salgado and Calvo, 1992; Gallina and Apesteguía, 2005; Rauhut et al., 2005; Schwarz et al., 2007b; Schwarz-Wings, 2009; Whitlock, 2011a; Carballido et al., 2012b; Mannion et al., 2012; Schwarz-Wings and Böhm, in press	
Suuwassea emilieae ANS 21122	yes	Harris, 2006a, b, c, 2007; Whitlock and Harris, 2010; Whitlock, 2011a; Carballido et al., 2012b; Mannion et al., 2012	D. Lovelace, 2012
Diplodocidae indet. SMA 0087	yes	Klein and Sander, 2008	O. Mateus, 2011
Diplodocidae indet. SMA 0011	limited	Klein and Sander, 2008	O. Mateus, 2011
Dyslocosaurus polyonychius AC 663	yes	McIntosh et al., 1992; Harris, 2007	
Apatosaurus ajax YPM 1860	yes	Marsh, 1877a, 1896; Osborn, 1898; McIntosh and Berman, 1975; Berman and McIntosh, 1978; McIntosh, 1995; Upchurch et al., 2004b; Harris, 2006a, b; Whitlock et al., 2010; Mannion, 2011	
Apatosaurus laticollis YPM 1861	yes	Marsh, 1879, 1896; McIntosh and Berman, 1975; McIntosh 1990a, b, 1995; Upchurch et al. 2004b; Taylor and Wedel, 2012	

Table 6.1: continued.

Brontosaurus excelsus YPM 1980	yes	Marsh, 1879, 1880, 1881, 1896; Osborn, 1898; Riggs, 1901; Ostrom and McIntosh, 1966; Berman and McIntosh, 1978; McIntosh 1990a, 1995; Wilson and Sereno, 1998; Bonnan, 2001; Upchurch et al., 2004a, b; Mannion et al., 2012; Taylor and Wedel, 2012; Tschopp and Mateus, 2012a	
Brontosaurus amplus YPM 1981	limited	Marsh, 1881; Ostrom and McIntosh, 1966; McIntosh and Berman, 1975; Berman and McIntosh, 1978; McIntosh, 1990b, 1995; Bonnan, 2001; Wilhite, 2003; Upchurch et al., 2004a, b	
Apatosaurus louisae CM 3018	yes	Holland, 1915a; Gilmore, 1936; McIntosh, 1990b, 2005; Wedel et al., 2000; Bonnan, 2001, 2003, 2007; Wilhite, 2003; Upchurch et al., 2004b; Harris 2006b, 2007; Mannion, 2011; Whitlock, 2011a, c; Carballido et al., 2012a; Mannion et al., 2012; Hedrick et al., in press	
Atlantosaurus immanis YPM 1840	limited	Marsh, 1878, 1879, 1896; Osborn, 1898; McIntosh and Berman, 1975; Berman and McIntosh, 1978; McIntosh, 1981, 1990b, 1995, 2005; Upchurch et al., 2004b; Harris, 2006b	
Elosaurus parvus CM 566	limited	Peterson and Gilmore, 1902; Carpenter and McIntosh, 1994; Bonnan, 2001, 2003, 2007; Wilhite, 2003; Upchurch et al., 2004b; Schwarz et al., 2007c; Whitlock, 2011a	
Apatosaurus parvus UW 15556		Hatcher, 1902; Gilmore, 1936; Berman and McIntosh, 1978; McIntosh, 1981, 1990b; Curry, 1999; Bonnan, 2001, 2003; Wilhite, 2003; Upchurch et al., 2004b; Harris, 2006b, 2007; Lovelace et al., 2007; Mannion et al., 2012; Hedrick et al., in press	D. Lovelace, 2012
Apatosaurus minimus AMNH 675	yes	Osborn, 1904; Mook, 1917; McIntosh, 1990b; Harris, 2006b; Whitlock, 2011a; Mannion et al., 2012	M. Taylor, 2012
Eobrontosaurus yahnahpin Tate-001		Filla and Redman, 1994; Bakker, 1998; Bonnan, 2001, 2003, 2007; Harris, 2006b, 2007	T. Ikejiri, 2008; P. Mannion, 2011; D. Lovelace, 2012
Apatosaurus ajax NSMT-PV 20375		Upchurch et al., 2004b; Harris, 2006b, 2007; Mannion et al., 2012	O. Mateus, 2011
Apatosaurus sp. CM 11162	yes	Holland, 1924; Berman and McIntosh, 1978; McIntosh, 1981; Harris, 2006b; Mannion, 2011; Whitlock, 2011a, c; Carballido et al., 2012b; Whitlock and Lamanna, 2012; Tschopp and Mateus, 2012b	J. Whitlock, 2012
Apatosaurus sp. AMNH 460	limited	Matthews, 1905; McIntosh and Berman, 1975; McIntosh, 1990b; Wedel and Sanders, 2002; Upchurch et al., 2004b; Whitlock, 2011a	O. Mateus, 2011; C. Hendrickx, 2012
Apatosaurus sp. CM 3378	limited	Holland, 1915b; Gilmore, 1936; McIntosh and Berman, 1975; Berman and McIntosh, 1978; McIntosh, 1981; Curtice, 1996; Upchurch et al., 2004b; Harris, 2006b; Whitlock, 2011a	
Apatosaurus sp. FMNH P25112		Riggs, 1903; McIntosh, 1990b; Bonnan, 2001, 2007; Wilhite, 2003; Upchurch et al., 2004b	M. Wedel, 2012; W. Simpson, 2013
Apatosaurus sp. ML 418	yes	Antunes and Mateus, 2003; Mannion et al., 2012	O. Mateus, 2012
Supersaurus vivianae holotype		Jensen, 1985, 1987; Curtice, 1996; Curtice and Stadtman, 2001; Harris, 2007; Lovelace et al., 2007	D. Lovelace, 2012; R. Wilhite, 2012
Supersaurus vivianae BYU		Jensen, 1985, 1987; Paul 1988; Curtice, 1995, 1996; Curtice and Curtice, 1996; Curtice et al., 1996; Curtice and Stadtman, 2001; McIntosh, 2005; Harris, 2006b, 2007; Lovelace et al., 2007	D. Lovelace, 2012; R. Wilhite, 2012
Supersaurus vivianae WDC DMJ-021	limited	Lovelace et al., 2007; Mannion et al., 2012	O. Mateus, 2011; D. Lovelace, 2012
Dystylosaurus edwini BYU 4503		Jensen, 1985; Curtice and Stadtman, 2001; Lovelace et al., 2007	O. Mateus, 2011; R. Wilhite 2012
Dinheirosaurus lourinhanensis ML 414	yes	Bonaparte and Mateus, 1999; Mannion et al., 2012	O. Mateus, 2011
Kaatedocus siberi SMA 0004	yes	Ayer, 2000; Klein et al., 2012; Tschopp et al. 2013	O. Mateus, 2011
Tornieria africana holotype	MB.R.2672, 2713, 2728	Fraas, 1908; Janensch, 1961; Remes, 2006, 2009; Bonnan, 2007; Whitlock, 2011a	
Tornieria africana skeleton k	MB.R.2386, 2572, 2586, 2669, 2673, 2726, 2730, 2733, 2913, 3816	Janensch, 1929b, 1935, 1961; Heinrich, 1999; Harris, 2006b, 2007; McIntosh, 2005; Remes, 2006, 2007, 2009; Bonnan, 2007; Mannion, 2011; Whitlock, 2011a; Knoll et al., 2012	
Diplodocus longus YPM 1920	yes	Marsh, 1878; Curtice, 1996; McIntosh and Carpenter, 1998	
Diplodocus lacustris YPM 1922	yes	Marsh, 1884; McIntosh and Berman, 1975; Whitlock et al., 2010	
Diplodocus carnegii CM 84	yes	Hatcher, 1901; McIntosh, 1981, 1990b, 2005; Curtice, 1996; McIntosh and Carpenter, 1998; Wilhite, 2003; Harris, 2006b, 2007; Taylor et al., 2011; Whitlock, 2011a, c; Carballido et al., 2012a, b; Mannion et al., 2012	
Diplodocus carnegii CM 94	yes	Hatcher, 1901; Gilmore, 1936; McIntosh, 1981, 1990b, 2005; McIntosh et al., 1992; Curtice, 1996; McIntosh and Carpenter, 1998; Wilhite, 2003; Bedell and Trexler, 2005; Harris, 2006b, 2007; Bonnan, 2007; Schwarz et al., 2007a; Whitlock, 2011a; Carballido et al., 2012a, b; Hedrick et al., in press	
Diplodocus sp. AMNH 223	yes	Osborn, 1899; McIntosh, 1990b, 2005; Gillette, 1991; Curtice, 1996; McIntosh and Carpenter, 1998	
Diplodocus sp. USNM 10865	limited	Gilmore, 1932; McIntosh, 1990b, 2005; Gillette, 1991; McIntosh et al., 1992; Curtice, 1996; Wilhite, 2003; Harris, 2007; Whitlock, 2011a	
Diplodocus sp. DMNS 1494	yes	McIntosh, 1981, 2005; Gillette, 1991; Curtice, 1996; McIntosh and Carpenter, 1998	D. Lovelace, 2012
Diplodocus sp. AMNH 969	limited	Holland, 1906, 1924; Berman and McIntosh, 1978; Barrett and Upchurch, 1994; Upchurch and Barrett, 2000	
Diplodocus sp. CM 11161	yes	Holland, 1924; McIntosh and Berman, 1975; Berman and McIntosh, 1978; McIntosh, 1981; Harris, 2006b; Mannion, 2011; Knoll et al., 2012; Schmitt, 2012; Young et al., 2012	
Diplodocus sp. CM 3452	limited	Holland, 1924; McIntosh and Berman, 1975; Berman and McIntosh, 1978; McIntosh, 1981; Harris, 2006a, b; Holliday and Witmer, 2008; Witmer et al., 2008; Whitlock et al., 2010; Whitlock and Harris, 2010; Knoll et al., 2012	L. Witmer 2012

Table 6.1: continued.

Diplodocus sp. USNM 2672	yes	Marsh, 1884, 1896; Holland, 1906, 1924; McIntosh and Berman, 1975; Berman and McIntosh, 1978; McIntosh, 1990b; Harris, 2006b	
Diplodocus sp. WDC-FS001A	limited	Bedell and Trexler, 2005	
Diplodocus hayi HMNS 175	limited	Hatcher, 1903; Holland, 1906, 1924; Berman and McIntosh, 1978; McIntosh, 1981, 2005; Curtice, 1996; Bonnan, 2001, 2005, 2007; Harris, 2006a, 2007	C. Hendrickx, 2012
Seismosaurus hallorum NMMNH 3690		Gillette, 1991; Curtice, 1996; Harris, 2006b; Herne and Lucas, 2006; Lucas et al., 2006; Lovelace et al., 2007	O. Mateus, 2011; S. Lucas, 2012
Barosaurus lentus YPM 429	yes	Marsh, 1890, 1896; Lull, 1919; Curtice, 1996; Wedel et al., 2000; McIntosh, 2005; Harris, 2006b, 2007; Remes, 2006; Lovelace et al., 2007	
Barosaurus affinis YPM 419	yes	Lull, 1919; Bonnan, 2001; McIntosh, 2005	
Barosaurus sp. AMNH 6341	yes	Gillette, 1991; Curtice, 1996; Bonnan, 2001, 2007; Wilhite, 2003; McIntosh, 2005; Lovelace et al., 2007; Schwarz et al., 2007c; Nair and Salisbury, 2012; Hedrick et al., in press	O. Mateus, 2011
Barosaurus sp. AMNH 7530	yes		O. Mateus, 2011
Barosaurus sp. CM 11984	limited	McIntosh, 1981, 2005; Wedel et al., 2000	
Barosaurus sp. AMNH 7535	yes		

Table 6.2: Anatomical overlap of the OTUs used in the phylogenetic analysis.

Taxon	OTU	Specimen(s)
Shunosaurus lii	-	-
Spinophorosaurus nigerensis	-	-
Omeisaurus	-	-
Mamenchisaurus	-	-
Jobaria tiguidensis	-	-
Turiasaurus riodevensis	-	-
Losillasaurus giganteus	type	MCNV Lo-1 to 26
Cetiosauriscus stewarti	-	NHMUK R3078
Dystrophaeus viaemalae	-	USNM 2364
Camarasaurus	-	-
Amphicoelias latus	-	AMNH 5765
Apatosaurus grandis	-	YPM 1901
Lourinhasaurus alenquerensis	lectotype	MIGM 4956-57, 4970, 4975, 4979-80, 4983-84, 5780-81
Giraffatitan brancai	-	-
Brachiosaurus sp.	-	SMA 0009
Brachiosaurus altithorax	-	-
Australodocus bohetii	type	MB.R.2454-55
Ligabuesaurus leanzai	-	-
Isisaurus colberti	-	-
Haplocanthosaurus priscus	-	-
Limaysaurus tessonei	-	-
Cathartesaura anaerobica	-	-
Zapalasaurus bonapartei	-	-
Nigersaurus taqueti	-	-
Demandasaurus darwini	-	-
Amphicoelias altus	-	AMNH 5764
Amphicoelias altus	type ext	AMNH 5764
Dicraeosaurus hansemanni	-	-
Brachytrachelopan mesai	-	-
Amargasaurus cazaui	-	-
Suuwassea emilieae	-	ANS 21122
Diplodocidae indet.	-	SMA 0087
Diplodocidae indet.	-	SMA 0011
Dyslocosaurus polyonychius	-	AC 663
Apatosaurus ajax	-	YPM 1860
Apatosaurus laticollis	-	YPM 1861
Brontosaurus excelsus	-	YPM 1980
Brontosaurus amplus	-	YPM 1981
Apatosaurus louisae	-	CM 3018
Atlantosaurus immanis	-	YPM 1840
Elosaurus parvus	-	CM 566
Apatosaurus parvus	-	UW 15556
Apatosaurus minimus	-	AMNH 675
Eobrontosaurus yahnahpin	-	Tate-001
Apatosaurus ajax	-	NSMT-PV 20375
Apatosaurus sp.*	-	CM 11162
Apatosaurus sp.	-	AMNH 460
Apatosaurus sp.	-	CM 3378
Apatosaurus sp.	-	FMNH P25112
Apatosaurus sp.	-	ML 418
*Supersaurus vivianae**	holotype	BYU 12962
Supersaurus vivianae	BYU	BYU 4503, 4839, 9024-25, 9044-45, 9085, 10612, 12424, 12555, 12639, 12819, 12861, 12946, 12962, 13016, 13018, 13981, 16679, 17462
Supersaurus vivianae	-	WDC DMJ-021
*Dystylosaurus edwini**	-	BYU 4503
Dinheirosaurus lourinhanensis	-	ML 414
Kaatedocus siberi	-	SMA 0004
Tornieria africana	holotype	MB.R.2672, 2713, 2728; SMNS 12140, 12141a, 12142, 12143, 12145a, c
Tornieria africana	skeleton k	MB.R.2386, 2572, 2586, 2669, 2673, 2726, 2730, 2733, 2913, 3816
Diplodocus longus	-	YPM 1920
Diplodocus lacustris	-	YPM 1922
Diplodocus carnegii	-	CM 84
Diplodocus carnegii	-	CM 94
Diplodocus sp.	-	AMNH 223
Diplodocus sp.	-	USNM 10865
Diplodocus sp.	DMNS 1494	CM 21763; DMNS 1494
Diplodocus sp.	-	AMNH 969
Diplodocus sp.	-	CM 11161
Diplodocus sp.	-	CM 3452
Diplodocus sp.	-	USNM 2672
Diplodocus sp.	-	WDC-FS001A
Diplodocus hayi	-	HMNS 175
Seismosaurus hallorum	-	NMMNH 3690
Barosaurus lentus	-	YPM 429
Barosaurus affinis	-	YPM 419
Barosaurus sp.	-	AMNH 6341
Barosaurus sp.	-	AMNH 7530
Barosaurus sp.	-	CM 11984
Barosaurus sp.	AMNH 7535	AMNH 7535, 30070

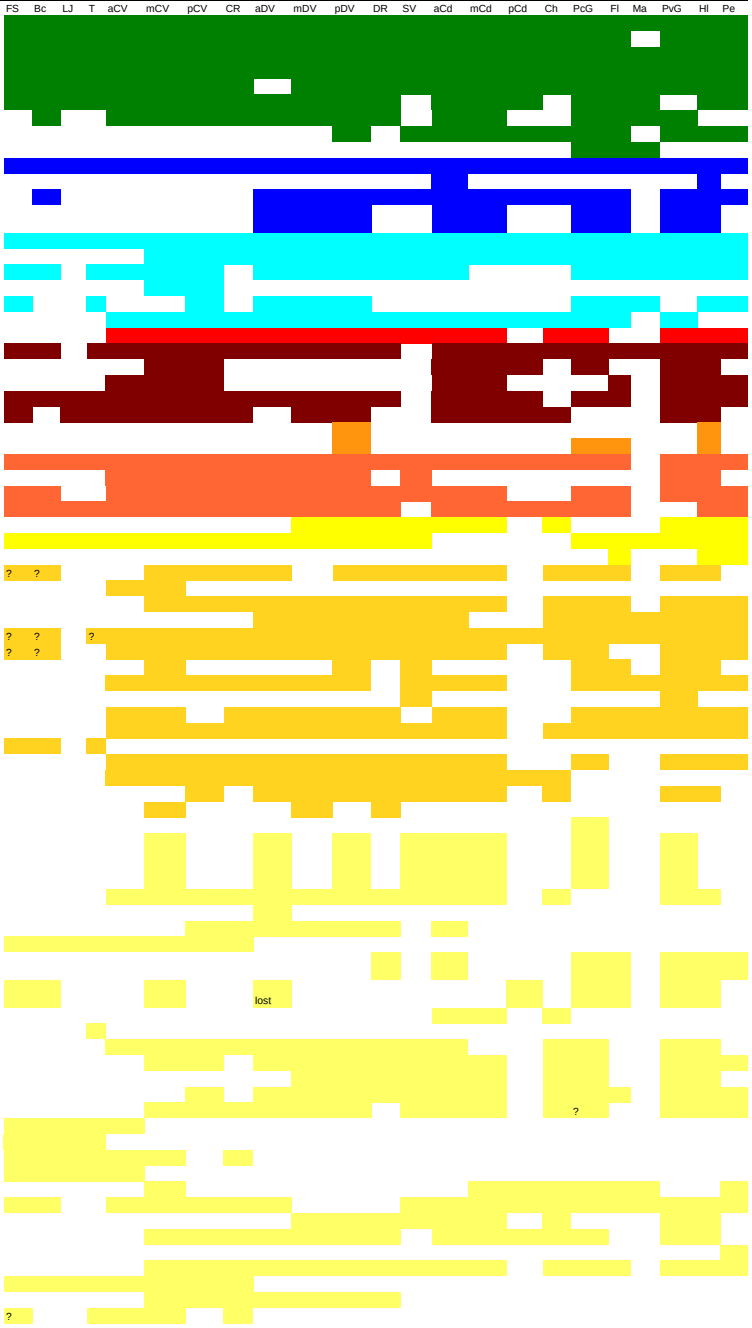

Taxa marked with an asterisk are joined with more complete specimens (see text). Question marks mark dubious assignments. Abbreviations: aCd, anterior caudal vertebrae; aCV, anterior cervical vertebrae; aDV, anterior dorsal vertebrae; Bc, braincase; Ch, chevrons; CR, cervical ribs; DR, dorsal ribs; Fl, forelimb; FS, facial skull; Hl, hindlimb; LJ, lower jaw; Ma, manus; mCd, mid-caudal vertebrae; mCV, mid-cervical vertebrae; mDV, mid-dorsal vertebrae; pCd, posterior caudal vertebrae; PcG, pectoral girdle; pCV, posterior cervical vertebrae; pDV, posterior dorsal vertebrae; Pe, Pes; PvG, pelvic girdle; SV, sacral vertebrae; T, teeth.

In order to quantify overlap within the single clades recovered, an overlap index was created together with F. Tschopp (Jona, Switzerland), indicating how many characters of the total 477 are available for analysis between the ingroup species. Overlaps were defined as the number of specimens for which a character was scorable, minus one, because if only one specimen of the group preserves a certain bone, no anatomical overlap is present in order to compare with other specimens of the same group. The index increases when more characters are scored in at least two specimens, or when the number of specimens scorable for the same character is enlarged. It thus combines a measure for the completeness of the matrix with the comparability of single characters within specimens of a single group. Thereby, it gives an idea of the strength of the matrix to recover certain clades. However, it

does not provide a measure for the significance of the result, as incomplete specimens might still bear taxonomically highly significant characters, which allow to identify it even to genus or species level. The overlap index is thus especially useful to evaluate taxa changing their positions between different trees. By calculating the overlap index for the sister group arrangements including the questionable taxon, researchers get an idea of how well the arrangement is supported based on overlapping skeletal material.

Positional terms for vertebrae

Serial variation within the vertebral column is highly developed in sauropods, and of taxonomical importance (Wilson, 2002, 2012). The high variability requires detailed character descriptions restricted not only to cervical, dorsal or caudal vertebrae, but even to areas within the respective portions of the column. It is thus general use in phylogenetic analyses that characters are restricted to anterior cervical vertebrae, or mid- and posterior caudal vertebrae, for example (Wilson, 2002; Upchurch et al., 2004a, b; Whitlock, 2011a; Mannion et al., 2012; Tschopp and Mateus, 2012b). However, a majority of the papers using phylogenetic analyses do not state how they define these subdivisions. The definitions used in the present analysis mostly follow the ones proposed by Mannion et al. (2013), and are summarized in table 6.3.

Table 6.3: Definitions of positional terms for vertebrae.

Vertebrae	Subdivision	Definition	Example *Apatosaurus louisae*
Cervical	Anterior	The division is made numerically	CV 1-5
	Mid-cervicals		CV 6-10
	Posterior		CV 11-15
Dorsal	Anterior	Parapophysis still touching centrum	DV 1-2
	Mid-dorsals	Numerical subdivision	DV 3-6
	Posterior		DV 7-10
Caudal	Anterior-most	With transverse processes extending onto neural arch	Cd 1-6
	Anterior	With normal transverse process	Cd 7-14
	Mid-caudal	without transverse processes, but still well-developed neural spine	Cd 15-28
	Posterior	Postzygapophyses reduced	Cd 29-42
	Distal	Neural arch reduced	Cd 43-82

Material

Ingroup specimens phylogenetic analysis

The following individual, presumed diplodocid, specimens were included in the ingroup of the phylogenetic analysis. All of these are reasonably complete specimens of reputed diplodocid species, or constitute the holotypes of taxa, irrespective of completeness, which have been either referred or associated to Diplodocidae. Previous classifications and assignments, as well as comments on the likelihood that they represent singular individuals, are given below, alphabetically ordered. Outgroups comprise species-, or genus-level taxa from non-neosauropod Eusauropoda, Macronaria, as well as closely related Diplodocoidea. They are not further discussed here.

***Amphicoelias altus*, AMNH 5764 and AMNH 5764 ext.** The holotype of *Amphicoelias altus* originally included a tooth, two dorsal vertebrae, a pubis, and a femur (Cope, 1877a). A scapula, coracoid, and an ulna were later provisionally referred to the specimen (Osborn and Mook, 1921). However, the strongly expanded distal end of the scapula, and the relatively deep notch anterior to the glenoid on the coracoid actually resemble more *Camarasaurus* than any diplodocid (pers. obs.). The same accounts for the single tooth stored at AMNH (Osborn and Mook, 1921). The tooth has already been excluded from scores of *A. altus* in recent phylogenetic analyses (Whitlock, 2011a; Mannion et al., 2012), which is followed here. Two different preliminary phylogenetic analyses were performed with the reduced and the extended holotype material (including the scapula, coracoid, and ulna). As both analyses yielded the same position for the specimens, the reduced holotype was preferred in the final analysis, given that it appeared to yield enough phylogenetically important information to resolve its position. The risk of adding dubious information from potentially wrongly referred material was thus circumvented. However, more detailed analysis is needed in order to refine these assignments.

'*Amphicoelias*' *latus*, AMNH 5765. This is a fragmentary specimen comprising four caudal vertebrae and a right femur from the same site as the holotypes of *Camarasaurus supremus* and *Amphicoelias altus* (Cope, 1877a; Osborn and Mook, 1921; Carpenter, 2006). Both the vertebrae and the femur show greater resemblance with *Camarasaurus* than to *Amphicoelias*, which led Osborn and Mook (1921) to synonymize *A. latus* with *C. supremus*.

***Apatosaurus ajax*, YPM 1860.** The holotype of *Apatosaurus ajax* also constitutes the genoholotype of *Apatosaurus*. During collection and shipping it became intermingled with YPM 1840, the holotype of *Atlantosaurus immanis* (McIntosh, 1995). As a result, it is currently difficult to distinguish the two individuals, even though they come from different quarries. I follow the suggestions of Berman and McIntosh (1978) and McIntosh (1995), in deciding which elements of the mingled taxa presently comprise the holotype of *Apatosaurus ajax*. The only material not confidently referable to either specimen is a braincase currently labeled 'YPM 1860'. In order to investigate the taxonomic implications of the attribution of this braincase to the types of *Apatosaurus ajax* or *Atlantosaurus immanis*, two supplementary analyses were performed with scores of the braincase added to YPM 1840 and 1860, respectively. Adding the information from the braincase to YPM 1840, tree length increases but positions of the two specimens remain the same. An assignment of the braincase to the holotype of *Apatosaurus ajax* appears thus more parsimonious, indicating that it was labeled right.

***Apatosaurus ajax*, AMNH 460.** This specimen was recovered as *Apatosaurus ajax* in the specimen-based phylogenetic analysis of Upchurch et al. (2004b). Because AMNH 460 is mounted with reconstructed contribution of other specimens, caution has to be used, in order to not code characters based on reconstructed bones or elements actually belonging to other specimens (for a list of bones belonging to AMNH 460, see table 6.1).

***Apatosaurus ajax*, NSMT-PV 20375.** Described by Upchurch et al. (2004b), this specimen is the only fully described skeleton previously referred to *A. ajax*. It is relatively complete, although abnormal length ratios of the humerus, radius and metacarpal III suggest that NSMT-PV 20375 might be composed of more than one individual, possibly including bones of the *Camarasaurus* specimens found intermingled in the quarry (Upchurch et al., 2004b). These forelimb elements were thus excluded from scores of the OTU in the present analysis.

'*Apatosaurus*' *grandis*, YPM 1901. Marsh (1877a) initially assigned this species to *Apatosaurus*, but subsequently referred it to *Morosaurus* (Marsh, 1878; later synonymized with *Camarasaurus*: Mook, 1914). There is some confusion about the correct assignment of several bones to either the holotype YPM 1901 or the referred specimens YPM 1902 or YPM 1905 from the same quarry (see Ostrom and McIntosh, 1966). Herein, scores are included from all elements potentially belonging to YPM 1901 (according to Ostrom and McIntosh, 1966). As all three specimens were referred to *Camarasaurus*, this should have no influence on the ingroup relationships of the current phylogenetic analysis.

***Apatosaurus laticollis*, YPM 1861.** *Apatosaurus laticollis* is based on a single, fragmentary cervical vertebra (Marsh, 1879). Subsequent studies proposed that this vertebra actually belongs to the same individual as the holotype material of *Atlantosaurus immanis* (YPM 1840), which were both found in the Lakes Quarry 1 (McIntosh, 1995). Here, the specimens were kept apart in order to evaluate this hypothesis.

***Apatosaurus louisae*, CM 3018 (holotype) and CM 11162.** The most complete specimen of *Apatosaurus* is CM 3018, a postcranial skeleton that was preliminarily described as new species by Holland (1915a) and followed by a detailed monographic treatment by Gilmore (1936). An obvious diplodocid skull (CM 11162) was found near it, but the historical referral of the latter specimen remained confused for a time (Holland, 1915b, 1924; Berman and McIntosh, 1978). Because *Apatosaurus* was thought to have a more *Camarasaurus*-like skull at the time, Holland's proposal that CM 11162 was the actual skull of CM 3018 (Holland, 1915b, 1924) was largely unaccepted by others (e.g. Gilmore, 1936). Only with the detailed description and study of the specimen by Berman and McIntosh (1978) did CM 11162 become the now widely accepted skull-form of *Apatosaurus*. Given the small distance between skull and postcrania in the quarry, as well as the perfectly fitting size of the cranial occipital

condyle and postcranial atlas, the probability that the two belong to the same individual is very high (Holland, 1915b; Berman and McIntosh, 1978). Accordingly, the OTU representing the holotype of *Apatosaurus louisae* in the present analysis comprises scoring from both CM 3018 and 11162.

***Apatosaurus louisae*, CM 3378.** The specimen was identified as *Apatosaurus louisae* in the analysis of Upchurch et al. (2004b). Although never described in detail, CM 3378 yields important information on the number of vertebrae in *Apatosaurus*, as this specimen is the only known with an articulated, uninterrupted vertebral column from the mid-cervical region to the last caudal vertebra (Holland, 1915b; McIntosh, 1981). CM 3378 was found at the Dinosaur National Monument, associated with a diplodocid skull (CM 11161; interpreted as *Diplodocus*), as well as appendicular elements. However, according to McIntosh (1981), these materials cannot be attributed to the same individual as CM 3378 with certainty, and no scores from them were thus included in this OTU.

'*Apatosaurus*' *minimus*, AMNH 675. Initially described as new species of *Apatosaurus* (Mook, 1917), AMNH 675 is now *g*enerally considered an indeterminate sauropod, with affinities to Titanosauriformes, based on the shape of the ilia and the six sacral vertebrae (McIntosh, 1990a). In order to test this, *Isisaurus colberti* was added to the analysis. *Isisaurus* has the typical titanosaurian sacrum with six vertebrae and the preacetabular lobe oriented perpendicular to the vertebral axis (Jain and Bandyopadhyay, 1997), as is the case in AMNH 675. At AMNH, a diplodocid chevron is also accessioned in AMNH 675. However, because AMNH record indicate it was 'found loose with other Bone Cabin Quarry material', I excluded scoring it as part of *A. minimus*.

***Apatosaurus parvus*, UW 15556.** This specimen was found by the Carnegie Museum, intermingled with the holotype specimen of *Elosaurus parvus*, CM 566 (Hatcher, 1902; Peterson and Gilmore, 1902). It first bore the specimen number CM 563, but was later transferred to the University of Wyoming (McIntosh, 1981). Usually identified as *A. excelsus* (Gilmore, 1936), a specimen-based phylogenetic analysis supported the retention of the species *parvus* for CM 566 and UW 15556 (Upchurch et al., 2004b).

***Apatosaurus* sp., FMNH P25112.** Riggs (1903) described this specimen (formerly FMNH 7163) as *A. excelsus*, which led him to two important conclusions: 1) *Brontosaurus* is a junior synonym of *Apatosaurus*, and 2) during ontogeny, additional vertebrae are added from the dorsal and caudal series to the sacrum. Later, the specimen-based phylogenetic analysis of Upchurch et al. (2004b) recovered it on a disparate branch within *Apatosaurus*, suggesting that FMNH P25112 represents a novel species.

***Apatosaurus* sp., ML 418.** This specimen is very badly preserved. One dorsal vertebra has been prepared and was identified as a possible *Apatosaurus* or *Dinheirosaurus* (Antunes and Mateus, 2003; Mateus, 2005; Mannion et al., 2012). Additional unprepared material includes dorsal rib fragments, and a partial tibia. A mid- or posterior cervical vertebra of the same individual was lost due to the friable preservation, and scores concerning the cervical vertebrae therefore base on photographs.

***Atlantosaurus immanis*, YPM 1840.** This is possibly the same individual as YPM 1861 (*Apatosaurus laticollis*), and it was mingled with YPM 1860 (*Apatosaurus ajax*) during shipping (see above). McIntosh (1995) tried to separate them based on their color, and on the sparse field notes. In the YPM collections, the specimens remain tagged as they have been before McIntosh's study, therefore it is difficult to reproduce his results. Scores for an ischium of YPM 1840 are based on personal observation, whereas cervical and dorsal vertebral characters are derived from the literature (Marsh, 1896; Ostrom and McIntosh, 1966; Upchurch et al., 2004b).

***Australodocus bohetii*, holotype and paratype.** The holotype and paratype are two successive mid-cervical vertebrae from the same individual (Remes, 2007). Mannion et al. (2013) suggested *Australodocus* to be a non-lithostrotian titanosaur. Accordingly, *Ligabuesaurus leanzai* was added to the taxon list in order to include a possible closely related derived titanosauriform that has anatomical overlap with *A. bohetii*.

***Barosaurus affinis*, YPM 419.** The holotype of *B. affinis* consists only of pedal material, and has no overlap with the holotype of *B. lentus* (Marsh, 1890, 1899). Because they come from the same quarry,

the two species were usually regarded as synonyms (Lull, 1919; McIntosh, 2005). McIntosh (2005) identified the elements as mt I and partial mt II, but the latter is herein interpreted to represent the proximal portion of mt V instead. The bone is widely expanded, and has the typical 'paddle'-shape of the metatarsal V in sauropods (pers. obs., 2011).

***Barosaurus lentus*, YPM 429.** Although this specimen is the genoholotype of *Barosaurus* (Marsh, 1890; Lull, 1919), most characterization of *Barosaurus* is based on another, more complete, and articulated specimen (AMNH 6341, see below). YPM 429 as presently available has a high degree of reconstruction, especially in some cervical vertebrae.

***Barosaurus* sp., AMNH 6341.** This specimen is the most complete probable *Barosaurus* (McIntosh, 2005). It was collected in three parts and subsequently separated by different institutions (USNM, CM, and UUVP), but later brought together by B. Brown for the AMNH (Bird, 1985). Some doubts exist concerning the correct attribution of a tibia-fibula pair, which might also belong to a *Diplodocus* specimen found in the vicinity of AMNH 6341 (McIntosh, 2005).

***Barosaurus* sp., AMNH 7530.** Both the holotype specimen of *Kaatedocus siberi* (SMA 0004) and AMNH 7530 were found at Howe Quarry (Michelis, 2004; Tschopp and Mateus, 2012b). The latter specimen is tagged as *Barosaurus* on display at AMNH, probably based on a tentative identification made by Brown (1935), but without detailed study. AMNH 7530 is an important specimen for diplodocid taxonomy because it includes articulated anterior and mid-cervical vertebrae and a partial skull.

***Barosaurus* sp., AMNH 7535.** This specimen was recovered with *Kaatedocus siberi* SMA 0004 and AMNH 7530 at Howe Quarry (Michelis, 2004; Tschopp and Mateus, 2012b), and has been simply cataloged as *Barosaurus* in the collections of the AMNH (likely by B. Brown; Brown, 1935). AMNH 7535 largely preserves the same elements as SMA 0004 and AMNH 7530, and appears to be of about the same size. A partial tail is also accessioned under AMNH 7535, but given the chaotic distribution of specimens in the quarry (Fig. 4.1), it is impossible to confidently attribute disparate and disarticulated portions to any single common individual. A diplodocid quadrate that was initially cataloged under AMNH 7535 now bears the number AMNH 30070. Since the original attribution of this quadrate to AMNH 7535 was probably based on their vicinity in the quarry, two analyses were performed with and without the information of this bone, yielding the same phylogenetic position in both iterations. On both instances, information from the caudal series were omitted from scores of AMNH 7535. Scores on the quadrate were retained in the final analysis because AMNH 30070 shows some differences with the quadrates known from *Kaatedocus* (e.g. lack of the small fossa dorsomedially on the quadrate shaft, pers. obs., 2011), as do also the cervical vertebrae.

***Barosaurus* sp., CM 11984.** Together with YPM 429 and AMNH 6341, CM 11984 represents a third, relatively complete, likely *Barosaurus* specimen (McIntosh, 2005). Some of the material of CM 11984 still is unprepared, and further crucial information on *Barosaurus* can be expected once these are freed from matrix. In addition to the vertebral column, a pes is accessioned under CM 11984, which McIntosh (2005) considered to have a dubious association with the remaining material. Therefore, this pes is not considered as part of the scoring of CM 11984.

***Brachiosaurus* sp., SMA 0009.** Initially described as a diplodocid (Schwarz et al., 2007c), a reassessment of the systematic position of SMA 0009 after further preparation of the mid-cervical vertebrae revealed probable titanosauriform affinities (Carballido et al., 2012a). Because Carballido et al. (2012a) suggested that SMA 0009 represents an immature *Brachiosaurus*, *B. altithorax* (Riggs, 1904; Taylor, 2009) was included in the dataset.

***Brontosaurus amplus*, YPM 1981.** The type of *B. amplus* (Marsh, 1881) is generally accepted as synonym to *Apatosaurus excelsus* (Gilmore, 1936; McIntosh, 1990a, 1995; Upchurch et al., 2004b), but has never been described in detail.

***Brontosaurus excelsus*, YPM 1980.** The holotype of *Brontosaurus excelsus* (now commonly synonymized with *Apatosaurus*) was the first to be published with a reconstruction of the entire

skeleton (Marsh, 1883), and is still one of the best preserved diplodocid specimens worldwide. For the mount at YPM it was extensively reconstructed, such that special care has to be taken when scoring its characters from the original specimen.

***Cetiosauriscus stewarti*, NHMUK R3078.** The holotype specimen was first described in the early 1900s (Woodward, 1905) as *Cetiosaurus leedsi*. However, Huene (1927) identified '*Cetiosaurus*' *leedsi* as a separate genus, *Cetiosauriscus*, and highlighted the then referred specimen NHMUK R3078 as exemplifying the new genus. NHMUK R3078 was made the holotype of *Cetiosauriscus stewarti* (Charig, 1980), which later was instated as the type species of *Cetiosauriscus* (Charig, 1993). It was included in Diplodocidae by McIntosh (1990b), based on pedal morphology, but subsequent analyses proposed a closer relationship with the non-neosauropod eusauropods *Mamenchisaurus* or *Omeisaurus*, as well as with *Tehuelchesaurus* (Heathcote and Upchurch, 2003). *Mamenchisaurus* and *Omeisaurus* were thus included in the present analysis in order to test these competing hypotheses. A detailed restudy of the material is in preparation by P. Mannion and P. Upchurch (pers. comm., 2011, 2012), and will doubtlessly reveal more valid characters. Since personal observation of the caudal vertebrae of *Spinophorosaurus nigerensis* revealed high similarity with *Cetiosauriscus*, *S. nigerensis* was added to the matrix, in order to appraise the phylogenetic role of their morphological similarities.

***Dinheirosaurus lourinhanensis*, ML 414.** The holotype of *Dinheirosaurus lourinhanensis* was originally referred to *Lourinhasaurus alenquerensis* by Dantas et al. (1998), but Bonaparte and Mateus (1999) realized that ML 414 represents a different genus. Contrary to the phylogenetic assignment of *L. alenquerensis*, which is now thought to be a basal macronarian (see below), the diplodocid affinities of *D. lourinhanensis* are well supported by four phylogenetic analyses (Rauhut et al., 2005; Whitlock, 2011a; Mannion et al., 2012; Tschopp and Mateus, 2012b).

***Diplodocus carnegii*, CM 84.** The holotype of *D. carnegii* is one of few specimens of *Diplodocus* that includes cervical vertebrae. It is mounted at CM, and completed with bones from various other specimens: CM 94, 307, 21775, 33985, HMNS 175, USNM 2673, and AMNH 965 (McIntosh, 1981; Curtice, 1996). Scores of the holotype of *D. carnegii* are based on this mounted specimen, with effort taken to ensure that only material from CM 84 was included. *D. carnegii* was erected based on comparisons to AMNH 223, which showed some differences in caudal neural spine orientation. If compared with the original type material, the differences are not as clear, and were in fact disputed by Gilmore (1932).

***Diplodocus carnegii*, CM 94.** This specimen was described as a paratype of *D. carnegii* (Hatcher, 1901). Both holotype and paratype specimens were found in the same quarry, from where also material of other genera was recovered (Hatcher, 1901). Oddly, CM 94 includes two pairs of ischia, which casts some doubt on the true attribution of bones to individual specimens (McIntosh, 1981; pers. obs., 2011). As both pairs of ischia show the same characteristics, I included the entire material excluding one pair of ischia from the OTU representing CM 94 (including some bones mounted with the holotype of *Galeamopus hayi* HMNS 175, see below). However, further studies are needed in order to definitively assign the various bones among the at-least two individuals present.

***Diplodocus* cf. *carnegii*, WDC-FS001A.** This specimen has not been described entirely, but is the most complete referral to *Diplodocus* that has a manus with associated hindlimb and axial material (Bedell and Trexler, 2005). The specimen was found in two spatial clusters in the quarry, but the lack of duplicated bones, the two similarly sized humeri, and osteological indications of a single ontogenetic stage led Bedell and Trexler (2005) to identify the materials as belonging to a single individual with affinities to *D. carnegii* (see below).

***Diplodocus hayi*, HMNS 175.** The holotype specimen was initially housed at CM (as CM 662), prior to residing in Cleveland for a time (formerly CMNH 10670). Holland (1924) described it as a novel species based solely on cranial characters. At that time, *Apatosaurus* was thought to bear a *Camarasaurus*-like skull (see Berman and McIntosh, 1978), which probably influenced researchers to identify any elongate, diplodocid skull as *Diplodocus*. McIntosh (1990a), amongst others, later suggested that *D. hayi* might actually not be a *Diplodocus*, but a unique genus, based on various

similarities with *Apatosaurus* in the cranium, forelimb, and tail. Because the specimen is mounted at HMNS (together with reconstructions and original bones from CM 94; McIntosh, 1981), it is only of limited accessibility.

***Diplodocus longus*, YPM 1920.** YPM 1920 constitutes the genoholotype of *Diplodocus* (Marsh, 1878), and has thus special scientific importance. Unfortunately, it is highly incomplete, with only two nearly complete caudal vertebrae, and few additional fragmentary anterior to mid-caudal vertebrae identifiable in the YPM collections. A chevron was reported as belonging to the same individual (Marsh, 1878; McIntosh and Carpenter, 1998), but it could not have been located at YPM. Other articulated vertebrae were found in the field but discarded due to their friable preservation (McIntosh and Carpenter, 1998). Extraneous materials were once assigned to the same specimen, including a skull, femur, tibia, fibula, astragalus, and five metatarsals (still accessioned under YPM 1920), as well as an ulna, radius, and partial manus assigned YPM 1906 (McIntosh and Carpenter, 1998). However, only the caudal series and the chevron can be surely identified as belonging to the holotypic individual (McIntosh and Carpenter, 1998), as scored in the present analysis.

***Diplodocus lacustris*, YPM 1922.** The original type material of *D. lacustris* comprises teeth, a premaxilla, and a maxilla (Marsh, 1884). However, personal observations at YPM reveal that the cranial bones clearly belong to *Camarasaurus* or a morphologically similar taxon, and that there is no relationship between them and the teeth. Therefore, in the present analysis, only the teeth were scored for *D. lacustris*.

***Diplodocus* sp., AMNH 223.** The specimen was first described as *Diplodocus longus* (Osborn, 1899). It was the first reasonably articulated specimen of *Diplodocus* and thus became one of the important specimens to base comparisons to (see Hatcher, 1901). Three partial cervical neural arches, described and figured by Osborn (1899), could not be located at AMNH (pers. obs., 2010, 2011). Coding of these elements is thus based entirely on Osborn (1899).

***Diplodocus* sp., AMNH 969.** This skull and associated atlas and axis were identified as *D. longus*, based on an earlier report of a skull allegedly belonging to the holotype specimen of *D. longus*, YPM 1920 (Marsh, 1884; Holland, 1906). However, the only reported *Diplodocus* specimen with an articulated skull and anterior cervical vertebrae is CM 3452, of which only the skull has been described (Holland, 1924). Since no anterior cervical vertebrae are definitely attributable to *D. longus*, the only comparison that can be made is with the *D. carnegii* type specimens, of which only CM 84 preserves the axis. As will be seen later, AMNH 969 is clearly distinguishable from any of these.

***Diplodocus* sp., CM 3452.** On display at CM, this specimen is the only probable *Diplodocus* with articulated skull and anterior cervical vertebrae (McIntosh and Berman, 1975). However, the cervical vertebrae have not been described, and no detailed study has been done in order to identify the species CM 3452 belongs to. Comparison with other specimens referred to *Diplodocus* is hampered due to very little anatomical overlap.

***Diplodocus* sp., CM 11161.** This specimen is only a skull. It was described as *Diplodocus longus* by Holland (1924) and McIntosh and Berman (1975), based on comparisons with the earlier reported putative *Diplodocus* skulls AMNH 969, USNM 2672 and 2673. However, because all of them were disarticulated and found in quarries that also produced other diplodocid genera, care must be taken concerning these identifications. Our knowledge of diplodocid skulls to date suggests that they are extremely similar to each other, and very few distinguishing characters have yet been proposed (Berman and McIntosh, 1978; McIntosh, 2005; Harris, 2006a; Remes, 2006; Whitlock et al., 2010; Whitlock, 2011b; Tschopp and Mateus, 2012b; Whitlock and Lamanna, 2012). Thus, it is refrained here from referring CM 11161 to any species of *Diplodocus* until postcranial diagnostic traits are robustly linked to cranial morphologies.

***Diplodocus* sp., DMNS 1494.** This specimen is a relatively complete, articulated find from the Dinosaur National Monument. The only disarticulated elements are the right scapulacoracoid and the left hindlimb. These elements were not included in the present analysis because DMNS 1494 was

found intermingled with other skeletons (V. Tidwell, pers. comm., 2010). DMNS 1494 was collected by the Carnegie Museum, and later transferred to DMNS for exhibit. A right fibula and astragalus of the same specimen remained at CM (presently CM 21763; McIntosh, 1981). The specimen has never been formally described, but is ascribed to *D. longus* (e.g. Gillette, 1991). Together with CM 84, DMNS 1494 is the only *Diplodocus* specimen included here with articulated, and well-preserved cervical vertebrae.

***Diplodocus* sp., USNM 2672.** Like AMNH 969, USNM 2672 preserves a partial skull and atlas. It was the first diplodocid skull to be reported, and was initially included among the holotype of *D. longus*, YPM 1920 (Marsh, 1884). However, the skull and holotypic caudal vertebrae were not found in articulation or even close association, therefore this attribution has to be regarded as questionable (McIntosh and Carpenter, 1998).

***Diplodocus* sp., USNM 10865.** Although USNM 10865 is one of the most complete *Diplodocus* specimens, it has only been preliminarily described and was tentatively referred to *D. longus* by Gilmore (1932). USNM 10865 was found close to the articulated *Barosaurus* AMNH 6341 ('#340' in Gilmore, 1932; McIntosh, 2005). According to McIntosh (2005), two sets of left lower legs of different lengths were found associated with USNM 10865. The shorter set was mounted by Gilmore (1932), but McIntosh (2005) suggests that this assignment might have been wrong. For the character relating to the tibia/femur length, the higher ratio was therefore used, following McIntosh (2005).

***Dyslocosaurus polyonychius*, AC 663.** The only specimen of this putative diplodocid sauropod consists of solely appendicular elements of dubious origin and association (McIntosh et al., 1992). No field notes exist, but personal observations of differing color and preservation led to the conclusion that at least the supposed php III-1 was probably not collected at the same place as the rest of the holotype specimen. It is therefore excluded from scores of *Dyslocosaurus* in this phylogenetic analysis. A more detailed reassessment of this specimen is in progress (Tschopp and Nair, in prep.), and might reveal additional information on its taxonomic affinities. The phylogenetic position yielded in the present analysis is regarded as preliminary.

***Dystrophaeus viaemalae*, USNM 2364.** This specimen is highly fragmentary, but was identified as possibly diplodocoid by McIntosh (1990b); his 'Diplodocidae' conforms to the current use of the Diplodocoidea). The type material is only partly prepared, which largely impedes identifying crucial character states. The type locality was relocated in the mid-1990s, and more material of the probable holotypic individual was excavated, of which only a phalanx has been identifiable (Gillette, 1996a, b). However, Gillette (1996a, b) states that more material is probably present, such that additional information on *Dystrophaeus* might be forthcoming. Both in the initial description (Cope, 1877b) and a reassessment (Huene, 1904), several of the bones were misidentified: metacarpal V (according to Huene, 1904) is most probably a metacarpal I, based on the angled distal articular surface (McIntosh, 1997; pers. obs., 2011). Cope (1877b) correctly identified a partial scapula (contra Huene, 1904, who thought it was a pubis), but misidentified a complete ulna and a partial radius as humerus and ulna, respectively, as already recognized by Huene (1904).

***Dystylosaurus edwini*, BYU 4503.** The holotype of *Dystylosaurus edwini* is an anterior dorsal vertebra (Jensen, 1985). There is some doubt concerning its taxonomic affinities: it has been identified as either brachiosaurid (Paul, 1988; McIntosh, 1990b; Upchurch et al., 2004a; Chure et al., 2006) or diplodocid, possibly even from the same individual as the *Supersaurus vivianae* holotype scapulacoracoid (Curtice and Stadtman, 2001; Lovelace et al., 2007). It was included in a preliminary analysis as an OTU independent from *Supersaurus vivianae* BYU and WDC DMJ-021 in order to clarify its taxonomic status. The results yielded 102 most parsimonious trees, where *Dystylosaurus* always grouped with the two *Supersaurus* OTUs, which sometimes include *Dinheirosaurus* ML 414, *Diplodocus hayi* HMNS 175, *Barosaurus affinis* YPM 419, or *Diplodocus lacustris* YPM 1922 within the same branch. In 31 out of 102 most parsimonious trees *Dystylosaurus* and the two *Supersaurus* OTUs formed sister taxa. This result corroborates the hypothesis of Curtice and Stadtman (2001) and Lovelace et al. (2007) that the *Dystylosaurus* holotypic vertebra is *Supersaurus*, and most probably from the same individual as the *Supersaurus* holotype. In the definitive analysis BYU 4503 was thus included as part of the

combined OTU representing the BYU specimens of *Supersaurus vivianae*.

***Elosaurus parvus*, CM 566.** CM 566 is a small juvenile that is generally referred to *Apatosaurus excelsus* (McIntosh, 1995), or constitutes the independent species *Apatosaurus parvus* together with an adult specimen (UW 15556; Upchurch et al., 2004b), with which it was found associated (Peterson and Gilmore, 1902).

***Eobrontosaurus yahnahpin*, Tate-001.** Initially described as *Apatosaurus yahnahpin* (Filla and Redman, 1994), a separate genus was erected for the specimen (Bakker, 1998), partly based on differences in coracoid morphology to *Apatosaurus*. The specimen has been considered a camarasaurid (Upchurch et al., 2004a), but more recently, Mannion (2010) suggested diplodocid affinities. The taxon has never been included in any phylogenetic analysis, but a detailed description of the entire material appears to be in preparation (R. Bakker, pers. comm., cited in Mannion, 2010).

***Kaatedocus siberi*, SMA 0004.** Before its detailed examination, the holotype of *Kaatedocus siberi* was generally reported as *Diplodocus* (Ayer, 2000) or *Barosaurus* (Michelis, 2004). A description and phylogenetic reappraisal of SMA 0004 as part of this Ph.D. revealed its generic separation from *Diplodocus* and *Barosaurus* (Tschopp and Mateus, 2012b).

***Losillasaurus giganteus*, MCNV Lo-1 to 26.** The OTU represents an individual containing the holotypic caudal vertebra, Lo-5 and the paratypes Lo-10 and Lo-23. All the bones of MCNV Lo-1 to 26 were found associated and no duplication of elements occurred (Casanovas et al., 2001). *Turiasaurus* was added as recent phylogenetic studies proposed them to be sister taxa (Royo-Torres et al., 2006, 2009; Royo-Torres and Upchurch, 2012).

***Lourinhasaurus alenquerensis*, lectotype.** The species was first described by Lapparent and Zbyszewski (1957) as referable to *Apatosaurus*, but later included into *Camarasaurus* (McIntosh, 1990a). Subsequently, Dantas et al. (1998) erected a new genus for the species, but only Antunes and Mateus (2003) clearly assigned a specific type specimen to the species. The genus was usually recovered as basal macronarian in phylogenetic analyses (Upchurch et al., 2004a; Royo-Torres and Upchurch, 2012; Mocho et al., 2013).

***Seismosaurus hallorum*, NMMNH 3690.** The holotype of *S. hallorum* was initially described as *S. halli*, and as one of the largest sauropods ever (Gillette, 1991). However, this was mainly based on an incorrect assignment of the position of some mid-caudal vertebrae (Curtice, 1996; Herne and Lucas, 2006). Subsequent reanalysis of the specimen revealed that it is indistinguishable from *Diplodocus*, and that it probably belongs to the same species as AMNH 223 and USNM 10865 (Lucas et al., 2006; Lovelace et al., 2007). Gillette (1994) corrected to species name from *halli* to *hallorum*, as he did not apply the right latin ending for the plural in the initial description (Gillette, 1991, 1994). Herne and Lucas (2006) added a femur (NMMNH 25079) to the holotype individual, which is also used to score the taxon in the analysis herein.

***Supersaurus vivianae* BYU.** *Supersaurus vivianae* is based on a scapulacoracoid (Jensen, 1985; Curtice et al., 1996; Curtice and Stadtman, 2001; Lovelace et al., 2007). It was found at the Dry Mesa Quarry, intermingled with other large bones of both diplodocid and brachiosaurid affinities (Jensen, 1985, 1987; Curtice and Stadtman, 2001). Jensen (1985) described three new taxa based on this material: *Supersaurus vivianae*, *Dystylosaurus edwini*, and *Ultrasauros macintoshi*. Subsequent study of the Dry Mesa specimens indicates that the holotypic dorsal vertebra of *Dystylosaurus*, as well as a dorsal vertebra referred to *Ultrasauros* by (Jensen, 1985, 1987) probably belonged to the same individual as the holotypic scapulacoracoid of *Supersaurus vivianae* (Curtice and Stadtman, 2001). Lovelace et al. (2007) revised this referral based on a new find from Wyoming, agreeing in large parts with Curtice and Stadtman (2001). Since a preliminary analysis of the phylogenetic affinities of *Dystylosaurus* (see above) further corroborated this referral, a combined OTU was used for the final analysis.

***Supersaurus vivianae* WDC DMJ-021.** WDC DMJ-021 is a reasonably articulated skeleton and represents the most complete specimen of *S. vivianae* (Lovelace et al., 2007). It is not directly

comparable with the holotype, because no scapulacoracoid was found. Nevertheless, based on the overlap with additional material attributed to the holotypic individual (see above; Lovelace et al., 2007), the identification of WDC DMJ-021 as *S. vivianae* has been widely accepted.

***Suuwassea emilieae*, ANS 21122.** *Suuwassea* was initially identified as flagellicaudatan with uncertain affinities to Diplodocidae or Dicraeosauridae (Harris and Dodson, 2004). Further analyses pointed to a closer relationship with the Dicraeosauridae (Whitlock and Harris, 2010; Whitlock, 2011a), which would mean that *Suuwassea* is the only North American representative of this taxon.

***Tornieria africana*, holotype.** The holotype specimen was found at the locality A at Tendaguru, Tanzania (Fraas, 1908; Remes, 2006). *Tornieria* was initially described as *Gigantosaurus africanus* Fraas, 1908, but (Sternfeld, 1911) noted that this generic name was preoccupied, proposing the combination *Tornieria africana* a replacement. Janensch (1922) suggested synonymy of *Tornieria* and *Barosaurus*, resulting in the combination *Barosaurus africanus*, and later referred much more material from various quarries to the same genus (Janensch, 1935, 1961). However, in a reassessment of the entire material, which also resurrected the name *Tornieria africana*, only two or three individuals were positively identified as belonging to *Tornieria* (Remes, 2006). Remes (2006) identified additional material from the same quarry, and most probably from the same individual as the holotype. I therefore follow Remes (2006) by including all the *Tornieria* material found at locality A in the holotypic OTU.

***Tornieria africana*, skeleton k.** A second specimen of *T. africana* comes from the k-quarry at Tendaguru and was the only individual found at that site (Heinrich, 1999; Remes, 2006). Initially relatively complete with semi-articulated vertebral column and numerous appendicular elements, much of it has been lost or was destroyed during World War II (Remes, 2006). For these elements, descriptions and figures in Janensch (1929b) were used to complement the scoring.

Character list

Skull

C1: Premaxillary anterior margin, shape: without step (0); with marked but short step (1); with marked and long step (2) (Upchurch, 1998; Wilson and Sereno, 1998; modified by Carballido et al., 2012b; Fig. 6.1).

Comments. The character describes the presence and development of a horizontal portion of the premaxilla, which lies anterior to the nasal process. The step, when present, is best visible in lateral view. It was initially proposed by Upchurch (1998), who scored the Diplodocoidea as unknown or inapplicable, due to a supposed absence of the ascending process. However, some diplodocoids, (e.g. *Suuwassea*) clearly show a distinction between the anterior main body and the posterior ascending process in dorsal view, where they show an abrupt narrowing (Harris, 2006a; ANS 21122, pers. obs., 2011). Diplodocoidea should therefore be scored as '0'. A third state was added in order to distinguish Brachiosauridae from other macronarian sauropods (Carballido et al., 2012b). The character is treated as ordered, due to the gradual change in morphology.

C2: Premaxilla, external surface: without anteroventrally orientated vascular grooves originating from an opening in the maxillary contact (0); vascular grooves present (1) (Wilson, 2002; Sereno et al., 2007; Fig. 6.2).

Comments. The presence of these grooves was previously found as a synapomorphy of Dicraeosauridae (Whitlock, 2011a; Mannion et al., 2012). However, faint grooves originating at the premaxillary-maxillary contact are also visible in *Nigersaurus* (Sereno et al., 2007) and in some diplodocid specimens. Here they fade anteriorly, shortly after the suture (e.g. in CM 11161, 11162, SMA 0011, USNM 2672). In the present analysis, all of these specimens are scored as apomorphic.

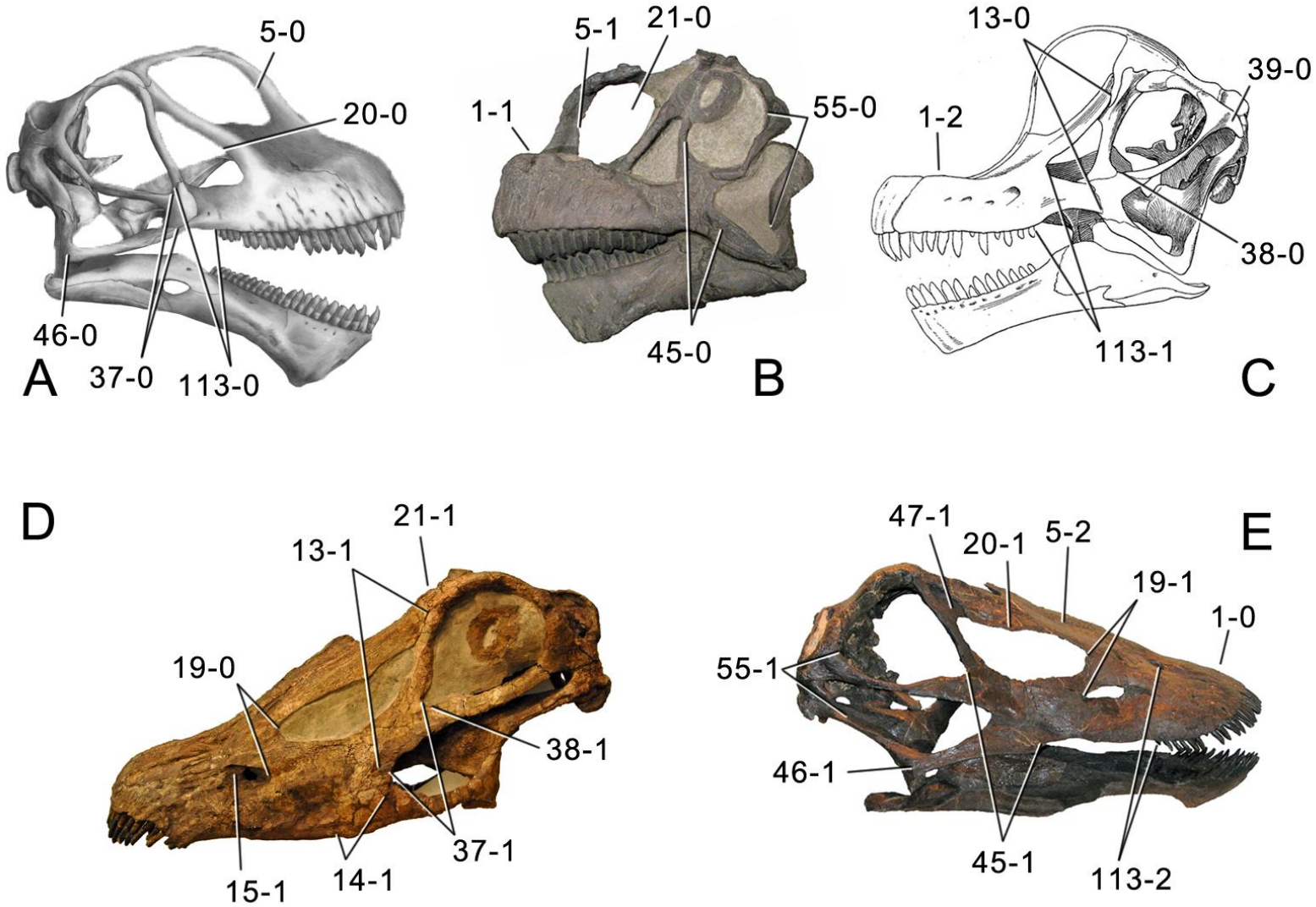

Figure 6.1: Skulls of *Mamenchisaurus youngi* (A; modified from Ouyang and Ye, 2002), *Camarasaurus* sp. USNM 13786 (B; photo from O. Mateus), *Giraffatitan brancai* (C; modified from Janensch, 1935), *Diplodocus* sp. CM 11161 (D), and *Galeamopus shellensis* SMA 0011 (E) in lateral view, illustrating the states of the characters 1, 5, 13, 14, 15, 19, 20, 21, 37, 38, 39, 45, 46, 55, 113. Not to scale.

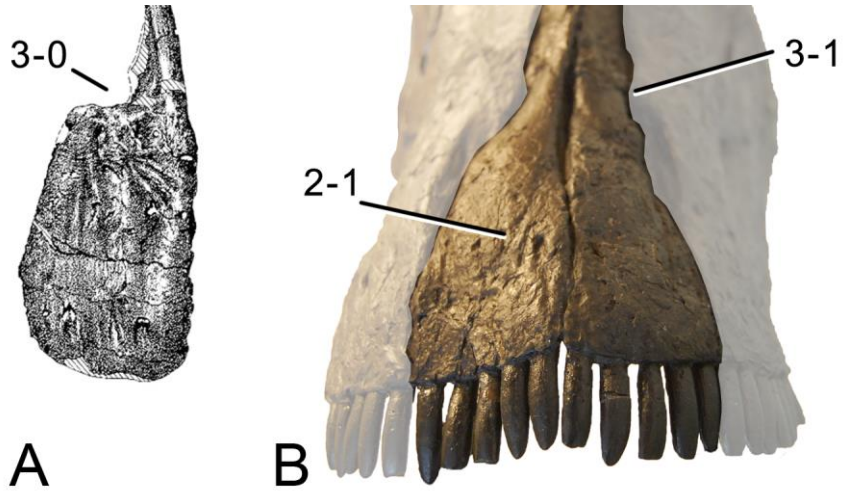

Figure 6.2: Anterior portions of premaxillae of *Camarasaurus* (A; modified from Madsen et al., 1995) and *Galeamopus shellensis* SMA 0011 (B) in anterodorsal view, illustrating the states of characters 2 and 3. Not to scale.

C3: Premaxilla, shape in dorsal view: main body is massive, with proportionally short ascending process distinct (0); single elongate unit, distinction between body and process nearly absent (1) (Upchurch, 1998; wording modified; Fig. 6.2).

Comments. Upchurch (1998) formulated this character differently, based on his interpretation that the ascending process of the premaxilla was absent in Diplodocoidea. As stated above, this is not the case. The wording of the derived state was thus changed accordingly.

C4: Premaxilla, angle between lateral and medial margins of premaxilla as seen in dorsal view: > 40° (0); 17°-40° (1); < 17° (2) (Upchurch, 1999; modified; Tab. 6.4).

Comments. Upchurch (1999) was the first to note significant differences in these angles between diplodocoids (around 10°), nemegtosaurids (18°), and remaining taxa (e.g. *Giraffatitan*, 30°; Upchurch, 1999: fig. 7). He used this character (with two states) as one of several that supported the inclusion of Nemegtosauridae within Diplodocoidea (Upchurch, 1999), a view now falsified by nearly complete finds of new nemegtosaurids that show them to be deeply nested titanosaurians, but with convergences with Diplodocoidea (Wilson, 2002; Curry Rogers, 2005; Zaher et al., 2011). The OTUs included in this dataset were rescored for this character based on figures or on original material. Because the lateral margin is concave to sinuous in most taxa, a straight line was drawn from the anterior-most point of the premaxillary-maxillary contact to the point where the lateral edge curves medially, at the base of the ascending process. The results (Tab. 6.4) indicate that the distribution of the character scores is not as straightforward as previously thought: *Shunosaurus*, as well as some specimens of *Camarasaurus* appear to show similarly narrow angles as *Dicraeosaurus* and *Suuwassea*. A third state was thus added, such that diplodocid and rebbachisaurids OTUs now score in the narrow-most range, and *Mamenchisaurus* and *Jobaria* are classed as significantly wide-angled taxa. Because the plesiomorphic state is state one, the character was left unordered.

C5: Premaxilla, posteroventral edge of ascending process in lateral view: concave (0); straight and dorsally oriented (1); straight, and directed posterodorsally (2) (Whitlock, 2011a; wording modified; Fig. 6.1).

Comments. Whitlock (2011a: p.35) described the character as follows: 'Ascending process of the premaxilla, shape in lateral view: convex (0); concave, with a large dorsal projection (0); sub-rectilinear and directed posterodorsally (1)'. This formulation is misleading and the states overlap with those of character 1, which describes the premaxillary 'step'. Varying morphologies of the ascending process, following the states of Whitlock (2011a), were observed among the included taxa regarding the posteroventral edge of the ascending process – the margin that delimits the nasal opening anteriorly. The description of the character was adapted, reducing the character to only encompass the orientation of the posteroventral edge, thereby avoiding overlap with character 1. The directional terms in the states are meant in relation to a horizontally oriented ventral edge of the maxilla. Since no state is obviously intermediate relative to the other two, the character is unordered.

Table 6.4: Premaxilla, angle between medial and lateral margin in dorsal view.

Taxon	Specimen	Angle	Mean	Reference
Shunosaurus lii	ZG 65430, R	18,2	18	Zheng 1996
	ZG 65430, L	17,9		Zheng 1996
Omeisaurus	T5702, R	30	30	He et al. 1988
Mamenchisaurus	ZDM 0083, R	50,6	54	Ouyang & Ye 2002
	ZDM 0083, L	57,2		Ouyang & Ye 2002
Jobaria tiguidensis	MNN TIG 3-5	63,4	63	Sereno et al. 1999
Camarasaurus	CM 11338	39,5	26	Wilson & Sereno 1998
	SMA 0002, L	20,5		pers. obs.
	DNM 28, R	20,1		Chatterjee & Zheng 2005
	DNM 28, L	18,7		Chatterjee & Zheng 2005
Giraffatitan brancai	MB.R.2181	30	30	Upchurch 1999
Nigersaurus taqueti		4,5	5	Whitlock 2011feeding
Demandasaurus darwini	MDS-RVII 275, R	10,9	11	Torcida Fernandez-Baldor et al. 2011
Dicraeosaurus hansemanni	MB.R.2337, R	23	23	pers. obs.
Suuwassea emilieae ANS 21122	ANS 21122, R	20,7	21	pers. obs.
Apatosaurus louisae CM 11162	CM 11162, R	15,9	16	pers. obs.
	CM 11162, L	15,8		pers. obs.
Kaatedocus siberi SMA 0004	SMA 0004, R	11,6	12	pers. obs.
Galeamopus shellensis AMNH 969	AMNH 969, R	12,6	13	pers. obs.
	AMNH 969, L	14,3		pers. obs.
Diplodocus sp. CM 11161	CM 11161, L	10,3	10	pers. obs.
	CM 11161, R	8,9		pers. obs.
Barosaurus sp. CM 3452	CM 3452, R	9,4	13	pers. obs.
	CM 3452, L	15,8		pers. obs.
Diplodocus sp. USNM 2672	USNM 2672, R	10,8	14	pers. obs.
	USNM 2672, L	17,8		pers. obs.
Galeamopus shellensis SMA 0011	SMA 0011, R	6,5	10	pers. obs.
	SMA 0011, L	13,8		pers. obs.

C6: Premaxilla, posterolateral process and the lateral process of the maxillary, shape: without midline contact (0); with midline contact forming a marked narial depression, subnarial foramen not visible laterally (1) (Wilson and Sereno, 1998; Fig. 6.3).

Comments. Whitlock (2011a) reversed the polarity of this character, due to a more limited outgroup sampling. With the inclusion of *Shunosaurus* (Mannion et al., 2012), the most basal OTU again lacks the midline contact, as is the case in Diplodocoidea. The original phrasing of Wilson and Sereno (1998) is therefore preferred.

C7: Premaxilla, dorsoventral depth of anterior portion: remains the same as posteriorly, or widens gradually (0); widens considerably, and abruptly (1) (Harris, 2006a; Fig. 6.4).

Comments. Harris (2006a) stated this difference as useful to distinguish *Suuwassea* (which retains the same depth) from *Diplodocus* (which widens). A similar, narrow premaxilla is furthermore present in *Kaatedocus* (Tschopp and Mateus, 2012b). The character is difficult to observe in articulated skulls, but single elements do show a significant difference.

C8: Subnarial foramen and anterior maxillary foramen, position: well distanced from one another (0); separated by narrow bony isthmus (1) (Wilson, 2002; Fig. 6.5).

C9: Maxilla, large foramen anterior to the preantorbital fossa, separated by a narrow bony bridge: absent (0); present (1) (Zaher et al., 2011; wording modified; Fig. 6.3).

Comments. Generally, sauropod maxillae are pierced by a number of small foramina anteriorly, probably for innervation or blood supply of the replacement teeth. The foramen described by Zaher et al. (2011) in *Tapuiasaurus*, however is relatively large, and closely attached to the preantorbital fossa. The same is the case in *Dicraeosaurus hansemanni* MB.R.2336 (Janensch, 1935), but not in Diplodocidae.

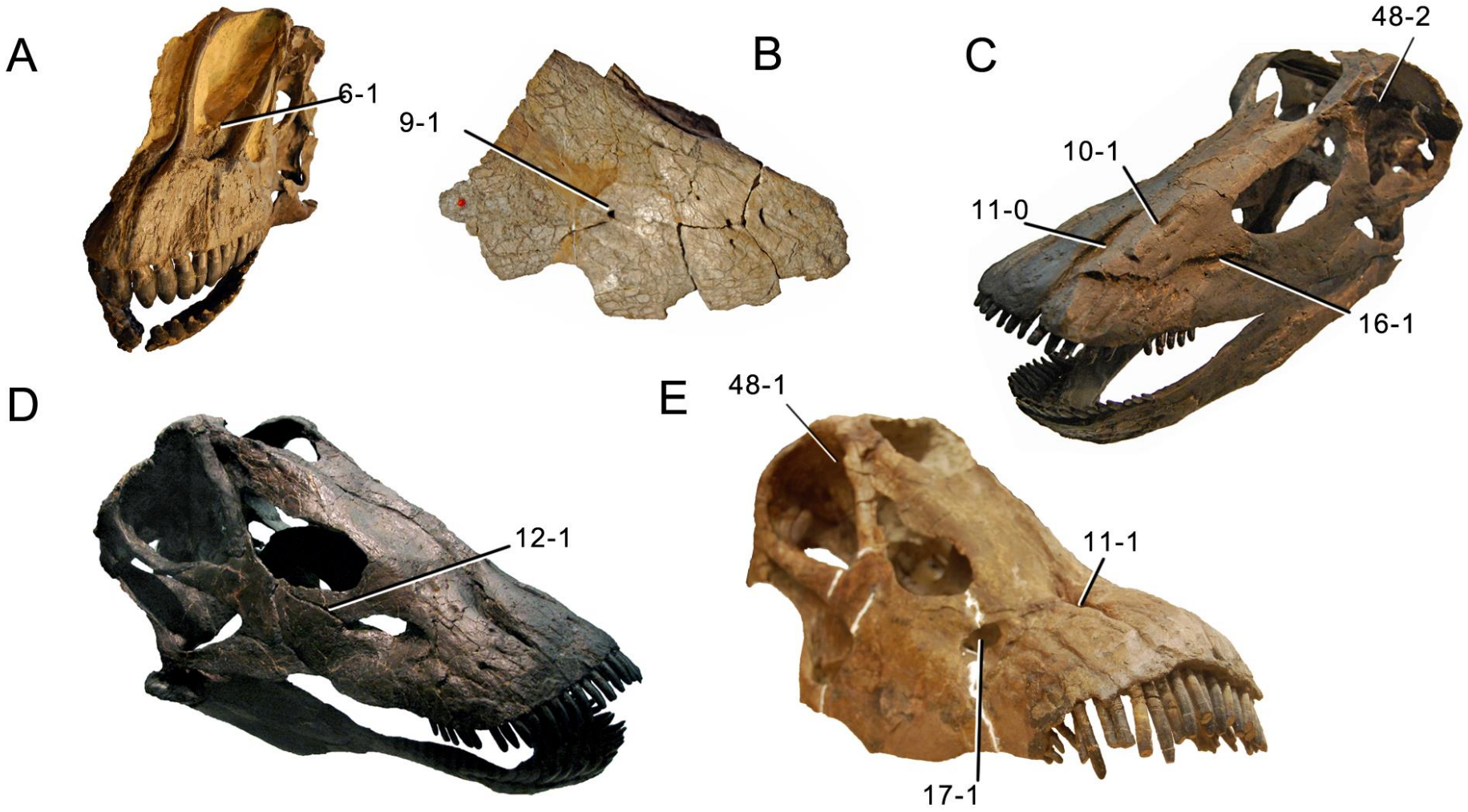

Figure 6.3: Skulls (A, C-E) or maxilla (B) of *Camarasaurus* sp. SMA 0002 (A; photo by O. Mateus), *Dicraeosaurus hansemanni* MB.R.2336 (B), *Kaatedocus siberi* SMA 0004 (C), *Galeamopus shellensis* SMA 0011 (D; photo by O. Mateus), and *Diplodocus* sp. CM 11161 (E) in anterolateral view, illustrating the states of the characters 6, 9, 10, 11, 12, 16, 17, 48. Not to scale.

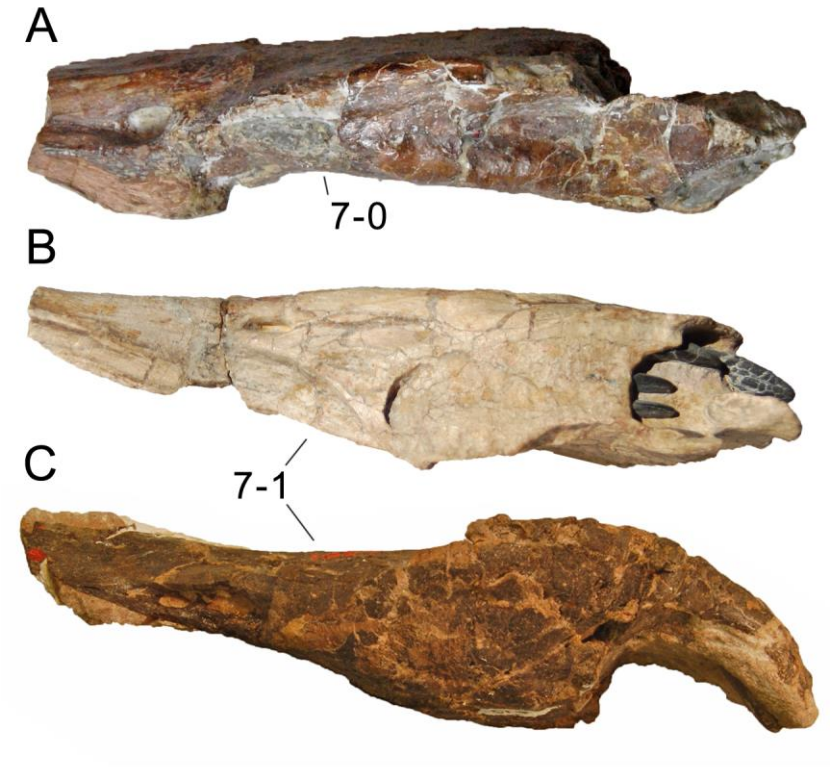

Figure 6.4: Premaxillae of *Suuwassea emilieae* ANS 21122 (A), *Dicraeosaurus hansemanni* MB.R.2337 (B), and *Diplodocus* sp. USNM 2673 (C, left element reversed) in lateral view, illustrating the states of character 7. Not to scale.

C10: Maxilla, large foramen posterior to anterior maxillary foramen, dorsal to preantorbital fossa: absent (0); present (1) (New; Fig. 6.3).

Comments. Few diplodocid specimens show a large foramen posterior to the anterior maxillary foramen (e.g. *Kaatedocus* SMA 0004). This foramen cannot be the same as the one described in character 9, given that both are present in *Dicraeosaurus*.

C11: Anterior maxillary foramen, location: detached from maxillary-premaxillary boundary, facing dorsally (0); lies on medial edge of maxilla, opening medially into the premaxillary-maxillary boundary (1) (New; Fig. 6.3).

Comments. Usually, diplodocids have the subnarial and the anterior maxillary foramina enclosed within a single, elongated fossa at the maxillary-premaxillary boundary (Wilson and Sereno, 1998; Whitlock, 2011b). However, in *Kaatedocus*, the anterior maxillary foramen is detached and laterally positioned, within a unique, small fossa. It thus resembles the plesiomorphic state present in *Jobaria* or *Camarasaurus* (Wilson and Sereno, 1998; Sereno et al., 1999), although it is still much closer to the subnarial foramen. Primitive outgroup taxa (those normally basal to *Jobaria*) were coded as unknown, as it is unclear if the intermaxillary foramen that is present in these taxa (e.g. He et al., 1988; Ouyang and Ye, 2002) is homologous to the anterior maxillary foramen or the subnarial foramen.

C12: Maxilla, canal connecting the antorbital fenestra and the preantorbital fossa: absent (0); present (1) (New; Fig. 6.3).

Comments. Such a canal is only present in SMA 0011, and is thus interpreted as autapomorphy of *Galeamopus shellensis*. Taxa without a preantorbital fossa were scored as unknown in order to avoid absence coding.

C13: Maxilla, dorsal process, posterior extent: anterior to or even with posterior process (0); extending posterior to posterior process (1) (Whitlock, 2011a; Fig. 6.1).

Comments. The character is applied to skulls in lateral view, with the ventral edge of the maxillary oriented horizontally.

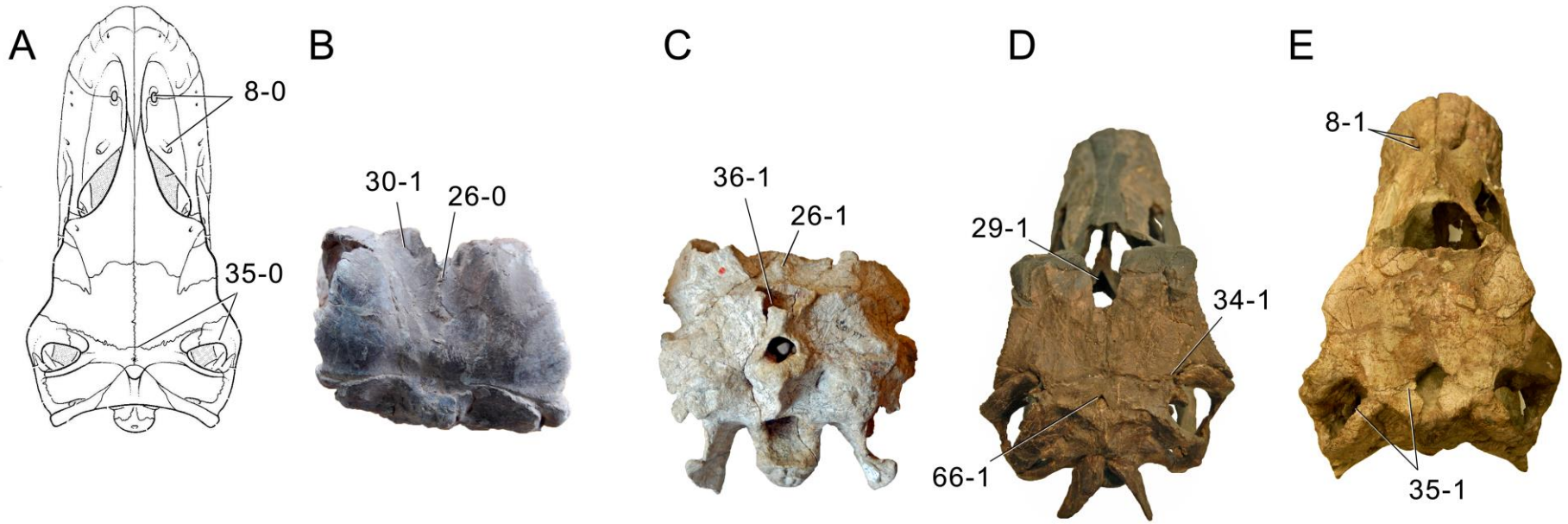

Figure 6.5: Skulls of *Camarasaurus* (A; modified from Wilson and Sereno, 1998), *Limaysaurus tessonei* MUCPv-205 (B; photo by J. Whitlock), *Dicraeosaurus hansemanni* MB.R.2379 (C), *Kaatedocus siberi* SMA 0004 (D) and *Diplodocus* sp. CM 11161 (E) in dorsal view, illustrating the states of the characters 8, 26, 29, 30, 34, 35, 36, 66. Not to scale.

C14: Maxilla-quadratojugal contact: absent or small (0); broad (1) (Yu, 1993; Fig. 6.1).
Comments. Upchurch (1998) reported some difficulties in scoring some taxa to his version of this character, which was defined as a simple absence-presence feature. Reduced, small contacts are present in *Camarasaurus*, but only diplodocids are known to have developed a broad area where the maxilla touches the quadratojugal (Upchurch, 1998; Wilson and Sereno, 1998). Therefore, Whitlock (2011a) redefined the states, such that the apomorphic state now describes a synapomorphy of at least Diplodocidae (it is unknown in Dicraeosauridae and Rebbachisauridae). The derived state appears to be a convergence in some nemegtosaurids (Upchurch, 1998; Wilson, 2005).

C15: Preantorbital fossa: absent (0); present (1) (Tschopp and Mateus, 2012b; Fig. 6.1).
Comments. Although some flagellicaudatan taxa have reduced to entirely closed preantorbital fenestrae, all show a distinct fossa, which is otherwise only present in some nemegtosaurids (Wilson, 2005).

C16: Preantorbital fossa, if present: with relatively indistinct borders (0); dorsally capped by a thin, distinct crest (1) (Wilson, 2002; modified; Fig. 6.3).
Comments. Wilson (2002) originally proposed the presence of a dorsally capped preantorbital fenestra as autapomorphy of *Diplodocus*. A broader survey of this character shows that the absence of this dorsal crest is instead autapomorphic for *Apatosaurus* (within Flagellicaudata). This observation, to date, it is only known from one skull (CM 11162), and thus might represent an autapomorphy of *Apatosaurus louisae* in future.

C17: Preantorbital fenestra: reduced to absent (0); present, occupying at least 50% of the preantorbital fossa (1) (Berman and McIntosh, 1978; Fig. 6.4).
Comments. Upchurch (1995) was the first to use this feature in a phylogenetic analysis. Tschopp and Mateus (2012b) modified the character, and included the dorsal crest as well. However, since these two features are not correlated (*Kaatedocus* has a dorsal crest but a reduced to absent fenestra), the states were adjusted, and a ratio is given to distinguish the small opening in *Dicraeosaurus* from the large ones in *Diplodocus*, for example. Large preantorbital fenestrae are convergently present in nemegtosaurids (Wilson, 2005; Zaher et al., 2011).

C18: Antorbital fenestra, maximum diameter: much shorter than orbital maximum diameter, less than 90% of orbit (0); subequal to orbital maximum diameter, greater than 90% orbit (1) (Yu, 1993; modified; Tab. 6.5).
Comments. Wilson (2002) proposed the character without any clear state boundaries, which were later added by Whitlock (2011a), and changed herein from 85% to 90% in order to have *Mamenchisaurus* within the plesiomorphic state.

C19: Antorbital fenestra, anterior extension: is restricted posterior to preantorbital fossa (0); reaches above preantorbital fossa (1) (New; Fig. 6.1).
Comments. The character has to be scored with the ventral border of the maxilla oriented horizontally. Within flagellicaudatans, the derived state is most developed in *Kaatedocus* SMA 0004, but nemegtosaurids like *Rapetosaurus* have extremely elongated antorbital fenestrae that even reach anterior to the entire preantorbital fossa (Curry Rogers and Forster, 2004).

C20: Antorbital fenestra, shape of dorsal margin: straight or convex (0); concave (1) (Whitlock, 2011a; Fig. 6.1).
Comments. The diplodocid skull AMNH 969 appears to have a convex dorsal margin at first glance. However, the presence of a lateral projection in the upper half of this edge indicates that the convex shape might be due to deformation. The lateral projection in AMNH 969 is at the same location, and has the same shape as the osteological feature producing the concave dorsal edge of the antorbital fenestra in CM 11161. AMNH 969 is thus interpreted to be derived and thus share the flagellicaudatan synapomorphy.

C21: External nares, position: retracted to level of orbit, facing laterally (0); retracted to position between orbits, facing dorsally or dorsolaterally (1) (McIntosh, 1989; Upchurch, 1995; modified by Whitlock, 2011a; Fig. 6.1).
Comments. Upchurch (1995) was the first to include this character in a phylogenetic analysis, based on observations made by McIntosh (1989). Whitlock (2011a) adjusted the state description, since the reduced taxon sampling made a third state redundant (anterior to orbit, the plesiomorphic state in Sauropoda; Upchurch, 1995).

Table 6.5: Antorbital fenestra, maximum diameter/orbit, maximum diameter.

Taxon	Specimen	Ratio	Mean	Reference	Comments
Shunosaurus lii	T5401	0,48	0,48	Zhang 1988	
Omeisaurus	T5702, R	0,48	0,48	He et al. 1988	
Mamenchisaurus	ZDM 0083	0,86	0,86	Ouyang & Ye 2002	
Jobaria tiguidensis		0,61	0,61	Sereno et al. 1999	estimated
Camarasaurus	CM 11338, L	0,58	0,68	Wilson & Sereno 1998	
	SMA 0002, L	0,71		pers. obs.	
	YPM 1905, L	0,64		Madsen et al. 1995	
	USNM 13786, L	0,70		Madsen et al. 1995	
	DNM 975, L	0,76		Madsen et al. 1995	
Giraffatitan brancai	MB.R.2181, R	0,51	0,51	pers. obs.	
Nigersaurus taqueti		1,18	1,18	Sereno et al. 2007	
Apatosaurus louisae CM 11162	CM 11162, R	1,01	1,04	pers. obs.	estimated
	CM 11162, L	1,07		pers. obs.	deformed
Kaatedocus siberi SMA 0004	SMA 0004, L	1,04	1,04	pers. obs.	estimated
Diplodocus sp. CM 11161	CM 11161	1,07	1,07	pers. obs.	
*Barosaurus*sp. CM 3452	CM 3452, R	1,22	1,12	pers. obs.	estimated
	CM 3452, L	1,02		Berman & McIntosh 1978	
Diplodocus sp. USNM 2672	USNM 2672, L	1,31	1,29	pers. obs.	
	USNM 2672, R	1,28		pers. obs.	
Galeamopus shellensis SMA 0011	SMA 0011, R	1,12	1,12	pers. obs.	

C22: External nares, maximum diameter: shorter than orbital maximum diameter (0); longer than orbital maximum diameter (1) (Upchurch, 1995; modified by Wilson and Sereno, 1998).

Comments. Upchurch (1995) initially defined the character states in relation to skull length, but later, Wilson and Sereno (1998) changed them to relate with orbital diameter. The latter has since been widely used and is thus retained here.

C23: Prefrontal, medial margin, shape: without distinct anteromedial projection (0); curving distinctly medially anteriorly to embrace the anterolateral corner of the frontal (1) (New; Fig. 6.6).

Comments. In some basal sauropods, the prefrontal is located entirely anterior to the frontal. These cases are scored as plesiomorphic.

C24: Prefrontal, posterior process size: small, not projecting far posterior of frontal-nasal suture (0); elongate, approaching parietal (1) (Wilson, 2002; Fig. 6.7).

Comments. This character is not as straight-forward as it seems. Care has to be taken that one observes the frontal and prefrontal in exactly perpendicular view. In some reconstructed dorsal views of the skull of *Diplodocus* (Wilson and Sereno, 1998; Whitlock, 2011b), the posterior extension of the prefrontal is remarkable, but this is due to the view, in which the reconstruction is drawn. The frontal slants posteriorly, and more posterior distances therefore appear shorter. In direct dorsal view, differences in distance between taxa diminish. However, the character remains informative: in diplodocids like *Apatosaurus* or *Diplodocus*, the posterior process of the prefrontal almost reaches or surpasses the midlength of the frontal, whereas in Rebbachisauridae or in *Kaatedocus* and *Tornieria*, it remains restricted to about the anterior third (Fig. 6.7).

C25: Prefrontal, posterior process shape: straight (0); hooked (1) (Wilson, 2002; modified; Fig. 6.7).

Comments. As the posterior elongation of the prefrontal, also this character was initially defined in a somewhat ambiguous way (flat/hooked). *Nigersaurus* does have a posteriorly facing, pointed prefrontal. The description 'flat' therefore does not fit very well, and it is replaced by 'straight'. Hooked is herein interpreted to describe a medially curving posterior process, such that its posterior end forms the medial-most extension of the prefrontal.

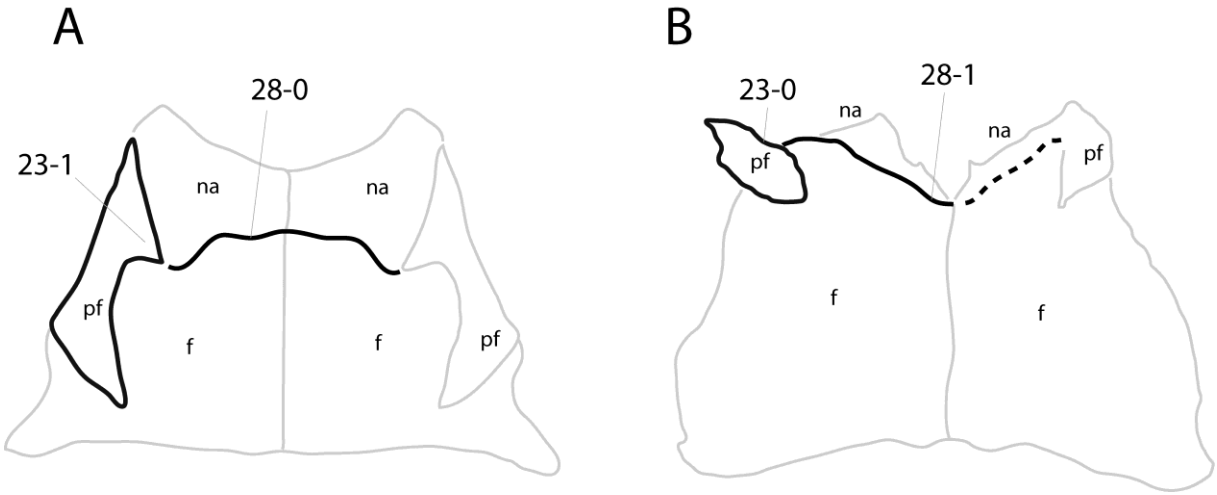

Figure 6.6: Skull roof of *Diplodocus* sp. CM 11161 (A; based on Wilson and Sereno, 1998) and *Limaysaurus tessonei* MUCPv-205 (B; based on Calvo and Salgado, 1995) in dorsal view. Note the anteromedial hook in the prefrontal of CM 11161 (A; C23-1), and the differently shaped frontal-nasal suture (straight to anteriorly bowed in A, C28-0; bowed posteriorly in B, C28-1). Abb.: f, frontal; na, nasal; pf, prefrontal. Scaled to the same skull roof length.

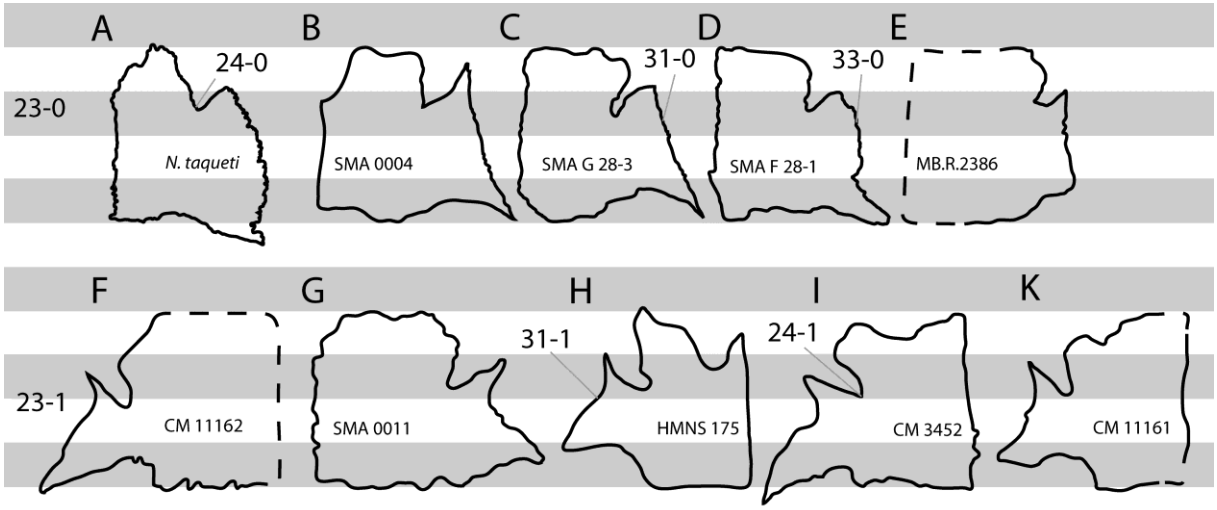

Figure 6.7: Left (F, H-K) and right (A-E, G) diplodocoid frontals in dorsal view, anterior to the front. The upper row shows elements with an anteriorly restricted posterior process of the prefrontal (C23-0), the lower row have elongated posterior processes (C23-1). Additional states are illustrated from the characters 24, 31, 33. Frontals figured in strict perpendicular view, and scaled to the same anteroposterior length.

C26: Frontals, midline contact (symphysis): patent suture (0); fused in adult individuals (1) (Salgado and Calvo, 1992; Yu, 1993; Fig. 6.5).

Comments. Fusion of skull bones is usually considered an ontogenetic feature (Varricchio, 1997; Whitlock et al., 2010). However, the ontogenetic stages, when fusion begins, might still be different between taxa and thus phylogenetically significant. This appears to be the case here, where the braincases of *Dicraeosaurus* and *Amargasaurus* have completely obliterated sutures between the frontals, whereas large-sized diplodocid skulls do not (e.g. CM 11161). Nonetheless, it remains possible that non-dicraeosaurid sauropods fuse their frontals at an old age. In future, it might be helpful to constrict the character to a specific age-range (possibly subadult or early adult), but to date, the exact individual age of the specimens showing the fused frontals remains unknown.

C27: Frontal, anteroposterior length: long, > 1.4 times minimum transverse width (0); short, 1.4 or less times minimum transverse width (1) (Gauthier, 1986; modified; Tab. 6.6).

Comments. This character was widely used in phylogenetic analyses of sauropod dinosaurs (Upchurch, 1998; Wilson, 2002; Whitlock, 2011a; Mannion et al., 2012; Tschopp and Mateus, 2012b),

with varying definitions of the state boundaries. In addition, it was often unclear if minimum or maximum transverse width was intended (e.g. Whitlock, 2011a; Tschopp and Mateus, 2012b). As shown in table 6.6, there are significant differences in the ratios, with more distinct changes when comparing frontal length and minimum transverse width. Therefore, state boundaries were herein defined numerically, which also led to some differential scorings compared to Tschopp and Mateus (2012b). *Kaatedocus*, for example, is now well within the ratios for the apomorphic state.

C28: Frontal-nasal suture, shape: flat or slightly bowed anteriorly (0); v-shaped, pointing posteriorly (1) (Whitlock, 2011a; Fig. 6.6).

Comments. The frontals of *Galeamopus hayi* might have a posteriorly pointing nasal contact as well (Holland, 1906). However, the nasals are not preserved in this specimen, and it seems thus more appropriate to code HMNS 175 as unknown.

C29: Frontals, distinct anterior notch medially between the two elements: absent (0); present (1) (Tschopp and Mateus, 2012b; modified; Fig. 6.5).

Comments. The shape description of the notch was excluded from the character in order to include also *Spinophorosaurus*, and SMA 0011 in the apomorphic state. The frontal usually becomes extremely thin in this part, and it is thus easily broken. Since in these three taxa/specimens, the notch still appears genuine, the character was retained. Tschopp and Mateus (2012b) mentioned this feature as autapomorphy of *Kaatedocus*. Given that a similar notch is present in SMA 0011, this character might actually be more widespread within Diplodocidae. In fact, many specimens (e.g. *Apatosaurus* CM 11162) show broken anteromedial edges in the frontal, which makes it difficult to evaluate this character. Additional, new finds of diplodocid frontals might shed some more light on the distribution of this character.

C30: Frontals, dorsal surface: without paired grooves facing anterodorsally (0); grooves present, extend on to nasal (1) (Whitlock, 2011a; Fig. 6.5).

Comments. Grooves appear to be present on the frontals of the dicraeosaurid *Amargasaurus cazaui* (Salgado and Calvo, 1992: fig. 2B), but these extend onto the prefrontals and not the nasals, and do not extend as far posteriorly as in *Limaysaurus* (J. Whitlock, pers. comm., 2013). *Amargasaurus* is thus scored as plesiomorphic, following Whitlock (2011a).

C31: Frontal, lateral edge in dorsal view: relatively straight (0); deeply concave (1) (New; Fig. 6.7).

Comments. This character has a somewhat ambiguous distribution. There is some difference in the shapes taken together in the plesiomorphic state as well: Rebbachisauridae, in contrast with most other taxa, have a weakly convex lateral frontal edge. Diplodocids exhibit varying shapes: *Apatosaurus* and *Diplodocus* have concave edges, whereas *Kaatedocus* or *Tornieria* have straight margins.

C32: Frontal, contribution to dorsal margin of orbit: less than 1.5 times the contribution of prefrontal (0); at least 1.5 times the contribution of prefrontal (1) (Whitlock, 2011a; modified by Mannion et al., 2012; Tab. 6.7).

Comments. The lengths of the frontal and prefrontal are measured in a straight line in lateral view, from the mid-point of the frontal-prefrontal articulation to the anterior-most (prefrontal) or posterior-most (frontal) point. Whitlock (2011a) proposed the character leaving a gap between plesiomorphic and apomorphic states (subequal, or twice), which was changed by Mannion et al. (2012). A comparative analysis of the included specimens confirms the utility of the boundary proposed by Mannion et al. (2012).

C33: Frontal, free lateral margin: rugose (0); smooth (1) (Tschopp and Mateus, 2012b; Fig. 6.7).

Comments. Rugosities are present around the dorsal margin of almost all sauropods, but in some cases, they are shifted onto the prefrontal or the postorbital. Tschopp and Mateus (2012b) hypothesized that the rugosities served for an attachment of a palpebral element.

C34: Frontal, contribution to margin of supratemporal fenestra/fossa: present (0); absent, frontal excluded from anterior margin of fenestra/fossa (1) (Wilson and Sereno, 1998; Fig. 6.5).

Comments. In the derived state, the frontal is excluded from a contribution to the margin of the supratemporal fenestra by a contact between the medial process of the postorbital and the anterolateral process of the parietal.

Table 6.6: Frontal, length/transverse width.

Taxon	Specimen	ratio (maxW)	mean (maxW)	ratio (minW)	mean (minW)	Reference	Comments
Shunosaurus lii	ZG 65430	1,2	1,2	1,6	1,6	Zheng 1996	based on reconstruction
Spinophorosaurus nigerensis	GCP-CV-4229, R	0,9	1,0	1,2	1,3	Knoll et al. 2012	
	NMB-1698-R, R	1,1		1,3		pers. obs.	
Omeisaurus	T5702, R	0,9	0,9	1,7	1,7	He et al. 1988	real ratios higher, not measured from strictly dorsally
Mamenchisaurus	ZDM 0083	0,8	0,8	1,3	1,3	Ouyang & Ye 2002	based on reconstruction
Jobaria tiguidensis	MNN TIG 3-5	0,9	0,9	1,3	1,3	Sereno et al. 1999	based on reconstruction
Turiasaurus riodevensis	CPT-1211	0,8	0,8	1,0	1,0	Royo-Torres & Upchurch 2012	based on reconstruction
Camarasaurus	DNM 28	0,9	0,9	1,4	1,2	Chatterjee & Zheng 2005	
	CM 11338	0,9		1,1		Wilson & Sereno 1998	based on reconstruction
Giraffatitan brancai	MB.R. S66, R	0,8	0,9	1,0	1,0	Janensch 1935	Ratios probably slightly higher due to incomplete anteromedial tip
		1,0		1,0		Janensch 1935	based on reconstruction
Limaysaurus tessonei	MUCPv-205, L	1,2	1,2	1,5	1,5	J. Whitlock, pers. comm.	
Nigersaurus taqueti		1,3	1,3	1,8	1,8	J. Whitlock, pers. comm.	minimum width measured at anteriormost point of lateral edge
Dicraeosaurus hansemanni	MB.R.2379, L	0,8	0,8	1,0	1,0	Janensch 1935	possibly slightly higher due to breakage of anterior edge, but not much, as indicated by prefrontal
Amargasaurus cazaui	MACN N-15, R	0,4	0,4	0,4	0,4	Salgado & Calvo 1992	
Apatosaurus louisae	CM 11162	CM 11162, L	0,7	0,7	1,0	1,0	J. Whitlock, pers. comm.
Kaatedocus siberi	SMA 0004	SMA 0004, R	1,0	1,1	1,4	1,5	pers. obs.
		SMA 0004, L	1,2		1,5		pers. obs.
Tornieria africana	skeleton k	MB.R.2386, R	0,9	0,9	1,0	1,0	pers. obs.
Diplodocus	sp. CM 11161	CM 11161, L	0,8	0,8	1,2	1,2	pers. obs.
Barosaurus	sp. CM 3452	CM 3452, L	0,9	0,9	1,3	1,3	pers. obs.
Diplodocus	sp. USNM 2672	USNM 2672, L	0,8	0,8	1,1	1,1	Harris 2006a
Galeamopus hayi	HMNS 175	HMNS 175, L	1,0	1,0	1,3	1,3	pers. obs.	based on CT scan on digimorph.org
Galeamopus shellensis	SMA 0011	SMA 0011, R	0,8	0,8	1,0	1,0	pers. obs.
		SMA 0011, L	0,8		1,0		pers. obs.

Table 6.7: Frontal, contribution to orbital margin compared to prefrontal.

Taxon	Specimen	Ratio	Mean	Reference	Comments
Shunosaurus lii	T5401, R	1,7	1,7	Zhang 1988	
Omeisaurus	T5702, R	1,2	1,2	He et al. 1988	based on reconstruction
Mamenchisaurus	ZDM 0083	1,0	1,0	Ouyang & Ye 2002	
Camarasaurus	CM 11338	0,6	0,8	Wilson & Sereno 1998	based on reconstruction
	CM 11338, L	0,2		Madsen et al. 1995	
	SMA 0002, L	0,9		pers.obs.	
	DNM 28, L	1,6		Zheng 1996	
Giraffatitan brancai		1,1	1,1	Wilson & Sereno 1998	based on reconstruction
Limaysaurus tessonei	MUCPv-205, L	2,6	2,6	Calvo & Salgado 1995	
Dicraeosaurus hansemanni	MB.R.2379, L	0,5	0,5	Janensch 1935	
Amargasaurus cazaui	MACN-N 15, R	0,9	1,0	Salgado & Bonaparte 1991	
	MACN-N 15, L	1,0		Salgado 1999	
Apatosaurus louisae CM 11162	CM 11162, L	0,8	0,8	Whitlock & Lamanna 2012	estimated
Kaatedocus siberi SMA 0004	SMA 0004, L	1,9	2,3	pers.obs.	
	SMA 0004, R	2,7			
Diplodocus sp. CM 11161	CM 11161, L	0,9	0,9	pers.obs.	
Barosaurus sp. CM 3452	CM 3452, L	1,1	1,1	Berman & McIntosh 1978	
Diplodocus sp. USNM 2672	USNM 2672, L	1,9	1,4	pers.obs.	possibly too high, sutures not well visible
	USNM 2672, R	0,8		pers.obs.	
Galeamopus hayi HMNS 175	HMNS 175, L	1,0	1,0	Holland 1906	
Galeamopus shellensis SMA 0011	SMA 0011, R	1,4	1,3	pers.obs.	
	SMA 0011, L	1,3		pers.obs.	
Kaatedocus siberi AMNH 7530	AMNH 7530, R	1,7	1,7	pers.obs.	

C35: Frontal-parietal suture, position of medial portion: closer to anterior extension of supratemporal fenestra (0); closer to posterior extension (1) (Tschopp and Mateus, 2012b; modified; Fig. 6.5).

Comments. Tschopp and Mateus (2012b) formulated the character inspired by Remes (2006), who mentioned the position of the fronto-parietal suture as a feature to distinguish *Tornieria* from *Diplodocus*. They used a three-partite character, with an intermediate state close the the central portion of the supratemporal fenestra (Tschopp and Mateus, 2012b). The position of the suture is difficult to assess in some diplodocid specimens, because it describes a strongly sinuous curve (e.g. CM 11161, Fig. 6.7). The character is thus restricted to the medial portion of the suture herein. By doing so, it becomes clear that the majority of *Diplodocus* skulls shifted the suture backwards, whereas all other specimens have it anteriorly located. The posterior dislocation might thus prove to be an autapomorphy of *Diplodocus.* The intermediate state becomes redundant.

C36: Pineal (parietal) foramen between frontals and parietals: present (0); absent (1) (Yu, 1993; modified; Fig. 6.5).

Comments. This character was proposed combined with the presence of a postparietal foramen (Yu, 1993). The two are herein separated in two characters, because *Kaatedocus* SMA 0004 has a postparietal but no pineal foramen (Tschopp and Mateus, 2012b). The presence of a pineal foramen is often difficult to assess due to breakage of the area around the fronto-parietal suture (McIntosh, 1990b; Upchurch et al., 2004a; Harris, 2006a). However, in some specimens, the presence or absence of this feature is genuine, and it thus appears appropriate to include this character. Specimens, where the presence of the foramen has been doubted previously are scored as 'unknown'. At the current state of knowledge, the presence seems to be a retained plesiomorphy characterizing the Dicraeosauridae, but in many diplodocid specimens its presence cannot be dismissed yet.

C37: Orbit, anterior-most point: anterior to the anterior extremity of lateral temporal fenestra (0); roughly even with or posterior to anterior extent of lateral temporal fenestra (1) (Gauthier, 1986; Upchurch, 1995; modified by Whitlock, 2011a; Fig. 6.1).

Comments. The original character was a multistate character (Upchurch, 1995). Given the limited taxon sampling of Whitlock (2011a) and the herein presented analysis, the third state becomes redundant (infratemporal fenestra restricted posterior to orbit).

C38: Orbital ventral margin, anteroposterior length: broad, with subcircular orbital margin (0);

reduced, with acute orbital margin (1) (Wilson and Sereno, 1998; Fig. 6.1).

Comments. The derived state results in a teardrop-shape of the orbit. With the ventral margin of the maxilla held horizontally, the 'ventral margin' would be better described with 'anteroventral corner'.

C39: Postorbital, posterior process: present (0); absent (1) (Wilson, 2002; Fig. 6.1).

Comments. The postorbital is usually a triradiate bone, with a relatively short posterior process that overlaps the squamosal. The latter is absent in rebbachisaurids (Wilson, 2002; Whitlock, 2011a).

C40: Jugal, contribution to antorbital fenestra: very reduced or absent (0); large, bordering approximately one-third of its perimeter (1) (Berman and McIntosh, 1978; Upchurch, 1995; modified by Whitlock, 2011a; Fig. 6.8).

Comments. Recognized as distinctive feature of Diplodocoidea by Berman and McIntosh (1978), the contribution of the jugal to the antorbital fenestra was first used as phylogenetic character by Upchurch (1995). Whitlock (2011a) defined the state boundaries quantitatively.

C41: Jugal, contact with ectopterygoid: present (0); absent (1) (Upchurch, 1995; Fig. 6.9).

Comments. The development of this character is barely known in sauropods. If preserved, the osteology of the palatal complex is often left obscured by matrix due to stability reasons. At the current state of knowledge, the ectopterygoid becomes anteriorly dislocated in Neosauropoda, and contacts the maxilla instead of the jugal. Future CT scanning of additional skulls will yield more detailed results.

C42: Jugal, posteroventral process: short and broad (0); narrow and elongate (1) (New; Fig. 6.8).

Comments. This character shows varying shapes in the skulls traditionally identified as *Diplodocus* (CM 11161 has a short process, whereas in all other skulls they are elongated). However, too few diplodocid jugals are preserved entirely in order to evaluate the distribution of this character to date.

C43: Jugal, dorsal process: present (0); absent (1) (Yu, 1993; polarity inverted; Fig. 6.8).

Comments. Yu (1993) proposed the dorsal process as a synapomorphy for Diplodocidae. However, no jugal is known from dicraeosaurids, and such a process is also present in *Shunosaurus*, *Omeisaurus*, and *Mamenchisaurus* (Janensch, 1935; He et al., 1988; Salgado and Calvo, 1992; Chatterjee and Zheng, 2002; Ouyang and Ye, 2002). Since the latter basal taxa show dorsal processes of the jugal, the character polarity was inverted relative to the original version (Yu, 1993). Although they are scored the plesiomorphic state, Diplodocidae are still distinguishable from *Shunosaurus* and the other taxa by the strong development of the dorsal process, and its anterior displacement. In *Omeisaurus*, e.g., the dorsal process is short and located at midlength of the jugal-lacrimal suture (He et al., 1988).

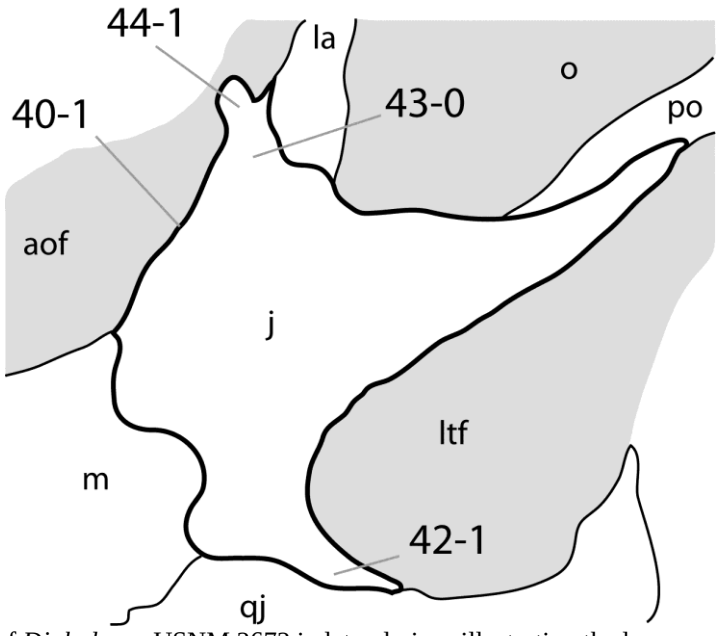

Figure 6.8: Left jugal of *Diplodocus* USNM 2672 in lateral view, illustrating the large contribution of the jugal to the antorbital fenestra (C40-1), the narrow and elongate posteroventral process (C42-1), the dorsal process of the jugal (C43-0), and the anterior spur (C44-1). Abb.: aof, antorbital fenestra; j, jugal; la, lacrimal; ltf, latero-temporal fenestra; m, maxilla; o, orbit; po, postorbital; qj, quadratojugal.

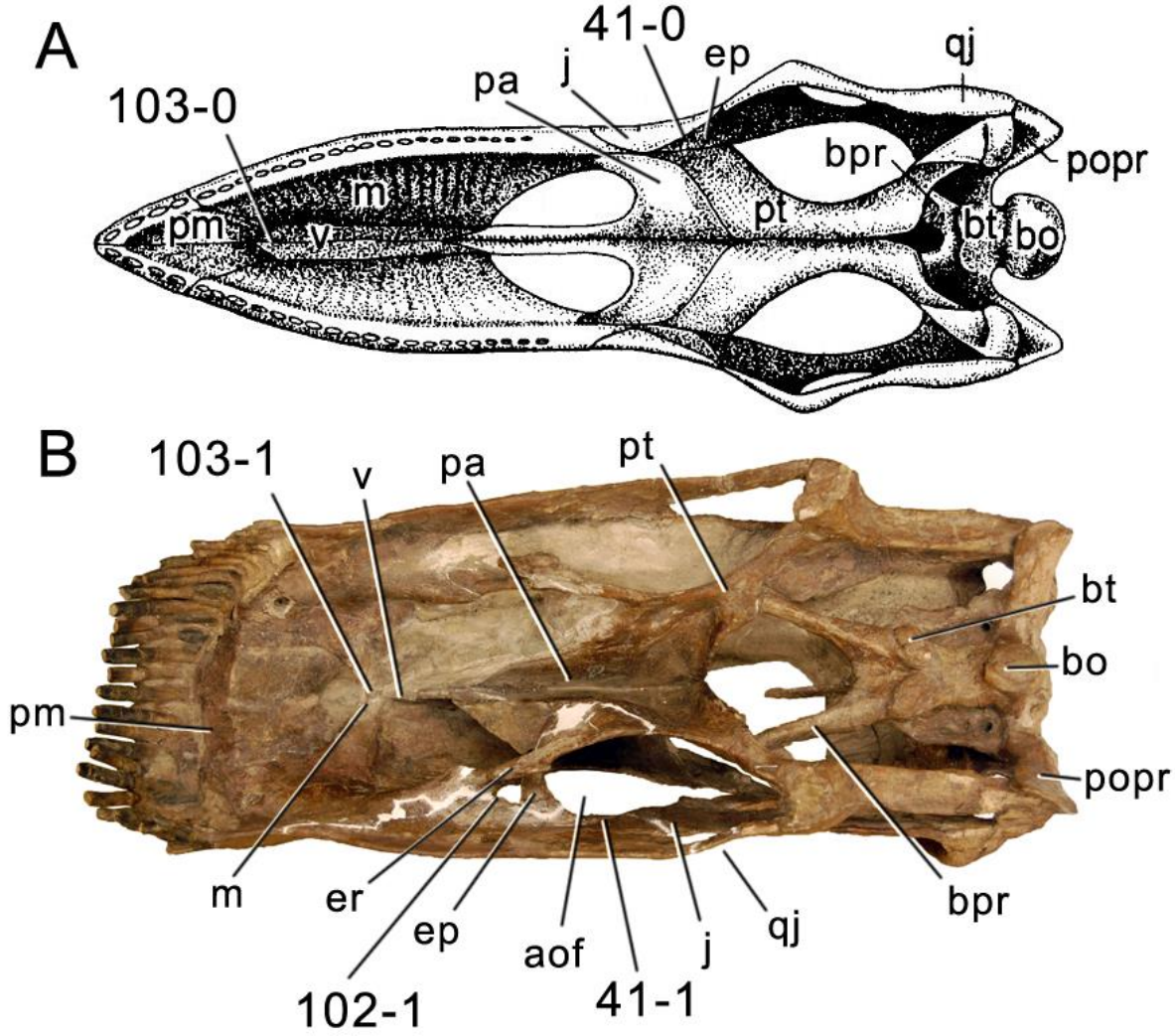

Figure 6.9: Skulls of *Shunosaurus lii* ZG 65430 (A; modified from Chatterjee and Zheng, 2002) and *Diplodocus* sp. CM 11161 (B) in ventral view. Note the anteriorly displaced position of the ectopterygoid ramus of the pterygoid, and the ectopterygoid itself, in *Diplodocus* (B; C41-1 and C102-1), as well as the vomer that articulates with the premaxilla in *Shunosaurus* (A; C103-0), but with the maxilla in *Diplodocus* (B; C103-1). Abb.: aof, antorbital fenestra; bo, basioccipital; bpr, basipterygoid process; bt, basal tuber; ep, ectopterygoid; er, ectopterygoid ramus; j, jugal; m, maxilla; pa, palate; pm, premaxilla; popr, paroccipital process; pt, pterygoid; qj, quadratojugal; v, vomer. Pictures scaled to the same skull length.

C44: Jugal, anterior spur dorsally, which projects into antorbital fenestra: absent (0); present (1) (New; Fig. 6.8).

Comments. Such a spur is present in many diplodocid specimens, although in USNM 2672, it only occurs on the left side (pers. obs., 2011). However, the possibility to develop such a spur still appears to be restricted to Diplodocidae, and the character is thus used in the analysis. USNM 2672 is scored as 'present'.

C45: Quadratojugal, position of anterior terminus: anterior margin of orbit or posteriorly restricted (0); beyond anterior margin of orbit (1) (Whitlock, 2011a; Fig. 6.1).

Comments. The character is coded with the ventral margin of the maxilla held horizontally. State boundaries by Whitlock (2011a): posterior to middle of orbit, anterior margin or beyond) were adjusted because all diplodocoids show strongly elongated anterior processes that end significantly anterior to the orbit. On the other hand, in *Mamenchisaurus* or *Brachiosaurus*, they reach the anterior margin of the orbit (Janensch, 1935; Ouyang and Ye, 2002), which would request a coding as apomorphic when following the description of Whitlock (2011a).

C46: Quadratojugal, angle between anterior and dorsal processes: less than or equal to 90°, so

that the quadrate shaft is directed dorsally (0); greater than 90°, approaching 130°, so that the quadrate shaft slants posterodorsally (1) (Gauthier, 1986; Upchurch, 1995; Fig. 6.1).

Comments. The angle between the quadratojugal processes reach their maximum in the large skulls CM 11161 and 11162. In smaller skulls (of both ontogenetically younger as well as phylogenetically more basal specimens), the angle is of approximately 110° (e.g. *Kaatedocus* SMA 0004, Tschopp and Mateus (2012b), but still clearly in the derived state.

C47: Lacrimal, anterior process: absent (0); present (1) (Wilson, 2002; polarity reversed by Mannion et al., 2013; Fig. 6.1).

Comments. Wilson (2002) initially proposed the character with inverted polarity. This was changed by Mannion et al. (2013), and herein in order to have the chosen outgroups showing the plesiomorphic state. An anterior process is usually interpreted to be absent in diplodocoids. However, SMA 0011 and *Dicraeosaurus* do have one. On the other hand, it is possible that the feature is more widespread among Diplodocoidea, but that the anterior process is obscured by the posterodorsal process of the maxilla. The latter partly overlaps the anterior process of the lacrimal in SMA 0011. The presence of an anterior process of the lacrimal would otherwise be one of the distinguishing characteristics between diplodocoids and nemegtosaurids (Wilson, 2005).

C48: Lacrimal, dorsal portion of lateral edge: flat (0); bears dorsoventrally elongate, shallow ridge (1); bears a dorsoventrally short laterally projecting spur (2) (Tschopp and Mateus, 2012b; Fig. 6.3).

Comments. There is some evidence that this character is ontogenetically controlled (Tschopp and Mateus, 2012b): only small skulls show the laterally projecting spur. The character is retained here in order to test its validity. The character is treated as ordered due to intermediate morphologies.

C49: Quadrate, articular surface shape: quadrangular in ventral view, orientated transversely (0); roughly triangular in shape (1); thin, crescent-shaped surface with anteriorly directed medial process (2) (Whitlock, 2011a; Fig. 6.10).

Comments. The character is treated as ordered as state '1' is intermediate in morphology.

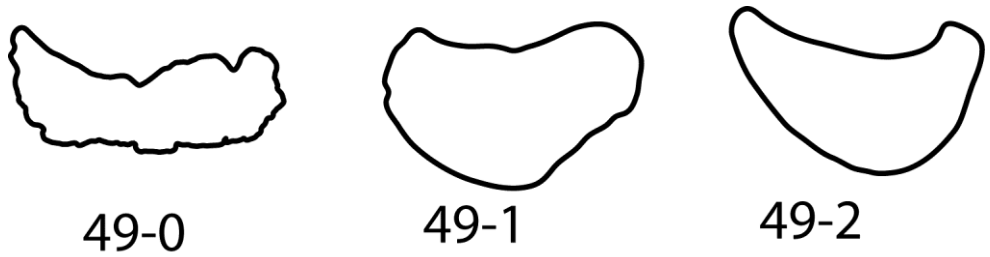

Figure 6.10: Quadrate articular surface shapes of *Camarasaurus* sp. SMA 0002 (left, quadrangular, C49-0), *Suuwassea emilieae* ANS 21122 (center, roughly triangular, C49-1), and *Nigersaurus taqueti* GAD512-7 (right, crescent-shaped, C49-2). Figures of *Suuwassea* and *Nigersaurus* traced from Harris (2006a) and Sereno et al. (2007), respectively.

C50: Quadrate, short transverse ridge medially on posterior side of ventral ramus, close to the articular surface with the lower jaw: absent (0); present (1) (New; Fig. 6.11)

Comments. This ridge is a small detail which appears to be synapomorphic for Diplodocidae. Most of the diplodocid quadrates could not have been investigated in original for this character. Therefore a more detailed evaluation of this character has to be undertaken in order to corroborate the presence or absence of such a ridge, and its taxonomic utility.

C51: Quadrate fossa, depth: shallow (0); deeply invaginated (1) (Russell and Zheng, 1993; Fig. 6.11).

C52: Quadrate, shallow, second fossa medial to pterygoid flange on quadrate shaft (not the quadrate fossa): absent (0); present, becoming deeper towards its anterior end (1) (Tschopp and Mateus, 2012b; wording modified; Fig. 6.12).

Comments. The medial surface of the pterygoid flange is nearly always concave, but concave dorsoventrally. In SMA 0004, as well as some other diplodocid specimens, the second fossa is transversely concave, lies anteriorly on the posterior shaft, medial to where the pterygoid flange originates. There is a chance that the character might be ontogenetic, given that no large-sized skull

has yet been identified to bear this second fossa. The character was slightly reworded from its original version (Tschopp and Mateus, 2012b) in order to describe the location of the fossa better.

C53: Quadrate, dorsal margin: concave, such that pterygoid flange is distinct from quadrate shaft (0); straight, without clear distinction of posterior extension of pterygoid flange (1) (New; Fig. 6.12).

C54: Quadrate, posterior end (posterior to posterior-most extension of pterygoid ramus): short and stocky (0); elongate and slender (1) (New; Fig. 6.12).

C55: Squamosal, anterior extent: restricted to postorbital region (0); extends well past posterior margin of orbit (1); extends beyond anterior margin of orbit (2) (Whitlock, 2011a; Fig. 6.1).

Comments. The anterior extent of the squamosal is measured with the ventral border of the maxilla oriented horizontally. The character is treated as ordered.

C56: Squamosal-quadratojugal contact: present (0); absent (1) (Upchurch, 1995; Fig. 6.13).

Comments. In diplodocids, where no contact is present, the distance between the squamosal and the quadratojugal varies (Whitlock et al., 2010; Whitlock and Lamanna, 2012). However, most of the diplodocid specimens do not preserve the entire anterior ramus of the squamosal (pers. obs., 2011) and it seems thus premature to include the distance as a phylogenetic character.

C57: Squamosal, posteroventral margin: smooth, or with short and blunt ventral projection (0); with prominent, ventrally directed 'prong' (1) (Whitlock, 2011a; modified; Fig. 6.13).

Comments. The original character description of Whitlock (2011a) was modified, and an additional binary character was added (see below) in order to describe better the state in *Kaatedocus*, where a short ventral projection of the squamosal is present.

C58: Squamosal, posteroventral margin: smooth, without ventral projection (0); ventral projection present (1) (Whitlock, 2011a; modified; Fig. 6.13).

Comments. A short projection is present in almost all preserved flagellicaudatan skulls. On the contrary, most non-flagellicaudatan sauropods do have smooth posteroventral margins of the squamosal.

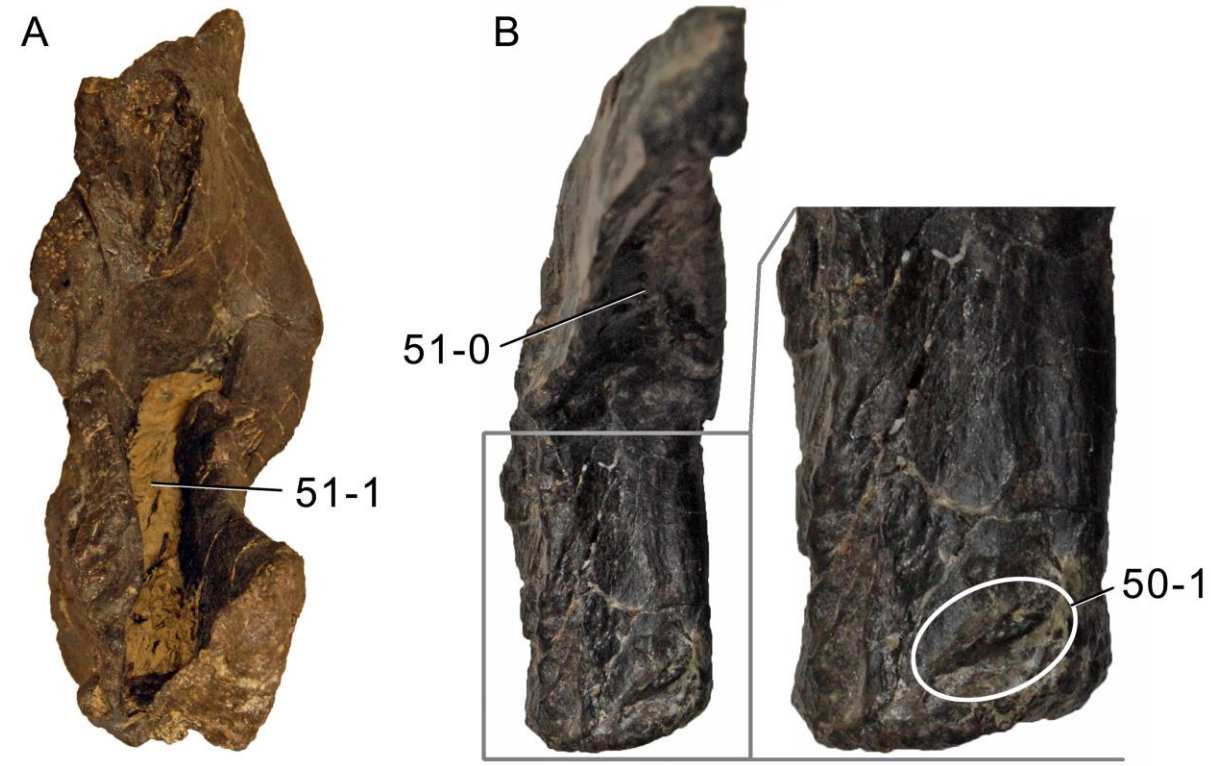

Figure 6.11: Quadrates of *Camarasaurus* sp. SMA 0002 (A) and Diplodocidae indet. SMA D27-7 (B) in posterior view, illustrating the transverse ridge (B, inlet; C50-1), and the deep (A; C51-0) versus shallow (B; C51-1) quadrate fossa. Not to scale.

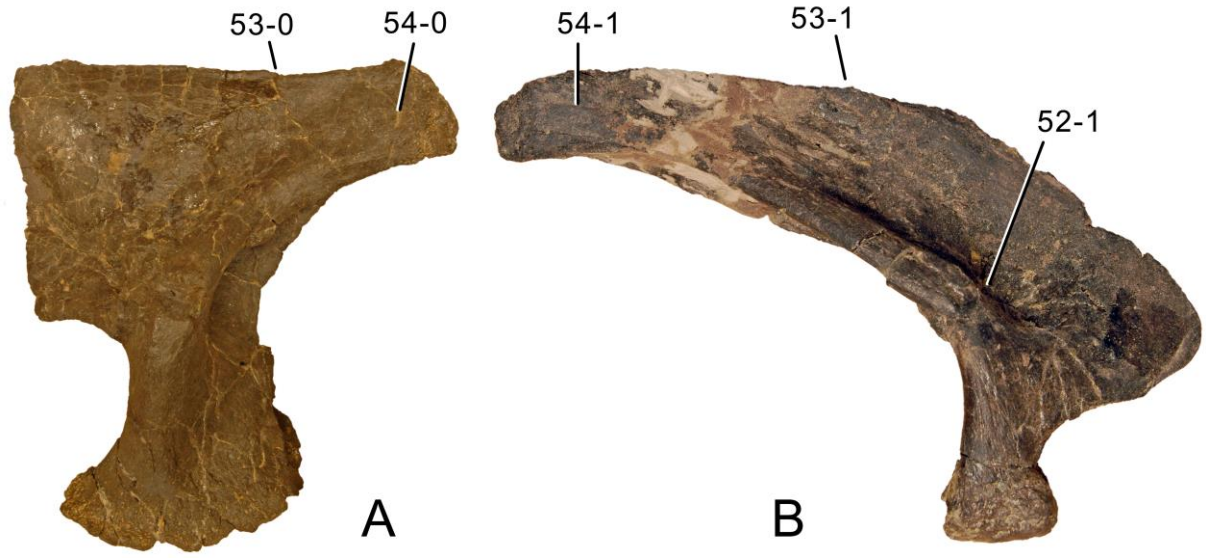

Figure 6.12: Quadrates of *Camarasaurus* sp. SMA 0002 (A) and Diplodocidae indet. SMA D27-7 (B) in medial view, illustrating the second medial fossa (B; C52-1), the shape of the dorsal margin (C53, concave versus convex), and the stocky versus slender posterior ramus (C54). Scaled to the same height.

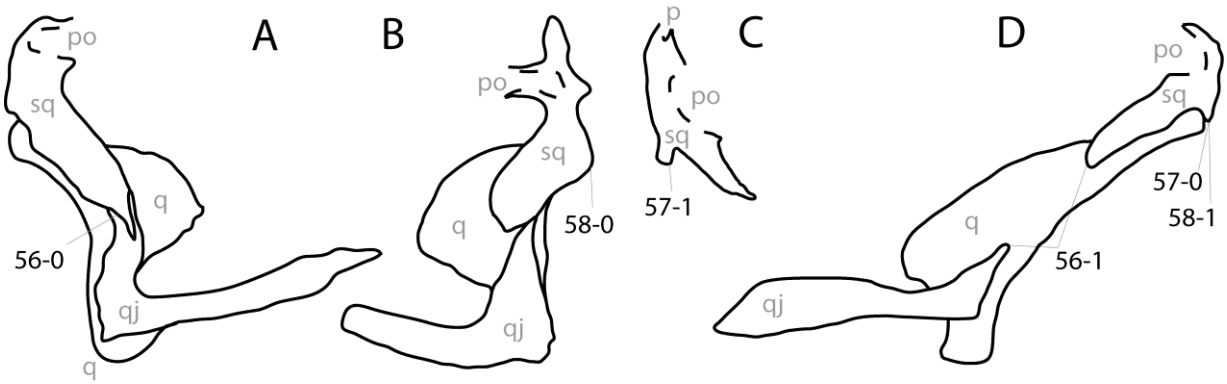

Figure 6.13: Squamosal and adjacent bones in *Mamenchisaurus youngi* (A; traced from Ouyang and Ye, 2002), *Camarasaurus lentus* CM 11338 (B; traced from Madsen et al., 1995), *Amargasaurus cazaui* MACN-N15 (C; traced from Salgado an Bonaparte, 1991), and Diplodocinae indet. CM 3452 (D; traced from a 3D model from L. Witmer), in right (A, C) and left (B, D) lateral view; illustrating the states of the characters 56, 57, and 58. Abb.: po, postorbital; q, quadrate; qj, quadratojugal; sq, squamosal. Not to scale.

C59: Parietal, contribution to post-temporal fenestra: present (0); absent (1) (Wilson, 2002; Fig. 6.14).

Comments. The absence of parietal contribution to the posttemporal fenestra is sometimes difficult to observe due to imperfectly preserved or distorted skulls. All diplodocid skulls have exoccipitals that bear a dorsolateral spur, which forms the dorsomedial end of the posttemporal fenestra (the 'posttemporal process' of Harris, 2006a). Additionally, most of them have dorsally extended distal ends of the paroccipital processes, which curve back towards the exoccipital spur. These two prominences are interconnected by the squamosal in complete diplodocid skulls (CM 11161, pers. obs., 2011).

C60: Parietal, portion contributing to skull roof, anteroposterior length/transverse width: wide, > 50% (0); narrow, 7-50% (1); practically nonexistent, < 7% (2) (New; Tab. 6.8).

Comments. In some taxa, the posterior-most point of the fronto-parietal suture is located posterior to the supratemporal fenestra. The minimum values are compared in this ratio. The character was treated as ordered in the present analysis.

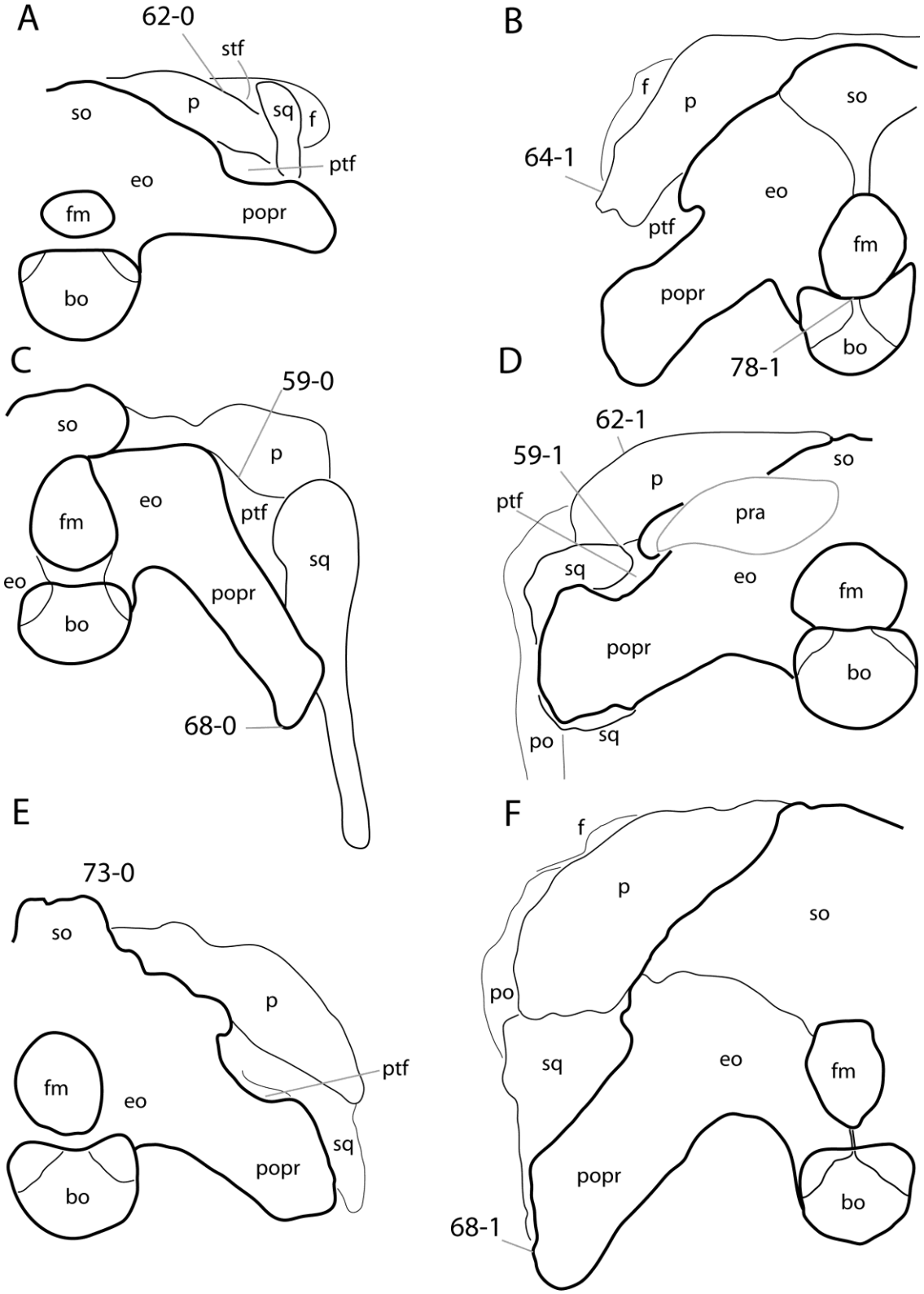

Figure 6.14: Sauropod skulls of *Spinophorosaurus nigerensis* GCP-CV-4229 (A; traced from Knoll et al. 2012); *Suuwassea emilieae* ANS 21122 (B; traced from Harris, 2006a); *Limaysaurus tessonei* MUCPv-205 (C; after Calvo and Salgado, 1995); *Kaatedocus siberi* SMA 0004 (D); *Apatosaurus louisae* CM 11162, (E, reversed); *Diplodocus* sp. CM 11161 (F) in posterior view. Note the participation (C; C59-0) or exclusion (D; C59-1) of the parietal to the posttemporal fenestra; the straight (A; C62-0) or convex (D; C62-1) dorsal edge of the posterolateral process of the parietal; the outwards curve of the distal end of the posterolateral process of the parietal (B; C64-1); the distally expanded (C; C68-0) or straight paroccipital processes (F; C68-1); the dorsally vaulted supraoccipital (E; C73-0); and the narrow contribution of the basioccipital to the dorsal surface of the condyle (B; C78-1). Skulls scaled to the same occipital condyle width.

Table 6.8: Parietal, dorsal portion contributing to skull roof: minimum anteroposterior length/minimum transverse width.

Taxon	Specimen	Ratio	Mean	Reference	Comments
Shunosaurus lii	ZG 65430	1,065	1,06	Zheng 1996	measured from reconstruction
Spinophorosaurus nigerensis	GCP-CV-4229, L	0,592	0,57	Remes et al. 2009	measured from photo
	GCP-CV-4229, R	0,549		Remes et al. 2009	measured from photo
Omeisaurus	T5702, L	0,887	1,17	He et al. 1988	measured from drawing
	T5702, R	1,456		He et al. 1988	measured from drawing
Mamenchisaurus	ZDM 0083, L	1,523	1,35	Ouyang & Ye 2002	measured from drawing
	ZDM 0083, R	1,175		Ouyang & Ye 2002	measured from drawing
Jobaria tiguidensis	MNN TIG 3-5	1,817	1,82	Sereno et al. 1999	measured from reconstruction
Turiasaurus riodevensis	CPT-1211	2,111	2,11	Royo-Torres & Upchurch 2012	measured from reconstruction
Camarasaurus	CM 11338, L	0,140	0,24	Madsen et al. 1995	measured from drawing
	CM 11338, R	0,126		Madsen et al. 1995	measured from drawing
	UUVP 10070, L	0,294		Madsen et al. 1995	measured from drawing
	UUVP 10070, R	0,275		Madsen et al. 1995	measured from drawing
	UUVP 4286, L	0,430		Madsen et al. 1995	measured from drawing
	UUVP 4286, R	0,291		Madsen et al. 1995	measured from drawing
	UUVP 3568, L	0,219		Madsen et al. 1995	measured from drawing
	UUVP 3568, R	0,182		Madsen et al. 1995	measured from drawing
Giraffatitan brancai	MB.R. S66, L	0,306	0,29	Janensch 1935	measured from drawing
	MB.R. S66, R	0,282		Janensch 1935	measured from drawing
Limaysaurus tessonei	MUCPv-205, L	0,040	0,03	J. Whitlock, pers. comm. 2012	measured from photo
	MUCPv-205, R	0,015		J. Whitlock, pers. comm. 2012	measured from photo
Nigersaurus taqueti	L	0,033	0,06	Sereno et al. 2007	measured from 3D model
	R	0,081		Sereno et al. 2007	measured from 3D model
Dicraeosaurus hansemanni	MB.R.2379, L	0,654	0,65	Janensch 1935	measured from drawing
	MB.R.2379, R	0,645		Janensch 1935	measured from drawing
Amargasaurus cazaui	MACN-N 15, L	0,113	0,08	Salgado & Calvo 1992	measured from drawing
	MACN-N 15, R	0,046		Salgado & Calvo 1992	measured from drawing
Suuwassea emilieae ANS 21122	ANS 21122, L	0,184	0,16	pers. obs.	measured from photo
	ANS 21122, R	0,134		pers. obs.	measured from photo
Apatosaurus ajax YPM 1860	YPM 1860, L	0,204	0,20	pers. obs.	measured from photo
Apatosaurus louisae CM 11162	CM 11162, L	0,328	0,32	Berman & McIntosh 1978	measured from photo
	CM 11162, L	0,304		J. Whitlock, pers. comm. 2012	measured from photo
Kaatedocus siberi SMA 0004	SMA 0004, L	0,276	0,31	pers. obs.	measured from photo
	SMA 0004, R	0,353		pers. obs.	measured from photo
Tornieria africana skeleton k	MB.R.2386, R	0,223	0,22	pers. obs.	measured from photo
Diplodocus sp. CM 11161	CM 11161, L	0,145	0,16	pers. obs.	measured from photo
	CM 11161, R	0,165		pers. obs.	measured from photo
Barosaurus sp. CM 3452	CM 3452, L	0,063	0,09	Berman & McIntosh 1978	measured from photo
	CM 3452, R	0,079		Berman & McIntosh 1978	measured from photo
	CM 3452, L	0,157		L. Witmer, pers. comm. 2012	measured from 3D model
	CM 3452, R	0,072		L. Witmer, pers. comm. 2012	measured from 3D model
Galeamopus hayi HMNS 175	HMNS 175, L	0,029	0,03	Holland 1906	measured from drawing
	HMNS 175, R	0,028		Holland 1906	measured from drawing
Galeamopus shellensis SMA 0011	SMA 0011, L	0,085	0,06	pers. obs.	
	SMA 0011, R	0,039		pers. obs.	

C61: Parietal, distance separating supratemporal fenestrae: less than 1.5 times the width of the long axis of the supratemporal fenestra (0); at least 1.5 times the length of the long axis of the supratemporal fenestra (1) (Wilson, 2002; modified by Mannion et al., 2012; Tab. 6.9).

Comments. The original character states of Wilson (2002) left a gap (subequal, or double). The distance between the supratemporal fenestrae in many diplodocid specimens does not reach two times the maximum diameter of the fenestra, which led Mannion et al. (2012) to adjust the state boundaries. Specimens were remeasured where possible (Tab. 6.9), for others scorings of Wilson (2002) or Mannion et al. (2012) were used. The new measurements show that the ratios are often overestimated, and that there seem to be three clusters of taxa (less than one: *Brachiosaurus*, and probably *Mamenchisaurus*, *Omeisaurus*, *Jobaria*, *Turiasaurus*; between one and 1.6 times: *Spinophorosaurus*, *Camarasaurus*, *Kaatedocus*, CM 11161 and 11162; more than 1.6 times, *Suuwassea*, CM 3452, SMA 0011, and probably Rebbachisauridae and Dicraeosauridae). However, a more inclusive study of this character should be performed in order to recognize the most useful state boundaries for phylogenetic analyses. At the moment it seems wisest to stay with the proposed version of Mannion et al. (2012).

Table 6.9: Distance between supratemporal fenestra, compared to maximum diameter of supratemporal fenestra.

Taxon	Specimen	Ratio	Mean	Reference	Comments
Shunosaurus		1	1	Mannion et al., in press	
Spinophorosaurus nigerensis	GCP-CV-4229, R	1,344	1,3	Knoll et al. 2012	measured from picture
Omeisaurus		0,800	0,8	Mannion et al., in press	
Mamenchisaurus		0,700	0,7	Mannion et al., in press	
Camarasaurus	CM 11338	1,309	1,5	Gilmore 1925; Madsen et al. 1995	parietal width measured from drawing in Madsen et al. (1995)
		1,700		Mannion et al., in press	
Giraffatitan brancai	MB.R. t1, R	0,520	0,5	Janensch 1935	
	MB.R. t1, L	0,433		Janensch 1935	
		0,500		Mannion et al., in press	
Suuwassea emilieae ANS 21122	ANS 21122	1,964	2,0	pers. obs.	
Apatosaurus louisae CM 11162	CM 11162	1,294	1,3	pers. obs.	
Kaatedocus siberi SMA 0004	SMA 0004, L	1,416	1,5	pers. obs.	measured from 3D model
	SMA 0004, L	1,370		pers. obs.	
	SMA 0004, R	1,621		pers. obs.	measured from 3D model
	SMA 0004, R	1,537		pers. obs.	
Diplodocus sp. CM 11161	CM 11161, R	1,319	1,4	pers. obs.	
	CM 11161, L	1,406		pers. obs.	
Barosaurus sp. CM 3452	CM 3452, L	1,802	1,9	L. Witmer, pers. comm. 2012	measured from 3D model
	CM 3452, R	1,906		L. Witmer, pers. comm. 2012	measured from 3D model
Galeamopus shellensis SMA 0011	SMA 0011, L	1,981	1,8	pers. obs.	
	SMA 0011, R	1,635		pers. obs.	

C62: Parietal, posterolateral process, dorsal edge in posterior view: straight, and ventrolaterally oriented, so that the supratemporal fenestra is slightly facing posteriorly as well (0); convex, so that the postorbital and thus the supratemporal fenestra are not visible (1) (Tschopp and Mateus, 2012b; Fig. 6.14).

Comments. The posterior view of the skull corresponds to the view parallel to the long axis of the occipital condylar neck, which is thought to be oriented as the lateral semicircular canal, thus indicating the neutral head position (Schmitt, 2012).

C63: Parietal, occipital process, dorsoventral height: low, subequal to less than the diameter of the foramen magnum (0); high, nearly twice the diameter of the foramen magnum (1) (Wilson, 2002; modified; Tab. 6.10).

Comments. Measurements are taken in strict posterior view (see above). Height is measured vertically between the dorsal-most and ventral-most extension of the occipital process, and the foramen magnum. In case of the occipital process, the dorsal- and ventral-most points are usually transversely shifted against each other. The measurement are therefore taken between horizontal lines intersecting the extremes. The state boundaries are tentatively set at 1.5, but more inclusive analyses would have to be undertaken in order to score this character adequately.

C64: Parietal, occipital process, distal end: ventrolaterally oriented, such that dorsolateral edge is straight or convex (0); curving laterally, such that dorsolateral edge becomes concave distally (1) (New; Fig. 6.14).

Comments. The distal end of the posterolateral process of the parietal of non-diplodocine flagellicaudatans curves outwards to meet the squamosal. This is not the case in the diplodocine skulls examined for this analysis.

C65: Parietal, distinct horizontal ridge separating dorsal from posterior portion: absent, transition more or less confluent (0); present, creating a distinct nuchal fossae below the ridge (1) (Tschopp and Mateus, 2012b; wording modified; Fig. 6.15).

Comments. This character is best observable in oblique posterolateral view, if one does not have the specimens at hand. In the derived state, the transverse ridge caps the nuchal fossa dorsally, creating a distinct concavity below it. Given that small skulls appear to have this feature most expressed (AMNH 7530, CM 3452, SMA 0004), there is some possibility that the nuchal fossae become shallower during ontogeny.

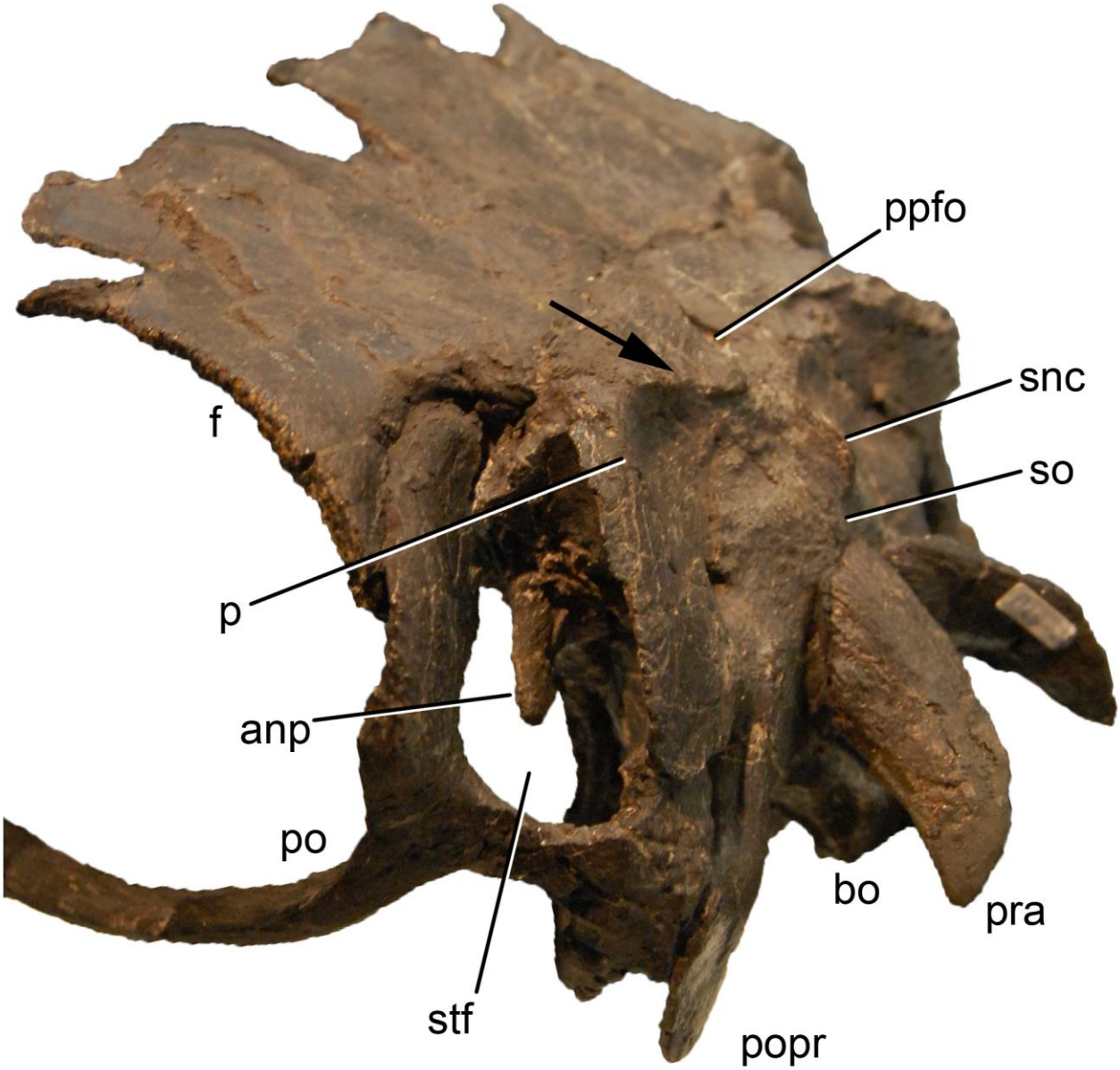

Figure 6.15: Transverse ridge of the parietal (arrow, C65-1) of *Kaatedocus siberi* SMA 0004 in posterolateral view. Abb.: anp, antotic process; bo, basioccipital; f, frontal; p, parietal; ppfo, postparietal foramen; po, post-orbital; popr, paroccipital process; pra, proatlas; snc, sagittal nuchal crest; so, supraoccipital; stf, supratemporal fenestra.

C66: Postparietal foramen: absent (0); present (1) (Upchurch, 1995; Fig. 6.5).

Comments. Postparietal foramina have been interpreted to be a dicraeosaurid synapomorphy (Whitlock, 2011a), but were recently shown to be present as well in Diplodocidae (Tschopp and Mateus, 2012b). The opening is located at the posteromedial corner of the two parietals, where they meet the supraoccipital. It might be associated with a vertical groove internally on the supraoccipital (Remes, 2006; see below), but additional CT studies would have to be performed in order to check for the presence or absence of this groove in specimens without the postparietal foramen. Many diplodocid specimens are damaged in this region of the skull, which makes it difficult to verify the presence of the foramen, and impedes an evaluation of its distribution among flagellicaudatans. The definitive presence in *Kaatedocus*, and the unknown state in the two *Apatosaurus* skulls CM 11162 and YPM 1860 (due to crushing, pers. obs.), indicates that it might be plesiomorphic for Flagellicaudata, subsequently lost in *Tornieria* and *Diplodocus*.

Table 6.10: Dorsoventral height of posterolateral, occipital process of parietal/height of foramen magnum.

Taxon	Specimen	Ratio	Mean	Reference	Comments
Shunosaurus lii	ZG 65430, L	0,855	0,8	Chatterjee & Zheng 2002	measured on reconstruction
	ZG 65430, R	0,700		Chatterjee & Zheng 2002	measured on reconstruction
Spinophorosaurus nigerensis	GCP-CV-4229	1,875	1,9	Knoll et al. 2012	measured on figure
Omeisaurus	T5702, R	5,131	5,1	He et al. 1988	measured from drawing, deformed
Mamenchisaurus	ZDM 0083, R	1,659	1,4	Ouyang & Ye 2002	measured from drawing
		1,100		Mannion et al., in press	
Turiasaurus riodevensis	CPT-1211	1,720	1,7	Royo-Torres & Upchurch 2012	measured on reconstruction
Camarasaurus	UUVP 4286, L	1,558	1,5	Madsen et al. 1995	measured from drawing
	UUVP 4286, R	1,379		Madsen et al. 1995	measured from drawing
	CM 11338, R	1,907		Madsen et al. 1995	measured from drawing
		1,300		Mannion et al., in press	
Giraffatitan brancai	MB.R. S66, R	1,094	1,1	Janensch 1935	measured from drawing
		1,100		Mannion et al., in press	
Brachiosaurus altithorax	USNM 5730, R	1,712	1,7	Carpenter & Tidwell 2001	measured from photo
Limaysaurus tessonei	MUCPv-205, L	0,915	0,9	Calvo & Salgado 1995	measured from drawing
	MUCPv-205, R	0,840		Calvo & Salgado 1995	measured from drawing
Nigersaurus taqueti	L	0,803	0,8	Sereno et al. 2007	measured from 3D model
	R	0,792		Sereno et al. 2007	measured from 3D model
Dicraeosaurus hansemanni	MB.R.2379, L	1,897	2,0	pers. obs.	
	MB.R.2379, R	2,129		pers. obs.	
Amargasaurus cazaui	MACN-N 15, R	1,360	1,4	Salgado & Calvo 1992	measured from drawing
Suuwassea emilieae ANS 21122	ANS 21122, L	1,947	1,9	Harris 2006cranial	measured from photo, parietal incomplete
	ANS 21122, R	1,824		Harris 2006cranial	measured from photo, parietal incomplete
Apatosaurus louisae CM 11162	CM 11162, L	1,365	1,4	pers. obs.	
Kaatedocus siberi SMA 0004	SMA 0004, L	1,750	1,6	pers. obs.	
	SMA 0004, R	1,500		pers. obs.	
Tornieria africana skeleton k	MB.R.2386, L	1,444	>1.4	Janensch 1935	measured from drawing, parietal incomplete
Galeamopus shellensis AMNH 969	AMNH 969, L	2,388	2,6	Holland 1906	measured from photo
	AMNH 969, R	2,837		Holland 1906	measured from photo
Diplodocus sp. CM 11161	CM 11161	1,762	1,8	pers. obs.	
Barosaurus sp. CM 3452	CM 3452, L	1,426	1,6	L. Witmer, pers. comm. 2012	measured from 3D model
	CM 3452, R	1,752		L. Witmer, pers. comm. 2012	measured from 3D model
Galeamopus hayi HMNS 175	HMNS 175, R	1,434	1,4	Digimorph	measured from 3D model
Galeamopus shellensis SMA 0011	SMA 0011, L	1,588	1,6	pers. obs.	
	SMA 0011, R	1,618		pers. obs.	

C67: Paroccipital process (popr), posterior face: smooth/flat (0); with longitudinal ridge along popr body extending from dorsomedial to ventrolateral corners (1) (Tschopp and Mateus, 2012b; Fig. 6.16).

Comments. Most of the specimens examined have a slightly convex posterior face of the paroccipital processes. However, few have such a distinct ridge as is present in *Kaatedocus*. In the latter, this ridge is accompanied by a rugose area at its dorsomedial origin. None of these structures are present in CM 11161, for example.

C68: Paroccipital process distal terminus: expanded vertically (0); not expanded (dorsal and ventral edges are subparallel) (1) (Upchurch, 1998; modified; Fig. 6.14).

Comments. Upchurch (1998) included two morphologies in one character: the dorsoventral expansion, and the rounded or straight distal edge. The shape of the distal edge is difficult to assess qualitatively, as many specimens have slightly convex, or somewhat triangular lateral ends of the paroccipital process (e.g. *Suuwassea* ANS 21122, or *Kaatedocus* SMA 0004, Fig. 6.14). Therefore, the character description was limited to the distal expansion.

C69: Paroccipital process, distal end in lateral view: straight (0); curved (1) (New; Fig. 6.17).

Comments. Due to the slight posteriorly orientation of the paroccipital processes in many sauropod taxa, a strict lateral view of the skull does often not allow for an accurate coding of this character. Also, on pictures of articulated skulls it is often difficult to see the distal end of the paroccipital process well enough, because it is partly obscured by the squamosal. In most cases, a posterolateral instead of lateral view would thus be more helpful.

C70: Supratemporal fenestra: present, relatively large (anteroposterior diameter is at least 5% of occiput width) (0); absent, or greatly reduced (so that anteroposterior diameter is less than 5% of occipital width) (1) (Wilson, 2002; modified by Mannion et al., 2012).

Comments. Wilson (2002) proposed this feature as present/absent character, but Mannion et al. (2012) showed that one of Wilson's (2002) derived taxa (*Limaysaurus*) actually has a supratemporal fenestra, although an extremely reduced one. Since this is a derived state of Rebbachisauridae, and all diplodocid skulls show large openings, no additional measuring was done for this analysis.

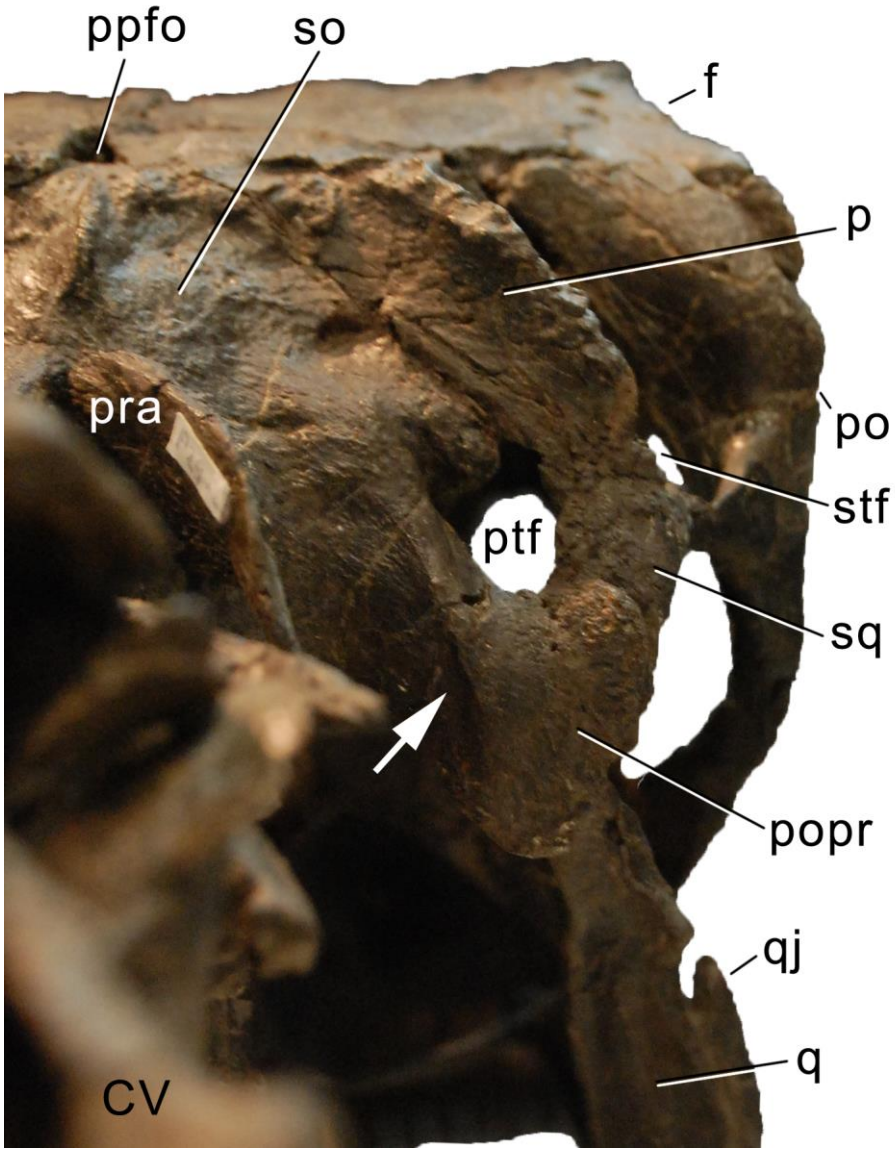

Figure 6.16: Oblique ridge on paroccipital process (arrow, C67-1) of *Kaatedocus siberi* SMA 0004 in posterior view. Abb.: CV, cervical vertebrae; f, frontal; p, parietal; ppfo, postparietal foramen; po, postorbital; popr; paroccipital process; pra, proatlas; ptf, post-temporal fenestra; q, quadrate; qj, quadratojugal; so, supraoccipital; sq, squamosal; stf, supratemporal fenestra.

C71: Supratemporal fenestra, maximum diameter: more than 1.2 times greatest diameter of foramen magnum (0); less than 1.2 times the greatest length of foramen magnum (1) (Yu, 1993; modified by Mannion et al., 2012).

Comments. Mannion et al. (2012) introduced the quantitative state boundaries to the original description (Yu, 1993). Basically, this character is an extension of the previous one, with the exception that *Nigersaurus* is impossible to score due to the complete absence of the supratemporal fenestra in this taxon. In addition to *Limaysaurus*, the quantitative boundaries of Mannion et al. (2012) also include the dicraeosaurids *Dicraeosaurus* and *Amargasaurus*, which have reduced supratemporal fenestra as well, but not to the extent shown by Rebbachisauridae. As stated above, the difference in relative size of the supratemporal fenestrae between the mentioned taxa and Diplodocidae is large, and thus no additional measurements were taken in order to test the boundaries proposed by Mannion et al. (2012).

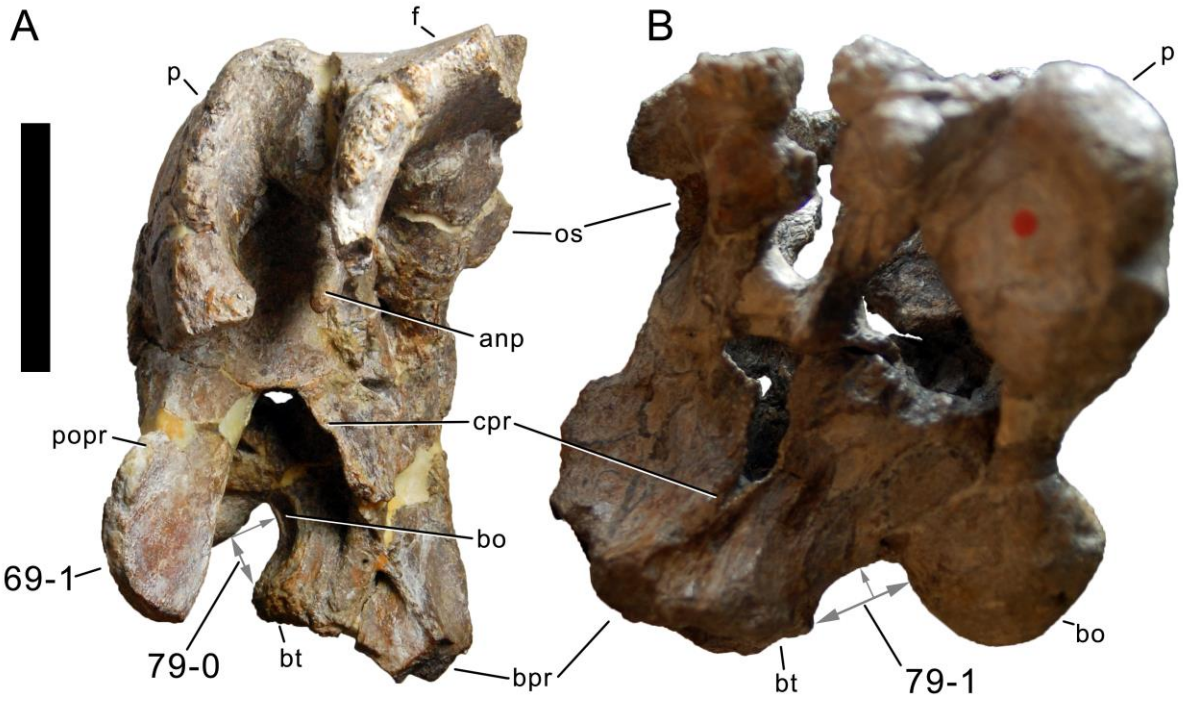

Figure 6.17: Braincase of *Suuwassea emilieae* ANS 21122 (A) and *Tornieria africana* MB.R.2386 (B) in right (A) and left (B) lateral view, illustrating the curved lateral end of the paroccipital process (A; C68-1), and the short (A; C79-0) and elongate basioccipital (B; C79-1). Abb.: anp, antotic process; bo, basioccipital; bpr, basipterygoid process; bt, basal tuber; cpr, crista prootica; f, frontal; os, orbitosphenoid; p, parietal; popr, paroccipital process. Scale bar = 5 cm.

C72: Supraoccipital, anterodorsal margin: internally concave, associated with a channel extending ventrally on the internal face (0); straight (1) (Remes, 2006; Fig. 6.18).

Comments. The channel was proposed by Remes (2006) as a distinguishing character between *Tornieria* and Dicraeosauridae, where the presence of the canal is coupled with the presence of a postparietal fenestra. However, as shown in *Kaatedocus*, these two features are not necessarily correlated. A separate coding for the two characters is thus justifiable. This is the first analysis to include this character.

C73: Supraoccipital, dorsal extension: high and vaulted, such that the dorsolateral edges are strongly sinuous (0); low, with the dorsolateral edges straight (1) (Remes, 2006; Fig. 6.14).

Comments. Remes (2006) used this character in order to distinguish *Tornieria* from *Apatosaurus*, but did not include it into his phylogenetic analysis. The present analysis is thus the first one to do so.

C74: Supraoccipital: sagittal nuchal crest: broad, weakly developed (0); narrow, sharp, and distinct (1) (Whitlock, 2011a; Fig. 6.19).

Comments. The nuchal crest lies on the midline of the supraoccipital, extending dorsoventrally. A narrow, sharp crest was previously thought to be a synapomorphy for Dicraeosauridae, but Tschopp and Mateus (2012b) showed that it also occurs in certain diplodocids.

C75: Supraoccipital, foramen close to contact with parietal: absent (0); present (1) (Tschopp and Mateus, 2012b; Fig. 6.19).

Comments. This foramen is called external occipital foramen by Balanoff et al. (2010), and is sometimes located entirely on the supraoccipital (*Dicraeosaurus hansemanni* MB.R.2379, Janensch, 1935), and in other cases on the suture with the parietal (*Kaatedocus siberi* SMA 0004, pers. obs., 2010). Only taxa with well visible foramina are coded as apomorpic.

C76: Crista prootica, size: rudimentary (0); expanded laterally into dorsolateral process (1) (Salgado and Calvo, 1992; Upchurch, 1995; Fig. 6.20).

Comments. Although diplodocids have a laterally protruding crista prootica (e.g. SMA 0011), only dicraeosaurids develop distinct lateral processes at the anteroventral ends of the crista prootica.

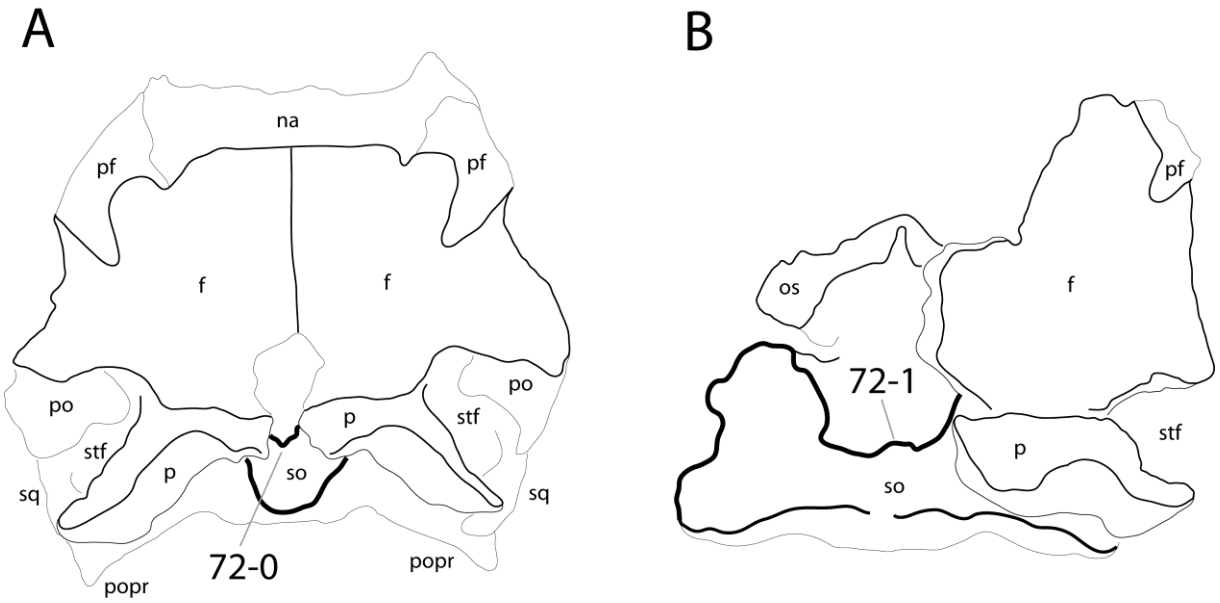

Figure 6.18: Braincase of *Diplodocus* sp. CM 11161 (A) and *Tornieria africana* MB.R.2386 (B) in dorsal view. Note the concave anterior margin of the supraoccipital in *Diplodocus* (A; C72-0), in contrast to the convex edge of *Tornieria* (B; C72-1). The left frontal of MB.R.2386 is lacking. Abb.: f, frontal; na, nasal; os, orbitosphenoid; p, parietal; pf, prefrontal; po, postorbital; popr, paroccipital process; so, supraoccipital; sq, squamosal; stf, supratemporal fenestra. Not to scale.

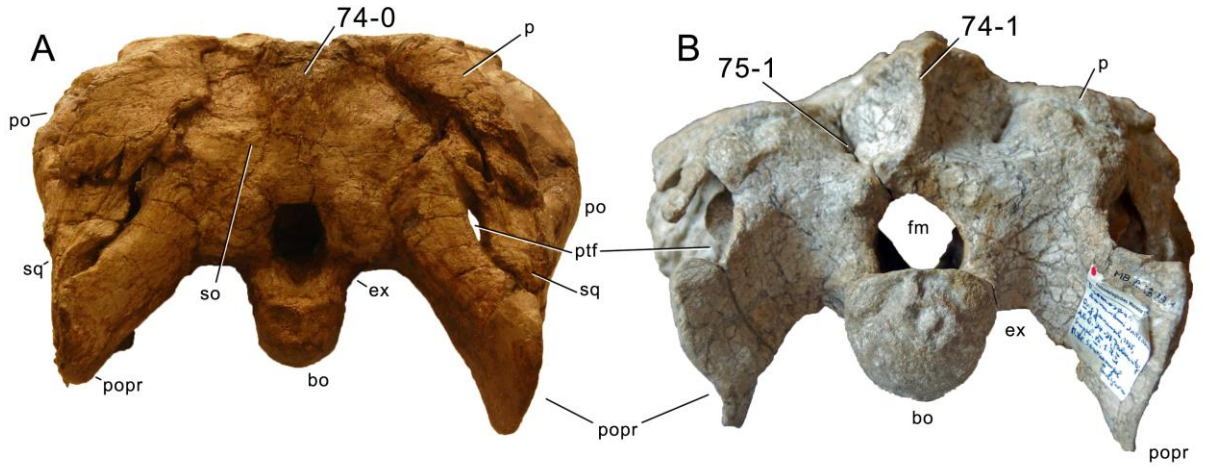

Figure 6.19: Skulls of *Diplodocus* sp. CM 11161 (A) and *Dicraeosaurus hansemanni* MB.R.2379 (B) in posterior view, illustrating the development of the sagittal nuchal crest (C74), and the supraoccipital foramina (C75). Abb.: bo, basioccipital; ex, exoccipital; fm, foramen magnum; p, parietal; po, postorbital; popr, paroccipital process; ptf, post-temporal fenestra; so, supraoccipital; sq, squamosal. Skulls scaled to the same skull width.

C77: Occipital condyle, articular surface: well offset from condylar neck (0); continuously grading into condylar neck (1) (New; Fig. 6.21).

Comments. Whereas in more basal sauropods the articular surface of the occipital condyle is usually well delimited, and offset from the condylar neck by a distinct ridge, diplodocids generally do not have such a clear distinction. The character states are most easily distinguished in dorsal view.

C78: Basioccipital, contribution to dorsal side of occipital condylar neck: present and broad, around 1/3 of entire dorsal side (0); reduced to absent (1) (Harris and Dodson, 2004; Fig. 6.14).

Comments. Harris and Dodson (2004) proposed the narrow contribution of the basioccipital to the dorsal face of the occipital condyle as characteristic for *Suuwassea*. A wider survey of the distribution of this character showed that the contribution of the basioccipital to the dorsal side of the occipital condylar neck is reduced in some diplodocid taxa as well.

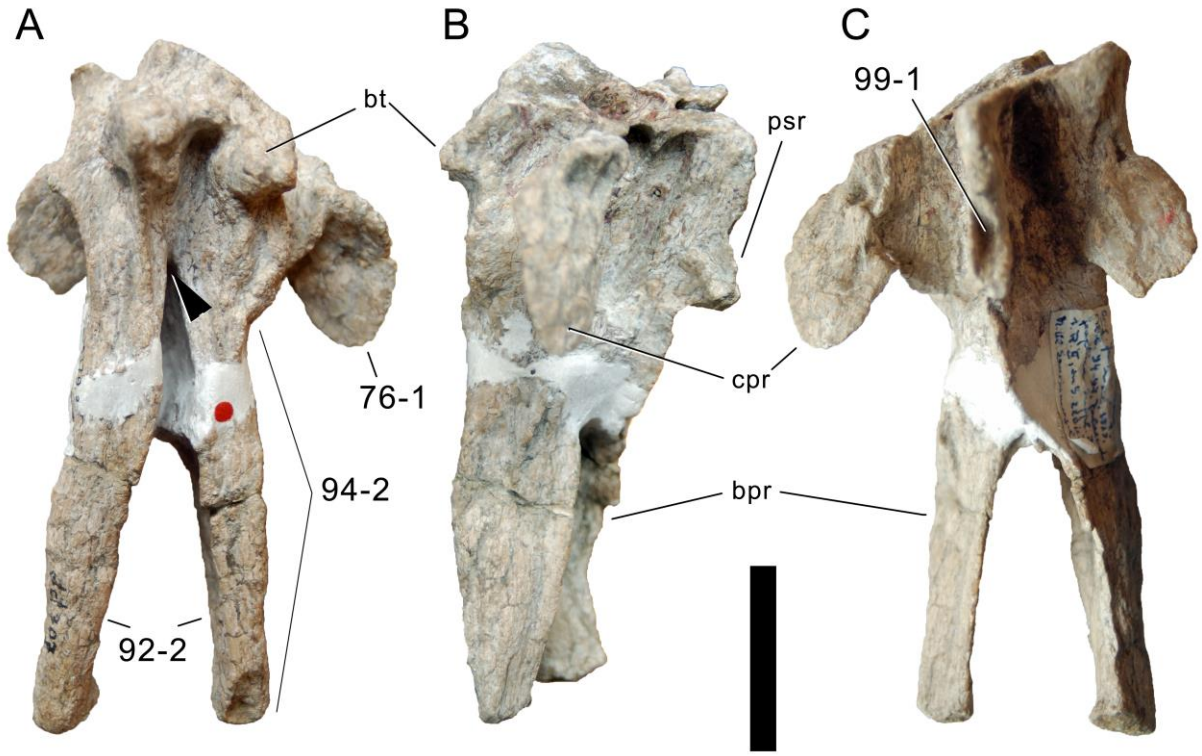

Figure 6.20: Basal tubera and basisphenoid of *Dicraeosaurus hansemanni* MB.R.2379 in posteroventral (A), left lateral (B), and anterodorsal view (C). Note the lateral expansion of the anteroventral end of the crista prootica (C76-1), the narrowly diverging, and elongate basipterygoid processes (C92-2 and C94-2, respectively), the deep slot-like cavity separating the bases of the processes (A, arrowhead; C95-1), and the groove on the dorsal surface of the parasphenoid rostrum (C; C99-1). Abb.: bt, basal tuber; bpr, basipterygoid process; cpr, crista prootica; psr, parasphenoid rostrum. Scale bar = 5 cm.

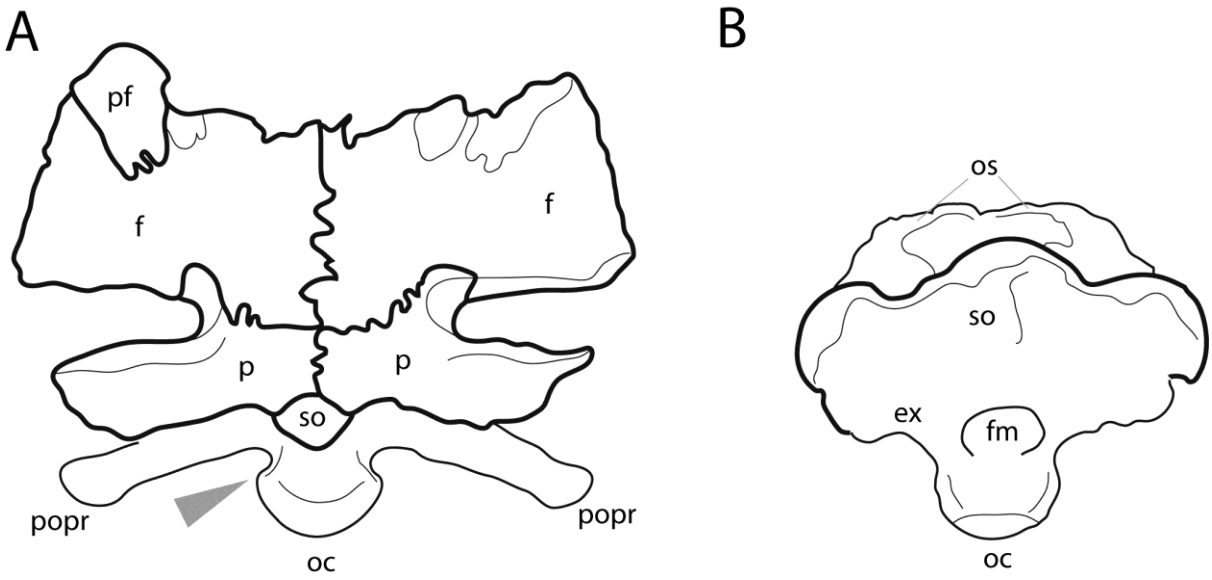

Figure 6.21: Braincase of *Camarasaurus* sp. UUVP 4286 (A; modified from Madsen et al., 1995) and *Tornieria africana* MB.R.2386 (B) in a view perpendicular to the dorsal surface of the occipital condyle, illustrating the distinctly offset articular surface (arrow in A; C77-0), in contrast to the derived condition of diplodocoids (B; C77-1). Abb.: ex, exoccipital; f, frontal; fm, foramen magnum; oc, occipital condyle; os, orbitosphenoid; p, parietal; pf, prefrontal; popr, paroccipital process. Skulls scaled to same breadth of occipital condyle.

C79: Basioccipital, distance from base of occipital condyle to base of basal tubera (best visible in lateral view): short, such that area is gently U-shaped in lateral view (0); elongate, with a flat portion between occipital condyle and basal tubera (1) (Tschopp and Mateus, 2012b; wording modified; Fig. 6.17).

Comments. The distance is measured relative to the height of the basal tuber, creating a narrow U-shape or a shallow, wide concavity in lateral view (Fig. 6.17).

C80: Basioccipital depression between foramen magnum and basal tubera: absent (0); present (1) (Wilson, 2002; Fig. 6.22).

Comments. The depression is a concave area on the posterolateral sides of the basioccipital, which is different from the concavity on the posterior face of the basal tubera described in another character.

C81: Basioccipital, pit between occipital condyle and basal tubera: absent (0); present (1) (New; Fig. 6.23).

Comments. Various pits can be present in the area around the basal tubera: YPM 1860 bears one within the notch between the tubera (see below), and a second one on the basioccipital posterior to the tubera (which is the one described here). Moreover, also the basipterygoid recess is located close by, but anterior to the basal tubera on the basisphenoid, instead of the basioccipital (J. Wilson, pers. comm., 2013).

C82: Basal tubera: globular (0); box-like (1) (Whitlock et al., 2010; Fig. 6.24).

Comments. Whitlock et al. (2010) used this character as one of the features distinguishing the juvenile diplodocid skull CM 11255 from *Apatosaurus*. It is herein used for the first time as a phylogenetic character.

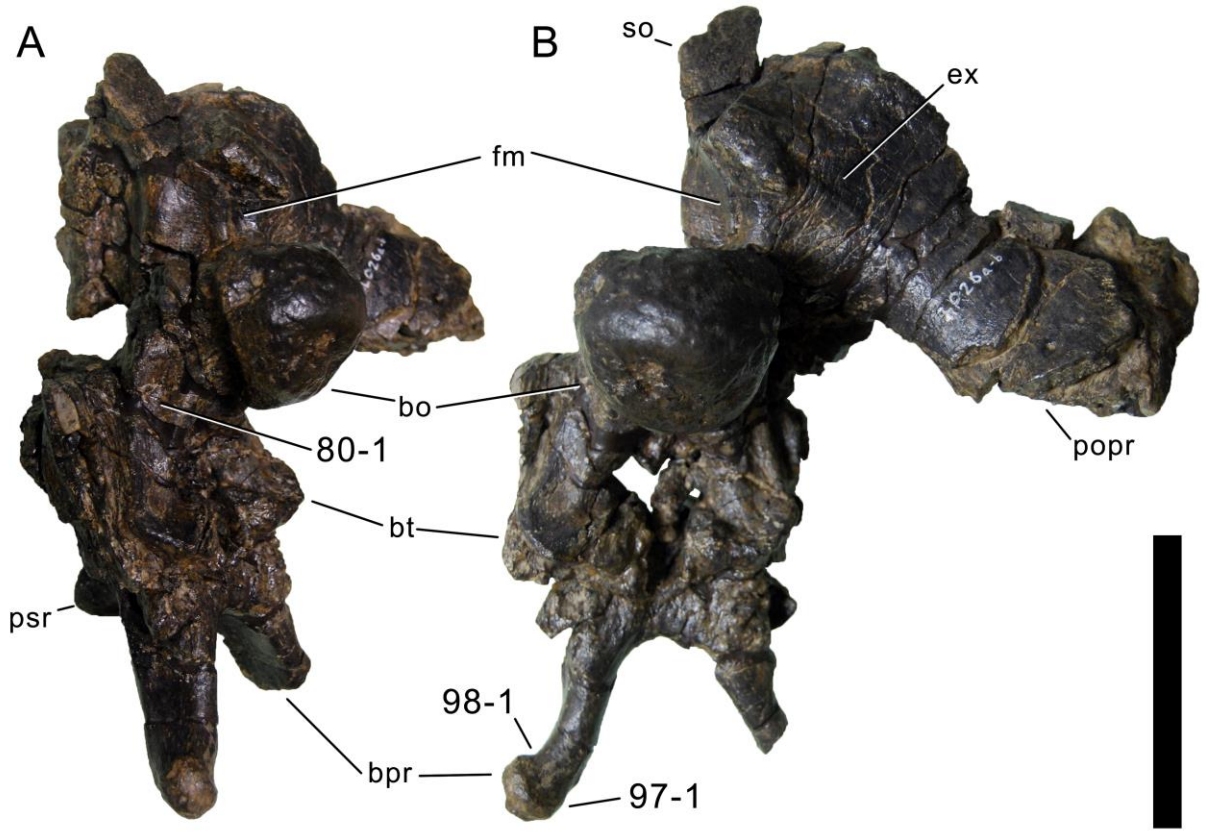

Figure 6.22: Braincase of *Losillasaurus giganteus* MCNV Lo-26 in posterolateral (A) and posterior (B) view. Note the lateral basioccipital depression between the foramen magnum and the basal tubera (A; C80-1); the laterally curving distal ends of the basipterygoid processes (B; C97-1), as well as their distinct transverse expansion (B; 98-1). Abb.: bo, basioccipital; bpr, basipterygoid process; bt, basal tuber; ex, exoccipital; fm, foramen magnum; popr, paroccipital process; psr, parasphenoid rostrum; so, supraoccipital. Scale bar = 10 cm.

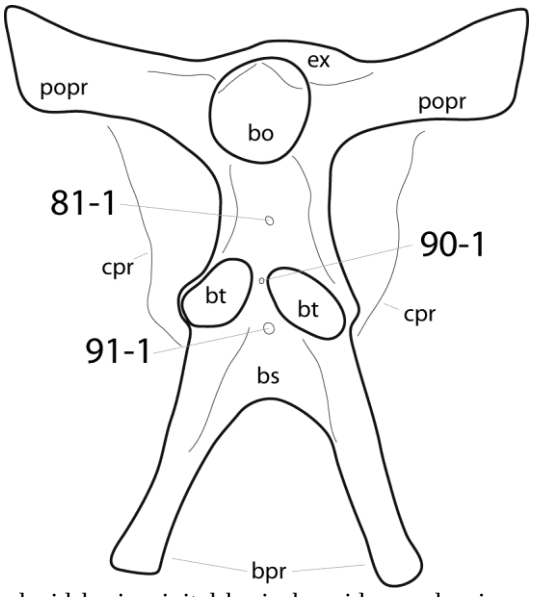

Figure 6.23: Hypothetical diplodocid basioccipital-basisphenoid complex in posteroventral view, showing the locations of pits sometimes present in diplodocid specimens: between occipital condyle and basal tubera (C81-1), in the notch between basal tubera (C90-1), and on the basisphenoid, between the bases of the basipterygoid processes (termed 'basipterygoid recess' by Wilson, 2002; C91-1). Abb.: bo, basioccipital; bpr, basipterygoid process; bs, basisphenoid; bt, basal tuber; cpr, crista prootica; ex, exoccipital; popr, paroccipital process.

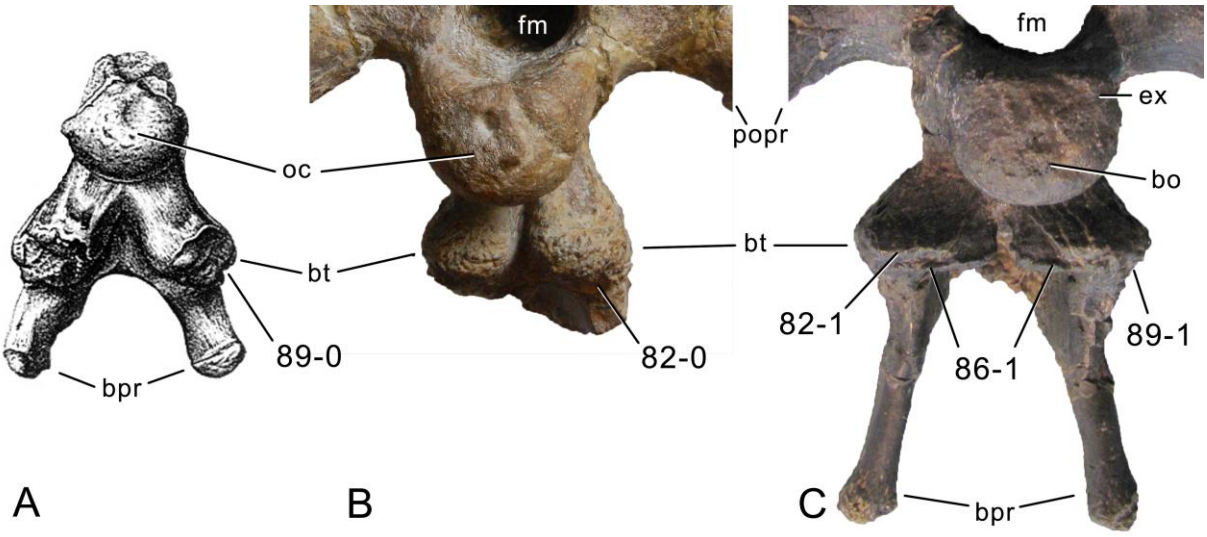

Figure 6.24: Basal tubera of *Camarasaurus grandis* YPM 1905 (A; modified from Madsen et al., 1995), *Suuwassea emilieae* ANS 21122 (B), and *Kaatedocus siberi* SMA 0004 (C; photo by J. Marinheiro) in posterior view. Note the globose (B; C82-0) compared to the box-like shape (C; C82-1) of the tubera, the transverse ridge on their posterior face (C; C86-1), and the ventrolateral (A; C89-0) in contrast to ventral orientation (C; C89-1). Abb.: bo, basioccipital; bpr, basipterygoid process; bs, basisphenoid; bt, basal tuber; ex, exoccipital; fm, foramen magnum; oc, occipital condyle; popr, paroccipital process. Pictures scaled to same distance between dorsal face of occipital condyle and basal tubera.

C83: Basal tubera, breadth: <1.3 times (0); 1.3-1.85 times (1); >1.85 times occipital condyle width (2) (Wilson, 2002; modified; Tab. 6.11).

Comments. The character was initially defined without clear state borders, and only with two states (Wilson, 2002). Mannion (2011) suggested that it might make sense to further subdivide the character, based on a wider survey of this ratio among sauropods. Mannion's (2011) table was here extended and the character state boundaries were modified following higher-level taxonomy and gaps in the distribution of the values.

Table 6.11: Width basal tubera/occipital condyle.

Taxon	Specimen	Ratio	Mean	Reference	Comments
Shunosaurus lii	ZG 65430	1	1,2	Zheng 1996	
		1,4		Mannion et al., in press	
Mamenchisaurus		1,2	1,2	Mannion et al., in press	
Turiasaurus riodevensis	CPT-1211	1,33	1,33	Royo-Torres & Upchurch 2012	
Losillasaurus giganteus type	MCNV Lo-26	1,51	1,51	pers. obs.	
Camarasaurus	YPM 1905	1,72	1,56	Mannion 2011	
	YPM 1907	1,42		Mannion 2011	
	CM 11338	1,32		Mannion 2011	
	AMNH 673	1,44		Mannion 2011	
	AMNH 5761	1,84		Mannion 2011	
		1,6		Mannion et al., in press	
Apatosaurus grandis YPM 1901	YPM 1901	1,59	1,59	Mannion 2011	
Giraffatitan brancai	MB.R. S66	1,05	1,17	Mannion 2011	
	MB.R. Y1	1,26		Mannion 2011	
		1,2		Mannion et al., in press	
Limaysaurus tessonei	MUCPv 205	1,17	1,17	Mannion 2011	
Nigersaurus taqueti	MNN GAD512	1,24	1,37	Mannion 2011	
		1,5		Mannion et al., in press	
Dicraeosaurus hansemanni	MB.R.2378	0,74	0,83	Mannion 2011	
	MB.R.2379	0,92		Mannion 2011	
Amargasaurus cazaui	MACN PV N15	1,12	1,12	Mannion 2011	
Suuwassea emilieae ANS 21122	ANS 21122	1,29	1,29	pers. obs.	
Apatosaurus ajax YPM 1860	YPM 1860	1,34	1,34	Mannion 2011	
Apatosaurus louisae CM 11162	CM 11162	1,49	1,49	Mannion 2011	
Kaatedocus siberi SMA 0004	SMA 0004	1,89	1,87	pers. obs.	measured from 3D model
	SMA 0004	1,86		pers. obs.	
Tornieria africana skeleton k	MB.R.2386	1,02	1,02	Mannion 2011	
Galeamopus shellensis SMA 0011	SMA 0011	1,02	1,02	pers. obs.	

C84: Basal tubera: distinct from basipterygoid (0); reduced to slight swelling on ventral surface of basipterygoid (1) (Whitlock, 2011a; Fig. 6.25).

Comments. The use of this character and its coding overlaps with an additional character proposed by Wilson (2002): 'Basal tubera, anteroposterior depth: approximately 33%, or more, of dorsoventral height (0); sheetlike, less than 33% (normally around 20%) dorsoventral height (1)'. Whitlock's (2011a) character is herein preferred as the directional terms used in Wilson (2002) are sometimes confusing due to varying orientations of the basal tubera of Diplodocoidea and non-diplodocoid sauropods.

C85: Basal tubera, shape of posterior face: convex (0); flat (1); slightly concave (2) (Whitlock, 2011a; modified by Tschopp and Mateus, 2012b; Fig. 6.25).

Comments. The 'posterior face' of the basal tubera is herein intended to be the side facing the occipital condyle. The concavity described herein is different from the concavity sometimes present on the lateral side of the basioccipital (see above).

C86: Basal tubera, posteroventral face: continuous (0); marked by a distinct transverse ridge (1) (New; Fig. 6.25).

Comments. The surface of the basal tubera is usually regularly rugose, and without distinct structuring. SMA 0004, however, bears a distinct transverse ridge on the posteroventral face of its basal tubera.

C87: Basal tubera, longest axes: parallel (0); in an angle to each other, pointing towards the occipital condyle (1) (New; Fig. 6.26).

Comments. The character is to be coded based on a view perpendicular to the orientation of the basipterygoid processes. It is inspired by the character of Tschopp and Mateus (2012b) describing the anterior margin of the tubera as V- or U-shaped, which included two differing morphologies in the same character (orientation of the tubera and shape of the anterior margin). The two morphologies are here treated as different characters (see below). In some cases (e.g. CM 11162), the outline of the tubera is subtriangular, with a more or less right angle pointing posterolaterally. These cases were treated as apomorphic, because the longest distance follows the obliquely oriented hypotenuse of the triangle.

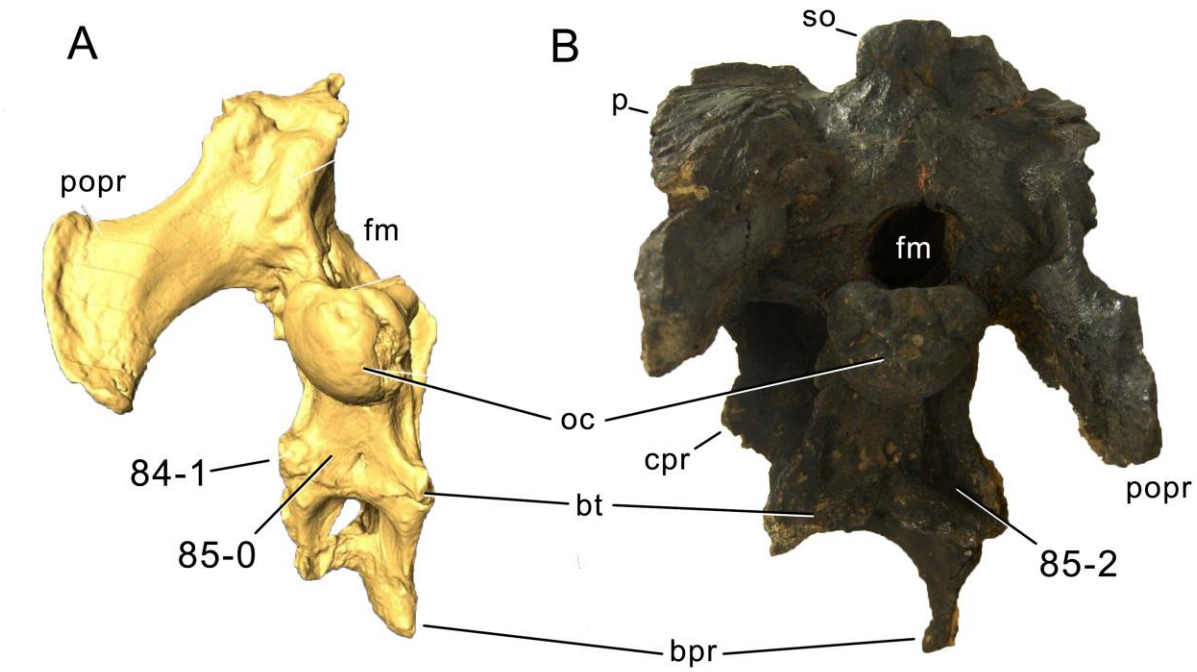

Figure 6.25: Skulls of *Nigersaurus taqueti* (A; modified from Schmitt, 2012) and *Diplodocus* sp. USNM 2673 (B) in occipital view. Note the reduced basal tubera in *Nigersaurus* (A; C84-1), and the convex (A; C 85-0), or concave (B; C85-2) posterior face of the tubera. Abb.: bpr, basipterygoid process; bt, basal tuber; cpr, crista prootica; fm, foramen magnum; oc, occipital condyle; popr, paroccipital process; so, supraoccipital. Skulls scaled to same occipital condyle height.

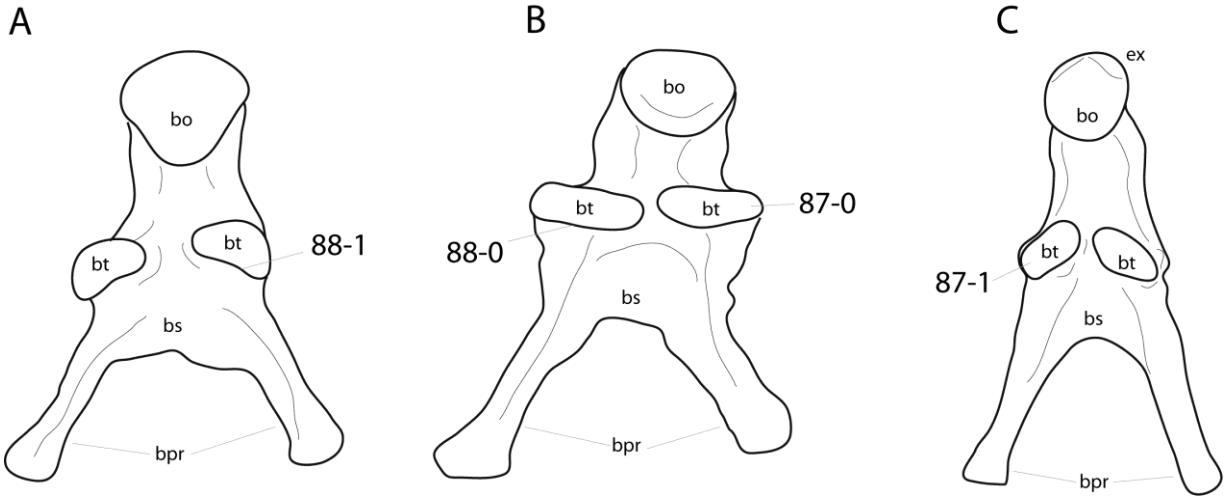

Figure 6.26: Basioccipital-basispenoid complex of *Apatosaurus louisae* CM 11162 (A), *Kaatedocus siberi* SMA 0004 (B; traced from a photo by J. Marinheiro), and *Diplodocus* sp. CM 11161 (C) in posteroventral view. Note the differing orientations of the longest axes of the basal tubera (B; C87-0; in contrast to C; C87-1), as well as the concave (A; C88-1) versus the straight to slightly convex anterior edge of the tubera (B; C88-0). Abb.: bo, basioccipital; bpr, basipterygoid process; bs, basisphenoid; bt, basal tuber; ex, exoccipital. Drawings not to scale.

C88: Basal tubera, anterior edge: straight or convex (0); concave (1) (Tschopp and Mateus, 2012b; Fig. 6.26).

Comments. The second of the two characters inspired by Tschopp and Mateus' (2012b) character about the anterior margin of the basal tubera. The anterior edge is the one facing towards the basipterygoid processes, which in non-diplodocoid sauropods is oriented rather anteroventrally. In specimens with angled basal tubera (see above), the anterior margin is oriented obliquely.

C89: Basal tubera in posterior view: facing ventrolaterally (0); facing straight ventrally, forming a horizontal line (1) (Tschopp and Mateus, 2012b; wording modified; Fig. 6.24).

Comments. Some specimens (in particular non-flagellicaudatans) have rounded basal tubera which extend onto the lateral surface of the basioccipital. These are treated as plesiomorphic, as the line projecting through the medial- and lateral-most points of the tubera is oblique in these cases.

C90: Basal tubera, foramen in notch that separates the two tubera: absent (0); present (1) (Tschopp and Mateus, 2012b; Fig. 6.23).

Comments. This foramen is one of three openings that can be present in this area (see above and below). However, the pit described in this character cannot be homologous to the other ones because it is present together with the basipterygoid recess in HMNS 175 (Holland, 1906), and together with the basioccipital pit in YPM 1860 (pers. obs., 2011).

C91: Basisphenoid/basipterygoid recess: absent (0); present (1) (Wilson, 2002; polarity inverted; Fig. 6.23)

Comments. The basipterygoid recess is a pit located anteriorly to the basal tubera, on the basisphenoid. Its absence was considered autapomorphic for *Apatosaurus*, representing a reversal to the plesiomorphic state in Sauropoda (Wilson, 2002). However, in the phylogenetic analysis, *Apatosaurus* was scored as having a recess, sharing this state with basal sauropods like *Shunosaurus* Wilson (2002). The character was organized as a presence/absence character, but with the presence being plesiomorphic (Wilson, 2002). Assuming that the discussion of the autapomorphies is right, polarity of the character states was inverted herein. The basipterygoid recess might be confused with the pits located in the notch between the tubera or the one posterior to them (see above), so it is important to state that it lies anterior to the tubera, between the bases of the basipterygoid processes. Although Wilson (pers. comm., 2013) himself is not convinced of the phylogenetic validity of this character, it was retained herein, as a specimen-based phylogenetic analysis also allows for the detection of possible individual variation.

C92: Basipterygoid processes: widely diverging (> 60°) (0); intermediate, 31°-60° (1); narrowly diverging (< 31°) (2) (Yu, 1993; modified; Fig. 6.20; Tab. 6.12).

Comments. There are several modes to measure the angle between the processes, and no previous analysis defines how this angle should be measured. Here, divergence is measured between lines drawn from the basisphenoid center, where the bases of the basipterygoid processes meet, to the anteromedial-most point of the processes. This is preferably done in posterior or posteroventral view, perpendicular to the longitudinal axis of the processes. The present measuring technique yields slightly different results compared to earlier studies, but general trends are similar.

C93: Basipterygoid processes, orientation: directed more than 75° to skull roof (normally perpendicular) (0); angled less than 75° to skull roof (normally approximately 45°) (1) (McIntosh, 1990b; modified; Tab. 6.13).

Comments. New numeric state boundaries were established, because a survey of diplodocoid braincases showed that there is more variety than previously recognized (Tab. 6.13). However, the difference was already recognized as taxonomically important by McIntosh (1990b). The angle is measured between the skull roof and a line through the center of the proximal and distal ends. This is important, as especially macronarian basipterygoid processes tend to curve backwards at their distal ends, thereby increasing the angle as measured here.

There is some possibility that this character is correlated with the large angle between the anterior and dorsal quadratojugal processes and the backwards inclination of the ventral ramus of the quadrate. This entire region is interconnected by the pterygoid, and the anterior shifting of the basisphenoid-pterygoid articulation due to the changed orientation of the basipterygoid processes might have been caused by, or the reason for the more anteriorly orientated ventral ramus of the quadrate, and therefore also the widening of the angle between the quadratojugal processes. However, since few to no skulls are known of basal diplodocoid taxa, which might show intermediate states, if they were present, the characters are retained separate here, lacking definitive evidence of correlation.

Furthermore, there is some indication that the character could be ontogenetically controlled: the two relatively small diplodocine skulls CM 3452 and SMA 0004 have both somewhat larger angles compared to larger specimens (Tab. 6.13), and lower angles in the quadratojugal. However, further studies are needed to decide if this is really ontogenetic, or if it could be taxonomically significant.

Table 6.12: Angle between basipterygoid processes.

Taxon	Specimen	Angle	Mean	Reference	Comments
Shunosaurus lii		50	70	Yu 1993	not personally measured
	ZG65430	90,6		Zheng 1996	measured from reconstruction
Spinophorosaurus nigerensis	GCP-CV-4229	84,4	84	Knoll et al. 2012	measured from photo
Omeisaurus		60	60	Yu 1993	not personally measured
Mamenchisaurus	ZDM 0083	48,8	49	Ouyang & Ye 2002	measured from drawing
Turiasaurus riodevensis	CPT-1211	51,3	51	Royo-Torres & Upchurch 2012	measured from photo
Losillasaurus giganteus type	MCNV Lo-26	55,4	55	pers. obs.	
Camarasaurus		55	65	Yu 1993	not personally measured
	BYU 601-9048	73		O. Mateus, pers. comm. 2010	measured from photo
	UUVP 10070	69,8		Madsen et al. 1995	measured from drawing
	UUVP 10795	56		Madsen et al. 1995	measured from drawing
	YPM 1905	68,7		Madsen et al. 1995	measured from drawing
Apatosaurus grandis YPM 1901	YPM 1901	89	89	Madsen et al. 1995	measured from drawing
Giraffatitan brancai		55	58	Yu 1993	not personally measured
	MB.R. S66	48,6		Janensch 1935	measured from drawing
	MB.R. T1	68,9		Janensch 1935	measured from drawing
Limaysaurus tessonei	MUCPv-205	74,8	75	Calvo & Salgado 1995	measured from drawing
Nigersaurus taqueti		38,6	39	Sereno et al. 2007	measured from 3D model
Dicraeosaurus hansemanni		25	20	Yu 1993	not personally measured
	MB.R.2379	14,2		pers. obs.	
Amargasaurus cazaui		25	21	Yu 1993	
	MACN-N 15	16,4		Salgado & Bonaparte 1991	measured from drawing
Apatosaurus louisae CM 11162	CM 11162	64,2	64	pers. obs.	
Kaatedocus siberi SMA 0004	SMA 0004	51,2	51	pers. obs.	
Diplodocus sp. CM 11161	CM 11161	54,7	55	pers. obs.	
Barosaurus sp. CM 3452	CM 3452	36,6	38	L. Witmer, pers. comm. 2013	estimated from 3D model, measuring both processes
	CM 3452	40,2		L. Witmer, pers. comm. 2013	calculated from 3D model, measuring only visible right process
Diplodocus sp. USNM 2672	USNM 2672	59,8	60	pers. obs.	
Galeamopus hayi HMNS 175	HMNS 175	82,7	83	Digimorph, 2013	measured from 3D model

C94: Basipterygoid processes, ratio of length:basal transverse diameter: < 4 (0); = or > 4.0 (1) (Wilson, 2002; modified; Fig. 6.20; Tab. 6.14).

Comments. The character was initially defined as ratio of length to maximum basal diameter (Wilson, 2002). However, maximum basal diameter is often oriented dorsoventrally (at least in diplodocids, pers. obs.), which means that one cannot take the measurements in a picture of the processes in ventral view only. Also, dorsoventral height changes considerably, and continuously towards the base of the processes in some specimens (e.g. *Dicraeosaurus hansemanni* MB.R.2379; Janensch, 1935); Fig. 6.20), and in lateral view, it is sometimes difficult to decide where exactly the base of the process is situated. Therefore, and because ventral views are obtainable more frequently than lateral views, the ratio length/basal transverse diameter is preferred herein. The dimensions should be measured perpendicular to each other. Wilson (2002) initially left a gap in the definition of the states (2 or less, 4 or more), which was corrected for by Mannion et al. (2012). However, as a more rigorous assessment of these ratios shows (Tab. 6.14), the state boundary should rather be set to four, the derived, elongate state resulting as a shared synapomorphy for Diplodocinae and Dicraeosauridae.

Measuring the basipterygoid processes in such a way leads to much higher elongation ratios for the holotype of *Kaatedocus siberi* (SMA 0004) than reported in its initial description (Tschopp and Mateus, 2012b). The low ratio also served as local autapomorphy for the genus (Tschopp and Mateus, 2012b). Following the results presented herein, this might have been an artifact based on differing measurement protocols, as Tschopp and Mateus (2012b) compared length with dorsoventral height, which is the maximum basal diameter in SMA 0004 (Tschopp and Mateus, 2012b). The current measurements show that *Kaatedocus* is actually well in the range of Diplodocinae, which can easily be distinguished from *Apatosaurus louisae* CM 11162 (Tab. 6.14).

C95: Basipterygoid, area between the basipterygoid processes and parasphenoid rostrum: is a mildly concave subtriangular region (0); forms a deep slot-like cavity that passes posteriorly between the bases of the basipterygoid processes (1) (Upchurch, 1995, 1998; Fig. 6.20).

Table 6.13: Angle between basipterygoid processes and skull roof in lateral view.

Taxon	Specimen	Angle	Mean	Reference	Comments
Shunosaurus lii	T5401, R	96,6	89	Zhang 1988	measured from drawing
	T5401, L	82,1		Zhang 1988	measured from drawing
Spinophorosaurus nigerensis	GCP-CV-4229, L	154,9	156	Knoll et al. 2012	measured from photo
	GCP-CV-4229, R	156,6		Knoll et al. 2012	measured from photo
Mamenchisaurus	ZDM 0083	104,8	105	Ouyang & Ye 2002	estimated from reconstruction
Turiasaurus riodevensis	CPT-1211	„ventrolaterally“	90	Royo-Torres & Upchurch 2012	
Losillasaurus giganteus type	MCNV Lo-26	87	87	pers. obs.	estimated, skull roof absent
Camarasaurus	DNM 28	102,8	102	Madsen et al. 1995	measured from drawing
	DNM 28	101,7		Chatterjee & Zheng 2005	measured from drawing
	UUVP 10070	102,5		Madsen et al. 1995	measured from drawing
Giraffatitan brancai	MB.R. S66	110,9	112	Janensch 1935	measured from drawing
	MB.R. t1	114		Janensch 1935	measured from drawing
Brachiosaurus altithorax	USNM 5730	130,1	130	Carpenter & Tidwell 2001	measured from photo
Limaysaurus tessonei	MUCPv-205	„anteriorly“	45	Calvo & Salgado 1995	
Nigersaurus taqueti	MNN GAD512-8	51,6	52	Sereno et al. 2007	measured from 3D model
Dicraeosaurus hansemanni	MB.R.2379	24,3	24	Janensch 1935	measured from drawing
Amargasaurus cazaui	MACN-N 15	21,1	21	Salgado & Calvo 1992	measured from drawing
Suuwassea emilieae ANS 21122	ANS 21122	35,1	35	pers. obs.	estimated, only bases of processes present
Apatosaurus louisae CM 11162	CM 11162	47,3	47	pers. obs.	estimated, processes partly hidden in lateral view
Kaatedocus siberi SMA 0004	SMA 0004	70,3	70	pers. obs.	estimated, braincase deformed
Galeamopus shellensis AMNH 969	AMNH 969	52,1	52	Holland 1906	measured from photo
Diplodocus sp. CM 11161	CM 11161	43	43	pers. obs.	estimated, processes partly hidden in lateral view
Barosaurus sp. CM 3452	CM 3452	66,7	68	L. Witmer, pers. comm. 2013	measured from 3D model
Diplodocus sp. USNM 2672	USNM 2672	56,3	56	McIntosh & Berman 1975	measured from drawing
Galeamopus hayi HMNS 175	HMNS 175	50,6	51	Digimorph, 2013	measured from 3D model
Galeamopus shellensis SMA 0011	SMA 0011	50,2	50	pers. obs.	estimated, processes wrongly mounted

C96: Basipterygoid processes, orientation of proximal-most portions: same as central portion of shaft (0); parallel to each other, outwards curve of shaft happens only more anteriorly (1) (New; Fig. 6.27).

Comments. The development of this character is best seen in ventral view. In the derived state, the parallel portion of the basipterygoid processes are often interconnected dorsomedially by a thin sheet of bone. On the other hand, a similar sheet can also be present if the processes are entirely straight.

C97: Basipterygoid processes, distal end: straight (0); curving outwards (1) (New; Fig. 6.22).

Comments. This character compares the distal end of the basipterygoid process with the central portion. It is thus different from the feature described in character 96.

C98: Basipterygoid processes, distal lateral expansion: absent (0); present (1) (New; Fig. 6.22).

Comments. Only abrupt distal expansions are coded as apomorphic, gradually extending processes are treated as plesiomorphic.

C99: Parasphenoid rostrum, groove on dorsal edge: absent (0); present (1) (Upchurch, 1995, 1998; modified; Fig. 6.20).

Comments. Upchurch (1995, 1998) proposed the character combining the presence of a dorsal groove with the lateral shape of the rostrum, thereby implying that the dorsoventrally thin parasphenoids of diplodocoids would not bear dorsal grooves. However, a more detailed study of diplodocoids shows that the groove is actually present in most of them.

C100: Optic foramen: paired (0); unpaired (1) (Berman and McIntosh, 1978; Sander et al., 2006; Fig. 6.28).

Comments. The optic foramen is lying close to the midline, within the orbitosphenoid in most sauropod taxa. Generally, they are separated medially by a narrow bony bridge, which is absent in some diplodocoid specimens (e.g. *Suuwassea*, Harris, 2006a). Sander et al. (2006) were the first to include the character into a phylogenetic analysis.

C101: Palatobasal contact, shape: pterygoid with small facet (0); dorsomedially orientated hook (1) (Wilson, 2002; modified by Tschopp and Mateus, 2012b; Fig. 6.29).

Comments. Tschopp and Mateus (2012b) deleted a third state present in the original character, which describes the specific rocker-like morphology of this region in nemegtosaurid sauropods (Wilson, 2002). Since no taxon of this clade is included, the additional state is redundant.

Table 6.14: Basipterygoid process length/maximum transverse width at base.

Taxon	Specimen	Ratio	Mean	Reference	Comments
Shunosaurus lii	ZG 65430	1,799	1,90	Chatterjee & Zheng 2002	measured from reconstruction
		2,000		Mannion et al., in press	
Spinophorosaurus nigerensis	GCP-CV-4229, R	2,912	2,91	Knoll et al. 2012	measured from photo
Mamenchisaurus	ZDM 0083, R	2,312	2,63	Ouyang & Ye 2002	measured from drawing
	ZDM 0083, L	3,065		Ouyang & Ye 2002	measured from drawing
		2,500		Mannion et al., in press	
Turiasaurus riodevensis	CPT-1211, L	3,075	3,07	Royo-Torres & Upchurch 2012	
Losillasaurus giganteus type	MCNV Lo-26, L	3,085	3,08	pers. obs.	
Camarasaurus	BYU 601-9048, L	1,792	1,79	O. Mateus, pers. comm. 2010	measured from photo
	DNM 28, R	1,669		Madsen et al. 1995	measured from drawing
	UUVP 10070, R	1,908		Madsen et al. 1995	measured from drawing
	UUVP 10070, L	1,406		Madsen et al. 1995	measured from drawing
	UUVP 4286, R	1,849		Madsen et al. 1995	measured from drawing
		2,100		Mannion et al., in press	
Apatosaurus grandis YPM 1901	YPM 1901, L	1,612	1,82	Madsen et al. 1995	measured from drawing
	YPM 1901, R	2,024		Madsen et al. 1995	measured from drawing
Giraffatitan brancai	MB.R. t1	3,000	2,96	Janensch 1935	unclear if right measurements, taken from text
	MB.R. t1, R	3,271		Janensch 1935	measured from drawing
	MB.R. S66, L	2,283		Janensch 1935	measured from drawing
		3,300		Mannion et al., in press	
Limaysaurus tessonei	MUCPv-205, R	3,529	3,41	Calvo & Salgado 1995	measured from drawing
	MUCPv-205, L	3,282		Calvo & Salgado 1995	measured from drawing, lateral edge reconstructed
Nigersaurus taqueti	MNN GAD512-8, R	3,773	3,89	Sereno et al. 2007	measured from 3D model
		4,000		Mannion et al., in press	
Dicraeosaurus hansemanni	MB.R.2379, L	5,678	6,44	pers. obs.	
	MB.R.2379, R	7,203		pers. obs.	
Amargasaurus cazaui	MACN-N 15, R	6,068	6,07	Salgado & Bonaparte 1991	measured from drawing
Apatosaurus louisae CM 11162	CM 11162, L	3,852	3,57	pers. obs.	
	CM 11162, R	3,291		pers. obs.	estimated, distorted
Kaatedocus siberi SMA 0004	SMA 0004, L	4,932	4,94	G. Dzemski, pers. comm. 2010	measured from 3D model
	SMA 0004, L	5,429		pers. obs.	
	SMA 0004, R	5,129		G. Dzemski, pers. comm. 2010	measured from 3D model
	SMA 0004, R	4,286		pers. obs.	
Diplodocus sp. CM 11161	CM 11161, L	4,645	4,94	pers. obs.	
	CM 11161, R	5,239		pers. obs.	
Barosaurus sp. CM 3452	CM 3452, R	6,128	6,03	L. Witmer, pers. comm. 2013	measured from 3D model
	CM 3452, L	5,928		L. Witmer, pers. comm. 2013	estimated, distal end of process obliterated in ventral view
Diplodocus sp. USNM 2672	USNM 2672	4,667	4,67	pers. obs.	
Galeamopus hayi HMNS 175	HMNS 175, L	5,000	4,19	Digimorph, 2013	measured from 3D model
	HMNS 175, R	3,375		Digimorph, 2013	measured from 3D model
Galeamopus shellensis SMA 0011	SMA 0011, L	5,182	5,14	pers. obs.	width estimated
	SMA 0011, R	5,100		pers. obs.	

C102: Pterygoid, transverse flange (i.e. ectopterygoid process) position: between orbit and antorbital fenestra (0); anterior to antorbital fenestra (1) (Upchurch, 1995; Fig. 6.9).

Comments. The transverse flange of the pterygoid connects to the maxilla through the ectopterygoid (Upchurch et al., 2004a).

C103: Vomer, anterior articulation: maxilla (0); premaxilla (1) (Wilson, 2002; polarity inverted; Fig. 6.9).

Comments. Polarity was inverted compared to Wilson's (2002) character due to the limited taxon sampling.

C104: Dentary, anteroventral margin shape: gently rounded (0); sharply projecting triangular process or 'chin' (1) (Upchurch, 1998; Fig. 6.30).

Comments. Usually considered a flagellicaudatan synapomorphy, also some specimens of *Camarasaurus* show a weak ventral expansion at the anterior extreme of the lower jaw. However, this never reaches the chin-like state as present in *Diplodocus*, and *Camarasaurus* is thus included in the plesiomorphic state here.

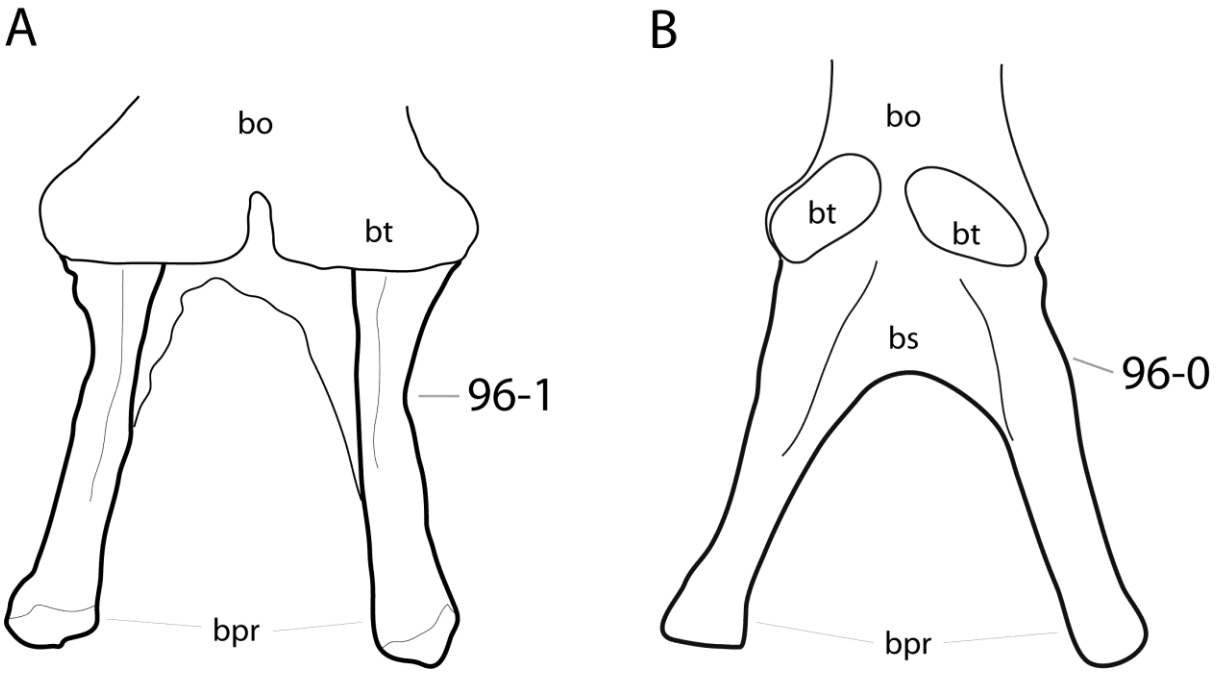

Figure 6.27: Basisphenoid of *Kaatedocus siberi* SMA 0004 (A; traced from a photo by J. Marinheiro), and *Diplodocus* sp. CM 11161 (B) in posteroventral view. Note the parallel proximal portion of the basipterygoid processes and the accompanying outwards curve in *Kaatedocus* (A; C96-1), in contrast to the straight processes of CM 11161 (B; C96-0). Abb.: bo, basioccipital; bpr, basipterygoid process; bs, basisphenoid; bt, basal tuber. Scaled to the same process length.

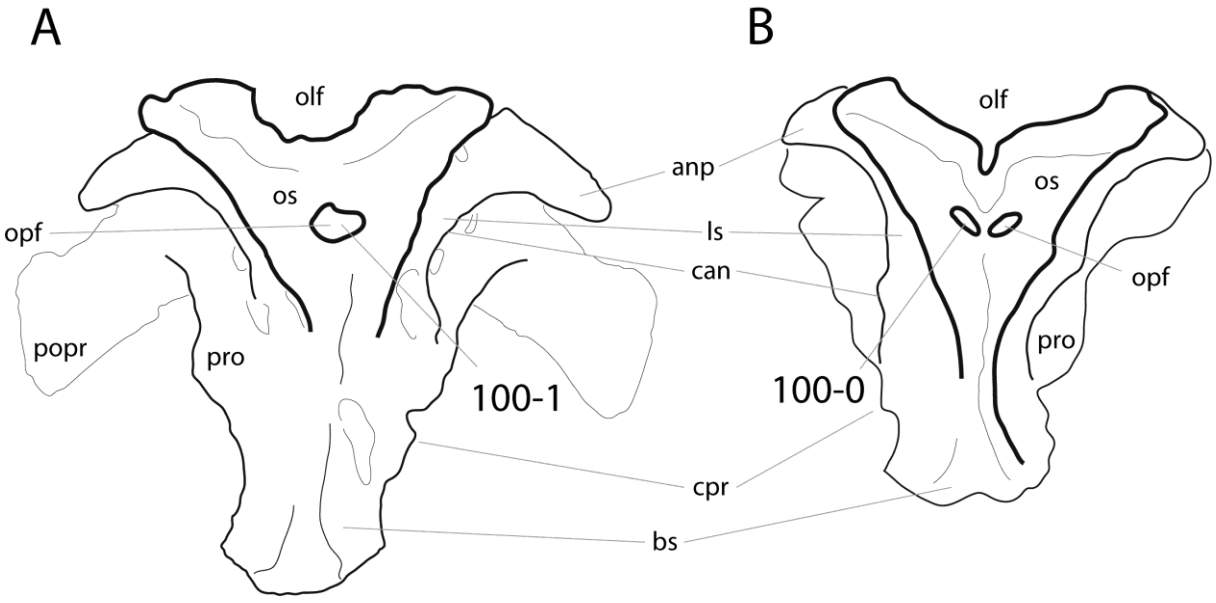

Figure 6.28: Braincases of *Suuwassea emilieae* ANS 21122 (A), and *Tornieria africana* MB.R.2386 (B; traced from Janensch, 1935) in anterior view. Note the unpaired optic foramen of *Suuwassea* (A; C100-1), in contrast to the paired foramen in *Tornieria* (B; C100-0). Abb.: anp, antotic process; bs, basisphenoid; can, crista antotica; cpr, crista prootica; ls, laterosphenoid; olf, olfactory foramen; opf, optic foramen; os, orbitosphenoid; popr, paroccipital process; pro, prootic. Scaled to the same width of the orbitosphenoids.

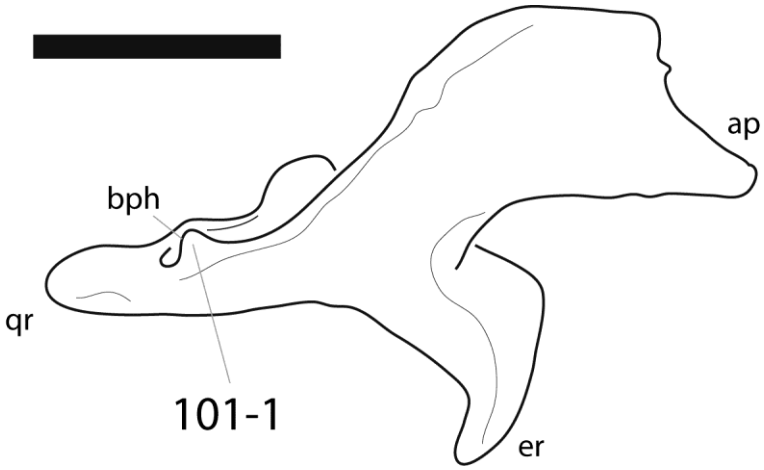

Figure 6.29: Left pterygoid of *Camarasaurus lentus* DNM 28 in medial view. Note the presence of a hook-like process at the articulation surface for the basipterygoid process (C101-1). Diplodocidae, on the other hand, only have shallow articular facets without hooks. Abb.: ap, anterior process; bph, basipterygoid hook; er, ectopterygoid ramus; qr, quadrate ramus. Picture traced from Madsen et al. (1995). Scale bar = 10 cm.

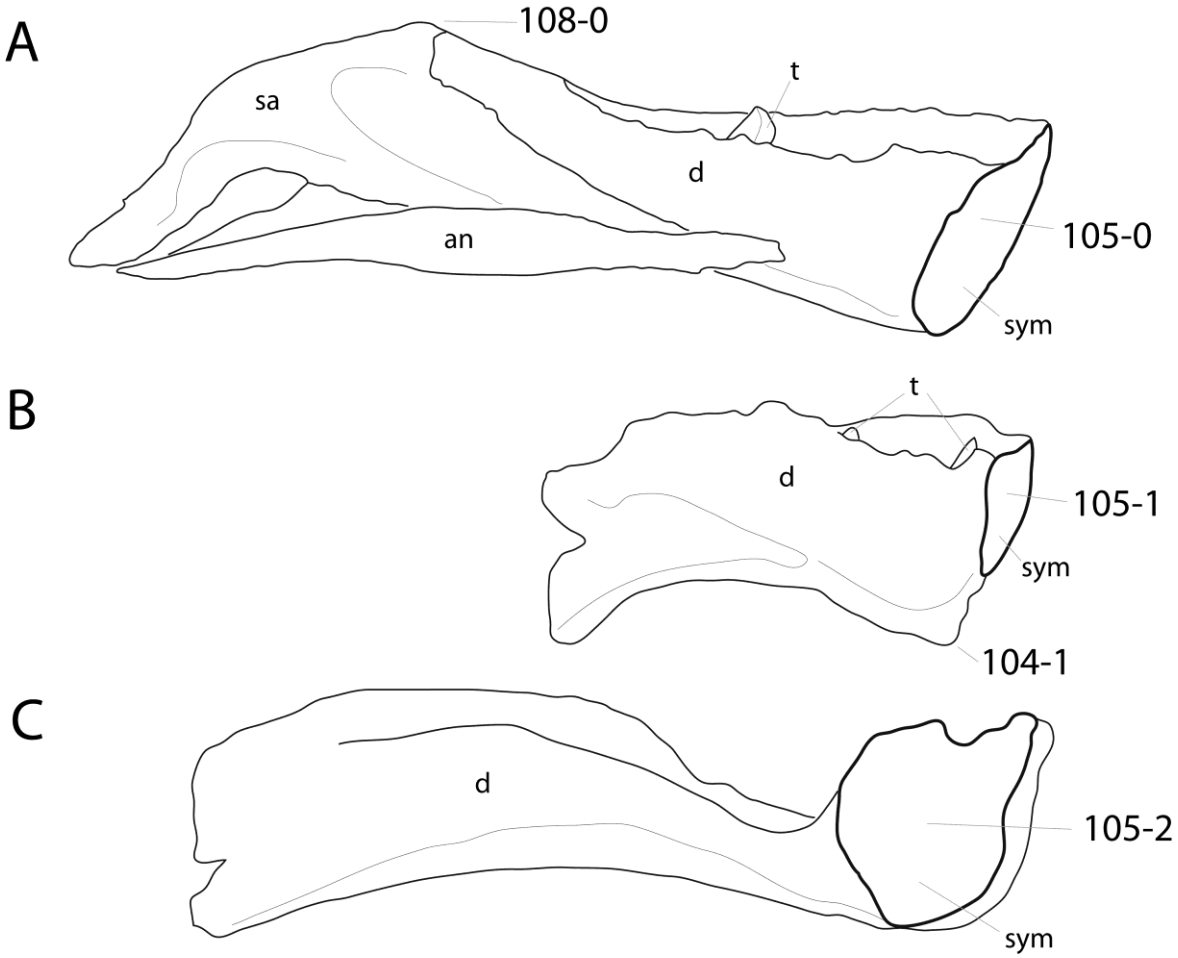

Figure 6.30: Left dentary of *Camarasaurus lentus* DNM 28 (A; traced from Madsen et al., 1995), *Dicraeosaurus hansemanni* MB.R.2372 (B; traced from Janensch, 1935), and *Nigersaurus taqueti* MNN GAD512-10 (C; traced from Sereno et al., 2007) in lingual view. Note the chin-like ventral process in *Dicraeosaurus* (B; C104-1), the different shapes of the symphysis (C105-1 to 3), and the high elevation of the coronoid eminence in *Camarasaurus* (A; C108-0). Abb.: an, angular; d, dentary; sa, surangular; sym, symphysis; t, tooth. Scaled to the same anteromedial height of the dentary.

C105: Dentary, cross-sectional shape of symphysis: oblong or rectangular (0); subtriangular, tapering sharply towards ventral extreme (1); subcircular (2) (Whitlock, 2011a; Fig. 6.30).
Comments. Diplodocids have ventrally tapering symphyses, but they do not taper to a point as in dicraeosaurids (Whitlock and Harris, 2010) and have thus still to be scored as plesiomorphic.

C106: Dentary, tuberosity on labial surface near symphysis: absent (0); present (1) (Whitlock and Harris, 2010; reworded by Whitlock, 2011a; Fig. 6.31).
Comments. This character was originally proposed by Whitlock and Harris (2010) to unite *Suuwassea* and *Dicraeosaurus*.

C107: Dentary, anterolateral corner: not expanded laterally beyond mandibular ramus (0); expanded beyond lateral mandibular ramus (1) (Whitlock, 2011a; Fig. 6.31).
Comments. The derived state of this character describes the extreme case of the character concerning the shape of the tooth row (see below). To date, it is only known in the rebbachisaurid *Nigersaurus* (Sereno et al., 2007).

C108: Mandible, coronoid eminence: strongly expressed, clearly rising above plane of dentigerous portion (0); absent (1) (Whitlock, 2011a; Fig. 6.30).
Comments. Some diplodocids have dorsally expanded coronoid areas, but they do not reach above the plane of the dentigerous portion.

C109: Surangular foramen: absent (0); present (1) (New; Fig. 6.32).
Comments. The location of the surangular foramen can vary in different taxa. Usually, it is situated in the anterior, horizontally oriented portion, but in some cases it is shifted posteriorly.

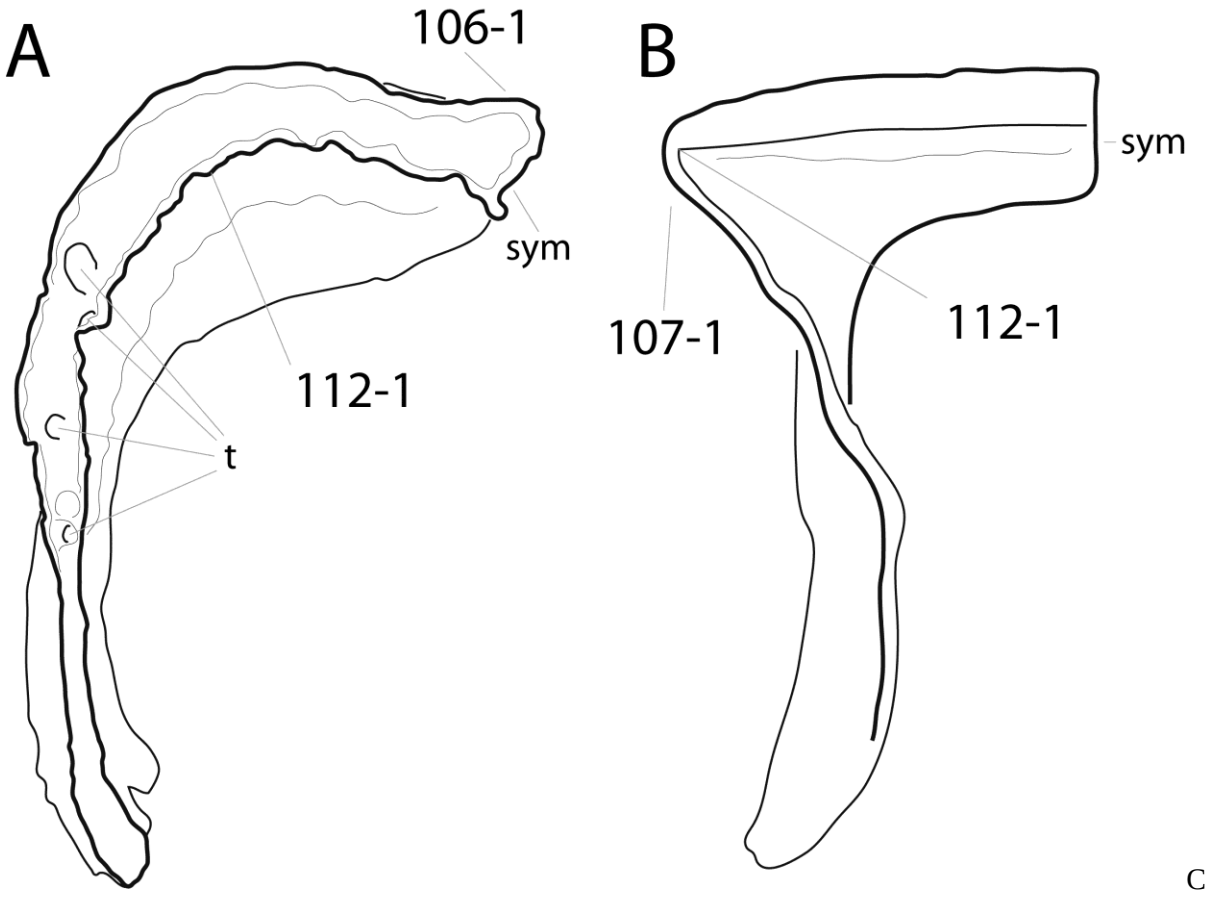

Figure 6.31: Left dentary of *Dicraeosaurus hansemanni* MB.R.2372 (A), and *Nigersaurus taqueti* MNN GAD512-10 (B; traced from Sereno et al., 2007) in dorsal view. Note the labial tubercle in *Dicraeosaurus* (A; C106-1), the dentigerous portion that expands laterally in *Nigersaurus* (B; C107-1), and the anterolaterally displaced tooth row, compared to the usual curvature in both taxa (C112-1). Abb.: sym, symphysis; t, tooth. Scaled to the same anteroposterior length.

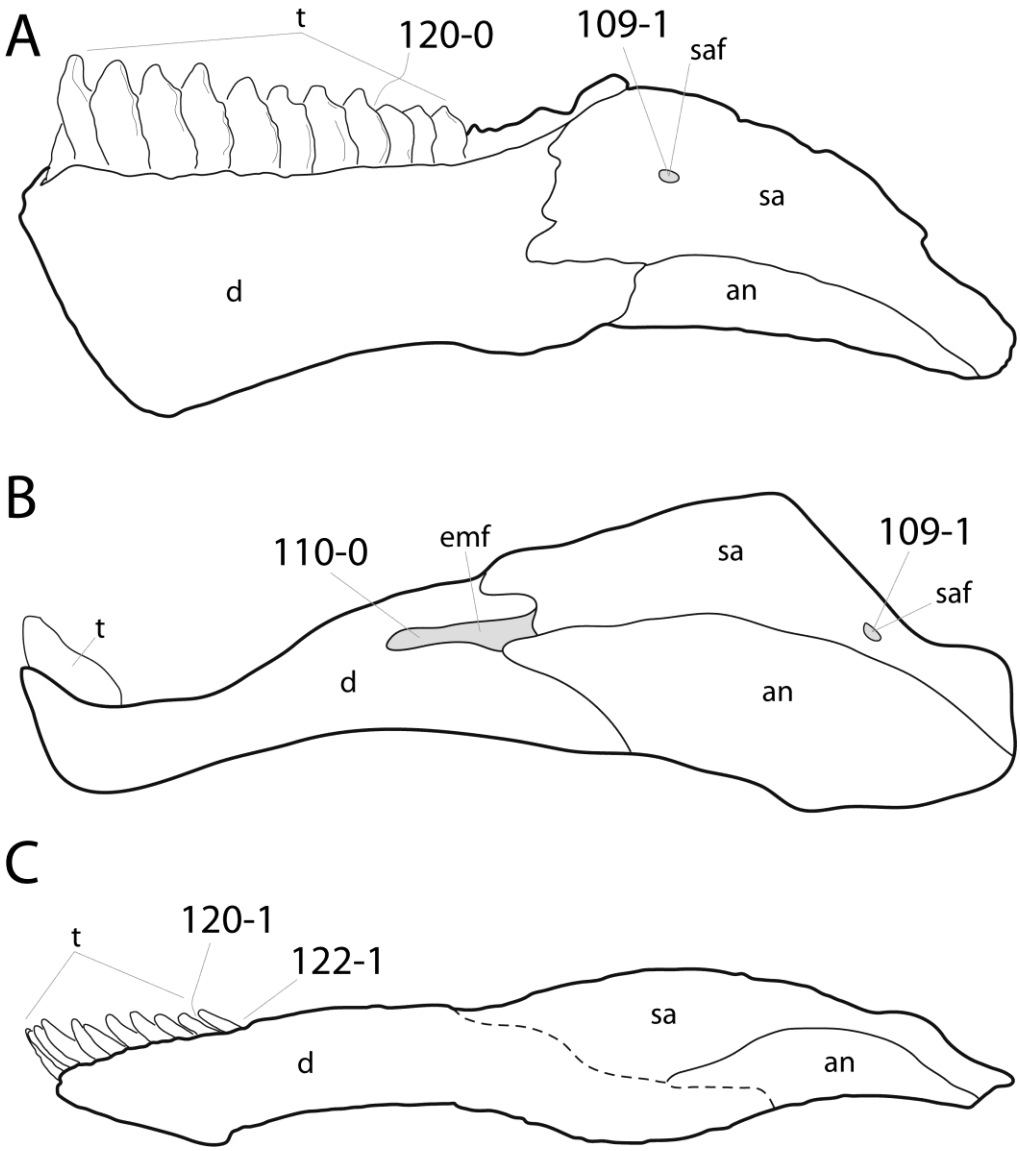

Figure 6.32: Left lower jaw of *Camarasaurus lentus* CM 11338 (A; modified from Madsen et al., 1995), *Nigersaurus taqueti* MNN GAD-512 (B; traced from Sereno et al., 2007), and SMA 0011 (C; traced from a photo by O. Mateus) in lateral view. Note the surangular foramen in A and B (C109-1), the external mandibular fenestra in *Nigersaurus* (B; C110-0), the strongly overlapping teeth of *Camarasaurus* (A; C120-0) in contrast to the more widely spaced teeth of diplodocids (C; C120-1), and the anterior inclination of the the diplodocid teeth in respect to the jaw axis (C; C122-1). Abb.: an, angular; d, dentary; emf, external mandibular fenestra; sa, surangular; saf, surangular foramen; t, tooth. Scaled to the same mandibular length.

110: External mandibular fenestra: present (0); absent (1) (McIntosh, 1990b; Russell and Zheng, 1993; Fig. 6.32).

Comments. The presence is a retained plesiomorphy, shared with early sauropodomorphs (Wilson, 2002).

C111: Snout shape in dorsal view: premaxilla-maxilla index (PMI; Whitlock et al., 2010) < 67% (0); 67-85% (1); > 85% (2) (Upchurch, 1998; Whitlock, 2011a; modified; Tab. 6.15).

Comments. In order to avoid gaps, an intermediate state was added to Whitlock's (2011a) version. The state boundaries were chosen following high-level phylogenetic differences. Measurements taken on photos from slightly different angles of the skulls CM 3452, 11161, 11162, and SMA 0011 show that the orientation of the skull has a relatively high influence on the measured PMI (Tab. 6.15). In order to avoid this, the same measurements were taken in more than one picture of the same skulls, where possible. In future, one should check and remeasure this ratio in all diplodocid skulls, making

sure that they are always taken in exactly the same orientation. Best results are to be expected with the ventral maxillary edge oriented horizontally.
Whitlock et al. (2010) reported that the snout becomes more squared during ontogeny in diplodocids. It might thus be possible that more juvenile specimens become artificially grouped closer to more basal taxa when including this character. The character was treated as ordered.

Table 6.15: PMI (sensu Whitlock et al., 2010).

Taxon	Specimen	Ratio	Mean	Reference	Comments
Shunosaurus lii		58%	33,6%	Whitlock 2011b	
	ZG 65430, R	21%		Zheng 1996	measured from reconstruction
	ZG 65430, L	22%		Zheng 1996	measured from reconstruction
Mamenchisaurus	ZDM 0083	32%	32,0%	Ouyang & Ye 2002	measured from reconstruction
Jobaria tiguidensis		55%	54,1%	Whitlock 2011b	
	MNN TIG3-5	53%		Sereno et al. 1999	measured from reconstruction
Turiasaurus riodevensis	CPT-1211	66%	65,7%	Royo-Torres & Upchurch 2012	measured from reconstruction
Camarasaurus		63%	51,8%	Whitlock 2011b	
	CM 11338, L	51%		Madsen et al. 1995	measured from drawing
	CM 11338, R	54%		Madsen et al. 1995	measured from drawing
	DNM 28	39%		Chatterjee & Zheng 2005	measured from reconstruction
Giraffatitan brancai		68%	66,7%	Whitlock 2011b	
		71%		Janensch 1935	measured from reconstruction
		61%		Wilson & Sereno 1998	measured from reconstruction
Nigersaurus taqueti		95%	96,1%	Whitlock 2011b	
		97%		Sereno et al. 2007	measured from reconstruction
		97%		Whitlock 2011b	measured from reconstruction
Dicraeosaurus hansemanni		74%	74,7%	Whitlock 2011b	
		75%		Whitlock 2011b	measured from reconstruction
Suuwassea emilieae ANS 21122	ANS 21122	74%	74,8%	Whitlock 2011b	based on reconstruction
	ANS 21122	76%		Whitlock 2011b	measured from reconstruction
Apatosaurus louisae CM 11162	CM 11162, L	88%	82,7%	Whitlock & Lamanna 2012	measured from photo
	CM 11162, R	88%		Whitlock & Lamanna 2012	measured from photo
	CM 11162, L	73%		pers. obs.	measured from photo
	CM 11162, R	82%		pers. obs.	measured from photo
	CM 11162, L	82%		Berman & McIntosh 1978	measured from photo
	CM 11162, R	84%		Berman & McIntosh 1978	measured from photo
Kaatedocus siberi SMA 0004	SMA 0004	68%	68,0%	Tschopp & Mateus, in press	
Galeamopus shellensis AMNH 969	AMNH 969, L	83%	80,1%	O. Mateus, pers. comm. 2010	measured from photo
	AMNH 969, R	77%		O. Mateus, pers. comm. 2010	measured from photo
Diplodocus sp. CM 11161	CM 11161, L	75%	75,6%	pers. obs.	measured from photo
	CM 11161, R	81%		pers. obs.	measured from photo
	CM 11161, L	73%		pers. obs.	measured from photo
	CM 11161, R	73%		pers. obs.	measured from photo
Barosaurus sp. CM 3452	CM 3452	79%	74,7%	pers. obs.	
	CM 3452, R	74%		L. Witmer, pers. comm. 2013	measured from 3D model
	CM 3452, L	71%		L. Witmer, pers. comm. 2013	measured from 3D model
Galeamopus shellensis SMA 0011	SMA 0011	72%	70,3%	pers. obs.	measured from photo
	SMA 0011, R	74%		pers. obs.	measured from photo
	SMA 0011, L	65%		pers. obs.	measured from photo

Teeth

C112: Shape of tooth row in occlusal view: follows curvature of dentary (0); anterolateral corner of tooth row displaced labially (1) (Whitlock and Harris, 2010; Fig. 6.31).

Comments. In dicraeosaurids, it seems to be the tooth row, which is mostly responsible for the squared appearance of the lower jaw. The ventral portions of the dentary would be much more rounded (Whitlock and Harris, 2010). The diplodocid AMNH 969 has a similar development as *Suuwassea*.

C113: Tooth rows, length: restricted anterior to orbit (0); restricted anterior to antorbital fenestra (1); restricted anterior to subnarial foramen (2) (Gauthier, 1986; modified by Whitlock, 2011a; Fig. 6.1).

Comments. In order to score this character, the skull should be hold with the ventral margin of the maxilla oriented horizontally. The tooth row is usually more anteriorly restricted in the lower jaw than in the maxilla. Here, the maxillary tooth row is used as a reference. As the snout shape, also the anterior restriction of the tooth row was interpreted as juvenile feature (Whitlock et al., 2010). The character is treated as ordered.

C114: Dentary teeth, number: greater than 17 (0); 10-17 (1); 9 or fewer (2) (Wilson and Sereno, 1998; modified by Carballido et al., 2012b; Tab. 6.16).

Comments. Carballido et al. (2012b) added a third state to distinguish *Demandasaurus* and *Suuwassea* from other sauropod specimens. Since the reduction of the number of dentary teeth was accomplished and reversed several times, it is not entirely clear how evolution worked in this case. The character was therefore left unordered.

C115: Replacement teeth per alveolus, number: three or fewer (0); four or more (1) (Wilson, 2002).

Comments. The number of replacement teeth appears to change between the tooth-bearing bones of the same individual (Schwarz-Wings, pers. comm., 2012). However, maximum number of replacement teeth is still informative, and therefore the character was retained.

C116: Teeth, crown-to-crown occlusion: present (0); absent (1) (Wilson and Sereno, 1998; polarity reversed by Whitlock, 2011a).

C117: Teeth, wear facets shape: v-shaped (0); planar (1) (Wilson and Sereno, 1998; modified; Fig. 6.33).

Comments. The initial character (Wilson and Sereno 1998) was first adapted by Sereno et al. (2007), in order to include the paired planar facets of *Nigersaurus*. Here, the shape and number of wear facets are considered independent characters (see character 118).

C118: Teeth, occlusal pattern: paired wear facets (0); single facet (1) (Wilson and Sereno, 1998; modified; Fig. 6.34).

Comments. See character 117.

C119: Teeth, SI values for tooth crowns: < 3.4 (0); 3.4 or greater (1) (McIntosh, 1989; Upchurch, 1998; modified; Tab. 6.17).

Comments. The SI value describes the slenderness of the teeth. It was defined as crown length/mesiodistal width (Upchurch, 1998). The state borders were changed, following large gaps apparently corresponding to higher-level taxonomy (Tab. 6.17).

Table 6.16: Number of dentary teeth.

Taxon	Specimen	Number	Mean	Reference	Comments
Shunosaurus lii	ZG 65430	>25	23	Chatterjee & Zheng 2002	
	T5401, R	22		Zhang 1988	based on drawing
	T5401, L	20		Zhang 1988	based on drawing
		25		Mannion et al., in press	
Omeisaurus	T5703, R	15	19	He et al. 1988	
		23		Mannion et al., in press	
Mamenchisaurus	ZDM 0083, L	24	24	Ouyang & Ye 2002	based on drawing
	ZDM 0083, R	24		Ouyang & Ye 2002	based on drawing
		23		Mannion et al., in press	
Jobaria tiguidensis	MNN TIG 3-5	?20	20	Sereno et al. 1999	
Camarasaurus	DNM 28, L	13	13	Madsen et al. 1995	based on drawing
	DNM 975, L	14		Madsen et al. 1995	based on photo
	CM 11338, L	13		Madsen et al. 1995	based on drawing
	SMA 0002, L	13		pers. obs.	
		13		Mannion et al., in press	
	USNM 13786	13		Janensch 1935	
	AMNH 467	13		Janensch 1935	
Giraffatitan brancai	MB.R. T1	13	14	Janensch 1935	based on reconstruction
	MB.R. S66	14			
	MB.R. S116, L	14			
	MB.R. S116, R	15			
		13		Mannion et al., in press	
Brachiosaurus altithorax	USNM 5730, R	14	14	Carpenter & Tidwell 2001	
Nigersaurus taqueti	MNN GDF512	34	34	Sereno et al. 1999	
		34		Mannion et al., in press	
Demandasaurus darwini	MDS-RVII,443, L	9	9	Torcida Fernández-Baldor et al. 2011	
Dicraeosaurus hansemanni	MB.R.2372, L	16	16	pers. obs.	
Suuwassea emilieae ANS 21122	ANS 21122, L	9	9	pers. obs.	
Kaatedocus siberi SMA 0004	SMA 0004	12 to 13	13	Tschopp & Mateus, in press	
Galeamopus shellensis AMNH 969	AMNH 969	10	10	pers. obs.	
Diplodocus sp. CM 11161	CM 11161	11	11	pers. obs.	
Barosaurus sp. CM 3452	CM 3452	11 to 12	12	pers. obs.	
Diplodocus sp. USNM 2672	USNM 2672	10 to 11	11	pers. obs.	
Galeamopus shellensis SMA 0011	SMA 0011	11 to 12	12	pers. obs.	

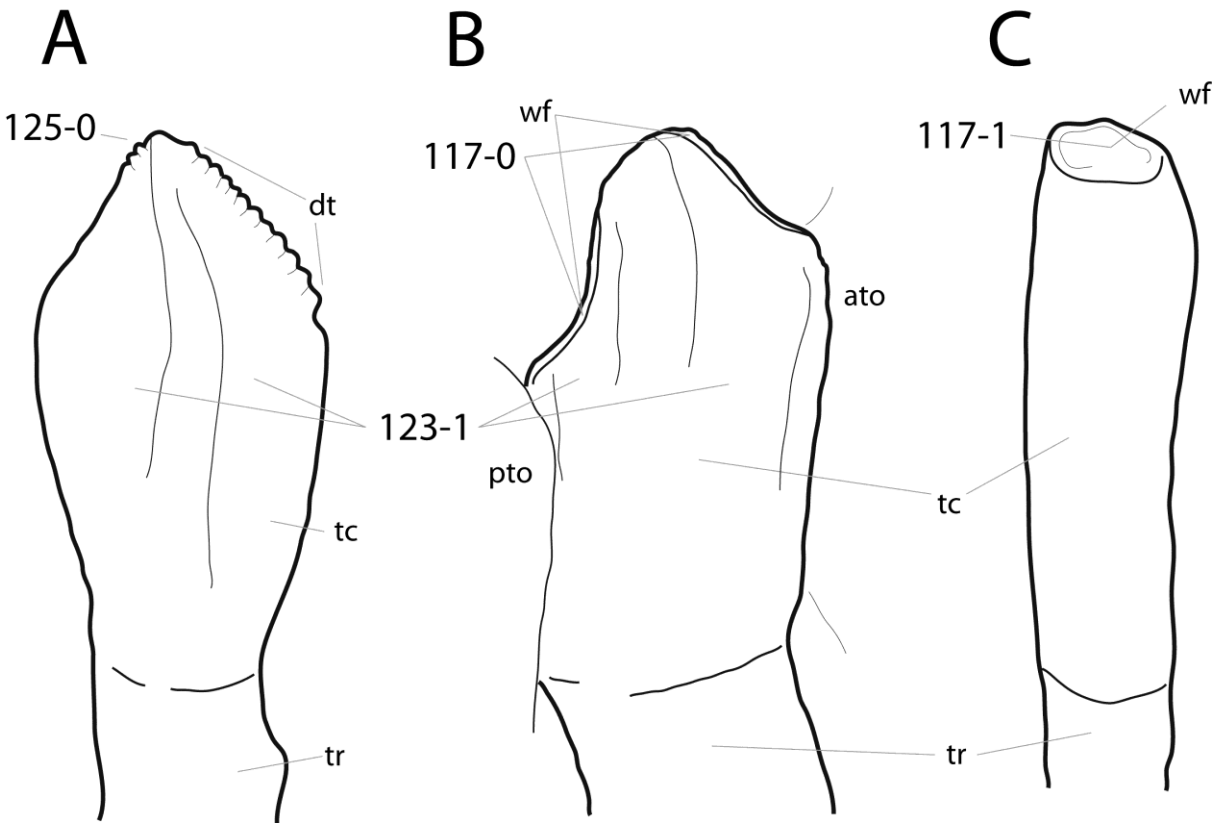

Figure 6.33: Tooth of *Omeisaurus tianfuensis* T5705 (A; traced from He et al., 1998), *Camarasaurus* sp. SMA 0002 (B; traced from a photo by O. Mateus), and Diplodocinae indet. CM 3452 (C) in lingual view. Note the V-shaped wear facets in *Camarasaurus* (B; C117-0), in contrast to the single, planar facet in diplodocids (C; C117-1), the longitudinal grooves in *Omeisaurus* and *Camarasaurus* (A, B; C123-1), and the marginal tooth denticles in *Omeisaurus* (A; C125-0). Abb.: ato, anterior tooth; dt, denticles; pto, posterior tooth; tc, tooth crown; tr, tooth root; wf, wear facet. Teeth scaled to the same crown length.

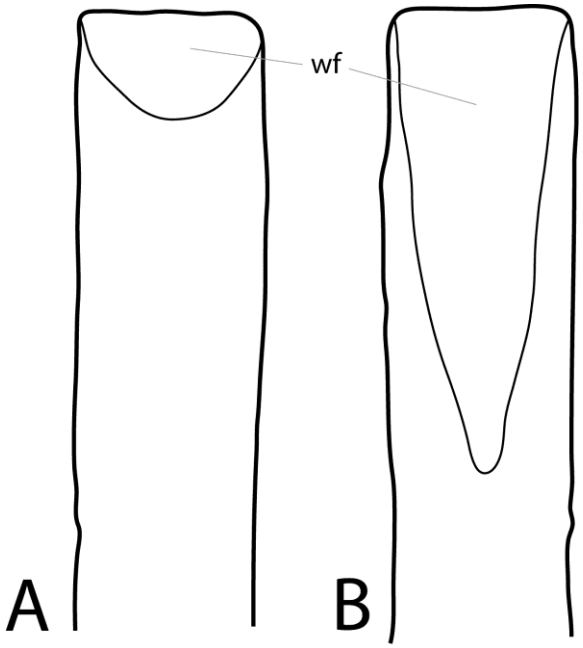

Figure 6.34: Tooth of *Nigersaurus* in labial (A) and lingual (B) view, showing the paired, planar wear facets typical for Rebbachisauridae (C117-1; C118-0). Abb.: wf, wear facet. Figure traced from Whitlock (2011b).

Table 6.17: Slenderness indices of teeth.

Taxon	Specimen	Ratio	Mean	Reference	Comments
Shunosaurus lii		2,3	2,3	Mannion et al., 2013	
		2,31		Chure et al. 2010	
		3 to 4		Carballido et al. 2012b	unclear, which one is true
Omeisaurus		1,9	2,1	Mannion et al., 2013	
		2,23		Chure et al. 2010	
		<3		Carballido et al. 2012b	
Mamenchisaurus		2,9	2,7	Mannion et al., 2013	
		2,42		Chure et al. 2010	
		<3		Carballido et al. 2012b	
Jobaria tiguidensis		1,36	1,4	Chure et al. 2010	
		<3		Carballido et al. 2012b	
Turiasaurus riodevensis		1,25	1,4	Chure et al. 2010	
	CPT	1,45		Royo-Torres & Upchurch 2012	
	CPT	1,53		Royo-Torres & Upchurch 2012	
	CPT-1213	1,28		Royo-Torres & Upchurch 2012	
		<3		Carballido et al. 2012b	
Camarasaurus		2	1,6	Mannion et al., 2013	
	SMA 0002	1,37		K. Wiersma, pers. comm. 2012	min SI pm
	SMA 0002	1,77		K. Wiersma, pers. comm. 2012	max SI pm
	SMA 0002	1,03		K. Wiersma, pers. comm. 2012	min SI m
	SMA 0002	1,84		K. Wiersma, pers. comm. 2012	max SI m
	SMA 0002	1,2		K. Wiersma, pers. comm. 2012	min SI d
	SMA 0002	1,86		K. Wiersma, pers. comm. 2012	max SI d
		1,92		Chure et al. 2010	
		<3		Carballido et al. 2012b	
Giraffatitan brancai		2,3	3,1	Mannion et al., 2013	
	MB.R. S116	3,98		Janensch 1935	last maxillary tooth
		3 to 4		Carballido et al. 2012b	
Brachiosaurus altithorax	USNM 5730	1,69	1,7	Carpenter & Tidwell 1998	measured from photo
		3 to 4		Carballido et al. 2012b	unclear, which one is true, USNM 5730 might not be *Brachiosaurus* (Mannion et al., 2013)
Ligabuesaurus leanzai		2,70	2,3	Mannion et al., 2013	
		1,96		Chure et al. 2010	
		3 to 4		Carballido et al. 2012b	unclear, which one is true
Limaysaurus tessonei		5,23	5,2	Chure et al. 2010	
		>5		Carballido et al. 2012b	
Nigersaurus taqueti		5,00	5,0	Mannion et al., 2013	
		4,96		Chure et al. 2010	
		>5		Carballido et al. 2012b	unclear, which one is true
Demandasaurus darwini	MDS-RVII,436	4,33	3,0	Torcida Fernández-Baldor et al. 2011	length estimated
	MDS-RVII,340	2,73		Torcida Fernández-Baldor et al. 2011	length estimated
	MDS-RVII,437	3,36		Torcida Fernández-Baldor et al. 2011	
	MDS-RVII,438	2,82		Torcida Fernández-Baldor et al. 2011	
	MDS-RVII,440	2,42		Torcida Fernández-Baldor et al. 2011	
	MDS-RVII,441	2,40		Torcida Fernández-Baldor et al. 2011	
		>5		Carballido et al. 2012b	probably wrong, given the above measurements
Dicraeosaurus hansemanni		4,52	4,3	Chure et al. 2010	
		4,77		Janensch 1935	
		3,47		Janensch 1935	
		>5		Carballido et al. 2012b	unclear, which one is true
Apatosaurus louisae CM 11162	CM 11162	4,19	4,9	pers. obs.	measured from photo
	CM 11162	5,68		pers. obs.	measured from photo
Diplodocus lacustris YPM 1922	YPM 1922	4,60	4,4	pers. obs.	measured from photo
	YPM 1922	4,84		pers. obs.	measured from photo
	YPM 1922	3,89		pers. obs.	measured from photo
Galeamopus shellensis AMNH 969	AMNH 969	4,69	4,4	pers. obs.	measured from photo
	AMNH 969	3,58		pers. obs.	measured from photo
	AMNH 969	4,18		pers. obs.	measured from photo
	AMNH 969	4,71		pers. obs.	measured from photo
	AMNH 969	4,85		pers. obs.	measured from photo
Diplodocus sp. CM 11161	CM 11161	5,56	4,3	pers. obs.	measured from photo
	CM 11161	4,47		pers. obs.	measured from photo
	CM 11161	3,88		pers. obs.	measured from photo
	CM 11161	3,10		pers. obs.	measured from photo
Diplodocinae indet. CM 3452	CM 3452	3,13	3,5	pers. obs.	measured from photo
	CM 3452	3,79		pers. obs.	measured from photo
Diplodocus sp. USNM 2672	USNM 2672	4,15	4,1	O. Mateus, pers. comm. 2010	measured from photo
	USNM 2672	4,00		pers. obs.	measured from photo
Galeamopus shellensis SMA 0011	SMA 0011	3,89	4,0	pers. obs.	measured from photo
	SMA 0011	4,17		pers. obs.	
	SMA 0011	4		pers. obs.	

C120: Tooth crowns, orientation: aligned slightly anterolingually, tooth crowns overlap (0); aligned along jaw axis, crowns do not overlap (1) (Wilson and Sereno, 1998; polarity reversed by Whitlock, 2011a; Fig. 6.32).

C121: Tooth crowns, cross-sectional shape at midcrown: D-shaped (0); cylindrical (1) (Russell and Zheng, 1993; modified by Wilson and Sereno, 1998; Fig. 6.35).

Comments. Unworn diplodocoid teeth often have ellipsoid cross-sections. However, this is different from the spatulate non-diplodocoid teeth as e.g. typical for *Camarasaurus*. Teeth of the latter genus have a slightly concave lingual face, unlike the convex surface of diplodocoids. In the absence of nemegtosaurid titanosaurs, which show similarly shaped teeth (Upchurch, 1999; Wilson, 2005), the derived state thus results as unambiguous synapomorphy of Diplodocoidea.

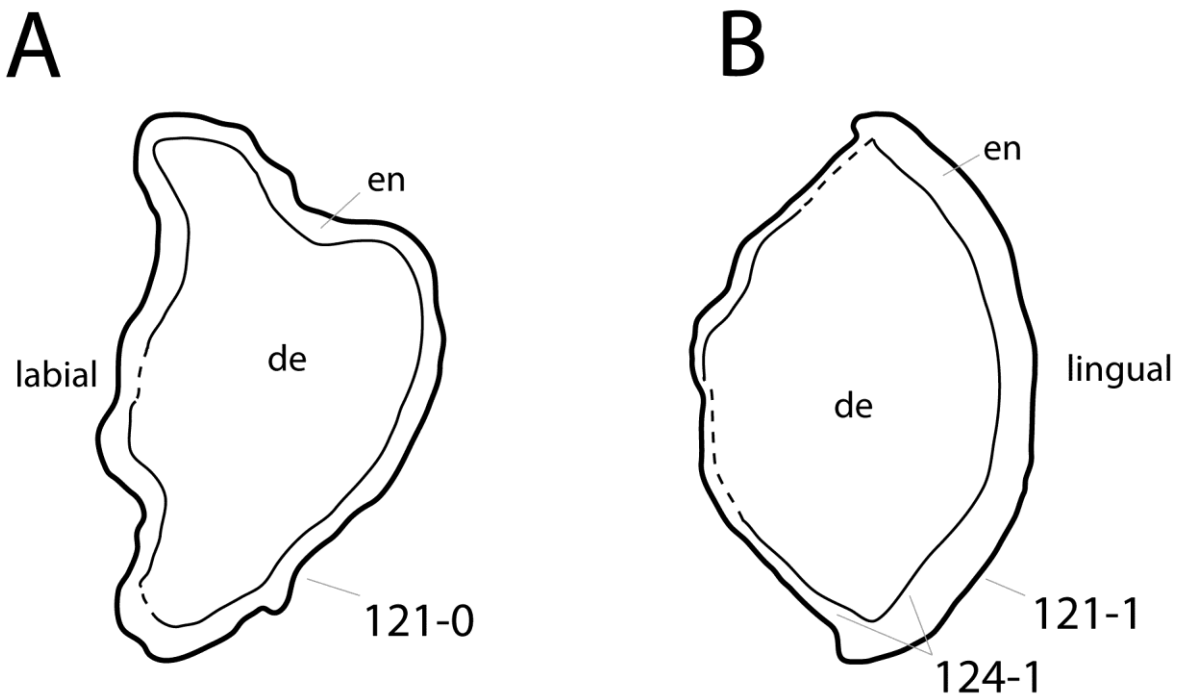

Figure 6.35: Tooth cross-section of *Camarasaurus* sp. AMNH 5764 (A), and *Demandasaurus darwini* MDS-RVII,438 (B; traced from Torcida Fernández-Baldor et al., 2011). Note the D-shaped crown of *Camarasaurus* (A; C121-0) in contrast with the rounded cross-section of diplodocoids (B; C121-0), and the asymmetric disposition of the enamel typical for rebbachisaurids (B; C124-1). The camarasaur tooth has the same specimen number as *Amphicoelias altus* holotype, but not the same individual (see text). Abb.: de, dentin; en, enamel. Scaled to the same mesiodistal width.

C122: Teeth, orientation relative to long axis of jaw: perpendicular (0); oriented anteriorly (procumbent) (1) (Upchurch, 1998; Fig. 6.32).

Comments. Tooth orientation is best recognized in the posterior-most teeth in the maxilla and dentary.

C123: Teeth, longitudinal grooves on lingual aspect: absent (0); present (1) (Wilson, 2002; Fig. 6.33).

Comments. Wilson (2002) initially scored only rebbachisaurids with the derived state. However, several non-diplodocoid taxa with spatulate teeth actually have a midline ridge on the lingual face of their teeth, creating two grooves mesially and distally to it (e.g. Osborn and Mook, 1921; Ouyang and Ye, 2002). Consequently, these taxa are scored as derived here as well.

C124: Teeth, thickness of enamel asymmetric labiolingually: absent (0); present (1) (Whitlock, 2011a; Fig. 6.35).

Comments. This feature can be observed easily in wear facets or cross-sections.

C125: Teeth, marginal denticles: present (0); absent (1) (McIntosh, 1990b; Fig. 6.33).

Comments. There is some morphological variation in the location of the denticles (Carballido et al., 2012b), but as no diplodocid shows denticles, this simplified version of the character is used herein.

Cervical vertebrae

C126: Presacral neural spines, bifurcation: absent (0); present (1) (McIntosh, 1989; Wilson, 2002; modified; Tab. 6.18).

Comments. Wilson (2002) divided this character into the different regions, where the bifurcation can be present. However, like this, taxa with unbifurcated neural spines are coded several times for the same state. In the present analysis, presence of bifurcation and the first bifid element are treated as two different characters (see character 140).

C127: Number of cervical vertebrae: < 13 (0); 14-15 (1); 16 or more (2) (McIntosh, 1990b; modified; Tab. 6.19).

Comments. The character is used in various versions in different phylogenetic analyses (Upchurch, 1998; Wilson, 2002; Whitlock, 2011a), depending on their specific focus. Herein, the states are adjusted to fit the included taxa, excluding redundancy. Only very few diplodocid specimens preserve complete necks (CM 84, 3018), and even here, the possibility of lacking elements cannot be ruled out entirely, due to gaps between certain cervical vertebrae as they were found (McIntosh, 2005). However, as the more anterior and posterior elements in these cases fit well together, I followed McIntosh (2005) in assuming that no vertebra was lost at the position of these gaps in CM 84 and 3018. McIntosh (2005) suggested that *Barosaurus* had 16 cervical vertebrae, instead of 15 as *Apatosaurus* and *Diplodocus*. The assumption was primarily based on the fact that AMNH 6341 only has nine dorsal vertebrae, and that the neosauropod presacral column generally consists of 25 elements (McIntosh, 2005). Since none of the *Barosaurus* specimens preserves an entire neck, none of the *Barosaurus* OTUs can be coded for this character. The inability to code incomplete specimens might be circumvented by using additive binary characters (Upchurch, 1998). However, this would imply that the corresponding multi-state character is continuous (Wilson, 2002), which means that the number of cervical vertebrae could not increase directly by more than one element during speciation. Given that the contrary is shown to be possible in dorsal and sacral vertebrae of mice (Wellik and Capecchi, 2003; C. Boehmer, pers. comm., 2013), it seems reasonable to argue that the same accounts for sauropod cervical vertebrae. The character is thus treated as unordered herein. This also indicates that 'analysis 1' of Mannion et al. (2012), where these characters are treated as unordered, should be preferred over 'analysis 2'.

C128: Cervical vertebrae width to height ratio: less than 0.5 (0); 0.5-1.5 (1); more than 1.5 (2) (Upchurch et al., 2004b; modified; Tab. 6.20)

Comments. Upchurch et al. (2004b: p. 105) defined the ratio as follows: „Height is measured from the top of the neural spine to the ventral surface of the centrum. Width is defined as the distance between the distal tips of the diapophyses." A third state was added (less than 0.5) as dicraeosaurids have a distinctly lower ratio compared to other flagellicaudatans. Given that evolution appears to have worked in both directions, the character is left unordered.

C129: Cervical pneumatopores (pleurocoels): absent (0); present (1) (McIntosh, 1990b; Upchurch, 1995; Fig. 6.36).

Comments. McIntosh (1990b) already used this character to distinguish advanced sauropods from the most basal forms, but Upchurch (1995) was the first to include it into a phylogenetic analysis.

C130: Cervical centra, internal pneumaticity: absent (0); present with single and wide cavities (1); present, with several small and complex internal cavities (2) (Upchurch, 1998; Wilson and Sereno, 1998; modified by Carballido et al., 2012b; Fig. 6.37).

Comments. Introduced as character by Upchurch (1998) and Wilson and Sereno (1998), only Wedel et al. (2000) and Wedel (2003) analyzed the distribution of this feature in detail. Carballido et al. (2012b) divided the original character, which did not discriminate between cervical and dorsal vertebrae (Upchurch, 1998; Wilson and Sereno, 1998).

C131: Cervical vertebrae, small fossa on posteroventral corner: absent (0); shallow, anteroposteriorly elongate fossa present, posteroventral to pleurocoel (1) (Whitlock, 2011a; Fig. 6.36).

Comments. *Kaatedocus siberi* SMA 0004, AMNH 7530, and the apatosaurines YPM 1980 and AMNH 460 have shallow depressions at the same place, but they do not create distinct fossae as in *Barosaurus* or *Diplodocus* (see Hatcher, 1901; McIntosh, 2005), and are thus coded as plesiomorphic.

Table 6.18: Presacral neural spine bifurcation.

Taxon	Specimen	Present	Position	Summary	Reference	Comments
Shunosaurus lii	T5402	no		unbifurcated	Zhang 1988	
		no			Harris 2006c	
Spinophorosaurus nigerensis	holotype	no		unbifurcated	Remes et al. 2009	
	paratype	no			Remes et al. 2009	
Omeisaurus	T5701	no		unbifurcated	He et al. 1984	
	T5703	?	CV 11 single		He et al. 1988	more posterior elements not shown/known
		no			Harris 2006c	
Mamenchisaurus	AL 001	yes	pCV bifid	pCV bifid	He et al. 1996	
	holotype M. hochuanensis	yes	anterior pCV bifid		Young & Zhao 1972	
		yes	pCV bifid		Harris 2006c	
	ZDM 0083	yes	CV 17		Ouyang & Ye 2002	
Jobaria tiguidensis		no		unbifurcated	Harris 2006c	
Turiasaurus riodevensis		yes			Royo-Torres et al. 2006	position unclear
Losillasaurus giganteus	type	no		unbifurcated	Harris 2006c	
Camarasaurus		yes	pCV bifid	reaching at least CV 7 (mCV)	Harris 2006c	
	CM 11338	yes	CV 7		Wedel & Taylor 2013	
	YPM 1905	yes	CV 3 bifid		Wedel & Taylor 2013	
	GMNH-PV 101	yes	CV 5		Wedel & Taylor 2013	CV 3 notched
	AMNH 5671	yes	CV 7		Wedel & Taylor 2013	CV 5 notched, unclear if single individual
	BYU 9047	yes	CV 3		Wedel & Taylor 2013	
Apatosaurus grandis	YPM 1901	yes	present in aDV		Wilson & Sereno 1998	no CV preserved
Giraffatitan brancai		no		unbifurcated	Janensch 1950	
Brachiosaurus	sp. SMA 0009	?	aCV and mCV single		Carballido et al. 2012a	state unknown in pCV
Australodocus bohetii	type MB.R.2454-2455	yes	CV 6 bifid		Remes 2007	only CV 6 and 7 preserved
Ligabuesaurus leanzai	MCF-PVPH-233	no		unbifurcated	Bonaparte et al. 2006	only pCV preserved
Isisaurus colberti	ISIR355	no		unbifurcated	Jain & Bandyopadhyay 1997	
Haplocanthosaurus priscus		no		unbifurcated	Harris 2006c	
	CM 879	no			Wedel & Taylor 2013	
Limaysaurus tessonei		no		unbifurcated	Harris 2006c	
	MUCPv-205	no			Calvo & Salgado 1995	
Cathartesaura anaerobica	MPCA-232	no		unbifurcated	Gallina & Apesteguía 2005	only pCV preserved
Zapalasaurus bonapartei		?	mCV or pCV single		Salgado et al. 2006	only one partial CV preserved
Nigersaurus taqueti		no		unbifurcated	Harris 2006c	
Amphicoelias altus	AMNH 5764	yes	present in aDV		Osborn & Mook 1921	no CV preserved
Dicraeosaurus hansemanni		yes	anterior to CV 6	reaching CV 3	Harris 2006c	
	MB.R.4886	yes	CV 3		pers. obs.	
Brachytrachelopan mesai	MPEF PV 1716	yes	CV 5 bifid		Rauhut et al. 2005	more anterior elements not preserved
Amargasaurus cazaui		yes	anterior to CV 6	reaching CV 3	Harris 2006c	
	MACN-N 15	yes	CV 3		Salgado & Bonaparte 1991	
Suuwassea emilieae	ANS 21122	yes	CV 6		Harris 2006c	
	ANS 21122	yes	CV 6		Wedel & Taylor 2013	CV 2 notched
Apatosaurus ajax	YPM 1860	YPM 1860	yes		pers. obs.	position unclear
Apatosaurus laticollis	YPM 1861	YPM 1861	yes		pers. obs.	position unclear
Brontosaurus excelsus	YPM 1980	YPM 1980	yes		pers. obs.	position unclear
Apatosaurus louisae	CM 3018	CM 3018	yes	CV 6 bifid	includes all mCV	Wedel & Taylor 2013	more anterior elements damaged
Atlantosaurus immanis	YPM 1840	YPM 1840	yes		Ostrom & McIntosh 1966	position unclear
Apatosaurus parvus	CM 566	CM 566	yes		pers. obs.	position unclear
Apatosaurus parvus	UW 15556	UW 15556	yes	CV 6 or 7	includes all mCV	Wedel & Taylor 2013	CV 6 lacking
Eobrontosaurus yahnahpin	Tate-001	Tate-001	yes	CV 4 single		P. Mannion, pers. comm., 2012	more posterior elements not preserved
Apatosaurus ajax	NSMT-PV 20375	NSMT-PV 20375	yes	CV 4, 5, or 6	includes all mCV	Wedel & Taylor 2013	CV 4 and 5 lacking
Apatosaurus	sp. AMNH 460	AMNH 460	yes			pers. obs.	position unclear
Apatosaurus	sp. FMNH P25112	FMNH P25112	yes	present in aDV		Wedel & Taylor 2013	no CV preserved
Apatosaurinae indet.	SMA 0087	SMA 0087	yes	present in aDV		pers. obs.	no CV preserved
Supersaurus vivianae	BYU	BYU 9024	yes			R. Wilhite, pers. comm., 2012	position unclear
Dinheirosaurus lourinhanensis	ML 414	ML 414	no		unbifurcated	Mannion et al. 2012	
Kaatedocus siberi	SMA 0004	SMA 0004	yes	CV 8	reaching mCV	Tschopp & Mateus, in press	
Diplodocus carnegii	CM 84	CM 84	yes	CV 3, 4, 5, or 6	includes all mCV	Wedel & Taylor 2013	CV 3 to 5 lacking
Diplodocus carnegii	CM 94	CM 94	yes			pers. obs.	position unclear
Diplodocus	sp. AMNH 223	AMNH 223	yes	present in aDV		pers. obs.	no CV preserved
Diplodocus	sp. USNM 10865	USNM 10865	yes	present in aDV		Wedel & Taylor 2013	no CV preserved
Diplodocus	sp. DMNS 1494	DMNS 1494	yes	CV 11 bifid		pers. obs.	more anterior elements not preserved
Diplodocinae indet.	CM 3452	CM 3452	?	CV 6 single	reaching mCV	pers. obs.	more posterior elements not preserved
Galeamopus hayi	HMNS 175	HMNS 175	yes	CV 5 bifid	includes all mCV	pers. obs.	more anterior elements damaged
Seismosaurus hallorum	NMMNH 3690	NMMNH 3690	yes	present in aDV		Gillette 1991	no CV preserved
Galeamopus shellensis	SMA 0011	SMA 0011	yes	CV 9	reaching mCV	pers. obs.	could also be CV 8 or 10
Barosaurus lentus	YPM 429	YPM 429	yes			pers. obs.	position unclear
Barosaurus	sp. AMNH 6341	AMNH 6341	yes	CV 9	reaching mCV	McIntosh 2005	
Barosaurus	sp. AMNH 7530	AMNH 7530	yes	CV 9	reaching mCV	pers. obs.	
Barosaurus	sp. CM 11984	CM 11984	yes			pers. obs.	position unclear
Barosaurus	sp. AMNH 7535	AMNH 7535	yes	CV 9	reaching mCV	pers. obs.	

C132: Cervical centra, midline keels on ventral surface: prominent and plate-like (0); reduced to low ridges (1) (Upchurch, 1998; Upchurch et al., 2004a; modified; Fig. 6.38).

Comments. Since the presence or absence is already coded for in following characters, the complete absence is here excluded from the original character description (Upchurch, 1998; Upchurch et al., 2004a), and taxa without ventral ridges are scored as unknown.

C133: Cervical vertebrae, longitudinal sulcus on ventral surface: absent (0); present (1) (Upchurch, 1995, 1998; Fig. 6.38).

Comments. Due to the lateroventral projecting cervical parapophyses of *Apatosaurus*, cervical vertebrae of this genus have a concave anterior portion of the ventral surface. However, this is the case in almost all sauropod taxa, and therefore only specimens with transversely concave ventral surfaces throughout the entire length of the centrum are herein scored as apomorphic.

Table 6.19: Number of cervical vertebrae.

Taxon	Specimen	Number	Mean	Reference
Shunosaurus lii		13	13	Mannion et al., 2013
		13		Remes et al. 2009
		13		Taylor 2009
Spinophorosaurus nigerensis		13	13	Remes et al. 2009
Omeisaurus		17	17	Mannion et al., 2013
Mamenchisaurus		18	18	Mannion et al., 2013
Jobaria tiguidensis		12	12 to 13	Carballido et al. 2012b
		13		Remes et al. 2009
		12		Taylor 2009
Camarasaurus		12	12	Mannion et al., 2013
	BYU 9047	12		McIntosh et al. 1996b
	CM 11338	12		Gilmore 1925
	USNM 13786	12		pers. obs.
	SMA 0002	12		pers. obs.
		12		Remes et al. 2009
Giraffatitan brancai		13	13	Remes et al. 2009
		13		Taylor 2009
Nigersaurus taqueti		13	13	Mannion et al., 2013
Dicraeosaurus hansemanni		12	12	Carballido et al. 2012b
		12		Remes et al. 2009
Amargasaurus cazaui		12	12 to 13	Carballido et al. 2012b
		13		Remes et al. 2009
		13		Taylor 2009
Apatosaurus louisae CM 3018	CM 3018	15	15	pers. obs.
Kaatedocus siberi SMA 0004	SMA 0004	14+	14+	pers. obs.
Diplodocus carnegii CM 84	CM 84	15	15	pers. obs.
Galeamopus shellensis SMA 0011	SMA 0011	13+	13+	pers. obs.

Table 6.20: Cervical width/height ratio.

Taxon	Specimen	Ratio	Mean	Reference	Comments
Shunosaurus lii	T5402, CV 12	0,624	0,62	Zhang 1988	measured from drawing
Spinophorosaurus nigerensis	NMB-1698-R, CV 2	0,767	0,76	pers. obs.	measured from digital model
	NMB-1698-R, CV 3	0,734		pers. obs.	measured from digital model
	NMB-1698-R, mCV	0,878		pers. obs.	measured from digital model
	NMB-1698-R, mCV	0,669		pers. obs.	measured from digital model
Mamenchisaurus	ZDM 0083, CV 17	0,939	0,94	Ouyang & Ye 2002	measured from drawing
	ZDM 0083, CV 18	0,943		Ouyang & Ye 2002	measured from drawing
Losillasaurus giganteus type	MCNV Lo-17, CV ?3	0,375	0,38	pers. obs.	measured from photo
Camarasaurus	GMNH-PV 101, CV 2	0,381	0,47	McIntosh et al. 1996a	
	GMNH-PV 101, CV 3	0,412		McIntosh et al. 1996a	
	GMNH-PV 101, CV 4	0,520		McIntosh et al. 1996a	
	GMNH-PV 101, CV 5	0,604		McIntosh et al. 1996a	
	GMNH-PV 101, CV 6	0,569		McIntosh et al. 1996a	
	GMNH-PV 101, CV 8	0,456		McIntosh et al. 1996a	
	BYU 9047, CV 2	0,354		McIntosh et al. 1996a	
	BYU 9047, CV 3	0,419		McIntosh et al. 1996a	
	BYU 9047, CV 4	0,468		McIntosh et al. 1996a	
	BYU 9047, CV 5	0,587		McIntosh et al. 1996a	
	BYU 9047, CV 7	0,532		McIntosh et al. 1996a	
	BYU 9047, CV 8	0,671		McIntosh et al. 1996a	
	YPM 1905, CV 2	0,327		McIntosh et al. 1996a	
	YPM 1905, CV 3	0,431		McIntosh et al. 1996a	
	YPM 1905, CV 4	0,447		McIntosh et al. 1996a	
	YPM 1905, CV 5	0,420		McIntosh et al. 1996a	
Giraffatitan brancai		0,526	0,65	pers. obs.	
		0,526		pers. obs.	
		0,667		pers. obs.	
		0,909		pers. obs.	
		0,667		pers. obs.	
		0,625		pers. obs.	
Ligabuesaurus leanzai	MCF-PVPH-233/2, pCV	1,632	1,63	Bonaparte et al. 2006	width estimated

Table 6.20: continued.

Isisaurus colberti	ISIR 335/2	1,160	1,08	Jain & Bandhyopadhyay 1997	estimated
	ISIR 335/8	1,000		Jain & Bandhyopadhyay 1997	
Haplocanthosaurus priscus	CM 879, CV ?4	1,132	1,00	Hatcher 1903	
	CM 879, CV ?8	1,094		Hatcher 1903	
	CM 879, CV ?10	0,980		Hatcher 1903	
	CM 879, CV ?11	0,907		Hatcher 1903	
	CM 879, CV ?12	0,918		Hatcher 1903	
	CM 879, CV ?13	0,974		Hatcher 1903	
Nigersaurus taqueti	GAD512-13, CV 3	0,784	0,89	Sereno et al. 2007	measured from digital model
	GAD512-14, CV 5	0,786		Sereno et al. 2007	measured from digital model
	GAD512-15, CV 6	1,091		Sereno et al. 2007	measured from digital model
Dicraeosaurus hansemanni	MB.R.4886, CV 2	0,322	0,43	Janensch 1929a	
	MB.R.4886, CV 3	0,490		Janensch 1929a	
	MB.R.4886, CV 4	0,319		Janensch 1929a	
	MB.R.4886, CV 5	0,330		Janensch 1929a	width slightly too short
	MB.R.4886, CV 6	0,356		Janensch 1929a	
	MB.R.4886, CV 7	0,401		Janensch 1929a	
	MB.R.4886, CV 8	0,438		Janensch 1929a	
	MB.R.4886, CV 9	0,520		Janensch 1929a	Width slightly too short
	MB.R.4886, CV 11	0,546		Janensch 1929a	left diapophysis reconstructed
	MB.R.4886, CV 12	0,626		Janensch 1929a	left diapophysis reconstructed
Amargasaurus cazaui	MACN-N 15, CV 2	0,313	0,29	Salgado & Bonaparte 1991	measured from drawing
	MACN-N 15, CV 6	0,192		Salgado & Bonaparte 1991	measured from drawing
	MACN-N 15, CV 8	0,362		Salgado & Bonaparte 1991	measured from drawing
Suuwassea emilieae ANS 21122	ANS 21122, CV 2	0,335	0,41	Harris 2006	deformed
	ANS 21122, CV 2	0,395		pers. obs.	
	ANS 21122, CV 3	0,464		Harris 2006	broken
	ANS 21122, CV 5	0,407		Harris 2006	deformed
	ANS 21122, CV 6	0,455		Harris 2006	deformed
Apatosaurus laticollis YPM 1861	YPM 1861	2,240	2,24	Upchurch et al. 2004b	
Brontosaurus excelsus YPM 1980	YPM 1980	1,000	1,00	Upchurch et al. 2004b	
Apatosaurus louisae CM 3018	CM 3018	1,330	1,33	Upchurch et al. 2004b	
Atlantosaurus immanis YPM 1840	YPM 1840	1,720	1,72	Upchurch et al. 2004b	
Apatosaurus parvus UW 15556	UW 15556	1,270	1,27	Upchurch et al. 2004b	
Eobrontosaurus yahnahpin Tate-001	Tate-001, CV ?7	1,615	1,62	Filla & Redman 1994	
Apatosaurus ajax NSMT-PV 20375	NSMT-PV 20375	1,770	1,77	Upchurch et al. 2004b	
Kaatedocus siberi SMA 0004	SMA 0004, CV 3	0,483	0,65	Tschopp & Mateus, in press	
	SMA 0004, CV 4	0,620		Tschopp & Mateus, in press	
	SMA 0004, CV 5	0,649		Tschopp & Mateus, in press	
	SMA 0004, CV 6	0,639		Tschopp & Mateus, in press	
	SMA 0004, CV 7	0,612		Tschopp & Mateus, in press	
	SMA 0004, CV 8	0,761		Tschopp & Mateus, in press	
	SMA 0004, CV 9	0,677		Tschopp & Mateus, in press	
	SMA 0004, CV 10	0,689		Tschopp & Mateus, in press	
	SMA 0004, CV 11	0,619		Tschopp & Mateus, in press	
	SMA 0004, CV 12	0,624		Tschopp & Mateus, in press	
	SMA 0004, CV 13	0,728		Tschopp & Mateus, in press	
	SMA 0004, CV 14	0,744		Tschopp & Mateus, in press	
Diplodocus carnegii CM 84	CM 84, CV 13	0,788	0,87	Hatcher 1901	
	CM 84, CV 15	0,959		Hatcher 1901	
Galeamopus shellensis AMNH 969	AMNH 969, CV 2	0,711	0,71	pers. obs.	measured from photo
Diplodocinae indet. CM 3452	CM 3452, CV 4	1,029	0,93	pers. obs.	measured from photo
	CM 3452, CV 6	0,837		pers. obs.	measured from photo
Barosaurus lentus YPM 429	YPM 429, pCV	1,421	1,42	pers. obs.	
Barosaurus sp. AMNH 6341	AMNH 6341, CV 8	0,817	0,82	McIntosh 2005	
	AMNH 6341, CV 9	0,813		McIntosh 2005	
	AMNH 6341, CV 10	0,846		McIntosh 2005	
	AMNH 6341, CV 11	0,799		McIntosh 2005	
	AMNH 6341, CV 12	0,807		McIntosh 2005	
	AMNH 6341, CV 13	0,832		McIntosh 2005	
	AMNH 6341, CV 14	0,808		McIntosh 2005	
	AMNH 6341, CV 15	0,813		McIntosh 2005	
	AMNH 6341, CV 16	0,822		McIntosh 2005	
Barosaurus sp. AMNH 7530	AMNH 7530, CV 2	0,427	0,58	pers. obs.	
	AMNH 7530, CV 3	0,580		pers. obs.	
	AMNH 7530, CV 5	0,720		pers. obs.	
Barosaurus sp. CM 11984	CM 11984, pCV	0,608	0,67	pers. obs.	
	CM 11984, pCV	0,630		pers. obs.	
	CM 11984, pCV	0,781		pers. obs.	
Barosaurus sp. AMNH 7535	AMNH 7535, CV 2	0,431	0,69	pers. obs.	
	AMNH 7535, CV 3	0,843		pers. obs.	
	AMNH 7535, CV 4	0,717		pers. obs.	
	AMNH 7535, CV 5	0,881		pers. obs.	
	AMNH 7535, CV 6	0,820		pers. obs.	
	AMNH 7535, CV 7	0,622		pers. obs.	
	AMNH 7535, CV 8	0,603		pers. obs.	
	AMNH 7535, CV 9	0,569		pers. obs.	

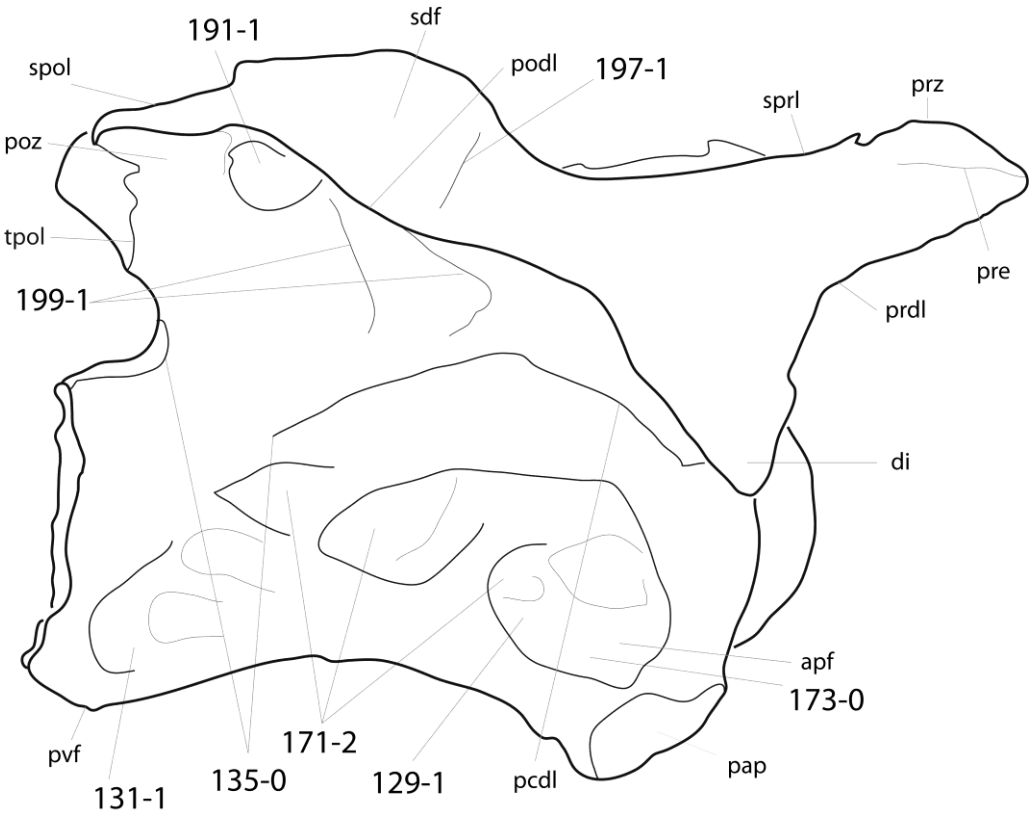

Figure 6.36: Posterior cervical vertebra (CV ?12) of SMA 0011 in right lateral view, showing the pleurocoel typical for advanced eusauropods (C129-1), but highly subdivided (C171-2), the elongate posteroventral fossa present in diplodocines (C131-1), the anteriorly restricted pcdl (C135-0), in contrast to the more posteriorly reaching pcdl of *Apatosaurus*, the dorsally excavated parapophysis (C173-0), the large foramen connecting the pocdf and the spof (C191-1), and the accessory laminae connecting the podl and the sprl (C197-1), and the pcdl and the podl (C199-1). Abb.: apf, anterior pneumatic fossa; di, diapophysis; pap, parapophysis; pcdl, posterior centrodiapophyseal lamina; pocdf, postzygapophyseal centrodiapophyseal fossa; podl, postzygodiapophyseal lamina; poz, postzygapophysis; prdl, prezygodiapophyseal lamina; pre, pre-epipophysis; prz, prezygapophysis; pvf, posteroventral flange; sdf, spinodiapophyseal fossa; spof, spinopostzygapophyseal fossa; spol, spino-postzygapophyseal lamina; sprl, spinoprezygapophyseal lamina; tpol, interpostzygapophyseal lamina.

C134: Cervical vertebra, posterior projection on transverse processes: present (0); absent (1) (Remes et al., 2009; polarity reversed; Fig. 6.39).

Comments. A distinct, triangular posterior projection marks the transverse process of *Spinophorosaurus* and many diplodocines. Posteriorly convex transverse processes are not considered projections. Due to reduced taxon sampling, the character polarity of the original version (Remes et al., 2009) was inverted here.

C135: Cervical vertebrae, posterior extension of posterior centrodiapophyseal lamina: is anteriorly restricted (0); reaches below posterior end of neural canal (1) (New; Figs 6.36, 6.40).

Comments. *Apatosaurus* specimens appear to have a consistently more developed pcdl compared to Diplodocinae. The only apatosaur specimen with an anteriorly restricted pcdl is the juvenile holotype of *Elosaurus parvus*, CM 566. The development of vertebral laminae has previously been linked with ontogeny (Carballido and Sander, 2013; Schwarz et al., 2007b).

C136: Cervical vertebrae, short second posterior centrodiapophyseal lamina ventral to the one uniting with the dorsal shelf of the diapophysis: absent (0); present (1) (New; Fig. 6.41).

Comments. The presence of a short accessory pcdl appears to be linked with the bifurcation of the pcdl in more posterior elements in '*Diplodocus*' *hayi* HMNS 175, as well as in SMA 0011 (pers. obs.). However, bifurcated pcdl also occur in some apatosaur specimens which do not have an additional pcdl in more anterior elements (e.g. UW 15556; Gilmore, 1936), and therefore, these morphologies are treated as independent characters.

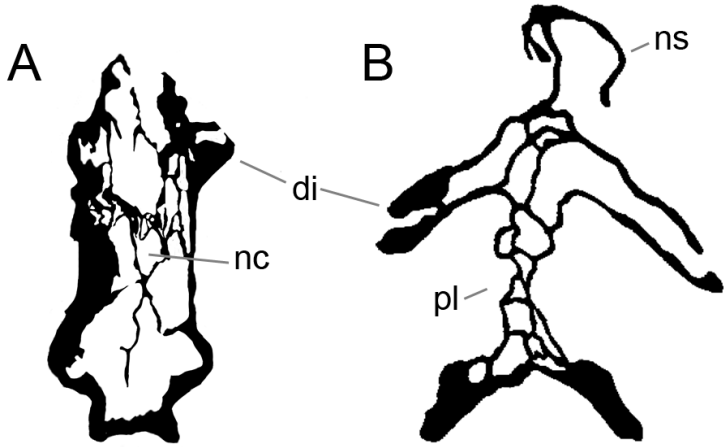

Figure 6.37: Mid- to posterior cervical vertebrae cross-section of *Supersaurus vivianae* WDC DMJ-021 (A; modified from Lovelace et al., 2007), and *Brachiosaurus* sp. BYU 12866 (B; modified from Wedel, 2009). Sections at base of diapophysis. Note the different internal pneumatic structure, with few but large cavities in *Supersaurus* (A; C128-1), in contrast to the many irregularly small fossa typical for titanosauriforms (B; C128-2). The differences shown here in cervical vertebrae apply as well for dorsal vertebrae (C228). Pictures scaled to the same centrum height. Abbreviations see page XXXII.

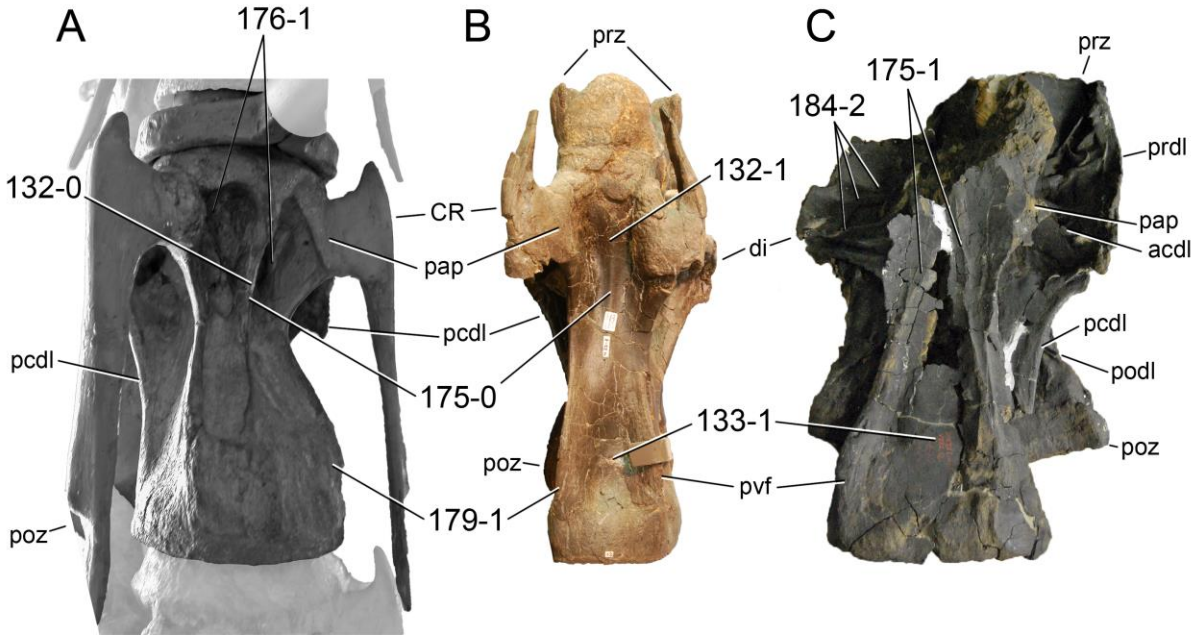

Figure 6.38: Mid- to posterior cervical vertebrae of *Dicraeosaurus hansemanni* MB.R.4886 (A; photo by J. Harris), *Kaatedocus siberi* SMA 0004 (B), and *Barosaurus lentus* YPM 429 (C) in ventral view (anterior to the top). Note the different developments of the ventral keels (prominent in *Dicraeosaurus*, A, C132-0; shallow, single in *Kaatedocus*, B, C132-1 and 175-0; double in *Barosaurus*, C, C175-1), the ventral sulcus typical for diplodocines (B, C; C133-1), the pneumatic foramina accompanying the ventral keel in *Dicraeosaurus* (A; C176-1), the posteroventral flanges (C179-1), and the numerous accessory laminae subdividing the pre-zygapophyseal centrodiapophyseal fossa in *Barosaurus* (C; C184-2). Vertebrae scaled to same centrum length. Abbreviations see page XXXII.

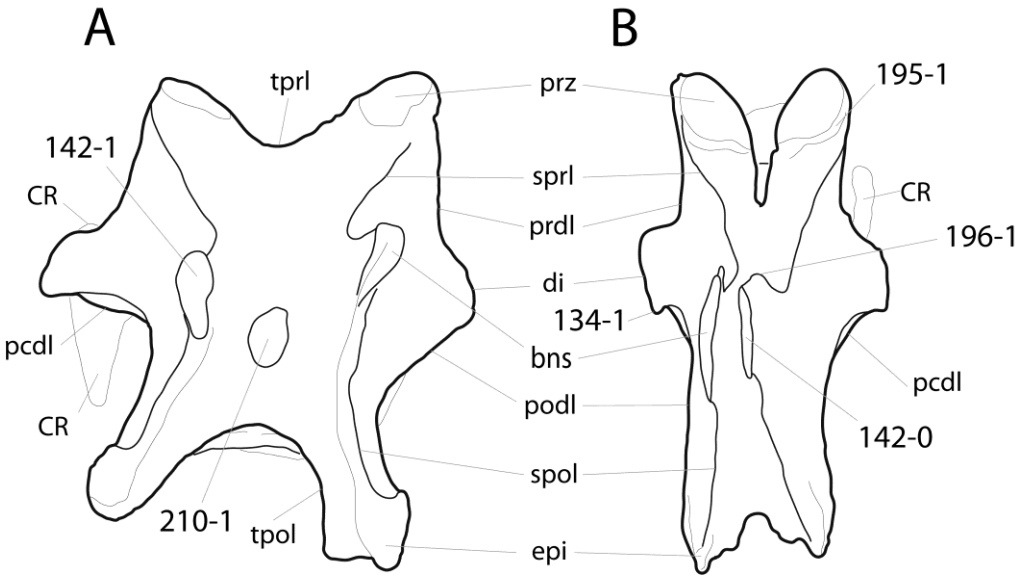

Figure 6.39: Mid- to posterior cervical vertebrae of *Apatosaurus ajax* YPM 1860 (A; traced from a photo by M. Taylor), and *Kaatedocus siberi* SMA 0004 (B; CV 13, traced from Tschopp and Mateus, in press) in dorsal view (anterior to the top). Note the triangular posterior projection on the diapophysis in *Kaatedocus* (B; C134-1), the transversely compressed (B; C142-0) in contrast to rounded (A; C142-1) neural spine summits, the transverse sulcus accompanying the prezygapophyseal facet posteriorly in *Kaatedocus* (B; C195-1), the anterior bulge of the sprl, just below the spine summit, characterizing most diplodocines (B; C196-1), and the median tubercle visible in *Apatosaurus* (A; C210-1). Abb.: bns, bifid neural spine; CR, cervical rib; di, diapophysis; epi, epipophysis; pcdl, posterior centrodiapophyseal lamina; podl, postzygodiapophyseal lamina; prdl, prezygodiapophyseal lamina; prz, prezygapophysis; spol, spinopostzygapophyseal lamina; sprl, spinoprezygapophyseal lamina; tpol, interpostzygapophyseal lamina; tprl, interprezygapophyseal lamina. Vertebrae scaled to same total length.

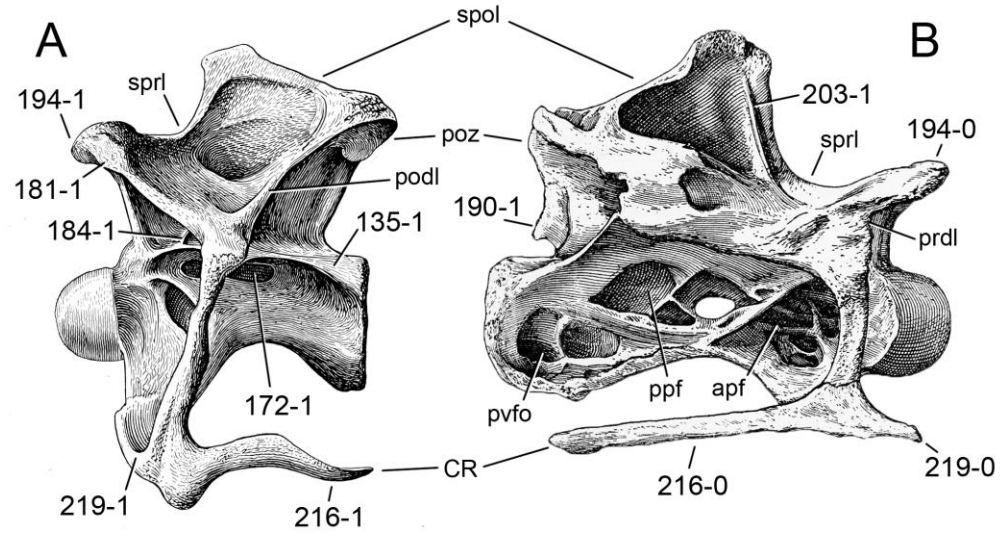

Figure 6.40: Cervical vertebra 11 of *Apatosaurus louisae* CM 3018 (A; modified from Gilmore, 1936) and *Diplodocus carnegii* (B; modified from Hatcher, 1901) in left (A) and right (B) lateral view. Note the posteriorly extending posterior centrodiapophyseal lamina in *Apatosaurus* (A; C135-1), the anteriorly restricted pneumatic foramen typical for most apatosaurs (A; C172-1), the pre-epipophysis (A; C181-1), the subdivided prezygapophyseal centrodiapophyseal fossa, characterizing *A. louisae* (A; C184-1), the posteriorly expanded interpostzygapophyseal lamina of *Diplodocus* (B; C190-1), the posteriorly restricted prezygapophysis of *A. louisae* (A; C194-1), compared to the state in *Diplodocus*, where it reaches the anterior edge of the condyle (B; C194-0), the vertical accessory spinal lamina marking *Diplodocus* (B; C203-1), the different positions of the cervical ribs (ventrally projecting, A, C216-1; or level with centrum, B, C216-0), and the absence (A; C219-1) or presence (B; C219-0) of the anterior process of the cervical rib. Vertebrae scaled to same posterior cotyle height. Abbreviations see page XXXII.

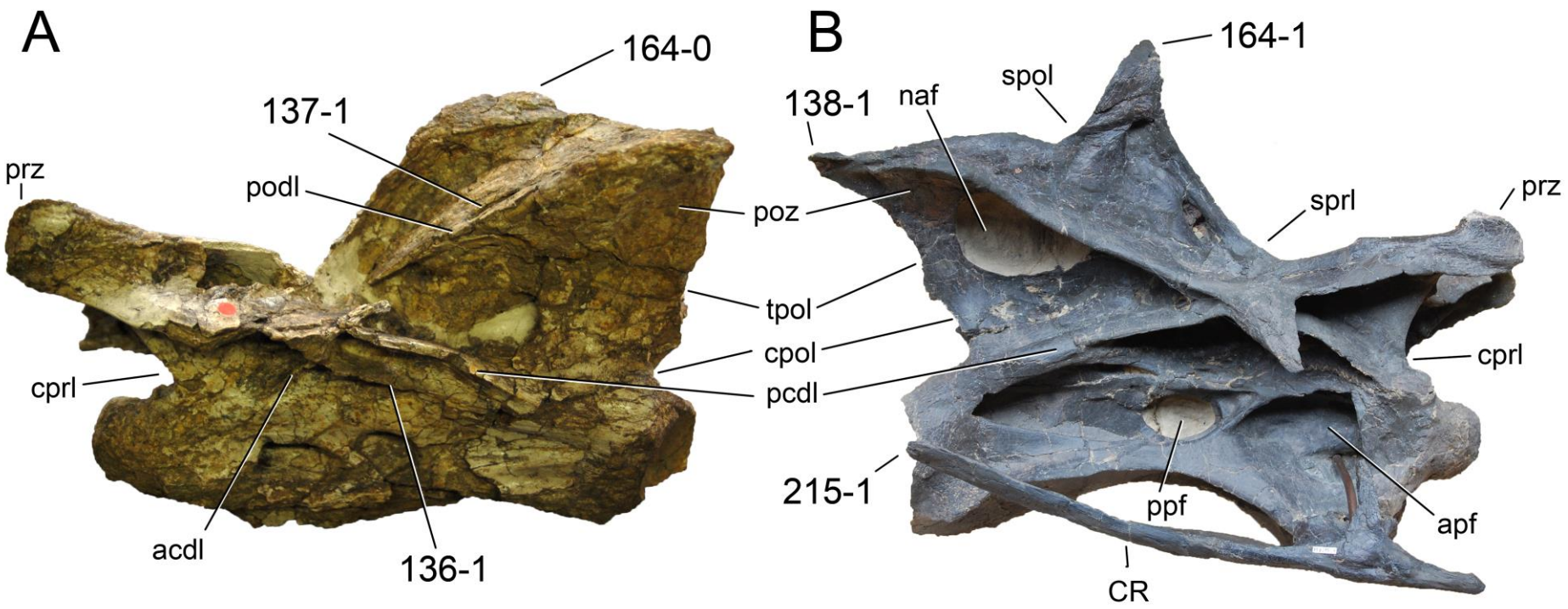

Figure 6.41: Cervical vertebra 6 of *Australodocus bohetii* MB.R.2455 (A) and SMA 0011 (B) in left (A) and right (B) lateral view. Note the short second pcdl in *Australodocus* (A; C136-1), the foramen piercing the podl (A; C137-1), the projection formed by the epipophysis (B; C138-1), the low (A; C164-0), and high (B; C164-1) neural spines, and the cervical rib, which is slightly longer than the centrum in SMA 0011 (B; C215-1). Abb.: acdl, anterior centrodiapophyseal lamina; apf, anterior pneumatic fossa; cpol, centropostzygapophyseal lamina; cprl, centroprezygapophyseal lamina; CR, cervical rib; naf, neural arch foramen; pcdl, posterior centrodiapophyseal lamina; podl, postzygodiapophyseal lamina; poz, postzygapophysis; ppf, posterior pneumatic fossa; prz, prezygapophysis; spol, spinopostzygapophyseal lamina; sprl, spino-prezygapophyseal lamina; tpol, interpostzygapophyseal lamina. Vertebrae scaled to the same centrum length.

C137: Cervical vertebrae, foramen on dorsal side of postzygodiapophyseal lamina, just anterior to base of neural spine process: absent (0); present (1) (Remes, 2007; Fig. 6.41).

Comments. Distinct foramina in the sdf are usually considered typical for brachiosaurids, and their presence in *Australodocus* was therefore one of the reasons why Whitlock (2011c) reinterpreted *Australodocus bohetii* as a titanosauriform, instead of a diplodocine as initially proposed (Remes, 2007). However, also *Barosaurus* sometimes shows small foramina in similar positions (YPM 429, pers. obs.), but they are usually less prominent. The putative juvenile *Brachiosaurus* specimen SMA 0009 does not have such foramina, but since the development of pneumatic structures appears to be ontogenetically controlled (Carballido and Sander, 2013; Schwarz et al., 2007c), this might be explained like that.

C138: Cervical vertebrae, epipophysis: reduced to absent (0); pronounced, forming a distinct projection above the postzygapophysis (1) (Remes et al., 2009; modified; Fig. 6.41)

C139: Cervical vertebrae, pneumatized epipophyses: absent (0); present (1) (New; Fig. 6.42).

Comments. The pneumatic foramen can be situated anteriorly as in *Diplodocus carnegii* (CM 84, 94, pers. obs.), or posteriorly as in *Barosaurus lentus* YPM 429 (pers. obs.).

C140: Cervical neural spines, first bifid element, if present: CV 3 (0); first mCV (1); posterior mCV (2); restricted to pCV (3) (Wilson, 2002; modified; Tab. 6.18).

Comments. Taxa with unbifurcated neural spines are scored as unknown. The subdivision into anterior, mid-, and posterior cervical vertebrae depends on the number of elements in the column (Tab. 6.3). Absolute numbers other than CV 3, which is the first postaxial cervical element would thus be misleading and are avoided here. The character is treated as ordered.

C141: Cervical vertebrae, unbifurcated neural spines in anterior/posterior view: with parallel lateral edges or converging (0); distal end expanded laterally (1) (New; Fig. 6.43).

Comments. The real distribution of this character within Diplodocidae is difficult to assess to date, as there are only few specimens reported that preserve complete neural spines of anterior, unbifurcated neural spines.

C142: Cervical vertebrae, summits of bifid neural spines: are laterally compressed (0); are rounded (1) (Upchurch et al., 2004b; Fig. 6.39).

Comments. The derived state of this character is shared by some *Apatosaurus* specimens and *Suuwassea*. The spine summits in most other taxa with bifurcated spines are generally anteroposteriorly elongate, and transversely compressed, resulting in narrow sheets of bone. In *Suuwassea* as well as some *Apatosaurus* specimens, the lateral edge of the spine summit is distinctly convex, producing a semi-circular outline. Some other taxa (e.g. *Kaatedocus*; Tschopp and Mateus, 2012b) have medial ridges connecting the summit with the base, but these are always relatively shallow, and do not form rounded outlines.

C143: Proatlas, distal end: broadly rounded (0); narrow and elongate, almost pointed (1) (New; Fig. 6.44).

C144: Atlantal intercentrum, anteroventral lip: absent, anterior edge of intercentrum straight in lateral view (0); present, anterior edge of intercentrum concave (1) (Wilson, 2002; modified; Fig. 6.45).

Comments. Initially regarded as flagellicaudatan synapomorphy (Wilson, 2002), the presence of an anteroventral lip is now known to be present in *Mongolosaurus* as well (Mannion, 2011). Following the original description of the character states (Wilson, 2002: intercentrum shape in lateral view: rectangular or ventrally longer than dorsally), also *Camarasaurus* and other non-flagellicaudatan taxa would have to be scored as apomorphic. However, they do not show a distinct anteroventral lip, resulting in a strongly concave anterior edge of the intercentrum, when seen in lateral view.

C145: Atlantal intercentrum, foramen between posterior ventrolateral processes: absent (0); present (1) (New; Fig. 6.45).

C146: Atlantal neurapophyses, anteromedial process: weakly developed (0); well-developed and distinct from posterior wing (1) (New; Fig. 6.46).

Comments. The anteromedial process corresponds to the prezygapophyses of more posterior elements. It articulates with the posterior end of the proatlas. In *Kaatedocus*, this process is relatively short transversely, and curves gradually into the posterior process, whereas in SMA 0011 and AMNH 969, the anteromedial process is distinct and at least as wide transversely as long anteroposteriorly.

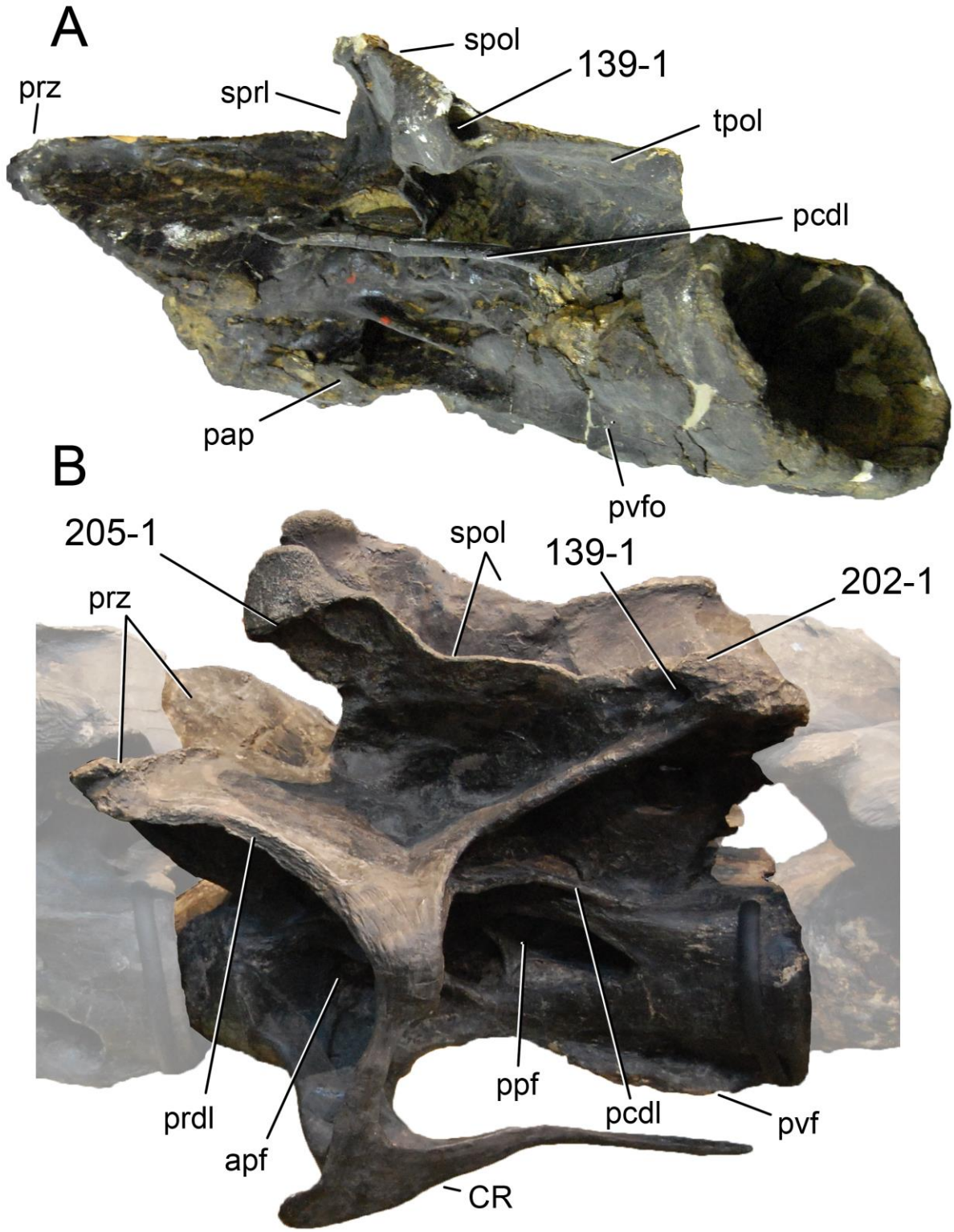

Figure 6.42: Mid- to posterior cervical vertebrae of *Barosaurus lentus* YPM 429 (A) and *Diplodocus carnegii* CM 84 (B) in left posterolateral (A) and left dorsolateral view (B). Note the differently pneumatized epipophyses (C139-1), the transversely compressed epipophysis (B; C202-1), and the horizontal ridge below the neural spine summit in *Diplodocus* (B; C205-1). The cervical vertebra of *B. lentus* is partly covered by matrix and plaster. Abb.: apf, anterior pneumatic fossa; CR, cervical rib; pap, parapophysis; pcdl, posterior centrodiapophyseal lamina; ppf, posterior pneumatic fossa; prdl, prezygodiapophyseal lamina; prz, prezygapophysis; pvf, posteroventral flange; pvfo, posteroventral fossa; spol, spinopostzygapophyseal lamina; sprl, spinoprezygapophyseal lamina. Vertebrae scaled to the same posterior cotyle height.

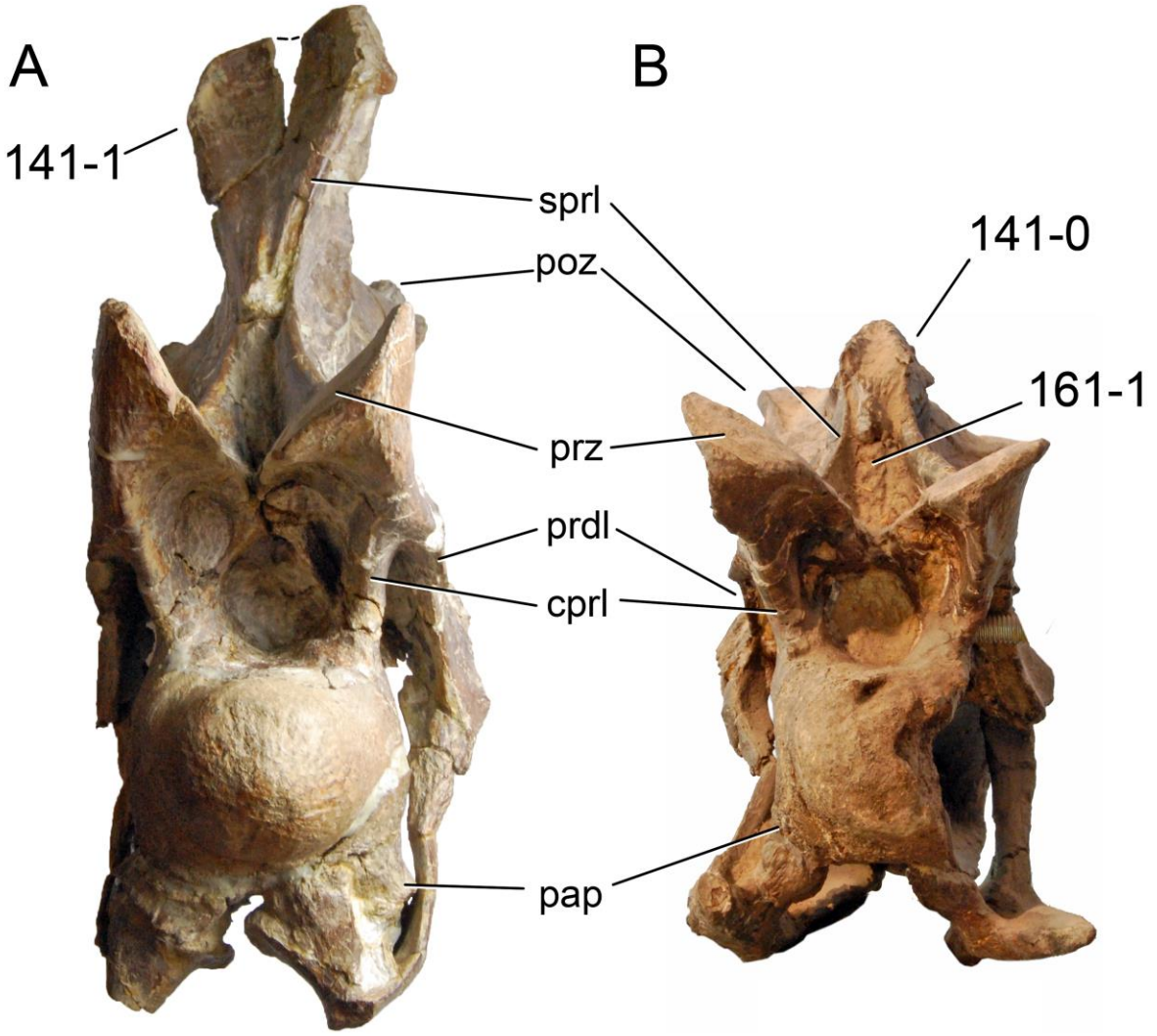

Figure 6.43: Cervical vertebra 5 of *Suuwassea emilieae* ANS 21122 (A) and *Kaatedocus siberi* SMA 0004 (B; modified from Tschopp and Mateus, in press) in anterior view. Note the transversely widening (A; C141-1) instead of straight (B; C141-0) neural spine, and the presence of a prespinal lamina in *Kaatedocus* (B; C161-1). The neural spine of *Suuwassea* (A) is not bifurcated, but broken (as indicated by the dashed line). Abb.: cprl, centroprezygapophyseal lamina; pap, parapophysis; poz, postzygapophysis; prdl, prezygodiapophyseal lamina; prz, prezygapophysis; sprl, spinoprezygapophyseal lamina. Vertebrae scaled to the same anterior condyle length.

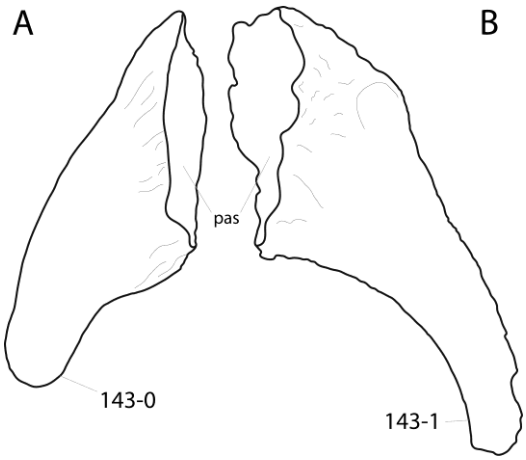

Figure 6.44: Proatlas of ?*Kaatedocus* SMA P29-1 (A) and SMA 0011 (B) in medial view, illustrating the broad (A; C143-0) and narrow distal tips (B; C143-1). Abb.: pas, proximal articular surface. Scaled to the same articular surface height.

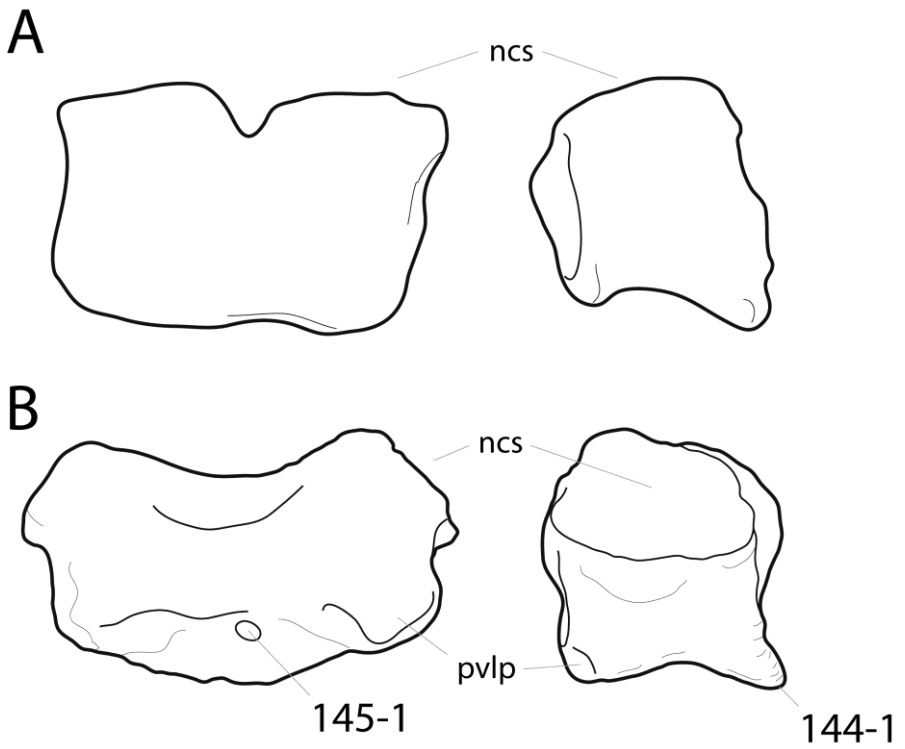

Figure 6.45: Atlas of *Camarasaurus* sp. UUVP 10070 (A; modified from Madsen et al., 1995), and *Galeamopus shellensis* AMNH 969 (B) in posterior (left) and right lateral view (right, A shows left side reversed). Note the distinct anteroventral lip characterizing diplodocids (B; C144-1), and the foramen between the posterior ventrolateral processes in AMNH 969 (B; C144-1). Abb.: ncs, neurocentral synchondrosis; pvlp, posterior ventrolateral process. Scaled to the same centrum height.

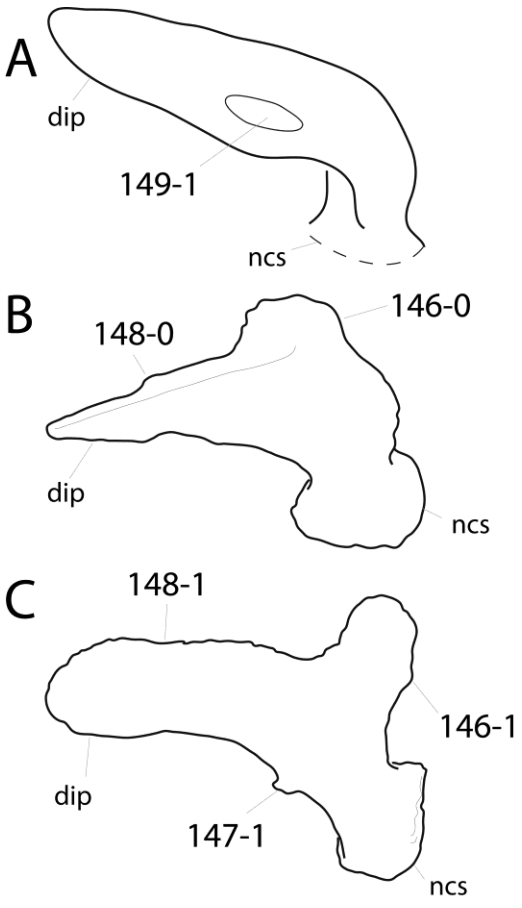

Figure 6.46: Neurapophyses of *Apatosaurus louisae* CM 3018 (A; modified from Gilmore, 1936), *Kaatedocus siberi* SMA 0004 (B; traced from 3D model provided by G. Dzemski), and SMA 0011 (C) in lateral (A; left side reversed), and dorsolateral view (B, C). Note the weak (B; C146-0) in contrast to well-developed medial process (C; C146-1), the subtriangular lateral spur in SMA 0011 (C; C147-1), the different shapes of the distal process (tapering, B, C148-0; wide, C, C148-1), and the foramen characterizing *A. louisae* (A; C149-1). Abb.: dip, distal process; ncs, neurocentral synchondrosis. Scaled to the same anteroposterior length.

C147: Atlantal neural arch, small subtriangular, laterally projecting spur at base: absent (0); present (1) (New; Fig. 6.46).

Comments. When present, this spur is located at the base of the neurapophysis, opposite to the position of the anteromedial process, and much smaller. It is also present in some, but not all *Camarasaurus* specimens (Ikejiri, 2004).

C148: Atlantal neurapophyses, posterior wing: gradually tapering along its length (0); of subequal width along most of its length (1) (New; Fig. 6.46).

Comments. The posterior wing of the neurapophysis articulates with the prezygapophysis of the axis.

C149: Atlantal neural arch: without foramen (0); with foramen (1) (Wilson, 2002; Whitlock, 2011a; Fig. 6.46).

Comments. Wilson (2002) proposed the presence of such a foramen as an autapomorphy of *Apatosaurus*, and it was included as character in the phylogenetic analysis of Whitlock (2011a). Due to the small number of preserved atlantal neurapophyses, only one specimen can currently be positively assigned to the apomorphic state (*Apatosaurus louisae* CM 3018). It could thus also represent a species autapomorphy, instead of being valid for the entire genus.

C150: Axial centrum, pneumatic fossae on ventrolateral edges, right posterior to parapophyses: absent (0); present (1) (New; Fig. 6.47).

Comments. Many specimens have a well-developed median keel on their ventral surfaces. In lateral view, this sometimes appears like a bifurcation of the ventrolateral edge, although this is not the case. The apomorphic state of the character proposed herein only includes fossae bordered by ridges that originate at the parapophysis anteriorly.

C151: Axis, prespinal lamina: of constant width (0); developing a transversely expanded, knob-like tuberosity at its anterior end (1) (New; Fig. 6.48).

C152: Axis, postspinal lamina: absent (0); present (1) (Harris and Dodson, 2004; Fig: 6.47).

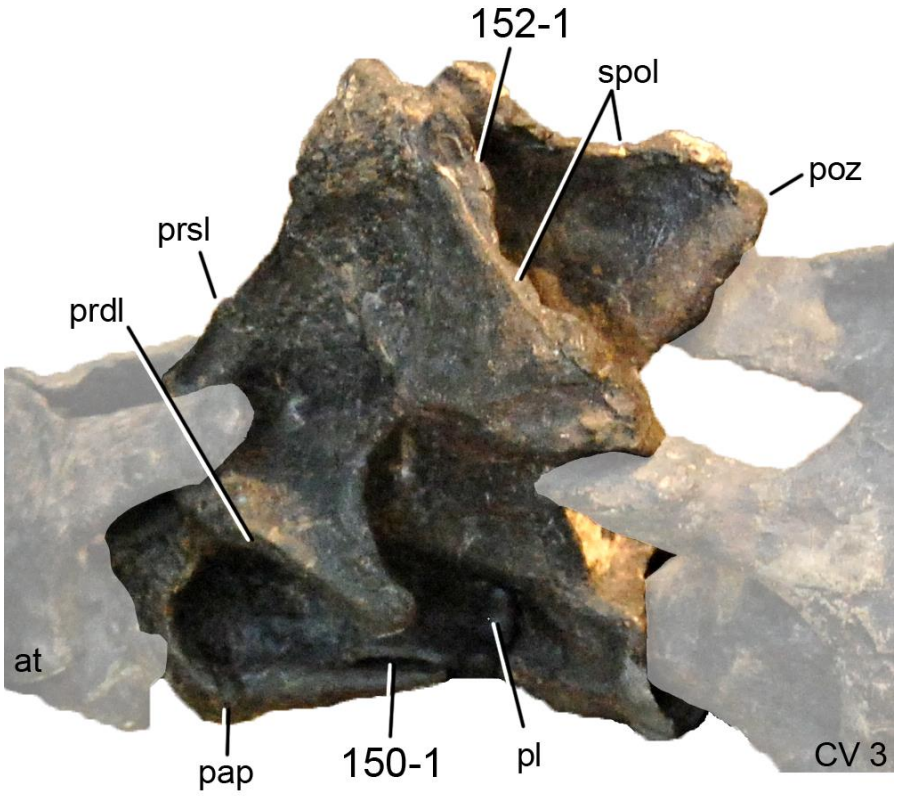

Figure 6.47: Axis of *Diplodocus carnegii* CM 84 in posterolateral view, illustrating the pneumatic slot-like fossa posterior to the parapophysis (C150-1), and the presence of a postspinal lamina (C152-1). Abb.: at, atlas; CV 3, cervical vertebra 3; pap, parapophysis; pl, pleurocoel; poz, postzygapophysis; prdl, prezygodiapophyseal lamina; prsl, prespinal lamina; spol, spinopostzygapophyseal lamina.

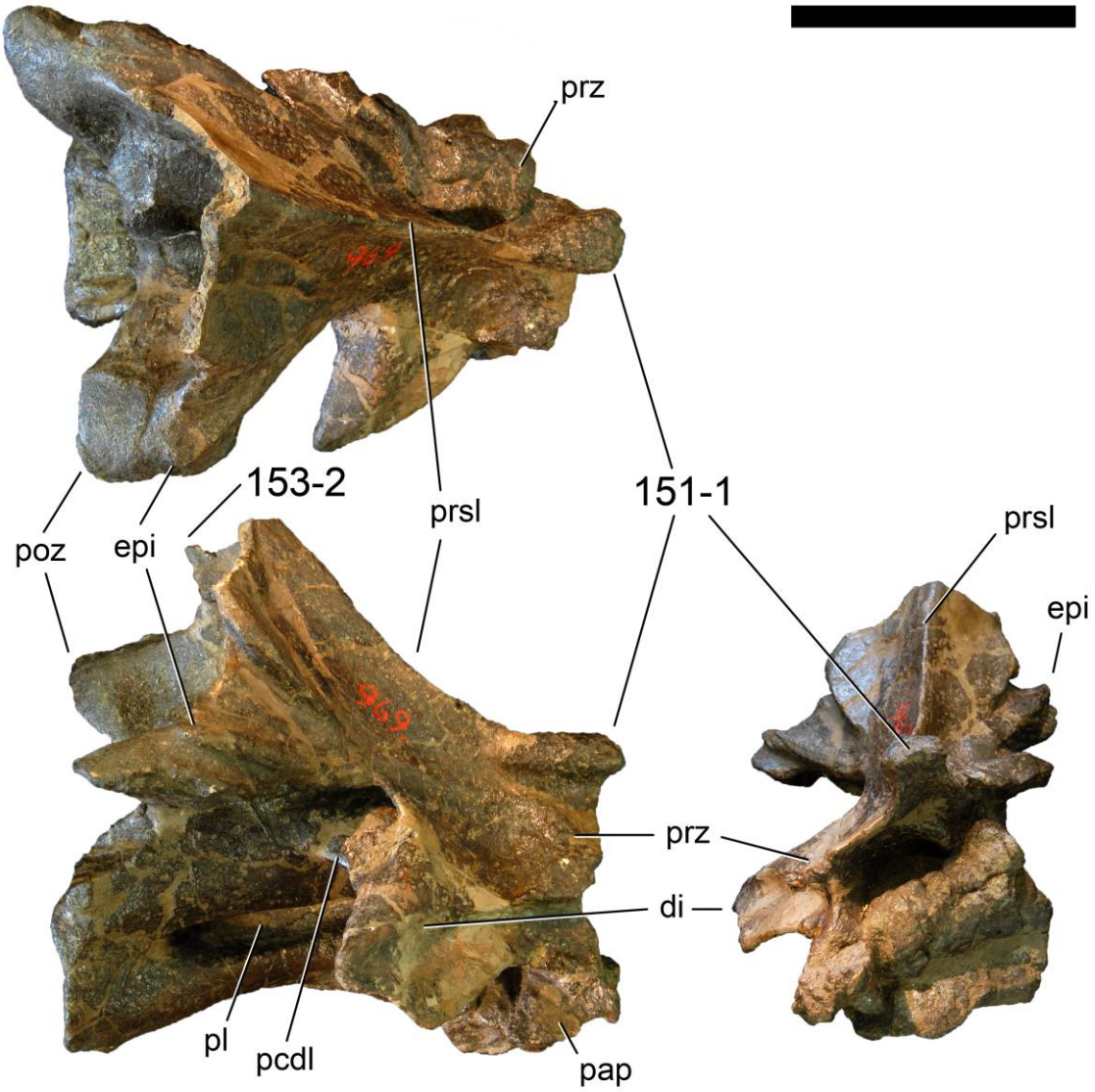

Figure 6.48: Axis of *Galeamopus shellensis* AMNH 969 in dorsal (top), right lateral (bottom left), and anterior (bottom right) view, illustrating the anteriorly expanded prespinal lamina (C151-1), and the anteriorly restricted neural spine summit (C153-2). Abb.: di, diapophysis; epi, epipophysis; pap, parapophysis; pcdl, posterior centrodiapophyseal lamina; pl, pleurocoel; poz, postzygapophysis; prsl, prespinal lamina; prz, prezygapophysis. Scale bar = 10 cm.

C153: Axis neural spine: projects beyond posterior border of centrum (0); terminates in front of or at posterior border of centrum (1); is restricted anterior to postzygapophyseal facets (2) (New; Fig. 6.48).

Comments. Due to intermediate morphologies, this character is treated as ordered.

C154: Anterior cervical vertebrae, total height/centrum length ratio: < 0.9 (0); 0.9-1.2 (1); > 1.2 (usually around 1.5) (1) (Whitlock, 2011a; modified; Tab. 6.21).

Comments. Total height is herein measured between the ventral-most expansion of the centrum (usually the parapophysis or posterior cotyle). A third state was added in order to distinguish *Apatosaurus* from *Diplodocus*. Given the high amount of changes in ratios during evolution, as indicated by the analysis, the character is left unordered.

C155: Cervical vertebrae 2 and 3, centrum length: moderate length increase, CV3 < 1.3 x CV 2 (0); length increases considerably CV 3 at least 1.3 x CV 2 (1) (Russell and Zheng, 1993; Tab. 6.22).

Comments. Even though this does not seem to follow higher-level taxonomy, there are two groups with ratios well separated from each other (Tab. 6.22). The state boundaries are therefore set in order to distinguish between these two groups.

Table 6.21: Anterior cervical vertebrae, height/centrum length.

Taxon	Specimen	Ratio	Mean	Reference	Comments
Shunosaurus lii	T5402, CV 2	1,20	1,2	Zhang 1988	measured from drawings
	T5402, CV 3	1,44		Zhang 1988	measured from drawings
	T5402, CV 4	0,99		Zhang 1988	
Spinophorosaurus nigerensis	NMB-1698-R, CV 2	0,81	0,8	pers. obs.	measured from 3D models
	NMB-1698-R, CV 3	0,73		pers. obs.	measured from 3D models
Omeisaurus	T5701, CV 2	0,61	0,5	He et al. 1988	
	T5701, CV 3	0,46		He et al. 1988	
	T5701, CV 4	0,42		He et al. 1988	
	T5703, CV 2	0,47		He et al. 1988	total height estimated
	T5703, CV 3	0,54		He et al. 1988	
	T5703, CV 4	0,41		He et al. 1988	
	T5703, CV 5	0,34		He et al. 1988	
Mamenchisaurus	ZDM 0083, CV 2	0,56	0,7	Ouyang & Ye 2002	total height damaged, number slightly too low
	ZDM 0083, CV 3	0,79		Ouyang & Ye 2002	
	ZDM 0083, CV 5	0,63		Ouyang & Ye 2002	
	ZDM 0083, CV 6	0,75		Ouyang & Ye 2002	
Jobaria tiguidensis			~1	R. Kosma, pers. comm., 2011	
Losillasaurus giganteus type	MCNV Lo-17, CV ?3	~1	~1	pers. obs.	incomplete
Camarasaurus	BYU 9047, CV 2	1,15	1,2	McIntosh et al. 1996b	
	BYU 9047, CV 3	1,09		McIntosh et al. 1996b	
	BYU 9047, CV 4	0,91		McIntosh et al. 1996b	
	GMNH-PV 101, CV 2	1,30		McIntosh et al. 1996a	
	GMNH-PV 101, CV 3	1,36		McIntosh et al. 1996a	
	GMNH-PV 101, CV 4	1,02		McIntosh et al. 1996a	
	YPM 1905, CV 2	1,65		McIntosh et al. 1996a	
	YPM 1905, CV 3	1,41		McIntosh et al. 1996a	
	YPM 1905, CV 4	1,04		McIntosh et al. 1996a	
Giraffatitan brancai	MB.R. S 71, CV 2	1,09	0,8	Janensch 1950	
	MB.R. S 51, CV 3	0,88		Janensch 1950	
	MB.R. S 70, CV 4	0,71		Janensch 1950	
	MB.R. be1, CV 2	0,78		Janensch 1950	
	MB.R. be2, CV 3	0,63		Janensch 1950	
Isisaurus colberti	ISIR 335/1	1,20	1,2	Jain & Bandyopadhyay 1997	
Haplocanthosaurus priscus	CM 879, CV ?4	1,00	1,0	Hatcher 1903	measured from drawings
Limaysaurus tessonei	MUCPv-205, aCV	1,50	1,5	Calvo & Salgado 1995	
Zapalasaurus bonapartei	Pv-6127-MOZ	~1	~1	Salgado et al. 2006	incomplete, estimated from drawings
Nigersaurus taqueti	GAD512-13, CV 3	1,02	1,0	Sereno et al. 2007	measured from 3D models
Demandasaurus darwini	MDS−RVII,606, CV 2	1,80	1,3	Torcida Fernández-Baldor et al. 2011	
	MDS−RVII,589, a to mCV	0,74		Torcida Fernández-Baldor et al. 2011	less indicative due to unclear position, estimated height
Dicraeosaurus hansemanni	MB.R.4886, CV 2	1,58	1,5	Janensch 1929a	
	MB.R.4886, CV 3	1,23		Janensch 1929a	
	MB.R.4886, CV 4	1,69		Janensch 1929a	
Amargasaurus cazaui	MACN-N 15, CV 2	> 2	> 2	Salgado & Bonaparte 1991	estimated from drawing
Suuwassea emilieae ANS 21122	ANS 21122, CV 2	1,40	1,3	Harris 2006b	
	ANS 21122, CV 3	1,16		Harris 2006b	deformed, height larger
Apatosaurus louisae CM 3018	CM 3018, CV 2	1,36	1,2	Gilmore 1936	height estimated, measured from drawing
	CM 3018, CV 3	1,20		Gilmore 1936	height estimated, measured from drawing
	CM 3018, CV 4	1,19		Gilmore 1936	height estimated, measured from drawing
Apatosaurus parvus UW 15556	UW 15556, CV 3	1,26	1,2	Gilmore 1936	
	UW 15556, CV 4	1,20		Gilmore 1936	
	UW 15556, CV 5	1,11		Gilmore 1936	
Eobrontosaurus yahnahpin Tate-001	Tate-001, CV 2	1,50	1,4	P. Mannion, pers. comm., 2012	measured from photo
	Tate-001, CV 3	1,39		P. Mannion, pers. comm., 2012	measured from photo
	Tate-001, CV ?4	1,29		P. Mannion, pers. comm., 2012	measured from photo
Apatosaurus ajax NSMT-PV 20375	NSMT-PV 20375, CV 3	0,91	0,9	Upchurch et al. 2004b	
Kaatedocus siberi SMA 0004	SMA 0004, CV 3	0,66	0,6	Tschopp & Mateus, in press	height measured to ventral surface, total height slightly higher
	SMA 0004, CV 4	0,61		Tschopp & Mateus, in press	height measured to ventral surface, total height slightly higher
	SMA 0004, CV 5	0,47		Tschopp & Mateus, in press	height measured to ventral surface, total height slightly higher
Diplodocus carnegii CM 84	CM 84, CV 2	1,04	0,8	Hatcher 1901	centrum length, ratio slightly lower
	CM 84, CV 3	0,82		Hatcher 1901	centrum length, ratio slightly lower
	CM 84, CV 4	0,73		Hatcher 1901	centrum length, ratio slightly lower
	CM 84, CV 5	0,63		Hatcher 1901	centrum length, ratio slightly lower
Galeamopus shellensis AMNH 969	AMNH 969, CV 2	~1	~1	pers. obs.	incomplete
Diplodocinae indet. CM 3452	CM 3452, CV 5	0,75	0,7	pers. obs.	measured from photo
Galeamopus hayi HMNS 175	HMNS 175, CV 3	1,40	1,1	pers. obs.	measured from photo
	HMNS 175, CV 4	1,02		pers. obs.	measured from photo
	HMNS 175, CV 5	0,81		pers. obs.	measured from photo
Galeamopus shellensis SMA 0011	SMA 0011, CV 2	1,58	1,3	pers. obs.	height measured to ventral surface, total height slightly higher
	SMA 0011, CV 3	1,29		pers. obs.	height measured to ventral surface, total height slightly higher
	SMA 0011, CV 4	1,25		pers. obs.	height measured to ventral surface, total height slightly higher
	SMA 0011, CV 5	1,25		pers. obs.	height measured to ventral surface, total height slightly higher

Table 6.21: continued.

Barosaurus sp. AMNH 7530	AMNH 7530, CV 2	0,84	0,8	pers. obs.	height measured to ventral surface, total height slightly higher
	AMNH 7530, CV 3	0,82		pers. obs.	height measured to ventral surface, total height slightly higher
	AMNH 7530, CV 4	0,74		pers. obs.	height measured to ventral surface, total height slightly higher
	AMNH 7530, CV 5	0,64		pers. obs.	height measured to ventral surface, total height slightly higher
Barosaurus sp. AMNH 7535	AMNH 7535, CV 2	0,73	0,7	pers. obs.	height measured to ventral surface, total height slightly higher
	AMNH 7535, CV 3	0,80		pers. obs.	height measured to ventral surface, total height slightly higher
	AMNH 7535, CV 4	0,67		pers. obs.	height measured to ventral surface, total height slightly higher
	AMNH 7535, CV 5	0,59		pers. obs.	height measured to ventral surface, total height slightly higher

Table 6.22: Centrum length ratio CV 3/CV 2

Taxon	Specimen	Ratio	Mean	Reference	Comments
Shunosaurus lii	T5402	1,184	1,18	Zhang 1988	
Spinophorosaurus nigerensis	NMB-1699-R	1,147	1,15	Remes et al. 2009	
Omeisaurus	T5701	1,486	1,45	He et al. 1988	
	T5703	1,418		He et al. 1988	
Mamenchisaurus	IVPP V10603	1,700	1,47	Russell & Zheng 1993	
	type *M. hochuanensis*	1,350		Young & Zhao 1972	
	ZDM 0083	1,371		Ouyang & Ye 2002	
Jobaria tiguidensis	MNN TIG	1,205	1,21	J. Carballido, pers. comm. 2013	measured from photo
Camarasaurus	BYU 9047	1,043	1,08	McIntosh et al. 1996b	
	GMNH-PV 101	1,117		McIntosh et al. 1996a	
Giraffatitan brancai	MB.R.2180	1,319	1,42	Janensch 1950	
	MB.R. be	1,517		Janensch 1950	
Dicraeosaurus hansemanni	MB.R.4886	1,127	1,13	Janensch 1929a	
Suuwassea emilieae ANS 21122	ANS 21122	1,173	1,17	Harris 2006b	
Apatosaurus louisae CM 3018	CM 3018	1,474	1,47	Gilmore 1936	
Eobrontosaurus yahnahpin Tate-001	Tate-001	1,139	1,14	P. Mannion, pers. comm. 2012	measured from photo
Diplodocus carnegii CM 84	CM 84	1,473	1,47	Hatcher 1901	
Galeamopus shellensis SMA 0011	SMA 0011	1,512	1,51	pers. obs.	
Barosaurus sp. AMNH 7530	AMNH 7530	1,152	1,15	pers. obs.	
Barosaurus sp. AMNH 7535	AMNH 7535	1,195	1,19	pers. obs.	

C156: Anterior cervical vertebrae, posterior edge of anterior condyle: anteriorly inclined (0); posteriorly inclined (1) (New; Fig. 6.49).

Comments. This character is strictly applicable to anterior cervical vertebrae. In SMA 0011, which has apomorphic anterior vertebrae, CV 6 and more posterior elements show the usual anteriorly inclined edge.

C157: Anterior cervical centra, pleurocoels: single (0); subdivided (1) (New; Fig. 6.49).

Comments. The subdivision of the pleurocentral cavity is sometimes regarded as ontogenetically controlled (Carballido and Sander, 2013; Schwarz et al., 2007b). However, given that the completely mature anterior cervical vertebrae (sensu Carballido and Sander, 2013) of the *Kaatedocus siberi* holotype SMA 0004 have undivided pleurocoels, in contrast to the still immature vertebrae of other specimens like SMA 0011 (pers. obs.), at least some taxonomic differences appear to be present.

C158: Anterior cervical vertebrae, pleurocoel extending onto dorsal surface of parapophysis: absent (0); present (1) (Upchurch, 1998; modified by Whitlock, 2011a; polarity reversed; Fig. 6.49).

Comments. Upchurch (1998) distinguished between continuous extensions or fossae that are separated from the main anterior pneumatic fossa or pleurocoel by a transverse ridge. The latter distinction was abandoned by Whitlock (2011a), who instead divided the character into the different regions (anterior and mid- and posterior cervical vertebrae, see below). Character polarity was herein reversed as basal outgroups used in the present analysis do have expanded pleurocoels.

C159: Anterior cervical vertebrae, longitudinal ridge on ventral surface: present (0); absent (1) (Upchurch, 1998; modified).

Comments. The ventral ridge (if present) can have various morphologies in diplodocid specimens, which is accounted for in other characters of this analysis. In addition to the original version of Upchurch (1998; character 132 herein), a strict presence-absence character was included for both anterior and mid- and posterior cervical vertebrae in the present analysis. The subdivision is necessary as in some specimens, the presence of a ventral keel is restricted to anterior elements only (*Suuwassea*

ANS 21122, *Eobrontosaurus* Tate-001, *Galeamopus shellensis* SMA 0011). This indicates that incomplete necks without ventral keels on posterior cervical vertebrae might still bear midline ridges anteriorly. For the various developments of the keels see Fig. 6.38, which shows mid- and posterior cervical vertebrae, but the morphology is the same in anterior elements.

C160: Anterior cervical vertebrae, paired pneumatic fossae on ventral surface: absent (0); present (1) (Whitlock, 2011a).

Comments. Like the ventral keel, also the paired pneumatic foramina are sometimes restricted to the anterior cervical vertebrae (e.g. in SMA 0011, pers. obs.). Whereas the presence of paired pneumatic foramina imply the presence of a ventral keel as well, this does not apply the other way around, as shown by the anterior cervical vertebrae of *Kaatedocus* SMA 0004 (Tschopp and Mateus, 2012b). The characters are therefore retained as independent. The morphology of the foramina is equal in anterior and mid- and posterior cervical vertebrae, where present (see Fig. 6.38).

C161: Anterior cervical vertebrae, prespinal lamina: absent (0); present (1) (Carballido et al., 2012b; Figs 6.43, 6.49).

Comments. In some diplodocid specimens, it appears that the prespinal lamina in undivided vertebrae gives rise to the median tubercle in divided, more posterior elements. However, given the presence of a prespinal lamina in *Camarasaurus* (Madsen et al., 1995), which does not have a median tubercle between bifurcated neural spines, these two characters should be treated as independent.

C162: Anterior and mid-cervical centra, pleurocoel pierced by one or two large, rounded foramina around centrum midlength: absent (0); present (1) (New; Fig. 6.50).

Comments. Such a foramen is not present in the anterior-most elements, but very distinct in CV 5 or 6 of SMA 0011, whereas it disappears again by CV 8 or 9. In SMA 0011, these foramina are situated at the anterior end of the posterior pneumatic fossa. Taxa where CV 5 to 7 or 8 are not preserved, and other elements do not show such a development, are scored as unknown. Similarly distinct, rounded foramina are only present in *Supersaurus* (Lovelace et al., 2007), and *Australodocus* (pers. obs., 2011).

C163: Anterior and mid-cervical vertebrae, spinoprezygapophyseal lamina: continuous as a lamina (0); reduced to ridge or totally interrupted in the middle (at base of prezygapophysis) (1) (Tschopp and Mateus, 2012b; Fig. 6.51).

C164: Anterior and mid-cervical neural spines height: high (project well above the level of postzygapophyses) (0); low (terminates level with postzygapophyses) (1) (Upchurch et al., 2004b; modified; Fig. 6.41).

Comments. This character is similar to character 168. It was added because it includes anterior cervical vertebrae, which are different in height among diplodocids and within Diplodocinae, and because it would have differing state boundaries, if it would be treated numerically.

C165: Anterior and mid-cervical neural spines, dorsoventrally elongate coel on lateral surface: absent (0); present (1) (Mannion et al., 2012; modified; Fig. 6.50).

Comments. The presence of a dorsoventrally elongate fossa in the spinodiapophyseal fossa is usually used as derived character for posterior cervical vertebrae only (Mannion et al., 2012). However, there are differences in anterior and mid-cervical neural arches as well, which appear to be phylogenetically significant.

C166: Mid-cervical centra, anteroposterior length/height of posterior face: 2.5-3.2 (0); 3.3-4.4 (1); 4.5+ (2) (Upchurch, 1995; modified; Tab. 6.23).

Comments. Elongation index as used herein is measured following the protocol of Wilson and Sereno (1998: total centrum length/height posterior cotyle). The mean elongation index is used for this metric. *Tornieria* specimen k is scored '2' as the centrum length to width ratio is very high (5.4; Remes, 2006), and thus a high EI as used herein can be expected with confidence.

C167: Mid-cervical pre-epipophyses anterior extreme: about the same as prezygapophyseal facet (0); projects considerably anterior to articular facet, forming a distinct spur (1) (Sereno et al., 1999; Fig. 6.51).

Comments. A distinct anterior extension of the pre-epipophysis was used as autapomorphy for *Australodocus bohetii* within Diplodocidae (Remes, 2007). However, it has since been shown to be present in *Kaatedocus* as well, as also in some non-diplodocid sauropods (Sereno et al., 1999; Ksepka and Norell, 2006; Tschopp and Mateus, 2012b). Taxa without pre-epipophyses are scored as unknown.

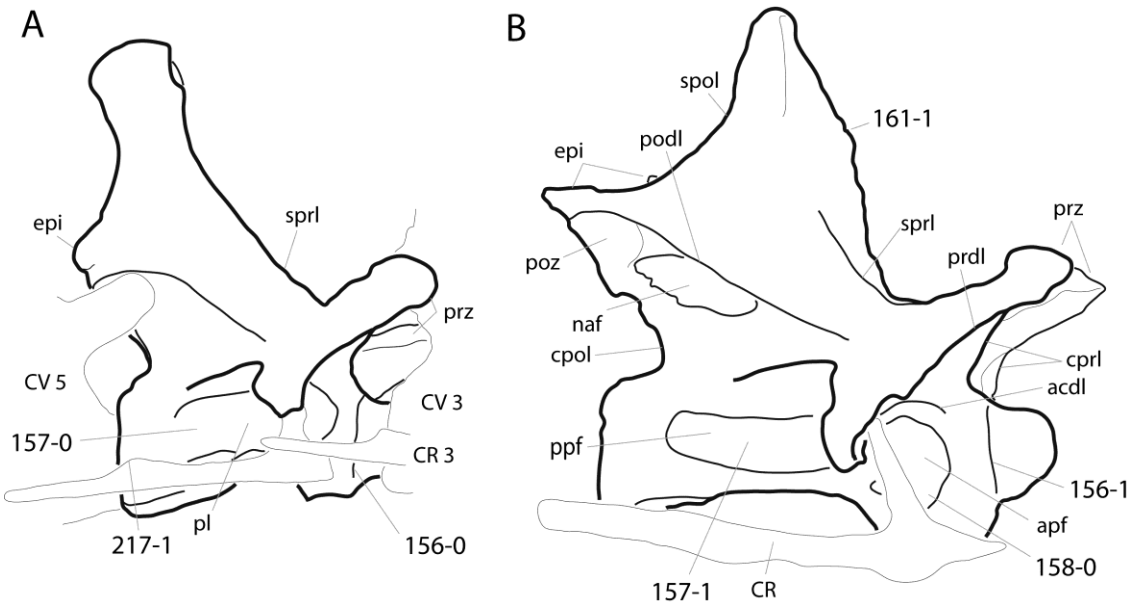

Figure 6.49: Cervical vertebra 4 of *Dicraeosaurus hansemanni* MB.R.4886 (A) and SMA 0011 (B) in right lateral view. Note the differently inclined posterior border of the anterior condyle (A, C156-0; B, C156-1), the subdivision of the pleurocoel in SMA 0011 (B; C157-1), which is absent in anterior cervical vertebrae of *Dicraeosaurus* (A; C157-0), the anterior pneumatic fossa that extends onto the parapophysis (B; C158-0), the presence of a prespinal lamina in SMA 0011 (B; C161-1), and the posteriorly projecting spur on the dorsal edge of the posterior process of the cervical rib of *Dicraeosaurus* (A; C217-1). Abb.: acdl, anterior centrodiapophyseal lamina; apf, anterior pneumatic fossa; cprl, centroprezygapophyseal lamina; CR 3, cervical rib 3; CV 3, cervical vertebra 3; epi, epipophysis; naf, neural arch foramen; pl, pleurocoel; podl, postzygodiapophyseal lamina; poz, postzygapophysis; ppf, posterior pneumatic fossa; prdl, prezygodiapophyseal lamina; prz, prezygapophysis; spol, spinopostzygapophyseal lamina; sprl, spinoprezygapophyseal lamina. Vertebrae scaled to the same cotyle height.

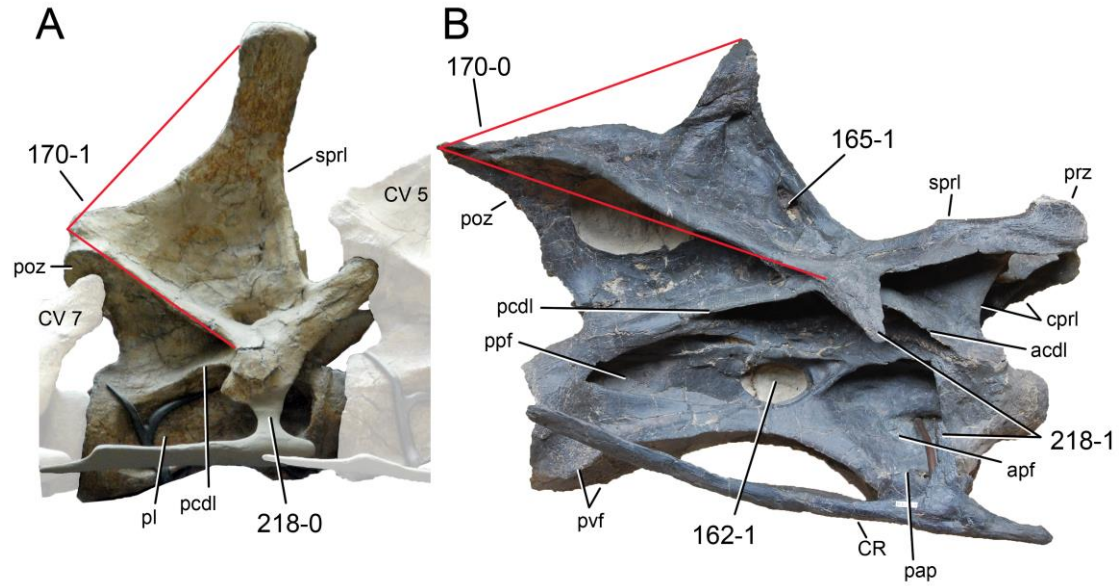

Figure 6.50: Cervical vertebra 6 of *Dicraeosaurus hansemanni* MB.R.4886 (A) and SMA 0011 (B) in right lateral view. Note the large, rounded pneumatic foramen marking the anterior end of the posterior pneumatic fossa in SMA 0011 (B; C162-1), the elongate foramen in the neural spine (B; C165-1), the right (A; C170-1), or acute angles (B; C170-0) between the spinopostzygapophyseal and the postzygodiapophyseal laminae, and the vertical (A; C218-0) or posteriorly inclined tuberculum (B; C218-1). Abb.: acdl, anterior centrodiapophyseal lamina; apf, anterior pneumatic fossa; cprl, centroprezygapophyseal lamina; CR, cervical rib; CV 5, cervical vertebra 5; pap, parapophysis; pl, pleurocoel; poz, postzygapophysis; ppf, posterior pneumatic fossa; prz, prezygapophysis; pvf, posteroventral flanges; sprl, spinoprezygapophyseal lamina. Scaled to the same cotyle height.

Table 6.23: Elongation indices mid-cervical centra (including condyle)

Taxon	Specimen	EI	Mean	Reference	Comments
Shunosaurus lii	T5401, CV 5	2,13	2,1	Zhang, 1988	
	T5401, CV 6	2,08		Zhang, 1988	
	T5401, CV 7	2,00		Zhang, 1988	
	T5401, CV 8	1,84		Zhang, 1988	
	T5402, CV 5	2,43		Zhang, 1988	
	T5402, CV 6	2,00		Zhang, 1988	
Spinophorosaurus nigerensis	NMB-1699-R, CV 6	3,55	3,5	A. Ritter, pers. comm. 2011	measured from 3D models
	NMB-1699-R, CV 9	3,47		A. Ritter, pers. comm. 2011	height estimated
Omeisaurus	T5701, CV 7	3,48	4,6	He et al., 1988	
	T5703, CV 7	5,98		He et al., 1988	
	T5703, CV 9	4,81		He et al., 1988	
	T5703, CV 10	4,76		He et al., 1988	
	T5704, CV 11	3,79		He et al., 1988	
Mamenchisaurus	CCG V 20401, CV 7	2,90	3,2	Ksepka & Norell, 2006	
	CCG V 20401, CV 8	2,70		Ksepka & Norell, 2006	
	ZDM 0083, CV 7	3,63		Ouyang & Ye, 2002	
	ZDM 0083, CV 8	3,49		Ouyang & Ye, 2002	
	ZDM 0083, CV 9	3,28		Ouyang & Ye, 2002	
	ZDM 0083, CV 10	3,14		Ouyang & Ye, 2002	
	ZDM 0083, CV 11	3,32		Ouyang & Ye, 2002	
	ZDM 0083, CV 12	3,07		Ouyang & Ye, 2002	
Jobaria tiguidensis	MNN TIG, CV 5	2,09	2,3	J. Carballido, pers. comm., 2013	measured from photo
	MNN TIG, CV 6	2,42		J. Carballido, pers. comm., 2013	measured from photo
	MNN TIG, CV 7	2,10		J. Carballido, pers. comm., 2013	measured from photo
	MNN TIG, CV 8	2,42		J. Carballido, pers. comm., 2013	measured from photo
Turiasaurus riodevensis	CPT	2,26	2,3	Royo-Torres et al., 2006	measured from figure
Camarasaurus	AMNH 5671, CV 5	2,30	2,9	Ksepka & Norell, 2006	
	AMNH 5671, CV 7	3,10		Ksepka & Norell, 2006	
	AMNH 5671, CV 8	3,50		Ksepka & Norell, 2006	
	BYU 9047, CV 5	2,90		Wedel et al., 2000	
	BYU 9047, CV 6	2,80		Wedel et al., 2000	
	BYU 9047, CV 7	3,00		Wedel et al., 2000	
	BYU 9047, CV 8	3,00		Wedel et al., 2000	
Giraffatitan brancai	MB.R.2181, CV 5	5,40	4,3	Ksepka & Norell, 2006	
	MB.R.2181, CV 6	5,00		Ksepka & Norell, 2006	
	MB.R.2181, CV 7	4,40		Ksepka & Norell, 2006	
	MB.R.2181, CV 8	4,00		Ksepka & Norell, 2006	
		3,92		Whitlock 2011c	
	MB.R.2180, CV 5	3,80		Wedel et al., 2000	
	MB.R.2180, CV 6	4,40		Wedel et al., 2000	
	MB.R.2180, CV 7	3,50		Wedel et al., 2000	
Brachiosaurus sp. SMA 0009	SMA 0009, CV 8?	2,82	2,9	Schwarz et al., 2007c	
	SMA 0009, CV 9?	3,02		Schwarz et al., 2007c	
Brachiosaurus altithorax	BYU 12866, CV 5?	3,10	3,1	Wedel et al., 2000	
Australodocus bohetii type	MB.R.2455, CV 6?	4,76	4,4	Remes, 2007	
	MB.R.2454, CV 7?	3,97		pers. obs.	
	MB.R.2454, CV 7?	4,00		Remes, 2007; Whitlock, 2011c	
Isisaurus colberti	ISIR 335/2, mCV	1,18	1,2	Jain & Bandyopadhyay, 1997	measured from figure
Haplocanthosaurus priscus	CM 879, CV 6?	2,94	2,9	Hatcher 1903	measured from figure, CV 8 according to Hatcher 1903
	CM 879, CV 7?	3,05		Hatcher 1903	measured from figure, CV 9 according to Hatcher 1903
	CM 879, CV 8?	2,72		Hatcher 1903	measured from figure, CV 10 according to Hatcher
Limaysaurus tessonei					
Nigersaurus taqueti	MNN-GAD 512, CV 5	4,24	4,2	Wilson et al., 2011	measured from figure
Demandasaurus darwini	MDS-RVII,589	2,84	2,8	Torcida Fernández-Baldor et al., 2011	
Dicraeosaurus hansemanni	MB.R.4886, CV 5	2,22	2,3	Janensch 1929	
	MB.R.4886, CV 6	2,38		Janensch 1929	
	MB.R.4886, CV 7	2,28		Janensch 1929	
	MB.R.4886, CV 8	2,13		Janensch 1929	
Brachytrachelopan mesai	MPEF-PV 1716	~1	1,0	Rauhut et al., 2005	
Amargasaurus cazaui	MACN-N 15, CV 6	2,40	2,2	Salgado & Bonaparte, 1991	measured from figure
	MACN-N 15, CV 8	2,00		Salgado & Bonaparte, 1991	measured from figure
Suuwassea emilieae ANS 21122	ANS 21122, CV 6	3,45	3,4	Harris 2006	
Apatosaurus ajax YPM 1860	YPM 1860, mCV	2,20	2,2	pers. obs.	measured from photo
Brontosaurus excelsus YPM 1980	YPM 1980, CV 8	2,50	2,5	pers. obs.	

Table 6.23: continued.

Apatosaurus louisae CM 3018	CM 3018, CV 6	3,20	2,9	Ksepka & Norell, 2006	
	CM 3018, CV 6	3,27		Whitlock 2011c	
	CM 3018, CV 6	3,36		pers. obs.	
	CM 3018, CV 7	3,14		Whitlock 2011c	
	CM 3018, CV 7	2,57		pers. obs.	
	CM 3018, CV 8	2,90		Ksepka & Norell, 2006	
	CM 3018, CV 8	3,30		Whitlock 2011c	
	CM 3018, CV 8	3,00		pers. obs.	
	CM 3018, CV 9	2,90		Wedel et al., 2000	
	CM 3018, CV 9	2,80		pers. obs.	
	CM 3018, CV 10	2,40		Wedel et al., 2000	
	CM 3018, CV 10	2,39		pers. obs.	
Apatosaurus parvus UW 15556	UW 15556, CV 7	2,50	2,4	Wedel et al., 2000	
	UW 15556, CV 7	2,40		pers. obs.	
	UW 15556, CV 8	2,30		Wedel et al., 2000	
	UW 15556, CV 8	2,45		pers. obs.	
	UW 15556, CV 9	2,20		Wedel et al., 2000	
	UW 15556, CV 9	2,23		pers. obs.	
	UW 15556, CV 10	2,40		Wedel et al., 2000	
	UW 15556, CV 10	2,64		pers. obs.	
Apatosaurus ajax NSMT-PV 20375	NSMT-PV 20375, CV 6	2,55	2,6	Upchurch et al., 2004b	
	NSMT-PV 20375, CV 7	2,71		Upchurch et al., 2004b	
	NSMT-PV 20375, CV 8	2,72		Upchurch et al., 2004b	
	NSMT-PV 20375, CV 9	2,42		Upchurch et al., 2004b	
Apatosaurus sp. AMNH 460	AMNH 460	ca. 2,5	2,5	pers. obs.	
Apatosaurus sp. CM 3378	CM 3378	3,18	3,2	pers. obs.	
Apatosaurus sp. ML 418	ML 418, mCV	3,00	3,0	pers. obs.	measured from photo, length estimated
Supersaurus vivianae BYU	BYU 9024	3,70	3,7	R. Wilhite, pers. comm. 2012	measured from photo
Supersaurus vivianae WDC DMJ-021	WDC DMJ-021, mCV	4,56	4,6	D. Lovelace, pers. comm. 2013	measured from photo
Kaatedocus siberi SMA 0004	SMA 0004, CV 6	4,13	3,5	Tschopp & Mateus, in press	
	SMA 0004, CV 7	3,66		Tschopp & Mateus, in press	
	SMA 0004, CV 8	3,31		Tschopp & Mateus, in press	
	SMA 0004, CV 9	3,51		Tschopp & Mateus, in press	
	SMA 0004, CV 10	3,00		Tschopp & Mateus, in press	
Tornieria africana , skeleton k	MB.R. k3	5,83	5,8	Remes, 2007	
Diplodocus carnegii CM 84	CM 84, CV 6	4,70	4,3	Hatcher 1901; Wedel et al. 2000	
	CM 84, CV 7	4,95		Hatcher 1901; Wedel et al. 2000	
	CM 84, CV 8	4,27		Hatcher 1901; Wedel et al. 2000	
	CM 84, CV 9	3,80		Hatcher 1901; Wedel et al. 2000	
	CM 84, CV 10	3,58		Hatcher 1901; Wedel et al. 2000	
Diplodocus carnegii CM 94	CM 94, CV 8?	4,00	3,8	pers. obs.	
	CM 94, CV 9?	4,00		pers. obs.	
	CM 94, CV 10?	3,53		pers. obs.	
Diplodocinae indet. CM 3452	CM 3452, CV 6	~4	4,0	pers. obs.	measured from photo
Galeamopus hayi HMNS 175	HMNS 175, CV 6	3,09	3,1	pers. obs.	measured from photo
	HMNS 175, CV 7	3,35		pers. obs.	measured from photo
	HMNS 175, CV 8	3,08		pers. obs.	measured from photo
	HMNS 175, CV 9	3,24		pers. obs.	measured from photo
	HMNS 175, CV 10	2,69		pers. obs.	measured from photo
Galeamopus shellensis SMA 0011	SMA 0011, CV 6	4,36	4,4	pers. obs.	
	SMA 0011, CV 8	3,98		pers. obs.	
	SMA 0011, CV 9	4,78		pers. obs.	
Barosaurus sp. AMNH 6341	AMNH 6341, CV 8	5,37	5,0	McIntosh 2005	
	AMNH 6341, CV 9	5,07		McIntosh 2005	
	AMNH 6341, CV 10	5,01		McIntosh 2005	
	AMNH 6341, CV 11	4,70		McIntosh 2005	
Barosaurus sp. AMNH 7530	AMNH 7530, CV 6	3,53	3,7	pers. obs.	
	AMNH 7530, CV 7	3,69		pers. obs.	
	AMNH 7530, CV 8	3,76		pers. obs.	
	AMNH 7530, CV 9	4,00		pers. obs.	
	AMNH 7530, CV 10	3,30		pers. obs.	
Barosaurus sp. CM 11984	CM 11984, mCV	5,07	5,1	pers. obs.	
Barosaurus sp. AMNH 7535	AMNH 7535, CV 6	3,51	4,7	pers. obs.	
	AMNH 7535, CV 7	5,04		pers. obs.	
	AMNH 7535, CV 8	5,30		pers. obs.	
	AMNH 7535, CV 9	4,80		pers. obs.	

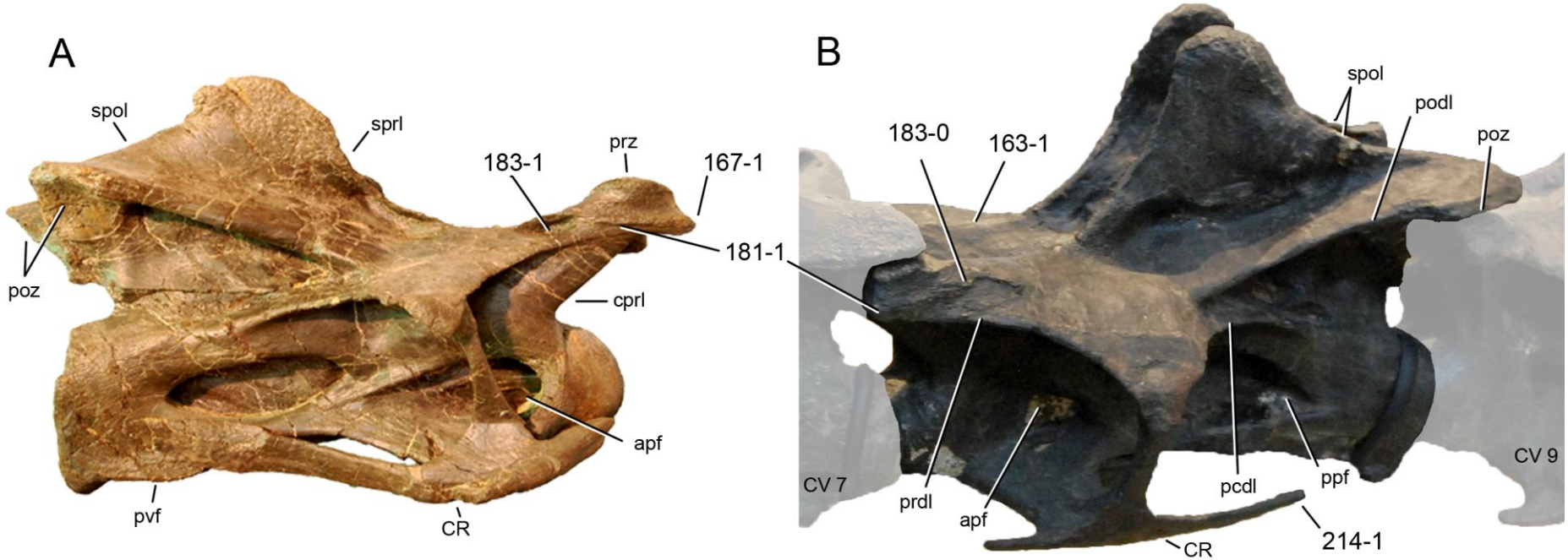

Figure 6.51: Mid-cervical vertebrae of *Kaatedocus siberi* SMA 0004 (A; CV 10, modified from Tschopp and Mateus, in press) and *Diplodocus carnegii* CM 84 (B; CV 8) in right lateral (A) and left laterodorsal view (B). Note the reduced spinoprezygapophyseal lamina (B; C163-1), the pre-epipophysis (C181-1), which is anteriorly expanded in *K. siberi* (A; C167-1), the distinct fossa posterolaterally to the prezygapophysis (A; C183-1), which is absent in CM 84 (B; C183-0), and the short cervical ribs (B; 214-1). Abb.: apf, anterior pneumatic fossa; cprl, centroprezygapophyseal lamina; CR, cervical rib; CV 7, cervical vertebra 7; podl, postzygodiapophyseal lamina; poz, postzygapophysis; ppf, posterior pneumatic fossa; prz, prezygapophysis; pvf, posteroventral flanges; spol, spinopostzygapophyseal lamina; sprl, spinoprezygapophyseal lamina. Not to scale.

C168: Mid-cervical neural spine height: considerably shorter than height of neural arch, <0.45 (0); subequal to height of neural arch, 0.45-1.6 (1); considerably higher than neural arch, >1.6 (2) (Rauhut et al., 2005; modified; Tab. 6.24).

Comments. Neural arch height is measured in a vertical line from the centrum to the dorsal edge of the postzygapophyses, neural spine height from dorsal edge of the postzygapophyses to the spine summit. The centrum is oriented such that the ventral floor of the neural canal is horizontal. The majority of the ratios were measured from photos or figures in lateral view. As exemplified by CV 6 of *Suuwassea* ANS 21122, this approach can yield major differences depending on slight changes in perspective (or left and right lateral views; CV 6 of ANS 21122 has ratios ranging from 0.91-1.27; Tab. 6.24). Although such differences are partly avoided by using mean ratios, it would be unwise to use closely spaced numerical state boundaries in this case. Therefore, only two steps were regarded as phylogenetically significant, and objective enough. The character left unordered due to diverging evolutionary trends.

C169: Mid-cervical neural spines, orientation: vertical (0); anteriorly inclined (1) (Rauhut et al., 2005; Fig. 6.52).

Comments. The neural spine is interpreted to be anteriorly inclined, when the anterior end of the summit reaches further anterior than the posterior-most point of the sprl.

C170: Mid-cervical vertebrae, angle between postzygodiapophyseal and spinopost-zygapophyseal laminae: acute (0); right angle (1) (Rauhut et al., 2005; Fig. 6.50).

Comments. Angles are measured between lines connecting the posterior-most point of podl and spol (often the epipophyses) with their opposing ends.

C171: Mid- and posterior cervical centra, pleurocoels: single without division (0) divided by a bone septum, resulting in an anterior and a posterior lateral excavation (1); divided in three or more lateral excavations, resulting in a complex morphology (2) (Carballido et al., 2012b; modified; Fig. 6.36).

Comments. The original character (Carballido et al., 2012b) includes a fourth character state, which describes the shallow posterior pneumatic fossa. As such, it overlaps with character 172, introduced by Whitlock (2011a). Furthermore, subdivision of the pleurocoel is not correlated with the depth of the single pneumatic fossae in diplodocids. Therefore, the fourth state was omitted here.

C172: Mid- and posterior cervical vertebrae, pneumatization of lateral surface of centra: large, divided pleurocoel over approximately half of centrum (0); reduced, large fossa but sharp-bordered coel, if present, restricted to area above parapophysis (1) (Whitlock, 2011a; Fig. 6.40).

Comments. Taxa with single pleurocoels are scored as unknown.

C173: Mid- and posterior cervical vertebrae, pleurocoel extending onto dorsal surface of parapophysis: present (0); absent (1) (Upchurch, 1998; modified by Mannion et al., 2012, based on Whitlock, 2011a; Fig. 6.36).

C174: Mid- and posterior cervical vertebrae, longitudinal ridge on ventral surface: present (0); absent (1) (New).

C175: Mid- and posterior cervical vertebrae, ventral keel: single (0); bifid, connects posterolaterally to the ventrolateral edges of the centrum (1) (New; Fig. 6.38).

Comments. Taxa without ventral keels are scored as unknown.

C176: Mid- and posterior cervical vertebrae, paired pneumatic fossae on ventral surface, separated by ventral midline keel: absent (0); present (1) (New; Figs 6.38, 6.53).

Comments. Usually, these fossae are situated anteriorly between the parapophyses, separated by a ventral keel. Some apatosaur specimens (e.g. YPM 1861, pers. obs.) show paired pneumatic fossae located posterior to the parapophyses, facing ventrolaterally, and not separated by a keel. This morphology is considered different, and accounted for in character 177.

C177: Mid- and posterior cervical vertebrae, lateral edge posterior to parapophysis: continuous (0); marked by a deep groove extending anteroposteriorly along the edge (1) (New; Fig. 6.53).

Comments. Such a groove was proposed as autapomorphic for *Dinheirosaurus* (Mannion et al., 2012). However, it is also present in *Supersaurus vivianae* WDC DMJ-021, *Apatosaurus laticollis* YPM 1861, and *Dicraeosaurus hansemanni* MB.R.4886. As in most of these specimens, such a groove appears together with more centrally placed ventral pneumatic foramina (see character 176), two different characters are used.

Table 6.24: Mid-cervical neural spine/neural arch height.

Taxon	Specimen	Ratio	Mean	Reference	Comments
Shunosaurus lii	T5402, CV 6	1,069	1,18	Zhang 1988	measured from figure, lateral view
	T5402, CV 9	1,293		Zhang 1988	measured from figure, lateral view
Spinophorosaurus nigerensis	NMB-1699-R, CV 6	0,694	0,82	A. Ritter, pers. comm. 2011	measured from figure, lateral view
	NMB-1699-R, CV 9	0,945		A. Ritter, pers. comm. 2011	measured from figure, lateral view
Omeisaurus	T5703, CV 8	1,538	1,17	He et al. 1988	measured from figure, lateral view
	T5703, CV 9	1,241		He et al. 1988	measured from figure, lateral view
	T5704, CV 11	0,733		He et al. 1988	measured from figure, lateral view
Mamenchisaurus	ZDM 0083, CV 7	0,609	0,99	Ouyang & Ye, 2002	measured from figure, lateral view
	ZDM 0083, CV 8	0,919		Ouyang & Ye, 2002	measured from figure, lateral view
	ZDM 0083, CV 9	1,455		Ouyang & Ye, 2002	measured from figure, lateral view
	ZDM 0083, CV 10	0,958		Ouyang & Ye, 2002	measured from figure, lateral view
	ZDM 0083, CV 11	0,902		Ouyang & Ye, 2002	measured from figure, lateral view
	ZDM 0083, CV 12	1,125		Ouyang & Ye, 2002	measured from figure, lateral view
Jobaria tiguidensis	MNN TIG, CV 5	0,314	0,63	J. Carballido, pers. comm., 2013	measured from photo, lateral view
	MNN TIG, CV 6	0,715		J. Carballido, pers. comm., 2013	measured from photo, lateral view
	MNN TIG, CV 7	0,543		J. Carballido, pers. comm., 2013	measured from photo, lateral view
	MNN TIG, CV 8	0,934		J. Carballido, pers. comm., 2013	measured from photo, lateral view
Turiasaurus riodevensis	CPT, mCV	1,386	1,39	Royo-Torres et al. 2006	measured from figure, lateral view
Camarasaurus	AMNH 5671, CV 5	0,400	0,65	Osborn & Mook, 1921	measured from figure, lateral view
	AMNH 5671, CV 7	1,423		Osborn & Mook, 1921	measured from figure, lateral view
	AMNH 5671, CV 8	0,651		Osborn & Mook, 1921	measured from figure, lateral view
	BYU 9047, CV 6	1,108		McIntosh et al. 1996b	measured from figure, lateral view
	BYU 9047, CV 7	0,533		McIntosh et al. 1996b	measured from figure, lateral view
	WDC A, CV 5	0,515		Ikejiri 2004	measured from figure, lateral view
	WDC A, CV 6	0,391		Ikejiri 2004	measured from figure, lateral view
	WDC A, CV 7	0,208		Ikejiri 2004	measured from figure, lateral view
	WDC A, CV 8	0,597		Ikejiri 2004	measured from figure, lateral view
Giraffatitan brancai	MB.R.2180, CV 5	0,676	0,91	Janensch 1950	measured from figure, lateral view
	MB.R.2180, CV 6	0,962		Janensch 1950	measured from figure, lateral view
	MB.R.2180, CV 7	0,737		Janensch 1950	measured from figure, lateral view
	MB.R.2181, CV 8	1,250		Janensch 1950	measured from figure, lateral view
Brachiosaurus sp. SMA 0009	SMA 0009, CV 5?	0,147	0,15	Carballido et al., 2012	measured from figure, lateral view
Australodocus bohetii type	MB.R.2455, CV 6?	0,650	0,53	pers. obs.	measured from photo, lateral view
	MB.R.2455, CV 6?	0,365		Remes 2007	measured from figure, lateral view
	MB.R.2454, CV 7?	0,579		Remes 2007	measured from figure, lateral view
Isisaurus colberti	ISIR335/2, mCV	1,320	1,32	Jain & Bandyopadhyay 1997	measured from figure, lateral view
Haplocanthosaurus priscus	CM 879, CV 6?	0,630	0,62	Hatcher 1903	measured from figure, lateral view, CV 8 according to Hatcher 1903
	CM 879, CV 7?	0,793		Hatcher 1903	measured from figure, lateral view, CV 9 according to Hatcher 1903
	CM 879, CV 8?	0,444		Hatcher 1903	measured from figure, lateral view, CV 10 according to Hatcher 1903
Zapalasaurus bonapartei	Pv-6127-MOZ, mCV	1,239	1,24	Salgado et al. 2006	measured from figure, lateral view
Nigersaurus taqueti	MNN-GAD 512, CV 5	0,229	0,61	Wilson et al. 2011	measured from figure, lateral view
	MNN-GAD 512, CV 7	1,000		Wilson et al. 2011	measured from figure, lateral view, centrum reconstructed
Dicraeosaurus hansemanni	MB.R.4886, CV 5	2,114	2,22	Harris 2006	measured from figure, lateral view
	MB.R.4886, CV 6	2,058		Harris 2006	measured from figure, lateral view
	MB.R.4886, CV 7	2,398		pers. obs.	measured from photo, lateral view
	MB.R.4886, CV 8	2,297		pers. obs.	measured from photo, lateral view
Brachytrachelopan mesai	MPEF PV 1716, CV 8	0,976	0,98	Rauhut et al. 2005	measured from figure, lateral view
Amargasaurus cazaui	MACN-N 15, CV 6	5,892	5,10	Salgado & Bonaparte, 1991	measured from figure, lateral view
	MACN-N 15, CV 8	4,299		Salgado & Bonaparte, 1991	measured from figure, lateral view
Suuwassea emilieae ANS 21122	ANS 21122, CV 6	0,981	1,07	D. Lovelace, pers. comm. 2013	measured from photo, lateral view
	ANS 21122, CV 6	1,135		pers. obs.	measured from photo, lateral view
	ANS 21122, CV 6	1,270		Harris 2006	measured from figure, R lateral view
	ANS 21122, CV 6	0,913		Harris 2006	measured from figure, L lateral view
Apatosaurus ajax YPM 1860	YPM 1860, mCV	0,203	0,36	pers. obs.	measured from photo, R lateral view
	YPM 1860, mCV	0,514		pers. obs.	measured from photo, L lateral view
Apatosaurus louisae CM 3018	CM 3018, CV 8	1,172	1,17	Gilmore 1936	measured from figure, L lateral view
Atlantosaurus immanis YPM 1840	YPM 1840, mCV	0,268	0,27	Ostrom & McIntosh 1999	measured from figure, L lateral view, centrum reconstructed
Apatosaurus parvus CM 566	CM 566, mCV	1,551	1,24	Peterson & Gilmore 1902	measured from figure, R lateral view
	CM 566, mCV	0,935		pers. obs.	measured from photo, L lateral view
Apatosaurus parvus UW 15556	UW 15556, CV 8	1,327	1,19	Gilmore 1936	measured from figure, R lateral view
	UW 15556, CV 9	1,060		Gilmore 1936	measured from figure, R lateral view
Apatosaurus ajax NSMT-PV 20375	NSMT-PV 20375, CV 6	0,338	0,43	Upchurch et al. 2004	measured from figure, R lateral view
	NSMT-PV 20375, CV 7	0,310		Upchurch et al. 2004	measured from figure, R lateral view
	NSMT-PV 20375, CV 7	0,722		Upchurch et al. 2004	measured from figure, L lateral view
Apatosaurus sp. ML 418	ML 418, mCV	1,077	1,08	Antunes & Mateus, 2003	measured from figure, R lateral view
Supersaurus vivianae BYU	BYU 9024, mCV	0,581	0,58	R. Wilhite, pers. comm. 2012	measured from photo, L lateral view
Supersaurus vivianae WDC DMJ-021	WDC DMJ-021, mCV	0,778	0,78	D. Lovelace, pers. comm. 2013	measured from photo, L lateral view

Table 6.24: continued.

Kaatedocus siberi SMA 0004	SMA 0004, CV 6	0,285	0,54	pers. obs.	measured from photo, R lateral view
	SMA 0004, CV 7	0,680		pers. obs.	measured from photo, R lateral view
	SMA 0004, CV 8	0,546		pers. obs.	measured from photo, R lateral view
	SMA 0004, CV 9	0,486		pers. obs.	measured from photo, R lateral view
	SMA 0004, CV 10	0,708		pers. obs.	measured from photo, R lateral view
Diplodocus carnegii CM 84	CM 84, CV 6	1,037	0,94	Hatcher 1901	measured from figure, R lateral view
	CM 84, CV 7	0,930		Hatcher 1901	measured from figure, R lateral view
	CM 84, CV 8	0,973		Hatcher 1901	measured from figure, R lateral view
	CM 84, CV 9	1,055		Hatcher 1901	measured from figure, R lateral view
	CM 84, CV 10	0,726		Hatcher 1901	measured from figure, R lateral view
Galeamopus shellensis SMA 0011	SMA 0011, CV 6	0,649	0,45	pers. obs.	measured from photo, R lateral view
	SMA 0011, CV 8	0,251		pers. obs.	measured from photo, R lateral view
Barosaurus sp. AMNH 6341	AMNH 6341, CV 8	1,192	0,97	McIntosh 2005	measured from figure, L lateral view
	AMNH 6341, CV 9	0,806		McIntosh 2005	measured from figure, L lateral view
	AMNH 6341, CV 10	1,054		McIntosh 2005	measured from figure, L lateral view
	AMNH 6341, CV 11	0,826		McIntosh 2005	measured from figure, L lateral view
Barosaurus sp. AMNH 7530	AMNH 7530, CV 6	0,437	0,79	pers. obs.	measured from photo, R lateral view
	AMNH 7530, CV 7	0,534		pers. obs.	measured from photo, R lateral view
	AMNH 7530, CV 8	0,829		pers. obs.	measured from photo, R lateral view
	AMNH 7530, CV 9	1,228		pers. obs.	measured from photo, R lateral view
	AMNH 7530, CV 10	0,905		pers. obs.	measured from photo, R lateral view
Barosaurus sp. CM 11984	CM 11984, CV 9	0,895	0,90	McIntosh 2005	measured from figure, R lateral view
Barosaurus sp. AMNH 7535	AMNH 7535, CV 6	0,117	0,52	pers. obs.	measured from photo, R lateral view
	AMNH 7535, CV 6	0,746		pers. obs.	measured from photo, L lateral view
	AMNH 7535, CV 7	0,650		pers. obs.	measured from photo, R lateral view
	AMNH 7535, CV 7	0,224		pers. obs.	measured from photo, L lateral view
	AMNH 7535, CV 8	0,566		pers. obs.	measured from photo, R lateral view
	AMNH 7535, CV 8	0,448		pers. obs.	measured from photo, L lateral view
	AMNH 7535, CV 9	0,618		pers. obs.	measured from photo, R lateral view
	AMNH 7535, CV 9	0,797		pers. obs.	measured from photo, L lateral view

C178: Mid- and posterior cervical vertebrae, rugose tuberosity on anterodorsal corner of lateral side: absent (0); present (1) (Tschopp and Mateus, 2012b; modified; Fig. 6.52).

Comments. The character description was extended to mid-cervical vertebrae in order to include *Suuwassea emilieae*. In the latter, the distinct rugose tubercles appear in mid-cervical vertebrae, whereas in *Kaatedocus siberi*, mid-cervical vertebrae only have very shallow tubercles. An additional character for serial variation is avoided as it could only be scored for these two taxa, and would thus not be phylogenetically significant.

C179: Mid- and posterior cervical centra with longitudinal flanges in the lateroventral edge on the posterior part of the centrum: absent (0); present (1) (Tschopp and Mateus, 2012b; Fig. 6.38).

Comments. These flanges are mainly responsible for the posterior portion of the ventral sulcus typical for diplodocines. However, also some apatosaur specimens have weak flanges, but no continuous ventral sulcus marking the ventral surface.

C180: Mid- and posterior cervical prezygapophyses, articular surfaces flat (0); articular surfaces strongly convex transversely (1) (Upchurch, 1995, 1998; Fig. 6.54).

C181: Mid- and posterior cervical vertebrae, pre-epipophysis: absent (0); present (1) (Remes, 2007; Figs 6.40, 6.51).

Comments. The pre-epipophysis is herein defined as a rugose, horizontal ridge laterally below the prezygapophyseal facet, which connects with the prdl anteriorly.

C182: Mid- and posterior cervical vertebrae, spinoprezygapophyseal lamina, anterior end: remains vertical, with the free edge facing dorsally (0); is strongly inclined laterally (sometimes roofing a lateral fossa in the prezygapophyseal process (1) (Tschopp and Mateus, 2012b; modified; Fig. 6.55).

Comments. At a first glance, it appears possible that this character is correlated with the occurrence of transversely convex prezygapophyseal facets. However, this is not the case, as can be seen in the several varying scores for these two characters.

C183: Mid- and posterior cervical neural arches, lateral fossae on the prezygapophysis process: absent (0); present (1) (Harris, 2006b; Tschopp and Mateus, 2012b; Figs 6.51, 6.55).

Comments. Where such a lateral fossa is present, it is dorsally roofed by a laterally tilted anterior end of the spinoprezygapophyseal lamina. However, not all specimens with a laterally tilted lamina also bear these fossae, which justifies the use of two independent characters. The character was first used in a phylogenetic analysis by Tschopp and Mateus (2012b).

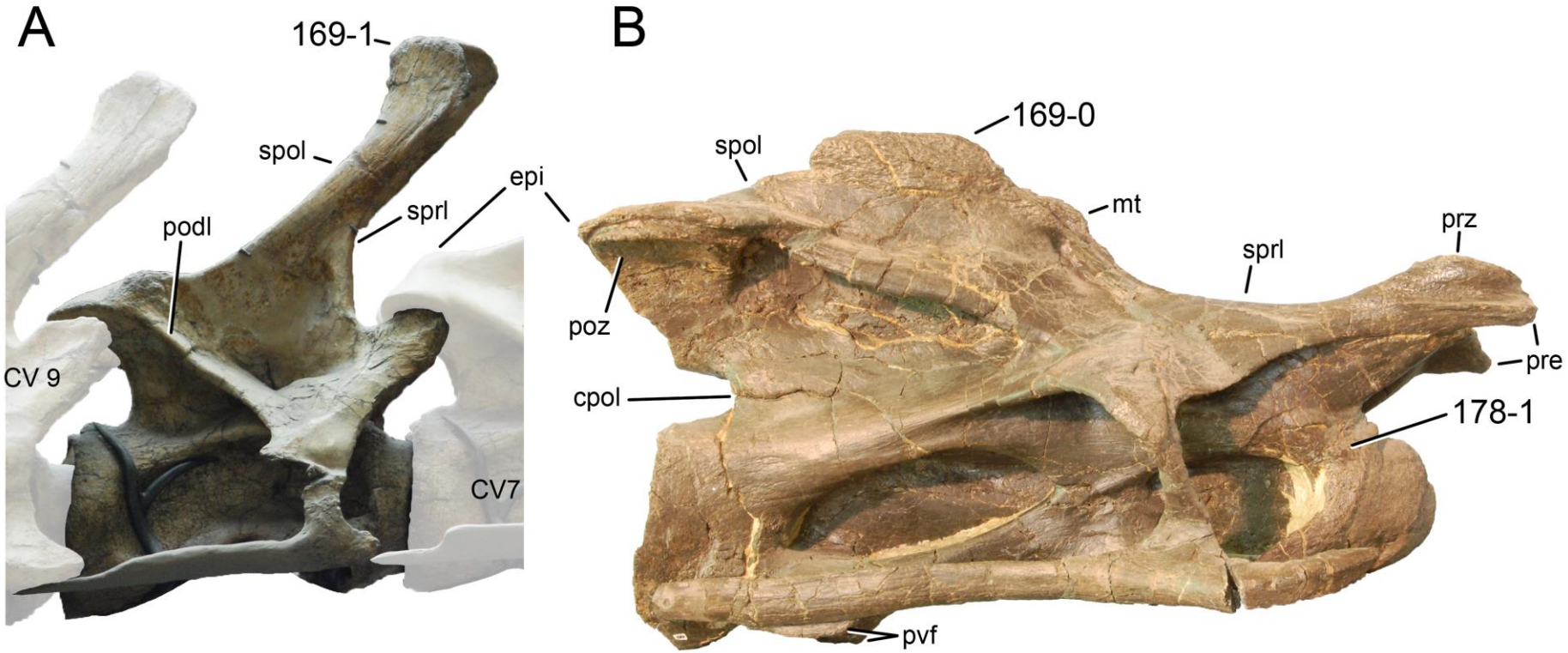

Figure 6.52: Cervical vertebra 8 of *Dicraeosaurus hansemanni* MB.R.4886 (A) and *Kaatedocus siberi* SMA 0004 (B) in right lateral view. Note the different inclinations of the neural spine (C169), and the small tuberosity marking the anterodorsal corner of the centrum in *Kaatedocus* (B; C178-1). Abb.: cpol, centropostzygapophyseal lamina; CV 7, cervical vertebra 7; epi, epipophysis; mt, median tubercle; podl, postzygodiapophyseal lamina; poz, postzygapophysis; pre, pre-epipophysis; prz, prezygapophysis; pvf, posteroventral flanges; spol, spinopostzygapophyseal lamina; sprl, spinoprezygapophyseal lamina. Scaled to the same cotyle height.

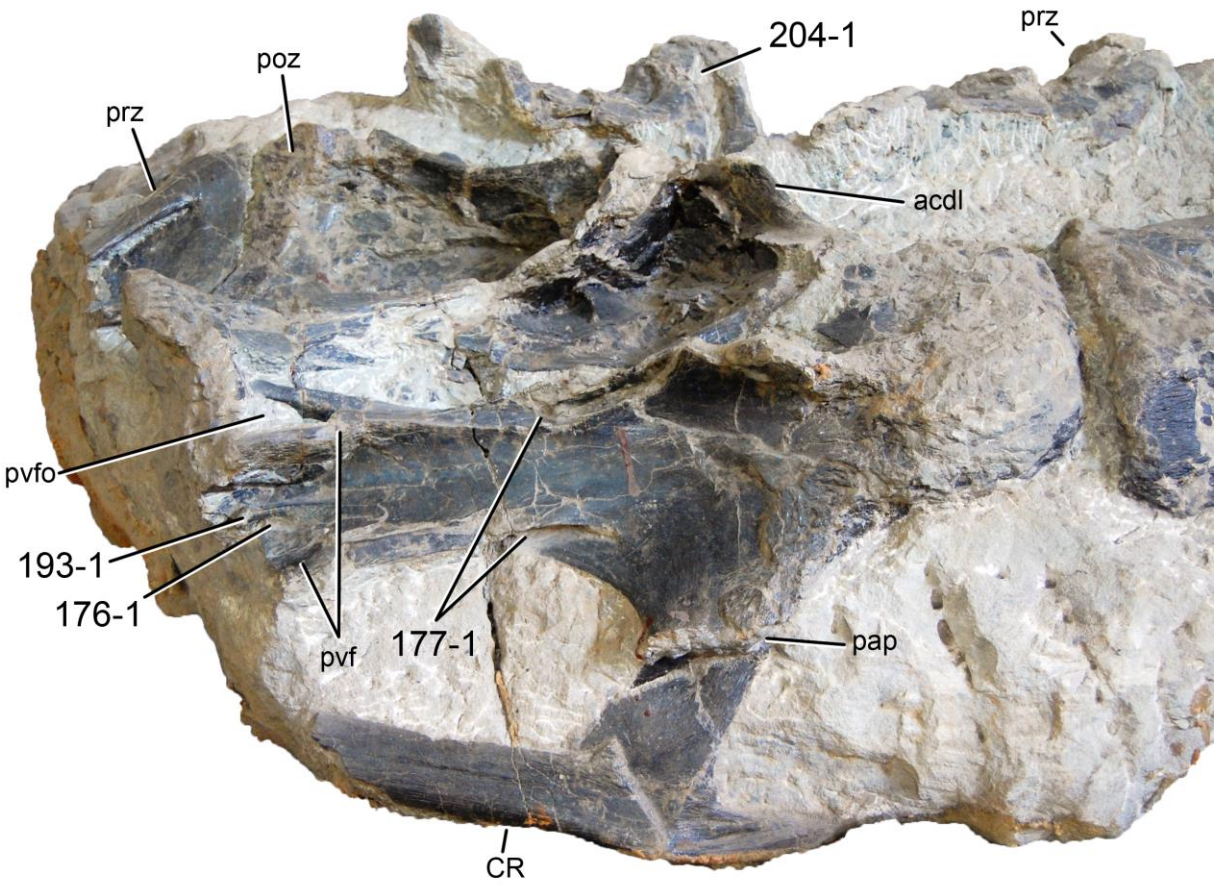

Figure 6.53: Cervical vertebra 14 of *Dinheirosaurus lourinhanensis* ML 414 in lateroventral view, illustrating the particular ventral morphology with posteriorly located paired pneumatic foramina (C176-1), lateral grooves posterior to the parapophyses (C177-1), a posteriorly restricted ventral keel (C193-1), and the elongated lateral spinal cavity (C204-1). Abb.: acdl, anterior centrodiapophyseal lamina; CR, cervical rib; pap, parapophysis; poz, postzygapophysis; prz, prezygapophysis; pvf, posteroventral flanges; pvfo, posteroventral fossa.

C184: Mid- and posterior cervical vertebrae, prezygapophyseal centrodiapophyseal fossa: single cavity (0); subdivided into two cavities by a ridge (1); several accessory laminae subdivide the fossa into various smaller partitions (2) (Gilmore, 1936; Upchurch et al., 2004b; modified; Figs 6.38, 6.40).
Comments. A third state was added in order to be able to accurately code the holotype specimen of *Barosaurus lentus* (YPM 429), as well as a few other specimens. The character is treated as ordered, as an increase in lamination is thought to happen step-wise. Two specimens coded as '0' actually only preserve mid-cervical vertebrae (AMNH 7535, CM 3452, pers. obs., 2011). It would thus be possible that more posterior elements of these cervical columns had subdivided prcdf.

C185: Mid- and posterior cervical neural arches, centroprezygapophyseal lamina: single (0); dorsally divided, resulting in a lateral and medial lamina, the medial lamina being linked with the interprezygapophyseal lamina and not with the prezygapophysis (1); divided, resulting in the presence of a "true" divided centroprezygapophyseal lamina, which is dorsally connected to the prezygapophysis (2) (Upchurch, 1995; modified by Carballido et al., 2012b; Fig. 6.54).
Comments. Usually, taxa with "true" divided cprl also have a lamina connecting from the base of the cprl to the tprl.

C186: Mid- and posterior cervical transverse processes: posterior centrodiapophyseal lamina (pcdl) and postzygodiapophyseal laminae (podl) meet at base of transverse process (0); pcdl and podl do not meet anteriorly, postzygapophyseal centrodiapophyseal fossa extends onto posterior face of transverse process (1) (New; Fig. 6.56).

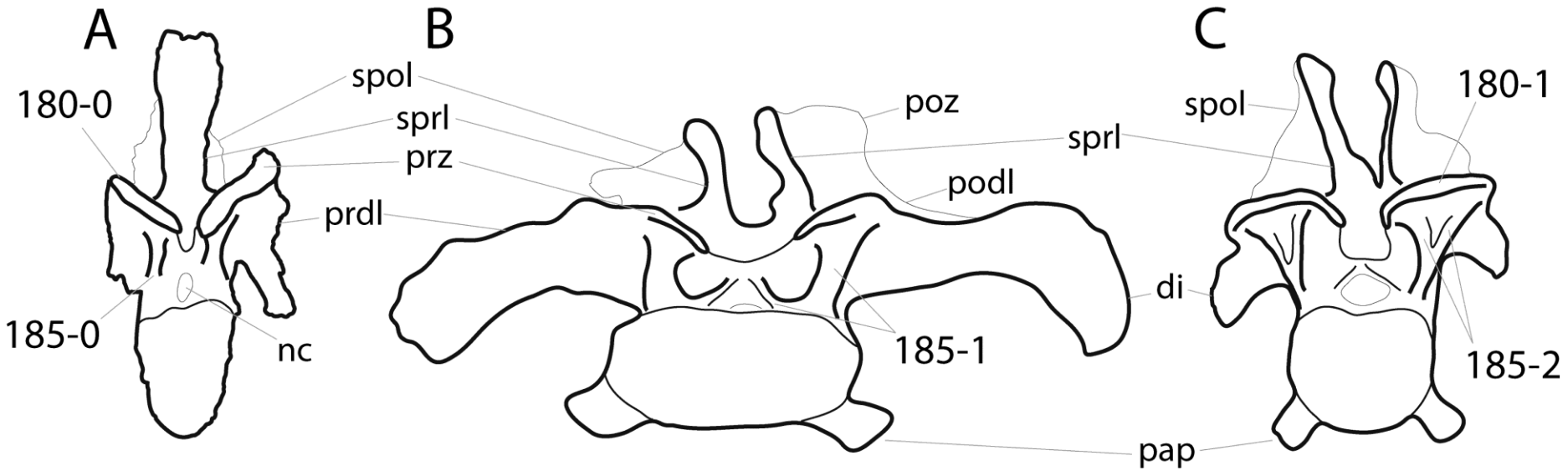

Figure 6.54: Cervical vertebra 11 of *Jobaria tiguidensis* MNN TIG (A; traced from photo by J. Carballido), *Camarasaurus supremus* AMNH 5671 (B; based on Osborn and Mook, 1921), and *Diplodocus carnegii* CM 84 (C; based on Hatcher, 1901) in anterior view. Note the straight (A; C180-0), in contrast to convex prezygapophyseal facet (C; C180-1), and the different morphologies of the centroprezygapophyseal lamina (single, A, C185-0; divided, and connecting to tprl, B, C185-1; divided with both branches connecting to prezygapophysis, C, C185-2). Abb.: di, diapophysis; nc, neural canal; pap, parapophysis; podl, postzygodiapophyseal lamina; poz, postzygapophysis; prdl, prezygodiapophyseal lamina; prz, prezygapophysis; spol, spinopostzygapophyseal lamina; sprl, spinoprezygapophyseal lamina. Scaled to the same condyle height.

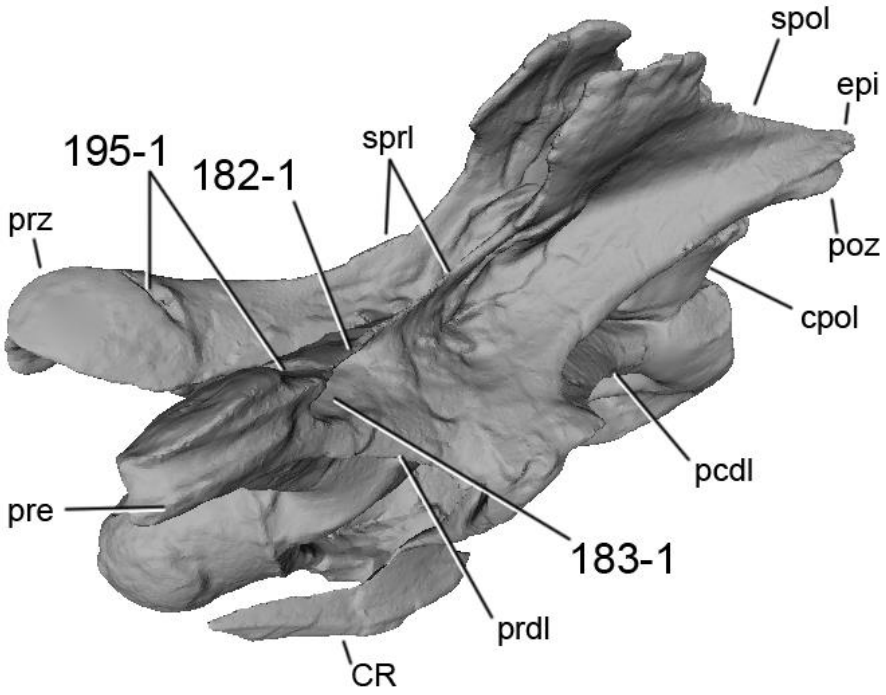

Figure 6.55: Cervical vertebra 12 of *Kaatedocus siberi* SMA 0004 in lateral anterodorsal view. Note the laterally tilted anterior portion of the sprl (C182-1), the lateral fossa marking the anterior end of the spinodiapophyseal fossa (C183-1), and the transverse sulcus accompanying the prezygapophyseal facet posteriorly (C195-1). Abb.: cpol, centropostzygapophyseal lamina; CR, cervical rib; epi, epipophysis; poz, postzygapophysis; prdl, prezygodiapophyseal lamina; pre, pre-epipophysis; prz, prezygapophysis; spol, spinopostzygapophyseal lamina; sprl, spinoprezygapophyseal lamina. 3D digital model provided by G. Dzemski.

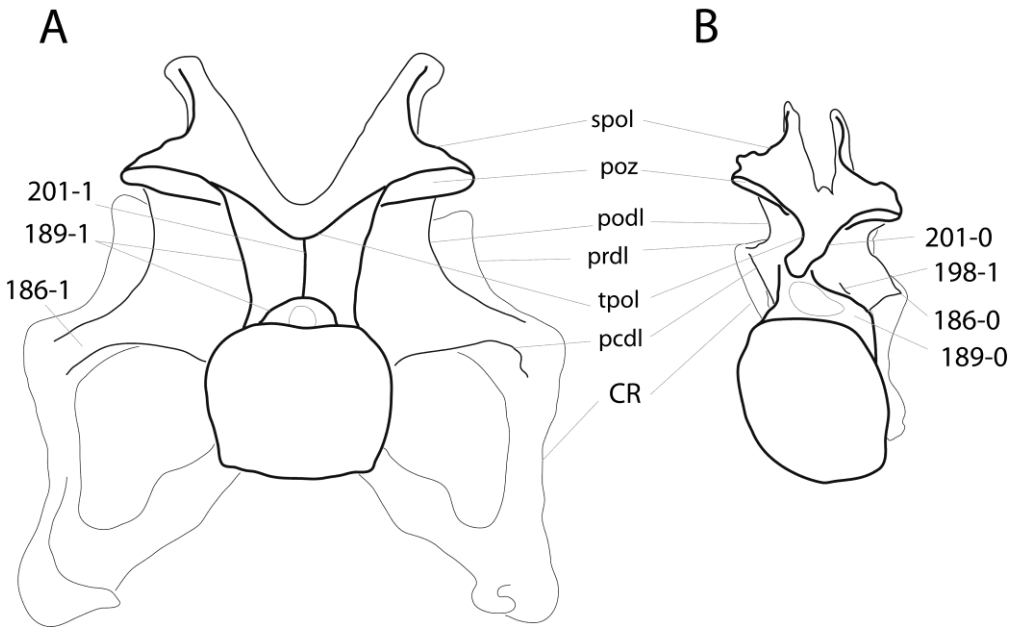

Figure 6.56: Cervical vertebra 12 of *Apatosaurus louisae* CM 3018 (A; based on Gilmore, 1936), and *Kaatedocus siberi* SMA 0004 (B; based on Tschopp and Mateus, in press) in posterior view. Note the separated (A; C186-1) or connected pcdl and podl (B; C186-0), the divided (A; C189-1) or single cpol (B; C189-0), the accessory lamina in the postzygapophyseal centrodiapophyseal fossa (B; C198-1), and the tpol that connects directly (B; C201-0) or indirectly with the neural canal roof (A; C201-1). Abb.: CR, cervical rib; pcdl; posterior centrodiapophyseal lamina; podl, postzygodiapophyseal lamina; poz, postzygapophysis; prdl, prezygodiapophyseal lamina; spol, spinopostzygapophyseal lamina; tpol, interpostzygapophyseal lamina. Scaled to the same posterior cotyle height.

C187: Mid- and posterior cervical vertebrae, accessory horizontal lamina in center of spinodiapophyseal fossa, not connected with any surrounding laminae: absent (0); present (1) (New; Fig. 6.57).

Comments. This accessory lamina could be a vestigial version of the epipophyseal-prezygapophyseal lamina (sensu Wilson, 2012) or the accessory lamina connecting the podl with the sprl (as used herein, following Carballido et al., 2012b). However, as no connection exists to any surrounding lamina, this cannot be definitely confirmed in the cases included here. The use of an independent character is thus preferred. The lamina is generally situated in the center of the sdf.

C188: Mid- and posterior cervical vertebrae, posterior centrodiapophyseal lamina: is single (0); bifurcates towards its anterior end (1) (Upchurch et al., 2004b; wording modified; Fig. 6.57).

Comments. Evidence from SMA 0011 shows that the presence of anteriorly bifurcated pcdl sometimes are a precursor of entirely double pcdl (see above). However, as in various specimens only bifurcated, and no entirely double pcdl exist, the character was retained as independent from the one describing the single or double pcdl (see character 136).

C189: Mid- and posterior cervical vertebrae, centropostzygapophyseal lamina (cpol): single (0); divided, with the medial part contacting the interpostzygapophyseal lamina (1) (Carballido et al., 2012b; Fig. 6.56).

C190: Mid- and posterior cervical neural arches, interpostzygapophyseal lamina projects beyond the posterior margin of the neural arch (including the centropostzygapophyseal lamina), forming a prominent subrectangular projection in lateral view: absent (0); present (1) (D'Emic, 2012; modified by Mannion et al., 2013; Fig. 6.40).

Comments. A reduced subrectangular projection is present in mid-cervical vertebrae of *Supersaurus* WDC DMJ-021. Generally, the development of this feature increases in more posterior elements (e.g. in *Diplodocus carnegii* CM 84; Hatcher, 1901). *Supersaurus* WDC DMJ-021 was thus scored as apomorphic, although it is not prominent in the preserved vertebrae. On the other hand, *Apatosaurus louisae* CM 3018, where only CV 13-15 bear weak projections, was coded as plesiomorphic.

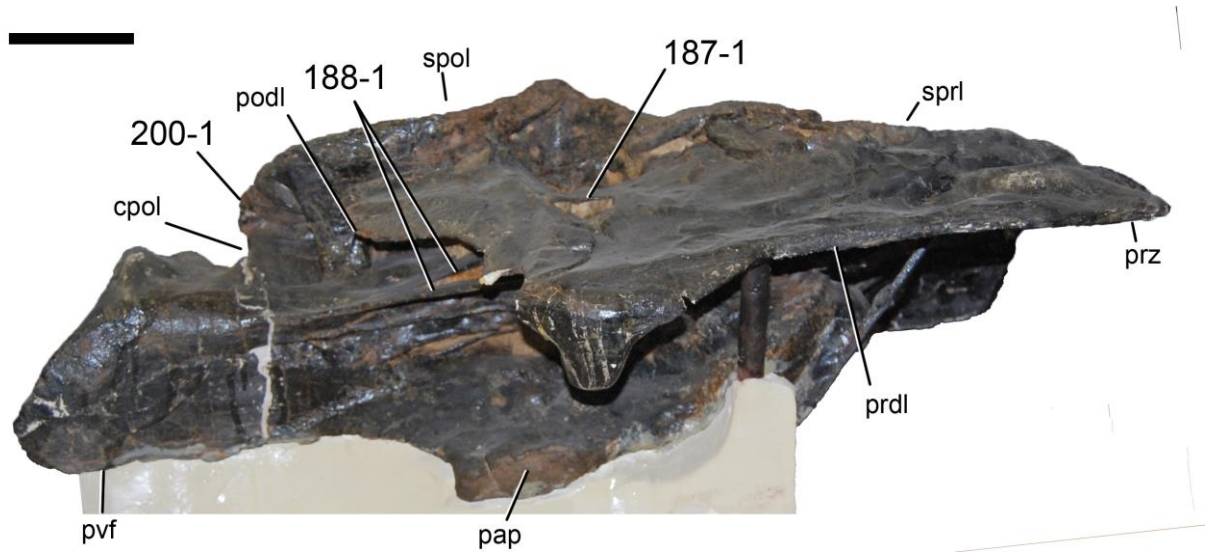

Figure 6.57: Posterior cervical vertebra of *Barosaurus lentus* YPM 429 in right lateral view, illustrating the short horizontal accessory lamina within the spinodiapophyseal fossa (C187-1), the anteriorly bifurcated posterior centrodiapophyseal lamina (C188-1), and the anteriorly restricted postzygapophyses (C200-1). Abb.: cpol, centropostzygapophyseal lamina; pap, parapophysis; podl, postzygodiapophyseal lamina; prdl, prezygodiapophyseal lamina; prz, prezygapophysis; pvf, posteroventral flanges; spol, spinopostzygapophyseal lamina; sprl, spinoprezygapophyseal lamina. Scale bar = 10 cm.

C191: Mid- and posterior cervical vertebrae, postzygapophyseal centrodiapophyseal fossa and spinopostzygapophyseal fossa: entirely separated (0); connected by a large foramen (1) (New; Fig. 6.36).

Comments. The laminae in this area are very thin and might brake easily. In fact, many specimens do show an opening here, but most of them also show broken margins around this opening, making it impossible to decide if the feature is genuine or not. Often, possible foramina are also closed with plaster or similar material during preparation, probably due to stability reasons, and because the presence of such foramina has never been reported before. In fact, only SMA 0011 can be confidently scored as apomorphic to date.

C192: Posterior cervical vertebrae, Elongation Index (cervical centrum length, excluding condyle, divided by posterior centrum height): less than 2.0 (0); 2.0 - 2.6 (1); higher than 2.6 (2) (Gauthier, 1986; Mannion et al., 2012; modified; Tab. 6.25).

Comments. In vertebrae with inclined posterior edges of the anterior condyle, a vertical line is drawn through the posterior-most point of the posterior edge, and the horizontal distance from this vertical line to a second vertical line through the posterior-most extension of the centrum is measured and taken as centrum length in this case. In some cases, only measurements of the complete centrum length were available, and the EI for the centrum length without anterior ball was calculated based on the mean difference between EI with and without condyle. Singular ratios given in table 6.25 have to be taken with care, as they differ considerably within posterior cervical centra (decreasing towards posterior). Ratios basing only on anterior posterior cervical vertebrae have thus to be corrected to a lower ratio (e.g. in UW 15556, Tab. 6.25).

C193: Posterior cervical vertebrae, ventral keel: anteriorly placed (0); restricted to posterior portion of the centrum (1) (New; Fig. 6.53).

Comments. Taxa without ventral ridges are scored as unknown.

C194: Posterior cervical prezygapophyses: terminate with or in front of the articular ball of the centrum (0); terminate well behind the articular ball (1) (Upchurch et al., 2004b; modified; Fig. 6.40).

Comments. The neural canal should be held horizontally, in order to accurately assess the expansion of the prezygapophysis.

C195: Posterior cervical vertebrae, prezygapophysis articular facet posterior margin: confluent with prezygapophyseal process (0); bordered posteriorly by conspicuous transverse sulcus (1) (Tschopp and Mateus, 2012b; Figs 6.39, 6.55).

Comments. The distribution of this character is dubious, as it is difficult to observe in photos and drawings. To date, only the holotype specimen of *Kaatedocus siberi* (SMA 0004) was reported to bear such a sulcus. The character in its present state thus does not contribute to the resolution of the tree. It was retained because more work on actual specimens has to be performed in order to confirm or discard this character as an unambiguous autapomorphy of *K. siberi*.

C196: Posterior cervical vertebrae, spinoprezygapophyseal lamina: continuous (0); developing an anterior projection (just beneath but independent from the spine summit) (1) (Tschopp and Mateus, 2012b; Fig. 6.39).

Comments. Sometimes the spine summit projects anteriorly, which is not what this character describes. Diplodocines often have an anterior projection below the summit, which forms the most anterior point of the spine.

C197: Posterior cervical vertebrae, accessory lateral lamina connecting postzygodiapophyseal and spinoprezygapophyseal laminae: absent (0); present (1) (Gallina and Apesteguía, 2005; Fig. 6.36).

Comments. This lamina was termed epipophyseal-prezygapophyseal lamina by Wilson and Upchurch (2009), but there are different ways of how to unite the epipophysis with the prezygapophysis (Carballido et al., 2012b; Wilson, 2012). Therefore, the description of Carballido et al. (2012b) was preferred herein.

C198: Posterior cervical vertebrae, accessory, subvertical lamina in the postzygapophyseal centrodiapophyseal fossa, with free edge facing laterally: absent (0); present (1) (New; Fig. 6.56).

Comments. There are two types of accessory laminae present in the pocdf of certain sauropod taxa: 1) laterally facing, relatively broad laminae, which are mostly located posteriorly, marking the lateral wall of the neural canal, and 2) more distinct, posteriorly facing laminae connecting the pcdl and podl anteriorly, at the base of the transverse process. The present character describes the presence of the first type, the second type is accounted for in the character 199.

Table 6.25: Elongation index posterior cervical vertebrae.

Taxon	Specimen	EI (-cd)	EI (+cd)	Mean EI (-cd)	Mean EI (+cd)	Difference	Reference	Comments
Shunosaurus lii	T5401, CV 9		1,75	1,6	1,9	85%	Zhang, 1988	
	T5401, CV 10		1,82				Zhang, 1988	
	T5402, CV 9	1,79					Zhang, 1988	measured from figure
	T5402, CV 10		2,38				Zhang, 1988	
	T5402, CV 11		1,68				Zhang, 1988	
	T5404, CV 12	1,47					Zhang, 1988	measured from figure
Omeisaurus	T5701, CV 12	3,14	3,26	2,3	2,3		He et al. 1988	EI (-cd) measured from figure
	T5701, CV 13	2,68	2,71				He et al. 1988	EI (-cd) measured from figure
	T5701, CV 14	2,81	2,38				He et al. 1988	EI (-cd) measured from figure
	T5701, CV 15	2,30	2,27				He et al. 1988	EI (-cd) measured from figure
	T5701, CV 16	2,06	1,89				He et al. 1988	EI (-cd) measured from figure
	T5701, CV 17	2,17					He et al. 1988	measured from figure
	T5704, CV 12		3,24				He et al. 1988	
	T5704, CV 13		2,60				He et al. 1988	
	T5704, CV 14		2,14				He et al. 1988	
	T5704, CV 15		2,19				He et al. 1988	
	T5704, CV 16		1,61				He et al. 1988	
	T5704, CV 17	1,17	1,16				He et al. 1988	EI (-cd) measured from figure
Mamenchisaurus	ZDM 0083, CV 13	2,69	2,59	2,1	2,2	96%	Ouyang & Ye 2002	EI (-cd) measured from figure
	ZDM 0083, CV 14	3,01	2,80				Ouyang & Ye 2002	EI (-cd) measured from figure
	ZDM 0083, CV 15	2,04	2,34				Ouyang & Ye 2002	EI (-cd) measured from figure
	ZDM 0083, CV 16	2,06	2,15				Ouyang & Ye 2002	EI (-cd) measured from figure
	ZDM 0083, CV 17	1,62	1,81				Ouyang & Ye 2002	EI (-cd) measured from figure
	ZDM 0083, CV 18	1,28	1,58				Ouyang & Ye 2002	EI (-cd) measured from figure
Jobaria tiguidensis	MNN TIG, CV 9	2,08	2,25	1,5	1,8	85%	J. Carballido, pers. comm. 2013	measured from photo
	MNN TIG, CV 10	1,44	1,68				J. Carballido, pers. comm. 2013	measured from photo
	MNN TIG, CV 11	1,53	1,70				J. Carballido, pers. comm. 2013	measured from photo
	MNN TIG, CV 12	0,99	1,44				J. Carballido, pers. comm. 2013	measured from photo
Camarasaurus	AMNH 5760, CV 10		3,39	1,7	2,4	72%	Osborn & Mook 1921	
	BYU 9047, CV 9	2,27	3,05				McIntosh et al. 1996b	
	WDC A, CV 9	1,96	2,44				Ikejiri 2004	
	WDC A, CV 10	1,63	1,95				Ikejiri 2004	
	WDC A, CV 11	1,58	2,05				Ikejiri 2004	
	WDC A, CV 12	1,08	1,38				Ikejiri 2004	
Brachiosaurus sp. SMA 0009	SMA 0009, CV 10		3,02	2,5	3,0		Schwarz et al. 2007	corresponds to Cep-7 in Schwarz et al. 2007
Ligabuesaurus leanzai	MCF-PVPH-233, pCV	2,15	2,62	2,1	2,6	82%	Bonaparte et al. 2006	measured from figure, posterior portion reconstructed
Isisaurus colberti	ISIR335/8, pCV	1,03	1,36	1,0	1,4	76%	Jain & Bandyopadhyay 1997	measured from figure, restored
Haplocanthosaurus priscus	CM 879, CV 10	2,02	2,34	2,0	2,5	81%	Hatcher 1903	measured from figure, CV 11 in Hatcher 1903
	CM 879, CV 11	2,27	2,72					measured from figure, CV 12 in Hatcher 1903
	CM 879, CV 12	1,89	2,44					measured from figure, CV 13 in Hatcher 1903
	CM 879, CV 13	1,96	2,51					measured from figure, CV 14 in Hatcher 1903

Table 6.25: continued.

Limaysaurus tessonei	MUCPv-205, pCV	2,40	3,09	2,4	3,1	78%	Calvo & Salgado 1995	measured from figure
Cathartesaura anaerobica	MPCA-232, pCV	2,27	2,54	2,3	2,5	89%	Gallina & Apesteguía, 2005	measured from figure
Nigersaurus taqueti	MNN, CV 11	2,05		2,1			Mannion et al. 2012	
Dicraeosaurus hansemanni	MB.R.4886, CV 9	1,57	1,96	1,3	1,7	76%	Janensch, 1929a	
	MB.R.4886, CV 10	1,50	1,89				Janensch, 1929a	
	MB.R.4886, CV 11	1,16	1,63				Janensch, 1929a	
	MB.R.4886, CV 12	1,09	1,50				Janensch, 1929a	
Brachytrachelopan mesai	MPEF-PV 1716	<1		<1			Rauhut et al. 2005	
Amargasaurus cazaui	MACN-N 15, CV 13	1,51		1,5			Mannion et al. 2012	
Apatosaurus ajax YPM 1860	YPM 1860, pCV	1,99	2,53	1,5	1,9	80%	pers. obs.	measured from photo
	YPM 1860, pCV	1,06	1,28				pers. obs.	measured from photo
Apatosaurus laticollis YPM 1861	YPM 1861	1,13		1,1			pers. obs.	
Apatosaurus louisae CM 3018	CM 3018, CV 11	1,83	2,39	1,5	2,0	77%	Gilmore 1936	measured from figure
	CM 3018, CV 12	1,67	2,10				Gilmore 1936	measured from figure
	CM 3018, CV 13	1,58	2,04				Gilmore 1936	measured from figure
	CM 3018, CV 14	1,38	1,78				Gilmore 1936	measured from figure
	CM 3018, CV 15	1,16	1,55				Gilmore 1936	measured from figure
Apatosaurus parvus UW 15556	UW 15556, CV 10	2,18	2,61	2,2	2,6	83%	Gilmore 1936	measured from figure, ratio for pCV lower, probably <2
Apatosaurus ajax NSMT-PV 20375	NSMT-PV 20375, CV 12	1,78	2,16	1,7	2,1	80%	Upchurch et al. 2004	centrum length estimated
	NSMT-PV 20375, CV 14	1,57	2,05				Upchurch et al. 2004	
Apatosaurus sp. AMNH 460	AMNH 460, CV 11	2,10		2,0			pers. obs.	EI (-cd) measured from photo
	AMNH 460, CV 12	2,30					pers. obs.	EI (-cd) measured from photo
	AMNH 460, CV 13	1,50					pers. obs.	EI (-cd) measured from photo
Apatosaurus sp. FMNH P25112	FMNH P25112, CV 15		1,76	1,4	1,8		Riggs, 1903	
Dinheirosaurus lourinhanensis ML 414	ML 414, CV 14	2,09		2,5	3,0	84%	Mannion et al. 2012	
	ML 414, CV 14	2,92	2,99				pers. obs.	Mannion et al. (2012) did not take distortion into account in posterior centrum height
Kaatedocus siberi SMA 0004	SMA 0004, CV 11	2,53	2,98	2,3	2,8	83%	Tschopp & Mateus, in press	
	SMA 0004, CV 12	2,59	3,08				Tschopp & Mateus, in press	
	SMA 0004, CV 13	2,15	2,58				Tschopp & Mateus, in press	
	SMA 0004, CV 14	2,07	2,64				Tschopp & Mateus, in press	
Diplodocus carnegii CM 84	CM 84, CV 11	2,85	3,45	2,5	3,0	82%	Hatcher 1901	measured from figure
	CM 84, CV 12	2,66	3,10				Hatcher 1901	measured from figure
	CM 84, CV 13	2,49	2,94				Hatcher 1901	measured from figure
	CM 84, CV 14	2,45	3,00				Hatcher 1901	measured from figure
	CM 84, CV 15	2,00	2,62				Hatcher 1901	measured from figure
Diplodocus carnegii CM 94	CM 94, CV ?12	2,63		2,6			pers. obs.	
Galeamopus hayi HMNS 175	HMNS 175, CV 11	2,10		2,0			pers. obs.	measured from photo
	HMNS 175, CV 12	2,15					pers. obs.	measured from photo
	HMNS 175, CV 13	1,87					pers. obs.	measured from photo
	HMNS 175, CV 14	1,83					pers. obs.	measured from photo

Table 6.25: continued.

Galeamopus shellensis	SMA 0011	SMA 0011, CV 11	2,59		2,3		
		SMA 0011, CV 12	2,21				
		SMA 0011, CV 15	2,00				
Barosaurus lentus	YPM 429	YPM 429, pCV		3,72	2,8	3,5	pers. obs.
		YPM 429, pCV		3,15			pers. obs.
		YPM 429, CV 13		3,41			McIntosh, 2005
		YPM 429, CV 16		3,60			McIntosh, 2005
Barosaurus	sp. AMNH 6341	AMNH 6341, CV 12	3,76		3,2		McIntosh, 2005
		AMNH 6341, CV 13	3,30				McIntosh, 2005
		AMNH 6341, CV 14	3,31				McIntosh, 2005
		AMNH 6341, CV 15	2,81				McIntosh, 2005
		AMNH 6341, CV 16	2,58				McIntosh, 2005
Barosaurus	sp. AMNH 7530	AMNH 7530, CV 11	2,63		2,6		pers. obs.
		AMNH 7530, CV 12	2,56				pers. obs.

C199: Posterior cervical vertebrae, accessory, subvertical lamina in the postzygapophyseal centrodiapophyseal fossa, with free edge facing posteriorly: absent (0); present (1) (Gilmore, 1936; Upchurch et al., 2004b; modified; Fig. 6.36).

Comments. Rarely, these accessory laminae can appear as a parallel pair as in SMA 0011 (Fig. 6.36). *Jobaria* has posteriorly facing laminae in the posterior portion of the pocdf, connecting to the postzygapophyses (J. Carballido, pers. comm., 2013). They are herein interpreted as lateral cpol, which are somewhat anteriorly shifted. *Jobaria* is thus scored as plesiomorphic in this character.

C200: Posterior cervical postzygapophyses: terminate at or beyond the posterior edge of the centrum (0); terminate in front of the posterior edge of the centrum (1) (Upchurch et al., 2004b; modified by Tschopp and Mateus, 2012b; Fig. 6.57).

C201: Posterior cervical neural arch, interpostzygapophyseal lamina (tpol): connects directly with roof of neural canal (0); vertical lamina connects tpol with neural canal roof (1) (New; Fig. 6.56).

Comments. Carballido and Sander (2013) termed this vertical lamina 'single intrapostzygapophyseal lamina' (stpol).

C202: Posterior cervical neural arches, epipophyses: transversely compressed (0); dorsoventrally compressed (1) (New; Fig. 6.42).

Comments. Two different morphologies of the epipophyses are present in diplodocids: 1) dorsoventrally compressed, usually forming a horizontal, rugose ridge above the postzygapophyseal facet, on the lateral side of the spol, and 2) transversely compressed, such that it is formed by a dorsal expansion of the posterior end of the spol, in some cases (e.g. *Diplodocus carnegii* CM 84) forming a rugose, vertical plate above the zygapophyseal facet, but never accompanied by a horizontal ridge. Taxa without epipophyses are scored as 'unknown'.

C203: Posterior cervical neural arches, accessory spinal lamina: absent (0); present, running vertically just posterior to spinoprezygapophyseal lamina (1) (Whitlock, 2011a; Fig. 6.40).

Comments. This lamina could represent a reduced spdl. The presence of a distinct lamina is restricted to advanced diplodocines, but a reduced lamina is present in *Spinophorosaurus* as well (NMB-1699-R, pers. obs., 2011).

C204: Posterior cervical neural spines, dorsoventrally elongate coel on lateral surface: absent (0); present (1) (Mannion et al., 2012; Fig. 6.53).

C205: Posterior cervical neural spine, horizontal, rugose ridge right below spine summit on lateral surface: absent (0); present, serves as distinct dorsal edge of the spinodiapophyseal fossa (1) (Tschopp and Mateus, 2012b; Fig. 6.42).

Comments. The ridge can be slightly curved in some taxa. When absent (plesiomorphic state), the sdf fades dorsally.

C206: Posterior bifid, cervical neural spines, medial surface: marked by a distinct, dorsoventral ridge from the base to the spine summit (0); smooth (1) (New; Fig. 6.58).

C207: Posterior cervical neural and/or anterior-most dorsal neural spines: vertical (0); anteriorly inclined (1) (Rauhut et al., 2005).

Comments. See comments in character 169 for definition of inclined.

C208: Posterior cervical and anterior dorsal vertebrae, roughened lateral aspect of prezygodiapophyseal lamina: absent (0); present (1) (Whitlock, 2011a; Fig. 6.59).

Comments. The rugose area in the derived taxa lies ventrolateral to the pre-epipophysis, where present.

C209: Posterior cervical and anterior dorsal vertebrae, prespinal lamina: absent (0), present (1) (Salgado et al., 1997; Fig. 6.60).

Comments. The presence of a prespinal lamina does not imply the presence of a median tubercle or vice versa. However, a dorsally expanded prespinal lamina can form a median tubercle (see below). In anterior dorsal vertebrae of *Diplodocus carnegii* CM 94, the median tubercle leans anteriorly, but no lamina is present connecting it with the base of the notch between the metapophyses (pers. obs., 2011).

C210: Posterior cervical and anterior dorsal bifid neural spines, median tubercle: absent (0); present (1) (McIntosh, 1990b; Upchurch, 1995; Fig. 6.39).

Comments. The median tubercle can be either an independent structure in the trough between the metapophyses, or a dorsal projection of the prespinal lamina.

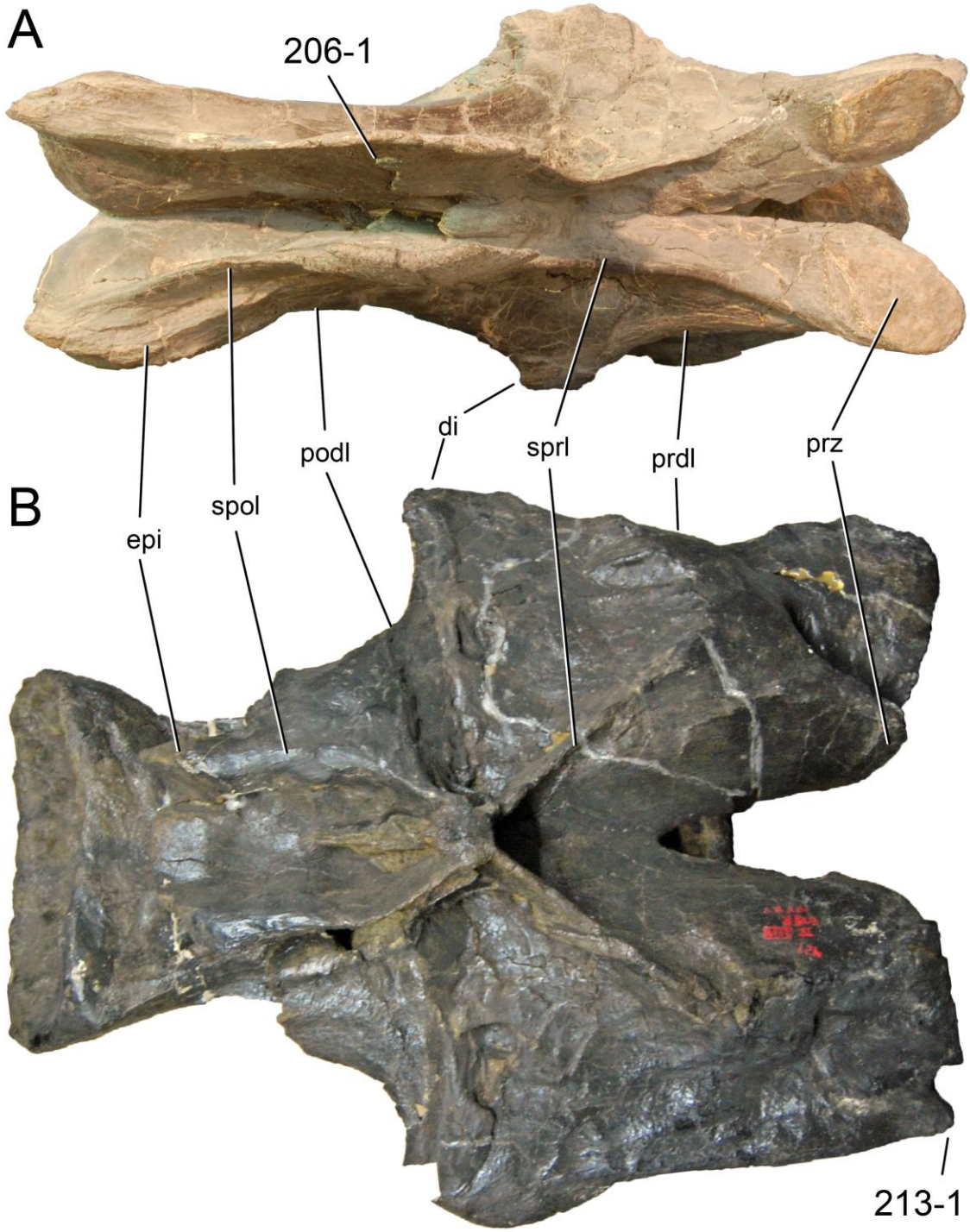

Figure 6.58: Posterior cervical vertebrae of *Kaatedocus siberi* SMA 0004 (A), and *Barosaurus lentus* YPM 429 (B) in dorsal view. Note the dorsoventral ridge on the medial side of the metapophysis (A; C206-1) and the anterior projection lateral to the prezygapophyseal facet (B; C213-1). Abb.: di, diapophysis; epi, epipophysis; podl, postzygodiapophyseal lamina; prdl, prezygodiapophyseal lamina; prz, prezygapophysis; spol, spinopost-zygapophyseal lamina; sprl, spinoprezygapophyseal lamina. Scaled to the same total length.

C211: Posterior cervical and anterior dorsal bifid neural spines, orientation: diverging (0); parallel to converging (1) (Rauhut et al., 2005; modified; Fig. 6.60).

Comments. Some taxa have diverging neural spines, with only their summits approaching an almost parallel orientation (e.g. CM 11984 or USNM 10865). They are scored as plesiomorphic herein. The character was initially proposed including the rate of divergence (Rauhut et al., 2005). The character was divided as orientation and distance between the metapophyses are not regarded to be dependent characters.

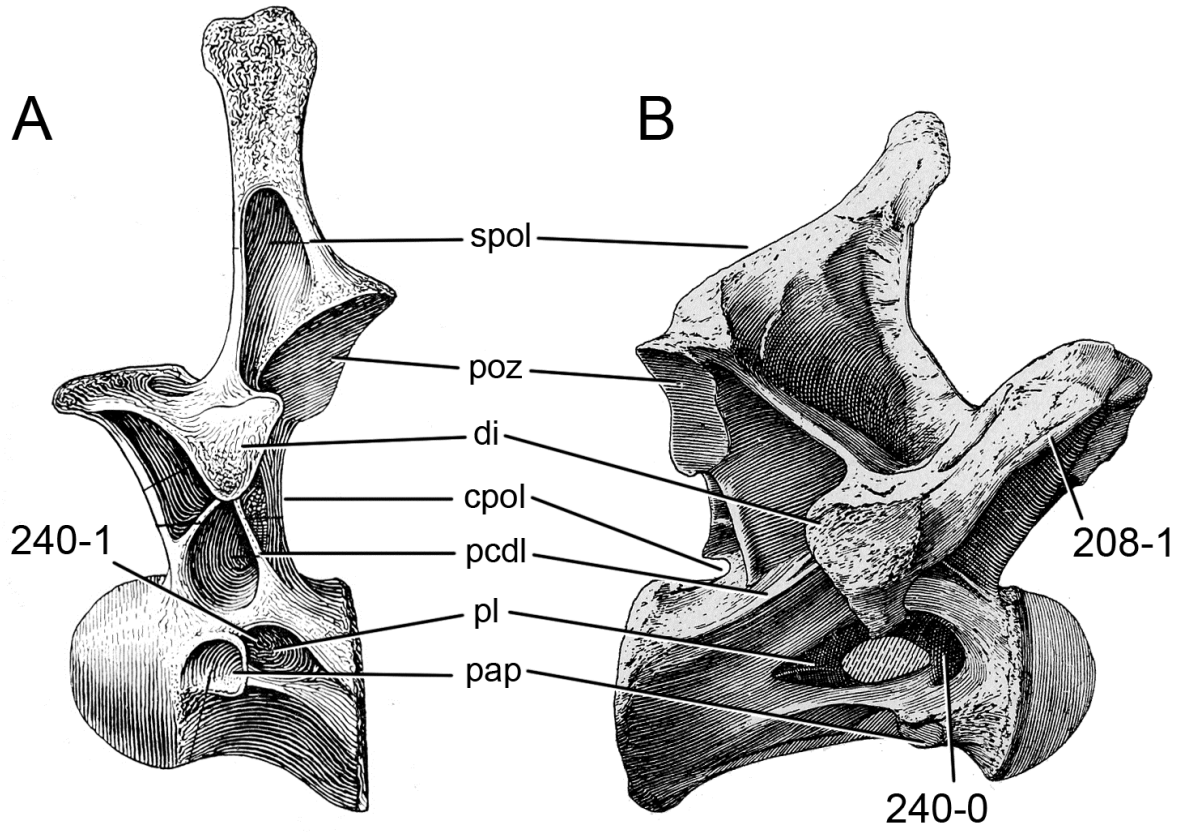

Figure 6.59: Dorsal vertebra 1 of *Apatosaurus louisae* CM 3018 (A; modified from Gilmore, 1936), and *Diplodocus carnegii* CM 84 (B; modified from Hatcher, 1901) in left and right lateral view, respectively. Note the roughened prdl (B; C208-1), and the different location of the pleurocoels (C240). Abb.: cpol, centro-postzygapophyseal lamina; di, diapophysis; pap, parapophysis; pcdl; posterior centrodiapophyseal lamina; pl, pleurocoel; poz, postzygapophysis; spol, spinopostzygapophyseal lamina. Scaled to same posterior cotyle height.

C212: Posterior cervical and anterior dorsal bifid neural spines, divergence: wide (0); narrow, distance between spine summits subequal to neural canal width (1) (Rauhut et al., 2005; modified; Fig. 6.60).

Comments. This is the second part of the character proposed by (Rauhut et al., 2005; see character 211).

C213: Posterior cervical, and anterior and mid-dorsal vertebrae, anterior projection of diapophysis right lateral to prezygapophysis: absent (0); present (1) (New; Fig. 6.58).

Comments. The projection described herein is not to be confused with the projection sometimes formed by the pre-epipophysis, which is posteriorly accompanied by a horizontal, rugose ridge.

C214: Cervical ribs, length: long, reaching posterior to posterior end of centrum (0); short, not reaching posterior end of centrum (1) (Russell and Zheng, 1993; modified; Fig. 6.51).

Comments. An additive binary version describing cervical rib length is preferred herein over the multi-state character of Whitlock (2011a).

C215: Cervical ribs, length: overlapping several centra posterior (0); overlapping no more than the next cervical vertebra in sequence (1) (Russell and Zheng, 1993; modified; Fig. 6.41).

C216: Cervical ribs, position relative to centrum: not projecting far beneath centrum (0); projecting well beneath centrum, such that length of posterior process is subequal in length to fused diapophysis/tuberculum (1) (Wilson, 2002; Whitlock, 2011a; modified; Fig. 6.40).

Comments. Whitlock (2011a) included two characters describing the length of the ventral projection (from Wilson, 2002) and comparing the length of the posterior process with the length of the fused diapophysis/tuberculum. However, the length of the fused diapophysis and tuberculum depends on how far the cervical ribs project ventrally, and the length of the posterior process is accounted for in the characters defining cervical rib length. Wilson (2002) defined the ventral projection as strong when it leads to a vertebral height that exceeds its length. Such a ratio is also present in dicraeosaurids, but

because of their highly elevated neural spines. The ventral projection of the cervical rib of dicraeosaurids is minimal as in all taxa other than *Apatosaurus*. Therefore, the two characters of Wilson (2002) and Whitlock (2011a) are herein combined, in order to define ventral projection compared to the length of the posterior process of the cervical rib.

C217: Cervical ribs, posteriorly projecting spur on dorsolateral edge of posterior shaft: absent (0); present (1) (New; Fig. 6.49).

Comments. The spur was proposed as autapomorphic for *Turiasaurus* (Royo-Torres et al., 2006), but it is also present in some apatosaurs and *Dicraeosaurus* (pers. obs.).

C218: Anterior and mid-cervical ribs, tuberculum in lateral view: is directed nearly vertically (0); is directed upwards and backwards (1) (Upchurch et al., 2004b; modified; Fig. 6.50).

Comments. The orientation of the tuberculum tends to become more vertical in more posterior elements. Some apatosaurs scored as plesiomorphic here actually do not have any anterior cervical vertebrae preserved, which means that they could still have inclined tubercula in the anterior elements. However, as others have distinctly inclined tubercula in mid-cervical ribs as well, a differential coding is still justifiable. Taxa that do not preserve cervical ribs were coded based on the relative positions of diapophysis and parapophysis.

C219: Posterior cervical ribs, anterior process: present (0); absent (1) (Upchurch et al., 2004b; modified; Fig. 6.40).

C220: Posterior cervical ribs, anterior process: distinct, much longer anteroposteriorly than high dorsoventrally (0); reduced to a short bump-like process or absent (1) (New; Fig. 6.61).

Comments. The last two characters serve as additive binary characters describing the reduction of the anterior process in *Apatosaurus* in general and its complete absence in some specimens (e.g. CM 3018; Gilmore, 1936; Wedel and Sanders, 2002).

C221: Posterior cervical ribs, anterior process: is rounded in lateral view (0); has an acute pointed tip in lateral view (1) (Upchurch et al., 2004b; modified; Fig. 6.61).

Comments. The anterior processes of cervical ribs can be rounded in dorsal view, but dorsoventrally compressed (as in SMA 0011, pers. obs., 2012). Therefore, they are still pointed in lateral view.

C222: Posterior cervical ribs, rounded sub-triangular process in lateral view, immediately below tuberculum: absent (0); present (1) (Wedel and Sanders, 2002; Upchurch et al., 2004b; modified; Fig. 6.61).

Comments. Upchurch et al. (2004b) scored the holotypic cervical vertebra of *Apatosaurus laticollis* YPM 1861 as plesiomorphic. However, as Wedel and Sanders (2002) showed, a process is clearly present in this specimen.

C223: Posterior cervical rib shafts: are nearly straight and are directed backward and a little upwards (0); are initially directed in the same direction but turn to run a little downwards toward the distal tip (1) (Upchurch et al., 2004b; Fig. 6.61).

Dorsal vertebrae

C224: Number of dorsal vertebrae: 13 or more (0); 12 (1); 10 (2); 9 (3) (McIntosh, 1990b; Russell and Zheng, 1993; modified; Tab. 6.26).

Comments. *Amargasaurus* was initially described to have 9 dorsal vertebrae (Salgado and Bonaparte, 1991), but their first dorsal has the parapophysis positioned dorsally to the pleurocoel, which is highly unusual in sauropods (Carballido et al., 2012a). Generally, this position marks the second or third dorsal vertebrae, which means that there would be at least 10 dorsal elements, which was the coding used by Mannion et al. (2012). Herein, a coding as unknown is preferred, following Carballido et al. (2012b).

C225: Dorsal centrum length (excluding articular 'ball'), remains approximately the same along the sequence (0); shortens from anterior to posterior dorsal vertebrae (1) (Mannion et al., 2012; Tab. 6.27).

Comments. The exclusion of the articular ball for measuring centrum length for this character is crucial, as anterior dorsal vertebrae often have considerably larger anterior condyles than posterior elements. In taxa lacking measurements or good figures to compare between anterior and posterior elements, scores of Mannion et al. (2012) were used (e.g. *Omeisaurus*).

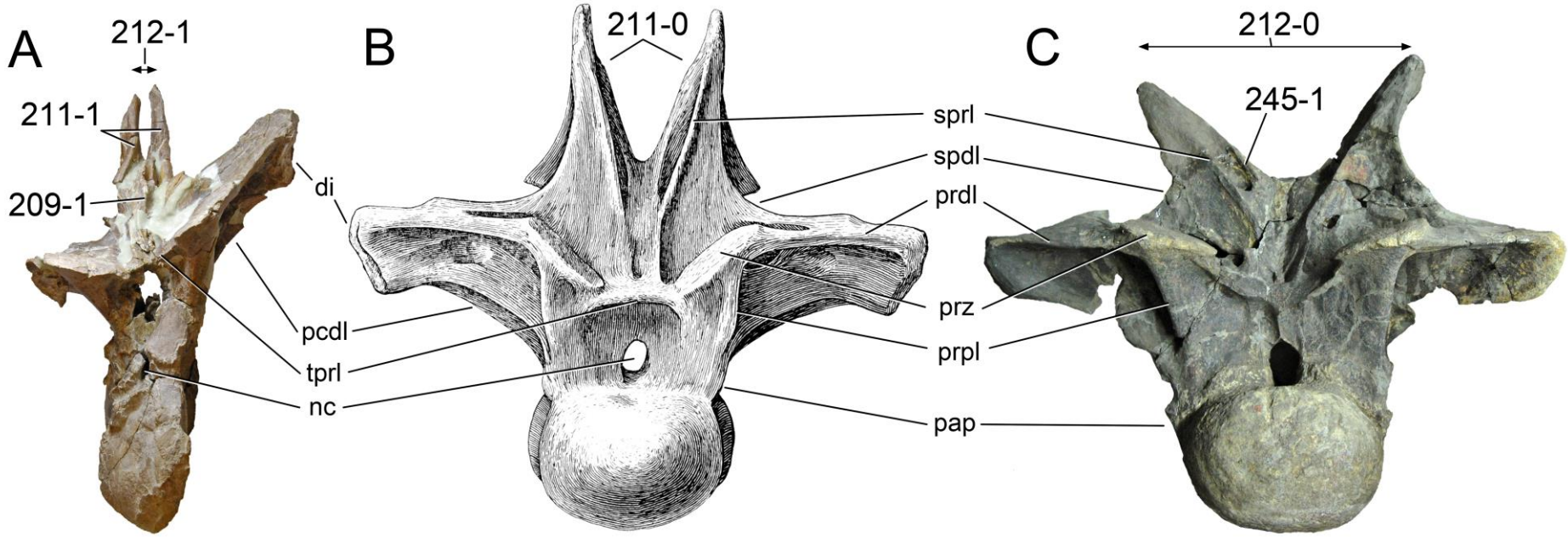

Figure 6.60: Anterior dorsal vertebrae of *Suuwassea emilieae* ANS 21122 (A), *Apatosaurus* sp. UW 15556 (B; modified from Gilmore, 1936), and *Apatosaurus ajax* YPM 1860 (C) in anterior view. Note the prespinal lamina (A and C; C209-1), the diverging (B; C211-0) or parallel neural spines (A; C211-1), the wide (C; C212-0) or narrow (A; C212-1) distance between the spine tops, and the ridge on the medial side of the neural spine (C; C245-1). Abb.: di, diapophysis; nc, neural canal; pap, parapophysis; pcdl; posterior centrodiapophyseal lamina; prdl, prezygodiapophyseal lamina; prpl, prezygoparapophyseal lamina; prz, prezygapophysis; sprl, spinoprezygapophyseal lamina; tprl, interprezygapophyseal lamina. Scaled to same anterior condyle height.

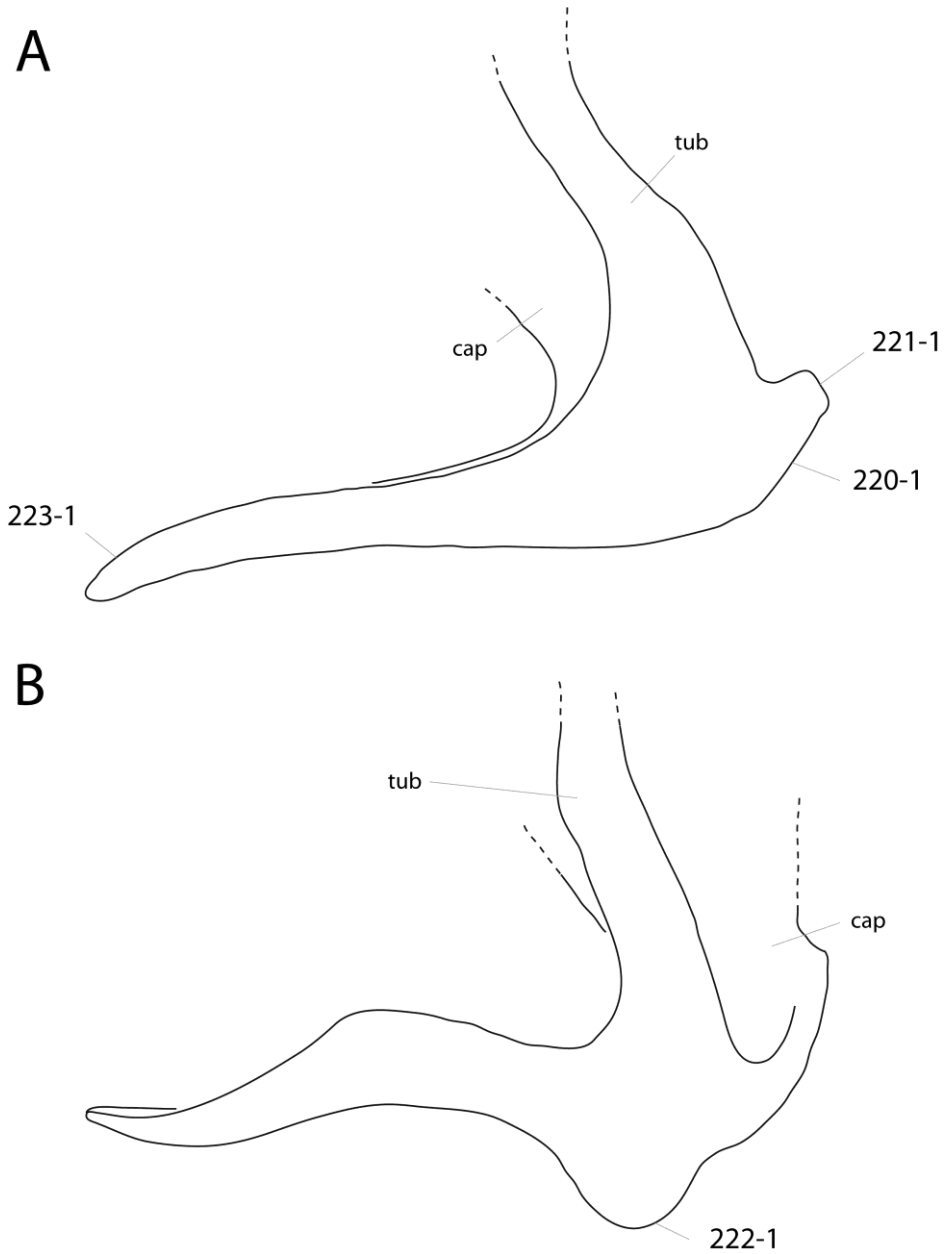

Figure 6.61: Posterior cervical ribs of *Apatosaurus* sp. UW 15556 (A; after Gilmore, 1936) and *A. louisae* CM 3018 (B; after Gilmore, 1936) in right lateral view (B inverted). Note the short, reduced anterior projection (A; C220-1), the pointed anterior process (A; C221-1), the ventrolateral process (B; C222-1), and the downwards curving posterior process (A; C223-1). Abb.: cap, capitulum; tub, tuberculum. Scaled to same length.

C226: Dorsal vertebrae, opisthocoely (including a prominent anterior articular 'ball') disappears: between D2 and D3 (0); between D3 and D4 or more posteriorly (1) (Holland, 1915a; Gilmore, 1936; Upchurch et al., 2004b; Tab. 6.28).

Comments. The definition of 'prominent anterior ball' is somewhat ambiguous. However, a new definition is not given here, as the character is interpreted to describe a significant change within the same vertebral column. These changes can be of different absolute size if one compares between specimens, but are relatively obvious within the same individual. The decrease is thus relative to its development in more anterior elements, but can be low in an absolute sense.

C227: Dorsal pneumatopores (pleurocoels): present (0); absent (1) (Gauthier, 1986; McIntosh, 1990b; Upchurch, 1995; polarity reversed; Fig. 6.62).

Comments. The dorsal centra of all included sauropod taxa have pleurocoel-like depressions on their lateral side, but in some taxa they do not bear a foramen.

Table 6.26: Number of dorsal vertebrae.

Taxon	Specimen	Number	Reference	Comments
Shunosaurus lii		13	Mannion et al., 2013	
Spinophorosaurus nigerensis	GCP-CV-4229	12	Remes et al. 2009	
Omeisaurus		12	Mannion et al., 2013	
Mamenchisaurus		12	Mannion et al., 2013	
Jobaria tiguidensis		13	Sereno et al. 1999	
Camarasaurus		12	Mannion et al., 2013	
Giraffatitan brancai		12	Taylor, 2009	
Brachiosaurus altithorax		12	Taylor, 2009	
Haplocanthosaurus priscus		13	Mannion et al., 2012	
Limaysaurus tessonei		12	Calvo and Salgado, 1995	
Nigersaurus taqueti		12	Mannion et al., 2013	
Dicraeosaurus hansemanni		12	Mannion et al., 2012	
Brachytrachelopan mesai		12	Carballido et al., 2012	
Amargasaurus cazaui		10	Mannion et al., 2012	questionable
		9	Salgado and Bonaparte, 1991	questionable
Brontosaurus excelsus YPM 1980	YPM 1980	10	pers. obs.	
Apatosaurus louisae CM 3018	CM 3018	10	pers. obs.	
Apatosaurus ajax NSMT-PV 20375	NSMT-PV 20375	10	Upchurch et al. 2004b	
Apatosaurus sp. CM 3378	CM 3378	10	Upchurch et al. 2004b	
Apatosaurus sp. FMNH P25112	FMNH P25112	10	Riggs, 1903	
Diplodocus carnegii CM 84	CM 84	10	pers. obs.	
Diplodocus sp. USNM 10865	USNM 10865	10	pers. obs.	
Diplodocus sp. DMNS 1494	DMNS 1494	10	pers. obs.	
Barosaurus sp. AMNH 6341	AMNH 6341	9	McIntosh, 2005	

C228: Dorsal centra, pneumatic structures: absent, dorsal centra with solid internal structure (0); present, dorsal centra with simple and big air spaces (1); present, dorsal centra with small and complex air spaces (2) (Carballido et al., 2011; modified by Carballido et al., 2012b; Fig. 6.37).

C229: Dorsal neural arches, paired, subdivided pneumatic chambers dorsolateral to neural canal: absent (0), present (1) (Sereno et al., 1999; Whitlock, 2011a; Fig. 6.63).

Comments. Paired pneumatic foramina are present in some diplodocids (e.g. UW 15556, YPM 1840), but they are not subdivided and far less deep than in *Nigersaurus* or *Demandasaurus*. The latter are thus the only taxa with the apomorphic state.

C230: Dorsal transverse processes, orientation: horizontal or only slightly inclined dorsally (0); more than 30° inclined dorsally from the horizontal (1) (Yu, 1993; modified by Upchurch, 1998; Fig. 6.63).

Comments. The angle of the transverse processes is easily affected by diagenetic distortion, as can be seen in dorsal vertebra 3 of *Suuwassea* ANS 21122, which most probably would actually have horizontal transverse processes.

C231: Dorsal vertebrae, single (not bifid) neural spines, spinoprezygapophyseal laminae: separate along entire length (0); joined distally, forming single prespinal lamina (1) (Upchurch, 1995; modified by Whitlock, 2011a; Fig. 6.64).

Comments. In some taxa (e.g. *Losillasaurus* or *Camarasaurus*), the spinoprezygapophyseal laminae unite dorsally with the prespinal lamina, but remain separate up to that point. Here, only taxa, where the prespinal lamina is formed by the junction of the two sprl, are scored as apomorphic.

C232: Dorsal vertebrae, spinodiapophyseal webbing: laminae follow curvature of neural spine and diapophysis in anterior view (0); laminae 'festooned' from spine, dorsal margin does not closely follow shape of neural spine and diapophysis (1) (Sereno et al., 2007; Fig. 6.65).

C233: Dorsal vertebrae with single neural spines, middle single fossa projected through the midline of the neural spine: present (0); absent (1) (Carballido et al., 2012b; Fig. 6.64).

Comments. The fossa described herein is a distinctly confined area within the spinoprezygapophyseal fossa, restricted to the anterior edge of the neural spine process.

C234: Dorsal (single) neural spines, postspinal lamina, dorsal end: flat to convex transversely (0); concave transversely (1) (New; Fig. 6.66).

Table 6.27: Dorsal centrum length (excluding articular 'ball').

Taxon	Specimen	Length	Difference	Reference	Comments
Shunosaurus lii	T5401, DV 3	106,6	-21	Zhang 1988	measured from drawings
	T5401, DV 11	127,9		Zhang 1988	measured from drawings
Omeisaurus			subequal	Mannion et al., 2012	taken from phylogenetic analysis
Mamenchisaurus	ZDM 0083, DV 2	200,7	-3	Ouyang & Ye 2002	measured from drawings
	ZDM 0083, DV 12	204,0		Ouyang & Ye 2002	measured from drawings
Camarasaurus	AMNH 5760/5761 series I, DV 3	180,0	-10	Osborn & Mook 1921	
	AMNH 5760/5761 series I, DV 10	190,0		Osborn & Mook 1921	
	CM 11338, DV 1	70,0	0	Gilmore, 1925	
	CM 11338, DV 12	70,0		Gilmore, 1925	
Lourinhasaurus alenquerensis lectotype	MIGM		subequal	pers. obs.	no measurements available
Giraffatitan brancai	MB.R. SII, DV 1	460,0	166	Janensch, 1950	
	MB.R. SII, DV 7	294,0		Janensch, 1950	
Brachiosaurus sp. SMA 0009	SMA 0009, DV 1	41,0	-8	Schwarz et al., 2007c	
	SMA 0009, DV 6	48,6		Schwarz et al., 2007c	
Haplocanthosaurus priscus			longer	Hatcher, 1903; Mannion et al., 2012	no measurements available
Dicraeosaurus hansemanni	MB.R.4886, DV 1	130,0	-10	Janensch, 1929	
	MB.R.4886, DV 12	140,0		Janensch, 1929	
Brachytrachelopan mesai	MPEF PV 1716, DV 2	122,9	-18	Rauhut et al. 2005	measured from drawings
	MPEF PV 1716, DV 11	140,7		Rauhut et al. 2005	measured from drawings
Amargasaurus cazaui	MACN-N 15, aDV	129,6	-18	Salgado & Bonaparte, 1991	measured from drawings
	MACN-N 15, last DV	147,2		Salgado & Bonaparte, 1991	measured from drawings
Suuwassea emilieae ANS 21122	ANS 21122, DV 2	268,0	99	Harris, 2006	
	ANS 21122, DV 4	168,9		Harris, 2006	no pDV present, but clear trend
Apatosaurus ajax YPM 1860	YPM 1860		subequal	pers. obs.	no measurements available
Brontosaurus excelsus YPM 1980	YPM 1980, DV 3	189,6	-68	Ostrom & McIntosh, 1966	measured from drawings
	YPM 1980, DV 5	257,1		Ostrom & McIntosh, 1966	measured from drawings
Apatosaurus louisae CM 3018	CM 3018, DV 1	213,0	-24	Gilmore, 1936	measured from drawings
	CM 3018, DV 10	237,5		Gilmore, 1936	measured from drawings
Apatosaurus parvus UW 15556	UW 15556		longer	Gilmore, 1936	no measurements available
Apatosaurus ajax NSMT-PV 20375	NSMT-PV 20375, DV 1	245,0	90	Upchurch et al., 2004	
	NSMT-PV 20375, DV 10	155,0		Upchurch et al., 2004	
Apatosaurus sp. AMNH 460	AMNH 460		subequal	pers. obs.	no measurements available
Apatosaurus sp. FMNH P25112	FMNH P25112		longer	pers. obs.	based on photos by W. Simpson
Dinheirosaurus lourinhanensis ML 414	ML 414, DV 1	234,0	3	Mannion et al., 2012	
	ML 414, DV 9	231,0		Mannion et al., 2012	
Diplodocus carnegii CM 84	CM 84		longer	Hatcher, 1901	no measurements available
Diplodocus carnegii CM 94	CM 94		longer	pers. obs.	no measurements available
Diplodocus sp. USNM 10865	USNM 10865		longer	pers. obs.	no measurements available
Diplodocus sp. DMNS 1494	DMNS 1494		longer	pers. obs.	no measurements available
Galeamopus hayi HMNS 175	HMNS 175		longer	pers. obs.	no measurements available
Galeamopus shellensis SMA 0011	SMA 0011, DV 1	310,0	135	pers. obs.	
	SMA 0011, DV 10	175,0		pers. obs.	
Barosaurus lentus YPM 429	YPM 429, DV 2	328,0	88	McIntosh 2005	
	YPM 429, DV 9	240,0		McIntosh 2005	
Barosaurus sp. AMNH 6341	AMNH 6341, DV 1	500,0	285	McIntosh 2005	
	AMNH 6341, DV 9	215,0		McIntosh 2005	

C235: Dorsal vertebrae, transition from bifid to single neural spines: gradual (0); abrupt (1) (New).

Comments. Gradual transitions go from deeply bifid, to shallowly bifid, to notched, to unsplit, as defined by Wedel and Taylor (2013). If one of the intermediate states is lacking, the taxon is scored as derived. Obviously, only specimens with articulated dorsal vertebrae can be scored for this character. Taxa without spine bifurcation are scored as unknown.

C236: Dorsal neural arches, hyposphene-hypantrum articulations: present (0); absent (1) (Gauthier, 1986; Salgado et al., 1997; Tab. 6.29).

C237: Dorsal vertebrae, hyposphene first appears: on D3 (0); on D4 or more posteriorly (1) (Upchurch et al., 2004b; modified; Tab. 6.29).

Comments. Both in *Apatosaurus* and *Camarasaurus* there are differences in the appearance of the hyposphene (Ikejiri, 2004; Upchurch et al., 2004b). Since the genotype species, *C. supremus*, appears to show the plesiomorphic state, the genus was scored as such as well. Ikejiri (2004) suggests that the development of the hyposphene might depend on ontogeny, based on observations in the juvenile specimen CM 11338. However, the latter specimen is articulated, and the region with the hyposphene is obliterated, such that its presence or absence is difficult to assess (McIntosh et al., 1996a).

Table 6.28: First dorsal vertebra without prominent anterior ball.

Taxon	Specimen	Position	Reference	Comments
Shunosaurus lii	T5401, T5404	DV 2 or 3	Zhang 1988	DV 1 of T5401 has an anterior ball, DV 3 of T5404 has not
Omeisaurus	T5701	DV 4 or 5	He et al. 1988	DV 4 not figured
		DV 4	Upchurch et al. 2004b	taken from phylogenetic matrix, but character does not allow more posterior loss
Mamenchisaurus	ZDM 0083	DV 5 or 6	Ouyang & Ye 2002	DV 5 articulated with DV 4, articular ball not visible
Camarasaurus	AMNH 5760/5761	DV 5	Osborn & Mook 1921	arbitrary assignment of vertebrae to specimen and position
	AMNH 5760/5761	DV 6	Osborn & Mook 1921	arbitrary assignment of vertebrae to specimen and position
Apatosaurus grandis YPM 1901	YPM 1901	posterior to DV 4	Wilson & Sereno 1998	Mid-dorsal vertebra with hypantrum still has distinct ball, hypantrum indicates position 4 or more posterior
Lourinhasaurus alenquerensis lectotype	MIGM	DV 4	pers. obs	
Giraffatitan brancai	MB.R. SII	DV 4	Janensch 1950	
Brachiosaurus sp. SMA 0009	SMA 0009	DV 4	pers. obs	
Ligabuesaurus leanzai	MCF-PVPH-233	not lost	Bonaparte et al. 2006	pDV are strongly opisthocoelous, according to Bonaparte et al. 2006
Isisaurus colberti	ISIR335	posterior to DV 4	Jain & Bandyopadhyay 1997	Mid-dorsal vertebra still has distinct ball
Haplocanthosaurus priscus	CM 879	DV 5	Hatcher 1903	DV 5 has a dorsally displaced anterior ball, but still somewhat disinct
Dicraeosaurus hansemanni	MB.R.4886	DV 4	pers. obs	
Suuwassea emilieae ANS 21122	ANS 21122	posterior to DV 3	pers. obs	only DV 1-3 preseved
Apatosaurus ajax YPM 1860	YPM 1860	posterior to DV 3	pers. obs	3 DV present with distinct anterior balls
Brontosaurus excelsus YPM 1980	YPM 1980	DV 5	Ostrom & McIntosh 1966	
Apatosaurus louisae CM 3018	CM 3018	DV 3	Gilmore 1936; Upchurch et al. 2004	
Atlantosaurus immanis YPM 1840	YPM 1840	posterior to DV 3	Ostrom & McIntosh 1966	
Apatosaurus parvus UW 15556	UW 15556	DV 4	Gilmore 1936; Upchurch et al. 2004	
Apatosaurus sp. AMNH 460	AMNH 460	DV 5	pers. obs	
Apatosaurus sp. FMNH P25112	FMNH P25112	DV 3	Upchurch et al. 2004	
Dinheirosaurus lourinhanensis ML 414	ML 414	DV 4	Mannion et al. 2012; pers. obs	
Diplodocus carnegii CM 84	CM 84	DV 5	Hatcher 1901	
Diplodocus carnegii CM 94	CM 94	posterior to DV 3	pers. obs	
Diplodocus sp. USNM 10865	USNM 10865	posterior to DV 3	pers. obs	
Diplodocus sp. DMNS 1494	DMNS 1494	posterior to DV 3	pers. obs	
Galeamopus hayi HMNS 175	HMNS 175	posterior to DV 3	pers. obs	
Galeamopus shellensis SMA 0011	SMA 0011	DV 4	pers. obs	
Barosaurus lentus YPM 429	YPM 429	posterior to DV 3	pers. obs	
Barosaurus sp. AMNH 6341	AMNH 6341	DV 4	McIntosh 2005	

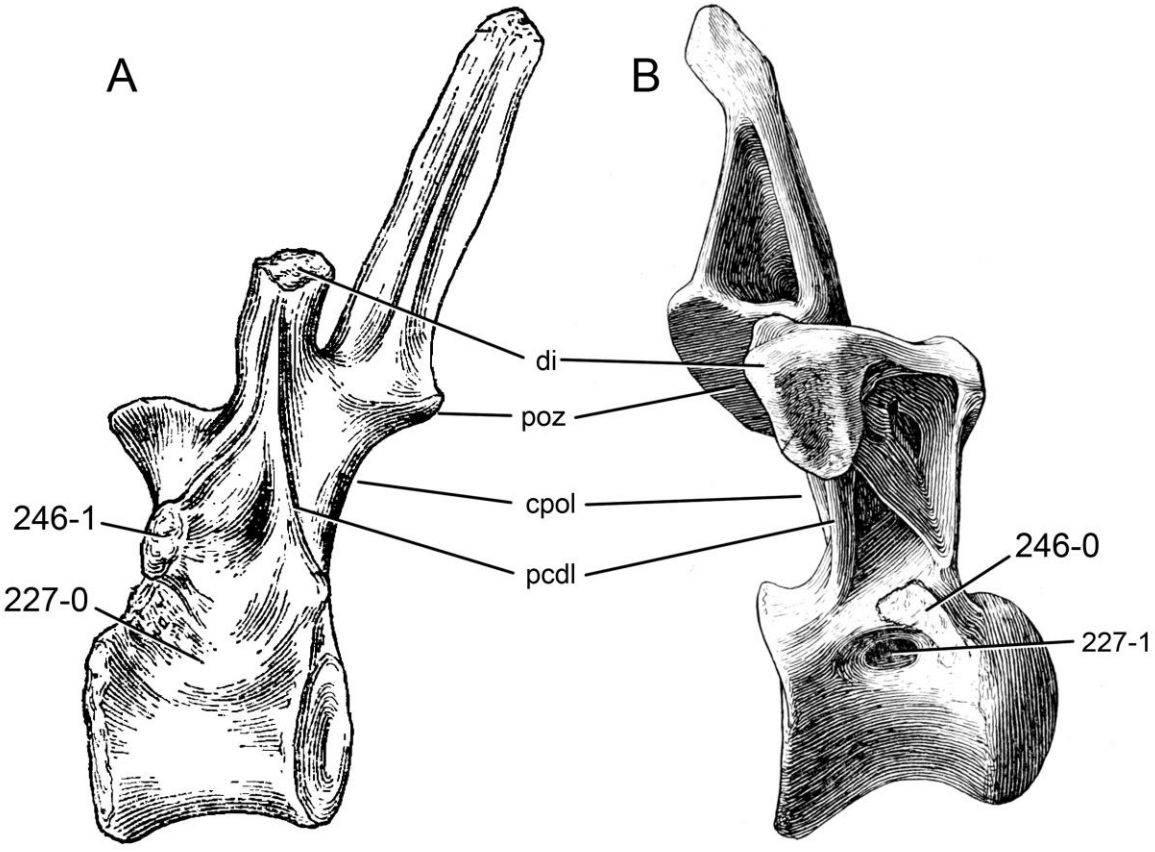

Figure 6.62: Dorsal vertebra 3 of *Shunosaurus lii* T5401 (A; modified from Zhang, 1988), and *Apatosaurus* sp. UW 15556 (B; modified from Gilmore, 1936) in left (A) and right (B) lateral view. Note the slightly concave lateral surface of the centrum in *Shunosaurus* (A; C227-0), in contrast to the well-defined pneumatopore in *Apatosaurus* (B; C227-1), and the different locations of the parapophyses (C246). Abb.: cpol, centro-postzygapophyseal lamina; di, diapophysis; pcdl, posterior centrodiapophyseal lamina; poz, postzygapophysis. Scaled to the same total vertebral height.

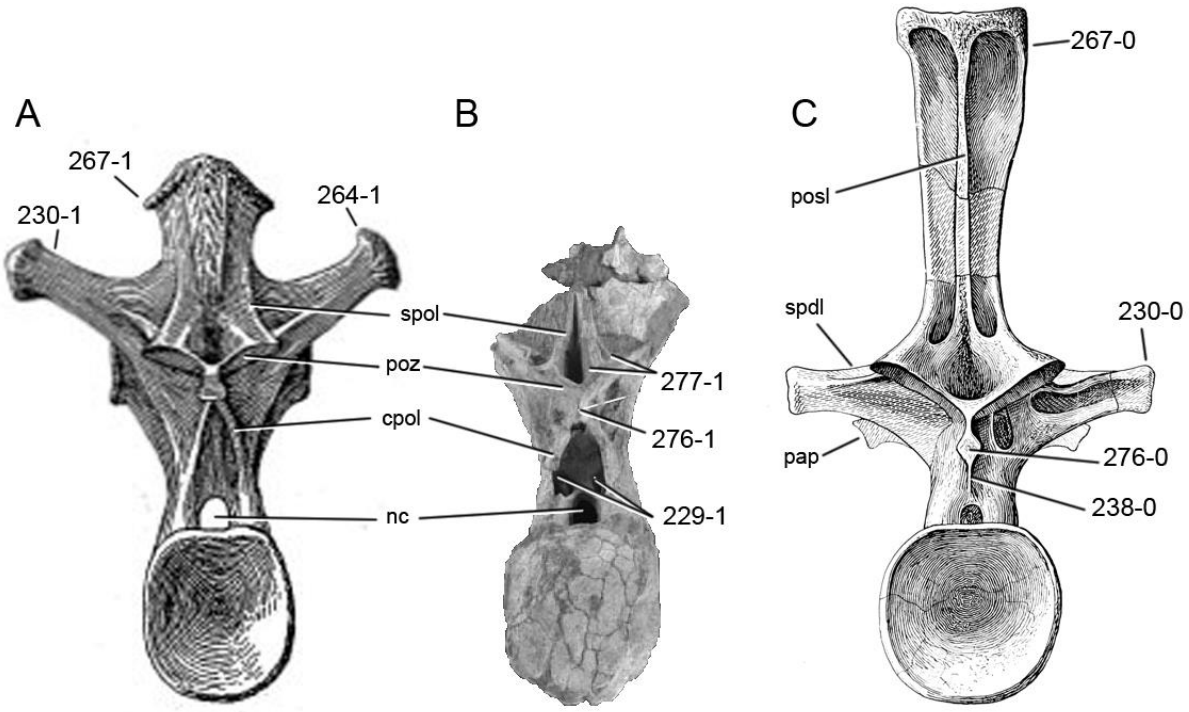

Figure 6.63: Posterior dorsal vertebrae of *Haplocanthosaurus priscus* CM 572 (A; modified from Hatcher, 1903), *Demandasaurus darwini* MDS-RVII 798 (B; modified from Torcida Fernández-Baldor et al., 2011), and *Apatosaurus louisae* CM 3018 (C; modified from Gilmore, 1936) in posterior view. Note the paired pneumatic foramen dorsolateral to the neural canal in *Demandasaurus* (B; C229-1), the different orientations of the diapophyses in *Haplocanthosaurus* (A; C230-1) and *Apatosaurus* (C; C230-0), the single lamina that supports the hyposphene from below (C; C238-0), the dorsal spur on the tip of the transverse process (A; C264-1), the small triangular lateral projections at the spine top (A; C267-1), or their absence (C; C267-0), the rhomboid (C; C276-0) in contrast to laminar (B; C276-1) hyposphene, and the ventrally forked spol (B; C277-1). Abb.: cpol, centropostzygapophyseal lamina; nc, neural canal; pap, parapophysis; posl, postspinal lamina; poz, postzygapophysis; spdl, spinodiapophyseal lamina; spol, spinopostzygapophyseal lamina. Scaled to same posterior centrum height.

C238: Dorsal vertebrae, single vertical lamina supporting the hyposphene from below: absent (0); present (1) (Gilmore, 1936; Upchurch et al., 2004b; modified; Fig. 6.63).

Comments. The original character description (Upchurch et al., 2004b) interfered with the character proposed by Wilson (2002) distinguishing between single and double cpol in mid- and posterior dorsal vertebrae (see character 261). The character of Upchurch et al. (2004b) was thus simplified, and polarity was reversed due to the differential taxon sampling. The lamina described herein corresponds to the stpol (Carballido and Sander, 2013). Taxa without hyposphene are scored as unknown.

C239: Dorsal vertebrae 1 and 2, centrum length: DV 1 > DV 2 (0); DV 2 > DV 1 (1) (Upchurch et al., 2004b; modified; Tab. 6.30).

Comments. The character was originally defined implying that either DV 1 or 2 were the longest in the series (Upchurch et al., 2004b), which is not always the case (see Tab. 6.30).

C240: First dorsal vertebrae, pleurocoel location: occupy the anterior and middle part of the centrum (0); occupy the posterior part of the centrum (1) (Holland, 1915a; Gilmore, 1936; Upchurch et al., 2004b; modified; Fig. 6.59).

Comments. The character was restricted to the first dorsal, as also in *Apatosaurus louisae*, for which this character was proposed as species autapomorphy (Holland, 1915a; Gilmore, 1936; Upchurch et al., 2004b), DV 2 and 3 already have a centrally placed pleurocoel (CM 3018, pers. obs., 2011).

C241: Anterior dorsal vertebrae, pleurocoels in first few centra: become larger along the series (0); become smaller (1) (Gilmore, 1936; Upchurch et al., 2004b; wording modified; Tab. 6.31).

Comments. Taxa without dorsal pleurocoels are scored as unknown.

C242: Anterior dorsal vertebrae, ventral keel: absent (0); present (1) (Mannion et al., 2012; Fig. 6.67).

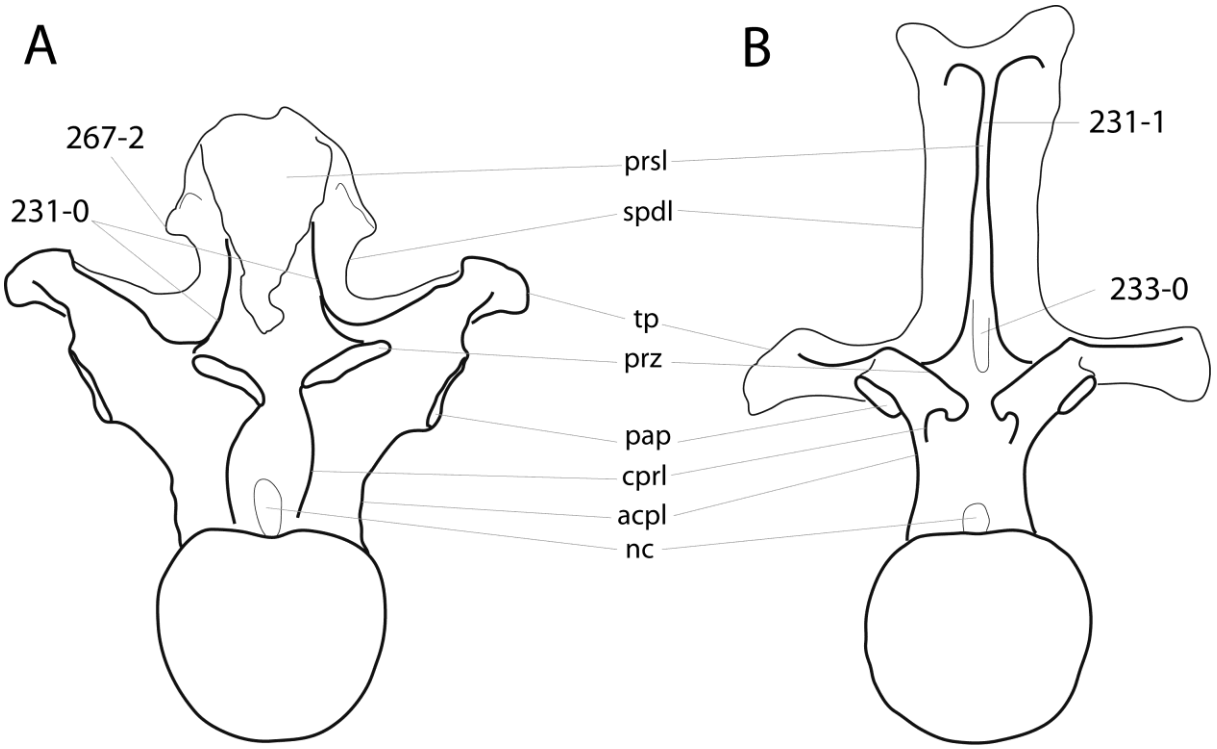

Figure 6.64: Dorsal vertebra 8 of *Camarasaurus supremus* AMNH 5760 (A; traced from Osborn and Mook, 1921) and *Apatosaurus louisae* CM 3018 (B; traced from Gilmore, 1936) in anterior view. Note the separated (A; C231-0) or dorsally united spinoprezygapophyseal laminae (B; C231-1), the fossa between them (B; C233-0), and the triangular processes of the neural spine, that project further than the zygapophyses (A; C267-2). Abb.: acpl, anterior centroparapophyseal lamina; cprl, centroprezygapophyseal lamina; nc, neural canal; pap, parapophysis; prsl, prespinal lamina; prz, prezygapophysis; spdl, spinodiapophyseal lamina; tp, transverse process. Scaled to same anterior condyle height.

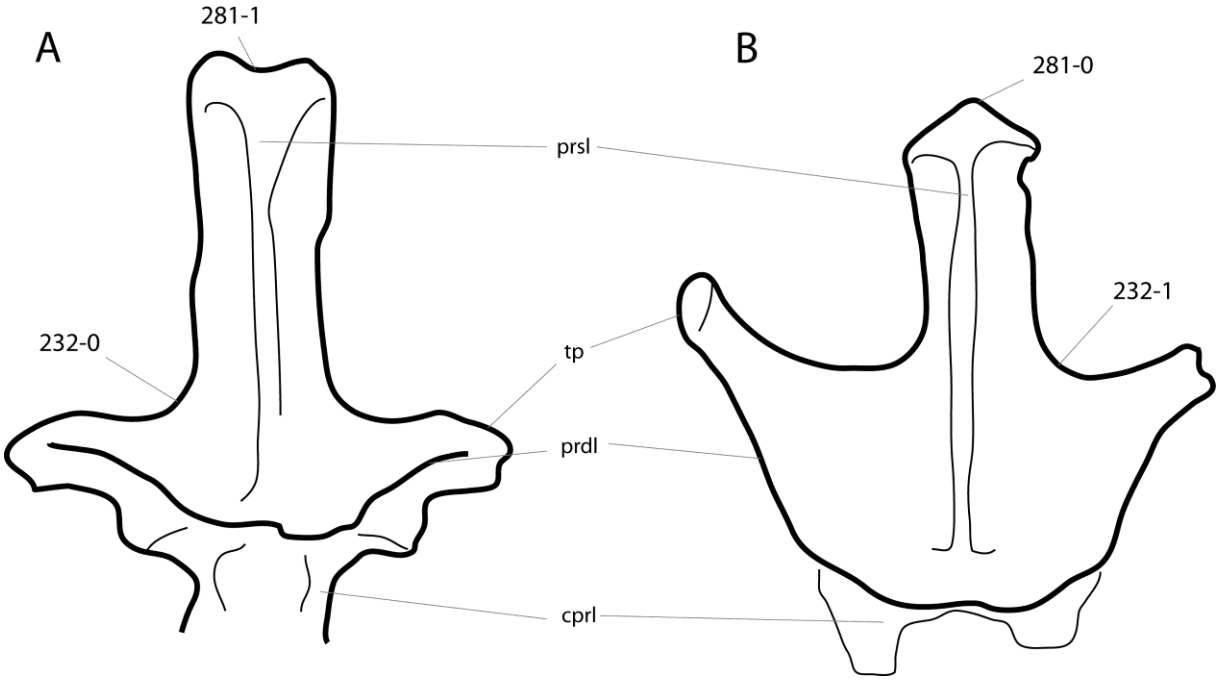

Figure 6.65: Dorsal neural arches of *Diplodocus carnegii* CM 84 (A; traced from Hatcher, 1901) and *Nopcsaspondylus alarconensis* holotype specimen (B; traced from Nopcsa, 1902) in anterior view. Note the festooned spdl typical for rebbachisaurids (B; C232-1), in contrast to the plesiomorphic state (A; C232-0), and the notched (A; C281-1), or straight to convex spine summits (B; C281-0). Abb.: cprl, centroprezygapophyseal lamina; prdl, prezygodiapophyseal lamina; prsl, prespinal lamina; tp, transverse process. Not to scale.

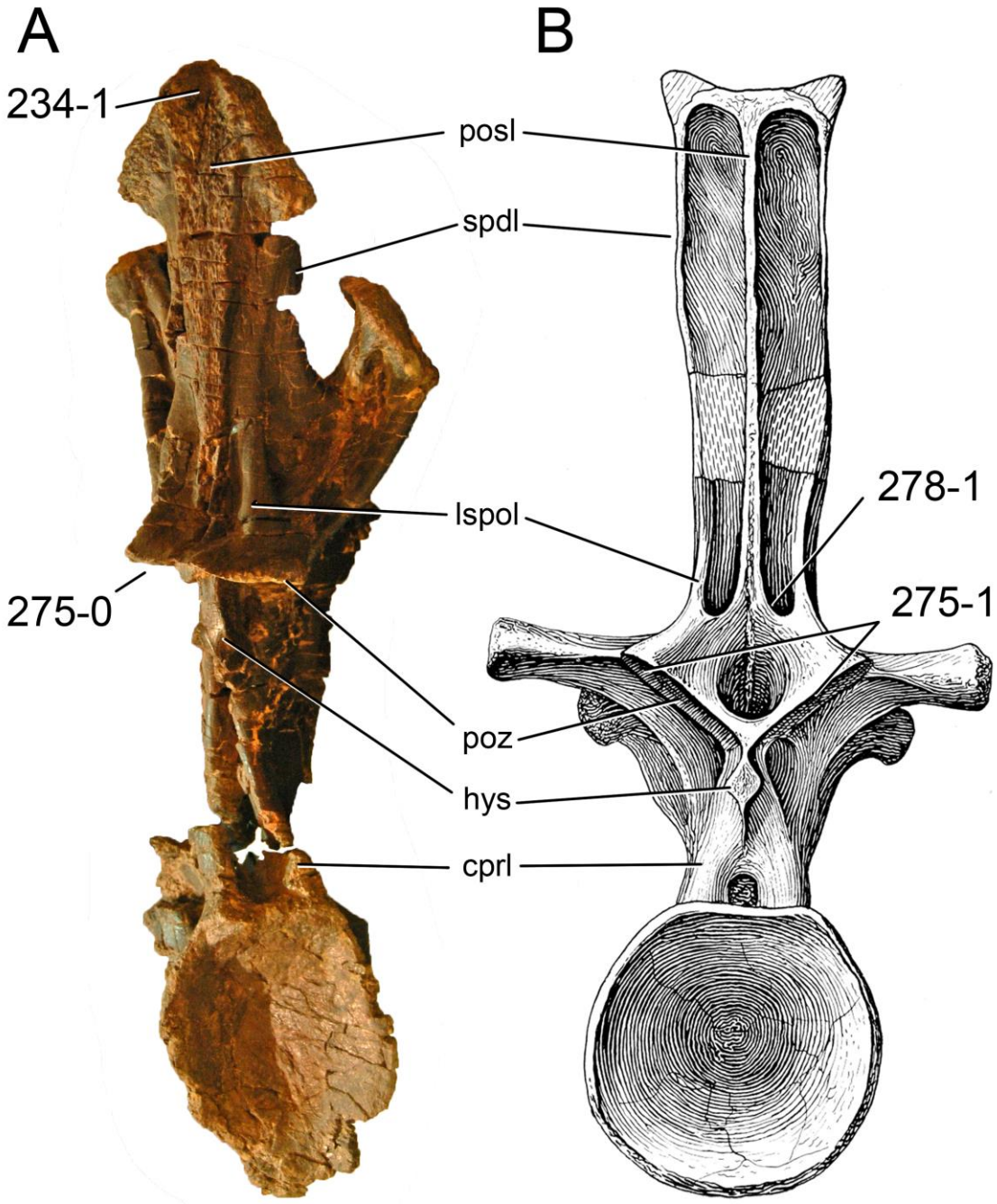

Figure 6.66: Posterior dorsal vertebrae of *Losillasaurus giganteus* MCNV Lo-11 (A), and *Apatosaurus louisae* CM 3018 (B; modified from Gilmore, 1936) in posterior view. Note the concave dorsal end of the posl (A; C234-1), the horizontal (A; C275-0), instead of angled (B; C275-1) postzygapophyseal facets, and the medial spinopostzygapophyseal lamina (B; C278-1). Abb.: cprl, centroprezygapophyseal lamina; hys, hyposphene; lspol, lateral spinopostzygapophyseal lamina; posl, postspinal lamina; poz, postzygapophysis; spdl, spino-diapophyseal lamina. Scaled to same posterior cotyle height.

C243: Anterior dorsal transverse process position: high, considerably above dorsal edge of posterior cotyle (0); low, ventral edge about level to dorsal edge of posterior cotyle (1) (Gilmore, 1936; Fig. 6.68).

Comments. The differing dorsoventral extension of the transverse processes in the anterior-most dorsal vertebrae was proposed as character to distinguish *Apatosaurus louisae* CM 3018 from the supposed *Apatosaurus excelsus* UW 15556 (Gilmore, 1936). It is here applied for the first time in a phylogenetic analysis. In most taxa, position of the transverse process rises considerably in the first few dorsal vertebrae. Therefore, this description applies best for the first element in the series.

Table 6.29: Dorsal vertebrae, hyposphene development.

Taxon	Specimen	Occurrence	First appearance	Morphology aDV-mDV	pDV	Widest	Reference	Comments
Shunosaurus lii		present		rhomboid	rhomboid		Carballido et al., 2012b	
Spinophorosaurus nigerensis		present					Remes et al., 2009	
Omeisaurus	T5701	present	DV 3	laminar			He et al., 1988; Upchurch et al. 2004b	pDV lacking
Mamenchisaurus	ZDM 0083	present		laminar	laminar	subequal	Ouyang and Ye, 2002	
Jobaria tiguidensis		present		rhomboid	rhomboid		Carballido et al., 2012b	
Turiasaurus riodevensis	CPT	present		rhomboid			pers. obs.	position unclear
Losillasaurus giganteus type	MCNV	present			laminar		pers. obs.	position unclear
Camarasaurus	AMNH 5760/5761	present	DV 3	rhomboid	laminar	anterior half	Osborn and Mook, 1921; Upchurch et al., 2004b	might be different individuals
	BYU 9047	present		rhomboid	rhomboid		McIntosh et al., 1996b	
	KUVP 129716	present	DV 4				Ikejiri, 2004	
	WDC A	present	DV 3	rhomboid	laminar to absent	anterior half	Ikejiri, 2004	found intermingled with second specimen
Apatosaurus grandis YPM 1901	YPM 1901	present		rhomboid			Wilson and Sereno, 1998	
Giraffatitan brancai		present		rhomboid	laminar	anterior half	Apesteguía, 2005; Taylor, 2009	
Brachiosaurus altithorax	FMNH P25107	present		rhomboid	rhomboid		Riggs, 1904; D. Lovelace, pers. comm., 2013	aDV lacking
Ligabuesaurus leanzai	MCF-PVPH-233	present		rhomboid	rhomboid		Bonaparte et al., 2006; Carballido et al., 2012b	
Isisaurus colberti	ISIR335	absent					Jain and Bandyopadhyay, 1997	
Haplocanthosaurus priscus	CM 572	present		rhomboid	laminar	anterior half	Hatcher, 1903	
	CM 879	present	DV 5				Hatcher, 1903	
Limaysaurus tessonei		absent					Calvo and Salgado, 1995	
Nigersaurus taqueti		present			laminar		Carballido et al., 2012b	
Demandasaurus darwini	MDS-RVII	present			laminar		Carballido et al., 2012b	
Amphicoelias altus AMNH 5764	AMNH 5764	present			rhomboid		Osborn and Mook, 1921; pers. obs.	
Dicraeosaurus hansemanni	MB.R.4886	present	DV 3	rhomboid	laminar	anterior half	Janensch, 1929; Upchurch et al. 2004b	
Brachytrachelopan mesai	MPEF PV 1716	present	DV 3	rhomboid			J. Carballido, pers. comm. 2013	
Apatosaurus ajax YPM 1860	YPM 1860	present			rhomboid	anterior half	pers. obs.	
Brontosaurus excelsus YPM 1980	YPM 1980	present	DV 4	rhomboid			Ostrom and McIntosh, 1966; Upchurch et al. 2004b	
Brontosaurus amplus YPM 1981	YPM 1981	present					pers. obs.	
Apatosaurus louisae CM 3018	CM 3018	present	DV 3	rhomboid	rhomboid	anterior half	Gilmore, 1936; Upchurch et al. 2004b	
Atlantosaurus immanis YPM 1840	YPM 1840		after DV 3				Ostrom and McIntosh, 1966	only DV 3 preserved, but unclear on what serial position is based
Elosaurus parvus CM 566	CM 566	present			rhomboid		Peterson and Gilmore, 1902	
Apatosaurus parvus UW 15556	UW 15556	present	DV 4	rhomboid	rhomboid	anterior half	Gilmore, 1936; Upchurch et al. 2004b	
Eobrontosaurus yahnahpin Tate-001	Tate-001	present			rhomboid		P. Mannion, pers. comm., 2012	
Apatosaurus ajax NSMT-PV 20375	NSMT-PV 20375	present	DV 4	rhomboid	rhomboid	anterior half	Upchurch et al. 2004b	
Apatosaurus sp. AMNH 460	AMNH 460	present	DV 3	rhomboid	rhomboid		pers. obs.	
Apatosaurus sp. FMNH P25112	FMNH P25112	present	DV 3	rhomboid	rhomboid		Riggs, 1903; Upchurch et al. 2004b	
Apatosaurus sp. ML 418	ML 418	present			rhomboid		pers. obs.	
Apatosaurinae indet. SMA 0087	SMA 0087	present		rhomboid	rhomboid	subequal	pers. obs.	
Supersaurus vivianae BYU	BYU 4503, BYU 9044	present	DV 3	rhomboid	rhomboid		Jensen, 1985	not entire dorsal series preserved, position of DV 4 inferred from height of parapophysis
Supersaurus vivianae WDC DMJ-021	WDC DMJ-021	present		rhomboid	rhomboid		D. Lovelace, pers. comm., 2013	
Dystylosaurus edwini BYU 4503	BYU 4503	present	DV 3	rhomboid			Jensen, 1985	only DV 4 preserved, position inferred from height of parapophysis

Table 6.29: continued.

Dinheirosaurus lourinhanensis ML 414	ML 414	present	DV 3		rhomboid		Mannion et al., 2012
Diplodocus carnegii CM 84	CM 84	present	DV 4	rhomboid	rhomboid	anterior half	Hatcher, 1901
Diplodocus carnegii CM 94	CM 94	present		rhomboid	rhomboid		pers. obs.
Diplodocus sp. AMNH 223	AMNH 223	present		rhomboid	rhomboid		Osborn, 1899
Diplodocus sp. USNM 10865	USNM 10865	present	DV 4		rhomboid		pers. obs.
Diplodocus sp. DMNS 1494	DMNS 1494	present	DV 4	rhomboid			D. Lovelace, pers. comm., 2013
Galeamopus shellensis SMA 0011	SMA 0011	present					pers. obs.
Seismosaurus hallorum NMMNH 3690	NMMNH 3690	present		rhomboid	rhomboid		Herne and Lucas, 2006
Barosaurus lentus YPM 429	YPM 429	present		rhomboid	rhomboid		Lull, 1919; pers. obs.
Barosaurus sp. AMNH 6341	AMNH 6341	present	DV 4	rhomboid	rhomboid	subequal	McIntosh, 2005
Barosaurus sp. CM 11984	CM 11984	present			rhomboid		pers. obs.
Cetiosauriscus stewarti NHMUK R3078	NHMUK R3078	present			laminar		pers. obs.

Table 6.30: Dorsal vertebrae 1 and 2, centrum length, and longest element in series.

Taxon	Specimen	DV 1	DV 2	longest	Reference	Comments
Shunosaurus lii	T5401	110	115	DV 2	Zhang, 1988	
Omeisaurus	T5701	249	233	DV 1	He et al., 1988	
	T5704	250	250	DV 1 & 2	He et al., 1988	
Mamenchisaurus	ZDM 0083	200	180	DV 1	Ouyang & Ye, 2002	
Camarasaurus	WDC A	281	205	DV 1	Ikejiri, 2004	
	WDC B	252	246	DV 1	Ikejiri, 2004	
Giraffatitan brancai	MB.R. SII	460	360	DV 1	Janensch, 1950	without ball, measurements of pDV lacking
Brachiosaurus sp.	SMA 0009	41	46,5	DV 5	Schwarz et al., 2007c; Carballido et al., 2012a	without ball, pDV lacking
Haplocanthosaurus priscus	CM 879	200	120	DV 1	Hatcher, 1903	DV 1 and 2 correspond to DV 2 and 3 as interpreted by Hatcher (1903)
Dicraeosaurus hansemanni	MB.R.4886	184	174	DV 7	Janensch, 1929	
Suuwassea emilieae	ANS 21122	307	259	-	Harris, 2006	identification based on position of pap
Brontosaurus excelsus	YPM 1980			DV 1	pers. obs.	no measurements available
Apatosaurus louisae	CM 3018	310	315	DV 2	Gilmore, 1936	
Apatosaurus parvus	UW 15556	345	285	DV 1	Gilmore, 1936	
Apatosaurus ajax	NSMT-PV 20375	340	220	DV 1	Upchurch et al. 2004	
Apatosaurus sp.	AMNH 460			DV 1	pers. obs.	no measurements available
Apatosaurus sp.	CM 3378			DV 2	Upchurch et al. 2004	no measurements available
Apatosaurus sp.	FMNH P25112	370	360	DV 1	Gilmore, 1936	
Diplodocus carnegii	CM 84	510	416	DV 1	Hatcher, 1901	
Diplodocus sp.	USNM 10865	460	376	DV 1	Gilmore, 1932	
Diplodocus sp.	DMNS 1494			DV 1	pers. obs.	no measurements available
Galeamopus hayi	HMNS 175			DV 1	pers. obs.	no measurements available
Galeamopus shellensis	SMA 0011		355	DV 1	pers. obs.	DV 1 distorted, but clearly longest
Barosaurus sp.	AMNH 6341	565	422	DV 1	McIntosh, 2005	

Table 6.31: Anterior dorsal vertebrae, pleurocoel length.

Taxon	Specimen	ppl	longest	Reference	Comments
Mamenchisaurus	ZDM 0083		DV 3	Ouyang and Ye, 2002	measured from photo
Camarasaurus	AMNH 5760/5761		DV 3	Osborn and Mook, 1921	measured from figure
	WDC B		DV 3	Ikejiri, 2004	measured from photo
Giraffatitan brancai	MB.R. SII, DV 2	70		Janensch, 1950	
	MB.R. SII, DV 4	140		Janensch, 1950	
Brachiosaurus sp.	SMA 0009		DV 1	pers. obs.	
Isisaurus colberti	ISIR335		DV 1	Jain and Bandyopadhyay, 1997	measured from photo
Haplocanthosaurus priscus	CM 879		DV 1	Hatcher, 1903	measured from figure
Limaysaurus tessonei			pDV	Calvo and Salgado, 1995	mentioned in text
Suuwassea emilieae	ANS 21122, DV 1	181,2	DV 1	Harris, 2006	
	ANS 21122, DV 3	43,2		Harris, 2006	
Apatosaurus ajax	YPM 1860		DV 1	pers. obs.	
Brontosaurus excelsus	YPM 1980		DV 1	pers. obs.	
Apatosaurus louisae	CM 3018		DV 3	Gilmore, 1936	measured from figure
Apatosaurus parvus	UW 15556		DV 1	Gilmore, 1936	measured from figure
Apatosaurus ajax	NSMT-PV 20375		DV 1	Upchurch et al., 2004b	
Apatosaurus sp.	AMNH 460		DV 3	pers. obs.	
Apatosaurus sp.	FMNH P25112		DV 3	Upchurch et al., 2004b	
Dinheirosaurus lourinhanensis	ML 414		DV 1	pers. obs.	
Diplodocus carnegii	CM 84		DV 1	Hatcher, 1901	measured from figure
Diplodocus carnegii	CM 94		DV 3	pers. obs.	DV 1 not preserved, dubious
Diplodocus sp.	USNM 10865		DV 1	pers. obs.	
Diplodocus sp.	DMNS 1494		DV 1	pers. obs.	
Galeamopus hayi	HMNS 175		DV 1	pers. obs.	
Galeamopus shellensis	SMA 0011, DV 1	185	DV 1 & 2	pers. obs.	
	SMA 0011, DV 3	65			
Barosaurus lentus	YPM 429, DV 1	195	DV 1	Lull, 1919	DV 2 and 3 lacking
	YPM 429, DV 4	60			
Barosaurus sp.	AMNH 6341		DV 1	McIntosh, 2005	measured from figure

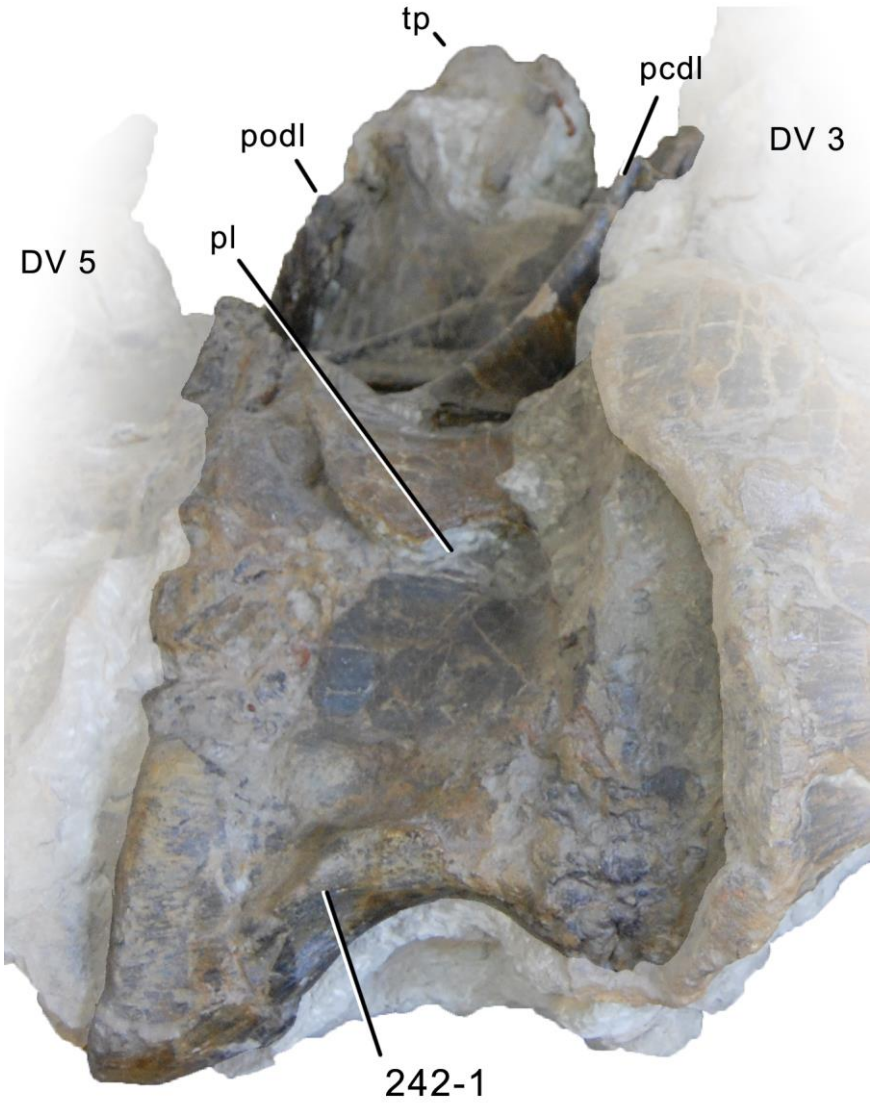

Figure 6.67: Dorsal vertebra 4 of *Dinheirosaurus lourinhanensis* ML 414 in ventral view, illustrating the ventral keel (C242-1) in anterior dorsal vertebrae. Abb.: DV, dorsal vertebra; pcdl, posterior centrodiapophyseal lamina; pl, pleurocoel; podl, postzygodiapophyseal lamina; tp, transverse process.

C244: Anterior, bifid dorsal vertebrae, base of notch between metapophyses: wide and rounded (0); narrow, V-shaped (1) (Gilmore, 1936; Fig. 6.68).

Comments. As *Apatosaurus*, also *Camarasaurus* appears to show intrageneric variation: *C. lewisi* has narrow troughs throughout its bifurcated presacral vertebrae, whereas other *Camarasaurus* species have wide bases (Jensen, 1988; McIntosh et al., 1996b). Herein, *Camarasaurus* was scored as plesiomorphic, because new evidence from material at SMA suggests that *C. lewisi*, which was initially described as new genus (*Cathetosaurus*), was actually erroneously referred to *Camarasaurus* (Mateus and Tschopp, 2013).

C245: Anterior dorsal, bifid neural spines, medial surface: gently rounded transversely (0); subtriangular (1) (New; Fig. 6.60).

Comments. Some diplodocid specimens bear a dorsoventral ridge on the medial surface of the anterior dorsal neural spines, similar to the ridge present in some diplodocid posterior cervical neural spines. The ridge results in a subtriangular shape of the medial surface.

C246: Dorsal vertebra 3, parapophysis: lies at the top of the centrum (0); lies mid-way between the top of the centrum and the level of the prezygapophyses (1) (Gilmore, 1936; Upchurch et al., 2004b; modified; Fig. 6.62).

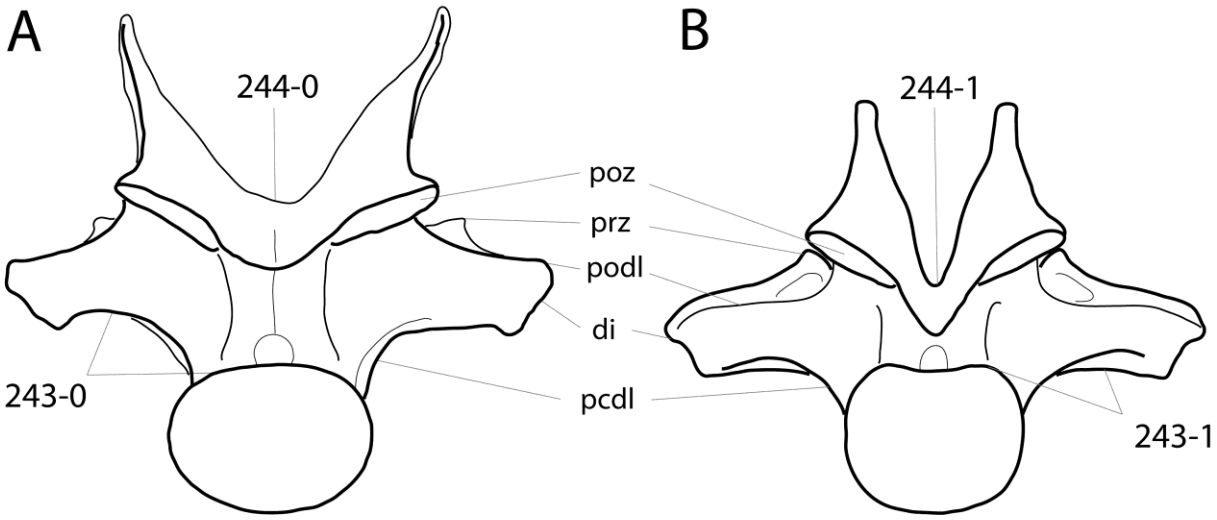

Figure 6.68: Dorsal vertebra 1 of *Apatosaurus louisae* CM 3018 (A) and *A.* sp. UW 15556 (B; both traced from Gilmore, 1936) in posterior view. Note the different positions of the transverse processes (high, A, C243-0; low, B, C243-1), and the varying width of the base of the bifurcated spines (wide, A, C244-0; narrow, B, C244-1). Abb.: di, diapophysis; pcdl, posterior centrodiapophyseal lamina; podl, postzygodiapophyseal lamina; poz, postzygapophysis; prz, prezygapophysis. Scaled to same posterior cotyle height.

C247: Anterior and mid-dorsal centra, pleurocoels: situated entirely on centrum (0); invade neural arch pedicels (1) (Holland, 1915a; Fig. 6.69).

Comments. Holland (1915a) proposed this morphology as diagnostic for *Apatosaurus louisae*, but it is included in a phylogenetic analysis for the first time here. Taxa without dorsal pleurocoels are scored as unknown.

C248: Anterior and mid-dorsal neural arch, hyposphene shape: rhomboid (0); laminar (1) (New; Tab. 6.29).

Comments. Hyposphene shape can change considerably from front to back, as is seen in specimens of *Camarasaurus* (Osborn and Mook, 1921; McIntosh et al., 1996b). In the present analysis, two different characters are thus used to code for the anterior and mid-dorsal vertebrae, as well as for the posterior elements, which are often less developed (see character 276). See figure 6.63 for an example of a laminar hyposphene.

C249: Mid-dorsal neural arches, height above postzygapophyses (neural spine) to height below (pedicel): 2.1 or greater (0); < 2.1 (1) (Whitlock, 2011a; modified; Tab. 6.32).

Comments. Pedicel height is measured from the neural canal floor to the ventral-most point of the postzygapophyseal facets, neural spine height from there to the spine top. Both measurements are taken vertically, ignoring spine inclination. The ratio changes considerably between mid- and posterior dorsal vertebrae, therefore the original character of Whitlock (2011a) was divided in two (see character 272). Furthermore, a numerical boundary was introduced.

C250: Mid-dorsal neural spines, form: single, bifid form (if present) does not extend past the second or third dorsal (0); bifid, inclusive of at least the fifth dorsal vertebrae (1) (Whitlock, 2011a; Tab. 6.33).

Comments. Notched and unsplit neural spines (sensu Wedel and Taylor, 2013) are counted as single, shallowly and deeply bifurcated spines as bifid. An additional character is used to account for the notched spines. The taxon scores are thus slightly different from the ones in Whitlock (2011a).

C251: Mid-dorsal neural spines, oblique accessory lamina connecting posl with spol: absent (0); present (1) (New; Fig. 6.69).

Comments. In *Supersaurus* and *Dinheirosaurus*, this accessory lamina extends posterodorsally-anteroventrally from near the dorsal end of the posl to the junction of the spol with the spdl.

C252: Mid- and posterior dorsal vertebrae, lateral pleurocoels present in centra: absent (0); present (1) (Gauthier, 1986; McIntosh, 1990b; Upchurch, 1995; modified by Whitlock, 2011a).

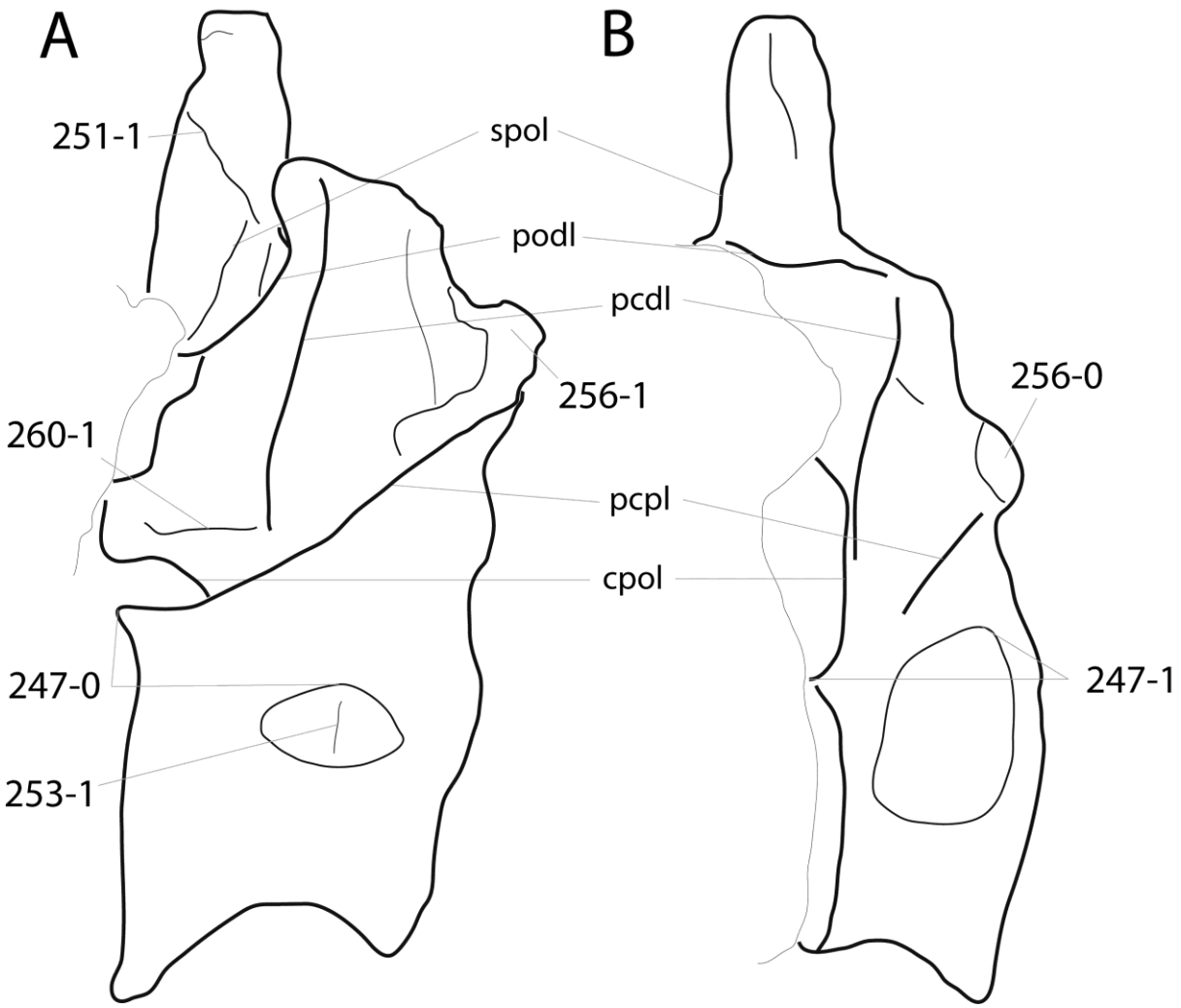

Figure 6.69: Mid-dorsal vertebrae of *Dinheirosaurus lourinhanensis* ML 414 (A; traced from photo by O. Mateus) and *Galeamopus shellensis* SMA 0011 (B) in lateral view. Note the pleurocoels that are entirely situated on the centrum (A; C247-0), or invade the neural arch (B; C247-1), the accessory spinal lamina connecting to the junction of spol and spdl (A; C251-1), the vertical lamina subdividing the pleurocoel (A; C253-1), the anteriorly displaced parapophysis (A; C256-1) in contrast to its usual position above the anterior edge (B; C256-0), and the horizontal accessory lamina connecting the hyposphene with the pcdl (A; C260-1). Abb.: cpol, centropost-zygapophyseal lamina; pcdl, posterior centrodiapophyseal lamina; pcpl, posterior centroparapophyseal lamina; podl, postzygodiapophyseal lamina; spol, spinopostzygapophyseal lamina. Scaled to same vertebral height.

C253: Mid- and posterior dorsal vertebrae, vertically oriented rod-like struts divide the lateral pneumatic foramina: absent (0); present (1) (Mannion et al., 2012; Fig. 6.69).

Comments. Mannion et al. (2012) proposed the presence of such a strut as synapomorphy for the clade uniting *Supersaurus* and *Dinheirosaurus*. However, similar struts are present as well in some apatosaurs. The pleurocoel is often not completely liberated from matrix during preparation, potentially obscuring the presence or absence of this structure.

C254: Mid- and posterior dorsal vertebrae, height of neural arch below the postzygapophyses (pedicel) divided by posterior cotyle height: <0.8 (0); 0.8 or greater (1) (Gallina and Apesteguía, 2005; modified; Tab. 6.34).

Comments. Neural arch height is measured from the neural canal floor to where the postzygapophyseal facets meet medially, above the hyposphene, where present.

C255: Mid- and posterior dorsal neural arches, prezygoparapophyseal lamina (prpl): present (0); absent (1) (Wilson, 2002; Fig. 6.70).

Table 6.32: Mid- and posterior dorsal neural arches, spine height/pedicel height.

Taxon	Specimen	Ratio	Mean tot	Mean mDV	Mean pDV	Reference	Comments
Shunosaurus lii	T5401, DV 7	2,669	2,38	2,67		Zhang, 1988	measured from figure
	T5401, DV 11	2,101			2,10	Zhang, 1988	measured from figure
Spinophorosaurus nigerensis	GCP-CV-4229, pDV	2,727	2,73		2,73	Remes et al., 2009	measured from figure
Omeisaurus	T5701, DV 6	2,021	2,37	2,37		He et al., 1988	measured from figure
	T5701, DV 7	2,716				He et al., 1988	measured from figure
Mamenchisaurus	ZDM 0083, DV 6	1,886	1,42	1,41		Ouyang and Ye, 2002	measured from figure
	ZDM 0083, DV 8	0,933				Ouyang and Ye, 2002	measured from figure
	ZDM 0083, DV 10	1,444			1,44	Ouyang and Ye, 2002	measured from figure
	ZDM 0083, DV 11	1,433				Ouyang and Ye, 2002	measured from figure
Jobaria tiguidensis	F144, DV 8	2,581	2,60	2,58		O. Mateus, pers. comm., 2010	measured from photo
	F145, DV 9	2,597			2,62	O. Mateus, pers. comm., 2010	measured from photo
	F146, DV 10	2,634				O. Mateus, pers. comm., 2010	measured from photo
Losillasaurus giganteus type	MCNV Lo-11	1,688	1,69		1,69	pers. obs.	measured from photo
Camarasaurus	AMNH 5760/5761, DV 4	1,264	2,02	1,89	2,14	Osborn and Mook, 1921	measured from figure
	AMNH 5760/5761, DV 5	2,549				Osborn and Mook, 1921	measured from figure
	AMNH 5760/5761, DV 7	1,800				Osborn and Mook, 1921	measured from figure
	AMNH 5760/5761, DV 8	2,000				Osborn and Mook, 1921	measured from figure
	AMNH 5760/5761, DV 9	2,083				Osborn and Mook, 1921	measured from figure
	AMNH 5760/5761, DV 10	2,128				Osborn and Mook, 1921	measured from figure
	AMNH 5760/5761, DV 11	2,000				Osborn and Mook, 1921	measured from figure
	WDC A, DV 6	1,828				Ikejiri, 2004	measured from figure
	WDC A, DV 9	2,085				Ikejiri, 2004	measured from figure
	WDC A, DV 12	2,123				Ikejiri, 2004	measured from figure
	WDC B, DV 12	2,394				Ikejiri, 2004	measured from figure
Apatosaurus grandis YPM 1901	YPM 1901, mDV	0,728	0,73	0,73		Wilson and Sereno, 1998	measured from figure
Giraffatitan brancai	MB.R. ?, DV 4	1,755	2,08	1,64		Taylor, 2009	measured from figure
	MB.R.3824, DV 8	1,519				pers. obs.	measured from photo
	MB.R. ?, DV 10	3,238			2,52	Taylor, 2009	measured from figure
	MB.R. ?, DV 12	1,800				Taylor, 2009	measured from figure
Brachiosaurus altithorax	FMNH P25107, DV 6	1,976	1,71	1,75		Taylor, 2009	measured from figure
	FMNH P25107, DV 8	1,525				Taylor, 2009	measured from figure
	FMNH P25107, DV 10	1,615			1,62	Taylor, 2009	measured from figure
Isisaurus colberti	ISIR355-15, mDV	3,857	3,86	3,86		Jain and Bandyopadhyay, 1997	measured from figure
Haplocanthosaurus priscus	CM 572, DV 6	1,025	1,16	1,08		Hatcher, 1903	measured from figure
	CM 572, DV 7	1,160				Hatcher, 1903	measured from figure
	CM 572, DV 8	1,065				Hatcher, 1903	measured from figure
	CM 572, DV 9	1,076			1,21	Hatcher, 1903	measured from figure
	CM 572, DV 10	1,153				Hatcher, 1903	measured from figure
	CM 572, DV 11	1,417				Hatcher, 1903	measured from figure
	CM 572, DV 12	1,152				Hatcher, 1903	measured from figure
	CM 572, DV 13	1,269				Hatcher, 1903	measured from figure
Limaysaurus tessonei	MUCPv-206, pDV	3,104	3,10		3,10	Calvo and Salgado, 1995	measured from figure
Amphicoelias altus AMNH 5764	AMNH 5764, pDV	2,712	2,71		2,71	Osborn and Mook, 1921	measured from figure
Dicraeosaurus hansemanni	MB.R.4886, DV 4	3,883	3,55	3,88		Schwarz-Wings, 2009	measured from figure
	MB.R.4886, DV 8	3,220			3,220	Schwarz-Wings, 2009	measured from figure
Brachytrachelopan mesai	MPEF PV 1716, mDV	3,264	3,35	3,26		J. Carballido, pers. comm., 2013	measured from photo
	MPEF PV 1716, pDV	3,437			3,437	J. Carballido, pers. comm., 2013	measured from photo
Apatosaurus ajax YPM 1860	YPM 1860, pDV	2,215	2,22		2,22	pers. obs.	measured from photo
Brontosaurus excelsus YPM 1980	YPM 1980, DV 5	2,351	3,15	2,35		Ostrom and McIntosh, 1966	measured from figure
	YPM 1980, DV 8	3,944			3,944	Ostrom and McIntosh, 1966	measured from figure
Apatosaurus louisae CM 3018	CM 3018, DV 3	1,891	3,02	2,34		Gilmore, 1936	measured from figure
	CM 3018, DV 4	1,657				Gilmore, 1936	measured from figure
	CM 3018, DV 5	2,474				Gilmore, 1936	measured from figure
	CM 3018, DV 6	3,326				Gilmore, 1936	measured from figure
	CM 3018, DV 7	3,980			3,94	Gilmore, 1936	measured from figure
	CM 3018, DV 8	4,122				Gilmore, 1936	measured from figure
	CM 3018, DV 9	3,709				Gilmore, 1936	measured from figure
Apatosaurus parvus UW 15556	UW 15556, DV 4	2,067	2,07	2,07		Gilmore, 1936	measured from figure
Eobrontosaurus yahnahpin Tate-001	Tate-001, pDV	2,902	2,90		2,902	P. Mannion, pers. comm., 2012	measured from photo
Apatosaurus ajax NSMT-PV 20375	NSMT-PV 20375, DV 4	2,194	2,41	2,34		Upchurch et al., 2004b	
	NSMT-PV 20375, DV 7	2,492				Upchurch et al., 2004b	
	NSMT-PV 20375, DV 10	2,536			2,536	Upchurch et al., 2004b	
Apatosaurus sp. FMNH P25112	FMNH P25112, DV 4	2,825	3,57	3,27		Riggs, 1903	measured from photo, height of poz estimated
	FMNH P25112, DV 5	2,618				Riggs, 1903	measured from photo, height of poz estimated
	FMNH P25112, DV 6	3,323				Riggs, 1903	measured from photo, height of poz estimated
	FMNH P25112, DV 7	4,301				Riggs, 1903	measured from photo, height of poz estimated
	FMNH P25112, DV 8	3,342			3,98	Riggs, 1903	measured from photo, height of poz estimated
	FMNH P25112, DV 9	4,057				Riggs, 1903	measured from photo, height of poz estimated
	FMNH P25112, DV 10	4,529				Riggs, 1903	measured from photo, height of poz estimated

Table 6.32: continued.

Apatosaurus sp. ML 418	ML 418, pDV	3,620	3,62		3,620	Mannion et al., 2012	measured from figure
Apatosaurinae indet. SMA 0087	SMA 0087, DV 5	2,300	2,50	2,40	2,78	pers. obs.	
	SMA 0087, DV 6	2,111				pers. obs.	
	SMA 0087, DV 7	2,800				pers. obs.	
	SMA 0087, DV 8	2,781				pers. obs.	
Supersaurus vivianae BYU	BYU 4503, mDV	1,911	2,68	1,91		Jensen, 1988	measured from figure
	BYU 9044, pDV	3,453			3,453	D. Lovelace, pers. comm., 2013	measured from figure
Supersaurus vivianae WDC DMJ-021	WDC DMJ-021, pDV	3,404	3,40		3,404	D. Lovelace, pers. comm., 2013	measured from photo
Dystylosaurus edwini BYU 4503	BYU 4503, mDV	1,911	1,91	1,91		Jensen, 1988	measured from figure
Dinheirosaurus lourinhanensis ML 414	ML 414		high	high	high	pers. obs.	no measurements available
Diplodocus carnegii CM 84	CM 84, DV 5	1,759	2,01	2,08		Hatcher, 1901	measured from figure
	CM 84, DV 6	2,167				Hatcher, 1901	measured from figure
	CM 84, DV 7	2,324				Hatcher, 1901	measured from figure
	CM 84, DV 8	1,830			1,94	Hatcher, 1901	measured from figure
	CM 84, DV 9	1,887				Hatcher, 1901	measured from figure
	CM 84, DV 10	2,103				Hatcher, 1901	measured from figure
Diplodocus sp. USNM 10865	USNM 10865, DV 10	2,310	2,31		2,310	Gilmore, 1932	measured from figure
Seismosaurus hallorum NMMNH 3690	NMMNH 3690, DV 8	2,484	2,48		2,484	Herne and Lucas, 2006	measured from figure
Galeamopus shellensis SMA 0011	SMA 0011, DV 5	1,134	1,23	0,95		pers. obs.	measured from photo
	SMA 0011, DV 6	0,863				pers. obs.	measured from photo
	SMA 0011, DV 7	0,840				pers. obs.	measured from photo
	SMA 0011, DV 8	1,333			1,51	pers. obs.	measured from photo
	SMA 0011, DV 9	1,561				pers. obs.	measured from photo
	SMA 0011, DV 10	1,639				pers. obs.	measured from photo
Barosaurus lentus YPM 429	YPM 429, DV 8	1,929	1,93		1,929	Lull, 1919	measured from figure
Barosaurus sp. AMNH 6341	AMNH 6341, DV 5	1,739	1,85	1,78		McIntosh, 2005	measured from figure
	AMNH 6341, DV 6	1,826				McIntosh, 2005	measured from figure
	AMNH 6341, DV 7	1,678			1,92	McIntosh, 2005	measured from figure
	AMNH 6341, DV 8	2,140				McIntosh, 2005	measured from figure
	AMNH 6341, DV 9	1,938				McIntosh, 2005	measured from figure
Barosaurus sp. CM 11984	CM 11984, pDV	2,723	2,72		2,723	pers. obs.	measured from photo

C256: Mid- and posterior dorsal parapophyses, location: above centrum, posterior to anterior edge of centrum (0); straight above anterior edge of centrum, or anteriorly displaced (1) (New; Figs 6.69, 6.70).

Comments. The anterior edge of the centrum corresponds to the rim of the anterior condyle in opisthocoelous elements. In some taxa, the position of the parapophysis changes from front to back, these taxa are scored for the majority of the elements in the series (e.g. *Haplocanthosaurus*, where DV 10 has a posteriorly placed parapophysis, but the majority of the mid- and posterior dorsal vertebrae have anteriorly displaced parapophyses; Hatcher, 1903).

C257: Mid- and posterior dorsal neural arches, anterior centroparapophyseal lamina: absent (0); present (1) (Upchurch et al., 2004a; Fig. 6.70).

C258: Mid- and posterior dorsal neural arches, posterior centroparapophyseal lamina: absent (0); present as single lamina (1); present, double (2) (Salgado et al., 1997; modified after Mannion et al., 2013; Figs 6.70, 6.71).

Comments. In taxa, where the pcpl is double, the more dorsal branch often connects to the pcdl. Mannion et al. (2013) defined the third state as 'two parallel laminae', but in certain specimens (e.g. *Diplodocus carnegii* CM 84), the dorsal branch becomes more horizontal (Hatcher, 1901). The character is treated as ordered, as it codes for both presence/absence and morphology.

C259: Mid- and posterior dorsal vertebrae, accessory laminae in the region between the posterior centrodiapophyseal lamina (pcdl) and posterior centroparapophyseal lamina (pcpl): absent (0); present (1) (Mannion et al., 2012; Fig. 6.71).

Comments. This character is somewhat ambiguous. Some of these accessory laminae might actually represent dorsal branches of the pcpl (see character 258) or dislocated ppdl. Here, only laminae not directly connecting to any specifying landmark (see Wilson, 1999) are considered accessory. More studies are needed to see if these are homologous to the above mentioned laminae.

C260: Mid- and posterior dorsal vertebrae, accessory lamina linking the hyposphene with base of the posterior centrodiapophyseal lamina: absent (0); present (1) (New; Figs 6.69, 6.71).

Comments. The presence of such an accessory lamina was proposed as autapomorphic for *Dinheirosaurus* (Mannion et al., 2012), but is herein interpreted to be present in other diplodocids as well. The accessory lamina can easily be confused with the lateral branch of the cpol, but the latter connects directly with the postzygapophyseal facet, and not with the hyposphene. The accessory lamina described herein is thus situated between the two branches of the cpol.

Table 6.33: Distribution of bifurcated, notched and unsplit dorsal neural spines.

Taxon	Specimen	Bifurcated	Notched	Unsplit	Reference	Comments
Shunosaurus lii				all	Zhang, 1988	
Spinophorosaurus nigerensis				all	Remes et al., 2009	
Omeisaurus				all	He et al., 1988	
Mamenchisaurus	ZDM 0083	DV 1-2	DV 3-4	DV 5-12	Ouyang and Ye, 2002	
Jobaria tiguidensis				all	Sereno et al., 1999	
Turiasaurus riodevensis	CPT		mDV		Royo-Torres et al., 2006	
Losillasaurus giganteus type	MCNV			all	Casanovas et al., 2001	
Camarasaurus	CM 11338	DV 1-5	DV 6	DV 7-12	Wedel and Taylor, 2013	
	GMNH-PV 101		DV 6-7	DV 8-12	Wedel and Taylor, 2013	
	AMNH 5761	DV 1-6	DV 7-8	DV 9-12	Wedel and Taylor, 2013	
	BYU 9047	DV 1-10	DV 11-12	none	Wedel and Taylor, 2013	
Apatosaurus grandis YPM 1901	YPM 1901		mDV		Wilson and Sereno, 1998	
Giraffatitan brancai				all	Janensch, 1950	
Brachiosaurus sp. SMA 0009	SMA 0009			all	Schwarz et al., 2007c	
Brachiosaurus altithorax				all	Riggs, 1904	
Ligabuesaurus leanzai				all	Bonaparte et al., 2006	
Isisaurus colberti				all	Jain and Bandyopadhyay, 1997	
Haplocanthosaurus priscus				all	Wedel and Taylor, 2013	
Limaysaurus tessonei				all	Calvo and Salgado, 1995	
Nigersaurus taqueti				all	Sereno et al., 1999	
Amphicoelias altus AMNH 5764	AMNH 5764			pDV	Osborn and Mook, 1921	
Dicraeosaurus hansemanni	MB.R.4886	DV 1-7	DV 8	DV 9-12	Janensch, 1929a	
Brachytrachelopan mesai	MPEF PV 1716	DV 1-6	DV 7	DV 8-12	Rauhut et al., 2005	
Amargasaurus cazaui	MACN-N 15	DV 1-9		DV 10	Salgado and Bonaparte, 1991	unclear how many DV. Only last DV unsplit, penultimate bifurcate
Suuwassea emilieae ANS 21122	ANS 21122	DV 1-3			Wedel and Taylor, 2013	only aDV preserved
Apatosaurus ajax YPM 1860	YPM 1860	DV 1-4			pers. obs.	more posterior elements incompletely preserved
Brontosaurus excelsus YPM 1980	YPM 1980	DV 1-3	DV 5	DV 8	Ostrom and McIntosh, 1966	DV 4, 6-7, 9-10 incompletely preserved
Apatosaurus louisae CM 3018	CM 3018	DV 1-3	DV 4-6	DV 7-9	Wedel and Taylor, 2013	
Atlantosaurus immanis YPM 1840	YPM 1840	DV 1-3			Ostrom and McIntosh, 1966	more posterior elements incompletely preserved
Apatosaurus parvus UW 15556	UW 15556	DV 1-3	DV 4		Wedel and Taylor, 2013	more posterior elements incompletely preserved
Apatosaurus ajax NSMT-PV 20375	NSMT-PV 20375	DV 1-5	DV 6	DV 7-10	Wedel and Taylor, 2013	
Apatosaurus sp. AMNH 460	AMNH 460	DV 1-4	DV 5		pers. obs.	more posterior elements incompletely preserved
Apatosaurus sp. FMNH P25112	FMNH P25112	DV 1-5	DV 6	DV 7-10	Wedel and Taylor, 2013	
Apatosaurus sp. ML 418	ML 418			pDV	pers. obs.	
Apatosaurinae indet. SMA 0087	SMA 0087	DV 5	DV 6	DV 7-10	pers. obs.	
Supersaurus vivianae BYU	BYU 4503, BYU 9044			DV 4-10	Lovelace et al., 2007	
Supersaurus vivianae WDC DMJ-021	WDC DMJ-021			pDV	Lovelace et al., 2007	aDV and mDV incompletely preserved
Dystylosaurus edwini BYU 4503	BYU 4503			DV 4	Lovelace et al., 2007	
Dinheirosaurus lourinhanensis ML 414	ML 414		pDV		Mannion et al., 2012	no bifurcation present, according to Mannion et al., 2012
Tornieria africana skeleton k	MB.R. k	aDV			Janensch, 1929b	only drawing of one aDV preserved
Diplodocus carnegii CM 84	CM 84	DV 1-6	DV 7-9	DV 10	Wedel and Taylor, 2013	
Diplodocus carnegii CM 94	CM 94	DV 2			pers. obs.	remaining DV incompletely preserved
Diplodocus sp. AMNH 223	AMNH 223	DV 1-6	DV 7-9	DV 10	Osborn, 1899	
Diplodocus sp. USNM 10865	USNM 10865	DV 1-5	DV 6-8	DV 9-10	Wedel and Taylor, 2013	
Diplodocus sp. DMNS 1494	DMNS 1494	DV 1-7			pers. obs.	more posterior elements incompletely preserved, but not bifurcate
Galeamopus hayi HMNS 175	HMNS 175	DV 1-5			pers. obs.	more posterior elements incompletely preserved
Seismosaurus hallorum NMMNH 3690	NMMNH 3690	DV 1-6?	DV 7?-8		Herne and Lucas, 2006	more posterior elements incompletely preserved
Galeamopus shellensis SMA 0011	SMA 0011	DV 1-5			pers. obs.	more posterior elements incompletely preserved
Barosaurus lentus YPM 429	YPM 429	DV 1-5		DV 6-9	Wedel and Taylor, 2013	
Barosaurus sp. AMNH 6341	AMNH 6341	DV 1-5	DV 6-8	DV 9	McIntosh, 2005	
Barosaurus sp. CM 11984	CM 11984		DV 6	DV 7	McIntosh, 2005	unclear on what identification of serial position bases

C261: Mid- and posterior dorsal neural arches, centropostzygapophyseal lamina: single (0); divided, lateral branch connecting to pcdl (1) (Wilson, 2002; wording modified; Fig. 6.70).

Comments. The lateral branch is often only visible in lateral view.

C262: Mid- and posterior dorsal neural arches, infradiapophyseal pneumatopore between acdl and pcdl: absent (0); present (1) (Wilson, 2002; Fig. 6.71).

Comments. Even though the development of pneumatic structures has been shown to depend on the ontogenetic stage (Wedel, 2003; Schwarz et al., 2007c), the early juvenile brachiosaur SMA 0009 already has this pneumatopore.

C263: Mid- and posterior dorsal transverse processes, length: short (0); long (projecting < 1.3 times posterior cotyle width) (1) (Carballido et al., 2012b; modified; Tab. 6.35).

Comments. The length of a single transverse process is compared to the maximum width of the posterior cotyle. Transverse process length is measured in a horizontal plane. Measurements taken from figures in posterior view generally underestimate the ratio, which has to be accounted for when scoring the taxa. In the case of *Brachiosaurus altithorax* FMNH P25107, true ratios based on the

measurements by Riggs (1904) are about 120 % of the ratios taken from published figures (Taylor, 2009), whereas in *Apatosaurus* NSMT-PV 20375 or *Diplodocus* CM 84, they are only 103 % higher. This percentage depends on the relative position of the transverse processes above the centrum. Ratios generally decrease from anterior to posterior dorsal vertebrae. Taxa or specimens that preserve only posterior elements (e.g. *Amphicoelias altus* AMNH 5764) should thus have higher actual ratios than shown in Tab. 6.35.

Table 6.34: Mid- and posterior dorsal neural arches, height below postzygapophyses/height of centrum at posterior cotyle.

Taxon	Specimen	Ratio	Mean	Reference	Comments
Shunosaurus lii	T5401, DV 7	0,790	0,93	Zhang, 1988	measured from figure
	T5401, DV 11	1,062		Zhang, 1988	measured from figure
Spinophorosaurus nigerensis	GCP-CV-4229, pDV	0,440	0,44	Remes et al., 2009	measured from figure
Omeisaurus	T5701, DV 6	0,646	0,60	He et al., 1988	measured from figure
	T5701, DV 7	0,550		He et al., 1988	measured from figure
Mamenchisaurus	ZDM 0083, DV 6	0,820	0,83	Ouyang and Ye, 2002	measured from figure
	ZDM 0083, DV 8	0,965		Ouyang and Ye, 2002	measured from figure
	ZDM 0083, DV 10	0,885		Ouyang and Ye, 2002	measured from figure
	ZDM 0083, DV 11	0,647		Ouyang and Ye, 2002	measured from figure
Jobaria tiguidensis	F144, DV 8	0,683	0,59	O. Mateus, pers. comm., 2010	measured from photo
	F145, DV 9	0,540		O. Mateus, pers. comm., 2010	measured from photo
	F146, DV 10	0,542		O. Mateus, pers. comm., 2010	measured from photo
Losillasaurus giganteus type	MCNV Lo-11	1,019	1,02	pers. obs.	measured from photo
Camarasaurus	AMNH 5760/5761, DV 4	0,635	0,54	Osborn and Mook, 1921	measured from figure
	AMNH 5760/5761, DV 5	0,757		Osborn and Mook, 1921	measured from figure
	AMNH 5760/5761, DV 7	0,494		Osborn and Mook, 1921	measured from figure
	AMNH 5760/5761, DV 8	0,586		Osborn and Mook, 1921	measured from figure
	AMNH 5760/5761, DV 9	0,494		Osborn and Mook, 1921	measured from figure
	AMNH 5760/5761, DV 10	0,411		Osborn and Mook, 1921	measured from figure
	AMNH 5760/5761, DV 11	0,517		Osborn and Mook, 1921	measured from figure
	AMNH 5760/5761, DV 12	0,528		Osborn and Mook, 1921	measured from figure
	WDC A, DV 6	0,615		Ikejiri, 2004	measured from figure
	WDC A, DV 9	0,574		Ikejiri, 2004	measured from figure
	WDC A, DV 12	0,378		Ikejiri, 2004	measured from figure
	WDC B, DV 12	0,463		Ikejiri, 2004	measured from figure
Apatosaurus grandis YPM 1901	YPM 1901, mDV	1,072	1,07	Wilson and Sereno, 1998	measured from figure
Giraffatitan brancai	MB.R. ?, DV 4	1,176	0,71	Taylor, 2009	measured from figure
	MB.R.3824, DV 8	0,452		pers. obs.	measured from photo
	MB.R. ?, DV 10	0,391		Taylor, 2009	measured from figure
	MB.R. ?, DV 12	0,812		Taylor, 2009	measured from figure
Brachiosaurus altithorax	FMNH P25107, DV 6	0,733	0,72	Taylor, 2009	measured from figure
	FMNH P25107, DV 8	0,700		Taylor, 2009	measured from figure
	FMNH P25107, DV 10	0,726		Taylor, 2009	measured from figure
Isisaurus colberti	ISIR355-15, mDV	0,429	0,43	Jain and Bandyopadhyay, 1997	measured from figure
Haplocanthosaurus priscus	CM 572, DV 6	1,466	1,18	Hatcher, 1903	measured from figure
	CM 572, DV 7	1,311		Hatcher, 1903	measured from figure
	CM 572, DV 8	1,365		Hatcher, 1903	measured from figure
	CM 572, DV 9	1,323		Hatcher, 1903	measured from figure
	CM 572, DV 10	1,084		Hatcher, 1903	measured from figure
	CM 572, DV 11	0,881		Hatcher, 1903	measured from figure
	CM 572, DV 12	1,026		Hatcher, 1903	measured from figure
	CM 572, DV 13	0,974		Hatcher, 1903	measured from figure
Limaysaurus tessonei	MUCPv-206, pDV	1,105	1,10	Calvo and Salgado, 1995	measured from figure, centrum reconstructed
Nigersaurus taqueti	DV 9	1,118	1,12	Carballido et al., 2012b	measured from figure
Demandasaurus darwini	pDV	0,929	0,93	Carballido et al., 2012b	measured from figure
Amphicoelias altus AMNH 5764	AMNH 5764, mDV	0,760	0,75	Osborn and Mook, 1921	measured from figure
	AMNH 5764, pDV	0,747		Osborn and Mook, 1921	measured from figure
Dicraeosaurus hansemanni	MB.R.4886, DV 4	0,842	0,89	Schwarz-Wings, 2009	measured from figure
	MB.R.4886, DV 8	0,937		Schwarz-Wings, 2009	measured from figure
Brachytrachelopan mesai	MPEF PV 1716, mDV	1,076	1,09	J. Carballido, pers. comm., 2013	measured from photo
	MPEF PV 1716, pDV	1,108		J. Carballido, pers. comm., 2013	measured from photo
Apatosaurus ajax YPM 1860	YPM 1860, pDV	0,744	0,74	pers. obs.	measured from photo
Brontosaurus excelsus YPM 1980	YPM 1980, DV 4	0,788	0,74	Ostrom and McIntosh, 1966	measured from figure
	YPM 1980, DV 5	0,824		Ostrom and McIntosh, 1966	measured from figure
	YPM 1980, DV 8	0,615		Ostrom and McIntosh, 1966	measured from figure
Apatosaurus louisae CM 3018	CM 3018, DV 3	0,844	0,72	Gilmore, 1936	measured from figure
	CM 3018, DV 4	1,045		Gilmore, 1936	measured from figure
	CM 3018, DV 5	0,764		Gilmore, 1936	measured from figure
	CM 3018, DV 6	0,618		Gilmore, 1936	measured from figure
	CM 3018, DV 7	0,610		Gilmore, 1936	measured from figure
	CM 3018, DV 8	0,560		Gilmore, 1936	measured from figure
	CM 3018, DV 9	0,624		Gilmore, 1936	measured from figure

Table 6.34: continued.

Elosaurus parvus CM 566	CM 566, pDV	1,027	1,03	pers. obs.	measured from photo
Apatosaurus parvus UW 15556	UW 15556, DV 4	0,729	0,79	Gilmore, 1936	measured from figure
	UW 15556, DV 5	0,960		Gilmore, 1936	measured from figure
	UW 15556, DV 6	0,767		Gilmore, 1936	measured from figure
	UW 15556, DV 7	0,793		Gilmore, 1936	measured from figure
	UW 15556, DV 8	0,908		Gilmore, 1936	measured from figure
	UW 15556, DV 9	0,605		Gilmore, 1936	measured from figure
Eobrontosaurus yahnahpin Tate-001	Tate-001, pDV	0,746	0,75	P. Mannion, pers. comm., 2012	measured from photo
Apatosaurus ajax NSMT-PV 20375	NSMT-PV 20375, DV 4	0,596	0,86	Upchurch et al., 2004b	
	NSMT-PV 20375, DV 5	0,832		Upchurch et al., 2004b	
	NSMT-PV 20375, DV 6	1,274		Upchurch et al., 2004b	
	NSMT-PV 20375, DV 7	0,789		Upchurch et al., 2004b	
	NSMT-PV 20375, DV 8	0,897		Upchurch et al., 2004b	
	NSMT-PV 20375, DV 10	0,778		Upchurch et al., 2004b	
Apatosaurus sp. FMNH P25112	FMNH P25112		low	Riggs, 1903	no measurements available, pictures only in anterior view
Apatosaurus sp. ML 418	ML 418, pDV	0,581	0,58	Mannion et al., 2012	measured from figure
Apatosaurinae indet. SMA 0087	SMA 0087, DV 5	0,918	1,01	pers. obs.	
	SMA 0087, DV 6	1,098		pers. obs.	
	SMA 0087, DV 7	1,031		pers. obs.	
	SMA 0087, DV 8	0,988		pers. obs.	
Supersaurus vivianae BYU	BYU 4503, mDV	0,543	0,59	Jensen, 1988	measured from figure
	BYU 9044, pDV	0,640		D. Lovelace, pers. comm., 2013	measured from figure
Supersaurus vivianae WDC DMJ-021	WDC DMJ-021, mDV	0,707	0,59	D. Lovelace, pers. comm., 2013	measured from photo
	WDC DMJ-021, pDV	0,550		D. Lovelace, pers. comm., 2013	measured from photo
	WDC DMJ-021, pDV	0,522		D. Lovelace, pers. comm., 2013	measured from photo
Dystylosaurus edwini BYU 4503	BYU 4503, mDV	0,543	0,54	Jensen, 1988	measured from figure
Dinheirosaurus lourinhanensis ML 414	ML 414, DV 5	0,657	0,83	Mannion et al., 2012	
	ML 414, DV 6	0,739		Mannion et al., 2012	
	ML 414, DV 7	0,719		Mannion et al., 2012	
	ML 414, DV 8	0,935		Mannion et al., 2012	
	ML 414, DV 9	1,091		Mannion et al., 2012	
Diplodocus carnegii CM 84	CM 84, DV 5	0,833	0,81	Hatcher, 1901	measured from figure
	CM 84, DV 6	0,778		Hatcher, 1901	measured from figure
	CM 84, DV 7	0,707		Hatcher, 1901	measured from figure
	CM 84, DV 8	0,822		Hatcher, 1901	measured from figure
	CM 84, DV 9	0,801		Hatcher, 1901	measured from figure
	CM 84, DV 10	0,898		Hatcher, 1901	measured from figure
Diplodocus carnegii CM 94	CM 94, pDV	1,115	1,12	pers. obs.	measured from photo
Diplodocus sp. USNM 10865	USNM 10865, DV 10	0,616	0,62	Gilmore, 1932	measured from figure
Seismosaurus hallorum NMMNH 3690	NMMNH 3690, DV 8	0,712	0,71	Herne and Lucas, 2006	measured from figure
Galeamopus shellensis SMA 0011	SMA 0011, DV 6	1,571	1,43	pers. obs.	
	SMA 0011, DV 7	1,533		pers. obs.	
	SMA 0011, DV 8	1,467		pers. obs.	
	SMA 0011, DV 9	1,368		pers. obs.	
	SMA 0011, DV 10	1,204		pers. obs.	
Barosaurus lentus YPM 429	YPM 429, DV 4	0,989	0,86	Lull, 1919	measured from figure
	YPM 429, DV 8	0,735		Lull, 1919	measured from figure
Barosaurus sp. AMNH 6341	AMNH 6341, DV 5	1,036	0,96	McIntosh, 2005	measured from figure
	AMNH 6341, DV 6	0,950		McIntosh, 2005	measured from figure
	AMNH 6341, DV 7	1,040		McIntosh, 2005	measured from figure
	AMNH 6341, DV 8	0,957		McIntosh, 2005	measured from figure
	AMNH 6341, DV 9	0,835		McIntosh, 2005	measured from figure
Barosaurus sp. CM 11984	CM 11984, pDV	0,686	0,69	pers. obs.	measured from photo

C264: Mid- and posterior dorsal transverse processes, dorsal edge: straight, or curving downwards at distal end (0); developing a distinct dorsal bump or spur (1) (New; Fig. 6.63).

Comments. Spurs are usually situated at the distal tip, whereas bumps are located more medially.

C265: Mid- and posterior dorsal neural spines, anteroposterior width: approximately constant along the height of the spine, with subparallel anterior and posterior margins (0); narrows dorsally to form a triangular shape in lateral view, with the base approximately twice the width of the dorsal tip (1) (New; Fig. 6.71).

C266: Middle and posterior dorsal neural spines, breadth at summit: much narrower (0); equal to or broader (1) transversely than anteroposteriorly (Wilson, 2002; modified).

Comments. Neural spine width can change considerably from the spine bottom to the top. The character was thus divided in two.

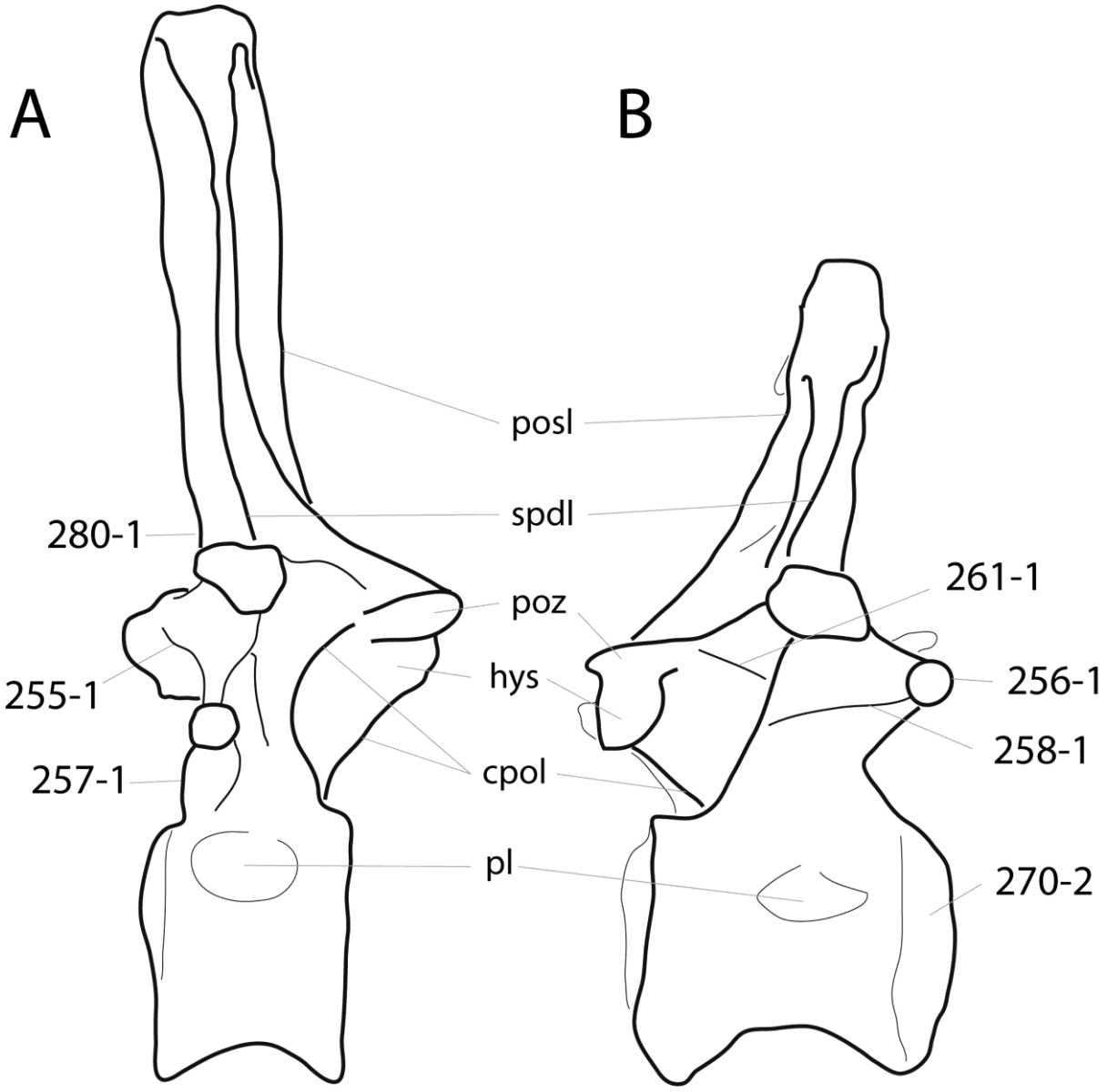

Figure 6.70: Posterior dorsal vertebrae of *Apatosaurus louisae* CM 3018 (A; traced from Gilmore, 1936) and *Supersaurus vivianae* BYU 9044 (B; traced from Jensen, 1985) in left (A) and right (B) lateral view. Note the prpl (A; C255-1), the anteriorly displaced parapophysis (B; C256-1), the acpl (A; C257-1), the pcpl (B; C258-1), the lateral branch of the cpol (B; C261-1), the pronounced opisthocoely (B; C270-2), and the anteriorly inclined base of the neural spine (A; C280-1). Abb.: cpol, centropostzygapophyseal lamina; hys, hyposphene; pl, pleurocoel; posl, postspinal lamina; poz, postzygapophysis; spdl, spinodiapophyseal lamina. Scaled to same posterior cotyle height.

C267: Mid- and posterior dorsal neural spines, triangular aliform processes: absent (0); present but do not project far laterally (not as far as postzygapophyses) (1); present, project at least as far laterally as postzygapophyses (2) (Carballido et al., 2012b; Figs 6.63, 6.64).

Comments. The character is treated as ordered.

C268: Posterior dorsal centra, total length/height of posterior articular surface: 1.0 or greater (0); short, < 1.0 (1) (New; Tab. 6.36).

C269: Posterior dorsal centra: subequal width and height, or higher than wide (0); wider than high (1) (Gilmore, 1936; Tab. 6.36).

Comments. Width and height are measured at the posterior cotyle. The boundary is set between 1.0 and 1.1 in the present study, because it was suggested by Gilmore (1936) to distinguish *Apatosaurus louisae* from *A. ajax* and *A. excelsus*.

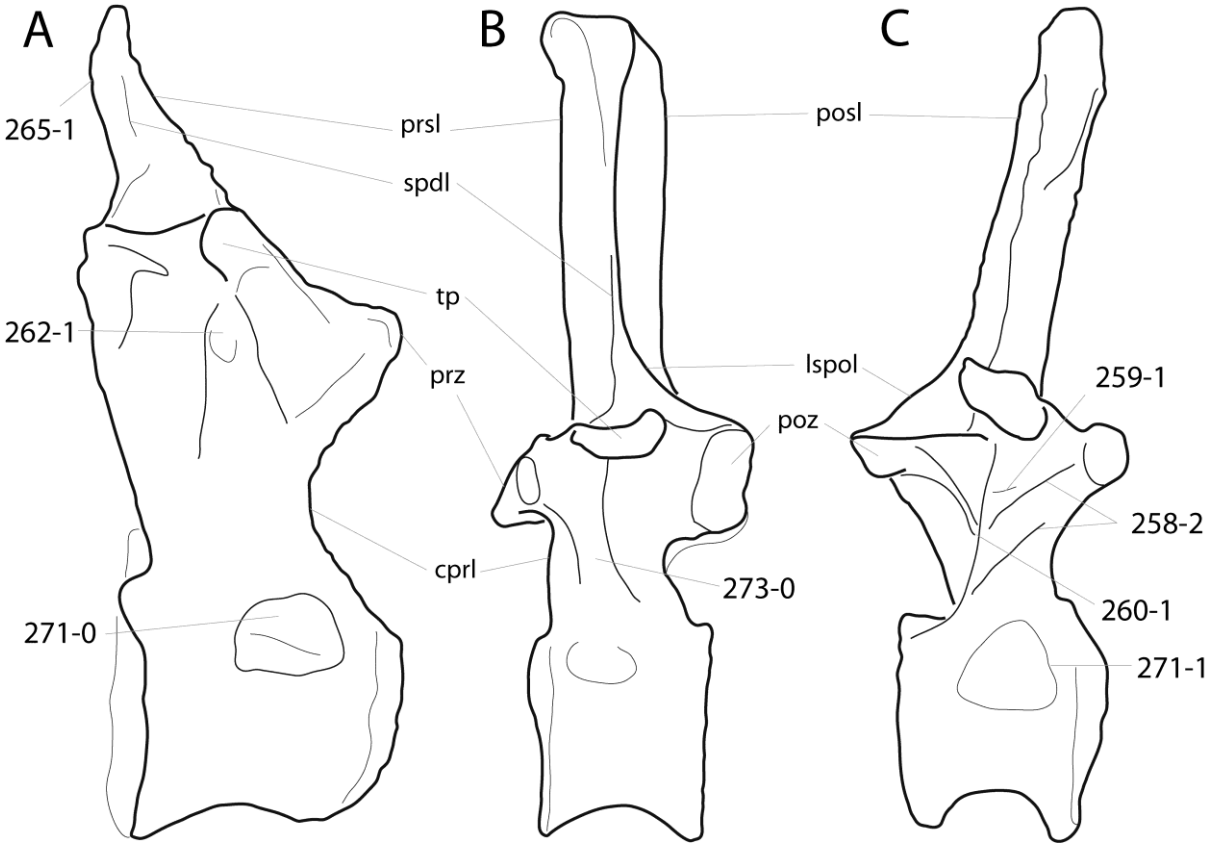

Figure 6.71: Posterior dorsal vertebrae of *Giraffatitan brancai* MB.R.3822 (A), *Apatosaurus louisae* CM 3018 (B; traced from Gilmore, 1936), and *Diplodocus carnegii* CM 84 (C; traced from Hatcher, 1901) in right lateral view. Note the double pcpl (C; C258-2), the accessory lamina in the parapophyseal centrodiapophyseal fossa (C; C259-1), the accessory lamina connecting the hyposphene with the pcdl (C; C260-1), the infradiapophyseal pneumatic foramen (A; C262-1), the dorsally tapering neural spine (A; C265-1), the different shapes of the pleurocoels (C271), and the ventrally open parapophyseal, centrodiapophyseal fossa (B; C273-0). Abb.: cprl, centroprezygapophyseal lamina; lspol, lateral spinopostzygapophyseal lamina; posl, postspinal lamina; poz, postzygapophysis; prsl, prespinal lamina; prz, prezygapophysis; spdl, spinodiapophyseal lamina; tp, transverse process. Scaled to same total height.

C270: Posterior dorsal centra, articular face shape: amphicoelous (0); slightly opisthocoelous (1); strongly opisthocoelous (2) (Yu, 1993; wording modified by Carballido et al., 2012b; Fig. 6.70).
Comments. Slightly opisthocoelous means that the condyle is either ventrally or dorsally restricted, but still visible in lateral view. Strongly opisthocoelous vertebrae have anterior balls that reach from the dorsal to the ventral edge of the centrum. In *Apatosaurus ajax* YPM 1860, no anterior articulation surface of a posterior dorsal vertebrae is observable, but the posterior articulation surface of a posterior element has a small, but distinct fossa marking its upper half. This indicates a slightly opisthocoelous centrum in the following element.

C271: Posterior dorsal vertebrae, pleurocoel shape: oval to circular (0); subtriangular with apex dorsally (1) (New; Fig. 6.71).
Comments. Taxa without dorsal pleurocoels are scored as unknown.

C272: Posterior dorsal neural arches, height above postzygapophyses (neural spine) to height below (pedicel): < 3.1 (0); 3.1 or greater (1) (Whitlock, 2011a; modified; Tab. 6.32).
Comments. See character 249.

C273: Posterior dorsal neural arches, parapophyseal centrodiapophyseal fossa: ventrally open, relatively shallow (0); deep, triangular (1) (Gallina and Apesteguía, 2005; Fig. 6.71).
Comments. The apomorphic state is applied to specimens with the pcpl connecting to the pcdl or acdl, thus creating a ventrally closed, triangular fossa between them and the ppdl or prdl. In plesiomorphic taxa, the pcpl fades out posteroventrally or connects to the centrum anterior to the ventral end of the pcdl.

Table 6.35: Mid- and posterior dorsal vertebrae, transverse process length/centrum width posterior cotyle.

Taxon	Specimen	Ratio	Mean	corrected mean	Reference	Comments
Shunosaurus lii			short		Carballido et al., 2012b	no measurements available, nor pictures in posterior view
Omeisaurus	T5701, DV 6	0,91	0,9		He et al., 1988	measured from figure
	T5701, DV 7	0,87			He et al., 1988	measured from figure
Mamenchisaurus	ZDM 0083, DV 6	1,21	0,9	higher	Ouyang and Ye, 2002	measured from figure
	ZDM 0083, DV 8	0,91			Ouyang and Ye, 2002	measured from figure
	ZDM 0083, DV 10	0,82			Ouyang and Ye, 2002	measured from figure
	ZDM 0083, DV 11	0,82			Ouyang and Ye, 2002	measured from figure
Jobaria tiguidensis			short		Carballido et al., 2012b	no measurements available, nor pictures in posterior view
Turiasaurus riodevensis			short		Carballido et al., 2012b	no measurements available, nor pictures in posterior view
Losillasaurus giganteus type			short		Carballido et al., 2012b	strongly deformed
Camarasaurus	BYU 9047, DV 7	1,01	1,1		McIntosh et al., 1996b	
	BYU 9047, DV 8	1,03			McIntosh et al., 1996b	
	BYU 9047, DV 9	1,00			McIntosh et al., 1996b	
	BYU 9047, DV 10	1,04			McIntosh et al., 1996b	
	BYU 9047, DV 11	0,90			McIntosh et al., 1996b	
	WDC A, mDV	1,10			Ikejiri, 2004	
	WDC A, mDV	1,02			Ikejiri, 2004	
	WDC A, mDV	1,38			Ikejiri, 2004	
	WDC A, mDV	1,02			Ikejiri, 2004	
	WDC A, pDV	1,20			Ikejiri, 2004	
	WDC A, pDV	1,10			Ikejiri, 2004	
	WDC A, pDV	0,86			Ikejiri, 2004	
	WDC B, pDV	1,66			Ikejiri, 2004	
	WDC B, pDV	1,23			Ikejiri, 2004	
Apatosaurus grandis YPM 1901	YPM 1901, mDV	1,21	1,2		Wilson and Sereno, 1998	measured from figure
Giraffatitan brancai	MB.R. SII, DV 4	2,08	1,4	1,6	Taylor, 2009	measured from figure; corrected mean based on discrepancy in ratios from figures or table in *B. altithorax*
	MB.R. SII, DV 10	1,20			Taylor, 2009	measured from figure
	MB.R. SII, DV 12	0,83			Taylor, 2009	measured from figure
Brachiosaurus sp. SMA 0009	SMA 0009, DV 4	1,79	1,7	lower	Schwarz et al., 2007	Do-6 in Schwarz et al., 2007
	SMA 0009, DV 5	1,76			Schwarz et al., 2007	Do-7 in Schwarz et al., 2007
	SMA 0009, DV 6	1,71			Schwarz et al., 2007	Do-8 in Schwarz et al., 2007
	SMA 0009, DV 7	1,66			Schwarz et al., 2007	Do-9 in Schwarz et al., 2007
Brachiosaurus altithorax	FMNH P25107, DV 6	1,50	1,3		Riggs, 1904	mean does not include measurements from figure
	FMNH P25107, DV 7	1,30			Riggs, 1904	
	FMNH P25107, DV 9	1,00			Riggs, 1904	
	FMNH P25107, DV 6	1,20			Taylor, 2009	measured from figure
	FMNH P25107, DV 9	0,88			Taylor, 2009	measured from figure
Ligabuesaurus leanzai	MCF-PVPH-233/4, pDV	1,00	1,0	higher	Bonaparte et al., 2006	width across diapophyses estimated
Isisaurus colberti	ISIR335/15, mDV	0,80	0,9	higher	Jain and Bandyophadhyay, 1997	width across diapophyses compressed
	ISIR335/16, mDV	1,07			Jain and Bandyophadhyay, 1997	estimated

Table 6.35: continued.

Haplocanthosaurus priscus	CM 572, DV 5	1,56	1,4		Hatcher, 1903	DV 6 in Hatcher, 1903
	CM 572, DV 6	1,58			Hatcher, 1903	DV 7 in Hatcher, 1903
	CM 572, DV 7	1,52			Hatcher, 1903	DV 8 in Hatcher, 1903
	CM 572, DV 8	1,48			Hatcher, 1903	DV 9 in Hatcher, 1903
	CM 572, DV 9	1,44			Hatcher, 1903	DV 10 in Hatcher, 1903
	CM 572, DV 10	1,34			Hatcher, 1903	DV 11 in Hatcher, 1903
	CM 572, DV 11	1,19			Hatcher, 1903	DV 12 in Hatcher, 1903
	CM 572, DV 12	1,07			Hatcher, 1903	DV 13 in Hatcher, 1903
	CM 572, DV 13	1,01			Hatcher, 1903	DV 14 in Hatcher, 1903
	CM 879, DV 4	1,57			Hatcher, 1903	DV 5 in Hatcher, 1903
Limaysaurus tessonei			long		Carballido et al., 2012b	no measurements available, nor pictures in posterior view
Nigersaurus taqueti			long		Carballido et al., 2012b	no measurements available, nor pictures in posterior view
Amphicoelias altus AMNH 5764	AMNH 5764, pDV	1,11	1,1	1,1	Osborn and Mook, 1921	measured from figure; corrected mean based on discrepancy in ratios from figures or table in *Apatosaurus* NSMT-PV 20375
Dicraeosaurus hansemanni	MB.R.4886, DV 5	1,64	1,4	higher	Janensch, 1929	width across diapophyses compressed
	MB.R.4886, DV 6	1,64			Janensch, 1929	width across diapophyses compressed
	MB.R.4886, DV 7	1,60			Janensch, 1929	width across diapophyses compressed
	MB.R.4886, DV 8	1,41			Janensch, 1929	width across diapophyses compressed
	MB.R.4886, DV 9	1,30			Janensch, 1929	width across diapophyses compressed
	MB.R.4886, DV 10	1,21			Janensch, 1929	width across diapophyses compressed
	MB.R.4886, DV 11	1,12			Janensch, 1929	width across diapophyses compressed
	MB.R.4886, DV 12	0,98			Janensch, 1929	width across diapophyses compressed
Brachytrachelopan mesai	MPEF PV 1716, DV 5	1,44	1,4	higher	J. Carballido, pers. comm., 2013	measured from photo, width across diapophyses compressed
Amargasaurus cazaui			long		Carballido et al., 2012b	no measurements available, nor pictures in posterior view
Brontosaurus excelsus YPM 1980	YPM 1980, DV 4	1,10	1,1	1,1	Ostrom and McIntosh, 1966	measured from figure; corrected mean based on discrepancy in ratios from figures or table in *Apatosaurus* NSMT-PV 20375
	YPM 1980, DV 5	1,11			Ostrom and McIntosh, 1966	measured from figure
Apatosaurus louisae CM 3018	CM 3018, DV 3	1,27	1,1	1,1	Gilmore, 1936	measured from figure; corrected mean based on discrepancy in ratios from figures or table in *Apatosaurus* NSMT-PV 20375
	CM 3018, DV 4	1,24			Gilmore, 1936	measured from figure
	CM 3018, DV 5	1,06			Gilmore, 1936	measured from figure
	CM 3018, DV 6	0,99			Gilmore, 1936	measured from figure
	CM 3018, DV 7	1,03			Gilmore, 1936	measured from figure
	CM 3018, DV 8	0,85			Gilmore, 1936	measured from figure
	CM 3018, DV 9	1,08			Gilmore, 1936	measured from figure

Table 6.35: continued.

Apatosaurus parvus UW 15556	UW 15556, DV 4	1,23	1,1	1,1	Gilmore, 1936	measured from figure; corrected mean based on discrepancy in ratios from figures or table in *Apatosaurus* NSMT-PV 20375
	UW 15556, DV 5	1,25			Gilmore, 1936	measured from figure
	UW 15556, DV 7	1,03			Gilmore, 1936	measured from figure
	UW 15556, DV 8	0,91			Gilmore, 1936	measured from figure
	UW 15556, DV 9	0,93			Gilmore, 1936	measured from figure
Apatosaurus ajax NSMT-PV 20375	NSMT-PV 20375, DV 4	1,40	1,2		Upchurch et al., 2004b	mean does not include measurements from figure
	NSMT-PV 20375, DV 10	1,07			Upchurch et al., 2004b	
	NSMT-PV 20375, DV 4	1,35			Upchurch et al., 2004b	measured from figure
	NSMT-PV 20375, DV 10	1,05			Upchurch et al., 2004b	measured from figure
Apatosaurus sp. FMNH P25112	FMNH P25112, DV 4	1,23	1,0		Riggs 1903	
	FMNH P25112, DV 5	1,15			Riggs 1903	
	FMNH P25112, DV 6	1,05			Riggs 1903	
	FMNH P25112, DV 7	0,98			Riggs 1903	
	FMNH P25112, DV 8	0,89			Riggs 1903	
	FMNH P25112, DV 9	0,82			Riggs 1903	deformed
	FMNH P25112, DV 10	0,93			Riggs 1903	deformed
Apatosaurus sp. ML 418	ML 418, pDV	0,87	0,9	0,9	Mannion et al., 2012	measured from figure; corrected mean based on discrepancy in ratios from figures or table in *Apatosaurus* NSMT-PV 20375
Apatosaurinae indet. SMA 0087	SMA 0087, DV 5	0,98	0,9		pers. obs.	deformed
	SMA 0087, DV 6	1,07			pers. obs.	deformed
	SMA 0087, DV 8	0,71			pers. obs.	deformed
Supersaurus vivianae BYU	BYU 4503, mDV	1,03	1,3	lower	Jensen, 1985	measured from figure
	BYU 9044, pDV	1,50			Curtice et al., 1996	deformed
	BYU 9044, pDV	1,26			Curtice et al., 1996	retrodeformed
Dystylosaurus edwini BYU 4503	BYU 4503, mDV	1,03	1,0	higher	Jensen, 1985	measured from figure
Dinheirosaurus lourinhanensis ML 414	ML 414		short		pers. obs.	no measurements available, nor pictures in posterior view
Diplodocus carnegii CM 84	CM 84, DV 4	1,05	1,0		Hatcher, 1901	
	CM 84, DV 5	1,08			Hatcher, 1901	
	CM 84, DV 6	1,18			Hatcher, 1901	
	CM 84, DV 7	1,10			Hatcher, 1901	
	CM 84, DV 8	0,96			Hatcher, 1901	
	CM 84, DV 9	0,96			Hatcher, 1901	
	CM 84, DV 10	0,85			Hatcher, 1901	
	CM 84, DV 4	1,07			Hatcher, 1901	measured from figure
	CM 84, DV 10	0,80			Hatcher, 1901	measured from figure
Diplodocus sp. AMNH 223			short		pers. obs.	no measurements available, nor pictures in posterior view
Diplodocus sp. USNM 10865			short		pers. obs.	no measurements available, nor pictures in posterior view
Diplodocus sp. DMNS 1494			short		pers. obs.	no measurements available, nor pictures in posterior view
Seismosaurus hallorum NMMNH 3690	NMMHN 3690, DV 8	0,99	1,0	1,0	Herne and Lucas, 2006	measured from figure; corrected mean based on discrepancy in ratios from figures or table in *Diplodocus* CM 84
Barosaurus sp. AMNH 6341	AMNH 6341, DV 8	0,74	0,7	higher	McIntosh, 2005	
Barosaurus sp. CM 11984	CM 11984, pDV	0,79	0,8	0,8	pers. obs.	measured from photo, corrected mean based on discrepancy in ratios from figures or table in *Diplodocus* CM 84

Table 6.36: Posterior dorsal centrum ratios.

Taxon	Specimen	cl/hct	Mean 1	wct/hct	Mean 2	Reference	Comments
Shunosaurus lii	T5401, DV 10	1,07	1,0	0,73	0,8	Zhang, 1988	
	T5401, DV 11	0,95		0,68		Zhang, 1988	
	T5401, DV 12	0,86		0,64		Zhang, 1988	
	T5401, DV 13	0,73		0,50		Zhang, 1988	
	T5403, DV 10	1,12		0,99		Zhang, 1988	
	T5403, DV 11	1,06		1,03		Zhang, 1988	
	T5403, DV 12	1,12		1,12		Zhang, 1988	
	T5403, DV 13	0,93		1,07		Zhang, 1988	
Spinophorosaurus nigerensis	GCP-CV-4229, pCV	0,65	0,7			Remes et al., 2009	measured from figure
	GCP-CV-4229, pCV	0,84				Remes et al., 2009	measured from figure
Omeisaurus	T5701, DV 9	0,81	0,7	0,67	0,7	He et al., 1988	
	T5701, DV 10	0,78		0,72		He et al., 1988	
	T5701, DV 11	0,82		0,61		He et al., 1988	
	T5701, DV 12	0,78				He et al., 1988	
	T5704, DV 9	0,58		0,51		He et al., 1988	
	T5704, DV 10	0,67		1,00		He et al., 1988	
	T5704, DV 11	0,77		0,88		He et al., 1988	
	T5704, DV 12	0,67		0,64		He et al., 1988	
	T5705, DV 9	0,74		0,57		He et al., 1988	
	T5705, DV 10	0,69		0,77		He et al., 1988	
	T5705, DV 11	0,56		0,62		He et al., 1988	
	T5705, DV 12	0,81		1,00		He et al., 1988	
Mamenchisaurus	ZDM 0083, DV 9	0,60	0,6	0,79	0,8	Ouyang and Ye, 2002	
	ZDM 0083, DV 10	0,63		0,77		Ouyang and Ye, 2002	
	ZDM 0083, DV 11	0,54		0,69		Ouyang and Ye, 2002	
	ZDM 0083, DV 12	0,57		0,75		Ouyang and Ye, 2002	
Jobaria tiguidensis	F144, DV 8	1,06	0,9	high		O. Mateus, pers. comm., 2010	measured from photo
	F145, DV 9	0,90				O. Mateus, pers. comm., 2010	measured from photo
	F146, DV 10	0,75				O. Mateus, pers. comm., 2010	measured from photo
Losillasaurus giganteus type	MCNV Lo-11, pDV	0,78	0,8	0,80	0,8	pers. obs.	measured from photo
Camarasaurus	BYU 9047, DV 9	0,86	0,8	1,05	1,2	McIntosh et al., 1996b	
	BYU 9047, DV 10	0,86		1,02		McIntosh et al., 1996b	length estimated
	BYU 9047, DV 11	0,85		1,08		McIntosh et al., 1996b	
	BYU 9047, DV 12	0,84		1,15		McIntosh et al., 1996b	
	WDC A, pDV	1,09		1,30		Ikejiri, 2004	
	WDC A, pDV	0,69		1,29		Ikejiri, 2004	
	WDC A, pDV	0,69		1,38		Ikejiri, 2004	
	WDC B, pDV	1,09		1,02		Ikejiri, 2004	
	WDC B, pDV	0,67		1,21		Ikejiri, 2004	
	WDC B, pDV	0,75		1,07		Ikejiri, 2004	
Lourinhasaurus alenquerensis lectotype	MIGM		short			pers. obs.	no measurements available
Giraffatitan brancai	MB.R.3822, pDV	0,93	1,0		1,8	pers. obs.	measured from photo
	MB.R. ?, DV 10			1,78		Taylor, 2009	measured from figure
	MB.R. ?, DV 12	1,17		1,91		Taylor, 2009	measured from figure
Brachiosaurus sp. SMA 0009	SMA 0009, pDV	1,84	1,8			Carballido et al., 2012a	measured from figure
Brachiosaurus altithorax	FMNH P25107, DV 9	1,39	1,6	1,07	1,1	Riggs, 1904	
	FMNH P25107, DV 10	1,62		1,19		Riggs, 1904	
	FMNH P25107, DV 11	1,63		1,11		Riggs, 1904	
	FMNH P25107, DV 12	1,59		1,11		Riggs, 1904	
Haplocanthosaurus priscus	CM 879, DV 10	0,73	0,8			Hatcher, 1903	measured from figure
	CM 879, DV 11	0,79				Hatcher, 1903	measured from figure
	CM 879, DV 12	0,78				Hatcher, 1903	measured from figure
	CM 879, DV 13	0,79				Hatcher, 1903	measured from figure
	CM 572, DV 9			0,78	0,9	Hatcher, 1903	measured from figure
	CM 572, DV 10			0,89		Hatcher, 1903	measured from figure
	CM 572, DV 11			0,92		Hatcher, 1903	measured from figure
	CM 572, DV 12			0,99		Hatcher, 1903	measured from figure
Nigersaurus taqueti	DV 9			1,04	1,0	Carballido et al., 2012b	measured from figure
Demandasaurus darwini	MDS-RVII.798, pDV	0,94	0,9	0,94	0,9	Torcida Fernández-Baldor et al., 2011	
Amphicoelias altus AMNH 5764	AMNH 5764, pDV	1,14	1,1	0,95	0,9	Osborn and Mook, 1921	measured from figure
Dicraeosaurus hansemanni	MB.R.4886, DV 9	1,14	1,0	0,86	0,9	Janensch, 1929	
	MB.R.4886, DV 10	1,00		0,82		Janensch, 1929	
	MB.R.4886, DV 11	1,03		0,88		Janensch, 1929	
	MB.R.4886, DV 12	0,90		0,98		Janensch, 1929	
Brachytrachelopan mesai	MPEF PV 1716, DV 9	0,74	0,8			J. Carballido, pers. comm., 2013	measured from photo
	MPEF PV 1716, DV 10	0,83				J. Carballido, pers. comm., 2013	measured from photo
Amargasaurus cazaui	MACN-N 15, pDV	1,30	1,2			Salgado and Bonaparte, 1991	measured from figure
	MACN-N 15, pDV	1,17				Salgado and Bonaparte, 1991	measured from figure
Apatosaurus ajax YPM 1860	YPM 1860, pDV			wide		pers. obs.	
Brontosaurus excelsus YPM 1980	YPM 1980, DV 8			1,29	1,3	Ostrom and McIntosh, 1966	measured from figure
Apatosaurus louisae CM 3018	CM 3018, DV 7	0,85	0,8	1,01	1,0	Gilmore, 1936	measured from figure
	CM 3018, DV 8	0,85		0,95		Gilmore, 1936	measured from figure
	CM 3018, DV 9	0,78		0,95		Gilmore, 1936	measured from figure
Apatosaurus parvus UW 15556	UW 15556, DV 8	0,96	0,9	1,37	1,3	Gilmore, 1936	measured from figure
	UW 15556, DV 9	0,83		1,28		Gilmore, 1936	measured from figure
Eobrontosaurus yahnahpin Tate-001	Tate-001, pDV	0,93	0,9	subequal		P. Mannion, pers. comm., 2012	measured from photo

Table 6.36: continued.

Apatosaurus ajax NSMT-PV 20375	NSMT-PV 20375, DV 8	0,90	0,7	1,10	1,1	Upchurch et al. 2004b	
	NSMT-PV 20375, DV 9	0,61		1,00		Upchurch et al. 2004b	
	NSMT-PV 20375, DV 10	0,69		1,12		Upchurch et al. 2004b	
Apatosaurus sp. AMNH 460	AMNH 460, DV 10	1,02	1,0			O. Mateus, pers. comm., 2010	measured from photo
Apatosaurus sp. FMNH P25112	FMNH P25112, DV 8	0,81	0,7	1,11	1,0	Riggs 1903	centrum length deformed
	FMNH P25112, DV 9	0,64		1,05		Riggs 1903	
	FMNH P25112, DV 10	0,61		0,98		Riggs 1903	
Apatosaurus sp. ML 418	ML 418, pDV			1,22	1,2	Mannion et al., 2012	measured from figure
Apatosaurinae indet. SMA 0087	SMA 0087, DV 5	0,99	1,0	0,7	0,8	pers. obs.	transversely compressed
	SMA 0087, DV 6	1,04		0,69		pers. obs.	transversely compressed
	SMA 0087, DV 7	1,01				pers. obs.	transversely compressed
	SMA 0087, DV 8	0,82		0,94		pers. obs.	transversely compressed
	SMA 0087, DV 9	0,90		0,88		pers. obs.	transversely compressed
Supersaurus vivianae BYU	BYU 9044, pDV	1,22	1,2	1,05	1,1	Jensen, 1985; D. Lovelace, pers. comm., 2013	measured from figure
Supersaurus vivianae WDC DMJ-021	WDC DMJ-021, pDV	1,16	1,2	1,20	1,2	D. Lovelace, pers. comm., 2013	measured from photo
	WDC DMJ-021, pDV	1,25		1,15		D. Lovelace, pers. comm., 2013	measured from photo
Dinheirosaurus lourinhanensis ML 414	ML 414, DV 7	1,27	1,3			Mannion et al., 2012	centrum length without ball
	ML 414, DV 8	1,51				Mannion et al., 2012	centrum length without ball
	ML 414, DV 9	1,19				Mannion et al., 2012	centrum length without ball
Diplodocus carnegii CM 84	CM 84, DV 9	0,98	0,9	1,04	1,1	Hatcher, 1901	width measured from figure
	CM 84, DV 10	0,86		1,12		Hatcher, 1901	width measured from figure
Diplodocus carnegii CM 94	CM 94, pDV		short			pers. obs.	no measurements available
Diplodocus sp. USNM 10865	USNM 10865, DV 10	0,86	0,9			Gilmore, 1932	measured from figure
Diplodocus sp. DMNS 1494	DNMS 1494, pDV		short			pers. obs.	no measurements available
Seismosaurus hallorum NMMNH 3690	NMMNH 3690, DV 8	0,91	0,9			Herne and Lucas, 2006	measured from figure
Galeamopus shellensis SMA 0011	SMA 0011, DV 8	0,72	0,8	high		pers. obs.	centrum length without ball
	SMA 0011, DV 9	0,75				pers. obs.	centrum length without ball
	SMA 0011, DV 10	0,81				pers. obs.	centrum length without ball
Barosaurus lentus YPM 429	YPM 429, DV 8	0,76	0,8	1,09	1,1	Lull, 1919	DV 9 according to Lull, 1919
	YPM 429, DV 9			1,04		Lull, 1919	DV 10 according to Lull, 1919
Barosaurus sp. AMNH 6341	AMNH 6341, DV 7	0,95	0,9	1,00	1,0	McIntosh, 2005	
	AMNH 6341, DV 8	0,92		0,98		McIntosh, 2005	
	AMNH 6341, DV 9	0,79		0,88		McIntosh, 2005	
Barosaurus sp. CM 11984	CM 11984, DV 7	1,27	1,3	1,16	1,2	McIntosh, 2005	measured from figure
Cetiosauriscus stewarti NHMUK R3078	NHMUK R3078, pDV	0,49	0,5	0,95	0,9	Woodward, 1905	measured from figure
Dystrophaeus viaemalae USNM 2364	USNM 2364, DV			1,0	1,0	pers. obs.	measured from photo, width estimated

C274: Posterior dorsal vertebrae, spinoprezygapophyseal lamina: absent or greatly reduced (0); present (1) (Upchurch et al., 2007; modified; Fig. 6.72).

Comments. Reduced sprl fade out anteroventrally and/or join the prsl at a very ventral level.

C275: Posterior dorsal postzygapophyses: almost horizontal, such that the two articular facets include a wide angle (0); articular facets oblique, including an almost 90° angle (1) (New; Fig. 6.66).

Comments. Some diplodocine taxa have curved facets. These are interpreted as horizontal.

C276: Posterior dorsal vertebrae, hyposphene-hypantrum system: well developed, rhomboid shape up to last element (0); weakly developed, mainly as a laminar articulation (1) (Carballido et al., 2012b; modified; Fig. 6.63; Tab. 6.29).

Comments. Taxa without hyposphenes are scored as unknown.

C277: Posterior dorsal neural arches: spinopostzygapophyseal laminae (spol) single (0); spol divided near postzygapophyses (1) (Wilson, 2002; Fig. 6.63).

Comments. The spol can bifurcate in two ways in different taxa: rebbachisaurids have ventrally forked laminae, whereas in some diplodocids the spol bifurcates dorsally, creating a medial and a lateral branch. The presence of a medial spol is accounted for in character 278, the present one describes the ventral bifurcation.

C278: Posterior dorsal vertebrae, medial spinopostzygapophyseal lamina (mspol): absent (0); present and forms part of the median posterior lamina (1) (Carballido et al., 2012b; Fig. 6.66).

Comments. The mspol can either be connected with the lspol ventrally or they can remain separated.

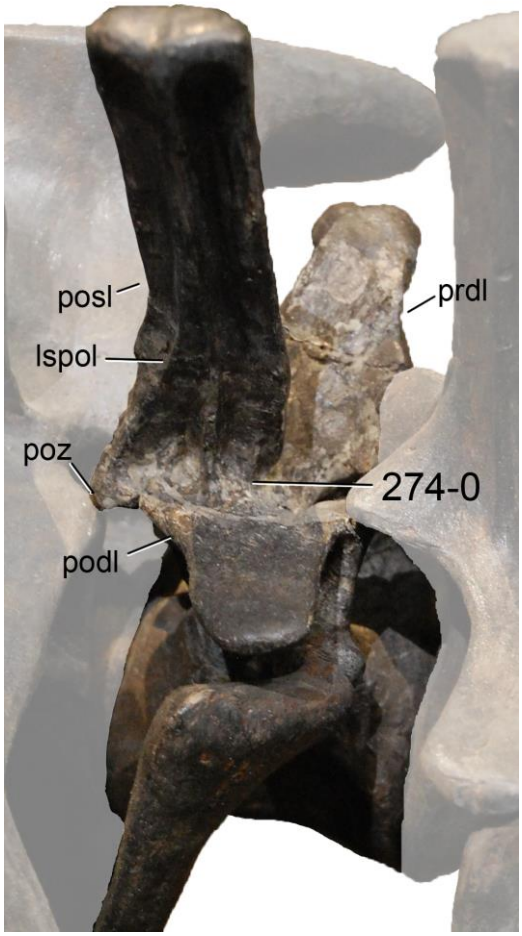

Figure 6.72: Posterior dorsal vertebra of *Elosaurus parvus* CM 566 in lateral anterodorsal view. Note the greatly reduced spinoprezygapophyseal lamina, which does not reach the prezygapophysis (C274-0). Only the base of the neural arch is preserved (see Peterson and Gilmore, 1902). Abb.: lspol, lateral spinopostzygapophyseal lamina; podl, postzygodiapophyseal lamina; posl, postspinal lamina; poz, postzygapophysis; prdl, prezygodiapophyseal lamina.

C279: Posterior dorsal vertebrae, base of neural spines just above transverse processes: longer than wide (0); subequal in width and length (1) (New).

Comments. This is the second character about spine width to length, inspired by a character from Wilson (2002) (see character 266).

C280: Posterior dorsal neural spines, orientation at its base: vertical (0); anteriorly inclined (1) (New; Fig. 6.70).

Comments. Anterior inclination can be restricted to the very base of the neural spine, as is the case in *Apatosaurus louisae* CM 3018 (Fig. 6.70A). The best indication for the inclination is the prsl in lateral view.

C281: Posterior dorsal neural spines, midline cleft along the dorsal surface: absent (0); present (1) (Mannion et al., 2012; modified; Fig. 6.65; Tab. 6.33).

Comments. The midline cleft described herein corresponds to the notched spines of Wedel and Taylor (2013). Not all posterior dorsal spines have to be notched in order to be scored as apomorphic.

C282: Posterior dorsal and/or sacral neural spines (not including arch), height: less than 2 times centrum length (0); 2 to 3 times centrum length (1); more than 3 times centrum length (2) (Mannion et al., 2012; modified; Tab. 6.37).

Comments. Neural spine height is measured from the top of the postzygapophyses to the highest point of the spine, vertically. Centrum length does not include the anterior ball. The original version (Mannion et al., 2012) was restricted here to posterior dorsal and sacral vertebrae only, as mid-dorsal elements of diplodocids considerably lower the ratio in some cases (Tab. 6.37). Also, state boundaries are adapted. The character is treated as ordered.

Table 6.37: Mid- and posterior dorsal, and sacral vertebrae, neural spine height (not including arch)/centrum length without ball.

Taxon	Specimen	Ratio	Mean mDV	Mean pDV	Mean SV	Mean pDV + SV	Mean tot	Reference	Comments
Shunosaurus lii	T5401, DV 7	1,583	1,58			1,77	1,73	Zhang, 1988	measured from figure
	T5401, DV 11	1,670		1,89				Zhang, 1988	measured from figure
	T5401, DV 12	2,109						Zhang, 1988	measured from figure
	T5401, SV 1	1,803			1,65			Zhang, 1988	measured from figure
	T5401, SV 4	1,500						Zhang, 1988	measured from figure
Spinophorosaurus nigerensis	GCP-CV-4229, pDV	1,337		1,34		1,34	1,34	Remes et al., 2009	measured from figure
Omeisaurus	T5701, DV 6	1,243	1,22				1,22	He et al., 1988	measured from figure
	T5701, DV 7	1,189						He et al., 1988	measured from figure
Mamenchisaurus	ZDM 0083, DV 6	1,027	1,08			1,19	1,15	Ouyang and Ye, 2002	measured from figure
	ZDM 0083, DV 8	1,139						Ouyang and Ye, 2002	measured from figure
	ZDM 0083, DV 10	1,082		1,15				Ouyang and Ye, 2002	measured from figure
	ZDM 0083, DV 11	1,188						Ouyang and Ye, 2002	measured from figure
	ZDM 0083, DV 12	1,168						Ouyang and Ye, 2002	measured from figure
	ZDM 0083, SV 5	1,322			1,32			Ouyang and Ye, 2002	measured from figure
Jobaria tiguidensis	F144, DV 8	1,778	1,78			1,95	1,89	O. Mateus, pers. comm., 2010	measured from photo
	F145, DV 9	1,881		1,95				O. Mateus, pers. comm., 2010	measured from photo
	F146, DV 10	2,012						O. Mateus, pers. comm., 2010	measured from photo
Losillasaurus giganteus type	MCNV Lo-11	1,278		1,28		1,28	1,28	pers. obs.	measured from photo
Camarasaurus	AMNH 5760/5761, DV 4	0,694	0,92	1,53	1,17	1,47	1,19	Osborn and Mook, 1921	measured from figure
	AMNH 5760/5761, DV 5	0,756						Osborn and Mook, 1921	measured from figure
	AMNH 5760/5761, DV 6	1,039						Osborn and Mook, 1921	measured from figure
	AMNH 5760/5761, DV 7	1,139						Osborn and Mook, 1921	measured from figure
	AMNH 5760/5761, DV 8	1,315						Osborn and Mook, 1921	measured from figure
	AMNH 5760/5761, DV 9	1,493						Osborn and Mook, 1921	measured from figure
	AMNH 5760/5761, DV 10	1,944						Osborn and Mook, 1921	measured from figure
	AMNH 5760/5761, DV 11	1,963						Osborn and Mook, 1921	measured from figure
	AMNH 5760/5761, SV 5	1,167						Osborn and Mook, 1921	measured from figure
	BYU 9047, DV 11	1,165						Jensen, 1988	measured from figure
	WDC A, DV 5	0,416						Ikejiri, 2004	measured from figure
	WDC A, DV 6	1,046						Ikejiri, 2004	measured from figure
	WDC A, DV 12	1,325						Ikejiri, 2004	measured from figure
	WDC B, DV 12	1,267						Ikejiri, 2004	measured from figure
Apatosaurus grandis YPM 1901	YPM 1901, mDV	0,724	0,72				0,72	Wilson and Sereno, 1998	measured from figure
Giraffatitan brancai	MB.R.3822, pDV	0,947	1,46	1,16		1,16	1,31	pers. obs.	measured from photo
	MB.R. ?, DV 4	1,685						Taylor, 2009	measured from figure
	MB.R. ?, DV 8	1,235						Taylor, 2009	measured from figure
	MB.R. ?, DV 12	1,375						Taylor, 2009	measured from figure

Table 6.37: continued.

Brachiosaurus sp. SMA 0009	SMA 0009, pDV	0,969		0,97		0,97	0,97	Carballido et al., 2012a	measured from figure
Brachiosaurus altithorax	FMNH P25107, DV 6	0,986	0,97			0,91	0,94	Taylor, 2009	measured from figure
	FMNH P25107, DV 8	0,952						Taylor, 2009	measured from figure
	FMNH P25107, DV 10	0,852		0,91				Taylor, 2009	measured from figure
	FMNH P25107, DV 12	0,977						Taylor, 2009	measured from figure
Isisaurus colberti	ISIR355/15, mDV	1,880	1,88				1,88	Jain and Bandyopadhyay, 1997	measured from figure
Haplocanthosaurus priscus	CM 879, DV 5	1,295	1,55			1,71	1,62	Hatcher, 1903	measured from figure
	CM 879, DV 6	1,672						Hatcher, 1903	measured from figure
	CM 879, DV 7	1,578						Hatcher, 1903	measured from figure
	CM 879, DV 8	1,575						Hatcher, 1903	measured from figure
	CM 879, DV 9	1,637						Hatcher, 1903	measured from figure
	CM 879, DV 10	1,749		1,71				Hatcher, 1903	measured from figure
	CM 879, DV 11	1,736						Hatcher, 1903	measured from figure
	CM 879, DV 12	1,556						Hatcher, 1903	measured from figure
	CM 879, DV 13	1,781						Hatcher, 1903	measured from figure
Limaysaurus tessonei							2 – 4	Carballido et al., 2012b	
Nigersaurus taqueti							2 – 4	Carballido et al., 2012b	
Demandasaurus darwini							> 4	Carballido et al., 2012b	
Amphicoelias altus AMNH 5764	AMNH 5764, pDV	2,243		2,24		2,24	2,24	Osborn and Mook, 1921	measured from figure
Dicraeosaurus hansemanni	MB.R.4886, DV 4	2,949	2,73				2,73	Schwarz-Wings, 2009	measured from figure
	MB.R.4886, DV 8	2,511						Schwarz-Wings, 2009	measured from figure
Brachytrachelopan mesai	MPEF PV 1716, DV 5	3,071	3,01			3,25	3,09	J. Carballido, pers. comm., 2013	measured from photo
	MPEF PV 1716, DV 7	2,955						J. Carballido, pers. comm., 2013	measured from photo
	MPEF PV 1716, SV 1	3,250			3,25			J. Carballido, pers. comm., 2013	measured from photo
Amargasaurus cazaui	MACN-N 15, pDV	2,918		3,36		3,36	3,36	Salgado and Bonaparte, 1991	measured from figure
	MACN-N 15, pDV	3,807						Salgado and Bonaparte, 1991	measured from figure
Apatosaurus ajax YPM 1860	YPM 1860, pDV	2 – 4					2 – 4	pers. obs.	no measurements available
Brontosaurus excelsus YPM 1980	YPM 1980, DV 5	1,444	1,44				1,44	Ostrom and McIntosh, 1966	measured from figure
Apatosaurus louisae CM 3018	CM 3018, DV 3	1,260	1,63			2,71	2,17	Gilmore, 1936	measured from figure
	CM 3018, DV 4	1,422						Gilmore, 1936	measured from figure
	CM 3018, DV 5	1,890						Gilmore, 1936	measured from figure
	CM 3018, DV 6	1,967						Gilmore, 1936	measured from figure
	CM 3018, DV 7	2,426		2,66				Gilmore, 1936	measured from figure
	CM 3018, DV 8	2,530						Gilmore, 1936	measured from figure
	CM 3018, DV 9	3,032						Gilmore, 1936	measured from figure
	CM 3018, SV 5	2,846			2,85			Gilmore, 1936	measured from figure
Apatosaurus parvus UW 15556	UW 15556, DV 4	1,820	1,82				1,82	Gilmore, 1936	measured from figure
Apatosaurus minimus AMNH 675	AMNH 675, SV 6	2,236			2,24	2,24	2,24	Mook, 1917	measured from figure
Eobrontosaurus yahnahpin Tate-001	Tate-001, pDV	1,924		1,92		1,92	1,92	P. Mannion, pers. comm., 2012	measured from photo
Apatosaurus ajax NSMT-PV 20375	NSMT-PV, DV 7	2,120	2,12			2,21	2,16	Upchurch et al., 2004b	measured from figure
	NSMT-PV, DV 10	2,207		2,21				Upchurch et al., 2004b	measured from figure

Table 6.37: continued.

Apatosaurinae indet. SMA 0087	SMA 0087, DV 5	1,851	2,18		2,31	2,22	pers. obs.	
	SMA 0087, DV 7	2,516					pers. obs.	
	SMA 0087, DV 8	2,306		2,31			pers. obs.	
Supersaurus vivianae BYU	BYU 4503, mDV	1,322	1,32		1,49	1,41	Curtice and Stadtman, 2001	measured from figure
	BYU 9044, pDV	1,488		1,49			Jensen, 1985	measured from figure
Supersaurus vivianae WDC DMJ-021	WDC DMJ-021, pDV	1,788		1,79	1,79	1,79	D. Lovelace, pers. comm., 2013	measured from photo
Dystylosaurus edwini BYU 4503	BYU 4503, mDV	1,322	1,32			1,32	Curtice and Stadtman, 2001	measured from figure
Dinheirosaurus lourinhanensis ML 414	ML 414, DV 7	1,724	1,72			1,72	Mannion et al., 2012	
Diplodocus carnegii CM 84	CM 84, DV 5	1,862	1,77		2,23	2,00	Hatcher, 1901	measured from figure
	CM 84, DV 6	1,638					Hatcher, 1901	measured from figure
	CM 84, DV 7	1,825					Hatcher, 1901	measured from figure
	CM 84, DV 8	2,087		2,23			Hatcher, 1901	measured from figure
	CM 84, DV 9	2,268					Hatcher, 1901	measured from figure
	CM 84, DV 10	2,347					Hatcher, 1901	measured from figure
Diplodocus sp. USNM 10865	USNM 10865, DV 10	2,404		2,40	2,40	2,40	Gilmore, 1932	measured from figure
Seismosaurus hallorum NMMNH 3690	NMMNH 3690, DV 8	1,613		1,61	1,61	1,61	Herne and Lucas, 2006	measured from figure
Galeamopus shellensis SMA 0011	SMA 0011, DV 5	1,545	1,55		1,53	1,54	pers. obs.	measured from photo
	SMA 0011, DV 8	1,477		1,53			pers. obs.	measured from photo
	SMA 0011, DV 9	1,584					pers. obs.	measured from photo
Barosaurus lentus YPM 429	YPM 429, DV 8	1,921		1,92	1,92	1,92	Lull, 1919	measured from figure
Barosaurus sp. AMNH 6341	AMNH 6341, DV 5	1,362	1,32		1,51	1,43	McIntosh, 2005	measured from figure
	AMNH 6341, DV 6	1,274					McIntosh, 2005	measured from figure
	AMNH 6341, DV 7	1,248		1,51			McIntosh, 2005	measured from figure
	AMNH 6341, DV 8	1,567					McIntosh, 2005	measured from figure
	AMNH 6341, DV 9	1,702					McIntosh, 2005	measured from figure
Barosaurus sp. CM 11984	CM 11984, DV 7	1,598		1,60	1,60	1,60	McIntosh, 2005	measured from figure

C283: Dorsal ribs, rib head: area between capitulum and tuberculum flat (0); oblique ridge present that connects medial and lateral edge at the base of the rib head (1) (New; Fig. 6.73).
Comments. The ridge marks the posterior surface of the rib head of advanced diplodocines.

C284: Dorsal ribs, proximal pneumatopores: absent (0); present (1) (Wilson, 2002; Fig. 6.73).
Comments. In some taxa, only one rib of the entire series bears a pneumatopore. However, the ability to develop pneumatized ribs appears to be restricted to certain diplodocid groups, therefore the character was applied to this analysis.

C285: Mid-dorsal ribs, orientation of tuberculum: spreading outside from rib shaft (0); following straight direction of rib shaft (1); following medial bend of rib shaft (2) (Gallina and Apesteguía, 2005; Fig. 6.73).

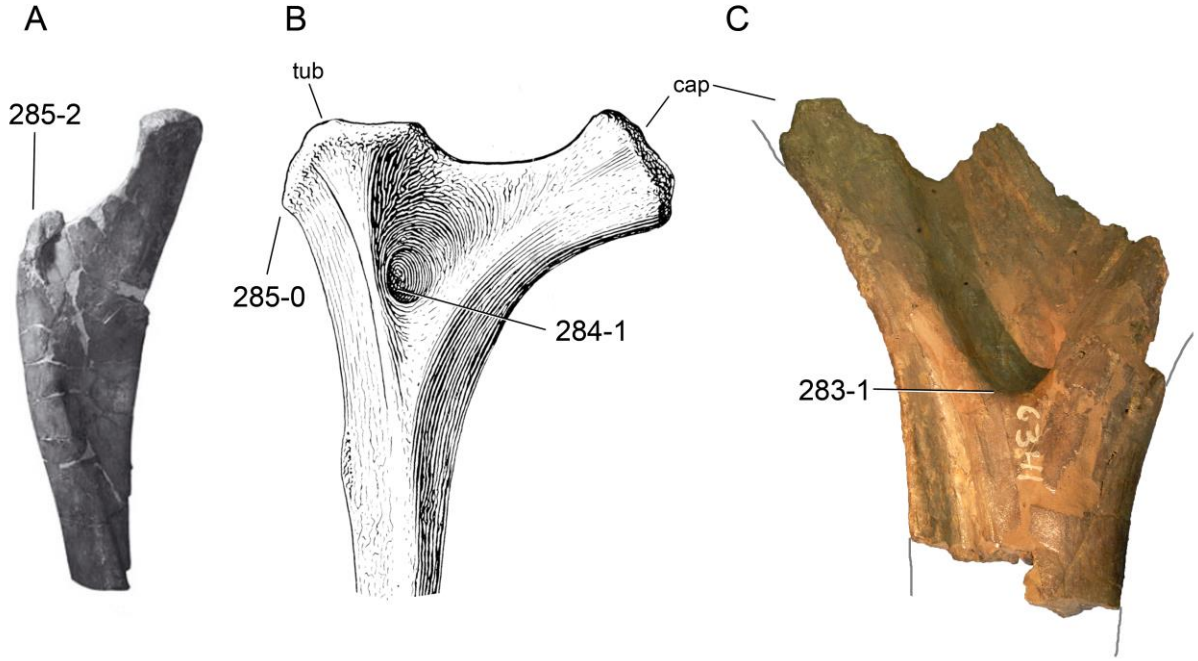

Figure 6.73: Dorsal rib heads of *Suuwassea emilieae* ANS 21122 (A; modified from Harris, 2006b), *Apatosaurus louisae* CM 3018 (B; modified from Gilmore, 1936) and *Barosaurus* sp. AMNH 6341 (C, fragment) in anterior (A, B) and posterior (C) view. Note the transverse ridge (C; C283-1), the pneumatic foramen (B; C284-1), and two of three different orientations of the tuberculum in respect to the rib shaft (C285). Grey lines in C indicate the continuation of the rib if complete. Abb.: cap, capitulum; tub, tuberculum. Not to scale.

Sacral vertebrae

C286: Sacral vertebrae, number: 4 (0); 5 (1); 6 (2) (Salgado et al., 1997; modified; Tab. 6.38).
Comments. Some *Camarasaurus* specimens appear to have six sacral vertebrae, which is usually considered a synapomorphy of advanced titanosauriforms (Tidwell et al., 2005). The addition of a sacral vertebra was suggested to be a sign of very old age (Tidwell et al., 2005). The unusual six sacral vertebrae in the holotype of '*Apatosaurus*' *minimus* AMNH 675 (Mook, 1917) might thus also be ontogenetic.

C287: Sacral vertebral centra, pleurocoels: absent (0); present (1) (Upchurch et al., 2004a; wording modified).

C288: Sacral rib III, ventral surface: smooth (0); with oblique ridge (1) (Mook, 1917; Fig. 6.74).
Comments. The presence of an oblique ridge was proposed as synapomorphy of *Apatosaurus* by Mook (1917), but later regarded as ambiguous and thus of little use to diagnose the genus (McIntosh, 1995). The presence of this ridge is herein used for the first time as phylogenetic character, in order to test its utility. According to Mook (1917), the ridge marks the ventral face of sacral rib II. However, as shown in the holotype specimen if *Brontosaurus amplus* YPM 1981 (Ostrom and McIntosh, 1966), among others, the ridge actually lies on sacral rib III. Some *Camarasaurus* specimens bear oblique ridges on their sacral ribs (e.g. AMNH 690; Osborn, 1904), but not the genotype specimen AMNH 5761. In the present analysis, *Camarasaurus* was thus scored as plesiomorphic.

Table 6.38: Number of sacral vertebrae.

Taxon	Specimen	Number	Reference
Shunosaurus lii		4	Mannion et al., 2013
Spinophorosaurus nigerensis		4	Remes et al., 2009
Omeisaurus		5	Mannion et al., 2013
Mamenchisaurus		5	Mannion et al., 2013
Jobaria tiguidensis	NMB-1695-R	5	pers. obs.
Camarasaurus		5	Mannion et al., 2013
	BYU 9047	5	O. Mateus, pers. comm., 2010
Giraffatitan brancai		5	Mannion et al., 2013
Brachiosaurus sp. SMA 0009	SMA 0009	5	pers. obs.
Brachiosaurus altithorax	FMNH P25107	5	Riggs, 1904
Isisaurus colberti	ISIR335/31	6	Jain and Bandypadhyay, 1997
Haplocanthosaurus priscus	CM 572	5	Hatcher, 1903
Dicraeosaurus hansemanni	MB.R.4886	5	pers. obs.
Amargasaurus cazaui	MACN-N 15	5	Salgado and Bonaparte, 1991
Brontosaurus excelsus YPM 1980	YPM 1980	5	Galiano and Albersdörfer, 2010
Apatosaurus louisae CM 3018	CM 3018	5	Gilmore, 1936
Apatosaurus parvus UW 15556	UW 15556	5	Hatcher, 1903
Apatosaurus minimus AMNH 675	AMNH 675	6	Mook, 1917
Apatosaurus ajax NSMT-PV 20375	NSMT-PV 20375	5	Upchurch et al., 2004b
Apatosaurus sp. FMNH P25112	FMNH P25112	5	Riggs, 1904
Apatosaurinae indet. SMA 0087	SMA 0087	5	pers. obs.
Supersaurus vivianae BYU	BYU 13018	5	Lovelace et al., 2007
Diplodocus carnegii CM 84	CM 84	5	pers. obs.
Diplodocus carnegii CM 94	CM 94	5	Hatcher, 1903
Diplodocus sp. AMNH 223	AMNH 223	5	Osborn, 1899
Diplodocus sp. USNM 10865	USNM 10865	5	pers. obs.
Diplodocus sp. DMNS 1494	DMNS 1494	5	pers. obs.
Galeamopus hayi HMNS 175	HMNS 175	5	pers. obs.
Seismosaurus hallorum NMMNH 3690	NMMNH 3690	5	Lucas et al., 2006
Barosaurus sp. AMNH 6341	AMNH 6341	5	McIntosh, 2005

C289: Sacral neural spines, lateral side, towards the summit: flat, with only the spdl well-developed (0); with distinct horizontal accessory laminae that connect the spdl to the pre- and/or the postspinal lamina (1) (New; Fig. 6.75).

C290: Sacral neural spines, lateral view, spinodiapophyseal lamina: reduced to absent, does not connect the summit and the diapophysis (0); present and distinct, connects spine summit with diapophysis (1) (New; Fig. 6.75).

C291: Sacral neural spines, lateral view, spdl: remain vertical and thus parallel to each other (0); spdl of neighboring spines converge (1) (New; Fig. 6.75).

Comments. Diplodocinae develop a very distinct dorsal widening of the sacral spdl. Together with the inclination of the spines towards the central portion of the sacrum, this often leads to a fusion of these anteroposteriorly widened dorsal ends of the spdl.

Caudal vertebrae

C292: Caudal neural spines, elliptical depression between lateral spinal lamina and postspinal lamina on dorsolateral surface: absent (0); present (1) (Sereno et al., 2007; modified; Fig. 6.76).

Comments. Sereno et al. (2007) initially defined the character as follows: 'elliptical depression between spinodiapophyseal lamina and postspinal lamina on lateral neural spine'. However, the spinal lamina they were most probably referring to (herein called lateral spinal lamina) is usually the united spol and sprl (at least in diplodocids). The character description has thus been reworded in order to clarify this. Sereno et al. (2007) recovered the presence of such a depression as synapomorphy of Nigersaurinae, but actually it is present in any taxon with transversely widened posl, and spol that either fuse with the spdl or the posl. Anterior caudal vertebrae of *Diplodocus* are a good example for this, although they were scored as plesiomorphic by Sereno et al. (2007). Taxa without spdl or posl are scored as unknown.

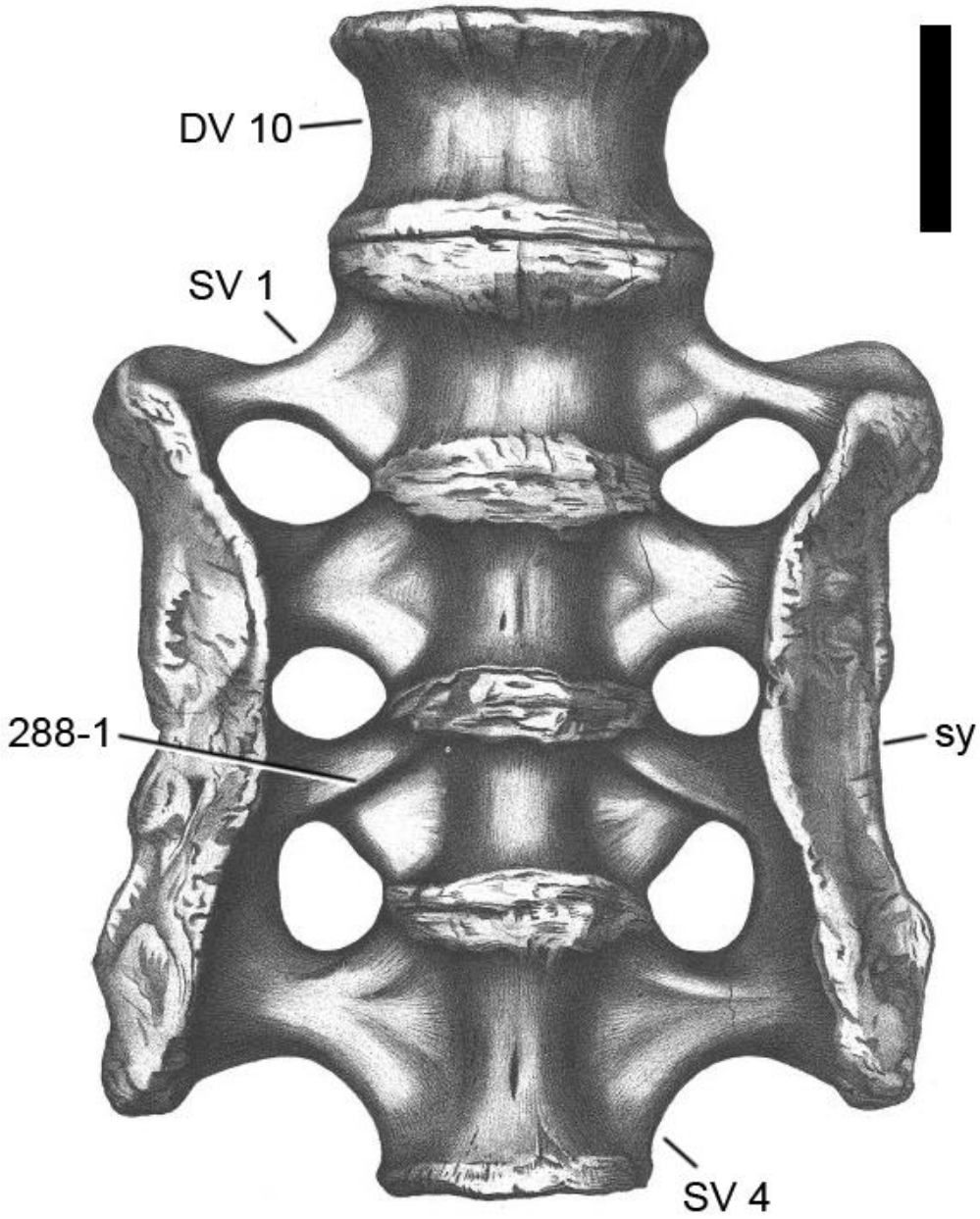

Figure 6.74: Sacrum of *Brontosaurus amplus* YPM 1981 in ventral view (modified from Ostrom and McIntosh 1966), illustrating the oblique ridge on sacral rib III (C288-1). Abb.: DV, dorsal vertebra; SV, sacral vertebra, sy, sacricostal yoke. Scale bar = 20 cm.

C293: Caudal neural spines with triangular lateral processes: absent (0); present (1) (Sereno et al., 2007; Fig. 6.77).

Comments. These processes correspond to the triangular lateral processes of dorsal neural spines, but do not appear to be correlated.

C294: Posterior dorsal, sacral and anterior caudal neural spines, shape in anterior/posterior view: rectangular through most of length (0); 'petal' shaped, expanding transversely through 75% of its length and then tapering (1) (Calvo and Salgado, 1995; Upchurch, 1998; Fig. 6.77).

Comments. Plesiomorphic caudal neural spines can still be transversely expanded at their ends. Also, taxa with gradually expanding neural spines that do not taper dorsally are herein scored as plesiomorphic, as without the tapering, the spines do not develop the 'petal' shape typical for rebbachisaurs and dicraeosaurs.

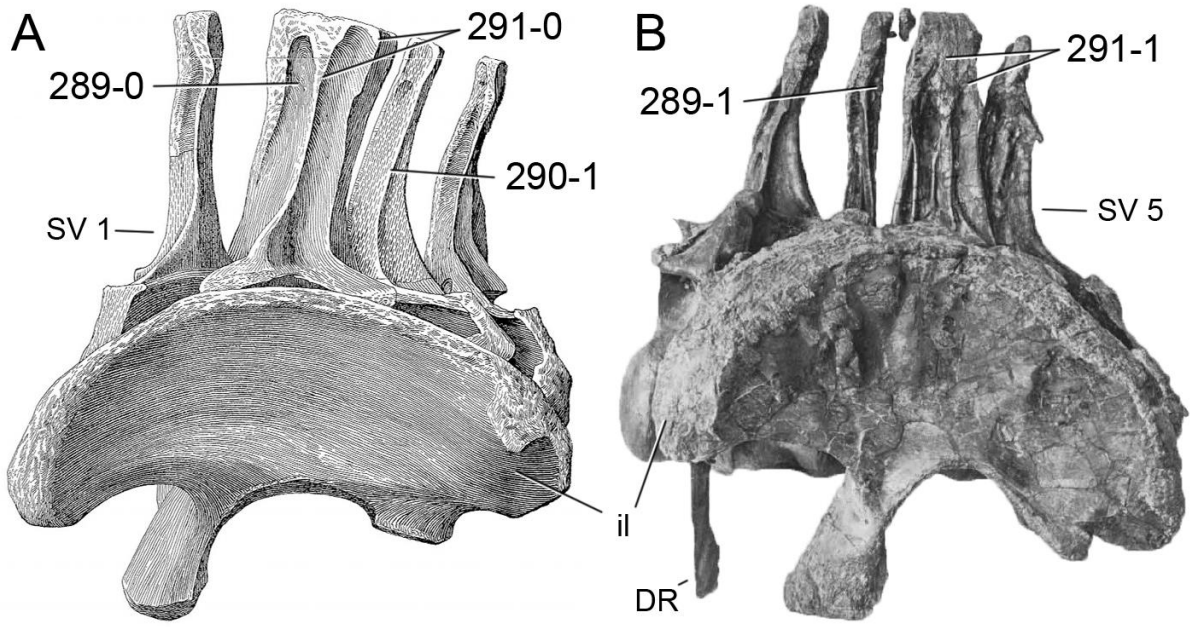

Figure 6.75: Sacra of *Apatosaurus* sp. UW 15556 (A; modified from Hatcher, 1903) and *Diplodocus* sp. AMNH 223 (B; modified from Osborn, 1899) in left lateral view. Note the flat (A; C289-0) instead of ornamented sacral neural spine top (B; C289-1), the spdl that extends ventrally to the diapophysis (A; C290-1), and the parallel (A; C291-0) in contrast to converging neural spines (B; C291-1). Abb.: DR, dorsal rib; il, ilium; SV, sacral vertebra. Scaled to the same height.

C295: First caudal centrum, articular face shape: flat (0); procoelous (1); opisthocoelous (2) (Wilson, 2002; modified).

Comments. The fourth state (biconvex) of Wilson (2002) was deleted as no used OTU has biconvex first caudal vertebrae. The probable brachiosaurid SMA 0009 and *Demandasaurus* have platycoel first caudal vertebrae (Torcida Fernández-Baldor et al., 2011; Carballido et al., 2012a), and are herein scored as opisthocoelous rather than flat.

C296: Anterior-most caudal centra, transverse cross-section: sub-circular with rounded ventral margin (0); 'heart'-shaped with an acute ventral ridge (1) (Gilmore, 1936; Upchurch et al., 2004b; wording modified; Fig. 6.78).

Comments. Taxa with ventral hollows in their anterior caudal centra are scored as plesiomorphic, because the presence of the ventral ridge is regarded as the crucial trait this character codes for.

C297: Anterior-most caudal centra, pneumatic fossae: reduced to absent (0); large pleurocoels (1) (New; Fig. 6.76).

Comments. Some apatosaur specimens and *Supersaurus* have distinct pleurocoels in their anterior-most caudal centra, whereas in anterior centra (as defined in table 6.3), pleurocoels are reduced to foramina in these taxa (see e.g. Riggs, 1903). The current character is thus added to the usual one coding for pleurocoels in anterior caudal vertebrae in general.

C298: Anterior-most caudal vertebrae, additional pneumatic fossa on posterodorsal corner of centrum: absent (0); present (1) (New; Fig. 6.76).

Comments. In lateral views, these additional pneumatic foramina are often obscured by the transverse process.

C299: Anterior-most caudal transverse processes, shape: triangular, tapering distally (0); wing-like (1) (McIntosh, 1990b; Yu, 1993; modified; Fig. 6.77).

Comments. A transverse process is herein interpreted as wing-like if it has a distinct shoulder, i.e. an angled bump on its dorsolateral edge.

C300: Anterior-most caudal vertebrae, transition from 'fan'-shaped to ' normal' caudal ribs: between Cd 1 and 2 (0); Cd4 and Cd5 (1); Cd5 and Cd6 (2); Cd6 and Cd7 (3); Cd7 and Cd8 or more posteriorly (4) (Upchurch et al., 2004b; modified; Tab. 6.39).

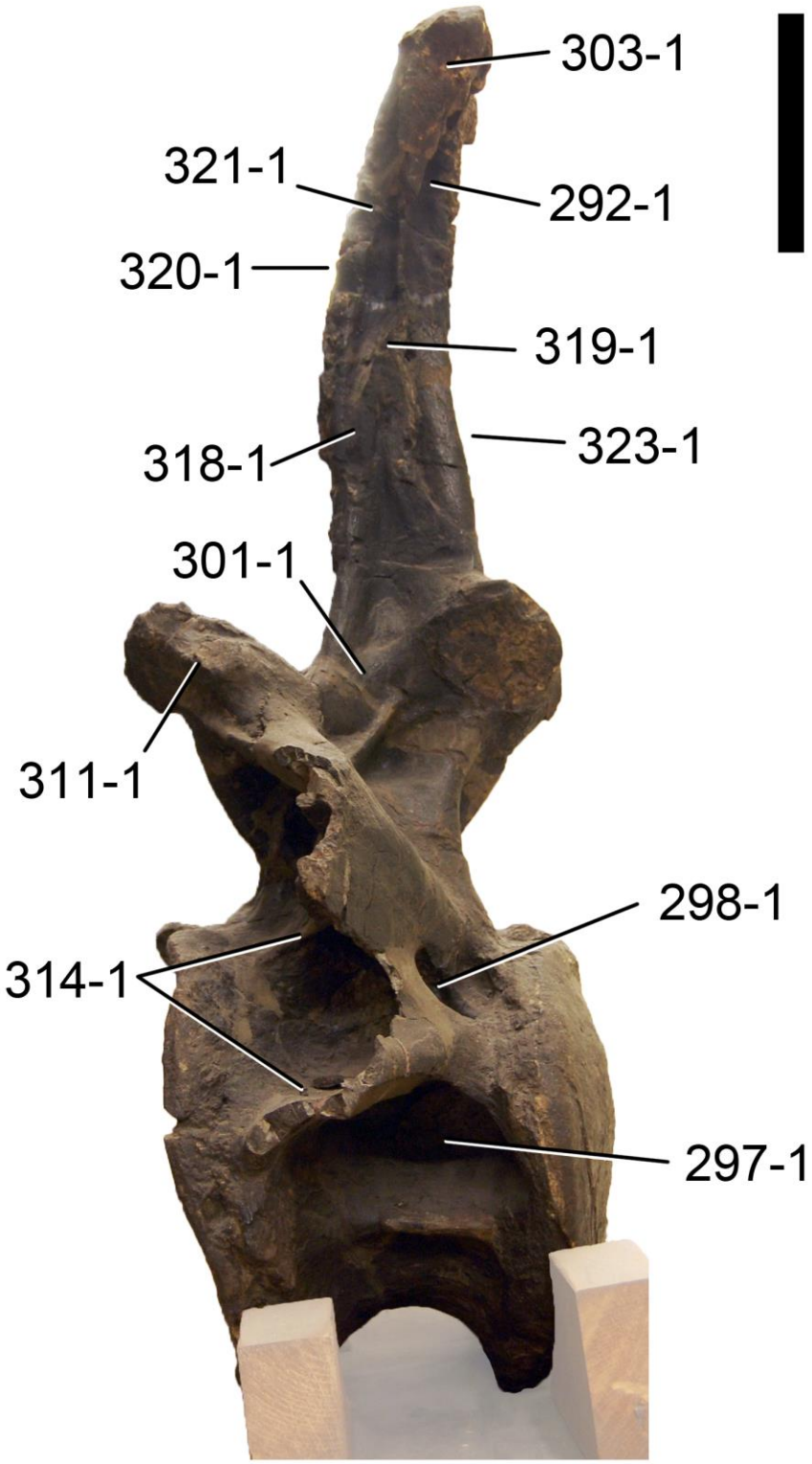

Figure 6.76: Anterior caudal vertebra of *Diplodocus carnegii* CM 94 in left lateral view, illustrating various characters typical for the genus: a depression between the lateral spinal lamina and the postspinal lamina (C292-1), the large pleurocoel (C297-1), an additional pneumatic foramen posterodorsally in the caudal centrum (C298-1), the accessory lamina between pre- and postzygapophysis (C301-1), a dorsally widened lateral spinal lamina (C303-1), a pre-epipophysis (C311-1), the double anterior centrodiapophyseal lamina (C314-1), the distinct spinoprezygapophyseal lamina that extends onto the lateral surface of the spine (C318-1) and contacts the spinopostzygapophyseal lamina (C319-1), the presence of a prespinal lamina (C320-1) with a thickened anterior rim (C321-1), and the presence of a postspinal lamina (C323-1). Scale bar = 10 cm.

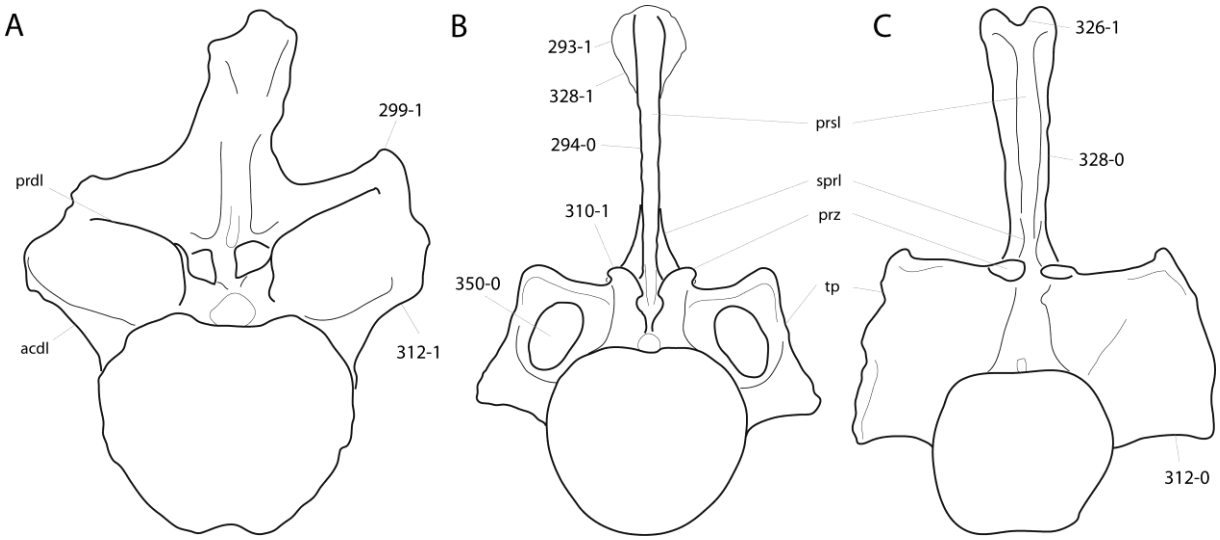

Figure 6.77: Anterior caudal vertebrae of *Demandasaurus darwini* MDS-RVII,610 (A; traced from Torica Fernandéz-Baldor et al., 2011), *Brontosaurus excelsus* YPM 1980 (B; traced from Ostrom and McIntosh, 1966), and *Diplodocus carnegii* CM 84 (C; traced from Hatcher, 1901) in anterior view. Note the lateral triangular processes (B; C293-1), the mostly rectangular outline of the spine (B; C294-0), the wing-like transverse processes (A; C299-1), the convex prezygapophyses (B; C310-1), the laterally (C; C312-0) or dorsally directed ventral surface of the transverse process (A; C312-1), the notched neural spine top (C; C326-1), the gradual (C; C328-0) or abrupt distal expansion of the spine (B; C328-1), and the foramen piercing the transverse process (B; C350-0). Abb.: prsl, prespinal lamina; prz, prezygapophysis; sprl, spinoprezygapophyseal lamina; tp, transverse process. Scaled to same total height.

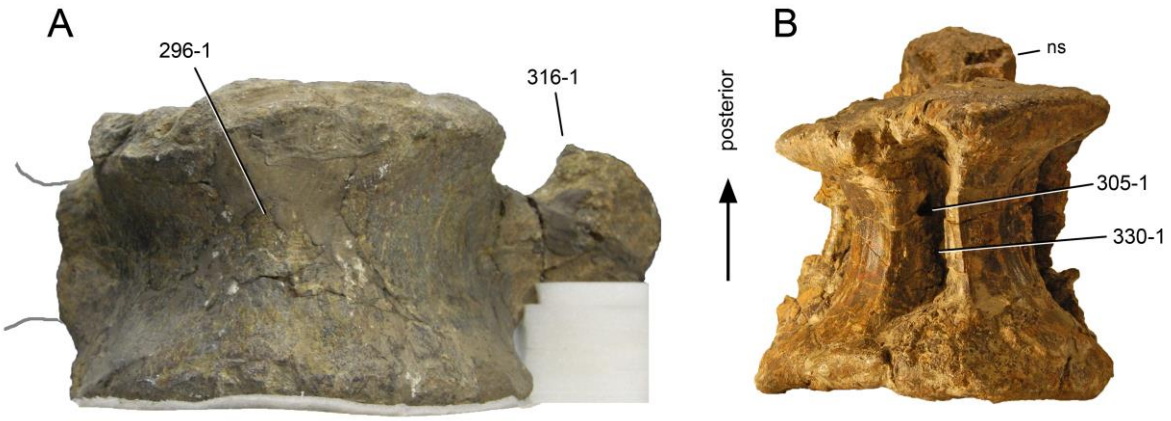

Figure 6.78: Anterior caudal vertebrae of *Apatosaurus ajax* YPM 1860 (A) and *Diplodocus* sp. DMNS 462 (B) in ventral view. Note the ventral keel (A; C296-1), the ventral foramen (B; C305-1) within the ventral longitudinal hollow (B; C330-1), and the anteroposteriorly expanded distal end of the transverse process (A; C316-1). Abb.: ns, neural spine. Scaled to same centrum length.

C301: Anterior-most caudal neural arches, accessory lamina connecting the pre- and postzygapophyses: absent (0); present (1) (New; Fig. 6.76).

Comments. This accessory lamina usually connects the postzygapophysis with the sprl.

C302: Anterior-most caudal neural spine (not including arch), height: less than 1.5 times centrum height (0); 1.5 times centrum height or more (1) (Yu, 1993; modified after Upchurch and Mannion, 2009; Tab. 6.40).

Comments. Neural spine height is measured from the dorsal edge of the postzygapophyses to the spine top, vertically. Centrum height is measured at the posterior articular surface. Yu (1993) used the entire neural arch height for the ratio, and formulated it as a multi-state character, restricted to the first

two caudal vertebrae. The ratio is herein adapted following Upchurch and Mannion (2009), but keeping the restriction to the anterior-most elements, instead of including all anterior caudal vertebrae as Upchurch and Mannion (2009).

C303: Anterior-most caudal neural spines, lateral spinal lamina: has the same anteroposterior width ventrally and dorsally (0); expands anteroposteriorly towards its distal end, and becomes rugose (1) (Upchurch et al., 2004a; wording modified; Fig. 6.76).

Comments. Apatosaurs usually have a more dorsally restricted anteroposterior expansion of the lateral spinal lamina, compared to diplodocines. SMA 0087 appears to show the plesiomorphic state, which could be an autapomorphic reversal. However, due to the bad preservation of the bones, the true morphology of the lateral spinal lamina is difficult to assess, and it might actually turn out to be widened as well, once all the material is prepared, or better specimens are found.

C304: Anterior caudal centra (excluding the first), articular surface shape: amphiplatyan or amphicoelous (0); procoelous/distoplatyan (1); slightly procoelous (2); procoelous (3) (McIntosh, 1990b; Russell and Zheng, 1993; modified after González Riga et al., 2009; Tab. 6.39).

Comments. Slightly procoelous is herein defined as the slightly opisthocoelous in posterior dorsal centra (see character 270). In diplodocids, the centra change their shape in anterior to middle caudal vertebrae from slightly procoelous to procoelous/distoplatyan to amphicoelous/amphiplatyan. In *Diplodocus* this change occurs more posteriorly than in *Apatosaurus*, for example, therefore specimens of the former genus have to be scored as slightly procoelous for this character, whereas *Apatosaurus* specimens are scored as procoelous/distoplatyan. However, more detailed studies about this transition is needed in order to score this character appropriately, as the specimens used herein generally show some correlation (within Flagellicaudata) of the development of procoely and the presence of wing-like transverse processes, which also mark more caudal vertebrae in *Diplodocus* than in less derived Flagellicaudata.

C305: Anterior caudal centra, ventral surface: without irregularly placed foramina (0); irregular foramina present on some anterior caudals (1) (Whitlock, 2011a; Fig. 6.78).

Comments. Foramina can also be present in anterior caudal vertebrae without concave ventral surfaces (see *Suuwassea emilieae* ANS 21122; Harris, 2006b).

C306: Anterior caudal centra, pneumatopores (pleurocoels): absent (0); present (1) (McIntosh, 1990b; Yu, 1993; modified).

Comments. Small pneumatopores also mark the lateral surfaces of non-diplodocine sauropods (e.g. *Lourinhasaurus alenquerensis* MIGM specimen, pers. obs., 2012). The development of the pneumatopores as foramina or deep coels is described in character 307.

C307: Anterior caudal centra, pneumatopores: restricted to foramina (0); large coels present (1) (Tschopp and Mateus, 2012b; modified; Fig. 6.79).

Comments. This character only codes for the anterior caudal vertebrae, excluding the anterior-most elements with wing-like transverse processes. The presence of a large coel in the latter is coded for in character 297. Taxa without pneumatopores are scored as unknown.

C308: Anterior caudal centra, pneumatopores: disappear by caudal 15 (0); present until caudal 16 or more (1) (McIntosh, 2005; Tab. 6.39).

Comments. McIntosh (2005) recognized this as distinguishing character between *Diplodocus* and *Barosaurus*, but it is applied for the first time as phylogenetic character.

C309: Anterior caudal centra, length: subequal amongst first 20 (0); more or less doubling over first 20 (1) (Upchurch, 1998; modified; Tab. 6.41).

Comments. Lengths were compared between the shortest element among the first three, and the longest preserved vertebrae within Cd 17 and 22 (or if this part of the tail is lacking, the longest element preserved). Taxa with a ratio of 1.5 or more are scored as derived.

C310: Anterior caudal vertebrae, concavo-convex zygapophyseal articulation: absent (0); present (1) (Wilson, 2002; Whitlock, 2011a; Fig. 6.77).

Comments. This character is like the one for cervical vertebrae, which describes the flat versus convex prezygapophyses of diplodocine cervical vertebrae. Wilson (2002) suggested that convex prezygapophyses and concave postzygapophyses are diagnostic for *Diplodocus*, but Whitlock (2011a) showed that also *Barosaurus* showed the derived state. During the current study, also some apatosaur specimens were observed to have the apomorphic condition.

Table 6.39: Caudal vertebrae, serial variation.

Taxon	Specimen	Centrum shape	Pneumatopores	Wing-like tp	Normal tp	Reference	Comments
Shunosaurus lii	T5401		absent	Cd 1		Zhang, 1988	no dCd
Spinophorosaurus nigerensis			absent		Cd 1-15	pers. obs.	no anterior-most Cd, dCd
Omeisaurus	T5701	Cd 1-15+, amc	absent	Cd 1	Cd 2-14	He et al., 1988	
Mamenchisaurus	ZDM 0083	Cd 1-7+, prc; Cd ?21-?, amp-amc	absent	Cd 1-?	loss before Cd 21	Ouyang and Ye, 2002	no dCd
Jobaria tiguidensis	NMB-1695-R		absent		Cd ?2-12	pers. obs.	
Turiasaurus riodevensis	CPT	pCd, opc				Royo-Torres et al., 2006	
Losillasaurus giganteus type	MCNV	Cd 1-?, prc; mCd, amc	absent	Cd 1-?		Casanovas et al., 2001	
Camarasaurus			absent	Cd 1	Cd 2-12	Curtice, 1996	
	BYU 9047	Cd 1-13, amc; Cd 14-?, amp	absent			McIntosh et al., 1996b	
	CM 11338		absent		Cd 2-11	McIntosh et al., 1996b	
Apatosaurus grandis YPM 1901	YPM 1901	amp-amc	absent		Cd ?-13	M. Fox, pers. comm., 2012	
Amphicoelias latus AMNH 5765	AMNH 5764	aCd, amc	absent			Cope, 1878	
Lourinhasaurus alenquerensis lectotype	MIGM	aCd, amc; mCd, amc	pnf			pers. obs.	
Giraffatitan brancai	MB.R. Aa		pnf		Cd 1-?15	Janensch, 1950	no anterior-most Cd
Brachiosaurus sp. SMA 0009	SMA 0009	aCd, amp-amc	absent		Cd 1-8	pers. obs.	no anterior-most Cd
Brachiosaurus altithorax	FMNH P25107	aCd, amc	absent		Cd 1-?	Riggs, 1904	no anterior-most Cd
Isisaurus colberti	ISIR335	prc	absent			Jain and Bandyopadhyay, 1997	
Haplocanthosaurus priscus	CM 572	amc	amCd, pl; aCd, pnf (< Cd 15)	Cd 1	Cd 2-13	Hatcher, 1903	
Limaysaurus tessonei		ptc	Cd 1-5?, pl	Cd 1-3?		Calvo and Salgado, 1995	
Cathartesaura anaerobica	MPCA-232	amp	absent	Cd 1-3?		Gallina and Apesteguía, 2005	
Zapalasaurus bonapartei	Pv-6127-MOZ	amc	absent				
Nigersaurus taqueti		mCd, amp-amc; dCd, bic	absent			Sereno et al., 2007	
Demandasaurus darwini	MDS-RVII	Cd 1, opc; aCd, amc;	absent	Cd 1-?		Torcida Fernandéz-Baldor et al., 2011	
Dicraeosaurus hansemanni	MB.R.4886	Cd 1-14, prc; Cd 15-?, amc	absent	Cd 1-4	Cd 5-12	Janensch, 1929	
Amargasaurus cazaui	MACN-N 15	aCd, amp; mCd, amp				Salgado and Bonaparte, 1991	
Suuwassea emilieae ANS 21122	ANS 21122	aCd, prc; mCd, amc; dCd, amp	aCd, pnf			Harris, 2006a	
Apatosaurus ajax YPM 1860	YPM 1860	aCd-mCd, amp-amc	amCd, pnf; aCd, pnf			pers. obs.	
Brontosaurus excelsus YPM 1980	YPM 1980	Cd 2-5, prc	amCd, pnf; aCd, pnf	Cd 1-5	Cd 6-12	Ostrom and McIntosh, 1966; Upchurch et al., 2004b; pers. obs.	
Brontosaurus amplus YPM 1981			aCd, pnf			pers. obs.	
Apatosaurus louisae CM 3018	CM 3018	Cd 1-7, prc; Cd 8-34, amc; Cd 35-?, bic	amCd, pl; aCd, pnf (< Cd 15)	Cd 1-6	Cd 7-14	Gilmore, 1936	

Table 6.39: continued.

Atlantosaurus immanis	YPM 1840	YPM 1840	aCd, prc			pers. obs.	
Apatosaurus parvus	UW 15556	UW 15556	Cd 1, amp; Cd 2-?, prc	amCd, pl; aCd, pnf (< Cd 15)	Cd 1-4	Cd 5-13?	Gilmore, 1936	found disarticulated, Cd 14 and 15 lacking
Eobrontosaurus yahnahpin	Tate-001	Tate-001	aCd, amc; mCd, amp-amc	aCd, pnf			P. Mannion, pers. comm., 2012	
Apatosaurus ajax	NSMT-PV 20375	NSMT-PV 20375	amc	amCd, pl; aCd, pnf (< Cd 15)	Cd 1-4	Cd 5-12	Upchurch et al., 2004b	
Apatosaurus sp.	AMNH 460	AMNH 460	amc	amCd, pnf; aCd, pnf	Cd 1-4	Cd 5-11	Gilmore, 1936	found disarticulated
Apatosaurus sp.	CM 3378	CM 3378	Cd 1-7, prc; Cd 8-34, amc; Cd 35-83, bic	aCd, pnf	Cd 1-6	Cd 7-14	Gilmore, 1936	
Apatosaurus sp.	FMNH P25112	FMNH 25112	Cd 2-?, prc	amCd, pl; aCd, pnf (< Cd 15)	Cd 1-5	Cd 6-12	Upchurch et al., 2004b	
Apatosaurinae indet.	SMA 0087	SMA 0087	aCd, prc; mCd, amc	amCd, pnf; aCd, pnf (< Cd 15)	Cd 1-6	Cd 7-13	pers. obs.	
Supersaurus vivianae	BYU	BYU 9045; BYU 10612	aCd, prc; mCd, amc; dCd, amp	amCd, pl; aCd, pnf			Jensen, 1985; D. Lovelace, pers. comm., 2013	
Supersaurus vivianae	WDC DMJ-021	WDC DMJ-021	aCd, prc; mCd, amc	amCd, pl; aCd, pnf			Lovelace et al., 2007	
Dinheirosaurus lourinhanensis	ML 414	ML 414	aCd, amc	aCd, pl				
Tornieria africana	holotype	SMNS 12141a;	aCd, prc	aCd, pl			Remes, 2006	
Tornieria africana	skeleton k	MB.R. K?	mCd, amp-amc				Remes, 2006	
Diplodocus longus	YPM 1920	YPM 1920	aCd-mCd, amc	aCd, pl			pers. obs.	
Diplodocus carnegii	CM 84	CM 84	aCd, prc	Cd 1-12+, pl	Cd 1-12?		Hatcher, 1901	only Cd 1-12 preserved
Diplodocus carnegii	CM 94	CM 94	aCd, prc; mCd, amp	Cd 1-16+, pl	Cd 1-9+	Cd ?-?20	pers. obs.	
Diplodocus sp.	AMNH 223	AMNH 223	aCd, prc; mCd, amc	Cd 1-18, pl	Cd 1-12	Cd 13-18	Osborn, 1899; pers. obs.	
Diplodocus sp.	USNM 10865	USNM 10865		Cd 1-19?, pl	Cd 1-12	Cd 13-19	Gilmore, 1932; pers. obs.	
Diplodocus sp.	DMNS 1494	DNMS 1494		Cd 1-17, pl	Cd 1-12	Cd 13-19	pers. obs.	
Diplodocus sp.	WDC-FS001A	WDC-FS001A	mCd, amp-amc				pers. obs.	
Galeamopus hayi	HMNS 175	HMNS 175	mCd, amp-amc	aCd, pl			pers. obs.	
Seismosaurus hallorum	NMMNH 3690	NMMNH 3690	mCd, amc	Cd 1-18?, pl	Cd 1-8+	Cd ?-19	Herne and Lucas, 2006	
Barosaurus lentus	YPM 429	YPM 429	aCd, prc; mCd, amc; dCd, bic	aCd, pl			Lull, 1919; pers. obs.	
Barosaurus sp.	AMNH 6341	AMNH 6341	aCd, prc; mCd, amp	Cd 1-14, pl	Cd 1-6	Cd 7-15	McIntosh, 2005	
Cetiosauriscus stewarti	NHMUK R3078	NHMUK R3078	aCd, prc; mCd amp	aCd, pnf (< Cd 15)	Cd 1-?4		Woodward, 1905; pers. obs.	Cd 5-10? not preserved

Table 6.40: Anterior caudal neural spine ratios.

Taxon	Specimen	1) hsp/hcd	Mean 1	2) max w/apl	Mean 2	3) max w/min w	Mean 3	Reference	Comments
Shunosaurus lii	T5401, Cd 1	1,759	1,76		0,90	1,002	1,00	Zhang, 1988	measured from figures
				0,900		1,000		Mannion et al., 2013	
Spinophorosaurus nigerensis	NMB-1698-R, Cd 6			0,843	0,85	3,105	3,14	A. Ritter, pers. comm. 2011	no anterior-most caudal; measured on 3D model
	NMB-1698-R, Cd 7			0,857		3,176		A. Ritter, pers. comm. 2011	no anterior-most caudal; measured on 3D model
Omeisaurus	T5701, Cd 1	1,020	1,02		0,89	1,842	1,89	He et al., 1988	measured from figures
	T5701, Cd 3			0,972		2,095		He et al., 1988	measured from figures
	T5701, Cd 6			0,788		1,731		He et al., 1988	measured from figures
				0,900		1,900		Mannion et al., 2013	
Mamenchisaurus	ZDM 0083, Cd 1	1,156	1,16	0,666	0,75	1,270	1,37	Ouyang and Ye, 2002	measured from figures
	ZDM 0083, Cd 7			0,788		1,454		Ouyang and Ye, 2002	measured from figures
				0,800		1,400		Mannion et al., 2013	
Jobaria tiguidensis	NMB-1695-R				<1		subequal	pers. obs.	
Losillasaurus giganteus type	MCNV Lo-5	1,011	1,01	1,227	1,22	3,049	2,20	Casanovas et al., 2001	measured from figures
	MCNV Lo-12			1,206		1,345		Casanovas et al., 2001	measured from figures
Camarasaurus	AMNH 5760/5761, Cd 1	1,101	0,99	1,881	1,59	1,690	2,29	Osborn and Mook, 1921	measured from figures
	AMNH 5760/5761, Cd 1	0,949		1,008		1,730		Osborn and Mook, 1921	measured from figures
	AMNH 5760/5761, Cd 5			1,346		2,360		Osborn and Mook, 1921	measured from figures
	AMNH 5760/5761, Cd 6			1,388		2,063		Osborn and Mook, 1921	measured from figures
	AMNH 5760/5761, Cd 8			2,103		2,706		Osborn and Mook, 1921	measured from figures
	BYU 9047, Cd 1	0,914		1,810		1,918		McIntosh et al., 1996b	1 and 3 measured from figures
	BYU 9047, Cd 5			1,836		2,519		McIntosh et al., 1996b	3 measured from figures
	BYU 9047, Cd 6			1,830		2,631		McIntosh et al., 1996b	3 measured from figures
	BYU 9047, Cd 8			1,291		2,314		McIntosh et al., 1996b	3 measured from figures
				1,400		3,000		Mannion et al., 2013	
Apatosaurus grandis YPM 1901	YPM 1901, aCd					2,596	3,05	M. Fox, pers. comm., 2012	measured from photo
	YPM 1901, aCd					3,600		M. Fox, pers. comm., 2012	measured from photo
	YPM 1901, aCd					2,759		M. Fox, pers. comm., 2012	measured from photo
	YPM 1901, aCd					2,738		M. Fox, pers. comm., 2012	measured from photo
	YPM 1901, aCd					3,558		M. Fox, pers. comm., 2012	measured from photo
Amphicoelias latus AMNH 5765	AMNH 5765, aCd			1,014	1,01	1,857	1,86	Cope, 1878	measured from figures
Giraffatitan brancai	MB.R. D, Cd 1			0,454	0,37	1,286	1,24	Janensch, 1950	no anterior-most caudal; measured from figure
	MB.R. D, Cd 4			0,522		1,456		Janensch, 1950	no anterior-most caudal; measured from figure
	MB.R. D, Cd 7			0,274		1,000		Janensch, 1950	no anterior-most caudal; measured from figure
	MB.R. D, Cd 10			0,308		1,275		Janensch, 1950	no anterior-most caudal; measured from figure
				0,300		1,200		Mannion et al., 2013	no anterior-most caudal

Table 6.40: continued.

Brachiosaurus sp. SMA 0009	SMA 0009				<1		low, <2	pers. obs.	no anterior-most caudal; no detailed measurements possible
Brachiosaurus altithorax	FMNH P25107, Cd 1			1,100	0,97		2,75	Riggs, 1904	no anterior-most caudal
	FMNH P25107, Cd 2			0,900		2,708		Riggs, 1904	no anterior-most caudal; 3 measured from figure
				0,900		2,800		Mannion et al., 2013	no anterior-most caudal
Isisaurus colberti	ISIR335/32, aCd			0,846	0,85	1,359	1,36	Jain and Bandyopadhyay, 1997	measured from figures
Haplocanthosaurus priscus	CM 572, Cd 1	0,852	0,85	0,821	0,53	1,857	1,46	Hatcher, 1903	measured from figures
	CM 572, Cd 4			0,597		1,682		Hatcher, 1903	measured from figures
	CM 572, Cd 7			0,443		1,299		Hatcher, 1903	measured from figures
	CM 572, Cd 10			0,276		1,000		Hatcher, 1903	measured from figures
Limaysaurus tessonei	MUCPv-153, Cd 4	2,339	2,34		1,33		1,80	Calvo and Salgado, 1995	measured from figures
	MUCPv-153, Cd 5			1,326		1,800		Calvo and Salgado, 1995	measured from figures
Nigersaurus taqueti				1,000	1,00	1,600	1,60	Mannion et al., 2013	
Demandasaurus darwini	MDS-RVII,605, Cd 1	1,842	1,62		1,55	1,656	2,18	Torcida Fernandéz-Baldor et al., 2011	measured from figures
	MDS-RVII,15, aCd	1,407		1,545		2,698		Pereda Suberbiola et al., 2003	3 measured from figures
Dicraeosaurus hansemanni	MB.R. ?, aCd	2,481	2,48		1,01	3,193	2,86	McIntosh, 1990a	measured from figures
	MB.R.3774, aCd			1,008		2,518		pers. obs.	measured from photo
Apatosaurus ajax YPM 1860	YPM 1860, aCd			1,100	1,37	2,348	2,06	pers. obs.	measured from photo
	YPM 1860, aCd	1,087	1,09	1,641		1,768		pers. obs.	measured from photo
Brontosaurus excelsus YPM 1980	YPM 1980, Cd 2		1,23		1,43	4,043	3,31	Ostrom and McIntosh, 1966	measured from figures
	YPM 1980, Cd 5	1,229		1,427		2,571		Ostrom and McIntosh, 1966	measured from figures
Apatosaurus louisae CM 3018	CM 3018, Cd 8			1,667	0,98	2,429	1,83	Gilmore, 1936	measured from figures
	CM 3018, Cd 10			0,917		1,654		Gilmore, 1936	measured from figures
	CM 3018, Cd 13			0,358		1,411		Gilmore, 1936	measured from figures
Apatosaurus parvus UW 15556	UW 15556, Cd 1	1,588	1,38	3,408	1,96		1,80	Gilmore, 1936	measured from figures
	UW 15556, Cd 3	1,167		2,426		1,724		Gilmore, 1936	measured from figures
	UW 15556, Cd 5			1,849		1,570		Gilmore, 1936	measured from figures
	UW 15556, Cd 8			1,696		2,211		Gilmore, 1936	measured from figures
	UW 15556, Cd 11			0,441		1,709		Gilmore, 1936	measured from figures
Eobrontosaurus yahnahpin Tate-001	Tate-001, aCd			2,017	2,02	3,718	3,72	P. Mannion, pers. comm., 2012	measured from photo
Apatosaurus ajax NSMT-PV 20375	NSMT-PV 20375, Cd 1	1,691	1,36	2,096	1,46	1,431	1,55	Upchurch et al., 2004b	1 and 3 measured from figures
	NSMT-PV 20375, Cd 4	1,032		1,286		1,947		Upchurch et al., 2004b	1 and 3 measured from figures
	NSMT-PV 20375, Cd 6			1,814		1,605		Upchurch et al., 2004b	1 and 3 measured from figures
	NSMT-PV 20375, Cd 9			0,660		1,207		Upchurch et al., 2004b	3 measured from figures
Apatosaurus sp. FMNH P25112	FMNH P25112, Cd 1	1,267	1,27		>1	1,644	1,64	Riggs, 1903	measured from figures

Table 6.40: continued.

Apatosaurinae indet. SMA 0087	SMA 0087, Cd 3		1,14	0,559	0,58	1,583	1,85	pers. obs.	transversely compressed
	SMA 0087, Cd 4			0,553		1,424		pers. obs.	transversely compressed
	SMA 0087, Cd 5	1,145		0,719		1,917		pers. obs.	transversely compressed; 1 measured from photo
	SMA 0087, Cd 6			0,662		1,720		pers. obs.	transversely compressed
	SMA 0087, Cd 7			0,690		2,000		pers. obs.	transversely compressed
	SMA 0087, Cd 8			0,569		1,762		pers. obs.	transversely compressed
	SMA 0087, Cd 9			0,630		2,000		pers. obs.	transversely compressed
	SMA 0087, Cd 10			0,582		2,000		pers. obs.	transversely compressed
	SMA 0087, Cd 11			0,709		2,167		pers. obs.	transversely compressed
	SMA 0087, Cd 12			0,371		1,769		pers. obs.	transversely compressed
	SMA 0087, Cd 13			0,333		2,000		pers. obs.	transversely compressed
Supersaurus vivianae BYU	BYU 9045, aCd	1,167	1,06	1,839	1,84	1,579	1,63	D. Lovelace, pers. comm., 2013	measured from photo
	BYU 12819, aCd	0,945				1,685		R. Wilhite, pers. comm., 2012	measured from photo
Supersaurus vivianae WDC DMJ-021	WDC DMJ-021, aCd	1,290	1,29	2,822	2,82	1,741	1,76	Lovelace et al., 2007	measured from figures
	WDC DMJ-021, aCd					1,782		D. Lovelace, pers. comm., 2013	measured from photo
Diplodocus carnegii CM 84	CM 84, Cd 1	1,739	1,39	2,374	2,30	2,621	2,08	Hatcher, 1901	measured from figures
	CM 84, Cd 4	1,540		2,727		1,826		Hatcher, 1901	measured from figures
	CM 84, Cd 7	1,173		2,471		1,895		Hatcher, 1901	measured from figures
	CM 84, Cd 10	1,240		2,231		2,334		Hatcher, 1901	measured from figures
	CM 84, Cd 12	1,252		1,685		1,719		Hatcher, 1901	measured from figures
Diplodocus carnegii CM 94	CM 94, Cd 4?	1,417	1,42	3,255	3,25	3,556	3,56	pers. obs.	measured from photo
Diplodocus sp. AMNH 223	AMNH 223, Cd 1	1,562	1,39	1,820	1,72	2,250	1,86	Osborn, 1899	measured from figures
	AMNH 223, Cd 5	1,387		2,559		2,093		Osborn, 1899	measured from figures
	AMNH 223, Cd 10	1,230		1,765		1,798		Osborn, 1899	measured from figures
	AMNH 223, Cd 14			0,726		1,284		Osborn, 1899	measured from figures
Diplodocus sp. USNM 10865	USNM 10865, aCd		<1,5		>1			pers. obs.	no detailed measurements possible
Diplodocus sp. DMNS 1494	DMNS 1494, aCd		<1,5		>1			pers. obs.	no detailed measurements possible
Galeamopus hayi HMNS 175	HMNS 175, aCd		<1,5		>1			pers. obs.	no detailed measurements possible
Seismosaurus hallorum NMMNH 3690	NMMNH 3690, aCd			1,858	1,36	2,903	2,36	Lucas et al., 2006	measured from figures
	NMMNH 3690, Cd 12?			0,871		1,813		Gillette, 1991	measured from figure; min spine width estimated
Barosaurus lentus YPM 429	YPM 429, Cd 3	1,535	1,53	1,511	1,51	1,530	1,53	Lull, 1919	1 and 3 measured from figures
Barosaurus sp. AMNH 6341	AMNH 6341, Cd 4	2,130	2,04					McIntosh, 2005	
	AMNH 6341, Cd 6	1,952						McIntosh, 2005	
	AMNH 6341, aCd				>1		>2	pers. obs.	no detailed measurements possible
Cetiosauriscus stewarti NHMUK R3078	NHMUK R3078, aCd	0,882	0,88	0,747	0,74	1,440	1,37	Woodward, 1905	measured from figures
	NHMUK R3078, aCd			0,731		1,300		Woodward, 1905	measured from figures

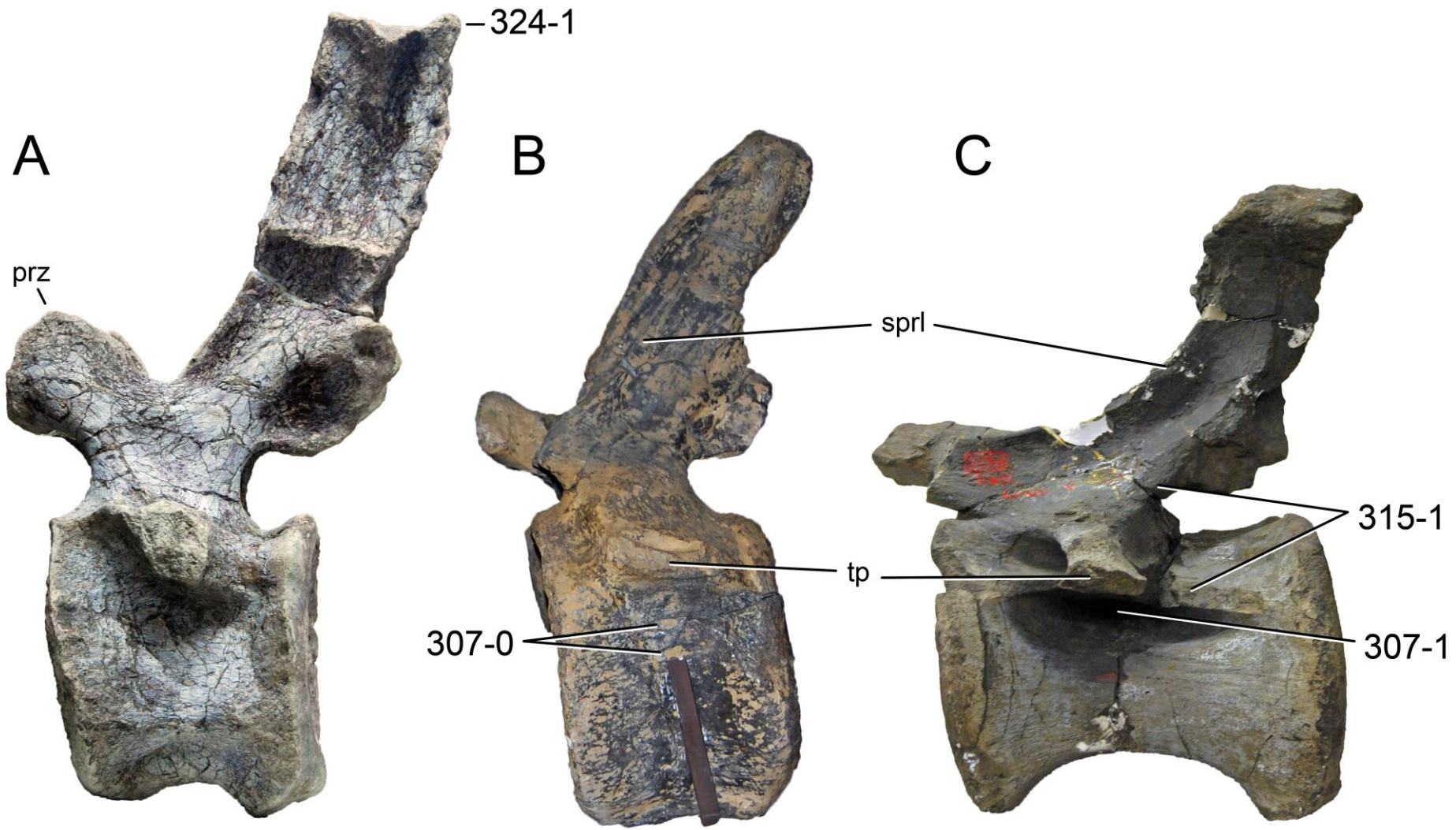

Figure 6.79: Anterior caudal vertebrae of *Dicraeosaurus hansemanni* MB.R.3774 (A), *Apatosaurus* sp. NHMUK R.3211 (B), and *Barosaurus lentus* YPM 429 (C) in left lateral view. Note the reduced (B; C307-0) or large pneumatopores (C; C307-1), the distinct posterior centrodiapophyseal and postzygodiapophyseal laminae (C; C315-1), and the postspinal lamina that projects dorsally (A; C324-1). Abb.: prz, prezygapophysis; sprl, spinoprezygapophyseal lamina; tp, transverse process. Scaled to same posterior centrum height.

Table 6.41: Caudal centra, ratios.

Taxon	Specimen	1) Cd 1-20, length	2) mCd, cl/cph	Mean 2	3) mCd-pCd, cw/ch	Mean 3	4) dCd, cl/cph	Mean 4	5) vlh depth	Mean 5	References	Comments
Shunosaurus lii	T5401, Cd 1-19	1,1									Zhang, 1988	Cd 18, 19 longest
	T5402, Cd 1-22	0,9									Zhang, 1988	Cd 1 longest
	T5401, Cd 16		1,27	1,3	0,94	1,1					Zhang, 1988	3) posterior
	T5401, Cd 19		1,46		0,95						Zhang, 1988	3) posterior
	T5401, Cd 22		1,40		1,06						Zhang, 1988	3) posterior
	T5401, Cd 25		1,53		1,05						Zhang, 1988	3) posterior
	T5401, Cd 28				1,27						Zhang, 1988	3) posterior
	T5401, Cd 32				1,26						Zhang, 1988	3) posterior
	T5402, Cd 16		0,98		0,97						Zhang, 1988	3) posterior
	T5402, Cd 19		1,10		1,00						Zhang, 1988	3) posterior
	T5402, Cd 22		1,38		1,03						Zhang, 1988	3) posterior
	T5402, Cd 25		1,40		1,04						Zhang, 1988	3) posterior
	T5402, Cd 28				1,13						Zhang, 1988	3) posterior
	T5402, Cd 32				1,05						Zhang, 1988	3) posterior
Spinophorosaurus nigerensis	GCP-CV-4229, aCd-pCd	1,4									Remes et al., 2009	exact position unclear
	GCP-CV-4229, HB 48, Cd 23?		1,89	2,1	0,96	0,8					A. Ritter, pers. comm., 2011	exact position unclear; measured from 3D model; 3) posterior
	GCP-CV-4229, HB 50, Cd 26?		1,95		0,81						A. Ritter, pers. comm., 2011	exact position unclear; measured from 3D model; 3) posterior
	GCP-CV-4229, HB 52, Cd 29		2,48		0,86						A. Ritter, pers. comm., 2011	measured from 3D model; 3) posterior
	GCP-CV-4229, HB 54, Cd 31				0,87						A. Ritter, pers. comm., 2011	measured from 3D model; 3) posterior
	GCP-CV-4229, HB 57, Cd 34				0,71						A. Ritter, pers. comm., 2011	measured from 3D model; 3) posterior
Omeisaurus	T5701, Cd 1-18	0,9									He et al., 1988	Cd 1 longest
	T5704, Cd 2-20	1,1									He et al., 1988	Cd 1 not preserved
	T5701, Cd 15		0,97	1,2	0,71	0,8					He et al., 1988	3) posterior
	T5701, Cd 20		1,26		0,89						He et al., 1988	3) posterior
	T5701, Cd 25		1,48		0,81						He et al., 1988	3) posterior
	T5704, Cd 15		0,88		0,86						He et al., 1988	3) posterior
	T5704, Cd 20		1,22		0,88						He et al., 1988	3) posterior
	T5704, Cd 25		1,50		0,88						He et al., 1988	3) posterior
	T5704, Cd 30				0,81						He et al., 1988	3) posterior
	T5704, Cd 35				0,73						He et al., 1988	3) posterior
Mamenchisaurus	ZDM 0083, Cd 1-21?	0,9									Ouyang and Ye, 2002	position of Cd 21 unclear; Cd 1 longest preserved element
	ZDM 0083, Cd 21?		1,22	1,3	0,91	1,0					Ouyang and Ye, 2002	3) posterior
	ZDM 0083, Cd 24?		1,46		0,98						Ouyang and Ye, 2002	3) posterior
	ZDM 0083, Cd 27?				1,00						Ouyang and Ye, 2002	3) posterior
Jobaria tiguidensis	NMB-1695-R, mCd	subequal	1,55	1,5		higher					pers. obs.	2) measured from photo, posterior mid-caudal, true mean probably lower
Losillasaurus giganteus type	MCNV, aCd-mCd	subequal									pers. obs.	positions unclear
	MCNV, Lo-32, mCd		1,44	1,4	1,10	1,1					pers. obs.	measured from photo

Table 6.41: continued.

Camarasaurus	CM 11338, Cd 1-20	0,9								Gilmore, 1925	Cd 7 longest
	GMNH-PV 101, Cd 3-17	1,0								McIntosh et al., 1996a	Cd 6 longest, Cd 1-2 not preserved
	BYU 9047, Cd 1-17	1,0								McIntosh et al., 1996b	Cd 6 longest
	GMNH-PV 101, Cd 13		0,75	1,1	0,85	1,0				McIntosh et al., 1996a	3) posterior
	GMNH-PV 101, Cd 17		0,93		0,88					McIntosh et al., 1996a	3) posterior
	GMNH-PV 101, Cd 21		1,11		1,00					McIntosh et al., 1996a	3) posterior
	GMNH-PV 101, Cd 24		1,19		0,99					McIntosh et al., 1996a	3) posterior
	GMNH-PV 101, Cd 28		1,33		1,00					McIntosh et al., 1996a	3) posterior
	GMNH-PV 101, Cd 33				1,00					McIntosh et al., 1996a	3) posterior
	GMNH-PV 101, Cd 37				1,04					McIntosh et al., 1996a	3) posterior
	GMNH-PV 101, Cd 41				0,95					McIntosh et al., 1996a	3) posterior
	GMNH-PV 101, Cd 45				1,13					McIntosh et al., 1996a	3) posterior
	GMNH-PV 101, Cd 49						1,57	2,2		McIntosh et al., 1996a	3) posterior
	GMNH-PV 101, Cd 52						2,92			McIntosh et al., 1996a	3) posterior
	BYU 9047, Cd 13		0,81	1,1	1,02	1,0				McIntosh et al., 1996b	3) posterior
	BYU 9047, Cd 16		0,89		0,94					McIntosh et al., 1996b	3) posterior
	BYU 9047, Cd 20		1,04		0,99					McIntosh et al., 1996b	3) posterior
	BYU 9047, Cd 24		1,21		1,05					McIntosh et al., 1996b	3) posterior
	BYU 9047, Cd 28?		1,44		1,05					McIntosh et al., 1996b	position unclear; 3) posterior
	BYU 9047, Cd 33?				1,03					McIntosh et al., 1996b	position unclear; 3) posterior
	BYU 9047, Cd 36?				1,08					McIntosh et al., 1996b	position unclear; 3) posterior
	BYU 9047, Cd 39?				1,03					McIntosh et al., 1996b	position unclear; 3) anterior
Apatosaurus grandis YPM 1901	YPM 1901, aCd-mCd	subequal								M. Fox, pers. comm., 2012	
	YPM 1901, Cd 14?		1,11	1,4		1,0				M. Fox, pers. comm., 2012	position unclear; posterior height estimated; measured from photo
	YPM 1901, Cd 21?		1,32							M. Fox, pers. comm., 2012	position unclear; posterior height estimated; measured from photo
	YPM 1901, Cd 24?		1,47							M. Fox, pers. comm., 2012	position unclear; posterior height estimated; measured from photo
	YPM 1901, Cd 28?		1,62							M. Fox, pers. comm., 2012	position unclear; posterior height estimated; measured from photo
	YPM 1901, Cd 29?				1,03					M. Fox, pers. comm., 2012	position unclear; measured from photo
	YPM 1901, Cd 31?		1,70							M. Fox, pers. comm., 2012	position unclear; posterior height estimated; measured from photo
ourinhasaurus alenquerensis lectotype	MIGM, aCd-mCd	subequal								pers. obs.	
	MIGM, mCd			short						pers. obs.	
Giraffatitan brancai	MB.R. Aa, Cd 1-18	1,0								Janensch, 1950	Cd 7 longest
	MB.R. D, Cd 1-18	1,0								Janensch, 1950	Cd 5 and 13 longest
	MB.R. D, Cd 16		1,13	1,3	1,13	1,2				Janensch, 1950	3) posterior
	MB.R. D, Cd 18		1,20		1,13					Janensch, 1950	3) posterior
	MB.R. D, Cd 20		1,33		1,21					Janensch, 1950	3) posterior
	MB.R. D, Cd 22		1,41		1,24					Janensch, 1950	3) posterior
Brachiosaurus sp. SMA 0009	SMA 0009, Cd 1-mCd	1,2								Schwarz et al., 2007	position of mCd unclear, but longest element preserved
	SMA 0009, Cd A		1,26	1,3	1,29	1,2				Schwarz et al., 2007	position unclear; 3) posterior
	SMA 0009, Cd C		1,49		1,59					Schwarz et al., 2007	position unclear; 3) posterior
	SMA 0009, Cd F		1,18							Schwarz et al., 2007	position unclear; 3) posterior
	SMA 0009, pCd				0,78				shallow	pers. obs.	position unclear; 3) posterior; measured from photo
Isisaurus colberti	ISIR335, aCd-mCd	0,7								Jain and Bandyopadhyay, 1997	position unclear, longest aCd and mCd taken for ratio
	ISIR335/42, mCd		1,55	1,7	0,93	1,0			shallow	Jain and Bandyopadhyay, 1997	position unclear; 3) posterior; measured from figure
	ISIR335/44, mCd		1,74		1,02				shallow	Jain and Bandyopadhyay, 1997	position unclear; 3) posterior; measured from figure
	ISIR335/46, mCd		1,84		0,98				shallow	Jain and Bandyopadhyay, 1997	position unclear; 3) posterior; measured from figure

Table 6.41: continued.

Haplocanthosaurus priscus	CM 572, Cd 1-19	0,9								Hatcher, 1903	Cd 10 longest (114mm)
	CM 572, Cd 14		0,89	0,9	0,85	0,9				Hatcher, 1903	measured from figure; 3) posterior
	CM 572, Cd 17		0,89		0,86					Hatcher, 1903	measured from figure; 3) posterior
	CM 572, Cd 19		0,86		0,87					Hatcher, 1903	measured from figure; 3) posterior
Limaysaurus tessonei	MUCPv-205, mCd		1,59	1,6						Calvo and Salgado, 1995	measured from figure
	MUCPv-205, dCd						4,44	4,2		Calvo and Salgado, 1995	measured from figure
	MUCPv-205, dCd						3,98			Calvo and Salgado, 1995	measured from figure
Cathartesaura anaerobica	MPCA-232, mCd		1,61	1,6						Gallina and Apesteguía, 2005	measured from figure
Zapalasaurus bonapartei	Pv-6127-MOZ, Cd 1-17	2,9								Salgado et al., 2006	
	Pv-6127-MOZ, Cd 13		2,32	2,6	0,89	0,8				Salgado et al., 2006	
	Pv-6127-MOZ, Cd 15		2,28		0,72					Salgado et al., 2006	
	Pv-6127-MOZ, Cd 17		3,15		0,85					Salgado et al., 2006	
Nigersaurus taqueti	MNN GAD, mCd		2,76	2,8						Sereno et al., 2007	measured from figure
	MNN GAD, dCd						3,81	3,8		Sereno et al., 2007	measured from figure
Demandasaurus darwini	MDS-RVII, Cd 1-mCd	1,3							very deep	Torcida Fernandéz-Baldor et al., 2011	position of mCd unclear, but longest element preserved
	MDS-RVII,3, mCd		1,11	1,8	1,00	1,2				Torcida Fernandéz-Baldor et al., 2011	
	MDS-RVII,216, mCd		2,64		1,50					Torcida Fernandéz-Baldor et al., 2011	
	MDS-RVII,218, mCd		1,52		1,09					Torcida Fernandéz-Baldor et al., 2011	
Dicraeosaurus hansemanni	MB.R.4886, Cd 1-22?	1,2								Janensch, 1929	position of Cd 22 unclear, but longest element preserved
	MB.R.4886, Cd 13		0,95	1,2	0,97	1,0				Janensch, 1929	3) posterior
	MB.R.4886, Cd 16		1,06		1,01					Janensch, 1929	3) posterior
	MB.R.4886, Cd 19		1,25		1,02					Janensch, 1929	3) posterior
	MB.R.4886, Cd 22?		1,70		1,11					Janensch, 1929	3) posterior
	MB.R. dd, dCd						3,63	3,6		Harris, 2006a	measured from figure
Suuwassea emilieae ANS 21122	ANS 21122, aCd-mCd	1,6								Harris, 2006a	ratio between longest element preserved (mCd) and shortest aCd
	ANS 21122, mCd		1,55	2,1	1,09	1,0				Harris, 2006a	3) posterior
	ANS 21122, mCd		2,58		1,00					Harris, 2006a	possibly also a pCd; 3) posterior
	ANS 21122, pCd				0,99					Harris, 2006a	3) posterior
	ANS 21122, pCd				1,01					Harris, 2006a	3) posterior
	ANS 21122, dCd						3,30	3,9		Harris, 2006a	
	ANS 21122, dCd						4,53			Harris, 2006a	
Apatosaurus ajax YPM 1860	YPM 1860, aCd-mCd	subequal								pers. obs.	positions unclear
	YPM 1860, mCd		1,43	1,4	0,93	0,9				pers. obs.	measured from photo
Brontosaurus excelsus YPM 1980	YPM 1980, Cd 1-19	subequal				subequal				pers. obs.	
	YPM 1980, Cd 15		1,10	1,3						pers. obs.	measured from photo
	YPM 1980, Cd 17		1,45							pers. obs.	measured from photo
	YPM 1980, Cd 19		1,32							pers. obs.	measured from photo

Table 6.41: continued.

Apatosaurus louisae CM 3018	CM 3018, Cd 1-20	0,8								Gilmore, 1936	Cd 1 longest
	CM 3018, Cd 15		1,12	1,3	0,96	1,0				Gilmore, 1936	measured from figure; 3) posterior
	CM 3018, Cd 19		1,25		1,14					Gilmore, 1936	measured from figure; 3) posterior
	CM 3018, Cd 23		1,19		0,97					Gilmore, 1936	measured from figure; 3) posterior
	CM 3018, Cd 27		1,49		0,98					Gilmore, 1936	measured from figure; 3) posterior
	CM 3018, Cd 31				1,02					Gilmore, 1936	measured from figure; 3) posterior
	CM 3018, Cd 35				0,96					Gilmore, 1936	measured from figure; 3) posterior
	CM 3018, Cd 39				1,04					Gilmore, 1936	measured from figure; 3) posterior
	CM 3018, Cd 43						3,90	4,2		Gilmore, 1936	measured from figure
	CM 3018, Cd 47						5,00			Gilmore, 1936	measured from figure
	CM 3018, Cd 51						3,90			Gilmore, 1936	measured from figure
	CM 3018, Cd 55						4,12			Gilmore, 1936	measured from figure
	CM 3018, Cd 59						3,95			Gilmore, 1936	measured from figure
	CM 3018, Cd 63						4,53			Gilmore, 1936	measured from figure
Apatosaurus parvus UW 15556	UW 15556, Cd 1-16	1,4								Gilmore, 1936	Cd 16 longest element preserved
	UW 15556, Cd 16		1,10	1,3	0,83	0,9				Gilmore, 1936	measured from figure; 3) posterior
	UW 15556, Cd 23		1,33		0,88					Gilmore, 1936	measured from figure; 3) posterior
	UW 15556, Cd 26		1,56		0,95					Gilmore, 1936	measured from figure; 3) posterior
	UW 15556, Cd 31				0,97					Gilmore, 1936	measured from figure; 3) posterior
Eobrontosaurus yahnahpin Tate-001	Tate-001, mCd		1,26	1,3	1,05	1,1				P. Mannion, pers. comm., 2012	measured from photo; 3) posterior
Apatosaurus ajax NSMT-PV 20375	NSMT-PV 20375, Cd 1-20	0,9								Upchurch et al., 2004b	Cd 1 longest
	NSMT-PV 20375, Cd 13		0,87	1,2	0,97	1,1				Upchurch et al., 2004b	2) cl/hca; 3) anterior
	NSMT-PV 20375, Cd 16		1,15		0,98				very shallow	Upchurch et al., 2004b	2) cl/hca; 3) anterior
	NSMT-PV 20375, Cd 19		1,04		1,09					Upchurch et al., 2004b	2) cl/hca; 3) anterior
	NSMT-PV 20375, Cd 22		1,31		1,13					Upchurch et al., 2004b	2) cl/hca; 3) anterior
	NSMT-PV 20375, Cd 25		1,40		1,14					Upchurch et al., 2004b	2) cl/hca; 3) anterior
	NSMT-PV 20375, Cd 29		1,56		1,07					Upchurch et al., 2004b	2) cl/hca; 3) anterior
	NSMT-PV 20375, Cd 31				0,98					Upchurch et al., 2004b	3) anterior
Apatosaurus sp. AMNH 460	AMNH 460, Cd 3-19	subequal								pers. obs.	
	AMNH 460, mCd			<1,5						pers. obs.	
Apatosaurus sp. CM 3378	CM 3378, Cd 3-20	1,3								Gilmore, 1936	Cd 20 longest element preserved
	CM 3378, mCd		1,04	1,3	0,92	0,9			shallow	pers. obs.	measured from photo; 3) anterior
	CM 3378, mCd		1,46		0,88				shallow	pers. obs.	measured from photo; 3) posterior
	CM 3378, Cd 37						3,93	4,8		Harris, 2006a	measured from figure
	CM 3378, Cd 38						3,31			pers. obs.	
	CM 3378, Cd 39						4,80			pers. obs.	
	CM 3378, Cd 40						3,82			pers. obs.	
	CM 3378, Cd 41						5,00			pers. obs.	
	CM 3378, Cd 42						4,92			pers. obs.	
	CM 3378, Cd 43						4,80			pers. obs.	
	CM 3378, Cd 44						5,65			pers. obs.	
	CM 3378, Cd 47						5,38			pers. obs.	
	CM 3378, Cd 53						5,26			pers. obs.	
	CM 3378, Cd 58						5,65			pers. obs.	
	CM 3378, Cd 62						5,65			pers. obs.	

Table 6.41: continued.

Apatosaurus sp. FMNH P25112	FMNH P25112, Cd 1-18	1,5							Gilmore, 1936	Cd 18 longest
	FMNH P25112, Cd 13		0,95	1,2	1,19	1,1			Riggs 1903	3) posterior
	FMNH P25112, Cd 14		1,05		1,10				Riggs 1903	3) posterior
	FMNH P25112, Cd 15		1,10		1,10				Riggs 1903	3) posterior
	FMNH P25112, Cd 16		1,16		1,11				Riggs 1903	3) posterior
	FMNH P25112, Cd 17		1,22		1,17				Riggs 1903	3) posterior
	FMNH P25112, Cd 18		1,29		1,18				Riggs 1903	3) posterior
	FMNH P25112, Cd 19		1,22		1,17				Riggs 1903	3) posterior
	FMNH P25112, Cd 20		1,35		1,12				Riggs 1903	3) posterior
	FMNH P25112, Cd 21		1,38		1,13				Riggs 1903	3) posterior
	FMNH P25112, Cd 22		1,47		1,13				Riggs 1903	3) posterior
	FMNH P25112, Cd 23		1,50		1,21				Riggs 1903	3) posterior
Apatosaurinae indet. SMA 0087	SMA 0087, Cd 2-17	1,1							pers. obs.	no measurements available for Cd 1, Cd 14 longest (148 mm)
	SMA 0087, Cd 14		0,99	1,1	0,54	0,6			pers. obs.	transversely compressed
	SMA 0087, Cd 17		1,22		0,68				pers. obs.	transversely compressed
Supersaurus vivianae BYU	BYU 9085, mCd		1,64	1,7	1,15	1,1		shallow	D. Lovelace, pers. comm., 2013	measured from photo; 3) anterior
	BYU 10612, mCd		1,72		1,00			shallow	D. Lovelace, pers. comm., 2013	measured from photo; 3) anterior
Supersaurus vivianae WDC DMJ-021	WDC DMJ-021, aCd-mCd	subequal							pers. obs.	
	WDC DMJ-021, mCd		1,30	1,7	0,90	1,0		shallow	D. Lovelace, pers. comm., 2013	measured from photo; 3) posterior
	WDC DMJ-021, mCd		1,99		1,10			shallow	D. Lovelace, pers. comm., 2013	measured from photo; 3) posterior
	WDC DMJ-021, mCd		1,47		1,05			shallow	D. Lovelace, pers. comm., 2013	measured from photo; 3) posterior
	WDC DMJ-021, mCd		1,87		1,04			shallow	D. Lovelace, pers. comm., 2013	measured from photo; 3) posterior
Tornieria africana holotype	SMNS 12141a, Cd 2							deep	Remes, 2006	
Tornieria africana skeleton k	MB.R.2913, mCd		2,35	2,4	1,12	1,1		shallow	Remes, 2006	3) posterior
Diplodocus longus YPM 1920	YPM 1920, mCd		1,66	1,7	1,03	1,0	20,0		Curtice, 1996; pers. obs.	2 and 3) measured from photo; 3) posterior
	YPM 1920, mCd		1,72		0,98		32,0		Curtice, 1996; pers. obs.	2 and 3) measured from photo; 3) posterior
Diplodocus carnegii CM 84	CM 84, Cd 1-12	1,6						deep	Hatcher, 1901	only Cd 1-12 preserved, Cd 20 probably longer
Diplodocus carnegii CM 94	CM 94, Cd 1-20	~2						deep	pers. obs.	
	CM 94, mCd		2,29	2,2	1,35	1,3			pers. obs.	3) anterior; measured from photo
	CM 94, mCd		2,11						pers. obs.	
Diplodocus sp. AMNH 223	AMNH 223, Cd 1-18	2,1						deep	Osborn, 1899; pers. obs.	Cd 18 longest
	AMNH 223, Cd 19		1,85	2,3	1,04	1,0			Osborn, 1899	
	AMNH 223, Cd 21		1,98		1,00				Osborn, 1899	
	AMNH 223, Cd 23		2,35		0,98				Osborn, 1899	
	AMNH 223, Cd 25		2,53		0,92				pers. obs.	measured from photo; 3) anterior
	AMNH 223, Cd 27		2,59		0,88				Osborn, 1899	

Table 6.41: continued.

Diplodocus sp. USNM 10865	USNM 10865, Cd 1-18	2,0						Gilmore, 1932	Cd 18 longest
	USNM 10865, Cd 22		2,06	2,2		subequal	deep	pers. obs.	measured from photo
	USNM 10865, Cd 25		2,27				deep	pers. obs.	measured from photo
Diplodocus sp. DMNS 1494	DMNS 1494, aCd-mCd	~2				subequal	deep	pers. obs.	
	DMNS 1494, mCd			~2				pers. obs.	
Diplodocus sp. WDC-FS001A	WDC-FS 9A		1,54	1,6	1,12	~1	shallow	pers. obs.	2) measured from photo
	WDC-FS 193		1,65		<1		shallow	pers. obs.	measured from photo
Galeamopus hayi HMNS 175	HMNS 175, mCd		1,66	1,7		<1	shallow	pers. obs.	measured from photo
Seismosaurus hallorum NMMNH 3690	NMMNH 3690; Cd 1-16?	1,8					~30	Curtice, 1996; Herne and Lucas, 2006	centrum length Cd 1 estimated, position Cd 16 estimated, but longest element preserved
Barosaurus lentus YPM 429	YPM 429, Cd 1-17?	1,5					<5	Curtice, 1996; McIntosh, 2005	Cd 17? last element preserved with complete centrum, position not without doubt, might also be more anterior and ratio higher
	YPM 429, Cd 17?		1,68	1,7	1,24	1,3		McIntosh, 2005	3) posterior
	YPM 429, Cd 18?				1,29			McIntosh, 2005	3) posterior
Barosaurus sp. AMNH 6341	AMNH 6341, Cd 1-18	1,8					becoming shallower	McIntosh, 2005	Cd 18 longest element preserved
	AMNH 6341, Cd 16		1,49	2,1	1,23	1,3		McIntosh, 2005	3) posterior
	AMNH 6341, Cd 18		1,85		1,23			McIntosh, 2005	3) posterior
	AMNH 6341, Cd 20		1,87		1,22			McIntosh, 2005	3) posterior
	AMNH 6341, Cd 22		2,41		1,40			McIntosh, 2005	3) posterior
	AMNH 6341, Cd 24		2,20		1,17			McIntosh, 2005	3) posterior
	AMNH 6341, Cd 26		2,51		1,39			McIntosh, 2005	3) posterior
	AMNH 6341, Cd 28		2,39		1,29			McIntosh, 2005	3) posterior
Cetiosauriscus stewarti NHMUK R3078	NHMUK R3078, aCd-mCd	1,8						Woodward, 1905	positions unclear
	NHMUK R3078, Cd 11?		1,17	1,5	0,91	0,9		pers. obs.	position unclear; 3) posterior
	NHMUK R3078, Cd 14?		1,09					pers. obs.	position unclear
	NHMUK R3078, Cd 18?		1,28		0,83			pers. obs.	position unclear; 3) posterior
	NHMUK R3078, Cd 21?		1,33					pers. obs.	position unclear
	NHMUK R3078, Cd 25?		1,56		0,84			pers. obs.	position unclear; 3) posterior
	NHMUK R3078, Cd 29?		1,83					pers. obs.	position unclear
	NHMUK R3078, Cd 32?		2,23					pers. obs.	position unclear

C311: Anterior caudal prezygapophyses, pre-epipophysis laterally below articular facet: absent (0); present (1) (New; Fig. 6.76).

Comments. A rugose horizontal ridge marks the lateral surface of the prezygapophysis of *Diplodocus* and very few other taxa, below the articular facet. The position corresponds to where the pre-epipophysis of cervical vertebrae is located and is thus termed equally here.

C312: Anterior caudal vertebrae, transverse processes: ventral surface directed laterally or slightly ventrally (0); directed dorsally (1) (Whitlock, 2011a; Fig. 6.77).

Comments. This character describes the orientation of the ventral edge of the transverse process in anterior or posterior view.

C313: Anterior caudal transverse processes, anterior diapophyseal laminae (acdl, prdl): reduced or absent (0); present, well defined (1) (Wilson, 2002; modified; see Fig. 6.79 for equivalent in posterior diapophyseal laminae).

Comments. The original character (Wilson, 2002) was split in two, as the development of the posterior centrodiapophyseal and the postzygodiapophyseal laminae differs between *Apatosaurus* and *Diplodocus*.

C314: Anterior caudal transverse processes, anterior centrodiapophyseal lamina (acdl), shape: single (0); divided (1) (Wilson, 2002; Fig. 6.76).

Comments. In contrast to dicraeosaurids or more basal diplodocoids, diplodocids have wing-like transverse processes, which are anteriorly supported by two independent laminae, which both originate on the centrum and thus classify as acdl (and the latter thus as divided or double). In advanced diplodocines, the lower of the two acdl is furthermore branching in two towards the transverse process.

C315: Anterior caudal transverse processes, posterior diapophyseal laminae (pcdl, podl): reduced or absent (0); present, well defined (1) (Wilson, 2002; modified; Fig. 6.79).

C316: Anterior caudal transverse processes, anteroposteriorly expanded lateral extremities: absent (0); present (1) (New; Fig. 6.78).

Comments. Backwards curving transverse processes are not necessarily anteroposteriorly expanded.

C317: Anterior caudal neural spines, maximum mediolateral width to anteroposterior length ratio: < 1.0 (0); 1.0 or greater (1) (Upchurch, 1998; modified by Mannion et al., 2013; Tab. 6.40).

Comments. The anteroposterior length of the spine is measured at the same level as the maximum mediolateral width, perpendicular to the inclination of the neural spine. The unusual plesiomorphic state of SMA 0087 within the apatosaur specimens might be due to diagenetic transverse compression.

C318: Anterior caudal neural spines, sprl: absent, or present as small short ridges that rapidly fade out into the anterolateral margin of the spine (0); present, extending onto lateral aspect of neural spine (1) (Wilson, 2002), modified by (Mannion et al., 2012; Fig. 6.76).

C319: Anterior caudal neural spines, spinoprezygapophyseal laminae (sprl)-spol contact: absent (0); present (1) (Wilson, 2002; Fig. 6.76).

C320: Anterior caudal neural arches, prespinal lamina: absent (0); present (1) (Upchurch, 1995; Fig. 6.76).

Comments. Sauropod anterior caudal neural spines are generally rugose anteriorly and posteriorly, but only derived eusauropods develop distinct ridges or laminae.

C321: Anterior caudal neural spines, thickened anterior rim of prespinal lamina: absent (0); present (1) (Gallina and Apesteguía, 2005; Fig. 6.76).

Comments. Specimens without prespinal lamina are scored as unknown.

C322: Anterior caudal neural spines, prespinal lamina or rugosity: terminate at or beneath dorsal margin of neural spine (0); project dorsally above neural spine (1) (Whitlock, 2011a; modified; see Fig. 6.79 for equivalent in postspinal lamina).

Comments. The original character (Whitlock, 2011a) was split in two, because in the anterior caudal vertebrae of *Cetiosauriscus stewarti* NHMUK R.3078 only the postspinal rugosity expands dorsally above the spine summit (Woodward, 1905). The character description was slightly changed in order to include taxa without distinct prsl.

C323: Anterior caudal neural arches, postspinal lamina: absent (0); present (1) (Upchurch, 1995; Fig. 6.76).

Comments. See character 320. The two characters coding for the presence of pre- or postspinal laminae, are scored equally in the present analysis, as also in Wilson (2002), and might thus prove correlated in future. They were both retained herein as they distinguish between basal and derived non-neosauropod eusauropods and should thus have no influence on the relationships between ingroup diplodocids.

C324: Anterior caudal neural spines, postspinal lamina or rugosity: terminate at or beneath dorsal margin of neural spine (0); project dorsally above neural spine (1) (Whitlock, 2011a; modified; Fig. 6.79).

Comments. See character 322.

C325: Anterior caudal neural arches; hyposphenal ridge on posterior face of neural arch; present (0); absent (1) (Mannion et al., 2012; Fig. 6.80).

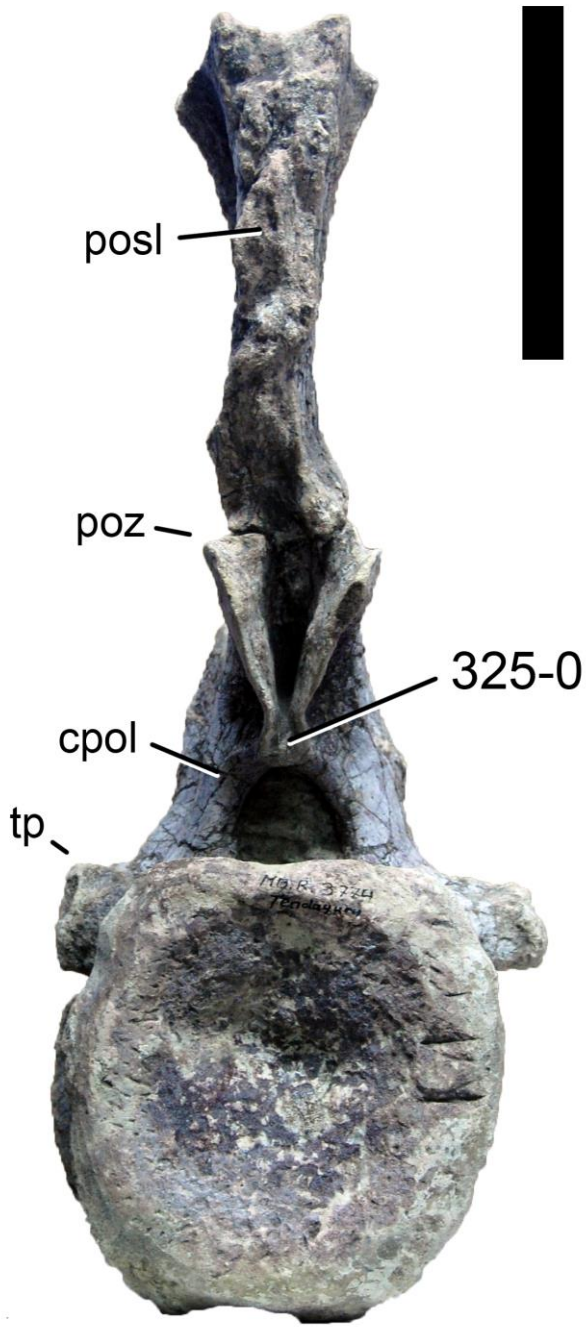

Figure 6.80: Anterior caudal vertebra of *Dicraeosaurus hansemanni* MB.R.3774 in posterior view, illustrating the hyposphenal ridge (C325-0). Abb.: cpol, centropostzygapophyseal lamina; posl, postspinal lamina; poz, postzygapophysis; tp, transverse process. Scale bar = 10 cm.

C326: Anterior caudal neural spines, shape: single (0); slightly bifurcate anteriorly (1) (Whitlock, 2011a; Fig. 6.77).

Comments. Anterior caudal neural spines can be bifid in two ways: anteroposteriorly and transversely. The former is coded for in characters 322 and 324, whereas the latter is described in the present character.

C327: Anterior caudal neural spines, maximum mediolateral width to minimum mediolateral width ratio: < 2.0 (0); 2.0 or greater (1) (Canudo et al., 2008; Taylor, 2009; modified by Mannion et al., 2013; Tab. 6.40).

C328: Anterior caudal neural spines, lateral expansion at distal end: gradual, expanding through the last third of the neural spine (0); abrupt, restricted to distal fourth of neural spine (1) (New; Fig. 6.77).

C329: Anterior and mid-caudal vertebrae, ventrolateral ridges: absent (0); present (1) (Upchurch et al., 2004a; Fig. 6.81).

Comments. There are two horizontal ridges marking some diplodocid caudal centra: the lateral ridge and the ventrolateral ridge. Usually, only one of the two is present, which is interpreted as the lateral ridge. The ventrolateral ridge as used herein does not describe the borders of the ventral longitudinal hollow of advanced diplodocines.

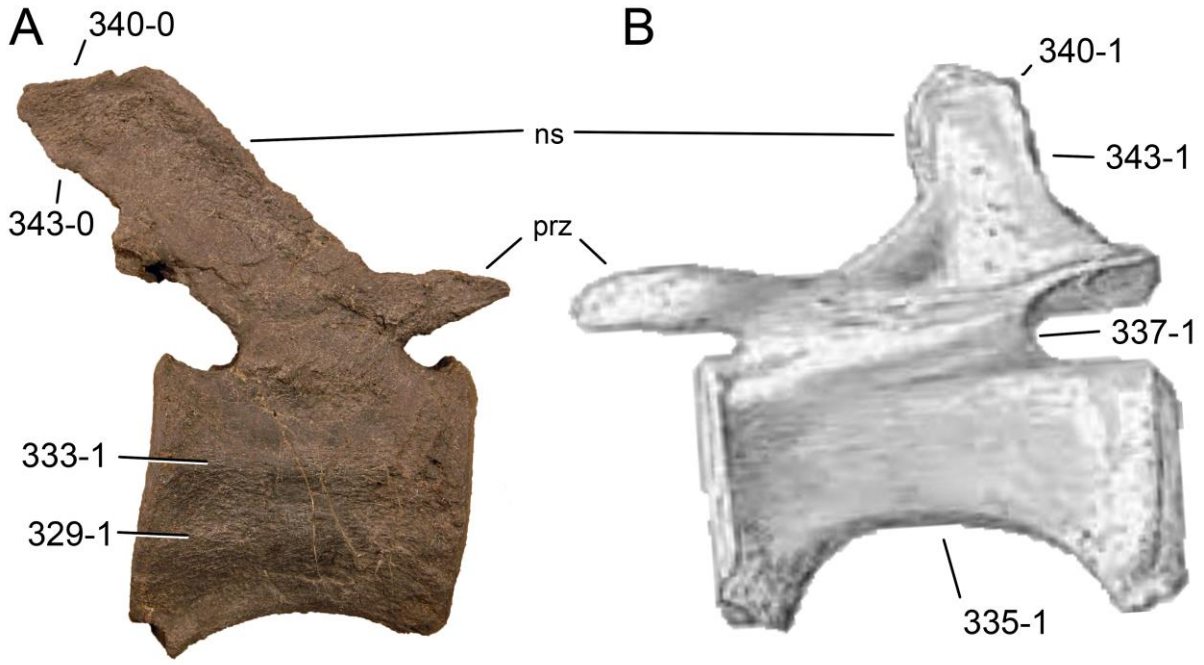

Figure 6.81: Mid-caudal vertebra of SMA 0087 (A) and *Diplodocus* sp. AMNH 223 (B) in right (A) and left (B) lateral view. Note the ventrolateral (A; C329-1) and lateral ridges (A; C333-1), the flat ventral border of the centrum (B; 335-1), the anteriorly shifted neural arch (B; C337-1), the differing inclinations of the neural spine (C340), which overhang the postzygapophyses (A; C343-0), or not (B; C343-1). Abb.: ns, neural spine; prz, prezygapophysis. Scaled to the same anterior articular surface height.

C330: Anterior and mid-caudal centra, ventral longitudinal hollow: absent (0); present (1) (McIntosh, 1990b; Yu, 1993; Fig. 6.78).

Comments. A ventral hollow is herein interpreted to be longitudinal concavity occupying the entire ventral surface. Various taxa have very distinct posterior chevron facets, with distinct ridges leading to them, thus creating a posteriorly concave ventral surface. However, these ridges often fade anteriorly. In some anterior diplodocine caudal centra, the ventral hollow is subdivided by longitudinal struts (e.g. *Tornieria africana* SMNS 12141a; Remes, 2006).

C331: Anterior- and mid-caudal vertebrae, ventral hollow depth: shallow, 10mm or less (0); deep, >10mm (1) (Curtice, 1996; Tab. 6.41).

Comments. Ventral hollow depth is used as distinguishing character between *Diplodocus* and *Baro-*

saurus (Curtice, 1996; McIntosh, 2005). Curtice (1996) showed that a caudal centra with a ventral hollow depth of more than 10 mm can be confidently identified as *Diplodocus*, whereas shallower centra are typical for less derived diplodocines. Only very limited measurements were available, and the scoring was mainly based on descriptions and thus the subjective opinion of the respective authors. An interesting case is present in *Tornieria*, where the only preserved caudal vertebra of the holotype specimen (SMNS 12141a, Cd 2) has a deep ventral hollow, whereas the medial caudal vertebra of skeleton k (MB.R.2913) is only shallowly excavated (Remes, 2006). More detailed research is needed in order to sort this out.

C332: Mid-caudal vertebrae, ratio of centrum length to posterior height: < 1,7 (0); 1,7 or greater (1) (Yu, 1993; modified; Tab. 6.41).

Comments. Usually, this character is included in analyses with its state boundary set at 2. In the present analysis, it was retained more useful to put the boundary at 1.7, as some diplodocine taxa have ratios between 1.7 and 2. Generally, the ratio increases in more posterior elements, therefore specimens with only anterior mid-caudal vertebrae preserved (e.g. *Diplodocus longus* YPM 1920, see McIntosh and Carpenter, 1998) most probably would have higher ratios than indicated in the table.

C333: Mid-caudal vertebrae, lateral surface of centra: without longitudinal ridge at mid-height (0); longitudinal ridge present, centra hexagonal in anterior/posterior view (1) (Upchurch and Martin, 2002; Fig. 6.81).

Comments. This ridge is not the same as the ventrolateral ridge described above, which is located below midheight.

C334: Mid-caudal centra, articular surface shape: cylindrical (0); quadrangular (1); trapezoidal (2); with flat ventral margin but rounded lateral edges (3) (Wilson, 2002; Gallina and Apesteguía, 2005; modified after Carballido et al., 2012b; Fig. 6.82).

Comments. The character was modified in order to be able to code for the various intermediate states between cylindrical, quadrangular, and triangular as described by earlier workers.

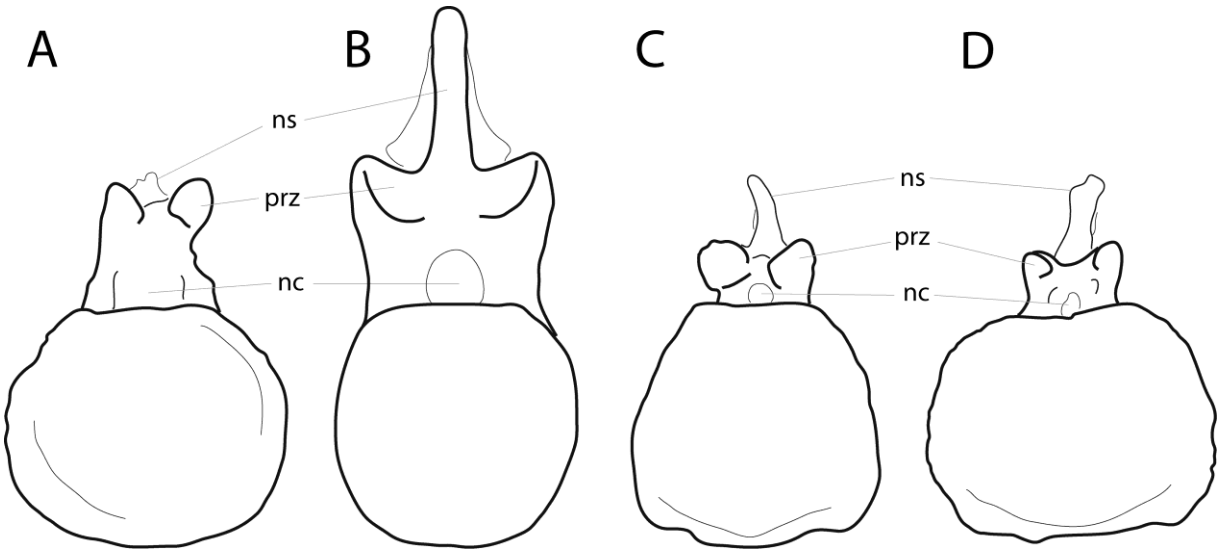

Figure 6.82: Mid-caudal vertebrae of *Losillasaurus giganteus* MCNV Lo-32 (A), *Isisaurus colberti* ISIR335/42 (B; traced from Jain and Bandyopadhyay, 1997), *Diplodocus* sp. AMNH 655 (C), and *Barosaurus lentus* AMNH 6341 (D) in anterior view, illustrating the four states of character 334 (A, circular; B, quadrangular; C, trapezoidal; D, flat ventral margin with rounded lateral edges). Abb.: nc, neural canal; ns, neural spine; prz, prezygapophysis. Scaled to same anterior surface height.

C335: Mid-caudal centra ventral surface in lateral view: gently curved (0); greater portion straight, with expansions on both ends to form the chevron facets restricted to about last fourth of centrum length (1) (New; Fig. 6.81).

Comments. This description applies especially for anterior mid-caudal elements, more posterior vertebrae of derived specimens tend to develop a more gentle curvature. This can create problems in taxa preserving only posterior mid-caudal vertebrae, as e.g. *Tornieria* specimen k, which is herein

scored as plesiomorphic for this character. Caudal vertebrae from trench dd, however, indicate that *Tornieria* actually might show the derived state, but these have not been found in articulation, and because anatomical overlap with the referred specimens included herein is minimal, their attribution to the species should be regarded as doubtful.

C336: Mid-caudal posterior articular surface: concave (0); flat (1); convex (2) (New; Tab. 6.39).

C337: Mid-caudal neural arches: over the midpoint of the centrum with approximately subequal amounts of the centrum exposed at either end (0); on the anterior half of the centrum (1) (Huene, 1929; Salgado et al., 1997; Fig. 6.81).

Comments. For this character, the distance between pre- and postzygapophyses and their location above the vertebral centrum is regarded as reference. The pedicels can still be dislocated anteriorly in plesiomorphic taxa. It is generally used as titanosauriform synapomorphy (Salgado et al., 1997; Wilson, 2002), but convergently present in some *Diplodocus* specimens (e.g. AMNH 223, or USNM 10865).

C338: Mid-caudal prezygapophyses: free (0); posteriorly interconnected by a transverse ridge, creating a triangular fossa together with the spinoprezygapophyseal laminae (1) (New; Fig. 6.83).

Comments. This transverse lamina marks the caudal vertebrae of *Diplodocus longus* YPM 1920, and might prove a valid autapomorphy for the species in future.

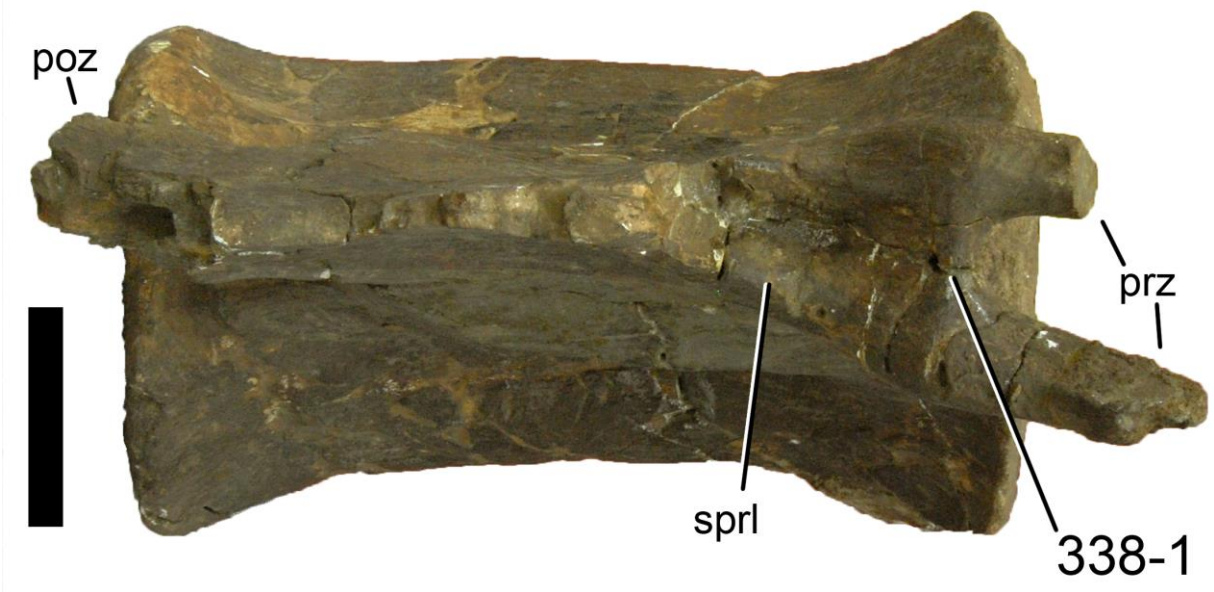

Figure 6.83: Mid-caudal vertebra of *Diplodocus longus* YPM 1920 in dorsal view, illustrating the transverse ridge connecting the prezygapophyses posteriorly (C338-1). Abb.: poz, postzygapophysis; prz, prezygapophysis; sprl, spinoprezygapophyseal lamina. Scale bar = 5 cm.

C339: Mid-caudal prezygapophyses position: terminate at or behind anterior edge of centrum (0); project considerably beyond anterior edge of centrum (1) (New).

Comments. Only taxa where the prezygapophyses clearly overhang the centrum (i.e. recognizable without any need of measuring) are scored as derived.

C340: Mid-caudal neural spines, orientation: directed posteriorly (0); vertical (1) (McIntosh, 1990a; Salgado et al., 1997; modified after Carballido et al., 2012b; Fig. 6.81).

C341: Mid-caudal neural arch, anterior extreme of spine summit: smooth (0); developing a short anterior or anterodorsal projection, such that anterior edge of spine becomes slightly concave (1) (New; Fig. 6.84).

Comments. Such a spur might also be interpreted as pathologic or ontogenetic. However, its presence in the juvenile to subadult *Apatosaurus* (= *Camarasaurus*) *grandis* YPM 1901 suggests that ontogeny can probably be excluded as a cause. More studies are needed in order to confirm or refuse pathological reasons, in the meanwhile the character is kept in the analysis.

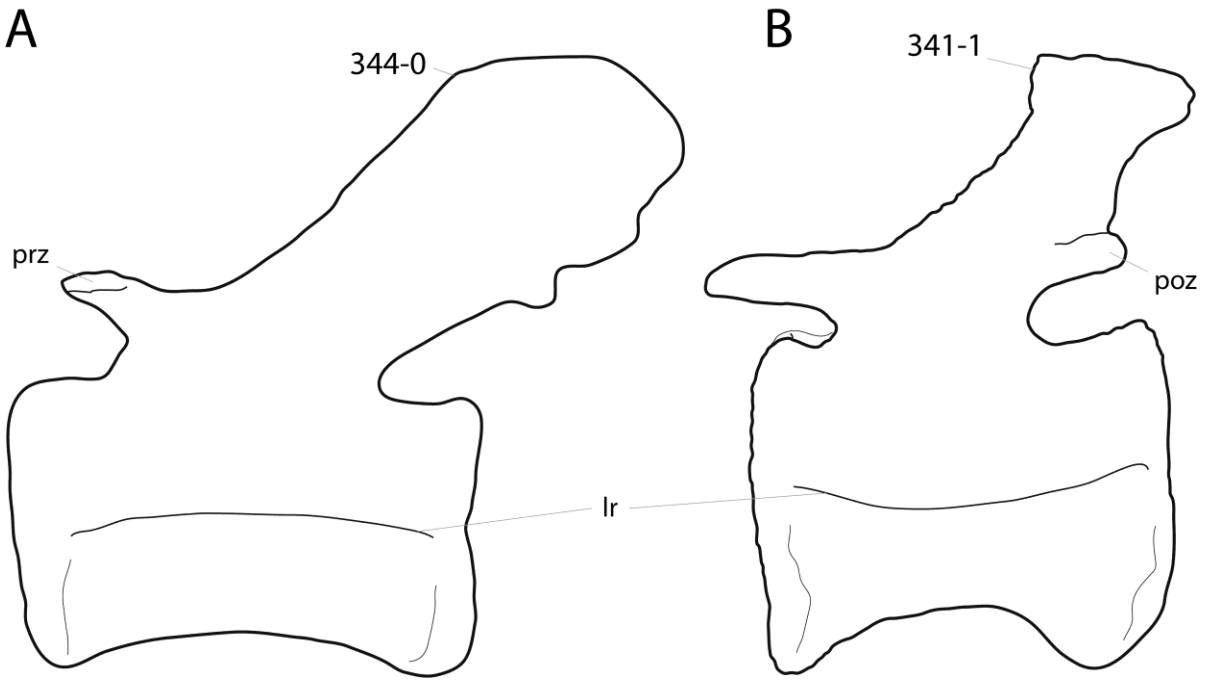

Figure 6.84: Mid-caudal vertebrae of *Cetiosauriscus stewarti* NHMUK R.3078 (A; traced from Woodward, 1905) and *Supersaurus vivianae* WDC DMJ-021 (B; traced from a photo by D. Lovelace) in left lateral view, illustrating the anterodorsal projection on the spine top (B; C341-1), and the posteriorly elongated neural spine (A; C344-0). Abb.: lr, lateral ridge; poz, postzygapophysis; prz, prezygapophysis. Scaled to same total vertebral height.

C342: Mid- and posterior caudal vertebral centra, articular surfaces: subequal in width and height or higher than wide (0); considerably wider than high (1) (Salgado et al., 1997; modified; Tab. 6.41).

Comments. A ratio of 1.2 or greater is regarded as considerably wider than high.

C343: Mid- and posterior caudal neural spines: spine summit overhangs postzygapophyses considerably posteriorly (0); posterior end of spine summit more or less straight above postzygapophyses (1) (New; Fig. 6.81).

C344: Mid- and posterior caudal spines: elongate and strongly caudally directed, extending over more than 50% of the length of the succeeding vertebral centrum (0); short, not extending far beyond the caudal articular facet of the centrum (1) (Remes et al., 2009; polarity reversed; Fig. 6.84).

C345: Posterior caudal prezygapophyses position: terminate at or behind anterior edge of centrum (0); project beyond anterior edge of centrum (1) (New).

C346: Distal-most caudal centra, articular face shape: platycoelous (0); biconvex (1) (Wilson et al., 1999; Tab. 6.39).

Comments. Taxa without distal caudal vertebrae are scored as unknown.

C347: Distal-most caudal centra, length-to-height ratio: < 4.0 (0); 4.0-6.5 (1); > 6.5 (2) (Upchurch, 1998), modified after (Wilson et al., 1999; Tab. 6.41).

C348: Distal-most caudal centra, number: ten or fewer (0); more than 30 (1) (Wilson, 2002; modified).

Comments. The character was modified such that it was not restricted to distal-most 'biconvex' caudal centra as in Wilson (2002).

C349: Caudal ribs, last occurs on: Cd 12 or more anteriorly (0); Cd 13 (1); Cd 14 (2); Cd 15-17 (3); Cd 18 or more posteriorly (4) (Holland, 1915a; Gilmore, 1936; Upchurch et al., 2004b; modified; Tab. 6.39).

Comments. Upchurch et al. (2004b), who were the first to include this positional character into a phylogenetic analysis, only distinguished between two states: Cd 14 and/or Cd 12. However, enlarging the taxon list, a higher variety becomes evident (Tab. 6.39). The state description was thus adapted accordingly. The character is left unordered as no obvious step-like evolution is recognizable.

C350: Anterior, 'fan'-shaped caudal ribs, foramen: present (0); absent (1) (Gilmore, 1936; Upchurch et al., 2004b; polarity reversed; Fig. 6.77).
Comments. Polarity was reversed herein given the different taxon sampling compared to Upchurch et al. (2004b).

Chevrons

C351: Chevrons, 'crus' bridging haemal canal: absent in some (0); present in all (1) (Yu, 1993; modified after Mannion et al., 2012).
Comments. Additive binary coding is preferred here in order to be able to code incomplete tails (following Mannion et al., 2012).

C352: Chevrons, 'crus' bridging haemal canal: present in some (0); absent in all (1) (Yu, 1993; modified after Mannion et al., 2012; Fig. 6.85).
Comments. See character 351.

C353: Chevrons with anterior and posterior projections: present (0); absent (1) (McIntosh, 1989; Russell and Zheng, 1993; modified; Fig. 6.86).
Comments. This character describes the often called 'forked chevrons' that inspired Marsh (1878) to name the specimen YPM 1920 *Diplodocus* (= double beam).

Figure 6.85: Anterior chevron of *Apatosaurus ajax* YPM 1860 in anterior, right lateral, and posterior view (left to right). Note the crus bridging the haemal canal dorsally (broken here; C352-0), the anterior, longitudinal median ridge (C354-1), and the step-like posterior expansion of the distal blade (C355-1). Abb.: db, distal blade; hc, haemal canal. Scale bar = 10 cm.

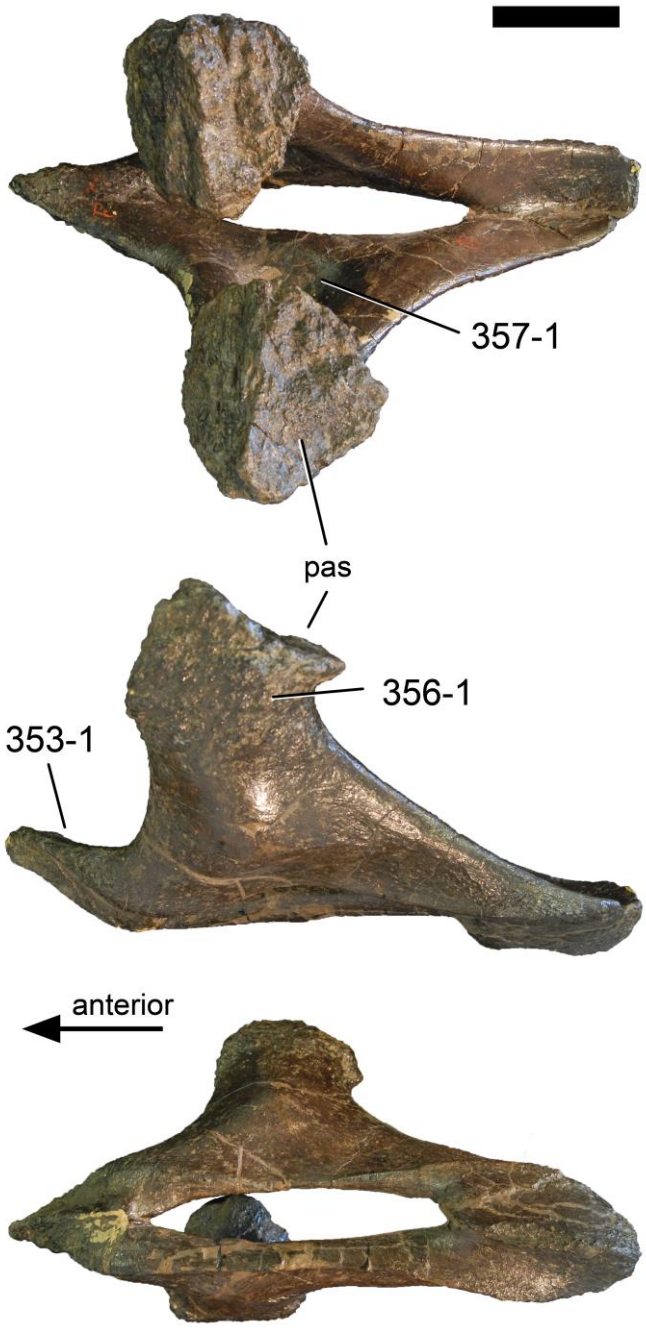

Figure 6.86: Mid-chevron of *Diplodocus* sp. AMNH 223 in dorsal, left lateral, and ventral view (top-bottom). Note the anterior and posterior projections (C353-1), the rugose horizontal ridge (C356-1), and the medial fossa (C357-1). Abb.: pas, proximal articular surface. Scale bar = 5 cm.

C354: Anterior chevrons, longitudinal median ridge on anterior surface: absent (0); present (1) (New; Fig. 6.85).

Comments. The ridge extends proximodistally.

C355: Anterior chevrons, posterior edge of distal blade in lateral view: continuous (0); posteriorly expanded in a step-like fashion (1) (New; Fig. 6.85).

C356: Anterior mid-chevrons, lateral surface: smooth (0); marked by a horizontal ridge right below articulation surfaces (1) (New; Fig. 6.86).

Comments. The ridge can be quite broad, but it is always rugose. Anterior mid-chevrons are meant to be the first elements with anterior projections on the distal blade.

C357: Middle chevrons, distinct fossae on medial surfaces of proximal branches: absent (0); present (1) (New; Fig. 6.86).

C358: Forked chevrons, anteroposterior length: short, about 50% of relative vertebral centrum length (0); elongate, approaching corresponding vertebral centrum length (1) (McIntosh, 1995).

Comments. The increased relative length of the chevron compared to its corresponding caudal vertebra was proposed as useful character to distinguish *Diplodocus* from *Apatosaurus* by McIntosh (1995), and is herein used for the first time in a phylogenetic analysis.

Pectoral girdle

C359: Scapular length/minimum blade breadth: > 5.5 (0); 5.5 or less (1) (Carballido et al., 2012b; polarity reversed; Tab. 6.42).

Comments. Measurements are taken from figures in lateral view, ignoring the proximodistal curve of the scapula. Greatest length follows the long axis of the scapula, such that orientation within the articulated skeleton is not taken into account, as this is still debated (see Schwarz et al., 2007a; Remes, 2008; Hohn, 2011). Minimum blade breadth is measured perpendicular to the long axis.

C360: Scapular acromion length/scapular length: > 0.54 (0); 0.46-0.54 (1); < 0.46 (2) (Gallina and Apesteguía, 2005; modified; Tab. 6.42).

Comments. Measurements were taken from figures in lateral view. Acromion length is measured perpendicular to scapular length, between horizontal lines extending through the ventral- and dorsal-most points of the acromion, with the distal blade oriented horizontally. The character is treated as ordered.

C361: Scapula, orientation of scapular, angle with coracoid articulation: > 80° (0); 80° or less (1) (Wilson, 2002; modified; Tab. 6.42).

Comments. The angle is measured from figures or photos in lateral view.

C362: Scapula, angle between acromial ridge and distal blade: < 70° (0); 70°-81° (1); > 81° (2) (Riggs, 1903; Carpenter and McIntosh, 1994; Upchurch et al., 2004b; modified; Tab. 6.42).

Comments. The angle to be measured lies between the dorsal half of the acromial ridge, and the long axis of the scapular blade. An additional state was added to the original version (Upchurch et al., 2004b), in order to be able to score specimens with intermediate ratios. The character is left unordered as no obvious evolutionary trend is observable.

C363: Scapular acromion process, dorsal part of posterior margin: convex or straight (0); U-shaped concavity (1) (Wilson, 2002; modified by Whitlock, 2011a; Fig. 6.87).

C364: Scapular, acromial process position: lies near the glenoid level (0); lies nearly at midpoint of scapular body (1) (Carballido et al., 2012b; Fig. 6.87).

Comments. The position of the acromial process relative to the glenoid has to be checked with the long axis of the distal blade oriented horizontally.

C365: Scapula, area posterior to acromial ridge and distal blade: is excavated (0); is flat or slightly convex (1) (Upchurch et al., 2004b; Fig. 6.88).

Comments. This character describes the area posterior to the acromial ridge, and dorsal to the distal blade, where the two meet.

C366: Scapular glenoid, orientation: relatively flat or laterally facing (0); strongly beveled medially (1) (Wilson and Sereno, 1998).

Comments. The medially beveled glenoid surface was proposed as autapomorphy for *Apatosaurus* (Wilson, 2002), but Upchurch et al. (2004b) showed that the orientation was actually variable within *Apatosaurus* specimens, which is confirmed herein.

C367: Scapular blade, acromial edge: straight (0); rounded expansion at distal end (1); racquet-shaped (2) (Wilson, 2002; wording modified; Fig. 6.87).

C368: Scapular blade, ventral edge in lateral view: is straight (0); curves ventrally towards its distal end (1) (Upchurch et al., 2004b; wording modified; Fig. 6.87).

Comments. Whereas the original character (Upchurch et al., 2004b) described the entire blade, the derived ventral curving is here restricted to the ventral edge of the blade.

C369: Scapula: without semi-ovate, flat muscle scar just distal to glenoid on scapular shaft (0); scar present (1) (Whitlock, 2011a; Fig. 6.88).

Comments. The scar described herein lies on the lateral side of the blade.

Table 6.42: Scapular ratios and angles.

Taxon	Specimen	Ratios			Angles		Means					Reference	Comments
		1) gl/min w db	2) acl/gl	3) db max w/min w	4) ca-db	5) ac-db	1	2	3	4	5		
Shunosaurus lii				2,00			6,6		2,0	90		Mannion et al., 2013	
	T5401, R	6,59		1,92	90							Zhang, 1988	measured from figure
Spinophorosaurus nigerensis	GCP-CV-4229, L			1,81	64,6	79,9			1,8	65	80	Remes et al., 2009	measured from figure
Omeisaurus				1,80			5,4	0,55	1,8	103		Mannion et al., 2013	
	T5701, R	5,42	0,55	1,76	103,1							He et al., 1988	measured from figure
Mamenchisaurus				2,20					2,2	72	69	Mannion et al., 2013	
	ZDM 0083, L				71,8	69,2						Taylor et al., 2011	measured from figure
Camarasaurus				2,20			6,5	0,58	2,1	74	85	Mannion et al., 2013	
	AMNH 5761	6,31	0,63	2,32		82,4						Osborn and Mook, 1921	measured from Fig. 74
	AMNH 5761	6,25	0,56	2,17		87,9						Osborn and Mook, 1921	measured from Fig. 75
	SMA 0002, L	6,61	0,58	2,24	75,3	85,6						O. Mateus, pers. comm., 2010	measured from photo
	SMA 0002, L	6,45	0,58	2,18	76,2	84,9						O. Mateus, pers. comm., 2010	measured from photo
	USNM 13768	5,60	0,54	1,68	61,3	81,9						O. Mateus, pers. comm., 2010	measured from photo
	WDC A, R	7,95	0,57	2,20	82,5	86,1						Ikejiri, 2004	measured from figure
Apatosaurus grandis YPM 1901	YPM 1901, L	6,05	0,55	2,16	81,8	73,8	6,1	0,55	2,2	82	74	Wilson and Sereno, 1998	measured from figure
Lourinhasaurus alenquerensis lectotype	MIGM, L	6,68	0,66	2,11		89,3	6,7	0,66	2,1		89	pers. obs.	measured from photo
Giraffatitan brancai				2,20			6,8	0,53	2,1	88	87	Mannion et al., 2013	
	MB.R.2727, L	6,75	0,55	1,94	85,9							pers. obs.	measured from photo; distal end reconstructed
	MB.R. Sa 9, L	6,90	0,51	2,25	90	87,4						Taylor et al., 2011	measured from figure
Brachiosaurus sp. SMA 0009	SMA 0009, L					90	7,6	0,39	2,0	77	86	Schwarz et al. 2007c	
	SMA 0009, L	7,64	0,39	2,00	77,4	81,4						Schwarz et al. 2007c	measured from figure
Ligabuesaurus leanzai				1,70			6,2	0,58	1,7	70	93	Mannion et al., 2013	
	MCF-PVPH-233, R	6,22	0,58	1,64	69,5	93,1						Bonaparte et al., 2006	measured from figure
Isisaurus colberti	ISIR335/57, L	4,17		1,59			4,2		1,6			Jain and Bandyopadhyay, 1997	measured from figure
Haplocanthosaurus priscus	CM 879, L	6,19		2,84	88,8	88,9	6,2		2,8	89	89	Hatcher, 1903	measured from figure
Limaysaurus tessonei	MUCPv-205, L	4,89		2,03	64,1		4,9		2,0	64		Calvo and Salgado, 1995	measured from figure
Cathartesaura anaerobica	MPCA-232	4,25			52,4	45,5	4,3			52	46	Gallina and Apesteguía, 2005	measured from figure
Nigersaurus taqueti				2,50			5,3	0,45	2,6	90		Mannion et al., 2013	
	MNN GAD	5,33	0,45	2,63	90							Sereno et al., 1999	measured from figure
Dicraeosaurus hansemanni	MB.R. E 19	6,84	0,53	1,78	77,8	92,8	6,8	0,53	1,8	78	93	Janensch, 1961	D. sattleri; measured from figure

Table 6.42: Scapular ratios and angles.

Suuwassea emilieae ANS 21122	ANS 21122					80	6,6	0,48	1,8	65	75	Schwarz et al. 2007c	
	ANS 21122	6,62	0,48	1,76	65,3	70						Harris, 2006	measured from figure; distal end reconstructed
Apatosaurus ajax YPM 1860	YPM 1860, L	5,78	0,50		90	85,1	5,8	0,50		90	85,1	Marsh, 1896	measured from figure
Brontosaurus excelsus YPM 1980	YPM 1980, L	7,48	0,50	1,83	83,9	79,6	7,5	0,50	1,8	84	80	Marsh, 1881	measured from figure
Apatosaurus louisae CM 3018	CM 3018, L	6,74	0,49	1,79	78,6	70	6,7	0,49	1,8	79	70	Gilmore, 1936	measured from figure
Elosaurus parvus CM 566	CM 566					90	5,8	0,56	1,6	77	93	Schwarz et al. 2007c	
	CM 566, R	5,84	0,56	1,56	77,1	95						pers. obs.	measured from photo
Apatosaurus parvus UW 15556	UW 15556					90	6,9	0,51		75	85	Schwarz et al. 2007c	
	UW 15556, L	6,89	0,51		74,8	80,9						Gilmore, 1936	measured from figure
Eobrontosaurus yahnahpin Tate-001	Tate-001	5,99	0,55	1,70	74	85,7	6,0	0,55	1,7	74	86	D. Lovelace, pers. comm., 2013	measured from photo
Apatosaurus ajax NSMT-PV 20375	NSMT-PV 20375	6,58	0,51	1,48	85	61,5	6,6	0,51	1,5	85	62	Upchurch et al., 2004b	measured from figure
Supersaurus vivianae holotype	BYU 12962	5,89	0,52	2,00	60,3	88,2	5,9	0,52	2,0	60	88	D. Lovelace, pers. comm., 2013	measured from photo
Supersaurus vivianae BYU	BYU 9025	5,94	0,51	1,98	77,2	77,3	5,9	0,52	2,0	69	83	Lovelace et al., 2007	measured from figure
	BYU 12962	5,89	0,52	2,00	60,3	88,2						D. Lovelace, pers. comm., 2013	measured from photo
Tornieria africana holotype	MB.R.2728, L	6,04	0,51	1,46	71,9	63,7	6,0	0,51	1,5	72	64	Remes, 2006	measured from figure
Tornieria africana skeleton k	MB.R.2730, L	7,02	0,50	1,63	64,9	60	7,0	0,50	1,6	65	60	Remes, 2006	measured from figure
Diplodocus carnegii CM 84	CM 84, L	6,66	0,47	1,67	71,5	76,4	6,7	0,47	1,7	72	76	pers. obs.	measured from photo
Diplodocus carnegii CM 94	CM 94					80	7,3	0,49	1,8	75	78	Schwarz et al. 2007c	
	CM 94, L	7,26	0,49	1,82	74,5	76,3						pers. obs.	measured from photo
Diplodocus sp. AMNH 223	AMNH 223, R	5,36	0,50	1,64		69,7	5,4	0,50	1,6		70	Osborn, 1899	measured from figure
	AMNH 223, R					69,7						pers. obs.	measured from photo
Diplodocus sp. USNM 10865	USNM 10865, R	5,84	0,53	1,84	71,7	81,3	5,8	0,53	1,8	72	81	Taylor et al., 2011	measured from figure
Galeamopus hayi HMNS 175	HMNS 175, R	6,16	0,47	1,83	78,8	78,3	6,2	0,47	1,8	79	78	pers. obs.	measured from photo
Galeamopus shellensis SMA 0011	SMA 0011, R	7,69			66,1		7,7			66		pers. obs.	measured from photo
Barosaurus sp. AMNH 6341	AMNH 6341, R					70	6,7	0,49	1,9	59	63	Schwarz et al. 2007c	
	AMNH 6341, R	6,71	0,49	1,88	59,1	56,5						McIntosh, 2005	measured from figure
Cetiosauriscus stewarti NHMUK R3078	NHMUK R3078	6,64					6,6					pers. obs.	incomplete, measured from photo

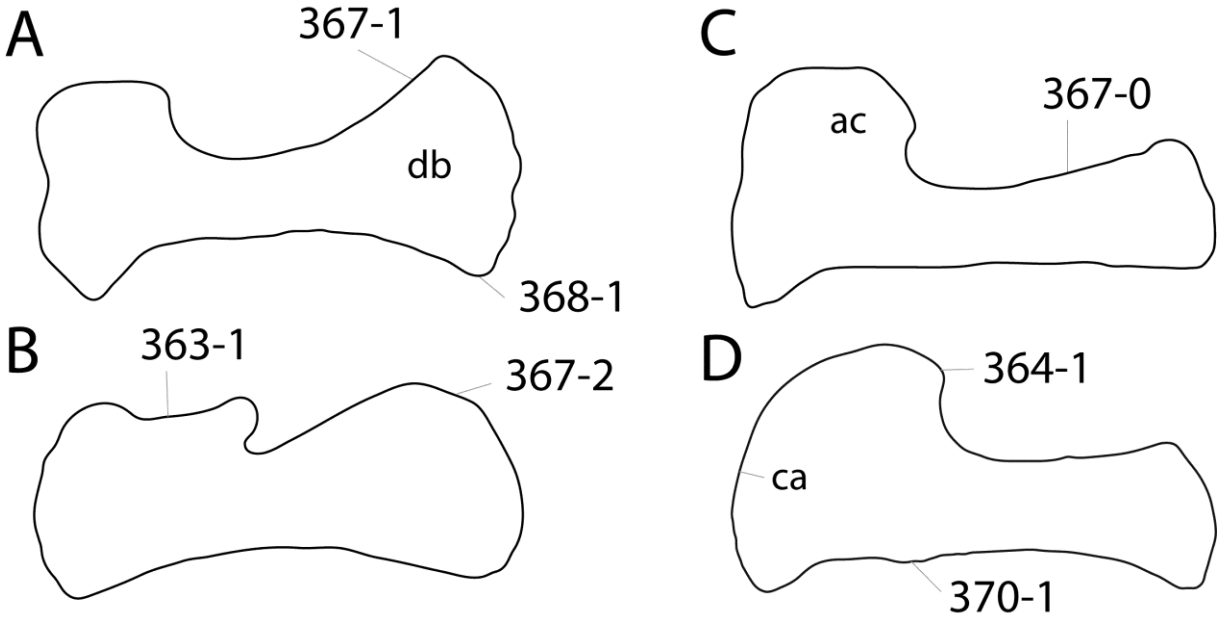

Figure 6.87: Scapula outlines of *Haplocanthosaurus priscus* CM 879 (A), *Limaysaurus tessonei* MUCPv-205 (B), *Apatosaurus louisae* CM 3018 (C; all traced from Mannion, 2009), and *Diplodocus* sp. AMNH 223 (D; traced from Osborn, 1899). Note the concave dorsal border of the acromion process (B; C363-1), the acromion process that reaches almost half the scapular length (D; C364-1), the different shapes of the acromial edge (straight, C, C367-0; with rounded expansion distally, A, C367-1; raquet-shaped, B, C367-2), the ventrally curving ventral margin (A; C368-1), and the subtriangular process (D; C370-1). Abb.: ac, acromion; ca, coracoid articulation; db, distal blade. Scaled to same scapular length.

C370: Scapular blade, subtriangular projection on anterior portion of ventral edge: absent (0); present (1) (Gallina and Apesteguía, 2005; Fig. 6.87).

Comments. In *Diplodocus* sp. AMNH 223, there are two eminences close to each other (pers. obs., 2011).

C371: Scapular blade, expansion of the distal end: wide (at least 2 times narrowest width of shaft in lateral view) (0); narrow (< 2 times narrowest width of shaft) (1) (Yu, 1993; modified; Tab. 6.42).

Comments. Measurements are taken perpendicular to the long axis of the blade.

C372: Coracoid, anteroventral margin shape: rounded (0); rectangular (1) (Bakker, 1998; Wilson, 2002; Fig. 6.89).

C373: Coracoid, infraglenoid groove: reduced to absent (0); present and distinct (1) (Carballido et al., 2012b; modified; Fig. 6.89).

C374: Sternal plates, shape: subcircular or oval (0); subtriangular with widened posterior border (1); elliptical to crescentic, with concave lateral margin (2) (Calvo and Salgado, 1995; modified; Fig. 6.90).

Comments. The subtriangular shape was added to the original version of Calvo and Salgado (1995) in order to better describe the difference between typical basal neosauropod or macronarian, and diplodocid shape. The character is treated as unordered, because none of the states can convincingly be interpreted as intermediate.

C375: Sternal plate, ridge on the ventral surface: absent (0); broad and shallow, or elongate and prominent (1) (Upchurch et al., 2004a; wording modified; Fig. 6.90).

C376: Sternal plate, anterior end: expanded dorsoventrally (0); flat, not expanded (1) (Tschopp and Mateus, 2012a; modified; Fig. 6.90).

C377: Sternal plate, posterior border: convex (0); straight (1) (González Riga, 2002; modified; Fig. 6.90).

Comments. The true shape of the posterior border can sometimes be obscured due to the presence of fused sternal ribs (Tschopp and Mateus, 2012a).

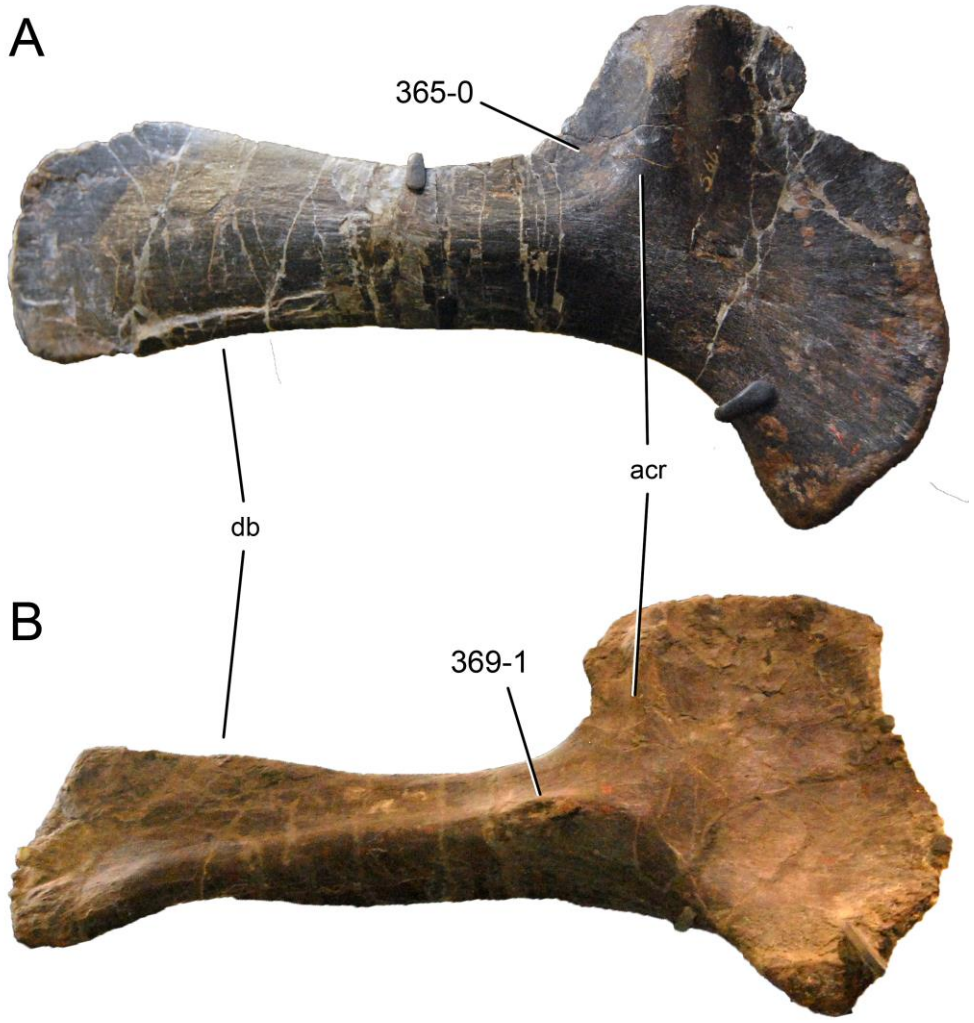

Figure 6.88: Right scapulae of *Elosaurus parvus* CM 566 (A) and *Brontosaurus excelsus* YPM 1980 (B) in lateral view. Note the excavated area between the acromial edge and the distal blade (A; C365-0) and the flat muscle scar at the base of the distal blade (B; C369-1). Abb.: acr, acromial ridge; db, distal blade. Scaled to same length.

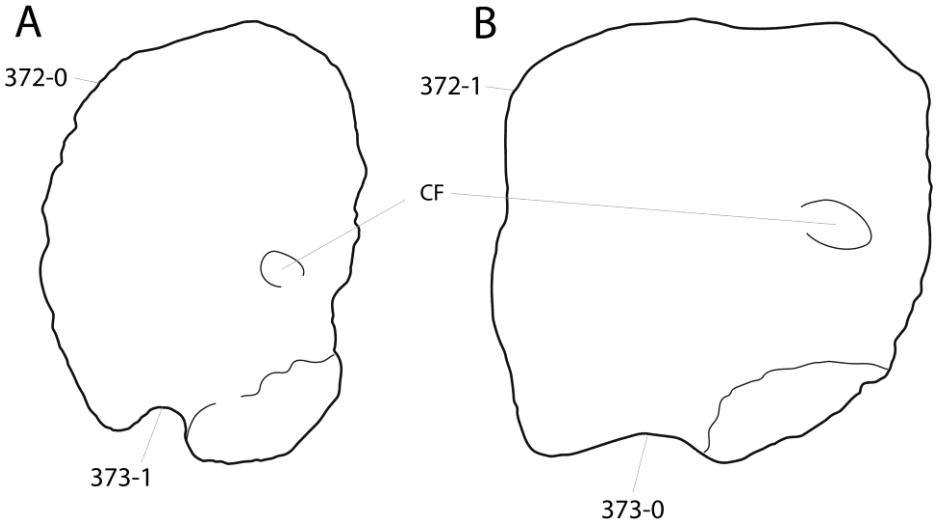

Figure 6.89: Left coracoids of *Amphicoelias altus* AMNH 5764? (A) and *Apatosaurus ajax* YPM 1860 (B; traced from Bakker, 1998) in anterolateral view. Note the rounded (A; C372-0) instead of rectangular shape (B; C372-1), and the deep (A; C373-1) in contrast to shallow infraglenoid groove (B; C373-0). Abb.: CF, coracoid foramen. Scaled to the same height.

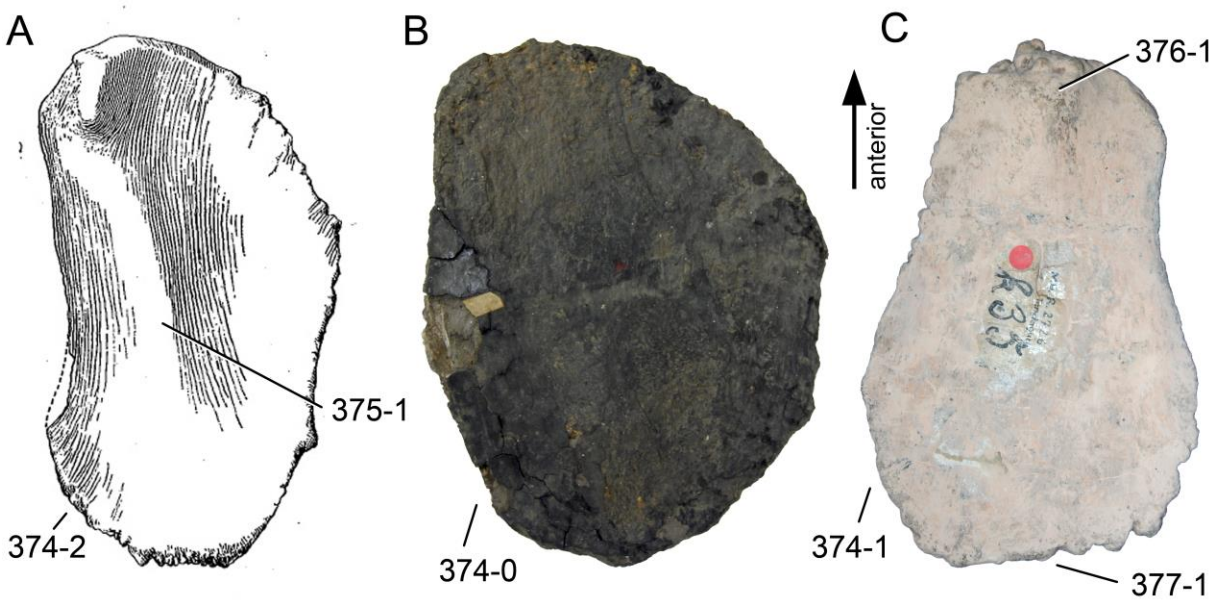

Figure 6.90: Right (A, B) and left (C) sternal plates of *Giraffatitan brancai* MB.R.2181 (A; modified from Janensch, 1961), *Brontosaurus amplus* YPM 1981 (B), and *Tornieria africana* MB.R.2726 (C) in ventral view. Note the different shapes (oval, B, C374-0; triangular, C, C374-1; crescentic, A, C374-2), the longitudinal ridge (A; C375-1), the anterior dorsoventral thickening (C; C376-1), and the straight posterior border (C; C377-1). Scaled to same length.

Forelimb

C378: Forelimb: hindlimb length ratio: 0.76 or greater (0); less than 0.76 (1) (Upchurch, 1995, 1998; modified; Tab. 6.43).

Comments. Forelimb length is the sum of the lengths of the humerus, radius, and metacarpal III, hindlimb length the sum of the lengths of femur, tibia, and metatarsal III.

C379: Humerus-to-femur ratio: < 0.7 (0); 0.7-0.77 (1); 0.77-0.90 (2); = or > 0.90 (3) (McIntosh, 1990a; modified; Tab. 6.44).

Comments. State boundaries are chosen such that the generally accepted genera *Apatosaurus* and *Diplodocus* can be distinguished from *Tornieria* and *Barosaurus*. The character is treated as ordered.

C380: Humerus, RI (sensu Wilson and Upchurch, 2003): gracile (less than 0.27) (0); medium (0.28-0.32) (1); robust (more than 0.33) (2) (Carballido et al., 2012b; Tab. 6.45).

Comments. The humerus RI was defined as the mean between proximal, distal, and midshaft transverse widths, divided by humerus length (Wilson and Upchurch, 2003). Scores for taxa where no measurements were available were taken from Carballido et al. (2012b). The character is herein treated as ordered.

C381: Humerus, shaft twist: minor to absent (0); high, distal articular surface twisted by at least 30° compared to proximal articular surface (1) (Gilmore, 1932; Tab. 6.45).

Comments. This angle is difficult to measure due to lacking references. It was proposed as distinguishing feature of *Diplodocus* (Gilmore, 1932) and is here included into a phylogenetic analysis for the first time.

C382: Humerus, midshaft cross-section, shape: circular, transverse diameter: anteroposterior diameter ratio is 1.5 or lower (usually close to 1.3) (0); elliptical, transverse diameter: anteroposterior diameter ratio is greater than 1.5 (usually close to 1.8) (1) (Wilson, 2002; modified by Mannion et al., 2012; Tab. 6.45).

C383: Humerus, pronounced proximolateral corner: absent (0); present (1) (Upchurch, 1998; Fig. 6.91).

Comments. A pronounced proximolateral corner forms a weak hump in anterior or posterior view.

C384: Humerus, proximal expansion: more or less symmetrical (0); asymmetrical, proximo-medial corner much more pronounced than proximolateral one (1) (Wilhite, 2005; Fig. 6.91).

Comments. The differing expansions were found to be taxonomically significant (Wilhite, 2005), but have not been previously included in any phylogenetic analysis. This character forms an additive binary character together with character 385.

Table 6.43: Forelimb/hindlimb ratio.

Taxon	Specimen	Ratio	Reference	Comments
Shunosaurus lii	T5402	0,64	Zhang, 1988	left and right elements mixed
Mamenchisaurus	ZDM 0083	0,79	Ouyang and Ye, 2002	mt II instead of III, left and right elements mixed
Camarasaurus	KUVP 129716	0,86	Bonnan, 2001	left and right elements mixed
Brachiosaurus sp.	SMA 0009, L	0,79	Schwarz et al., 2007	
Apatosaurus louisae	CM 3018	0,72	Bonnan, 2001	left and right elements mixed
Galeamopus shellensis	SMA 0011	0,72	pers. obs.	left and right elements mixed

Table 6.44: Humerus/femur length.

Taxon	Specimen	Ratio	Mean	Reference
Shunosaurus lii	T5402	0,56	0,62	Zhang, 1988
		0,60		Yu, 1993
		0,70		Mannion et al., 2013
Omeisaurus	T5701	0,82	0,82	He et al., 1988
	T5704	0,81		He et al., 1988
	T5705	0,85		He et al., 1988
		0,82		Yu, 1993
		0,80		Mannion et al., 2013
Mamenchisaurus		0,71	0,71	Ouyang and Ye, 2002
		0,70		Mannion et al., 2013
Jobaria tiguidensis		0,76	0,76	Sereno et al., 1999
Camarasaurus		0,75	0,74	Yu, 1993
		0,70		Mannion et al., 2013
	GMNH-PV 101	0,76		McIntosh et al., 1996a
	YPM 1910	0,73		McIntosh et al., 1996a
	CM 11338	0,76		McIntosh et al., 1996a
Apatosaurus grandis	YPM 1901	0,75	0,75	McIntosh et al., 1996a
Lourinhasaurus alenquerensis	lectotype	0,85	0,85	Raath and McIntosh, 1987
Giraffatitan brancai	MB.R.2181	1,02	1,02	Janensch, 1961
		1,05		Yu, 1993
		1,00		Mannion et al., 2013
Brachiosaurus sp.	SMA 0009	0,81	0,81	Schwarz et al., 2007c
Brachiosaurus altithorax		1,00	1,00	Janensch, 1929
		1,00		Mannion et al., 2013
Ligabuesaurus leanzai	MCF-PHV-233	0,90	0,90	Bonaparte et al., 2006
Limaysaurus tessonei	MUCPv-205	0,63	0,63	Calvo and Salgado, 1995
Amargasaurus cazaui	MACN-N 15	0,69	0,69	Salgado and Bonaparte, 1991
		0,68		Yu, 1993
Brontosaurus excelsus	YPM 1980	0,63	0,63	Upchurch et al., 2004b
		0,62		Bonnan, 2001
Brontosaurus amplus	YPM 1981	0,64	0,64	McIntosh, 1995
Apatosaurus louisae	CM 3018	0,64	0,64	Gilmore, 1936
Elosaurus parvus	CM 566	0,67	0,67	Bonnan, 2001
Apatosaurus parvus	UW 15556	0,64	0,64	Bonnan, 2001
Tornieria africana	holotype	0,72	0,72	Remes, 2006
Tornieria africana	skeleton k	0,71	0,72	Remes, 2006
		0,72		Janensch, 1929b
Diplodocus sp.	USNM 10865	0,63	0,63	Gilmore, 1932
Galeamopus shellensis	SMA 0011	0,64	0,64	pers. obs.
Barosaurus sp.	AMNH 6341	0,71	0,73	McIntosh, 2005
		0,75		Schwarz et al., 2007c
Cetiosauriscus stewarti	NHMUK R3078	0,71	0,70	pers. obs.
		0,69		Janensch, 1929b

Table 6.45: Humerus ratios.

Taxon	Specimen	1) RI	Mean 1	2) min w/ min apd	Mean 2	3) shaft twist	Reference	Comments
Shunosaurus lii	T5402, L	0,340	0,32				Zhang, 1988	
	T5402, R	0,295					Zhang, 1988	
Spinophorosaurus nigerensis	NMB-1698-R, R	0,250	0,25			22,6	Remes et al., 2009; O. Mateus, pers. comm. 2011	measured from photos
Omeisaurus			0,29	1,640	1,62		Young 1939	
				1,600			Mannion et al., in press	
	T5701, L	0,289					He et al., 1988	
	T5702, L	0,304					He et al., 1988	
	T5703, R	0,305					He et al., 1988	
	T5704, L	0,276					He et al., 1988	
	T5705, L	0,286					He et al., 1988	
Mamenchisaurus	ZDM 0083, L	0,285	0,29				Ouyang and Ye, 2002	
	ZDM 0083, R	0,293					Ouyang and Ye, 2002	
Jobaria tiguidensis	MNN-TIG			1,310			Mannion et al. 2012	
Turiasaurus riodevensis	CPT-1195-1210			1,990			Mannion et al. 2012	
Losillasaurus giganteus type	MCNV Lo-7			1,830			Mannion et al. 2012	
Camarasaurus			0,29	1,260	1,36		Ostrom & McIntosh 1966	
				1,300			Mannion et al., in press	
	AMNH 664, L	0,305		1,455			Bonnan, 2001	
	BYU 9047	0,262				'not twisted'	McIntosh et al. 1996a, b	
	CM 21781, L	0,345		1,627			Bonnan, 2001	
	FMNH P25182, R	0,311					Bonnan, 2001	
	GMNH-PV 101	0,251				nearly parallel	McIntosh et al. 1996a, fig. 62c	
	YPM 1910	0,333					McIntosh et al. 1996a	
	YPM 5858, L	0,258		1,167			Bonnan, 2001	
Apatosaurus grandis YPM 1901	YPM 1901	0,299	0,28		1,17		McIntosh et al. 1996a	
	YPM 1901, L	0,256		1,167			Bonnan, 2001	
	YPM 1901, L	0,300					Wilhite, 2003	
Lourinhasaurus alenquerensis lectotype	MIGM		0,25	1,210	1,21		Mannion et al. 2012	
	MIGM	0,250					pers. obs.	measured from photo
Giraffatitan brancai			0,22	1,400	1,40		Janensch, 1961	
				1,400			Mannion et al., in press	
	MB.R. F2, R	0,210					Janensch, 1961	
	MB.R. I 1, R	0,251					Janensch, 1961	
	MB.R. Ki 130					35	Janensch, 1961	
	MB.R.2181, R	0,210					Janensch, 1961	
Brachiosaurus sp. SMA 0009	SMA 0009	0,290	0,29				Schwarz et al., 2007	
Brachiosaurus altithorax	FMNH P25107, R	0,221	0,22				Wilhite, 2003	distal end damaged, ratio slightly higher
Ligabuesaurus leanzai	MCF-PHV 233		0,22	1,200	1,20		Mannion et al. 2012	
				1,200			Mannion et al., in press	
	MCF-PHV 233	0,221					Bonaparte et al., 2006	
Isisaurus colberti	ISIR335/59	0,252	0,25				Jain and Bandypadhyay, 1997	
Limaysaurus tessonei	MUCPv-205		0,26	1,830	1,83		Mannion et al. 2012	
	MUCPv-205	0,260					Wilson and Upchurch, 2003	
Nigersaurus taqueti	MNN GAD			1,250	1,28		Mannion et al. 2012	
				1,300			Mannion et al., in press	
Dicraeosaurus hansemanni			0,32	1,380	1,38		Janensch, 1961	
	MB.R. Q 11, R	0,331					Janensch, 1961	
	MB.R. St53, R	0,315					Janensch, 1961	
Amargasaurus cazaui	MACN-N 15		0,31	1,880	1,88	'not very pronounced'	Salgado and Bonaparte, 1991; Mannion et al., 2012	
	MACN-N 15	0,310					Wilson and Upchurch, 2003	
Suuwassea emilieae ANS 21122	ANS 21122	0,362	0,36	1,270	1,27	'gently twisted'	Harris 2007	
Brontosaurus excelsus YPM 1980	YPM 1980, L		0,33		1,25	'straight appearance'	Bedell & Trexler 2005	confirmed by pictures
	YPM 1980	0,367					McIntosh, 1995	
	YPM 1980, L	0,291		1,250			Bonnan, 2001	
Brontosaurus amplus YPM 1981	YPM 1981	0,323	0,33				McIntosh, 1995	
	YPM 1981, L	0,327					Wilhite, 2003	
Apatosaurus louisae CM 3018	CM 3018		0,36	1,280	1,28		Gilmore 1936	
	CM 3018, L	0,359					Wilhite, 2003	
	CM 3018, L	0,361		1,280			Bonnan, 2001	
	CM 3018, R	0,354					Wilhite, 2003	
	CM 3018					gentle	pers. obs.	
Elosaurus parvus CM 566	CM 566, R	0,336	0,33	1,088	1,09		Bonnan, 2001	
	CM 566, R	0,336					Wilhite, 2003	
	CM 566, L	0,329		1,091			Bonnan, 2001	
	CM 566, L	0,323					Wilhite, 2003	
Apatosaurus parvus UW 15556	UW 15556, R	0,370	0,37				Hatcher, 1902	
Eobrontosaurus yahnahpin Tate-001	Tate-001		0,35	1,390	1,45	23,6	Mannion et al., 2012; P. Mannion, pers. comm. 2012	
	Tate-001	0,342					Filla and Redman, 1994	
	Tate-001	0,363		1,517			Bonnan, 2001	
Tornieria africana holotype	MB.R.2672, R	0,316	0,32				Janensch, 1961	
Tornieria africana skeleton k	MB.R.2673, R		0,31	1,300	1,30	31,05	pers. obs.	measured from photo
	MB.R.2673, R	0,314					Janensch, 1961	
Diplodocus sp. USNM 10865	USNM 10865		0,28			45	Gilmore 1932	
	USNM 10865, L	0,284					Wilhite, 2003	
	USNM 10865, L	0,283					McIntosh, 2005	
	USNM 10865				<1,5		pers. obs.	
Diplodocus sp. WDC-FS001A	WDC-FS001A, R	0,268	0,27	0,983	1,00	'nearly 45°'	Bedell and Trexler, 2005; pers. obs.	measured from photo
Galeamopus hayi HMNS 175	HMNS 175, L	0,323	0,32	1,758	2,18		Bonnan, 2001	
	HMNS 175, L	0,318					McIntosh, 2005	
	HMNS 175, R	0,326		2,606			Bonnan, 2001	
	HMNS 175, R	0,322					McIntosh, 2005	
	HMNS 175					gentle	pers. obs.	
Galeamopus shellensis SMA 0011	SMA 0011, L	0,367	0,37	2,486	2,49		pers. obs.	min apd estimated
Barosaurus sp. AMNH 6341	AMNH 6341, R		0,24		1,69	55,4	pers. obs.	
	AMNH 6341, R	0,246		1,695			Bonnan, 2001	
	AMNH 6341	0,246					Wilhite, 2003	
	AMNH 6341	0,239					McIntosh, 2005	
Cetiosauriscus stewarti NHMUK R3078	NHMUK R3078		0,32	1,550	1,44		Mannion et al. 2012	
	NHMUK R3078	0,316		1,333			Woodward, 1905	

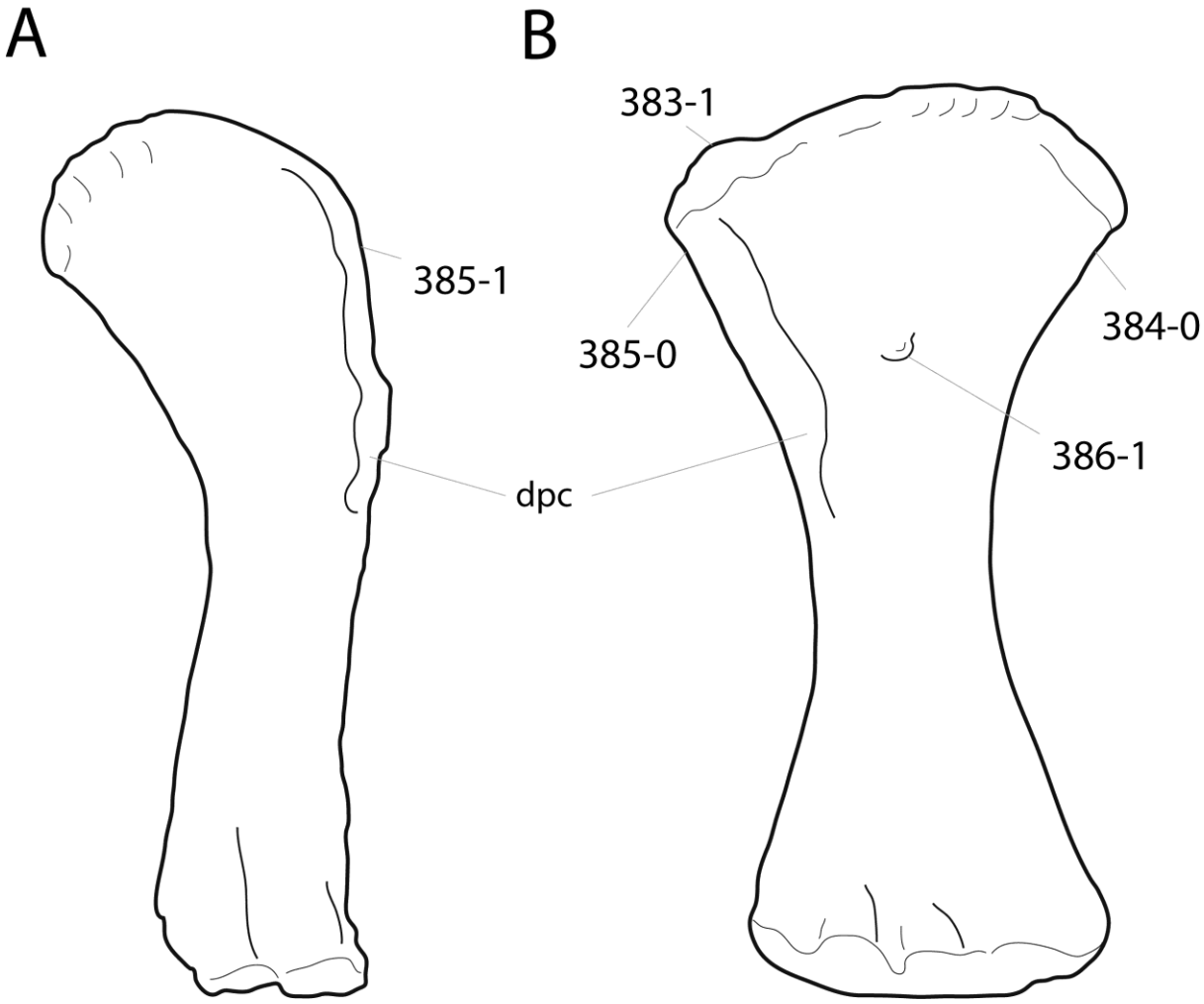

Figure 6.91: Humeri of *Turiasaurus riodevensis* CPT 1195-1210 (A; traced from Royo-Torres et al., 2006) and *Suuwassea emilieae* ANS 21122 (B; traced from Harris, 2007) in anterior view. Note the pronounced proximo-lateral corner (B; C383-1), the symmetrical proximal transverse expansion (B; C384-1), the unexpanded (A; C385-1) or expanded lateral edges (B; C385-0), and the tubercle marking the center of the proximal concavity (B; C386-1). Abb.: dpc, deltopectoral crest. Scaled to same length.

C385: Humerus, proximal end expanded laterally in anterior/proximal view: expanded, lateral margin concave in anterior/posterior view (0); not expanded (1) (Curry Rogers, 2005; polarity reversed; Fig. 6.91).

Comments. Polarity was reversed compared to the original description (Curry Rogers, 2005), due to the differing taxon sampling.

C386: Humerus, shallow, but distinct rugose tubercle at the center of the concave proximal portion of the anterior surface: absent (0); present (1) (New; Fig. 6.91).

C387: Ulna to humerus length: < 0.65 (0); 0.66-0.76 (1); > 0.76 (2) (Janensch, 1929; Tab. 6.46).

Comments. The states were defined in order to include the majority of diplodocids in the same state. The character is treated as ordered.

C388: Ulna, proximal condylar processes: subequal in length (0); anterior arm longer (1) (Wilson, 2002; Tab. 6.47).

Comments. The state boundary is here set at 1.1, as this follows best higher-level taxonomy.

C389: Ulna, proximal articular surface, angle between anterior and lateral branch: 90° (0); acute (1) (New; Tab. 6.47).

Comments. Taxa with angles greater than 83° were scored as plesiomorphic.

Table 6.46: Ulna/humerus length.

Taxon	Specimen	Ratio	Mean	Reference	Comments
Shunosaurus lii	T5402, R	0,722	0,71	Zhang 1988	
	T5402, L	0,704		Zhang 1988	
Omeisaurus	T5702, L	0,696	0,79	He et al. 1988	
	T5703, R	0,787		He et al. 1988	
	T5704, L	0,803		He et al. 1988	
	T5705, L	0,869		He et al. 1988	
Mamenchisaurus	ZDM 0083, R	0,691	0,69	Ouyang & Ye 2002	
	ZDM 0083, L	0,694		Ouyang & Ye 2002	
Turiasaurus riodevensis		0,704	0,70	Royo-Torres et al. 2006	
Losillasaurus giganteus type		0,566	0,57	Royo-Torres et al. 2006	
Camarasaurus	AMNH 664, L	0,701	0,77	Bonnan 2001	
	AMNH 711, L	0,800		Bonnan 2001	
	BYU 9047	0,761		McIntosh et al. 1996b	
	CM 11338	0,687		Gilmore 1925; Wilhite 2003	
	FMNH P25182, R	0,767		Bonnan 2001	
	KUVP 129716, R	0,894		Bonnan 2001	
Apatosaurus grandis YPM 1901	YPM 1901, L	0,743	0,74	Bonnan 2001; Wilhite 2003	
Lourinhasaurus alenquerensis lectotype		0,707	0,71	Royo-Torres et al. 2006	
Giraffatitan brancai		0,610	0,61	Janensch 1929b	
Brachiosaurus sp. SMA 0009	SMA 0009	0,750	0,75	Schwarz et al. 2007c	
Isisaurus colberti	ISIR 335	0,560	0,56	Jain & Bandhyapadhyay 1997	
Limaysaurus tessonei	MUCPv-205	0,733	0,73	Calvo & Salgado 1995	
Dicraeosaurus hansemanni		0,700	0,70	Janensch 1929b	*D. sattleri*
Amargasaurus cazaui	MACN-N 15	0,611	0,61	Salgado & Bonaparte 1991	
Brontosaurus excelsus YPM 1980	YPM 1980, L	0,756	0,76	Bonnan 2001	
Apatosaurus louisae CM 3018	CM 3018, L	0,739	0,74	Bonnan 2001	
Elosaurus parvus CM 566	CM 566, R	0,741	0,74	Bonnan 2001; Wilhite 2003	
Apatosaurus parvus UW 15556	UW 15556, R	0,673	0,67	Hatcher 1902; Gilmore 1936	
Eobrontosaurus yahnahpin Tate-001	Tate-001, L	0,701	0,70	Bonnan 2001; Wilhite 2003	
Tornieria africana skeleton k		0,750	0,75	Janensch 1929b	
Diplodocus sp. USNM 10865	USNM 10865, R	0,733	0,73	Gilmore 1932	
Galeamopus hayi HMNS 175	HMNS 175, L	0,819	0,82	Bonnan 2001	
Galeamopus shellensis SMA 0011	SMA 0011	0,693	0,69	pers. obs.	
Cetiosauriscus stewarti NHMUK R3078	NHMUK R3078	0,809	0,81	Royo-Torres et al. 2006	

C390: Ulna, distal transverse expansion: slight, < 1.3 times min sw (0); wide, 1,3 times min sw or greater (1) (New; Tab. 6.47).

Comments. Some width measurements published do not state explicitly if they are taken transversely or anteroposteriorly, they just report maximum distal width. Anteroposterior width is often much greater than transverse width in distal surfaces of the sauropod ulnae. This leads to exaggerated ratios, if erroneously included here. Also, especially disarticulated ulnae, where both proximal processes are equally long, are difficult to orient properly. Nonetheless, the differences in these ratios still appear significant.

C391: Radius, maximum diameter of the proximal end divided by greatest length: < 0.3 (0); 0.3 or greater (1) (McIntosh, 1990a; modified by Mannion et al., 2013; Tab. 6.48).

Comments. Maximum diameter can be width or depth.

C392: Radius, distal articular surface for ulna: reduced and relatively smooth (0); well developed with one or two distinct longitudinal ridges (1) (New; Fig. 6.92).

C393: Radius, distal condyle orientation in anterior view: perpendicular or beveled less than 15° to long axis of shaft (0); beveled at least 15° to long axis of shaft (1) (Curry Rogers and Forster, 2001; Wilson, 2002; modified; Tab. 6.48).

Comments. As stated by Mannion et al. (2013), the beveling of the distal surface often only affects the lateral half of the distal end. Given the different scope of the phylogenetic analysis, character state boundaries are different herein compared to Mannion et al. (2013).

C394: Radius, distal breadth: <1.8 times larger than midshaft breadth (0); at least 1.8 times midshaft breadth (1) (Wilson, 2002; modified).

Comments. Breadth is measured mediolaterally.

Table 6.47: Ulnar ratios and angles.

Taxon	Specimen	1) pw/pd	Mean 1	2) dw/min sw	Mean 2	angle cond proc	Reference	Comments
Shunosaurus lii	T5402, R		subequal	1,09	1,1		Zhang, 1988	
Omeisaurus		1,30	1,2		1,5		Mannion et al., 2013	
	T5703, R			1,31			He et al., 1988	
	T5704, L	1,10		1,69		86,5	He et al., 1988	1) and 3) measured from figure
	T5705, L			1,37			He et al., 1988	
Mamenchisaurus		1,00	1,0		1,7		Mannion et al., 2013	
	ZDM 0083, L	1,05		1,67		55,9	Ouyang and Ye, 2002	1) and 3) measured from figure
Jobaria tiguidensis	MNN TIG	1,42	1,4	1,35	1,4	59,3	O. Mateus, pers. comm., 2009; J. Carballido, pers. comm., 2013	measured from photos
Turiasaurus riodevensis	CPT			1,87	1,9		Royo-Torres et al., 2006	measured from figure
Losillasaurus giganteus type	MCNV Lo-8, L			1,38	1,4		Casanovas et al., 2001	
Camarasaurus		1,30	1,3		1,3		Mannion et al., 2013	
	AMNH 711, L			1,27			Bonnan, 2001	
	CM 11393, R			1,46			Bonnan, 2001	
	FMNH P25182, R			1,10			Bonnan, 2001	
	WDC A, R	1,26				47,7	Ikejiri, 2004	
Apatosaurus grandis YPM 1901	YPM 1901, L		1,2	1,29	1,3		Bonnan, 2001	
	YPM 1901, L	1,17				70,1	Wilson and Sereno, 1998	measured from figure
Lourinhasaurus alenquerensis lectotype	MIGM		>1				pers. obs.	
Giraffatitan brancai		1,40	1,3		1,5		Mannion et al., 2013	
	MB.R.2181, R	1,19		1,49		81,5	Janensch, 1961	2) and 3) measured from figure
Brachiosaurus sp. SMA 0009	SMA 0009, L			1,74	1,7		Schwarz et al., 2007c	
	SMA 0009, R			1,66			Schwarz et al., 2007c	
Isisaurus colberti	ISIR335/60, L	1,45	1,4	1,43	1,4	73,1	Jain and Bandyopadhyay, 1997	measured from figure
Limaysaurus tessonei			>1				Carballido et al., 2012b	
Zapalasaurus bonapartei	MOZ-Pv 1243, R	1,16	1,2	1,56	1,6	75,9	Salgado et al., 2012	2) and 3) measured from figure
Nigersaurus taqueti		1,20	1,2				Mannion et al., 2013	
Amphicoelias altus AMNH 5764	AMNH 5764-a, L	1,09	1,1	1,20	1,2	75,2	Osborn and Mook, 1921	measured from figure
Dicraeosaurus hansemanni	MB.R. O7	1,24	1,2	1,24	1,2	64,5	Janensch, 1961	D. sattleri; 2) and 3) measured from figure
Amargasaurus cazaui	MACN-N 15	1,07	1,1			45,8	Salgado and Bonaparte, 1991	measured from figure
Apatosaurus ajax YPM 1860	YPM 1860, L		1,4	1,34	1,3		Bonnan, 2001	
	YPM 1860, L	1,45				66,5	pers. obs.	measured from photos
Apatosaurus louisae CM 3018	CM 3018, L	1,03	1,0		1,1	67,6	Gilmore, 1936	measured from figure
	CM 3018, L			1,07			Bonnan, 2001	
Elosaurus parvus CM 566	CM 566, R	1,28	1,3		1,1	68,9	Carpenter and McIntosh, 1994	measured from figure
	CM 566, R			1,10			Wilhite, 2003	
Apatosaurus parvus UW 15556	UW 15556, L	1,47	1,5	1,35	1,4	100	Hatcher, 1902	measured from figure
Eobrontosaurus yahnahpin Tate-001	Tate-001, L		1,1	1,24	1,2		Bonnan, 2001	
	Tate-001, L	1,12				73,1	P. Mannion, pers. comm., 2012	

Table 6.47: continued.

Apatosaurus ajax NSMT-PV 20375	NSMT-PV 20375, R	1,05	1,0	2,20	2,2	80,1	Upchurch et al., 2004b	2) and 3) measured from figure
Tornieria africana skeleton k	MB.R.2586		1,2	1,39	1,5		McIntosh, 2005	
	MB.R.2586	1,19		1,59		66,9	Janensch, 1961	
	MB.R.2586	1,18					pers. obs.	
Diplodocus sp. USNM 10865	USNM 10865, L			1,26	1,3		McIntosh, 2005	
	USNM 10865, R			1,41			McIntosh, 2005	
	USNM 10865		subequal				pers. obs.	
Galeamopus hayi HMNS 175	HMNS 175	1,01	1,0		1,4	71,1	Hatcher, 1903	measured from figure
	HMNS 175, L			1,18			Bonnan, 2001	
	HMNS 175, L			1,57			McIntosh, 2005	
Galeamopus shellensis SMA 0011	SMA 0011, L	1,65	1,6	1,28	1,3	acute	pers. obs.	
Dyslocosaurus polyonychius AC 663	AC 663			1,41	1,4		pers. obs.	measured from photo
Dystrophaeus viaemalae USNM 2364	USNM 2364, R		1,5	1,06	1,1		Cope, 1877	
	USNM 2364, R	1,54				86,3	McIntosh, 1997	measured from figure

Table 6.48: Radius, ratios and angles.

Taxon	Specimen	1) pw/l	Mean 1	2) dw/min sw	Mean 2	angle dist cond	Reference	Comments
Shunosaurus lii		0,30	0,3	1,70	1,7	0	Mannion et al., 2013	
	T5402	0,33		1,65			Zhang, 1988	
Omeisaurus		0,20	0,2	2,00	1,9		Mannion et al., 2013	
	T5701	0,20		2,00		18	He et al., 1988	3) measured from figure
	T5703	0,21		1,87			He et al., 1988	
	T5704	0,21		1,97			He et al., 1988	
	T5705	0,18		1,56			He et al., 1988	
Mamenchisaurus		0,20	0,2	1,80	1,7	0	Mannion et al., 2013	
	ZDM 0083, L	0,21		1,62			Ouyang and Ye, 2002	
	ZDM 0083, R			1,66			Ouyang and Ye, 2002	
Jobaria tiguidensis	MNN TIG	0,25	0,2	1,88	1,9	15	J. Carballido, pers. comm., 2013	measured from photo
Turiasaurus riodevensis	CPT	0,21	0,2	2,29	2,3	4	Royo-Torres et al., 2006	measured from figure
Losillasaurus giganteus type	MCNV Lo-9, L			1,94	1,9		Casanovas et al., 2001	
Camarasaurus		0,30	0,3	2,30	1,9	10	Mannion et al., 2013	
	AMNH 823, L	0,26		1,59			McIntosh et al., 1996b	
	AMNH 823, R	0,28		1,69			McIntosh et al., 1996b	
	BYU 9047, R	0,24		1,79		11	McIntosh et al., 1996b	3) measured from figure
	FMNH P25182, R	0,22		2,29			Wilhite, 2003	
Apatosaurus grandis YPM 1901	YPM 1901, L	0,26	0,3	2,08	1,8		McIntosh et al., 1996b	
	YPM 1901, L					8	Wilson and Sereno, 1998	measured from figure
	YPM 1901, L	0,27		1,29			Bonnan, 2001	
	YPM 1901, L	0,24		2,11			Wilhite, 2003	
Giraffatitan brancai		0,20	0,2	2,00	2,0	16	Mannion et al., 2013	
	MB.R.2181, R	0,25		1,96			Janensch, 1961	
Brachiosaurus sp. SMA 0009	SMA 0009, L	0,20	0,2	1,48	1,5	0	Schwarz et al., 2007	3) measured from figure

Table 6.48: continued.

Limaysaurus tessonei	MUCPv-205, L	0,24	0,2	1,83	1,8		Calvo and Salgado, 1995	measured from figure
Zapalasaurus bonapartei	MOZ-Pv 1255, L	0,26	0,3	2,00	2,0	8	Salgado et al., 2012	2) measured from figure
Nigersaurus taqueti		0,20	0,2	1,70	1,7	0	Mannion et al., 2013	
Dicraeosaurus hansemanni	MB.R. G83, L	0,24	0,2	1,54	1,5	8	Janensch, 1961	D. sattleri; 3) measured from figure
Amargasaurus cazaui	MACN-N 15, L	0,26	0,3	1,69	1,7		Salgado and Bonaparte, 1991	measured from figure
Brontosaurus excelsus YPM 1980	YPM 1980, R	0,32	0,3	2,09	2,1	6	Ostrom and McIntosh, 1966	measured from photo
Apatosaurus louisae CM 3018	CM 3018, L	0,30	0,3	1,86	2,0	22	Gilmore, 1936	3) measured from figure
	CM 3018, L	0,30		2,25			Bonnan, 2001	
	CM 3018, L	0,29		1,93			Wilhite, 2003	
Apatosaurus parvus UW 15556	UW 15556	0,32	0,3	1,81	1,8	11	Hatcher, 1902	3) measured from figure
	UW 15556, L	0,31		1,73			Wilhite, 2003	
Eobrontosaurus yahnahpin Tate-001	Tate-001, L	0,26	0,3	1,64	1,4		Bonnan, 2001	
	Tate-001, L	0,33		1,07			Wilhite, 2003	
	Tate-001, L					19	P. Mannion, pers. comm., 2012	measured from photo
Diplodocus sp. USNM 10865	USNM 10865, R	0,23	0,2	1,56	1,6		Wilhite, 2003	
Diplodocus sp. WDC-FS001A	WDC-FS001A	0,16	0,2	1,35	1,4	0	pers. obs.	measured from photo
Galeamopus hayi HMNS 175	HMNS 175, R		0,2		1,6	21	Hatcher, 1903	measured from figure
	HMNS 175, L	0,23		1,78			Bonnan, 2001	
	HMNS 175, R	0,26		1,47			Bonnan, 2001	
Galeamopus shellensis SMA 0011	SMA 0011, L	0,27	0,3	1,60	1,6	6	pers. obs.	
Dyslocosaurus polyonychius AC 663	AC 663			1,59	1,6	0	pers. obs.	measured from photo
Dystrophaeus viaemalae USNM 2364	USNM 2364			> 1.97	> 1,97	18	pers. obs.	measured from photo

Figure 6.92: Distal half of radius of *Dyslocosaurus polyonychius* AC 663 illustrating the very weak ridges for the articulation with the ulna (C392-0). Scale bar = 10 cm.

C395: Carpus, number of carpal bones: 3 or more (0); 2 (1); 1 or less (2) (McIntosh, 1990b; Upchurch, 1998; modified).

Comments. The character was initially proposed with only two character states (three or more, two or less; Upchurch, 1998). A third state was added here in order to distinguish *Apatosaurus* from the remaining taxa (Bonnan, 2003). Even though SMA 0011 was found with only one carpal preserved, its articulated position directly below the radius, and articulating with the first two to three metacarpals suggest that a second element was present. Such a presence is also indicated by the proximodistal width of the preserved element, which in articulation would create a large gap between the ulna and the lateral metacarpals. A similar case can be seen in the putative *Diplodocus* manus described by Bedell and Trexler (2005). The opposite can be seen in *Apatosaurus*, where the only carpal lies above mc II to IV, is proximodistally flattened, and metacarpals I and V are proximally dislocated in respect to the inner elements (CM 3018, UW 15556; Hatcher, 1902; Gilmore, 1936; Bonnan, 2003). Due to the probable gradual decrease in the number of carpal bones the character is treated as ordered.

C396: Carpals: block-like (0); proximodistally compressed discs (1) (New; Fig. 6.93).

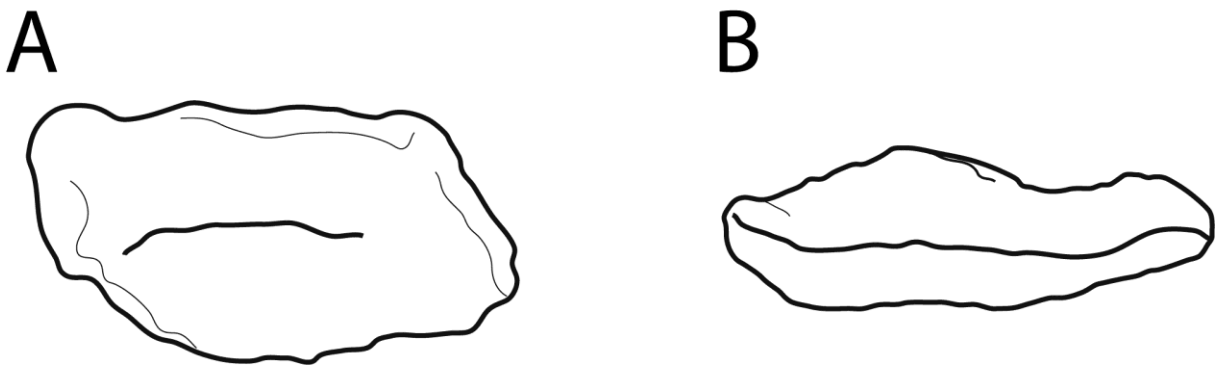

Figure 6.93: Carpal elements of SMA 0011 (A) and *Apatosaurus* sp. UW 15556 (B; traced from Bonnan, 2003) in anterior view, illustrating the two different shapes described in C396: 0) block-like (A), and 1) disc-like (B). Scaled to the same transverse width.

C397: Metacarpus, shape: spreading (0); bound, with subparallel shafts and articular surfaces that extend half their length (1) (Wilson, 2002).

C398: Metacarpals, shape of proximal surface in articulation: gently curving, forming a 90° arc (0); U-shaped, subtending a 270° arc (1) (Wilson, 2002).

C399: Metacarpus, ratio of longest metacarpal to radius: < 0.40 (0); 0.40 or greater (1) (Calvo and Salgado, 1995; modified by Mannion et al., 2013; Tab. 6.49).

Comments. The longest metacarpal is usually mc II or mc III.

C400: Metacarpal I, length: shorter than IV (0); longer than IV (1) (Wilson and Sereno, 1998; Tab. 6.49).

Comments. The state boundary applied herein lies at 1.0.

C401: Metacarpal I, proximal end dorsoventral height to mediolateral width ratio: < 1.8 (0); 1.8 or greater (1) (Apesteguía, 2005; Mannion and Calvo, 2011; Mannion et al., 2013; Tab. 6.49).

Comments. Mannion et al. (2013) were the first to include this ratio in a phylogenetic analysis.

C402: Metacarpal III, robustness (length/distal transverse width): robust, <2.9 (0); intermediate, 2.9-3.5 (1); slender, > 3.5 (2) (Bedell and Trexler, 2005; Tab. 6.49).

Comments. Suggested as distinguishing character between *Diplodocus* and *Apatosaurus*, and especially between WDC-FS001A and *Galeamopus hayi* HMNS 175 (Bedell and Trexler, 2005), which are both probably not *Diplodocus* (see next chapter), metacarpal robustness is herein used for the first time as a character in a phylogenetic analysis. The character is treated as ordered.

C403: Metacarpal V, proximal articular surface: subequal to smaller than (0); or significantly larger than proximal articular surface of mc III and IV (1) (Janensch, 1929b; Fig. 6.94).

Comments. An enlarged proximal articular surface of mc V can be seen in *Apatosaurus louisae* CM 3018 (Gilmore, 1936). However, this does not seem to be the case in another apatosaur specimen (NSMT-PV 20375; Upchurch et al., 2004b), such that the derived state might prove an autapomorphy of the species *A. louisae*. A similar development can be seen in the manus of *Janenschia robusta* (Janensch, 1922).

C404: Manual phalanx I-1, flange-like sheet of bone projecting from the proximoventral margin: absent (0); present (1) (Hatcher, 1902; Gilmore, 1936; Upchurch et al., 2004b; Fig. 6.95).

Pelvic girdle

C405: Ilium, ratio of blade height above pubic peduncle to anteroposterior length: <0.40 (0); 0.40 or more (1) (New; Tab. 6.50).

Comments. Blade height is measured vertically above the base of the pubic pedicel, with the ischiadic tubercle and the anteroventral-most point of the preacetabular process oriented on a horizontal line.

C406: Iliac preacetabular process, shape: sharply pointed (0); blunt to semicircular anterior margin (1) (Salgado et al., 1997; Fig. 6.96).

Comments. A strict lateral view of the ilium is often misleading, given the anterolateral to lateral orientation of the preacetabular lobe.

Table 6.49: Metacarpus ratios.

Taxon	Specimen	1) mc/r	Mean 1	2) mc I/IV	Mean 2	3) mc I, pd/pw	Mean 3	4) mc III, gl/dw	Mean 4	Reference	Comments
Shunosaurus lii		0,300	0,33	0,700	0,7	1,600	1,6			Mannion et al., 2013	
	T5402	0,354		0,750				2,615	2,6	Zhang 1988	
Omeisaurus			0,35	0,800	0,9	1,200	1,2			Mannion et al., 2013	
	T5701, L	0,371						3,333	3,2	He et al. 1988	
	T5703, R	0,345		1,101				3,257		He et al. 1988	
	T5704, R	0,327		0,817				3,050		He et al. 1988	
Mamenchisaurus	ZDM 0083	0,410	0,41	0,800	0,8		1,6			Mannion et al., 2013	
	ZDM 0083, R					1,570		3,485	3,4	Ouyang and Ye, 2002	3) measured from figure
	ZDM 0083, L	0,413		0,820				3,385		Ouyang and Ye, 2002	
Jobaria tiguidensis	MNN TIG		0,38		shorter		1,6	3,277	3,3	O. Mateus, pers. comm. 2013	measured from photo
	MNN TIG3	0,375				1,558		2,939		Sereno et al., 1999; Bonnan and Wedel, 2004	3) measured from figure
Turiasaurus riodevensis	CPT	0,380	0,37		shorter					Mannion et al., 2013; pers. obs.	
	CPT	0,369								Royo-Torres et al., 2006	
Losillasaurus giganteus type	MCNV	0,420	0,42							Royo-Torres et al., 2006	estimated
Camarasaurus			0,50	1,000	0,9	1,500	1,9			Mannion et al., 2013	
	AMNH 664, L	0,475		0,977				3,766	4,7	Bonnan, 2001	
	AMNH 712, L			0,906				3,827		Bonnan, 2001	
	BYU 9047, R	0,443		0,965				11,815		McIntosh et al., 1996b	
	FMNH P25120, R			0,958				5,145		Bonnan, 2001	
	KUVP 129713, R			0,936				3,731		Bonnan, 2001	
	KUVP 129716, R	0,467		0,855				3,551		Bonnan, 2001	
	SMA 0002, R	0,573		0,864				3,542		Tschopp 2008	
	SMA 0002, L	0,544		0,871				5,067		Tschopp 2008	
	YPM 1910, L			0,894		1,644		3,442		Ostrom and McIntosh, 1966	measured from drawings
	YPM 4633, L			0,964		2,462		3,590		Ostrom and McIntosh, 1966	measured from drawings

Table 6.49: continued.

Giraffatitan brancai		0,510	0,51	1,000	1,0	1,700	1,9			Mannion et al., 2013	
	MB.R.2181, R	0,511		1,024		2,058		3,596	3,6	Janensch, 1922, 1961; Bonnan and Wedel, 2004	Length estimated
Brachiosaurus sp. SMA 0009	SMA 0009, L	0,338	0,34		shorter			2,980	3,0	Schwarz et al., 2007; pers. obs.	
Brachiosaurus altithorax	OMNH 01138							4,099	4,1	Bonnan and Wedel, 2004	
Ligabuesaurus leanzai	MCF-PHV-233, L							3,429	3,4	Bonaparte et al. 2006	
Limaysaurus tessonei	MUCPv-206	< 0,33	< 0,33							Calvo and Salgado, 1995	
					shorter					Mannion et al., 2013	
Apatosaurus louisae CM 3018	CM 3018, L	0,366	0,36	1,082	1,1	1,750	1,8	2,254	2,2	Gilmore 1936	
	CM 3018, L	0,354		1,034				2,128		Bonnan, 2001	
Apatosaurus parvus UW 15556	UW 15556, R	0,377	0,38	1,071	1,0	1,645	1,6	2,395	2,4	Gilmore 1936	
	UW 15556, R			0,945				2,383		Bonnan, 2001	
Eobrontosaurus yahnahpin Tate-001	Tate-001, L	0,437	0,44		1,0			2,431	2,4	Bonnan, 2001	
Apatosaurus ajax NSMT-PV 20375	NSMT-PV 20375, R			0,947	0,9	1,333	1,3	3,059	3,1	Upchurch et al. 2004b	
Diplodocus sp. WDC-FS001A	WDC-FS001A	0,365	0,36	0,764	0,8	1,909	1,9	3,046	3,0	Bedell and Trexler 2005; pers. obs.	comparing R with L
Galeamopus hayi HMNS 175	HMNS 175, L	0,306	0,31		0,8			2,667	2,7	Bonnan, 2001	
Galeamopus shellensis SMA 0011	SMA 0011, L	0,383	0,38	0,894	0,9			2,674	2,7	pers. obs.	
Dystrophaeus viaemalae USNM 2364	USNM 2364, L					2,001	2,0	2,799	2,9	McIntosh 1997	measured from drawings
	USNM 2364, L							2,948		pers. obs.	measured from photo

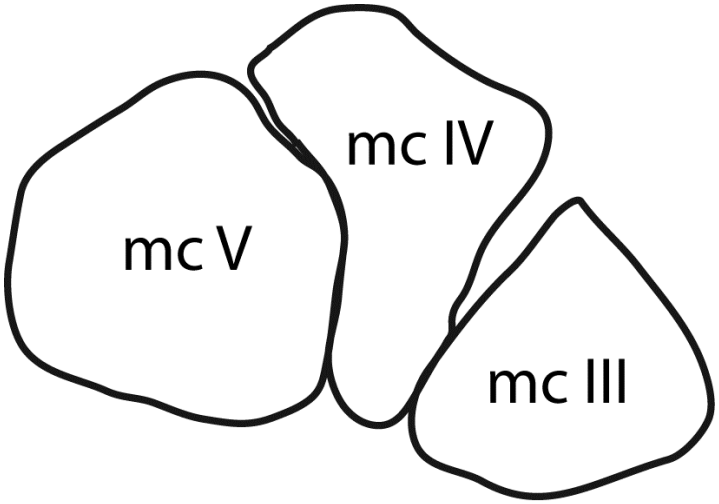

Figure 6.94: Articulated metacarpals III-V of *Apatosaurus louisae* CM 3018 in proximal view (traced from Gilmore, 1936), showing the greatly enlarged mc V, in comparison to mc III and IV (C403-1).

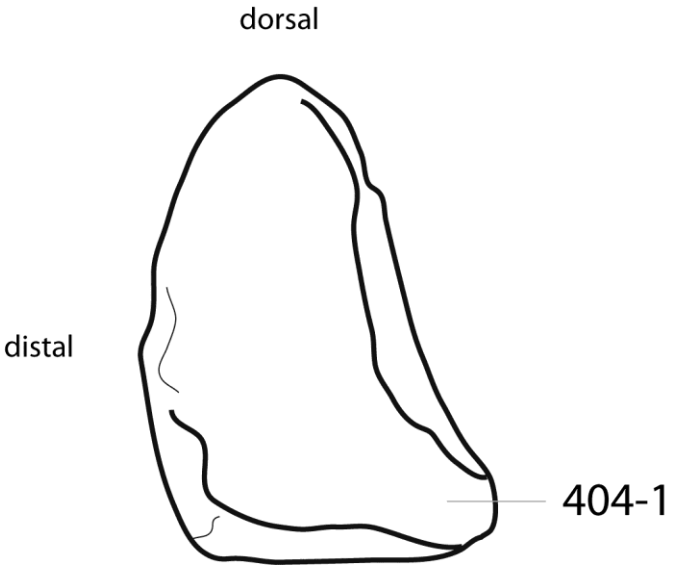

Figure 6.95: Manual phalanx phm I-1 of *Apatosaurus* sp. NSMT-PV 20375 in medial view (traced from Upchurch et al., 2004b), showing the proximoventral lip-like projection (C404-1).

C407: Ilium, preacetabular process orientation: anterolateral to body axis (0); perpendicular to body axis (1) (Salgado et al., 1997).

Comments. The perpendicular orientation of the preacetabular process is generally considered synapomorphic for derived titanosauriforms (Salgado et al., 1997; Wilson, 2002), but they also occur in the holotype of '*Apatosaurus*' *minimus* AMNH 675 (Mook, 1917).

C408: Ilium, angle between the ventral edge of anterior iliac lobe and the anterior surface of the pubis process: is ~90° (0); is acute (1) (Gilmore, 1936; Upchurch et al., 2004b).

C409: Ilium, dorsal margin shape: flat to slightly convex (0); semicircular (1) (Wilson, 2002; modified; Fig. 6.96).

Comments. Derived taxa have uniformly convex dorsal margins, apomorphic ones generally have a large straight portion.

C410: Ilium, highest point on the dorsal margin: lies posterior to the base of the pubic process (0); lies anterior to the base of the pubic process (1) (Upchurch et al., 2004a; Fig. 6.96).

Comments. The position of the highest point in respect to the pubic peduncle is assessed with the ischiadic tubercle and the anteroventral-most point of the preacetabular process lying on a horizontal line.

Table 6.50: Ilium, ratios.

Taxon	Specimen	1) pabh/gl	Mean 1	2) ppapd/ppw	Mean 2	Reference	Comments
Shunosaurus lii	T5401	0,330	0,33	1,018	1,02	Zhang, 1988	measured from figure
Omeisaurus	T5704		< 0,37	0,822	0,82	He et al., 1988	measured from figure
Mamenchisaurus	ZDM 0083	0,350	0,35			Ouyang and Ye, 2002	measured from figure
Jobaria tiguidensis	NMB-1695-R		low		wider	O. Mateus, pers. comm., 2010	
Camarasaurus			0,35	0,700	0,66	Mannion et al., 2013	
		0,340				pers. obs.	
	AMNH 5761, II 1	0,402		0,643		Osborn and Mook, 1921	measured from figure
	DNM 1253, R			0,632		Wilhite, 2003	measured from figure
	SMA 0002, L	0,303				pers. obs.	measured from photo
Apatosaurus grandis YPM 1901	YPM 1901, R	0,370	0,37	0,667	0,67	Wilson and Sereno, 1998	measured from figure
Lourinhasaurus alenquerensis lectotype	MIGM	0,380	0,38	0,765	0,76	pers. obs.	measured from photo
Giraffatitan brancai	MB.R. J1	0,360	0,36			Janensch, 1961	measured from figure
Brachiosaurus sp. SMA 0009	SMA 0009, L		< 0,33			pers. obs.	measured from photo; anterior portion lacking
Brachiosaurus altithorax	FMNH P25107, R	0,410	0,41			Riggs, 1904	measured from figure
Isisaurus colberti	ISIR335/31		low		wider	Jain and Bandyopadhyay, 1997	
Haplocanthosaurus priscus	CM 572	0,330	0,33	0,594	0,59	Hatcher, 1903	measured from figure
Limaysaurus tessonei	MUCPv-205				wider	Calvo and Salgado, 1995	
Dicraeosaurus hansemanni	MB.R.4886, R	0,400	0,40			pers. obs.	measured from photo
Brachytrachelopan mesai	MPEF PV 1716, L	0,420	0,42			Rauhut et al., 2005	measured from figure
Amargasaurus cazaui	MACN-N 15, L	0,400	0,40			Salgado and Bonaparte, 1991	measured from figure
Brontosaurus amplus YPM 1981	YPM 1981, L	0,432	0,43			Ostrom and McIntosh, 1966	measured from figure
Apatosaurus louisae CM 3018	CM 3018, L	0,363	0,36			Gilmore, 1936	measured from figure
Apatosaurus parvus UW 15556	UW 15556	0,350	0,35			Gilmore, 1936	measured from figure
Apatosaurus minimus AMNH 675	AMNH 675, L	0,271	0,27			M. Taylor, pers. comm., 2010	measured from photo
	AMNH 675, R	0,262				M. Taylor, pers. comm., 2010	measured from photo
Apatosaurus ajax NSMT-PV 20375	NSMT-PV 20375, L	0,320	0,31	0,752	0,63	Upchurch et al., 2004b	
	NSMT-PV 20375, R	0,290		0,502		Upchurch et al., 2004b	
Apatosaurus sp. FMNH P25112	FMNH P25112	0,320	0,32			Riggs, 1903	measured from figure
Supersaurus vivianae BYU	BYU 13018, R	0,380	0,38			Lovelace et al., 2007	measured from figure
Tornieria africana holotype	MB.R.2713, R	0,320	0,32			Janensch, 1961	measured from figure
Diplodocus carnegii CM 84	CM 84	0,400	0,40			pers. obs.	measured from figure
Diplodocus carnegii CM 94	CM 94, L		0,40	0,880	0,87	Hatcher, 1901	measured from figure
	CM 94, R	0,400		0,859		Hatcher, 1901	measured from figure
Diplodocus sp. AMNH 223	AMNH 223	0,420	0,42			Osborn, 1899	measured from figure
Galeamopus hayi HMNS 175	HMNS 175	0,350	0,35			pers. obs.	measured from photo
Galeamopus shellensis SMA 0011	SMA 0011, R			0,875	0,88	pers. obs.	
Barosaurus sp. AMNH 6341	AMNH 6341, R			0,883	0,88	McIntosh, 2005	measured from figure

C411: Ilium, pubic peduncle (measured at the articular surface), anteroposterior to mediolateral width ratio: > 0.80 (0); 0.80 or less (1) (Taylor, 2009; Mannion et al., 2013; modified; Tab. 6.50).

Comments. Mannion et al. (2013) was the first to include this character in a phylogenetic analysis, based on observations made by Taylor (2009). State boundaries are adapted herein from 0.5 to 0.8, given the different scope and thus taxon sampling of the present analysis.

C412: Ilium, triangular fossa laterally at base of pubic peduncle: absent (0); present (1) (New; Fig. 6.96).

Comments. The apex of this fossa is pointing ventrally.

C413: Ilium, distinct tubercle in the postacetabular region: absent (0); present (1) (Carballido et al., 2012a; Fig. 6.96).

Comments. The herein described tubercle is not the transverse widening of the dorsal edge towards its posterior end, but a second rugose area laterally on the blade (see Schwarz et al., 2007c; Carballido et al., 2012a).

C414: Pubis, ambiens process development: small, confluent, not differentiated from anterior border of the pubis (0); evident, but not especially developed (1); prominent, hook-like (2) (McIntosh, 1990b; Yu, 1993; wording modified; Fig. 6.97).

Comments. The hook-like ambiens process is interpreted to represent an increased development of the incipient shape. The character is thus treated as ordered.

C415: Pubis, length of puboischial contact: less than 0.41 total length of pubis (0); 0.41 or more of total length of pubis (1) (Salgado et al., 1997; modified; Tab. 6.51).

Comments. Mannion et al. (2012) used a ratio of 0.45 as state boundary, but as shown in table 6.51, for the present set of taxa, 0.41 appears more appropriate.

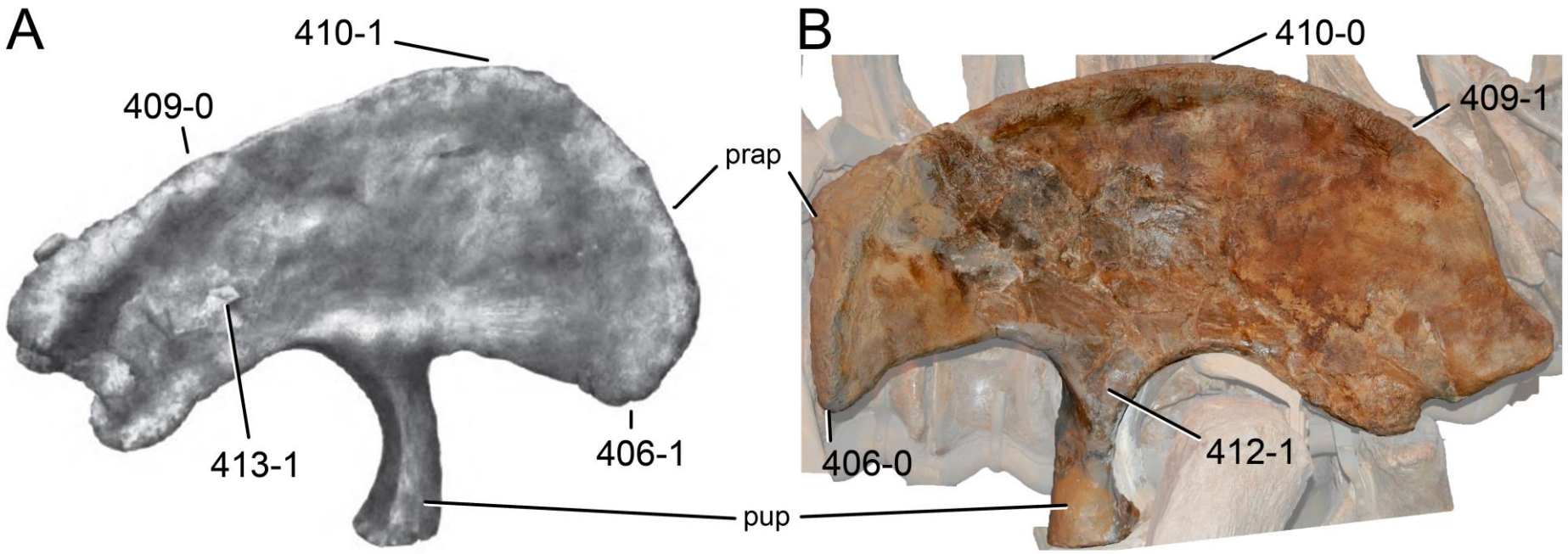

Figure 6.96: Right (A) and left (B) ilium of *Brachiosaurus altithorax* FMNH P25107 (A; modified from Riggs, 1904) and *Diplodocus* sp. DMNS 1494 (B) in lateral view. Note the pointed (B; C406-0) or semicircular preacetabular process (A; C406-1), the straight (A; C409-0) or strongly convex dorsal edge (B; C409-1), the location of the highest point (anterior to pubic peduncle, A, C410-1; posterior to pubis peduncle, B, C410-1), the triangular fossa on the pubic peduncle base (B; C412-1), and the tubercle in the postacetabular region (A; C413-1). Abb.: prap, preacetabular process; pup, pubic peduncle. Scaled to same height.

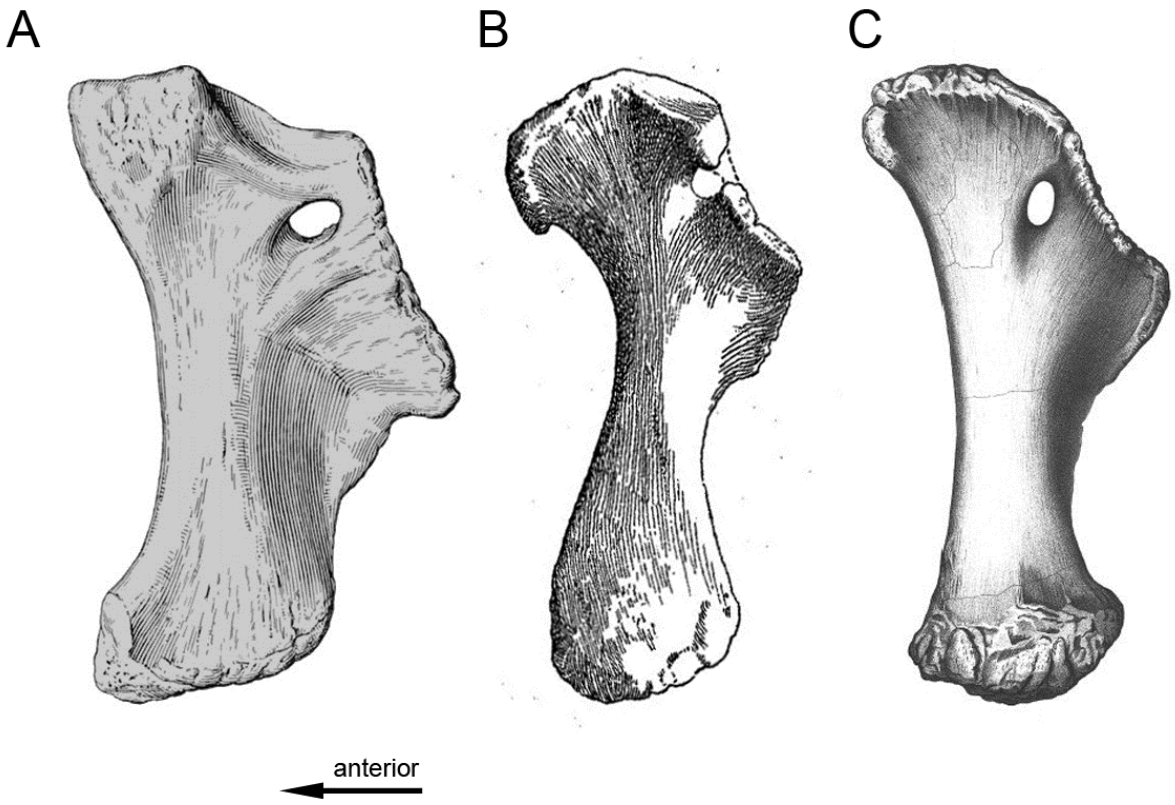

Figure 6.97: Left (A, C) and right (B, reversed) pubis of *Camarasaurus supremus* AMNH 5761 (A; modified from Osborn and Mook, 1921), *Dicraeosaurus hansemanni* MB.R.4886 (B; modified from Janensch, 1961), and *Brontosaurus excelsus* YPM 1980 (C; modified from Ostrom and McIntosh, 1966) in lateral view. Note the different sizes of the ambiens process (C414, arrowheads: absent, A; hook-like, B; incipient, C). Abb.: ac, acetabular surface; ias, ischial articular surface; ip, iliac peduncle; of, obturator foramen. Scaled to same length.

C416: Pubis, participation in acetabulum: subequal to larger, compared to ischium (0); significantly smaller (1) (Janensch, 1961; Tab. 6.52).

Comments. A state boundary of 0.8 was used herein as the used OTU show a large step from ratios below 0.75 to ratios greater than 0.83. The character was proposed as potentially useful to distinguish taxa by Janensch (1961). It is included in a phylogenetic analysis for the first time.

C417: Ischium, acetabular articular surface: maintains approximately the same transverse width throughout its length (0); is transversely narrower in its central portion and strongly expanded as it approaches the iliac and pubic articulations (1) (Mannion et al., 2012).

Comments. The narrow acetabular surface is only present in some rebbachisaurids (Mannion et al., 2012).

C418: Ischium, acetabular margin, in lateral view: flat or mildly concave (0); strongly concave, such that the pubic articular surface forms an anterodorsal projection (1) (D'Emic, 2012; modified by Mannion et al., 2013; Fig. 6.98).

Comments. In some diplodocids (e.g. *Apatosaurus excelsus* YPM 1980, see Fig. 6.98), the lateroventral edge of the acetabular surface is strongly concave, whereas the mediodorsal margin forms a bony sheet extending straight from the iliac to the pubic articular surfaces. In lateral view, this configuration appears straight and was thus scored as plesiomorphic herein.

C419: Ischium, iliac peduncle: iliac peduncle straight or widening in smooth curve distally (0); narrow, with distinct 'neck' (1) (Sereno et al., 2007; Fig. 6.98).

Table 6.51: Pubis, length of ischial articulation surface/greatest length.

Taxon	Specimen	Ratio	Mean	Reference	Comments
Shunosaurus lii		0,400	0,40	Mannion et al., 2013	
Spinophorosaurus nigerensis	GCP-CV-4229, L	0,374	0,37	Remes et al., 2009	measured from figure
Omeisaurus		0,400	0,37	Mannion et al., 2013	
	T5704, R	0,350		He et al., 1988	measured from figure
Mamenchisaurus		0,400	0,40	Mannion et al., 2013	
Jobaria tiguidensis	NMB-1695-R	0,345	0,35	O. Mateus, pers. comm., 2010	measured from photo
Camarasaurus		0,500	0,45	Mannion et al., 2013	
	AMNH 5761, L	0,418		Osborn and Mook, 1921	measured from figure
	CM 11393	0,430		Ikejiri, 2004	measured from figure
	YPM 1910, R	0,440		Wilson and Sereno, 1998	measured from figure
Lourinhasaurus alenquerensis lectotype	MIGM	0,277	0,28	pers. obs.	measured from photo
Giraffatitan brancai		0,400	0,42	Mannion et al., 2013	
	MB.R. J2	0,449		Janensch, 1961	measured from figure
Haplocanthosaurus priscus	CM 572, L	0,193	0,19	Hatcher, 1903	measured from figure
Limaysaurus tessonei	MUCPv-205, L	0,228	0,23	Calvo and Salgado, 1995	measured from figure
Zapalasaurus bonapartei	Pv-6127-MOZ, L		low	Salgado et al., 2006	
Dicraeosaurus hansemanni	MB.R.4886, R	0,275	0,27	Janensch, 1961	measured from figure
Brontosaurus excelsus YPM 1980	YPM 1980, L	0,278	0,32	Ostrom and McIntosh, 1966	measured from figure
	YPM 1980	0,370		pers. obs.	
Brontosaurus amplus YPM 1981	YPM 1981	0,404	0,40	pers. obs.	
Apatosaurus louisae CM 3018	CM 3018, L	0,370	0,37	Gilmore, 1936	measured from figure
Atlantosaurus immanis YPM 1840	YPM 1840, L	0,304	0,30	Marsh, 1896	measured from figure
Apatosaurus parvus UW 15556	UW 15556, L	0,322	0,32	Hatcher, 1903	measured from figure
Apatosaurus minimus AMNH 675	AMNH 675	0,443	0,44	Mook, 1917	measured from figure
Apatosaurus ajax NSMT-PV 20375	NSMT-PV 20375, L	0,286	0,29	Upchurch et al., 2004b	
Apatosaurus sp. FMNH P25112	FMNH P25112, R	0,378	0,38	Riggs, 1903	measured from figure
Supersaurus vivianae BYU	BYU 12424, L	0,378	0,38	Lovelace et al., 2007	measured from figure
Diplodocus carnegii CM 94	CM 94, L	0,233	0,23	Hatcher, 1903	measured from figure
Galeamopus hayi HMNS 175	HMNS 175, R	0,311	0,31	pers. obs.	measured from photo
Seismosaurus hallorum NMMNH 3690	NMMNH 3690	0,423	0,42	Lucas et al., 2006	measured from figure
Galeamopus shellensis SMA 0011	SMA 0011	0,383	0,38	pers. obs.	
Barosaurus sp. AMNH 6341	AMNH 6341	0,308	0,31	pers. obs.	measured from photo

Table 6.52: Pubis to ischium ratios.

Taxon	Specimen	1) ac lengths	Mean 1	2) greatest lengths	Mean 2	Reference	Comments
Shunosaurus lii	T5402	0,895	0,89	0,984	1,0	Zhang, 1988	1) measured from figure
Spinophorosaurus nigerensis	GCP-CV-4229, L	0,552	0,55	0,824	0,8	Remes et al., 2009	measured from figure
Omeisaurus	T5701, L	0,737	0,74	0,771	0,9	He et al., 1988	1) measured from figure
	T5701, R			0,794		He et al., 1988	
	T5704, L			0,900		He et al., 1988	
	T5704, R			0,848		He et al., 1988	
	T5705, L			0,932		He et al., 1988	
	T5705, R			0,890		He et al., 1988	
Mamenchisaurus	ZDM 0083, L			0,987		Ouyang and Ye, 2002	
Jobaria tiguidensis	MNN TIG	0,751	0,75	0,938	0,9	O. Mateus, pers. comm., 2009	measured from photo
Camarasaurus	GMNH-PV 101, L	0,946	0,97	0,821	0,8	McIntosh et al., 1996a	
	GMNH-PV 101, R	0,763		0,828		McIntosh et al., 1996a	
	SMA 0002, L	1,208				O. Mateus, pers. comm., 2009	measured from photo
Giraffatitan brancai	MB.R. Sa9			0,962	1,0	Janensch, 1961	
	MB.R.2181			0,962		Janensch, 1961	
Isisaurus colberti	ISIR 335			1,120	1,1	Jain and Bandyopadhyay, 1997	
Haplocanthosaurus priscus	CM 572, L	0,660	0,66	0,910	0,9	Hatcher, 1903	measured from figure
Limaysaurus tessonei	MUCPv-205	0,400	0,40	1,043	1,0	Calvo and Salgado, 1995	1) measured from figure
Dicraeosaurus hansemanni	MB.R.4886, R	0,745	0,74	1,060	1,1	Janensch, 1961	1) measured from figure
Brontosaurus excelsus YPM 1980	YPM 1980	0,543	0,54	1,045	1,0	Osborn, 1898	3) estimated
Apatosaurus louisae CM 3018	CM 3018	0,696	0,70	0,933	0,9	Gilmore, 1936	1) measured from figure
Atlantosaurus immanis YPM 1840	YPM 1840, L	0,666	0,67	0,963	1,0	Marsh, 1896	measured from figure
Apatosaurus parvus UW 15556	UW 15556, L	0,628	0,63	0,884	0,9	Hatcher, 1903; Gilmore, 1936	1) measured from figure
Apatosaurus minimus AMNH 675	AMNH 675	0,825	0,83	1,000	1,0	Mook, 1917	measured from figure
Apatosaurus ajax NSMT-PV 20375	NSMT-PV 20375, L			1,063	1,0	Upchurch et al. 2004b	
	NSMT-PV 20375, R			1,007		Upchurch et al. 2004b	
Apatosaurus sp. FMNH P25112	FMNH P25112	0,867	0,87	1,034	1,0	Riggs, 1903	1) measured from figure
Supersaurus vivianae BYU	BYU 12424, 12946	0,653	0,65	0,991	1,0	Lovelace et al., 2007	comparing R and L; measured from figure
Diplodocus carnegii CM 84	CM 84			1,064	1,1	Hatcher, 1901	
Diplodocus carnegii CM 94	CM 94, L	0,650	0,65			Hatcher, 1903	1) measured from figure
Diplodocus sp. USNM 10865	USNM 10865			0,943	0,9	Gilmore, 1932	
Galeamopus shellensis SMA 0011	SMA 0011	0,830	0,83			pers. obs.	measured from photo
Barosaurus sp. AMNH 6341	AMNH 6341			1,019	1,0	McIntosh, 2005	

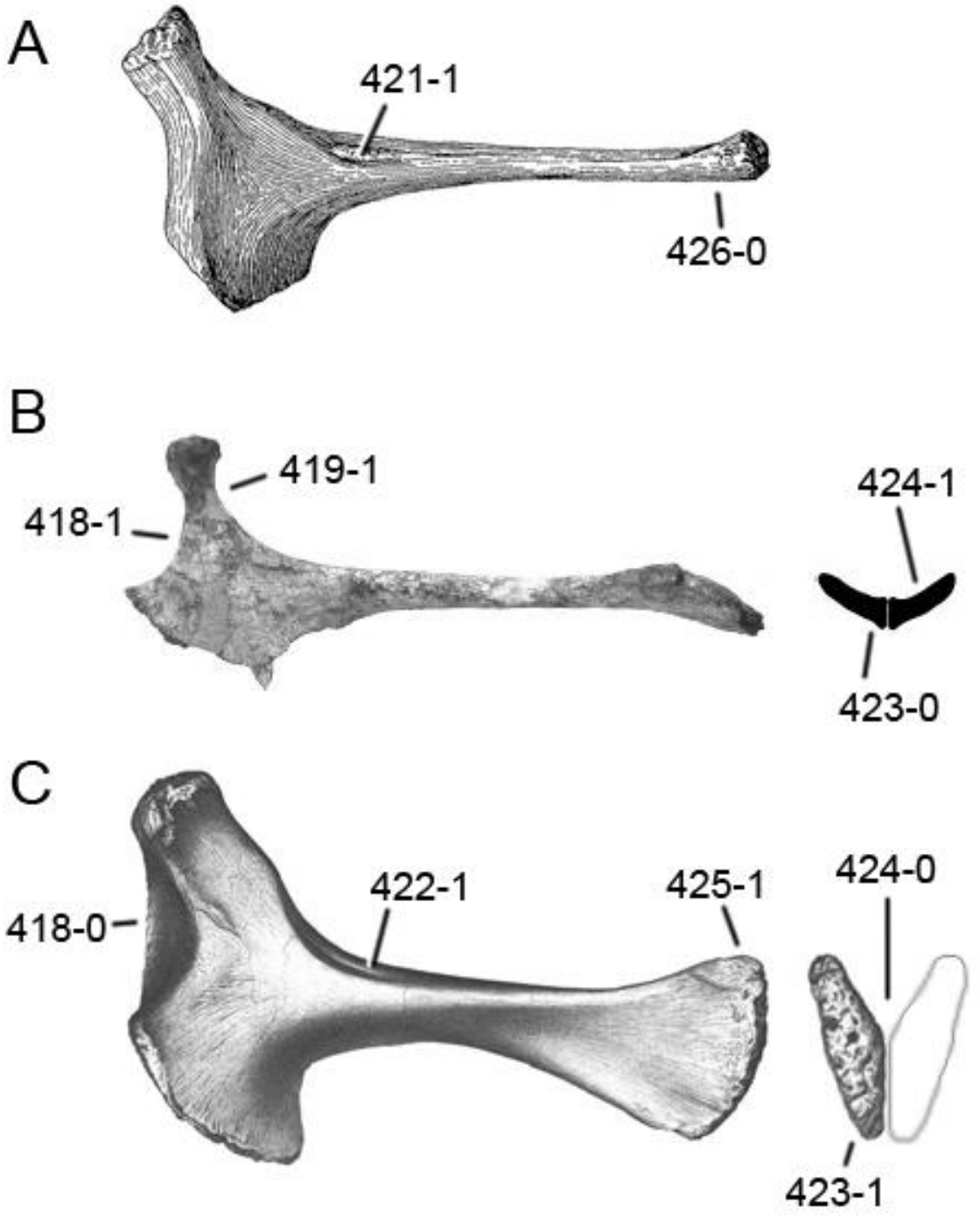

Figure 6.98: Left ischium of *Haplocanthosaurus priscus* CM 572 (A; modified from Hatcher, 1903), *Demandasaurus darwini* MPS-RVII,18 (B; modified from Pereda Suberbiola et al., 2003), and *Brontosaurus excelsus* YPM 1980 (C; modified from Ostrom and McIntosh, 1966) in lateral (left) and distal (right) view. Note the flat (C; C418-0) in contrast to strongly concave acetabular margin (B; C418-1), the constricted neck of the iliac tubercle (B; C419-1), the elongate muscle scar on the proximal shaft (A; C421-1), the lateral fossa at the base of the blade (C; C422-1), the blade-like (B; C423-0) or medially expanded distal ends (C; C423-1), which form a more or less straight line (B; C424-1) or a V (C; C424-0), and can be straight (A; C426-0) or expanded dorsoventrally as well as transversely (C; C425-1). The light gray line in B indicates the distal view of the right ischium. Scaled to same length.

C420: Ischia pubic articulation/anteroposterior length of pubic pedicel: < 1.5 (0); 1.5 or greater (1) (Salgado et al., 1997; modified; Tab. 6.53).

Comments. Anteroposterior length of the pubic pedicel is measured perpendicular to the articular surface, from its ventral-most point, to the point where it intersects with a line following the ventral edge of the distal shaft. A numerical state boundary was added to the original version of Salgado et al. (1997), which separates Macronaria from basal Eusauropoda, and most diplodocines from most apatosaurs (Tab. 6.53).

C421: Ischium, elongate muscle scar on proximal end: absent (0); present (1) (Sereno et al., 2007; Fig. 6.98).

Comments. I follow Mannion et al. (2012), in that the presence of a distinct ridge on the dorsolateral edge qualifies for the apomorphic state.

C422: Ischium, lateral fossa at base of shaft: absent (0); present (1) (Wilson, 2002; Fig. 6.98).

Comments. The fossa is longitudinally oriented, and marks the dorsolateral edge.

C423: Ischial distal shaft, shape: blade-like, medial and lateral depths subequal (0); triangular, depth of ischial shaft increases medially (1) (Wilson, 2002; Fig. 6.98).

C424: Ischial distal shafts, cross-sectional shape: V-shaped, forming an angle of nearly 50° with each other (0); flat, nearly coplanar (1) (Upchurch, 1998; Wilson and Sereno, 1998; Fig. 6.98).

C425: Ischial shaft, transverse distal expansion: absent (0); present (1) (Whitlock, 2011a; Fig. 6.98).

Comments. Due to the V-shaped distal end of the ischia, 'transverse' and 'posterodorsal' do not apply very well to the ingroup specimens. However, given the twist of the ischial shaft in the taxa with coplanar distal shafts, which results in almost horizontally oriented distal ends, the main expansion of diplodocid ischia should be regarded as transverse, even though in lateral view it would appear rather dorsoventral.

Table 6.53: Ischium, pubic articulation/anteroposterior length pubic peduncle.

Taxon	Specimen	Ratio	Mean	Reference	Comments
Shunosaurus lii	T5401, R	1,263	1,3	Zhang, 1988	measured from figure
Spinophorosaurus nigerensis	GCP-CV-4229, L	1,193	1,2	Remes et al., 2009	measured from figure
Omeisaurus			<1	Carballido et al., 2012b	
Mamenchisaurus	ZDM 0083, R	2,500	2,5	Ouyang and Ye, 2002	measured from figure
Jobaria tiguidensis	NMB-1695-R, R	2,220	2,2	O. Mateus, pers. comm., 2010	measured from photo
Camarasaurus	AMNH 5760	2,330	2,2	Osborn and Mook, 1921	measured from figure
	GMNH-PV 101, R	1,860		McIntosh et al., 1996a	measured from figure
	YPM 1905, R	2,262		Wilson and Sereno, 1998	measured from figure
Apatosaurus grandis YPM 1901	YPM 1901, R	2,081	2,1	M. Fox, pers. comm., 2012	measured from photo
Lourinhasaurus alenquerensis lectotype	MIGM, R	1,564	1,6	pers. obs.	measured from photo
Giraffatitan brancai	MB.R. J3, R	7,731	7,7	Janensch, 1961	measured from figure
Isisaurus colberti	ISIR335/65, R	4,433	4,4	Jain and Bandyopadhyay, 1997	measured from figure
Haplocanthosaurus priscus	CM 572, L	0,648	0,6	Hatcher, 1903	measured from figure
Limaysaurus tessonei	MUCPv-153, R	1,435	1,7	Calvo and Salgado, 1995	measured from figure
	MUCPv-205, L	1,913		Calvo and Salgado, 1995	measured from figure
Zapalasaurus bonapartei	Pv-6127-MOZ, L	0,525	0,5	Salgado et al., 2006	measured from figure
Demandasaurus darwini	MPS-RVII,18, L	1,072	1,1	Pereda Suberbiola et al., 2003	measured from figure
Dicraeosaurus hansemanni	MB.R.4886, R	1,771	1,8	Janensch, 1961	measured from figure
Brontosaurus excelsus YPM 1980	YPM 1980, L	1,833	1,8	Ostrom and McIntosh, 1966	measured from figure
Apatosaurus louisae CM 3018	CM 3018, L	1,476	1,5	Gilmore, 1936	measured from figure
Atlantosaurus immanis YPM 1840	YPM 1840, R	3,924	3,9	pers. obs.	measured from photo
Apatosaurus parvus UW 15556	UW 15556, L	1,493	1,5	Hatcher, 1903	measured from figure
Apatosaurus minimus AMNH 675	AMNH 675	2,600	2,6	M. Taylor, pers. comm., 2011	measured from photo
Apatosaurus ajax NSMT-PV 20375	NSMT-PV 20375, R	0,964	1,0	Upchurch et al., 2004b	measured from figure
Apatosaurus sp. FMNH P25112	FMNH P25112, R	0,913	0,9	Riggs, 1903	measured from figure
Supersaurus vivianae BYU	BYU 12555, R	0,704	0,8	Jensen, 1985	measured from figure
	BYU 12946, L	0,851		Lovelace et al., 2007	measured from figure
Tornieria africana holotype	SMNS 12143, R	1,968	2,0	Remes, 2006	measured from figure
Tornieria africana skeleton k	MB.R.2733, R	1,778	1,8	Remes, 2006	measured from figure
Diplodocus carnegii CM 94	CM 94, L	0,892	0,9	Hatcher, 1903	measured from figure
Diplodocus sp. DMNS 1494	DMNS 1494, L	1,086	1,1	pers. obs.	measured from photo
Galeamopus shellensis SMA 0011	SMA 0011, L	1,212	1,2	pers. obs.	measured from photo

C426: Ischium, posterodorsal expansion of distal end: absent (0); present (1) (Lovelace et al., 2007; Fig. 6.98).
Comments. See comment on transverse expansion in character 425.

Hindlimb

C427: Femur, robustness index (sensu Wilson and Upchurch, 2003): gracile, <0.22 (0); intermediate, 0.22-0.25 (1); robust, > 0.25 (2) (Janensch, 1961; Tab. 6.54).
Comments. Due to the gradual increase, this character is treated as ordered.

C428: Femur, lateral bulge (marked by the lateral expansion and a dorsomedial orientation of the laterodorsal margin of the femur, which starts below the femur head ventral margin): absent (0); present (1) (Salgado et al., 1997; modified; Fig. 6.99).
Comments. The definition of this character changed in different phylogenetic analyses (e.g. Salgado et al., 1997; Mannion et al., 2012). Here, we follow Mannion et al. (2012) in that we also score incipient lateral bulges as apomorphic.

C429: Femoral shaft, lateral margin shape: straight (0); proximal one-third deflected medially (1) (Wilson, 2002; Fig. 6.99).
Comments. The fact that the probable brachiosaurid juvenile SMA 0009 does not show any medial deflection might indicate that this character changes during ontogeny. This might be correlated with the weak development of the articular surface in juvenile specimens (Ikejiri et al., 2005; Schwarz et al., 2007c).

C430: Femur, cross-sectional shape: subequal to anteroposterior diameter (0); 125-150% anteroposterior diameter (1); at least 185% anteroposterior diameter (2) (Wilson and Smith, 1996; Tab. 6.54).
Comments. The character was added in order to distinguish between titanosauriforms, but it is also useful for the distinction of *Amphicoelias altus* AMNH 5764. Taxa scored but without entries in table 6.54 are taken from Carballido et al. (2012b). The character is treated as ordered.

C431: Femoral head, position of highest point in anterior view: above point of maximum curvature of ventral edge of femoral head (0); laterally shifted, above main portion of the shaft (1) (New; Fig. 6.99).

C432: Femur, ventral surface of head: confluent with shaft (0); stepped (1) (New; Fig. 6.99).

C433: Femur, greatest anteroposterior thickness of shaft: less than or approximately equal to half the anteroposterior depth of the distal articular condyles (0); much greater than half the anteroposterior depth of the distal articular condyles (1) (Whitlock, 2011a; Tab. 6.54).
Comments. The state boundary used herein is 0.6. Taxa scored for this character, but not having any values in table 6.54 are taken from Whitlock (2011a).

C434: Femur, large nutrient foramen opening midshaft anteriorly on femur: absent (0); present (1) (Wilson, 2002; Fig. 6.99).

C435: Femur, pronounced ridge on posterior surface between greater trochanter and head: absent (0); present (1) (Sereno et al., 2007).
Comments. The derived state is a synapomorphy for Nigersaurinae.

C436: Femur, fourth trochanter: not visible in anterior view (0); prominent, visible in anterior view (1) (Gallina and Apesteguía, 2005; modified by Whitlock, 2011a; Fig. 6.99).
Comments. In certain taxa, a small bulge is visible on the medial edge in anterior view, which represents the medially positioned, and prominent fourth trochanter.

C437: Femoral fourth trochanter, present as low rounded ridge (0); greatly reduced so that it is virtually absent (1) (Mannion et al., 2012).
Comments. A reduced fourth trochanter is synapomorphic for rebbachisaurs and some titanosauriforms (Torcida Fernández-Baldor et al., 2011; Mannion et al., 2012). The reduced fourth trochanter of the juvenile *Elosaurus parvus* CM 566 implies that the development of this structure happens during ontogeny.

C438: Femur, fourth trochanter, position: distally displaced (0); on proximal half of shaft (1) (Schwarz-Wings and Böhm, 2012; Tab. 6.54).
Comments. Distance between femoral head and fourth trochanter is measured to the distal end of the trochanter. Taxa with ratios of 0.4 are scored as apomorphic.

Table 6.54: Femur ratios.

Taxon	Specimen	1) RI	Mean 1	2) min sw/apd	Mean 2	3) min apd/dapd	Mean 3	4) ptr/gl	Mean 4	Reference	Comments
Shunosaurus lii	T5401, R	0,220	0,21							Zhang, 1988	
	T5401, L	0,200								Zhang, 1988	
Spinophorosaurus nigerensis	GCP-CV-4229 (HB 62), L	0,220	0,22					0,530	0,5	Remes et al. 2009	4) measured from figure
Omeisaurus	T5701, L	0,230	0,25		1,40				0,5	He et al., 1988	
	T5704, L	0,240								He et al., 1988	
	T5704, R	0,250								He et al., 1988	
	T5705, L	0,250								He et al., 1988	
	T5705, R	0,260								He et al., 1988	
	O. tianfuensis							0,517		Ouyang and Ye, 2002	measured from figure
				1,400						Mannion et al., 2013	
Mamenchisaurus	ZDM 0083, R	0,200	0,23					0,519	0,5	Ouyang and Ye, 2002	4) measured from figure
	M. hochuanensis	0,257						0,511		Ouyang and Ye, 2002	measured from figure
Jobaria tiguidensis	MNN TIG	0,246	0,25							J. Carballido, pers. comm. 2013	measured from photo
Camarasaurus	CM 11338, L	0,296	0,26	1,738	1,57		0,6	0,417	0,4	Bonnan, 2001	juvenile
	CM 11338, L	0,271								Wilhite, 2003	
	CM 36664, L	0,232						0,434		Bonnan, 2001	
	CM 36664, L	0,231								Wilhite, 2003	
	DNM 3735, R	0,261						0,454		Bonnan, 2001	
	GMNH-PV 101, R	0,250								McIntosh et al. 1996a	
	UMNH 5286, L	0,266		1,618				0,449		Bonnan, 2001	
	WDC B, R	0,263		1,339		0,562				Ikejiri, 2004	
				1,600						Mannion et al., 2013	
Apatosaurus grandis YPM 1901	YPM 1901, L	0,290	0,28	1,912	1,91	0,330	0,3	0,525	0,5	Wilson and Sereno, 1998	juvenile, measured from figure
	YPM 1901, L	0,272								Wilhite, 2003	
Amphicoelias latus AMNH 5765	AMNH 5765, L	0,270	0,27	1,791	1,79	0,437	0,4	0,493	0,5	Osborn and Mook, 1921	measured from figure, gl estimated
Lourinhasaurus alenquerensis lectotype	MIGM, L	0,270	0,27					0,505	0,5	pers. obs.	measured from photo
Giraffatitan brancai	MB.R. II 27e, R	0,260	0,24		2,13		0,4		0,4	Janensch, 1961	
	MB.R. IX 1, L	0,230								Janensch, 1961	juvenile
	MB.R. XV 1, R	0,220								Janensch, 1961	
	MB.R. Ng 21, R	0,220								Janensch, 1961	juvenile
	MB.R. St 134, R	0,230								Janensch, 1961	juvenile
	MB.R. XX 5, R	0,260								Janensch, 1961	juvenile
	MB.R. Nr. 12, R	0,240								Janensch, 1961	
	MB.R. t 6, L	0,230								Janensch, 1961	
	MB.R. St 291, R	0,250		2,056		0,380		0,434		Janensch, 1961	2) to 4) measured from figure
				2,200						Mannion et al., 2013	

Table 6.54: continued.

Brachiosaurus sp. SMA 0009	SMA 0009, L	0,260	0,26							Schwarz et al. 2007	juvenile
Brachiosaurus altithorax	FMNH P25107, R	0,250	0,25		2,10					Wilhite, 2003	
				2,100						Mannion et al., 2013	
Ligabuesaurus leanzai	MCF-PHV-233, R	0,210	0,21		2,40					Bonaparte et al. 2006	
				2,400						Mannion et al., 2013	
Haplocanthosaurus priscus	CM 572, L	0,230	0,22							Hatcher, 1903	
	CM 572, L	0,206								Wilhite, 2003	
Limaysaurus tessonei	MUCPv-205, L	0,220	0,22							Calvo and Salgado, 1995	
Cathartesaura anaerobica	MPCA- 232, R	0,250	0,25							Gallina and Apesteguía, 2005	
Nigersaurus taqueti				1,300	1,30					Mannion et al., 2013	
Demandasaurus darwini	MPS-RVII,16, L	0,236	0,24	2,077	2,08			0,472	0,5	Torcida Fernández-Baldor et al., 2011	
Amphicoelias altus AMNH 5764	AMNH 5764, R	0,180	0,18	0,968	0,97	0,519	0,5	0,534	0,5	Osborn and Mook, 1921	2) to 4) measured from figure
Dicraeosaurus hansemanni	MB.R.4886, R	0,230	0,23	1,194	1,19	0,463	0,5	0,505	0,5	Janensch, 1961	2) to 4) measured from figure
Amargasaurus cazaui	MACN-N 15, L	0,230	0,23							Salgado and Bonaparte, 1991	
Brontosaurus excelsus YPM 1980	YPM 1980, L	0,262	0,26	1,457	1,50	0,395	0,4	0,567	0,5	Ostrom and McIntosh, 1966	measured from figure
	YPM 1980	0,258								McIntosh, 1995	
	YPM 1980, L	0,260		1,538				0,471		Bonnan, 2001	
Brontosaurus amplus YPM 1981	YPM 1981	0,256	0,26							McIntosh, 1995	
Apatosaurus louisae CM 3018	CM 3018, R	0,270	0,27	1,485	1,48	0,496	0,5	0,557	0,5	Gilmore 1936	2) to 4) measured from figure
	CM 3018, R							0,462		Bonnan, 2001	
Atlantosaurus immanis YPM 1840	YPM 1840, L	0,240	0,24	1,429	1,43					Marsh 1896	
Elosaurus parvus CM 566	CM 566, R	0,220	0,23	1,225	1,23		0,6	0,417	0,4	Bonnan, 2001	juvenile
	CM 566, R	0,243								Wilhite, 2003	juvenile
	CM 566, R					0,563				pers. obs.	measured from photo
Apatosaurus parvus UW 15556	UW 15556, R	0,260	0,26							Gilmore 1936	
Apatosaurus ajax NSMT-PV 20375	NSMT-PV 20375, R	0,260	0,26	1,500	1,50	0,348	0,3	0,532	0,5	Upchurch et al., 2004b	2) and 3) measured from drawing
Apatosaurus sp. FMNH P25112	FMNH P25112	0,268	0,27	2,100	2,10	0,580	0,6		0,4	Riggs, 1903	2) and 3) measured from drawing
	FMNH P25112	0,261						0,423		Bonnan, 2001	
	FMNH P25112	0,277								Wilhite, 2003	
Tornieria africana holotype	SMNS 12140, R	0,240	0,24	1,286	1,29	0,373	0,4	0,525	0,5	Fraas, 1908	2) to 4) measured from figure
Tornieria africana skeleton k	MB.R.2669, L		>0.21							Remes 2006	
Diplodocus carnegii CM 84	CM 84, R	0,250	0,25							Hatcher 1901; Wilhite 2003	
Diplodocus carnegii CM 94	CM 94, L	0,250	0,25	1,287	1,56		0,4	0,537	0,5	Bonnan, 2001	
	CM 94, R					0,432				Hatcher, 1901	measured from figure
	CM 94, R	0,240		1,824				0,448		Bonnan, 2001	
Diplodocus sp. USNM 10865	USNM 10865, L	0,200	0,20							Wilhite, 2003	
Galeamopus shellensis SMA 0011	SMA 0011, L	0,240	0,24					0,480	0,5	pers. obs.	
Barosaurus sp. AMNH 6341	AMNH 6341, R	0,240	0,24	1,413	1,41			0,492	0,5	Bonnan, 2001	
	AMNH 6341, R	0,238								Wilhite, 2003	
Cetiosauriscus stewarti NHMUK R3078	NHMUK R3078, L	0,210	0,21	1,345	1,30			0,522	0,5	Woodward, 1905	4) measured from figure
		0,210		1,253						pers. obs.	

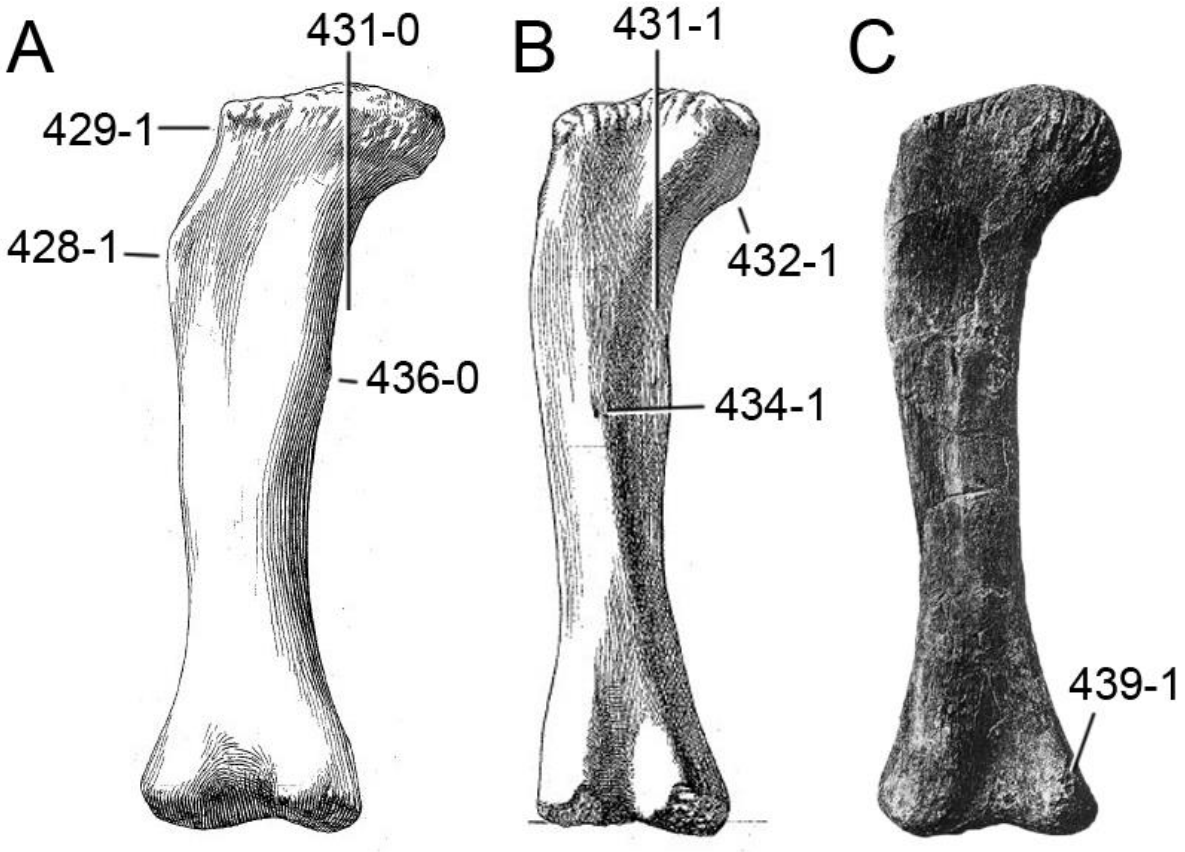

Figure 6.99: Right femur of *Giraffatitan brancai* MB.R. St291 (A), *Dicraeosaurus hansemanni* MB.R.4886 (B; both modified from Janensch, 1961), and *Tornieria africana* SMNS 12140 (C; modified from Fraas, 1908) in anterior view. Note the lateral bulge (A; C428-1), the medial deflection of the femoral head (A; C429-1), the different positions of the highest point of the femoral head (C431), the stepped ventral margin of the head (B; C432-1), the nutrient foramen (B; C434-1), the fourth trochanter, which is visible in anterior view (A; C436-0), and the anteriorly extended distal articular surface of the condyle (C; C439-1). Scaled to same length.

C439: Femur, shape of distal condyles: articular surface restricted to distal portion of femur (0); expanded onto anterior portion of femoral shaft (1) (Wilson and Carrano, 1999; Wilson, 2002; Fig. 6.99).

C440: Tibia to femur length: < 0.68 (0); 0.68 or greater (1) (New; Tab. 6.55).

C441: Tibia, proximal articulation surface, shape: subcircular to transversely compressed (0); anteroposteriorly compressed (1) (Wilson, 2002; modified; Fig. 6.100).

Comments. Character descriptions was slightly changed such that the subcircular surfaces are now scored together with the transversely compressed, instead of the anteroposteriorly compressed as in (Wilson, 2002).

C442: Tibia, proximal articular surface, shape: subrectangular (0); subtriangular (1) (Harris and Dodson, 2004; Fig. 6.100).

Comments. Rhomboid or suboval outlines are scored as plesiomorphic.

C443: Tibia, short transverse ridge on anteromedial surface of distal end: absent (0); present (1) (New; Fig. 6.101).

C444: Tibia, cnemial crest in anterior view: widely rounded (0); subtriangular (1) (New; Fig. 6.102).

C445: Tibia, posterior surface of cnemial crest: smooth (0); bears a distinct fibular trochanter (1) (Harris, 2007; Fig. 6.103).

Comments. A distinct fibular trochanter marks the posterior face of the cnemial crest of *Suuwassea* (Harris, 2007). The character is herein included in a phylogenetic analysis for the first time.

Table 6.55: Tibia to femur length.

Taxon	Specimen	Ratio	Mean	Reference
Shunosaurus lii	T5402	0,57	0,57	Zhang, 1988
Spinophorosaurus nigerensis	GCP-CV-4229	0,58	0,58	Remes et al., 2009
Omeisaurus	T5701	0,63	0,63	He et al., 1988
Mamenchisaurus	ZDM 0083	0,57	0,57	Ouyang and Ye, 2002
Jobaria tiguidensis	MNN TIG3	0,60	0,60	Sereno et al., 1999
Camarasaurus	CM 11338	0,62	0,64	Gilmore, 1925
	GMNH-PV 101	0,64		McIntosh et al., 1996a
	SMA 0002	0,65		Tschopp, 2008
Lourinhasaurus alenquerensis lectotype	MIGM	0,63	0,63	O. Mateus, pers. comm., 2009
Giraffatitan brancai	MB.R.2181	0,58	0,58	Janensch, 1961
Brachiosaurus sp. SMA 0009	SMA 0009	0,83	0,83	Schwarz et al. 2007c
Ligabuesaurus leanzai	MCF-PHV-233	0,63	0,63	Bonaparte et al., 2006
Limaysaurus tessonei	MUCPv-205	0,59	0,59	Calvo and Salgado, 1995
Dicraeosaurus hansemanni		0,64	0,64	Janensch, 1961
Amargasaurus cazaui	MACN-N 15	0,61	0,61	Salgado and Bonaparte, 1991
Brontosaurus excelsus YPM 1980	YPM 1980	0,61	0,67	McIntosh, 1995
	YPM 1980	0,72		Bonnan, 2001
Brontosaurus amplus YPM 1981	YPM 1981	0,63	0,63	McIntosh, 1995
Apatosaurus louisae CM 3018	CM 3018	0,62	0,63	Schwarz et al. 2007c
	CM 3018	0,63		Upchurch et al., 2004b
Apatosaurus parvus UW 15556	UW 15556	0,59	0,59	Gilmore, 1936
Apatosaurus ajax NSMT-PV 20375	NSMT-PV 20375	0,64	0,64	Upchurch et al., 2004b
Apatosaurinae indet. SMA 0087	SMA 0087	0,62	0,62	pers. obs.
Tornieria africana skeleton k	MB.R.2572, 2669		< 0,64	Remes, 2006
Diplodocus carnegii CM 94	CM 94	0,72	0,70	McIntosh, 2005
	CM 94	0,67		Schwarz et al. 2007c
Diplodocus sp. USNM 10865	USNM 10865	0,75	0,75	McIntosh, 2005
Galeamopus shellensis SMA 0011	SMA 0011	0,62	0,62	pers. obs.
Barosaurus sp. AMNH 6341	AMNH 6341	0,74	0,75	McIntosh, 2005
	AMNH 6341	0,75		Schwarz et al. 2007c

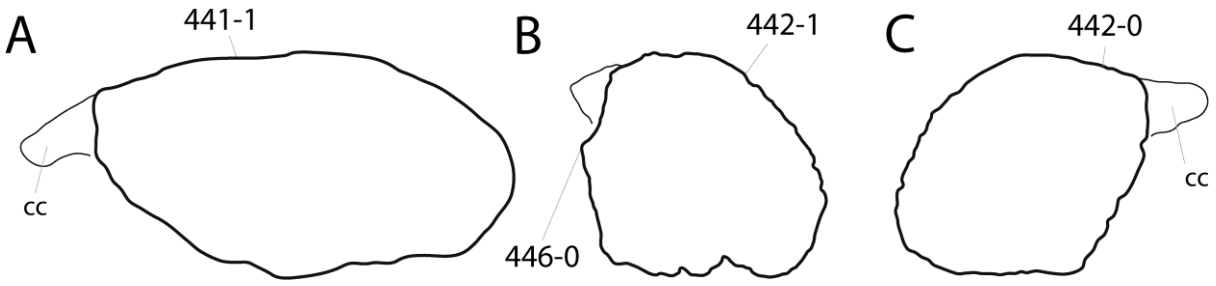

Figure 6.100: Tibia of *Omeisaurus tianfuensis* T5701 (A; traced from He et al., 1988), *Dyslocosaurus polyonychius* AC 663 (B), and *Apatosaurus louisae* CM 3018 (C; traced from Gilmore, 1936) in proximal view. Note the different outlines (anteroposteriorly compressed, A, C441-1; subtriangular, B, C442-1; subrectangular, C, C442-0), and the projection posterior to the cnemial crest (B; C446-0). Abb.: cc, cnemial crest. Scaled to same anteroposterior length.

C446: Tibia, lateral edge of proximal end forms a pinched out projection, posterior to cnemial crest (the 'second cnemial crest' of Bonaparte et al., 2000): present (0); absent (1) (Mannion et al., 2013; Fig. 6.100).

C447: Fibula, proximal end with anteromedially directed crest extending into a notch behind the cnemial crest of the tibia: absent (0); present (1) (Wilson and Upchurch, 2009; D'Emic, 2012; modified by Mannion et al., 2013).

Comments. Most sauropods have ellipsoid proximal articular surfaces of the fibula. However, some diplodocid specimens (as well as some titanosauriforms; Wilson and Upchurch, 2009; D'Emic, 2012; Mannion et al., 2013) develop a distinct, narrow, anteromedial crest.

C448: Fibula, insertion of the M. iliofibularis: located approximately at mid-shaft (0); proximal, located above midshaft (1) (Whitlock, 2011a; Tab. 6.56).

Comments. Distance from the proximal articular surface to the center of the tubercle was measured and compared to greatest length. Values of 0.4 or lower were scored as derived.

C449: Astragalus, morphology in anterior view: rectangular (0); wedge-shaped, narrowing medially (1) (Upchurch, 1995, 1998; modified by Nair and Salisbury, 2012; Fig. 6.104).

C450: Astragalus, anteroposterior dimension as seen in dorsal view: widens medially or does not change in width (0); narrows medially (1) (Cooper, 1984; Upchurch, 1998; Fig. 6.104).

Comments. The taxonomic significance of this character was recognized by Cooper (1984), but included into a phylogenetic analysis for the first time by Upchurch (1998).

Figure 6.101: Distal end of tibia of *Dyslocosaurus polyonychius* AC 663 in medial view, illustrating the transverse ridge on the anteromedial surface, close to the distal end (C443-1). Scale bar = 10 cm.

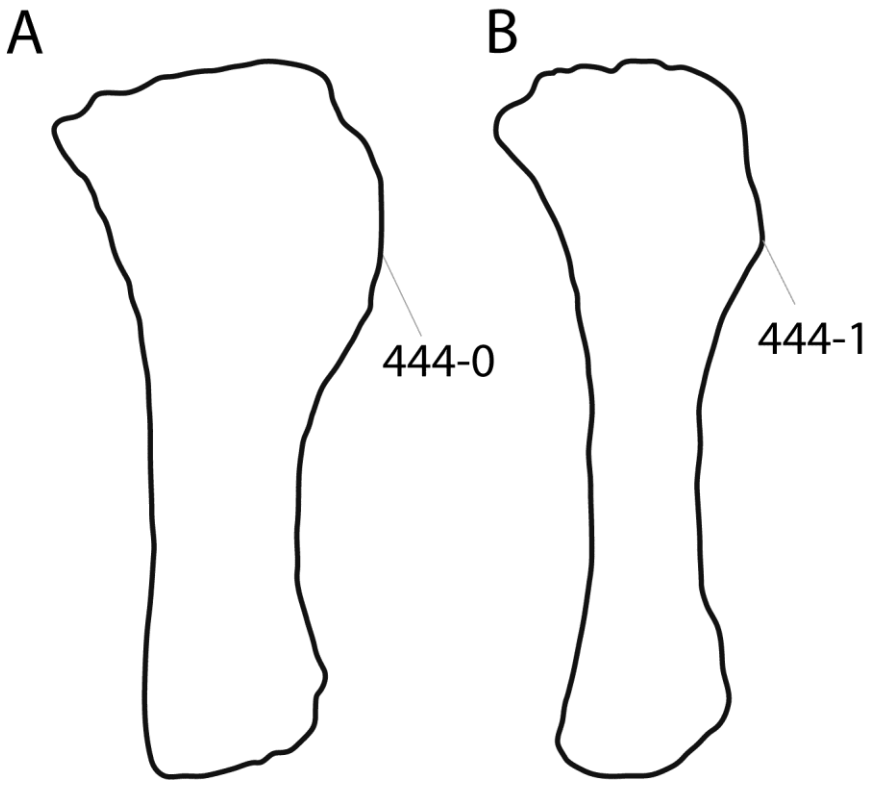

Figure 6.102: Tibia of *Zapalasaurus* sp. MOZ-Pv 1244 (A; traced from Salgado et al., 2012) and *Tornieria africana* MB.R.2572 (B; traced from Remes, 2006) in anterolateral view, illustrating the different shapes of the cnemial crest (widely rounded, A, C444-0; triangular, B, C444-1). Scaled to same length.

Figure 6.103: Proximal end of the tibia of *Suuwassea emilieae* ANS 21122 in posterolateral view, showing the distinct fibular trochanter on the posterior surface of the cnemial crest (C445-1). Scale bar = 10 cm.

Table 6.56: Fibula, position of insertion M. iliofibularis

Taxon	Specimen	Ratio	Mean	Reference	Comments
Shunosaurus lii	T5402, R	0,36	0,4	Zhang, 1988	measured from figure
Omeisaurus			midshaft	Mannion et al., 2012	
Camarasaurus	AMNH 217, L	0,42	0,5	Bonnan, 2001	
	CM 11339, L	0,48		Bonnan, 2001	
	KUVP 129716, R	0,60		Bonnan, 2001	
Lourinhasaurus alenquerensis lectotype	MIGM		midshaft	pers. obs.	no measurements available
Giraffatitan brancai	MB.R. St149	0,45	0,4	Janensch, 1961	measured from figure
Ligabuesaurus leanzai	MCF-PVPH-233, R	0,51	0,5	Bonaparte et al., 2006	measured from figure
Limaysaurus tessonei	MUCPv-205, L	0,49	0,5	Calvo and Salgado, 1995	measured from figure
Zapalasaurus bonapartei	MOZ-Pv 1245, L	0,48	0,5	Salgado et al., 2012	measured from figure
Nigersaurus taqueti			proximal	Mannion et al., 2012	
Dicraeosaurus hansemanni			midshaft	Mannion et al., 2012	
Amargasaurus cazaui			midshaft	Mannion et al., 2012	
Suuwassea emilieae ANS 21122	ANS 21122	0,52	0,5	pers. obs.	
Apatosaurus ajax YPM 1860			midshaft	pers. obs.	no measurements available
Brontosaurus excelsus YPM 1980	YPM 1980	0,45	0,5	Bonnan, 2001	
Brontosaurus amplus YPM 1981	YPM 1981	0,47	0,5	Bonnan, 2001	
Apatosaurus louisae CM 3018	CM 3018	0,51	0,5	Bonnan, 2001	
Elosaurus parvus CM 566	CM 566, L	0,41	0,4	pers. obs.	measured from photo
Eobrontosaurus yahnahpin Tate-001	Tate-001	0,45	0,5	Bonnan, 2001	
Apatosaurus ajax NSMT-PV 20375	NSMT-PV 20375, R	0,44	0,4	Upchurch et al., 2004b	
Apatosaurinaeindet. SMA 0087	SMA 0087		midshaft	pers. obs.	no measurements available
Supersaurus vivianae WDC DMJ-021	WDC DMJ-021	0,42	0,4	Lovelace et al., 2007	measured from figure
Tornieria africana holotype	SMNS 12142, R	0,44	0,4	Remes, 2006	measured from figure
Diplodocus carnegii CM 94	CM 94	0,41	0,4	Bonnan, 2001	
	CM 94	0,41		pers. obs.	
Diplodocus sp. USNM 10865	USNM 10865	0,42	0,4	pers. obs.	
Diplodocus sp. DMNS 1494	DMNS 1494, L	0,50	0,5	pers. obs.	measured from photo
Galeamopus hayi HMNS 175	HMNS 175	0,44	0,4	Bonnan, 2001	
Galeamopus shellensis SMA 0011	SMA 0011	0,41	0,4	pers. obs.	
Barosaurus sp. AMNH 6341	AMNH 6341	0,42	0,4	Bonnan, 2001	

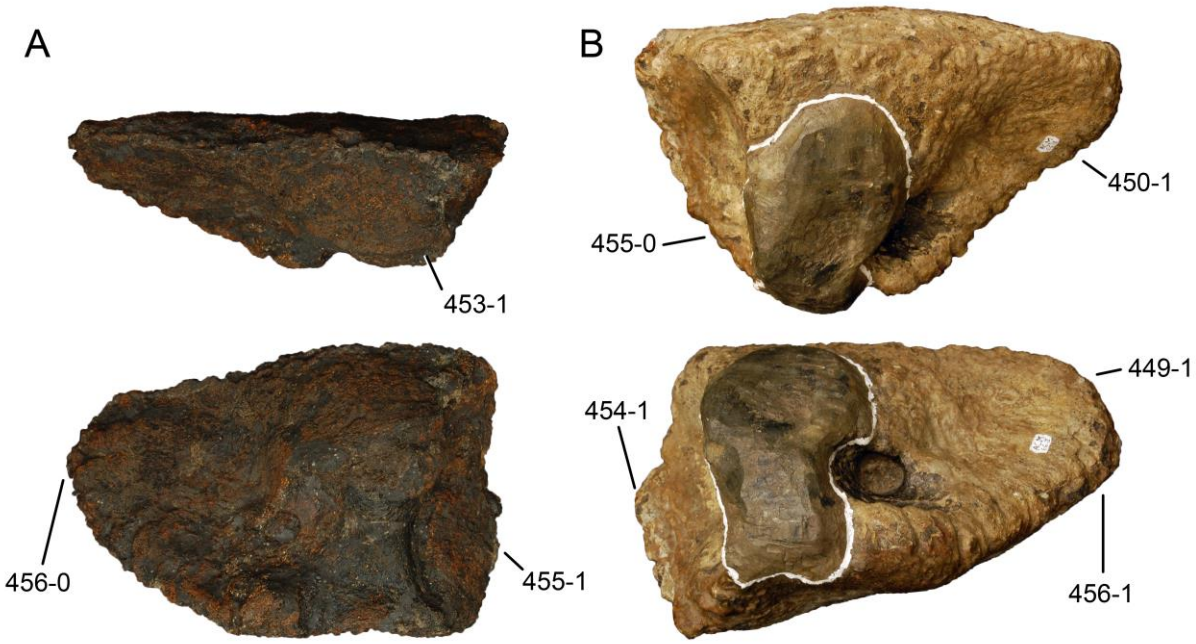

Figure 6.104: Astragalus of SMA 0087 (A) and *Dyslocosaurus polyonychius* AC 663 (B) in dorsal (top) and posterior (bottom) view. Note the triangular shape in both views (B; C449-1, C450-1), the ascending process that reaches the posterior border (A; C453-1), the anterior border of the fibular facet, which is visible in posterior view (B; C454-1), the presence (B; C455-0) or absence (A; 455-1) of a sheet underlying the fibula, and the blunt (A; C456-0) in contrast to elongate medial end (B; C456-1). Scaled to the same proximodistal height.

C451: Astragalus, proximodistal length/transverse breadth: < 0.55 (0); 0.55 or greater (1) (McIntosh et al., 1992; Tab. 6.57).

Comments. This ratio was used by McIntosh et al. (1992) to distinguish *Dyslocosaurus* from *Diplodocus*, but is here included in a phylogenetic analysis for the first time.

C452: Astragalus, mediolateral width to maximum anteroposterior length ratio: 1.6 or greater (0); < 1.6 (1) (Sander et al., 2006; modified; Tab. 6.57).

C453: Astragalus, ascending process length: limited to anterior two-thirds of astragalus anteroposterior width (0); extends beyond two-thirds of astragalus anteroposterior width (normally to posterior margin of astragalus) (1) (Wilson and Sereno, 1998; Wilson, 2002; modified by Mannion et al., 2012; Fig. 6.104).

C454: Astragalus, fibular facet: faces laterally (0); faces posterolaterally, anterior margin visible in posterior view (1) (Whitlock, 2011a; Fig. 6.104).

C455: Astragalus, laterally directed ventral shelf underlies the distal end of the fibula: present (0); absent (1) (Mannion et al., 2013; based on Wilson and Upchurch, 2009; Fig. 6.104).

Comments. The ventral shelf only underlies a part of the fibula.

C456: Astragalus, anteromedial corner in posterior view: short and blunt (0); elongate and narrow (1) (New; Fig. 6.104).

Comments. The short and blunt shape is a somewhat intermediate state between triangular and rectangular outlines, as described in character 449.

C457: Calcaneum: proximodistally compressed (0); globular (1) (Harris and Dodson, 2004).

Comments. *Suuwassea* has a globular calcaneum, whereas most other sauropods that preserve calcanea have dorsoventrally compressed elements. These bones are very rarely preserved, and were even proposed to be absent in diplodocids (McIntosh, 1990b; Upchurch, 1998). However, Bonnan (2000) reported a probable calcaneum from *Diplodocus*, and also an apatosaur specimen from Como Bluff, Wyoming (NHMUK R.3215) appears to show such an element (pers. obs., 2011).

Table 6.57: Astragalus, ratios.

Taxon	Specimen	1) pdl/tw	Mean 1	2) tw/apd	Mean 2	Reference	Comments
Spinophorosaurus nigerensis	GCP-CV-4229, L	0,54	0,54			Remes et al. 2009	
Omeisaurus	T5701, L	0,44	0,49	1,72	1,7	He et al. 1988	
	T5704, R	0,50		1,65		He et al. 1988	
	T5705, R	0,53		1,72		He et al. 1988	
				1,80		Mannion et al., 2013	
Mamenchisaurus				1,60	1,6	Mannion et al., 2013	
Camarasaurus	CM 21777, L	0,45	0,50	1,48	1,7	Bonnan, 2001	
	KUVP 129716, L	0,51		2,06		Bonnan, 2001	
	OMNH 10342, L	0,42		1,67		Bonnan, 2001	
	SMA 0002, R	0,51				Tschopp 2008	
	SMA 0002, L	0,60				Tschopp 2008	
				1,50		Mannion et al., 2013	
Apatosaurus grandis YPM 1901	YPM 1901, L	0,61	0,61	1,72	1,7	Bonnan, 2001	
Giraffatitan brancai	MB.R. St 150, R	0,61	0,59	1,54	1,6	Janensch 1961	
	MB.R. Y 25, R	0,56		1,84		Janensch 1961	
	MB.R. Z 68, L	0,52		1,53		Janensch 1961	
	MB.R. X 24, L	0,62		1,45		Janensch 1961	
	MB.R. XII 7, L	0,62		1,68		Janensch 1961	
				1,50		Mannion et al., 2013	
Dicraeosaurus hansemanni	MB.R. 4886, L	0,66	0,66	1,30	1,3	Janensch 1961	
Brontosaurus excelsus YPM 1980	YPM 1980, L	0,59	0,59	1,33	1,3	Ostrom and McIntosh, 1966	measured from figure
Brontosaurus amplus YPM 1981	YPM 1981, L	0,63	0,63	1,42	1,4	Bonnan, 2001	
Apatosaurus louisae CM 3018	CM 3018, R	0,33	0,33	0,94	0,9	Bonnan, 2001	
Eobrontosaurus yahnahpin Tate-001	Tate-001, L	0,90	0,90	1,31	1,3	Bonnan, 2001	
Apatosaurus ajax NSMT-PV 20375	NSMT-PV 20375, R	0,48	0,48	1,62	1,6	Upchurch et al. 2004b	
Apatosaurinae indet. SMA 0087	SMA 0087, R	0,31	0,31	1,95	2,0	pers. obs.	
Diplodocus carnegii CM 94	CM 94		0,47	1,63	1,6	Hatcher, 1901	
	CM 94, L	0,60		1,41		McIntosh et al. 1992	
	CM 94, R	0,34		1,66		Bonnan, 2001	
Diplodocus sp. WDC-FS001A	WDC-FS001A, R	0,62	0,62			R. Wilhite, pers. comm.	measured on photo
Galeamopus hayi HMNS 175	HMNS 175, L	0,66	0,66	1,92	1,9	Bonnan, 2001	
Galeamopus shellensis SMA 0011	SMA 0011, L	0,40	0,40	2,38	2,4	pers. obs.	
Barosaurus sp. AMNH 6341	AMNH 6341, R	0,61	0,61	1,49	1,5	Bonnan, 2001	
Dyslocosaurus polyonychius AC 663	AC 663, L	0,50	0,50	1,43	1,4	McIntosh et al. 1992	

C458: Metatarsals, metatarsal I to metatarsal V proximodistal length ratio: 1.0 or greater (0); < 1.0 (1) (Mannion et al., 2013; polarity reversed; Tab. 6.58).

Comments. Length is measured between parallel lines through the proximal- and distal-most points of the metatarsals.

C459: Metatarsal I, dorsal/anterior surface: without foramina (0); several foramina present (1) (New; Fig. 6.105).

C460: Metatarsal I proximal articular surface, transverse axis orientation: angled ventromedially approximately 15º to (0); perpendicular to axis of shaft (1) (Wilson, 2002; modified by Carballido et al., 2012b; polarity reversed; Fig. 6.105).

Comments. The original character (Wilson, 2002) was split into two by Carballido et al. (2012b), because some specimens have one of the two articular surfaces in an angle to the long axis of the shaft, and the other one perpendicular. Herein, polarity was reversed due to the different taxon sampling.

C461: Metatarsal I, robustness (proximal transverse width/greatest length): relatively gracile, < 0.8 (0); robust, 0.8 or more (1) (Upchurch et al., 2004a; modified; Tab. 6.59).

C462: Metatarsal I distal articular surface, transverse axis orientation: angled dorsomedially to (0); perpendicular to axis of shaft (1) (Wilson, 2002; modified by Carballido et al., 2012b; polarity reversed; Fig. 6.105).

C463: Metatarsal I distal condyle, posterolateral projection: absent (0); present (1) (Berman and McIntosh, 1978; see Fig. 6.105).

Comments. All taxa where the posterolateral corner of the distal articular surface can be seen in anterior view are scored as apomorphic.

C464: Metatarsal I, distolateral projection, if present: small and blunt, not projecting considerably lateral to dorsal edge of distal articular surface (0); prominent and pointed, reaching significantly more laterally than dorsal edge of distal articular surface (1) (McIntosh, 1990b; Fig. 6.105).

Comments. Usually, a prominent posterolateral or distolateral projection exceeds the lateral expansion of the proximal articular surface in anterior view.

C465: Metatarsals I-III, rugosities on dorsolateral margins near distal ends: absent (0); present (1) (Upchurch, 1995).

Comments. A second character (C468) accounts for the strength of the rugosity on mt II (see Fig. 6.106).

Table 6.58: Metatarsals, mt I to mt V proximodistal length ratio.

Taxon	Specimen	Ratio	Mean	Reference	Comments
Shunosaurus lii		1,000	1,0	Mannion et al., 2013	
	T5402, L	0,982		Zhang, 1988	
Omeisaurus		1,000	1,0	Mannion et al., 2013	
	T5701, L	1,016		He et al., 1988	
	T5704, R	0,917		He et al., 1988	
Camarasaurus		1,200	1,1	Mannion et al., 2013	
	CM 11338, L	1,167		Gilmore, 1925	
	GMNH-PV 101, R	1,036		McIntosh et al., 1996a	
	SMA 0002, R	1,046		Tschopp, 2008	
Apatosaurus grandis YPM 1901	YPM 1901, L	1,015	1,0	Bonnan, 2001	
Brachiosaurus sp. SMA 0009	SMA 0009, L	1,032	1,0	Schwarz et al., 2007	
Ligabuesaurus leanzai		0,800	0,8	Mannion et al., 2013	
	MCF-PVPH-233, R	0,778		Bonaparte et al., 2006	
Limaysaurus tessonei	MUCPv-205, R	0,626	0,6	Calvo and Salgado, 1995	measured from figure
Dicraeosaurus hansemanni	MB.R. dd113	0,867	0,9	Janensch, 1961	measured from figure, L and R compared
Eobrontosaurus yahnahpin Tate-001	Tate-001, L	1,050	1,0	Bonnan, 2001	
Apatosaurus ajax NSMT-PV 20375	NSMT-PV 20375, R	0,843	0,8	Upchurch et al., 2004b	
Apatosaurinae indet. SMA 0087	SMA 0087, R	0,726	0,7	pers. obs.	
Diplodocus carnegii CM 94	CM 94	1,313	1,3	Hatcher, 1901	
Galeamopus shellensis SMA 0011	SMA 0011, L	0,804	0,8	pers. obs.	
Barosaurus affinis YPM 419	YPM 419		shorter	pers. obs.	
Barosaurus sp. AMNH 6341	AMNH 6341, R	0,800	0,8	McIntosh, 2005	
Cetiosauriscus stewarti NHMUK R3078	NHMUK R3078, L	0,813	0,8	pers. obs.	

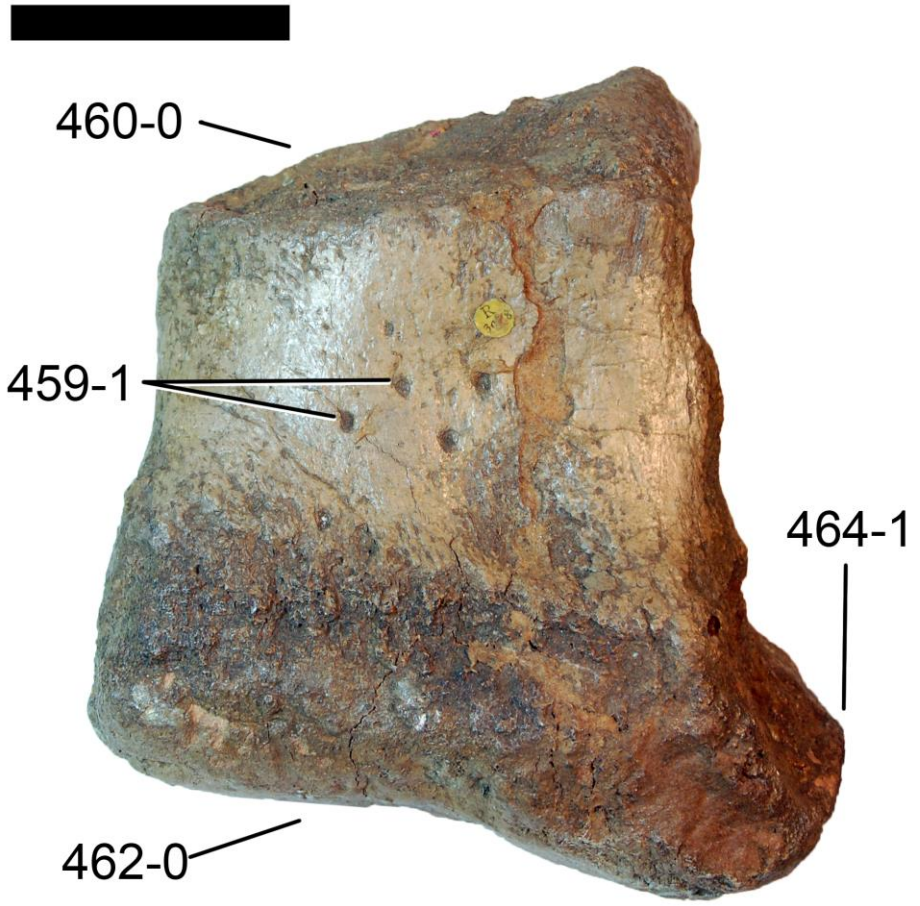

Figure 6.105: Metatarsal I of *Cetiosauriscus stewarti* NHMUK R3078 in dorsal/anterior view. Note the foramina (C459-1), the angled proximal (C460-0) and distal articular surfaces (C462-0), and the distinct posterolateral process on the distal articular surface (C464-1). Scale bar = 5 cm.

C466: Metatarsal II, robustness (mean proximal and distal transverse breadth /maximum length): slender, <0.53 (0); intermediate, 0.53-0.65 (1); robust, >0.65 (2) (McIntosh et al., 1992; Tab. 6.59).

Comments. The robustness of metatarsal II was used by McIntosh et al. (1992) to distinguish between diplodocids, but has never been included in a phylogenetic analysis. The character is treated as ordered.

C467: Metatarsal II, lateral margin in proximal view: concave (0); straight (1) (Mannion et al., 2013; Fig. 6.107).

Comments. The medial margin is usually concave. With the lateral margin being concave as well, the outline of the proximal articular surface of mt II becomes somewhat hourglass-shaped.

C468: Metatarsal II, rugosity on dorsolateral margin near distal end (if present): shallow (0); well-developed, extending to center of shaft (1) (New; Fig. 6.106).

Comments. The development of the rugosities in mt I to III differs within the pes (mt II bearing the most prominent ridge), but more so between taxa. This is exemplified by the well-developed, rugose ridge of *Dyslocosaurus polyonychius* AC 663, which extends almost to the center of the shaft. Taxa without any rugosities are scored as unknown.

C469: Metatarsal II distal condyle, posterolateral projection: absent (0); present (1) (New; Fig. 6.106).

Comments. The distribution of the posterolateral projection in mt II was discussed by Nair and Salisbury (2012).

C470: Metatarsal IV, proximal articular surface, outline: L- to V-shaped, with distinctly concave posterolateral edge (0); subtriangular (1) (New; Fig. 6.108).

C471: Metatarsal V, proximal articular surface, shape: triangular (0); rhomboid (1) (New; Fig. 6.109).

Table 6.59: Metatarsal ratios.

Taxon	Specimen	1) mt I pw/gl	Mean 1	2) mt II, rob	Mean 2	3) mt V, pw/dw	Mean 3	Reference	Comments
Shunosaurus lii	T5402, L	1,00	1,0	0,57	0,57	1,47	1,6	Zhang 1988	
						1,70		Mannion et al., 2013	
Omeisaurus	T5701, L	0,49	0,6	0,55	0,56	2,43	2,8	He et al. 1988	
	T5704, R	0,79		0,57		3,19		He et al. 1988	
						2,50		Mannion et al., 2013	
Mamenchisaurus	ZDM 0083, R	0,55	0,6	0,40	0,40		2,1	Ouyang and Ye, 2002	underestimated due to lacking proximolateral portion
						2,10		Mannion et al., 2013	
Camarasaurus	GMNH-PV 101, L		0,7	0,47	0,54		2,0	McIntosh et al., 1996a	
	GMNH-PV 101, R	0,62						McIntosh et al., 1996a	
	SMA 0002, L			0,56		2,20		Tschopp, 2008	
	SMA 0002, R	0,76		0,59		1,98		Tschopp, 2008	
						1,80		Mannion et al., 2013	
Apatosaurus grandis YPM 1901	YPM 1901, R			0,52	0,52			M. Fox, pers. comm.	
Giraffatitan brancai	MB.R. XX 12, R			0,47	0,47			Janensch, 1961	
Brachiosaurus sp. SMA 0009	SMA 0009, L		0,5	0,47	0,47			Schwarz et al., 2007	
	SMA 0009, R	0,46						Schwarz et al., 2007	
Ligabuesaurus leanzai	MCF-PHV-233, R	0,93	0,9	0,63	0,63	2,07	1,9	Bonaparte et al. 2006	
						1,80		Mannion et al., 2013	
Limaysaurus tessonei	MUCPv-205, R	0,83	0,8	0,66	0,66	1,67	1,7	Calvo and Salgado, 1995	measured from figure
Zapalasaurus bonapartei	MOZ-Pv 1257, R	1,03	1,0					Salgado et al. 2012	
	MOZ-Pv 1232, L	1,03						Salgado et al. 2012	
Nigersaurus taqueti						1,70	1,7	Mannion et al., 2013	
Dicraeosaurus hansemanni	MB.R. dd113, L	0,68	0,7		0,58	1,60	1,6	Janensch, 1961	
	MB.R. St 593, R			0,58				Janensch, 1961	
Suuwassea emilieae ANS 21122	ANS 21122, R	0,69	0,7	0,56	0,56			Harris 2007	
Apatosaurus louisae CM 3018	CM 3018, L	0,75	0,8	0,75	0,75			Gilmore 1936	
	CM 3018, L	0,85						Upchurch et al. 2004b	
Apatosaurus sp. UW 15556	UW 15556, R			0,70	0,70			D. Lovelace, pers. comm., 2013	measured from photo
Apatosaurus ajax NSMT-PV 20375	NSMT-PV 20375, R	0,84	0,8	0,63	0,63	1,72	1,7	Upchurch et al. 2004b	
Apatosaurinae indet. SMA 0087	SMA 0087, R	0,80	0,8	0,55	0,55	1,84	1,8	pers. obs.	
Diplodocus carnegii CM 94	CM 94, L	0,60	0,6	0,52	0,52		1,5	McIntosh et al. 1992	
						1,52		pers. obs.	measured from photo
Diplodocus sp. USNM 10865	USNM 10865, L			0,56	0,56			pers. obs.	measured from photo
Diplodocus sp. WDC-FS001A	WDC-FS001A, R					1,75	1,8	R. Wilhite, pers. comm., 2012	measured from photo
Galeamopus hayi HMNS 175	HMNS 175, R					1,53	1,5	pers. obs.	measured from photo
Galeamopus shellensis SMA 0011	SMA 0011, L	0,81	0,8	0,76	0,76			pers. obs.	
Barosaurus affinis YPM 419	YPM 419, L	0,62	0,6					McIntosh 2005	
Barosaurus sp. AMNH 6341	AMNH 6341, R	0,74	0,7	0,56	0,56	1,46	1,5	McIntosh 2005	
Cetiosauriscus stewarti NHMUK R3078	NHMUK R3078, L	0,67	0,7	0,53	0,53	1,69	1,7	pers. obs.	
Dyslocosaurus polyonychius AC 663	AC 663, L	0,70	0,7	0,58	0,58			McIntosh et al. 1992	

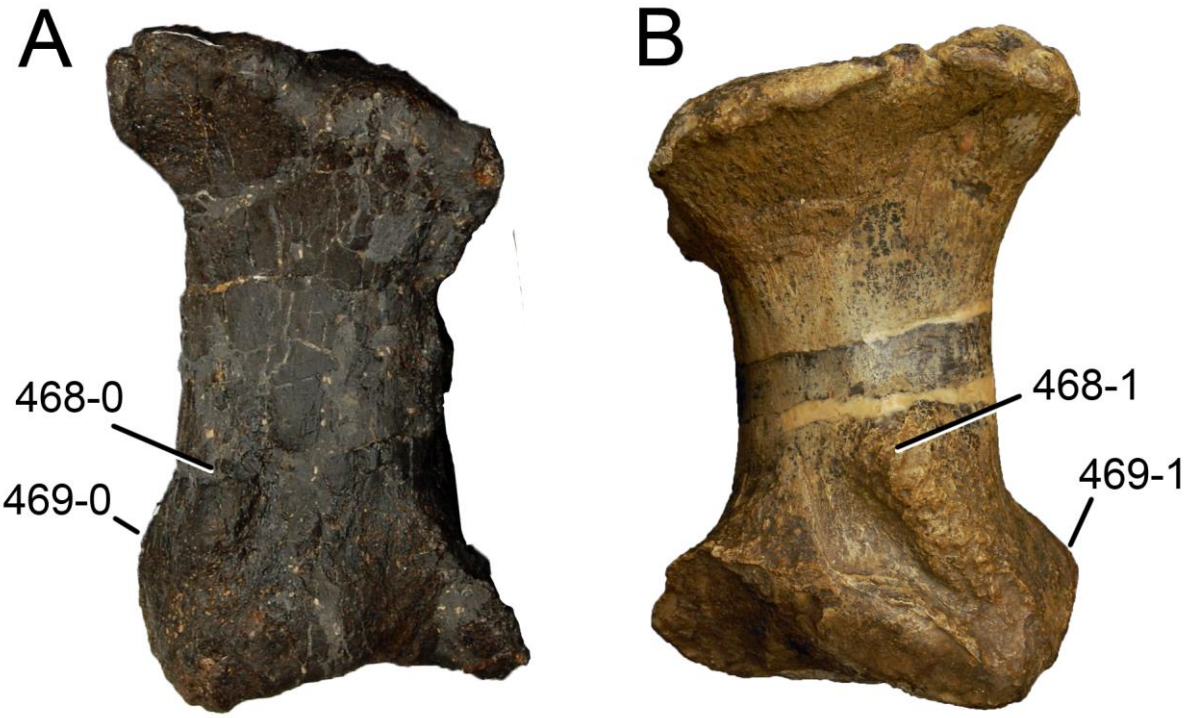

Figure 6.106: Right (A) and left (B) metatarsal II of SMA 0087 (A) and *Dyslocosaurus polyonychius* AC 663 in dorsal/anterior view. Note the dorsolateral rugosity (C465-1) with its different developments (reduced, laterally, A, C468-0; prominent, reaching center or shaft, B, C468-1), or the posterolateral process (absent, A, C469-0; present, B, C469-1). Scaled to same proximodistal length.

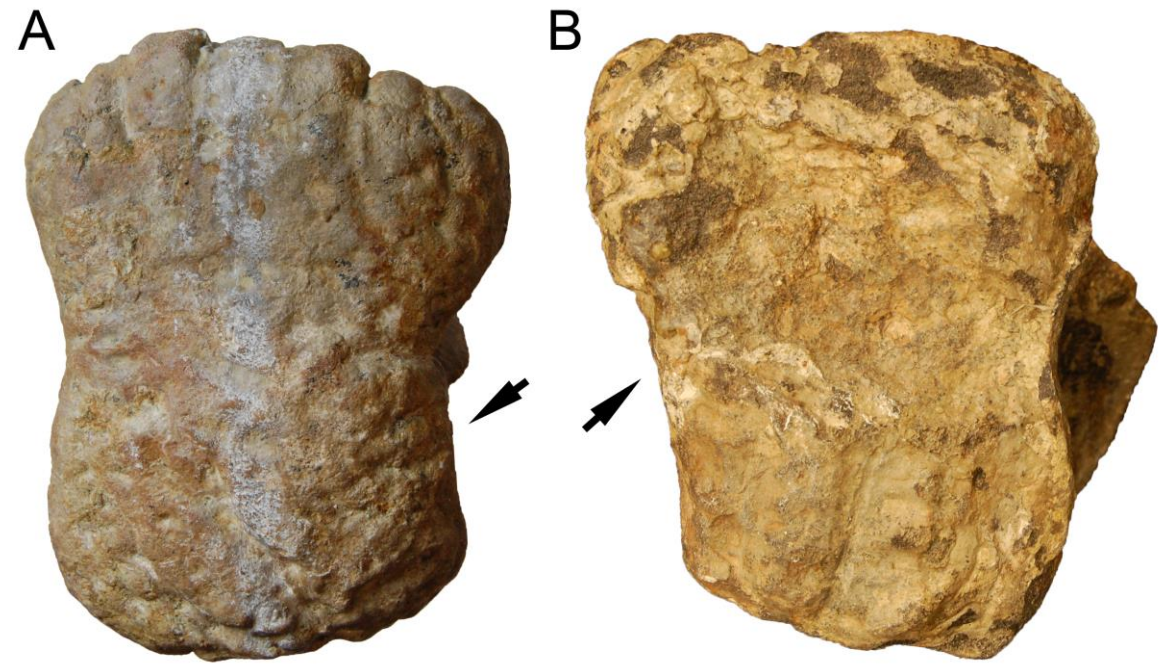

Figure 6.107: Right (A) and left (B) metatarsal II of *Suuwassea emilieae* ANS 21122 (A) and *Dyslocosaurus polyonychius* AC 663 (B) in proximal view, illustrating the concave (A) and straight (B) lateral margins (arrows; C467). Scaled to the same dorsoventral height.

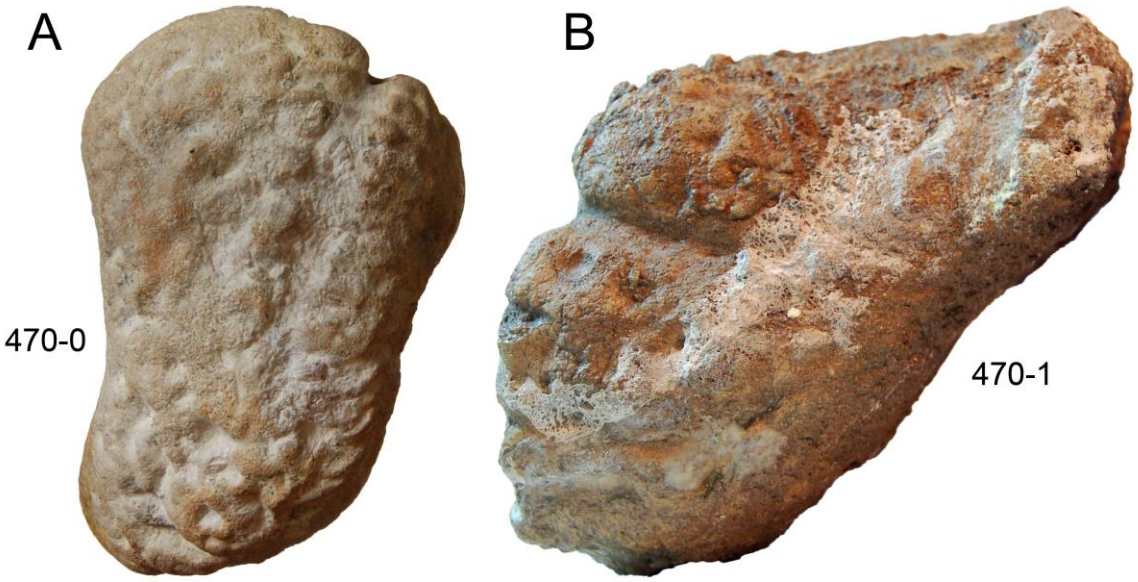

Figure 6.108: Right (A) and left (B) metatarsal IV of *Suuwassea emilieae* ANS 21122 (A) and *Cetiosauriscus stewarti* NHMUK R3078 (B) in proximal view, illustrating the curved (A; C470-0) and subtriangular outlines (B; C470-1). Scaled to the same dorsoventral height.

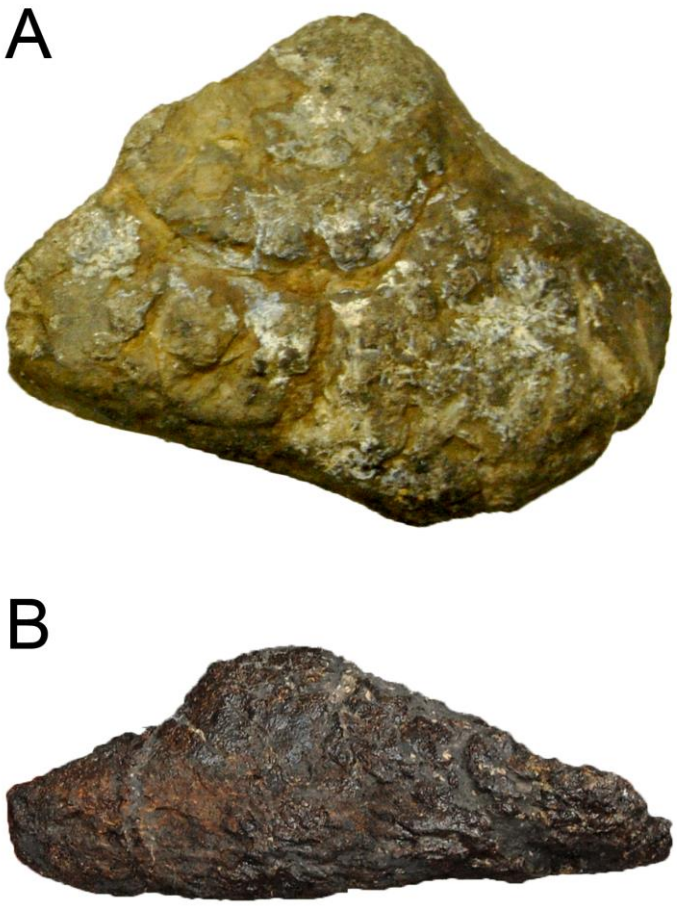

Figure 6.109: Metatarsal V of *Barosaurus affinis* YPM 419 (A) and SMA 0087 (B) in proximal view, illustrating the rhomboid (A; C471-1) or triangular outline of the articular surface (B; C471-0). Scaled to the same transverse width.

C472: Metatarsal V proximal end to distal end maximum mediolateral width ratio: 1.6 or greater (0); < 1.6 (Mannion et al., 2013; Tab. 6.59).

Comments. Transverse width was measured between parallel vertical lines through the medial- and lateral-most points of the articular surfaces.

C473: Pes, phalanx I-1: proximal and ventral surfaces meet at approximately 90° (0); proximoventral corner drawn out into thin plate underlying metatarsal I (1) (McIntosh et al., 1992; Fig. 6.110).

C474: Pes, phalanx I-1, distal articular surface shape: wide, maximum transverse width > 1.1 times anteroposterior height (0); narrow, maximum transverse width 1.1 times anteroposterior height or less (1) (New; Tab. 6.60).

C475: Pes, phalanx II-2: well developed and subrectangular in dorsal view (0); reduced, with an irregular D-shaped outline and proximal and distal articular surfaces that meet virtually along the dorsal and plantar margins (1) (McIntosh et al., 1992).

C476: Pes, phalanges III-1 and IV-1: equal to longer than wide (0); wider than long (1) (McIntosh et al., 1992; Tab. 6.60).

Comments. The greatly elongate php IV-1 of the early juvenile SMA 0009 indicates that phalanges grow allometrically during early ontogeny.

C477: Pedal unguals, groove on lateral surface: follows curvature of claw (0); straight horizontally (1) (New; Fig. 6.111).

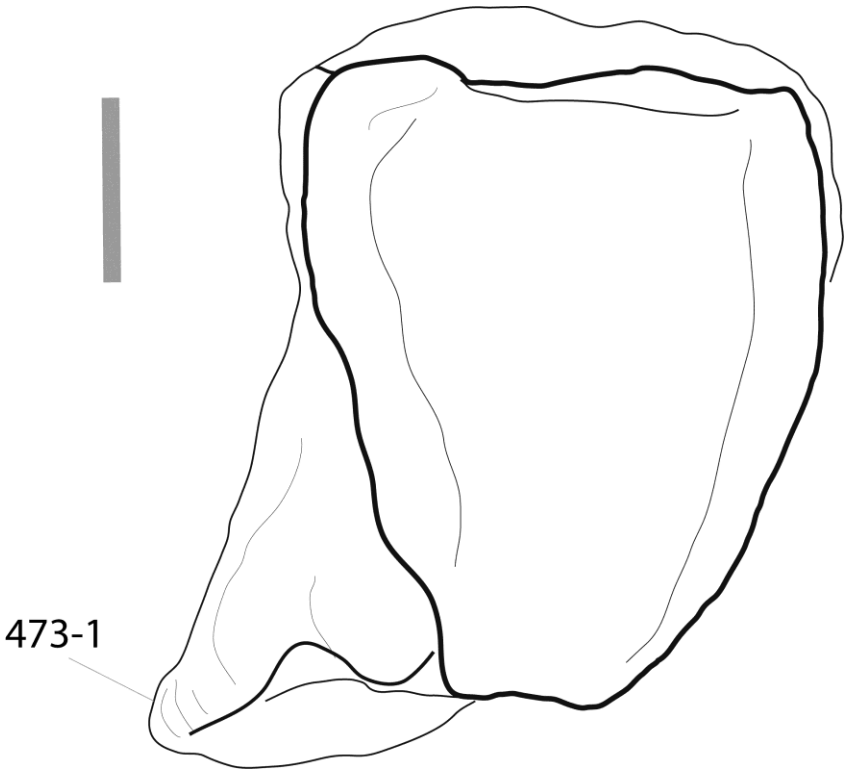

Figure 6.110: Pedal phalanx I-1 of *Apatosaurus* sp. NHMUK R3215 in medial view, illustrating the ventral shelf (C473-1). Scale bar = 2 cm.

Table 6.60: Pedal phalanges, ratios.

Taxon	Specimen	php I-1		php III-1-IV-1		Reference	Comments
		1) dw/dh	Mean 1	2) gl/max w	Mean 2		
Shunosaurus lii	T5402	1,056	1,1		0,7	Zhang, 1988	
	T5402, III-1			0,688		Zhang, 1988	
	T5402, IV-1			0,625		Zhang, 1988	
Omeisaurus	T5701	1,620	1,6		1,0	He et al., 1988	measured from figure
	T5704, III-1			1,000		He et al., 1988	
	T5704, IV-1			0,931		He et al., 1988	
Mamenchisaurus	ZDM 0083, III-1			0,815	0,8	Ouyang and Ye, 2002	
Turiasaurus riodevensis	CPT				wider	pers. obs.	no measurements available
Camarasaurus	GMNH-PV 101, III-1		1,2	0,545	0,6	McIntosh et al., 1996a	
	GMNH-PV 101, IV-1			0,429		McIntosh et al., 1996a	
	SMA 0002, L	1,111				Tschopp, 2008	
	SMA 0002, R	1,352				Tschopp, 2008	
	SMA 0002, L, III-1			0,831		Tschopp, 2008	
	SMA 0002, L, IV-1			0,787		Tschopp, 2008	
	SMA 0002, R, III-1			0,825		Tschopp, 2008	
	SMA 0002, R, IV-1			0,429		Tschopp, 2008	
Apatosaurus grandis YPM 1901	YPM 1901			0,925	0,9	M. Fox, pers. comm., 2012	probably php III-1, measured from photo
Giraffatitan brancai	MB.R. i7	1,498	1,4		0,7	Janensch, 1961	measured from figure
	MB.R. JR19	1,398				Janensch, 1961	measured from figure
	MB.R. JR20, IV-1			0,637		Janensch, 1961	measured from figure
	MB.R. TL4, III-1			0,849		Janensch, 1961	measured from figure
	MB.R. U11, III-1			0,798		Janensch, 1961	measured from figure
	MB.R. XX15, IV-1			0,706		Janensch, 1961	measured from figure
	MB.R. XX16, III-1			0,801		Janensch, 1961	measured from figure
	MB.R.2181, IV-1			0,695		Janensch, 1961	measured from figure
Brachiosaurus sp. SMA 0009	SMA 0009, L, IV-1			3,000	3,0	Schwarz et al., 2007	
Suuwassea emilieae ANS 21122	ANS 21122			1,015	1,0	Harris, 2007	not sure which element
Apatosaurus louisae CM 3018	CM 3018	1,130	1,1		0,9	Gilmore, 1936	measured from figure
	CM 3018, III-1			0,938		Gilmore, 1936	
	CM 3018, IV-1			0,891		Gilmore, 1936	
Eobrontosaurus yahnahpin Tate-001	Tate-001, L, IV-1			0,815	0,8	P. Mannion, pers. comm., 2012	measured from photo
Apatosaurus ajax NSMT-PV 20375	NSMT-PV 20375, R	1,450	1,5		0,7	Upchurch et al., 2004b	
	NSMT-PV 20375, R, III-1			0,680		Upchurch et al., 2004b	
	NSMT-PV 20375, R, IV-1			0,774		Upchurch et al., 2004b	
Apatosaurinae indet. SMA 0087	SMA 0087, R	1,061	1,1			pers. obs.	
Diplodocus carnegii CM 94	CM 94, L				longer	pers. obs.	no measurements available
Diplodocus sp. USNM 10865	USNM 10865, L		higher		0,8	pers. obs.	
	USNM 10865, L, III-1			0,846		pers. obs.	measured from figure
Diplodocus sp. WDC-FS001A	WDC-FS001A, III-1			0,990	0,9	R. Wilhite, pers. comm., 2012	measured from photo
	WDC-FS001A, IV-1			0,837		R. Wilhite, pers. comm., 2012	measured from photo
Galeamopus shellensis SMA 0011	SMA 0011, L, III-1			1,100	1,1	pers. obs.	
Barosaurus sp. AMNH 6341	AMNH 6341, R	0,970	1,0			pers. obs.	
Cetiosauriscus stewarti NHMUK R3078	NHMUK R3078, L	1,104	1,1		1,0	pers. obs.	
	NHMUK R3078, L, III-1			1,064		pers. obs.	
	NHMUK R3078, L, IV-1			1,000		pers. obs.	
Dyslocosaurus polyonychius AC 663	AC 663, L	1,105	1,1			pers. obs.	measured from photo

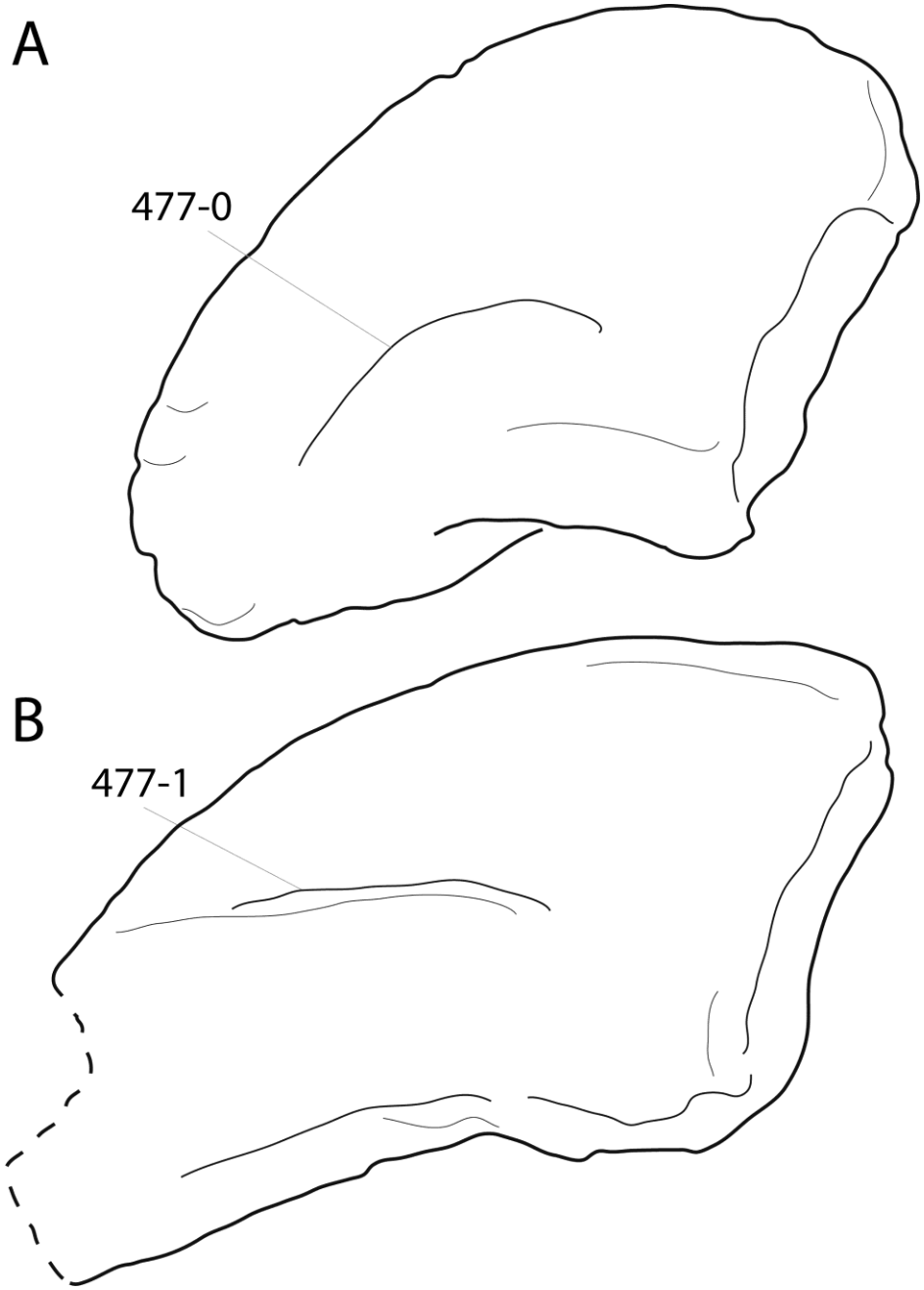

Figure 6.111: Pedal ungual I of *Cetiosauriscus stewarti* NHMUK R3078 (A) and *Dyslocosaurus polyonychius* AC 663 (B) in lateral view, illustrating the two different courses of the canals (curved, A, C477-0; straight, B, C477-1). Dotted lines indicates the broken tip. Scaled to same proximal articular surface height.

Results

The first iteration of the analysis yielded 184 most parsimonious trees with a score of 1897 steps. The second iteration using the command bbreak increased this number to 41000 (more was not possible due to computer limitations). Overall CI and RI were calculated in WinClada (version 1.00.08, www.cladistics.com), and are equal to 27, and 58, respectively. The strict consensus tree had 12 nodes, which are exclusively located outside Diplodocidae, meaning that all ingroup specimens formed one big polytomy (Fig. 6.112). Deleting the six most unstable taxa a posteriori, the higher-level clades within Flagellicaudata can be observed (Dicraeosauridae, Apatosaurinae, and Diplodocinae; Fig. 6.113). The equally weighted reduced consensus tree includes 51 from the originally 76 taxa. The classical diplodocid genera as used in earlier phylogenetic analyses (Whitlock, 2011a; Mannion et al., 2012; Tschopp and Mateus, 2012b) are all visible (Fig. 6.114).

Diplodocoidea forms the sister-taxon to Titanosauriformes, with *Camarasaurus* and Turiasauria forming a more basal clade. This result contradicts most of the recent analyses on sauropod, and in particular studies on early macronarian phylogenetic relationships (Carballido et al., 2012b; D'Emic, 2012; Mannion et al., 2013), and appears to corroborate preliminary results from Upchurch (2009) and Mateus et al. (2011), which recovered Macronaria as polyphyletic. However, many important taxa and characters usually defining Macronaria are missing in the present tree, due to the focus on Diplodocoidea. Since diplodocoid synapomorphies are often shared with derived titanosauriforms, these characters probably pulled the entire clade into a closer relationship with Diplodocoidea.

Within Diplodocoidea, Rebbachisauridae forms the most basal clade, followed by Dicraeosauridae (including *Suuwassea emilieae*), and the Diplodocidae. Diplodocidae are divided into Apatosaurinae and Diplodocinae. The newly described genera *Kaatedocus* and *Galeamopus* are deeply nested within Diplodocinae, but SMA 0087 has an ambiguous position at the base of Apatosaurinae or Diplodocinae.

Specimens included, which are recovered outside Diplodocoidea in the equally weighted reduced strict consensus tree are the following: *Amphicoelias latus* AMNH 5765 (Camarasauridae), *Apatosaurus grandis* YPM 1901 (*Camarasaurus*), *Losillasaurus giganteus* type (Turiasauria), and *Brachiosaurus* sp. SMA 0009 (Neosauropoda). *Cetiosauriscus stewarti* NHMUK R3078 (non-flagellicaudatan Diplodocoidea) and *Suuwassea emilieae* ANS 21122 (Dicraeosauridae) are recovered as non-diplodocid Diplodocoidea. Important specimens not represented in the equally weighted reduced consensus tree are YPM 1920 (genoholotype of *Diplodocus*), YPM 1980 (genoholotype of *Brontosaurus*), and CM 566 (genoholotype of *Elosaurus*). The specimen SMA 0087, preliminarily described herein, also lacks in the reduced strict consensus tree.

One by one addition to the reduced consensus tree of the single specimens used in the ingroup revealed non-flagellicaudatan phylogenetic positions for the following specimens: *Lourinhasaurus alenquerensis* MIGM (non-diplodocoid, non-titanosauriform neosauropod), *Australodocus bohetii* type (possibly brachiosaurid titanosauriform), '*Apatosaurus*' *minimus* AMNH 675 (non-flagellicaudatan, non-rebbachisaurid, non titanosauriform neosauropod), and *Dystrophaeus viaemalae* USNM 2364 (non-flagellicaudatan, non-rebbachisaurid, non titanosauriform eusauropod).

The single most unstable taxon as recovered by the pruned trees approach was *Diplodocus lacustris* YPM 1922. By excluding this taxon from the strict consensus tree, 12 more nodes were resolved (*Australodocus* in a trichotomy with *Brachiosaurus* and *Giraffatitan*, a polytomous Dicraeosauridae including *Dyslocosaurus* and *Suuwassea*, *Dinheirosaurus* + *Supersaurus*, an apatosaur clade comprising the new sister arrangement *Elosaurus parvus* CM 566 + UW 15556, and a diplodocine clade including a branch with CM 3452, *Barosaurus*, and *Kaatedocus*). *Diplodocus lacustris* YPM 1922 was shown to group with a large number of OTUs, mostly within Flagellicaudata, as exemplified by the large polytomy of the reduced consensus tree including the specimen. As YPM 1922 is a teeth-only specimen, the result mentioned above indicates that flagellicaudatan teeth cannot be distinguished at the present state of knowledge.

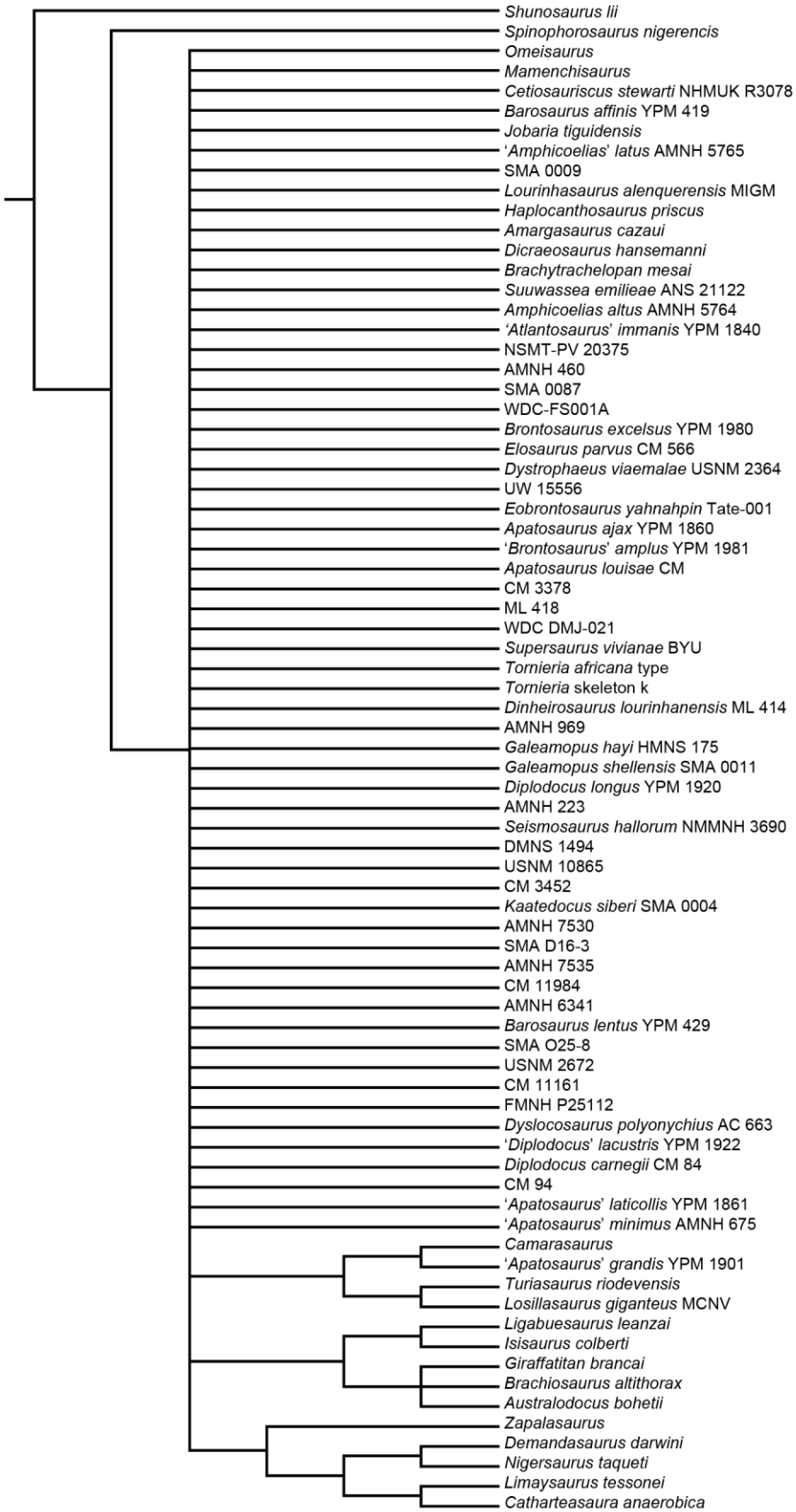

Figure 6.112: Strict consensus tree of the complete analysis with equal weighting. OTUs with species names and specimen numbers are type specimens. Tree length is 1897 steps. Note the brachiosaurid affinities of *Australodocus*.

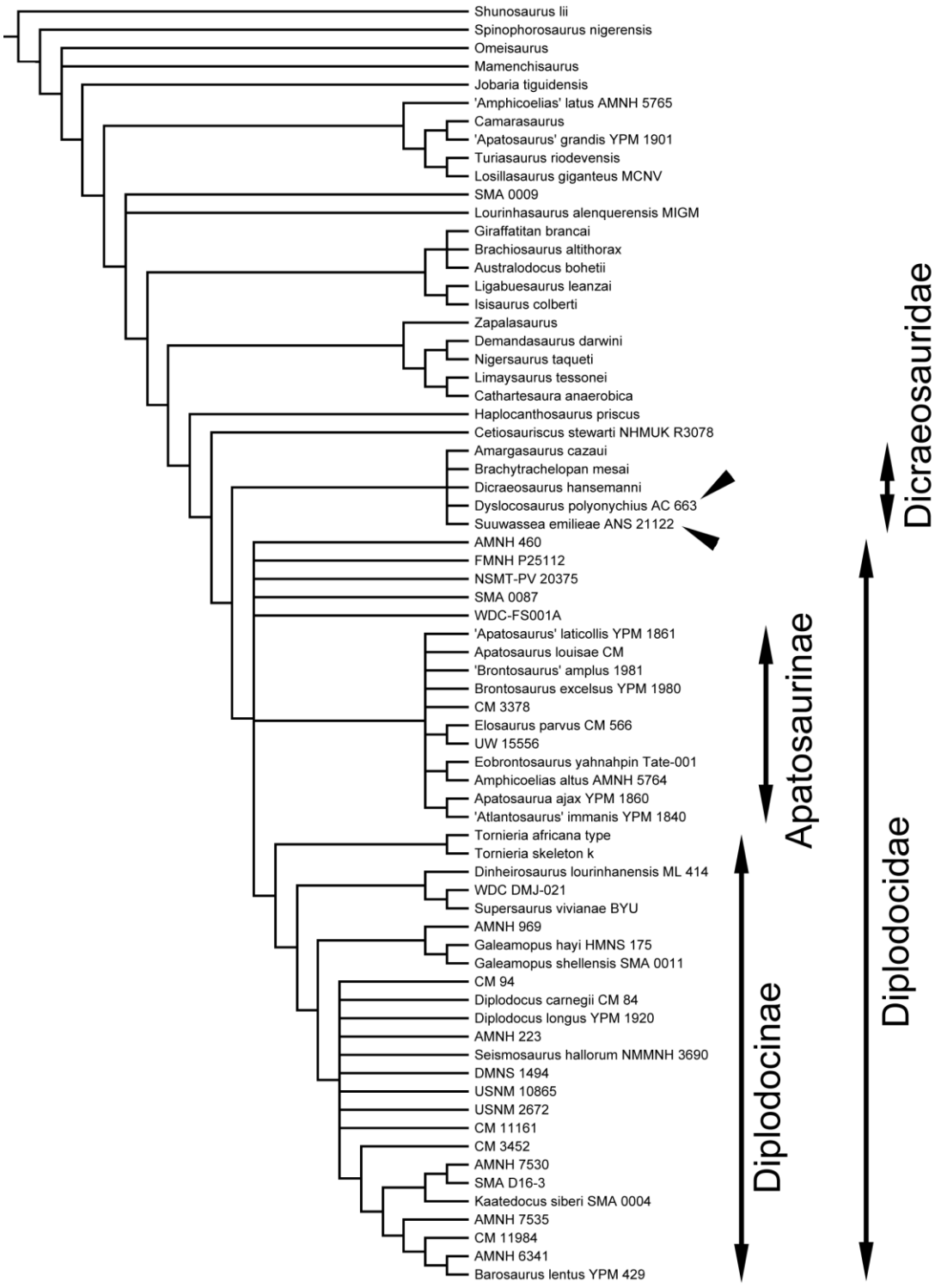

Figure 6.113: Pruned strict consensus tree obtained by equal weighting, after the a posteriori deletion of '*Apatosaurus*' *minimus* AMNH 675, '*Barosaurus*' *affinis* YPM 419, '*Diplodocus*' *lacustris* YPM 1922, *Dystrophaeus viaemalae* USNM 2364, ML 418, and SMA O25-8. Note the dicraeosaurid affinities of *Dyslocosaurus* and *Suuwassea* (arrowheads).

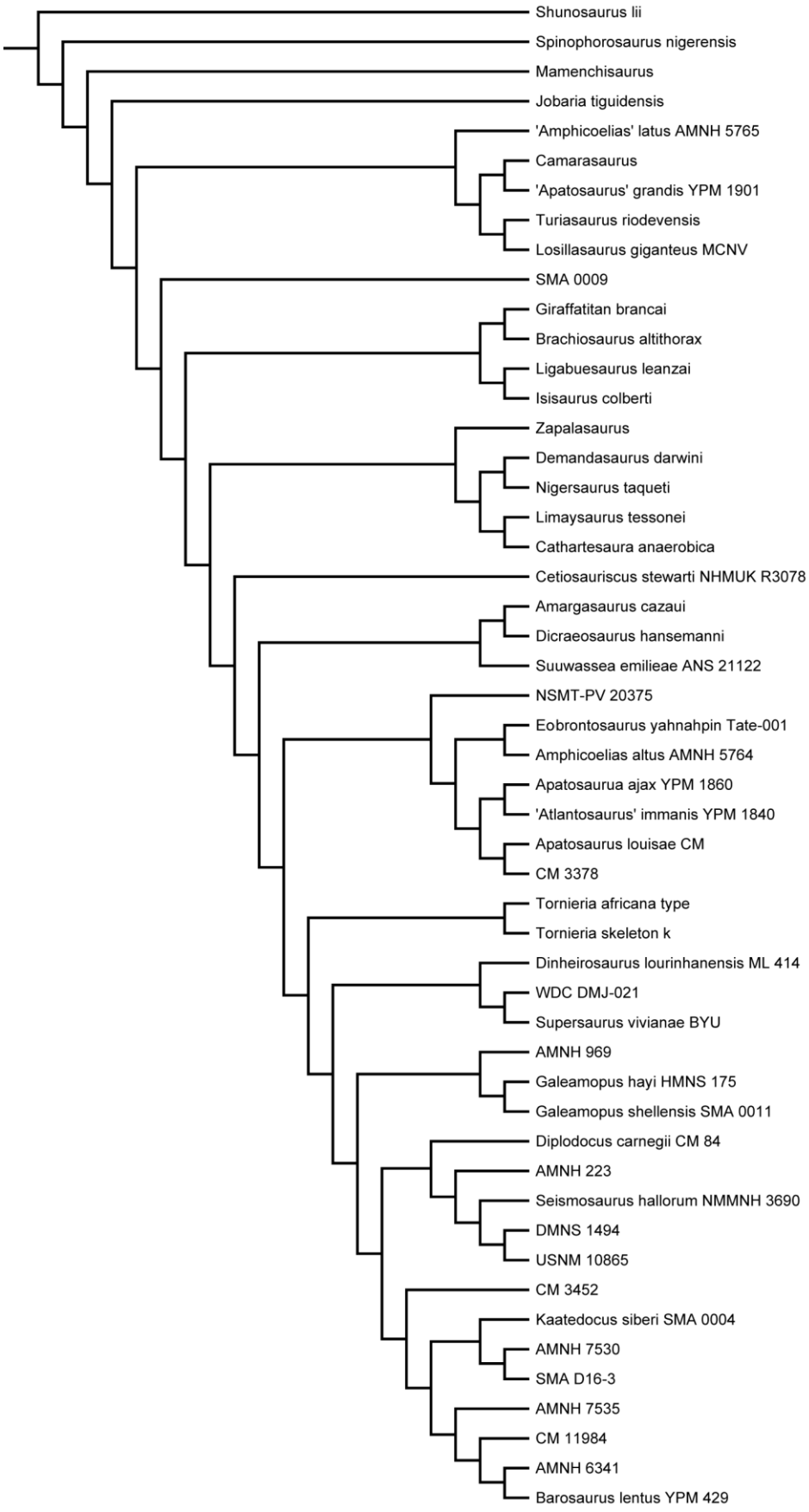

Figure 6.114: Reduced consensus tree obtained by equal weighting, after the a posterior deletion of 25 OTUs.

The analysis done under implied weighting yielded 202 most parsimonious trees of a length of 187.97214, but the number was increased by the second iteration of tree branch swapping to 41000, as in the first analysis with equal weighting. However, the strict consensus tree preserved 24 nodes, the double of the first version (Fig. 6.115). The pruned tree analysis with implied weights confirmed that the *Diplodocus lacustris* holotype specimen (YPM 1922) is the least stable. Deletion of YPM 1922 results in 29 gained nodes, compared to the strict consensus tree. Omission of the least stable quartet (*D. lacustris* YPM 1922, the diplodocine skulls CM 11161 and USNM 2672, and the braincase SMA O25-8) resulted in a pruned consensus tree with 36 nodes more than the complete strict consensus tree, and 17 nodes more than the pruned tree with equal weighting, where six specimens were deleted a posteriori (Fig. 6.116). The reduced consensus tree with implied weights includes 66 taxa, 15 more than the equally weighted reduced consensus tree (Fig. 6.117).

Implied weighting leads to an exclusion of *Cetiosauriscus stewarti* and *Barosaurus affinis* from Diplodocoidea, and even Neosauropoda. '*Apatosaurus*' *minimus* is recovered within Somphospondyli, and within Diplodocinae, *Dinheirosaurus* is separated from *Supersaurus*, which groups with *Australodocus* instead. The clade *Eobrontosaurus* + *Amphicoelias* is split here, with the latter resolved as most basal diplodocid. Finally, an apatosaurine clade including the genoholotypes of *Brontosaurus*, *Dystrophaeus* and *Elosaurus* is found.

Symmetric resampling did not find much support for ingroup clades (Tab. 6.61), most probably due to the little anatomical overlap. However, it found support for three clades that were not recovered in any of the six main trees: the grouping of the two diplodocine skulls USNM 2672 and CM 11161 (resampling value of 12), a dichotomy of holotype and paratype of *Diplodocus carnegii* (CM 84 and 94, resampling value 8), and a clade including the holotypes of *Apatosaurus louisae* and *A. laticollis*, as well as the specimen CM 3378 (resampling value of 15). The latter two clades are actually found in trees excluding *D. longus* YPM 1920 or *Brontosaurus amplus* YPM 1981, respectively. The grouping of the two skulls CM 11161 and USNM 2672 indicates that they are more similar to each other than to any other diplodocine skull.

Table 6.61: Clades recovered, support values, and differences.

Clade	recovered by		equivalent to	Resampling	Overlap	Synapomorphies		Differencies ew-iw	
						total	unique	ingroup	outgroup
Diplodocoidea	S_ew								AuBo
	P_ew	✓	Diplodocimorpha		33%	27	19	CeSt	AuBo
	R_ew	✓	Diplodocimorpha		36%	28	20	CeSt	
	S_iw	✓	H. priscus + mdD		31%			AuBo	CeSt
	P_iw	✓	H. priscus + mdD		32%	5	2	AuBo	CeSt
	R_iw	✓	H. priscus + mdD		32%	4	2	AuBo	CeSt
Diplodocimorpha	S_ew								AuBo
	P_ew	✓	Diplodocoidea		33%	27	19	CeSt, HaPr	AuBo
	R_ew	✓	Diplodocoidea		36%	28	20	CeSt	
	S_iw	✓			31%			AuBo	CeSt, HaPr
	P_iw	✓			32%	6	4	AuBo	CeSt, HaPr
	R_iw	✓			32%	6	4	AuBo	CeSt, HaPr
Rebbachisauridae	S_ew	✓			28%				
	P_ew	✓			28%	9	0		
	R_ew	✓			28%	8	0		
	S_iw	✓		56	28%				
	P_iw	✓			28%	8	0		
	R_iw	✓			28%	7	0		
Nigersaurinae + Limaysaurinae	S_ew	✓			32%				
	P_ew	✓			32%	5	2		
	R_ew	✓			32%	5	2		
	S_iw	✓		17	32%				
	P_iw	✓			32%	4	2		
	R_iw	✓			32%	4	2		
Nigersaurinae	S_ew	✓			24%				
	P_ew	✓			24%	3	1		
	R_ew	✓			24%	3	1		
	S_iw	✓		18	24%				
	P_iw	✓			24%	3	1		
	R_iw	✓			24%	3	1		
Limaysaurinae	S_ew	✓			19%				
	P_ew	✓			19%	3	0		
	R_ew	✓			19%	3	0		
	S_iw	✓		64	19%				
	P_iw	✓			19%	3	0		
	R_iw	✓			19%	3	0		

Table 6.61: continued.

Haplocanthosaurus + mdD	S_ew								
	P_ew	✓			33%	4	1	CeSt	Rebbachisauridae
	R_ew								
	S_iw	✓	Diplodocoidea		31%			Rebbachisauridae, AuBo	CeSt
	P_iw	✓	Diplodocoidea		32%	5	2	Rebbachisauridae, AuBo	CeSt
	R_iw	✓	Diplodocoidea		32%	4	2	Rebbachisauridae, AuBo	CeSt
Cetiosauriscus + mdD	S_ew								
	P_ew	✓			32%	4	0		
	R_ew	✓			35%	5	0		
	S_iw								
	P_iw								
	R_iw								
Flagellicaudata	S_ew								
	P_ew	✓			32%	9	2		AuBo
	R_ew	✓			35%	6	1		
	S_iw								
	P_iw	✓			31%	30	10	AuBo	
	R_iw	✓			31%	28	10	AuBo	
Dicraeosauridae	S_ew								
	P_ew	✓			31%	36	5		
	R_ew	✓			45%	11	2		
	S_iw								
	P_iw	✓			31%	36	6		
	R_iw	✓			39%	15	3		
Brachytrachelopan + (Amargasaurus + Dicraeosaurus)	S_ew								
	P_ew								
	R_ew			34					
	S_iw								
	P_iw								
	R_iw	✓			37%	8	0		
Amargasaurus + Dicraeosaurus	S_ew								
	P_ew								
	R_ew	✓		38	48%	13	1		
	S_iw								
	P_iw								
	R_iw	✓			48%	4	1		
Diplodocidae	S_ew								
	P_ew	✓			31%	32	9		AuBo
	R_ew	✓			33%	15	5		
	S_iw								
	P_iw	✓			30%	5	0	AuBo	
	R_iw	✓			29%	4	0	AuBo	
Apatosaurinae + Diplodocinae	S_ew								
	P_ew								
	R_ew	✓	Diplodocidae		33%	15	5	AmAl	
	S_iw								
	P_iw	✓			30%	3	1	AuBo	AmAl
	R_iw	✓			30%	3	1	AuBo	AmAl
Apatosaurinae	S_ew								
	P_ew	✓			27%	25	2	AmAl	WDC-FS001A, SMA 0087, FMNH P25112, AMNH 460, NSMT-PV 20375
	R_ew	✓			31%	7	1	AmAl, NSMT-PV 20375	
	S_iw								
	P_iw	✓			29%	11	1	NSMT-PV 20375, AMNH 460, WDC-FS001A, SMA 0087, FMNH P25112	AmAl
	R_iw	✓			30%	11	1	NSMT-PV 20375, AMNH 460, WDC-FS001A, SMA 0087	AmAl
NSMT-PV 20375 + A. immanis YPM 1840	S_ew								
	P_ew								
	R_ew								
	S_iw								
	P_iw	✓			15%	4	0		
	R_iw	✓			15%	5	0		
AMNH 460 + mdA	S_ew								
	P_ew								
	R_ew								
	S_iw								
	P_iw	✓			28%	3	0		
	R_iw	✓			29%	4	0		
SMA 0087 + mdA	S_ew								
	P_ew								
	R_ew								
	S_iw								
	P_iw	✓			27%	2	0		
	R_iw	✓			29%	1	0		
WDC-FS001A + SMA 0087	S_ew								
	P_ew								
	R_ew								
	S_iw								
	P_iw	✓			8%	2	0		
	R_iw	✓			8%	2	0		

Table 6.61: continued.

B. excelsus + mdA	S_ew								
	P_ew								
	R_ew								
	S_iw								
	P_iw	✓		28%	10	1			
	R_iw	✓		30%	9	1			
Brontosaurus + (Elosaurus + Dystrophaeus)	S_ew								
	P_ew								
	R_ew								
	S_iw								
	P_iw	✓		24%	5	1			
	R_iw	✓		22%	4	0			
Elosaurus + Dystrophaeus	S_ew								
	P_ew								
	R_ew								
	S_iw								
	P_iw								
	R_iw	✓		10%	3	0			
E. parvus + UW 15556	S_ew								
	P_ew	✓		17%	7	0			
	R_ew								
	S_iw								
	P_iw								
	R_iw								
Dystrophaeus + UW 15556	S_ew								
	P_ew								
	R_ew								
	S_iw								
	P_iw								
	R_iw	✓		4%	1	0			
Eobrontosaurus + mdA	S_ew								
	P_ew								
	R_ew	✓		25%	8	0	AmAl, AtIm		
	S_iw								
	P_iw	✓		24%	3	0		AmAl, AtIm	
	R_iw	✓		28%	3	0		AmAl, AtIm	
Eobrontosaurus + Amphicoelias	S_ew								
	P_ew	✓		7%	2	0			
	R_ew	✓		7%	2	0			
	S_iw								
	P_iw								
	R_iw								
A. ajax + mdA	S_ew								
	P_ew								
	R_ew	✓		25%	3	0	AtIm		
	S_iw								
	P_iw	✓		21%	6	0		AtIm	
	R_iw	✓		25%	7	0		AtIm	
A. ajax + A. immanis	S_ew								
	P_ew	✓		13%	4	0			
	R_ew	✓		13%	4	0			
	S_iw								
	P_iw								
	R_iw								
B. amplus + mdA	S_ew								
	P_ew								
	R_ew								
	S_iw								
	P_iw								
	R_iw	✓		14%	1	0			
A. louisae + CM 3378	S_ew								
	P_ew								
	R_ew	✓	23	13%	7	0			
	S_iw								
	P_iw								
	R_iw	✓		13%	2	0			
Diplodocinae	S_ew								
	P_ew	✓		29%	16	2		AuBo	
	R_ew	✓		30%	8	2		AuBo	
	S_iw								
	P_iw	✓		28%	2	0	AuBo		
	R_iw	✓		26%	2	0	AuBo		
Supersaurus + mdD	S_ew								
	P_ew	✓		30%	2	0		AuBo, ToAf	
	R_ew	✓		31%	3	0		AuBo, ToAf	
	S_iw								
	P_iw	✓		29%	2	0	AuBo, ToAf		
	R_iw	✓		27%	2	0	AuBo, ToAf		

Table 6.61: continued.

Australodocus + Supersaurus	S_ew										
	P_ew										
	R_ew										
	S_iw										
	P_iw	✓			16%	4	0				
	R_iw	✓			16%	4	0				
Dinheirosaurus + Supersaurus	S_ew										
	P_ew	✓			21%	7	1				
	R_ew	✓		3	21%	5	1				
	S_iw										
	P_iw										
	R_iw										
S. vivianae + WDC-DMJ 021	S_ew										
	P_ew	✓			25%	6	0				
	R_ew	✓		36	25%	7	0				
	S_iw										
	P_iw	✓			25%	1	0				
	R_iw	✓			25%	1	0				
Tornieria + mdD	S_ew										
	P_ew	✓	Diplodocinae		29%	16	2	SuVi			
	R_ew	✓	Diplodocinae		30%	8	2	SuVi			
	S_iw										
	P_iw	✓			29%	3	2			SuVi	
	R_iw	✓			27%	3	2			SuVi	
T. africana + MB.R. Skeleton k	S_ew										
	P_ew	✓			6%	5	0				
	R_ew	✓		4	6%	3	0				
	S_iw										
	P_iw	✓			6%	3	0				
	R_iw	✓			6%	3	0				
Dinheirosaurus + mdD	S_ew										
	P_ew	✓	Supersaurus + mdD		30%	2	0	SuVi			
	R_ew	✓	Supersaurus + mdD		31%	3	0	SuVi			
	S_iw										
	P_iw	✓			31%	1	0			SuVi	
	R_iw	✓			28%	1	0			SuVi	
Galeamopus + mdD	S_ew										
	P_ew	✓			30%	11	2				
	R_ew	✓			32%	6	2				
	S_iw										
	P_iw	✓			31%	6	0				
	R_iw	✓			29%	5	0				
AMNH 969 + (SMA 0011 + G. hayi)	S_ew										
	P_ew	✓			31%	4	2				
	R_ew	✓		2	31%	3	2				
	S_iw										
	P_iw	✓			31%	3	2				
	R_iw	✓			31%	3	2				
SMA 0011 + G. hayi	S_ew										
	P_ew	✓			39%	3	0				
	R_ew	✓			39%	1	0				
	S_iw										
	P_iw	✓			39%	1	0				
	R_iw	✓			39%	1	0				
Diplodocus + mdD	S_ew										
	P_ew	✓			27%	17	1				
	R_ew	✓			28%	6	1				
	S_iw										
	P_iw	✓			28%	8	1				
	R_iw	✓			24%	6	1				
D. carnegii + md Diplodocus	S_ew										
	P_ew										
	R_ew	✓			30%	7	1				
	S_iw										
	P_iw	✓			29%	7	1				
	R_iw										
D. longus + md Diplodocus	S_ew										
	P_ew										
	R_ew										
	S_iw										
	P_iw	✓	D. carnegii + md Diplodocus		29%	7	1				
	R_iw	✓			21%	1	0				

Table 6.61: continued.

AMNH 223 + D. halli	S_ew						
	P_ew						
	R_ew	✓	6	26%	5	1	
	S_iw						
	P_iw	✓		26%	6	1	
	R_iw	✓		26%	3	1	
D. halli + md Diplodocus	S_ew						
	P_ew						
	R_ew	✓	6	24%	1	0	
	S_iw						
	P_iw	✓		24%	1	0	
	R_iw	✓		24%	1	0	
DMNS 1494 + USNM 10865	S_ew						
	P_ew						
	R_ew	✓	9	24%	1	0	
	S_iw						
	P_iw	✓		24%	1	0	
	R_iw	✓		24%	0	0	
CM 3452 + mdD	S_ew						
	P_ew	✓		22%	11	1	
	R_ew	✓		22%	2	0	
	S_iw						
	P_iw	✓		22%	3	0	
	R_iw	✓		22%	2	0	
Kaatedocus + Barosaurus	S_ew						
	P_ew	✓		20%	3	0	
	R_ew	✓		20%	2	0	
	S_iw						
	P_iw	✓		20%	3	0	
	R_iw	✓		20%	1	0	
K. siberi + (SMA D16-3 + AMNH 7530)	S_ew						
	P_ew	✓		17%	9	0	
	R_ew	✓	14	17%	8	0	
	S_iw						
	P_iw	✓		17%	8	0	
	R_iw	✓		17%	7	0	
SMA D16-3 + AMNH 7530	S_ew						
	P_ew	✓		5%	0	0	
	R_ew	✓	20	5%	0	0	
	S_iw						
	P_iw	✓		5%	0	0	
	R_iw	✓		5%	0	0	
AMNH 7535 + mdD	S_ew						
	P_ew	✓		21%	1	0	
	R_ew	✓		21%	1	0	
	S_iw						
	P_iw	✓		21%	1	0	
	R_iw	✓		21%	1	0	
CM 11984 + (AMNH 6341 + B. lentus)	S_ew						
	P_ew	✓		27%	2	0	
	R_ew	✓	13	27%	2	0	
	S_iw						
	P_iw	✓		27%	2	0	
	R_iw	✓		27%	2	0	
AMNH 6341 + B. lentus	S_ew						
	P_ew	✓		33%	4	0	
	R_ew	✓	32	33%	4	0	
	S_iw						
	P_iw	✓		33%	4	0	
	R_iw	✓		33%	4	0	
C. stewarti + B. affinis	S_ew						
	P_ew						
	R_ew		3				
	S_iw	✓		2%			
	P_iw	✓		2%	3	0	
	R_iw	✓		2%	3	0	
USNM 2672 + CM 11161	S_ew						
	P_ew						
	R_ew		12	21%			
	S_iw						
	P_iw						
	R_iw						
D. carnegii + CM 94	S_ew						
	P_ew						
	R_ew		8	39%	5	0	CM 94 added
	S_iw						
	P_iw						
	R_iw						
A. laticollis + (A. louisae + CM 3378)	S_ew						
	P_ew						
	R_ew		15	10%			
	S_iw						
	P_iw						
	R_iw						

Figure 6.115: Strict consensus tree of the complete analysis with implied weighting. OTUs with species names and specimen numbers are type specimens. Tree length is 187.97214 steps. Note the basal position of *Barosaurus affinis*, *Cetiosauriscus stewarti*, and the somphospondylian affinities of '*Apatosaurus*' *minimus*.

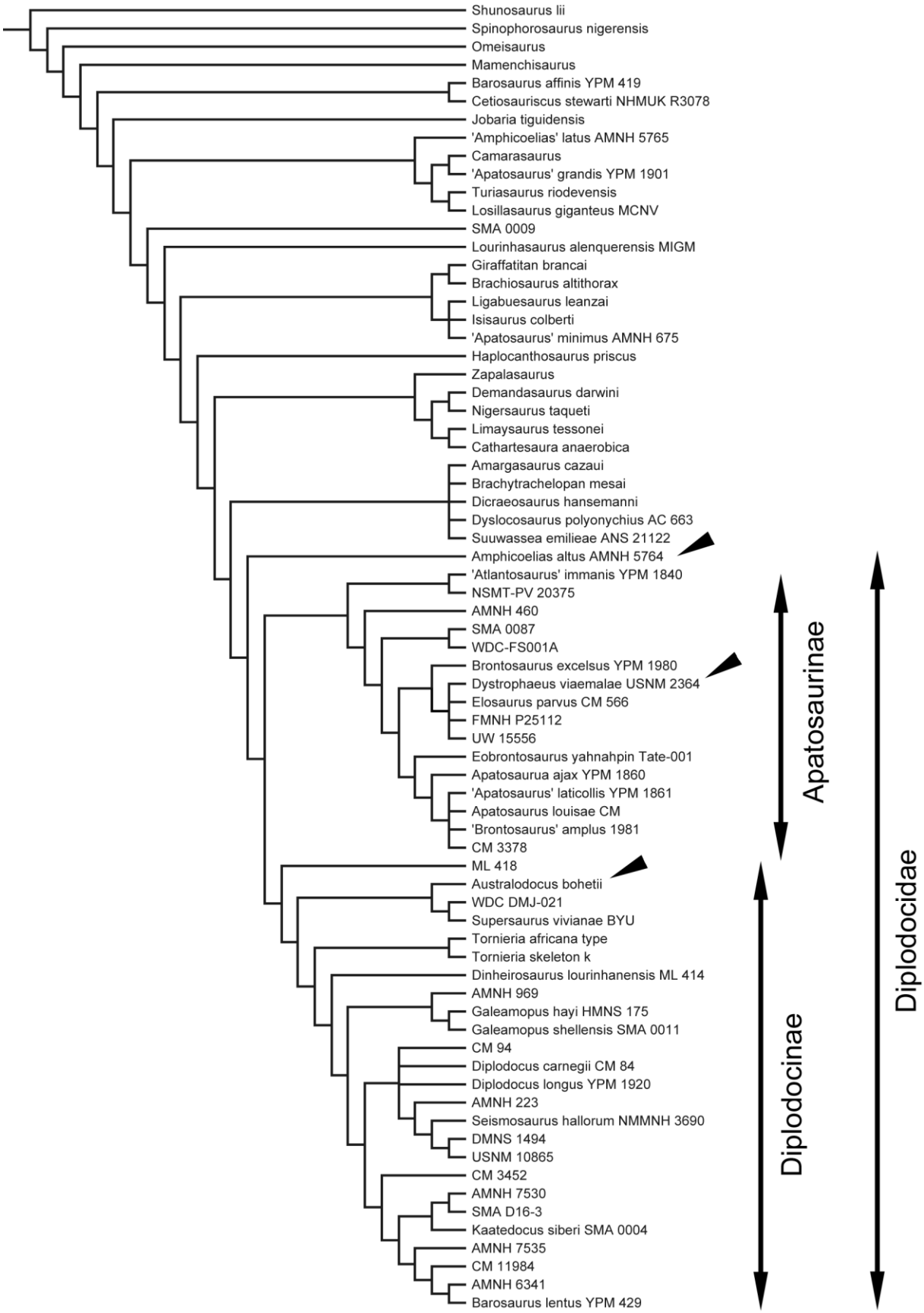

Figure 6.116: Pruned strict consensus tree obtained by implied weighting, after the a posteriori deletion of the skull-only specimens, YPM 1922, CM 11161, USNM 2672, and SMA O25-8. Note the position of *Amphicoelias altus* as most basal diplodocid, *Dystrophaeus viaemalae* within Apatosaurinae, and *Australodocus bohetii* as a diplodocine (arrowheads).

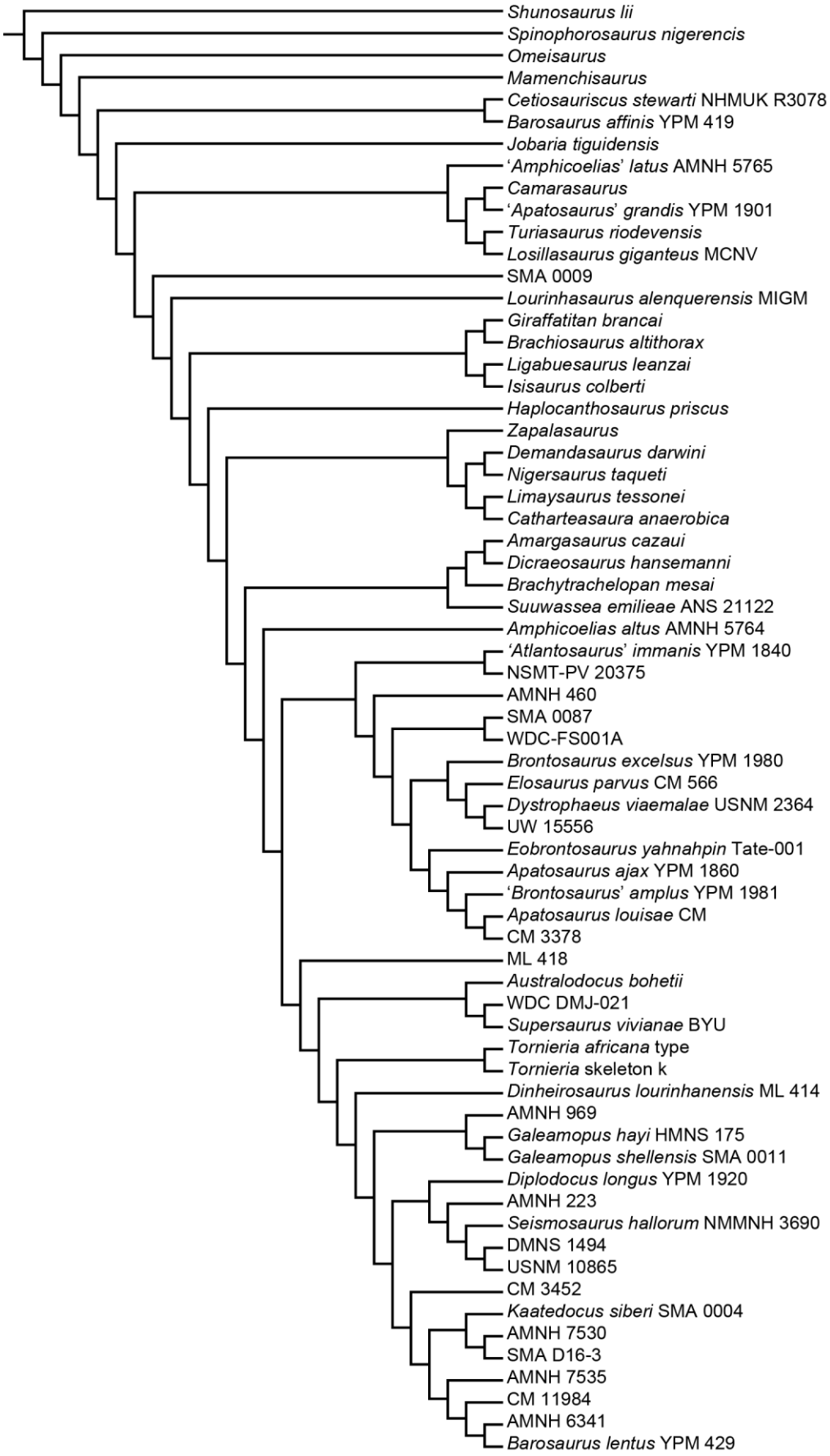

Figure 6.117: Reduced consensus tree obtained by implied weighting, after the a posteriori deletion of 10 OTUs.

Discussion

The phylogenetic history of Diplodocidae

Earlier phylogenetic studies of sauropods mostly just included the three genera *Apatosaurus*, *Diplodocus*, and *Barosaurus* (e.g. Upchurch, 1998; Wilson, 2002; Upchurch et al., 2004a). More recent analyses with a narrower focus on diplodocoid intrarelationships included more diplodocid species (Upchurch et al., 2004b; Rauhut et al., 2005; Remes, 2006; Lovelace et al., 2007; Sereno et al., 2007; Whitlock, 2011a; Carballido et al., 2012b; Mannion et al., 2012; Tschopp et al., 2012b). However, other than Upchurch et al. (2004b), all of them included the genera *Apatosaurus* and *Diplodocus* as OTU, and no analysis was ever done with all proposed diplodocid species (Fig. 6.118). Basic relationships between diplodocid taxa generally remained the same among the studies, which is probably a consequence of the fact that most were based on Wilson (2002), with only minor changes (Rauhut et al., 2005; Remes, 2006; Lovelace et al., 2007; Sereno et al., 2007). The greatest changes between these four phylogenetic analyses occur in the position of *Suuwassea*, which is recovered within Apatosaurinae (Lovelace et al., 2007), in a polytomy with *Apatosaurus* and Diplodocinae (Remes, 2006), just outside Apatosaurinae + Diplodocinae (Rauhut et al., 2005), or in a trichotomy with Diplodocidae and Dicraeosauridae (Sereno et al., 2007). Of the remaining diplodocid taxa other than *Apatosaurus*, *Diplodocus*, or *Barosaurus*, only *Tornieria* was included in more than one of these four analyses, and found within Diplodocinae (Rauhut et al., 2005; Remes, 2006).

Due to their strong focus on interspecific relationships of *Apatosaurus*, Upchurch et al. (2004b) had a very reduced dataset, with only 16 taxa and 32 characters. The character list was assembled based on earlier descriptions and diagnoses of the different species (mostly Riggs, 1903; Holland, 1915a; Gilmore, 1936), with some original characters added (Upchurch et al., 2004b). Whitlock (2011a), although basing on Wilson (2002), can be considered a new analysis as well, given the large number of modifications and added characters, and the largely increased number of taxa in order to be able to resolve diplodocoid intrarelationships. Subsequently published analyses (Mannion et al., 2012; Tschopp and Mateus, 2012b) thus consequently based on Whitlock (2011a).

The present analysis further increases both taxon and character list of Whitlock (2011a) by almost 300% and 250%, respectively (76 versus 26 OTUs, 477 versus 189 characters), and can thus be considered independent as well. Nonetheless, most of the positions of the common genera included in the analyses remained the same. The analyses thus generally corroborate each other's results.

Difficulties and possibilities of a specimen-based analysis

A specimen-based phylogenetic analysis has both drawbacks and advantages. One of the major problems is the lacking anatomical overlap, most importantly between incomplete historic holotype specimens. In particular in diplodocid sauropods, the majority of the type specimens was described by Marsh and Cope during the so-called Bone Wars (Cope, 1877a, b; Marsh, 1877a, 1878, 1879, 1881, 1884, 1890, 1899). New species were rushed into press without detailed description, sometimes even lacking illustrations (e.g. Marsh, 1881, 1899). In certain cases, subsequent studies revealed that different species were erected based on different bones of possibly the same skeleton ('*Atlantosaurus*' *immanis* YPM 1840 and *Apatosaurus laticollis* YPM 1861; Marsh, 1877a, 1879; McIntosh, 1995). More complete skeletons were later recovered, but many of these still lack a description, and were identified as a particular genus or species without any detailed study (e.g. '*Diplodocus longus*' DMNS 1494). Now, more and more nearly complete specimens are becoming available for study (e.g. Harris and Dodson, 2004; Upchurch et al., 2004b; Tschopp and Mateus, 2012b; Barrett et al., 2011). Complete, articulated specimens, or parts of skeletons preserving portions underrepresented in earlier finds (e.g. skulls attached to their necks, transitions from cervical to dorsal vertebrae, articulated manus or pedes), are crucial for a specimen-based phylogenetic analysis. They provide the anchorage with which fragmentary specimens can be compared, thereby allowing for indirect comparisons. Care has to be taken to include articulated specimens and exclude information from portions of the skeleton for which an unambiguous association with the specimen to be studied cannot be ascertained. The most valuable documents to assure genuine association of skeletal parts to one individual are detailed quarry maps and field notes, but these often lack in historic type specimens. However, efforts were made lately to unravel excavation stories and bone associations of the most important holotype specimens (e.g. McIntosh, 1990a, 1995; McIntosh and Carpenter, 1998). The present study heavily

relies on these earlier studies to confirm or discard bone associations. However, certain specimens would still need such a detailed overhaul, and their phylogenetic positions has still to be regarded provisional (see below).

An additional problem for quantitative characters in particular, are deformed specimens. Whereas brittle deformation can be readily identified due to the introduced cracks, plastic deformation results in unfractured, but distorted fossils (Tschopp et al., 2013). If plastic deformation happens symmetrically, it is almost impossible to identify, and least of all to quantify. Retrodeformation can yield some information on how bones were deformed, but only in bilaterally symmetrical elements (Arbour and Currie, 2012; Tschopp et al., 2013). For species- or genus-level phylogenetic analyses, mean ratios can be taken from different individuals of the same taxon, thereby approaching more closely the ratios generally typical for that taxon. In specimen-based analyses, such an approach is not possible. However, if a specimen is deformed in such a way that it would be scored differently from closely related species, or specimens from the same species, it increases homoplasy of this single character, and decreases its consistency index. By using implied weighting, as was done in the second analysis herein, this can be partly accounted for.

During the study of single specimens, one usually records and describes morphological details unique to the animal, which might or might not be taxonomically significant. If the phylogenetic analysis accompanying the description recovers the new specimen on a separate branch and thus as new taxon, these traits are generally interpreted as autapomorphic for the new taxon. The confirmation of such an interpretation can only be made with the discovery of additional specimens of the same species, preserving the same portions of the skeleton. Before that, variation due to any pre- or post-mortem processes (ontogeny, individual variation, sexual dimorphism, or taphonomic deformation) cannot be excluded with certainty as a cause for the morphological disparity found in the fossil. Specimen-based phylogenetic analyses are the only way to test for such variation. As mentioned above, highly homoplastic characters are describing the most variation, in the case of a specimen-based analysis between individuals. They are thus the most probable to code for individual variation, and should thus either be deleted or downweighted compared to the less variable characters, as is done by implied weighting (Goloboff, 1993). Because it cannot be excluded that characters describing individual variation in some groups actually code for taxonomically significant differences in other taxa, downweighting the characters in question appears more accurate than deleting them entirely. Finally, by scoring single specimens of a species, and thereby detecting individual variation in some characters, researchers create a firmer base for how to score species- or even genus-level OTUs.

Validity of recovered diplodocoid subclades

The following discussion includes only the clades recovered within Diplodocoidea, as the present analysis was designed for the study of diplodocid intrarelationships, and is thus not suitable for inferring phylogenetic positions and definitions for clades recovered outside Diplodocoidea. The systematic affinities of single specimens included in the analysis, which are recovered outside Diplodocoidea, are discussed below. Definitions of the clade names follow Taylor and Naish (2005) and Whitlock (2011a).

In order to avoid entirely subjective assessments of the validity of species and genera, a quantitative approach was chosen, based on the number and quality of synapomorphies and autapomorphies. Synapomorphies are separated into four, qualitatively different categories. Unambiguous synapomorphies are shared by all ingroup members of the respective clade, and only by them. Exclusive synapomorphies only mark ingroup members, but not all of them. Shared synapomorphies are present in all ingroup members, but also occasionally occur in taxa outside the clade in question. Ambiguous synapomorphies are neither exclusive, nor shared by all ingroup members, but still recovered as synapomorphies by at least one analysis with equal and one with implied weighting. Ambiguous synapomorphies recovered by only one type of analysis (equal or implied weighting) are not considered reliable, as are synapomorphies only found by one reduced consensus tree only.

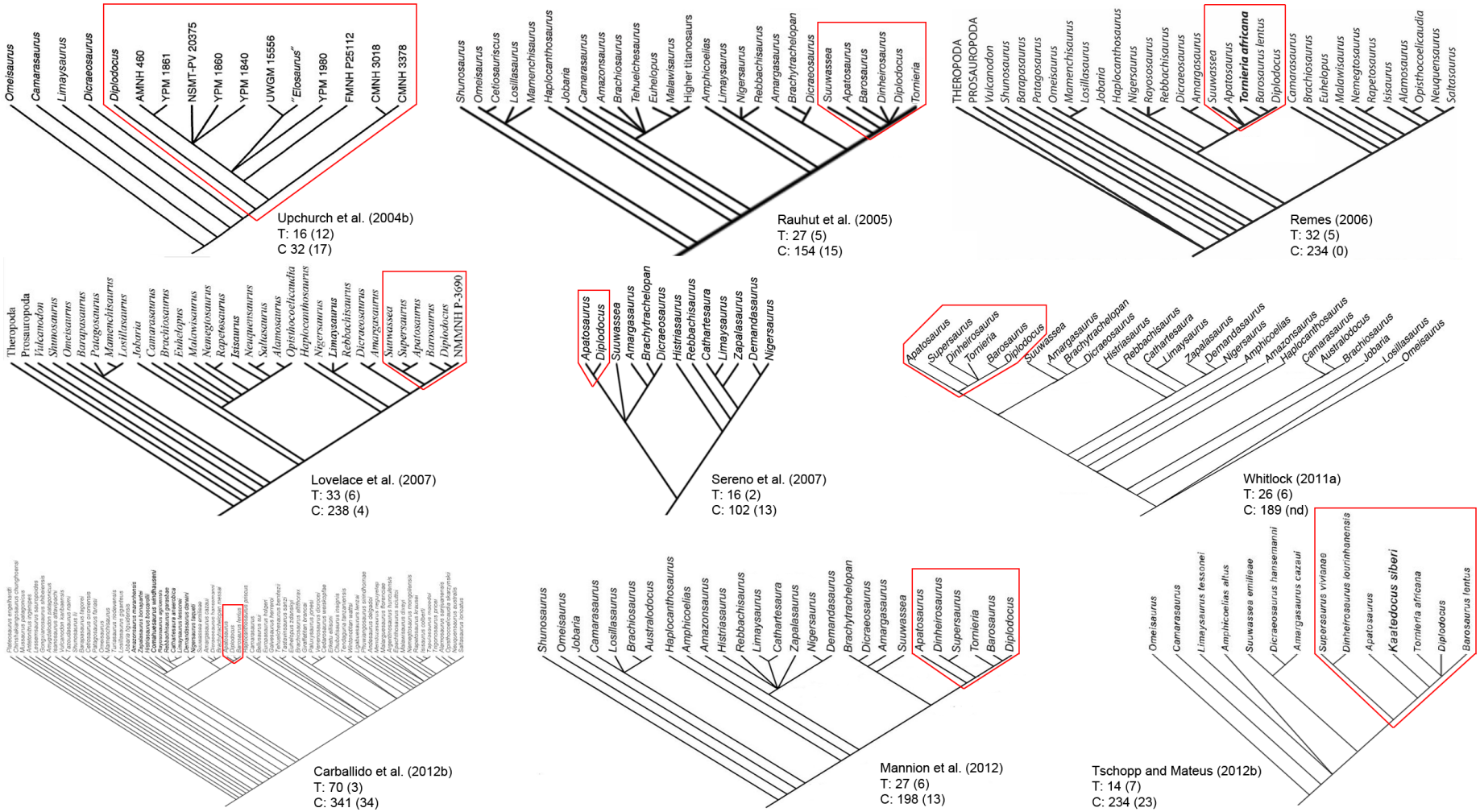

Figure 6.118: Strict consensus trees of previous phylogenetic analyses with special focus on diplodocoid intrarelationships, with the number of taxa (T) and characters (C) indicated. In brackets the number of diplodocid taxa and newly proposed characters. Taxon names were changed according to more recent publications, and diplodocid OTU highlighted with the red box.

Specimen autapomorphies are divided into unambiguous, or ambiguous (shared with other taxa). Autapomorphies found by only reduced consensus trees, but no pruned tree are considered invalid, or at least dubious, as more specimens potentially bearing the same morphology are excluded from reduced trees compared to pruned trees. Also, autapomorphies of apatosaurine specimens, which are shared with other apatosaurine specimens or clades (or diplodocine with diplodocine) are interpreted as inappropriate for species recognition.

Synapomorphies of diplodocid genera and species generally considered valid were then counted and summed between sister taxa (specimens or clades, in this case). A minimum number of synapomorphies was defined for justifying specific or generic separation. The minimum number of needed differences for generic separation was chosen based on the count obtained from the well-established sister genera *Dinheirosaurus* and *Supersaurus*, which are also geographically separated (Portugal, and USA, respectively). The ten differences obtained here were compared with the sum of changes between two species of *Apatosaurus* (*A. ajax* and *A. louisae*) or *Diplodocus* (*D. carnegii* and *D. hallorum*), which were both found to be lower (8 and 9, respectively). A minimum of ten differences is thus considered enough for genus-level separation, whereas for species, a margin of five changes is given in order to account for individual variation (which is already accounted for by the evaluation of the validity of the autapomorphies, but a wider margin is preferred herein in order to be more cautious).

The discussion of the various clades recovered is done following a bottom-up approach, starting with dichotomies between single specimens. This is preferred over a top-down approach, because it is the specimens that define the taxa, not the taxa that determine the affiliation of the specimen. Based on the validity of the recovered dichotomies between single specimens, species and finally genera and higher-level taxa can be evaluated more accurately.

***Barosaurus lentus* YPM 429 + AMNH 6341.** These two specimens were recovered as sister taxa in all pruned and reduced trees. It has a relatively high resampling value and is supported by four shared synapomorphies: 1) presence of a foramen on the dorsal side of the postzygodiapophyseal lamina of the cervical vertebrae, just anterior to the base of the neural spine process (137-1); 2) presence of lateral fossae on the prezygapophysis process of mid- and posterior cervical neural arches (183-1); 3) the posterior centrodiapophyseal lamina of mid- and posterior cervical vertebrae bifurcates towards its anterior end (188-1); and 4) posterior cervical postzygapophyses that terminate in front of the posterior edge of the centrum (200-1). All four synapomorphies were resulting as such by every analysis recovering this clade. Whereas the first and fourth synapomorphy are only shared with taxa outside Diplodocoidea (with the possible exception of *Australodocus bohetii*, see below), the other two synapomorphies are also shared with various specimens within Diplodocidae, or even Diplodocinae. The two specimens are separated by one change only, indicating that they belong to the same species.

CM 11984 + (*Barosaurus lentus* YPM 429 + AMNH 6341). All four trees show this grouping, and found one shared and an ambiguous synapomorphy defining it: 1) pneumatization of the lateral surface of mid- and posterior cervical centra is reduced, with a large fossa but a sharp-bordered coel, if present, restricted to area above parapophysis (172-1); and 2) prezygapophyseal centrodiapophyseal fossa of mid- and posterior cervical vertebrae subdivided into various smaller partitions by several accessory laminae (184-2). The latter is not the case in a mid-cervical vertebra in storage at AMNH, but the determination of presence or absence of accessory laminae was not possible for posterior cervical vertebrae on public display. Further studies are needed to clarify this. Both of these synapomorphies are shared with other diplodocine specimens, and do therefore not classify as species autapomorphies. No valid autapomorphy separates the two groups, which are thus interpreted to belong to the same species.

AMNH 7535 + (CM 11984 + (*Barosaurus lentus* YPM 429 + AMNH 6341)). As the two clades discussed above, also the present arrangement was recovered by all four trees. Statistical support for it is lower, and only one shared synapomorphy is found: mid-cervical centra, anteroposterior length/height of posterior face 4.5 or greater (166-2). This character is the best known and most widely used trait to distinguish *Barosaurus* from *Diplodocus* (e.g. McIntosh, 2005). The lack of other synapomorphies is probably due to the very restricted overlap in the four specimens of this clade, but

also with the closest sister group (*Kaatedocus siberi* SMA 0004 + (SMA D16-3 + AMNH 7530)), which is only known from neck and skull material. Neither delayed nor accelerated transition (DELTRAN and ACCTRAN, respectively) approaches are thus able to find more synapomorphies for either clade, but probably more will be recovered when it will be possible to add more specimens preserving overlapping material. The number of changes does not allow the erection of different species. Since the entire clade only includes the holotype specimen of *Barosaurus lentus* (YPM 429), all specimens are herein referred to that species.

SMA D16-3 + AMNH 7530. This clade is not supported by any synapomorphy, but recovered in all four trees. The latter is mainly due to the fact that SMA 0004 (the sister specimen of the current clade) has some morphological features in common with more basal diplodocine specimens, which are not present in SMA D16-3 or AMNH 7530. Given that both specimens of this group do not show any specimen autapomorphies, a referral to the same species can be regarded well-supported.

***Kaatedocus siberi* SMA 0004 + (SMA D16-3 + AMNH 7530).** The current triplet constitutes the sister group to the *Barosaurus lentus* clade discussed above. It is found in all four trees, and supported by a resampling value of 14, one higher than the clade CM 11984 + (YPM 429 + AMNH 6341). Nine shared synapomorphies are recovered: 1) absence of a small fossa on the posteroventral corner of cervical centra (131-0); 2) presence of a rugose tuberosity on the anterodorsal corner of the lateral side of mid- and posterior cervical centra (178-1); 3) presence of lateral fossae on the prezygapophysis process of mid- and posterior cervical neural arches (183-1); 4) dorsoventrally compressed epipophyses in posterior cervical neural arches (202-1); 5) absence of an accessory spinal lamina extending vertically in posterior cervical neural arches (203-0); 6) absence of a horizontal, rugose ridge right below spine summit on the lateral surface of posterior cervical neural spines (205-0); 7) parallel to converging posterior cervical and anterior dorsal bifid neural spines (211-1); 8) distance between spine summits of posterior cervical and anterior dorsal bifid neural spines subequal to neural canal width (212-1); and 9) cervical ribs that reach posterior to the posterior end of centrum (214-0). One additional unambiguous autapomorphy of the genus was proposed by Tschopp and Mateus (2012b), but not recovered as such by the present analyses: a transverse sulcus bordering the prezygapophyseal facets of posterior cervical vertebrae posteriorly. This feature was impossible to code for in the other two specimens of *Kaatedocus siberi*, which was probably the reason why it was not found as synapomorphy or autapomorphy. However, SMA 0004 is the only specimen positively scored for its presence in the current analysis, indicating that one more synapomorphy, possibly unambiguous for this clade, might be present. Not counting this, the nine shared synapomorphies of *K. siberi* plus the single synapomorphy of the sister clade *Barosaurus lentus* sum to ten, which is deemed enough for generic separation (see above). Within *Kaatedocus*, one change separates SMA 0004 from the other two specimens, which are thus referred to the type species *K. siberi*.

***Kaatedocus* + *Barosaurus*.** The sister arrangement of *Barosaurus* and *Kaatedocus* is herein recovered by both analyses, supported by three shared synapomorphies: 1) pleurocoels in anterior cervical centra single (157-0); 2) low anterior and mid-cervical neural spines that terminate level with the postzygapophyses (164-1); and 3) a dorsoventrally elongate coel on the lateral surface of anterior and mid-cervical neural spines (165-1). These traits are somewhat problematical, as many other specimens within Diplodocidae do not preserve anterior cervical vertebrae, and AMNH 7535 is the only specimen recovered as *Barosaurus* in the present analysis that preserves anterior cervical vertebrae. Furthermore, overlap between the two genera is low. However, differences in height of anterior neural spines are very pronounced when comparing *Kaatedocus* SMA 0004 with *Diplodocus* CM 84 or *Galeamopus* SMA 0011, the two genera most closely related to *Kaatedocus* + *Barosaurus* within Diplodocidae. Dorsoventrally elongate coels on the lateral side of the neural spines are typical for posterior cervical vertebrae of *Diplodocus*, among others, but in this genus, these coels are not present in anterior elements. In *Kaatedocus* and *Barosaurus* AMNH 7535 the serial pattern is inverted, and the coels only mark anterior elements. Additional synapomorphies, in particular from appendicular bones, might be found once a more complete specimen of *Kaatedocus siberi* is described.

CM 3452 + (*Kaatedocus* + *Barosaurus*). Before the description of *Kaatedocus siberi* SMA 0004, the specimen CM 3452 was the only diplodocid preserving an almost complete skull in articulation with

the most anterior cervical vertebrae. Although generally identified as *Diplodocus* (Holland, 1924; McIntosh and Berman, 1975; Whitlock et al., 2010), CM 3452 is recovered as sister taxon to *Barosaurus* + *Kaatedocus* in all four trees found here. The affiliation of CM 3452 with this group is supported by one unambiguous, nine shared, and one ambiguous synapomorphies. None of these are present in any specimen recovered within the *Diplodocus* clade. The synapomorphies are the following: 1) external surface of the premaxilla without anteroventrally orientated vascular grooves originating from an opening in the maxillary contact (2-0, shared); 2) presence of a large foramen in the maxilla, posterior to anterior maxillary foramen, and dorsal to preantorbital fossa (10-1, shared); 3) the antorbital fenestra reaches above the preantorbital fossa anteriorly (19-1, shared); 4) the dorsal portion of the lateral edge of the lacrimal bears a dorsoventrally short, laterally projecting spur (48-2, unambiguous); 5) the quadrate bears a shallow, second fossa medial to pterygoid flange on quadrate shaft, which becomes deeper towards its anterior end (52-1, shared); 6) a distinct horizontal ridge separates the dorsal from the posterior portion of the parietal, creating a distinct nuchal fossae below the ridge (65-1, shared); 7) the posterior face of the paroccipital process bears a longitudinal ridge along its body, extending between the dorsomedial and ventrolateral corners (67-1, shared); 8) presence of a posterior projection on the transverse processes of cervical vertebrae (134-0, shared); 9) the first bifid element of the cervical neural spines is a posterior mCV (140-2, shared); 10) the anterior end of the spinoprezygapophyseal lamina of mid- and posterior cervical vertebrae is strongly inclined laterally, sometimes roofing a lateral fossa in the prezygapophyseal process (182-1, shared); and 11) the prezygapophyseal centrodiapophyseal fossa of mid- and posterior cervical vertebrae is a single cavity (184-0, ambiguous). The lateral lacrimal spur recovered as unambiguous synapomorphy for this clade was proposed as autapomorphy of *Kaatedocus* (Tschopp and Mateus, 2012b), and is actually not unambiguous among sauropods: Tschopp and Mateus (2012b) reported a specimen of *Camarasaurus* (SMA 0002), which shows a similar trait, as do some other camarasaur lacrimals (Madsen et al., 1995). However, within Diplodocidae, of the few skulls known, only CM 3452, SMA 0004, and CM 11255 bear such a spur (Tschopp and Mateus, 2012b). If the feature gets confirmed to diagnose this group, also CM 11255 would have to be referred to it, instead of being identified as *Diplodocus* (Whitlock et al., 2010). Although tree topologies suggests that CM 3452 constitutes its own genus, the low number of four changes between the specimen and the *Kaatedocus* + *Barosaurus* clade does not support an erection of a new genus nor a species. The status of CM 3452 will be discussed in more detail below.

DMNS 1494 + USNM 10865. These two specimens traditionally referred to *Diplodocus* (Gilmore, 1932; McIntosh, 2005) are recovered in both trees obtained with implied weighting, as well as the reduced consensus with equal weighting. The equally weighted pruned consensus tree shows a polytomy formed by all putative *Diplodocus* specimens and the clade CM 3452 + mdD. This is probably a consequence of the incompleteness of important specimens like *D. longus* YPM 1920, or the skulls CM 11161 and USNM 2672. The clade DMNS 1494 + USNM 10865 is supported by a resampling value of nine, and one shared synapomorphy: mid- and posterior dorsal neural arches, pcpl present as single lamina (258-1). Other *Diplodocus* specimens have two parallel pcpl. As only one change separates DMNS 1494 from USNM 10865, the two specimens are referred to the same species.

***Seismosaurus hallorum* NMMNH 3690 + (DMNS 1494 + USNM 10865).** The current triplet is found in the equally weighted reduced consensus tree, as well as in both pruned and reduced consensus trees when applying implied weights. It has a resampling value of six, and is supported by one shared synapomorphy: distal end of the ischium posterodorsally expanded (426-1). The four changes separating *S. hallorum* from the clade DMNS 1494 + USNM 10865 are not enough to justify the erection of two different species, therefore entire triplet is referred to the same species.

AMNH 223 + (*Seismosaurus hallorum* NMMNH 3690 + (DMNS 1494 + USNM 10865)). As the two clades discussed above, the present quartet of specimens is recovered in all trees but the equally weighted pruned tree. It has a resampling value of six, and one unambiguous and five shared synapomorphies, which distinguish it from the other *Diplodocus* specimens: 1) a transversely concave dorsal end of the postspinal lamina of single dorsal neural spines (234-1, shared); 2) mid-caudal neural arches situated on the anterior half of the centrum (337-1, shared); 3) vertical mid-caudal neural spines

(340-1); 4) posterior end of the spine summit of mid- and posterior caudal neural spines lies more or less straight above the postzygapophyses (343-1, shared); 5) middle chevrons bear distinct fossae on the medial surfaces of the proximal branches (347-1, shared); and 6) the presence of a subtriangular projection on the anterior portion of the ventral edge of the scapular blade (370-1, shared). Of these synapomorphies, only the subtriangular process on the scapular blade also occurs in other diplodocines. Three changes are recovered between AMNH 223 and the remaining triplet, indicating that they belong to the same species, as was already suggested by McIntosh (2005).

The presence of an unambiguous synapomorphy (vertical mid-caudal neural spines) allows the erection of its own species or genus. Sister specimens recovered as such are *D. longus* YPM 1920 in the reduced consensus using implied weighting, and *D. carnegii* CM 84 + CM 94 in the equally weighted reduced consensus tree with CM 94 added. Nine changes lie between the *D. carnegii* pair and the clade discussed herein, whereas only six changes are recovered between the current clade and *D. longus*. As both of these remain below the 10 changes set as sufficient for genus-level separation, *Seismosaurus* is here considered a synonym of *Diplodocus*, but as its own species *D. hallorum*, including the specimens AMNH 223, DMNS 1494, NMMNH 3690, and USNM 10865.

***Diplodocus longus* YPM 1920 + *Diplodocus hallorum*.** Of the four main trees, only the reduced consensus tree with implied weighting recovered this arrangement, but by substituting *D. carnegii* CM 84 by *D. longus* YPM 1920 in the equally weighted reduced consensus tree, the same result is obtained. Such a grouping, where *D. longus* + *D. hallorum* form the sister clade to *D. carnegii* CM 84 + CM 94 is not supported by any synapomorphy, in fact, when adding either the holotype or the paratype specimen, a polytomy is recovered between CM 84, CM 94, YPM 1920 and *Diplodocus hallorum*, as can be seen in the pruned consensus tree using implied weighting.

***Diplodocus carnegii* CM 84 + CM 94.** Although not recovered in the four main trees discussed here, symmetric resampling yielded a value of eight for this clade, and indeed, when deleting YPM 1920 and adding CM 84 and CM 94 to the reduced consensus trees, the clade discussed here forms the sister group to *D. hallorum* as discussed above. The clade is supported by three shared synapomorphies, which are all absent in any specimen referred to *D. hallorum* above: 1) presence of pneumatized epipophyses in cervical vertebrae (139-1); 2) absence of an accessory, subvertical lamina in the postzygapophyseal centrodiapophyseal fossa of posterior cervical vertebrae, the free edge of which is facing posteriorly (199-0); and 3) pleurocoels of anterior and mid-dorsal centra that invade the neural arch pedicels (247-1). Together with the six synapomorphies of the *D. hallorum* clade, this amounts to nine changes, which allows erection of different species but not genera, following the guidelines established above. The recovery of this clade in the extended reduced consensus trees confirms Hatcher's (1901) assignment of CM 94 as paratype of the species *D. carnegii*. Both specimens were found in the same stratigraphic level of the same quarry (Hatcher, 1901).

***Diplodocus carnegii* + *Diplodocus hallorum*.** The grouping of these two species within the genus *Diplodocus* occurs in all trees excluding the skull specimens CM 11161 and USNM 2672. When including *D. longus* YPM 1920 as well, the grouping of CM 84 and 94 is broken, and a polytomy is formed as explained above. All these specimens are united by six shared and one unambiguous synapomorphies: 1) anterior end of the spinoprezygapophyseal lamina of mid- and posterior cervical vertebrae remains vertical, with the free edge facing dorsally (182-0, shared); 2) anteroposterior width of mid- and posterior dorsal neural spines remains approximately constant along the height of the spine, with subparallel anterior and posterior margins (265-0, shared); 3) base of posterior dorsal neural spines is anteriorly inclined (280-1, shared); 4) pneumatopores of anterior caudal centra are present until caudal 16 or further posteriorly (308-1, unambiguous); 5) anterior- and mid-caudal vertebrae have a ventral hollow with a depth of more than 10 mm (331-1, shared); 6) posterior articular surfaces of mid-caudal vertebrae are flat (336-1, shared); and 7) the rugosity on the dorsolateral margin of metatarsal II, near its distal end (if present) is well-developed, and extends to the center of the shaft (468-1, shared). Only one of these synapomorphies is shared with one single specimen of *Barosaurus lentus* (265-0, shared with YPM 429), and an additional one is shared with *Galeamopus*, the genus forming the sister taxon to *Diplodocus* + mdD (182-0, with SMA 0011). Also in this case, the trait is only shared with one single specimen, and not the entire taxon. As all trees

recovered also include *D. longus* YPM 1920 within this clade, and because *D. longus* is currently regarded type species of the genus *Diplodocus* (but see below for a more detailed assessment of YPM 1920), the specimens included in the clade are herein referred to that genus. It is separated from its sister clade CM 3452 + mdD by 18 changes, and both groups are diagnosed with an unambiguous synapomorphy. One of the synapomorphies for the *Diplodocus* clade is shared with the holotype specimen of *Barosaurus lentus* (265-0), and seven synapomorphies of the clade CM 3452 + mdD are based on cranial material, none of which is definitely attributable to the *Diplodocus* clade (2-0, 10-1, 19-1, 48-2, 52-1, 65-1, 67-1). All of these traits are different from the two included skulls CM 11161 and USNM 2672, which probably belong to the genus *Diplodocus* (see below for a discussion of their taxonomic affinities). The synapomorphies are thus tentatively retained in the count for the changes between the clades, and the remaining 17 changes (excluding the one shared with YPM 429) still confidently justify generic separation.

***Diplodocus* + mdD.** *Diplodocus* is recovered as sister taxon to the clade with *Kaatedocus* and *Barosaurus* in all four principal trees discussed here. It is diagnosed by 13 synapomorphies, of which one is unambiguous, ten are shared, and two are ambiguous: 1) a straight distal end of the paroccipital process in lateral view (69-0, shared); 2) the absence of a basioccipital depression between the foramen magnum and the basal tubera (80-0, shared); 3) anterior cervical vertebrae with a total height to centrum length ratio of less than 0.9 (154-0, shared); 4) the spinoprezygapophyseal lamina of posterior cervical vertebrae bears an anterior projection just beneath, but independent from the spine summit (196-1, shared); 5) posterior dorsal centra that are wider than high (269-1, ambiguous); 6) absence of a longitudinal ridge at mid-height on the lateral surface of the mid-caudal centra (333-0, shared); 7) the ventral surface of mid-caudal centra is mostly straight horizontal in lateral view, with expansions on both ends to form the chevron facets restricted to about last fourth of centrum length (335-1, unambiguous); 8) scapular blade has a straight acromial edge (367-0, ambiguous); 9) presence of a subtriangular projection on the anterior portion of the ventral edge of the scapular blade (370-1, shared); 10) a distal humeral shaft end that is twisted by at least 40° compared to proximal articular surface (381-1, shared); 11) a ratio of iliac blade height above the pubic peduncle to anteroposterior length of 0.40 or greater (405-1, shared); 12) a tibia to femur length of 0.68 or greater (440-1, shared); and 13) relatively gracile metatarsal I, with a proximal transverse width to greatest length ratio of less than 0.8 (461-0, shared). Four of the shared synapomorphies are unique within Diplodocidae (69-0, 80-0, 154-0, and 440-1), and five more within Diplodocinae (196-1, 269-1, 367-0, 381-1, 405-1).

SMA 0011 + *Galeamopus hayi*. All four principal trees show this clade, which is supported by one shared synapomorphy (if strictly following the qualitative assignment of synapomorphies mentioned above): the position of the medial portion of the frontal-parietal suture is closer to posterior extension of the supratemporal fenestra (35-1). However, all three trees recovering this synapomorphy exclude the skulls CM 11161, SMA O25-8, and USNM 2672, which all have the same position of the frontal-parietal suture. When added to the reduced consensus trees, these skulls form polytomies with specimens from *Diplodocus* (CM 11161 and USNM 2672), or *Barosaurus* (SMA O25-8). As also the skull CM 3452 shows the same morphology, an interpretation of this synapomorphy as diagnosing the clade SMA 0011 + *Galeamopus hayi* is highly questionable. The clade is thus not diagnosable by any synapomorphy. The two specimens are separated from each other by nine changes, including one unambiguous autapomorphy diagnosing SMA 0011. The high number of differences allows the erection of two species, as suggested in the descriptive part of the thesis: *Galeamopus hayi* as the type species, and *G. shellensis*.

AMNH 969 + (*Galeamopus hayi* + *G. shellensis*). The triplet is recovered in all main trees, and shows a resampling value of two. It is supported by two unambiguous and two shared synapomorphies: 1) presence of an anterior process on the lacrimal (47-1, shared); 2) well-developed anteromedial processes of the atlantal neurapophyses, which are very distinct from the posterior wing (146-1, shared); 3) a posterior wing of the atlantal neurapophyses that is of subequal width along most of its length (148-1, unambiguous); and 4) the prespinal lamina of the axis bears a transversely expanded, knob-like tuberosity at its anterior end (151-1, unambiguous). Due to the rare finds of atlantes and axes, these synapomorphies are somewhat dubious, and will have to be assessed in more detail once

more complete specimens become available for study. However, the continuous recovery of the same triplet in the same position of all four trees, as well as its higher resampling value compared with most other clades indicates that this grouping forms its own genus. Two changes lie between AMNH 969 and the clade with *G. hayi* + *G. shellensis*, therefore not allowing the erection of a third species. The affinities of AMNH 969 will be discussed in more detail below.

***Galeamopus* + mdD.** All four trees show the new genus *Galeamopus* as first sister taxon to the clade with *Diplodocus*, *Kaatedocus*, and *Barosaurus*. Two unambiguous, six shared, and two ambiguous synapomorphies diagnose this group: 1) the spinoprezygapophyseal lamina of anterior and mid-cervical vertebrae is reduced to a ridge or totally interrupted at the base of prezygapophysis (163-1, shared); 2) presence of an accessory, subvertical lamina in the postzygapophyseal centrodiapophyseal fossa of posterior cervical vertebrae, with its free edge facing laterally (198-1, ambiguous); 3) presence of an accessory spinal lamina in posterior cervical neural arches, running vertically just posterior to spinoprezygapophyseal lamina (203-1, ambiguous); 4) a low position of anterior dorsal transverse processes, with their ventral edge being about level to the dorsal edge of the posterior cotyle (243-1, shared); 5) bifid mid-dorsal neural spines, inclusive of at least the fifth dorsal vertebrae (250-1, shared); 6) a ratio of the height of posterior dorsal neural arches above postzygapophyses (neural spine) to the height below (pedicel) of less than 3.1 (272-0, shared); 7) posterior dorsal postzygapophyses almost horizontal, such that the two articular facets include a wide angle (275-0, shared); 8) presence of an additional pneumatic fossa on the posterodorsal corner of anterior-most caudal centra (298-1, unambiguous); 9) well defined posterior diapophyseal laminae (pcdl, podl) in anterior caudal vertebrae (315-1, unambiguous); and 10) a widely rounded tibial cnemial crest in anterior view (444-0, shared). Only one of the shared synapomorphies is present in other diplodocines as well (275-0, in ML 418 and *Supersaurus vivianae*), whereas one ambiguous synapomorphy is unique within the sampled Neosauropoda (203-1), but *Kaatedocus* autapomorphically bears the reversed state. Between *Galeamopus* and its sister clade *Diplodocus* + mdD, 16 differences are present. One is shared between *Galeamopus* and *Kaatedocus* (47-1), one between *Galeamopus* and the putative *Barosaurus* SMA O25-8 (80-0), a third is present in both SMA 0011 and AMNH 6341 (269-0), and a fourth is shared with CM 94 (367-0). Deleting them from the 16 changes, the remaining twelve are still sufficient for a generic separation.

***Dinheirosaurus* + mdD.** Although *Dinheirosaurus* is recovered in the same relative position in both analyses with equal and implied weighting, the first major difference between the trees of these two analyses is encountered here. Whereas the equally weighted trees show a sister genera arrangement of *Dinheirosaurus* and *Supersaurus*, the analyses using implied weighting results in a more basal position of *Supersaurus*. In this paragraph, only the clade excluding *Supersaurus* will be discussed, recovered by applying implied weights. The more parsimonious position of *Supersaurus* will be assessed below. Only one shared synapomorphy supports such an arrangement to the exclusion of *Supersaurus*: mid- and posterior cervical neural arches have 'true', divided centroprezygapophyseal laminae, which are both dorsally connected to the prezygapophysis (185-2). The equally weighted analysis recovers this feature as synapomorphic for the entire Diplodocidae (in the pruned consensus tree), with a reversal in *Tornieria*. The state is unknown in *Supersaurus*, due to insufficient information in descriptions, and lacking figures in anterior view. Future personal observations of the BYU specimen might clarify its morphology. The present arrangement yields 10 changes between *Dinheirosaurus* and its sister clade *Galeamopus* + mdD, four more synapomorphies of *Galeamopus* + mdD are not preserved in the known material from *Dinheirosaurus*.

***Tornieria africana* holotype + skeleton k.** The earlier referral of these two specimens to *Tornieria* (Remes, 2006, 2009) is confirmed by both analyses performed herein. They show a resampling value of four, and five shared synapomorphies: 1) an angle between the acromial ridge of the scapula and the distal blade of less than 70° (362-0); 2) a humerus to femur ratio between 0.7 and 0.77 (379-1); 3) the acetabular margin of the ischium is strongly concave in lateral view, such that the pubic articular surface forms an anterodorsal projection (418-1); 4) the ratio of the pubic articulation to the anteroposterior length of the pubic pedicel of the ischium is 1.5 or greater (420-1); and 5) a posterodorsally expanded distal end of the ischium (426-1). The apparent lack of vertebral characters

is due to the destruction of most putative *Tornieria* vertebrae during World War II (Remes, 2006; Whitlock, 2011a). A series of caudal vertebrae from trench dd from Tendaguru (MB.R.2956), referred to *Tornieria* by Remes (2006) was not included into the analysis as concerns of their attribution to the same individual were raised by Remes (2006). No valid autapomorphies are recovered for either *Tornieria* specimen, confirming the referral of skeleton k to the species *T. africana*.

***Tornieria* + mdD.** A clade with *Tornieria* and more derived Diplodocoidea to the exclusion of other diplodocine specimens was only recovered in the analysis using implied weighting, and including all specimens. With equal weights, or by excluding *Australodocus bohetii* from the analysis with implied weighting a priori, *Tornieria* + mdD corresponds to Diplodocinae. In the following, the find of the main trees by using implied weights is discussed. One unambiguous, one exclusive, and one shared synapomorphy are found for this clade: 1) cervical vertebrae bear a shallow, anteroposteriorly elongate fossa, posteroventral to the pleurocoel (131-1, exclusive); 2) anterior caudal centra (excluding the first) slightly procoelous (304-2, shared); and 3) pneumatopores of anterior caudal centra are large coels (307-1, unambiguous). *Supersaurus* has no shallow fossa posteroventral to its cervical pleurocoels, distoplatyan anterior caudal centra, without large coels (these are restricted to the anterior-most caudal centra in *Supersaurus*). Of the synapomorphies proposed for *Tornieria* + mdD by the analysis using implied weighting, the first (131-1) and third (307-1) are also recovered by the equally weighted trees (for the clade Diplodocinae), with the difference that the unambiguous synapomorphy becomes exclusive. The same happens when excluding *Australodocus bohetii* from the implied weights analysis a priori. In the main trees from the analysis with implied weighting, seven changes separate *Tornieria* from the clade *Dinheirosaurus* + mdD, nine changes are between *Tornieria* and *Dinheirosaurus*, when adding the autapomorphies of *Dinheirosaurus* comparable with their states in *Tornieria*. In the equally weighted trees, where the clade *Tornieria* + mdD corresponds to Diplodocinae, six changes are recovered between *Tornieria* and *Supersaurus* + mdD. This would not allow the erection of a different genus for *Tornieria*, but see below for a more detailed taxonomic assessment.

***Supersaurus vivianae* BYU + WDC DMJ-021.** The unity of the two *Supersaurus* specimens included in the present analysis is well supported. All four trees show this arrangement, and resampling yielded a value of 36, which is the highest value reported within Diplodocidae. Seven shared synapomorphies define the clade: 1) cervical vertebrae without small fossa on posteroventral corner (131-0); 2) presence of a short second posterior centrodiapophyseal lamina ventral to the one uniting with the dorsal shelf of the diapophysis of cervical vertebrae (136-1); 3) pneumatization of the lateral surface of mid- and posterior cervical centra is reduced, with a large fossa but the sharp-bordered coel, if present, restricted to the area above the parapophysis (172-1); 4) a deep groove extending anteroposteriorly within the lateral edge posterior to the parapophysis of mid- and posterior cervical vertebrae (177-1); 5) spinoprezygapophyseal laminae of single dorsal neural spines separate along their entire length (231-0); 6) anterior-most caudal centra are 'heart'-shaped with an acute ventral ridge (296-1); and 7) pneumatopores anterior caudal centra reduced to foramina (307-0). Recovery of these synapomorphies highly depends on tree topology, and thus the type of analysis performed. In the main trees obtained through implied weighting, where *Supersaurus* lies outside *Tornieria* + mdD, only the fourth synapomorphy (177-1) was found to unite the two specimens. The split ventrolateral edge is shared with *Dinheirosaurus*, with which *Supersaurus* groups in all other trees, including the one obtained by implied weighting, and excluding *Australodocus bohetii* a priori. On the other hand, from the other six synapomorphies, three are shared with *Australodocus bohetii* (131-0, 136-1, 172-1), and two of them result as synapomorphies of this clade as recovered by the main implied weights trees (see below). In any case, attribution of the two specimens to *Supersaurus* appears well-supported, and the absence of any valid differences between the specimens confirms the referral of WDC DMJ-021 to the type species *S. vivianae*, and in turn also corroborates the assignment of the single bones in the BYU collection to the same individual, as suggested by Lovelace et al. (2007).

***Dinheirosaurus* + *Supersaurus*.** A sister taxon relationship of these two taxa to the exclusion of others is only recovered by using equal weights, or by pruning *Australodocus bohetii* from the implied weights analysis a priori. In the latter analysis, *Dinheirosaurus* + *Supersaurus* is the sister clade to the

specimen ML 418, with which it forms the sister group to *Galeamopus* + mdD. Where *Dinheirosaurus* and *Supersaurus* form a clade, they are located within Diplodocinae, in a position more derived than *Tornieria*. *Dinheirosaurus* + *Supersaurus* is supported by a resampling value of three, as well as six shared and one unambiguous synapomorphies: 1) presence of paired pneumatic fossae on the ventral surface of mid- and posterior cervical vertebrae, separated by a ventral midline keel (176-1, shared); 2) a deep groove extending anteroposteriorly along the lateral edge of mid- and posterior cervical vertebrae, posterior to the parapophysis (177-1, shared); 3) mid-dorsal neural spines are single, bifid form (if present) does not extend past the second or third dorsal (250-0, shared); 4) presence of an oblique accessory lamina connecting the posl with the spol in mid-dorsal neural spines (251-1, unambiguous); 5) posterior dorsal centra with a ratio of total length to height of posterior articular surface of 1.0 or greater (268-0, shared); 6) posterior dorsal neural arches with a ratio of height above the postzygapophyses (neural spine) to height below (pedicel) of 3.1 or greater (272-1, shared); and 7) dorsal ribs with proximal pneumatopores (284-1, shared). Of the shared synapomorphies, the high ratio of neural spine to pedicel height, is present as well in ML 418. *Dinheirosaurus* is separated from *Supersaurus* by ten changes, and was the main pair of genera on which the numerical approach of specific and generic distinction was based, given the geographical distance between the two genera.

Australodocus bohetii* type + *Supersaurus. Such a group was only recovered in the main trees of the analysis with implied weighting. There, it is located basal to *Tornieria*, within Diplodocinae, and thus contrasts with the position of *Supersaurus* when associated with *Dinheirosaurus*. The more basal position of the clade *Australodocus* + *Supersaurus* is probably due to the several traits *Australodocus* shares with titanosauriform sauropods. Resampling does not support the current clade, which is specified by four shared synapomorphies: 1) presence of a short second posterior centrodiapophyseal lamina in cervical vertebrae, ventral to the one uniting with the dorsal shelf of the diapophysis (136-1); 2) the pleurocoel of anterior and mid-cervical centra is pierced by one or two large, rounded foramina around centrum midlength (162-1); 3) pneumatization of the lateral surface of mid- and posterior cervical centra is reduced, with a large fossa, but the sharp-bordered coel, if present, restricted to an area above the parapophysis (172-1); and 4) the presence of lateral fossae on the prezygapophysis process of mid- and posterior cervical neural arches (183-1). The latter two are shared with brachiosaurid titanosauriforms, and actually diagnose the brachiosaurid clade including *Australodocus* in the pruned tree with equal weighting. The first two synapomorphies recovered for an *Australodocus* + *Supersaurus* clade (136-1 and 162-1) are not shared with any included taxon outside Diplodocidae. The two genera are only separated by six changes, which would not allow generic separation. However, this would only apply if *Australodocus* really would represent the sister taxon to *Supersaurus*, which is highly questionable, as will be discussed in more detail below.

***Supersaurus* + mdD.** Depending on the analysis, this clade includes *Tornieria* or represents its sister group. Therefore, also the combination of synapomorphies change in the different trees. Whereas none can be considered valid (based on the guidelines established above) for the main trees recovered with implied weighting – thus including *Tornieria* – one shared synapomorphy describes *Supersaurus* + mdD with the exclusion of *Tornieria* in the equally weighted trees: mid-caudal prezygapophyses project considerably beyond the anterior edge of the centrum (339-1). This synapomorphy is not found in the agreement subtree of the analysis with implied weights excluding *Australodocus bohetii* a priori, where the position of *Supersaurus* + mdD is the same as in the equally weighted trees, but furthermore includes ML 418. In this tree, another shared synapomorphy unites the clade: ratio of the pubic articulation length of the ischium to the anteroposterior length of the pubic pedicel is less than 1.5 (420-0). However, measurements were only obtainable for four specimens within *Supersaurus* + mdD, and the validity of this synapomorphy will have to be addressed in more detail in future. In any case, the only probably valid synapomorphies are found in the trees excluding *Tornieria* from *Supersaurus* + mdD. In the equally weighted trees, *Dinheirosaurus* + *Supersaurus* are separated from *Galeamopus* + mdD by 16 changes. *Australodocus* + *Supersaurus* distinguish only seven changes from their sister clade *Tornieria* + mdD.

Diplodocinae. The composition of Diplodocinae is almost equal in all main trees. The only taxon changing between diplodocine, and non-diplodocine affinities is *Australodocus bohetii*, as already

mentioned above. Due to the incompleteness of ML 418, which was recovered as most basal diplodocine in the main trees by using implied weights, the number of synapomorphies for the entire clade is much reduced compared to the main equally weighted trees, where ML 418 was excluded from both the pruned and reduced consensus trees. Applying the guidelines for assessing the significance of synapomorphies, two exclusive and eight shared synapomorphies are found by the two analyses: 1) box-like basal tubera (82-1, shared); 2) presence of a basisphenoid/basipterygoid recess present (91-1, shared); 3) cervical vertebrae bear a small, shallow, anteroposteriorly elongate fossa posteroventral to the pleurocoel (131-1, exclusive); 4) a longitudinal sulcus marks the ventral surface of the cervical vertebrae (133-1, shared); 5) the tuberculum of anterior and mid-cervical ribs is directed upwards and backwards in lateral view (218-1, shared); 6) an oblique ridge connects the medial and lateral edges at the base of the rib head in dorsal ribs (283-1, shared); 7) large coels mark the anterior caudal centra (307-1, exclusive); 8) presence of a ventral longitudinal hollow in anterior and mid-caudal centra (330-1, shared); 9) a ratio of centrum length to posterior height in mid-caudal vertebrae of 1.7 or greater (332-1, shared); and 10) the scapular acromial process that lies nearly at midpoint of the scapular body (364-1, shared). Three of these synapomorphies are shared with certain apatosaurine specimens (218-1, 283-1, 330-1). Upwards and backwards directed tubercula of anterior and mid-cervical ribs are not present in *Australodocus*, such that in the improbable case of diplodocine affinities of this taxon, this character state would become an ambiguous synapomorphy of Diplodocinae, instead of shared. In the trees, where ML 418 represents the most basal diplodocine taxon, it is separated from the more derived group by just two changes, which does not allow the erection of a new species. This is supported by the fact that ML 418 was among the six most unstable taxa in the equally weighted analysis, and that it switches to a position within the clade *Dinheirosaurus* + *Supersaurus* when excluding *Australodocus* a priori from the analysis applying implied weighting.

***Apatosaurus louisae* CM 3018 + CM 3378.** A clade only including these two specimens is recovered in both reduced consensus trees, and supported by a relatively high resampling value of 23. The pruned consensus tree of the analysis using implied weighting shows a polytomy with these two specimens and the holotype specimens of *Apatosaurus laticollis* (YPM 1861) and *Brontosaurus amplus* (YPM 1981). When adding these two specimens to the reduced consensus tree of the equally weighted analysis, *A. laticollis* forms a trichotomy with the *A. louisae* specimens, whereas *B. amplus* is recovered more basally within Apatosaurinae. Two shared synapomorphies are considered reliable: 1) the pleurocoel of the first dorsal vertebra occupies the posterior part of the centrum (240-1); 2) presence of an oblique ridge that connects the medial and lateral edges of dorsal ribs at the base of the rib head (283-1). The latter synapomorphy is otherwise typical for diplodocines. One change lies between the two specimens, confirming the previous referrals to the same species (e.g. McIntosh, 1981; Upchurch et al., 2004b).

***Brontosaurus amplus* YPM 1981 + mdA.** This clade is only recovered by the reduced consensus tree obtained applying implied weighting. Adding *A. laticollis* YPM 1861 to the tree, a polytomy is created between *B. amplus*, *A. laticollis*, *A. louisae*, and CM 3378, as visible in the pruned consensus tree with implied weights. In the analysis with implied weights excluding *Australodocus* a priori, *B. amplus* groups with *Apatosaurus ajax* YPM 1860 to form the sister clade to the two *A. louisae* specimens. When excluding *A. laticollis*, only one shared synapomorphy is found: dorsal ribs bear proximal pneumatopores (284-1). If *A. laticollis* is added, one unambiguous and three shared synapomorphies are added to the one mentioned above: 1) posterior cervical prezygapophyses terminate well behind the articular ball (194-1, shared); 2) absence of an accessory, subvertical lamina in the postzygapophyseal centrodiapophyseal fossa of posterior cervical vertebrae, with the free edge facing posteriorly (199-0, shared); 3) posterior cervical ribs lack an anterior process (219-1, shared); and 4) presence of a rounded sub-triangular process immediately below the tuberculum of posterior cervical ribs (222-1, unambiguous). However, it was not possible to score *B. amplus* for any these added synapomorphies. They thus mostly describe the grouping of *A. laticollis* with the two *A. louisae* specimens. Four changes lie between *B. amplus* YPM 1981 and the two *A. louisae* specimens, two changes separate *A. laticollis* YPM 1861 from the *A. louisae* holotype, and a single change from CM 3378. This would indicate that all four specimens belong to the same species, but see below for a more detailed assessment of the affinities of YPM 1861 and 1981.

***Apatosaurus ajax* YPM 1860 + *'Atlantosaurus' immanis* YPM 1840.** The unity of these two specimens is only shown in the equally weighted trees. In the tree obtained with implied weighting, the holotype specimen of '*Atlantosaurus*' *immanis* groups together with NSMT-PV 20375, which was described as belonging to *Apatosaurus ajax* (Upchurch et al. 2004b), but does not group with the holotype YPM 1860 in any of the trees recovered here. Four shared synapomorphies support the clade *Apatosaurus ajax* + *'Atlantosaurus' immanis*: 1) summits of bifid neural spines of cervical vertebrae are rounded (142-1); 2) mid-cervical neural spine is less than 0.45 times the height of the neural arch (168-0); 3) posterior cervical vertebrae have an accessory, subvertical lamina in the postzygapophyseal centrodiapophyseal fossa, with the free edge facing laterally (198-1); and 4) the distal end of the ischium is posterodorsally expanded (426-1). All four synapomorphies are shared with other specimens within Apatosaurinae. Two are shared with the putative *Apatosaurus ajax* specimen NSMT-PV 20375 (168-0, 426-1), and one with the holotype of *Apatosaurus laticollis*, YPM 1861 (198-1). Considering the low overlap index of 13%, and the inability to recover this group by resampling, support for this clade is very low. Six changes lie between the two specimens, which indicate that they are different species, but not different genera.

***Apatosaurus ajax* + mdA.** Such a clade is found with both methods. It is present in the reduced consensus tree from the equally weighted analysis, and both main trees obtained with implied weighting. The only difference lies in the position of *'Atlantosaurus' immanis* YPM 1840, which is included in the equally weighted reduced consensus tree, but excluded in the trees with implied weights. This appears to have an influence on the number of synapomorphies found in the different trees, with the equally weighted reduced consensus tree showing less than half of the synapomorphies recovered by implied weighting. In total, eight shared synapomorphies were found: 1) prezygodiapophyseal lamina of posterior cervical and anterior dorsal vertebrae smooth laterally (208-0); 2) vertically oriented, rod-like struts divide the lateral pneumatic foramina of mid- and posterior dorsal vertebrae (253-1); 3) pleurocoel of posterior dorsal vertebrae oval to circular (271-0); 4) caudal neural spines without triangular lateral processes (293-0); 5) anterior caudal neural spines gradually expanding distally (328-0); 6) anterior and mid-caudal vertebrae without ventrolateral ridges (329-0); 7) a flat or slightly convex area posterior to the acromial ridge and the distal blade of the scapula (365-1); and 8) a straight ventral edge of the scapular blade in lateral view (368-0). Only one of these characters is preserved in YPM 1840 as well (208), but the latter specimen does not show the plesiomorphic state. Consequently, this synapomorphy was only found by the trees obtained with implied weights, and excluding YPM 1840 from the clade *Apatosaurus ajax* + mdA. Three synapomorphies are shared with NSMT-PV 20375 (271-0, 293-0, 365-1), an additional one with the apatosaur UW 15556 (208-0). Three synapomorphies are not present in any other apatosaur specimen (253-1, 328-0, 368-0). In the equally weighted reduced tree, *Apatosaurus ajax* YPM 1860 + *'Atlantosaurus' immanis* YPM 1840 is separated from the sister clade *Apatosaurus louisae* CM 3018 + CM 3378 by six changes, whereas *Apatosaurus ajax* YPM 1860 and *Brontosaurus amplus* + mdA are distinguished by a sum of eleven apomorphies. The difference mainly lies in the high number of autapomorphies found for YPM 1860, which contrasts with the low number of synapomorphies of the clade YPM 1860 + YPM 1840. Two of the autapomorphies are from the braincase included in YPM 1860, which cannot definitively be attributed to the same specimen (McIntosh, 1995). Excluding these info, the number of changes between *Apatosaurus ajax* and *Brontosaurus amplus* + mdA drops to nine. At this stage, an assignment to two different species appears thus better supported than an erection of a different genus for the sister clade of *Apatosaurus ajax*.

***Eobrontosaurus* + *Amphicoelias*.** Both the pruned and reduced consensus trees of the equally weighted analysis recover these two genera as sister taxa within Apatosaurinae. If applying implied weighting, *Amphicoelias* results as the most basal diplodocid sauropod, sister taxon to Diplodocinae + Apatosaurinae, whereas *Eobrontosaurus* is still found well within Apatosaurinae. Two shared synapomorphies are found for the clade *Eobrontosaurus* +*Amphicoelias*: 1) mid- and posterior dorsal neural spines narrow dorsally to form a triangular shape in lateral view, with the base approximately twice the width of the dorsal tip (265-1); and 2) the neural spines of posterior dorsal vertebrae are longer than wide at their base, just above transverse processes (279-0). Whereas the first does not occur in other apatosaurines, the second synapomorphy is shared with *Elosaurus parvus* CM 566 and the

specimen UW 15556. The longer than wide bases of the posterior dorsal neural spines are recovered as autapomorphic for *Amphicoelias* in the trees obtained with implied weighting. The low overlap index of seven percent casts further doubts on the validity of this grouping. If confirmed, two changes would separate the two specimens, not justifying the erection of two different species.

***Eobrontosaurus* + mdA.** Such a clade is recovered in both main trees with implied weights, as well as the equally weighted reduced consensus tree. It always includes the clade with *Apatosaurus ajax* and *Apatosaurus louisae*, and excludes the specimens NSMT-PV 20375, SMA 0087, and WDC-FS001A. *'Atlantosaurus' immanis* YPM 1840 switches positions in the two analyses from *A. ajax* to a sister taxon arrangement with NSMT-PV 20375. When excluding *Australodocus bohetii* from the implied weights analysis a priori, *Eobrontosaurus* + mdA becomes more inclusive as compared to the complete implied weights trees. Without *Australodocus*, it also includes AMNH 460, as well as the clade including the holotype specimens of *Dystrophaeus viaemalae*, *Brontosaurus excelsus*, and *Elosaurus parvus*. The unstable taxa are thus *Eobrontosaurus* and AMNH 460, as the clade with *Brontosaurus* also results sister clade to *Apatosaurus ajax* + *Apatosaurus louisae* if excluding *Eobrontosaurus*. The result of the analysis without *Australodocus* can be neither confirmed nor rejected by the equally weighted reduced consensus tree, as none of the doubtful specimens are recovered there.

Combining the information of the main trees, nine shared synapomorphies are found: 1) absence of any longitudinal ridge on the ventral surface of mid- and posterior cervical vertebrae (174-1); 2) dorsal vertebrae have a single vertical lamina supporting the hyposphene from below (238-1); 3) a ratio of the height of mid- and posterior dorsal neural arches below the postzygapophyses (pedicel) to posterior cotyle height of less than 0.8 (254-0); 4) transverse cross-section of anterior-most caudal centra 'heart'-shaped, with an acute ventral ridge (296-1); 5) a strongly medially beveled scapular glenoid (366-1); 6) a distal condyle of the radius that is beveled at least 15° to the long axis of shaft, in anterior view (393-1); 7) a metacarpal I that is longer than mc IV (400-1); 8) presence of an anteromedially directed crest at the proximal end of the fibula, extending into a notch behind the cnemial crest of the tibia (447-1); and 9) a ratio of mediolateral width to maximum anteroposterior length of the astragalus of less than 1.6 (452-1). All but one of these synapomorphies are unique within Apatosaurinae, the single lamina supporting the hyposphene is also present in AMNH 460. This character, as well as two more (400-1, 452-1) are also found as synapomorphies for the more inclusive clade *Eobrontosaurus* + mdA in the implied weights analysis excluding *Australodocus bohetii* a priori. Three more shared and one unambiguous synapomorphies are found in the tree without *Australodocus*. None of these were possible to code for AMNH 460, with the result that all of them are recovered as synapomorphies for *Brontosaurus* + mdA in the complete implied weights analyses.

In the equally weighted reduced consensus tree, *Eobrontosaurus* + *Amphicoelias* and its sister clade are separated by five changes. The trees obtained by implied weighting yield distances of 15 (pruned) and 14 (reduced) changes from *Eobrontosaurus* to *Apatosaurus ajax* + mdA. The tree without *Australodocus* shows nine changes between *Eobrontosaurus* and AMNH 460 + mdA. Whereas *Eobrontosaurus* or *Eobrontosaurus* + *Amphicoelias* can thus be confidently considered a new species, support for being a different genus is dubious. The taxonomic status of *Eobrontosaurus* and *Amphicoelias* will be assessed with further detail below.

***Dystrophaeus viaemalae* USNM 2364 + UW 15556.** The unity of these two specimens to the exclusion of any other is only seen in the reduced consensus tree applying implied weights. Support from overlap index is extremely low, being only four percent. A single shared synapomorphy is recovered: angle between the anterior and lateral branches of the ulnar proximal articular surface is 90° (389-0). The addition of the single specimen FMNH P25112 to the reduced consensus tree with implied weights results in a polytomy between *Dystrophaeus viaemalae*, *Elosaurus parvus*, UW 15556, and FMNH P25112. Six changes are found between *Dystrophaeus viaemalae* USNM 2364 and UW 15556, but the states of all five autapomorphies recovered for UW 15556 are not known in *D. viaemalae*. The apomorphy count drops to one, indicating that the two specimens would represent the same species if they truly are sister taxa.

***Elosaurus parvus* CM 566 + UW 15556.** In the equally weighted pruned tree, the specimen UW

15556 is recovered together with the holotype specimen of *Elosaurus parvus* (CM 566), to the exclusion of all other taxa. *Dystrophaeus viaemalae* was excluded from that tree. When added to the equally weighted pruned tree, *Dystrophaeus* creates a large polytomy close to the base of the tree, and the unity of the two specimens CM 566 and UW 15556 remains. This clade was also recovered by Upchurch et al. (2004b), and interpreted as its own species within *Apatosaurus*, introducing the new combination *Apatosaurus parvus*. Seven shared synapomorphies are recovered for this clade, but only supported by the equally weighted pruned tree: 1) the prezygapophyseal centrodiapophyseal fossa of mid- and posterior cervical vertebrae is not subdivided (184-0); 2) posterior cervical vertebrae have an accessory lateral lamina connecting the postzygodiapophyseal and the spinoprezygapophyseal laminae (197-1); 3) absence of a single vertical lamina supporting the hyposphene in dorsal vertebrae from below (238-0); 4) a single centropostzygapophyseal lamina in mid- and posterior dorsal neural arches (261-0); 5) an absent or greatly reduced spinoprezygapophyseal lamina in posterior dorsal vertebrae (274-0); 6) a longer than wide base of the neural spines of posterior dorsal vertebrae, just above transverse processes (279-0); and 7) an acute angle between the ventral edge of the preacetabular lobe of the ilium and the anterior surface of the pubis process (408-1). Five of the seven synapomorphies are shared with other apatosaurines (184-0, 238-0, 261-0, 279-0, 408-1), the greatly reduced sprl in posterior dorsal vertebrae is unique within Diplodocoidea. The two specimens can be distinguished by a sum of four autapomorphies, which are also observable in the other specimen.

***Elosaurus parvus* CM 566 + (*Dystrophaeus* + UW 15556).** This triplet does only occur in the reduced implied weight trees, excluding the specimen FMNH P25112. In the pruned implied weight tree, where FMNH P25112 is present, the four specimens form a polytomy, with *Brontosaurus excelsus* YPM 1980 as sister taxon. Three shared synapomorphies are found by the reduced consensus tree, and five more are added in the pruned consensus tree with FMNH P25112. The eight shared synapomorphies found are the following: 1) dorsal centrum length (excluding the articular 'ball') shortens from anterior to posterior dorsal vertebrae (225-1); 2) mid- and posterior dorsal neural arches have single centropostzygapophyseal lamina (261-0); 3) spinoprezygapophyseal lamina of posterior dorsal vertebrae are absent or greatly reduced (274-0); 4) anterior-most caudal centra are sub-circular with a rounded ventral margin (296-0); 5) anterior-most caudal centra have large pleurocoels (297-1); 6) the angle between the ventral edge of the preacetabular lobe of the ilium and the anterior surface of the pubis process is acute (408-1); 7) the greatest anteroposterior thickness of the femoral shaft is much greater than half of the anteroposterior depth of the distal articular condyles (1); and 8) the fourth trochanter is positioned on the proximal half of the femoral shaft (438-1). Due to its incompleteness, *Dystrophaeus* cannot can be scored for any of these synapomorphies. The three synapomorphies found by the reduced implied weights tree are in fact also found by the equally weighted trees for the cluster *E. parvus* + UW 15556. In the reduced implied weight trees, *Elosaurus parvus* CM 566 is separated from the *Dystrophaeus* cluster by four changes, not justifying specific separation.

***Brontosaurus excelsus* YPM 1980 + (*Elosaurus* + *Dystrophaeus*).** A grouping of the holotype specimen of *Brontosaurus excelsus* with *Elosaurus* and other specimens, as sister clade to a clade including the type specimens of *Apatosaurus ajax* and *Apatosaurus louisae*, is only found by applying implied weights. The clade always contains three holotype specimens (*B. excelsus* YPM 1980, *E. parvus* CM 566, and *D. viaemalae* USNM 2364), as well as UW 15556. In the pruned consensus tree, also FMNH P25112 was recovered within this group. Five shared and one exclusive synapomorphies are recovered: 1) a single prezygapophyseal centrodiapophyseal fossa in mid- and posterior cervical vertebrae (184-0, shared); 2) absence of a median tubercle in posterior cervical and anterior dorsal bifid neural spines (210-0, shared); 3) hyposphene first appears on DV 4 or more posteriorly (237-1, shared); 4) the height above posterior dorsal postzygapophyses (neural spine) is at least 3.1 times greater than the height below (pedicel) (272-1, shared); 5) the transition from 'fan'-shaped to 'normal' caudal ribs occurs between Cd 5 and Cd 6 (300-2, exclusive); and 6) anterior, 'fan'-shaped caudal ribs are pierced by a foramen (350-1, shared). Two of the shared synapomorphies are also present in other apatosaurs (237-1, 272-1). The transition of fan-shaped to normal caudal ribs between Cd 5 and 6 does not appear to be shown in UW 15556, where it is between Cd 4 and 5, according to Gilmore (1936). However, the caudal vertebrae were found disarticulated, and the serial positions proposed by Gilmore

(1936) were based on comparisons with the type specimen of *Apatosaurus louisae* (Gilmore, 1936: p. 251). Therefore, it could be that an anterior-most caudal vertebra is missing, and it would thus probably be more accurate to score UW 15556 as unknown in this character. As with the previous clade, due to the fragmentary state of USNM 2364, it was not possible to score *Dystrophaeus* for any of the characters herein recovered as synapomorphies for *Brontosaurus* + (*Elosaurus* + *Dystrophaeus*). *Brontosaurus excelsus* is separated from the sister clade by twelve changes, justifying the use of two distinct genera (see below).

***Brontosaurus* + mdA.** This clade is found in the implied weights analysis only. Whereas the main trees show the *Brontosaurus* clade to be sister taxon to *Eobrontosaurus* + mdA, the reduced consensus tree obtained by excluding *Australodocus* a priori does show a more basal position for *Eobrontosaurus*. The clade is supported by eight shared and one unambiguous synapomorphies: 1) a ratio of total length of posterior dorsal centra to height of the posterior articular surface of less than 1.0 (268-1, shared); 2) short forked chevrons of about 50% of the corresponding vertebral centrum length (358-0, shared); 3) a humerus RI (sensu Wilson and Upchurch, 2003) of more than 0.33 (380-2, shared); 4) a ratio of maximum diameter of the proximal end of the radius divided by greatest length of 0.3 or greater (391-1, shared); 5) number of carpal bones reduced to one or less (395-2, unambiguous); 6) carpals are proximodistally compressed discs (396-1, shared); 7) metacarpal I is longer than mc IV (400-1, shared); 8) a ratio of mediolateral width of the astragalus to maximum anteroposterior length of less than 1.6 (452-1, shared); and 9) a ratio of mean transverse breadth of proximal and distal ends of metatarsal II to the maximum length of more than 0.65 (466-2, shared). Describing features of appendicular elements, which lack in several specimens included in the present analysis, six of the present synapomorphies diagnose the more inclusive *Eobrontosaurus* + mdA in the reduced consensus tree of the analysis excluding *Australodocus* a priori (380-2, 391-1, 395-2, 396-1, 400-1, 452-1). In the latter analysis, only one, but an unambiguous synapomorphy is found for *Brontosaurus* + mdA: posterior cervical rib shafts are initially directed in the same direction but turn to run a little downwards toward the distal tip (223-1). Including *Australodocus* in the analysis, 15 changes are recovered between the *Brontosaurus* clade and the *Eobrontosaurus* clade, whereas in the other analysis, eleven changes separate *Brontosaurus* from *Apatosaurus ajax* + mdA. Both counts support the use of different genera for the two clades.

WDC-FS001A + SMA 0087. The clustering of these two specimens is only found when using implied weighting. They have a very low overlap, indicated by the index of seven percent. Two shared synapomorphies characterize the clade: 1) a tibial cnemial crest that is widely rounded in anterior view (444-0); and 2) the presence of a distinct fibular trochanter on the posterior surface of the cnemial crest of the tibia (445-1). None of these traits are seen in other apatosaur specimens preserving the tibia. Two changes are separating the two specimens, indicating that they might belong to the same species. More detailed study of the material will be needed in order to definitely assess the systematic position of these two specimens.

SMA 0087 + mdA. As the clades discussed above, also this arrangement is only recovered in the trees obtained with implied weighting. Whereas AMNH 460 is found as sister taxon to the present clade in the trees obtained by the complete analysis, this specimen is included into SMA 0087 + mdA when *Australodocus* is deleted from the matrix a priori. No valid synapomorphies are found with the analysis including *Australodocus*, but one unambiguous synapomorphy characterizes this clade when *Australodocus* is excluded a priori: proximal articular surface of metacarpal V significantly larger than the proximal articular surface of mc III and IV (403-1). However, a very small percentage of all taxa preserve metacarpals III to V, such that only two ingroup specimens (out of 12) and 14.7 percent of the specimens in the entire analysis were scorable for this character. Support for such an arrangement is thus very low. Nonetheless, eleven changes separate the clade SMA 0087 + WDC-FS001A from *Brontosaurus* + mdA in the main implied weights trees, and eight in the case of the analysis without *Australodocus*. This relatively high number indicates the presence of a new, previously unrecognized taxon.

AMNH 460 + mdA. The composition of this clade as recovered by the implied weight analyses changes depending on in- or exclusion of *Australodocus*. The specimens changing their positions in

respect to this clade are *Eobrontosaurus yahnahpin* Tate-001, SMA 0087, and WDC-FS001A. They are nested within the present clade in the main trees, but fall outside when excluding *Australodocus*. A single valid, shared synapomorphy is found with the main, pruned consensus tree: absence of a longitudinal ridge on the ventral surface of mid- and posterior cervical vertebrae (174-1). This trait is not identified as synapomorphic for AMNH 460 + mdA in the analysis without *Australodocus*, as it shows the same development in *Eobrontosaurus*, which is recovered as sister taxon to the present clade, instead of being nested within. No changes separate AMNH 460 from the more derived clade SMA 0087 + mdA in the main implied weights trees, and one single change is found between AMNH 460 and *Brontosaurus* + mdA in the implied weights reduced consensus tree without *Australodocus*. Neither specific nor generic separation of AMNH 460 from its sister groups is thus warranted. The taxonomic affinities of AMNH 460 will be addressed below.

***'Atlantosaurus' immanis* YPM 1840 + NSMT-PV 20375.** The grouping of these two specimens is only recovered with implied weights. Both specimens are usually interpreted as belonging to *Apatosaurus ajax* (McIntosh, 1995; Upchurch et al., 2004b), but are here found as the most basal apatosaurines. Whereas NSMT-PV 20375 occupies the same position in the equally weighted trees, *'Atlantosaurus' immanis* YPM 1840 switches to a sister arrangement with the *Apatosaurus ajax* holotype YPM 1860. Overlap is low, as indicated by the index of 15%. Four valid, shared synapomorphies are found: 1) mid-cervical neural spine height less than 0.45 times than the height of the neural arch (168-0); 2) the posterior centrodiapophyseal lamina of mid- and posterior cervical vertebrae bifurcates towards its anterior end (188-1); 3) the hyposphene first appears on DV 4 or more posteriorly (237-1); and 4) the distal end of the ischium is posterodorsally expanded (426-1). All four synapomorphies are shared with other apatosaurines, and would thus not qualify as species autapomorphies. Two traits are also present in *Apatosaurus ajax* YPM 1860 (168-0, 426-1), which supports the earlier identifications, and casts additional doubt on the position recovered herein. If a true phylogenetic signal, the two specimens would be separated by one single change, not allowing specific separation.

Apatosaurinae. Whereas an apatosaurine clade was recovered in all four main trees, composition of it changes. Five putative apatosaur specimens are found outside Apatosaurinae, in a polytomy with the latter clade and Diplodocinae in the equally weighted pruned consensus tree: WDC-FS001A, SMA 0087, FMNH P25112, AMNH 460, and NSMT-PV 20375. When adding them one by one to the reduced consensus, only WDC-FS001A and SMA 0087 result in such a position, indicating that they are the main cause for the large polytomy in the pruned tree. *Amphicoelias altus* is found within Apatosaurinae applying equal weights, but remains outside when using implied weighting. Two unambiguous, one exclusive, 20 shared, and one ambiguous synapomorphies add to a total of 24 synapomorphies recovered for the clade: 1) dorsoventral height of the occipital process of the parietal is low, subequal to less than the diameter of the foramen magnum (63-0, shared); 2) presence of a foramen in the notch that separates the two basal tubera (90-1, shared); 3) posterior centrodiapophyseal lamina in cervical vertebrae reaches below the posterior end of the neural canal (135-1, ambiguous); 4) centroprezygapophyseal lamina of mid- and posterior cervical neural arches is divided, resulting in the presence of a 'true' divided centroprezygapophyseal lamina, which is dorsally connected to the prezygapophysis (185-2, shared); 5) posterior centrodiapophyseal lamina (pcdl) and postzygodiapophyseal laminae (podl) of mid- and posterior cervical transverse processes do not meet anteriorly, such that the postzygapophyseal centrodiapophyseal fossa extends onto the posterior face of the transverse process (186-1, shared); 6) cervical ribs projecting well beneath centrum, such that the length of the posterior process is subequal in length to the fused diapophysis/tuberculum (216-1, unambiguous); 7) anterior process of posterior cervical ribs is reduced to a short bump-like process or absent (220-1, shared); 8) posterior cervical rib shafts are initially directed in the same direction but turn to run a little downwards toward the distal tip (223-1, exclusive); 9) abrupt transition from bifid to single dorsal neural spines (235-1, shared); 10) bifid dorsal neural spines (if present) do not extend past the second or third dorsal (250-0, shared); 11) mid- and posterior dorsal parapophyses lie posterior to the anterior edge of centrum (256-0, shared); 12) absence of accessory laminae in the region between the posterior centrodiapophyseal lamina (pcdl) and posterior centroparapophyseal lamina (PCPL) of mid- and posterior dorsal vertebrae (259-0, shared); 13) posterior dorsal

postzygapophyses are oblique, including an almost 90° angle (275-1, shared); 14) forked chevrons are about 50% of the length of the corresponding vertebral centrum (358-0, shared); 15) humerus RI (sensu Wilson and Upchurch, 2003) is more than 0.33 (380-2, shared); 16) maximum diameter of the proximal end of the radius divided by the greatest length is 0.3 or greater (391-1, shared); 17) number of carpal bones reduced to one or less (395-2, unambiguous); 18) carpals are proximodistally compressed discs (396-1, shared); 19) metacarpal I is longer than mc IV (400-1, shared); 20) ratio of metacarpal III length to distal transverse width of less than 2.9 (402-0, shared); 21) ratio of the pubic articulation of the ischia to the anteroposterior length of the pubic pedicel of 1.5 or greater (420-1, shared); 22) ratio of mediolateral width of the astragalus to maximum anteroposterior length is less than 1.6 (452-1, shared); 23) ratio of mean transverse breadth of proximal and distal ends of the metatarsal II to maximum length is greater than 0.65 (466-2, shared); and 24) pedal phalanges III-1 and IV-1 are wider than long (476-1, shared). Seven of these traits result as synapomorphic for Diplodocidae in the equally weighted pruned tree (135-1, 185-2, 186-1, 216-1, 220-1, 256-0, 275-1), but this is because of the apatosaur specimens recovered outside Apatosaurinae in this tree (135-1, 186-1, 216-1, 220-1, 256-0, 275-1), or the changing positions of *Supersaurus* (185-2). Nine synapomorphies are recovered for the less inclusive *Brontosaurus* + mdA in the implied weight trees, and should thus not be used in diagnoses of Apatosaurinae (259-0, 358-0, 380-2, 391-1, 395-2, 396-1, 400-1, 452-1, 466-2). The reason for the discrepancy is that the specimens found basal to *Brontosaurus* are mostly the ones recovered outside Apatosaurinae in the equally weighted pruned tree. Of the latter nine, two result as synapomorphic for *Eobrontosaurus* + mdA in the equally weighted reduced tree (400-1, 452-1), and seven for the same clade in the implied weights analysis without *Australodocus* (380-2, 391-1, 395-2, 396-1, 400-1, 402-0, 452-1). The high number of synapomorphies for Apatosaurinae contrasts with the low number of generally accepted genera this clade includes (*Apatosaurus*, and possibly *Eobrontosaurus*). This is surprising, when compared to its sister clade Diplodocinae, which includes at least six different genera, but does not appear to be much more divers morphologically. An analysis of morphological disparity would probably be able to quantify the difference, but is out of the scope of this thesis. In any case, the numerical approach as chosen herein also indicates a higher generic diversity within Apatosaurinae, with at least three, possibly up to six valid genera.

The most basal taxon as recovered by this analysis, would be represented by NSMT-PV 20375 (equal weights) or *'Atlantosaurus' immanis* YPM 1840 + NSMT-PV 20375. These specimens are separated from more derived apatosaurs by 14 changes in the case of the equally weighted reduced tree, five in the case of the main implied weights trees, as well as the one without *Australodocus*. This difference is mainly due to the fact that many specimens recovered between *Eobrontosaurus* and NSMT-PV 20375 in the implied weight trees, are not present in the equally weighted reduced consensus tree, in which the 14 changes were found. However, the true number also depends on the systematic position of YPM 1840, which will be discussed in more detail below.

Apatosaurinae + Diplodocinae. The unity of these clades usually corresponds to Diplodocidae, but since the definitions of the two clades are stem-based, as is Diplodocidae (Taylor and Naish, 2005), additional taxa can be recovered basal to Apatosaurinae + Diplodocinae, but still within Diplodocidae. This is the case in the implied weights trees, where *Amphicoelias altus* AMNH 5764 is found to be the basal-most diplodocid. Two unambiguous, four exclusive, and two shared synapomorphies are found for this clade: 1) preantorbital fenestra occupies at least 50% of the preantorbital fossa (17-1, exclusive); 2) medial margin of the prefrontal is curving distinctly medially at its anterior end to embrace the anterolateral corner of the frontal (23-1, exclusive); 3) posterior process of the prefrontal is hooked (25-1, unambiguous); 4) ten dorsal vertebrae (224-2, exclusive); 5) presence of accessory laminae in the region between the posterior centrodiapophyseal lamina (pcdl) and the posterior centroparapophyseal lamina (pcpl) in mid- and posterior dorsal vertebrae (259-1, exclusive); 6) short mid- and posterior dorsal transverse processes (263-0, shared); 7) posterior dorsal, sacral and anterior caudal neural spines are rectangular through most of their length (294-0, shared); and 8) anterior centrodiapophyseal lamina (acdl) of anterior caudal vertebrae is divided (314-1, unambiguous). Seven of these are also recovered as synapomorphies of Diplodocidae (17-1, 23-1, 25-1, 224-2, 259-1, 263-0, 294-0, 314-1). Two traits are scored differently in *Amphicoelias* (characters 259 and 294), and should thus not be used to diagnose Diplodocidae. The sum of synapomorphies for Apatosaurinae and

Diplodocinae is 34.

Diplodocidae. As stated above, the implied weight trees recover *Amphicoelias* as sister taxon to Apatosaurinae + Diplodocinae, and thus as the most basal diplodocid genus. Sixteen synapomorphies are supported by the analysis, three unambiguous, six exclusive, five shared, and two ambiguous: 1) preantorbital fenestra occupies at least 50% of the preantorbital fossa (17-1, exclusive); 2) medial margin of the prefrontal is curving distinctly medially at its anterior end to embrace the anterolateral corner of the frontal (23-1, exclusive); 3) posterior process of the prefrontal is hooked (25-1, unambiguous); 4) shape of the posterior face of the basal tubera flat (85-1) or slightly concave (85-2, shared); 5) 14 to 15 cervical vertebrae (127-1, unambiguous); 6) cervical ribs projecting well beneath centrum, such that the length of the posterior process is subequal in length to the fused diapophysis/tuberculum (216-1, exclusive); 7) ten dorsal vertebrae (224-2, exclusive); 8) dorsal transverse processes horizontal or only slightly inclined dorsally (230-0, ambiguous); 9) posterior centroparapophyseal lamina of mid- and posterior dorsal neural arches present as single lamina (258-1, ambiguous); 10) presence of accessory laminae in the region between the posterior centrodiapophyseal lamina (pcdl) and the posterior centroparapophyseal lamina (pcpl) in mid- and posterior dorsal vertebrae (259-1, exclusive); 11) short mid- and posterior dorsal transverse processes (263-0, shared); 12) anterior centrodiapophyseal lamina (acdl) of anterior caudal vertebrae is divided (314-1, unambiguous); 13) anterior caudal transverse processes with anteroposteriorly expanded lateral extremities (316-1, shared); 14) spinoprezygapophyseal laminae (sprl) and spol contact each other on anterior caudal neural spines (319-1, shared); 15) anterior and mid-caudal vertebrae bear ventrolateral ridges (329-1, exclusive); and 16) presence of a lateral bulge on the femur (428-1, shared). One of the stated synapomorphies actually only occurs in apatosaurine specimens (216-1), and is recovered as a synapomorphy for that clade by all but the equally weighted pruned tree. It is thus more carefully treated as synapomorphy of Apatosaurinae, and should not be used in diagnoses of Diplodocidae. A similar case is character 259, where the derived state is recovered as diplodocid synapomorphy, but *Amphicoelias* is scored for the plesiomorphic state. If the basal position of *Amphicoelias* is confirmed, the derived state would only diagnose the clade Apatosaurinae + Diplodocinae, as already stated above. *Amphicoelias* – in such a position – is separated from more derived diplodocids by a sum of twelve changes, but only six are actually comparable due to the incomplete condition of the type specimen of *Amphicoelias*.

Flagellicaudata. The node-based taxon Flagellicaudata includes Diplodocidae and Dicraeosauridae. It is recovered by all four main trees, and supported by eight unambiguous, three exclusive, eight shared, and three ambiguous synapomorphies: 1) subnarial foramen and anterior maxillary foramen are separated by a narrow bony isthmus (8-1, unambiguous); 2) presence of a preantorbital fossa (15-1, unambiguous); 3) a shallow quadrate fossa (51-0, shared); 4) an elongate and slender posterior end of the quadrate (posterior to posterior-most extension of pterygoid ramus) (54-1, unambiguous); 5) the absence of any squamosal-quadratojugal contact (56-1, unambiguous); 6) the absence of a parietal contribution to the post-temporal fenestra (59-1, unambiguous); 7) the longest axes of the basal tubera are oriented in an angle to each other, pointing towards the occipital condyle (87-1, exclusive); 8) the anteroventral margin of the dentary bears a sharply projecting triangular process or 'chin' (104-1, unambiguous); 9) anteriorly oriented, procumbent teeth (122-1, unambiguous); 10) absence of longitudinal grooves on the lingual aspect of the teeth (123-0, shared); 11) mid- and posterior dorsal neural arches have divided centropostzygapophyseal lamina, with the lateral branch connecting to the pcdl (261-1, ambiguous); 12) the hyposphene-hypantrum system is well developed in posterior dorsal vertebrae, having a rhomboid shape up to last element (276-0, ambiguous); 13) the lateral spinal lamina of anterior-most caudal neural spines expands anteroposteriorly towards its distal end, and becomes rugose (303-1, exclusive); 14) the ventral surface is marked by irregular foramina on some anterior caudal centra (305-1, ambiguous); 15) anterior diapophyseal laminae (acdl, prdl) are well defined in in anterior caudal vertebrae (313-1, shared); 16) the spinoprezygapophyseal laminae of anterior caudal neural spines extend onto the lateral aspect of the neural spine (318-1, shared); 17) a 'crus' bridging the haemal canal is present in some chevrons (352-0, shared); 18) the posterior edge of the distal blade of anterior chevrons is posteriorly expanded in a step-like fashion (355-1, exclusive); 19) the distal shaft of the ischium is triangular, with its depth increasing medially (423-1,

unambiguous); 20) the cross-sectional shape of ischial distal shafts is V-shaped, forming an angle of nearly 50° with each other (424-0, shared); 21) the ischial shaft is transversely expanded distally (425-1, shared); and 22) the distal condyle of metatarsal I bears a posterolateral projection (463-1, shared). One of the above mentioned synapomorphies was recovered as diagnosing Diplodocimorpha in the implied weight trees, instead (318-1). The sprl also extends onto the lateral aspect of the caudal neural spines in rebbachisaurs. Since *Cetiosauriscus* and *Haplocanthosaurus* are recovered as diplodocoid sauropods more derived than rebbachisaurs in the equally weighted analysis, but have reduced caudal sprl, it results a shared synapomorphy of rebbachisaurs and flagellicaudatans. If – as in the trees found by using implied weighting – *Cetiosauriscus* and *Haplocanthosaurus* are found to be more basal to rebbachisaurs, the well-developed caudal sprl become a diagnosing feature for Diplodocimorpha as defined by Taylor and Naish (2005). Proximally closed haemal arches (352-0) are present as well in *Cetiosauriscus stewarti* NHMUK R3078. In the equally weighted pruned tree, where *C. stewarti* is recovered as diplodocoid more than Rebbachisauridae, this feature thus appears synapomorphic for a clade *C. stewarti* + mdD. The same occurs in character 463 describing the presence of a posterolateral projection on the distal condyle of metatarsal I, which is also present in *C. stewarti* and thus becomes a synapomorphy for the slightly more inclusive clade *C. stewarti* + mdD. Within Flagellicaudata, Dicraeosauridae and Diplodocidae are separated by 56 changes.

***Cetiosauriscus* + mdD.** Such a clade is only found with equal weighting, where *Cetiosauriscus stewarti* NHMUK R3078 is recovered in a position between Rebbachisauridae and Flagellicaudata. Three shared synapomorphies support this grouping: 1) sacral spinodiapophyseal lamina is present and distinct, and connects spine summit with diapophysis (290-1); 2) 'crus' bridging haemal canal present in some chevrons (352-0); and 3) presence of a posterolateral projection on the distal condyle of metatarsal I (463-1). All of these synapomorphies are shared with more basal taxa, close to the position where *Cetiosauriscus* is recovered in the implied weights trees, and are thus not conclusive evidence for diplodocoid affinities of *Cetiosauriscus*. The sum of apomorphies between *Cetiosauriscus* and Flagellicaudata is 30.

***Haplocanthosaurus* + mdD.** This clade corresponds to Diplodocoidea in the implied weights trees, but is more restricted when applying equal weighting. In the latter analysis, *Haplocanthosaurus* is recovered more derived than Rebbachisauridae. Such an arrangement is supported by one exclusive synapomorphy: the postspinal lamina or rugosity of anterior caudal neural spines projects dorsally above the neural spine (324-1). However, if the true phylogenetic position of *Cetiosauriscus* would be outside Diplodocoidea, this feature would not be useful anymore to define this clade, and indeed was not found as such in the implied weights analysis. *Haplocanthosaurus* is separated from *Cetiosauriscus* + mdD by 14 changes.

Diplodocimorpha. The present clade is often used in the same way as Diplodocoidea, but in fact has a node-based definition, whereas Diplodocoidea is stem-based. In the present analyses, Diplodocimorpha is only different from Diplodocoidea when using implied weighting, where *Haplocanthosaurus* is recovered more basal to Rebbachisauridae. In these cases, even the complete strict consensus tree finds Diplodocimorpha. One unambiguous, two exclusive, and one ambiguous synapomorphies are found to be reliable in the implied weights trees: 1) posterior dorsal, sacral and anterior caudal neural spines are 'petal' shaped in anterior/posterior view, expanding transversely through 75% of its length and then tapering (294-1, exclusive); 2) transition from 'fan'-shaped to 'normal' caudal ribs occurs between Cd 4 and Cd 5 (300-1, exclusive); 3) sprl extend onto lateral aspect of anterior caudal neural spines (318-1, unambiguous); and 4) a semicircular dorsal margin of the ilium (409-1, ambiguous). The semicircular dorsal margin of the ilium was the only characteristic also recovered as synapomorphic for Diplodocoidea by equal weighting. One of the synapomorphies was found to diagnose Rebbachisauridae in the equally weighted tree (294-1). The latter clade is distinct from Flagellicaudata (which is the sister taxon to Rebbachisauridae in the implied weight trees) by 27 changes.

Diplodocoidea. The clade Diplodocoidea is represented in all consensus trees but the complete strict consensus tree with equal weighting. Due to the more derived position of *Haplocanthosaurus priscus* in the equally weighted analyses compared to the analysis with implied weights, Diplodocoidea is

equivalent to Diplodocimorpha in the former analysis. Synapomorphies recovered include 14 unambiguous, five exclusive, five shared, and one ambiguous traits: 1) external surface of the premaxilla is marked by vascular grooves (2-1, exclusive); 2) premaxilla is a single elongate unit with nearly no distinction between the body and the nasal process (3-1, unambiguous); 3) posteroventral edge of the ascending process of the premaxilla is straight in lateral view, and directed posterodorsally (5-2, unambiguous); 4) the posterolateral process of the premaxilla and the lateral process of the maxillary are without any midline contact (6-0, shared); 5) the anterior maxillary foramen lies on the medial edge of the maxilla, opening medially into the premaxillary-maxillary boundary (11-1, exclusive); 6) the dorsal process of the maxilla extends posterior to the posterior process (13-1, unambiguous); 7) maximum diameter of the antorbital fenestra is subequal (greater than 90%) to the orbital maximum diameter (18-1, unambiguous); 8) the external nares are retracted to a position between the orbits, facing dorsally or dorsolaterally (21-1, unambiguous); 9) maximum diameter of the external nares is shorter than the orbital maximum diameter (22-0, shared); 10) a large contribution of the jugal to the antorbital fenestra, bordering approximately one-third of its perimeter (40-1, unambiguous); 11) the anterior terminus of the quadratojugal lies below the anterior margin of the orbit or beyond (45-1, unambiguous); 12) angle between anterior and dorsal processes of the quadratojugal is greater than 90°, approaching 130°, so that the quadrate shaft slants posterodorsally (46-1, unambiguous); 13) the articular surface of the quadrate is roughly triangular in shape (49-1, exclusive); 14) the articular surface of the occipital condyle is continuously grading into the condylar neck (77-1, shared); 15) the basipterygoid processes are angled less than 75° to the skull roof (normally approximately 45°) (93-1, unambiguous); 16) the transverse flange (i.e. ectopterygoid process) of the pterygoid lies anterior to the antorbital fenestra (102-1, unambiguous); 17) four or more replacement teeth per alveolus (115-1, unambiguous); 18) planar wear facets of the teeth (117-1, unambiguous); 19) SI values for tooth crowns are 3.4 or greater (119-1, exclusive); 20) cylindrical cross-sectional shape of the teeth at midcrown (121-1, unambiguous); 21) short cervical ribs, not reaching the posterior end of the centrum (214-1, exclusive); 22) cervical ribs overlap no more than the next cervical vertebra in sequence (215-1, shared); 23) the dorsal transverse processes are inclined dorsally more than 30° from the horizontal (230-1, ambiguous); 24) the proximal expansion of the humerus is more or less symmetrical (384-0, shared); and 25) the fibular facet of the astragalus faces posterolaterally, such that the anterior margin is visible in posterior view (454-1, unambiguous). Twenty of the synapomorphies mentioned describe cranial features, which are rarely preserved, as exemplified by the low percentage of ingroup specimens scored: nine of them are only known from less than 20% of all specimens included in the analysis, five from less than 15%. Their assignment as synapomorphies should thus be regarded provisional. The distance between *Haplocanthosaurus* and Diplodocimorpha amounts to 17 changes.

Validity and taxonomic assessment of the holotype specimens

Discussion of the taxonomic affinities of the holotype specimens is ordered based on date of description. By doing so, possible synonymy of the species and genera can be assessed in a more intuitive way. The specimens are listed with the initially proposed name.

***Dystrophaeus viaemalae* USNM 2364.** The phylogenetic position of *Dystrophaeus viaemalae* is dubious, mostly due to its fragmentary remains. In the present analysis, the holotype USNM 2364 was among the six most unstable, and thus pruned taxa in the equally weighted trees. The analysis using implied weighting recovered it consistently as sister taxon to UW 15556, closely related with the holotype of *Elosaurus parvus*. Validity and phylogenetic position of *Dystrophaeus viaemalae* is particularly important because it was the first sauropod to be described from North America, and would thus have priority over any possibly synonymous taxon. The present study is the first to include the specimen in a phylogenetic analysis. Earlier studies proposed diplodocid affinities (McIntosh, 1997), but that was mainly based on the plesiomorphically short and robust metacarpals (Upchurch et al., 2004a). The latter did not find any diagnostic feature in the fragmentary material, but refrained to classify *Dystrophaeus* as nomen dubium as it was found very low in stratigraphy, possibly even below the Morrison Formation.

One single, ambiguous autapomorphy was recovered for USNM 2364: ulnar articular surface on distal radius reduced and relatively smooth (392-0). The identification of the partial radius as distal is

debatable, however, as proximal and distal ends of the radius can be highly similar. McIntosh (1997), for example, identified the same piece as proximal radius, which would render the autapomorphy invalid. As recovered herein, it is shared with specimens from all major taxonomic groups included in the analysis. The fact that two specimens of the same diplodocine genus (*Galeamopus*) are scored differently for this character casts further doubt on its validity as autapomorphy. A single character ties *D. viaemalae* to UW 15556: a right angle lies between the arms of the ulnar proximal articular surface (389-0). This trait is shared with *Omeisaurus*, and possibly affected by deformation. Incompleteness of the specimen inhibits a scoring for any character providing synapomorphies of lower-level clades (below Apatosaurinae) recovered including *Dystrophaeus*. The holotype specimen can be scored for a single character producing a shared synapomorphy of Apatosaurinae (robust metacarpal III), but actually results in a controversial coding (intermediate robustness of metacarpal III), not shown in any other apatosaurine specimen. A differential scoring is also present in an ambiguous synapomorphy of Diplodocidae (posterior centroparapophyseal lamina absent instead of single or double in mid- and posterior dorsal neural arches). However, identification of laminae in the preserved partial dorsal vertebra of *Dystrophaeus* is very difficult, because distinction of bone from the still adherent matrix is not made without difficulty. The plesiomorphic coding for this character is furthermore shared by the type specimen *Elosaurus*, which groups with *Dystrophaeus* in the implied weights tree. No synapomorphy of higher-level clades as Flagellicaudata, Diplodocimorpha, or Diplodocoidea can be identified in USNM 2364. This implies that either USNM 2364 is not diagnostic, or not a diplodocoid sauropod. As a macronarian affinity appears to be improbable given the relatively short metacarpals (McIntosh, 1997; Upchurch et al., 2004a), the only reasonable identification would be a non-neosauropod eusauropod.

In order to test these interpretations, constrained tree searches with equal weights were performed forcing USNM 2364 into a position with *Elosaurus parvus* CM 566 and UW 15556 as found by the implied weight trees, as well as forcing it into a position outside Diplodocoidea. Minimum tree length obtained by imposing a grouping of USNM 2364 with CM 566 and UW 15556 is three steps higher (1900) than the most parsimonious trees (1897), and produces one synapomorphy recognizable in *Dystrophaeus* as well: distal end of the radius much wider than midshaft (394-1). The same trait has been identified as synapomorphy for Apatosaurinae (equally weighted pruned tree) or *Jobaria* + mdE (equally weighted reduced tree). The shortest tree constraining *Dystrophaeus* to a taxon outside Diplodocoidea resulted from a grouping with *Lourinhasaurus* or *Omeisaurus*, both producing the same tree length as the most parsimonious trees (1897). A single synapomorphy supports the grouping with *Lourinhasaurus*: presence of a subtriangular process on the ventral edge of the scapular blade (370-1) – which is present as well in several diplodocid specimens. The sister group arrangement with *Omeisaurus* yielded three synapomorphies: 1) a flat or slightly convex area posterior to the acromial ridge and the distal blade of the scapula (365-1); 2) the right angle between the two arms of the ulnar proximal articular surface (389-0); and 3) a beveled distal articular surface of the radius (393-1). Any of these traits are shared with diplodocid specimens as well. Forcing USNM 2364 into a non-diplodocoid position by using implied weights yielded a minimal tree length of 188.00488 when grouping with *Lourinhasaurus*, which is an increase of 0.03274 steps, compared to the most parsimonious trees. If forced to group with *Omeisaurus*, tree length increases to 188.3466. The synapomorphy found for *Lourinhasaurus* + *Dystrophaeus* is the same as in the equally weighted tree (370-1). A length increase of 0.16% is thus needed in the equally weighted trees to force *Dystrophaeus* into the position recovered with implied weighting, whereas a position outside Diplodocoidea results in the same length. On the other hand, using implied weighting, a tree length increase of 0.02% already supports a grouping of *Dystrophaeus* with *Lourinhasaurus*. A position outside Diplodocoidea seems thus better supported. More detailed studies are needed including basal Macronaria, Neosauropoda, as well as derived, non-neosauropod Eusauropoda, in order to resolve phylogenetic relationships of *Dystrophaeus viaemalae* and definitively assess its taxonomic validity.

***Amphicoelias altus* AMNH 5764.** The holotype of *Amphicoelias altus* is found in two different positions in the present analysis. Both positions contrast with the position it was found by Rauhut et al. (2005), Whitlock (2011a), Mannion et al. (2012) or Tschopp and Mateus (2012b): whereas it was found within Diplodocidae in the present analysis, all earlier assessments recovered it more basal than Dicraeosauridae, mostly even outside Diplodocimorpha (Rauhut et al., 2005; Whitlock, 2011a;

Mannion et al., 2012). The strict interpretation of the holotype as used in the present analysis (only including the dorsal vertebrae and the femur) possibly increased the diplodocid affinities, even though preliminary analyses recovered them in the same position. The positions recovered herein are in a dichotomy with *Eobrontosaurus yahnahpin*, within Apatosaurinae, or as basal-most diplodocid, neither apatosaurine nor diplodocine.

Four ambiguous autapomorphies were considered valid for the holotype, two of them for the position within Apatosaurinae (with equal weighting), and two as basal-most diplodocid (with implied weights): 1) posterior dorsal postzygapophyses almost horizontal, such that the two articular facets include a wide angle (275-0, equal weights); 2) posterior dorsal, sacral and anterior caudal neural spines 'petal' shaped, expanding transversely through 75% of its length and then tapering (294-1, equal weights); 3) femur gracile, robustness index (sensu Wilson and Upchurch, 2003) < 0.22 (427-0, implied weights); and 4) mediolateral width of the femur subequal to anteroposterior diameter (430-0, implied weights). The nearly horizontal postzygapophyses are widespread among sauropods, and thus probably not a meaningful autapomorphy. The 'petal' shape in the posterior dorsal of *A. altus* is less developed than in rebbachisaurs and dicraeosaurs, and an additional tree search was performed changing this single character state. In both equal and implied weights analyses, length of the MPTs was increased compared to the main trees (1900 and 188.32214 steps, respectively). Position of *Amphicoelias* remained the same, the interpretation of the neural spine shape is thus without influence. The gracile femur, with its mediolateral width subequal to anteroposterior depth describes the stove-pipe shape of this element, most often used as best way to distinguish *Amphicoelias* from other sauropods. In fact, these are the autapomorphies least shared with other taxa. On the other hand, the greatly deformed femur of SMA 0087 shows that ratios like transverse width to anteroposterior depth can be considerably distorted. However, in contrast to SMA 0087, the femur of AMNH 5764 does not show any sign of breakage, indicating that the preserved subcircular cross-section might at least approach the true shape in the living animal. The subcircular femoral cross-section, as well as the 'petal'-shaped posterior dorsal neural spines, and the horizontal posterior dorsal postzygapophyses are all traits shared with dicraeosaurids, whereas only one is shared with a single apatosaurine. In fact, the horizontal posterior dorsal postzygapophyses contrast with the state in all other Apatosaurinae, for which the implied weights analysis recovered a low angle as synapomorphy shared by all apatosaurine specimens. Moreover, *Amphicoelias* does not show an additional otherwise shared synapomorphy of Apatosaurinae: mid- and posterior dorsal parapophyses are not located above the centrum, but anteriorly displaced (256-1, instead of 256-0). One exclusive synapomorphy of Apatosaurinae + Diplodocinae, the accessory laminae in the region between the posterior centrodiapophyseal lamina (pcdl) and the posterior centroparapophyseal lamina (pcpl) of mid- and posterior dorsal vertebrae (259-1) is absent in *Amphicoelias*, but also in *Brontosaurus* + mdA, and in *Eobrontosaurus*. *Amphicoelias* shares the diplodocid synapomorphies of short posterior dorsal transverse processes, and the presence of a lateral bulge on the femur, both of which are not present in any other sampled diplodocoid sauropod. A diplodocid affiliation is thus probable. This is also supported by constrained searches testing the position of *Amphicoelias altus* recovered in the alternative analysis. When inhibiting a grouping of *Amphicoelias* with *Eobrontosaurus* in the equally weighted analysis, a tree of one step longer than the original is found (0.05% length increase), but relationships of *Amphicoelias* cannot be established beyond Diplodocidae indet. Tree length for a grouping of *Amphicoelias* and *Eobrontosaurus* using implied weights is 188.13188, which corresponds to a tree length increase of 0.08%. Such a constrain pulls *Amphicoelias* into Apatosaurinae, into the position corresponding to the one found in the equally weighted reduced consensus tree. However, given that relative tree length increase is lower when inhibiting instead of forcing such an interrelationship, the two taxa are herein considered distinct. Based on the lacking apatosaurine synapomorphies of *Amphicoelias*, and given that previous analyses agreed in a more basal position within Diplodocoidea, the position outside Apatosaurinae + Diplodocinae is herein interpreted as more reasonable.

***Amphicoelias latus* AMNH 5765.** All analyses performed agreed in a position of AMNH 5765 within Camarasauridae. *Amphicoelias latus* is generally synonymized with *Camarasaurus supremus*, following Osborn and Mook (1921).

No autapomorphies are found for *Amphicoelias latus*. The synapomorphies of *Camarasaurus* + Turiasauria, not shared with AMNH 5765 are the following: 1) maximum mediolateral width to

minimum mediolateral width of anterior caudal neural spines is 2.0 or greater (327-1), and 2) a prominent fourth trochanter on the femur, which is visible in anterior view (436-1). The first of these synapomorphies has actually been shown to be variable within *Camarasaurus* by Ikejiri (2004). The second is somewhat dubious, as AMNH 5765 was only scored based on the drawings in Cope (1877b) and Osborn and Mook (1921). Of the four synapomorphies recovered for *Camarasaurus* (92-0, 333-1, 392-1, 408-0), AMNH 5765 is not scorable for any of these. Furthermore, given that the present analysis is designed to resolve relationships within Diplodocidae, and that AMNH 5765 is highly incomplete (a femur and two anterior to middle caudal vertebrae), the more basal position compared to the other two *Camarasaurus* OTUs should not be considered significant. The present result can thus be regarded to corroborate the referral of Osborn and Mook (1921) of the holotype material of *Amphicoelias latus* to *Camarasaurus*.

***Apatosaurus ajax* YPM 1860.** As type specimen of the type species of *Apatosaurus*, YPM 1860 has special taxonomic importance. It is herein always recovered in the same tree branch as *Apatosaurus louisae* CM 3018. This is opposite to the finding of Upchurch et al. (2004b), where *Apatosaurus louisae* formed the sister group to all other apatosaur specimens included.

Six autapomorphies are found for YPM 1860, one of which unambiguous: 1) a shallow, second fossa marks the quadrate shaft medially to the pterygoid flange (not the quadrate fossa) (52-1, ambiguous); 2) box-like basal tubera (81-1, ambiguous); 3) longest axes of the basal tubera oriented parallel to each other (87-0, ambiguous); 4) medial surface of posterior bifid, cervical neural spines is smooth (206-1, unambiguous); 5) presence of an accessory lamina linking the hyposphene of mid- and posterior dorsal vertebrae with the base of the posterior centrodiapophyseal lamina (260-1, ambiguous); and 6) presence of an elliptical depression between the lateral spinal lamina of caudal neural spines and the postspinal lamina (292-1, ambiguous). Even when excluding the information of the braincase, the unambiguous synapomorphy would warrant specific separation. The specimen YPM 1860 can thus be regarded diagnostic, and the species *Apatosaurus ajax* valid. YPM 1860 is thus per definition an apatosaurine diplodocid.

***Apatosaurus grandis* YPM 1901.** The specimen YPM 1901 has long been known not to belong to *Apatosaurus*, but to typify its own species within *Camarasaurus* (Marsh, 1878; Osborn and Mook, 1921; McIntosh et al., 1996a, b; Ikejiri, 2004). It is herein consistently recovered as sister taxon to the genus-level OTU *Camarasaurus*, thereby confirming this identification.

Four ambiguous autapomorphies are considered valid: 1) last caudal rib occurs on Cd 13 (349-1); 2) sternal plates subtriangular with widened posterior border (374-1); 3) absence of a ridge on the ventral surface of the sternal plate (375-0); and 4) presence of foramina on the dorsal surface of mt I (459-1). Specific separation from *Camarasaurus* appears thus well-founded, and more detailed work on camarasaur intrarelationships will definitely produce more differences. *Apatosaurus grandis* is thus referred to *Camarasaurus*, as *Camarasaurus grandis*, with the type specimen being YPM 1901.

***Amphicoelias fragillimus* AMNH 5777.** This specimen was the only putative diplodocid holotype specimen not included into the present analysis. Given that it has been lost shortly after publication (Carpenter, 2006), and that no other material has yet been reported reaching anywhere near the same size as proposed in the initial description (Cope, 1878), it seems unwise to speculate about its phylogenetic position solely based on the single drawing and inadequate description of this extremely fragmentary specimen. *Amphicoelias fragillimus* is thus herein considered a nomen dubium.

***'Atlantosaurus' immanis* YPM 1840.** Generally considered synonymous to *Apatosaurus ajax* (McIntosh, 1995; Upchurch et al., 2004b), findings of this study are controversial (see above). No recovered autapomorphy for the specimen can be considered valid according to the guidelines established earlier. Both sister group arrangements with *Apatosaurus ajax* YPM 1860 and the putative *Apatosaurus ajax* NSMT-PV 20375 do not yield any synapomorphy not shared with any other apatosaur specimen. *'Atlantosaurus' immanis* YPM 1840 furthermore could not be scored for the single unambiguous autapomorphy found for *Apatosaurus ajax* YPM 1860 (smooth medial face of bifid posterior cervical neural spines). From the eight shared synapomorphies recovered for the clade *Apatosaurus ajax* + mdA, only one was scored for YPM 1840, but differently compared to the remaining ingroup specimens: presence instead of absence of a roughened lateral aspect of the prdl in

posterior cervical and anterior dorsal vertebrae (C208). YPM 1840 unambiguously classifies as Apatosaurinae due to the following preserved synapomorphies: true divided posterior cervical centroprezygapophyseal laminae (185-2, shared), and pcdl and podl of mid- and posterior cervical vertebrae that do not meet anteriorly (186-1, shared), cervical ribs projecting well beneath centrum (216-1, unambiguous), the bump-like anterior process of cervical ribs (220-1, shared), and the high ratio of the pubic articulation of the ischia to the anteroposterior length of the pubic pedicel (420-1, shared). However, placement within Apatosaurinae remains controversial.

Forcing YPM 1840 to group with NSMT-PV 20375 (as recovered with implied weighting) in the equally weighted analysis yielded minimal tree lengths of 1 step more than the most parsimonious trees, or a relative length increase of 0.05%. The strict reduced consensus tree shows three more taxa compared to the main equally weighted reduced consensus tree. The most important changes are the following: *Dystrophaeus* is found as most basal titanosauriform, thus further corroborating its non-diplodocoid affinities stated above; and *Brontosaurus excelsus*, together with UW 15556, now form the sister clade to *Apatosaurus ajax* + *Apatosaurus louisae*, which is the same arrangement as seen in the implied weights reduced consensus tree. Synapomorphies found for the union of YPM 1840 and NSMT-PV 20375 are the same as in the main implied weight trees. A constrained search with implied weighting, imposing a sister arrangement of YPM 1840 with YPM 1860 (as found by the equally weighted trees) resulted in a minimal tree length of 188.16879, which corresponds to a relative length increase of 0.1%. Apatosaurine intrarelationships changed considerably: NSMT-PV 20375 was found as sister taxon to YPM 1840 + YPM 1860, and together they formed the sister clade to SMA 0087 + mdA. The specimen AMNH 460 was recovered as most basal apatosaurine. The *Elosaurus parvus* group was pulled out of its relationship with *Brontosaurus excelsus*, and recovered as sister taxon to *Brontosaurus* + mdA, including *Brontosaurus excelsus*, *Brontosaurus amplus*, and *Eobrontosaurus yahnahpin* + FMNH P25112 as successive sister groups to a trichotomy with *Apatosaurus louisae*, *A. laticollis*, and CM 3378. Traits uniting NSMT-PV 20375 with *Apatosaurus ajax* + *'Atlantosaurus' immanis* are the following: 1) cervical vertebrae that are much wider than high (128-2); 2) mid-cervical neural spines that are shorter than the neural arches (168-0); 3) posterior dorsal centra wider than high (269-1); 4) the posterior edge of anterior chevrons expands in a step-like fashion (355-1); 5) an almost right angle between the scapular blade and the coracoid articular surface (361-0); 6) a flat or slightly convex area posterior to the acromial ridge and distal scapular blade (365-1); and 7) dorsoventrally expanded distal ends of the ischia (426-1). The low mid-cervical neural spines would qualify as unambiguous synapomorphy, and the dorsoventrally expanded distal end of the ischium would be unique within Apatosaurinae. All other traits are shared with other apatosaur specimens.

To summarize, concerning the phylogenetic position of YPM 1840, the present study best supports a grouping with NSMT-PV 20375, with or without participation of *Apatosaurus ajax* remains to be seen. These uncertainties, as well as the lacking autapomorphies for the specimen suggest that YPM 1840 has to be treated as undiagnostic, and classified as an indeterminate Apatosaurinae. *'Atlantosaurus' immanis* is thus a nomen dubium. As it has no taxonomic preference, and was usually synonymized with *Apatosaurus ajax*, such a treatment has no influence on apatosaur taxonomy.

***Diplodocus longus* YPM 1920.** This specimen is the most important for the entire taxon Diplodocoidea. Being the type specimen of the type species of the genus defining all names of the higher-level taxonomic units, validity of it is of particular importance. Nonetheless, results obtained herein raise considerable doubts about the diagnosability of the specimen.

Diplodocus longus YPM 1920 consistently groups with the other included specimens of *Diplodocus* in both types of analyses (equal and implied weighting). It is found as sister taxon to *Diplodocus hallorum* in the reduced consensus tree obtained by implied weighting, and is recovered in the same position, when added to the equally weighted reduced consensus tree. In all cases, if the tree also includes one or both specimens of *Diplodocus carnegii* (CM 84 or 94), a polytomy is formed with YPM 1920, the included specimen(s) of *D. carnegii*, and the *D. hallorum* clade. If *D. longus* is excluded, but both *D. carnegii* specimens are added, they form the sister clade to *D. hallorum*. This shows that *D. longus* YPM 1920 switches position between the two specimens of *D. carnegii*, and a position closer to *D. hallorum*, indicating that it is not diagnosable on its own. A single autapomorphy was recovered from the main trees, but considered invalid as it is shared with the *Diplodocus* specimen AMNH 223: presence of a transverse ridge interconnecting the mid-caudal prezygapo-

physeal rami (338-1). Given that no tree recovers this as a synapomorphy for a clade uniting YPM 1920 and AMNH 223 to the exclusion of all other *Diplodocus* specimens, this feature has probably to be interpreted as individual variation. A constrained search uniting these two specimens yielded an equally weighted tree of 1899 steps, and an implied weights tree of 188.14357 steps. Relative length increase thus amounts to 0.11% and 0.09%, respectively.

Although confidently identifiable as belonging to the same genus as the type specimens of *D. carnegii* and *Seismosaurus hallorum*, YPM 1920 does not appear to be diagnosable to the species level. This would mean that *Diplodocus longus* would have to be considered a nomen dubium, and that consequently also the names *Diplodocus*, Diplodocinae, Diplodocidae, and Diplodocoidea would have to be abolished. As *Diplodocus* is probably one of the most iconic dinosaurs, and generally considered to be one of the best known sauropod genera, based on numerous partly to nearly complete skeletons (McIntosh and Carpenter, 1998; Upchurch et al., 2004a), an abolition of these names just for the sake of strictly following ICZN rules is not advisable. A case to ICZN is thus being prepared to suggest the suppression of *D. longus* as type species of *Diplodocus*, and its replacement by *D. carnegii*. *D. carnegii* is typified by the nearly complete, and articulated type specimen CM 84, which includes a complete vertebral column from the second cervical to the twelfth caudal vertebra, as well as articulated fore- and hindlimb material. CM 84 is the most famous specimen of *Diplodocus*, constituting the largest part of the *Diplodocus* cast sent by Andrew Carnegie to various museums around the world in order to promote the activities of the newly founded Carnegie Museum (Nieuwland, 2010). The higher importance of this specimen compared to the holotype specimen of *D. longus*, YPM 1920, is also exemplified by the fact that important studies of diplodocoid interrelationships do not base on personal observations of YPM 1920, but mainly of CM 84 (e.g. Whitlock, 2011a). This shows that even if further studies would reveal YPM 1920 to be diagnosable, and that *D. longus* would therefore be valid, a suppression of the latter species in favor of CM 84 and *D. carnegii* as type for *Diplodocus* would still make sense due to the wider availability for study, as well as the much higher degree of completeness of the specimen. Consequently, and pending a decision on the prepared case to ICZN, it is hereby suggested to use *D. carnegii* as type species for *Diplodocus*. YPM 1920 is considered not diagnostic at species level, and *Diplodocus longus* has therefore to be regarded a nomen dubium. A similar case was announced by Upchurch and Martin (2003) for the substitution of *Cetiosaurus medius* by *C. oxoniensis* as type species, and submitted in 2009 (Upchurch et al., 2009). Their reasoning leading to the case was almost identical to the one presented herein.

***Brontosaurus excelsus* YPM 1980.** Differences between YPM 1980 and *Apatosaurus ajax* YPM 1860 are usually considered not abundant enough to justify generic distinction (Riggs, 1903), leading to a treatment of *Brontosaurus* as junior synonym of *Apatosaurus* (Riggs, 1903; Gilmore, 1936; McIntosh, 1995; Upchurch et al., 2004a, b). The specimen YPM 1980 is the genoholotype of *Brontosaurus*. Where recovered, it always forms the sister taxon to a clade including *Apatosaurus ajax* YPM 1860 and *Apatosaurus louisae* CM 3018.

Four ambiguous autapomorphies are found to be reliable: 1) the tuberculum of mid-dorsal ribs follows the straight direction of the rib shaft (285-1); 2) the posterior end of mid- and posterior caudal spine summits is more or less straight above the postzygapophyses (343-1); 3) presence of a large nutrient foramen at midshaft, anteriorly on the femur (434-1); and 4) presence of a short transverse ridge on the anteromedial surface of the distal end of the tibia (443-1). The last was found to be unique within Diplodocidae. Given the high number of differences with the *Elosaurus* clade, as well as with the *Apatosaurus ajax* clade, generic separation from both of these genera is herein regarded valid. The sum of differences needed for generic separation, as established above, was based on the differences between the European *Dinheirosaurus* and the North American *Supersaurus*, as it was seen that they exceed the sum of differences between species generally considered congeneric (see above). The decision for specific versus generic separation is somewhat arbitrary, in particular in paleontology, where no tests exist for the biological species concept (Carpenter, 2010). If qualitatively assessing the validity and significance of single characters, subjectivity of the interpretation as separate species or genus is even more increased. With a numerical approach as proposed herein, personal influence can be minimized, and the process of generic separation can be rendered more repeatable and thus scientifically sound.

Additional support for generic separation and thus a resurrection of *Brontosaurus* as a valid genus comes from the equally weighted tree, and the position recovered for *Amphicoelias altus* therein. *Amphicoelias altus* was described before any other putative apatosaurine genus (Cope 1877a), and would thus have priority over any genus recovered as sister taxon and considered to pertain to the same genus. In the equally weighted reduced consensus tree, *Amphicoelias altus* + *Eobrontosaurus yahnahpin* form the sister clade to *Apatosaurus ajax* + *Apatosaurus louisae*. When adding *Brontosaurus excelsus* to the tree, a trichotomy is formed between *Brontosaurus*, *Amphicoelias* + *Eobrontosaurus*, and *Apatosaurus*. If *Brontosaurus* would be considered synonymous to *Apatosaurus* in such an arrangement, *Apatosaurus* would have to be synonymized with *Amphicoelias* according to ICZN rules. The specimen YPM 1980 is thus herein considered diagnosable, and distinct enough to justify generic separation from *Apatosaurus*.

***Apatosaurus laticollis* YPM 1861.** Based on a single, fragmentary, mid- to posterior cervical vertebra, this specimen is one of the least complete included in the analysis. McIntosh (1995) suggested it to come from the same individual as YPM 1840, but evidence from two partial femur elements suggest that more than one individual was present in the quarry (McIntosh, 1995). The fact that no tree of the present analysis shows a sister taxon arrangement of YPM 1840 and 1861 casts further doubts on the proposal of McIntosh (1995). *Apatosaurus laticollis* YPM 1861 is herein consistently found as most closely related to *Apatosaurus louisae* CM 3018 and CM 3378. If true, and if YPM 1861 is considered diagnosable, this would indicate that the two species would be synonymous, and that *Apatosaurus laticollis* would therefore have priority over *Apatosaurus louisae*.

One ambiguous autapomorphy is found for *Apatosaurus laticollis* YPM 1861: the lateral edge of the ventral surface of mid- and posterior cervical centra is marked by a deep groove posterior to the parapophysis, extending anteroposteriorly along the edge (177-1). Such a groove is not found in any other apatosaur, thus also not in *A. louisae* CM 3018. As only two traits distinguish *A. laticollis* from *A. louisae*, specific separation cannot be justified, and the two traits are more cautiously interpreted as individual variation, at least in the present species. The fact that the two shared synapomorphies for CM 3018 + CM 3378 (and thus YPM 1861 as well) could not be scored in YPM 1861 indicates that the latter specimen does not exhibit any taxonomically significant character for the species it forms together with CM 3018 and CM 3378.

Forcing *Apatosaurus laticollis* YPM 1861 into close relationship with YPM 1840 (following McIntosh, 1995), recovered tree lengths are 1898 (length increase of 0.05%) with equal weighting, and 188.34011 (relative increase of 0.2%) with implied weighting. In both analyses, YPM 1861 is pulled into the clade where YPM 1840 was found in the unconstrained search. The fact that YPM 1861 readily changes position further indicates that it is not diagnosable to species level, and that *Apatosaurus laticollis* has to be considered a nomen dubium. Pending further detailed studies of the specimens YPM 1840 and 1861, YPM 1861 is herein referred to *Apatosaurus louisae*.

***Brontosaurus amplus* YPM 1981.** *Brontosaurus amplus* YPM 1981 is often considered synonymous to *Brontosaurus excelsus* (McIntosh, 1995; Upchurch et al., 2004b), although mostly stating that further studies are needed in order to assess its taxonomic affinities. The present study does not allow a much more detailed assessment, mostly because of limited personal observations of the specimen due to time constraints during the collection visit at YPM. However, some conclusions can be drawn from the trees recovered. Although not present in the equally weighted reduced consensus tree, addition of the specimen results in a polytomy with *Apatosaurus louisae* + CM 3378, *Eobrontosaurus* + *Amphicoelias*, and *Apatosaurus ajax* + YPM 1840. In the implied weights trees, *Brontosaurus amplus* does not group with *Brontosaurus excelsus*, but with *Apatosaurus louisae*.

Two ambiguous autapomorphies were recovered for YPM 1981: 1) ratio of iliac blade height above pubic peduncle to its anteroposterior length is 0.40 or greater (405-1); and 2) the highest point of the ilium lies anterior to the base of the pubic process (410-1). However, the four changes separating YPM 1981 from *Apatosaurus louisae* do not allow specific separation (see above). Also the polytomy recovered when adding *A. laticollis* to the reduced consensus tree obtained by implied weights indicates that all four specimens (CM 3018, CM 3378, YPM 1861, and YPM 1981) might belong to the same species. More detailed studies of YPM 1981 would be needed in order to confirm presence or absence of the five synapomorphies found for the clade uniting these four specimens.

Although no apatosaurine synapomorphies can be positively identified in YPM 1981 to date, the robust humerus (380-2) and astragalus (452-1) suggest that an identification of *B. amplus* as apatosaur more derived than *Eobrontosaurus* or *Brontosaurus* can be stated with some confidence.

Constraining the search to trees recovering a clade with *Brontosaurus excelsus* and *B. amplus* expulses both *Apatosaurus ajax* and *A. louisae* from the equally weighted reduced consensus tree. Tree length is 1898 steps, and three major clades are recovered within Apatosaurinae: the previously unrecognized combination of FMNH P25112 + (SMA 0087 + AMNH 460) forms the sister taxon to *Elosaurus* + *Brontosaurus*, which include CM 566 + UW 15556, and YPM 1980 + YPM 1981, respectively. When one of the *Apatosaurus* specimens is added, a large polytomy is formed including many diplodocine specimens as well. The same constraint in the implied weights analysis yields trees of a length of 187.98825 steps, which is only 0.01% longer than the most parsimonious trees. Several changes are introduced to apatosaurine interrelationships: SMA 0087 forms a clade together with AMNH 460, *Elosaurus parvus* CM 566 + UW 15556 are separated from *Brontosaurus*, and form the sister clade to *Apatosaurus ajax* + mdA, the two *Brontosaurus* type specimens form the sister group to *Apatosaurus ajax*, together forming the sister clade to *Eobrontosaurus* + (FMNH P25112 + (*Apatosaurus louisae* + CM 3378)). However, no valid synapomorphies unite YPM 1980 with YPM 1981 in that tree, and only one of the four found synapomorphies for the clade uniting them with *Apatosaurus ajax* is found as well in YPM 1981: the presence of a ridge on the ventral side of the third sacral rib (288-1). The latter trait has been proposed by Mook (1917), but regarded as unreliable for species identification within *Apatosaurus* by Upchurch et al. (2004b). Given this, although tree length is not increased much by the current constraint, morphological support for the recovered arrangement appears low. A closer relationship with *Apatosaurus louisae* seems thus better supported by the present analysis, but since YPM 1981 cannot be scored for any of the recovered species autapomorphies, it has to be considered a nomen dubium, pending restudy. It is tentatively referred to *Apatosaurus louisae*.

***Diplodocus lacustris* YPM 1922.** Marsh (1884) established this species based on more slender teeth compared to the ones present in the skull USNM 2672. Whereas this appears to be true (Tab. 6.17), both specimens are within the minimum and maximum values of the teeth of the skull CM 11161, which was only found after Marsh's death (Holland, 1924). The specimen YPM 1922 was found to be the least stable in both main analyses, being mainly responsible for the large polytomy within Diplodocoidea in the complete strict consensus tree.

Given that no characters are known that would allow an identification of diplodocid teeth at species level, and that both the premaxilla and maxilla referred to the type specimen are not diplodocid (see above), the teeth of the holotype specimen YPM 1922 can only be identified as Diplodocidae indet. *D. lacustris* should thus be regarded as a nomen dubium. It is thus also not available as type specimen for the substitution of the suppressed *D. longus* YPM 1920. The choice of *D. carnegii* and CM 84 to typify *Diplodocus* is thus further supported.

***Elosaurus parvus* CM 566.** The specimen CM 566 is a very juvenile individual, as exemplified by its small size and the lacking neurocentral fusion (Peterson and Gilmore, 1902; McIntosh, 1995; Upchurch et al., 2004b; Schwarz et al., 2007c). Until recently, it was generally referred to *Brontosaurus excelsus*, together with the adult specimen UW 15556, with which it was found (Gilmore, 1936; McIntosh, 1995). By means of a specimen-based phylogenetic analysis, Upchurch et al. (2004b) showed that specific separation of CM 566 and UW 15556 from other apatosaur species is justifiable. Recovered autapomorphies for the species were also shown in the juvenile specimen CM 566, leading Upchurch et al. (2004b) to propose the new combination *Apatosaurus parvus*. The present analysis also consistently recovers CM 566 together with UW 15556, and confirms the validity of the species autapomorphies found by Upchurch et al. (2004b), as well as their presence in CM 566. Position in the trees is generally close to the holotype of *Brontosaurus excelsus* (YPM 1980). Whereas at first sight, this might corroborate synonymy of *Elosaurus parvus* with *Brontosaurus excelsus*, the high number of differences between the two taxa not only allows specific, but also generic distinction (see above). *Elosaurus* is thus considered a valid genus, with *Elosaurus parvus* as its type species, and CM 566 as its genoholotype.

***Gigantosaurus africanus* various specimen numbers.** The holotype specimen of *Gigantosaurus africanus* consists of several bones excavated in the first expedition to Tendaguru, Tanzania, now housed at the Staatliches Museum für Naturkunde in Stuttgart, Germany. More elements from the same individual were found later and brought to the Museum für Naturkunde in Berlin, Germany (Remes, 2006). The taxon has a complex taxonomic history: *Gigantosaurus* being preoccupied, it was later renamed *Tornieria* (Sternfeld, 1911), and then synonymized with *Barosaurus* (Janensch, 1922). After a thorough redescription and study of all preserved material, Remes (2006) re-established it as the separate genus *Tornieria*, in the combination *Tornieria africana*, adapting the latinized species name to the female genus. Its generic distinction from *Barosaurus* has been shown to hold in phylogenetic analyses as well (Remes, 2006; Whitlock, 2011a; Mannion et al., 2012). The current study confirms this separation. Skeleton A, from which the holotype material is a part of, consistently clusters with a second specimen referred to the same species by Remes (2006), skeleton k, also from Tendaguru. Both together form a relatively basal clade within Diplodocinae, in many cases the most basal one. Five shared synapomorphies unite the two specimens, although only one of these qualifies as species autapomorphy, as all other four are shared with other diplodocine specimens: the ratio of the pubic articulation of the ischia to the anteroposterior length of the pubic pedicel is 1.5 or greater (420-1). The holotype specimen is thus diagnosable at species level, and *Tornieria africana* a valid species.

***Apatosaurus louisae* CM 3018.** The type specimen of *Apatosaurus louisae* is the most complete type specimen of the entire clade of Apatosaurinae. It is also one of the few diplodocid holotypes which has been decently described and figured (Gilmore, 1936). CM 3018 is thus probably the best known and most used reference specimen for *Apatosaurus*, even though it is not its genoholotype. In the recovered main trees, it consistently groups with CM 3378 and *Apatosaurus laticollis* YPM 1861, with which it forms the sister clade to *Apatosaurus ajax*.

Even though it is so complete, only one ambiguous autapomorphy was found for the single specimen: presence of a pre-epipophysis laterally below the articular facet of anterior caudal prezygapophyses (311-1). This indicates that the other specimens grouping with CM 3018 belong to the same species. As *A. laticollis* is herein considered a nomen dubium, the only available species name for this group is *Apatosaurus louisae*, as initially proposed for CM 3018 (Holland, 1915a). The specimen CM 3018 shows all the five synapomorphies found for the clade with CM 3018, CM 3378, YPM 1861, and YPM 1981 (see above). Of these, three qualify as valid autapomorphies for the species, not shared with any other apatosaur specimen (see updated diagnosis below). Following the numerical approach, generic separation from *Apatosaurus ajax* is not justified, corroborating all previous referrals of CM 3018 to *Apatosaurus*, as *Apatosaurus louisae*.

***Apatosaurus minimus* AMNH 675.** *Apatosaurus minimus* was described by Mook (1917), based on a sacrum and pelvic girdle. The specimen has generally been considered misidentified, and its diplodocoid affinities rejected (McIntosh, 1995; Upchurch et al., 2004b). Whereas pubis morphology strongly resembles *Camarasaurus*, the presence of six sacral vertebrae and widely splayed preacetabular lobes of the ilium are generally considered titanosauriform characteristics (McIntosh, 1990a; Upchurch et al., 2004a, b). Due to its incompleteness, the true identity of AMNH 675 still remains dubious. Other than confirming the non-flagellicaudatan (and probably non-diplodocoid) affinities of AMNH 675, the present study does not help much in resolving this issue. Whereas the equally weighted trees recovered AMNH 675 as one of the six most unstable taxa (thus deleted from the pruned consensus), implied weighting resolves AMNH 675 as somphospondylian titanosauriform, based on the two characteristics mentioned above. The three autapomorphies found for the specimen indicate that AMNH 675 probably shows a unique combination of features. Addition of AMNH 675 to the equally weighted reduced consensus tree results in a polytomy with *Cetiosauriscus stewarti*, SMA 0009, AMNH 5765, Titanosauriformes, Camarasaurus + Turiasauria, Rebbachisauridae, and Flagellicaudata.

Forcing *A. minimus* AMNH 675 into a titanosauriform position in the equally weighted analysis results in a tree three steps longer than the most parsimonious tree. *Dystrophaeus* is pulled into Titanosauriformes as well, and *Australodocus* is recovered as basal-most Diplodocinae. The same tree length is found when imposing apatosaurine affinities, with a completely unresolved clade as result.

Camarasaurid affinities are much more probable, given that a forcing into this group yields the same tree length as the equally weighted most parsimonious trees (1897 steps). Furthermore, also the presence of six sacral vertebrae has already been reported in a camarasaur (Tidwell et al., 2005), and was interpreted as an ontogenetic feature. Tree length of the implied weight trees increase to 188.23185 steps, or by a percentage of 0.14%, when restricting AMNH 675 to Apatosaurinae (where it grouped with *Dystrophaeus* and *Elosaurus*), and to 188.18066 (0.11%) when forcing it into Camarasauridae. Camarasaurid or titanosauriform affinities are thus the most probable for AMNH 675, but more detailed studies of those clades are needed in order to identify AMNH 675 properly.

***Diplodocus hayi* HMNS 175.** Described by Holland (1924) as *Diplodocus hayi*, HMNS 175 (initially CM 662) was often thought not to belong to *Diplodocus* (e.g. McIntosh, 1990b; Foster, 1998; Harris, 2006c), due to its relatively robust forelimbs, and the widely diverging basipterygoid processes – both traits that are generally interpreted to diagnose apatosaurs (Berman and McIntosh, 1978; McIntosh, 1990a; Upchurch et al., 2004a). The specimen HMNS 175 is one of the most complete specimens known from Diplodocinae, but has never been completely described. It preserves cranial material, cervical, dorsal, sacral, and caudal vertebrae, as well as a nearly complete forelimb and hindlimb (McIntosh, 1981; pers. obs.). The current analysis supports a generic separation from *Diplodocus*, as HMNS 175 consistently results in a clade more basal to *Diplodocus*, together with the specimens AMNH 969 and SMA 0011.

Autapomorphies for HMNS 175 amount to four, one of which unique within Diplodocidae, and a second one within Diplodocoidea: 1) dorsoventral height of the parietal occipital process is low, subequal to less than the diameter of the foramen magnum (63-0, shared with apatosaurs); 2) an ulna to humerus length of more than 0.76 (387-2, unique within Diplodocoidea); 3) distal articular surface for the ulna on the radius is reduced and relatively smooth (392-0, unique within Diplodocidae); and 4) the distal condyle of the radius is beveled at least 15° to the long axis of the shaft (393-1, shared with *Apatosaurus louisae* and *Eobrontosaurus yahnahpin*).

Forcing '*Diplodocus*' *hayi* HMNS 175 to group with the classical *Diplodocus* specimens, equally weighted analysis recovers shortest trees of 1904 steps, a length increase of seven steps of 0.37% compared to the unconstrained most parsimonious trees. Applying implied weights, tree length counts 188.70122 steps, corresponding to a relative increase of 0.39%. A generic separation from *Diplodocus* is thus well-supported. The specimen HMNS 175 is therefore regarded the type specimen of the species *Galeamopus hayi*, a diplodocine sauropod less derived than *Diplodocus*, *Kaatedocus*, and *Barosaurus*.

'*Apatosaurus*' *alenquerensis* MIGM various numbers (lectotype). As *Tornieria africana*, also '*Apatosaurus*' *alenquerensis* has had a complicated taxonomic history. After being referred to *Camarasaurus* (McIntosh, 1990b), Dantas et al. (1998) erected the new genus *Lourinhasaurus* for a number of specimens thought to belong to the same species. No specific type specimen was attributed to the name (only a skeleton was mentioned without specimen number; Dantas et al., 1998), until Antunes and Mateus (2003) established the first specimen found at Moinho do Carmo, Alenquer, Lourinhã, as lectotype specimen. In the meantime, the specimen on which Dantas et al. (1998) made most observations of differences between *Lourinhasaurus* and *Camarasaurus* was redescribed and referred to a new species and genus, *Dinheirosaurus lourinhanensis* (Bonaparte and Mateus, 1999). Even so, *Lourinhasaurus* remained accepted, and its generic separation subsequently justified by means of phylogenetic analyses, which did not recover the lectotype specimen in a position close to *Camarasaurus* or *Apatosaurus* (e.g. Upchurch et al., 2004a; Royo-Torres and Upchurch, 2012).

Two ambiguous autapomorphies are found to diagnose *Lourinhasaurus*: 1) the subtriangular projection on the ventral edge of the scapular blade, close to the acromion (370-1); and 2) the dorsoventrally expanded distal ends of the ischia (426-1). The fact that *Lourinhasaurus* consistently forms its own clade in any recovered tree indicates that it also exhibits a unique combination of traits. The lectotype specimen is thus considered diagnostic, and *Lourinhasaurus alenquerensis* valid.

Forcing *Lourinhasaurus* into the Camarasauridae clade, equal weighting results in a tree only one step longer than the most parsimonious trees. *Lourinhasaurus* is found to be in the turiasaur clade, not supported by any synapomorphy. Implied weighting recovers *Lourinhasaurus* basal to *Camarasaurus* + Turiasauria, with a tree length of 188.03513, an increase of 0.03%. A close

relationship with *Camarasaurus* can thus not be excluded, although generic separation is probably warranted. Although the precise phylogenetic position of *Lourinhasaurus* cannot be resolved herein, a position at the base of Neosauropoda appears the most supported.

***Cetiosauriscus stewarti* NHMUK R3078.** Phylogenetic position of *Cetiosauriscus stewarti* has been debated (Charig, 1980; McIntosh, 1990b; Heathcote and Upchurch, 2003; Upchurch et al., 2004a). Diplodocid affinities were purported several times (Charig, 1980; McIntosh, 1990b; Upchurch et al., 2004a), but mostly based on a second specimen containing a whip-lash tail, which has no overlapping bones with the holotype (Heathcote and Upchurch, 2003; Upchurch et al., 2004a). Diplodocid affinities of the holotype specimen are thus questionable, and consequently, a closer relationship to *Mamenchisaurus* or *Omeisaurus* was found by Heathcote and Upchurch (2003). The current analysis recovers NHMUK R3078 in two different positions depending on the weighting strategy applied. Equal weighting yields diplodocimorph affinities, more derived than Rebbachisauridae, whereas implied weighting recovers NHMUK R3078 as non-neosauropod eusauropod, close to *Mamenchisaurus* or *Omeisaurus* as proposed by Heathcote and Upchurch (2003).

No autapomorphies were found by the implied weights analysis, probably due to the sister relationship with *Barosaurus affinis* YPM 419. The incompleteness of the latter find inhibited the recovery of autapomorphies in its sister taxon *Cetiosauriscus*, as for many features the two specimens are not comparable. However, the recovered autapomorphies from the equally weighted trees were assessed in two ways, and their validity was tested based on both diplodocoid as well as non-neosauropod eusauropod affinities. Three traits qualified as ambiguous autapomorphy in both cases: 1) the gracility of the femur (427-0, shared with *Amphicoelias*, *Ligabuesaurus*, *Shunosaurus*, and USNM 10865); 2) the presence of foramina on the dorsal surface of metatarsal I (459-1, shared with some flagellicaudatans and *Camarasaurus grandis*); and 3) a rhomboid proximal articular surface of metatarsal V (471-1, shared with *Galeamopus hayi*, *Barosaurus affinis*, and NSMT-PV 20375). The fact that autapomorphies were found reliable independent from the phylogenetic position indicates that NHMUK R3078 is diagnosable, and *Cetiosauriscus stewarti* thus valid.

Imposing a sister arrangement of *Cetiosauriscus* and *Barosaurus affinis* YPM 419 in the equally weighted tree does not increase length, nor influence the position of *Cetiosauriscus*. Forced sister arrangements with *Omeisaurus* and *Mamenchisaurus* produced tree lengths of 1900 and 1903 steps or length increases of 0.16% and 0.32%, respectively. When forcing *Cetiosauriscus* into Apatosaurinae or Diplodocinae with implied weighting, tree lengths of 188.80886 or 189.29031 steps are recovered (length increase of 0.45% or 0.7%). Imposing dicraeosaurid or rebbachisaurid affinities results in tree lengths of 188.72199 or 188.99738, corresponding to an increase of 0.4% or 0.55%. Changing the position from diplodocoid to non-neosauropod eusauropod in the equally weighted tree (in particular close to *Omeisaurus*) appears thus more easy than imposing diplodocoid affinities of *Cetiosauriscus* in the implied weights analysis. *Cetiosauriscus stewarti* is thus herein interpreted as non-diplodocoid eusauropod, possibly closely related to *Omeisaurus*, as already proposed by Heathcote and Upchurch (2003).

***Supersaurus vivianae* BYU 12962.** The holotype specimen of *Supersaurus vivianae* is restricted to a scapula (Jensen, 1985), but other elements from the same quarry most probably belong to the same individual (Curtice and Stadtman, 2001; Lovelace et al., 2007). A scapula is not present in the second specimen referred to *Supersaurus vivianae* by Lovelace et al. (2007; WDC DMJ-021), which inhibited recognition of autapomorphies on the scapula by TNT. However, the fact that both referred specimens consistently group together in all trees indicates that identification of additional elements as belonging to the same individual as the type specimen (Curtice and Stadtman, 2001; Lovelace et al., 2007) was right. Even though the holotype might not be diagnostic, the individual it is part of definitely is.

No valid autapomorphies separate the type individual from the second specimen, WDC DMJ-021, indicating that they belong to the same species. Of the seven traits uniting the two specimens, only three can be considered valid autapomorphies for the species, as the other four also occur in other diplodocine specimens. The three species autapomorphies are: 1) spinoprezygapophyseal laminae of single (not bifid) dorsal neural spines are separate along their entire length (231-0, unique within Diplodocoidea); 2) 'heart'-shaped anterior-most caudal centra (296-1, unique within Diplodocinae); and 3) pneumatopores of anterior caudal centra are restricted to foramina (307-0, unique within

Diplodocinae).

Supersaurus vivianae forms a clade together with *Dinheirosaurus* when applying equal weighting, whereas implied weighting recovers it together with *Australodocus*, in a position more basal to *Dinheirosaurus*, and even *Tornieria*. The fact that trees excluding *Australodocus* a priori, or restricting it to Titanosauriformes, show *Supersaurus* again as sister taxon to *Dinheirosaurus*, in its more derived position, indicates that the change is mainly due to the instability of *Australodocus*. Furthermore, when restricting *Supersaurus* to *Dinheirosaurus* in the implied weights trees, *Australodocus* is pushed into Titanosauriformes. Tree length in this case is 188.02344, which is even shorter than the trees recovered when forcing *Australodocus* directly into Titanosauriformes (188.09844). The former tree length equals a length increase of 0.03%, which corresponds to less than a one-step increase in the equally weighted trees. The position more derived than *Tornieria* appears thus better supported by the present analysis, even though this is contrary to the findings of Whitlock (2011a), Mannion et al. (2012), or Tschopp and Mateus (in press).

***Dystylosaurus edwini* BYU 4503.** The holotype specimen of *Dystylosaurus edwini* was previously proposed to belong to the same individual as the *Supersaurus vivianae* holotype scapula (Curtice and Stadtman, 2001), a view supported by Lovelace et al. (2007), as well as preliminary analyses of the present study (see above). Therefore, *Dystylosaurus edwini* is herein considered a junior synonym of *Supersaurus vivianae*. Its type specimen BYU 4503 has thus not been included in the final analysis as separate slot, but was incorporated into the OTU called *Supersaurus vivianae* BYU+.

***Seismosaurus halli* NMMNH 3690.** Gillette (1991) named this new genus based on the specimen NMMNH 3690, and later changed to species name to *hallorum*, in order to correct it for wrongly applied latin grammar (Gillette, 1994). *Seismosaurus* was later synonymized with *Diplodocus* (Lucas et al., 2006; Lovelace et al., 2007), with uncertainties if it can be retained as separate species or if it should be regarded synonymous to *Diplodocus longus* (Lovelace et al., 2007). The latter statement was most probably based on previous identifications of the more complete specimens AMNH 223 and USNM 10865 as *Diplodocus longus* (Osborn, 1899; Gilmore, 1932), which was herein showed to be erroneous, or at least questionable. *Seismosaurus hallorum* NMMNH 3690 is consistently recovered in a group with AMNH 223, USNM 10865, and DMNS 1494, which has been shown to constitute its own species. Showing four of the six shared traits of the group, *Seismosaurus hallorum* NMMNH 3690 can be considered diagnostic. As it is the only type specimen in this cluster, and since the number of changes does not allow generic separation (see above), *Diplodocus hallorum* is the only valid, available name for this taxon.

***Dyslocosaurus polyonychius* AC 663.** Being based on very fragmentary appendicular material, assessment of the phylogenetic position is difficult for this taxon. Although initially described as diplodocid (McIntosh et al., 1992), the high number of probable pedal unguals resembles basal sauropods, as the loss of pedal phalanges and unguals is usually considered typical for Eusauropoda and more derived forms (Wilson, 2002; Upchurch et al., 2004a). However, almost no complete and articulated pes is known from any diplodocid, and of the included specimens, only few preserve pedal material. A positive confirmation of the absence of vestigial phalanges or unguals is very difficult, if not impossible. The true distribution of a high number of pedal phalanges can thus not be assessed with the present analysis.

Although reduced consensus trees omit *Dyslocosaurus polyonychius*, both pruned trees find it as dicraeosaurid. Five synapomorphies found for Dicraeosauridae are present in *Dyslocosaurus*, but four of them are only shared with one other dicraeosaurid taxon: 1) position of highest point of the femoral head is laterally shifted in anterior view, lying above the main portion of the shaft (431-1, shared with *Dicraeosaurus*); 2) presence of a short transverse ridge on the anteromedial surface of the distal end of the tibia (443-1, shared with *Dicraeosaurus*); 3) mediolateral width to maximum anteroposterior length in the astragalus is less than 1.6 (452-1, shared with *Dicraeosaurus*); 4) a gracile metatarsal I (461-0, shared with *Dicraeosaurus* and *Suuwassea*); and 5) a straight horizontal groove on the lateral surface of pedal unguals (477-1, shared with *Suuwassea*). None of these traits could be coded in *Amargasaurus* or *Brachytrachelopan*, and all of them are also present in certain diplodocid taxa. If *Dyslocosaurus* should not be a dicraeosaurid, only the gracility of the metatarsal I would possibly

remain as dicraeosaurid synapomorphy, pending further finds of dicraeosaurid hindlimb material.

Five ambiguous autapomorphies are found for AC 663 when considered a dicraeosaurid: 1) a subtriangular proximal articular surface of the tibia (442-1); 2) the lateral edge of the proximal end of the tibia forms a pinched out projection, posterior to the cnemial crest (the 'second cnemial crest' of Bonaparte et al., 2000) (446-0); 3) an elongate and narrow dorsomedial corner of the astragalus, in posterior view (456-1); 4) a well-developed rugosity on the dorsolateral margin of the metatarsal II near its distal end, extending to the center of the shaft (468-1); and 5) a subtriangular proximal articular surface of the metatarsal IV (470-1). Three of these autapomorphies are shared with apatosaur specimens (442-1, 468-1, 470-1), four also occur in diplodocines (442-1, 446-0, 456-1, 468-1). The fact that this specimen appears to unite apatosaur, diplodocine, and dicraeosaurid traits indicates that AC 663 – even though highly incomplete – is diagnostic, and *Dyslocosaurus polyonychius* thus a valid taxon.

Forcing *Dyslocosaurus* into a position within Apatosaurinae produced shortest trees of a length of 1902 (equal weighting) and 188.17813 (implied weighting) steps, an increase of 0.26% and 0.11%, respectively. When imposing diplodocine affinities, tree lengths of 1910 and 189.51146 steps are recovered, corresponding to length increases of 0.69% and 0.82%. Diplodocine affinities are thus the least parsimonious, followed by an identification as Apatosaurinae, which still appears improbable. Despite the shared characters with both diplodocid clades, an identification of *Dyslocosaurus* as dicraeosaurid diplodocoid is considerably better supported.

***Apatosaurus yahnahpin* Tate-001.** *Apatosaurus yahnahpin* Tate-001 has later been renamed *Eobrontosaurus yahnahpin* (Bakker, 1998), but it was never included in any phylogenetic analysis, and no detailed description has yet been published. Based on purportedly primitive conditions in the pectoral girdle and the cervical ribs, Bakker (1998) interpreted *Eobrontosaurus* as the basal-most apatosaurine. Upchurch et al. (2004a) stated that the specimen Tate-001 is practically indistinguishable from *Camarasaurus*, but personal comments of R. Wilhite (cited in Taylor et al., 2011) and P. Mannion (2012) implied that the taxon might be a valid diplodocid. The present analysis confirms the result of Bakker (1998): Tate-001 is consistently recovered as apatosaurine diplodocid. Whereas it forms the sister taxon to *Amphicoelias altus* in the equally weighted tree, its position within the clade is less clear when applying implied weighting: *Eobrontosaurus yahnahpin* is found as sister taxon to *Apatosaurus ajax* + mdA in the main trees, whereas an a priori deletion of *Australodocus*, or its forced titanosaurid affinities, result in a more basal position of *E. yahnahpin*, as sister taxon to AMNH 460 + mdA.

Eight ambiguous autapomorphies are considered valid for Tate-001: 1) presence of a longitudinal sulcus on the ventral surface of cervical vertebrae (133-1); 2) total height of anterior cervical vertebrae to centrum length ratio is greater than 1.2 (usually around 1.5) (154-2); 3) the medial surface of anterior dorsal, bifid neural spines is gently rounded transversely (245-0); 4) mid- and posterior dorsal neural spines narrow dorsally to form a triangular shape in lateral view, with the base approximately twice the width of the dorsal tip (265-1); 5) absence of a thickened anterior rim of anterior caudal prespinal lamina (321-0); 6) a rounded anteroventral margin of the coracoid (372-0); 7) a ratio of the longest metacarpal to radius length of 0.40 or greater (399-1); and 8) the distal articular surface of the metatarsal I being perpendicular to the axis of the shaft (462-1). Whereas this already justifies specific separation, support for generic separation depends on the position where it is recovered (see above). The least support for generic distinction is found if recovered as sister taxon to *Amphicoelias* (five changes), followed by the tree without *Australodocus* (nine changes). As *Amphicoelias* is more parsimoniously considered the basal-most diplodocid genus, instead of an Apatosaurinae, distance between *Eobrontosaurus* and its sister clade *Apatosaurus ajax* + mdA in the equally weighted tree increases to 16. Given that it is generally found as single slot, *Eobrontosaurus* is herein accepted as valid genus within Apatosaurinae.

Forcing *Eobrontosaurus* to lie outside AMNH 460 + mdA in the implied weight trees resulted in tree lengths of 188.00659 steps, an increase of 0.02%. Position of *Eobrontosaurus* is thus not very clear to date, and has to await publication of the promised detailed description (see above).

***Dinheirosaurus lourinhanensis* ML 414.** *Dinheirosaurus lourinhanensis* ML 414 was first described as *Lourinhasaurus alenquerensis* (Dantas et al., 1998), but a more detailed redescription showed that it

constitutes its own genus within Diplodocidae (Bonaparte and Mateus, 1999). Such a position was later confirmed by phylogenetic analyses, and refined to Diplodocinae (Rauhut et al., 2005; Whitlock, 2011a; Mannion et al., 2012). The present analysis supports this assignment, but recovered *Dinheirosaurus* in an even more derived position than Whitlock (2011a) or Mannion et al. (2012). Both analyses find *Dinheirosaurus* in a position within Diplodocinae, more derived than *Tornieria*. Differences occur in the relative position of *Supersaurus*, although a position as sister genus of *Dinheirosaurus* appears more probable, as discussed above.

Four ambiguous autapomorphies are found for ML 414, and thus for *Dinheirosaurus lourinhanensis*: 1) single posterior cervical and anterior dorsal neural spines (126-0, unique within Flagellicaudata); 2) ventral keel is restricted to the posterior portion of the posterior cervical centrum (193-1, unique within Flagellicaudata); 3) dorsal transverse processes more than 30° inclined dorsally from the horizontal (230-1, unique within Diplodocidae); and 4) the ventral surface of anterior caudal centra is without irregularly placed foramina (305-0, unique within Flagellicaudata). The ten changes found between *Dinheirosaurus* and *Supersaurus* or (in the case of a more basal position of the latter) *Galeamopus* + mdD are considered enough to justify generic separation, especially given that *Dinheirosaurus* is a Portuguese taxon, and thus also geographically separated from its closest relatives.

***Losillasaurus giganteus* MCNV Lo-5.** Whereas the holotype is restricted to an anterior caudal vertebrae, it actually belongs to a more complete individual (Casanovas et al., 2001) and was included as such in the present analysis. Initially regarded a basal diplodocoid (Casanovas et al., 2001), *Losillasaurus* was soon found to represent a non-diplodocoid, probably non-neosauropod eusauropod (Rauhut et al., 2005; Harris, 2006c). With the description of *Turiasaurus* (Royo-Torres et al., 2006), which has since been consistently recovered as sister genus to *Losillasaurus* (Royo-Torres et al., 2006, 2009; Barco, 2009; Carballido et al., 2012b; Royo-Torres and Upchurch, 2012), the more basal position has been generally accepted. The present study supports this view as well.

Two ambiguous autapomorphies are found: 1) presence of an infradiapophyseal pneumatopore between the acdl and the pcdl in mid- and posterior dorsal neural arches (262-1); and 2) a low ulna to humerus length ratio of less than 0.65 (387-0). Despite the low number of autapomorphies, the numerical approach is not applied here, as non-diplodocid OTUs have not been sampled with enough detail to apply the same standards as established for Diplodocidae. *Losillasaurus* is thus considered herein a valid, non-diplodocoid genus, probably a non-neosauropod eusauropod.

***Suuwassea emilieae* ANS 21122.** *Suuwassea emilieae* was initially described as indeterminate flagellicaudatan (Harris and Dodson, 2004). Whereas earlier studies showed more diplodocid affinities (Gallina and Apesteguia, 2005; Rauhut et al., 2005; Remes, 2006; Lovelace et al., 2007), the discovery of the dentary of the holotype specimen (Whitlock and Harris, 2010) subsequently resulted in an identification as dicraeosaurid (Whitlock, 2011a; Mannion et al., 2012; Tschopp and Mateus, 2012b). The present analysis supports the latter assignment: *Suuwassea emilieae* ANS 21122 is consistently found as basal-most dicraeosaurid sauropod.

Suuwassea emilieae ANS 21122 is herein diagnosed by 35 ambiguous autapomorphies: 1) the dorsal edge of the posterolateral process of the parietal is straight in posterior view, and ventrolaterally oriented, such that the supratemporal fenestra is slightly facing posteriorly as well (62-0); 2) a straight anterodorsal margin of the supraoccipital (72-1); 3) a slightly concave posterior face of the basal tubera (85-2); 4) a foramen in the notch that separates the two basal tubera (90-1); 5) an unpaired optic foramen (100-1); 6) nine or fewer dentary teeth (114-2); 7) a small fossa is present on the posteroventral corner of cervical vertebrae centra (131-1); 8) the posterior edge of the anterior condyle of anterior cervical vertebrae is posteriorly inclined (156-1); 9) the pleurocoel of anterior cervical vertebrae does not extend onto the dorsal surface of the parapophysis (158-1); 10) an intermediate elongation of mid-cervical centra; 11) an acute angle between the postzygodiapophyseal and spinopostzygapophyseal laminae of mid-cervical vertebrae (170-0); 12) absence of a longitudinal ridge on the ventral surface of mid- and posterior cervical vertebrae (174-1); 13) a continuous , single, ventrolateral edge of mid- and posterior cervical centra, posterior to the parapophysis (170-0); 14) a pre-epipophysis in mid- and posterior cervical vertebrae (181-1); 15) the interpostzygapophyseal lamina of mid- and posterior cervical neural arches projects beyond the posterior margin of the neural arch (190-1); 16) a prespinal lamina in posterior cervical and anterior dorsal vertebrae (209-1); 17) the

tuberculum of anterior and mid-cervical ribs is directed upwards and backwards (218-1); 18) dorsal centrum length (excluding articular 'ball') shortens from anterior to posterior dorsal vertebrae (225-1); 19) dorsal pneumatopores (227-1); 20) dorsal centra with simple and big air spaces internally (228-1); 21) dorsal transverse processes horizontal or only slightly inclined dorsally (230-0); 22) a ventral keel in anterior dorsal vertebrae (242-1); 23) the parapophysis of DV 3 lies at the top of the centrum (246-0); 24) 'heart'-shaped anterior-most caudal centra (296-1); 25) length of anterior caudal centra more or less doubling over first 20 (309-1); 26) elongate mid-caudal centra (332-1); 27) platycoelous distal-most caudal centra (346-0); 28) an angle between the scapular acromial ridge and the distal blade of 70°-81° (362-1); 29) the area posterior to the scapular acromial ridge and the distal blade is flat or slightly convex (365-1); 30) the acromial edge of the scapular blade has a rounded expansion at its distal end (367-1); 31) a very robust humerus (380-2); 32) an anteroposteriorly compressed proximal articulation surface of the tibia (441-1); 33) the posterior surface of the cnemial crest of the tibia bears a distinct fibular trochanter (445-1); 34) the dorsal surface of mt I is pierced by several foramina (459-1); and 35) a concave lateral margin of mt II in proximal view (467-0).

The high number of autapomorphies for *Suuwassea emilieae* reflect not only its diagnosability, but also the fact that the main dicraeosaurid OTUs were not studied in the same detail as the diplodocid sauropods. Given that the majority of the found autapomorphies are shared with certain diplodocid specimens, the difficulties in determining its dicraeosaurid affinities are not surprising. However, forcing *Suuwassea* into an apatosaurine clade (as found by Lovelace et al., 2007) yields trees of 1907 or 189.58814 steps (relative length increases of 0.53% and 0.86%, respectively). Diplodocine relationships are found in shortest trees of 1903 and 189.21056 steps, corresponding to increases in tree length of 0.32% and 0.66%. Apatosaurine or diplodocine affinities are thus much less parsimonious than an identification as dicraeosaurid.

***Australodocus bohetii* MB.R.2455.** Whereas the holotype only includes the single cervical vertebra MB.R.2455, a second, probably adjacent cervical vertebrae most probably belongs to the same animal (MB.R.2454; Remes, 2007). *Australodocus* was first described as diplodocid (Remes, 2007), but later found to represent a titanosauriform (Whitlock, 2011a, c; Mannion et al., 2012, 2013). The present analysis shows ambiguous results, with the equal weights analysis recovering it as brachiosaurid titanosauriform, but implied weighting finding diplodocine affinities. The incompleteness of the type individual complicates the recovery of a stable position for *Australodocus*.

Of the autapomorphies recovered for *Australodocus*, only two were found by both analyses: 1) mid-cervical pre-epipophyses project considerably anterior to the prezygapophyseal facet, forming a distinct spur (167-1); and 2) absence of a longitudinal ridge on the ventral surface of mid- and posterior cervical vertebrae (174-1). Both of these autapomorphies are shared with diplodocine specimens. In general, autapomorphies recovered for a brachiosaurid position are shared with diplodocines, and autapomorphies found for a diplodocine position with titanosauriforms. This indicates that the combination of traits is unique in *Australodocus*, which is thus regarded valid.

As mentioned in the discussion of *Supersaurus*, *Australodocus* pulls the former genus into a more basal position in the main implied weight trees. When forcing *Supersaurus* into a monophyletic group with *Dinheirosaurus*, *Australodocus* is recovered again as a brachiosaurid titanosauriform. The latter constrained search produced shortest trees of 188.02344 (a 0.03% length increase), whereas diplodocine affinities for *Australodocus* in the equally weighted trees finds trees of a length of 1898 steps, one more compared to the most parsimonious trees (an increase of 0.05%). In this case, however, *Supersaurus* remains united with *Dinheirosaurus*, instead of grouping with *Australodocus* as in the most parsimonious implied weight trees. The low number of titanosauriform OTUs in the present specimen lowers the capability of the analysis to recover *Australodocus* as belonging to that taxon, such that convergences found with Diplodocinae tend to get more important. Given that *Australodocus* is still recovered as titanosauriform in many trees, and that relative tree length increase to impose diplodocine affinities is slightly higher than the inverse direction in the implied weight trees, indicates that an identification as titanosauriform is more probable. Addition of titanosauriform specimens preserving cervical vertebrae would help to resolve this problem, but is not the scope of this analysis.

***Kaatedocus siberi* SMA 0004.** *Kaatedocus siberi* was initially described as diplodocine less derived than *Tornieria*, *Diplodocus*, and *Barosaurus* (Tschopp and Mateus, 2012b). In the present analysis, *Kaatedocus* is consistently recovered in a more derived position, as sister taxon to *Barosaurus lentus*.

The type specimen SMA 0004 bears one ambiguous autapomorphy: the posteroventral face of the basal tubera is marked by a distinct transverse ridge (86-1). As no synapomorphy was found for the sister clade AMNH 7530 + SMA D16-3, only one change separates SMA 0004 from the latter. The presence of such a transverse ridge is thus better interpreted as individual variation. Four of the nine synapomorphies found for the entire group of *Kaatedocus siberi* also qualify as species autapomorphies, not shared with other diplodocine specimens: 1) mid- and posterior cervical centra with a rugose tuberosity on the anterodorsal corner of the lateral side (178-1, unique within Diplodocidae); 2) the posterior cervical epipophyses are dorsoventrally compressed (202-1, unique within Flagellicaudata); 3) the posterior cervical and anterior dorsal bifid neural spines are parallel to converging (211-1, unique within Diplodocidae); and 4) the distance between the spine summits of posterior cervical and anterior dorsal bifid neural spines is subequal to the neural canal width (212-1, unique within Diplodocidae).

***Galeamopus shellensis* SMA 0011.** *Galeamopus shellensis* is herein reported and described for the first time and thus no comparisons with earlier studies exist. The holotype specimen SMA 0011 consistently groups with the holotype of *Galeamopus hayi*, HMNS 175, and the skull previously identified as *Diplodocus*, AMNH 969 (Holland, 1906).

The specimen SMA 0011 shows four ambiguous and three unambiguous autapomorphies, justifying specific separation from *Galeamopus hayi*: 1) horizontal canal connecting the preantorbital and the antorbital fenestra laterally on the maxilla (12-1, unambiguous; not recovered by the analysis, as the state in AMNH 969 or HMNS 175 cannot be discerned due to incomplete preservation. The trait could thus also be diagnostic for a more inclusive taxon, possibly the genus *Galeamopus*); 2) total height to centrum length ratio in anterior cervical vertebrae greater than 1.2 (usually around 1.5) (154-2, unique within Diplodocinae); 3) mid- and posterior cervical vertebrae with a large foramen connecting the postzygapophyseal centrodiapophyseal fossa and the spinopostzygapophyseal fossa (191-1, unambiguous); 4) a robust humerus (380-2, unique within Diplodocinae); 5) absence of a shallow, but distinct rugose tubercle at the center of the concave proximal portion of the anterior surface of the humerus (386-0, unique within Diplodocinae); and 6) the maximum diameter of the proximal end of the radius divided by its greatest length equals 0.3 or greater (391-1, unique within Diplodocinae).

Taxonomic affinities and identification of diplodocid non-type specimens

AMNH 223. Described as *Diplodocus longus* (Osborn, 1899), AMNH 223 readily became the mostly used reference specimen for this species (Hatcher, 1901; Gilmore, 1932). However, the present analysis does not recover AMNH 223 together with the holotype specimen YPM 1920, but as most basal OTU of a clade including the holotype of *Seismosaurus hallorum*.

Two ambiguous autapomorphies are found for this specimen: 1) scapular length to minimum blade breadth equals 5.5 or less (359-1); and 2) the scapula bears a semi-ovate, flat muscle scar just distal to the glenoid on the scapular shaft (369-1). The fact that only one of the other three specimens in the same clade preserves a scapula, and the low number of differences between AMNH 223 and the remaining triplet, indicates that these might represent individual variation, and that AMNH 223 is most parsimoniously identified as belonging to the same species, which would be *Diplodocus hallorum*.

AMNH 460. The specimen AMNH 460 has never been described, but was included in the specimen-level phylogenetic analysis of Upchurch et al. (2004b). In the latter, it has been identified as *Apatosaurus ajax*, which is not supported by the most parsimonious trees of the present analysis. In the equally weighted pruned tree, AMNH 460 is pulled outside Apatosaurinae due to unresolved relationships of SMA 0087 and WDC-FS001A. When applying implied weights, AMNH 460 is found within Apatosaurinae, as single slot between YPM 1840 + NSMT-PV 20375 and SMA 0087 + WDC-FS001A. When excluding *Australodocus* from Diplodocidae, AMNH 460 changes position within Apatosaurinae, and forms the sister taxon to *Brontosaurus* + *Apatosaurus*, still as single slot. The

found positions would imply that AMNH 460 represent a different taxon, but the fact that no found autapomorphy is unique within Apatosaurinae makes such an assignment questionable.

A constrained search forcing AMNH 460 into the clade including *Apatosaurus ajax* YPM 1860 yielded trees of a length of 1902 or 188.54847 steps, corresponding to relative length increases of 0.26% or 0.31%. AMNH 460 continues to be found as a single slot, more basal to *Apatosaurus ajax* YPM 1860. Imposed brontosaur affinities for AMNH 460 result in tree lengths of 1903 and 188.31076 steps, or relative increases of 0.32% and 0.18%. A sister clade arrangement with *Eobrontosaurus* produces tree lengths of 1900 and 188.10509 steps, relative increases of 0.16% and 0.07%. In both cases, the pair is recovered basal to the clade *Brontosaurus* + mdA. When forced into a triplet with SMA 0087 and WDC-FS001A, tree length stayed the same (1897) or increased by 0.01%, to 187.98825 steps. Equal weighting finds trees of 1903 steps (0.32% longer) if constrained by a unity of AMNH 460 with NSMT-PV 20375, whereas implied weighting results in trees 0.05% longer (188.06943 steps) if constraining the triplet AMNH 460, NSMT-PV 20375, and YPM 1840. A closer relationship with the specimens SMA 0087 and WDC-FS001A can thus not be excluded by the present analysis. Such a triplet would be supported by the following three ambiguous synapomorphies: 1) posterior dorsal centra longer than high (268-0, unique within Apatosaurinae); 2) a widely rounded cnemial crest of the tibia, in anterior view (444-0, unique within Apatosaurinae); and 3) the posterior surface of the tibial cnemial crest bears a distinct fibular trochanter (445-1, unique within Apatosaurinae). It thus possibly represents a yet unknown, apatosaurine taxon. However, none of the specimens included have yet been completely described, and it thus refrained herein to establish a new name at the moment. Relative positions are considered too unstable to confidently suggest a new taxon.

AMNH 969. This skull was generally considered to belong to *Diplodocus* (Holland, 1906, 1924; Berman and McIntosh, 1978), probably due to strong resemblances with the purported skulls of *Diplodocus longus* USNM 2672 and 2673. However, the latter two specimens cannot be confidently referred to the type species, as there is no overlap with the type specimen YPM 1920 (McIntosh and Carpenter, 1998). Furthermore, given the few differences in skull morphology between diplodocine and apatosaurine species, even less can be expected within one of the two clades only. Indeed, the present analysis recovers AMNH 969 consistently with the two type specimens of *Galeamopus hayi* and *G. shellensis*, indicating that it belongs to this genus. Constrained searches support this assignment, as a forced inclusion in *Diplodocus* yields shortest trees of 1901 or 188.61461 steps, a relative increase of 0.21% or 0.34%, respectively.

One ambiguous autapomorphy is found that distinguishes AMNH 969 from the other two specimens: the anterolateral corner of the tooth row in the dentary is displaced labially (112-1, unique within Diplodocidae). As the clade formed by the other two *Galeamopus* specimens does only show one shared synapomorphy, differences between the species are not enough to justify erection of a third species. When forcing AMNH 969 to group with either of the two species of *Galeamopus*, tree lengths for a *G. hayi* assignment are 1900 (equal weighting) and 188.21024 (implied weighting) steps, whereas affinities with *G. shellensis* are found with trees of a length of 1898 (equal weighting) and 188.1269 (implied weighting) steps. The skull and first two cervical vertebrae of AMNH 969 are thus herein tentatively referred to *Galeamopus shellensis*.

AMNH 6341. The specimen AMNH 6341 is the most complete specimen generally considered to be a *Barosaurus lentus*. As it is completely prepared, and appears largely undeformed (in contrast to the type specimen YPM 429), AMNH 6341 has generally been used as reference specimen for the genus (see Whitlock, 2011a). Although it was found early after the discovery of the Carnegie Quarry at what was later to be named Dinosaur National Monument (McIntosh, 2005), it was only described by McIntosh (2005), but still not in a very detailed way.

In the present analysis, AMNH 6341 was consistently found as sister taxon to the holotype specimen of *Barosaurus lentus*, YPM 429. Given that all the recovered autapomorphies cannot be considered valid, according to the guidelines established above, AMNH 6341 is most parsimoniously interpreted to belong to the same species as YPM 429. Previous assignments to *Barosaurus lentus* are thus corroborated by the current analysis.

AMNH 7530. The specimen AMNH 7530 was never described but is labeled as *Barosaurus* sp. on display at AMNH. It is herein consistently recovered together with *Kaatedocus siberi* SMA 0004. No autapomorphies are found for the specimen, probably due to the fragmentary preservation of the specimen with which it forms a dichotomy – which is a partial skull. Differences between AMNH 7530 and SMA 0004 exist in the shape of the dorsal edge of the parietal (C62), in the orientation of the longest axes of the basal tubera (C87), and in the development of the pre-epipophyseal anterior spur (C167). However, the sum of recovered autapomorphies between the specimens is too low to justify specific separation. The mentioned differences are thus interpreted as individual variation, contrary to the interpretation in Tschopp and Mateus (2012b), where the anterior spur of the pre-epipophysis was stated as autapomorphic for the species *Kaatedocus siberi*.

Forcing AMNH 7530 in a position with the other sampled *Barosaurus* specimens increased tree length by 0.42% (equal weighting) and 0.4% (implied weighting), to 1905 and 188.73208 steps, respectively. Such an assignment is thus considerably less parsimonious than an referral to *Kaatedocus siberi*.

AMNH 7535. As AMNH 7530, also AMNH 7535 was tentatively identified as *Barosaurus* in the AMNH data base, but was never described. In contrast to the specimen AMNH 7530, here identified as *Kaatedocus*, AMNH 7535 consistently groups with other *Barosaurus* specimens in the present analysis.

No autapomorphies were recovered for the specimen, and as stated above, the sum of differences between AMNH 7535 and its sister clade CM 11984 + mdD is too low to establish specific separation. Obvious differences between AMNH 7535 and the holotype specimen YPM 429 (as transverse width, or size of the cervical vertebrae) are herein interpreted to represent a combination of ontogenetic variation, deformation, and serial variation within the cervical column.

CM 94. This specimen was designated the paratype of *Diplodocus carnegii* (Hatcher, 1901). It complements the knowledge of *Diplodocus carnegii* in crucial parts as the mid-caudal vertebrae (thus allowing comparisons with the holotype specimen of *D. longus* YPM 1920), and appendicular elements. When excluding YPM 1920, CM 94 is herein consistently recovered as sister taxon to the holotype specimen of *D. carnegii*, CM 84.

Three autapomorphies are found reliable for the specimen CM 94: 1) scapular glenoid strongly beveled medially (366-1); 2) a metatarsal I to metatarsal V proximodistal length ratio of 1.0 or greater (458-0); and 3) a slender metatarsal II (466-0). Of these, only the first can be compared with CM 84, as the latter specimen does not preserve any pedal material. The sum of comparable differences thus amounts to one (no valid autapomorphies were found for CM 84), referral to the same species and thus an assignment of CM 94 as paratype for *Diplodocus carnegii* is justified.

CM 3378. The specimen CM 3378 was found together with the holotype of *Apatosaurus louisae* at Dinosaur National Monument, and preserves the most complete vertebral column of any of the specimens included herein (McIntosh, 1981). Nonetheless, it has only been described and figured in parts (Holland, 1915b; Gilmore, 1936). It was included into the specimen-based phylogenetic analysis of Upchurch et al. (2004b), and resulted as second specimen of *Apatosaurus louisae*. As none of the recovered autapomorphies for CM 3378 can be considered valid, the present analysis confirms this interpretation.

CM 3452. The specimen CM 3452 is one of very few preserving an almost complete skull in articulation with the first few cervical vertebrae. It was reported as juvenile to subadult *Diplodocus* specimen (Holland, 1924; McIntosh and Berman, 1975; Whitlock et al., 2010), but never described in detail. A referral to *Diplodocus* is questionable, as almost no overlapping material exists between CM 3452 and any type specimen of *Diplodocus*. Now that generic separation from *Diplodocus* is confirmed for *Galeamopus hayi*, the only other *Diplodocus* specimen preserving anterior cervical vertebrae is CM 84. With the description of two additional specimens preserving articulated skulls and cervical vertebrae (SMA 0004 and 0011), affinities of CM 3452 can be assessed more accurately. The present analysis consistently recovers CM 3452 as sister taxon to *Kaatedocus siberi* + *Barosaurus lentus*.

A single autapomorphy was found valid for CM 3452: basal tubera facing ventrolaterally in

posterior view (89-0). Summed differences between CM 3452 and its sister clade amount to four, not justifying specific separation. Constrained searches were thus performed in order to evaluate the most parsimonious identification. Forcing CM 3452 into *Diplodocus*, following earlier identifications, equal weighting finds shortest trees of 1905 steps, and implied weighting 188.82961 steps – relative length increases of 0.42% and 0.46%, respectively. Imposed affinities with *Kaatedocus* yield trees with a length of 1903 and 188.44375 steps, corresponding to an increase in length of 0.32% and 0.25%. A forced inclusion into the *Barosaurus* clade results in length increases of 0.11% and 0.04%, to 1899 and 188.04743 steps, respectively.

In the case of affinities to *Barosaurus*, CM 3452 is recovered as the basal-most specimen, united with the remaining quartet by a single synapomorphy: presence of an accessory horizontal lamina in the center of the spinodiapophyseal fossa of mid- and posterior cervical vertebrae, not connected with any surrounding lamina (187-1). This trait is shared with all included *Barosaurus* specimens but AMNH 7535, which was not scorable for this character. The only other diplodocine specimen showing the same development is *Diplodocus carnegii* CM 94. Distance between CM 3452 and the more derived clade amounts to a single difference, which does not allow specific separation. Therefore, CM 3452 is herein tentatively referred to *Barosaurus lentus*.

CM 11161. This skull-only specimen is generally referred to *Diplodocus* (Holland, 1915b, 1924; McIntosh and Berman, 1975; Berman and McIntosh, 1978; Whitlock et al., 2010; Whitlock and Lamanna, 2012), and has been used in numerous publications as model for feeding strategies or other ecological or behavioral studies concerning this genus (e.g. Haas, 1963; Barrett and Upchurch, 1994; Calvo, 1994; Upchurch and Barrett, 2000; Whitlock, 2011b; Young et al., 2012). However, as no overlap exists with any of the type specimens of *Diplodocus*, referral to that genus remains controversial. Given that all skulls with articulated vertebrae are herein identified as other diplodocine species (AMNH 969 and SMA 0011 as *Galeamopus shellensis*, CM 3452 as *Barosaurus lentus*, SMA 0004 as *Kaatedocus siberi*), only indirect evidence can be used for such an assignment, as exemplified by the present analysis, which is not able to resolve the position of CM 11161 due to the lacking overlap.

Two ambiguous autapomorphies are found for the specimen: 1) a short and broad posteroventral process of the jugal (42-0); and 2) the distance separating supratemporal fenestrae is less than 1.5 times the width of the long axis of the supratemporal fenestra (61-0). The latter trait was scored as unknown in the other putative *Diplodocus* skull, USNM 2672, due to lacking measurements. In another skulls not included in the present analysis, the mean ratio is 1.4 (USNM 2673), thus resembling CM 11161. The short posteroventral process of the jugal, however, is not present in USNM 2672 (pers. obs., 2011) and CM 11255, a putative juvenile *Diplodocus* skull (Whitlock et al., 2010; but see above).

Constrained searches were performed forcing CM 11161 to group with diplodocine taxa preserving articulated skull material. Imposed relationships with *Galeamopus* produced trees 0.16% and 0.18% longer than the most parsimonious trees, with lengths of 1900 and 188.31381 steps, respectively. A forced assignment to *Kaatedocus* yielded shortest trees of 1911 and 189.77095 steps, a relative increase in length of 0.74% and 0.96%. When constraining CM 11161 to group with *Barosaurus*, tree length increases by 0.58% and 0.62%, reaching 1908 and 189.12979 steps. Given that all these alternative assignments increase tree length by at least three steps (or almost the equivalent to it in implied weight trees), a referral to *Diplodocus* still remains the most parsimonious identification. However, given that nearly complete specimens including articulated skulls, vertebrae from anterior cervical to distal caudal elements, as well as appendicular elements including manual and pedal material are known from *Galeamopus*, the latter genus appears more appropriate as representative of the diplodocine clade in phylogenetic analyses.

CM 11984. The specimen CM 11984 was partly described as *Barosaurus lentus* by McIntosh (2005), but is largely unprepared. The present analysis finds CM 11984 in all most parsimonious trees as sister taxon to *Barosaurus lentus* YPM 429 + AMNH 6341.

Autapomorphies recovered for the specimen were all shared with other diplodocine specimens, and thus not considered reliable. The four synapomorphies found for the sister clade *Barosaurus lentus* YPM 429 + AMNH 6341 are thus not enough to erect a new species within *Barosaurus*. Therefore,

McIntosh's (2005) referral of this specimen to *Barosaurus lentus* is herein corroborated.

DMNS 1494. Although undescribed, DMNS 1494 is often considered a *Diplodocus longus* (McIntosh, 1981; Gillette, 1991), probably based on similarities with AMNH 223, the specimen described as *D. longus* by Osborn (1899). As the latter identification was herein rejected, also the referral of DMNS 1494 to *D. longus* appears questionable. In the present analysis DMNS 1494 is consistently found as sister taxon to USNM 10865.

A single ambiguous autapomorphy was found for the specimen: presence of a lateral fossa at the base of the ischial shaft (422-1, unique within Diplodocinae). As this is the only valid difference between DMNS 1494 and USNM 10865, the two are considered to belong to the same species. Following the reasoning stated above, this species will be *Diplodocus hallorum*.

FMNH P25112. The current specimens is one of the few non-type specimens, which was described (Riggs, 1903). Riggs (1903) referred it to *Apatosaurus excelsus* (herein reinterpreted as *Brontosaurus excelsus*), an identification which was accepted by Gilmore (1936). Upchurch et al. (2004b) recovered FMNH P25112 as a single OTU, proposing that it might belong to its own species within *Apatosaurus*. In the present analysis, FMNH P25112 is recovered in the same position as *Brontosaurus excelsus* when adding it to the equally weighted reduced consensus tree, whereas it groups with *Elosaurus* and *Dystrophaeus* in the implied weights pruned consensus tree.

Forcing FMNH P25112 into the clade with *Apatosaurus ajax* YPM 1860 (together with YPM 1840 in the equally weighted analysis, but alone when using implied weighting), tree lengths increase by 0.47% with equal weighting and 0.19% in the analysis with implied weights, to 1906 and 188.38266 steps, respectively. Imposing a dichotomy with *Brontosaurus excelsus* YPM 1980, shortest trees measure 1903 and 188.17315 steps, an increase of 0.32% and 0.11%. A grouping with *Elosaurus parvus* as proposed by the implied weights trees increases equally weighted tree lengths by 0.11%, to 1899 steps. When restricting FMNH P25112 to *Eobrontosaurus*, trees lengthen by 0.16% or 0.02%, to a length of 1900 or 188.01343 steps. A forced relationship with the putative new taxon including AMNH 460, SMA 0087, and WDC-FS001A (see above) is supported by trees of a length of 1897 or 188.11135 steps, a relative increase of 0% or 0.07% compared to the most parsimonious trees. Finally, imposing a relationship with NSMT-PV 20375 in the equally weighted trees, or with NSMT-PV 20375 and YPM 1840 in the implied weights trees produces shortest trees of 1897 or 187.99160 steps, respectively, corresponding to increases of 0% or 0.01%. According to these values, several different referrals appear similarly parsimonious: an identification as *Elosaurus*, as belonging to the same taxon as AMNH 460, SMA 0087, and WDC-FS001A, or as NSMT-PV 20375, possibly together with YPM 1840.

A single synapomorphy supports an assignment to *Elosaurus*: reduction of the spinoprezygapophyseal lamina in posterior dorsal vertebrae (274-0). The quartet FMNH P25112, AMNH 460, SMA 0087, and WDC-FS001A is united by the two synapomorphies diagnosing SMA 0087 + WDC-FS001A (444-0, 445-1). However, both FMNH P25112 and AMNH 460 could not have been scored for these two characters. The unity of FMNH P25112 with NSMT-PV 20375 in the equally weighted tree yields one synapomorphy: pubic articulation of the ischia to anteroposterior length of pubic pedicel is less than 1.5 (420-0). The triplet FMNH P25112, NSMT-PV 20375, and YPM 1840 in the implied weight trees is not supported by any valid synapomorphy. Taking all this together, an assignment to *Elosaurus* appears to be the best supported. Therefore, pending further studies on the involved specimens, FMNH P25112 is tentatively referred to *Elosaurus parvus*.

MB.R. skeleton k. Skeleton k is the second individual referred to *Tornieria africana* by Remes (2006). The individual includes a braincase (MB.R.2386), which was interpreted to not belong to that taxon by Harris (2006a). However, based on preserved quarry maps, referral to the same individual appears justified (Heinrich, 1999; Remes, 2006). The present analysis consistently recovers skeleton k with the holotype individual of *Tornieria africana*. As no autapomorphy was found distinguishing skeleton k from skeleton A, Remes' (2006) referral to the same species is herein corroborated.

ML 418. Consisting of very fragmentary material, ML 418 was identified as one of the six most unstable taxa in the equally weighted analysis. It was referred to *Dinheirosaurus* by Antunes and Mateus (2003), and later assigned to *Apatosaurus* sp. by Mateus (2005). Mannion et al. (2012) noted

that it cannot be confidently identified as either of these two taxa, as it lacks their autapomorphic traits, and identified it as indeterminate diplodocid. When added to the equally weighted reduced consensus tree, ML 418 produces a polytomy at the base of Diplodocinae, together with SMA 0011, *Galeamopus hayi* HMNS 175, AMNH 969, the two *Tornieria* skeletons, the clade uniting *Dinheirosaurus* with *Supersaurus*, and *Diplodocus* + mdD. In the most parsimonious implied weights trees, ML 418 occupies the most basal position within Diplodocinae, but switches to a position within the clade of *Dinheirosaurus* and *Supersaurus* when excluding *Australodocus* or restricting it to Titanosauriformes.

One ambiguous autapomorphy is found for the specimen: mid- and posterior dorsal transverse processes bear a distinct dorsal bump or spur (264-1). The fact that the sum of differences between ML 418 and the remaining diplodocines is just two does not allow an identification as separate species. Constrained searches forcing ML 418 into a dichotomy with *Dinheirosaurus* (as suggested by Antunes and Mateus, 2003) produce equally weighted trees of a length of 1900 steps, whereas implied weighting finds shortest trees of 188.09487 steps, corresponding to length increases of 0.16% and 0.07%, respectively. In both cases, no synapomorphies are found for the clade uniting them. This implies that Mannion et al. (2012) were right in considering it a possible second diplodocid taxon, although not diagnosable based on the preserved material. As ML 418 shows two shared synapomorphies of Diplodocinae (218-1, 283-1) and does not exhibit any of Apatosaurinae (275-0 instead of 275-1), it is herein considered an indeterminate Diplodocinae.

NSMT-PV 20375. The specimen NSMT-PV 20375 was described by Upchurch et al. (2004b) and identified as *Apatosaurus ajax*, by means of a specimen-based phylogenetic analysis. In the present analysis, it is never found in close relationship with the holotype specimen of *Apatosaurus ajax*. In fact, NSMT-PV consistently occupies the most basal position within Apatosaurinae, alone in the equally weighted trees, or together with YPM 1840 in the implied weights trees. A single, ambiguous autapomorphy is recovered for NSMT-PV 20375: presence of lateral fossae on the prezygapophyseal process of mid- and posterior cervical vertebrae (183-1).

Forcing NSMT-PV 20375 into a dichotomy together with YPM 1840 with the equally weighted analysis yielded trees one step longer (1898; 0.05%) than the most parsimonious trees. The resulting reduced consensus tree recovered *Elosaurus parvus*, *Apatosaurus ajax*, and *Apatosaurus louisae* in the same relative positions as the shortest implied weights trees. Imposing a grouping with *Apatosaurus ajax*, as found by Upchurch et al. (2004b) produced trees of 1899 and 188.10818 steps, a relative increase of 0.11% and 0.07%. In both cases, it has YPM 1840 as sister taxon, and is positioned relatively basal within Apatosaurinae, detached from *Apatosaurus louisae*. The same results are obtained when forcing the entire triplet (NSMT-PV 20375, YPM 1840 and YPM 1860) to cluster together, thus not imposing a sister taxon relationship between NSMT-PV 20375 and YPM 1860 a priori. The most parsimonious interpretation thus seems the arrangement found by the implied weights trees, with NSMT-PV 20375 and YPM 1840 forming the basal-most taxon within Apatosaurinae. It thus seems that two more, previously unrecognized taxa are present within Apatosaurinae. However, support for such a separation is low, and more detailed studies are needed to confirm such a hypothesis. No additional taxa shall thus be named herein.

SMA 0087. The specimen SMA 0087, described for the first time herein, forms a clade together with WDC-FS001A – if the analysis is able to resolve their position. In the equally weighted pruned tree, SMA 0087 is found outside Apatosaurinae, as also if added to the equally weighted reduced consensus tree. On the other hand, implied weighting finds SMA 0087 + WDC-FS001A within Apatosaurinae, more derived than NSMT-PV 20375 + YPM 1840.

No valid autapomorphy is found by the present analysis, but both shared synapomorphies between SMA 0087 and WDC-FS001A would qualify as species autapomorphies (444-0, 445-1), given that they are not shared with any other apatosaurine specimen. Apatosaurine affinities are indicated for SMA 0087 by the presence of two shared (256-0, 275-1) and two ambiguous synapomorphies (235-1, 250-0) of the clade. The absence of one exclusive (307-0 instead of 1) and three shared synapomorphies of Diplodocinae (283-0, 330-0, 332-0 instead of 283-1, 330-1, and 332-1) implies that an identification as apatosaurine is more probable.

When forcing SMA 0087 into a dichotomy with WDC-FS001A in the equally weighted trees,

tree length does not increase, but SMA 0087 + WDC-FS001A remains in a trichotomy with Apatosaurinae and Diplodocinae. Imposing apatosaurine affinities, two large polytomies are found to form the clade, with SMA 0087, WDC-FS001A, FMNH P25112, and AMNH 460 being the sister clade to a polytomy with all other apatosaurine specimens. Tree length is 1898, one step more than in the most parsimonious trees. When forcing SMA 0087 into Diplodocinae, tree length stays the same, and SMA 0087 is recovered together with WDC-FS001A as most basal diplodocine taxon. Five synapomorphies are found for Diplodocinae in such a case, but only one of these would be shared by all diplodocines, and not be present in any apatosaurine specimen: a subtriangular proximal articular surface of the tibia. However, the latter trait is not recognizable in the badly distorted tibia of SMA 0087. Given that previously established synapomorphies of Apatosaurinae and Diplodocinae favor an apatosaurine identification of SMA 0087, the latter is herein preferred over an assignment to Diplodocinae.

SMA D16-3. This partial skull has not been described in detail yet. It is herein consistently found as *Kaatedocus siberi*. No autapomorphies were found in any of the trees. A referral to *Kaatedocus siberi* is thus warranted.

SMA O25-8. The second isolated partial skull (besides SMA D16-3) from Howe Quarry exhibits both internal and external differences in braincase morphology, compared with the *Kaatedocus siberi* specimens (Schmitt et al., 2013). Being identified as one of the four most unstable taxa, it was excluded from all most parsimonious pruned and reduced consensus trees. When added, it consistently groups within the *Kaatedocus* + *Barosaurus* clade, but outside *Kaatedocus siberi*.

The specimen SMA O25-8 can be confidently identified as Diplodocidae due to the hook-shaped posterior process of the prefrontal and the slightly concave posterior face of the basal tubera, and as Diplodocinae given the box-like basal tubera and the presence of a basipterygoid recess. It is included in the *Kaatedocus* + *Barosaurus* clade based on the distinct nuchal fossae on the parietal, and the ridge on the posterior face of the paroccipital process.

Forcing SMA O25-8 into *Barosaurus lentus* does not increase tree length, but a confident assignment to this taxon is hampered by the lack of overlap with definitive *Barosaurus lentus* specimens. Indeed, recovered consensus trees show one large polytomy including all of the specimens. When further including CM 3452 into *Barosaurus lentus* (following the identification of CM 3452 above), tree lengths increase by 0.42% (equal weighting) and 0.31% (implied weighting), to 1905 and 188.55338 steps, respectively. Imposing a clustering with *Kaatedocus siberi* also does not increase tree length, but no synapomorphies are found for an inclusion into *Kaatedocus siberi*. Taking all the information into account, SMA O25-8 can be confidently identified as derived diplodocine, most closely related to either *Kaatedocus* or *Barosaurus*. The fact that a unity of CM 3452, SMA O25-8 and the definitive *Barosaurus* specimens is highly unparsimonious indicates that a third taxon might be present, or that morphological variety within *Kaatedocus* might be higher than acknowledged at present. Pending further studies, and given the differences found between SMA O25-8 and the known *Kaatedocus* braincases, SMA O25-8 is herein still tentatively referred to *Barosaurus*.

USNM 2672. The specimen USNM 2672 is the second skull usually identified as *Diplodocus* included in the study. It also preserves a partial atlas. The problem for a confident identification of USNM 2672 remains the same as in CM 11161, as no definitive *Diplodocus* specimen is known with either atlas or skull.

No autapomorphy was found in the equally weighted pruned consensus tree, the only tree to include USNM 2672. Nonetheless, the specimen can be confidently identified as diplodocid due to the broad contact between maxilla and quadratojugal, the large preantorbital fenestra, the concave dorsal margin of the antorbital fenestra, the medially curving anteromedial corner of the prefrontal, the hook-shaped posterior process of the prefrontal, the slightly concave posterior face of the basal tubera, the absence of a coronoid eminence, as well as absence of direct crown-to-crown occlusion in the teeth. Diplodocine affinities are confirmed by the box-like basal tubera.

The same constrained searches are performed as for CM 11161, in order to test affinities with species for which cranial material is known. Affinities with *Galeamopus* are found in trees of a length of 1900 or 188.43524 steps (an increase of 0.16% or 0.25%). Forcing an inclusion into the *Kaatedocus* clade yields trees of a length of 1911 and 189.61024 steps, corresponding to a 0.74% and 0.87% length

increase. When imposing an assignment to the clade uniting *Kaatedocus*, *Barosaurus*, and CM 3452, the trees are lengthened by 0.11% and 0.13%, reaching 1899 and 188.21381 steps. Taking everything together, USNM 2672 appears to be most parsimoniously referred to *Diplodocus*, but it remains unknown to what species.

USNM 10865. On display at USNM, the specimen USNM 10865 is the second, relatively complete skeleton referred to *Diplodocus longus* after AMNH 223 (Osborn, 1899; Gilmore, 1932). It has been partially described by Gilmore (1932). In the present analysis, USNM 10865 consistently forms a dichotomy with DMNS 1494.

No valid autapomorphy is found for the present specimen, and as stated above, specific distinction from DMNS 1494, AMNH 223, and most importantly the holotype of *Seismosaurus hallorum*, NMMNH 3690, is not warranted. As *Seismosaurus* was earlier synonymized with *Diplodocus*, the specimen USNM 10865 is herein referred to the species *Diplodocus hallorum*.

UW 15556. Described in detail by Hatcher (1902) and Gilmore (1936), the specimen UW 15556 (previously CM 563) is one of the best known apatosaur specimens. It was often referred to *Apatosaurus excelsus* (Hatcher, 1902; Gilmore, 1936; McIntosh, 1981, 1995), but found to constitute its own species within *Apatosaurus*, together with the holotype of *Elosaurus parvus*, CM 566 (Upchurch et al., 2004b). Upchurch et al. (2004) thus proposed the new combination *Apatosaurus parvus.* However, as showed earlier, generic separation of the two specimens can be justified due to several differences with the recovered sister taxon *Brontosaurus excelsus*. The specimen UW 15556 is thus herein referred to *Elosaurus parvus*.

WDC DMJ-021. The specimen WDC DMJ-021 was described by Lovelace et al. (2007), and identified as *Supersaurus vivianae*. Herein, it is always found together with the BYU specimen of *Supersaurus vivianae*, thus confirming the assignment of Lovelace et al. (2007).

No valid autapomorphies for the specimen are found by any of the trees, but seven shared synapomorphies unite the two specimens of *Supersaurus*. Three of them are unique within Diplodocinae, and can be considered autapomorphies of the species.

WDC-FS001A. Only the manus of the present specimen has been described in detail (Bedell and Trexler, 2005). The specimen was identified as *Diplodocus* cf. c*arnegii*, based on morphology of the caudal vertebra, which was different from the specimens generally considered '*Diplodocus longus*', and the general slenderness of the appendicular bones (Bedell and Trexler, 2005). The implied weights analysis finds WDC-FS001A together with SMA 0087, for which apatosaurine affinities are more probable than diplodocine (see above). On the other hand, equal weighting is not able to resolve the relationships of WDC-FS001A, finding affinities with both Apatosaurinae and Diplodocinae.

Two ambiguous autapomorphies are found for WDC-FS001A, both of them shared with *Diplodocus* specimens: 1) presence of a distinct fossa on the medial surface of the proximal branches of middle chevrons (357-1); and 2) a well-developed rugosity on the dorsolateral margin of metatarsal II, near its distal end, extending towards the center of the shaft (468-1). Apatosaurinae affinities are ambiguous, as WDC-FS001A shares one shared synapomorphy (476-1), but does not exhibit an ambiguous synapomorphy (402-1 instead of 0) of the clade. The first of these is shared with the *Diplodocus hallorum* USNM 10865, while the second is also present in the basal apatosaurine NSMT-PV 20375, though. Information is also ambiguous concerning diplodocine synapomorphies: whereas WDC-FS001A shows one shared synapomorphy (330-1), a second one is absent (332-0 instead of 1). Here, the first trait also occurs in apatosaurine specimens, but the second one is not shared by any diplodocine. Morphological evidence therefore slightly favors an assignment to Apatosaurinae.

A forced clustering with the two *Diplodocus carnegii* specimens (as proposed by Bedell and Trexler, 2005) produces tree lengths of 1903 and 188.65885 steps, an increase of 0.32% and 0.37%. Diplodocine affinities are found with shortest trees of 1898 and 188.28028 steps, corresponding to a lengthening of 0.05% and 0.16%, respectively. Imposing a grouping within Apatosaurinae (as found by the implied weight analysis) did not result in longer trees. Both morphological evidence as well as constrained searches thus indicate that apatosaurine affinities are more parsimonious for WDC-FS001A. Therefore, and following also the reasoning in the earlier paragraphs about the affinities of SMA 0087 and AMNH 460, WDC-FS001A is herein referred to one of the putative new apatosaurine

taxa, together with the specimens mentioned before.

Combined cladogram

Based on the identifications stated above, a combined cladogram was created to summarize the results (Fig. 6.119). The cladogram represents the latest species-level taxonomy of Diplodocidae. Diagnoses of the proposed clades, genera, and species are given below. Outgroup taxa are reduced considerably compared to the trees recovered by the main analyses, in order to increase the intended focus on Diplodocidae.

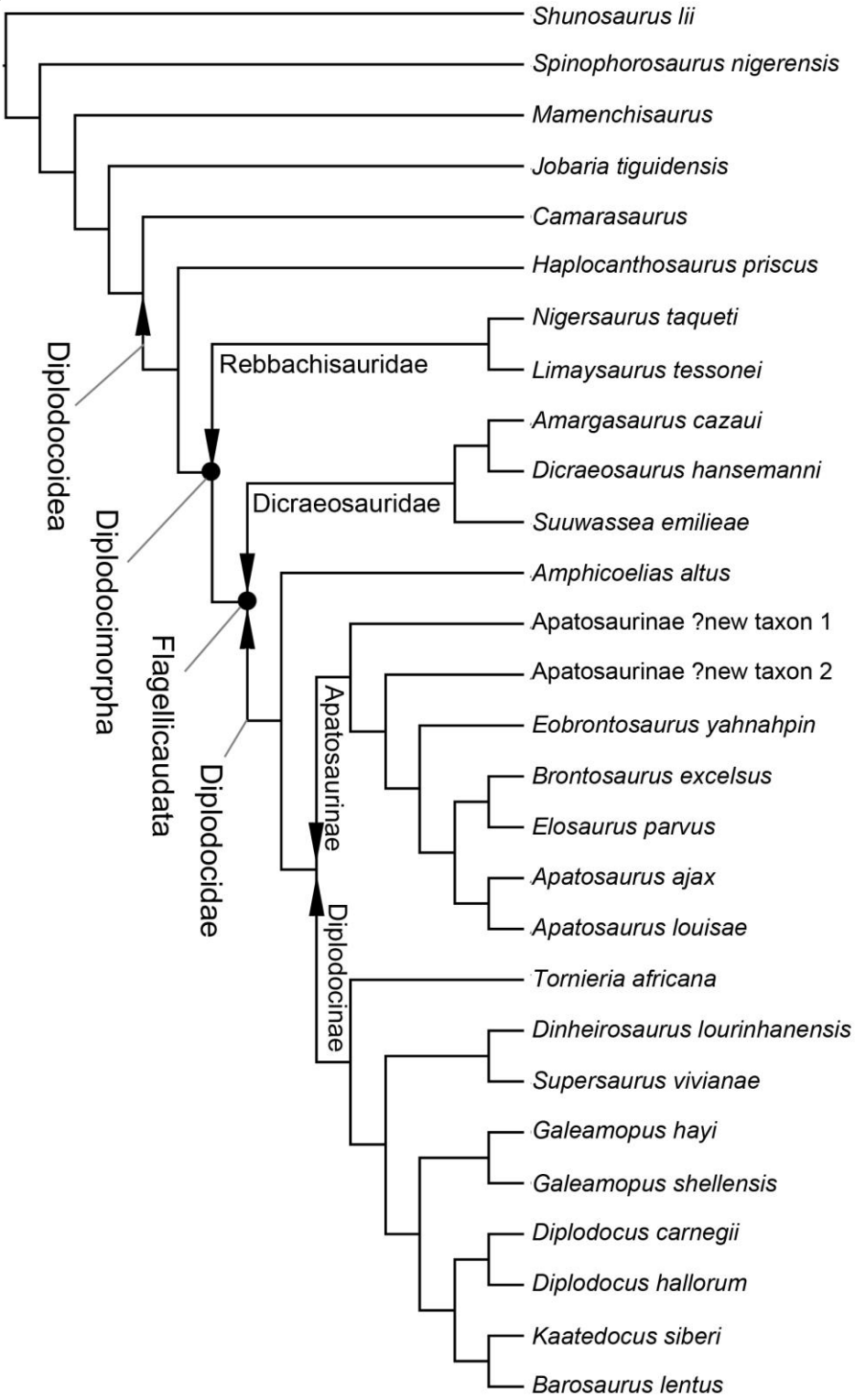

Figure 6.119: Combined cladogram of diplodocid species-level intrarelationships, summarizing the results of the present thesis. Stem-based higher-level taxa are marked by an arrowhead, node-based taxa by a dot.

Biostratigraphic and paleobiogeographical implications

The present analysis rejects diplodocid affinities of the only putative Middle Jurassic and Cretaceous diplodocid species, i.e. *Cetiosauriscus stewarti*, *Losillasaurus giganteus*, *Dystrophaeus viaemalae*, and *Dyslocosaurus polyonychius*. A single anterior caudal vertebra previously identified as Cretaceous diplodocid (Upchurch and Mannion, 2009) was subsequently shown to belong to Titanosauriformes (Whitlock et al., 2011), and therefore not included in the present analysis. Diplodocidae thus appear restricted to the Late Jurassic, with a caudal vertebra from the Oxfordian of Georgia being the first representative of the clade (Gabunia et al., 1998; Mannion et al., 2012). Given the high diversity, such a temporal restriction is remarkable. The Morrison Formation, from where the majority of diplodocids are known, is interpreted to represent a time span of about seven (Swierc and Johnson, 1996; Kowallis et al., 1998) to eleven million years (Platt and Hasiotis, 2006). Therefore, even though morphologically similar, at least two diplodocid species appear to have lived contemporaneously throughout the entire duration of the sedimentation of the Morrison Formation, and besides non-diplodocid sauropods like *Camarasaurus*, *Haplocanthosaurus*, *Brachiosaurus*, or others. If precise stratigraphical levels and geological ages would be known for all the sites where diplodocids were found, the present analysis would provide a good phylogenetic foundation on which hypotheses of speciation or niche partitioning within diplodocids from the Morrison Formation could be based. However, exact geological dating was rarely done, or has provided controversial results (in particular for the Howe Ranch sites, Tschopp and Mateus, 2012b). Therefore, and because no reliable marker beds appear to be present throughout the entire extent of the Morrison Formation (Trujillo, 2006; contra Turner and Peterson, 1999), long distance correlation between Morrison Formation quarries is nearly impossible at present. Proposed biostratigraphical zones within the formation (Bakker, 1998; Turner and Peterson, 1999; Foster, 2003; Ikejiri, 2004) have thus to be regarded questionable and provisional. Their validity is furthermore debatable because they heavily rely on species and genus referrals that have not been tested by means of phylogenetic analyses. Given that diversity appears to have been underestimated, as indicated by the present analysis, these referrals will have to be reconsidered. Notwithstanding the lack of knowledge concerning such specific stratigraphy and phylogeny, Diplodocidae as a whole appears to be a good candidate to serve for relative geological dating. Their presence in at least three continents, and restriction in time to the Late Jurassic, and more precisely the period of the Oxfordian to Tithonian qualifies them as age index fossils.

Diplodocidae is most divers in North America, but the earliest finds from Georgia suggest that the origin of the clade lies in Europe (Mannion et al., 2012). As the Georgian caudal vertebra, also the non-American diplodocid OTU included herein (ML 418, *Dinheirosaurus lourinhanensis*, *Tornieria africana*) can be referred to Diplodocinae (Mannion et al., 2012; this study). The fact that the latter two species lie at the base of the diplodocine radiation (Fig. 6.119) furthermore corroborates a hypothesis of an extra-American origin of this clade. Interestingly, apatosaurine specimens have only been recovered from North America to date, so that interpretations of their origin are more dubious.

Diagnoses

Updated diagnoses of the main diplodocoid subclades

The following lists of synapomorphies only includes the named nodes and stems in the recovered phylogenetic tree, which directly lead to Diplodocidae, as well as its sister clade Dicraeosauridae (Fig. 6.118). Synapomorphies are divided into their qualitative states as defined above, and ordered based on anatomical regions. Where conflicting interpretations exist between the analyses using equal or implied weighting, the synapomorphy is attributed to the less inclusive clade. Additional synapomorphies are added to the diagnoses following earlier studies, if supported by the data set, also in cases where the analysis did not recognize them as such. References for the synapomorphies credit the first recognition of the respective trait as synapomorphic for the taxon in question. Finally, previously proposed synapomorphies are discussed in the light of the new analysis.

Diplodocoidea Marsh, 1884.

Definition: *Diplodocus*, not *Saltasaurus* (stem-based; Wilson and Sereno, 1998).

Unambiguous synapomorphies:

1. premaxilla is a single elongate unit with nearly no distinction between the body and the nasal process (3-1; Upchurch et al., 2004a)
2. posteroventral edge of the ascending process of the premaxilla is straight in lateral view, and directed posterodorsally (5-2; Upchurch, 1995)
3. the dorsal process of the maxilla extends posterior to the posterior process (13-1; Wilson, 2002)
4. maximum diameter of the antorbital fenestra is subequal (greater than 90%) to the orbital maximum diameter (18-1; Wilson, 2002)
5. the external nares are retracted to a position between the orbits, facing dorsally or dorsolaterally (21-1; Marsh, 1898)
6. a large contribution of the jugal to the antorbital fenestra, bordering approximately one-third of its perimeter (40-1; Upchurch, 1995)
7. the anterior terminus of the quadratojugal lies below the anterior margin of the orbit or beyond (45-1; Rauhut et al., 2005)
8. angle between anterior and dorsal processes of the quadratojugal is greater than 90°, approaching 130°, so that the quadrate shaft slants posterodorsally (46-1; McIntosh, 1990b)
9. the basipterygoid processes are angled less than 75° to the skull roof (normally approximately 45°) (93-1; Calvo and Salgado, 1995)
10. the transverse flange (i.e. ectopterygoid process) of the pterygoid lies anterior to the antorbital fenestra (102-1; Upchurch, 1998)
11. four or more replacement teeth per alveolus (115-1; Wilson, 2002)
12. planar wear facets of the teeth (117-1)
13. cylindrical cross-sectional shape of the teeth at midcrown (121-1; Marsh, 1884)
14. the fibular facet of the astragalus faces posterolaterally, such that the anterior margin is visible in posterior view (454-1).

Exclusive synapomorphies:

15. external surface of the premaxilla is marked by vascular grooves (2-1)
16. the anterior maxillary foramen lies on the medial edge of the maxilla, opening medially into the premaxillary-maxillary boundary (11-1)
17. the articular surface of the quadrate is roughly triangular in shape (49-1)
18. SI values for tooth crowns are 3.4 or greater (119-1; McIntosh, 1990b)
19. short cervical ribs, not reaching the posterior end of the centrum (214-1; Berman and McIntosh, 1978).

Shared synapomorphies:

20. the posterolateral process of the premaxilla and the lateral process of the maxillary are without any midline contact (6-0; Wilson, 2002)
21. maximum diameter of the external nares is shorter than the orbital maximum diameter (22-0)

22. the articular surface of the occipital condyle is continuously grading into the condylar neck (77-1)
23. cervical ribs overlap no more than the next cervical vertebra in sequence (215-1)
24. the proximal expansion of the humerus is more or less symmetrical (384-0).

Ambiguous synapomorphies:

25. the dorsal transverse processes are inclined dorsally more than 30° from the horizontal (230-1).

Previously suggested synapomorphies:

- a very acute angle between medial and lateral margins of the premaxilla (Upchurch et al., 2004a). The character describing the angle between medial and lateral borders of the premaxilla was redefined herein, and the numeric boundary changed as to be able to distinguish between Dicraeosauridae and Diplodocidae. An angle lower than 17° would thus be synapomorphic for both Rebbachisauridae and Diplodocidae, but not for Dicraeosauridae. The same character was further found by Whitlock (2011a) to diagnose Diplodocimorpha.
- an elongate subnarial foramen (Upchurch et al., 2004a). The character describing the elongation of the subnarial foramen was not included in the present analysis, as it is impossible to code in most specimens. Even when rostral skull elements are preserved, the fossa containing the subnarial and the anterior maxillary foramina is often obliterated with matrix (e.g. USNM 2672), and only CT scanning would reveal the true shape.
- a strongly reduced anteroposterior diameter of the supratemporal fenestra (Upchurch et al., 2004a). The relation of anteroposterior diameter of the supratemporal to occipital width was not included in the present analysis, as it was not well explained what was measured for obtaining a value for the occiput width (Upchurch et al., 2004a). Also, anteroposterior diameter of supratemporal fenestrae seems to be variable within diplodocids, and relatively easily deformed (compare the two putative *Diplodocus* skulls CM 11161 and 11255).
- elongate basipterygoid processes (McIntosh, 1990b; Upchurch, 1998). This trait is recovered as diplodocimorph synapomorphy by Wilson (2002) and Whitlock (2011a). In fact, the difference is inexistent as Diplodocimorpha describes the same clade as Diplodocoidea in McIntosh (1990b) and Upchurch (1998). Whitlock (2011a) resolved it as diplodocimorph synapomorphy due to the basal diplodocoid position of *Haplocanthosaurus*, which does not preserve cranial bones, and applying the character state optimization strategy DELTRAN. In the present analysis, definition of the character was slightly changed, which lead to varying scores for diplodocid taxa. It can thus not be considered a synapomorphy for any clade herein.
- a rectangular snout (Upchurch et al., 2004a). The rectangular snout was herein included as diagnosing Diplodocimorpha, following Whitlock (2011a).
- dentary with ventrally projecting 'chin' (Wilson and Sereno, 1998). At the time Wilson and Sereno's (1998) monograph was published, no dentary was known from diplodocoids more basal than Flagellicaudata. The recovery of *Nigersaurus* and *Demandasaurus* dentaries showed that such a 'chin' was absent in rebbachisaurids (Sereno et al., 1999; Sereno and Wilson, 2005; Torcida Fernández-Baldor et al., 2011). Consequently, its presence was later found as synapomorphy for Flagellicaudata (Whitlock 2011a; this study).
- the anterior restriction of the tooth row (McIntosh, 1990a). The length of the tooth row is recovered as diplodocimorph synapomorphy by Whitlock (2011a), applying DELTRAN. In the present analysis, the number of states has been increased, compared to the definition of Whitlock (2011a), due to the recognition of a higher diversity within diplodocids. Also, brachiosaurid skulls have anteriorly restricted tooth rows (Janensch, 1935; Wilson and Sereno, 1998), which shows that this feature is present in diplodocoid outgroups as well.
- atlantal intercentrum with anteroventral lip (Wilson and Sereno, 1998). The same doubts apply here as for the presence of a 'chin' in the dentary (see above). The question is furthermore complicated as no rebbachisaurid atlas has been described to date. With the present dataset it is thus more cautious to add this trait as synapomorphy of Flagellicaudata.
- cervical and anterior dorsal vertebrae opisthocoelous (McIntosh, 1990a). Opisthocoel cervical and anterior dorsal vertebrae are actually widespread among sauropod dinosaurs, and represent the plesiomorphic condition. No phylogenetic analysis was thus able to support this

trait as a synapomorphy of Diplodocoidea.

- deeply divided V-shaped posterior cervical and anterior dorsal neural spines (McIntosh, 1990b). Subdivided cervical and dorsal neural spines are known from a variety of sauropod dinosaurs from different clades (Upchurch et al., 2004a; Wedel and Taylor, 2013). The shape of the subdivision was proposed as distinguishing feature between diplodocids and camarasaurs (V- versus U-shaped; McIntosh, 1990a), but has rarely been used in phylogenetic analyses. In the present analysis, a character is used to describe the base of the notch. Reducing the description to the base of the notch, occurrence of U-shaped notches is not restricted to camarasaurs, but also present in diplodocoid species (e.g. *Amargasaurus cazaui* or *Apatosaurus ajax* YPM 1860). It should thus not be used to diagnose Diplodocoidea.
- dorsal junction of the spinoprezygapophyseal laminae of dorsal vertebra (Whitlock, 2011a). Here, this feature is recovered as diagnosing a more inclusive clade, SMA 0009 + mdE, in the equally weighted reduced consensus tree, as well as in both main implied weights trees. The difference is a result of the addition of the titanosauriform species *Giraffatitan brancai*, *Ligabuesaurus leanzai*, and *Isisaurus colberti*, where spinoprezygapophyseal and prespinal laminae join dorsally (Janensch, 1950; Jain and Bandyopadhyay, 1997; Bonaparte et al., 2006).
- posterior dorsal centra are amphicoelous (McIntosh, 1990a). Detailed study of diplodocine posterior dorsal centra showed that most of them are actually slightly opisthocoelous (e.g. *Diplodocus carnegii* CM 84) to distinctly so (*Supersaurus vivianae*). The amphicoelous condition was thus herein recovered as synapomorphic for Apatosaurinae or less inclusive clades.
- arches of dorsal and caudal vertebrae tall (more than two and one-half times length of dorsoventral centrum height) (Wilson and Sereno, 1998). The present synapomorphy actually includes two characters as used by Whitlock (2011a) as well as in this study. They were both interpreted to diagnose Diplodocimorpha by Whitlock (2011a). In the present study, state boundaries for the dorsal neural arch height were changed, leading to differently scored diplodocid specimens, which actually show variable ratios. A detailed study of the ratio of diplodocid caudal neural spines showed that many specimens do not have neural spines that are 1.5 times taller than the posterior articular surface. Therefore, neither of the two characters was recovered as diplodocid or diplodocimorph synapomorphy.
- proximal caudal vertebrae with procoelous centra (McIntosh, 1990b). Procoelous centra were shown to have a much wider distribution than just Diplodocoidea (Carballido et al., 2012b; D'Emic, 2012; Mannion et al., 2013). Herein, the character describing caudal articular surface shape, is subdivided into four states, including slight and strong procoely (following Carballido et al., 2012b). Whereas most diplodocines have slightly procoelous anterior caudal centra, many other diplodocid specimens actually have flat posterior articular surfaces. To state that all diplodocoid taxa have procoelous centra would thus over simplify the variety of morphologies found.
- caudal vertebrae with wing-like transverse processes (McIntosh, 1990b). The same trait was found to diagnose Diplodocimorpha by Whitlock (2011a). Many non-diplodocid sauropod species do have dorsally expanded caudal transverse processes on their first caudal vertebra. These are herein interpreted as wing-like, but they do not have the same shape as diplodocoid taxa. The problem is best exemplified by a putative diplodocid anterior caudal from the Cretaceous of China (PMU R263; Upchurch and Mannion, 2009), which was later reidentified as somphospondylan titanosauriform (Whitlock et al., 2011). A more precise definition of wing-like would be beneficial for future analyses.
- presence of a whiplash tail (at least 30 elongate, biconvex posterior caudal vertebrae) (McIntosh, 1990a; Wilson and Sereno, 1998). Even though probably valid, the present analysis is not able to identify this feature as synapomorphic for any clade, due to the incompleteness of the included specimens. Only the two specimens of *Apatosaurus louisae* (CM 3018 and 3378) preserve a tail complete enough to confidently score them for this character. The trait was thus not included into any clade diagnosis.
- presence of forked chevrons (McIntosh, 1990b). Although named for this peculiar morphology

(Marsh, 1878), *Diplodocus*, as well as its higher-level clades are not the only taxa to have forked chevrons. In fact, recent studies and discovery of new basal sauropods show that it might actually be a retained plesiomorphy (Zhang, 1988; Ouyang and Ye, 2002; Remes et al., 2009).

- short metacarpals (McIntosh, 1990a). The same as for the forked chevrons accounts here: relatively short metacarpals are plesiomorphic for Sauropoda, whereas the elongate metacarpals diagnose macronarian and titanosauriform taxa (Wilson, 2002; Upchurch et al., 2004a; Tschopp, 2008).
- ischia have expanded distal ends (McIntosh, 1990b). The expanded distal ends of the ischia are in fact typical for all diplodocoid sauropods from which ischia were known in 1990. Now, rebbachisaurs are known to have distally unexpanded ischia, restricting this trait to diagnose Flagellicaudata.

Diplodocimorpha Calvo and Salgado, 1995.
Definition: *Diplodocus* + *Rebbachisaurus* (node-based; Taylor and Naish, 2005).
Unambiguous synapomorphies:

1. the anterior margin of the premaxilla does not have a step (1-0; Wilson, 2002. This synapomorphy was not found by the present analysis, but recovered as such by Wilson (2002) and Whitlock (2011a). As the data matrix indeed supports an identification of this trait as unambiguous synapomorphy for Diplocimorpha, it has been included in the present list)
2. squared (111-2) or blunted snout (111-1; Berman and McIntosh, 1978. As the first synapomorphy, also this one was found by Whitlock (2011a), but not directly confirmed by the present analysis, although supported by the data matrix)
3. sprl extend onto lateral aspect of anterior caudal neural spines (318-1).

Exclusive synapomorphies:

4. posterior dorsal, sacral and anterior caudal neural spines are 'petal' shaped in anterior/posterior view, expanding transversely through 75% of its length and then tapering (294-1)
5. transition from 'fan'-shaped to 'normal' caudal ribs occurs between Cd4 and Cd5 (300-1).

Ambiguous synapomorphies:

6. a semicircular dorsal margin of the ilium (409-1).

Previously suggested synapomorphies:

The analysis of Whitlock (2011a) produced a high number of synapomorphies for Rebbachisauridae + Flagellicaudata. Several of these are herein recovered as synapomorphic for Diplodocoidea: the straight, and posterodorsally directed nasal process of the premaxilla, the absence of a sharp distinction between the premaxillary main body and the nasal process, the lacking midline contact of the posterolateral process of the premaxilla and the lateral process of the maxilla, the dorsal process of the maxilla that extends posterior to the posterior process, the subequal diameters of the antorbital and orbital fenestra, the retracted external nares, the large contribution of the jugal to the antorbital fenestra, the anterior ramus of the quadratojugal that reaches anterior to the orbit, the wide angle between the anterior and the dorsal process of the quadratojugal, the low angle between basipterygoid processes and skull roof, the transverse flange of the pterygoid that reaches anterior to the antorbital fenestra, and the four or more replacement teeth per alveolus. As no skull is known for *Haplocanthosaurus*, the recovery of these synapomorphies for Diplodocidea or Diplodocimorpha depends on the method used. With ACCTRAN, they result synapomorphic for Diplodocoidea, whereas DELTRAN recovers them diagnosing Diplodocimorpha. Additional synapomorphies previously recovered for Diplodocimorpha are the following:

- parietal excluded from margin of posttemporal foramen (Calvo and Salgado, 1995; Upchurch, 1998; Wilson, 2002). The exclusion of the parietal from the posttemporal foramen is not recovered as synapomorphy for any clade herein, although the data set would support one for Flagellicaudata, as proposed by Whitlock (2011a) as well.
- squamosal extends anteriorly past posterior margin of orbit (Whitlock, 2011a). The anterior extension of the squamosal is restricted in *Kaatedocus* (Tschopp and Mateus, 2012b), which inhibited an identification of the anteriorly reaching squamosal as diplodocimorph synapomorphy in the present analysis.

- tooth crowns aligned along jaw axis, not overlapping (Wilson, 2002). Lacking overlap of tooth crowns is not restricted to Diplodocoidea, but also present in *Giraffatitan brancai*, for example (Janensch, 1935; Wilson and Sereno, 1998). It was thus not recovered as synapomorphy of any clade in the present analysis.
- mid-caudal vertebral centra length at least twice its height (Upchurch et al., 2004a). The mid-caudal centra are generally more elongate in diplodocoids, compared to other taxa. However, they only reach ratios of two times centrum height in advanced diplodocines, as a more detailed assessment of this character shows. It can thus not be regarded synapomorphic for Diplodocimorpha.
- biconvex distal-most caudal centra (Upchurch, 1998). Biconvex distal caudal vertebrae are exclusive to Diplodocimorpha in the present analysis (but absent in *Suuwassea*, Harris 2006a), which would favor an identification as synapomorphy, as in Whitlock (2011a). However, biconvex caudal vertebrae also occur in titanosauriforms (Wilson et al., 1999), and would thus only qualify for an ambiguous synapomorphy. Therefore, it was not included as such in the present diagnosis.
- distal-most caudal centra at least five times longer than tall (Wilson et al., 1999). The elongation of these distal caudal vertebrae was coded differently in Whitlock (2011a) and here, which resulted in *Apatosaurus* specimens being scored different than *Diplodocus*. The value of greater than five, as proposed by Whitlock (2011a) might thus still be valid, but cannot be recovered as synapomorphic with the present analysis due to varying state boundaries.
- proximal margin of humerus expanded, lateral margin concave in anterior/posterior view (Janensch, 1961). The last diplodocimorph synapomorphy recovered by Whitlock (2011a) describes the concave lateral border of the humerus. This feature is actually present as well in most of the basal sauropods used as outgroups herein. It is thus a plesiomorphic trait and cannot be used as synapomorphy of Diplodocimorpha.

Flagellicaudata Harris and Dodson, 2004.
Definition: *Dicraeosaurus* + *Diplodocus* (node-based; Harris and Dodson, 2004).
Unambiguous synapomorphies:

1. subnarial foramen and anterior maxillary foramen are separated by a narrow bony isthmus (8-1; Wilson, 2002)
2. presence of a preantorbital fossa (15-1)
3. an elongate and slender posterior end of the quadrate (posterior to posterior-most extension of pterygoid ramus) (54-1)
4. the absence of any squamosal-quadratojugal contact (56-1)
5. the absence of a parietal contribution to the post-temporal fenestra (59-1; Whitlock, 2011a)
6. vomer articulates with maxilla (103-1; Wilson, 2002. The recovery of this trait as synapomorphy for Flagellicaudata is supported by the present analysis but not recovered as such, probably due to the very low percentage of specimens scorable for the character)
7. the anteroventral margin of the dentary bears a sharply projecting triangular process or 'chin' (104-1; Wilson and Smith, 1996)
8. anteriorly oriented, procumbent teeth (122-1)
9. atlantal intercentrum bears an anteroventral lip (144-1. Recovered as diplodocoid synapomorphy by Wilson and Sereno (1998), the presence of the anteroventral lip can actually only be confirmed for Flagellicaudata, as no rebbachisaurid atlas has yet been reported. The data matrix supports an identification of the derived as diagnostic for Flagellicaudata, even though it was not recovered as such)
10. the distal shaft of the ischium is triangular, with its depth increasing medially (423-1).

Exclusive synapomorphies:

11. the longest axes of the basal tubera are oriented in an angle to each other, pointing towards the occipital condyle (87-1)
12. the lateral spinal lamina of anterior-most caudal neural spines expands anteroposteriorly towards its distal end, and becomes rugose (303-1)

13. the posterior edge of the distal blade of anterior chevrons is posteriorly expanded in a step-like fashion (355-1).

Shared synapomorphies:

14. a shallow quadrate fossa (51-0)
15. absence of longitudinal grooves on the lingual aspect of the teeth (123-0)
16. anterior diapophyseal laminae (acdl, prdl) are well defined in in anterior caudal vertebrae (313-1)
17. a 'crus' bridging the haemal canal is present in some chevrons (352-0; Wilson, 2002)
18. the cross-sectional shape of ischial distal shafts is V-shaped, forming an angle of nearly 50° with each other (424-0; Upchurch, 1998)
19. the ischial shaft is transversely expanded distally (425-1; Upchurch, 1998)
20. the distal condyle of metatarsal I bears a posterolateral projection (463-1; Berman and McIntosh, 1978).

Ambiguous synapomorphies:

21. presacral neural spine bifurcation present (126-1; McIntosh, 1990b; this synapomorphy was not found by the main analyses, but included in the list as it readily distinguishes derived diplodocoids from more basal forms as rebbachisaurs or *Haplocanthosaurus*)
22. mid- and posterior dorsal neural arches have divided centropostzygapophyseal lamina, with the lateral branch connecting to the pcdl (261-1)
23. the hyposphene-hypantrum system is well developed in posterior dorsal vertebrae, having a rhomboid shape up to last element (276-0)
24. the ventral surface is marked by irregular foramina on some anterior caudal centra (305-1).

Previously suggested synapomorphies:

- quadrate articular surface roughly triangular in shape (Whitlock, 2011a). The triangular articular surface of the quadrate was recovered as exclusive diplodocoid synapomorphy herein, with rebbachisaurids developing crescent-shaped surfaces. This is most probably due to the fact that the character was herein treated as ordered, thus assuming that a common ancestor of rebbachisaurs and flagellicaudatans must have had triangular articular surfaces.
- distance between supratemporal fenestrae twice the length of the longest axis of the supratemporal fenestrae (Salgado and Calvo, 1992). A detailed assessment of this ratio showed that most diplodocids do not reach a ratio of two. Even after redefining the state boundaries, variation between diplodocid specimens results in differential scorings. A high ratio, and thus wide distance between the supratemporal fenestrae can thus not be regarded synapomorphic for Flagellicaudata.
- ventrally directed occipital condyle (Upchurch, 1998). The orientation of the occipital condyle was not included in the present analysis, as it was found to be very difficult to define a character in an unambiguous way.
- single planar occlusal facet on teeth (Wilson, 2002). This synapomorphy includes two characters as used in the present analysis, the distinction between single and double occlusal facets, as well as the planar versus V-shaped facets. The planar facets were found herein as synapomorphy for Diplodocoidea, whereas the single facets are not found to be typical for any clade.
- 17 dentary teeth or fewer (Wilson, 2002). Whereas it is true that flagellicaudatans have less than 17 teeth, the same is true for basal macronarian dinosaurs (e.g. *Camarasaurus* or *Giraffatitan*; Gilmore, 1925; Janensch, 1935), as well as for the rebbachisaurid *Demandasaurus*. It thus seems more parsimonious to interpret the less than 17 dentary teeth as ancestral to all neosauropods, with subsequent reversal to a higher number of teeth in *Nigersaurus* (Sereno and Wilson, 2005).
- low-angled, planar wear facets on the teeth (Calvo, 1994). The angulation of the wear facets was not included as character in the present analysis, as an acute angle only characterizes rebbachisaurids, and enough characters were already used to resolve the position and relationship of that clade. Low angles are not restricted to diplodocids either, being also present as late stages in the wear of camarasaur teeth (e.g. SMA 0002; Wiersma, 2013).
- anterior cervical neural spines bifid (McIntosh, 1990b). Anterior neural spines are rarely

preserved in cervical vertebrae, even in nearly complete specimens like the holotypes of *Apatosaurus louisae* or *Diplodocus carnegii* (CM 3018 and 84, respectively; Wedel and Taylor, 2013). Diplodocid specimens preserving anterior neural spines actually all show the bifurcation to initiate posterior to CV 5 or 6, and thus not in the anterior elements. The only group positively confirming bifid neural spines in anterior cervical vertebrae are the Dicraeosauridae. Indeed, the present analysis recovered bifid anterior neural spines as synapomorphic for this taxon.

- presence of a median tubercle in bifurcated cervical and dorsal neural spines (Wilson, 2002). Although generally present in Flagellicaudata, some specimens do not show such a tubercle (e.g. *Amargasaurus cazaui*, or UW 15556). Also, the probable non-diplodocoid *Australodocus* does have a median tubercle, such that its presence could at most be interpreted as ambiguous synapomorphy. Since it was not recovered as such by the present analysis, it was not included in the diagnosis.
- anterior dorsal vertebrae with divided centropostzygapophyseal laminae (Wilson, 2002). A divided centropostzygapophyseal lamina was only positively identified in mid- and posterior dorsal vertebrae, but not in anterior ones. Therefore, the character was restricted to mid- and posterior elements.
- height of sacral neural spines nearly four times length of centrum (Wilson, 2002). This ratio was redefined and posterior dorsal vertebrae were included into the description. The apomorphic state of the new character (282-1) was found to diagnose Dicraeosauridae in the present analysis.
- anterior caudal neural arches with spinoprezygapophyseal lamina (sprl) on lateral aspect of neural spine (Wilson, 2002). The extension of the caudal spinoprezygapophyseal lamina onto the lateral side of the neural spine is actually a diplodocimorph synapomorphy, as also present in rebbachisaurids, but absent in *Haplocanthosaurus* (Hatcher, 1903; Sereno et al., 2007).
- procoelous first caudal centrum (Wilson, 2002). The first caudal centrum is actually flat posteriorly in many flagellicaudatan specimens (e.g. CM 84, pers. obs.), and only more posterior elements develop a slight convexity, if at all. This trait is thus not included as synapomorphic for any clade herein.
- pubis with prominent ambiens process (McIntosh, 1990b). In the present analysis, a distinction is made between the hook-like ambiens process as present in *Diplodocus* and *Dicraeosaurus* (Hatcher, 1901; Janensch, 1961), for example, and the less developed, but still prominent process of apatosaurines (Ostrom and McIntosh, 1966). The presence of a prominent ambiens process can thus still be confirmed as synapomorphic for Flagellicaudata, but as the morphology is different, it was not recovered as such in the present analysis.

Dicraeosauridae Huene, 1927.

Definition: *Dicraeosaurus*, not *Diplodocus* (stem-based; Sereno, 1998).

Unambiguous synapomorphies:

1. the crista prootica is expanded laterally into dorsolateral process (76-1; Salgado and Calvo, 1992)
2. basipterygoid processes are narrowly diverging (< 31°) (92-2; Wilson, 2002)
3. the area between the basipterygoid processes and parasphenoid rostrum forms a deep slot-like cavity that passes posteriorly between the bases of the basipterygoid processes (95-1; Upchurch et al., 2004a)
4. subtriangular cross-sectional shape of the symphysis of the dentary, tapering sharply towards its ventral extreme (105-1; Whitlock and Harris, 2010)
5. presence of a tuberosity on the labial surface of the dentary, near the symphysis (106-1; Whitlock and Harris, 2010)
6. the first bifid cervical neural spine is in CV 3 (140-0).

Shared synapomorphies:

7. frontal symphysis is fused in adult individuals (26-1; Salgado and Calvo, 1992)
8. presence of a pineal (parietal) foramen between frontals and parietals (36-0)
9. presence of a postparietal foramen (66-1; Salgado and Calvo, 1992)

10. the sagittal nuchal crest of the supraoccipital is narrow, sharp, and distinct (74-1)
11. the supraoccipital bears a foramen close to its contact with the parietal (75-1)
12. absence of a basioccipital depression between foramen magnum and basal tubera (80-0)
13. the anterolateral corner of the tooth row is displaced labially (112-1)
14. the width to height ratio of cervical vertebrae is less than 0.5 (128-0; Upchurch et al., 2004a)
15. the total height to centrum length ratio of anterior cervical vertebrae is greater than 1.2 (usually around 1.5) (154-2)
16. the pleurocoels of anterior cervical centra are undivided (157-0)
17. presence of paired pneumatic fossae on the ventral surface of anterior cervical centra (160-1)
18. mid-cervical neural spines are anteriorly inclined (169-1; Rauhut et al., 2005)
19. posterior cervical and anterior dorsal bifid neural spines are parallel to converging (211-1; Rauhut et al., 2005)
20. absence of an anterior, middle single fossa projected through the midline of single dorsal neural spines (233-1)
21. the transition from bifid to single dorsal neural spines is abrupt (235-1)
22. mid-dorsal neural spines are bifid, inclusive of at least the fifth dorsal vertebrae (250-1)
23. lateral pleurocoels are absent in mid- and posterior dorsal centra (252-0; Janensch, 1929a)
24. posterior dorsal centra are amphicoelous (270-0)
25. the ratio of height above postzygapophyses (neural spine) of posterior dorsal neural arches to height below (pedicel) is 3.1 or greater (272-1)
26. the height of posterior dorsal and/or sacral neural spines (not including arch) is more than 3 times centrum length (282-2; McIntosh, 1990a)
27. absence of pleurocoels in sacral vertebral centra (287-0)
28. the ventral surface of anterior caudal transverse processes is directed dorsally (312-1)
29. a ratio of blade height above pubic peduncle of the ilium to its anteroposterior length of 0.40 or more (405-1)
30. the position of the highest point of the femoral head is laterally shifted in anterior view, and lies above the main portion of the shaft (431-1)
31. presence of a short transverse ridge on the anteromedial surface of the distal end of the tibia (443-1)
32. a ratio of mediolateral width of the astragalus to maximum anteroposterior length of less than 1.6 (452-1)
33. metatarsal I is relatively gracile, proximal transverse width to greatest length is less than 0.8 (461-0)
34. the groove on the lateral surface of pedal unguals extends straight horizontally (477-1).

Ambiguous synapomorphies:

35. postzygodiapophyseal and spinopostzygapophyseal laminae of mid-cervical vertebrae form a right angle (170-1)
36. mid- and posterior cervical neural arches bear lateral fossae on the prezygapophysis process (183-1)
37. absence of dorsal pneumatopores (pleurocoels) (227-0)
38. the base of the notch between the metapophyses of anterior, bifid dorsal vertebrae is narrow and V-shaped (244-1)
39. the parapophysis of DV 3 lies mid-way between the top of the centrum and the level of the prezygapophyses (246-1).

Previously suggested synapomorphies:

- premaxilla with anteroventrally orientated vascular grooves originating from an opening in the maxillary contact (Wilson, 2002). The grooves are shown to be present as well in some diplodocid specimens (see above). An identification of this trait as dicraeosaurid synapomorphy is thus questionable.
- frontal contributes to margin of supratemporal fenestra (reversal; Wilson and Sereno, 1998). Although this is true for *Dicraeosaurus* and *Amargasaurus*, *Suuwassea* does not show any participation of the frontal in the supratemporal fenestra. Therefore, the present analysis was

not able to recover this reversal as synapomorphic for the entire clade Dicraeosauridae.

- supratemporal fenestra smaller than foramen magnum (Salgado and Calvo, 1992). The reduced size of the supratemporal fenestra has been found as synapomorphic for *Amargasaurus* + *Dicraeosaurus* by the equally weighted reduced consensus tree. However, this trait is shared with *Limaysaurus*, and it remains thus unclear how to interpret it (diplodocoid or diplodocimorph synapomorphy with reversals, or as convergently acquired traits of Rebbachisauridae and Dicraeosauridae).
- ventrally directed prong on squamosal (Whitlock, 2011a). A ventrally directed process is present in some diplodocids as well, and very similar to the state in *Dicraeosaurus* (see above). An enlarged prong-like structure is only present in *Amargasaurus*, which does not allow an identification of this feature as synapomorphic for Dicraeosauridae.
- basal tubera narrower than occipital condyle (Wilson, 2002). As shown by Mannion (2011), the ratio between basal tubera and occipital condyle width is highly variable. The state boundaries used herein do not allow to identify the lowest ratio as synapomorphic for Dicraeosauridae, although the ratios themselves indicate that it might be taxonomically significant.
- 'petal' shaped posterior dorsal neural spines (Wilson, 2002). The peculiar 'petal' shape of dorsal, and sacral neural spines of dicraeosaurids is also present in rebbachisaurids, which led to an identification of this feature as diplodocimorph synapomorphy herein.
- cervical vertebrae with longitudinal ridge on ventral surface (Sereno et al., 2007). The presence of a longitudinal ridge is a plesiomorphic feature within sauropods, and present as well in some diplodocid specimens (e.g. SMA 0004, YPM 429; Lull, 1919; Tschopp and Mateus, 2012b). Dicraeosaurids have well-developed keels in anterior cervical centra, shared with *Shunosaurus*, but also with *Galeamopus shellensis* SMA 0011 (see above). The presence of ventral ridges and keels is thus too variable as that a reversal to the plesiomorphic state could be recovered as synapomorphic for any clade.
- anterior caudal centra with irregularly placed foramina on ventral surface (Harris, 2007). The presence of ventral foramina in anterior caudal vertebrae is herein recovered as flagella-caudatan synapomorphy, as it is shared with numerous diplodocid specimens.
- mid-caudal vertebral centra with mid-height longitudinal ridge on lateral surface, centra hexagonal in anterior/posterior view (Whitlock, 2011a). Longitudinal ridges also mark the mid-caudal vertebrae of *Camarasaurus*, as well as many apatosaurine specimens (Gilmore, 1925, 1936). Their presence could thus only be interpreted as shared synapomorphy for Dicraeosauridae. Since it was not recovered as such, it is not included in the diagnosis herein.
- humerus with pronounced proximolateral corner (Wilson, 2002). This trait was recovered as neosauropod synapomorphy in the implied weights trees. As definition of 'pronounced' is somewhat vague, interpretation of this character might have been different in Wilson (2002). The herein used definition is explained and figured above.

Diplodocidae Marsh, 1884.
Definition: *Diplodocus*, not *Dicraeosaurus* (stem-based; Sereno, 1998).
Unambiguous synapomorphies:

1. maxilla-quadratojugal contact broad (14-1; Rauhut et al., 2005; not recovered by the present analysis, it is still supported by the data matrix. The reason why it was not recovered is probably the low percentage of specimens preserving these two bones)
2. antorbital fenestra with concave dorsal margin (20-1; Wilson, 2002; also this trait was not recovered as diplodocid synapomorphy, although supported by the specimens for which a scoring was possible. The reason is probably the same as in the previous synapomorphy)
3. posterior process of the prefrontal is hooked (25-1; Berman and McIntosh, 1978)
4. mandible without strong coronoid eminence (108-1; Whitlock, 2011a; as in the previous characters, the low number of specimens preserving the mandible probably precluded an identification of this character as synapomorphy for Diplodocidae, although supported by the data set)

5. direct crown-to-crown occlusion absent (116-1; Wilson, 2002; yet another trait not found as synapomorphic, probably due to low percentage of preservation, but supported by the dataset)
6. 14 to 15 cervical vertebrae (127-1; Huene, 1929)
7. anterior centrodiapophyseal lamina (acdl) of anterior caudal vertebrae is divided (314-1; Wilson, 2002).

Exclusive synapomorphies:

8. preantorbital fenestra occupies at least 50% of the preantorbital fossa (17-1)
9. medial margin of the prefrontal is curving distinctly medially at its anterior end to embrace the anterolateral corner of the frontal (23-1)
10. ten dorsal vertebrae (224-2; Huene, 1929)
11. anterior and mid-caudal vertebrae bear ventrolateral ridges (329-1).

Shared synapomorphies:

12. shape of the posterior face of the basal tubera flat (85-1) or slightly concave (85-2)
13. short mid- and posterior dorsal transverse processes (263-0)
14. posterior dorsal, sacral and anterior caudal neural spines rectangular through most of their length (294-0; Whitlock, 2011a; the current state represents a reversal to the plesiomorphic condition, and it was scored differently in *Amphicoelias altus* AMNH 5764, which has a dorsally expanded neural spine, somewhat resembling a 'petal' shape, although not to the extent as in dicraeosaurs or rebbachisaurs)
15. anterior caudal transverse processes with anteroposteriorly expanded lateral extremities (316-1)
16. spinoprezygapophyseal laminae (sprl) and spol contact each other on anterior caudal neural spines (319-1; Wilson, 1999)
17. presence of a lateral bulge on the femur (428-1).

Ambiguous synapomorphies:

18. dorsal transverse processes horizontal or only slightly inclined dorsally (230-0)
19. posterior centroparapophyseal lamina of mid- and posterior dorsal neural arches present as single lamina (258-1; Wilson, 2002).

Previously suggested synapomorphies:

- antorbital fenestra subequal to orbital maximum diameter (Wilson, 2002). The large antorbital fenestrae are recovered as diplodocid synapomorphy herein, as *Nigersaurus* also shows the apomorphic state (Sereno et al., 1999, 2007).
- prefrontal posterior process elongate (Wilson, 2002). Determination of the length of the posterior process of the prefrontal is highly influenced by the orientation of the skull roof, as shown previously. Taking this into account, elongated posterior processes of the prefrontal are not present in all diplodocid specimens. This trait was thus excluded from the diagnosis.
- no internarial bar (Upchurch et al., 2004a). An internarial bar also appears to be absent in dicraeosaurids (Janensch, 1935; Harris, 2006b). It would thus more appropriately be interpreted as flagellicaudatan synapomorphy, but was not included in the present analysis, as in most specimens it is difficult to distinguish true absence from incomplete preservation.
- frontal contribution to dorsal margin of orbit roughly equal to contribution of prefrontal (Whitlock, 2011a). Remeasuring the contribution of the frontal and prefrontal in various diplodocid skulls showed that variation occurs both within but also outside Diplodocidae. Neither one nor the other state can thus be confidently considered synapomorphic for any clade.
- quadrate fossa shallow (Wilson, 2002). A shallow quadrate fossa was later found in *Suuwassea* as well (Harris, 2006a), thus not being restricted to Diplodocidae. Consequently, it has here been found as flagellicaudatan synapomorphy.
- squamosal-quadratojugal contact absent (Wilson, 2002). Tschopp and Mateus (2012b) showed that a contact between the squamosal and the quadratojugal was also absent in *Suuwassea* (contrary to Harris, 2006a). Therefore, the present trait was herein recovered as flagellicaudatan synapomorphy.
- the jugal forms a substantial part of the caudoventral margin of the antorbital fenestra (Upchurch, 1998). The contribution of the jugal to the antorbital fenestra was recovered as

diplodocoid synapomorphy, as *Nigersaurus* shows the same morphology (Sereno and Wilson, 2005).

- an angle between the rostra1 and dorsal quadratojugal processes of 130° (Upchurch et al., 2004a). A wide angle between rostral and dorsal processes of the quadratojugal also occurs in *Nigersaurus* (Sereno and Wilson, 2005), leading to a recovery of this feature as diplodocoid synapomorphy herein.
- the distal end of the paroccipital process rounded and tongue-like (Upchurch et al., 2004a). This character was not used in the present analysis as it was unclear what tongue-like precisely means. It was substituted by a character describing dorsoventral expansion towards the distal ends of the paroccipital processes, which varies within Diplodocidae and does thus not qualify as reliable synapomorphy.
- the parasphenoid rostrum is a laterally compressed, thin spike lacking the longitudinal dorsal groove (Upchurch et al., 2004a). A dorsal groove is actually present on many diplodocid parasphenoid rostra (e.g. CM 11161, pers. obs.). Transverse compression of the parasphenoid rostrum is also apparent in *Camarasaurus* (Madsen et al., 1995). Generally, diplodocid parasphenoid rostra are more spike-like, or dorsoventrally compressed, compared to *Giraffatitan* or *Camarasaurus* (Janensch, 1935; Madsen et al., 1995), but that is difficult to translate into a valid phylogenetic character, and was thus not used as such herein.
- the ectopterygoid process of the pterygoid located below the antorbital fenestra (Upchurch et al., 2004a). Such an anterior position of the ectopterygoid process is shared with rebbachisaurs (Whitlock, 2011a) , and thus recovered as diplodocoid synapomorphy herein.
- the ectopterygoid process of the pterygoid reduced, so that it cannot be seen below the ventral margin of the skull in lateral view (Upchurch et al., 2004a). No such character was included in the present analysis. However, given the rareness of palatal complexes preserved in their true position, it remains doubtful if the analysis would have been capable to confidently resolve character state distributions.
- the breadth of the main body of the pterygoid at least 33% of pterygoid length (Upchurch et al., 2004a). Given that only one disarticulated diplodocid pterygoid was available for direct study (SMA 0011), no character was included in the present analysis to test the distribution of this trait. Generally, diplodocid pterygoids do appear more elongate compared to non-diplodocid taxa, but only rarely measurements can be taken directly from the specimen. It is thus not included in the diagnosis herein.
- cervical vertebrae with longitudinal sulcus on ventral surface (Upchurch, 1998). Presence of a ventral longitudinal sulcus in cervical vertebrae is uncommon in apatosaurs, if one does not consider the concave area between the strongly ventrally projecting parapophyses. Consequently, the sulcus is herein recovered as diplodocine synapomorphy.
- bifurcated centroprezygapophyseal lamina in cervical vertebrae, with a medial and a lateral ramus connecting to the zygapophysis (Wilson, 2002). As *Supersaurus* does not seem to have divided cprl, the current analysis recovered this trait as synapomorphic for both Apatosaurinae and Diplodocinae more derived than *Supersaurus*.
- 70-80 caudal vertebrae (Upchurch et al., 2004a). The high number of caudal vertebrae is difficult to score in a specimen-based phylogenetic analysis, as only very few specimens preserve reasonably complete caudal series. In the present analysis, only CM 3018 and 3378 positively confirm such a statement. Indirect evidence for an elongated tail also comes from the rod-like distal caudal vertebrae in some dicraeosaurid specimens, as well as in *Limaysaurus*. The number of caudal vertebrae is thus not included in the diagnosis here.
- presence of diapophyseal laminae on anterior caudal vertebrae (Upchurch, 1998). This character has been divided in the present analysis, distinguishing between anterior and posterior diapophyseal laminae. Apatosaurs, as well as *Supersaurus* tend to have much broader posterior diapophyseal laminae compared to diplodocines, thus not qualifying to be scored as 'distinct'. On the other hand, well-developed anterior diapophyseal laminae also occur in dicraeosaurs. Therefore, the latter were recovered as flagellicaudatan synapomorphy, whereas distinct posterior diapophyseal laminae were found to diagnose *Galeamopus* + mdD.

- humero-femoral length ratio is approximately 0.66 (Huene, 1927). Due to the lack of specimens preserving both complete fore- and hindlimbs, the distribution of this character state cannot be assessed in enough detail with the present analysis. While generally supporting the identification as diplodocid synapomorphy, the low number of only two specimens positively confirming this ratio for the entire clade Diplodocidae does not allow a well-founded inclusion of the trait into a diagnosis.
- insertion of the M. iliofibularis on the fibula located above midshaft (Wilson and Sereno, 1998). In fact, insertion of this muscle on the fibula is located further distally in apatosaurines and *Tornieria* than in more derived diplodocines, as a detailed assessment showed (see above). The proximal location of the insertion is thus recovered as synapomorphic for *Supersaurus* + mdD herein.
- an absence of a calcaneum (McIntosh, 1990b). The absence of a calcaneum as diplodocid synapomorphy is most probably a preservational artifact. As shown by Bonnan (2000), at least one pes of *Diplodocus* preserves a calcaneum, and personal observations in two putative apatosaur pedes (CM 30766 and NHMUK R3215) reveal the probable presence of such an element in apatosaurs as well. It is thus not included in the diagnosis of any clade.
- pedal phalanx I-1 having a proximoventral margin drawn out into a thin plate or heel that underlies the distal end of metatarsal I (Upchurch et al., 2004a). The distribution of this trait is more complicated: it is also present in the non-diplodocid *Turiasaurus* and *Cetiosauriscus stewarti*, and absent in *Apatosaurus louisae* CM 3018. Its presence would thus only qualify for an ambiguous synapomorphy, but was not recovered as such by the present analysis.
- pedal phalanx II-2 reduced in craniocaudal length and having an irregular shape (Upchurch et al., 2004a). Whereas all included diplodocid specimens preserving this element show a reduced craniocaudal length in php II-2, the same is also present in *Mamenchisaurus* (Ouyang and Ye, 2002). As no complete pes is known from any dicraeosaur or rebbachisaur, true distribution of this trait cannot be assessed to date, and it is thus excluded from the updated diagnosis of Diplodocidae.

Apatosaurinae Huene, 1927.
Definition: *Apatosaurus*, not *Diplodocus* (stem-based; Taylor and Naish, 2005).
Unambiguous synapomorphies:

1. cervical ribs projecting well beneath centrum, such that the length of the posterior process is subequal in length to the fused diapophysis/tuberculum (216-1).

Exclusive synapomorphies:

2. posterior cervical rib shafts are initially directed in the same direction but turn to run a little downwards toward the distal tip (223-1).

Shared synapomorphies:

3. dorsoventral height of the occipital process of the parietal is low, subequal to less than the diameter of the foramen magnum (63-0)
4. presence of a foramen in the notch that separates the two basal tubera (90-1)
5. centroprezygapophyseal lamina of mid- and posterior cervical neural arches is divided, resulting in the presence of a 'true' divided centroprezygapophyseal lamina, which is dorsally connected to the prezygapophysis (185-2)
6. posterior centrodiapophyseal lamina (pcdl) and postzygodiapophyseal laminae (podl) of mid- and posterior cervical transverse processes do not meet anteriorly, such that the postzygapophyseal centrodiapophyseal fossa extends onto the posterior face of the transverse process (186-1)
7. anterior process of posterior cervical ribs is reduced to a short bump-like process or absent (220-1)
8. mid- and posterior dorsal parapophyses lie posterior to the anterior edge of centrum (256-0)
9. posterior dorsal postzygapophyses are oblique, including an almost 90° angle (275-1)
10. ratio of the pubic articulation of the ischia to the anteroposterior length of the pubic pedicel of 1.5 or greater (420-1)
11. pedal phalanges III-1 and IV-1 are wider than long (476-1).

Ambiguous synapomorphies:

12. posterior centrodiapophyseal lamina in cervical vertebrae reaches below the posterior end of the neural canal (135-1)
13. abrupt transition from bifid to single dorsal neural spines (235-1)
14. bifid dorsal neural spines (if present) do not extend past the second or third dorsal (250-0)
15. ratio of metacarpal III length to distal transverse width of less than 2.9 (402-0).

Previously suggested synapomorphies:

To my knowledge, only one phylogenetic study is published recognizing an apatosaurine clade including more than just the genus *Apatosaurus*: Lovelace et al. (2007) also recover *Supersaurus* and *Suuwassea* as apatosaurine diplodocids, but do not provide a diagnosis for the clade. The current diagnosis is thus the first for Apatosaurinae based on a cladistic analysis.

Diplodocinae Marsh, 1884.

Definition: *Diplodocus*, not *Apatosaurus* (stem-based; Taylor and Naish, 2005).

Exclusive synapomorphies:

1. cervical vertebrae bear a small, shallow, anteroposteriorly elongate fossa posteroventral to the pleurocoel (131-1)
2. large coels mark the anterior caudal centra (307-1; Wilson, 2002).

Shared synapomorphies:

3. box-like basal tubera (82-1)
4. presence of a basisphenoid/basipterygoid recess (91-1)
5. a longitudinal sulcus marks the ventral surface of the cervical vertebrae (133-1)
6. the tuberculum of anterior and mid-cervical ribs is directed upwards and backwards in lateral view (218-1)
7. an oblique ridge connects the medial and lateral edges at the base of the rib head in dorsal ribs (283-1)
8. presence of a ventral longitudinal hollow in anterior and mid-caudal centra (330-1; Marsh, 1895)
9. a ratio of centrum length to posterior height in mid-caudal vertebrae of 1.7 or greater (332-1)
10. the scapular acromial process that lies nearly at midpoint of the scapular body (364-1).

Previously suggested synapomorphies:

- EI of mid-cervical vertebrae greater than 4.0 (Upchurch, 1998). State boundaries were changed herein in comparison to Upchurch (1998). However, a mean value of four or more is not reached by several diplodocine specimens, but convergently acquired by various outgroup taxa (Tab. 6.23). It is thus excluded from the diagnosis of Diplodocinae herein.
- quadrangular anterior articular surface of anterior caudal centra (Wilson, 2002). There is a wide range of articular surface shapes in these elements, and it is difficult to describe them qualitatively or divide them into only two categories, as was done by Wilson (2002: circular or quadrangular). Most of the diplodocine anterior caudal centra have a flat ventral edge (e.g. *Barosaurus lentus* YPM 429; Lull, 1919), but this is accounted for in other characters. The shape becomes gradually more quadrangular towards middle caudal vertebrae in *Diplodocus* (e.g. AMNH 223; Osborn, 1899), but not in *Barosaurus*, which keeps its rounded lateral edges (e.g. AMNH 6341; pers. obs., 2011). Although anterior caudal centra with flat ventral border can still be confidently assigned to Diplodocinae, more rounded centra cannot be excluded just based on this morphology. The 'quadrangular' shape of the anterior face should thus not be regarded a true synapomorphy of Diplodocinae.
- caudal centrum length doubles over first 20 vertebrae (Wilson, 2002). Caudal centra that are nearly doubling their length within the first 20 elements is not restricted to Diplodocinae. It is shared by *Cetiosauriscus stewarti* (NHMUK R3078, pers. obs., 2011), *Zapalasaurus bonapartei* (Salgado et al., 2006), as well as *Suuwassea emilieae* (Harris, 2006a) and the apatosaur FMNH P25112 (Gilmore, 1936). It is therefore not considered a diplodocine synapomorphy herein.
- middle caudal neural spines vertical (Wilson, 2002). Actually, the majority of diplodocine specimens preserving mid-caudal vertebrae have posterodorsally directed neural spines. The

only species with vertical mid-caudal neural spines is *Diplodocus hallorum*.

Updated diagnoses of valid diplodocid genera and species

The following diagnoses include autapomorphies found by the analysis as well as additional traits found to be unique at least within the respective higher-level clade (Apatosaurinae or Diplodocinae). Autapomorphies found only in one specimen are marked by an asterisk. Referred specimens as well as localities and horizons only include information from the present analysis. Specific or generic identification of other specimens is often not done with enough detail (i.e. without phylogenetic analysis or accurate description of the material), such that earlier referrals require a reappraisal before definitely including them in the species lists. Geographical and temporal distribution of the genera and species proposed herein have thus to be regarded as smallest possible ranges.

Systematic Paleontology

Dinosauria Owen, 1842.
Sauropoda Marsh, 1878.
Neosauropoda Bonaparte, 1986.
Diplodocoidea Marsh, 1884.
Flagellicaudata Harris and Dodson, 2004.
Diplodocidae Marsh, 1884.

***Amphicoelias* Cope, 1877a.**

Type and only referred species: *Amphicoelias altus* Cope, 1877a.

Invalid proposed species: *Amphicoelias latus* Cope, 1877a (= *Camarasaurus*); *Amphicoelias fragillimus* Cope, 1878 (nomen dubium).

Revised diagnosis: *Amphicoelias* is diagnosed by the following autapomorphies: posterior dorsal postzygapophyses almost horizontal, such that the two articular facets include a wide angle (275-0*, shared with Diplodocinae); posterior dorsal neural spines 'petal' shaped, expanding transversely through 75% of its length and then tapering (294-1*, unique within Diplodocidae); a gracile femur, with a robustness index (sensu Wilson and Upchurch, 2003) of less than 0.22 (427-0*, only shared with USNM 10865 within Diplodocidae); and a mediolateral width of the femur which is subequal to the anteroposterior diameter (430-0*, only shared with CM 566 and *Dicraeosaurus* within Diplodocoidea).

Comments: The characters initially used by Cope (1877a) to diagnose the genus are now known to be more widespread among sauropods, as the amphicoelous dorsal centra, or the weak development of the greater trochanter on the femur. Osborn and Mook (1921) first recognized the extreme slenderness of the femur of *Amphicoelias*, compared to other sauropods. Wilson and Smith (1996) reported two autapomorphies for the skull, based on a second specimen referred to the genus. However, no detailed description nor figures of the material have yet been published, such that the validity of these traits as autapomorphic features for *Amphicoelias* are herein regarded questionable. The assignment of the specimen to *Amphicoelias* was mainly based on the circular cross section of the femur midshaft (Wilson and Smith, 1996), which has been recovered as autapomorphic herein as well. Upchurch et al. (2004a) proposed the unusual, slightly posterodorsal orientation of the posterior dorsal neural spine as an autapomorphy of the genus. Although characters were included in the present analysis to code for this morphology (C265 and 280), none of them was found as autapomorphic for *Amphicoelias*, and both are shared with specimens from both Apatosaurinae and Diplodocinae.

Locality and horizon: Cope Quarry 12, Garden Park Area, Fremont County, Colorado. Upper-most Brushy Basin Member, Morrison Formation (probably Tithonian). Dinosaur zone 4 (Turner and Peterson, 1999), Zone 6 (Foster, 2003).

***Amphicoelias altus* Cope, 1877a.**

Type specimen: AMNH 5764.
Referred specimens: -

Diagnosis, locality, and horizon as genus.

Apatosaurinae Huene, 1927.
***Apatosaurus* Marsh, 1877a.**

Syn. *Brontosaurus amplus* Marsh, 1881.

Type species: *Apatosaurus ajax* Marsh, 1877a.
Referred species: *Apatosaurus louisae* Holland, 1915a.

Invalid proposed species: *Apatosaurus grandis* Marsh, 1877a (= *Camarasaurus grandis*), *A. laticollis* Marsh, 1879 (nomen dubium; =*A. louisae*), *A. minimus* Mook, 1917 (non-diplodocoid neosauropod), *A. alenquerensis* Lapparent and Zbyzewski, 1957 (= *Lourinhasaurus alenquerensis*), *A. yahnahpin* Filla and Redman, 1994 (= *Eobrontosaurus yahnahpin*).

Revised diagnosis: *Apatosaurus* is diagnosed by the following autapomorphies: presence of an accessory horizontal lamina in the spinodiapophyseal fossa of mid- and posterior cervical vertebrae, not connected to any surrounding lamina (187-1, unique within Apatosaurinae), vertical struts divide lateral pneumatic foramen of mid- and posterior dorsal centra (253-1, unique within Apatosaurinae); gradual transverse expansion of anterior caudal neural spines (328-0, unique within Diplodocidae); absence of ventrolateral ridges (329-0, unique within Apatosaurinae); and a straight scapular blade in lateral view (368-0, unique within Diplodocidae).

Comments: Berman and McIntosh (1978) proposed the relative positions of ectopterygoid and pterygoid as distinguishing character between the skulls CM 11161 and 11162. It was used as a phylogenetic character by Wilson (2002). However, there are only very few diplodocid skulls available, with the palatal complex articulated and complete. One of these is the juvenile probable *Diplodocus* skull CM 11255, which was interpreted to have an organization more similar to the state in *Apatosaurus* than to *Diplodocus* (Whitlock et al., 2010). However, recent studies appear to show that actually *Apatosaurus* CM 11162 has the same arrangement as *Diplodocus* CM 11161 (Whitlock and Lamanna, 2012). The distribution of this character thus seems very difficult to interpret. The fact that there are so few specimens preserving this area also decreases the phylogenetic value of this character. Therefore, until a more numerous sample of diplodocid skulls with articulated palatal complex is found, this feature should not be used in diagnoses. In general, autapomorphies previously proposed for the genus *Apatosaurus* most often describe a more inclusive clade in the present analysis, as many taxa previously included in the genus are actually better interpreted as forming their own genera (e.g. *Brontosaurus*, or *Elosaurus*). These traits are thus not further discussed here.

Locality and horizon: various sites in Colorado, Wyoming, and Utah. Middle to upper part of the Upper Jurassic Morrison Formation, Late Kimmeridgian to Early Tithonian. Apatosaurine intervals 2 and 3 (Bakker, 1998); Dinosaur zone 3B upper (Turner and Peterson, 1999); Zone 5 (Foster, 2003).

***Apatosaurus ajax* Marsh, 1877a.**
Syn.? *Brontosaurus amplus* Marsh, 1881

Type specimen: YPM 1860.
Referred specimens: ?YPM 1981

Revised diagnosis: *A. ajax* is diagnosed by the following autapomorphies: a shallow, second fossa marks the quadrate shaft medially to the pterygoid flange (not the quadrate fossa) (52-1*, unique within Apatosaurinae), box-like basal tubera (81-1*, unique within Apatosaurinae), longest axes of the basal tubera oriented parallel to each other (87-0*, unique within Apatosaurinae), medial surface of posterior bifid, cervical neural spines is smooth (206-1*, unambiguous), presence of an accessory lamina linking the hyposphene of mid- and posterior dorsal vertebrae with the base of the posterior centrodiapophyseal lamina (260-1*, unique within Apatosaurinae), and presence of an elliptical depression between the lateral spinal lamina of caudal neural spines and the postspinal lamina (292-1*, unique within Apatosaurinae).

Comments: In the most recent revised diagnosis of the species, Upchurch et al. (2004b) proposed four more autapomorphies of the species, which are not found in the present analysis, due to the differing set of referred specimens to the species. Upchurch et al. (2004b) also included the specimens AMNH 460, NSMT-PV 20375, YPM 1840, and 1861 within *A. ajax*, whereas the present analysis recovers the first three specimens as more basal, possibly new apatosaurine taxa, and YPM 1861 as *Apatosaurus louisae*. Wide cervical vertebrae, and low cervical neural spines are thus variable within Apatosaurinae. The dorsolateral process of the distal condyle of mt I, as well as the flange-like proximoventral process of php II-1might diagnose NSMT-PV 20375 instead.

Locality and horizon: Lakes' Quarry 10, Morrison, Gunnison County, Colorado (YPM 1860), and possibly Reed's Quarry 11, Como Bluff, Albany County, Wyoming (YPM 1981). Upper middle to upper-most Morrison Formation, Late Kimmeridgian to Early Tithonian. Apatosaurine intervals 2 and 3 (Bakker, 1998); Dinosaur zone 3B upper (Turner and Peterson, 1999); Zone 5 (Foster, 2003).

***Apatosaurus louisae* Holland, 1915a.**
Syn.? *Brontosaurus amplus* Marsh, 1881

Type specimen: CM 3018.
Referred specimens: CM 3378, CM 11162, YPM 1861, ?YPM 1981.

Revised diagnosis: *A. louisae* can be diagnosed by the following autapomorphies: presence of a dorsoventrally elongate coel on anterior and mid-cervical neural spines (165-1*, unique within Apatosauridae), posterior cervical prezygapophyses terminate well behind anterior ball (194-1, unique within Flagellicaudata), absence of a subvertical lamina in the postzygapophyseal centrodiapophyseal fossa of posterior cervical vertebrae, with the free edge facing posteriorly (199-0, unique within Apatosaurinae), presence of a rounded, subtriangular process on posterior cervical ribs, below the tuberculum (222-1, unambiguous), DV 2 is longer than DV 1 (239-1, unique within Diplodocoidea), pleurocoel on the first dorsal centra located posteriorly (240-1, unique within Apatosaurinae), parapophysis of DV 3 lies mid-way between centrum and prezygapophyses (246-1, unique among Diplodocidae), presence of an oblique ridge on the rib head of some dorsal ribs (283-1, unique within Apatosaurinae), slightly bifid anterior caudal neural spines (326-1*, unique within Apatosaurinae), and presence of a subtriangular projection on the ventral edge of the scapular blade (370-1*, unique among Apatosaurinae).

Comments: In their revised diagnosis, Upchurch et al. (2004b) also proposed the presence of pneumatopores in the dorsal ribs as autapomorphic for *A. louisae*. However, pneumatized dorsal ribs were already figured by Marsh (1896) from the holotype of *Brontosaurus excelsus*, YPM 1980, and are also present in YPM 1981 (pers. obs., 2011). The anterior restriction of the sacral ribs as interpreted to be present in the holotype specimen by Upchurch et al. (2004b) is herein regarded a questionable autapomorphy, as original matrix was left filling the space between the sacral ribs, which might thus partly be obliterated. Two more autapomorphies put forward by Upchurch et al. (2004b) are actually also present in other apatosaurine specimens: the heart-shaped anterior caudal centra, and the medially beveled glenoid surface of the scapula.

Locality and horizon: Dinosaur National Monument, Jensen, Uintah County, Utah (CM 3018, 3378, and 11162), and Lakes' Quarry 10, Morrison, Gunnison County, Colorado (YPM 1861). Upper middle to upper-most Morrison Formation, Late Kimmeridgian to Early Tithonian. Apatosaurine intervals 2 and 3 (Bakker, 1998); Dinosaur zone 3B upper (Turner and Peterson, 1999); Zone 5 (Foster, 2003).

***Brontosaurus* Marsh, 1879.**

Type and only species: *Brontosaurus excelsus* Marsh, 1879.

Invalid proposed species: *Brontosaurus amplus* Marsh, 1881 (= *Apatosaurus*).

Revised diagnosis: *Brontosaurus* can be diagnosed by the following autapomorphies: orientation of the tuberculum of mid-dorsal ribs follows the straight direction of the rib shaft (285-1*, unique among Apatosaurinae), the posterior end of mid- and posterior caudal neural spine summits lies more or less straight above the postzygapophyses (343-1*, unique among Apatosaurinae); presence of a large nutrient foramen opening on midshaft anteriorly on the femur (434-1*, unique among Apatosaurinae); presence of a short transverse ridge on the anteromedial surface of the distal end of the tibia (443-1*, unique among Diplodocidae).

Comments: The autapomorphies proposed for '*Apatosaurus*' *excelsus* by Upchurch et al. (2004b) are questionable. Cervical ribs that terminate in front of the posterior end of the centrum are widespread among Diplodocoidea, and are recovered as synapomorphic for that clade herein. The ventromedially projecting process on the anterior end of the cervical ribs is here reinterpreted as shortened anterior process of the cervical rib. The spine summits in anterior dorsal vertebrae are actually longer than wide (Ostrom and McIntosh, 1966: plates 17 and 18), and the slight medial widening is due to the presence of a medial ridge on the metapophyses, which is also present on other apatosaurine specimens (e.g. CM 3018, UW 15556; Gilmore, 1936).

Locality and horizon: Reed's Quarry 10, Como Bluff, Albany County, Wyoming. Middle (Bakker, 1998) to upper (Foster, 1998) Morrison Formation, Late Kimmeridgian to ?Early Tithonian. Dinosaur zone 3B upper (Turner and Peterson, 1999), Zone 5 (Foster, 2003).

***Brontosaurus excelsus* Marsh, 1879.**

Type specimen: YPM 1980.
Referred specimens: -

Diagnosis, locality, and horizon as genus.

***Elosaurus* Peterson and Gilmore, 1902.**

Type and only species: *Elosaurus parvus* Peterson and Gilmore, 1902.

Revised diagnosis: *Elosaurus* is diagnosed by the following autapomorphies: greatly reduced spinoprezygapophyseal laminae in posterior dorsal vertebrae (274-0, unique within Diplodocoidea), and absence of a shallow, but distinct rugose tubercle at the center of the concave proximal portion of the anterior surface of the humerus (386-0*, unique within Apatosaurinae).

Comments: In their revised diagnosis of '*Apatosaurus*' *parvus*, Upchurch et al. (2004b) further mentioned wider than high posterior dorsal centra, a right angle between acromial ridge and scapular blade, differences in length of the ulnar proximal branches, a constriction in the distal half of mc III, and subequal width and depth of the distal articular surface of mc V. Wider than high dorsal centra are also present in NSMT-PV 20375 (Upchurch et al., 2004b), an almost right angle between acromial ridge and distal blade can be seen in *Apatosaurus ajax* as well as in *Eobrontosaurus yahnahpin* (Filla and Redman, 1994), and different lengths of the ulnar branches also mark *Apatosaurus ajax* (Tab. 6.47). The characters from the manus could not have been positively identified in the specimens included, and were thus omitted from the revised diagnosis.

Locality and horizon: Sheep Creep Quarry E, Albany County, Wyoming, and possibly Riggs' Quarry 15, Dinosaur Hill, Mesa County, Colorado. Middle Morrison Formation, probably Late Kimmeridgian. Dinosaur zone 3B lower (Turner and Peterson, 1999), Zone 4 (Foster, 2003).

***Elosaurus parvus* Peterson and Gilmore, 1902.**

Type specimen: CM 566.
Referred specimens: UW 15556 (previously CM 563), FMNH P25112 (provisionally).

Diagnosis, locality, and horizon as genus.

Eobrontosaurus Bakker, 1998.

Type and only species: *Eobrontosaurus yahnahpin* (Filla and Redman, 1994). The species was initially described as belonging to *Apatosaurus*.

Revised diagnosis: *Eobrontosaurus* can be diagnosed by the following autapomorphies: presence of a longitudinal sulcus on the ventral surface of cervical vertebrae (133-1*, unique among Apatosaurinae), total height of anterior cervical vertebrae to centrum length ratio is greater than 1.2 (usually around 1.5) (154-2*, unique among Apatosaurinae), the medial surface of anterior dorsal, bifid neural spines is gently rounded transversely (245-0*, unique within Apatosaurinae), mid- and posterior dorsal neural spines narrow dorsally to form a triangular shape in lateral view, with the base approximately twice the width of the dorsal tip (265-1*, unique among Apatosaurinae), absence of a thickened anterior rim of anterior caudal prespinal lamina (321-0*, unique among Apatosaurinae), a rounded anteroventral margin of the coracoid (372-0*, unique among Apatosaurinae), a ratio of the longest metacarpal to radius length of 0.40 or greater (399-1*, unique among Diplodocoidea), and the distal articular surface of the metatarsal I being perpendicular to the axis of the shaft (462-1*, unique among Flagellicaudata).

Comments: Bakker (1998) mentioned three more diagnosing features: long cervical ribs, distal scapular blade expanded, and coracoid suture at right angle with the long axis of the scapular blade. The presence of long cervical ribs could not have been confirmed based on the available pictures of the type specimen. The distally expanded scapular blade is actually shared with many apatosaur specimens (e.g. CM 3018, UW 15556, Gilmore, 1936). The unexpanded state is primarily based on the type specimen of *Apatosaurus ajax*, YPM 1860, but personal observations showed that the edges of the distal end are broken, and that the true expansion can therefore not be assessed in its entirety. The angle between the coracoid articulation and the distal blade, measured from photographs, is 74° (Tab. 6.42). Even if that should be wrong, the specimen described by Upchurch et al. (2004b), NSMT-PV 20375 shows an almost right angle, which would thus impede an interpretation as autapomorphy for *Eobrontosaurus*.

Locality and horizon: Bertha Quarry, Como Bluff, Albany County, Wyoming. Lower Morrison Formation, Kimmeridgian. Apatosaurine interval 1 (Bakker, 1998), Dinosaur zone 2 (Turner and Peterson, 1999), Zone 2 (Foster, 2003).

Eobrontosaurus yahnahpin (Filla and Redman, 1994).

Type specimen: Tate-001.
Referred specimens: -

Diagnosis, locality, and horizon as genus.

Diplodocinae Marsh, 1884.

Diplodocus Marsh, 1878.

Syn. *Seismosaurus* Gillette, 1991

Type species: *Diplodocus carnegii* Hatcher, 1901 (suppressing the *D. longus* Marsh, 1878, see above).
Referred species: *Diplodocus hallorum* (Gillette, 1991).

Invalid proposed species: *Diplodocus longus* Marsh, 1878 (nomen dubium, previous type species, case to ICZN in preparation to propose *D. carnegii* as substitute), *D. lacustris* Marsh, 1884 (nomen dubium), *D. hayi* Holland, 1924 (= *Galeamopus hayi*).

Revised diagnosis: *Diplodocus* can be diagnosed by the following autapomorphies: base of posterior dorsal neural spines anteriorly inclined (280-1, unique within Diplodocinae), pneumatopores of anterior caudal centra persist until caudal 16 or more posteriorly (308-1, unambiguous), well-developed rugosity on dorsolateral margin of metatarsal II, near the distal end, extending to the center

of the shaft (468-1, unique among Diplodocidae).

Comments: Whitlock (2011a) proposes three cranial traits as autapomorphies of *Diplodocus*: a well-defined preantorbital fossa, the pterygoid that lies medial to the ectopterygoid, and the anteriorly inclined, procumbent teeth. As no skull can be definitely attributed to *Diplodocus*, these suggestions are questionable. Furthermore, distinct preantorbital fossae, and procumbent teeth are also present on other diplodocine taxa (e.g. *Galeamopus, Kaatedocus*), and the relative positions of the pterygoid and ectopterygoid are not established with enough certainty to use it as diagnostic character (see above). Upchurch et al. (2004a) also defines *Diplodocus* solely based on cranial traits, most of which are actually shared with other diplodocine species that have not been described or recognized at the time (*Galeamopus*, *Kaatedocus*). Wilson (2002) proposed the anteriorly expanded femoral distal condyles as autapomorphic for *Diplodocus*, as shared characteristic with advanced titanosauriforms. However, although the distal condyles are accompanied anteriorly by two distinct vertical ridges, the articular surface does not extend onto them as in *Rapetosaurus krausei* FMNH PR 2209, for example (Curry Rogers, 2009).

Locality and horizon: various sites in Colorado, New Mexico, Utah, and Wyoming. Middle Morrison Formation, probably Late Kimmeridgian. Apatosaurine interval 2 (Bakker, 1998), Dinosaur zones 3A to 3B upper (Turner and Peterson, 1999), Zones 3 to 5 (Foster, 2003).

***Diplodocus carnegii* Hatcher, 1901.**

Type specimen: CM 84.
Paratype: CM 94.
Referred specimens: -

Revised diagnosis: *Diplodocus carnegii* is diagnosed by the following autapomorphies: spinopostzygapophyseal laminae (spol) of posterior dorsal neural arches divided near the postzygapophyses (277-1, unique among Flagellicaudata), and slender metatarsal II (mean proximal and distal transverse breadth/maximum length <0.53) (465-0*, unique among Diplodocoidea).

Comments: Hatcher (1901) proposed two different characters to distinguish *D. carnegii* from *D. longus*: shorter cervical ribs, and more posteriorly directed caudal neural spines. However, comparisons were not based on the holotype of *D. longus*, but on two referred specimens (USNM 4712 and AMNH 223), which are now known not to belong to the species: the cervical vertebra Hatcher (1901) mentions (USNM 4712) actually has apatosaurine affinities (Hatcher, 1903, pers. obs. 2011), whereas the specimen AMNH 223, on which Hatcher (1901) based his comparisons, is herein interpreted to belong to *Diplodocus hallorum*. The short cervical ribs are widespread among Diplodocinae, and do thus not qualify as species autapomorphy. Caudal neural spine orientation is one of the main features distinguishing *D. carnegii* from *D. hallorum*, but the vertical spines from the latter species are herein found to be the derived state, such that the more posteriorly inclined spines in *D. carnegii* cannot be used to diagnose the species.

Locality and horizon: Sheep Creek Quarries D (CM 94) and D(3) (CM 84), Albany County, Wyoming. Middle Morrison Formation, Late Kimmeridgian. Dinosaur zone 3B lower (Turner and Peterson, 1999), Zone 4 (Foster, 2003).

***Diplodocus hallorum* (Gillette, 1991).**
Syn. *Seismosaurus hallorum*, *Seismosaurus halli*.

Type specimen: NMMNH 3690.
Referred specimens: AMNH 223, DMNS 1494, USNM 10865.

Revised diagnosis: *Diplodocus hallorum* can be diagnosed by the following autapomorphies: dorsal end of the postspinal lamina of single dorsal neural spines concave transversely (234-1,

unique among Diplodocoidea), mid-caudal neural arches are situated on the anterior half of the centrum (337-1, unique among Diplodocoidea), vertical mid-caudal neural spines (340-1, unambiguous), posterior end of mid- and posterior caudal neural spine summits lies more or less straight above the postzygapophyses (343-1, unique among Diplodocinae), presence of distinct fossae on the medial surfaces of the proximal branches of middle chevrons (357-1, unique among Diplodocinae), a gracile femur (robustness index (sensu Wilson and Upchurch, 2003) <0.22) (427-0*, unique among Diplodocinae), and the groove on the lateral surface of pedal unguals extends straight horizontally (477-1*, unique among Diplodocinae).

Comments: Lucas et al. (2006) in their taxonomic reappraisal of *Seismosaurus hallorum* proposed two more characters that distinguish the type specimen of *D. hallorum* from other species of *Diplodocus*: a more robust pubis, and paddle-shaped distal blades of the chevrons. Whereas the first is difficult to quantify and is thus provisionally omitted from the present diagnosis, the paddle shape of the chevrons is partly included in the character coding the posterior expansion of the chevron blade (C355), which is not present in the other specimens referred to *D. hallorum*. The specific chevron shape of NMMNH 3690 is thus herein regarded as individual variation.

Locality and horizon: Seismosaurus Quarry, Sandoval County, New Mexico (NMMNH 3690), Dinosaur National Monument Quarry, Uintah County, Utah (DMNS 1494, USNM 10865), and AMNH 223 Quarry, Como Bluff, Albany County, Wyoming (AMNH 223). Middle Morrison Formation, Late Kimmeridgian. Apatosaurine interval 2 (Bakker, 1998), Dinosaur zones 3B lower to upper (Turner and Peterson, 1999), Zones 4 to 5 (Foster, 2003).

***Barosaurus* Marsh, 1890.**

Type and only species: *Barosaurus lentus* Marsh, 1890.

Invalid proposed species: *Barosaurus affinis* Marsh, 1899 (nomen dubium), *Barosaurus gracilis* Russell et al., 1980 (nomen nudum).

Revised diagnosis: *Barosaurus* can be diagnosed by the following autapomorphies: pleurocoel not extending onto parapophysis in anterior cervical vertebrae (158-1*, unique among Diplodocidae), elongation index of posterior cervical vertebrae (without anterior condyle) greater than 2.6 (192-2*, unique among Diplodocoidea), an anterior projection on the prdl of posterior cervical, or anterior and mid-dorsal vertebrae, right lateral to the prezygapophysis (213-1, unique among Diplodocoidea), nine dorsal vertebrae (224-3*, unambiguous), transition from 'fan'-shaped to 'normal' caudal ribs occurs between Cd 6 and Cd 7 (300-3*, unique among Diplodocinae), pneumatopores of anterior caudal centra disappear by caudal 15 (308-0*, unique within Diplodocinae), depth of ventral hollow increasing from anterior to posterior caudal centra (the present trait could not have been assessed in the current analysis, but is provisionally included in the diagnosis of *Barosaurus* following Upchurch et al., 2004a).

Comments: Whitlock (2011a) does not list any autapomorphies for *Barosaurus*. McIntosh (2005) states four more diagnosing features for *Barosaurus*: bifurcation of cervical neural spines restricted to the posterior half of the neck, summits of caudal neural spines undivided, a proportionally shorter tail, and a less prominent ventral hollow in anterior and mid-caudal centra. However, all of these traits represent the basal diplodocid morphology, and are shared e.g. with *Kaatedocus* or *Supersaurus* (Lovelace et al., 2007; Tschopp and Mateus, 2012b). Upchurch et al. (2004a) suggested an additional autapomorphy: the parapophysis of DV 2 is situated at the bottom of the centrum. Such a low position of the parapophysis is also present in DV 2 of *Galeamopus shellensis*, and can thus not be regarded diagnostic for *Barosaurus*.

Locality and horizon: various sites in South Dakota, Utah, and Wyoming. Lower to middle Morrison Formation, Kimmeridgian. Apatosaurine intervals ?1 to 2 (Bakker, 1998), Dinosaur zones 2 to 3B upper (Turner and Peterson, 1999), Zones 2 to 5 (Foster, 2003).

***Barosaurus lentus* Marsh, 1890.**

Type specimen: YPM 429.
Referred specimens: AMNH 6341, AMNH 7535, CM 11984.

Diagnosis, locality, and horizon as genus.

***Tornieria* Sternfeld, 1911.**

Type and only species: *Tornieria africana* (Fraas, 1908). The species was originally assigned to *Gigantosaurus africanus* (Fraas, 1908).

Invalid proposed species: *Tornieria robustus* (Fraas, 1908) (=*Janenschia robusta*).

Revised diagnosis: *Tornieria* is diagnosed by the following autapomorphies: mid-caudal prezygapophyses terminate at or behind the anterior edge of the centrum (339-0*, unique among Diplodocinae), a straight posterior border of the sternal plate (377-1*, unique among Neosauropoda), and distal femoral condyles expand onto the anterior portion of the femoral shaft (439-1*, unambiguous).

Comments: Whitlock (2011a) listed a single autapomorphy for the genus: the absence of a ventral hollow in anterior and mid-caudal centra. Contrary to Whitlock (2011a), a ventral hollow is present in the preserved caudal vertebrae of both specimens included herein (Remes, 2006; pers. obs., 2011). In his revision of *Tornieria*, Remes (2006) proposed additional autapomorphies: frontal forms the entire dorsal margin of the orbit, prefrontal with a short posterior process, elongate cervical vertebrae, relatively long anterior caudal vertebrae, pleurocoel located on the upper third of the caudal centra, caudal transverse processes situated high on the centrum, caudal neural spines single, and lacking lateral processes, the distal blade of the scapula is only slightly expanded, unequal lengths of the proximal ulnar processes, robust ischial shaft, and a low tibia to femur length ratio. The traits of the frontal and prefrontal were later shown to be present in *Kaatedocus* as well (Tschopp and Mateus, 2012b). Elongate cervical vertebrae were developed several times within Diplodocinae (e.g. *Barosaurus*, *Supersaurus*; McIntosh, 2005; Lovelace et al., 2007). Centrum length increases from anterior-most towards middle caudal vertebrae in all diplodocines, making relative length a serially variable character. It was thus not included in the present analysis, and a detailed assessment of the relative position of the anterior caudal vertebrae in the *Tornieria* specimens would be needed before including relative centrum length as diagnosing trait for the genus. The position of the pleurocoel in the preserved anterior-most caudal vertebra of the holotype individual (SMNS 12141a) does not appear to be restricted to the upper third (Remes, 2006: fig. 4C). Pneumatic foramina are dorsally located in the referred caudal vertebrae from trench dd (MB.R.2956 to MB.R.2958; Remes, 2006), but as this trait appears different in the holotype, it should not be used in a diagnosis. The same accounts for the dorsal location of the transverse processes, which is most probably influenced by the position of the pleurocoel. Single caudal neural spines without lateral processes can only be observed in the referred caudal vertebrae, which were not included in the present analysis. However, these traits also occur in other diplodocine species, and are thus not reliable characters to distinguish *Tornieria*. A slight expansion of the scapular blade as well as robustness of the ischial shaft are difficult to quantify, but ratios do not appear to be significantly different from other diplodocine taxa. Unequally long ulnar proximal processes are shared with *Galeamopus shellensis* (Tab. 6.47), as is the low tibia to femur ratio (Tab. 6.55).

Locality and horizon: localities A and k, Upper Saurian Beds, Tendaguru, District of Lindi, Tanzania. Tithonian.

***Tornieria africana* (Fraas, 1908).**

Type specimen: SMNS 12141a, 12145a, 12143, 12140, and 12142. The individual also contains the specimens SMNS 12145c, MB.R.2672, 2713, and 2728 (Remes, 2006).
Referred specimens: MB.R.2386, 2572, 2586, 2669, 2673, 2726, 2730, 2733, 2913, and 3816

(all belonging to a single individual; Heinrich, 1999; Remes, 2006).

Diagnosis, locality, and horizon as genus.

***Supersaurus* Jensen, 1985.**

Syn. *Dystylosaurus* Jensen, 1985; *Ultrasauros* Olshevsky, 1991.

Type and only species: *Supersaurus vivianae* Jensen, 1985.

Revised diagnosis: *Supersaurus* can be diagnosed by the following autapomorphies: spinoprezygapophyseal laminae in single dorsal neural spines separate along their entire length (231-0, unique among Diplodocoidea), presence of an infradiapophyseal pneumatopore between the acdl and the pcdl of mid- and posterior dorsal neural arches (262-1*, unique among Diplodocinae), opisthocoelous posterior dorsal centra (270-2, unique among Diplodocoidea), 'heart'-shaped anterior-most caudal centra with an acute ventral ridge (296-1, unique among Diplodocinae), pneumatopores on anterior caudal centra restricted to foramina (307-0, unique among Diplodocinae), and an angle between the acromial ridge and the distal blade greater than 81° (362-2*, unique among Diplodocinae).

Comments: Lovelace et al. (2007) listed several additional diagnosing traits for *Supersaurus*: elongate cervical vertebrae, an extreme narrowing of the ventral surface of cervical centra, well-developed parallel keels that mark the ventral surface of cervical centra, pneumatic foramina present on the ventral surface of cervical centra, lateral pneumatopores on cervical centra small, located within a shallow coel, anterior dorsal vertebrae with a ventral keel, tall posterior dorsal neural spines, relatively low posterior dorsal neural arch, pneumatized dorsal ribs, and a dorsally expanded scapular blade. Most of these traits are actually shared with other diplodocine species: the elongate cervical vertebrae (e.g. *Tornieria*), the well-developed parallel keels (herein called posteroventral flanges), the ventral pneumatic foramina (e.g. in *Dinheirosaurus*), the restricted and small lateral pneumatic foramina of cervical vertebrae (e.g. *Galeamopus shellensis*), the ventral keel in anterior dorsal centra, the low dorsal neural arches, and the pneumatized dorsal ribs (e.g. *Dinheirosaurus*), the tall dorsal neural spines (typical for diplodocids in general), as well as the expanded scapular blade (e.g. *Galeamopus*). The extreme narrowing of the ventral surface of cervical centra is herein interpreted as a consequence of the centrum elongation, as a narrowing is generally seen relative to the centrum length.

Locality and horizon: Dry Mesa Quarry, Montrose County, Colorado, and Jimbo Quarry, Converse County, Wyoming. Middle Morrison Formation, Late Kimmeridgian to ?Early Tithonian. Dinosaur zone 3B lower (Turner and Peterson, 1999), Zone 4 (Foster, 2003).

***Supersaurus vivianae* Jensen, 1985.**

Syn. *Dystylosaurus edwini* Jensen, 1985; *Ultrasauros macintoshi* (Jensen, 1985).

Type specimen: BYU 12962. Individual probably also contains the specimens BYU 4503, 4839, 9024-25, 9044-45, 9085, 10612, 12424, 12555, 12639, 12819, 12861, 12946, 13016, 13018, 13981, 16679, and 17462 (Lovelace et al., 2007).
Referred specimens: WDC DMJ-021.

Diagnosis, locality, and horizon as genus.

***Dinheirosaurus* Bonaparte and Mateus, 1999.**

Type and only species: *Dinheirosaurus lourinhanensis* Bonaparte and Mateus, 1999.

Revised diagnosis: *Dinheirosaurus* can be diagnosed by the following autapomorphies: single posterior cervical and anterior dorsal neural spines (126-0*, unique among Flagellicaudata), the ventral keel is restricted to the posterior portion of the posterior cervical centrum (193-1*, unique within Flagellicaudata), three small fossae on the lateral face of the posterior cervical neural spine, posterior to the elongated coel (unambiguous; this trait was not included as character, as unambiguous autapomorphies of single OTUs do not bear any phylogenetic information), dorsal centrum length

(excluding articular 'ball') remains approximately the same along the sequence (225-0*, unique among Diplodocinae), dorsal transverse processes are more than 30° inclined dorsally from the horizontal (230-1*, unique among Diplodocidae), and the ventral surface of anterior caudal centra is without irregularly placed foramina (305-0*, unique within Flagellicaudata).

Comments: In their redescription of the species, Mannion et al. (2012) mention two additional autapomorphies: an accessory, subvertical lamina in the postzygapophyseal centrodiapophyseal fossa, and an accessory lamina linking the hyposphene to the posterior centrodiapophyseal lamina in mid- and posterior dorsal neural arches. A subvertical accessory lamina actually subdivides the pocdf in a variety of diplodocid and diplodocine taxa (e.g. *Galeamopus hayi*), whereas a lamina connecting hyposphene and pcdl is also present in posterior dorsal neural arches of *Supersaurus vivianae* (D. Lovelace, pers. comm., 2013).

Locality and horizon: Praia de Porto Dinheiro, Lourinhã, Portugal. Amoreira-Porto Novo Member, Lourinhã Formation, Late Kimmeridgian.

***Dinheirosaurus lourinhanensis* Bonaparte and Mateus, 1999.**

Type specimen: ML 414.
Referred specimens: -

Diagnosis, locality, and horizon as genus.

***Kaatedocus* Tschopp and Mateus, 2012b.**

Type and only species: *Kaatedocus siberi* Tschopp and Mateus, 2012b.

Revised diagnosis: *Kaatedocus* can be diagnosed by the following autapomorphies: anteriorly restricted squamosals (55-0*, unique among Diplodocoidea), a rugosity on the anterodorsal corner of the lateral side of mid- and posterior cervical centra (178-1, unique among Diplodocidae), posterior cervical prezygapophyseal facets are posteriorly followed by a transverse sulcus (195-1*, unambiguous), posterior cervical epipophyses are dorsoventrally compressed (202-1, unique among Flagellicaudata), posterior cervical neural spines parallel to converging (211-1, unique among Diplodocidae), and the distance between the bifid posterior cervical neural spine summits is subequal to neural canal width (212-1, unique among Diplodocidae).

Comments: Tschopp and Mateus (2012b) list several other autapomorphies as well: a U-shaped notch between the frontals, presence of a post-parietal foramen, a sharp, narrow sagittal nuchal crest, a straight anterior edge of the basal tubera, and the cervical pre-epipophysis that forms a distinct anterior spur. The notch is herein shown to be shared with *Galeamopus shellensis*. The presence of a post-parietal foramen is difficult to interpret in most diplodocid skulls, due to often fractured surfaces in this area of the skull. Moreover, it is present as well in another braincase from the Howe Quarry, SMA O25-8, which was tentatively referred to *Barosaurus* (Schmitt et al., 2013). A relatively sharp sagittal nuchal crest is present as well in the skull of *Galeamopus hayi* HMNS 175 (Holland, 1906). Straight to convex anterior margins of the basal tubera are shared with CM 3452 and *Galeamopus shellensis*. The development of the cervical pre-epipophysis is actually different in the holotype and the referred specimen AMNH 7530, where no distinct anterior spur is present. The presence or absence of a spur is thus better interpreted as individually variable within *Kaatedocus*, and thus not diagnostic for the present genus.

Locality and horizon: Howe Quarry, Shell, Bighorn County, Wyoming. Lower Morrison Formation, Kimmeridgian. Dinosaur zone 2 (Turner and Peterson, 1999), Zone 2 (Foster, 2003).

***Kaatedocus siberi* Tschopp and Mateus, 2012b.**

Type specimen: SMA 0004.
Referred specimens: AMNH 7530, SMA D16-3.

Diagnosis, locality, and horizon as genus.

***Galeamopus* Tschopp, 2013.**

Type species: *Galeamopus hayi* (Holland, 1924). The type species was originally assigned to *Diplodocus hayi*.

Diagnosis: *Galeamopus* is diagnosed by the following autapomorphies: portion of the parietal contributing to the skull roof is practically inexistent (60-2, unique among Flagellicaudata), a foramen in the notch that separates the two basal tubera (90-1, unique among Diplodocinae), well-developed anteromedial processes on the atlantal neurapophyses, which are distinct from the posterior wing (146-1, unique among Diplodocoidea), the posterior wing of atlantal neurapophyses remains of subequal width along most of its length (148-1, unambiguous), and the axial prespinal lamina develops a transversely expanded, knob-like tuberosity at its anterior end (151-1, unambiguous).

Locality and horizon: various sites in Wyoming. Lower to Middle Morrison Formation, Kimmeridgian. Apatosaurus interval 1 (Bakker, 1998), Dinosaur zone 2 to possibly 3 (Turner and Peterson, 1999), Zones 2 to possibly 3 or 4 (Foster, 2003).

***Galeamopus hayi* (Holland, 1924).**

Type specimen: HMNS 175 (previously CM 662).
Referred specimens: -

Diagnosis: *Galeamopus hayi* is diagnosed by the following autapomorphies: dorsoventral height of the parietal occipital process is low, subequal to less than the diameter of the foramen magnum (63-0*, unique among Diplodocinae), basipterygoid processes widely diverging (> 60°; 92-0*, unique among Diplodocinae), an ulna to humerus length of more than 0.76 (387-2*, unique within Diplodocoidea), distal articular surface for the ulna on the radius is reduced and relatively smooth (392-0*, unique within Diplodocidae), and the distal condyle of the radius is beveled at least 15° to the long axis of the shaft (393-1*, unique within Diplodocinae).

Locality and horizon: Quarry A, Red Fork of the Powder River, Johnson County, Wyoming. Lower Morrison Formation, Kimmeridgian. Apatosaurine interval 1 (Bakker, 1998).

***Galeamopus shellensis* Tschopp, 2013.**

Type specimen: SMA 0011.
Referred specimen: AMNH 969.

Diagnosis: *Galeamopus shellensis* can be diagnosed by the following autapomorphies: horizontal canal connecting the preantorbital and the antorbital fenestra laterally on the maxilla (12-1*, unambiguous), mid- and posterior cervical vertebrae with a large foramen connecting the postzygapophyseal centrodiapophyseal fossa and the spinopostzygapophyseal fossa (191-1*, unambiguous), a robust humerus (380-2*, unique within Diplodocinae), absence of a shallow, but distinct rugose tubercle at the center of the concave proximal portion of the anterior surface of the humerus (386-0*, unique within Diplodocinae), and the maximum diameter of the proximal end of the radius divided by its greatest length equals 0.3 or greater (391-1*, unique within Diplodocinae).

Locality and horizon: Howe-Scott Quarry, Shell, Bighorn County, Wyoming (SMA 0011), and Bone Cabin Quarry, Albany County, Wyoming (AMNH 969). Lower to Middle Morrison Formation, Kimmeridgian. Apatosaurus interval 1 (Bakker, 1998), Dinosaur zone 2 to possibly 3 (Turner and Peterson, 1999), Zones 2 to possibly 3 or 4 (Foster, 2003).

Future developments

Identification of new specimens
The current thesis sheds light on the phylogenetic relationships within Diplodocidae, the most divers and common clade in the well-known Morrison Formation. With the addition of new taxa to the count, up to 15 different diplodocid species have been present in this area. Only two species are recognized outside North America: *Tornieria africana*, and *Dinheirosaurus lourinhanensis*, although fragmentary material suggests that more might have been present in Europe and Asia (Gabunia et al., 1998; Upchurch and Mannion, 2009; Mannion et al., 2012; this study). The present analysis can thus be used as a base for the identification of more fragmentary, possibly diplodocid material.

The large increase of apatosaurine diversity as proposed herein is intended to be tested and verified by means of studies of morphological disparity within Apatosaurinae and Diplodocinae. Assuming that morphological disparity can serve as a proxy for taxonomic diversity, and that the relation between the two measures would be similar in the two sister taxa, the diversity of Apatosaurinae could be assessed comparing its disparity with the one present within Diplodocinae.

Paleoecological studies. The recovered trees form the base for an assessment of spatial and temporal restriction of single species. Hypothesized differing faunal compositions of northern and southern areas of the Morrison Formation (Harris, 2006c; Tschopp and Mateus, 2012b) can thus be tested more rigorously. One of the issues concerning this questions is the lack of reliable geological dates of most fossil sites in the Morrison Formation (see Trujillo, 2006). Thus, long distance correlation between sites has not yet been successful, notwithstanding the nearly 150 years of research in the area (Turner and Peterson, 1999, 2004; Trujillo, 2006). The given data in the locality and horizon sections of the diagnoses (see above) have thus to be interpreted with caution. Once temporal resolution of the Morrison Formation will be better known, also the question of how this ecosystem was able to support such a high diversity of sauropod dinosaurs, can be assessed in more detail. Clearly, not all 15 diplodocid species were present at the same time and place, but the exact spatial and temporal restriction remains unknown. The present study will be important for these future studies on biodiversity and niche partitioning as it provides a firm phylogenetic base.

Technical advances. Some approaches to interpret data from phylogenetic trees are proposed for the first time herein, in particular the numerical way how to decide if specific or generic separation is warranted. Further studies will be needed to refine this approach, and test its utility as well as its ease of use. As evolution does not occur at the same pace in all taxa, numerical borders for genus and species separation have to be adapted for every new analysis. Also, an inclusion of the rate of completeness of the specimen, or the homoplasy within the count could be imagined to improve such a numerical approach and further decrease subjectivity in the evaluation of taxonomic significance of single traits. However, this would increase the complexity of the approach significantly. It was thus herein preferred to stay with the more straightforward version, thereby also assuming that acquisition or loss of a trait always involves the same 'evolutionary costs', if individually variable within a species or actually taxonomically significant.

The present study also implies that the more detailed a phylogenetic analysis, the higher the number of differences and thus taxa. The adding of characters describing very specific morphological details appears to increase the chance of creation and inclusion of uninformative characters, or recognition of autapomorphies that are actually coding individual variation. This is a problem for species- or genus-level phylogenetic analysis, but not so much in a specimen-based analysis as performed herein. With the separate scoring of specimens from the same taxon, individually varying characters are detected. However, more theoretical studies are needed to explore the influence of the used characters on the phylogenetic relationships of the included taxa.

The retrodeformation study of the cervical vertebrae of SMA 0004 showed that it can be useful to test quantitative phylogenetic characters. Such an approach should be expanded to the rest of the vertebral column, and – if possible – to appendicular elements as well. The latter would require the development of new software able to recognize strains in non-symmetric elements as well and restoring a shape more close to the original.

Conclusions

A specimen-based phylogenetic analysis

The present thesis highly increases knowledge about the morphology and the phylogenetic relationships of diplodocid sauropods. Three new, partially complete specimens are described, two of them include nearly complete skulls, and represent new diplodocine species: *Kaatedocus siberi* and *Galeamopus shellensis*. In order to resolve their exact systematic position within Diplodocidae, a specimen-based phylogenetic analysis was performed, which included all holotypes that have been identified as belonging to a diplodocid sauropod at some point in history. Such an approach created problems, as many of the type specimens are largely incomplete, and without field notes, which would help to clarify if they really represent single individuals. The latter is crucial for a specimen-based analysis, as one of the main ideas behind such an approach, as well as one of its greatest potentials, is the recognition of individual variation within the same species or genera.

Individual variation

Individual variation can be caused by a variety of factors: ontogenetic variation, sexual dimorphism, pathologies, can all change the morphology of living tissue. If working with fossils, variation can also be introduced by taphonomic processes as deformation or scavenging. Whereas the effects of the latter are generally easily recognizable, in particular the amount of changes introduced by deformational processes are difficult to impossible to quantify. Retrodeformation studies as performed with the holotypic cervical vertebrae of *Kaatedocus siberi* (Tschopp et al., 2013) yielded some information about the influence of deformation on the scorings of phylogenetic characters. The validity and utility of numerical characters was thus assessed in more detail. However, for most traits, an evaluation of taxonomic utility versus individual variation remains difficult. By using single individuals as operational taxonomic units in a phylogenetic analysis, this can in part be accounted for. The characters coding for traits that are variable between individuals as thus expected to show the most homoplasy in the analysis. In order to account for this, the analysis was performed both with all characters being given the same weight, as well as by using the so-called implied weights analysis, where the weight and thus influence of a character on the phylogenetic relationships is calculated while performing the tree searches, and based on the rate of homoplasy of the single character.

An additional issue introduced by individual variation and its effects within a specimen-based phylogenetic analysis is where to decide if specific or generic separation of the included specimens is warranted. Given that the only applicable species concept in paleontology is based on morphological differences, the sum of differences can be the only way how to approach this issue. Basing on the assumption that the rate of evolution was similar in the two temporally as well as spatially coexisting taxa Diplodocinae and Apatosaurinae, accumulation of individually varying traits is assumed to lead to speciation with the same speed in both taxa. Thus, a numerical approach was introduced, including a three-step approach to account for individual variation: first, phylogenetic software does not find all potential autapomorphies for single specimens or synapomorphies for recovered clades, because the sister clades (specimens or taxa in the case of a specimen-based analysis) often do not preserve the same bones, and are thus not comparable. Second, the quality and thus validity of found apomorphies was assessed based on the number of taxa they were shared with, as well as the relative phylogenetic positions of these taxa with the specimen or clade in question. Finally, the number of valid apomorphies was summed between sister clades (sometimes specimens). Based on the relationship between *Supersaurus* and *Dinheirosaurus*, which have been continuously found as sister taxa (Mannion et al., 2012; Tschopp and Mateus, 2012b; this study), and where generic separation is further supported by the geographical separation (North America versus Portugal), a sum of ten steps was considered enough for generic separation. By comparing the sum of differences between generally accepted species of the same genus (*Apatosaurus ajax* and *Apatosaurus louisae*, or *Diplodocus carnegii* and *Diplodocus hallorum*) with the sum of differences between specimens often identified as belonging to the same species (*Apatosaurus louisae* CM 3018 and CM 3378, or *Diplodocus carnegii* CM 84 and CM 94), a sum of five steps was established as being enough for specific separation. Given the three-step approach to reduce influence of individual variation, the true sum of differences between

specimens or clades would even be higher in most cases. By applying these rules to all sister group arrangements found in the tree, validity of the included taxa was assessed in a more objective way.

Implications on taxonomy

Apatosaurinae. The numerical approach established in the present analysis allowed a reassessment of the validity of the numerous taxonomic names proposed within Diplodocidae. Thereby, it was found that apatosaurine diversity was particularly underestimated in the past. Two genera previously synonymized with *Apatosaurus* resulted valid based on the sum of differences with their recovered sister taxa: *Brontosaurus* and *Elosaurus*, which together form the sister clade to *Apatosaurus* in the present analysis. *Eobrontosaurus* was found to be valid as well, and two more clusters of specimens were recovered at the base of Apatosaurinae, which might even represent two additional apatosaurine genera. However, more detailed work has to be done on the specimens forming these clades before being able to confirm such an extraordinary increase in the number of apatosaurine genera. *Apatosaurus* was found to be the only apatosaurine genus with more than one species: *A. ajax*, and *A. louisae*. This results in four to six genera and five to seven species belonging to Apatosaurinae. In a less inclusive and less detailed specimen-based analysis of *Apatosaurus*, Upchurch et al. (2004b) found five species as probably valid, but did not include *Eobrontosaurus yahnahpin*. The species count thus remained more or less the same in the two analyses.

Diplodocinae. The intrarelationships of Diplodocinae were already well established before (Whitlock, 2011a; Mannion et al., 2012; Tschopp and Mateus, 2012b). However, by including single specimens, it became possible to furthermore assess the validity of the various species proposed in *Diplodocus*. Thereby, the type species *D. longus* was considered a nomen dubium, given the undiagnostic, fragmentary holotype specimen. This would lead to an abolishment of the generic name *Diplodocus*, and all the higher-level taxa based on the genus (Diplodocinae, Diplodocidae, Diplodocoidea). As this was not considered reasonable, a case is being prepared for submission to ICZN proposing *D. carnegii* as new type species, and suppressing *D. longus*. Furthermore, the holotype specimen of '*Diplodocus*' *hayi*, often mentioned to probably not belong to *Diplodocus* (McIntosh, 1990a; Curtice, 1996; Foster, 2003), was found to form its own genus (herein named *Galeamopus*), together with one of the newly described specimens, SMA 0011, and the diplodocine skull AMNH 969 – also the latter having previously been identified as *Diplodocus* (Holland, 1906, 1924; McIntosh and Berman, 1978). Interestingly, no diplodocine specimen preserving articulated skulls and postcranial elements was herein found to group with *Diplodocus*: AMNH 969 and '*Diplodocus*' hayi are referred to *Galeamopus*, and CM 3452, on which Holland (1924), McIntosh and Berman (1975), and Berman and McIntosh (1978) based their identification of the skull-only specimens as *Diplodocus*, is recovered as more closely related to *Barosaurus* and *Kaatedocus*, and provisionally referred to *Barosaurus*. Although essentially complete and well-preserved, skulls like CM 11161, or USNM 2672 can thus not be definitely identified as *Diplodocus*. However, their recovered intermediate position between *Galeamopus* and *Kaatedocus* + *Barosaurus* indicates that a referral to *Diplodocus* might be justifiable, even though direct evidence for it is lacking. In any case, given the completeness and articulation of the two *Galeamopus* specimens HMNS 175 and SMA 0011, as well as the presence of at least an additional, referred skull, the morphology of *Galeamopus* can be considered better preserved than *Diplodocus*, where information on skull, forelimb, or distal tail morphology is not available from type specimens. In total, nine different species in seven genera are recognized within Diplodocinae. Together with the probable non-apatosaurine, non-diplodocine diplodocid *Amphicoelias altus*, this amounts to a total of 15 to 17 valid diplodocid species, 13 to 15 of which from the Morrison Formation of the Western United States.

References

Angielczyk, K. D., and H. D. Sheets. 2007. Investigation of simulated tectonic deformation in fossils using geometric morphometrics. Paleobiology 33:125–148.

Antunes, M. T., and O. Mateus. 2003. Dinosaurs of Portugal. Comptes Rendus Palevol 2:77–95.

Apesteguía, S. 2005. Evolution of the titanosaur metacarpus; pp. 321–346 in V. Tidwell and K. Carpenter (eds.), Thunder-Lizards: The Sauropodomorph Dinosaurs. Indiana University Press, Bloomington.

Arbour, V. M., and P. J. Currie. 2012. Analyzing taphonomic deformation of ankylosaur skulls using retrodeformation and Finite Element Analysis. PLoS ONE 7:e39323.

Ayer, J. 2000. The Howe Ranch Dinosaurs. Sauriermuseum Aathal, Aathal, Switzerland, 96 pp.

Bader, K. S., S. T. Hasiotis, and L. D. Martin. 2009. Application of forensic science techniques to trace fossils on dinosaur bones from a quarry in the Upper Jurassic Morrison Formation, Northeastern Wyoming. PALAIOS 24:140–158.

Bakker, R. T. 1998. Dinosaur mid-life crisis; the Jurassic-Cretaceous transition in Wyoming and Colorado. Bulletin of the New Mexico Museum of Natural History and Science 14:67–77.

Balanoff, A. M., G. S. Bever, and T. Ikejiri. 2010. The braincase of *Apatosaurus* (Dinosauria: Sauropoda) based on Computed Tomography of a new specimen with comments on variation and evolution in sauropod neuroanatomy. American Museum Novitates 3677:1–32.

Barco, J. 2009. Sistemática e implicaciones filogenéticas y paleobiogeográficas del saurópodo *Galvesaurus herreroi* (Formación Villar del Arzobispo, Galve, España). 405 pp.

Barrett, P. M., and P. Upchurch. 1994. Feeding mechanisms of *Diplodocus*. Gaia 10:195–203.

Barrett, P. M., G. W. Storrs, M. T. Young, and L. M. Witmer. 2011. A new skull of *Apatosaurus* and its taxonomic and palaeobiological implications. 1606.

Bedell, M. W. J., and D. L. Trexler. 2005. First articulated manus of *Diplodocus carnegii*; pp. 302–320 in V. Tidwell and K. Carpenter (eds.), Thunder-Lizards: The Sauropodomorph Dinosaurs. Indiana University Press, Bloomington.

Benton, M. J., and A. D. Walker. 2002. *Erpetosuchus*, a crocodile-like basal archosaur from the Late Triassic of Elgin, Scotland. Zoological Journal of the Linnean Society 136:25–47.

Berman, D. S., and J. S. McIntosh. 1978. Skull and relationships of the Upper Jurassic sauropod *Apatosaurus* (Reptilia, Saurischia). Bulletin of the Carnegie Museum of Natural History 8:1–35.

Bird, R. T. 1985. Bones for Barnum Brown: Adventures of a Dinosaur Hunter. Texas Christian University Press, Fort Worth, 225 pp.

Birkemeier, T. 2011. Neurocentral suture closure in *Allosaurus* (Saurischia: Theropoda): sequence and timing. Journal of Vertebrate Paleontology, Program and Abstracts 2011:72A.

Bonaparte, J. F. 1986. The early radiation and phylogenetic relationships of the Jurassic sauropod dinosaurs, based on vertebral anatomy; pp. 247–258 in K. Padian (ed.), The Beginning of the Age of Dinosaurs. Cambridge University Press, Cambridge.

Bonaparte, J. F., and O. Mateus. 1999. A new diplodocid, *Dinheirosaurus lourinhanensis* gen. et sp. nov., from the Late Jurassic beds of Portugal. Revista Del Museo Argentino de Ciencias Naturales 5:13–29.

Bonaparte, J. F., B. J. González Riga, and S. Apesteguía. 2006. *Ligabuesaurus leanzai* gen. et sp. nov. (Dinosauria, Sauropoda), a new titanosaur from the Lohan Cura Formation (Aptian, Lower Cretaceous) of Neuquén, Patagonia, Argentina. Cretaceous Research 27:364–376.

Bonaparte, J. F., W.-D. Heinrich, and R. Wild. 2000. Review of *Janenschia* Wild, with the description of a new sauropod from the Tendaguru beds of Tanzania and a discussion on the systematic value of procoelous caudal vertebrae in the Sauropoda. Palaeontographica Abteilung A 256:25–76.

Bonnan, M. F. 2000. The presence of a calcaneum in a diplodocid sauropod. Journal of Vertebrate Paleontology 20:317–323.

Bonnan, M. F. 2001. The evolution and functional morphology of sauropod dinosaur locomotion. Ph.D. dissertation, Northern Illinois University., Dekalb, Illinois, 759 pp.

Bonnan, M. F. 2003. The evolution of manus shape in sauropod dinosaurs: implications for functional morphology, forelimb orientation, and phylogeny. Journal of Vertebrate Paleontology 23:595–613.

Bonnan, M. F. 2005. Pes anatomy in sauropod dinosaurs: Implications for functional morphology, evolution, and phylogeny; pp. 346–380 in V. Tidwell and K. Carpenter (eds.), Thunder-lizards: the Sauropodomorph dinosaurs. Indiana University Press, Bloomington.

Bonnan, M. F. 2007. Linear and geometric morphometric analysis of long bone scaling patterns in Jurassic neosauropod dinosaurs: their functional and paleobiological implications. The Anatomical Record: Advances in Integrative Anatomy and Evolutionary Biology 290:1089–1111.

Bonnan, M. F., and M. J. Wedel. 2004. First occurrence of *Brachiosaurus* (Dinosauria: Sauropoda) from the Upper Jurassic Morrison Formation of Oklahoma. PaleoBios 24:13–21.

Boyd, A. A., and R. Motani. 2008. Three-dimensional reevaluation of the deformation removal technique based on “jigsaw puzzling.”Palaeontologia Electronica 11:1–7.

Brinkmann, W., and H.-J. Siber. 1992. Dinosaurier in Aathal. Sauriermuseum Aathal, Aathal, 37 pp.
Brochu, C. A. 1996. Closure of neurocentral sutures during crocodilian ontogeny: Implications for maturity assessment in fossil archosaurs. Journal of Vertebrate Paleontology 16:49–62.
Brown, B. 1935. Sinclair dinosaur expedition, 1934. Natural History 36:2–15.
Calvo, J. O. 1994. Jaw mechanics in sauropod dinosaurs. Gaia 10:183–193.
Calvo, J. O., and L. Salgado. 1995. *Rebbachisaurus tessonei* sp. nov. A new sauropod from the Albian-Cenomanian of Argentina; new evidence on the origin of the Diplodocidae. Gaia 11:13–33.
Canudo, J. I., R. Royo-Torres, and G. Cuenca-Bescós. 2008. A new sauropod: *Tastavinsaurus sanzi* gen. et sp. nov. from the Early Cretaceous (Aptian) of Spain. Journal of Vertebrate Paleontology 28:712–731.
Carabajal, A. P., R. A. Coria, and L. M. Chiappe. 2008. An incomplete Upper Cretaceous titanosaur (Sauropoda) braincase: new insights on the dinosaurian inner ear and endocranium. Cretaceous Research 29:643–648.
Carballido, J. L., and P. M. Sander. 2013. Postcranial axial skeleton of *Europasaurus holgeri* (Dinosauria, Sauropoda) from the Upper Jurassic of Germany: implications for sauropod ontogeny and phylogenetic relationships of basal Macronaria. Journal of Systematic Palaeontology. 1–53.
Carballido, J. L., J. S. Marpmann, D. Schwarz-Wings, and B. Pabst. 2012a. New information on a juvenile sauropod specimen from the Morrison Formation and the reassessment of its systematic position. Palaeontology 55:567–582.
Carballido, J. L., L. Salgado, D. Pol, J. I. Canudo, and A. Garrido. 2012b. A new basal rebbachisaurid (Sauropoda, Diplodocoidea) from the Early Cretaceous of the Neuquén Basin; evolution and biogeography of the group. Historical Biology 24:631–654.
Carballido, J. L., O. W. M. Rauhut, D. Pol, and L. Salgado. 2011. Osteology and phylogenetic relationships of *Tehuelchesaurus benitezii* (Dinosauria, Sauropoda) from the Upper Jurassic of Patagonia. Zoological Journal of the Linnean Society 163:605–662.
Carpenter, K. 2010. Species concept in North American stegosaurs. Swiss Journal of Geosciences 103:155–162.
Carpenter, K., and J. McIntosh. 1994. Upper Jurassic sauropod babies from the Morrison Formation. Dinosaur Eggs and Babies 265–278.
Carpenter, K., and V. Tidwell. 1998. Preliminary description of a *Brachiosaurus* skull from Felch quarry 1, Garden Park, Colorado. Modern Geology 23:69–84.
Carrano, M. T. 2005. The evolution of sauropod locomotion: morphological diversity of a secondarily quadrupedal radiation; pp. 229–251 in The Sauropods: Evolution and Paleobiology. University of California Press, Berkeley, CA.
Casanovas, M. L., J. V. Santafé, and J. L. Sanz. 2001. *Losillasaurus giganteus* , un nuevo saurópodo del tránsito Jurásico-Cretácico de la cuenca de“ Los Serranos”(Valencia, España). Paleontologia i Evolució 99–122.
Charig, A. J. 1980. A diplodocid sauropod from the Lower Cretaceous of England; pp. 231–244 in L. L. Jacobs (ed.), Aspects of Vertebrate History. Essays in Honor of Edwin Harris Colbert. Museum of Northern Arizona Press, Flagstaff.
Chatterjee, S. 1978. A primitive parasuchid (phytosaur) reptile from the Upper Triassic Maleri Formation of India. Palaeontology 21:83–127.
Chatterjee, S., and Z. Zheng. 2002. Cranial anatomy of *Shunosaurus*, a basal sauropod dinosaur from the Middle Jurassic of China. Zoological Journal of the Linnean Society 136:145–169.
Chatterjee, S., and Z. Zheng. 2005. Neuroanatomy and dentition of *Camarasaurus lentus*; pp. 199–211 in V. Tidwell and K. Carpenter (eds.), Thunder-lizards. The sauropodomorph dinosaurs. Indiana University Press, Bloomington.
Chinnery, B. J., and D. B. Weishampel. 1998. *Montanoceratops cerorhynchus* (Dinosauria: Ceratopsia) and relationships among basal neoceratopsians. Journal of Vertebrate Paleontology 18:569–585.
Christiansen, N. A., and E. Tschopp. 2010. Exceptional stegosaur integument impressions from the Upper Jurassic Morrison Formation of Wyoming. Swiss Journal of Geosciences 103:163–171.
Chure, D., B. Britt, J. Whitlock, and J. Wilson. 2010. First complete sauropod dinosaur skull from the Cretaceous of the Americas and the evolution of sauropod dentition. Naturwissenschaften 97:379–391.
Chure, D. J., R. Litwin, S. T. Hasiotis, E. Evanoff, and K. Carpenter. 2006. The fauna and flora of the Morrison Formation: 2006. Paleontology and Geology of the Upper Jurassic Morrison Formation. New Mexico Museum of Natural History and Science Bulletin 36:233–249.
Claessens, L. P. A. M. 2004. Dinosaur gastralia; origin, morphology, and function. Journal of Vertebrate Paleontology 24:89–106.
Claessens, L. P. A. M., P. M. O’Connor, and D. M. Unwin. 2009. Respiratory evolution facilitated the origin of pterosaur flight and aerial gigantism. PLoS One 4:e4497.
Clark, J. M., M. Norell, and L. M. Chiappe. 1999. An oviraptorid skeleton from the late Cretaceous of Ukhaa Tolgod, Mongolia, preserved in an avianlike brooding position over an oviraptorid nest. American Museum Novitates 3265:1–36.
Cooper, M. R. 1981. The prosauropod dinosaur *Massospondylus carinatus* Owen from Zimbabwe: its biology,

mode of life and phylogenetic significance. Occas Pap Natl Monuments Rhod 6:690–840.
Cooper, M. R. 1984. A reassessment of *Vulcanodon karibaensis* Raath (Dinosauria: Saurischia) and the origin of the Sauropoda. Palaeontologia Africana 25:203–231.
Cooper, R. A. 1990. Interpretation of tectonically deformed fossils. New Zealand Journal of Geology and Geophysics 33:321–332.
Cope, E. D. 1877a. On *Amphicoelias*, a genus of saurians from the Dakota Epoch of Colorado. Paleontology Bulletin 27:1–5.
Cope, E. D. 1877b. On a dinosaurian from the Trias of Utah. Proceedings of the American Philosophical Society 16:579–584.
Cope, E. D. 1878. A new species of *Amphicoelias*. American Naturalist 12:563–564.
Curry, K. A. 1999. Ontogenetic histology of *Apatosaurus* (Dinosauria: Sauropoda): new insights on growth rates and longevity. Journal of Vertebrate Paleontology 19:654–665.
Curry Rogers, K. A. 2005. Titanosauria: a phylogenetic overview; pp. 51–103 in K. A. Curry Rogers and J. A. Wilson (eds.), The Sauropods: Evolution and Paleobiology. University of California Press, Berkeley, CA.
Curry Rogers, K. A. 2009. The postcranial osteology of *Rapetosaurus krausei* (Sauropoda: Titanosauria) from the Late Cretaceous of Madagascar. Journal of Vertebrate Paleontology 29:1046–1086.
Curry Rogers, K. A., and C. A. Forster. 2001. The last of the dinosaur titans: a new sauropod from Madagascar. Nature 412:530–534.
Curry Rogers, K. A., and C. A. Forster. 2004. The skull of *Rapetosaurus krausei* (Sauropoda: Titanosauria) from the Late Cretaceous of Madagascar. Journal of Vertebrate Paleontology 24:121–144.
Curtice, B. 1996. Codex of diplodocid caudal vertebrae from the Dry Mesa dinosaur quarry. Master Thesis, Brigham Young University. Department of Geology., 156 pp.
Curtice, B. D., and K. L. Stadtman. 2001. The demise of *Dystylosaurus edwini* and a revision of *Supersaurus vivianae*. Mesa Southwest Museum Bulletin 8:33–39.
Curtice, B. D., K. L. Stadtman, and L. J. Curtice. 1996. A reassessment of *Ultrasauros macintoshi* (Jensen, 1985). Museum of Northern Arizona Bulletin 60:87–95.
D'Emic, M. D. 2012. The early evolution of titanosauriform sauropod dinosaurs. Zoological Journal of the Linnean Society 166:624–671.
Dantas, P., J. Sanz, C. Marques da Silva, F. Ortega, V. Santos, and M. Cachão. 1998. *Lourinhasaurus* n. gen. novo dinossáurio saurópode do Jurássico superior (Kimeridgiano superior-Titoniano inferior) de Portugal. Actas Do V Congresso Nacional de Geologia.-Com. Inst. Geol. Mineiro 84:91–94.
Dilkes, D., and H.-D. Sues. 2009. Redescription and phylogenetic relationships of *Doswellia kaltenbachi* (Diapsida: Archosauriformes) from the Upper Triassic of Virginia. Journal of Vertebrate Paleontology 29:58–79.
Dodson, P., A. K. Behrensmeyer, R. T. Bakker, and J. S. McIntosh. 1980. Taphonomy and paleoecology of the dinosaur beds of the Jurassic Morrison Formation. Paleobiology 6:208–232.
Dong, Z., and Z. Tang. 1984. Note on a new mid-Jurassic sauropod (*Datousaurus bashanensis* gen. et sp. nov.) from Sichuan Basin, China. Vertebrata PalAsiatica 22:69–75.
Dong, Z., G. Peng, and D. Huang. 1989. The discovery of the bony tail club of sauropods. Vertebrata PalAsiatica 27:218–224.
Dong, Z., S. Zhou, and Y. Zhang. 1983. The dinosaurian remains from Sichuan basin, China. Palaeontologia Sinica. NSC 23:139–145.
Dunlavey, T., C. Mitchell, and H. D. Sheets. 2004. Retrodeformation is paramount to the accurate description of fossil taxa. Geological Society of America Abstracts with Programs 36:422.
Eaton, T. H., and P. L. Stewart. 1960. A new order of fishlike Amphibia from the Pennsylvanian of Kansas. Univ Kans Mus Nat Hist 12:217–240.
Filla, J., and P. D. Redman. 1994. *Apatosaurus yahnahpin*: a preliminary description of a new species of diplodocid dinosaur from the Late Jurassic Morrison Formation of Southern Wyoming, the first sauropod dinosaur found with a complete set of "belly ribs."159–178.
Foster, J. R. 1998. Aspects of vertebrate paleoecology, taphonomy, and biostratigraphy of the Morrison Formation (Upper Jurassic), Rocky Mountain region, western United States. University of Colorado, 466 pp.
Foster, J. R. 2003. Paleoecological analysis of the vertebrate fauna of the Morrison Formation (Upper Jurassic), Rocky Mountain Region, U.S.A. New Mexico Museum of Natural History and Science Bulletin 23:2–100.
Fraas, E. 1908. Ostafrikanische Dinosaurier. Palaeontographica 15:105–144.
Gabunia, L. K., G. Mchedlidze, V. M. Chkhikvadze, and S. G. Lucas. 1998. Jurassic sauropod dinosaur from the Republic of Georgia. Journal of Vertebrate Paleontology 18:233–236.
Galiano, H., and R. Albersdörfer. 2010. *Amphicoelias*" Brontodiplodocus", a New Sauropod, from the Morrison Formation, Big Horn Basin, Wyoming, with Taxonomic Reevaluation of *Diplodocus*, *Apatosaurus*,

Barosaurus and Other Genera. Dinosauria International, LLC, 50 pp.
Gallina, P. A. 2011. Notes on the axial skeleton of the titanosaur *Bonitasaura salgadoi* (Dinosauria-Sauropoda). Anais Da Academia Brasileira de Ciências 83:235–246.
Gallina, P. A. 2012. Histología ósea del titanosaurio *Bonitasaura salgadoi*(Dinosauria: Sauropoda) del Cretácico Superior de Patagonia. Ameghiniana 49:289–302.
Gallina, P. A., and S. Apesteguía. 2005. *Cathartesaura anaerobica* gen. et sp. nov., a new rebbachisaurid (Dinosauria, Sauropoda) from the Huincul Formation (Upper Cretaceous), Río Negro, Argentina. Revista Museo Argentino Ciencias Naturales Nueva Serie 7:153–166.
Gallina, P. A., and S. Apesteguía. 2011. Cranial anatomy and phylogenetic position of the titanosaurian sauropod *Bonitasaura salgadoi*. Acta Palaeontologica Polonica 56:45–60.
Galton, P., and J. Jensen. 1973. Skeleton of a hypsilophodontid dinosaur (*Nanosaurus* (?) *rex*) from the Upper Jurassic of Utah. Brigham Young University Geology Studies 20:137–157.
Gauthier, J. 1986. Saurischian monophyly and the origin of birds. Memoirs of the California Academy of Sciences 8:55.
Gillette, D. D. 1991. *Seismosaurus halli*, gen. et sp. nov., a new sauropod dinosaur from the Morrison Formation (Upper Jurassic/Lower Cretaceous) of New Mexico, USA. Journal of Vertebrate Paleontology 11:417–433.
Gillette, D. D. 1994. *Seismosaurus*: The Earth Shaker. Columbia University Press, New York, 205 pp.
Gillette, D. D. 1996a. Origin and early evolution of the sauropod dinosaurs of North America: the type locality and stratigraphic position of *Dystrophaeus viaemalae* Cope 1877. Utah Geological Association Guidebook 25:313–324.
Gillette, D. D. 1996b. Stratigraphic position of the sauropod *Dystrophaeus viaemalae* Cope 1877 and its evolutionary implications. Museum of Northern Arizona, Bulletin 60:59–68.
Gilmore, C. W. 1925. A nearly complete articulated skeleton of *Camarasaurus*, a saurischian dinosaur from the Dinosaur National Monument, Utah. Memoirs of the Carnegie Museum 10:347–384.
Gilmore, C. W. 1932. On a newly mounted skeleton of *Diplodocus* in the United States National Museum. Proceedings of the United States National Museum 81:1–21.
Gilmore, C. W. 1936. Osteology of *Apatosaurus*: with special reference to specimens in the Carnegie Museum. Memoirs of the Carnegie Museum 11:175–300.
Goloboff, P. A. 1993. Estimating character weights during tree search. Cladistics 9:83–91.
Goloboff, P. A., J. S. Farris, and K. C. Nixon. 2008. TNT, a free program for phylogenetic analysis. Cladistics 24:774–786.
Goloboff, P. A., J. S. Farris, M. Källersjö, B. Oxelman, M. J. Ramírez, and C. A. Szumik. 2003. Improvements to resampling measures of group support. Cladistics 19:324–332.
González Riga, B. J. 2002. Estratigrafía y Dinosaurios del Cretácico Tardío en el extremo sur de la provincia de Mendoza, Argentina. Ph.D. dissertation, National University of Córdoba, Argentina, 280 pp.
González Riga, B. J., E. Previtera, and C. A. Pirrone. 2009. *Malarguesaurus florenciae* gen. et sp. nov., a new titanosauriform (Dinosauria, Sauropoda) from the Upper Cretaceous of Mendoza, Argentina. Cretaceous Research 30:135–148.
Gow, C. E. 1990. Morphology and growth of the *Massospondylus* braincase (Dinosauria, Prosauropoda). Palaeontologia Africana 27:59–75.
Gunz, P., P. Mitteroecker, S. Neubauer, G. W. Weber, and F. L. Bookstein. 2009. Principles for the virtual reconstruction of hominin crania. Journal of Human Evolution 57:48–62.
Haas, G. 1963. A proposed reconstruction of the jaw musculature of *Diplodocus*. Annals of Carnegie Museum 36:139–157.
Haines, R. W. 1969. Epiphyses and sesamoids; pp. 81–115 in Biology of the Reptilia, Vol. 1: Morphology A. vol. 1. Academic Press, London.
Harris, J. D. 2006a. Cranial osteology of *Suuwassea emilieae* (Sauropoda: Diplodocoidea: Flagellicaudata) from the Upper Jurassic Morrison Formation of Montana, USA. Journal of Vertebrate Paleontology 26:88–102.
Harris, J. D. 2006b. The axial skeleton of the dinosaur *Suuwassea emilieae* (Sauropoda: Flagellicaudata) from the Upper Jurassic Morrison Formation of Montana, USA. Palaeontology 49:1091–1121.
Harris, J. D. 2006c. The significance of *Suuwassea emilieae* (Dinosauria: Sauropoda) for flagellicaudatan intrarelationships and evolution. Journal of Systematic Palaeontology 4:185–198.
Harris, J. D. 2007. The appendicular skeleton of *Suuwassea emilieae* (Sauropoda: Flagellicaudata) from the Upper Jurassic Morrison Formation of Montana (USA). Geobios 40:501–522.
Harris, J. D., and P. Dodson. 2004. A new diplodocoid sauropod dinosaur from the Upper Jurassic Morrison Formation of Montana, USA. Acta Palaeontologica Polonica 49:197–210.
Hatcher, J. B. 1901. *Diplodocus* (Marsh): its osteology, taxonomy, and probable habits, with a restoration of the skeleton. Memoirs of the Carnegie Museum 1:1–63.
Hatcher, J. B. 1902. Structure of the forelimb and manus of *Brontosaurus*. Annals of the Carnegie Museum

1:356–376.
Hatcher, J. B. 1903. Osteology of *Haplocanthosaurus*, with description of a new species and remarks on the probable habits of the Sauropoda and the age and origin of the *Atlantosaurus* beds: Additional remarks on *Diplodocus*. Memoirs of the Carnegie Museum 2:1–72.
He, X., C. Wang, S. Liu, F. Zhou, T. Liu, K. Cai, and B. Dai. 1998. A new species of sauropod from the Early Jurassic of Gongxian County, Sichuan. Acta Geologica Sichuan 18:1–6.
He, X., K. Li, and K. Cai. 1988. The Middle Jurassic Dinosaur Fauna from Dashanpu, Zigong, Sichuan. Vol. IV. Sauropod Dinosaurs (2) *Omeisaurus tianfuensis*. Sichuan Publishing House of Science and Technology, Chengdu, China, 143 pp.
He, X., K. Li, K. Cai, and Y. Gao. 1984. *Omeisaurus tianfuensis*—a new species of *Omeisaurus* from Dashanpu, Zigong, Sichuan. Journal of Chengdu College Geology, Supplement 2:13–32.
He, X., S. Yang, K. Cai, K. Li, and Z. Liu. 1996. A new species of sauropod, *Mamenchisaurus anyuensis* sp. nov. Proceedings of the 30th International Geological Congress 12:83–86.
Heathcote, J., and P. Upchurch. 2003. The relationships of *Cetiosauriscus stewarti* (Dinosauria; Sauropoda): implications for sauropod phylogeny. Journal of Vertebrate Paleontology 23:60A.
Hedrick, B., A. R. Tumarkin-Deratzian, and P. Dodson. 2012. Bone microstructure and relative age of the holotype specimen of the diplodocoid sauropod dinosaur *Suuwassea emilieae*. Acta Palaeontologica Polonica.
Heinrich, W.-D. 1999. The taphonomy of dinosaurs from the Upper Jurassic of Tendaguru (Tanzania) based on field sketches of the German Tendaguru Expedition (1909-1913). Fossil Record 2:25–61.
Herne, M. C., and S. G. Lucas. 2006. *Seismosaurus hallorum*: osteological reconstruction from the holotype. Bulletin of the New Mexico Museum of Natural History and Science 36:139–148.
Hocknull, S. A., M. A. White, T. R. Tischler, A. G. Cook, N. D. Calleja, T. Sloan, and D. A. Elliott. 2009. New mid-Cretaceous (latest Albian) dinosaurs from Winton, Queensland, Australia. PloS One 4:e6190.
Hohn, B. 2011. Walking with the shoulder of giants: biomechanical conditions in the tetrapod shoulder girdle as a basis for sauropod shoulder reconstruction; pp. 182–196 in N. Klein, K. Remes, C. T. Gee, and P. M. Sander (eds.), Biology of the Sauropod Dinosaurs: Understanding the Life of Giants., Life of the Past Indiana University Press, Bloomington.
Hohn-Schulte, B. 2010. Form and function of the shoulder girdle in sauropod dinosaurs: a biomechanical investigation with the aid of finite elements. Ruhr-Universität Bochum, Universitätsbibliothek, Bochum, 233 pp.
Holland, W. J. 1906. The osteology of *Diplodocus* Marsh. Memoirs of the Carnegie Museum 2:225–264.
Holland, W. J. 1915a. A new species of *Apatosaurus*. Annals of the Carnegie Museum 10:143–145.
Holland, W. J. 1915b. Heads and tails: a few notes relating to the structure of the sauropod dinosaurs. Annals of the Carnegie Museum 9:272–278.
Holland, W. J. 1924. The skull of *Diplodocus*. Memoirs of the Carnegie Museum 9:378–403.
Holliday, C. M., and L. M. Witmer. 2008. Cranial kinesis in dinosaurs: intracranial joints, protractor muscles, and their significance for cranial evolution and function in diapsids. Journal of Vertebrate Paleontology 28:1073–1088.
Huene, F. 1904. *Dystrophaeus viaemalae* Cope in neuer Beleuchtung. Separat-Abdruck Aus Dee Neuen Jahrbuch Fur Mineralogie, Geologie Und Palaeontologie, Stuttgart, Germany.
Huene, F. 1926. Vollständige Osteologie eines Plateosauriden aus dem schwäbischen Keuper. Geologische Und Palaeontologische Abhandlungen, Neue Folge 15:139–179.
Huene, F. 1927. Sichtung der Grundlagen der jetzigen Kenntnis der Sauropoden. Eclogae Geologicae Helvetiae 20:444–470.
Huene, F. 1929. Los Saurisquios y Ornithisquios de Cretaceo Argentine. Annales de Museo de La Plata 3 (Series 2):1–196.
Hughes, N. C., and P. A. Jell. 1992. A statistical/computer-graphic technique for assessing variation in tectonically deformed fossils and its application to Cambrian trilobites from Kashmir. Lethaia 25:317–330.
Ikejiri, T. 2004. Anatomy of *Camarasaurus lentus* (Dinosauria: Sauropoda) from the Morrison Formation (Late Jurassic), Thermopolis, central Wyoming, with determination and interpretation of ontogenetic, sexual dimorphic, and individual variation in the genus. Master Thesis, Fort Hays State University, Kansas, UMI pp.
Ikejiri, T. 2012. Histology-based morphology of the neurocentral synchondrosis in *Alligator mississippiensis* (Archosauria, Crocodylia). Anatomical Record 295:18–31.
Ikejiri, T., V. Tidwell, and D. L. Trexler. 2005. New adult specimens of *Camarasaurus lentus* highlight ontogenetic variation within the species; pp. 154–179 in Thunder-lizards: the Sauropodomorph dinosaurs. Indiana University Press, Bloomington.
Irmis, R. B. 2007. Axial skeleton ontogeny in the Parasuchia (Archosauria: Pseudosuchia) and its implications

for ontogenetic determination in archosaurs. Journal of Vertebrate Paleontology 27:350–361.
Jain, S. L., and S. Bandyopadhyay. 1997. New titanosaurid (Dinosauria: Sauropoda) from the Late Cretaceous of Central India. Journal of Vertebrate Paleontology 17:114–136.
Janensch, W. 1922. Das Handskelett von *Gigantosaurus robustus* und *Brachiosaurus brancai* aus den Tendaguru-Schichten Deutsch-Ostafrikas. Centralblatt Für Mineralogie, Geologie Und Paläontologie 15:464–480.
Janensch, W. 1929a. Die Wirbelsäule der Gattung *Dicraeosaurus*. Palaeontographica Supplement 7:38–133.
Janensch, W. 1929b. Material und Formengehalt der Sauropoden in der Ausbeute der Tendaguru-Expedition. Palaeontographica-Supplementbände 1–34.
Janensch, W. 1935. Die Schädel der Sauropoden *Brachiosaurus*, *Barosaurus* und *Dicraeosaurus* aus den Tendaguruschichten Deutsch-Ostafrikas. Palaeontographica Supplement 7:145–298.
Janensch, W. 1950. Die Wirbelsäule von *Brachiosaurus brancai*. Palaeontographica Supplement 7:27–93.
Janensch, W. 1961. Die Gliedmassen und Gliedmassengürtel der Sauropoden der Tendaguru-Schichten. Palaeontographica-Supplementbände 177–235.
Jensen, J. A. 1985. Three new sauropod dinosaurs from the Upper Jurassic of Colorado. Western North American Naturalist 45:697–709.
Jensen, J. A. 1987. New brachiosaur material from the Late Jurassic of Utah and Colorado. Western North American Naturalist 47:592–608.
Jensen, J. A. 1988. A fourth new sauropod dinosaur from the Upper Jurassic pf the Colorado Plateau and sauropod bipedalism. Western North American Naturalist 48:121–145.
Kazhdan, M., N. Amenta, S. Gu, D. F. Wiley, and B. Hamann. 2009. Symmetry restoration by stretching. 21st Canadian Conference on Computational Geometry, Vancouver, Canada. Unpaginated.
Klein, N., A. Christian, and P. M. Sander. 2012. Histology shows that elongated neck ribs in sauropod dinosaurs are ossified tendons. Biology Letters 8:1032–1035.
Klein, N., and M. Sander. 2008. Ontogenetic stages in the long bone histology of sauropod dinosaurs. Paleobiology 34:247-263.
Klima, P. D. M. 1973. Die Frühentwicklung des Schultergürtels und des Brustbeins bei den Monotremen (Mammalia: Prototheria). Advances in Anatomy, Embryology and Cell Biology 47:66–70.
Klima, P. D. M. 1987. Early development of the shoulder girdle and sternum in marsupials (Mammalia: Metatheria). Advances in Anatomy, Embryology and Cell Biology 109:1–91.
Knoll, F., L. M. Witmer, F. Ortega, R. C. Ridgely, and D. Schwarz-Wings. 2012. The braincase of the basal sauropod dinosaur *Spinophorosaurus* and 3D reconstructions of the cranial endocast and inner ear. PLoS ONE 7:e30060.
Kowallis, B. J., E. H. Christiansen, A. L. Deino, F. Peterson, C. E. Turner, M. J. Kunk, and J. D. Obradovich. 1998. The age of the Morrison Formation. Modern Geology 22:235–260.
Ksepka, D. T., and M. A. Norell. 2006. *Erketu ellisoni*, a long-necked sauropod from Bor Guvé (Dornogov Aimag, Mongolia). American Museum Novitates 3508:1–16.
Kvale, E. P., A. D. Johnson, D. L. Mickelson, K. Keller, L. C. Furer, and A. W. Archer. 2001. Middle Jurassic (Bajocian and Bathonian) dinosaur megatracksites, Bighorn Basin, Wyoming, USA. Palaios 16:233–254.
Lapparent, A. F. de, and G. Zbyszewski. 1957. Les dinosauriens du Portugal. Memoires Des Services Géologiques Du Portugal 2:1–63.
Lawing, A. M., and P. D. Polly. 2010. Geometric morphometrics: recent applications to the study of evolution and development. Journal of Zoology 280:1–7.
Linnaeus, C. 1758. Systema Naturae Per Regna Tria Naturae: Secundum Classes, Ordines, Genera, Species, Cum Characteribus, Differentiis, Synonymis, Locis. Impensis Direct. Laurentii Salvii, Holmiae: 911 pp.
Lovelace, D. M., S. A. Hartman, and W. R. Wahl. 2007. Morphology of a specimen of *Supersaurus* (Dinosauria, Sauropoda) from the Morrison Formation of Wyoming, and a re-evaluation of diplodocid phylogeny. Arquivos Do Museu Nacional 65:527–544.
Lucas, S. G., J. A. Spielman, L. A. Rinehart, A. B. Heckert, M. C. Herne, A. P. Hunt, J. R. Foster, and R. M. Sullivan. 2006. Taxonomic status of *Seismosaurus hallorum*, a Late Jurassic sauropod dinosaur from New Mexico. New Mexico Museum of Natural History and Science Bulletin 36:149–162.
Lull, R. S. 1919. The sauropodous dinosaur *Barosaurus* Marsh. Memoirs of the Connecticut Academy of Arts and Sciences 6:1–42.
Madsen, J. H., J. S. McIntosh, and D. S. Berman. 1995. Skull and atlas-axis complex of the Upper Jurassic sauropod *Camarasaurus* Cope (Reptilia: Saurischia). Bulletin of Carnegie Museum of Natural History 31:1–115.
Maidment, S. C. R., and L. B. Porro. 2010. Homology of the palpebral and origin of supraorbital ossifications in ornithischian dinosaurs. Lethaia 43:95–111.
Makovicky, P. J., and P. J. Currie. 1998. The presence of a furcula in tyrannosaurid theropods, and its phylogenetic and functional implications. Journal of Vertebrate Paleontology 18:143–149.

Mannion, P. D. 2009. A rebbachisaurid sauropod from the Lower Cretaceous of the Isle of Wight, England. Cretaceous Research 30:521–526.
Mannion, P. D. 2010. Environmental and geological controls on the diversity and distribution of the sauropodomorpha. Ph.D. Dissertation, University College London, London, 349 pp.
Mannion, P. D. 2011. A reassessment of *Mongolosaurus haplodon* Gilmore, 1933, a titanosaurian sauropod dinosaur from the Early Cretaceous of Inner Mongolia, People's Republic of China. Journal of Systematic Palaeontology 9:355–378.
Mannion, P. D., and J. O. Calvo. 2011. Anatomy of the basal titanosaur (Dinosauria, Sauropoda) *Andesaurus delgadoi* from the mid-Cretaceous (Albian–early Cenomanian) Río Limay Formation, Neuquén Province, Argentina: implications for titanosaur systematics. Zoological Journal of the Linnean Society.
Mannion, P. D., P. Upchurch, O. Mateus, R. N. Barnes, and M. E. H. Jones. 2012. New information on the anatomy and systematic position of *Dinheirosaurus lourinhanensis* (Sauropoda: Diplodocoidea) from the Late Jurassic of Portugal, with a review of European diplodocoids. Journal of Systematic Palaeontology 10:521–551.
Mannion, P. D., P. Upchurch, R. N. Barnes, and O. Mateus. 2013. Osteology of the Late Jurassic Portuguese sauropod dinosaur Lusotitan atalaiensis (Macronaria) and the evolutionary history of basal titanosauriforms. Zoological Journal of the Linnean Society 168:98–206.
Marsh, O. C. 1877a. Notice of some new dinosaurian reptiles from the Jurassic Formation. American Journal of Science (series 3) 14:514–516.
Marsh, O. C. 1877b. A new order of extinct Reptilia (Stegosauria) from the Jurassic of the Rocky Mountains. American Journal of Science, 3rd Series 14:34–35.
Marsh, O. C. 1878. Principal characters of American Jurassic dinosaurs, Part I. American Journal of Science (series 3) 16:411–416.
Marsh, O. C. 1879. Notice of new Jurassic reptiles. American Journal of Science (series 3) 18:510–505.
Marsh, O. 1880. The sternum in dinosaurian reptiles. American Journal of Science (Series 3) 19:395–396.
Marsh, O. C. 1881. Principle characters of American Jurassic dinosaurs. Part V. American Journal of Science (Series 3) 21:417–437.
Marsh, O. C. 1883. Principal characters of American Jurassic dinosaurs. Restoration of *Brontosaurus*. Geological Magazine (Decade II) 10:385–388.
Marsh, O. C. 1884. Principal characters of American Jurassic dinosaurs. Part VII. On the Diplodocidae, a new family of the Sauropoda. American Journal of Science (series 3) 27:160–168.
Marsh, O. C. 1890. Description of new dinosaurian reptiles. American Journal of Science (series 3) 39:81–86.
Marsh, O. C. 1895. On the affinities and classification of the dinosaurian reptiles. American Journal of Science 483–498.
Marsh, O. C. 1896. The dinosaurs of North America. US Geological Survey Annual Report 16:142–230.
Marsh, O. C. 1898. On the families of sauropodous Dinosauria. American Journal of Science 6:487–488.
Marsh, O. C. 1899. Footprints of Jurassic dinosaurs. American Journal of Science s4-7:227–232.
Martínez, R. N. 2009. *Adeopapposaurus mognai*, gen. et sp. nov. (Dinosauria: Sauropodomorpha), with comments on adaptations of basal Sauropodomorpha. Journal of Vertebrate Paleontology 29:142–164.
Martz, J. W. 2002. The Morphology and Ontogeny of *Typothorax coccinarum* (Archosauria, Stagonolepididae) from the Upper Triassic of the American Southwest. Master Thesis, Graduate Faculty, Texas Tech University, 297 pp.
Mateus, O. 2005. Dinossauros do Jurássico Superior de Portugal, com destaque para os saurísquios. Ph.D. dissertation, Universidade Nova de Lisboa, Lisboa 381 pp.
Mateus, O. and E. Tschopp. 2013. *Cathetosaurus* as a valid sauropod genus and comparisons with *Camarasaurus*. Journal of Vertebrate Paleontology, Programs and Abstracts: 173.
Mateus, O., L. L. Jacobs, A. S. Schulp, M. J. Polcyn, T. S. Tavares, A. Buta Neto, M. L. Morais, and M. T. Antunes. 2011. *Angolatitan adamastor*, a new sauropod dinosaur and the first record from Angola. Anais Da Academia Brasileira de Ciências 83:221–233.
Matthew, W. D. 1905. The mounted skeleton of *Brontosaurus*. American Museum Journal 5:63–71.
McIntosh, J. S. 1981. Annotated catalogue of the dinosaurs (Reptilia, Archosauria) in the collections of Carnegie Museum of Natural History. Bulletin of Carnegie Museum of Natural History 18:1–67.
McIntosh, J. S. 1989. The sauropod dinosaurs: a brief survey; pp. 85–99 in K. Padian and D. J. Chure (eds.), The Age of Dinosaurs., Short Courses in Paleontology Paleontological Society, Saint-Louis.
McIntosh, J. S. 1990a. Species determination in sauropod dinosaurs with tentative suggestions for their classification; pp. 53–69 in K. Carpenter and P. J. Currie (eds.), Dinosaur Systematics: Perspectives and Approaches. Cambridge University Press, New York.
McIntosh, J. S. 1990b. Sauropoda; pp. 345–401 in D. B. Weishampel, P. Dodson, and H. Osmólska (eds.), The Dinosauria. University of California Press, Berkeley, CA.
McIntosh, J. S. 1995. Remarks on the North American sauropod *Apatosaurus* Marsh. Short Papers 119–123.

McIntosh, J. S. 1997. The saga of a forgotten sauropod dinosaur. Dinofest International Proceedings 7–12.
McIntosh, J. S. 2005. The genus *Barosaurus* Marsh (Sauropoda, Diplodocidae); pp. 38–77 in V. Tidwell and K. Carpenter (eds.), Thunder-lizards: the Sauropodomorph dinosaurs. Indiana University Press, Bloomington.
McIntosh, J. S., and D. S. Berman. 1975. Description of the palate and lower jaw of the sauropod dinosaur *Diplodocus* (Reptilia: Saurischia) with remarks on the nature of the skull of *Apatosaurus*. Journal of Paleontology 49:187–199.
McIntosh, J. S., and K. Carpenter. 1998. The holotype of *Diplodocus longus*, with comments on other specimens of the genus. Modern Geology 23:85–110.
McIntosh, J. S., C. A. Miles, K. A. Cloward, and J. R. Parker. 1996a. A new nearly complete skeleton of *Camarasaurus*. Bulletin of the Gunma Museum of Natural History 1:1–87.
McIntosh, J. S., W. E. Miller, K. L. Stadtman, and D. D. Gillette. 1996b. The osteology of *Camarasaurus lewisi* (Jensen, 1988). Brigham Young University Geology Studies 41:73–116.
McIntosh, J. S., W. P. Coombs, and D. A. Russell. 1992. A new diplodocid sauropod (Dinosauria) from Wyoming, USA. Journal of Vertebrate Paleontology 12:158–167.
Michelis, I. 2004. Taphonomie des Howe Quarry's (Morrison-Formation, Oberer Jura), Bighorn County, Wyoming, USA. Ph.D. dissertation, Institute of Palaeontology, University of Bonn, Bonn, Germany, 41 pp.
Mocho, P., R. Royo-Torres, and F. Ortega. 2013. New approach to *Lourinhasaurus alenquerensis* (Macronaria, Camarasauromorpha) from the Portuguese Upper Jurassic. Abstract Book 91.
Molnar, J. L., S. E. Pierce, J. A. Clack, and J. R. Hutchinson. 2012. Idealized landmark-based geometric reconstructions of poorly preserved fossil material: a case study of an early tetrapod vertebra. Palaeontologia Electronica 15:1–18.
Mook, C. C. 1917. Criteria for the determination of species in the Sauropoda, with description of a new species of *Apatosaurus*. Bulletin of the American Museum of Natural History 37:355–358.
Motani, R. 1997. New technique for retrodeforming tectonically deformed fossils, with an example for ichthyosaurian specimens. Lethaia 30:221–228.
Motani, R., N. Amenta, and D. F. Wiley. 2005. Possibilities and limitations of three dimensional retrodeformation of a trilobite and plesiosaur vertebrae. PaleoBios 25:88.
Nair, J. P., and S. W. Salisbury. 2012. New anatomical information on *Rhoetosaurus brownei* Longman, 1926, a gravisaurian sauropodomorph dinosaur from the Middle Jurassic of Queensland, Australia. Journal of Vertebrate Paleontology 32:369–394.
Nesbitt, S. J. 2011. The early evolution of archosaurs: relationships and the origin of major clades. Bulletin of the American Museum of Natural History 1–292.
Nesbitt, S. J., A. H. Turner, M. Spaulding, J. L. Conrad, and M. A. Norell. 2009. The theropod furcula. Journal of Morphology 270:856–879.
Nieuwland, I. 2010. The colossal stranger. Andrew Carnegie and *Diplodocus* intrude European culture, 1904–1912. Endeavour 34:61–68.
Nopcsa, F. B. 1902. Notizen über die Cretacischen Dinosaurier. Pt. 3. Wirbel eines südamerikanischen Sauropoden. Sitzungsberichte der Berliner Akademie der Wissenschaften 3:108–114.
Nopcsa, F. B. 1905. Remarks on the supposed clavicle of the sauropodous dinosaur *Diplodocus*. Proceedings of the Zoological Society 2:289–294.
Novas, F. E. 1996. Dinosaur monophyly. Journal of Vertebrate Paleontology 16:723–741.
Ogihara, N., M. Nakatsukasa, Y. Nakano, and H. Ishida. 2006. Computerized restoration of nonhomogeneous deformation of a fossil cranium based on bilateral symmetry. American Journal of Physical Anthropology 130:1–9.
Olshevsky, G. 1991. A revision of the parainfraclass Archosauria Cope, 1869, excluding the advanced Crocodylia. Mesozoic Meanderings 2:1–196.
Osborn, H. F. 1898. Additional characters of the great herbivorous dinosaur *Camarasaurus*. Bulletin of the American Museum of Natural History 10:219–233.
Osborn, H. F. 1899. A skeleton of *Diplodocus*. Memoirs of the American Museum of Natural History 5:191–214.
Osborn, H. F. 1904. Manus, sacrum, and caudals of Sauropoda. Bulletin of the American Museum of Natural History 20:181–190.
Osborn, H. F., and C. C. Mook. 1921. *Camarasaurus*, *Amphicoelias*, and other sauropods of Cope. Memoirs of the American Museum of Natural History, New Series 3:249–387.
Ostrom, J. O., and J. S. McIntosh. 1966. Marsh's Dinosaurs: The Collection from Como Bluff. Vol. 1. Yale University Press, New Haven, 388 pp.
Ouyang, H., and Y. Ye. 2002. The First Mamenchisaurian Skeleton with Complete Skull, *Mamenchisaurus Youngi*. Sichuan Publishing House of Science and Technology, Chengdu, China, 138 pp.
Owen, R. 1842. Report on British Fossil Reptiles Pt. II. Report of the British Association for the Advancement of

Science 1841:60–204.
Parks, W. A. 1926. *Thescelosaurus warreni*, a new species of orthopodous dinosaur from the Edmonton Formation of Alberta. University of Toronto Studies (Geological Series) 21:1–42.
Paul, G. S. 1988. The brachiosaur giants of the Morrison and Tendaguru with a description of a new subgenus, *Giraffatitan*, and a comparison of the world's largest dinosaurs. Hunteria 2 (3):1–14.
Pereda Suberbiola, X., F. Torcida, L. A. Izquierdo, P. Huerta, D. Montero, and G. Pérez. 2003. First rebbachisaurid dinosaur (Sauropoda, Diplodocoidea) from the early Cretaceous of Spain: paleobiogeographical implications. Bulletin de La Societe Geologique de France 174:471–479.
Peterson, O. A., and C. W. Gilmore. 1902. *Elosaurus parvus*; a new genus and species of the Sauropoda. Annals of the Carnegie Museum 1:490–499.
Platt, B. F., and S. T. Hasiotis. 2006. Newly discovered sauropod dinosaur tracks with skin and foot-pad impressions from the Upper Jurassic Morrison Formation, Bighorn Basin, Wyoming, U.S.A. PALAIOS 21:249–261.
Polcyn, M. J., L. L. Jacobs, and A. Haber. 2005. A morphological model and CT assessment of the skull of *Pachyrhachis problematicus* (Squamata, Serpentes), a 98 million year old snake with legs from the Middle East. Palaeontologia Electronica 8:1–24.
Ponce de León, M. S., and C. P. Zollikofer. 1999. New evidence from Le Moustier 1: Computer-assisted reconstruction and morphometry of the skull. The Anatomical Record 254:474–489.
Raath, M. A., and J. S. McIntosh. 1987. Sauropod dinosaurs from the central Zambezi Valley, Zimbabwe, and the age of the Kadzi Formation. South African Journal of Geology 90:107–119.
Rauhut, O. W. M., K. Remes, R. Fechner, G. Cladera, and P. Puerta. 2005. Discovery of a short-necked sauropod dinosaur from the Late Jurassic period of Patagonia. Nature 435:670–672.
Reisz, R. R., D. Scott, H. D. Sues, D. C. Evans, and M. A. Raath. 2005. Embryos of an Early Jurassic prosauropod dinosaur and their evolutionary significance. Science 309:761–764.
Remes, K. 2006. Revision of the Tendaguru sauropod dinosaur *Tornieria africana* (Fraas) and its relevance for sauropod paleobiogeography. Journal of Vertebrate Paleontology 26:651–669.
Remes, K. 2007. A second Gondwanan diplodocid dinosaur from the Upper Jurassic Tendaguru beds of Tanzania, East Africa. Palaeontology 50:653–667.
Remes, K. 2008. Evolution of the pectoral girdle and forelimb in Sauropodomorpha (Dinosauria, Saurischia). Ph.D. dissertation, Fakultät für Geowissenschaften, LMU München, München, 355 pp.
Remes, K. 2009. Taxonomy of Late Jurassic diplodocid sauropods from Tendaguru (Tanzania). Fossil Record 12:23–46.
Remes, K., F. Ortega, I. Fierro, U. Joger, R. Kosma, J. M. M. Ferrer, O. A. Ide, and A. Maga. 2009. A new basal sauropod dinosaur from the Middle Jurassic of Niger and the early evolution of Sauropoda. PLoS ONE 4:e6924.
Rieppel, O. 1992. Studies on skeleton formation in reptiles. III. Patterns of ossification in the skeleton of *Lacerta vivipara* Jacquin (Reptilia, Squamata). Fieldiana Life Earth Sci 68:1–25.
Riggs, E. S. 1901. The fore leg and pectoral girdle of *Morosaurus*: with a note on the genus *Camarosaurus*. Field Columbian Museum, Geological Series 2 275–281.
Riggs, E. S. 1903. Structure and relationships of opisthocoelian dinosaurs: *Apatosaurus* Marsh. Field Columbian Museum, Geological Series 2 4:165–196.
Riggs, E. S. 1904. Structure and relationships of opisthocoelian dinosaurs: the Brachiosauridae. Field Columbian Museum, Geological Series 2 2:229–247.
Romer, A. 1956. Osteology of the Reptiles. University of Chicago Press, Chicago, 772 pp.
Royo-Torres, R., A. Cobos, and L. Alcalá. 2006. A giant European dinosaur and a new sauropod clade. Science 314:1925–1927.
Royo-Torres, R., A. Cobos, L. Lurque, A. Aberasturi, E. Espílez, I. Fierro, A. González, L. Mampel, and L. Alcalá. 2009. High European sauropod dinosaur diversity during Jurassic–Cretaceous transition in Riodeva (Teruel, Spain). Palaeontology 52:1009–1027.
Royo-Torres, R., and A. Cobos. 2004. Estudio sistemático de un ilion de Sauropoda del yacimiento Pino de Jarque 2 en Riodeva (Teruel). Geo-Temas 6:59–62.
Royo-Torres, R., and P. Upchurch. 2012. The cranial anatomy of the sauropod *Turiasaurus riodevensis* and implications for its phylogenetic relationships. Journal of Systematic Palaeontology 1–31.
Ruben, J. A., T. D. Jones, and N. R. Geist. 2003. Respiratory and reproductive paleophysiology of dinosaurs and early birds. Physiological and Biochemical Zoology 141–164.
Rushton, A. W. A., and M. Smith. 1993. Retrodeformation of fossils-a simple technique. Palaeontology 36:927–930.
Russell, D. A., and Z. Zheng. 1993. A large mamenchisaurid from the Junggar Basin, Xinjiang, People's Republic of China. Canadian Journal of Earth Sciences 30:2082–2095.
Russell, D. A., P. Béland, and J. S. McIntosh. 1980. Paleoecology of the dinosaurs of Tendaguru (Tanzania).

Mémoires de La Société Géologique de France 139:169–175.
Salgado, L. 1999. The macroevolution of the Diplodocimorpha (Dinosauria; Sauropoda): a developmental model. Ameghiniana 36:203–216.
Salgado, L., and J. Calvo. 1992. Cranial osteology of *Amargasurus cazaui* Salgado & Bonaparte (Sauropoda, Dicraeosuridae) from the Neocomian of Patagonia. Ameghiniana 29:337–346.
Salgado, L., and J. F. Bonaparte. 1991. Un nuevo saurópodo Dicraeosauridae, *Amargasaurus cazaui* gen. et sp. nov., de la Formación La Amarga, Neocomiano de la provincia del Neuquén, Argentina. Ameghiniana 28:333–346.
Salgado, L., I. S. Carvalho, and A. C. Garrido. 2006. *Zapalasaurus bonapartei*, un nuevo dinosaurio saurópodo de la Formación La Amarga (Cretácico Inferior), noroeste de Patagonia, Provincia de Neuquén, Argentina. Geobios 39:695–707.
Salgado, L., J. I. Canudo, A. C. Garrido, and J. L. Carballido. 2012. Evidence of gregariousness in rebbachisaurids (Dinosauria, Sauropoda, Diplodocoidea) from the Early Cretaceous of Neuquén (Rayoso Formation), Patagonia, Argentina. Journal of Vertebrate Paleontology 32:603–613.
Salgado, L., R. A. Coria, and J. O. Calvo. 1997. Evolution of titanosaurid sauropods: Phylogenetic analysis based on the postcranial evidence. Ameghiniana 34:3–32.
Sander, P. M., A. Christian, M. Clauss, R. Fechner, C. T. Gee, E. Griebeler, H. Gunga, J. Hummel, H. Mallison, S. F. Perry, H. Preuschoft, O. W. M. Rauhut, K. Remes, T. Tütken, O. Wings, and U. Witzel. 2011. Biology of the sauropod dinosaurs: the evolution of gigantism. Biological Reviews 86:117–155.
Sander, P. M., and C. Tückmantel. 2003. Bone lamina thickness, bone apposition rates, and age estimates in sauropod humeri and femora. Paläontologische Zeitschrift 77:161–172.
Sander, P. M., O. Mateus, T. Laven, and N. Knötschke. 2006. Bone histology indicates insular dwarfism in a new Late Jurassic sauropod dinosaur. Nature 441:739–741.
Schmitt, A., D. 2012. The inner ear of diplodocoid and basal macronarian sauropods: vestibular adaptations and paleobiological implications. Master, Rheinische Friedrich-Wilhelms-Universität, Bonn, Germany, 82 pp.
Schmitt, A., D., E. Tschopp, F. Knoll, and P. M. Sander. 2013. Paleoneuroanatomy and braincase morphology indicate the presence of at least two diplodocine taxa (Dinosauria: Sauropoda) at the Howe Ranch (Wyoming, USA). Journal of Vertebrate Paleontology, Program and Abstracts 206.
Schwarz, D., E. Frey, and C. A. Meyer. 2007a. Novel reconstruction of the orientation of the pectoral girdle in sauropods. The Anatomical Record: Advances in Integrative Anatomy and Evolutionary Biology 290:32–47.
Schwarz, D., E. Frey, and C. A. Meyer. 2007b. Pneumaticity and soft-tissue reconstructions in the neck of diplodocid and dicraeosaurid sauropods. Acta Palaeontologica Polonica 52:167–188.
Schwarz, D., T. Ikejiri, B. H. Breithaupt, P. M. Sander, and N. Klein. 2007c. A nearly complete skeleton of an early juvenile diplodocid (Dinosauria: Sauropoda) from the Lower Morrison Formation (Late Jurassic) of north central Wyoming and its implications for early ontogeny and pneumaticity in sauropods. Historical Biology 19:225–253.
Schwarz-Wings, D. 2009. Reconstruction of the thoracic epaxial musculature of diplodocid and dicraeosaurid sauropods. Journal of Vertebrate Paleontology 29:517–534.
Schwarz-Wings, D., and N. Böhm. 2012. A morphometric approach to the specific separation of the humeri and femora of *Dicraeosaurus* from the Late Jurassic of Tendaguru,Tanzania. Acta Palaeontologica Polonica.
Sdzuy, K. 1966. An improved method of analyzing distortion in fossils. Palaeontology 9:125–134.
Sereno, P. C. 1991. Basal archosaurs: phylogenetic relationships and functional implications. Journal of Vertebrate Paleontology 11:1–53.
Sereno, P. C. 1998. A rationale for phylogenetic definitions, with application to the higher-level taxonomy of Dinosauria. Neues Jahrbuch Für Geologie Und Paläontologie Abhandlungen 210:41–83.
Sereno, P. C., A. L. Beck, D. B. Dutheil, H. C. . Larsson, G. H. Lyon, B. Moussa, R. W. Sadleir, C. A. Sidor, D. J. Varricchio, and G. P. Wilson. 1999. Cretaceous sauropods from the Sahara and the uneven rate of skeletal evolution among dinosaurs. Science 286:1342–1347.
Sereno, P. C., and J. A. Wilson. 2005. Structure and evolution of a sauropod tooth battery; pp. 157–177 in K. Curry Rogers and J. A. Wilson (eds.), The Sauropods: Evolution and Paleobiology. University of California Press, Berkeley, CA.
Sereno, P. C., J. A. Wilson, L. M. Witmer, J. A. Whitlock, A. Maga, O. Ide, and T. A. Rowe. 2007. Structural extremes in a Cretaceous dinosaur. PLoS ONE 2:e1230.
Siber, H. J., and U. Möckli. 2009. The Stegosaurs of the Sauriermuseum Aathal. Sauriermuseum Aathal, Aathal, 56 pp.
Srivastava, D. C., and J. Shah. 2006. Digital method for strain estimation and retrodeformation of bilaterally symmetric fossils. Geology 34:593–596.
Stein, K., and E. Prondvai. 2013. Rethinking the nature of fibrolamellar bone: an integrative biological revision of sauropod plexiform bone formation. Biological Reviews n/a–n/a.

Sternfeld, R. 1911. Zur Nomenklatur der Gattung *Gigantosaurus* Fraas. Sitzungsberichte Der Gesellschaft Naturforschender Freunde Zu Berlin 8:398.
Steyer, J.-S., D. Heyler, and L. Guillot. 2000. Nouvelles données sur les stégocéphales du bassin de Souvigny. Revue Scientifique Du Bourbonnais et Du Centre de La France 1998:80–88.
Stovall, J. W. 1938. The Morrison of Oklahoma and its dinosaurs. The Journal of Geology 46:583–600.
Swierc, J. E., and G. D. Johnson. 1996. A local chronostratigraphy for the Morrison Formation, Northeastern Bighorn Basin, Wyoming. Wyoming Geological Association, 47th Annual Field Conference Guidebook 47:315–327.
Tang, F., X. Jing, X. Kang, and G. Zhang. 2001. [*Omeisaurus maoianus*: a complete sauropod from Jingyuan, Sichuan]. China Ocean Press, Beijing, China, 112 pp.
Taylor, M. P. 2009. A re-evaluation of *Brachiosaurus altithorax* Riggs 1903 (Dinosauria, Sauropoda) and its generic separation from *Giraffatitan brancai* (Janensch 1914). Journal of Vertebrate Paleontology 29:787–806.
Taylor, M. P. 2010. Sauropod dinosaur research: a historical review. Geological Society, London, Special Publications 343:361.
Taylor, M. P., and D. Naish. 2005. The phylogenetic taxonomy of Diplodocoidea (Dinosauria: Sauropoda). PaleoBios 25:1–7.
Taylor, M. P., and M. J. Wedel. 2013. Why sauropods had long necks; and why giraffes have short necks. PeerJ 1:e36.
Taylor, M. P., M. J. Wedel, and R. L. Cifelli. 2011. A new sauropod dinosaur from the Lower Cretaceous Cedar Mountain Formation, Utah, USA. Acta Palaeontologica Polonica 56:75–98.
Tidwell, V., K. L. Stadtman, and A. Shaw. 2005. Age-related characteristics found in a partial pelvis of *Camarasaurus*; pp. 180–186 in V. Tidwell and K. Carpenter (eds.), Thunder-Lizards: The Sauropodomorph Dinosaurs. Indiana University Press, Bloomington.
Torcida Fernández-Baldor, F., J. I. Canudo, P. Huerta, D. Montero, and X. Pereda Suberbiola. 2011. *Demandasaurus darwini*, a new rebbachisaurid sauropod from the Early Cretaceous of the Iberian Peninsula. Acta Palaeontologica Polonica 56:535–552.
Trujillo, K. C. 2006. Clay mineralogy of the Morrison Formation (Upper Jurassic-? Lower Cretaceous), and its use in long distance correlation and paleoenvironmental analysis. New Mexico Museum of Natural History and Science Bulletin 36:17–23.
Trujillo, K., D. Demar, J. Foster, and S. A. Bilbey. 2011. An exceptionally large juvenile *Camarasaurus* from the Morrison Formation (Upper Jurassic) of Albany County, WY, USA. Journal of Vertebrate Paleontology, Program and Abstracts Suppl. 2:205.
Tschopp, E. 2008. The complete set of autopodia of the *Camarasaurus* SMA 0002 and what it can tell about systematics, taphonomy, ontogeny, and footprint shape. Master Thesis, Paläontologisches Institut und Museum, Zürich, 185 pp.
Tschopp, E., and G. Dzemski. 2012. 3-dimensional reproduction techniques to preserve and spread paleontological material – a case study with a diplodocid sauropod neck. Journal of Paleontological Techniques 10:1–8.
Tschopp, E., and O. Mateus. 2012a. A sternal plate of a large-sized sauropod dinosaur from the Late Jurassic of Portugal. ¡Fundamental! 20:263–266.
Tschopp, E., and O. Mateus. 2012b. The skull and neck of a new flagellicaudatan sauropod from the Morrison Formation and its implication for the evolution and ontogeny of diplodocid dinosaurs. Journal of Systematic Palaeontology 1–36.
Tschopp, E., and O. Mateus. 2013. Clavicles, interclavicles, gastralia, and sternal ribs in sauropod dinosaurs: new reports from Diplodocidae and their morphological, functional and evolutionary implications. Journal of Anatomy 222:321–340.
Tschopp, E., J. Russo, and G. Dzemski. 2013. Retrodeformation as a test for the validity of phylogenetic characters: an example from diplodocid sauropod vertebrae. Palaeontologia Electronica 16:1–23.
Turner, C. E., and F. Peterson. 1999. Biostratigraphy of dinosaurs in the Upper Jurassic Morrison Formation of the Western Interior, USA; pp. 77–114 in Vertebrate Paleontology in Utah., Utah Geological Survey Miscellaneous Publication Salt Lake City.
Turner, C. E., and F. Peterson. 2004. Reconstruction of the Upper Jurassic Morrison Formation extinct ecosystem–a synthesis. Sedimentary Geology 167:309–355.
Upchurch, P. 1995. The evolutionary history of sauropod dinosaurs. Philosophical Transactions of the Royal Society of London. Series B: Biological Sciences 349:365.
Upchurch, P. 1998. The phylogenetic relationships of sauropod dinosaurs. Zoological Journal of the Linnean Society 124:43–103.
Upchurch, P. 1999. The phylogenetic relationships of the Nemegtosauridae (Saurischia, Sauropoda). Journal of Vertebrate Paleontology 19:106–125.

Upchurch, P. 2009. The sauropodomorph supermatrix: towards a global phylogeny of the largest terrestrial animals. Journal of Vertebrate Paleontology Suppl 1:194A.
Upchurch, P., and J. Martin. 2002. The Rutland *Cetiosaurus*: the anatomy and relationships of a Middle Jurassic British sauropod dinosaur. Palaeontology 45:1049–1074.
Upchurch, P., and P. D. Mannion. 2009. The first diplodocid from Asia and its implications for the evolutionary history of sauropod dinosaurs. Palaeontology 52:1195–1207.
Upchurch, P., and P. M. Barrett. 2000. The evolution of sauropod feeding mechanisms; pp. 79–122 in Evolution of herbivory in terrestrial vertebrates: perspectives from the fossil record., Cambridge University Press. Sues, H.-D., Cambridge.
Upchurch, P., P. M. Barrett, and P. Dodson. 2004a. Sauropoda; pp. 259–322 in D. B. Weishampel, P. Dodson, and H. Osmólska (eds.), The Dinosauria. Second edition. University of California Press, Berkeley, CA.
Upchurch, P., P. M. Barrett, and P. M. Galton. 2007. A phylogenetic analysis of basal sauropodomorph relationships: implications for the origin of sauropod dinosaurs. Evolution and Palaeobiology of Early Sauropodomorph Dinosaurs 57–90.
Upchurch, P., Y. Tomida, and P. M. Barrett. 2004b. A new specimen of *Apatosaurus ajax* (Sauropoda: Diplodocidae) from the Morrison Formation (Upper Jurassic) of Wyoming, USA. National Science Museum Monographs 26:1–118.
Varricchio, D. J. 1997. Growth and embryology; pp. 282–288 in Encyclopedia of Dinosaurs. Academic Press, London.
Vickaryous, M. K., and B. K. Hall. 2006. Homology of the reptilian coracoid and a reappraisal of the evolution and development of the amniote pectoral apparatus. Journal of Anatomy 208:263–285.
Vickaryous, M. K., and B. K. Hall. 2010. Comparative development of the crocodylian interclavicle and avian furcula, with comments on the homology of dermal elements in the pectoral apparatus. Journal of Experimental Zoology Part B: Molecular and Developmental Evolution 314:196–207.
Wedel, M. J. 2003. The evolution of vertebral pneumaticity in sauropod dinosaurs. Journal of Vertebrate Paleontology 23:344–357.
Wedel, M. J. 2009. Another mystery: embossed laminae and "unfossae." Sauropod Vertebra Picture of the Week. http://svpow.com/2009/12/07/another-mystery-embossed-laminae-and-unfossae/
Wedel, M. J., and M. P. Taylor. 2013. Neural spine bifurcation in sauropod dinosaurs of the Morrison Formation: ontogenetic and phylogenetic implications. PalArch's Journal of Vertebrate Palaeontology 10:1–34.
Wedel, M. J., and R. K. Sanders. 2002. Osteological correlates of cervical musculature in Aves and Sauropoda (Dinosauria: Saurischia), with comments on the cervical ribs of *Apatosaurus*. PaleoBios 22:1–12.
Wedel, M. J., R. L. Cifelli, and R. K. Sanders. 2000. Osteology, paleobiology, and relationships of the sauropod dinosaur Sauroposeidon. Acta Palaeontologica Polonica 45:343–388.
Weishampel, D. B., and R. Heinrich. 1992. Systematics of Hypsilophodontidae and basal Iguanodontia (Dinosauria: Ornithopoda). Historical Biology 6:159–184.
Wellik, D. M., and M. R. Capecchi. 2003. Hox10 and Hox11 genes are required to globally pattern the mammalian skeleton. Science 301:363–367.
Whitlock, J. A. 2011a. A phylogenetic analysis of Diplodocoidea (Saurischia: Sauropoda). Zoological Journal of the Linnean Society 161:872–915.
Whitlock, J. A. 2011b. Inferences of diplodocoid (Sauropoda: Dinosauria) feeding behavior from snout shape and microwear analyses. PLoS ONE 6:e18304.
Whitlock, J. A. 2011c. Re-evaluation of *Australodocus bohetii*, a putative diplodocoid sauropod from the Tendaguru Formation of Tanzania, with comment on Late Jurassic sauropod faunal diversity and palaeoecology. Palaeogeography, Palaeoclimatology, Palaeoecology 309:333–341.
Whitlock, J. A., and J. D. Harris. 2010. The dentary of *Suuwassea emilieae* (Sauropoda: Diplodocoidea). Journal of Vertebrate Paleontology 30:1637–1641.
Whitlock, J. A., and M. C. Lamanna. 2012. A reanalysis of CM 11162, a skull of *Apatosaurus* (Sauropoda: Diplodocidae). Journal of Vertebrate Paleontology Program and Abstracts:192.
Whitlock, J. A., J. A. Wilson, and M. C. Lamanna. 2010. Description of a nearly complete juvenile skull of *Diplodocus* (Sauropoda: Diplodocoidea) from the Late Jurassic of North America. Journal of Vertebrate Paleontology 30:442–457.
Whitlock, J. A., M. D. D'Emic, and J. A. Wilson. 2011. Cretaceous diplodocids in Asia? Re-evaluating the phylogenetic affinities of a fragmentary specimen. Palaeontology 54:351–364.
Wiersma, K. 2013. Morphology and function of the dentition of *Camarasaurus*. Bachelor Thesis, Universität Bonn, Bonn, Germany, 66 pp.
Wilborn, B. K. 2008. Paleoecology and stratigraphy of the Morrison and Cloverly Formations, Bighorn Basin, Wyoming. Ph.D. dissertation, The University of Oklahoma, Norman, Oklahoma, USA, 291 pp.
Wiley, D. F., N. Amenta, D. A. Alcantara, D. Ghosh, Y. J. Kil, E. Delson, W. Harcourt-Smith, F. J. Rohlf, K. St John, and B. Hamann. 2005. Evolutionary morphing. Visualization, 2005. VIS 05. IEEE 431–438.

Wilhite, D. R. 2003. Biomechanical reconstruction of the appendicular skeleton in three North American Jurassic sauropods. Ph.D. dissertation, Graduate Faculty of the Louisiana State University and Agricultural and Mechanical College 232 pp.

Wilhite, D. R. 2005. Variation in the appendicular skeleton of North American sauropod dinosaurs: taxonomic implications; pp. 268–301 in V. Tidwell and K. Carpenter (eds.), Thunder-lizards: the Sauropodomorph dinosaurs. Indiana University Press, Bloomington.

Williams, S. H. 1990. Computer-assisted graptolite studies; pp. 46–55 in Microcomputers in Palaeontology., Contributions from the Palaeontology Museum, University of Oslo vol. 370. Oslo.

Wilson, J. A. 1999. A nomenclature for vertebral laminae in sauropods and other saurischian dinosaurs. Journal of Vertebrate Paleontology 19:639–653.

Wilson, J. A. 2002. Sauropod dinosaur phylogeny: critique and cladistic analysis. Zoological Journal of the Linnean Society 136:215–275.

Wilson, J. A. 2005. Overview of sauropod phylogeny and evolution; pp. 15–49 in K. A. Curry Rogers and J. A. Wilson (eds.), The Sauropods: Evolution and Paleobiology. University of California Press, Berkeley, CA.

Wilson, J. A. 2012. New vertebral laminae and patterns of serial variation in vertebral laminae of sauropod dinosaurs. Contributions from the Museum of Paleontology, University of Michigan 32:91–110.

Wilson, J. A., and D. M. Mohabey. 2006. A titanosauriform (Dinosauria: Sauropoda) axis from the Lameta Formation (Upper Cretaceous: Maastrichtian) of Nand, central India. Journal of Vertebrate Paleontology 26:471–479.

Wilson, J. A., and M. B. Smith. 1996. New remains of *Amphicoelias* Cope (Dinosauria: Sauropoda) from the Upper Jurassic of Montana and diplodocoid phylogeny. Journal of Vertebrate Paleontology 16:73A.

Wilson, J. A., and M. T. Carrano. 1999. Titanosaurs and the origin of "wide-gauge" trackways: a biomechanical and systematic perspective on sauropod locomotion. Paleobiology 25:252–267.

Wilson, J. A., and P. C. Sereno. 1998. Early evolution and higher-level phylogeny of sauropod dinosaurs. Journal of Vertebrate Paleontology 18:1–79.

Wilson, J. A., and P. Upchurch. 2003. A revision of *Titanosaurus* Lydekker (Dinosauria-Sauropoda), the first dinosaur genus with a "Gondwanan"distribution. Journal of Systematic Palaeontology 1:125–160.

Wilson, J. A., and P. Upchurch. 2009. Redescription and reassessment of the phylogenetic affinities of *Euhelopus zdanskyi* (Dinosauria: Sauropoda) from the Early Cretaceous of China. Journal of Systematic Palaeontology 7:199–239.

Wilson, J. A., M. D. D'Emic, T. Ikejiri, E. M. Moacdieh, and J. A. Whitlock. 2011. A nomenclature for vertebral fossae in sauropods and other saurischian dinosaurs. PLoS ONE 6:e17114.

Wilson, J. A., R. N. Martinez, and O. Alcober. 1999. Distal tail segment of a titanosaur (Dinosauria: Sauropoda) from the Upper Cretaceous of Mendoza, Argentina. Journal of Vertebrate Paleontology 19:591–594.

Witmer, L. M., R. C. Ridgely, D. L. Dufeau, and M. C. Semones. 2008. Using CT to Peer into the Past: 3D Visualization of the brain and ear regions of birds, crocodiles, and nonavian dinosaurs; pp. 67–87 in H. Endo and R. Frey (eds.), Anatomical Imaging. Springer Japan, Tokyo.

Woodruff, D. C., and D. W. Fowler. 2012. Ontogenetic influence on neural spine bifurcation in Diplodocoidea (Dinosauria: Sauropoda): a critical phylogenetic character. Journal of Morphology 273:754–764.

Woodward, A. S. 1905. On parts of the skeleton of *Cetiosaurus leedsi*, a sauropodous dinosaur from the Oxford Clay of Peterborough. Proceedings of the Zoological Society of London 1:232–243.

Xing, L., Y. Yong, S. Chunkang, P. Guangzhao, and Y. Hailu. 2009. Structure, orientation and finite element analysis of the tail club of *Mamenchisaurus hochuanensis*. Acta Geologica Sinica - English Edition 83:1031–1040.

Yates, A. M., and C. C. Vasconcelos. 2005. Furcula-like clavicles in the prosauropod dinosaur *Massospondylus*. Journal of Vertebrate Paleontology 25:466–468.

Young, C. C. 1939. On a new Sauropoda, with notes on other fragmentary reptiles from Szechuan. Bulletin of the Geological Society of China 19:279–315.

Young, C. C. 1958. New sauropods from China. Vertebrata PalAsiatica 2:1–28.

Young, C. C., and X. Zhao. 1972. Description of the type material of *Mamenchisaurus hochuanensis*. Institute of Vertebrate Paleontology and Paleoanthropology Monograph Series I 8:1–30.

Young, M. T., E. J. Rayfield, C. M. Holliday, L. M. Witmer, D. J. Button, P. Upchurch, and P. M. Barrett. 2012. Cranial biomechanics of *Diplodocus* (Dinosauria, Sauropoda): testing hypotheses of feeding behaviour in an extinct megaherbivore. Naturwissenschaften 1–7.

Yu, C. 1993. The skull of *Diplodocus* and the phylogeny of the Diplodocidae. Ph.D. dissertation, Faculty of the Division of Biological Sciences and the Pritzker School of Medicine, University of Chicago, Chicago, 154 pp.

Zaher, H., D. Pol, A. B. Carvalho, P. M. Nascimento, C. Riccomini, P. Larson, R. Juarez-Valieri, R. Pires-Domingues, N. J. da Silva, and C. D. de Almeida. 2011. A complete skull of an Early Cretaceous sauropod and the evolution of advanced titanosaurians. PLoS ONE 6:e16663.

Zhang, Y. 1988. The Middle Jurassic Dinosaur Fauna from Dashanpu, Zigong, Sichuan, Vol. 1: Sauropod Dinosaur (I): *Shunosaurus*. Sichuan Publishing House of Science and Technology, Chengdu, China, 114 pp.

Zheng, Z. 1996. Cranial anatomy of *Shunosaurus* and *Camarasaurus* (Dinosauria: Sauropoda) and the phylogeny of the Sauropoda. Ph. D. dissertation, Texas Tech University, Lubbock, TX, USA, 208 pp.

Zollikofer, C. P., and M. S. Ponce de León. 2005. Virtual Reconstruction: a Primer in Computer-assisted Paleontology and Biomedicine. Wiley-Interscience, Hoboken, NJ, 333 pp.

Zollikofer, C. P., M. S. Ponce de León, and R. D. Martin. 1998. Computer-assisted paleoanthropology. Evolutionary Anthropology: Issues, News, and Reviews 6:41–54.

Zollikofer, C. P., M. S. Ponce de León, D. E. Lieberman, F. Guy, D. Pilbeam, A. Likius, H. T. Mackaye, P. Vignaud, and M. Brunet. 2005. Virtual cranial reconstruction of *Sahelanthropus tchadensis*. Nature 434:755–759.